Medical Radiology · Diagnostic Imaging
Series Editors: Hans-Ulrich Kauczor · Paul M. Parizel · Wilfred C. G. Peh

Filip M. Vanhoenacker
Mario Maas
Jan L. M. A. Gielen *Editors*

Imaging of Orthopedic Sports Injuries

Second Edition

Springer

Medical Radiology

Diagnostic Imaging

The book series Medical Radiology – Diagnostic Imaging provides accurate and up-to-date overviews about the latest advances in the rapidly evolving field of diagnostic imaging and interventional radiology. Each volume is conceived as a practical and clinically useful reference book and is developed under the direction of an experienced editor, who is a world-renowned specialist in the field. Book chapters are written by expert authors in the field and are richly illustrated with high quality figures, tables and graphs. Editors and authors are committed to provide detailed and coherent information in a readily accessible and easy-to-understand format, directly applicable to daily practice.

Medical Radiology – Diagnostic Imaging covers all organ systems and addresses all modern imaging techniques and image-guided treatment modalities, as well as hot topics in management, workflow, and quality and safety issues in radiology and imaging. The judicious choice of relevant topics, the careful selection of expert editors and authors, and the emphasis on providing practically useful information, contribute to the wide appeal and ongoing success of the series. The series is indexed in Scopus.

For further volumes: http://www.springer.com/series/4354

Filip M. Vanhoenacker • Mario Maas
Jan L. M. A. Gielen
Editors

Imaging of Orthopedic Sports Injuries

Second Edition

Springer

Editors
Filip M. Vanhoenacker
Department of Radiology
Antwerp University Hospital
Edegem, Belgium

Jan L. M. A. Gielen
Department of Radiology
Antwerp University Hospital
Edegem, Belgium

Mario Maas
Department of Radiology and Nuclear Medicine
Amsterdam University Medical Centres
Amsterdam, The Netherlands

ISSN 0942-5373 ISSN 2197-4187 (electronic)
Medical Radiology
ISBN 978-3-030-75361-0 ISBN 978-3-030-75362-7 (eBook)
https://doi.org/10.1007/978-3-030-75362-7

This Springer imprint is published by the registered company Springer Nature Switzerland AG
The registered company address is: Gewerbestrasse 11, 6330 Cham, Switzerland

Foreword to the Second Edition

Soon after we assumed Editorships of the Medical Radiology Series of *Springer Nature*, one of the first books that was targeted for an updated edition was *Imaging of Orthopedic Sports Injuries,* edited by Professors Filip Vanhoenacker, Mario Maas and Jan Gielen. When approached, lead editor Professor Vanhoenacker readily agreed to take on this task and after a period of planning, commenced on the project which took about 1 year to complete. This is a very efficient turnaround time by any standard, let alone for a monumental project such as this.

Following on the outstanding success of the original book published in 2007, Professors Vanhoenacker, Maas and Gielen have once again put together this truly excellent second edition. The new book has not only expanded in terms of additional chapters but also contains much new content that reflects the continued growth and updated knowledge of imaging and imaging-guided intervention of sports injuries. The authorship list of this book can be regarded a "Who's who" of musculoskeletal radiologists in Europe, with the exception of one chapter authored from Singapore and Australia!

It gives both of us great personal pleasure to be able to congratulate Filip for successfully overseeing the second edition of this book. Wilfred has known Filip for about 20 years, having been involved together as faculty in many annual congresses in Europe and North America organised by the European Society of Skeletal Radiology (ESSR) and the International Skeletal Society (ISS). Being fellow musculoskeletal radiologists with a strong sense of academic obligation, both have also contributed substantially to congresses and teaching programmes held in Asia under the auspices of the Asian Musculoskeletal Society, an organisation in which Wilfred served as the Founding President, as well as the ISS regional outreach programmes and meetings of other regional and national radiological societies in Asia. Wilfred and Filip have, more importantly, become firm friends over these many years.

Paul and Filip go back even further, having known each other since the beginning of their professional careers as radiologists in Belgium. Their professional collaboration has expanded far beyond the local and national level, onto the international and European arena. Throughout the years, both have collaborated on many projects, courses and meetings organised by the European Society of Radiology (ESR), the ESSR and the European Society of Neuroradiology (ESNR). Through serendipity, it so happened that in the year 2017, Filip was President of the ESSR while Paul was President of the

ESR, and this happy coincidence further enhanced their collaboration on many projects. Importantly, their collaboration on scientific projects has grown into a long-lasting friendship spanning several decades and built on a foundation of respect and mutual understanding.

Over the recent two decades or so, imaging has become increasingly important in the diagnosis, management, therapy guidance, and follow-up of patients with sports injuries. Healthcare professionals, and in particular orthopaedic surgeons, are increasingly reliant on imaging data to make clinical decisions. New developments in imaging technology have greatly advanced our insights into the pathophysiology of sports injuries. This progress has created not only new opportunities for radiologists and nuclear medicine physicians but also new challenges. We must learn to understand and speak the language of our clinical colleagues, and we need to acquire clinical background knowledge about mechanisms of injury and repair and about their pathophysiology. Together with orthopaedic surgeons, specialists in physical medicine and rehabilitation, physical therapists and many other healthcare professionals, radiologists and nuclear medicine physicians are an essential part of the multidisciplinary team that makes evidence-based decisions in patients with sports injuries. This book provides a comprehensive overview of the subject and shall prove to be equally useful to both imaging professionals and referring clinicians.

The second edition of *Imaging of Orthopedic Sports Injuries* is therefore very timely. We have no doubt that this book will be most successful and sought after as a "must-read" by everyone with an interest in and wishing to learn more about imaging of musculoskeletal sports injuries.

July 2020

Wilfred C. G. Peh
Department of Diagnostic Radiology
Khoo Teck Puat Hospital
Singapore, Singapore

Yong Loo Lin School of Medicine
National University of Singapore
Singapore, Singapore

Paul M. Parizel
Royal Perth Hospital &
University of Western Australia
Perth, Australia

Preface to the Second Edition

Today more than ever, sports activities are no longer the privilege of competitive and professional athletes or the "select happy few", but almost all sports disciplines are accessible to a large population in all age groups.

The sporting population is vulnerable to musculoskeletal lesions due to either acute trauma or overuse. It was already underscored in the first edition of this book that imaging of these patients plays an important role in diagnosis, grading, defining appropriate treatment regime, and follow-up.

Since the first edition in 2007, imaging techniques have been further refined, indications have expanded, and new insights in pathogenesis and imaging of musculoskeletal sports trauma evolved tremendously.

Therefore, we are very grateful that the series editors of Medical Radiology (Springer) professor Wilfred Peh and professor Paul Parizel entrusted us with the task to update our work.

Ultrasound is generally accepted as the "working horse" for the evaluation of trauma of the ligaments, tendons and muscles, particularly for dynamic evaluation of these structures. The overall availability of MRI has increased, and the technique is now a mature and indispensable diagnostic tool for the evaluation of internal joint derangement in every sports clinic.

Although CT is generally replaced by MRI, (Cone Beam) CT may be very useful for the diagnosis of occult fractures of (small) bones and is particularly important in the evaluation of maxillofacial sports trauma, where it completely replaced plain radiography.

Compared to the previous edition, the general structure of this book has been maintained, with a general part on basic sciences and general imaging principles, followed by an extensive topographic discussion of musculoskeletal sports injuries and lastly some special addenda.

The text of the book has been largely updated, and many new state-of-the-art images were added. We included new chapters on imaging-guided intervention of sports injuries and postoperative joint imaging in the sportive patient.

Furthermore, we dedicated one chapter to imaging of soccer injuries, as one of the most popular sports worldwide.

We are very grateful to all contributing authors, being internationally renowned experts in musculoskeletal imaging, for their willingness to deliver outstanding contributions.

Finally—on behalf of my co-editors—I would like to express our special thanks to Springer for giving us the opportunity to edit the second edition of this book.

We hope that this work will be helpful in the daily practice of general and musculoskeletal radiologists and everyone else involved in sports medicine and we hope you enjoy reading it.

Antwerp, Belgium
July 2020

Filip M. Vanhoenacker

Introduction

Endorsement on Behalf of the European Society of Musculoskeletal Radiology (ESSR)

Musculoskeletal (MSK) injuries occurring from sports play today an important role in the diagnosis and treatment of MSK disorders. Recent advances in imaging have greatly aided the diagnosis and treatment decision-making in patients with sports injuries. Imaging can be used to make diagnoses, define prognoses, influence treatment plans, or to preoperatively assess the severity of known pathology, and follow-up recovery of the injury. Let us simplify: imaging of sports injuries is challenging, interesting, and evolving. The use of imaging and its various modalities depends on the clinical information and availability of those modalities. The goal of musculoskeletal imaging is to provide as much information as possible to allow timely and appropriate patient care. The musculoskeletal radiologist plays a pivotal role and has a strong tool in hands to start managing sports injuries. A strong tool primarily assumes knowledge: Knowledge about body anatomy, pathophysiology, mechanism of injury, injuries pattern, advances and limitation of different imaging modalities as well as typical injuries for any specific sport. The aim of the European Society of Musculoskeletal Radiology and its Sports Subcommittee is to encourage the advancement of knowledge. Therefore, the publication of this book, *Imaging of Orthopedic Sports Injuries*, is an important highlight for the radiological profession and for all those involved in sports injuries management.

All parts of the book offer an invaluable wealth of fundamental insights and new achievements in sports injuries imaging.

The first part of the book contains information on relevant basic science and general imaging principles in sports traumatology. The second part comprises a topographic discussion of sports injuries and elaborates the merit of different imaging techniques and different clinical problems focused on a specific location. In the third part, monitoring and follow-up of sports injuries and their repair by imaging are discussed. The fourth part leads through imaging-guided intervention procedures and postoperative imaging of sports injuries.

This well-illustrated book will be of value for musculoskeletal radiologists, but it also represents valuable educational material that will improve and facilitate everyday work of orthopaedic surgeons, sports physicians, and everyone else involved in sports medicine.

Igor Boric
St. Catharine Specialty Hospital
Zagreb, Croatia

Contents

Part I

Relevant Basic Science and General Imaging Principles

The Clinician's Point of View

Babette M. Pluim and Sebastiaan J. Maresch

Contents

Abstract

In this chapter the role of musculoskeletal radiology in the diagnosis and management of sports injuries is discussed. The use of imaging techniques is an important tool for the sports physician to establish the correct diagnosis and to choose the appropriate treatment procedures. In addition, imaging techniques can be useful for the evaluation and monitoring of the healing process and the early identification of complications.

Good communication between the radiologist and the sports physician is essential. The information the sports physician provides to the radiologist regarding the history of injury, athlete's training program, and physical examination will help the radiologist choose the correct imaging technique. The sports physician should also share his/her knowledge of the special demands of the sport involved and the effects that this has on the musculoskeletal system of the athlete.

The radiologist should have a subspecialization in musculoskeletal radiology, preferably sports radiology. The department should be flexible enough to examine an athlete within 24 h to 5 days, if warranted. Detailed feedback from the radiologist to the sports physician will help the latter to make the correct interpretation of any abnormalities and direct him/her towards the appropriate form of treatment.

There is a risk of over-imaging, including finding nonsignificant abnormalities, imaging

B. M. Pluim (✉)
KNLTB, Amstelveen, The Netherlands
e-mail: B.Pluim@knltb.nl

S. J. Maresch
Sports Valley & Radiological Centre Topsport, Ede, The Netherlands

Med Radiol Diagn Imaging (2020)
https://doi.org/10.1007/174_2020_246, © Springer Nature Switzerland AG
Published Online: 08 December 2020

findings with no direct relation with clinical symptoms or different reports. The travelling athlete is an extra challenge, which can be reduced by having the athlete carry their own files, having an electronic database or sending the information electronically.

It is only as a result of teamwork between the sports physician and the radiologist that an optimal outcome can be achieved.

1 Introduction

Musculoskeletal (MSK) radiology has grown rapidly as an imaging subspecialty in the past years. Especially the improvement in magnetic resonance imaging (MRI) and ultrasonography has resulted in enhanced imaging of MSK structures, and led to a more important role for radiologists in the diagnosis and management of sports injuries (Coris et al. 2009).

The new technologies in ultrasound, multidetector computed tomography (CT), and MRI have made it possible to detect subtle findings, including muscle injury, stress reactions of the bones, tendinosis, and early stages of bone marrow edema (Hynes et al. 2018). Detection of early abnormalities has enabled further research in the prevention of tendon ruptures, osteoarthritis, and fractures of bone and has improved clinical management. An accurate diagnosis can often be made based on a history and physical examination alone but imaging techniques can be very helpful to confirm the clinical suspicion or if there is doubt about the diagnosis in trauma and overuse injuries. Imaging may be useful to refine the differential diagnosis. In addition, imaging is frequently used to determine the prognosis in elite professional athletes, but plays an increasingly important role in amateur sport at all levels and ages as well. Furthermore, imaging services are now provided at many sporting events and venues and not only in the traditional clinic/hospital setting.

In patients who do not respond to conservative management, imaging can be especially useful to acquire a better understanding of the extent of the lesion. However, over-imaging can cause problems in high-level athletes, who have easy access to imaging modalities when travelling abroad. This is particularly so when there is lack of communication between the various treating physicians and when an understanding of the mechanism of injury is essential in order to establish the correct diagnosis.

Sports medical care is a team effort in which a diversity of medical professionals from a variety of disciplines are involved, especially at elite level. The sport radiologist is an important part of the team, working in close collaboration with the sports medicine physician.

This chapter will review a number of situations, where good communication between the radiologist and sports physician can result in the correct choice of imaging technique and a greater chance of establishing the correct diagnosis. The specific demands that elite athletes and sports physicians may place on the radiologist and the radiology department are also discussed.

2 Role of Imaging

It should be noted that the patient population of the sports physician differs slightly from the normal population. In general, athletes tend to be highly motivated and are keen to resume sport as soon as possible. The majority of their injuries are caused by training overload; yet, they find it very difficult to reduce this load. There is always another match, another race, another goal to achieve. In a situation where a “normal” patient may be content to give his/her ankle sprain or stress fracture the required 3–6 weeks rest, an athlete will want to know if she or he can participate in next week’s tournament. When working with athletes, there is always time pressure.

This is where imaging can play an important role for both the sports physician and the athlete. Firstly, by specifying the diagnosis and the extent of injury, imaging can be conducive to a more tailor-made choice of treatment and return to play. Secondly, it is often very helpful to provide the athlete with visual evidence that a significant injury is present (e.g., stress fracture, muscle rupture, or meniscal lesion) and thereby convince him/her that rest is indeed essential. Hopefully,

this will also obviate the inclination of the athlete to get multiple opinions ("medical shopping"). Lastly, it may clarify if surgery is necessary. In cases where conservative management is indicated, imaging may also help determine the appropriate form of treatment, e.g., if calcifications are present, use of needle aspiration of calcium deposits may be indicated (Oudelaar et al. 2016). Despite the fact that corticosteroid injections are used less and less in sports medicine, there are still instances when this type of treatment is indicated and imaging can help in this choice, e.g., a tenosynovitis (trigger finger), ganglion cyst, or bursitis. Imaging (ultrasound) guided injections are increasingly used and are more accurate compared to blind injections (Daniels et al. 2018; Evers et al. 2017).

3 What Is Expected from the Radiologist?

When dealing with elite athletes, there are certain aspects that differentiate the general radiologist from the "sports" radiologist.

1. Subspecialization in musculoskeletal and preferably sports radiology with interest in sports and "feel" for the athlete. It is very important that the radiologist has an interest in sports and is able to place himself in the position of the athlete. For athletes, minor injuries can cause great distress and hamper the athlete in his or her training (e.g., a minor muscle strain in a long-distance runner). The radiologist has to be aware of this fact and needs to look for minor abnormalities that may have no clinical significance in a nonathletic patient. The sports-radiologist has to have knowledge of sports specific pathology, clinical irrelevant sports findings, and anatomical variations. It is essential that the radiologist is willing to analyze the problem with the sports physician and aid in the complex process of return to sports involving multiple factors, stakeholders, and everlasting time constraints.
2. Interest in the musculoskeletal system. The radiologist needs to be knowledgeable about the musculoskeletal system, because this is where the vast majority of the sporting injuries occur. Musculoskeletal radiology's role in the recent and continued evolution of sports medicine is expanding. Radiologists are playing a definite role in the clinical management of elite- and non-elite athletes.
3. Access to a broad network. The radiologist does not need to be an expert in every area himself, but should have a broad network of specialist colleagues who have an interest and/or knowledge of sports related problems.
4. An unbiased interpretation of imaging findings. It is recommended to have two radiologists interpret the images of elite athletes ("double-reading").
5. Knowledge and understanding of different imaging modalities and image-guided interventions. Image-guided injections, CT, and more often ultrasound are superior over blind-injections techniques.
6. Aid in return-to-play decision-making. It can be helpful to show the athlete (and sport physician) the images, if the setting allows this. Educating the athlete may lead to better understanding, increase their engagement, and improve their compliance.
7. Speed and accuracy of diagnosis. Of concern for both the professional and the amateur athlete. Although anatomical imaging remains the mainstay of MSK radiology, significant progress has been made in functional and molecular imaging as well as in hybrid imaging with an expanding armament of technologies becoming available or in development.

4 What Is Expected from the Radiology Department?

1. The full spectrum of MSK-imaging modalities has to be in the portfolio of the radiology department. The department should have an MSK radiologist with extensive expertise in MSK ultrasound including dynamic and ultrasound guided therapy, multidetector CT, MRI/MR-arthrography, scintigraphy, and knowledge of the latest techniques.

Rapid advancements are developing in the field of imaging of MSK disorders such as functional and molecular imaging, rapid image acquisition techniques, cartilage mapping, 3D imaging, diffusion-weighted imaging, perfusion imaging, diffusion tensor imaging, peripheral nerve imaging, kinematic CT, artificial intelligence, elastography, ultrasound tissue characterization, PET CT, and hybrid imaging.

2. The radiologist needs to work in a team willing to provide 24/7/365 sports radiology care when dealing with elite athletes. Since there is a lot of time pressure on elite athletes, flexibility and easy access are important. It is preferable if the department has slots open for elite athletes for diagnostics within 24 h to 5 days, if required. This is not always necessary, but can be essential when the athlete is competing in a tournament, or has to travel again within a short period of time. Pitch-side and sporting events radiology are more often requested, contributing to the demand of speed, onsite delivery, and image-guided therapies (Hynes et al. 2018).

5 What Is Expected from the Sports Physician?

1. To provide detailed information. The sports physician has to provide detailed information to the radiologist. For example, when referring an athlete with a high probability of a stress fracture, information regarding the nature of the activity or sport (e.g., jumping, hurdling, plyometrics) and the load on the athlete is very important in establishing the diagnosis. A detailed history, including a training history, is essential. Most radiologists should have a high level of suspicion of a fracture of the second metatarsal in military recruits or athletes. However, in order to detect high-risk or more uncommon stress fractures (such as a humeral stress fracture in a tennis player, a stress fracture of the lower back in a gymnast, or a stress fracture of the hip in a long-distance runner), good communication between the sports physician and radiologist is essential (McKinnis and Ramey 2016). This is particularly important because the sensitivity of plain radiographs in the early stages of a stress fracture is very low. In athletes where there is a high probability of a stress fracture, a normal radiograph should prompt further investigation with other imaging techniques (Kiel and Kaiser 2019).
2. Seek advice before referring. Since the choice of the imaging modality depends on the expected type of lesion, the sports physician should be willing to seek advice from the radiologist before referring an athlete. No clearer example can be given that the ideal imaging technique for examination of the shoulder joint (plain radiography, ultrasound, MR(-arthrography) or CT(-arthrography), bone scan) will differ along with the clinical problem (SLAP lesion, (partial) tendon rupture, bursitis, synovitis or fracture) (Beltran et al. 2015; Roy et al. 2015, 2016). Previous radiology exams can be essential in the interpretation of a radiology exam and form an integral part of the interpretation in every diagnostic imaging. Whenever possible, a previous exam should be provided. A central archive with easy and direct availability can be very helpful, especially in elite athletes.

6 Risks of Over-Imaging

When working with high-level athletes, there are certain situations that are less likely to occur in the general population or in lower level athletes.

1. No direct relation between clinical symptoms and imaging findings. Athletes are often tempted to repeat imaging to establish if "things are improving." The diagnosis is already established and imaging has already been carried out, so repeat studies should only be undertaken if symptomatic improvement is not taking place. Repeat studies often lead to confusion in the mind of the athlete and coach. He feels better, he is getting better, but that is

not confirmed by MRI, which may cause anxiety. Not performing an imaging study would have been a better decision for the patient, although the hospital finance department might not agree. If the diagnosis is already known, and the treatment plan has been determined, and performing an imaging study will have no influence on this, imaging is not necessary.

2. Nonsignificant abnormalities. Asymptomatic athletes may have abnormalities on plain radiographs, CT-scan, or MRI, but which have no clinical significance (Johansson et al. 2015). It is important to make this very clear to the athlete, in order not to disturb their positive body image.
3. Different reports. There is also the risk that serial imaging will produce slightly different reports. Again, this may have no clinical significance, but it is important to explain this clearly to the athlete and his/her coach. Ultrasound or MRI reports are not always black and white, so if the reporting radiologist focuses on slightly different areas than the previous radiologist, this may lead to a confused athlete. For example, when examining a shoulder with ultrasound, there may be a thickening of the supraspinatus tendon, some fluid in the bursa, and small calcifications present. If the (nonsignificant) calcifications were not mentioned the first time, this may put doubt in the athlete's mind that the injury is getting worse instead of better. The same may happen with an MRI of the lower back after a herniated disc. Clinical symptoms do not always coincide with MRI images, and one clinician may call the herniation "small," whereas the next report may mention a "significant" herniation. It is always recommended that previous imaging and reports are available when repeat imaging is being carried out.

7 The Travelling Athlete

An extra challenge may be encountered when dealing with elite athletes who are travelling regularly, or have just returned from travelling. Their documentation may be incomplete and the athlete may not know or remember whether they had a partial medial or lateral meniscectomy. Even the referring sports physician may not know the answer and this can make it very difficult for the radiologist who has to perform an MRI because of residual or recurrent symptoms.

This problem has been recognized at the international level, but has not yet led to a unified approach. Three options are currently available to tackle this problem:

1. The athlete carries his own medical files and takes them with him/her when they visit a doctor. This requires the athlete to be efficient and carry the medical information at all times.
2. The injuries are registered in an electronic database that is hosted by the (inter)national federation of the athlete's sport. The data need to be stored in a highly secure environment, whereby access is carefully controlled to ensure that data is available to relevant parties only.
3. The information is sent from the previous doctor to the current doctor electronically. This requires that the name of the previous doctor and hospital are known, that they can be traced, and that they are able to send this information very quickly.

In addition, there is sometimes a travelling sports physician accompanying elite athletes. It is therefore desirable that a medical database, including imaging files, can be accessed by health care professionals wherever an athlete may be competing in the world. This would ensure that other medical specialists could have access to the athlete's complete medical history, regardless of location.

8 Conclusions

The use of imaging techniques is an important tool for the sports physician in establishing the correct diagnosis and choosing the appropriate treatment procedures. In addition, imaging techniques can be useful for the evaluation and

monitoring of the healing process and the early identification of complications.

Good communication between the radiologist and the sports physician is essential. The information the sports physician provides to the radiologist regarding the history of injury, athlete's training program, and physical examination will help the radiologist choose the correct imaging technique. The sports physician should also share his/her knowledge of the special demands of the sport involved and the effects that this has on the musculoskeletal system of the athlete.

The radiologist should have an interest in sports and be willing to invest some extra time with the athlete for a detailed history and to communicate with the referring sports physician. The department should be flexible enough to examine athlete within 24 h to 5 days, if warranted. Detailed feedback from the radiologist to the sports physician will help the latter to make the correct interpretation of any abnormalities and direct him/her towards the appropriate form of treatment.

It is only as a result of teamwork between the sports physician and the radiologist that an optimal outcome can be achieved.

Things to Remember

1. The radiologist should have an interest in sports, preferably work in a team with MSK-/sports radiologists, specific knowledge of MSK- and sports radiology and availability of the necessary broad spectrum of imaging techniques and state-of-the-art equipment and be willing to invest extra time with the athlete for a detailed history and to communicate with the referring sports physician.
2. The use of imaging techniques is an important tool for the sports physician in establishing the correct diagnosis and choosing the appropriate treatment procedures. It is only as a result of teamwork between the sports physician and the radiologist that an optimal outcome can be achieved.

References

Beltran LS, Adler R, Stone T et al (2015) MRI and ultrasound imaging of the shoulder using positional maneuvers. Am J Radiol 205:W244–W254

Coris EE, Zwygart K, Fletcher M, Pescasio M (2009) Imaging in sports medicine: an overview. Sports Med Arthrosc Rev 17:2–12

Daniels EW, Cole D, Jacobs B et al (2018) Existing evidence on ultrasound-guided injections in sports medicine. Orthop J Sports Med 6(2):2325967118756576

Evers S, Bryan AJ, Sanders TL et al (2017) Effectiveness of ultrasound-guided injections compared to blind steroid injections in the treatment of carpal tunnel syndrome. Arthritis Care Res 69(7):1060–1065

Hynes JP, Walsh J, Farrell TP et al (2018) Role of musculoskeletal radiology in modern sports medicine. Semin Musculoskelet Radiol 22(5):582–591

Johansson FR, Skillgate E, Adolfsson A et al (2015) Asymptomatic elite adolescent tennis players' signs of tendinosis in their dominant shoulder compared with their nondominant shoulder. J Athl Train 50(12):1299–1305

Kiel J, Kaiser K (2019) Stress reactions and fractures. Source StaPearls [Internet]. StatPearls Publishing, Treasure Island (Fl)

McKinnis KC, Ramey LN (2016) High-risk stress fractures: diagnosis and management. PM R 8(3 suppl):S113–S124

Oudelaar BW, Schepers-Bok R, Ooms EM et al (2016) Needle aspiration of calcific deposits (NACD) for calcific tendinitis is safe and effective: six months follow-up of clinical results and complications in a series of 431 patients. Eur J Radiol 85(4): 689–694

Roy JS, Braën C, Leblond J et al (2015) Diagnostic accuracy of ultrasonography, MRI and MR arthrography in the characterisation of rotator cuff disorders: a systematic review and meta-analysis. Br J Sports Med 49:1316–1328

Roy EA, Cheyne I, Andrews GT, Forster B (2016) Beyond the cuff: MR imaging of labroligamentous injuries in the athletic shoulder. Radiology 278(2):316–332

Imaging Techniques and Procedures in Sports Injuries

E. De Smet, P. Van Dyck, J. Gielen, and F. M. Vanhoenacker

Contents

Abstract

In the evaluation of sport injuries, clinical findings may be non-specific and radiological imaging is often necessary to obtain an accurate diagnosis. This chapter describes the different imaging modalities available to evaluate sports injuries (radiography, ultrasound (US), computed tomography (CT) and magnetic resonance imaging (MRI)) as well as technical considerations and indications. Radiography is useful as a screening tool for bony abnormalities, such as degeneration or fractures. (Cone beam) CT can visualise these bony abnormalities even better or, combined with arthrography, may reveal labral or tendon abnormalities. US and MRI are able to visualise superficial and deep soft-tissue lesions, respectively. The optimal imaging pathway should be tailored to the patient and depends of the patient, radiologist and clinician.

E. De Smet (✉) · P. Van Dyck · J. Gielen
Department of Radiology, University of Antwerp, Edegem, Belgium
e-mail: eline.desmet2@uza.be

F. M. Vanhoenacker
Department of Radiology, University Hospital Antwerp, Edegem, Belgium

Department of Radiology, AZ St-Maarten, Mechelen, Belgium

Department of Radiology, Ghent University Hospital and Ghent University, Ghent, Belgium

Med Radiol Diagn Imaging (2021)
https://doi.org/10.1007/174_2020_239, © Springer Nature Switzerland AG
Published Online: 23 February 2021

1 Introduction

In the last decennia, sports medicine has become one of the most rapidly growing medical subspecialties (Johnson 2000).

Symptoms and clinical findings in sports injuries are often non-specific or unreliable, for example when patients are in too much pain to cooperate. Therefore, accurate diagnosis and optimal treatment planning are often dependent on imaging studies. It is important to realise that the "optimal" imaging modality or pathway probably does not exist and that the choice of imaging modality depends on the clinicians' and radiologists' comfort and experience with those modalities, financial costs, availability and invasiveness of each technique balanced against the diagnostic award. In many cases, the imaging pathway should be tailored to the individual patient.

In this chapter, the imaging strategies that can be employed to diagnose and grade sports injuries are reviewed, including the role of each imaging technique with its specific advantages and limitations. The reader will find some practical guidelines for the evaluation of sports injuries that, in our opinion, may be useful in daily clinical practice.

2 Plain Radiography and Conventional Arthrography

2.1 Plain Radiography

Radiography is often the first imaging modality performed for the evaluation of sport injuries and is capable of detecting fractures, joint degeneration and/or loose bodies.

Typically, two projections perpendicular to each other are sufficient to detect radiographic abnormalities. Occasionally, oblique (3/4) views may be helpful, e.g. to demonstrate fractures of the radial head or for detection of bone spurs in anterior ankle impingement. They are—however—not commonly used in daily clinical practice and have largely been replaced by cross-sectional imaging.

Stress views have additional value, in that they may provide indirect evidence of ligamentous injury, e.g. weight-bearing radiographs in ligamentous Lisfranc injury or stress views of the AC joint. However, the value of stress radiographs has declined in the previous centuries, as MRI is nowadays more and more available to provide direct visualisation of ligamentous injury. For example, the ACR appropriateness criteria (2017) prefer MRI to stress views of the ankle in the evaluation of suspected ankle instability (Chang et al. 2017). Stress radiographs are also painful or even impossible to obtain in the acute setting as patients are unable or reluctant to cooperate.

After the initial diagnosis, radiographs are essential to evaluate the surgical results: reduction of dislocations and alignment of displaced fracture fragments and position of internal or external fixation devices. It can also be useful in monitoring progress of fracture healing (callus formation) or detecting soft-tissue calcification after severe muscle trauma (e.g. myositis ossificans).

When complications of the healing process occur, such as infection or avascular necrosis, the role of plain radiography may be limited and other imaging techniques, such as bone scintigraphy and/or MRI, may be useful for confirming the diagnosis.

The lack of soft-tissue contrast resolution is a well-recognised limitation of plain radiography, but when present, soft-tissue changes can be used as indirect signs of osseous pathology.

2.2 Conventional Arthrography

For decades, conventional arthrography (after sterile preparation and injection of intra-articular contrast medium) was used for investigating intra-articular pathology. This imaging modality has now been largely replaced by cross-sectional imaging techniques and is only performed as part of CT or MR arthrography.

3 Ultrasound

Since approximately 30% of sports injuries deal with muscle and tendon injuries, ultrasound (US) plays a major role in sports traumatology, helping the clinician to decide whether the athlete should or should not return to training and competition (Peterson and Renstrom 1986).

Due to the excellence of spatial resolution and definition of muscle structure, US keeps its leading edge when dealing with muscle pathology, both in the initial phase for recognition of a lesion, but also for follow-up of lesions and search for healing problems such as fibrosis, muscle cysts, hernias or myositis ossificans (Sconfienza et al. 2018).

Major advantages of US are its low cost, availability at short notice, ease of examination, short examination times, lack of radiation exposure and dynamic imaging.

High-frequency (>10 MHz) linear array probes are used to perform musculoskeletal US examinations. Transverse and longitudinal slices are mandatory. US palpation is a very valuable tool, trying to find the point of maximal tenderness during the examination by a gentle but firm compression of the probe on the skin (Peetrons 2002). Dynamic US study may be very helpful for the correct diagnosis, e.g. to search for muscle hernia (during muscle contraction) or to evaluate the snapping hip syndrome (during hip flexion and lateral rotation). To avoid artefacts or pitfalls, comparison with the contralateral side is necessary.

The addition of colour-power Doppler imaging to US allows for the non-invasive study of blood flow and vascularity within anatomic structures and lesions. In patients with tendinosis, increased vascularity in the tendon may be correlated with clinical symptoms (Weiberg et al. 1998; Zanetti et al. 2003).

(Sono)elastography (SEL) is a relatively recent addition to musculoskeletal ultrasound and is based on evaluating tissue deformity, which depends on tissue composition and structure (Shiina et al. 2002). Inflammatory and degenerative processes alter these characteristics and can therefore be detected. Several SEL techniques are available (compression elastography, shear wave elastography and transient elastography), each with specific indications, limitations and artefacts. Although the techniques yield promising study results, clinical application is not yet widely spread due to lack of standardised imaging protocols and variable repeatability (Baumer et al. 2017).

Furthermore, US provides image guidance for interventional procedures such as drainage of fluid collections and cysts (Peetrons 2002). Recently, US-guided sclerosis of neovascularity in painful chronic tendinosis has been described as an effective treatment with significant reduction of pain during activity (Öhberg and Alfredson 2002; Lind et al. 2006; Sconfienza et al. 2019a, b, c).

The trade-off for the high-frequency, linear, musculoskeletal transducers is their limited depth of penetration and the small, static scan field. This is a disadvantage if the structure to be visualised is large (e.g. large intramuscular hematoma) or deeply localised (e.g. hip joint). Extended field-of-view ultrasonography (EFOVS) overcomes this disadvantage by generating a panoramic image. With this technique, sequential registration of images along a broad examination region and their subsequent combination into an image of larger dimension and format are obtained (Weng et al. 1997). EFOVS does not add much in diagnosis but is, however, easily interpretable by the novice and improves cross-specialty communication.

For evaluation of deeply localised structures, such as the hip joint in an obese patient, cross-sectional imaging modalities (mostly MRI) are often required.

Other disadvantages of ultrasound include operator dependency, selective and often incomprehensible documentation and inability to penetrate osseous structures.

4 Computed Tomography

4.1 Multi-Detector CT

CT imaging, by virtue of its excellent multiplanar capability, fast acquisition time and submillimetre spatial resolution due to the development of the spiral acquisition mode and current multi-detector row technology, is a valuable imaging tool for the evaluation of all kinds of sports injuries (Berland and Smith 1998).

It has proved to be an effective method of documenting injuries particularly in complex bony structures such as the wrist and pelvis, and may often show post-traumatic changes not shown by radiography.

For most musculoskeletal studies, slice thickness is 0.6 mm, reconstructed to 1 mm images with an increment of 0.5 mm. The images should be assessed using both bone and soft-tissue window settings.

From the three-dimensional data set, images can be reformatted in other planes (2D technique/multiplanar reconstruction) and used for volume rendering (3D technique).

2D reformatting of sagittal and coronal images from axial images is helpful in the detection of longitudinal fracture lines and can make it easier to evaluate horizontal interfaces, such as the acetabular roof.

Volume-rendering techniques provide a 3D model of the evaluated structure, which does not as much increase the detection rate of fractures but does offer a better 3D understanding of the image and is often used as a model for preoperative planning by orthopaedic surgeons.

All reconstruction methods offer a more effective display of complex anatomic and pathologic structures. It may be helpful for the assessment of comminuted fractures, improving visualisation of the fracture's extent and location, shape and position of the fracture fragments and condition of articular surfaces.

4.2 Dual-Energy CT

Dual-energy CT (DECT) is a relatively new technique which is able to provide information on tissue composition. Its best known application is the detection of urate depositions in patients with gout (Glazebrook et al. 2011; Choi et al. 2012). More recently, studies have described the value of DECT in the detection of bone marrow oedema. This makes DECT a valuable option for evaluating bone marrow oedema in post-traumatic situation (Pache et al. 2010; Guggenberger et al. 2012) or in autoimmune inflammatory joint disorders (Jans et al. 2018).

Additionally, the technique has the ability to reduce beam-hardening artefacts caused by metal implants (osteosynthesis of prosthetic material). This facilitates detection of periprosthetic fractures, (aseptic) loosening, implant failure/fracture or infection (Bamberg et al. 2011; Zhou et al. 2011).

4.3 Cone Beam CT

Cone beam CT, although first described in the 1980s, is a relatively new technique in the musculoskeletal imaging field. In contrast to conventional multi-detector CT, in which a fan-shaped beam and linear detector are used, CBCT makes use of a cone-shaped radiation beam and a flat-panel detector, which allows image acquisition in only one rotation of radiation beam and detector around the patient. The advantages of this technique include higher spatial resolution, ideally for evaluation of small joints (e.g. wrist, hand, foot) and reduction of metal artefacts. CBCT has also low radiation doses, although very state-of-the-art multi-detector CTs have comparable doses. Despite its disadvantages (longer scan time and therefore increased sensitivity to motion artefacts, smaller scan range and loss of contrast resolution), it has been proposed as a low-dose alternative to multi-detector CT in patients with high clinical suspicion of fracture but negative findings on standard radiography (De Smet et al. 2015; Vanhoenacker and Desimpel 2017; Posadzy et al. 2018).

4.4 CT Arthrography

CT arthrography (CTA) is performed by direct injection of iodine contrast within the joint cavity, using fluoroscopy or ultrasound as

guidance (Newberg et al. 1985). The volume of contrast medium injected depends on the joint examined: shoulder: 10–15 mL; wrist: 5 mL; hip: 10 mL; knee: 20 mL; and ankle: 6–12 mL. After injection of contrast material, patients are asked to perform full-range mobilisation of the joint to obtain homogeneous distribution of contrast within the joint. Thereafter, anteroposterior, lateral and oblique views are obtained to image the entire articular cavity. Subsequently, multi-detector CT is performed, preferably with multiplanar reconstructions.

The major advantage of CTA is its excellent conspicuity of focal cartilage lesions that results from the high spatial resolution and the high attenuation difference between the cartilage substance and the joint contrast filling the lesion. Vande berg et al. (2002) found, in a study with spiral CTA of cadaver knees, a better correlation for grading articular surfaces between macroscopic examination and spiral CTA than with MR imaging.

Other potential advantages of spiral CTA with respect to MR imaging are the short examination time, the availability at short notice (short waiting list) and the low sensitivity and limited degree of imaging artefacts related to the presence of microscopic metallic debris or air which may hinder MR imaging studies.

Limitations of CTA include its invasiveness, possible allergic reaction, use of ionising radiation and poor soft-tissue contrast resolution. Another major limitation of CTA imaging of the cartilage is its complete insensitivity to alterations of the deep layers of the cartilage or on articular sides of tendons (e.g. bursal sided rotator cuff tears).

5 Magnetic Resonance Imaging

5.1 Field Strength and Imaging Planes

The clinical MR imaging protocol will be greatly influenced by local preferences, time constraints and MR system available (field strength, local coil). For an in-depth discussion of the different MR imaging protocols, the reader is referred to subsequent chapters.

5.1.1 Field Strength

It is generally accepted that high-field-strength magnets (3 T or even higher) provide the highest quality images, although midfield (1.5 T or higher) is more than acceptable in clinical routine.

5.1.2 Imaging Planes

Although appropriate selection of imaging planes will depend on the location and desired coverage of the anatomical region to be examined and the pathology to be expected, a complete MR examination requires images obtained in the axial, coronal and sagittal planes. Of utmost importance is to respect the anatomical orthogonal planes since, with excessive rotation of a limb, inappropriate positioning of imaging planes may result in images which are difficult to interpret. Oblique planes may also be useful, e.g. in the shoulder (paracoronal and parasagittal images).

5.2 MRI Sequences

The number of pulse sequences and combinations (“hybrid techniques”) is almost infinitive however in musculoskeletal MR; the most commonly used sequences include turbo-spin echo (TSE) T1-, T2- and intermediate-weighted sequences and gradient echo (GRE) sequences.

TSE sequences are less susceptible to field inhomogeneity than SE and GRE sequences. Therefore, when metallic artefacts are present, such as in post-surgical patients, TSE sequences are preferred over GRE.

Intermediate-weighted sequences, such as proton density sequences, with fat suppression are the keystone of MSK imaging. With the correct parameters ((TR/TE = 75/30–40 ms), they depict anatomical structures in high detail. In addition, they are very sensitive to oedema (both bone or soft tissue) and therefore valuable in detecting pathology. Without fat suppression, the sensitivity for pathological fluid decreases, but the sequence remains valuable for the detection of meniscal and cartilage lesions due to its high resolution.

T1-weighted images excel at providing anatomical detail and are essential in evaluating bone marrow.

T2-weighted images have a lower resolution and are less sensitive in detecting pathology, especially without fat suppression. With fat suppression, sensitivity increases but signal-to-noise ratio decreases.

GRE sequences are used for the evaluation of articular cartilage and for dynamic contrast-enhanced imaging. They are also used in a limited number of T2* protocols (glenoid labrum, meniscus of the knee). As mentioned before however, these sequences are very vulnerable to artefacts, which may simulate pathology.

3D sequences could theoretically be used as an alternative to multiple 2D sequences and can be based on either GRE (FLAS, SPGR, DESS, SSPR, FISP) or TSE (SPACE or XETA) sequences. The advantage of 3D sequences is their thin slice thickness (0.5 mm or less), which reduces partial volume artefacts and interslice gap (Yao et al. 2007; Van Dyck et al. 2012). The major disadvantages include a longer imaging time and image blurring (due to the use of long echo train lengths) (Naraghi and White 2012). This latter may cause difficulties in evaluating low-contrast structures, such as menisci, and associated lesions (Subhas et al. 2011; Ristow et al. 2009). Therefore, 2D acquisition is still regarded as more reliable than 3D sequences.

Diffusion-weighted imaging (DWI) has not (yet) reached the same popularity in the field of MSK imaging as it has in the neuroradiology. DWI is based on the principle of Brownian motion of molecules and the alteration of normal diffusion in pathological processes (Huisman 2010; Chilla et al. 2015).

Diffusion tensor imaging (DTI), the next step after DWI, allows quantification of anisotropy in tissues to assess its microstructure, for example the organisation of muscle fibres (Galban et al. 2004; Yanagisawa et al. 2009; Van Donkelaar et al. 1999). Studies have demonstrated that DTI is useful in evaluating sports-related muscle injury (Froeling et al. 2015; Oudeman et al. 2016); however further research is warranted to increase its applications in routine clinical imaging.

Ultrashort echo time (UTE) sequences have been developed for better visualisation of tissues with very short transverse relaxation time, such as menisci, ligaments and tendons (Chang et al. 2015). Its value has been established in the evaluation of tendinopathy, alterations in deep cartilage layers (which are difficult to differentiate from subchondral bone on conventional sequences) and bone composition (Bae et al. 2010; Horch et al. 2012; Du et al. 2013; Chen et al. 2015; Liu and Kijowski 2017).

Parametric mapping sequences (T2 and T1ρ) are mostly implemented in the assessment of hyaline cartilage (Duvvuri et al. 2001; Akella et al. 2001; Dunn et al. 2004; Nishii et al. 2010; Zhong et al. 2016), especially in detecting early stages of degeneration not yet visible on conventional sequences.

5.3 Fat Suppression

Different fat suppression (FS) techniques are available.

In our institution, we prefer the spectral FS technique because of its better SNR and spatial resolution compared to the inversion recovery fat suppression techniques (Fleckenstein et al. 1991), unless in the presence of metallic hardware (see artefacts).

Dixon sequences have become quite popular in the last decennium, providing fat-only, water-only, in-phase and out-of-phase images in one time. They provide more reliable fat suppression than spectral or inversed recovery techniques, due to decreased sensitivity to field inhomogeneities.

5.4 Contrast Administration

Contrast-enhanced MR studies lead to a prolonged examination time and high costs, and therefore the use of intravenous contrast agents is not indicated when evaluating a sports lesion. It should be reserved for cases in which the results would influence patient care (Kransdorf and Murphey 2000). Application of intravenous gadolinium is indicated when dealing with a tumoural or pseudotumoural mass (Lunkiewicz et al. 2021) to detect neovascularisation and intralesional necrosis (which is a major parameter for malignancy), in cases of inflammation or as part of indirect arthrography. For detection of subtle areas of

contrast enhancement, we use subtraction images (TSE T1-WI with FS after minus TSE T1-WI with FS before gadolinium, static MR imaging).

5.5 Artefacts

The musculoskeletal system, especially in the extremities, is not influenced by motion, and as a consequence motion artefacts are rare. Infolding artefacts can be avoided by selecting an appropriate imaging matrix, saturating anatomical areas outside the region of interest and off-centre imaging. Artefacts due to distortions of the local magnetic field are attributable to ferromagnetic and, to a lesser degree, nonferromagnetic orthopaedic devices. In these cases, STIR is preferred to spectral fat suppression techniques. The use of surface coils will improve the SNR; smaller slice thickness and larger matrices are essential for soft-tissue imaging. The choice of small "field of view (FOV)" without changing the matrix size will increase the spatial resolution. Sometimes, imaging of the contralateral side may be useful, requiring a larger FOV and the use of a body coil.

5.6 Disadvantages

MRI has the disadvantage of not always being well accepted by patients, of being incompatible with dynamic manoeuvres and of not always being possible in emergency conditions. Furthermore, it provides the evaluation of an entire anatomical area—bone structures included—but is only good for the study of a limited part of the skeleton. This is in contrast to scintigraphy, with which the whole skeleton can be evaluated at once. Otherwise, MRI helps to elucidate the true nature of highly non-specific hotspots on scintigraphy.

5.7 Direct and Indirect Arthrography

MR arthrography is a technique which is mainly used in the shoulder, wrist, ankle, knee and hip joint. Two different techniques are described: direct and indirect MR arthrography.

5.7.1 Direct Technique

The contrast medium is a 2 mmol/L solution of gadolinium in 0.9% NaCl. Eventually 1–5 mL 1% lidocaine may be added. Fluoroscopy or ultrasound is used to bring the needle tip into a correct intra-articular position. If using fluoroscopy, 1–2 mL of 60% non-ionic contrast medium is added to the Gd mixture to assure correct needle position. The amount of the MR contrast medium injected depends on the selected joint (see CT arthrography). MR imaging (with FS TSE T1-WI) is preferably performed within 1 h after injection to minimise the absorption of contrast solution and the loss of capsular distension.

The clinical and radiological importance of the direct technique for the assessment of chondral and ligamentous lesions is well established. Major disadvantages of the direct technique are its invasiveness and insensitivity to lesions that lack contact with the joint (e.g. bursal sided rotator cuff tears in the shoulder).

5.7.2 Indirect Technique

Indirect arthrography relies on the intra-articular/synovial secretion of contrast medium after intravenous contrast administration (0.1 mmol Gd-DTPA/kg body weight), which causes shortening of the relaxation time of the synovial fluid. This process starts within minutes after the injection and is accelerated by joint movement (exercise). Therefore, patients are instructed to move the examined joint for 10–15 min after contrast administration. MR imaging (with FS SE T1-WI) is initiated within 30 min after injection, when maximal enhancement is reached.

This indirect technique has the advantage of not requiring direct access to the joint but lacks the advantages of joint distension. Another disadvantage of the indirect technique is the enhancement of extra-articular structures.

Therefore, direct arthrography is preferred in most scenarios, in particular in case of highly competitive athletes.

6 General Principles and Indications

As a general rule, MRI and US are most accurate for grading soft-tissue injuries while bone injury can be assessed with conventional radiography, CT and MRI. For internal derangements of joints, we prefer MRI because of its non-invasive character. In our institution, CT is used for better evaluation of fracture or fracture healing or for biometric views (e.g. anteversion femoral neck, Q-angle). We recommend that conventional radiography should always be the first diagnostic modality performed to depict (associated) skeletal or joint abnormalities.

Radiographic assessment of a stress fracture, an entity frequently encountered in sports men, can be insensitive, especially in the early stage of the condition and follow-up films may demonstrate abnormalities in only 50% (Spitz and Newberg 2002). Bone scintigraphy has a high sensitivity but low specificity and lacks spatial resolution and has been largely superseded by MRI, providing excellent sensitivity and specificity, as it can also identify alternative sources of pain, such as muscle tears or joint degeneration (Anderson and Greenspan 1996). Moreover, MRI is useful for follow-up of stress injury, with a return of normal bone marrow signal on T2-WI at 3 months compared to scintigraphy, which may show abnormal uptake for up to 10 months (Slocum et al. 1997).

Conventional arthrography has now been replaced by cross-sectional imaging techniques and is only performed as part of CT or MR arthrography.

For the diagnosis of muscle and tendon lesions, US is considered the best imaging modality, in the initial phase for recognition of a lesion, but also for the assessment of the various changes it undergoes until complete healing has been achieved. In most cases, MRI adds no additional diagnostic information. Well-established indications for US are summarised in Box 1 (Sconfienza et al. 2018).

If plain radiographs and/or US are negative or reveal unequivocal findings and clinical symptoms persist, MR imaging must be performed.

MR examinations most frequently requested are of the knee and shoulder. Well-established indications for MRI are summarised in Box 2.

Due to the recent developments in CT technology, multi-detector CTA has become a valuable alternative to MR imaging for the assessment of

Box 1 Well-Established Indications for US

Foot/ankle	Achilles tendinosis, plantar fasciitis, ligamentous injury
Shoulder	Rotator cuff disease, biceps tendon (dynamic evaluation), spinoglenoid cyst
Elbow	Common extensor, flexor and triceps brachii tendinosis
Wrist/hand	Tenosynovitis, synovial cyst
Hip/pelvis	Inguinal hernia, snapping hip, bursitis, avulsion injury
Knee	Collateral ligaments, patellar and quadriceps tendon, bursitis, meniscal cyst

Box 2 Well-Established Indications for MRI

Foot/ankle	Osteochondral lesion
Shoulder	Labral abnormalities, suprascapular nerve entrapment, quadrilateral space syndrome, Parsonage-Turner
Elbow	Osteochondral lesion, ligamentous injury, instability
Wrist/hand	Triangular fibro-cartilage complex (TFCC), avascular necrosis (AVN), distal radio-ulnar joint (DRUJ)
Hip/pelvis	Pubalgia, adductor strain, labral abnormalities, AVN
Knee	Meniscus, osteochondral lesion, cruciate ligaments, posterolateral corner

internal derangement of joints and has proved to be an accurate technique to detect articular cartilage lesions (Edwards et al. 1995). Major drawback of spiral CTA, however, is its invasive character.

The choice between multi-detector CTA and MR imaging for assessment of internal joint derangement is offered to the referring clinician, depending on the clinical situation. In general, children and young patients, patients with allergy to iodinated contrast, patients with suspicion of ligamentous lesions and patients with recent trauma (and haemarthrosis) are imaged with MR imaging. Multi-detector CTA is favoured in patients with chronic symptoms, suspected cartilage lesions or recurrent symptoms after surgery (e.g. post-operative meniscus). When MRI is contraindicated, bone marrow oedema can be detected by dual-energy CT.

7 Optimal Moment of Investigation

The ideal time for the US examination of fresh traumatic muscle lesions is between 2 and 48 h after trauma. Before 2 h, the haematoma is still in formation. After 48 h, the haematoma can be spread outside of the muscle (Peetrons 2002). However, with some muscles, it can stay for much longer. It is recommended that for lesions in the hamstrings the US examination be done as soon as possible after the 2-h delay. For rectus femoris and gastrocnemius lesions, the examination can be postponed as long as 2 or 3 days, or even longer sometimes (Brandser et al. 1995).

8 Safety, Availability and Economic Aspects

Because all ionising radiation is harmful and there is no safe lower threshold of radiation, consideration must be given to the radiation dose to the patient when plain radiography or a CT examination is requested. Examinations on children require an even higher level of justification since they are at greater risk from radiation than adults. Therefore, when clinically appropriate, the alternative use of safer non-ionising techniques (such as ultrasound and MRI) or of low-dose radiography/CT techniques must always be considered.

The number of sport participants, both amateur and professional athletes, has increased dramatically over recent decades. The benefits to health are debated but are generally accepted. However, more participation has led to more sports-related injuries. The increase has been in both acute and, even more, overuse injuries (Garrick and Requa 2003). Although some researchers and policymakers have expressed concern about the lack of high-quality evidence regarding the cost-effectiveness and efficiency of MRI, it was demonstrated that, in most diagnostic categories, MRI findings may have a significant impact on diagnosis and treatment planning (Hollingworth et al. 2000). For example, several studies have documented that MR imaging can be an accurate, cost-effective means of assessing injuries in the knee, preventing patients from undergoing unnecessary arthroscopy (Carmichael et al. 1997). Appropriate selection of patients will probably yield similar results in other anatomic locations. The advancements in MRI technology may expand the range of usefulness of this modality, leading to even greater utilisation of MR imaging in patients with sports injuries, and, eventually, to reduced costs and greater availability.

9 Conclusion

The diagnosis of sports injuries can be difficult owing to the degree of overlap of symptoms between different injuries, necessitating further imaging evaluation. Different imaging techniques, with their specific advantages and limitations, can be used to diagnose and grade such injuries. The correct use of these imaging modalities will lead to an early and accurate diagnosis preventing the development of chronic pain or other complications and thus avoiding waste of limited financial resources. The specific merit of each imaging modality in the evaluation of sports-related lesions will be further highlighted in the next chapters and summarised in schematic boxes.

Things to Remember

1. The imaging requirements for sports medicine physicians should begin with conventional radiography.
2. Ultrasound is considered the imaging technique of first choice for the diagnosis of muscle lesions. The examination must be performed between 2 h and 48 h after the muscle trauma to assess the extension of the haematoma and hence predict a grading of muscle lesions.
3. MR imaging has become the dominant imaging modality in the assessment of sports-related injury, because sports medicine and high-quality imaging are inextricably linked. There are, however, many findings on MRI that may not represent clinically significant disorders. Therefore, optimisation of image acquisition and interpretation require correlation with clinical findings.
4. Multi-detector CT arthrography is a valuable alternative to MR imaging for the assessment of internal derangement of joints. In daily, clinical practice, the choice between the two imaging modalities is offered to the referring clinician, depending on the clinical situation.

References

Akella SV, Regatte RR, Gougoutas AJ et al (2001) Proteoglycan-induced changes in T1ρ-relaxation of articular cartilage at 4T. Magn Reson Med 46:419–423

Anderson MW, Greenspan A (1996) Stress fractures. Radiology 199:1–12

Bae WC, Dwek JR, Znamirowski R et al (2010) Ultrashort echo time MR imaging of osteochondral junction of the knee at 3 T: identification of anatomic structures contributing to signal intensity. Radiology 254:837–845

Bamberg F, Dierks A, Nikolaou K et al (2011) Metal artifact reduction by dual energy computed tomography using monoenergetic extrapolation. Eur Radiol 21:1424–1429

Baumer TG, Davis L et al (2017) Shear wave elastography of the supraspinatus muscle and tendon: repeatability and preliminary findings. J Biomech 53:201–204

Berland LL, Smith JK (1998) Once again, technology creates new opportunities. Radiology 209:327–329

Brandser EA, El-Khoury GY, Kathol MH et al (1995) Hamstring injuries: radiographic, conventional tomographic, CT and MR imaging characteristics. Radiology 197:257–262

Carmichael I, MacLeod A, Travlos J (1997) MRI can prevent unnecessary arthroscopy. J Bone Joint Surg Br 79:624–625

Chang EY, Du J, Chung CB (2015) UTE imaging in the musculoskeletal system. J Magn Reson Imaging 41:870–883

Chang EY, Radros AY, Amini B et al (2017) ACR Appropriateness Criteria® Chronic Ankle Pain. Am Coll Radiol. https://acsearch.acr.org/docs/69422/Narrative. Accessed 23 Jan 2020

Chen J, Grogan SP, Shao H et al (2015) Evaluation of bound and pore water in cortical bone using ultrashort-TE MRI. NMR Biomed 28:1754–1762

Chilla G, Tan C, Xu C et al (2015) Diffusion weighted magnetic resonance imaging and its recent trend: a survey. Quant Imaging Med Surg 5:407–422

Choi H, Burns L, Shojania K et al (2012) Dual energy CT in gout: a prospective validation study. Ann Rheum Dis 71:1466–1471

De Smet E, De Praeter G, Verstraete KL et al (2015) Direct comparison of conventional radiography and cone beam-CT in small bone and joint trauma. Skelet Radiol 44:1111–1117

Du J, Carl M, Bae WC et al (2013) Dual inversion recovery ultrashort echo time (DIR-UTE) imaging and quantification of the zone of calcified cartilage (ZCC). Osteoarthr Cartil 21:77–85

Dunn TC, Lu Y, Jin H et al (2004) T2 relaxation time of cartilage at MR imaging: comparison with severity of knee osteoarthritis. Radiology 232:592–598

Duvvuri U, Charagundla SR, Kudchodkar SB et al (2001) Human knee: in vivo T1ρ-weighted MR imaging at 1.5 T—preliminary experience. Radiology 220:822–826

Edwards DJ, Lomas D, Villar RN (1995) Diagnosis of the painful hip by MRI and arthroscopy. J Bone Joint Surg 77:374–376

Fleckenstein JL, Archer BT, Barker BA et al (1991) Fast short-tau inversion-recovery MRI. Radiology 179:499–504

Froeling M, Oudeman J, Strijkers GJ et al (2015) Muscle changes detected with diffusion-tensor imaging after long-distance running. Radiology 274:548–562

Galban CJ, Maderwald S, Uffmann K et al (2004) Diffusive sensitivity to muscle architecture: a magnetic resonance diffusion tensor imaging study of the human calf. Eur J Appl Physiol 93:253–262

Garrick JG, Requa RK (2003) Sports and fitness activities: the negative consequences. J Am Acad Orthop Surg 11:439–443

Glazebrook K, Guimarães L, Murthy N et al (2011) Identification of intraarticular and periarticular uric acid crystals with dual-energy CT: initial evaluation. Radiology 261:516–524

Guggenberger R, Gnannt R, Hodler J et al (2012) Diagnostic performance of dual-energy CT for the detection of traumatic bone marrow lesions in the

ankle: comparison with MR imaging. Radiology 264:164–173
Hollingworth W, Todd CJ, Bell MI (2000) The diagnostic and therapeutic impact of MRI: an observational multi-centre study. Clin Radiol 55:825–831
Horch RA, Gochberg DF, Nyman JS et al (2012) Clinically compatible MRI strategies for discriminating bound and pore water in cortical bone. Magn Reson Med 68:1774–1784
Huisman TA (2010) Diffusion-weighted and diffusion tensor imaging of the brain, made easy Cancer Imaging 10(spec no A):163–171
Jans L, De Kock I, Herregods N et al (2018) Dual-energy CT: a new imaging modality for bone marrow oedema in rheumatoid arthritis. Ann Rheum Dis 77: 958–960
Johnson R (2000) Sports medicine in primary care. Saunders, Philadelphia, PA
Kransdorf MJ, Murphey MD (2000) Radiologic evaluation of soft tissue masses: a current perspective. AJR Am J Roentgenol 175:575–587
Lind B, Ohberg L, Alfredson H (2006) Sclerosing polidocanol injections in mid-portion Achilles tendinosis: remaining good clinical results and decreased tendon thickness at 2-year follow-up. Knee Surg Sports Traumatol Arthrosc 14:1327–1332
Liu F, Kijowski R (2017) Assessment of different fitting methods for in-vivo bi-component T2* analysis of human patellar tendon in magnetic resonance imaging. Muscles Ligaments Tendons J 7:163–172
Lunkiewicz M, Davies AM, Anderson SE (2021) Pseudotumors in sports. Med Radiol. https://doi.org/10.1007/174_2020_270
Naraghi A, White LM (2012) Three-dimensional MRI of the musculoskeletal system. AJR Am J Roentgenol 199:283–293
Newberg AH, Munn CS, Robbins AH (1985) Complications of arthrography. Radiology 155:605–606
Nishii T, Shiomi T, Tanaka H et al (2010) Loaded cartilage T2 mapping in patients with hip dysplasia. Radiology 256:955–965
Öhberg L, Alfredson H (2002) Ultrasound guided sclerosis of neovessels in painful chronic Achilles tendinosis: pilot study of a new treatment. Br J Sports Med 36:173–175
Oudeman J, Nederveen AJ, Strijkers GJ et al (2016) Techniques and applications of skeletal muscle diffusion tensor imaging: a review. J Magn Reson Imaging 43:773–788
Pache G, Krauss B, Strohm P et al (2010) Dual-energy CT virtual noncalcium technique: detecting posttraumatic bone marrow lesions—feasibility study. Radiology 256:617–624
Peetrons P (2002) Ultrasound of muscles. Eur Radiol 12:35–43
Peterson L, Renstrom P (1986) Trauma in sport. Nurs RSA 1:20–23
Posadzy M, Desimpel J, Vanhoenacker F (2018) Cone beam CT of the musculoskeletal system: clinical applications. Insights Imaging 9:35–45
Ristow O, Steinbach L, Sabo G et al (2009) Isotropic 3D fast spin-echo imaging versus standard 2D imaging at 3.0T of the knee—image quality and diagnostic performance. Eur Radiol 19:1263–1272
Sconfienza LM, Albano D, Allen G et al (2018) Clinical indications for musculoskeletal ultrasound updated in 2017 by European Society of Musculoskeletal Radiology (ESSR) consensus. Eur Radiol 28:5338–5351
Sconfienza LM, Adriaensen M et al (2019a) Clinical indications for image-guided interventional procedures in the musculoskeletal system: a Delphi-based consensus paper from the European Society of Musculoskeletal Radiology (ESSR)-part II, elbow and wrist. Eur Radiol. https://doi.org/10.1007/s00330-019-06545-6
Sconfienza LM, Adriaensen M et al (2019b) Clinical indications for image guided interventional procedures in the musculoskeletal system: a Delphi-based consensus paper from the European Society of Musculoskeletal Radiology (ESSR)-part III, nerves of the upper limb. Eur Radiol. https://doi.org/10.1007/s00330-019-06479-z. [Epub ahead of print]
Sconfienza LM, Adriaensen M et al (2019c) Clinical indications for image-guided interventional procedures in the musculoskeletal system: a Delphi-based consensus paper from the European Society of Musculoskeletal Radiology (ESSR)-part I, shoulder. Eur Radiol. https://doi.org/10.1007/s00330-019-06419-x. [Epub ahead of print]
Shiina T, Nitta N, Ueno E, Bamber JC (2002) Real time tissue elasticity imaging using the combined autocorrelation method. J Med Ultrason 29:119–128
Slocum KA, Gorman JD, Puckett ML et al (1997) Resolution of abnormal MR signal intensity in patients with stress fractures of the femoral neck. AJR Am J Roentgenol 168:1295–1299
Spitz D, Newberg A (2002) Imaging of stress fracture in the athlete. Radiol Clin N Am 40:313–331
Subhas N, Kao A, Freire M et al (2011) MRI of the knee ligaments and menisci: comparison of isotropic-resolution 3D and conventional 2D fast spin-echo sequences at 3T. AJR Am J Roentgenol 197: 442–450
Van Donkelaar CC, Kretzers LJ, Bovendeerd PH et al (1999) Diffusion tensor imaging in biomechanical studies of skeletal muscle function. J Anat 194:79–88
Van Dyck P, Gielen JL, Vanhoenacker FM et al (2012) Diagnostic performance of 3D SPACE for comprehensive knee joint assessment at 3T. Insights Imaging 3:603–610
Vande Berg BC, Lecouvet FE, Poilvache P et al (2002) Spiral CT arthrography of the knee: technique and value in the assessment of internal derangement of the knee. Eur Radiol 12:1800–1810

Vanhoenacker FM, Desimpel J (2017) Cone beam CT of trauma of small bones and joints. Semin Musculoskelet Radiol 21:290–302

Weiberg EP, Adams MJ, Hollenberg GM (1998) Color Doppler sonography of patellar tendinosis. AJR Am J Roentgenol 171:743–744

Weng L, Tirumalai AP, Lowery CM et al (1997) Ultrasound extended-field-of-view imaging technology. Radiology 203:877–880

Yanagisawa O, Shimao D, Maruyama K et al (2009) Diffusion-weighted magnetic resonance imaging of human skeletal muscles: gender-, age- and muscle-related differences in apparent diffusion coefficient. Magn Reson Imaging 27:69–78

Yao L, Pitts JT, Thomasson D (2007) Isotropic 3D fast spin-echo with proton-density-like contrast: a comprehensive approach to musculoskeletal MRI. AJR Am J Roentgenol 188:199–201

Zanetti M, Metzdorf A, Kundert H-P (2003) Achilles tendons: clinical relevance of neovascularization diagnosed on power Doppler US. Radiology 227: 556–560

Zhong H, Miller DJ, Urish KL (2016) T2 map signal variation predicts symptomatic osteoarthritis progression: data from the osteoarthritis initiative. Skelet Radiol 45:909–913

Zhou C, Zhao YE, Luo S et al (2011) Monoenergetic imaging of dual-energy CT reduces artifacts from implanted metal orthopedic devices in patients with factures. Acad Radiol 18:1252–1257

Muscle Injuries

J. L. M. A. Gielen, P. Robinson, P. Van Dyck,
A. Van der Stappen, and F. M. Vanhoenacker

Contents

J. L. M. A. Gielen (✉) · P. Van Dyck
A. Van der Stappen · F. M. Vanhoenacker
University of Antwerp, University Hospital, Edegem, Antwerp, Belgium
e-mail: Jan.gielen@uza.be; Pieter.vandyck@uza.be; Filip.vanhoenacker@telenet.be

P. Robinson
Department of Radiology, Musculoskeletal Centre, Chapel Allerton Hospital, Leeds Teaching Hospitals, Leeds, UK
e-mail: philip.robinson10@nhs.net

Abstract

Muscle damage is related to indirect/elongation mechanism, direct impact or dysfunction of the supporting connective tissue and is common in athletes. Muscle trauma can lead to changes that may be observed on US and MRI. MRI or US grading of muscle injury can be performed. In clinical practice the classic three-grade system of muscle trauma proved to be insufficient to predict recovery period and complication rate. Last decennium novel grading systems are developed taking into account new pathophysiological insights.

This chapter reviews the relevant imaging anatomy, ultrastructure and (patho)physiology of muscle as well as the radiological characteristics of normal and injured muscle as seen on ultrasound and MRI with emphasis on its clinical relevance introducing the novel grading systems.

Abbreviations

BAC	British Athletics Muscle Tear Classification System
CSA	Cross-sectional area

Med Radiol Diagn Imaging (2021)
https://doi.org/10.1007/174_2020_247, © Springer Nature Switzerland AG
Published Online: 23 February 2021

CT	Computed tomography
DOMS	Delayed onset muscle soreness
MRI	Magnetic resonance imaging
MTJ	Musculotendinous junction
MTU	Musculotendinous unit
US	Ultrasound
SI	Signal intensity

1 Introduction

Skeletal muscle comprises the largest tissue mass in the body, accounting for 40–45% of body mass (Best and Garrett 1994; Garrett and Best 1994). The muscle-tendon unit (MTU) is, in essence, a mechanical system that enables locomotion through contractions that alter length of sarcomeres.

Muscles are subject to traumatic processes that can compromise their function. Muscle trauma is common in athletes, it can lead to changes that may be observed on US and MRI, and that may manifest as abnormalities of muscle reflectivity respectively intensity and (ultra)structure as well as volume alterations. Muscle damage is related to indirect mechanism (overuse (DOMS) or stretching), direct impact (contusion of with penetration) or dysfunction of the supporting connective tissue (compartment syndrome and muscle herniation) (Flores et al. 2018).

Muscles were difficult to image with early techniques (radiographs, computerised tomography (CT) and low resolution ultrasound) because of low soft tissue contrast. With the advent of high resolution and compound ultrasound (US) and magnetic resonance imaging (MRI) it became much easier to diagnose injuries primarily affecting the soft tissues. More attention is paid to traumatic lesions of the MTU in radiological literature (Campbell and Wood 2002; El-Khoury et al. 2004; Flores et al. 2018; Dimmick and Linklater 2017). MRI or US grading of muscle injury can be performed, and follow-up studies can assess repair of muscle tissue and identify complications of the healing process. Some features such as vascularity and intralesional calcification may be more easily appreciated on ultrasound than MRI.

In clinical practice the classic three-grade system of muscle trauma (Table 1) proved to be insufficient to predict recovery period and complication rate (O'Donoghue 1962; Takebayashi et al. 1995; Peetrons 2002; Stoller 2007). This insufficiency is related to the lack of relation to aetiology the lack of subclassifications with the consequence that injuries with different aetiology, treatment pathway and different prognostic relevance are categorised in one group (Mueller-Wohlfahrt et al. 2013). Last decennium novel grading systems are developed taking into account new pathophysiological insights

Table 1 Three-grades muscle classification systems of elongation injury

O'Donoghue (1962) **anatomy-function** based	
Takebayashi et al. (1995)/Peetrons (2002) **US** based	
Stoller (2007) **MRI** based	
A.	**Grade 1**
	(a) Anatomy: No appreciable tearing, no loss of function or strength, low-grade inflammation
	(b) US: No abnormalities or diffuse bleeding with less than 5% or without focal fibre rupture
	(c) MRI: No structural damage, no SI abnormalities or oedema without haemorrhage
B.	**Grade 2**
	(a) Anatomy: Tissue damage, muscle strength reduced
	(b) US: Partial rupture: Focal fibre rupture more than 5% of the muscle involved, with or without fascial injury
	(c) MRI: Rupture up to 50%, hyperintense focal defect and partial retraction of fibres possible
C.	**Grade 3**
	(a) Anatomy: Complete muscle tear with complete loss of function
	(b) US: Complete muscle rupture with retraction, fascial injury is present
	(c) MRI: Complete tearing with or without retraction

(Mueller-Wohlfahrt et al. 2013; Pollock et al. 2014) (Tables 2 and 3).

This chapter reviews the imaging relevant anatomy, ultrastructure and (patho)physiology of muscle as well as the radiological characteristics of normal and injured muscle as seen on ultrasound and MRI with emphasis on its clinical relevance introducing the novel grading systems.

2 Anatomy, Ultrastructure and (Patho)Physiology with Imaging Correlation

The muscle fibre is the basic structural element of skeletal muscle; the sarcomere is the smallest contractile unit of muscle fibre. The muscle fibre is a long cell connected to the tendon or bone on

Table 2 Munich comprehensive classification system of acute muscle disorders and injuries

Mean lay of time: MLT from Ekstrand et al. (2013)
Indirect injury
A. Functional muscle disorders (MLT: 6 days)
Type 1: Overexertion related
(a) Fatigue induced
(b) DOMS
Type 2: Neuromuscular muscle disorders
(a) Spine related
(b) Muscle related
B. Structural muscle injuries
Type 3: Partial tears
(a) Minor tear: Less than fascicle or bundle (MLT 13 days)
(b) Moderate tear: Diameter greater than a fascicle or bundle with involvement of connective tissue (endomysium, perimysium and epimysium (fascia) (MLT 32 days)
Type 4: (sub)total tears/tendinous avulsions) (MTL 60 days)
Direct injury
Contusion
Laceration

Table 3 BAC classification system of muscle injury

This system combines two classification principles: Extent (grades 0–4) and location (suffix a–c). Rehabilitation period and complication rate climb with increased grades and suffix.
Grades:
Grade 0
(a) Focal neuromuscular injury with normal MRI
(b) Generalised muscle soreness with normal MRI or with characteristics of DOMS
Grade 1 involves <10% of the muscle CSA with length < 5 cm
Grade 2 involves 10–50% of the muscle CSA with length 5–15 cm
Grade 3 greater than 50% with length > 15 cm
Grade 4 complete tear
Location suffix:
(a) Myofascial
(b) MTJ
(c) Intratendinous
Acute muscle elongation trauma: 12 stages combined grade 0–4 with suffix a–c with increasing rehabilitation period from 1 to 12 weeks
0a
1a and 1b
2a, 2b and 2c
3a, 3b and 3c
4a, 4b and 4c

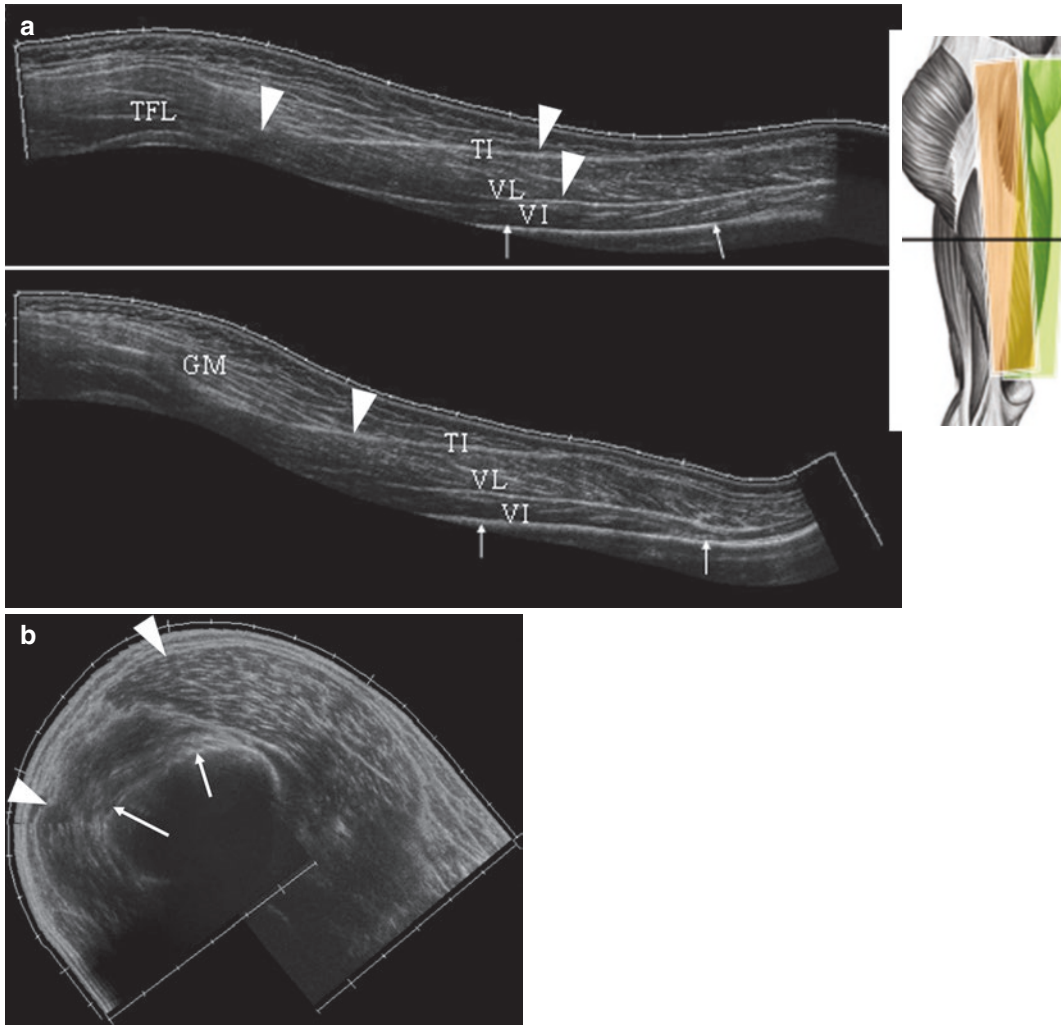

Fig. 1 (**a** and **b**) Thigh muscles and tractus iliotibialis. (**a**) Lateral longitudinal and (**b**) transverse extended field of view ultrasound images of the thigh muscles. Longitudinal posterior and anterior view with a total length of 40cm on top and bottom, respectively. The gluteus maximus (GM), vastus lateralis (VL) and vastus intermedius (VI) muscles and the tractus iliotibialis (TI) can be identified on longitudinal images. The four quadriceps heads including vastus medialis (VM) and rectus femoris (RF) can be identified on the transverse image. The reflective linear lines of the perimysium are best appreciated in the localised longitudinal ultrasound images. The reflective line between muscles corresponds to the epimysium (muscle fascia) (arrow heads). The deep reflective line (arrows) is formed by the cortical lining of the femur diaphysis and distal metaphysis

which it acts. The contractile filaments, myosin and actin filaments, are interswitched with an overlap. Greater overlap of these filaments produces muscle shortening-contraction. There are no end-to-end connections between muscle fibres. Muscles originate from and insert on bone or dense connective tissue either directly or via a tendon. A layer of fibrous connective tissue, the *endomysium*, surrounds each individual muscle fibre. These fibres are bundled into fascicles, which themselves are surrounded by perimysium. The *perimysium* is easily recognised on longitudinal ultrasound as linear reflective lines separating the hyposonant contractile fascicles (Peetrons 2002) (Fig. 1a). Transversely they appear as dotted reflective areas. Thicker reflective septa may occasionally be seen within the muscle belly, resulting in a reticular or

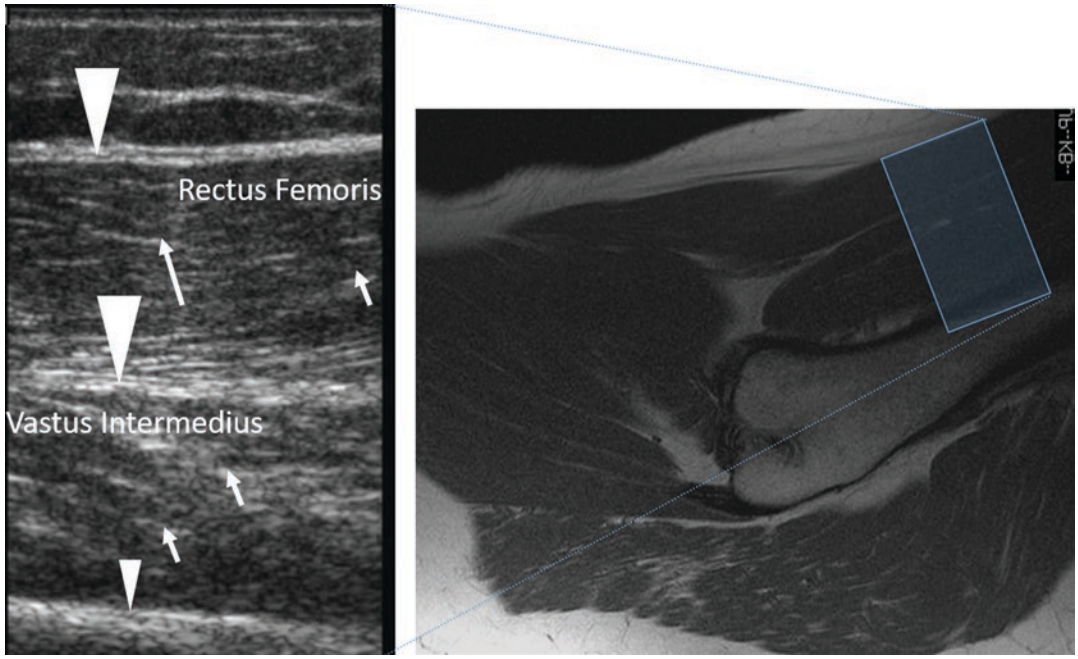

Fig. 2 Rectus femoris muscle, vastus intermedius and rectus femoris, proximal third, longitudinal view. Comparison US and MRI T1 WI. Cut out of US FOV projected on the MRI image. US: epimysium (muscle fascia): arrow heads, cortex femur: small arrow head, endomysium and perimysium: arrows. MRI: homogeneous aspect of muscle tissue on MRI: no discrimination collagen and muscle fibres, and thus no discrimination of individual bundles and fascicles. Hyperintense aspect of intramuscular, perimuscular, subcutaneous and endomedullary fat

honeycomb pattern on transverse images (Fornage 1995) (Fig. 1b). On MRI this fascicular structure is not appreciated. Muscular tissue produces a homogeneous intermediate SI on T1- and T2-weighted MR images (WI) with intermediate to slightly long T1 relaxation time and short T2 relaxation time. The fat along fascial and subcutaneous tissue planes allows identification of individual muscles (Fig. 2). The axial plane is particularly helpful for outlining specific muscle contours to determine location of lesions and to compare atrophy or expansion of muscle. Including the opposite side for comparison may be helpful (Kathol et al. 1990). The outer thicker layer or *epimysium* (muscle fascia) that surrounds the entire muscle belly is also reflective on US (Fig. 1a and b). This thick fascia may produce a low SI cocoon around the muscle belly on T1- and T2-WI MR images (Fig. 2).

These layers of connective tissue within the muscle belly are regarded as the connective tissue skeleton of the muscle (endo-, peri- and epimysium). At the myotendinous junction the contractile elements end and the connective tissue skeleton of the muscle belly continues in endo-, peri- and epitendineum of the tendons of attachment. This transition site of connection between the contractile muscle cells and the tendon is known as the myotendinous junction (MTJ) (Noonan and Garrett 1992). It is a specialised region of highly folded membranes at the muscle-tendon interface. The folding increases the junctional surface area by 10–20 times, decreasing the stress per unit area.

The orientation of reflective layers of perimysium on US depends on the orientation of the muscle fibre.

Pennate muscles have muscle fibres obliquely oriented to the epimysium and MTJ (Fig. 3a–g). Pennate muscles may have a unipennate (Fig. 3a, b), bipennate, circumpennate or multipennate (Fig. 3d, e) architecture (Table 4). In these cases, the myotendinous junction is often quite large, extending a long distance into (in bi- or

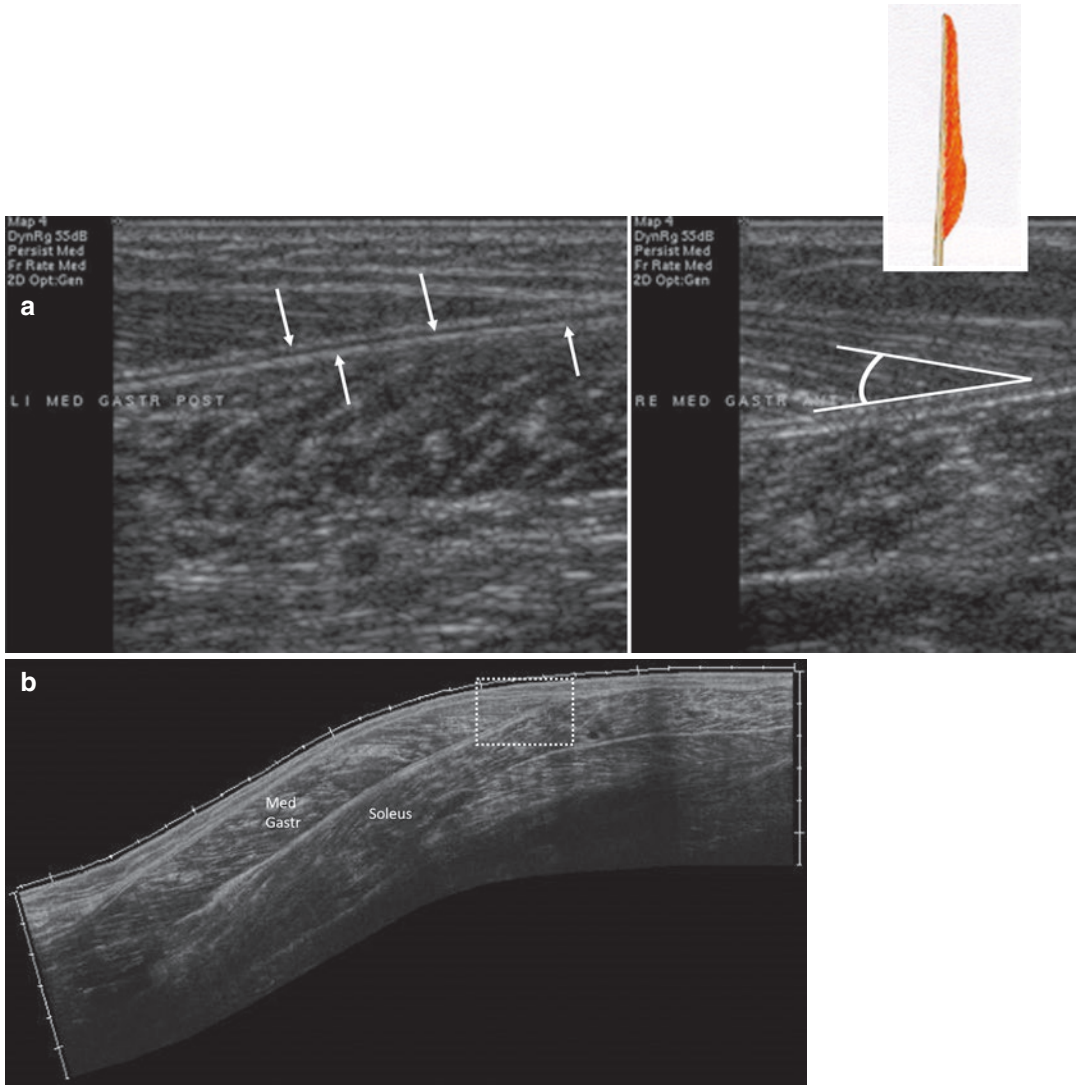

Fig. 3 (**a**–**h**) Ultrasound and diagram illustrating arrangement of muscle fibres. (**a** and **b**) Unipennate medial gastrocnemius muscle. (**a**) Distal third of left muscle and (**b**) extended field of view (left = proximal). White arrows point at the aponeurosis (eccentric tendon) of the distal MTJ. The pennation angle is measured at 20° (white angle on **a**). Extended field of view image (**b**) from the popliteal fossa (left side) to the Achilles tendon (right side). Panel (**a**) is the part at the dotted box in (**b**). (**c**) Diagrams illustrating the effect of muscle hypertrophy on force vector in line with the tendon. Left diagram with pennation angle of 45°, right diagram with pennation angle of 70°. Increased force generated by the hypertrophic muscle but similar resultant force vector in line of the tendon compared to non-hypertrophied muscle. (**d**–**g**) Circumpennate adductor longus muscle proximal MTJ [(**d**) transverse and (**e**) longitudinal imaging plane at the proximal third, (**f** and **g**) extended field of view]. The central reflective structure represents the tendon (arrow) that is surrounded by hypoechoic contractile elements, the reflective dots and lines between the contractile elements represent perimysium. Superficial thick reflective line is epimysium or superficial muscle fascia (arrow heads). (**h**) Parallel or fusiform muscle type, musculus biceps brachii. (US Left: longitudinal plane. Right transverse plane). Muscle fascia (arrow heads). The larger number of muscle fibres in a given cross-sectional area in the pennate muscle types allows for greater muscle strength, but less capacity for muscle shortening than in the parallel muscle type. Dynamic ultrasound during active muscle contraction demonstrates the change in muscle shape and fibre orientation in the longitudinal plane

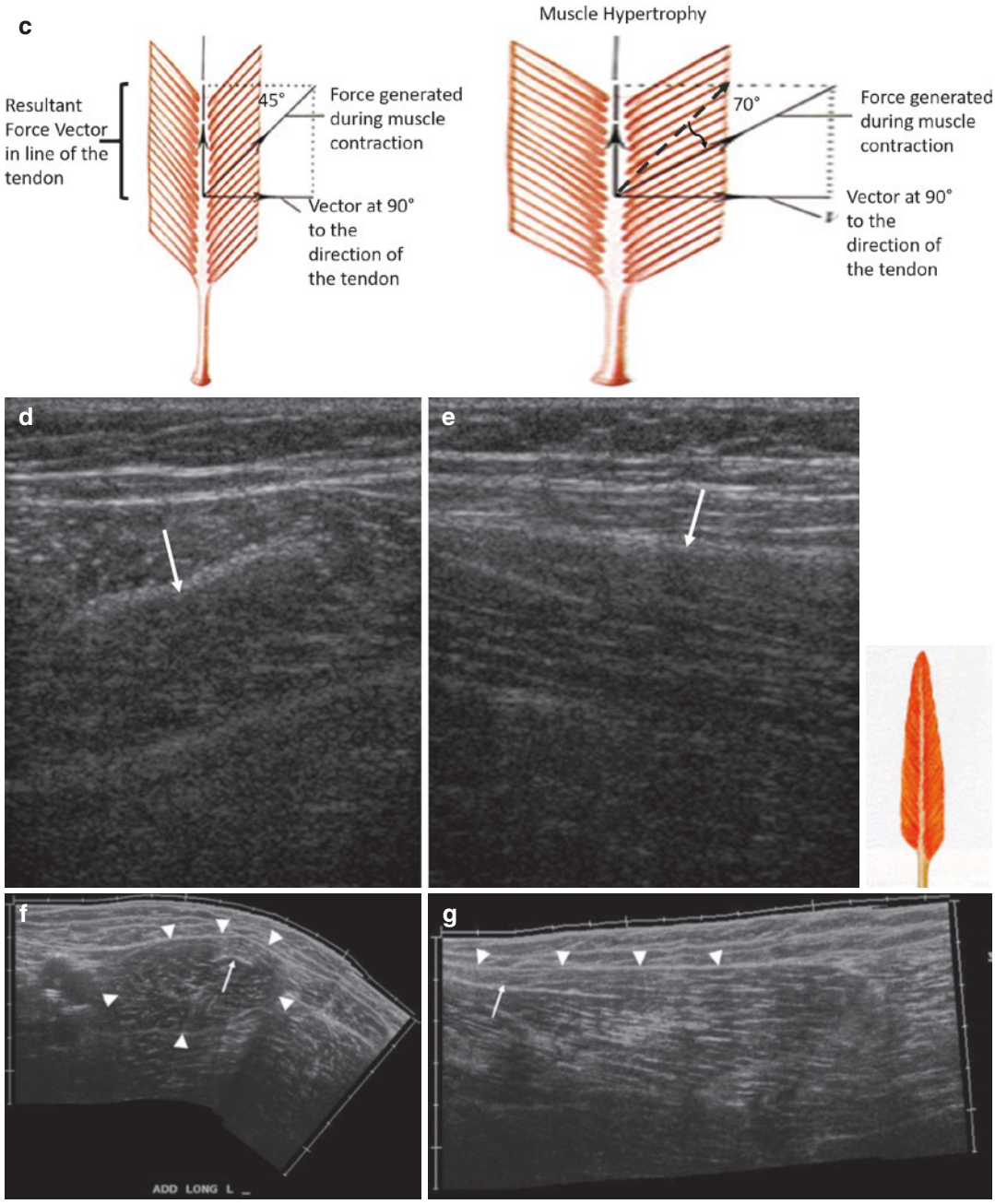

Fig. 1 (continued)

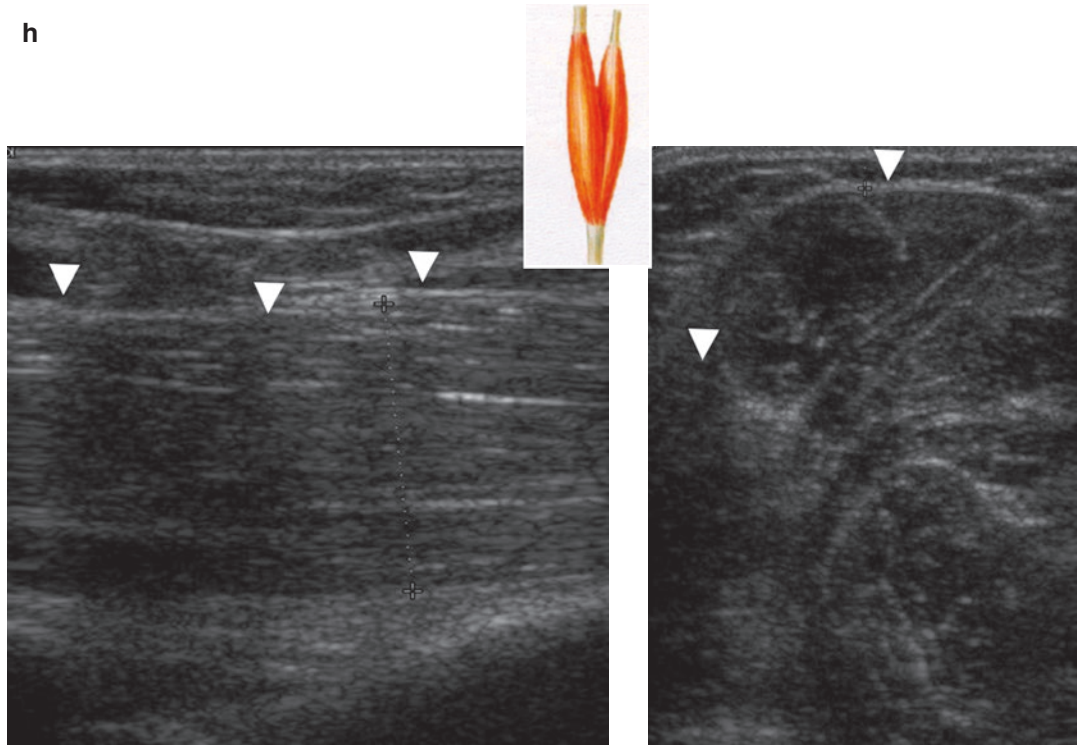

Fig. 247.3 (continued)

circumpennate architecture) or along the surface (in unipennate architecture) of the muscle belly. The pennate configuration allows for a large number of short muscle fibres packed in parallel in a given cross-sectional area (CSA), producing powerful muscles that resist elongation. In unipennate muscle the eccentric MTJ is often called aponeurosis and typically thin or membranous; it is continuous with the muscle fascia, and weak with high sensitivity to elongation injury. On imaging (ultrasound and MRI) no distinction is possible between fascia and aponeurosis. The pennation angle (angle of the muscle fibres to the tendon or aponeurosis) is easily appreciated on ultrasound; it increases in hypertrophied muscles as is the case in athletes, especially in body builders (Fig. 3a–c). Increased pennation angle results in increased number of muscle fibres/CSA and increased maximum force. However it is believed that resultant force vector parallel to the tendon diminishes in angulations over 45° resulting in lower muscle strength (Fig. 3c).

In a parallel or fusiform configuration, the muscle fibres are oriented with the long axis of the muscle, with a smaller number of longer muscle fibres in the same CSA (Fig. 3h). This allows a greater range of movement and maximum velocity of shortening, but less power.

Research in muscle biology has proved the existence of different types of muscle fibres with distinctly different structural, physiological and biochemical characteristics. Differences in fibre type are related to performance characteristics of certain muscles which reflect the speed of contraction and endurance of the muscle (Garrett et al. 1984).

The type I (slow twitch) fibre has slow contraction and relaxation times; it is, however, resistant to fatigue and has more mitochondria and capillaries per fibre. These type I fibres have a red colour related to the higher myoglobin content. Muscles active in postural activities are rich of type I fibres. The type II (fast twitch) fibre is divided into three subtypes (Type II A, B and C)

Table 4 Muscle architecture

Non limitative list!
Bold: Crossing two joints
Italics: Prone to elongation injury
Parallel, fusiform and convergent muscle structure
Biceps brachii distal MTJ short and ***long head proximal MTJ***
Sartorius proximal and distal MTJ
Rectus abdominis muscle proximal and distal MTJ
Sternocleidomastoid muscle proximal and distal MTJ
Psoas major muscle distal and proximal MTJ
Pectoralis major distal MTJ
Unipennate muscle: Membranous eccentric tendon
Gastrocnemius (*medial* and lateral) muscles distal MTJ
Soleus muscle distal MTJ
***Semimembranosus* proximal MTJ**
Rectus femoris straight head proximal MTJ
Lumbrical muscles distal MTJ
Interosseous muscles distal MTJ
Extensor digitorum longus of the leg and arm distal MTJ
Bipennate muscle
***Rectus femoris muscle reflected head* proximal MTJ**
Circumpennate and multipennate muscle
Deltoid muscle distal MTJ
***Adductor longus* muscle proximal MTJ**

but generally the type II fibre has lower mitochondrial content, functions glycolytically and is better adapted to intense movement activities of short duration. Type II muscle fibres have a white colour related to less myoglobin. More tension can developed in type II fibres than in the type I fibres. The amount of active tension that a muscle produces has been shown to be proportional to the fibre type content, so that muscles with higher proportion of type II fibres are able to generate more force. Low-intensity exercise selectively involves type I fibres, while more type II fibres are recruited as exercise intensity increases.

Slow and fast twitch fibre distribution is *genetically determined*, mean distribution is 45% slow and 55% fast twitch. About 20% of muscle fibres are undifferentiated, the endurance characteristics of these type IIC fibres can be altered as a result of training (Garrett 1990). People with genetic predominance of type II fibres are more successful in explosive sports activities whereas people with predominance of type I fibres are more successful in endurance sports activities. Muscle biopsies from sprinters are more likely to show a predominance of type II fibres (37% slow and 63% fast twitch), compared with long distance runners where type I fibres predominate (82% slow and 18% fast twitch). A non-invasive alternative to muscle biopsy for typing is quantification of muscle carnosine with *proton MR spectroscopy* (Ozdemir et al. 2007). Because of the low magnitude of carnosine spectroscopy peak MRS; quantification of carnosine needs big volumes and is prone to errors and available only in specialised (research and elite sports) centres.

Most muscles cross one joint but some cross two or more joints (Table 4). Those muscles that cross only one joint are located more deeply and are usually involved in postural activities (predominant type I fibres), with greater strength and slow speeds of contraction. Muscles that cross more than one joint produce higher speeds of contraction and a greater shortening index, but produce less tension over the full range of movement (predominant type II fibres). Typical muscles that cross two joints at the upper limb are the biceps brachii muscle, extensor carpi radialis brevis and longus muscles, triceps brachii (long head), long finger extensor and flexor muscles. At the lower limb: rectus femoris muscle, semitendinosis, semimembranosus and long head of biceps femoris muscles, medial and lateral gastrocnemius muscle, plantaris muscle, peroneal and long toe flexor and extensor muscles (Table 4).

Muscles that are located deeply, i.e. adjacent to bony structures, are more prone to crush (direct) trauma. Muscles that span more than one joint are more prone to elongation (indirect) injury.

Skeletal muscles are controlled by motor nerves. A motor unit is made up of a single nerve axon and all the muscle fibres it supplies. Muscle fibres in a motor unit have the same contractile and metabolic properties.

Muscle activation generates force within the muscle. If the resisting load is less than the force generated by the muscle, then the muscle

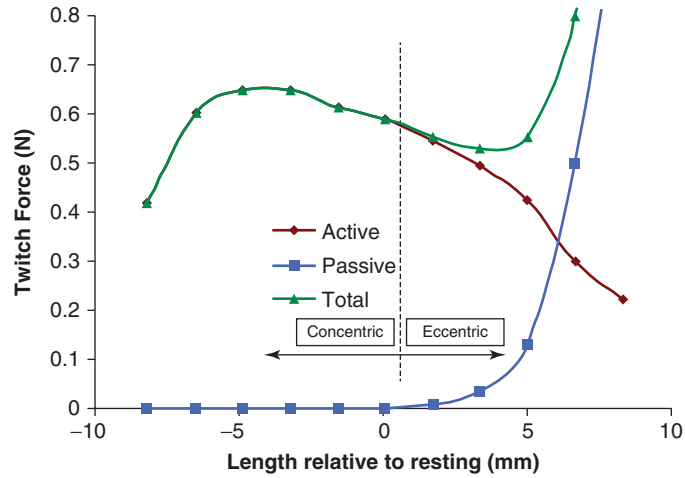

Fig. 4 Adapted MTU "length-tension" diagram by Mokele (not from real data) to illustrate a widely known biological concept. Licensed under Public Domain via commons

will shorten; this is referred to as *concentric contraction*. When the resisting force is greater than that generated by the muscle, the muscle will elongate; this is referred to as *eccentric elongation*. A large portion of muscle activity occurs in an eccentric fashion. Eccentric muscle activation can produce more force or tension within the muscle than when it is activated concentrically (Fig. 4), making it more susceptible to rupture or tearing. Dynamic US in a longitudinal plane during active muscle contraction demonstrates changes in muscle volume and fibre orientation in pennate muscle ultrastructure.

A tear in the MTU will occur when the tension in the unit exceeds the strength of the weakest structural element. From an imaging standpoint, the MTJ is an important region, because injuries involving the muscle belly tend to occur near, but not precisely at the true histological MTJ. This location is quoted with a suffix b in the BAC classification system (Pollock et al. 2014) (Table 3).

3 Muscle Trauma with Discussion of Grading Systems

A large segment of the population participates in sports activities resulting in injuries to a variety of muscles. In soccer hamstrings injuries and rectus femoris injuries are most frequent and players will have long periods of time lost (Ekstrand et al. 2011). The majority of muscle injuries are self-limited and imaging is not routinely indicated.

Not only for the sports physician but also for the radiologist it is recommended to start with a precise history of the occurrence, the circumstances, the symptoms, previous problems, followed by a careful clinical examination with inspection, palpation of the injured area, comparison to the other side and eventually testing of the function of the muscles. Palpation serves to detect (more superficial and larger) tears, perimuscular oedema and increased muscle tone (Askling et al. 2007; Jarvinen et al. 2005).

The Munich consensus statement comprehensive classification system developed in 2012 (Mueller-Wohlfahrt et al. 2013) differentiates indirect and direct (contusional) muscle injury as major groups with four types of indirect muscle injury (Table 2). The major discrimination in indirect trauma is functional and structural muscle disorders. Functional muscle disorders are typically disorders without macroscopic evidence (US or MRI) of fibre tear. Macroscopic evidence (US or MRI) of structural damage or fibre tear is found in structural muscle injuries. In this instrument for the first time that a large volume of data (referring to almost 400 thigh injuries in professional soccer players) has been used to test the classification and grading system (Grassi et al. 2016). Functional injuries were associated with a significantly shorter lay-off time compared to structural injuries (6 versus

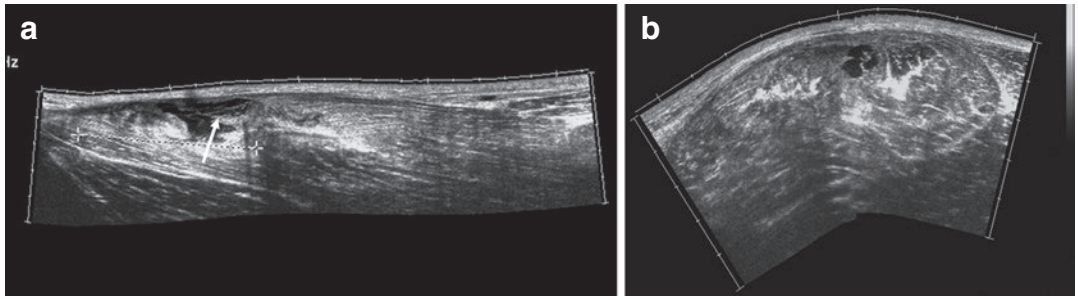

Fig. 5 (**a** and **b**) Adductor longus proximal MTJ muscle, circumpennate muscle type. Subacute partial tear at the muscle proximal at the myotendinous junction with organising haematoma BAC grade 2c/Munich type b. (**a**) Longitudinal US imaging plane, (**b**) axial US imaging plane. Hyporeflective serosanginous collection at the fibre discontinuity of the proximal MTJ, retracted muscle (**a** arrow). Distraction length of 7 cm. On transverse US (**b**) CSA of the collection of 10% of the whole muscle CSA. The torn end is evident by the presence of retracted muscle fibres surrounded by fluid (clapper bell sign, arrow). Perimysium tear with extramuscular fluid is evident

16 days). A significant difference was found also within the indirect injuries, with a median lay-off time of 13 days for Type 3a (minor partial muscle tears), 32 days for Type 3b (moderate partial muscle tears) and 60 days for Type 4 (complete muscle tears) (Ekstrand et al. 2013).

The Munich consensus statement also recommends to avoid elongation, pulled-muscle, hardening and hypertonus as these terms are either biomechanical, non-scientific or not well defined.

The British athletics muscle elongation classification system (BAC) is probably the most advanced in clinical practise as it introduces additional location characteristics that influence rehabilitation time and complication rate (Pollock et al. 2014) (Table 3).

US and MRI may be employed for the assessment of (professional and elite) sports injuries involving direct and structural muscle injury and in general population in muscle lesions prone to complications (muscle contusion and pennate muscle elongation trauma).

In the evaluation of muscle injury US may be performed in the subacute setting (24–48 h after the injury) to provide information about any existing disturbance of the muscle structure, particularly if there is any collection or haematoma to discriminate towards a *functional disorder* without evidence of structural damage (Mueller-Wohlfahrt et al. 2013). US is also performed to identify the muscle groups involved, to quantify the lesion and to identify involvement of the tendon (Fig. 5a, b). These abnormalities are thought to influence rehabilitation time and complication rate (Peetrons 2002). MRI is helpful in determining whether focal increased fluid signal is present, to assess the pattern, and if there is a structural lesion including its approximate size (Figs. 6 and 7a, b). Furthermore, MRI is also helpful in confirming the site of injury and any tendon involvement (Fig. 7a, b). However, it must be pointed out that MRI alone is not sensitive enough to measure the extent of muscle tissue damage accurately. For example, it is not possible to judge where oedema/haemorrhage (seen as high signal) is obscuring muscle tissue that has not been structurally damaged leading to oversizing the lesion (Mueller-Wohlfahrt et al. 2013). The latter is more accurately done with US.

Imaging during rehabilitation to monitor the healing response is generally regarded not useful if the clinical progress is as expected. Monitoring and natural history of muscle trauma will be discussed in Kilsdonk et al. (2021).

3.1 Acute Traumatic Muscle Injuries

Acute traumatic muscle injury occurs as a result of two mechanisms. Direct crush trauma or compressive injury that results in contusions and lacerations with haematomas. Indirect trauma with over-elongation of muscle fibres, during active

Fig. 6 Coronal MRI of both triceps surae at the posterior third, intermediate TE with FS. Muscle elongation trauma BAC grade O/Munich type 1 or 3a). Linear fluid signal at the right medial gastrocnemius distal MTJ with identification of fibrillary muscle architecture (arrows). No fluid signal at the intermuscular area between the medial gastrocnemius and the soleus is detected (arrowheads)

contraction or passive stretching, may lead to muscle tear.

Differentiation of direct and indirect muscle trauma is critical as they have typical clinical presentations, rehabilitation characteristics and specific complications.

3.1.1 Muscle Elongation Trauma

3.1.1.1 Biomechanical Basis

Muscle functions to initiate skeletal movement, but also resists and modifies other movements by transmitting forces to the skeleton through the tendons (Herzog 1996; Brinckmann et al. 2002).

Indirect muscle injuries, or muscle elongations, are frequently encountered following athletic activities; they represent a major reason for time lost from sports (Shellock et al. 1994). Muscle injuries occur during powerful eccentric contraction because more tension is generated within muscles during eccentric contraction than during concentric contraction.

Muscle and tendon injury occur at zones of anatomical or functional transition as these sites generate the greatest concentrations of intrinsic forces (Garrett et al. 1987; Nordin and Frankel 2001). Experimentally, muscle-tendon units stretched to failure, consistently disrupt near the myotendinous junction. Indeed already more than 60 years ago, McMaster (1933) showed experimentally that tendons does not rupture when a normal muscle-tendon unit is subjected to powerful elongation. This is also most often but not always true clinically and has been shown repeatedly on US and MRI studies, in adults muscles subjected to forceful eccentric contraction consistently disrupt at the muscular side near and not at the muscle-tendon junction or near the bone-tendon junction. However in clinical practice MTJ tear extending into the tendon (BAC classification suffix "c") and subfascial muscle tear (BAC classifications suffix "a") also occur and should be recognised (Pollock et al. 2014) (Table 3).

At the microscopic level initially an area of diluted haemorrhage is found. Twenty-four to 48 h after the injury, a pronounced inflammatory response is seen with fibre necrosis, capillary ingrowth, and a proliferation of disorganised fibroblasts (Nikolaou et al. 1987). The oedema and inflammatory response is resolved after 1–2 weeks. After 72 h collagen synthesis may be found that together with myotube bridges the injury site. Stress produces secondary remodelling of the muscle that goes on for months. It is obvious that the imaging aspect of muscle tears largely depends on the time interval to the injury. Imaging aspect of muscle tears also depends on the grade of elongation injury. Human imaging-histopathologic correlative studies to grade

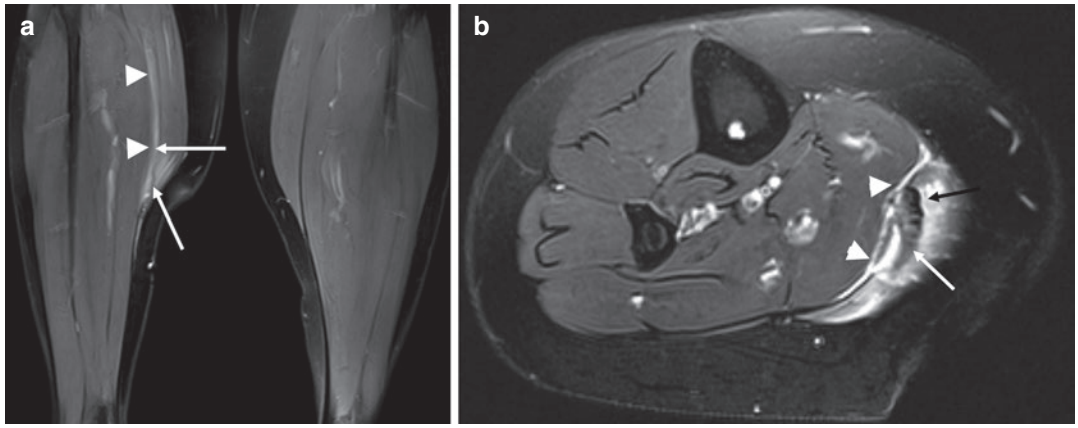

Fig. 7 (**a** and **b**) Coronal (**a**) and axial (**b**) MRI intermediate TE with FS. Medial gastrocnemius elongation trauma with recurrent tear BAC grade 2c/Munich type 3b. Coronal image (**a**) demonstrates fibrillary fluid infiltration between the fascicles of the right distal medial gastrocnemius with slackened aspect of the membranous tendon (arrow) and marked fluid infiltration between the medial gastrocnemius and soleus (arrowheads **a**, **b**). Fibrillary aspect of the fluid is not demonstrated on the axial image (**b**). Low SI sickle shaped fibrous old scar at the distal MTJ landmark of previous muscle tear with complication (arrows **b**)

muscle elongation lesions are not published yet. We propose the following hypothetic mechanism of distraction injury that is based on long-lasting ultrasound practice in acute and chronic lesions at different grades and stages. The BAC and Munich grading system are used to stratify the chapter on imaging (Table 3).

BAC Grade 0, Munich Type 1a

In a first stage of injury the myosin and actin filaments are powerfully contracted above their viscoelastic limits without being torn apart, and thus no filament or muscle fibre rupture is present. Capillary (blood and lymph) vessels at the contractile apparatus and at the surrounding endomysium may be injured, which results in diffuse bleeding (diluted haemorrhage). In this low-grade elongation, not tissue loss but swelling may be clinically apparent.

BAC Grade 1, Munich Grade 3a

Ongoing distraction forces will cause contractile fibres discontinuity. Individual muscle fibres/cells are microscopic, they have a diameter 60 µm and are not visible to the eye and neither documented on US. On ultrasound local bleeding/fluid collection is seen as hyporeflective areas without internal structure (Fig. 8a, b). MRI documents increased SI (Fig. 6). In these small lesions within the fascicle-bundle dimensions (less than 2–5 mm diameter) no destruction of the connective tissue skeleton of the muscle and no extension to the tendon is present. No fluid external to the superficial muscle fascia is detected.

BAC Grade 2 and 3, Munich Type 3b

Increasing distraction force causes discontinuity of the endomysium with subsequent tear of the perimysium and epimysium. Lesions over the size of an individual fascicle/bundle include damage to the connective tissue (Munich type 3b) and may be documented on US. As fibre architecture is not documented, small Munich type 3a and b and type 1a lesions are not easily discriminated on MRI.

The location of muscle elongation injury will vary along with the type of muscle.

Unipennate muscles are of special interest as the musculotendinous junction is located superficially and continues in a membranous tendon. A MTJ tear that stretches into the tendon is frequently encountered in this situation. The commonest example of this is “tennis leg”, occurring at the distal medial gastrocnemius muscle (Fig. 7). Some authors describe this particular variation of muscle rupture at the myotendinous

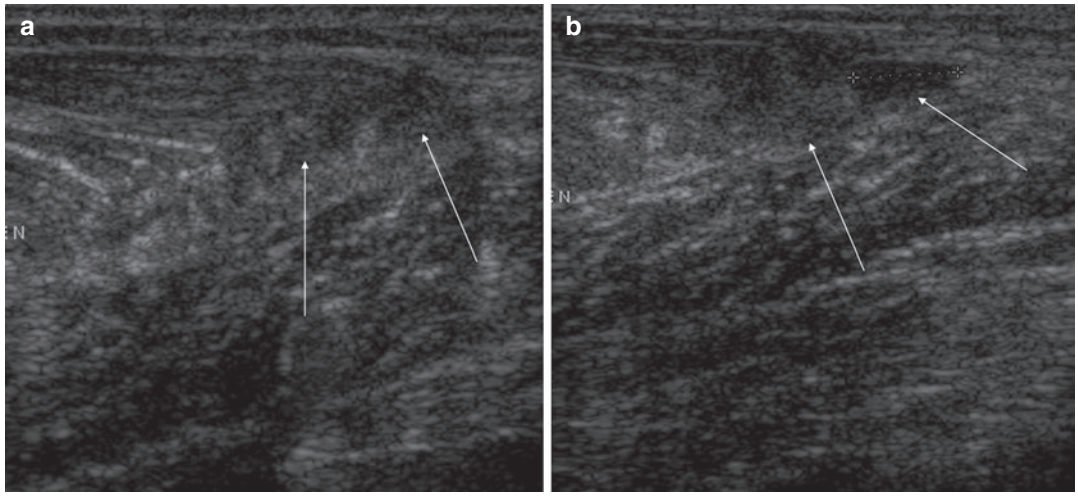

Fig. 8 (**a** and **b**) Acute BAC grade 1/Munich grade 3a injury of the medial gastrocnemius on longitudinal US. Unipennate muscle type. Typical example of "tennis leg". A small low reflective focal haematoma (arrows) with a few internal echoes replaces the retracted fibres at the distal musculotendinous junction. No fluid is documented between the soleus and gastrocnemius muscles. The soleus muscle lies immediately deep to the haematoma and is normal. Compare with Fig. 1a demonstrating the normal musculotendinous junction

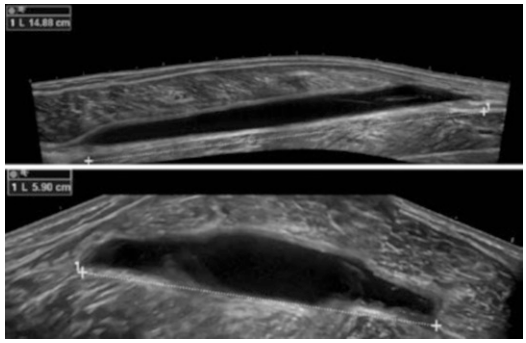

Fig. 9 Medial gastrocnemius tear with involvement of the aponeurosis and intermuscular fluid collection between the soleus and the medial gastrocnemius. Extended field of view ultrasound images with demonstration of major asonant collection in longitudinal (top, 15 cm) and transverse (bottom, 6 cm) orientation

junction as a muscle–aponeurosis avulsion. This lesion needs the suffix c in the BAC classification system and implies longer rehabilitation and complication risk (Table 3). Injury to the aponeurosis causes perimuscular fluid or bleeding and is often followed by scarring (Figs. 7b and 9). On the contrary, in parallel or circumpennate muscles fibre orientation tears are more frequently centrally located.

BAC Grade 4 or Munich Type 4

Ongoing distraction force may cause complete muscle rupture with injury of the epimysium/fascia. This corresponds to BAC grade 4 or Munich type 4 injury.

In BAC grade 3/ Munich type 3b and up, clinically, tissue loss with a gap is often felt at the rupture site. Occasionally, a subcutaneous ecchymosis can occur but this usually develops 12–24 h later (Peterson and Renstrom 1986). This ecchymosis is probably only found in cases of epimysium tear. It is located typically distally to the tear where the fascial planes abut the subcutis and gravitation brings it to the surface. Major haematoma is not often found in distraction injury, as the larger vessels are not involved. Clinical examination may be confusing in rare cases of extensive haematoma as it fills in the gap and may eventually give the impression of a swelling.

The forces experienced can be exacerbated by concurrent injury, fatigue and the severity of external forces as well as their speed of application (Mair et al. 1996; Brinckmann et al. 2002). Weakened or fatigued muscles absorb less energy and therefore are more likely to be injured. Muscles containing predominantly type II fibres

and muscles that cross more than one joint are at increased risk of elongations.

Recognising the tendon is important as a muscle tear that extends into the tendon results in significant prolonged rehabilitation and increased complication rate (BAC grading system suffix c). In this regard, the radiologist should focus to recognise the tendon, especially in unipennate muscles prone to elongation injury (Table 4). A muscle belly tear is less frequently located adjacent to the fascia (BAC grading system suffix a); these lesions tend to have a short revalidation period with lower complication rate compared to lesions at the MTJ (suffix b) and lesions with involvement of the tendon (suffix c).

The majority of athletes are skeletally mature with little tendon degeneration. In this setting excessive tensile forces across the musculoskeletal unit typically lead to failure near the myotendinous junction (Mink 1992; Taylor et al. 1993). This is in contrast to skeletally immature athletes in which the apophysis is the most sensible link (Patel et al. 2021) and athletes with tendinosis or weak tendons where the diseased tendon can fail rather than the myotendinous junction (Llopis et al. 2021) (Mink 1992; Taylor et al. 1993).

3.1.1.2 Clinical Presentation

Clinically, muscle elongation is characterised by immediate focal pain and decreased function that can be due to muscle disruption or associated reactive spasm in adjoining muscles (Nicholas and Hershman 1986; Peterson and Renstrom 1986; Speer et al. 1993; Noonan and Garrett 1992). Muscle elongations are *clinically* classified as either complete or partial based on whether the muscle-tendon unit is grossly disrupted or not (Zarins and Ciullo 1983). The most established clinical grading system has three components but it is recognised that differentiation of clinical grades can be difficult (O'Donoghue 1962 and 1984) (Table 1). Grade 1 injury is less than 5% loss of function with mild evidence of a haematoma or oedema (O'Donoghue 1962 and 1984). Grade 2 injury is more severe but with some function preserved. Grade 1 and 2 are characterised with increasing pain during muscle contraction. Grade 3 elongations are complete muscle tears with no objective function and occasionally a palpable gap in the muscle belly. After the acute moment pain is generally absent during rest and muscle activity (Table 1).

Most muscle elongations occur in the lower extremities with the *rectus femoris, biceps femoris* and *medial gastrocnemius* muscle being most commonly affected; they are followed by the *semitendinosus*, adductor, vastus medialis and soleus muscles (Greco et al. 1991). The muscles in *italics* span more than one joint (Table 4).

Previous incomplete injury, without total recovery of tensile strength, predisposes to more serious elongations.

3.1.1.3 Imaging

In experienced hands and with modern equipment MR imaging and ultrasound are both accurate techniques for the evaluation of lower limb muscle elongation (Steinbach et al. 1998; Van Holsbeeck and Introcaso 2001; Connell et al. 2004; Cross et al. 2004; Robinson 2004). When symptoms are localised, acute muscle injury is best evaluated with ultrasound. In comparison to MR imaging it is fast and allows dynamic stressing, which can be useful for differentiating large BAC grade 3 from BAC grade 4 tears (Van Holsbeeck and Introcaso 2001; Robinson 2004). However, the large muscle bulk often present in athletes means that the depth of resolution and field of view offered by ultrasound can be limiting, especially in the pelvis and proximal thigh. Therefore, MR imaging can be more accurate in these anatomical areas or when symptoms are diffuse. Ideally, the radiologist should be familiar with both techniques.

In the very acute stage within 2 h after the injury, haemorrhage and haematoma has a reflective aspect, in this stage the lesion is underestimated (Fig. 10a). After 48–72 h the lesion is correctly graded due to the anechoic aspect of the liquefaction (Fig. 10b).

MRI may also be used to assess muscle injury, but evaluation can be difficult as ultrastructure of muscles is not discriminated; thus, even minor elongation injuries can produce quite dramatic appearances that can be overestimated in their severity. The majority of acute muscle injuries

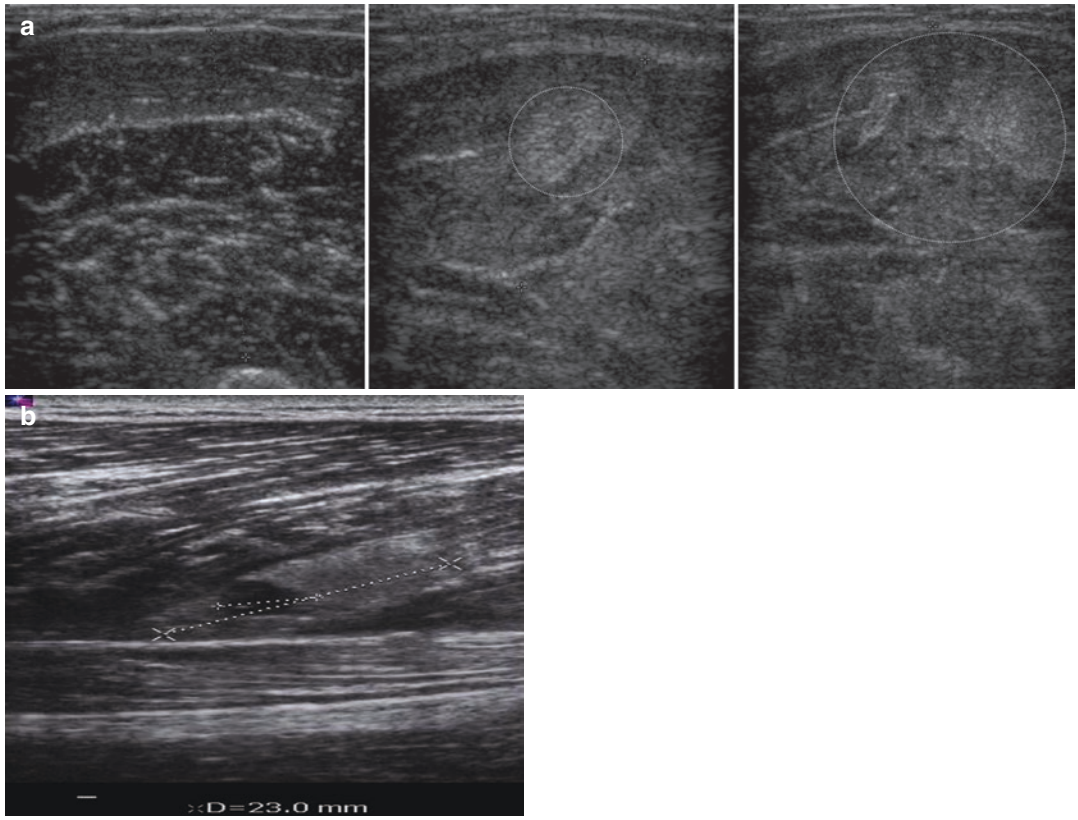

Fig. 10 (**a** and **b**) Hyperacute BAC grade 0/Munich type 1a injury. (**a**) Transverse US images of the biceps brachii muscle. Parallel muscle type. Left image represents normal right muscle, middle and right images represent side of the injury (left). Several small areas of low and high reflectivity adjacent to one of the intramuscular septa are seen in the long axis of the left muscle belly (dotted circles). (**b**) Longitudinal ultrasound image of the long head of biceps femoris muscle with diffuse reflective infiltration due to diffuse bleeding (long dotted line 23 mm) with central small liquefaction (short dotted line 7 mm)

have associated oedema and haemorrhage which cause prolongation of the T1 and T2 relaxation times of the injured tissue. Occasionally an added sequence utilising fat suppression may be required. T2-weighted MR images are ideal for the delineation of muscle tears; the bright signal from high water content stands out against the relatively low signal of muscle and intermediate signal of fat on T2-weighted MR images. T1-weighted MR images are less sensitive in depicting soft tissue abnormalities because most pathologic processes have long T1-relaxation times similar to muscle; the contrast between muscle and haemorrhage or between muscle and oedema may be imperceptible on T1-weighted MR images. T1-weighted MR imaging may be useful, however, in providing specificity in regard to the presence of haemorrhage or fat (Deutsch and Mink 1989).

The initial attempt of the imaging classification is to correlate with clinical evaluation resulting in grades 1–3 (Takebayashi et al. 1995; Peetrons 2002) using a US or MRI system varying from normal imaging findings up to complete muscle tears with retraction (Table 1). However in clinical practice, the most important aim of grading is prediction of rehabilitation period and complication risk. Novel Munich (Mueller-Wohlfahrt et al. 2013, Table 2) or BAC (Pollock et al. 2014, Table 3) grading systems are developed to enhance the efficacy of this prediction. Although these novel systems were not validated yet with clinical prospective studies it makes sense to introduce them in clinical practice. The Munich system is

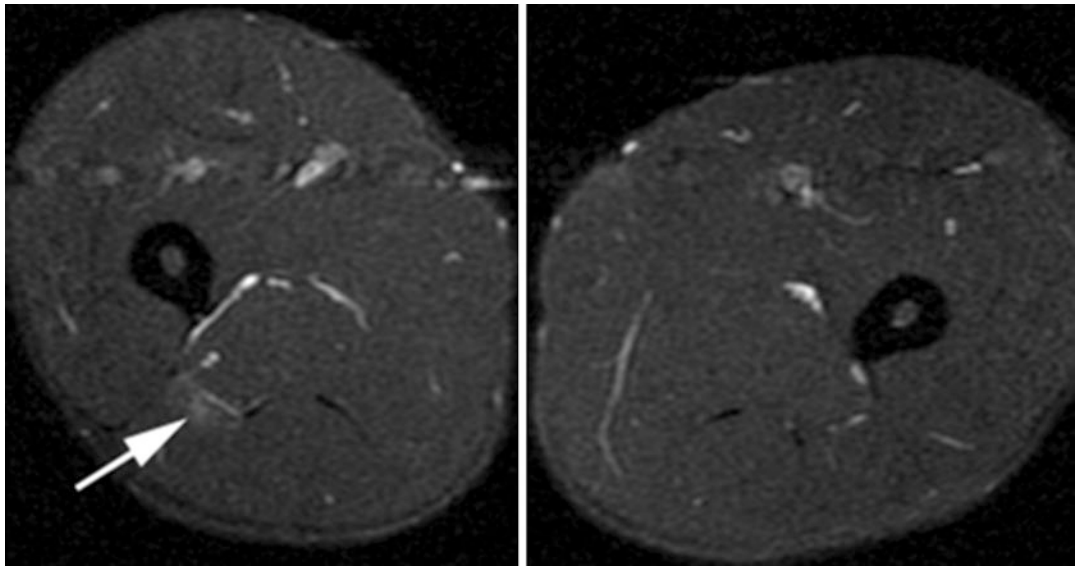

Fig. 11 Axial MRI with acute BAC grade0/Munich type 1a or 3a injury. Professional soccer player with acute onset thigh pain. Axial fat-suppressed T2-weighted MR shows minor area of oedema (arrow) within the long head of biceps femoris

retrospectively validated by Ekstrand (Ekstrand et al. 2013). The mean lay of time of muscle injury (MLT) of this validation is supplemented in Table 3. The BAC system is not validated yet but more advanced as it is quantifying not only the size but also the location of the tear. For this reason we use this system in clinical practice. The suffixes added to define the location are explained in Table 3. To discriminate suffix b and c lesions it is critical to differentiate tendon and muscle on imaging studies (US and MRI). Especially in unipennate muscle architecture the eccentric location of the tendon that is thinned into a membrane or aponeurosis should not be mixed up with a superficial muscle fascia. A suffix c (and not a) is added if a tear in this aponeurosis or membrane is present. Unipennate (medial gastrocnemius muscle distal MTJ) and bipennate (reflected head of rectus femoris proximal MTJ) are frequently torn muscles with increased rehabilitation periods and increased complication risk.

BAC Grade 0, Munich Type 1 and Type 3a

Minor elongation injuries, also called *claquage,* will either appear on US as normal, or as small areas of low reflective cavities (Fig. 10b), in which no disruption of the striated aspect is documented. A normal US with clinical history of a sharp stabbing pain that increases by muscle contraction is diagnostic for a grade BAC grade 0/Munich type 1 muscle elongation (Mink 1992; Van Holsbeeck and Introcaso 2001; Robinson 2004). MRI may have a normal appearance (type 1) or may present as a (small) area of oedema that presents as a diffuse area with prolonged T2-relaxation time (high SI) (type 3a).

In this grade of injury MR imaging can be superior to ultrasound (Figs. 6 and 11) (Gibbs et al. 2004). However, in daily clinical practice, a normal ultrasound is sufficient in most cases to exclude higher grade injury (Gibbs et al. 2004; Robinson 2004). BAC grade 0/Munich type1 injuries usually heal quickly within 1–2 weeks without complications.

BAC Grade 1 Suffix a and b/Munich Type 3b

More serious elongation injuries result in partial ruptures, and are evident by the discontinuity of muscle fibres and bundles, and by the presence haematomas and liquefaction (Fig. 8 US). In the BAC classification these injuries correspond to a partial tear with haematoma and muscle fibre disruption but not affecting the whole muscle belly (maximum 10% CSA and a length less

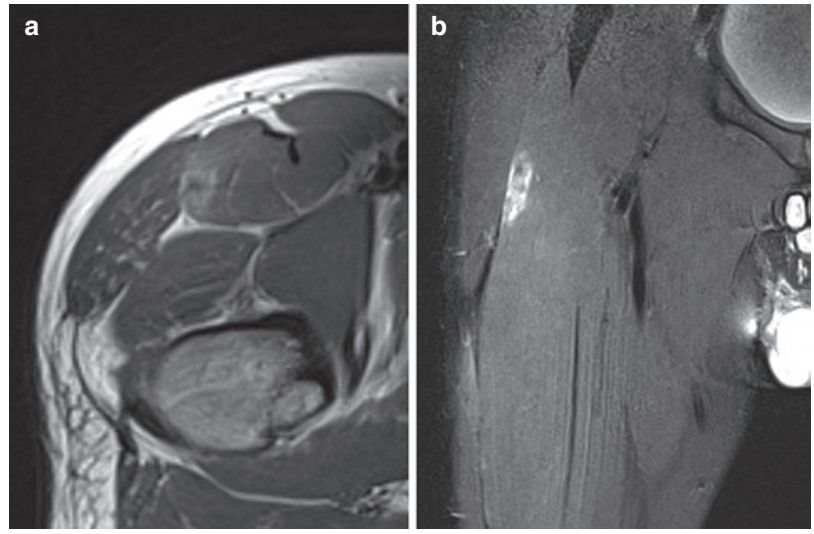

Fig. 12 (**a** and **b**) MRI examination in a 19-year-old soccer player with elongation trauma and tear of the right rectus femoris muscle, straight head, BAC Grade 1, suffix a/ Munich type 1 or 3b. (**a**) Axial T2 WI, (**b**) coronal intermediate TE with FS Blood infiltration with high SI located at the lateral subfascial area with involvement of <10% cross-sectional area (CSA) of the rectus femoris muscle

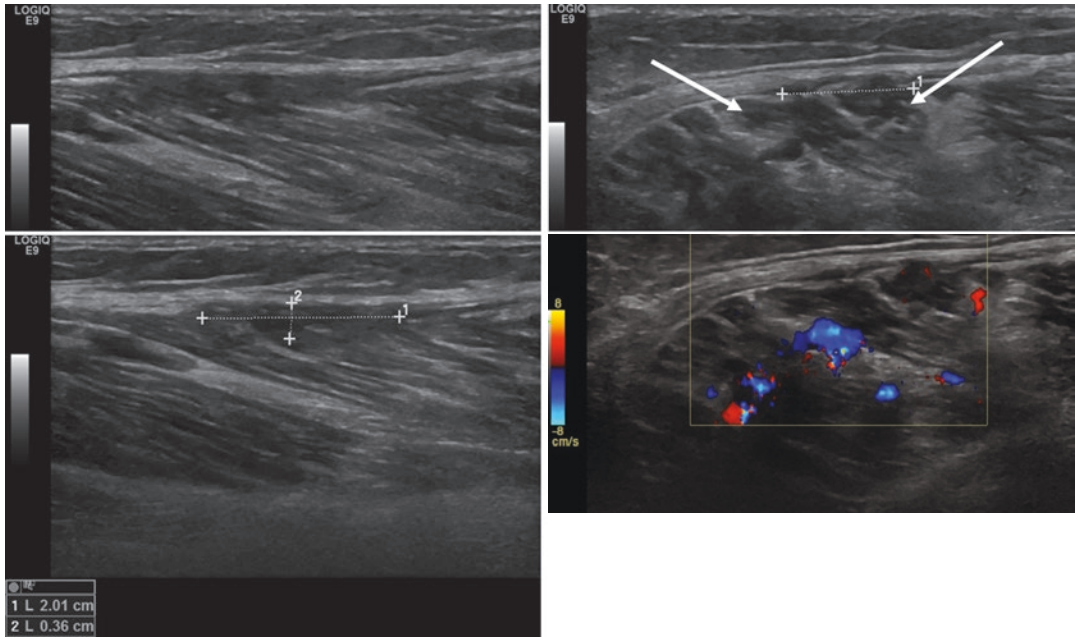

Fig. 13 Ultrasound examination in a 78-year-old woman with sudden snap at the calf with subfascial medial gastrocnemius tear. Longitudinal images (left images) document an area with disrupted fibrillary structure and hyporeflective aspect of the muscle belly of the medial gastrocnemius located adjacent to the superficial muscle fascia (area measured maximally 2 by 03 cm, between arrow). Axial images (right images) document the CSA less than 10%

than 5 cm). A suffix "a" is added if tear is located at the myofascial area of the muscle (Figs. 12a, b MRI and 13 US). The suffix "b" is added in MTJ tears (Fig. 8a US). "a" Lesions tend to heal easier with less complications compared to "b" lesions. The Munich classification can be misleading as a type 3b can describe a minor up to 95% muscle tear yet these two extremes will

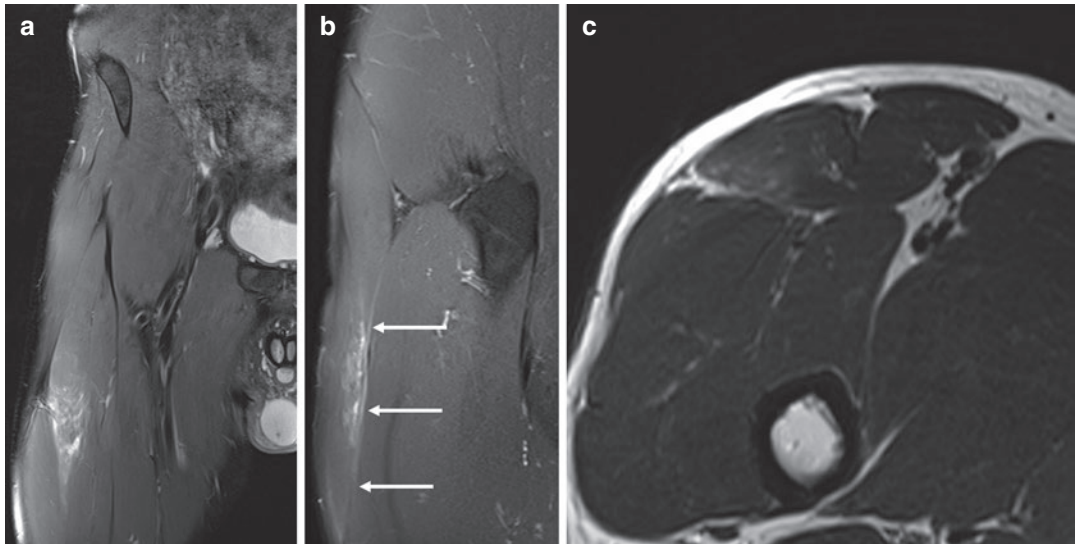

Fig. 14 (**a**–**c**) MRI examination in a 29-year-old soccer player with elongation trauma and tear at the straight head of the right rectus femoris muscle grade BAC 2a/Munich type 3b. (**a**) Coronal intermediate TE with FS, (**b**) sagittal intermediate TE with FS, (**c**) Axial T2 Fluid infiltration with high SI located at the posterior lateral subfascial area with involvement of 10–50% CSA of the rectus femoris muscle belly. Fluid signal along the fascia (arrows) as a sign of involvement of the fascia

have significantly different rehabilitation times. Therefore when describing a type 3b tear it is important to also convey the percentage volume of muscle disrupted and the length of injury (Verrall et al. 2001, 2003; Slavotinek et al. 2002; Connell et al. 2004; Cross et al. 2004; Gibbs et al. 2004). As these parameters increase, the severity of injury also increases implying the need for longer rehabilitation.

BAC Grade 2, Suffix a, b or c/ Munich Type 3b

BAC Grade 2 injuries are muscle tears with loss of muscle continuity for 10–50% CSA and length of 5–15 cm with marginal distraction. Ultrasound can visualise the torn ends of the muscle bundles, and retracted muscle tissue may be highlighted by the presence of refractile shadowing. In some cases of partial or complete rupture, the torn ends of the muscle can be seen floating within the haematoma ("clapper in the bell" sign) (Fig. 5a). It may be also helpful to ask the patient to actively contract the muscle, which will accentuate the retraction of muscle tissue facilitating the identification and sizing of the muscle tear. Related to the location of the tear a suffix a (myofascial) (Figs. 12–14), b (MTJ) (Fig. 15) or c (intratendinous extension) is added. Blood and oedema within the tear and surrounding fascial planes can also be seen. Recognising the tendon is the challenge for the radiologist in unipennate muscle architecture (Fig. 16) to depict aponeurosis lesions (Figs. 7 and 17a–c) referring to increasing rehabilitation period and increased complication rate. Regarding the Munich type 3b identical remark to the previous grade is made.

BAC Grade 3, Suffix a, b or c/ Munich Type 3b

BAC grade 3 injuries are muscle tears with loss of muscle continuity for over 50% but not the complete CSA and length of over 15 cm with distraction. Blood and oedema within the tear and surrounding fascial planes can also be seen. Related to the location of the tear a suffix a (myofascial), b (MTJ) or c (intratendinous extension) (Figs. 15a, b, 18a, b, 19a–e and 20a–c) referring to increasing rehabilitation period and increased complication rate. Regarding the Munich type 3b identical remark to the previous grades is made.

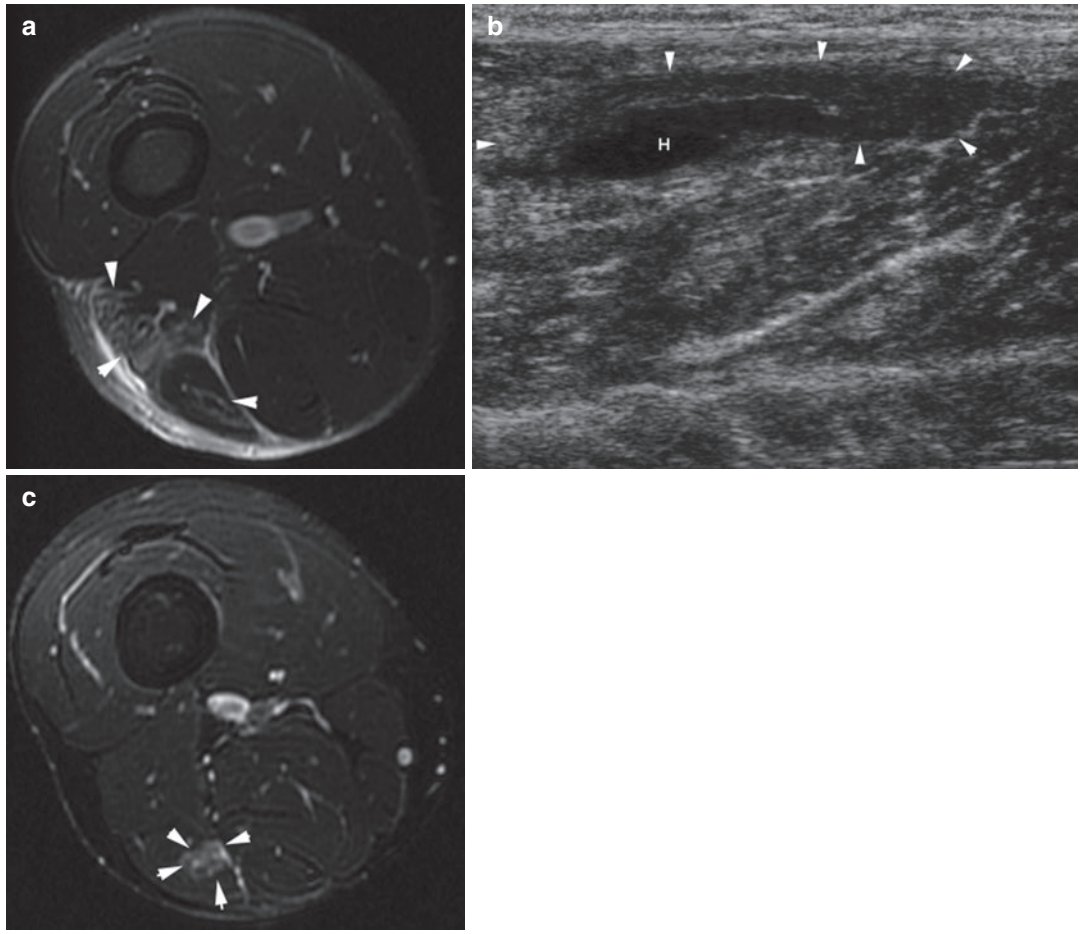

Fig. 15 Professional soccer player with recurrent hamstring injuries. BAC grade 2b/ Munich type 3b biceps femoris long head injury. Distal MTJ of the long head of the biceps femoris is unipennate with membranous flattening of the tendon. (**a**) Axial fat-suppressed T2-weighted MR image from 2002 shows an acute grade 2 injury involving the long head of biceps femoris (small arrowheads). (**b**) Corresponding longitudinal ultrasound image 1 week later shows a hypoechoic haematoma-collection (H) with an area (arrowheads) occupying 10–20% of the muscle diameter (BAC grade 2 injury). (**c**) Axial fat-suppressed T2-weighted MR image from new injury in 2005 shows marked oedema involving the myotendinous junction of the short and long heads (arrowheads) of biceps femoris

BAC Grade 4/Munich Type 4

This Grade 4/Type 4 lesions are complete tears (Fig. 21a–c). Differentiating acute high BAC grade 3 and 4 injuries can sometimes be problematic on T2-weighted MR images as it can be difficult to distinguish oedematous muscle from fluid within the tear (Fig. 21a, c). Occasionally this can be resolved by correlation with T1-weighted MR images or post-gadolinium images where the oedematous muscles enhance but fluid should not. In this situation it may be convenient to perform ultrasound evaluation as it is usually easier to distinguish oedematous muscle from haematoma during static and dynamic imaging (Fig. 22) (Van Holsbeeck and Introcaso 2001; Robinson 2004). A defect is detected at the

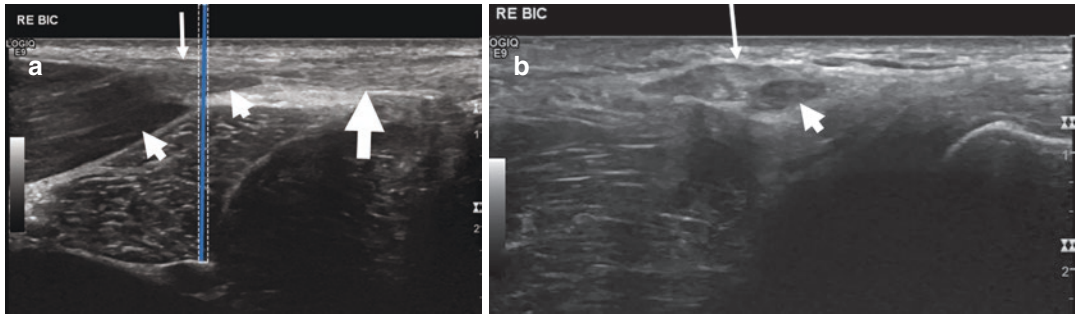

Fig. 16 (**a** and **b**) Long head of biceps femoris distal MTJ. US Anatomy of unipennate distal MTJ, longitudinal (**a**) and axial (**b**). Axial image (**b**) at the level of the dotted line on (**a**). Flattened membranous aspect of the tendon of the long head of the biceps (thin arrow on **a** and **b**) superficial to the muscle belly of the short head (short arrows on **a** and **b**). Thick combined tendon of short and longhead (thick arrow on **a**)

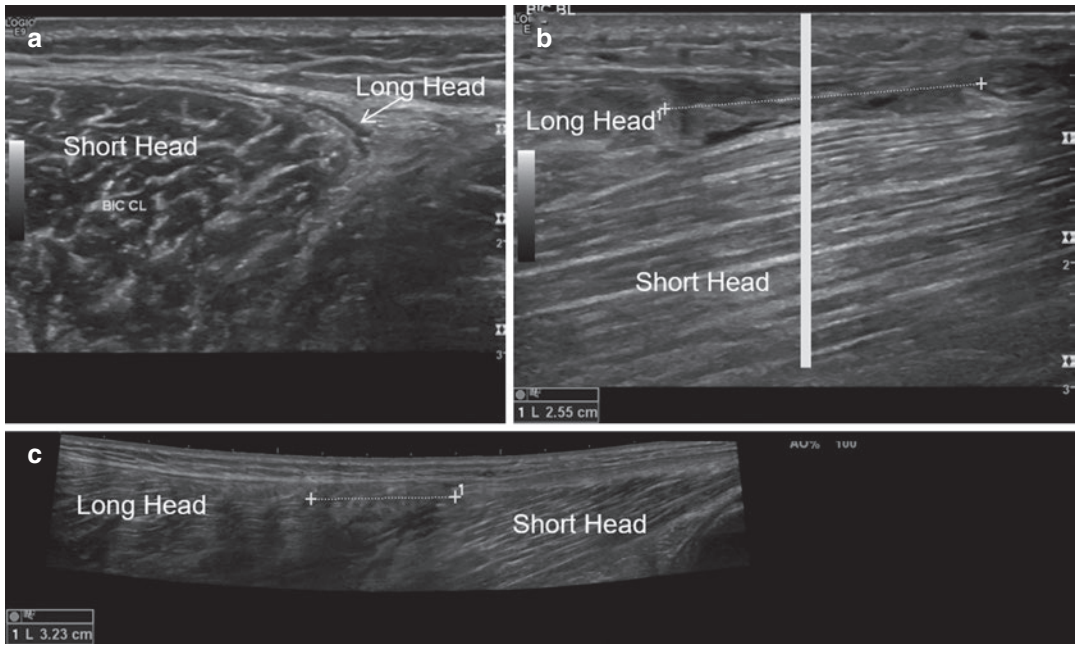

Fig. 17 (**a**–**c**) Ultrasound of tear of the long head of biceps with involvement of the aponeurosis/tendon. BAC grade 2c/Munich type 3b. (**a**) Axial US image at the level of the white line of (**b**). (**b**) Longitudinal image. (**c**) Longitudinal extended field of view. Thin hyporeflective collection (arrow **a**) at the level of the rupture of the aponeurosis of the long head. Located superficial to the short head of the biceps. (**b** and **c**) Dotted line marks retraction of the long head over 3.2 cm

site of the tear, and a mass which is isointense with normal muscle is detected due to retraction of the torn muscle.

Complete tears are more serious injuries and require longer periods of rehabilitation, from several weeks to months.

Haematomas and haemorrhage are a key sign of muscle rupture. Haematomas typically appear as circumscribed areas of low or absent US reflectivity, and, as cellular elements separate out, fluid–fluid levels may be seen. However, in the very early stages of a tear, the haemorrhage

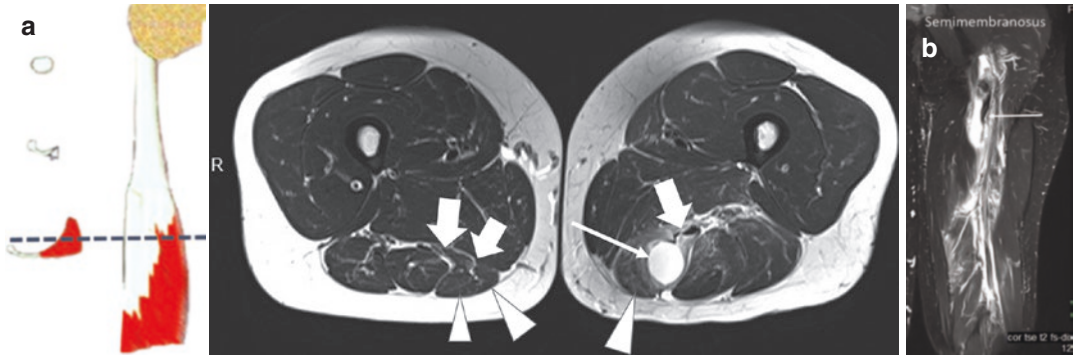

Fig. 18 (**a** and **b**) Semimembranosus tear. BAC grade 3c/Munich type 3b. (**a**) Axial MRI T2 WI, left semimembranosus tear, right normal semimembranosus for comparison. Diagram with dotted line at the level of the MRI. Diagram demonstrating solid tendon at the origin of the tuber ischiadium, more distally thinning of the tendon into a membrane. (**b**) Coronal intermediate TE with FS. Left semimembranosus tear. (**a**) Axial T1WI at the level of the musculotendinous junction. Membrane thick arrow, muscle belly: arrowheads. Left side shows fluid collection at the torn MTJ (thin arrow) with CSA of 50% of the CSA of the semimembranosus. Slackened aspect of the membrane (thick arrow). (**b**) Arrow points at the slackened and retracted semimembranosus tendon

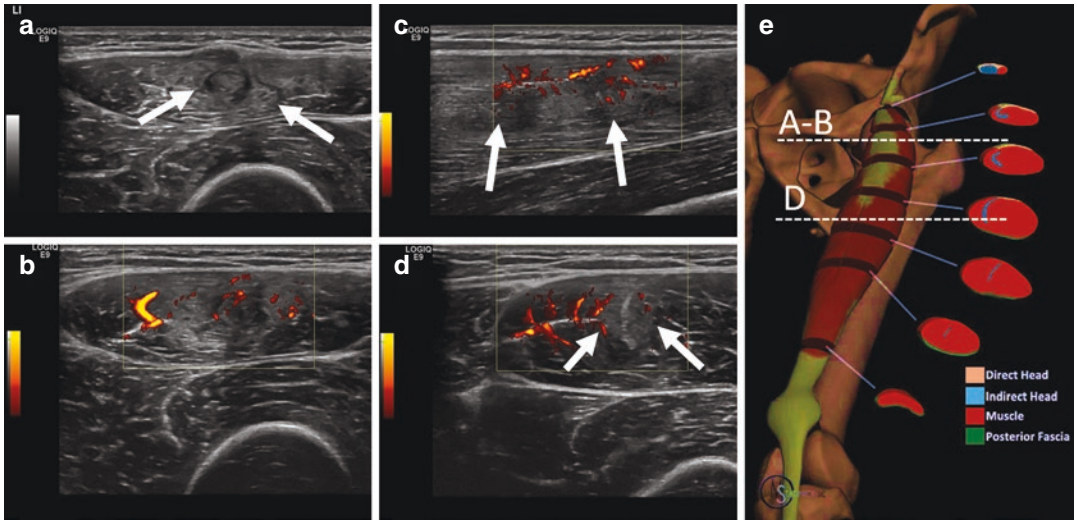

Fig. 19 (**a**–**e**) Fourteen-year-old male soccer player with acute elongation trauma 3 weeks ago. Rectus femoris proximal MTJ tear of the reflected head. BAC grade 3c. (**a**) Top left: proximal axial. (**b**) Bottom left: proximal axial with power Doppler. (**c**) Top right: proximal longitudinal. (**d**) Bottom right: mid axial. (**e**) Diagram adapted from Radsource.us. (Kerr 2014) Diagram (**e**): Unipennate proximal MTJ of the direct of straight head: membranous aspect of the proximal tendon of the direct/straight head (orange) with muscle belly at the periphery at the muscle belly. Bipennate proximal MTJ of the reflected head: proximal tendon (blue) of the reflected/indirect head that flattens to form a central membrane. This bipennate membrane forms the central located muscle belly of the reflected head. Distal MTJ of both heads form a unipennate posterior located membrane (green). (**a**–**d**) Reflected/indirect head of the rectus femoris is the central component of the muscle with bipennate proximal musculotendinous junction. Structural anomaly with mixed hyper- and hyporeflective aspect and increased power Doppler signal (arrows) is documented proximal (**a** and **b** axial and **c** longitudinal) with extension into the centrally located aponeurosis at the middle third of the muscle (**d**)

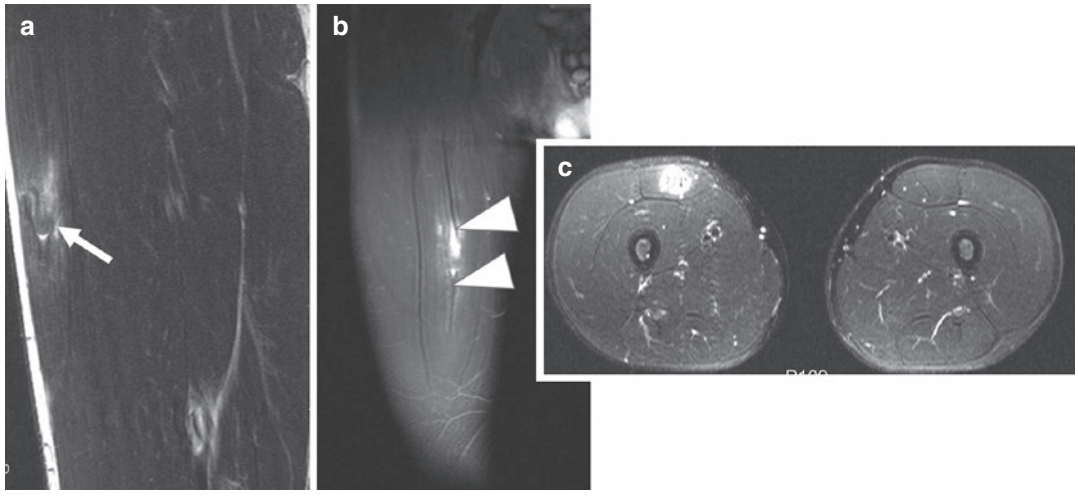

Fig. 20 (**a**–**c**) MRI of rectus femoris reflected head, proximal MTJ tear BAC grade 3c at the right side. (**a**) Sagittal T2. (**b**) Coronal intermediate TE FS. (**c**) Axial intermediate TE FS. Oedema and fluid at the proximal MTJ of the reflected head involving over 50% of CSA, arrows. Bell clappers sign (**a** arrow). Tear of the aponeurosis (**b** arrowheads)

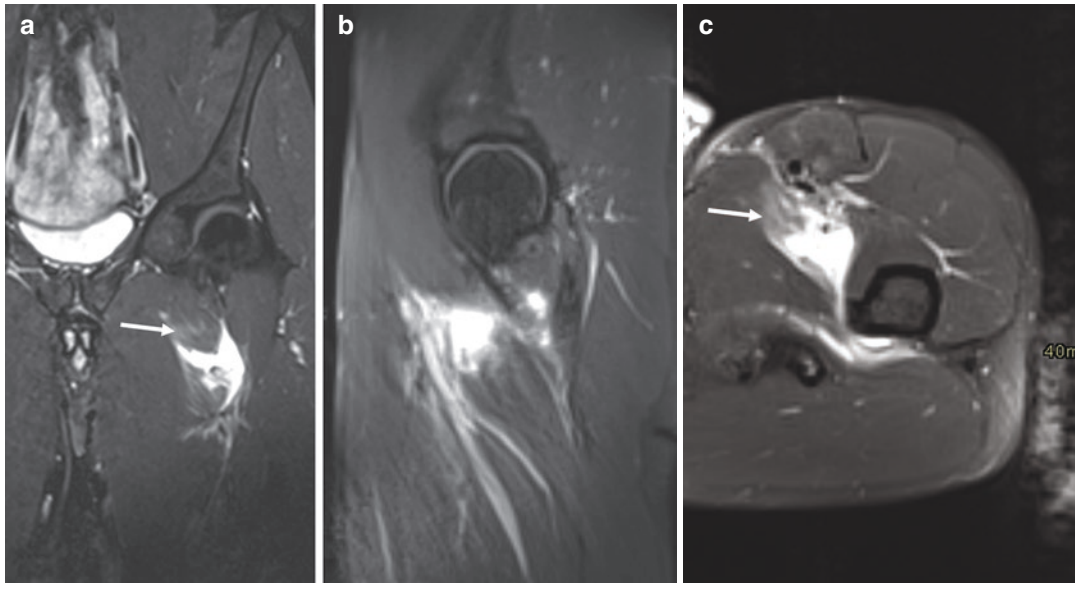

Fig. 21 (**a**–**c**) Left iliopsoas complete tear. BAC grade 4/Munich type 4. MRI intermediate with FS, coronal (**a** left), sagittal (**b** mid) and axial (**c** right). Complete disruption of the distal MTJ of the iliopsoas with oedematous infiltration along the muscle fascia. Homogeneous high SI collection at the tear, intermediate SI at the level of oedematous infiltration of the muscle (arrows)

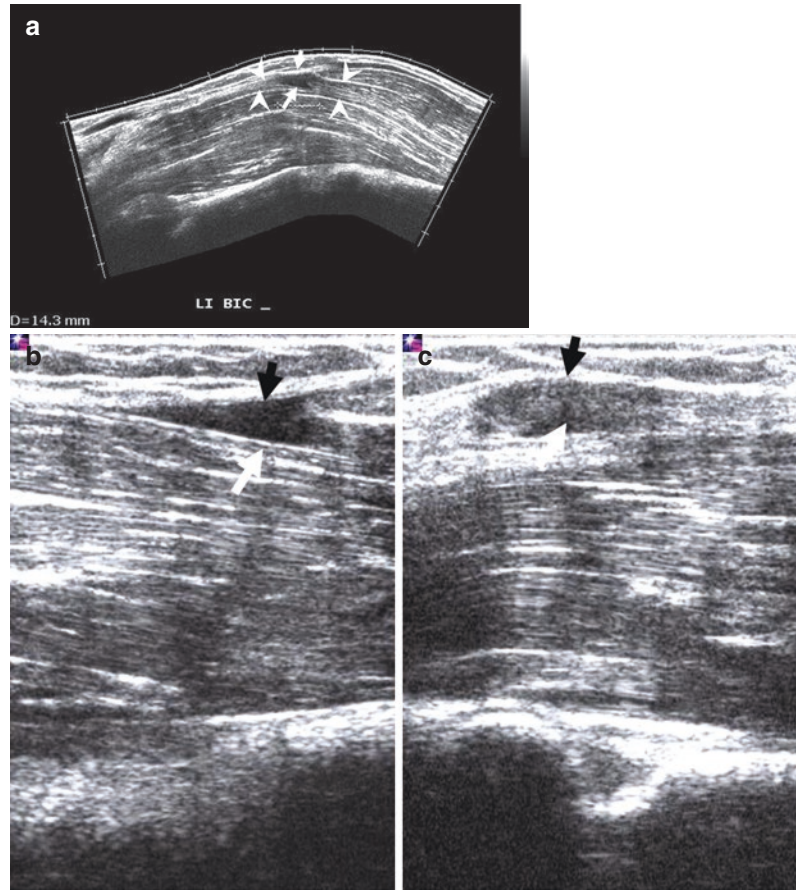

Fig. 22 (**a**–**c**) Early (age 24 h) biceps brachii tear BAC grade 4/ Munich type 4. Parallel muscle fibre type. (**a**) Longitudinal extended field of view. (**b**) Longitudinal view. (**c**) Transverse view. Tear at the lacertus fibrosus myotendinous junction (**a**, arrowheads). Demonstration of an ill-defined and hyporeflective fluid collection (**a**–**c**, arrows)

and haematoma may appear diffuse and hyperreflective (Takebayashi et al. 1995), or cause an increase in the separation of the reflective layers of perimysium. Blood and oedema may also insinuate between the fascial planes (Fleckenstein et al. 1989). If the epimysium or aponeurosis is torn, then the haematoma/fluid may extend beyond the boundaries of the muscle and may appear diffuse and indistinct and seen as high-signal intensity rimming the muscle on T2-weighted images (Figs. 12, 14 and 18a, b). Perifascial fluid is relatively common for BAC grades 2 and up of injury as any breach of the muscle aponeurosis allows blood to track along the fascial planes (Jarvinen et al. 2005).

MRI findings in muscle elongations not only depend on whether the tear is complete or incomplete but also on the duration of the tear. In the acute incomplete tear, blood and oedema may infiltrate between the muscle bundles, especially in the region of the myotendinous junction, giving a feathery appearance (Fig. 6). Acutely, a mass may be detected at the site of the injury; the mass is usually associated with abnormal signals from bleeding and oedema as well as muscle retraction (DeSmet 1993).

3.1.2 Crush Trauma

Muscle trauma resulting from direct trauma represents a crush injury of the muscle fibres. It causes predominant muscular haemorrhage and haematoma and less or no muscle fibre disruption. This usually results from muscle being compressed against bone but can also occur when superficial muscle is compressed against a contracted underlying muscle (Jarvinen et al. 2005). Anatomical boundary may be absent and multiple muscles may be involved. Muscle crush

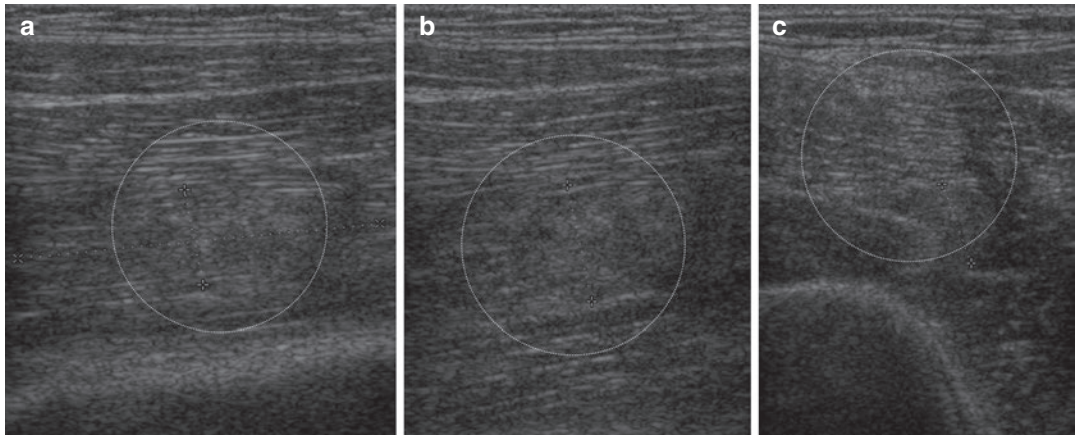

Fig. 23 (**a**–**c**) Crush trauma, vastus medialis. Ultrasound of hyperacute haemorrhage at the vastus medialis muscle. (**a** and **b**) Longitudinal imaging plane, (**c**) axial imaging plane. Diffuse hyperreflective area with unsharp margins and without retroacoustic shadowing (dotted circle)

trauma is commonly seen in contact sports. It is a clinical diagnosis obtained from patient history, muscle function is relatively normal given the degree of pain (Jackson and Feagin 1973; Zarins and Ciullo 1983; Armstrong 1984; Stauber 1988; Jarvinen et al. 2005).

In a similar manner to muscle elongation MR imaging or ultrasound can be used. The difficulty for either imaging modality is defining if there is muscle distraction especially if the clinical history is unclear.

Crush trauma may bring about Morel-Lavallée effusions. They are the result of the skin and subcutaneous fatty tissue abruptly separating from the underlying fascia, a traumatic lesion pattern that has been termed "closed deglovement injury". The lesion is located at the subcutaneous tissue, the muscle itself is typically not involved.

3.1.2.1 Muscle Contusion

Initially and in minor cases, interstitial bleeding or haemorrhage results in ill-defined areas of increased ultrasound reflectivity within the muscle belly (Fig. 23), which become better defined and poorly reflective over time. Depending on the timing of the ultrasound these lesions may be difficult to detect, and an appreciation of the overall increase in muscle size compared with the normal side may be the only ultrasound finding. An acute contusion (0–48 h) appears ill defined with irregular margins and marked echogenic swelling of the fascicles and entire muscle (Aspelin et al. 1992). MR imaging also demonstrates oedema and mixed intrinsic signal as the blood products develop. In anterior snapping hip an intrinsic cause of muscle contusion oedema at the psoas may be found (Fig. 24).

3.1.2.2 Muscle Haematoma

Intramuscular haematoma is a frequent finding in patients with athletic crush muscle injures. Haematomas are usually identifiable on ultrasound within a few hours of injury, or sooner in some cases. The timing of ultrasound examination of muscle injury is ideally between 2 and 48 h after trauma. More serious compressive injuries result in typical haematoma formation, a confined collection of blood; this wedges the muscle fibres away and gives the clinical impression of a mass; fibre rupture is not predominant in crush trauma (Figs. 25 and 26). It may cross aponeurotic boundaries representing the demarcation of the impact (Van Holsbeeck and Introcaso 2001; Robinson 2004). Dynamic ultrasound imaging confirms that a major tear is not present and documents the extent of muscle damage. At 48–72 h ultrasound appearances become better defined with the haematoma appearing

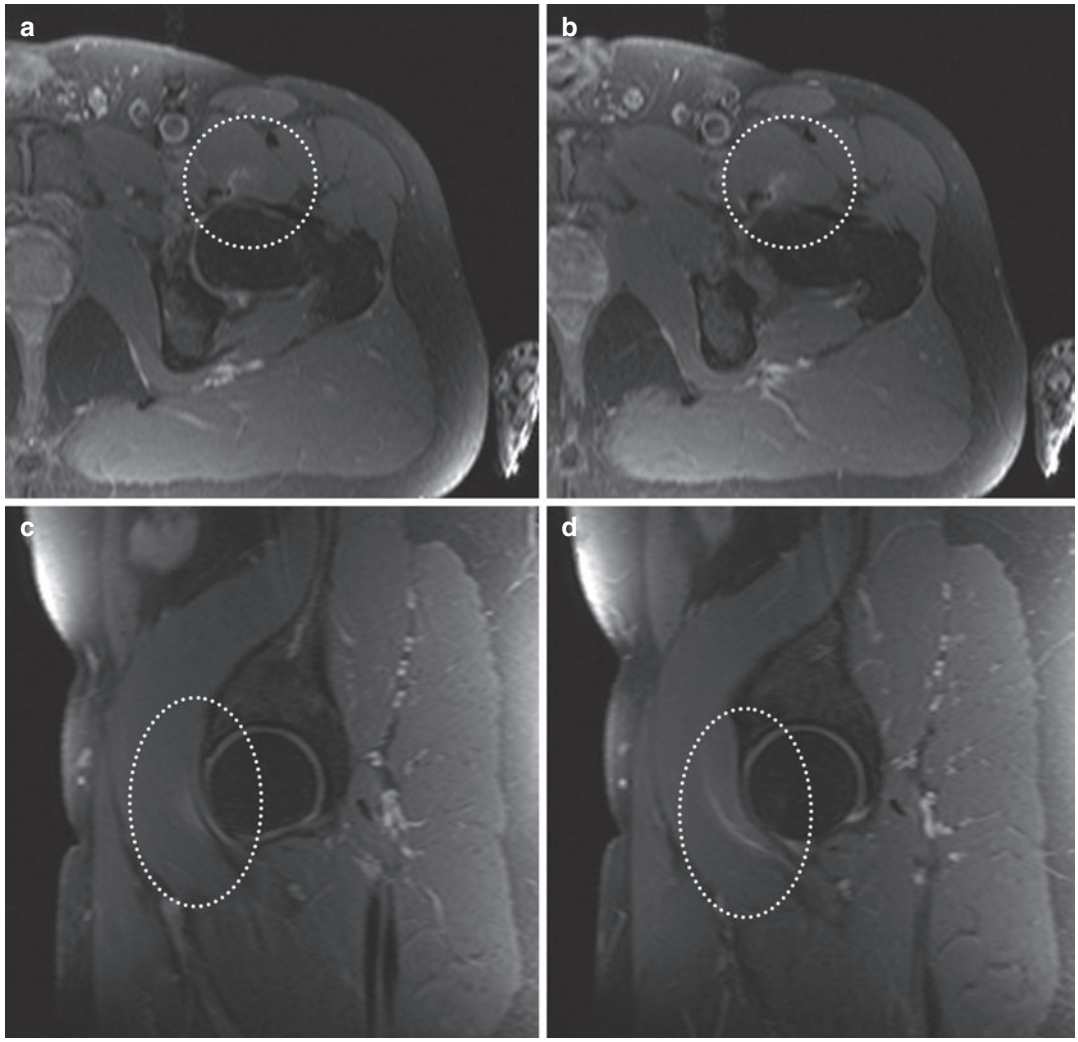

Fig. 24 (**a**–**d**) Anterior snapping hip. (**a** and **b**) Axial fat-suppressed TSE intermediate TE, (**c** and **d**) sagittal fat-suppressed TSE intermediate TE Prolonged T2-releaxation time due to oedema at the musculotendinous junction of the psoas muscle (region of the lacuna musculorum and hip joint capsule (dotted circles))

hypoechoic and a clearer circumscribed echogenic margin which expands centrally as the muscle repairs (Van Holsbeeck and Introcaso 2001; Robinson 2004). The content of the circumscribed lesion may be liquefied, mixed with areas of liquefaction and coagulated blood.

MR imaging also demonstrates these changes although the degree of adjacent muscle and soft tissue oedema can persist for some time.

MRI criteria for diagnosing intramuscular blood, whether haematoma or infiltrating haemorrhage, have been confusing. Blood degrades with time, resulting in changed signal characteristics. Thus, the age of a blood collection determines its signal characteristics on MRI (Fig. 27). Signal characteristics also vary with field strength. All haemoglobin compounds occurring in a muscular haematoma are paramagnetic except oxyhaemoglobin. Methaemoglobin is the only haemoglobin breakdown product encountered in a haematoma which is capable of significant T1 shortening by this mechanism.

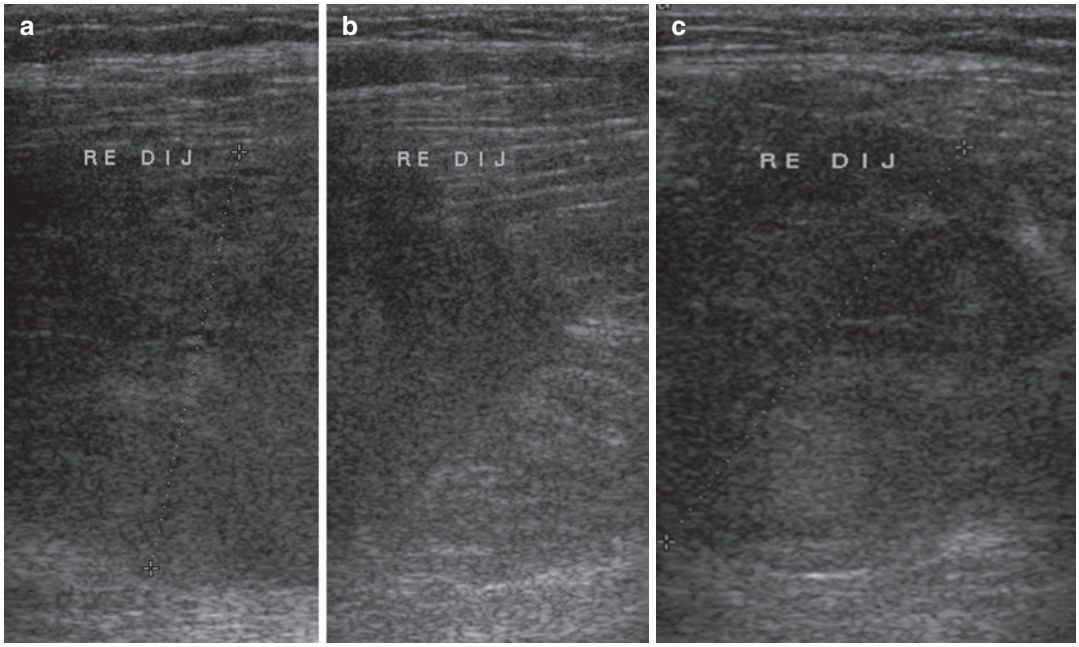

Fig. 25 (**a** and **b**) Right gluteus maximus haematoma, subacute phase. (**a**) Longitudinal ultrasound image of the buttock shows non homogeneous hypoechoic organising haematoma predominantly involving the gluteus maximus. (**b**) Axial imaging plane

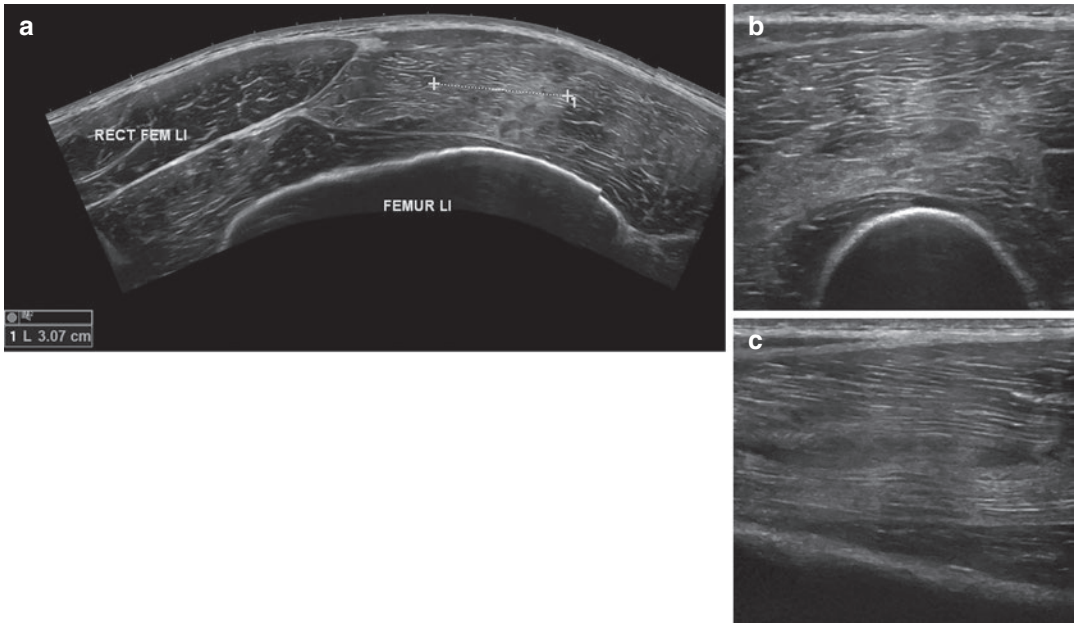

Fig. 26 (**a**–**c**) Ultrasound of subacute haematoma at the vastus medialis of the quadriceps. (**a**) Axial extended field of view. (**b**) Axial imaging plane. (**c**) Longitudinal imaging plane. Hypoechoic unsharp delineated collection wedging away muscle fibres. Surrounded with hyperreflective infiltrated area with transverse diameter 3 cm. No ruptured muscle fibres are visualised

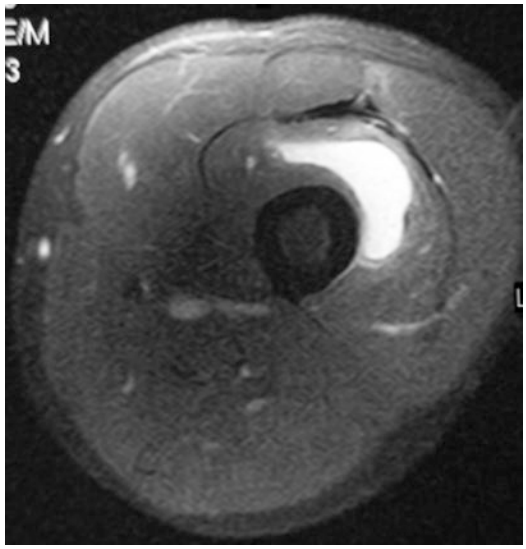

Fig. 27 MRI of subacute haematoma (<30 days) at the vastus intermedius. Axial T2-WI with FS shows homogeneous high SI at the haematoma

Haemosiderin, intracellular deoxyhaemoglobin, and intracellular methaemoglobin all cause T2 shortening. In the case of intracellular deoxyhaemoglobin and intracellular methaemoglobin, this effect is of importance only at high field strengths. The simultaneous presence of many haemoglobin breakdown products in a haematoma can result in very complex-appearing masses on MRI, but the recognition of the T1 shortening of methaemoglobin and/or the T2 shortening of haemosiderin can often suggest the diagnosis (Bush 2000).

Typically an intramuscular haematoma resorbs spontaneously over a period of 6–8 weeks, but on rare occasions it may persist for a long time as a seroma or cystic haematoma (Fig. 28a).

3.1.2.3 Morel Lavallée Effusions/Closed Deglovements

Morel Lavallée effusions are the result of the skin and subcutaneous fatty tissue abruptly separating from the underlying fascia. They are particularly common in the trochanteric region and proximal thigh, where they have been specifically referred to as Morel-Lavallée lesions. In this region, the dermis contains a rich vascular plexus that pierces the fascia lata. The disrupted capillaries and/or lymph vessels may continuously drain into the perifascial plane, filling up the virtual cavity with blood, lymph and debris. An inflammatory reaction commonly creates a peripheral capsule, which may account for the self-perpetuation and occasional slow growth of the process (Mellado et al. 2004).

Ultrasound is the primary technique to depict Morel-Lavallée lesions. In the acute stage diffuse hyporeflective fluid infiltration between subcutaneous fat lobules and the superficial muscle fascia is depicted (Fig. 29). In this stage ultrasound-guided aspiration is easily performed. The patient is treated after evacuation, before standing up, with elastic bandage. In the chronic stage a secreting wall has formed, in this stage evacuation is successful but generally not permanent (Fig. 30a–d).

Three different MR presentations of Morel-Lavallée effusions are discriminated. They may present with cyst-like, haematoma-like at the methaemoglobin degradation phase and haematoma-like with haemosiderotic wall and capillary ingrowth. Long-standing Morel-Lavallée lesions may present cyst-like MRI signal characteristics correlated with encapsulated serosanguinous fluid or seroma. The lesions appear homogeneously hypointense on T1-weighted MR sequences, hyperintense on T2-weighted MR sequences and are partially surrounded by a peripheral ring that appears hypointense on all pulse sequences (Figs. 30e–g and 31a–d).

Morel-Lavallée lesions may also show homogeneous hyperintensity on both T1- and T2-weighted MR sequences and appear surrounded by a hypointense peripheral ring. This T1 signal-intensity behaviour is probably related to the existence of methaemoglobin, characteristic of subacute haematomas (Fig. 32a–d).

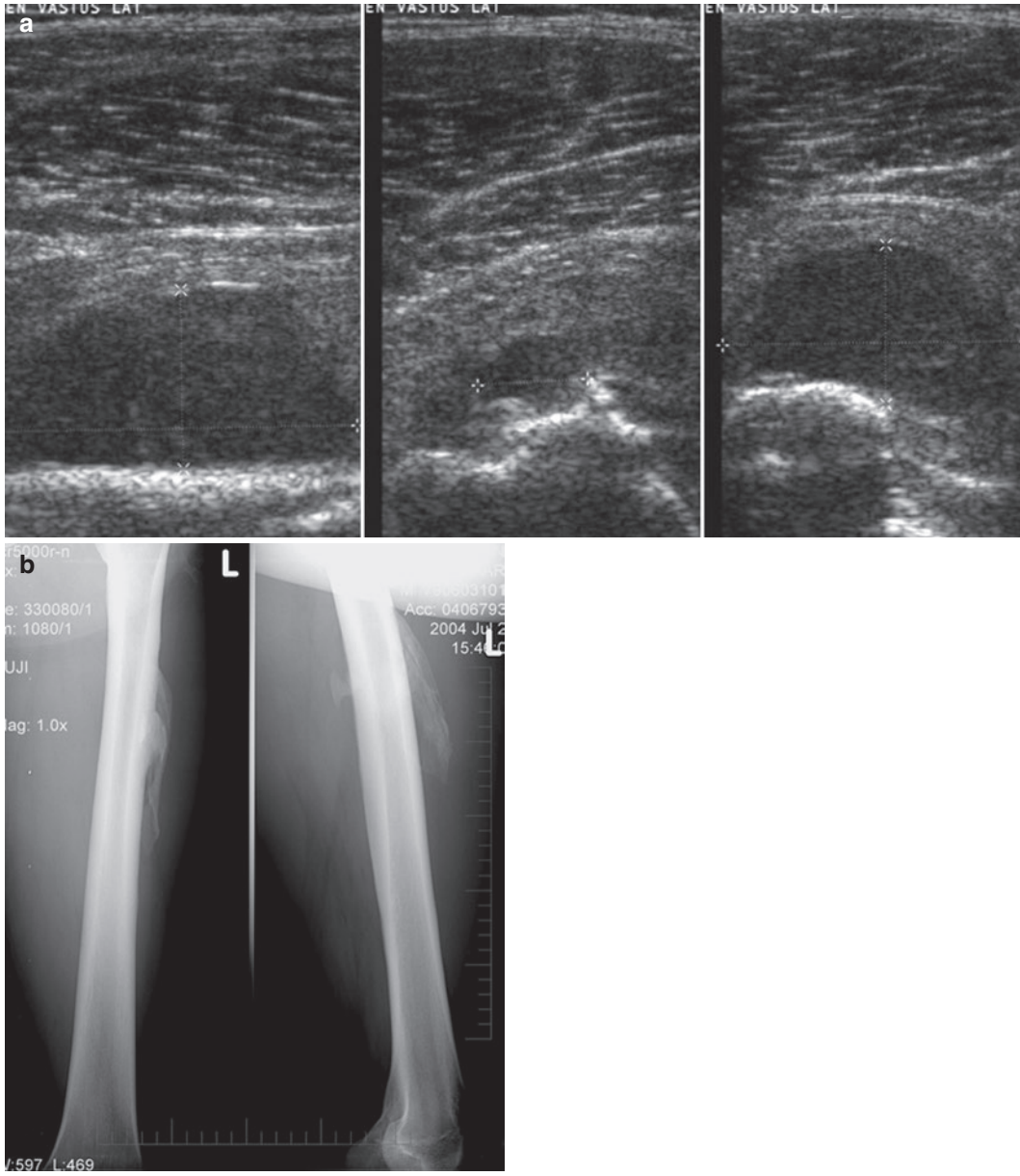

Fig. 28 (**a** and **b**) Male soccer player. Residual pain during play, palpable soft tissue mass at the thigh. Ultrasound, radiography 4 months after crush trauma at the left upper leg demonstrating myositis ossificans and seroma at the vastus intermedius muscle. (**a**) Ultrasound longitudinal (left) and axial (middle and right) images of the thigh. Hyperreflective irregular ossification with posterior acoustic shadowing at the vastus intermedius adjacent to the femur diaphysis. Superficial to this area a hyporeflective seroma is shown (between crosses) that wedges away muscle fibres. (**b**) Radiograph, AP and lateral view, obtained on the same day demonstrates a massive focus of mature ossification: adult stage of myositis ossificans

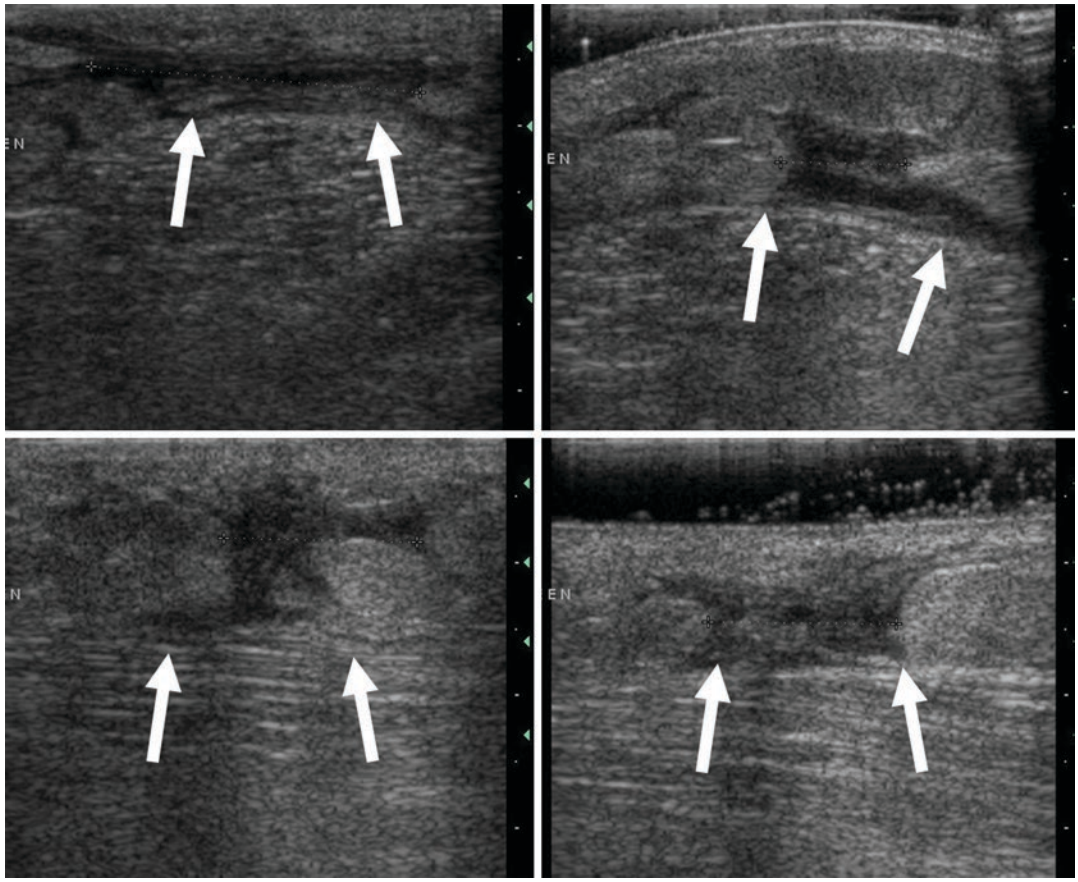

Fig. 29 Ultrasound of acute Morel-Lavallée perifascial fluid at the calf. Hyporeflective fluid at the subcutaneous compartment infiltrating between fat lobules and the superficial muscle fascia (arrows)

Methaemoglobin is first observed on the periphery of subacute haematomas and produces a "concentric ring" sign. As the haematoma evolves, it becomes progressively encapsulated and homogeneously hyperintense on T1-weighted MR sequences.

Long-standing Morel-Lavallée lesions may also show a third MRI pattern that includes variable signal intensity on T1-weighted MR images, heterogeneous hyperintensity on T2-weighted MR sequences, and a hypointense peripheral ring. Patchy internal enhancement and peripheral enhancement may also be present. The heterogeneous hyperintensity on T2-weighted MR sequences correlates with the existence of haemosiderin deposition, granulation tissue, necrotic debris, fibrin and blood clots characteristic of chronic organising haematoma. The hypointense peripheral ring has been found to represent a haemosiderin-laden fibrous capsule with mild inflammatory infiltrate. The internal enhancement after gadolinium administration on MRI and power Doppler signal is probably related to the capillary formation in the lesion. Differentiation of these lesions with soft tissue neoplasm with bleeding is difficult on MRI and US. In cases without a history of trauma specific attention is needed to avoid misdiagnosis of neoplasm with bleeding, i.e. synovial sarcoma, leiomyosarcoma and malignant peripheral nerve

sheath tumour. Also clear cell sarcoma may present with high SI on T1-weighted MR due to the presence of melanin. Every "haematoma" that grows with time or that not diminishes over a few weeks is suspect, it is examined by MRI and eventually biopsied prior to resection (Mellado et al. 2004).

3.2 Complications of Muscle Injury

Elongation injury and muscle contusion may give rise to specific complications (Table 5). The most frequent complication of elongation injury with tear and destruction of the muscular skele-

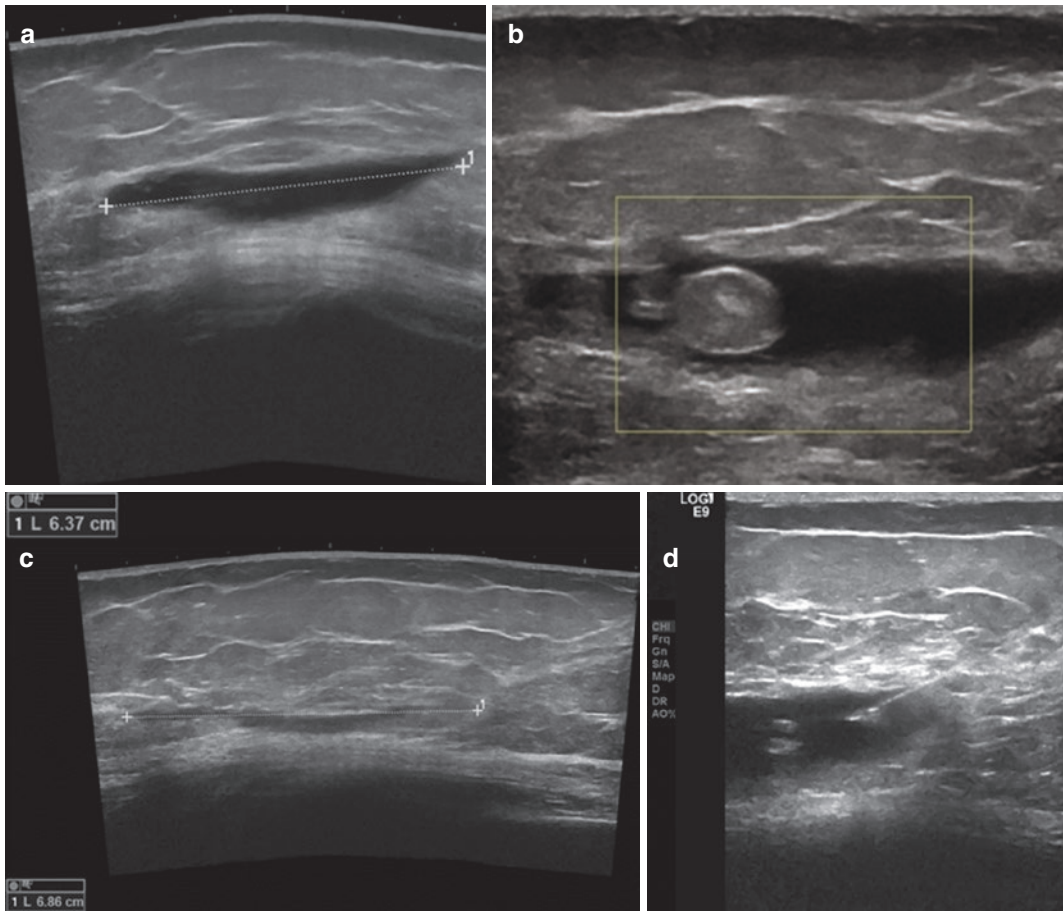

Fig. 30 Ultrasound and MRI of chronic Morel-Lavallée collection at the right thigh superficial to the iliotibial tract. A 58-year-old female with ski trauma 12 years ago. (**a**) US extended field of view, hyposonant collection with maximal dimension 6.4 cm. (**b**) US demonstrating intralesional fat lobules, (**c**) US empty cavity after evacuation, (**d**) US during evacuation with needle trajectory, (**e**) MRI coronal T1 WI, low SI collection superficial to the iliotibial tract, multiple rounded high SI fat drops in the lesion, (**f**) MRI coronal intermediate TE with fat suppression, high SI collection with supressed fat signal at the intralesional fat drops, (**g**) MRI axial T2 WI, high SI collection

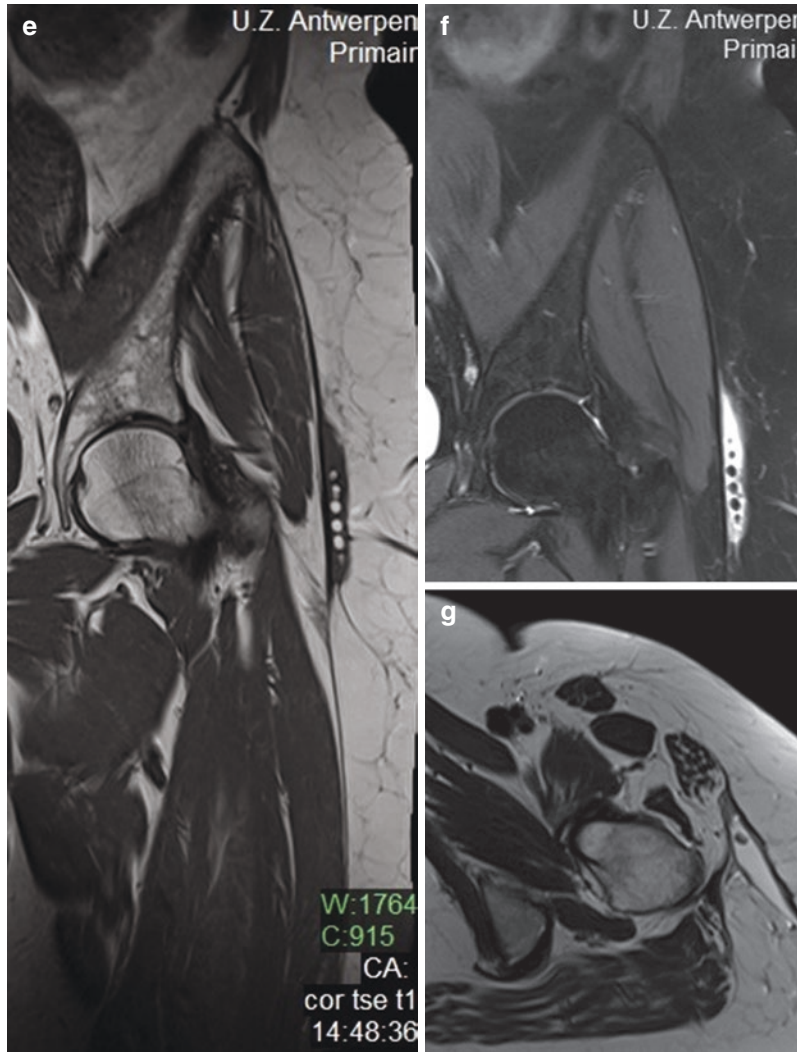

Fig. 247.30 (continued)

ton is fibrosis (Table 5a). Fibrosis is the main reason for retear or recurrence of muscle tear (Figs. 7b, 33, 34 and 35). Muscle atrophy is a complication of elongation injury. Muscle hernia may be caused by focal destruction or weakening of the superficial muscle fascia related to elongation trauma or direct trauma. The main clinical presentation of muscle hernia is not acute injury but chronic compartment syndrome (Figs. 36–38). Muscle hernia is discussed in paragraph 3.9.

The major complication of muscle contusion with laceration is the development of myositis ossificans/focal myositis. A tumour-like mass develops within muscle, which undergoes calcification followed by ossification (Figs. 39a, b and 40a–d). In focal myositis the relationship to an actual traumatic event is often not recalled by the patient. It is more frequent and typical in crush trauma and rare in muscle elongation. In our own experience, the proximal musculotendinous junction of the rectus femoris is the most frequent site

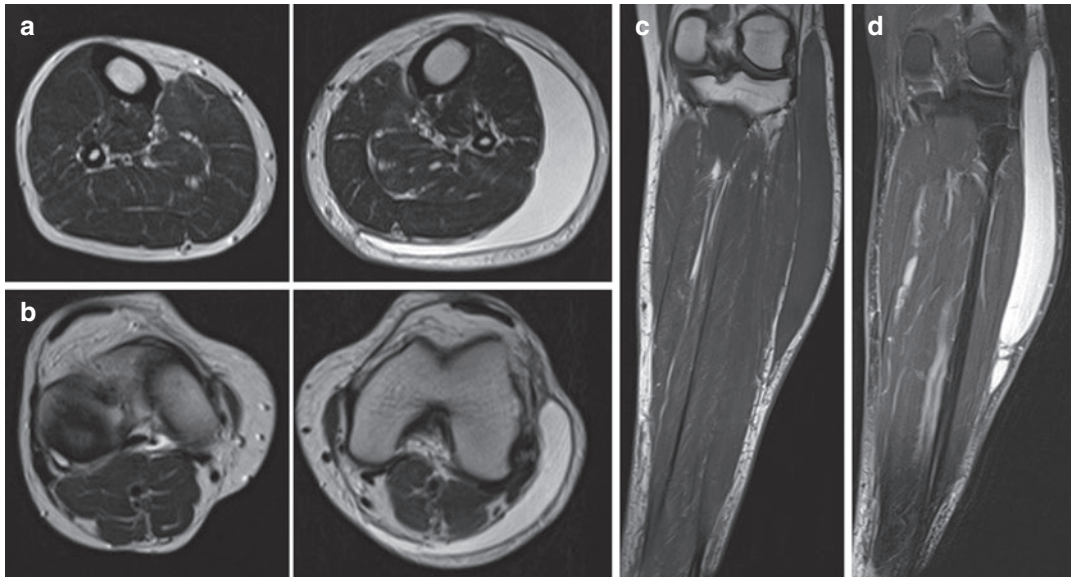

Fig. 31 (**a**–**d**) MRI of chronic Morel-Lavallée collection at the left knee and lower leg. (**a**) Axial T2 WI at the proximal third of the calf, (**b**) axial T2 WI at the knee, (**c**) coronal T1 WI, (**d**) coronal intermediate TE with FS Sharp sickle-like collection external to the superficial muscle fascia with thin regular hypointense wall, homogeneous hyperintense on T2 and low SI on T1 indicating serous fluid without blood degradation components

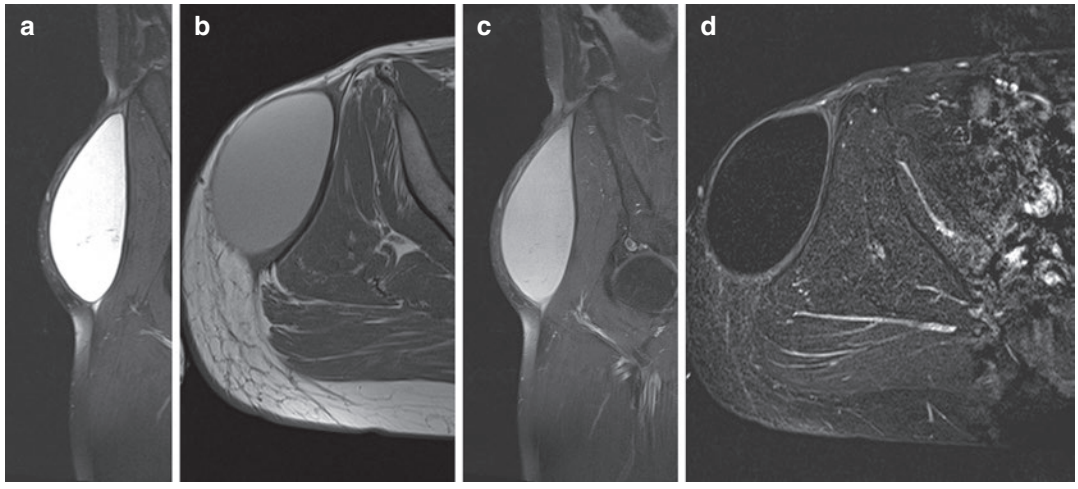

Fig. 32 (**a**–**d**) Six-month-old trauma of the right hip area in 37-year-old male patient with residual mass. MRI of chronic Morel-Lavallée collection superficial to the right iliotibial tract. (**a**) Coronal T2-WI FS, (**b**) axial T1-WI after IV gadolinium DTPA administration, (**c**) coronal T1-WI with FS after IV gadolinium DTPA administration, (**d**) axial T1-WI subtracted images before and after iv gadolinium DTPA injection. Almost homogeneous high SI on T2-WI with FS (**a**). High SI on T1-WI after gadolinium administration. The high SI is related to blood degradation products with high protein content (**b** and **c**). High protein content results in similar SI characteristics of T2 FS and T1 FS with interchangeable images. Enhancement is demonstrated on T1 subtracted images before and after gadolinium administration (**d**). A regular thick enhancing wall of the lesion but absent central enhancement excludes sarcoma (**d**)

of myositis ossificans in muscle elongation. Calcification becomes apparent sooner on ultrasound than on radiographs and typical acoustic shadowing is seen in an early stage (Fig. 40a) (Fornage and Eftekhari 1989). The calcification may develop along the plane of the muscle bundles (Peck and Metreweli 1988), or may be more irregular (Kramer et al. 1979) (Fig. 39a). At early stage, the imaging appearance may mimic a soft tissue sarcoma, and although the typical distribution of calcification at the periphery of myositis is different to the central calcification noted in tumours, it may be extremely difficult to make this distinction (Figs. 39b and 40a–d). Histological diagnosis has to be avoided at this stage, as an erroneous diagnosis of sarcoma is possible. If the diagnosis is unclear, it is recommended to repeat radiographs after an interval of a few weeks to demonstrate

Table 5 Complications of muscle injury in order of decreasing frequency

A. Indirect trauma or elongation with muscle tear	
1.	Fibrosis > retear
2.	Muscle atrophy
3.	Muscle hernia
4.	Myositis ossificans (rare: Rectus femoris)
B. Direct trauma with muscle laceration	
1.	Myositis ossificans/focal myositis
2.	Collection/seroma
3.	Muscle hernia
4.	Calcific myonecrosis (in history of compartment syndrome with muscle necrosis)

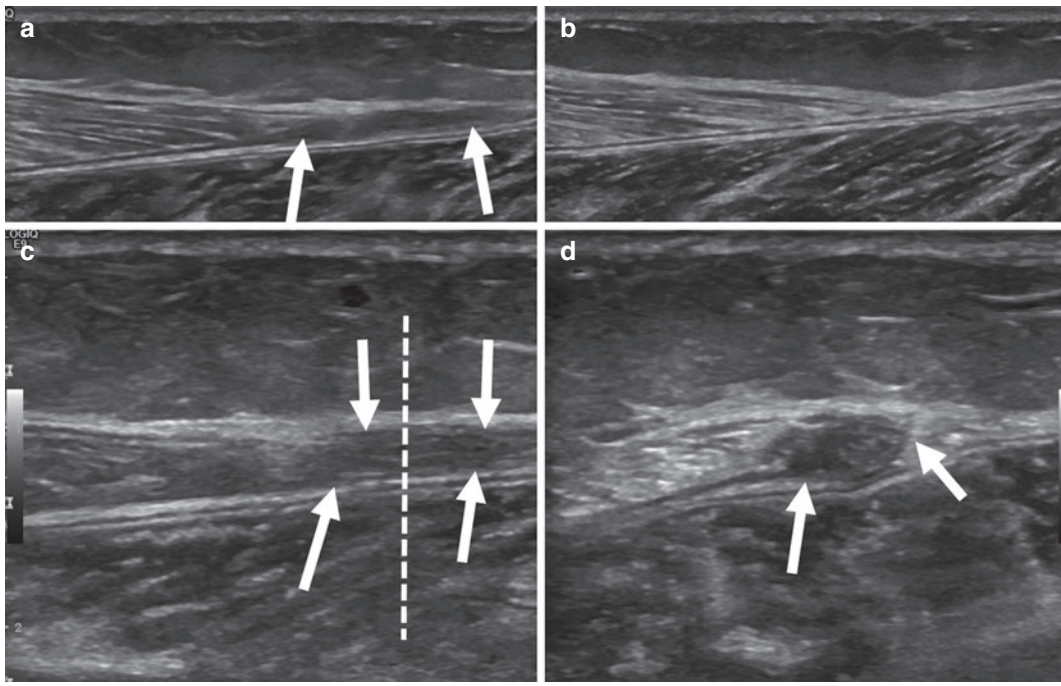

Fig. 33 (**a**–**d**) Fibrosis in a 38-year-old female 9 months after the acute elongation trauma with tennis leg at the right leg. (**a**) Right longitudinal view. (**b**) Right longitudinal view, magnification of (**a**). (**c**) Left longitudinal view for comparison. (**d**) Right transverse view at the level of the dotted line in (**b**) hyporeflective area without striated aspect in the distal aspect of the medial gastrocnemius aponeurosis (arrows **a**, **b** and **d**): old fibrosis

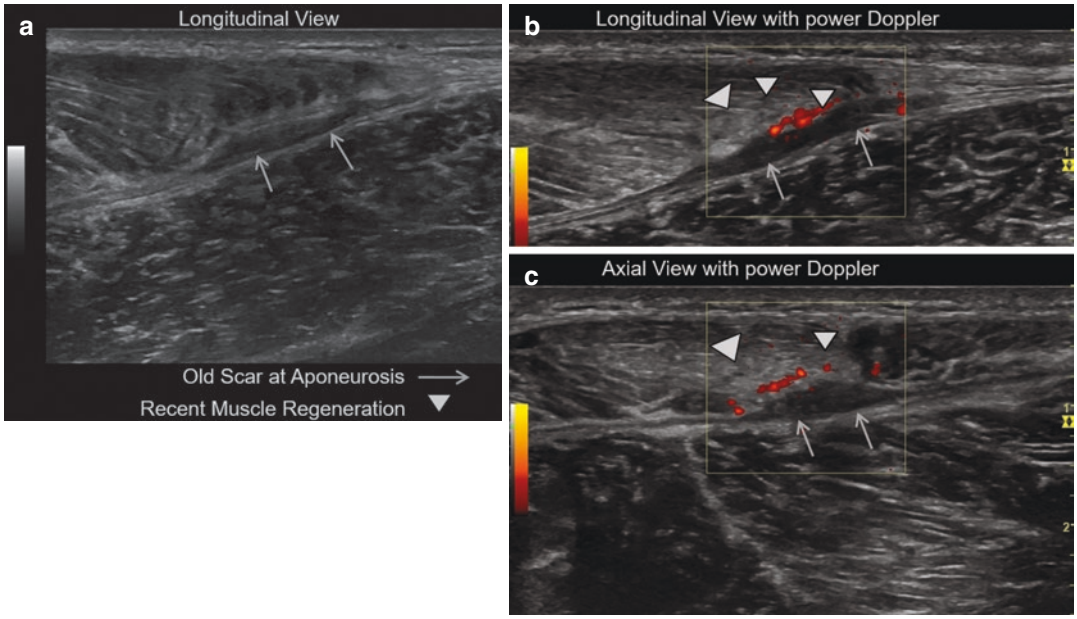

Fig. 34 (**a**–**c**) Recurrent tennis leg in a 38-year-old male patient. Ultrasound 2.5 weeks after the acute trauma. (**a**) Longitudinal view of distal third of the medial gastrocnemius, (**b**) longitudinal view (**a**) with power Doppler. (**c**) Transverse view. Old fibrosis (hyporeflective area) at the distal aponeurosis of the medial gastrocnemius (arrows on **a**, **b**, **c**). Local reflectivity and hypervascularity at the distal MTJ of the medial gastrocnemius: area of subacute elongation trauma (arrowheads on **b** and **c**)

maturation of the calcifying/ossifying process in case of myositis ossificans (Fig. 28b). In some instances large symptomatic lesions may be removed surgically, which is only performed in case of mature bone.

In direct muscle trauma with laceration occasionally intramuscular haematomas fail to resolve, and form chronic cysts (Table 5b). These lesions present on ultrasound as discrete areas of absent reflectivity with posterior acoustic enhancement (Fig. 28a), which can persist for several years and may be responsible for continued muscle pain.

Acute compartment syndrome may result from a single traumatic event, due to the presence of a large haematoma with mass effect. This can compromise vessels and nerves and lead to ischaemic necrosis. Especially the anterior and deep posterior compartment of the lower leg are at risk. Diffuse increased reflectivity of the muscles in the involved compartment may be seen in conjunction with an overall increase in muscle dimension. In later stages, areas of necrosis will develop that appear identical to rhabdomyolysis. Therefore prompt evacuation of haematoma is indicated in patients with increased compartment pressure.

Percutaneous needle aspiration of haematomas is possible. However, there is risk of infection in incompletely aspirated collections of blood, which provide a good medium for bacteria. Aspiration may be used if there is severe pain, or in an attempt to promote early healing. Ultrasound provides a useful means of evaluating haematoma to identify features that might result in failed or incomplete aspiration, such as extensive loculation of the haematoma during organisation.

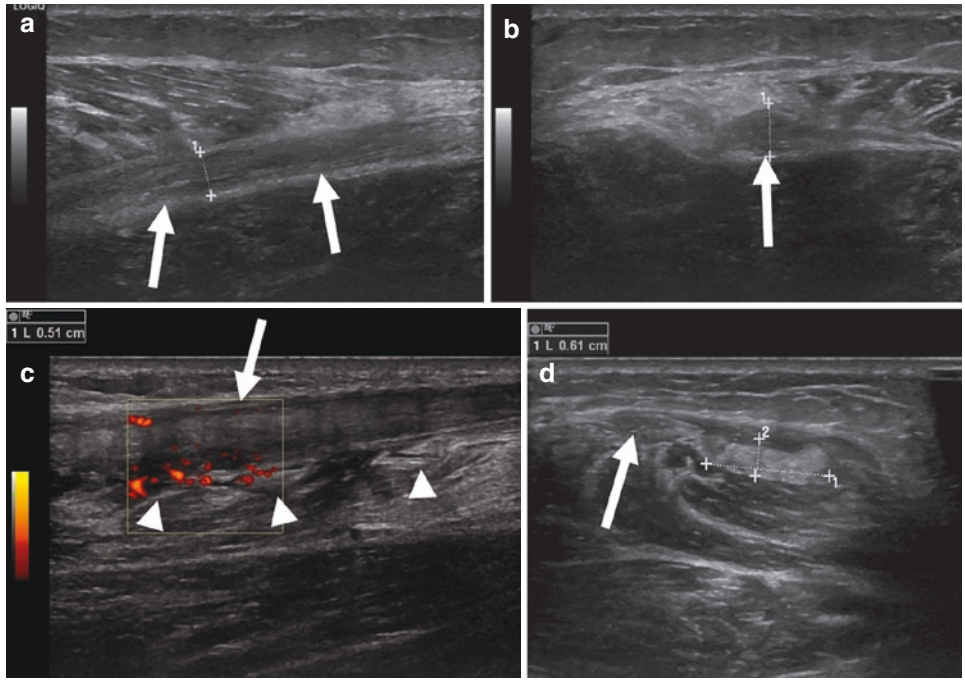

Fig. 35 (**a**–**d**) A 42-year-old male patient with history of old tennis leg and recurrent elongation in the soleus muscle. Ultrasound 2 weeks after the acute trauma. (**a**) Longitudinal view of distal third of the medial gastrocnemius. (**b**) Longitudinal view (**a**) with power Doppler. (**c**) Transverse view at the level of the distal MTJ of the medial gastrocnemius. (**d**) Transverse view at the level of the soleus. Old fibrosis (hyporeflective area) in the area between the distal aponeurosis of the medial gastrocnemius and soleus muscle (arrows on **a**, **b**, **c** and **d**) with adherence of both triceps surae components continuous with the Achilles tendon. Local reflectivity and hypervascularity at the MTJ of the soleus: area of subacute elongation trauma (arrowheads on **b**, cross marks on **d**)

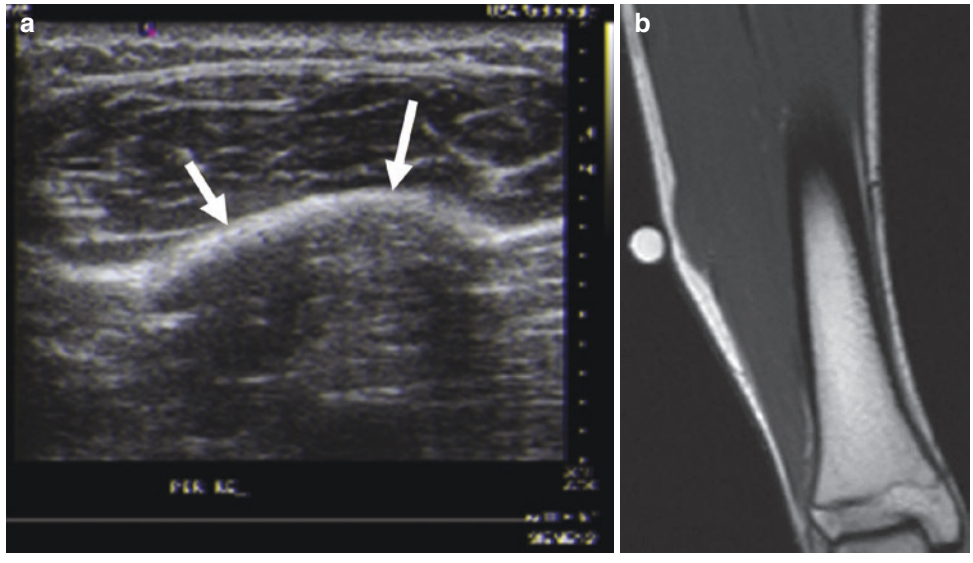

Fig. 36 (**a** and **b**) Muscle hernia in chronic compartment syndrome. (**a**) Patient in upright position. Longitudinal dynamic US with muscle activity with demonstration of muscle herniation at the anterior tibial muscle (arrows). Bulging of muscular tissue towards the subcutaneous tissue is obvious during muscular contraction. (**b**) Coronal T1-WI with muscle bulging to the subcutaneous tissue at the level of the vitamin A pearl

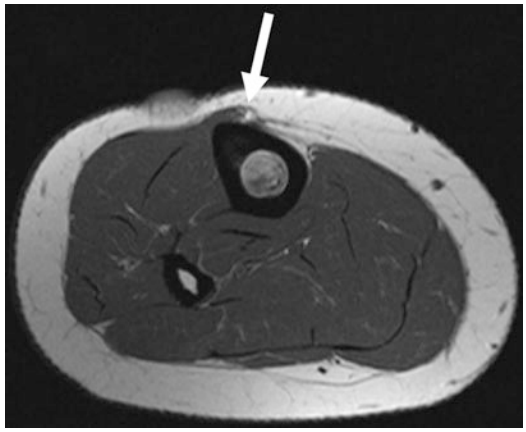

Fig. 37 Axial SE T1-weighted MRI of tibialis anterior muscle hernia. Bulging of tibialis anterior muscle in front of tibia diaphysis representing muscle hernia (arrow)

4 Ultrasound-Guided Aspiration of Traumatic Collections

In elite athletes early recovery of traumatic collections is promoted through ultrasound-guided aspiration. Evacuation or aspiration of fluid collections is most appropriate in closed deglovement and muscle tear. These are serous or serosanguinous collections that do not show clotting. In direct muscle trauma with haematoma intracavity fibrinolysis of the blood clot with urokinase drip is often necessary. As a general rule, the catheter should be maintained until the patient is free of fever, has no infection, and presents less than 10 cc of drainage during three consecutive days (del Cura 2008).

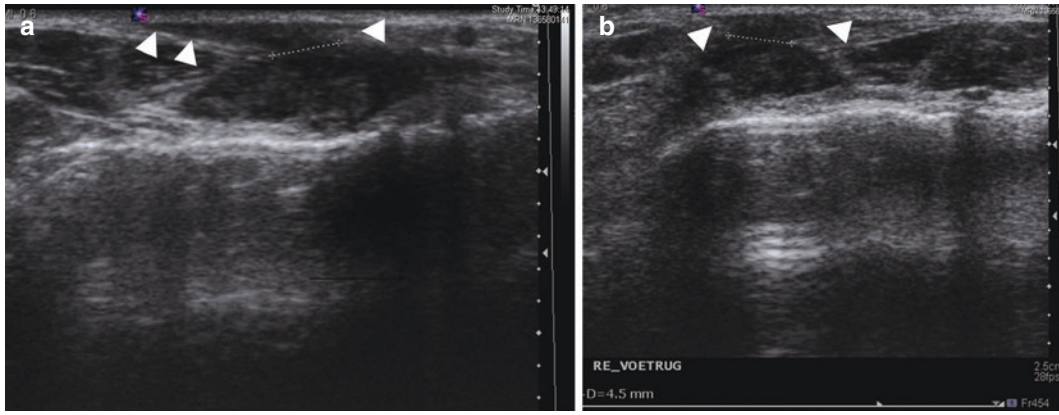

Fig. 38 (**a** and **b**) Muscle herniation at the dorsum of the right foot in a 36-year-old female. Direct trauma at the dorsum of the foot several years ago with persistent pain and swelling. Ultrasound examination demonstrates rent in the superficial muscle fascia of the extensor digiti quinti muscle with dimension 4.5 mm (between cross marks) with bulging of the muscle belly to the subcutaneous compartment (arrow heads)

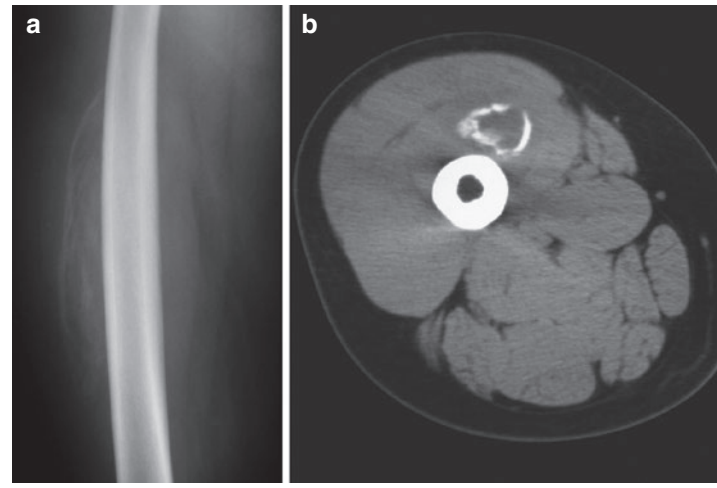

Fig. 39 (**a** and **b**) Focal myositis-myositis ossificans at the left vastus intermedius muscle, early stage. (**a**) Lateral radiograph of the femur diaphysis. Amorphous calcification at the soft tissue anterior to the diaphysis of the femur. (**b**) Axial CT at the mid third of the left leg. Ring-like calcification at the periphery of the area of muscle haematoma/laceration. This is a characteristic presentation of early focal myositis/myositis ossificans and excludes sarcoma with haematoma

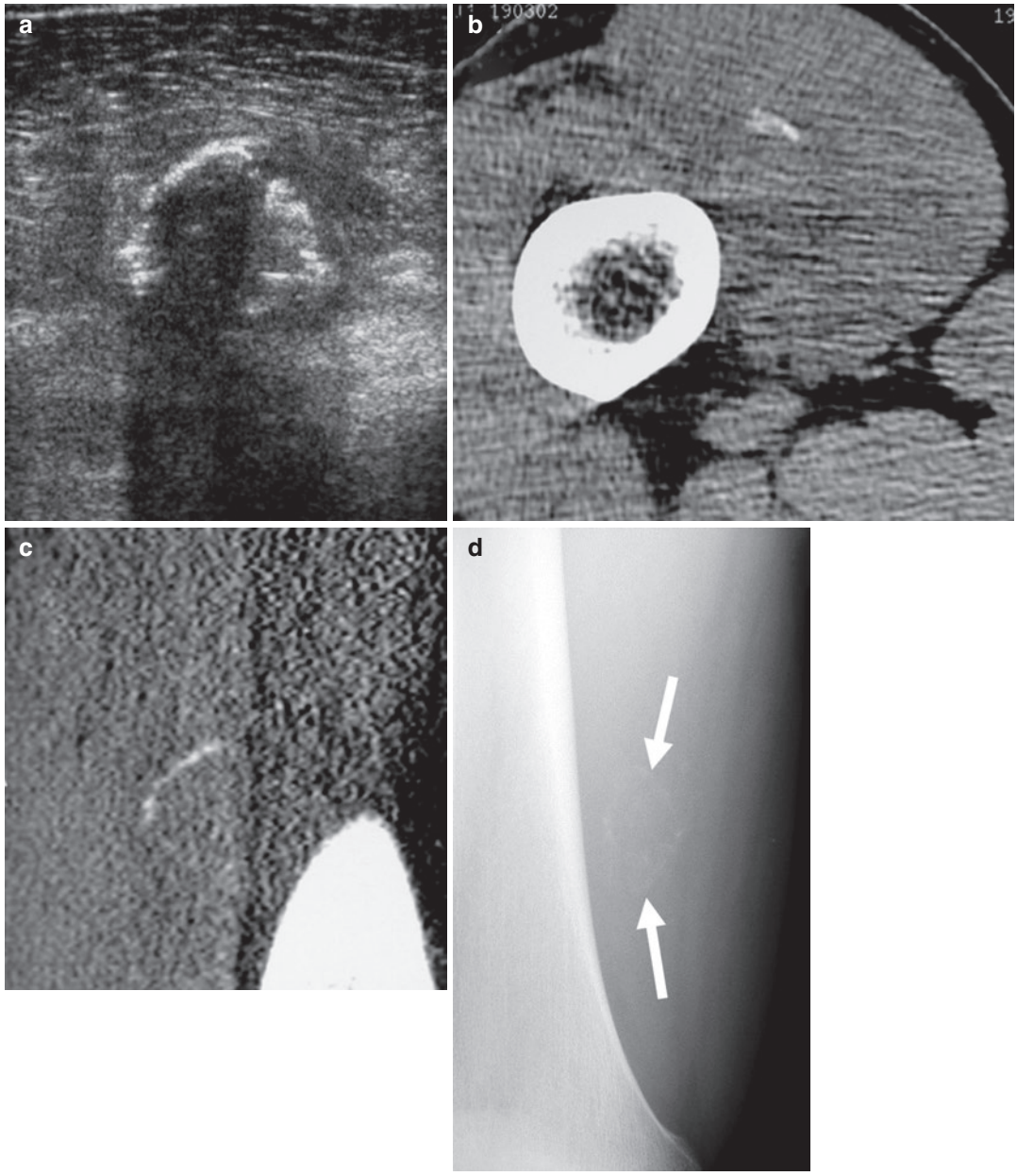

Fig. 40 (**a**–**d**) Early (1–2 weeks after the traumatic event) focal myositis in vastus intermedius muscle in three different patients. (**a**) Ultrasound demonstrating early calcification at the peripheral with irregular reflectivity (**b** and **c**) same patient. CT shows sickle-like parts of ring calcification of peripheral calcified haematoma. (**d**) Radiograph demonstrating rim calcification (arrows)

5 Delayed Onset Muscular Soreness (DOMS)

Delayed onset muscular soreness (DOMS) Munich type 1b, a common ailment, is another form of muscle injury. Regardless of a person's general level of fitness, nearly every healthy adult has experienced DOMS. Following unaccustomed muscular exertion, patients develop DOMS and experience a sensation of discomfort and pain in their skeletal muscles. For example, after prolonged downhill running

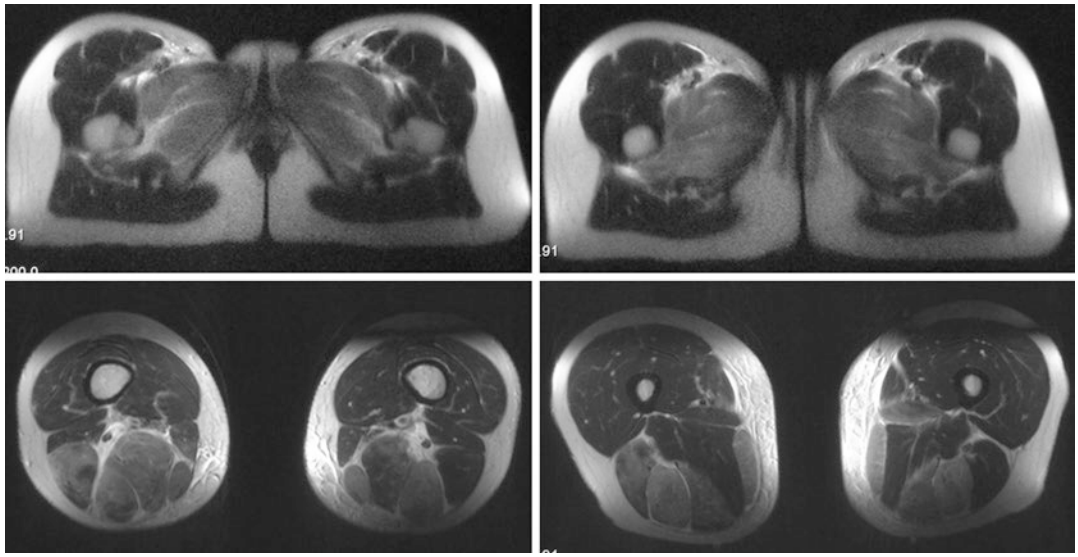

Fig. 41 Delayed onset muscular soreness in a 27-year-old female. Pain and muscle stiffness at the adductor and hamstrings area of both legs the day after a major water ski tournament. Axial T2 WI shows symmetric marked muscle oedema at the adductor and hamstrings muscles

(eccentric muscle activity) in an experimental setting, athletes experienced pain in all the extensor and flexor muscles groups around the hip, thigh and leg. Structural abnormalities in the Z band and a rise in the serum creatine kinase have been described by Nurenberg et al. (1992). Pain increases in intensity for the first 24 h after exercise, peaks between 24 and 72 h and then subsides in 5–7 days. Temporary loss of strength, up to 50%, can be present. The diminished performance results from reduced voluntary effort due to pain as well as reduced capacity of the muscle to produce force. The soreness is believed to be due to reversible structural damage at the cellular level. There is no associated long-term damage or reduced function in the muscles. Some authorities believe that the clinical syndrome of exertional rhabdomyolysis may represent a severe form of DOMS. US demonstrates no obvious abnormalities in either stage of DOMS.

MR imaging of DOMS is very rarely required. Experimental studies by Shellock et al. (Shellock et al. 1991) showed that DOMS follows a consistent pattern where signal intensity on T2-weighted images increases gradually over few days after initial eccentric exercises, peaks after several days, and gradually returns to normal over as long as 80 days. There is a high correlation between the increase in signal intensity on MR and the ultrastructural injury demonstrated in the Z bands. Because DOMS is not associated with bleeding, it is assumed that the MRI changes are primarily due to oedema. Muscle elongation and DOMS frequently have similar appearance, and the two clinical conditions are difficult to differentiate on the basis on the imaging findings alone (Fleckenstein and Shellock 1991). Muscle elongation often appears less extensive or uniform in its distribution within a muscle than DOMS by MRI (Fig. 41).

6 Chronic Exertional Compartment Syndrome

6.1 Definition, Clinical Presentation and Diagnosis

Compartment syndrome is defined as increased interstitial pressure within an anatomically confined compartment that interferes with neurovascular function. Normal pressures within a muscle compartment are between 0 and 4 mmHg and can peak above 60 mmHg on exercise but quickly

dissipate on cessation. However if this pressure is sustained above 15 mmHg blood flow is compromised and muscle ischaemia can occur (Zabetakis 1986).

Chronic exertional compartment syndrome commonly affects the anterior and deep posterior calf lower leg musculature (Martens et al. 1984; Peterson and Renstrom 1986; Zabetakis 1986). Elite motocross racers are at risk to develop bilateral chronic exertional compartment syndrome at the forearm (Gielen et al. 2009). It is thought that chronic traction on the muscle fascia alters its compliance and subsequent ability to accommodate volume change on exercise (Nicholas and Hershman 1986; Peterson and Renstrom 1986). The athlete usually presents with crescendo pain and paraesthesia after exercise which eases on ceasing activity and unlike popliteal artery syndrome is not posture dependant (Martens et al. 1984; Nicholas and Hershman 1986). There may also be muscle swelling and it is important to rule out an underlying muscle hernia. The diagnosis can sometimes be made with history alone but compartmental pressure measurements may be necessary. Pressure pre exercise of greater than 15 mmHg, or post exercise pressure greater than 30 mmHg at 1 min, or greater than 20 mmHg at 5 min confirm the diagnosis (Pedowitz et al. 1990).

6.2 Imaging

Appearances on imaging can be nonspecific and are not always reliable in confirming the diagnosis (Edwards Jr et al. 2005).

On ultrasound the muscle can appear echogenic with relative sparing of periseptal areas which are still receiving sufficient blood flow from the adjacent fascia (Van Holsbeeck and Introcaso 2001). Studies evaluating muscle cross-sectional area on ultrasound both before and after exercise describe two different patterns in symptomatic patients. In one group the muscle compartment cannot expand with a relatively rigid fascia compared to normal subjects (where muscle volume can increase by 10–15%). In the other symptomatic group, although the muscle compartment does expand during exercise, there is a slow reduction in volume post exercise compared to normal subjects (Van Holsbeeck and Introcaso 2001).

Post exercise MR imaging can show oedema related to eccentric muscle activity in the clinically affected muscles confirming the diagnosis (Gielen et al. 2009) (Figs. 42 and 43). However, like ultrasound, this technique is not completely sensitive or specific with oedema being found in asymptomatic athletes and normal muscle appearances occurring in athletes with objective

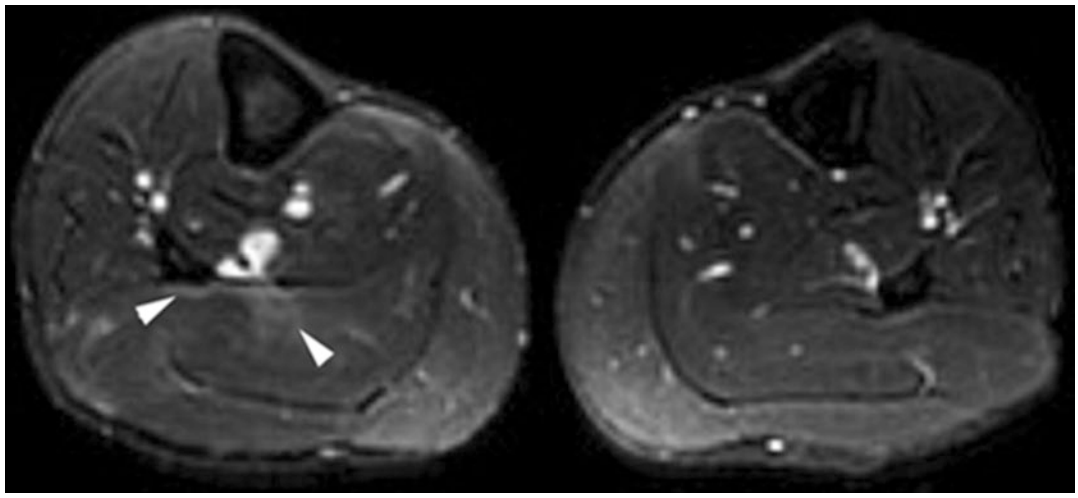

Fig. 42 Chronic compartment syndrome of right the calf. Running athlete with chronic exertional right leg pain. Axial T2-weighted fat-suppressed MR image post exercise shows persisting soleus oedema (arrowheads). The athlete was successful treated with fasciotomy

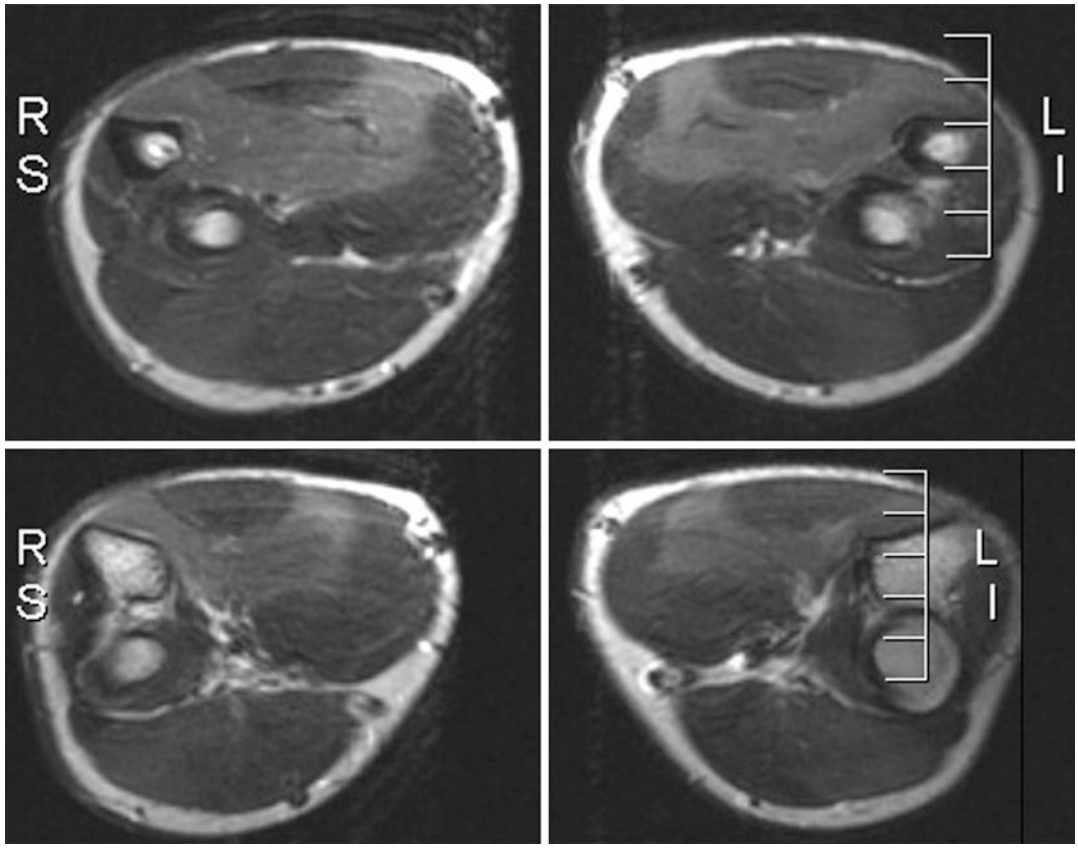

Fig. 43 Chronic compartment syndrome at the forearms in a 29-year-old professional motor cyclist. MRI with axial T2-WI performed immediately after exertion that provoked pain at the flexor compartments of both forearms demonstrates symmetric muscle oedema at the flexor digitorum superficialis

clinical features (Fleckenstein et al. 1989; Shellock et al. 1991).

The initial treatment of chronic exertional compartment syndrome includes training modifications and assessment for orthotics; however, if symptoms persist, fasciotomy of the muscle compartment is performed. Morbidity can potentially result if there is subsequent muscle herniation or scarring (Van Holsbeeck and Introcaso 2001).

7 Muscle Atrophy

Muscle atrophy may be secondary to disuse, muscle denervation, e.g. compressive neuropathy, muscle rupture or a consequence of a primary muscle disorder, e.g. muscular dystrophy. Varying degrees of atrophy exist and, where possible, comparison with normal muscle aids diagnosis as differences may be subtle. Discrepancies in muscle bulk may be easier to detect near the myotendinous junction. Atrophic muscle appears characteristically hyperreflective owing to the replacement of muscle fibres by fat (Hide et al. 1999). It may also be possible to detect a relative decrease in vascularity on Doppler ultrasound, especially after exercise. In cases of compressive neuropathy, ultrasound can be a useful means of identifying compressive lesions and may help in demonstrating the pattern of involved muscle groups. Function loss of the motor nerve leads to muscle paralysis that is easily demonstrated on

dynamic US investigation by the absence of motion at the muscle fibres during voluntary activation.

A specific cause of muscle atrophy is suprascapular nerve lesion resulting in weakness of the supraspinatus or infraspinatus muscle. It is found idiopathically in athletes and in relation to paralabral cyst with compression of the nerve at the level of the suprascapular notch.

Early phases of denervation present as diffuse muscle oedema, in chronic phases atrophy with lipomatous infiltration is found, these are demonstrated as high SI on T2-weighted MR imaging and T1-weighted MR imaging respectively.

For further discussion of muscle atrophy, see also Attard et al. (2021) and Kilsdonk et al. (2021).

8 Rhabdomyolysis

Rhabdomyolysis is a condition that results in necrosis of skeletal muscle. The causes include primary muscle injury, diabetes, burns, hypoxia secondary to peripheral vascular disease, infection, inflammation and drugs and toxins. Early diagnosis is important as complications include acute renal failure, hyperkalaemia and disseminated intravascular coagulation.

Ultrasound usually demonstrates a heterogeneous echo pattern within affected muscles (Lamminen et al. 1989; Fornage and Nerot 1986). The muscle often appears diffusely enlarged with loss of normal fibrillar architecture and thickening of the layers of perimysium. A hyporeflective inflammatory exudate engulfs necrotic muscle cells. Hyperreflective areas are due to gas within necrotic tissue. The aspiration of clear serous fluid under ultrasound guidance supports the diagnosis of uncomplicated rhabdomyolysis.

Ultrasound appearances must be interpreted in conjunction with clinical and haematological findings as similar features may be seen at ultrasound in cases of acute haematoma and pyomyositis.

9 Calcific Myonecrosis

Calcific myonecrosis is a rare, (very) late sequel of trauma with myonecrosis occurring almost exclusively in the lower extremity (anterior and posterior tibial compartment) which may be confused with an aggressive primary neoplasm (Gielen et al. 2008a, b). The platelike mineralisation pattern seen on radiographs is characteristic but not widely recognised by clinicians (Holobinko et al. 2003) (Fig. 44c, d). US shows diffuse calcifications encompassing a complete muscle or muscle compartment that is avascular on power Doppler colour duplex US (Fig. 44a, b). On MRI a tumour-like but avascular mass with bleeding components and fibrosis is found (Fig. 45a–d).

10 Muscle Herniation

Muscle herniation is a relative rare condition which is often diagnosed clinically, although occasionally the symptomatology is confusing. Elongation trauma and blunt trauma can produce a rent in the fascia, allowing the underlying muscle to protrude. However the main clinical presentation of muscle hernia is not acute injury but chronic compartment syndrome. It is usually seen in the leg, particularly over the anterior tibial compartment. Muscle hernias result in masses, which appear on active contraction of the muscle. MRI or ultrasound may offer an unequivocal diagnosis by demonstration of the fascial rent and characterisation of the protruding mass as being muscle tissue (Zeiss et al. 1989). Ultrasound can demonstrate the muscle bulge and defect in the fascia (Figs. 36a and 38a, b). The hernia may sometimes be reduced by pressure with the ultrasound probe.

It may be helpful to perform the ultrasound and MR scanning with the herniated muscle both relaxed and contracted in order to demonstrate a change in size of the herniated portion (Figs. 36 and 37). Muscle herniation will be discussed more in detail in Baur et al. (2021) and Karantanas (2021).

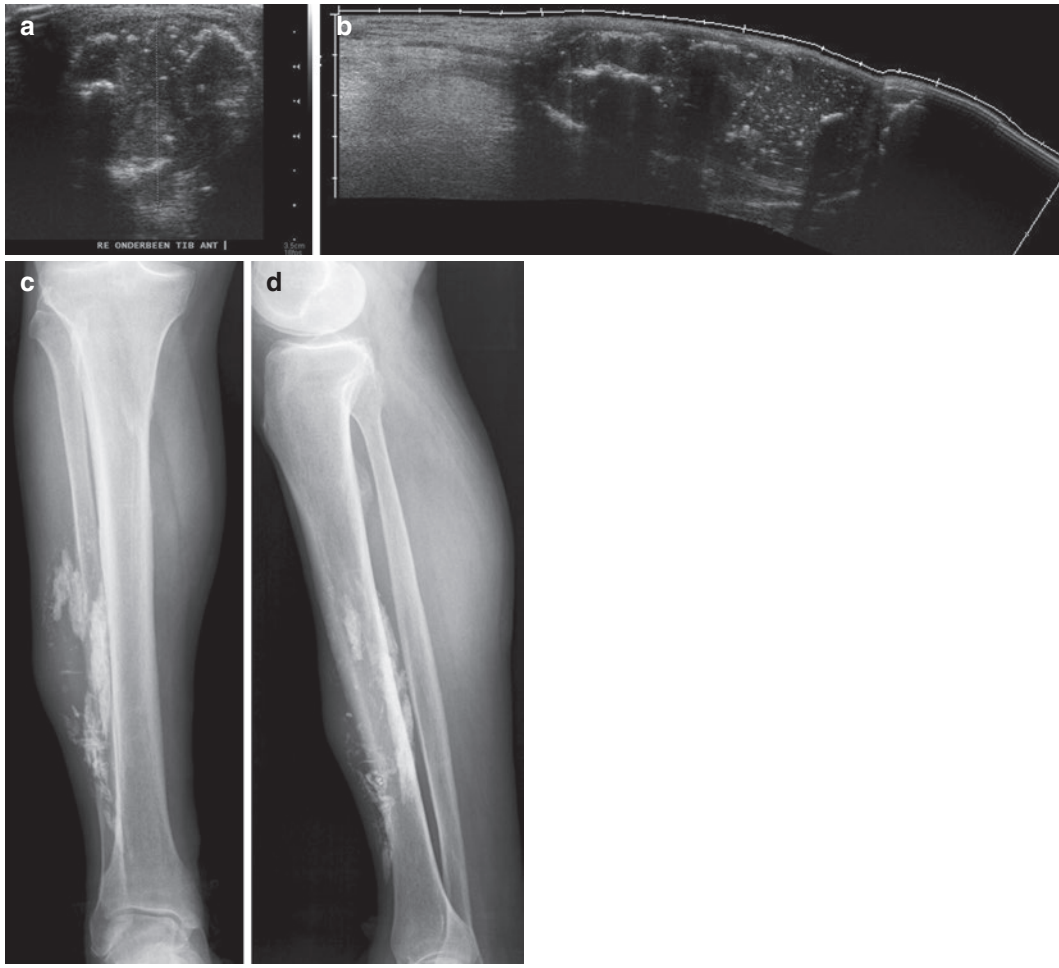

Fig. 44 (**a**–**d**) Eighty-four-year-old male with drop foot after blunt trauma 15 years ago. Development of painless, soft swelling at the right anterior tibial compartment since 2 months. Calcific myonecrosis of the right anterior tibial compartment detected. Axial (**a**) and longitudinal (**b**) extended field of view US images and radiographs (**c** and **d**), anteroposterior and lateral view, respectively). US reveals avascular non homogeneous hyporeflective mass lesion with intralesional reflective areas with acoustic shadowing. Radiograph shows amorphous calcifications with characteristic platelike aspect at the anterior tibial compartment. Central mass with smaller amorphous calcifications. No ossified parts are seen

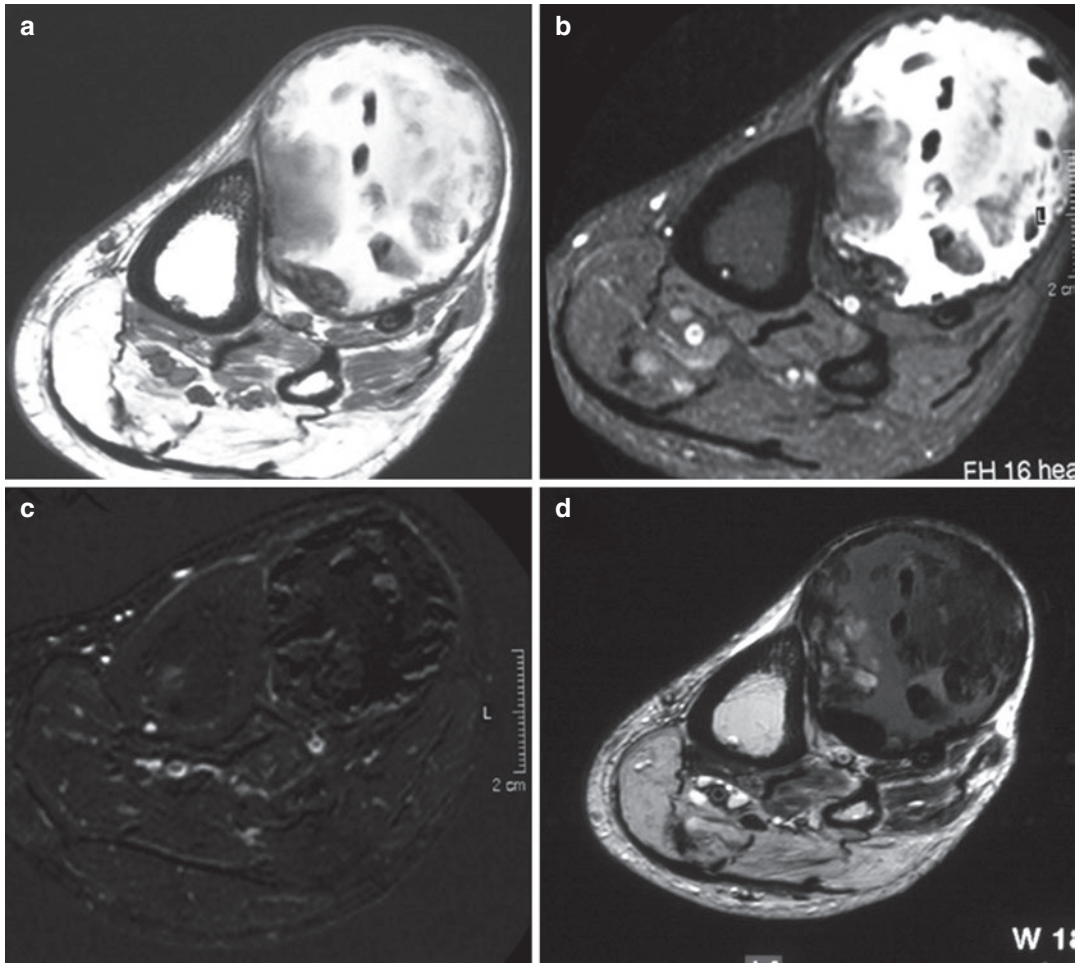

Fig. 45 (**a**–**d**) Calcific Myonecrosis in a 77-year-old patient with chronic drop foot since world war II related to severe contusional soccer trauma at the anterior tibial muscle compartment. Recent painless volume increase of the compartment. (**a**) Axial SE T1. (**b**) Axial SE T1 FS. (**c**) Axial T1 subtracted before and after iv gadolinium DTPA administration. (**d**) Axial TSE T2 Calcifications and fibrosis with low SI on all sequences. High SI on T1-weighted images with and without fat suppression: methaemoglobin blood degradation products. No enhancement at the mass lesion. Necrosis of all the muscles at the anterior tibial compartment

11 Conclusion

The ability of ultrasound, to study muscle tissue through a dynamic range of movements, to compare with normal structures in the contralateral limb, and lesion follow-up, make it a very versatile tool in clinical practice. MRI represents the main alternative imaging modality for the study of muscle trauma; however despite the better soft tissue contrast of MRI, US is the first choice because of better spatial resolution with evaluation of muscular ultrastructure and the still poor availability of MRI.

Although many muscle abnormalities share similar ultrasound and MRI features, imaging can provide an accurate diagnosis with proper BAC or Munich grading in many instances, when clinical findings are taken into account. Ultrasound can help confirm or exclude abnormality. A "dynamic" evaluation of muscle can be performed with ultrasound, which may detect abnormalities not appreciated on MRI.

Because the majority of muscle injuries are self limiting US investigation is limited to delineate the extent of the muscle injury in high-performance athletes and to evaluate lesions prone to complications in elongation trauma. This is the case in "tennis leg" and in crush trauma. It can be valuable for determining which patients will benefit from aspiration or surgery and which can be treated conservatively. It is used to provide a prompt diagnosis when rapid initiation of proper therapy is crucial and to evaluate obscure muscle pain, such as intermittent muscle herniation through a fascial rent. The use of MRI is limited to the evaluation of deeply located muscles and to assess the severity of DOMS or rhabdomyolysis.

Plain radiographs are only indicated for assessment of bony avulsions and to depict myositis ossificans and calcific myonecrosis.

Box 3.1 US

- Best technique for diagnosis of elongation and contusion.
- Evaluation of the muscular ultrastructure provides a good assessment to grade tears.
- Best technique for follow-up of elongation.

Box 3.2 MRI

- Best technique for detection of oedema.
- Time-dependent presentation of blood degradation products.

Box 3.3 Standard radiography

- Main role is evaluation of maturity of myositis ossificans and avulsion fractures.
- Characteristic in calcific myonecrosis.

Things to Remember

1. Many muscle abnormalities share similar ultrasound and MRI features, and therefore clinical findings have to be taken into account to obtain an accurate diagnosis.
2. US and MRI are excellent tools to evaluate muscle elongation in high-performance athletes. US is preferred because of its dynamic characteristics.
3. BAC and Munich advanced grading systems are comprehensive and may be used to predict.
4. A negative US examination with typical clinical presentation of elongation injury is diagnostic for BAC Grade 0a or functional muscle disorder Munich grade 1 elongation.
5. US is the imaging modality of choice to evaluate specific locations of muscle elongation prone to complications, i.e. tennis leg and rectus femoris elongation.
6. Muscle contusion is studied by a combination of US and radiographs to exclude complications, i.e. myositis ossificans and cyst formation.
7. In suspect cases hydrostatic pressure measurement is the only way to exclude early acute compartment syndrome.

References

Armstrong RB (1984) Mechanisms of exercise-induced delayed onset muscular soreness: a brief review. Med Sci Sports Exerc 16:529–538

Askling CM, Tengvar M, Saartok T et al (2007) Acute first-time hamstring strains during high-speed running: a longitudinal study including clinical and magnetic resonance imaging findings. Am J Sports Med 35:197–206

Aspelin P, Ekberg O, Thorsson O et al (1992) Ultrasound examination of soft tissue injury of the lower limb in athletes. Am J Sports Med 20:601–603

Attard V, Rowbotham E, Robinson P (2021) Acute and overuse lesions of the leg and calf. Med Radiol. https://doi.org/10.1007/174_2020_268

Baur OLG, Dahmen J, Kerkhoffs GMMJ, Maas M (2021) Ankle and foot: osteochondral injuries. Med Radiol. https://doi.org/10.1007/74_2020_258

Best TM, Garrett WE (1994) Muscle and tendon. In: DeLee JC, Drez D (eds) Orthopaedic sports medicine. WB Saunders, Philadelphia PA, pp 1–45

Brinckmann P, Frobin F et al (2002) Musculoskeletal biomechanics. Thieme, New York

Bush C (2000) The magnetic resonance imaging of musculoskeletal hemorrhage. Skelet Radiol 29:1–9

Campbell RS, Wood J (2002) Ultrasound of muscle. Imaging 14:229–240
Connell DA, Schneider-Kolsky ME, Hoving JL et al (2004) Longitudinal study comparing sonographic and MRI assessments of acute and healing hamstring injuries. Am J Roentgenol 183:975–984
Cross TM, Gibbs N, Houang MT et al (2004) Acute quadriceps muscle strains: magnetic resonance imaging features and prognosis. Am J Sports Med 32: 710–719
del Cura JL (2008) Ultrasound-guided therapeutic procedures in the musculoskeletal system. Curr Probl Diagn Radiol 37:203–218
DeSmet AA (1993) Magnetic resonance findings in skeletal muscle tears. Skelet Radiol 22:479–484
Deutsch AL, Mink JH (1989) Magnetic resonance imaging of musculoskeletal injuries. Radiol Clin N Am 27:983–1002
Dimmick S, Linklater JM (2017) Imaging of acute hamstring muscle strain injuries. Semin Musculoskelet Radiol 21:415–432. https://doi.org/10.1055/s-0037-1604005. Epub 2017 Aug 3
Edwards PH Jr, Wright ML, Hartman JF (2005) A practical approach for the differential diagnosis of chronic leg pain in the athlete. Am J Sports Med 33: 1241–1249
Ekstrand J, Hägglund M, Walden M (2011) Epidemiology of muscle injuries in professional football (soccer). Am J Sports Med 39:1226–1232
Ekstrand J, Askling C, Magnusson H et al (2013) Return to play after thigh muscle injury in elite football players: implementation and validation of the Munich muscle injury classification. Br J Sports Med 47:769–774
El-Khoury G, Brandser EA, Kathol MH et al (2004) Imaging of muscle injuries. Springer, Berlin Heidelberg New York
Fleckenstein JL, Shellock FG (1991) Exertional muscle injuries: magnetic resonance imaging evaluation. Top Magn Reson Imaging 3:50–70
Fleckenstein JL, Weatherall PT, Parkey PW et al (1989) Sports-related muscle injuries: evaluation with MR imaging. Radiology 172:793–798
Flores DV, Mejía Gómez C, Estrada-Castrillón M et al (2018) MR imaging of muscle trauma: anatomy, biomechanics, pathophysiology, and imaging appearance. Radiographics 38:124–148
Fornage B (1995) Muscular trauma. In: Fornage B (ed) Musculoskeletal ultrasound. Churchill Livingstone, New York, NY, pp 1–19
Fornage BD, Eftekhari F (1989) Sonographic diagnosis of myositis ossificans. J Ultrasound Med 8:463–466
Fornage BD, Nerot C (1986) Sonographic diagnosis of rhabdomyolysis. J Clin Ultrasound 14:389–392
Garrett WE Jr (1990) Muscle strain injuries: clinical and basic aspects. Med Sci Sports Exerc 22:436–443
Garrett WE Jr, Best TM (1994) Anatomy, physiology, and mechanics of skeletal muscle. In: Simon SR (ed) Orthopaedic basic science. American Academy of Orthopaedic Surgeons, Rosemont, IL, pp 89–126
Garrett WE Jr, Califf JC, Bassett FH III (1984) Histochemical correlates of hamstring injuries. Am J Sports Med 12:98–103
Garrett WE Jr, Safran MR, Seaber AV et al (1987) Biomechanical comparison of stimulated and non-stimulated skeletal muscle pulled to failure. Am J Sports Med 15:448–454
Gibbs NJ, Cross TM, Cameron M et al (2004) The accuracy of MRI in predicting recovery and recurrence of acute grade one hamstring muscle strains within the same season in Australian rules football players. J Sci Med Sport 7:248–258
Gielen J, Blom RM, Vanhoenacker F et al (2008a) An elderly man with a slowly growing painless mass in the soft tissues of the lower leg: presentation. Skelet Radiol 37:335
Gielen J, Blom RM, Vanhoenacker F et al (2008b) An elderly man with a slowly growing painless mass in the soft tissues of the lower leg: diagnosis and discussion. Skelet Radiol 37:337–338
Gielen J, Peersman B, Peersman G et al (2009) Chronic exertional compartment syndrome of the forearm in motorcross racers: findings on MRI. Skelet Radiol 38:1153–1161
Grassi A, Quaglia A, Canatia GL et al (2016) An update on the grading of muscle injuries: a narrative review from clinical to comprehensive systems. Joints 4:39–46
Greco A, McNamara MT, Escher RMB et al (1991) Spin-echo and STIR MR imaging of sports-related muscle injuries at 1.5T. J Comput Assist Tomogr 15: 994–999
Herzog W (1996) Muscle function in movement and sports. Am J Sports Med 24:S14–S19
Hide IG, Grainger AJ, Naisby GP et al (1999) Sonographic findings in the anterior interosseous nerve syndrome. J Clin Ultrasound 27:459–464
Holobinko JN, Damron TA, Scerpella PR et al (2003) Calcific myonecrosis: keys to early recognition. Skelet Radiol 32:35–40
Jackson DW, Feagin JA (1973) Quadriceps contusions in young athletes. Relation of severity of injury to treatment and prognosis. J Bone Joint Surg Am 55: 95–105
Jarvinen TA, Jarvinen TL, Kaariainen M et al (2005) Muscle injuries: biology and treatment. Am J Sports Med 33:745–764
Karantanas AH (2021) Natural history and monitoring of fractures and microfractures. Med Radiol. https://doi.org/10.1007/174_2020_271
Kathol MH, Moore TE, El-Khoury GY et al (1990) Magnetic resonance imaging of athletic soft tissue injuries. Iowa Orthop J 9:44–50
Kerr RG (2014) Mri of rectus femoris/quadriceps injury. MRI Web Clinic Radsource. https://radsource.us/rectus-femoris-quadriceps-injury/
Kilsdonk I, Dalili D, van der Made AD, Maas M (2021) Monitoring of muscle and tendon repair. Med Radiol. https://doi.org/10.1007/174_2020_264

Kramer FL, Kurtz AB, Rubin C et al (1979) Ultrasound appearance of myositis ossificans. Skelet Radiol 4:19–20

Lamminen AE, Hekali PE, Tiula E et al (1989) Acute rhabdomyolysis: evaluation with magnetic resonance imaging compared with computed tomography and ultrasonography. Br J Radiol 62:326–330

Llopis E, Aparisi P, Idoate F, Padrón M (2021) The aging athlete. Med Radiol. https://doi.org/10.1007/174_2020_265

Mair SD, Seaber AV et al (1996) The role of fatigue in susceptibility to acute muscle strain injury. Am J Sports Med 24:137–143

Martens MA, Backaert M, Vermaut G et al (1984) Chronic leg pain in athletes due to a recurrent compartment syndrome. Am J Sports Med 12:148–151

McMaster PE (1933) Tendon and muscle ruptures. J Bone J Surg 15:705–722

Mellado JM, Perez del Palomar L, Diaz L et al (2004) Long-standing Morel-Lavallee lesions of the trochanteric region and proximal thigh: MRI features in five patients. AJR Am J Roentgenol 182: 1289–1294

Mink JH (1992) Muscle injuries. In: Deutsch A, Mink JH, Kerr R MRI of the foot and ankle. Raven Press, New York. pp 281–312

Mueller-Wohlfahrt HW, Haensel L, Mithoefer K et al (2013) Terminology and classification of muscle injuries in sport: the Munich consensus statement. Br J Sports Med 47:342–350

Nicholas J, Hershman E (1986) The lower extremity and spine in sports medicine. Mosby, St Louis

Nikolaou PK, Macdonald BL, Glisson RR et al (1987) Biomechanical and histological evaluation of muscle after controlled strain injury. Am J Sports Med 15:9–14

Noonan TJ, Garrett WE Jr (1992) Injuries at the myotendinous junction. Clin Sports Med 11:783–806

Nordin M, Frankel VH (2001) Biomechanics of skeletal muscle. In: Nordin M, Frankel VH (eds) Basic biomechanics of the musculoskeletal system. Lippincott Williams and Wilkins, Philadelphia, pp 149–174

Nurenberg P, Giddings CJ, Stray-Gundersen J et al (1992) MR imaging-guided muscle biopsy for correlation of increased signal intensity with ultrastructural change and delayed-onset muscle soreness after exercise. Radiology 184:865–869

O'Donoghue D (1984) Principles in the management of specific injuries. In: O'Donoghue D (ed) Treatment of injuries to athletes. WB Saunders, Philadelphia, pp 39–91

O'Donoghue DO (1962) Treatment of injuries to athletes. WB Saunders, Philadelphia

Ozdemir MS, Reyngoudt H, De Deene Y et al (2007) Absolute quantification of carnosine in human calf muscle by proton magnetic resonance spectroscopy. Phys Med Biol 52:6781–6794

Patel A, Anderson SE, Davies AM (2021) Special considerations in the immature skeleton. Med Radiol. https://doi.org/10.1007/174_2020_266

Peck RJ, Metreweli C (1988) Early myositis ossificans: a new echographic sign. Clin Radiol 39:586–588

Pedowitz RA, Hargens AR, Mubarak SJ et al (1990) Modified criteria for the objective diagnosis of chronic compartment syndrome of the leg. Am J Sports Med 18:35–40

Peetrons P (2002) Ultrasound of muscles. Eur Radiol 12:35–43

Peterson L, Renstrom P (1986) Sports injuries. Year Book Medical, Chicago

Pollock N, James SLJ, Lee JC, Chakraverty R (2014) British athletics muscle injury classification: a new grading system. Br J Sports Med 48: 1347–1351

Robinson P (2004) Ultrasound of muscle injury. In: McNally E (ed) Practical musculoskeletal ultrasound. Churchill Livingston, London

Shellock FG, Fukunaga T, Mink JH et al (1991) Exertional muscle injury: evaluation of concentric versus eccentric actions with serial MR imaging. Radiology 179:659–664

Shellock FG, Mink J, Deutsch AL (1994) MR imaging of muscle injuries. Appl Radiol February:11–16

Slavotinek JP, Verrall GM, Fon GT (2002) Hamstring injury in athletes: using MR imaging measurements to compare extent of muscle injury with amount of time lost from competition. AJR Am J Roentgenol 179:1621–1628

Speer KP, Lohnes J, Garrett WE Jr (1993) Radiographic imaging of muscle strain injury. AM J Sports Med 21:89–95; discussion 96

Stauber W (1988) Eccentric action of muscles: physiology, injury, and adaption. In: Stauber W (ed) Exercise and sports sciences reviews. Franklin Institute, Philadelphia, pp 158–185

Steinbach L, Fleckenstein J, Mink J (1998) MR imaging of muscle injuries. Semin Musculoskeletal Radiol 1:128–141

Stoller DW (2007) MRI in orthopaedics and sports medicine, 3rd edn. Wolters Kluwer/Lippincott, Philadelphia

Takebayashi S, Takasawa H, Banzai Y et al (1995) Sonographic findings in muscle strain injury: clinical and MR imaging correlation. J Ultrasound Med 14:899–905

Taylor DC, Dalton JD Jr, Seaber AV et al (1993) Experimental muscle strain injury. Early functional and structural deficits and the increased risk for reinjury. Am J Sports Med 21:190–194

Van Holsbeeck MT, Introcaso JH (2001) Sonography of muscle. In: Van Holsbeeck MT, Introcaso JH (eds) Musculoskeletal ultrasound, 2nd edn. Mosby, St Louis, MI, pp 23–75

Verrall GM, Slavotinek JP, Barnes PG et al (2001) Clinical risk factors for hamstring muscle strain injury: a pro-

spective study with correlation of injury by magnetic resonance imaging. Br J Sports Med 35:435–439; discussion 440

Verrall GM, Slavotinek JP, Barnes PG et al (2003) Diagnostic and prognostic value of clinical findings in 83 athletes with posterior thigh injury: comparison of clinical findings with magnetic resonance imaging documentation of hamstring muscle strain. Am J Sports Med 31:969–973

Zabetakis P (1986) Muscle soreness and rhabdomyolysis. In: Nicholas J, Hershman E (eds) The lower extremity and spine in sports medicine. Mosby, St Louis, pp 59–81

Zarins B, Ciullo JV (1983) Acute muscle and tendon injuries in athletes. Clin Sports Med 2:167–182

Zeiss J, Ebraheim NA, Woldenberg LS (1989) Magnetic resonance imaging in the diagnosis of anterior tibialis muscle herniation. Clin Orthop 244:249–253

Cartilage Trauma

W. C. J. Huysse and K. L. Verstraete

Contents

Abstract

Cartilage injury in the athletic patient has been a challenge both for the clinician to treat and for the radiologist to image.

Continuous progress in anatomic and physiologic imaging of cartilage has resulted in accurate depiction of deep defects and extensive damage to the macromolecular structure of cartilage. Superficial abrasion or early disruption of ultrastructure is not seen on routine imaging of cartilage. Sophisticated imaging techniques are able to depict these early changes more and more accurately but remain too cumbersome and susceptible to imaging artefacts to be useful in routine imaging protocols.

Treatment of these cartilage lesions has come a long way, but the long-term results still leave room for improvement.

1 Basic Science

1.1 Composition, Organization and Function of Normal Articular Cartilage

1.1.1 Introduction

The articular surface of diarthrodal joints is covered by hyaline cartilage, a fibrous tissue made up of chondrocytes lying within an extracellular

W. C. J. Huysse (✉) · K. L. Verstraete
Ghent University, Ghent, Belgium
e-mail: wouter.huysse@ugent.be; koenraad.verstraete@ugent.be

Med Radiol Diagn Imaging (2020)
https://doi.org/10.1007/174_2020_248, © Springer Nature Switzerland AG
Published Online: 01 January 2021

matrix. This matrix is composed of tissue fluid containing dissolved electrolytes, gasses, small proteins and metabolites on the one hand and macromolecules such as collagens, proteoglycans and noncollagenous proteins on the other. The type of molecule and their distribution differ depending on the joint and the location within the joint (Gurr et al. 1985; Huber et al. 2000). They also change with age (Bayliss and Ali 1978; Meachim 2001; Krajewska-Włodarczyk et al. 2018).

1.1.2 The Structure of Articular Cartilage

Articular cartilage can be divided into four or five layers (Fig. 1) depending on the differentiation of the superficial layer in one or two compartments (Imhof et al. 2002). These two layers are the lamina splendens, composed of tightly packed bundles of collagen arranged parallel to each other and a second layer, made of collagen fibres perpendicular to the surface (Huber et al. 2000). The chondrocytes in the superficial region are flattened and tangential to the articular surface (Martinek 2003). There is a high water and low proteoglycan content.

The middle zone or the transitional zone contains more rounded chondrocytes and the collagen fibres are oriented randomly and are of larger diameter. Proteoglycan and glycosaminoglycan content is higher than in the superficial zone. In the deep or radial region chondrocytes are grouped in columns and proteoglycan content is highest. This region has the lowest density of cells. The diameter of collagen fibrils is maximal in this region (Poole 1997). The collagen fibres have an overall orientation towards the surface and are arranged in large bundles approximately 55 μm in diameter (Minns and Steven 1977). The water content in these three layers is a mirror image of the proteoglycan and glycosaminoglycan concentration with high water content in the superficial region and low water content in the deep region (Huber et al. 2000).

Underneath the radial region there is the calcified region, constituting approximately 5% of the total cartilage volume (Peterfy 2000). The two

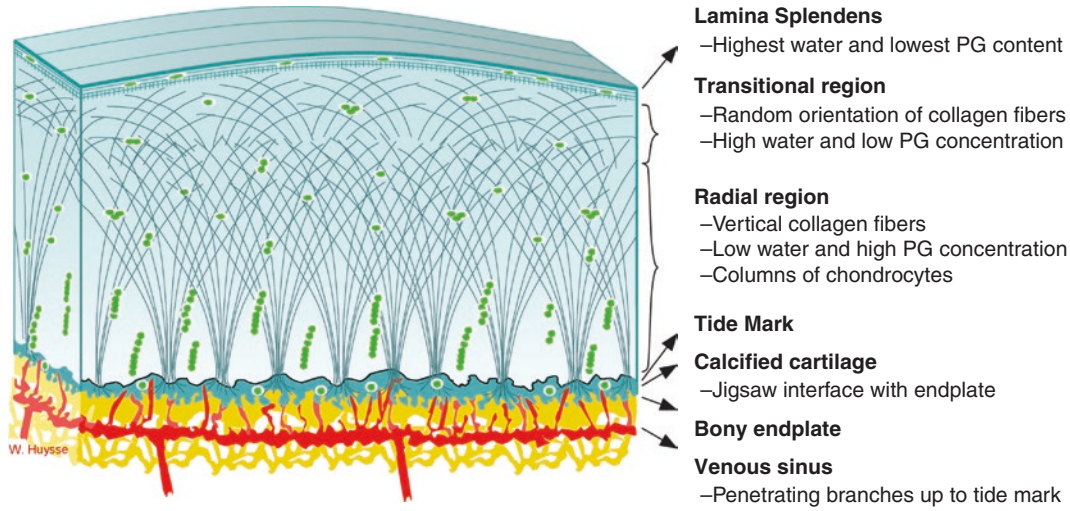

Fig. 1 Schematic representation of the different layers within articular cartilage. Hyaline cartilage is a fibrous tissue made up of chondrocytes lying within an extracellular matrix composed of tissue fluid containing dissolved electrolytes and macromolecules such as collagen II and proteoglycans. It is secured to the bony end plate in a jigsaw-like manner. Collagen fibrils are anchored in the calcified cartilage, have a largely vertical orientation in the radial zone and a more random orientation in the transitional zone. The top layer consists of densely packed collagen bundles parallel to the cartilage surface. Water content decreases towards the deeper regions and proteoglycan (PG) content increases, with the exception of the calcified cartilage, where no PG is found

are separated by the tide mark, a wavy line representing the mineralized front of the calcified cartilage.

The calcified zone is characterized by rounded chondrocytes surrounded by uncalcified lacunae (Huber et al. 2000). These chondrocytes have hardly any metabolic activity (Martinek 2003). There are no proteoglycans in the calcified zone. The collagen fibres run perpendicular to the articular surface and are anchored in a calcified matrix. This layer serves as a bridge between the upper layers of the cartilage and the subchondral bone.

Articular cartilage is closely connected to the subchondral bone plate, also called the cortical end plate or the articular bone plate. It penetrates in the recesses of the highly irregular bone plate, somewhat like the pieces of a jigsaw puzzle. The subchondral bone is situated underneath the end plate and contains fatty bone marrow and trabecular bone. In this subchondral region underneath the end plate many terminal arterial branches are found that end in a transverse sinus, located just below the end plate and formed by multiple venous branches (Imhof et al. 2000). The end plate is penetrated by small vascular branches originating from the subchondral bone region. These invade the calcified cartilage up to the tide mark. The distribution of these branches and the bony channels they run in is related to compressive forces acting on the cartilage and the subchondral bone. This vascularization also varies with age, individually and within joints. At least 50% of the oxygen and glucose required by the cartilage is supplied by these vessels (Imhof et al. 2000).

1.1.3 Function of Cartilage

In combination with synovial fluid, the smooth (Bloebaum and Radley 1995) surface of articular cartilage serves as a gliding surface with very low resistance. The elasticity of cartilage has only a limited role in cushioning compressive forces. The majority of load forces (30%) are taken up by the subchondral bone. Hyaline cartilage absorbs only 1–3% of compressive forces. The main function of cartilage in weight-bearing is dissipating the loading forces to a larger area (Imhof et al. 2002).

1.2 Composition and Function of Fibrocartilage

Although hyaline cartilage provides a frictionless surface in diarthrodal joint, many joints also contain fibrocartilaginous structures. These structures include the meniscus in the temporomandibular joint, the labrum in shoulder and hip joint, the triangular fibrocartilage in the wrist and both menisci in the knee. Occasionally, a meniscus can be found in the acromioclavicular joint. These structures have an important stabilizing function (Rath and Richmond 2000): a labrum significantly increases the surface area of the joint and adds to the depth of the joint socket (Parentis et al. 2002); menisci compensate joint congruency and aid in transmitting the load. The menisci in the knee have also been shown to improve lubrication and nutrition of the articular cartilage.

Like hyaline cartilage, a fibrocartilaginous structure relies on diffusion from the synovial fluid for an important part of its nutrition (Rijk 2004). Most vascular branches end in the peripheral rim and are connected to vessels in the periosteum or the joint capsule.

Fibrocartilage is made up of about 75% water, 20% collagen and a small amount of proteoglycan, elastin and cells. Type I collagen accounts for more than 90% of the total collagen present, but types II, III, V, and VI have also been shown to be present in small amounts (McDevitt and Webber 1990).

Most collagen fibres in a labrum or meniscus are arranged in a circumferential direction and woven together by smaller, radially oriented fibres. Due to this configuration, most tears tend to progress more or less tangentially to the free edge (Rath and Richmond 2000). For a more detailed description of the pathological conditions of fibrocartilage we refer to (Schäffeler 2020) (shoulder labrum), (Mascarenhas et al. 2020) (hip labrum) and (De Smet et al. 2020) (meniscus of the knee).

1.3 Mechanical Injury of Articular Cartilage: Mechanisms and Staging

1.3.1 Introduction

Articular cartilage injury is a common finding during arthroscopy (Curl et al. 1997). In the knee most of these injuries are associated with other problems, such as meniscal lesions and anterior cruciate ligament injury.

As there are an unknown number of people who sustain chondral lesions without seeking treatment, it is extremely difficult to uncover the natural progression of an untreated cartilage lesion. According to a number of investigators, many of these lesions, and especially the partial-thickness injuries, are non-progressive (Fuller and Ghadially 1972; Ghadially et al. 1977a, b; Mankin 1982).

1.3.2 Mechanism of Injury

Loading of articular surfaces causes movement of fluid within the cartilage matrix that dampens and distributes the load within the cartilage and to the subchondral bone (Buckwalter 2002). Increasing weight-bearing activity in athletes increases the volume and thickness of articular cartilage (McAdams et al. 2010) and also increases knee cartilage glycosaminoglycan content (Roos and Dahlberg 2005). However, this response reaches a threshold and activity beyond this threshold can result in maladaptation and injury of articular cartilage (Kiviranta et al. 1992; Arokoski et al. 1993).

If the force is great enough, the framework is ruptured, chondrocytes are damaged, and a degenerative process is initiated that can include loss of articular cartilage volume and decreased stiffness. This, in turn, will lead to elevation of contact pressures.

If the abnormal strain persists, the subchondral bone is fractured. Acute or repetitive blunt joint trauma can result in damage to the subchondral bone and the deeper regions of the cartilage without visual disruption of the surface (Buckwalter 2002). This damage will result in subchondral bone marrow oedema with or without associated microfractures (Fig. 2).

Fig. 2 Bone marrow oedema in a 32-year-old professional football player after traumatic contact with an opponent. Sagittal fat-suppressed T2-weighted image shows extensive bone marrow oedema (arrowheads) without disruption of the cartilage surface. Signal changes in the cartilages could arguably represent grade I cartilage damage

Fig. 3 Residual pain 2 years after bucket handle tear and osteochondral fracture of the medial femoral condyle. Coronal intermediate-weighted image shows collapse of the subcortical bone and subsequent sclerosis

Healing of these fractures will lead to microcallus formation and focal subchondral sclerosis (Fig. 3).

Severe or repetitive overloading leads to changes in uncalcified cartilage, such as fibrillation and production of abnormal matrix proteins. This initiates swelling in the deepest regions of the cartilage and can result in delamination of the articular surface if (repetitive) overloading persists (Imhof et al. 2000).

Repetitive microinjuries to subchondral bone and calcified cartilage may result in the activation of repair mechanisms. Increased activity of osteoblasts, osteoclasts and fibrovascular tissue results in the formation of subchondral sclerosis and establishment of one or more new tide marks (Imhof et al. 2002).

1.3.3 Staging of Cartilage Lesions

The most well-known arthroscopic staging method for articular cartilage is that proposed by Outerbridge in 1961 (Outerbridge et al. 1961) and modified by Shahriaree (Shahriaree 1985). Other systems to grade cartilage, osteoarthritis and cartilage repair procedures with imaging methods were developed, but most of these systems were proven to have only a moderate reproducibility (Mankin et al. 1971; O'Driscoll et al. 1988; van der Sluijs et al. 1992; Ostergaard et al. 1997, 1999; Biswal et al. 2002; Cameron et al. 2003).

A practical classification system, based on the system of Yulish (Yulish et al. 1987) and modified by Disler, Recht and Verstraete (Disler et al. 1995; Recht et al. 1996; Kramer and Recht 2002; Verstraete et al. 2004), uses four grades of chondromalacia:

- 0: normal cartilage
- I: slight swelling (not adequately assessable on routine MR and CT imaging)
- II: fissuring or cartilage defects less than 50% of cartilage thickness (Fig. 4)
- III: fissuring or cartilage defects more than 50% but less than 100% of cartilage thickness (Fig. 5)
- IV: cartilage defects and erosion with exposure of subchondral bone (Fig. 6)

A final grade V could be added to allow for differentiation between full-thickness lesions with intact subchondral bone or with penetration of the bony end plate (Fig. 7). These grade V lesions are often associated with focal areas of bone marrow oedema.

A similar arthroscopic grading system was proposed by the members of the International Cartilage Repair Society (Brittberg et al. 2000) and can be found on the ICRS website (http://www.cartilage.org).

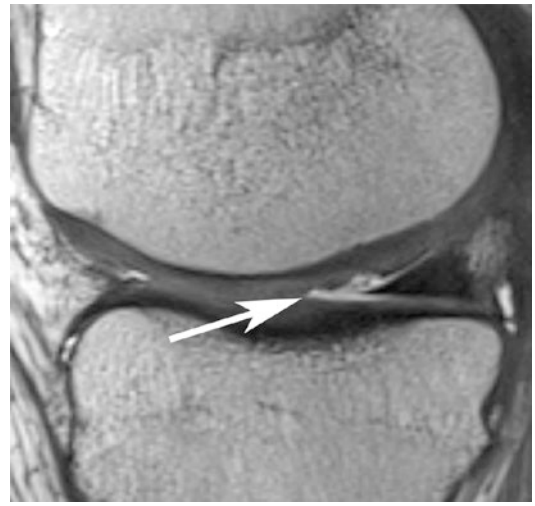

Fig. 4 Grade II cartilage defect. Sagittal 3D proton-density-weighted image demonstrating a partial-thickness defect of less than 50% of the cartilage width

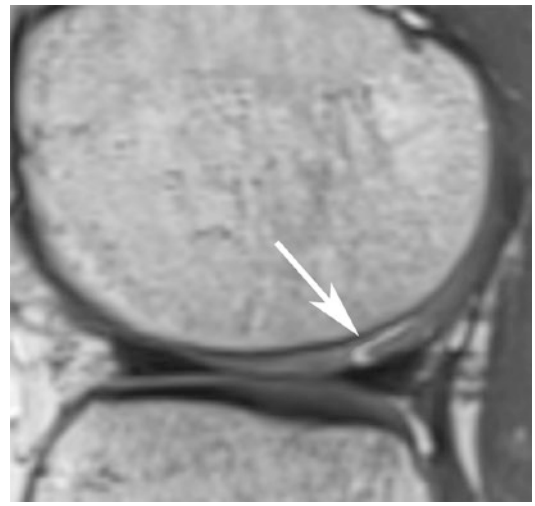

Fig. 5 Recent intracartilaginous tear in a recreational basketball player. Sagittal 3D proton-density-weighted image shows a residual basal layer of cartilage at the beginning of the tear. Less than 50% of the initial cartilage thickness remains making this a grade III lesion extending into a full-thickness defect further on

Limitations of this classification are the inability of CT and routine MR imaging to reliably demonstrate early degenerative changes (Peterfy 2000). Moreover, the size of a lesion is not taken into account in this classification as it is difficult to measure the diameter of an often irregular lesion.

Fig. 6 Recent cartilage defect after pivot-shift trauma. Coronal fat-suppressed intermediate-weighted image shows a grade IV cartilage lesion on the medial femoral condyle with acute margins (arrows)

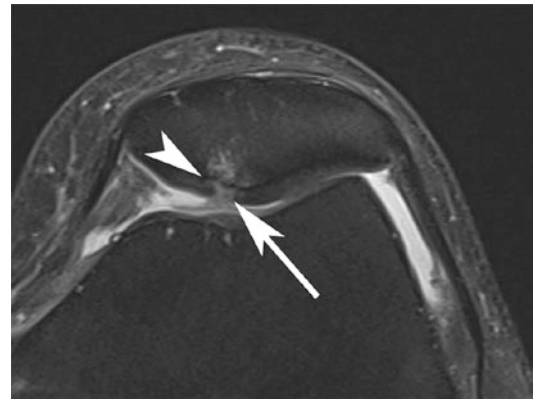

Fig. 7 Osteochondral fracture in the patella. Transverse fat-suppressed intermediate-weighted image shows a grade V cartilage defect with disruption and indentation of the subchondral bone plate (arrowhead). The cartilage defect has been filled in with a blood clot (arrow)

A comparison between the arthroscopic and MR classifications of cartilage defects is given in Table 1.

Table 1 Arthroscopic and MR classification system to grade cartilage lesions

Arthroscopic classification					
Outerbridge (Shahriaree)		ICRS		MR classification	
Grade 0	Normal	Grade 0	Normal	Grade 0	Normal
Grade 1	Softening or swelling	Grade 1a	Soft indentation	Grade 1	Normal contour ± abnormal signal
		Grade 1b	Superficial fissures and cracks		
Grade 2	Shallow fibrillation, cartilage defects (<50% of cartilage thickness) and blister like swelling	Grade 2	Lesions extending down to <50% of cartilage depth	Grade 2	Superficial fraying; erosion or cartilage defects of less than 50%
Grade 3	Surface irregularities and areas of thinning (>50% of cartilage thickness)	Grade 3a	Defects extending down >50% of cartilage depth	Grade 3	Partial-thickness defect of more than 50% but less than 100%
		Grade 3b	Defects extending down to the calcified layer		
		Grade 3d	Intracartilaginous tears/ blisters		
Grade 4	Cartilage defects and exposure of subchondral bone	Grade 3c	Defects down to the subchondral bone plate	Grade 4	Full-thickness cartilage loss
		Grade 4a	Interruption of the bony end plate	Grade 5	Full-thickness lesions with penetration of the bony end plate
		Grade 4b	Grade IVa with subcortical cyst formation		

2 Imaging

2.1 Imaging Articular Cartilage

2.1.1 Conventional Radiography and Arthrography

The overall status of the articular cartilage in a joint can be measured by the width of joint space. For the lower limbs, this is best evaluated in weight-bearing position. For many joints a normal range of width has been established (Keats and Sistrom 2001) and specific views have been developed to allow a better evaluation of the joint space.

Conventional X-ray images are very well suited for the evaluation of moderate or severe osteoarthritis, clearly depicting joint space narrowing, osteophytes and the presence of degenerative cysts (Figs. 8 and 9).

Indications for conventional arthrography have diminished significantly in recent years due to the higher availability and accuracy of other diagnostic methods, particularly MR imaging. For imaging articular cartilage, arthrography without subsequent CT or MR imaging is no longer indicated (Resnick 2002). Arthrography is often combined with CT (CT arthrography) because this technique is not impeded by superposition and allows displaying the lesions in several planes (multiplanar reconstruction; MPR).

Fluoroscopic guided joint puncture is still the most commonly used image guidance method, but the role of ultrasound is steadily increasing (Klaan et al. 2019).

2.1.2 CT Arthrography

After intra-articular administration of water-soluble iodine containing contrast agents (preferably non-ionic and of low osmolality) CT has a sensitivity and specificity comparable to MR imaging for detecting articular cartilage defects (Nishii et al. 2005; Waldt et al. 2005).

CT arthrography very well depicts surface lesions of cartilage (grade II–IV) in different imaging planes (Fig. 10).

In patients with osteochondritis dissecans the integrity of the cartilage and the attachment of the osteochondral lesion to the surrounding bone can be assessed with high accuracy (Fig. 11).

Fig. 8 Coxarthrosis. Standard radiography shows an osteophyte at the acetabular roof (hollow arrow), a small degenerative cyst (white arrow), and joint space narrowing (arrowheads)

CT arthrography can be advantageous in small joints (wrist, elbow, ankle) compared to MR arthrography due to its higher image resolution (Klaan et al. 2019).

A major drawback of routine CT is its inability to visualize associated subchondral bone marrow oedema, which may be the cause of the patient's pain. Dual-energy CT (DECT) in acute knee trauma has been shown to accurately depict traumatic bone marrow oedema (Booz et al. 2020). In CT arthrography, DECT has demonstrated the ability to reduce beam-hardening artefacts and separate contrast from cortical bone (An et al. 2014). However cartilage is usually the focus of analysis, which may be challenging to assess on DECT due to artefacts produced by adjacent cortical bone (Subhas et al. 2010). A limitation of DECT is that it is unable to evaluate BME in the immediate vicinity to cortical bone due to confusion with the cortex (Wong et al. 2018).

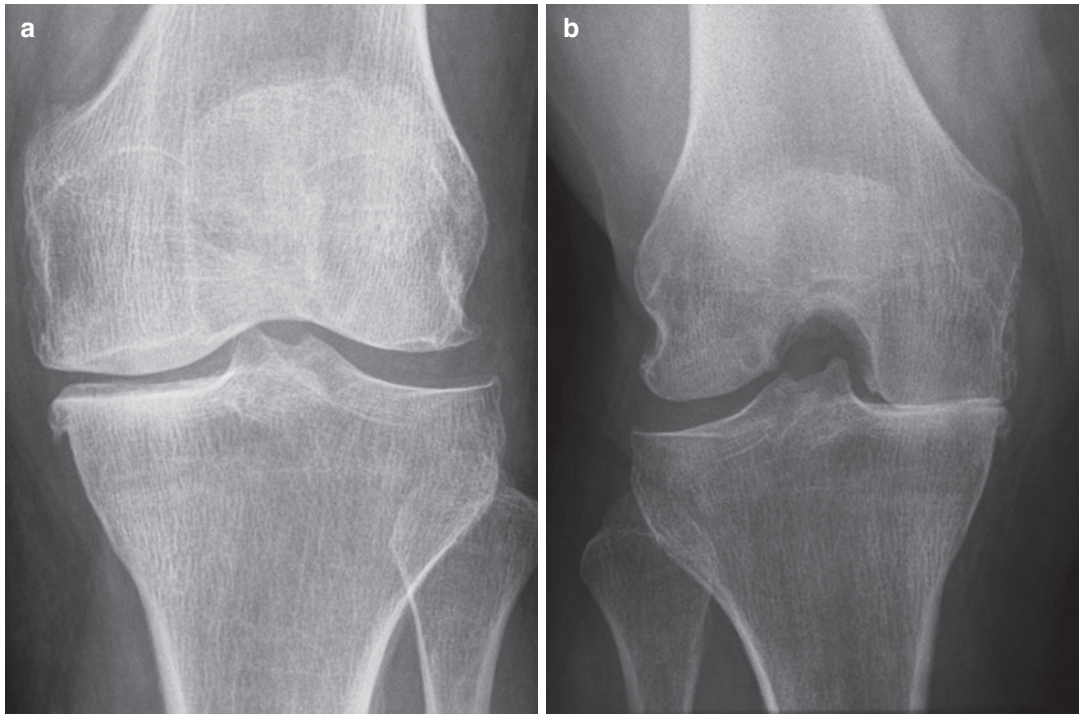

Fig. 9 (**a** and **b**) Gonarthrosis. (**a**) Standard AP and (**b**) PA radiographs. The PA radiograph with 30° flexion or "Schuss" position of the knee is used to evaluate the posterior third of the weight-bearing part of the femoral condyles. In this case there is marked thinning of the articular cartilage in this region, not visible on regular AP images

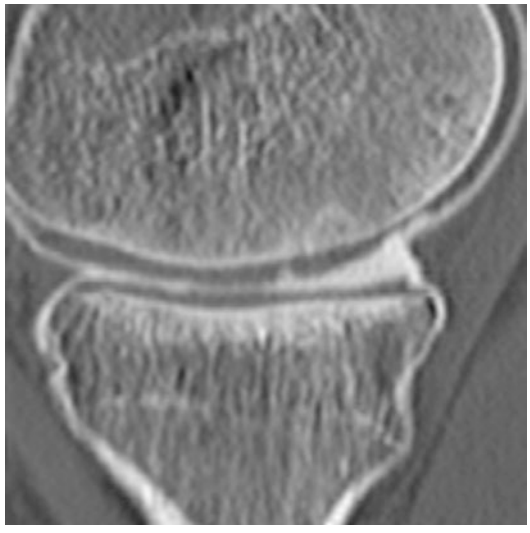

Fig. 10 Cartilage defect. Sagittal CT arthrography of the knee. Cartilage lesion starting with a full-thickness fissure anteriorly, followed by a grade II region which progresses to grade III posteriorly

Loose (cartilaginous) bodies on the other hand are more easily seen on a CT arthrography.

The radiation dose of CT arthrography used to be another disadvantages compared to MR imaging. With the advent of cone beam CT (CBCT), the radiation dose has been drastically reduced for imaging of the ankle, knee, wrist and elbow, to such a degree that it may be considered negligible. Furthermore, advances in imaging hardware now allow for weight-bearing CBCT of ankle, knee and hip, providing the added information of joint alignment (Boesen et al. 2017; Leardini et al. 2019).

The discomfort associated with intra-articular injections and the very rare potential complications associated with arthrography, such as septic arthritis and allergic reactions to iodine containing contrast media (Dupas et al. 2005), remain drawbacks of CT arthrography.

2.1.3 Morphologic MR Imaging of Cartilage

The ideal MR imaging sequence for the evaluation of articular cartilage should be able to:

1. Sharply delineate superficial and deep defects in the articular cartilage
2. Display cartilage with an optimal contrast resolution, high spatial resolution and/or allow segmentation, volume calculation and three-dimensional (3D) display
3. Show changes in the subchondral bone plate and display the exact thickness of the subchondral bone plate without magnetic susceptibility
4. Detect bone marrow oedema, subchondral cysts and granulation tissue
5. Detect changes in the internal structure (disruption of the collagen framework) and biochemical composition of articular cartilage (mainly depletion of proteoglycans and increase of water content), with high contrast between normal and abnormal cartilage, both in deep and in superficial layers

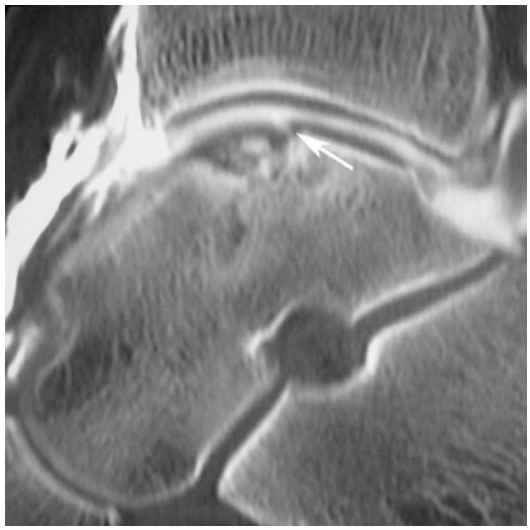

Fig. 11 Osteochondral defect of the talus. Sagittal CT arthrography of the ankle. Fissure in the cartilage overlying an osteochondral defect. The contrast medium infiltrates between the lesion and the surrounding subchondral bone over a short distance

To date, either 2D or 3D intermediate-weighted fast spine-echo (FSE) sequences are still the bedrock for MR imaging of the knee (Kassarjian et al. 2016). In respect to cartilage the addition of a 3D fat-suppressed T1-weighted gradient-echo (GRE) acquisition combined with the standard FSE sequences is still the most widely used imaging protocol (Trattnig et al. 2011).

More recently developed 3D FSE sequences, called SPACE (sampling perfection with application-optimized contrasts using different flip-angle evolutions), 3D Fast Spin-Echo Extended Echo Train Acquisition (FSE-XETA, also known as 3D FSE-CUBE), or VISTA, may provide accurate evaluation of cartilage and cartilage repair tissue as well as the other joint structures (Kijowski et al. 2009), especially in postoperative imaging (Fig. 12).

FSE images with a long repetition time (TR $\geq$ 2000 ms) with or without fat suppression have been shown to be accurate in the detection of chondral abnormalities, with high sensitivity and specificity (Broderick et al. 1994; Potter et al. 1998; Bredella et al. 1999; Sonin et al. 2002; Lang et al. 2005; Jung et al. 2009). In these sequences, articular cartilage shows an intermediate signal intensity (SI) compared to the high SI of the adjacent joint fluid and the low SI of the subchondral bone (Fig. 12).

Even in the absence of fluid, the borders of the cartilage are readily visible (Sonin et al. 2002; Lang et al. 2005). Moreover, these images can be obtained in a short acquisition time (1–5 min) with high resolution and allow simultaneous evaluation of other structures in the knee, such as menisci, ligaments and tendons. Therefore, in routine clinical practice, long TR FSE images are usually sufficient. Without fat suppression, the soft tissues, like menisci, tendons and ligaments are well displayed, in contrast to fat-suppressed FSE images, which are better for detection of bone marrow oedema (Fig. 2). A fat-suppressed sequence with a long TR and an echo time (TE) between that of a traditional proton-density (e.g. TE = 10–20 ms) and

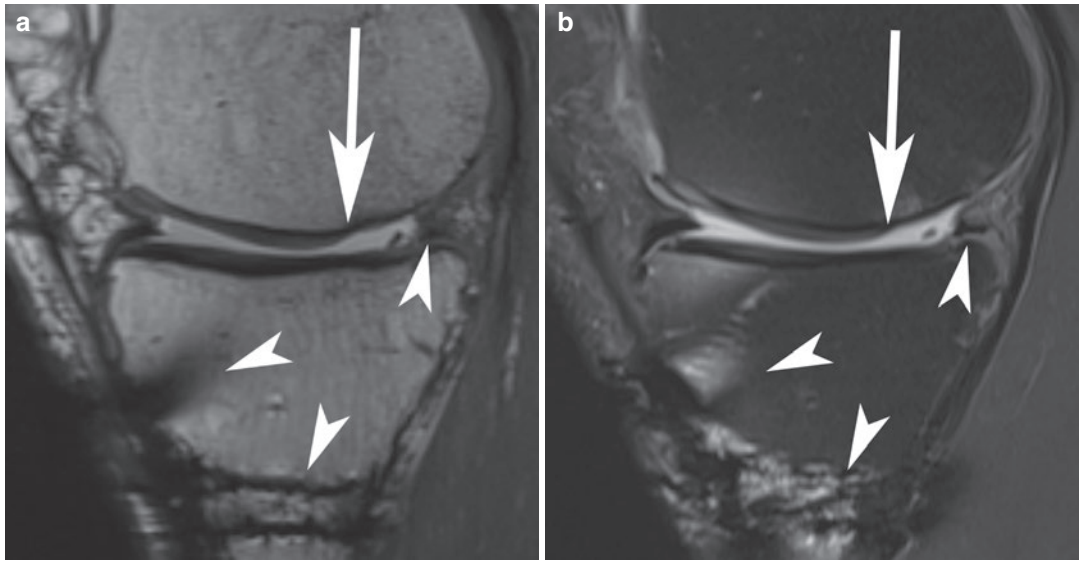

Fig. 12 (**a** and **b**) Chronic grade IV cartilage defect in a 40-year-old recreational football player with previous meniscectomy, high tibial osteotomy and ACL repair (arrowheads). (**a**) Sagittal 3D proton-density-weighted image, in this case a sampling perfection with application-optimized contrasts using different flip-angle evolutions (SPACE), demonstrates a long-standing full-thickness cartilage lesion with obtuse edges (arrow). Both the contour and the signal of the cartilage remain clearly visible despite the presence of metal artefact. (**b**) On the sagittal fat-suppressed intermediate-weighted image some distortion of the spectral fat suppression is visible

a traditional T2-weighted sequence (e.g. TE = 80–100 ms) has the advantage that the TE is short enough to maintain sufficient signal for visualization of the anatomy (like a proton-density) yet long enough to be more fluid sensitive (like a T2-weighted image).

As relaxation times in the deepest cartilage layers decrease (Gold et al. 2004), separating them from the subchondral bone is challenging for FSE sequences (Roemer et al. 2009; Kijowski et al. 2009). This results in an overestimation of the depth of a cartilage lesion. Therefore, more time-consuming high-resolution 3D GRE techniques have to be used whenever deep cartilage lesions are detected on the FSE images.

Currently, isotropic 3D, gradient-echo-based sequences have the potential of high-resolution imaging with a voxel dimension as small as 0.3 mm and can be reformatted in any plane. These acquisitions include SPGR (spoiled gradient echo), FLASH (fast-low angle shot), VIBE (volume-interpolated breath-hold examination), DESS (double-echo steady state), SSFP (steady-state free precession) and True-FISP (fast imaging with steady-state precession). They provide higher spatial and contrast resolution but require longer acquisition times and are more vulnerable to magnetic susceptibility artefacts.

All 3D sequences allow high-quality multiplanar reconstructions (MPR), which are useful for evaluating the cartilage with images perpendicular to the curved articular surface (Fig. 13).

In fat-suppressed 3D-SPGR and FLASH-3D we, articular cartilage has very high signal intensity, joint fluid has an intermediate to low signal intensity, and subchondral bone and bone marrow are dark. Reported sensitivity and specificity for detection of cartilage lesions are 75–85% and 95–97%, respectively (Disler et al. 1996; Recht et al. 1996; Ruehm et al. 1998; Trattnig et al. 2000). Deep cartilage layers and focal loss of trabecular bone is much better appreciated on 3D-fat-suppressed GRE images than on FSE images.

Moreover, thin-section volume acquisitions allow segmentation and accurate 3D reconstructions of articular cartilage (Fig. 14).

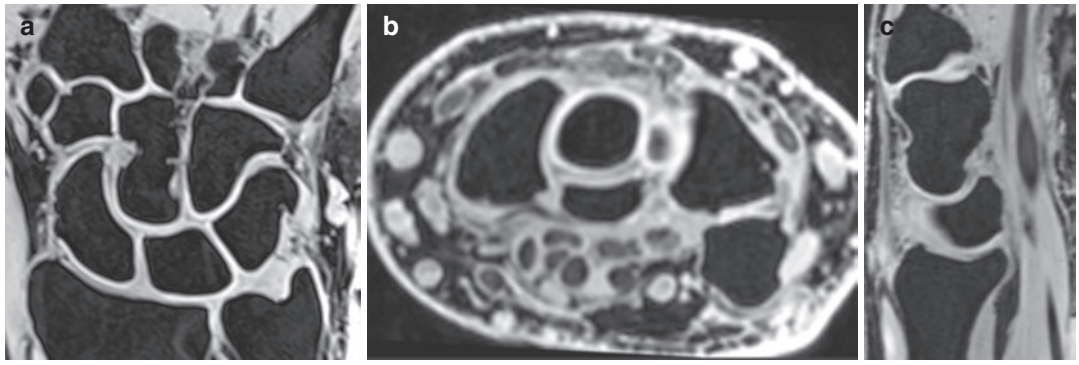

Fig. 13 (**a**–**c**) Type 2 lunate predisposing to osteoarthritis. (**a**) Coronal 3D T1-weighted VIBE (volume-interpolated breath-hold examination) with water excitation (we). The 0.3 mm isotropic voxels allow flawless reconstructions in the (**b**) transverse and (**c**) sagittal planes. Cartilage is visible as a white band between the dark subchondral end plate and the grey joint fluid

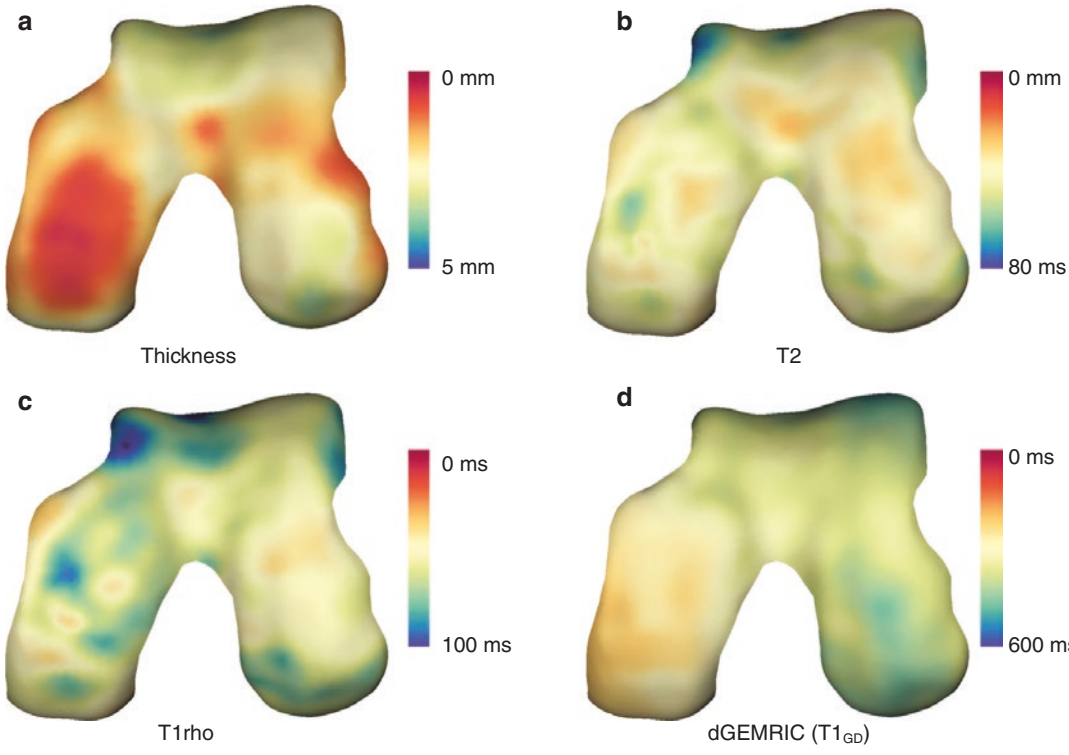

Fig. 14 3D cartilage surface mapping in a patient with moderate osteoarthritis of the knee. (**a**) Colour-coded thickness map generated from fat-saturated 3D spoiled gradient echo (3D SPGR) sequence (voxel size 0.3 × 0.3 x 1 mm) demonstrating cartilage loss on the weight-bearing portion of the medial femoral condyle (red area). (**b**–**d**) 3D surface maps demonstrating (**b**) higher T2 value, (**c**) higher T1ρ value and (**d**) increased gadolinium diffusion in the affected area on the medial condyle. [Courtesy of James W. MacKay and Tom D. Turmezei (MacKay et al. 2019)]

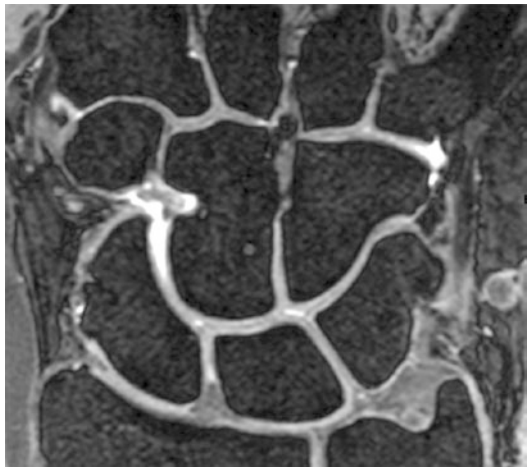

Fig. 15 Normal cartilage in a wrist joint with type 2 lunate predisposing to osteoarthritis. Coronal DESSwe 3D image. Cartilage is visible as a thin grey layer between the black bony end plate and white joint fluid

However, quantification of cartilage volume by manually summing the voxels containing cartilage using 3D imaging techniques is relatively time-consuming. Automated methods for segmentation are becoming available to make this tool valuable in routine daily practice (Boesen et al. 2017; Gatti 2018).

In the 3D-DESS sequence without fat suppression or water excitation (Fig. 15), the cartilage has intermediate signal intensity, but is well delineated because joint fluid exhibits very high signal intensity.

If there is not enough fluid present within the joint, delineation of cartilage may become problematic. Due to the intermediate signal intensity of cartilage, segmentation for volume measurements is not possible. The 3D-DESS sequence allows high-quality multiplanar reconstructions (MPR) and provides T1 contrast in the soft tissues. Therefore, it allows better visualization of menisci, muscles, ligaments and tendons than fat-suppressed 3D-SPGR (FLASH-3D we; DESS-3D we) that can only be used to evaluate the cartilage, because all other tissues are dark, and contrast is low.

Another drawback of the 3D GRE sequences is the significant image artefacts, which are much more pronounced than those on FSE images and tend to result in overestimation of cartilage disease (Lang et al. 2005) (Table 2).

Post-traumatic, early cartilage degeneration (grade 1) or focal cartilage contusion cannot be reliably demonstrated using any of these sequences.

2.1.4 Physiologic Imaging of Articular Cartilage

To evaluate early changes in water content, collagen structure or proteoglycan concentration compositional, physiological or biochemical MR imaging is needed.

2.1.4.1 dGEMRIC

Delayed gadolinium enhanced MRI of cartilage relies on the principle of fixed charge density.

Table 2 MR methods for evaluation of cartilage

Pulse sequences for routine clinical MR imaging of cartilage		
Pulse sequence	Signal of articular cartilage and fluid	Remarks
Proton-density- and T2-weighted fast spin-echo ± fat suppression	Articular cartilage has a lower SI than fluid	Other joint structures readily visible
Fat-suppressed T1-weighted spoiled gradient echo; fat-suppressed 3D spoiled gradient echo/FLASH-3D we/3D-T1-FFE WATSc	Articular cartilage has a very high SI; fluid has low SI	High resolution and contrast; MPR possible; assessment of other joint structures not possible
DESS-3D	Cartilage has intermediate SI; joint fluid has a very high SI	High resolution and contrast; MPR possible; other joint structures readily visible
DESS-3D we	Cartilage has intermediate SI; joint fluid has a very high SI	High resolution and contrast; MPR possible; assessment of other joint structures possible

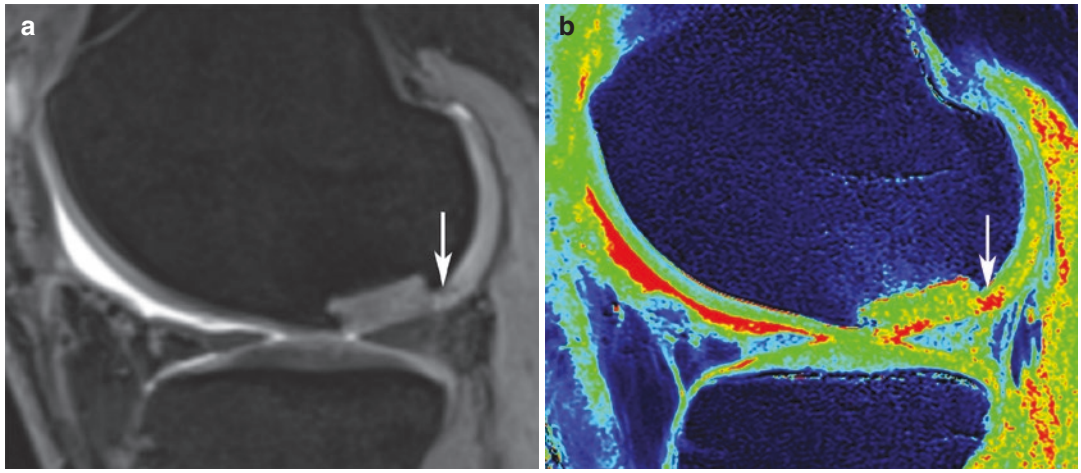

Fig. 16 (**a** and **b**) Six months after osteochondral repair with matrix-associated autologous stem cells and chondrocytes. (**a**) Sagittal 3D DESSwe shows adequate filling of the defect with a repair tissue that has the same signal intensity as native cartilage. However, there is increased signal at the interface between the implant and the native cartilage (arrow). (**b**) The T1 map produced after delayed gadolinium enhanced MRI of cartilage (dGEMRIC) confirms this is an area of decreased glycosaminoglycans and cartilage loss. The repair tissue itself has only slightly lower GAG-concentrations than native cartilage

Ions in the extracellular fluid are distributed in relation to the concentration of negatively charged glycosaminoglycans in cartilage. Accordingly, extracellular fluid has a lower concentration of anions and higher concentration of cations than are present in blood or synovial fluid. The difference between anion and cation concentrations in extracellular fluid is equal to the fixed charge density (Gray et al. 2008). Anions such as gadopentetate dimeglumine ($Gd\text{-}DTPA^{2-}$) are repelled by the negatively charged glycosaminoglycans, and as they diffuse into the cartilage extracellular matrix, they are distributed in inverse proportion to the local proteoglycan concentration. The increase of cartilage T1 after contrast agent equilibration is a measure of the $Gd\text{-}DTPA^{2-}$ and glycosaminoglycan concentrations (Trattnig et al. 2009) (Figs. 14 and 16).

2.1.4.2 T2 Mapping and T2* Mapping

The T2-relaxation time for a given tissue in a given magnetic field strength is constant. In cartilage, quantitative T2 mapping has been shown at both high-field and clinically relevant field strengths to correlate to collagen orientation (Xia et al. 2001). In native hyaline cartilage, there is a depth-wise variation of T2 relaxation times with shorter T2 values in the deeper, radial zone, where the collagen is highly ordered, and longer values in the transitional zone because of less organization of the collagen (Trattnig et al. 2011).

Changes in T2-relaxation times are dependent upon the quantity of water and the integrity of the proteoglycan–collagen matrix (Fig. 14).

Several in vivo studies have shown T2-relaxation times to correlate with collagen matrix and water changes (Poon and Henkelman 1992; Mosher et al. 2000). As collagen degradation occurs, water molecule content and motion increases. This results in high signal intensity on T2-weighted images and elevated T2-relaxation times (Braun and Gold 2011).

T2*-weighted imaging is similar to T2-weighted imaging, but gradient-echo signals are used instead of spin-echo signals. Shorter T2*values are thought to represent decreased water content, decreased collagen content and disruption of collagen fibre orientation (Bittersohl et al. 2015). The main advantages of T2* mapping are the reduced acquisition time and the possibility to acquire high-resolution 3D data in a reasonable acquisition time (Kolf et al. 2016). Main disadvantages are the increased sensibility to susceptibility artefacts and magic angle effects (Link et al. 2017).

2.1.4.3 T1ρ Mapping

T1ρ has been shown to reflect the glycosaminoglycan content in cartilage (Regatte et al. 2003; Wheaton et al. 2004; Mosher et al. 2011) and allows measurement of the interaction between motion-restricted water molecules and their extracellular environment (Li et al. 2007). T1ρ measurements are also affected by the magic angle effect of collagen fibres in articular cartilage (Guermazi et al. 2015). When proteoglycan depletion occurs, the physiochemical interactions in the macromolecule environment are disrupted and T1ρ relaxation time increases (Braun and Gold 2011) (Fig. 14).

Recently a method to automatically segment and calculate T1ρ values in the knee cartilage using voxel-based relaxometry was suggested (Pedoia et al. 2016).

2.1.4.4 Diffusion-Weighted and Diffusion Tensor Imaging

Diffusion-weighted imaging (DWI) is based on the motion of water molecules that is influenced by intracellular and extracellular barriers. When the extracellular matrix is disrupted, water molecules move more freely, increasing the signal intensity of cartilage on DWI (Burstein et al. 1993; Baur et al. 1998).

With the use of 3D DWI cartilage repair tissue can be differentiated from native cartilage and the diffusivity seems to decrease over time towards control healthy cartilage (Mamisch et al. 2008; Welsch et al. 2009c; Friedrich et al. 2010).

Diffusion tensor imaging (DTI) is a more advanced form of DWI capable of obtaining directionality and magnitude measurements of water diffusion.

Both DWI and DTI are challenging in vivo due to the long echo time required for diffusion sensitization and the sensitivity to motion (Braun and Gold 2011).

2.1.4.5 Sodium Imaging

Under normal circumstances sodium ($^{23}Na^{+}$) is one of the cations counteracting the negative charge of the glycosaminoglycans in the extracellular matrix. The distribution of $^{23}Na^{+}$ can therefore be used as a measure of the cartilage glycosaminoglycan content, with cartilage damage resulting in a decrease of $^{23}Na^{+}$ concentration (Madelin et al. 2014). Unsurprisingly, sodium imaging correlates well with dGEMRIC. The low concentrations of $^{23}Na^{+}$ in cartilage and the lower spin frequency of the nucleus, however, make it difficult to elicit signal during MRI, resulting in noisy images and long acquisition times. The signal-to-noise ratio gain in 7 T MRI is particularly useful for $^{23}Na^{+}$ imaging (Alizai et al. 2019). An additional limitation of this technique is the need for special transmit and receive coils to accommodate the lower concentration, lower resonant frequency and shorter T2-relaxation times of $^{23}Na^{+}$. Furthermore, the influence of sodium suspended in the synovial fluid has to be counteracted resulting in an even longer scan time and lower signal-to-noise ratio (Oei et al. 2018).

2.1.4.6 Magnetization Transfer Contrast/gagCEST

First described by Wolff et al. back in 1991 (Wolff et al. 1991) magnetization transfer imaging may provide a quantitative method for tissue characterization of basic macromolecular dynamics and chemistry.

The magnetization transfer effect is based on the interaction between the protons of unbound water, visible on MRI, and those of water that is bound to the macromolecules of the extracellular matrix. This has a very short T2 relaxation time and is therefore invisible on MRI. After saturation of the magnetization of bound water molecules by off-resonance or binomial pulses, the equilibrium is shifted to the unbound protons, which results in a reduction of the observable magnetization and, thus, in a reduction of the MR signal (Alizai et al. 2019).

With glycosaminoglycan Chemical Exchange Saturation Transfer (gagCEST) imaging, off-resonance radio frequent saturation pulses are designed specifically to saturate exchangeable protons residing on the hydroxyl groups of cartilage glycosaminoglycans. This technique correlates well with $^{23}Na^{+}$ imaging, and like $^{23}Na^{+}$ imaging, it is optimally performed at ultrahigh

field strength (7 T) magnets (Singh et al. 2012). Technical challenges in MTC and gagCEST imaging are the reduction of motion artefacts and the compensation for field inhomogeneities.

2.1.4.7 Ultrashort Echo Time Imaging

Ultrashort echo time (UTE) techniques facilitate imaging of tissues with short transverse relaxation times such as deep and calcified cartilage layers where T2 measurements were shown to be unreliable (Bae et al. 2010).

With the use of echo times that are 20–50 times shorter than conventional T2 sequences, high signal is acquired from tissues that typically produce little to no signal and increased signal sensitivity allows detection of layers or defects within the articular cartilage (Gatehouse et al. 2004).

Shortcomings of UTE imaging include lengthened scan times, difficulty in slice selection and sensitivity to magic angle effect (Chang et al. 2015).

2.1.5 MR Arthrography

In small joint and joints with thinner cartilage like the hip, 3D SPGR sequences, even with fat suppression or water excitation, do not achieve the same specificity and sensitivity as in the knee (Keeney et al. 2004). MR arthrography allows a better delineation of the articular cartilage surface and the detection of small cartilage lesions (Cerezal et al. 2005a, b). As the joint distends after the intra-articular administration of gadolinium solution, opposing cartilage surfaces become separated and more easily evaluated. The cartilage is also separated from surrounding tissues such as the synovium and meniscal structures (Fig. 17).

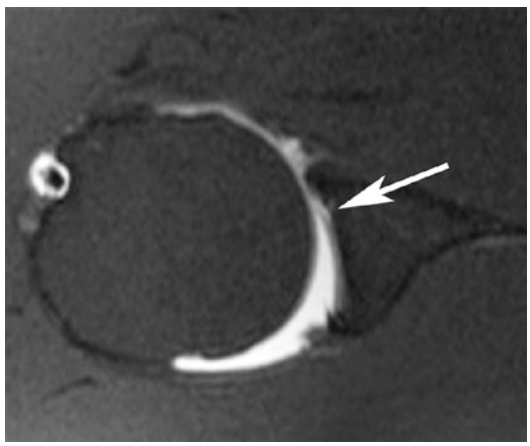

Fig. 17 Grade II–III cartilage defect. Transverse fat-suppressed T1-weighted image after intra-articular contrast administration. A small tear in the glenoidal cartilage seen on direct MR arthrography could easily have been missed on unenhanced MR imaging

In osteochondral lesions MR arthrography can be performed to differentiate more accurately between stable and unstable lesions.

MR arthrography can be performed in a direct or indirect manner. Direct arthrography implies the intra-articular injection of contrast solution under fluoroscopic visualization. Indirect MR arthrography takes advantage of the diffusion of contrast material from the blood vessels in the synovium into the synovial fluid. After 5–10 min of exercise, the concentration of gadolinium-base contrast agents in the synovial fluid is high enough to markedly shorten the T1-relaxation time of the fluid. Indirect arthrography in osteochondral lesions has the advantage that contrast is able to enter the bone-lesion interface as opacified synovial fluid or trough diffusion from hypervascular granulation tissue lining the interface. Both situations indicate instability. Another advantage is the enhancement of the extra-articular soft tissues and of possible hyperaemic sites underneath areas of cartilage contusion (Kramer et al. 1992, 1994; Kramer and Recht 2002; Recht and Kramer 2002).

The main drawback of indirect MR arthrography is the lack of joint distension. To overcome this, distraction techniques have been used to improve discrimination of opposing cartilage layers (Becce et al. 2010).

2.2 Imaging of Cartilage Trauma

2.2.1 Chondral Defects

Large defects diminish joint space width, but conventional radiography is not accurate. MR

Fig. 18 Recent cartilage defect. Sagittal CT arthrography. Traumatic grade IV cartilage defect (arrow) showing straight edges. Bone marrow oedema is not visible on CT imaging

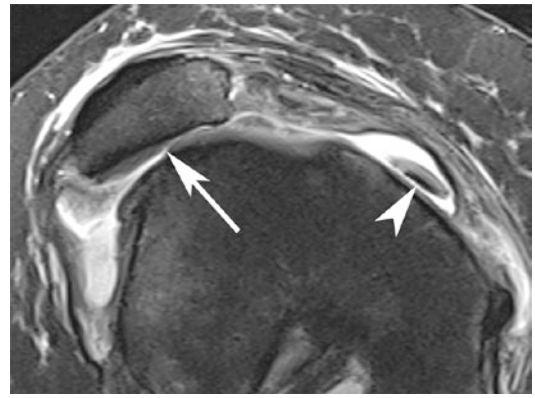

Fig. 19 Displaced chondral fragment in a 17-year-old recreational rugby player with predisposing trochlear dysplasia. The transverse fat-suppressed intermediate-weighted image shows a large cartilage defect on the medial patellar facet with an obtuse lateral margin (arrow). The displaced fragment can be seen in the medial patellar recess (arrowhead)

imaging and CT and MR arthrography reliably show chondromalacia and acute chondral defects, but all are incapable of demonstrating grade I lesions.

The outline of a cartilage lesion, best seen after direct or indirect arthrography but also appreciable on unenhanced MR imaging, allows to differentiate between acute and more chronic lesions. In general, if the edges are sharp (Fig. 18) and the cartilaginous lesion is accompanied by bone marrow oedema in the subjacent bone, an acute lesion must be suspected. A shallow lesion with wide margins, a more gradual slope to its edges and sclerosis of the subchondral bone suggest a chronic, degenerative lesion (Fig. 12).

An exception to this rule is seen in acute chondral and osteochondral lesions that arise due to excessive shear forces. In these cases, the edges of the lesion are also obtuse (Fig. 19).

2.2.2 Osteochondritis Dissecans and Osteochondral Lesions

Preferential places for osteochondral lesions and osteochondritis dissecans are the femoral condyles, talar dome and capitulum of humerus.

Possible aetiologies for osteochondral lesions in the knee are osteochondritis dissecans, post-traumatic osteochondral fractures or insufficiency fractures of an osteonecrotic area. Mechanically, these lesions are caused by repetitive and prolonged overloading or a sudden compressive stress of the articular surface and subchondral bone. These lesions can be classified in four stages.

Stage I lesions are stable, show no discontinuity between the lesion and the surrounding bone and are covered by intact cartilage. Stage II lesions are partially detached but stable. Stage III lesions are completely detached and considered unstable but not dislocated. In stage IV lesions, the fragment is displaced or loose within its bed (Brittberg et al. 2000). A summary of the stages is given in Table 3.

The role of imaging is first to identify the lesion and secondly to differentiate between stable and unstable lesions (Fig. 20). MR imaging has proven most accurate in doing this (Chung

Table 3 Stages of osteochondritis dissecans

Stage I	No discontinuity of bone and cartilage; covered by intact cartilage
Stage II	Partially detached osteochondral lesion but stable
Stage III	Completely detached osteochondral lesion but not dislocated
Stage IV	Displaced or loose osteochondral lesion within its bed

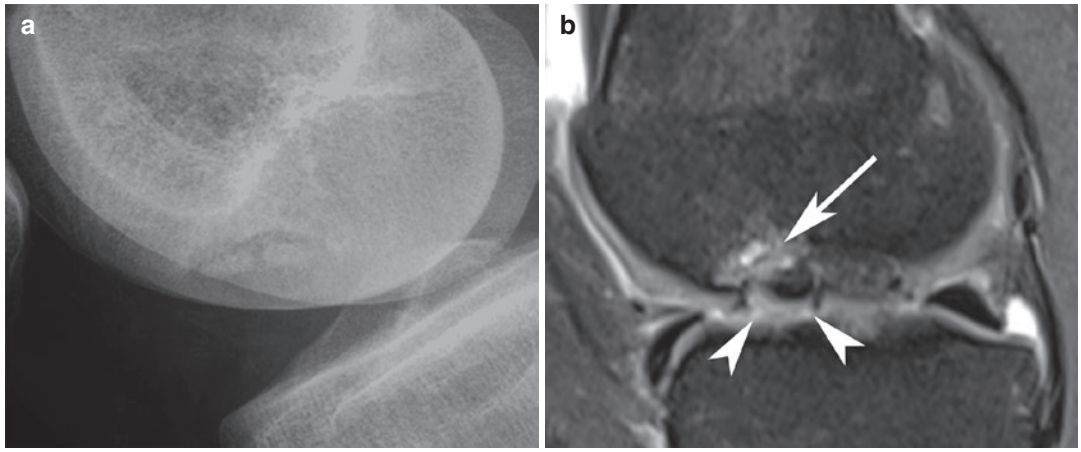

Fig. 20 (**a** and **b**) Osteochondritis dissecans. (**a**) Standard radiograph shows typically unstable osteochondral lesions of the femoral condyle: a radiolucent defect with sclerotic margins containing at least two loose bodies. (**b**) Sagittal fat-suppressed intermediate-weighted image shows an osteochondral lesion with a high signal intensity area between the loose fragment and the femoral condyle (white arrow). The cartilage covering the lesion shows several deep fissures (arrowheads). Note bone marrow oedema in the unstable osteochondral lesion and in the surrounding femoral condyle

et al. 2005). MR findings indicating an unstable lesion are a linear high signal deep to the lesion on T2-weighted images (which is the most important finding), an articular fracture indicated by a high signal passing through the end plate, a focal osteochondral defect and a fluid-filled cyst more than 5 mm in diameter (De Smet et al. 1990; Chung et al. 2005). The presence of intra-articular gadolinium contrast clearly improves the diagnostic accuracy of MR as the contrast solution outlines the (osteo)chondral defect from the surrounding bone.

At the talar dome "*osteochondral lesion of the talus*" is the common term for lesions like osteochondritis dissecans, osteochondral fractures and talar dome fractures. These lesions are caused by impaction of the dome during an inversion trauma and are preferentially located on the medial or lateral edge of the talar dome, depending on whether the impaction occurred during inversion combined with plantar flexion and external rotation of the tibia or inversion and dorsiflexion of the foot (Cerezal et al. 2005a). The most widely accepted classification of the lesions is that of Berndt and Harty (Berndt and Harty 1959; Beltran and Shankman 2001). It is similar to the classification of osteochondritis dissecans with an added grade (IIa) representing cystic degeneration of the lesion. Like in osteochondritis dissecans, it is important to distinguish between stable and unstable lesions. A linear high signal on T2-weighted images between the lesion and native bone represents fluid or granulation tissue (Fig. 21). When this area of bone resorption surrounding the osteochondral lesion abuts the cartilage, the lesion is classified as unstable. A linear signal of moderate intensity may represent fibrovascular tissue.

This is also considered as an unstable lesion, but healing can occur spontaneously or after a period of non-weight-bearing. Another criterion of instability is the presence of cystic degeneration larger than 5 mm.

In the capitulum of the humerus, osteochondral lesions are located at the anterolateral part and are typically seen in young baseball players and other throwing sports with valgus stress on the elbow (de Jonge et al. 2020). Aetiology, imaging findings and differentiation between stable and unstable lesions are the same as in osteochondral lesions of the talus and the femoral condyle (Fig. 22). Unstable osteochondritis dissecans lesions have a peripheral rim of high signal intensity or an underlying fluid-filled cyst on

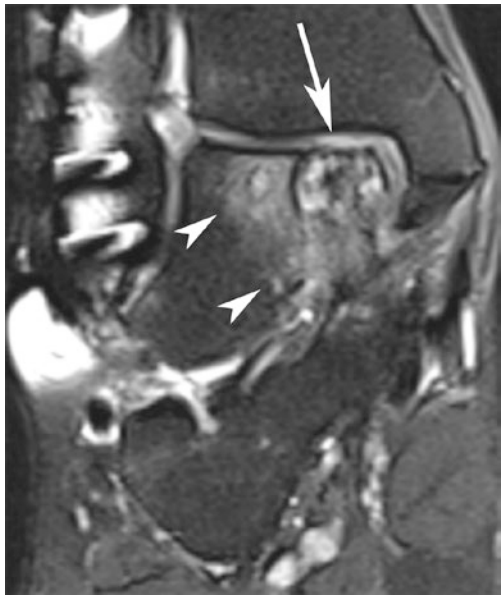

Fig. 21 Osteochondral lesion of the talus. Coronal fat-suppressed intermediate-weighted image shows extensive cartilage loss over the osteochondral defect (arrow) and subchondral cyst formation surrounded by bone marrow oedema (arrowheads)

Fig. 22 Osteochondritis dissecans. Standard AP radiograph of the right elbow. Plain radiography readily demonstrates the subcortical radiolucent area with sclerotic margin, typical for osteochondritis dissecans

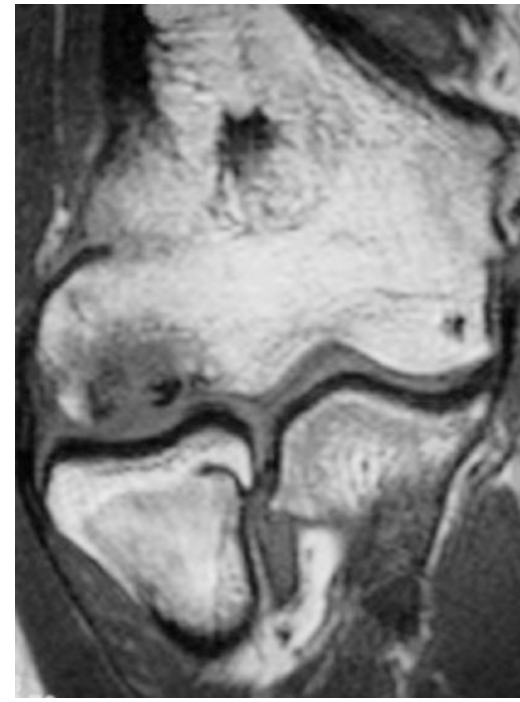

Fig. 23 Osteochondritis dissecans. Coronal T1-weighted image shows a large, unstable osteochondral lesion in the capitulum, with fragmentation

T2-weighted images (Fig. 23). The main pitfall in MR imaging of the elbow is the pseudodefect at the posterior rim of the capitulum. This is caused by the abrupt transition between the postero-inferior articular surface of the capitulum and the nonarticulating surface of the lateral epicondyle. This pseudodefect is a normal finding and should not be mistaken for osteochondritis-like lesions found more anteriorly within the capitulum (Nakagawa et al. 2001; Kijowski and De Smet 2005).

2.3 Modalities for Cartilage Repair

As no stem cells are found within hyaline cartilage, intrinsic repair capabilities of cartilage are limited. No meaningful repair of cartilage occurs in partial-thickness defects. Spontaneous repair is initiated if the subchondral bone plate is damaged and there is communication with the

subcortical marrow cavity (Shapiro et al. 1993). Given the poor intrinsic repair capabilities of adult articular cartilage, many different surgical repair techniques have been developed. These can be divided into three groups: the palliative (débridement or stabilization of loose articular cartilage), reparative (stimulation of repair from the subcortical bone) and restorative procedures (replacement of damaged cartilage).

The treatment goals of cartilage damage are symptom relief, improvement of joint congruence by restoring the joint surface with the best possible tissue, and prevention of further joint degeneration.

The palliative procedures are lavage, débridement and shaving. These procedures do not induce repair. Moreover, the therapeutic effects generally last only 1 year and are no better than those seen in sham surgery (Bruce Moseley et al. 2002).

Reparative procedures take advantage of the intrinsic repair response after opening the subchondral plate. This introduces all the vascular-mediated elements necessary for the classic healing response, such as fibrin clot, blood and marrow cells, cytokines, growth factors, and vascular invasion (Newman 1998; Redman et al. 2005). The most widely used is still microfracturing (Özmeriç et al. 2014) (Fig. 24), introduced by Steadman et al. in 1994 (Steadman et al. 1997). In most cases the defect is filled with collagen I rich fibrocartilage which does not resist compression and shear loads as predictably as hyaline cartilage does and is likely less durable over time.

The ideal patient for this type of repair procedure is young, has 2–4 cm^2, ICRS grade III cartilage lesion and a well-defined history of trauma. He or she is compliant with the demanding postoperative rehabilitation protocols and does not have mechanical axis malalignment.

Other reparative procedures such as Pridie drilling and abrasion arthroplasty have gone out of flavour. The effects and results of these are similar to those of microfracturing. However, superiority of one of these techniques over the other has never been established through robust comprehensive comparison (Gao et al. 2018).

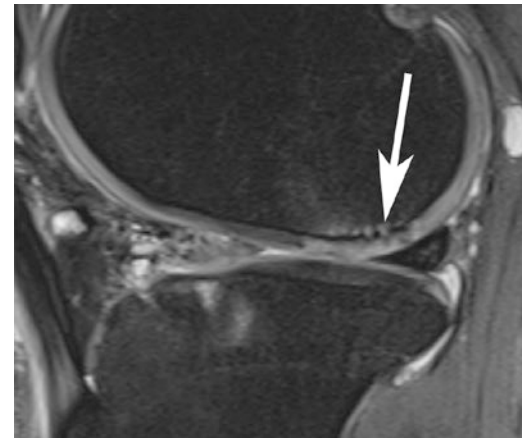

Fig. 24 Pridie microfracturing. Sagittal fat-suppressed intermediate-weighted image shows the result 6 months after microfracturing of a grade IV cartilage lesion on the weight-bearing part of the lateral femoral condyle. Note the irregular aspect of the subchondral bone plate (arrow)

The restorative procedures are more numerous and more diverse. They can be divided into several subgroups. First there are the soft tissue transplants. During these procedures perichondrium or periosteum is transferred to the defect after removal residual cartilage in the defect to create a full-thickness lesion and of 2–3 mm of subchondral bone. Periosteum is more widely used because it is more readily available.

Although preliminary results were encouraging, with one group reporting repair tissue with a collagen II content of 74% (Homminga et al. 1990), few other groups have pursued this further. Recently, costal cartilage was used as graft material (Farinelli et al. 2019). However, to date its therapeutic potential remains to be clearly defined by animal and clinical studies.

A second group encompasses all cell transplantation-based repair. This includes autologous chondrocyte implantation (ACI) (Fig. 25), allogeneic chondrocyte transplantation (ACT) and auto- or allogeneic stem cell transplantation (Fig. 16).

In later generations of this technique, the transplanted chondrocytes are no longer suspended in fluid that is injected underneath a periosteal flap but are grafted or cultured on a biodegradable membrane or scaffold prior to

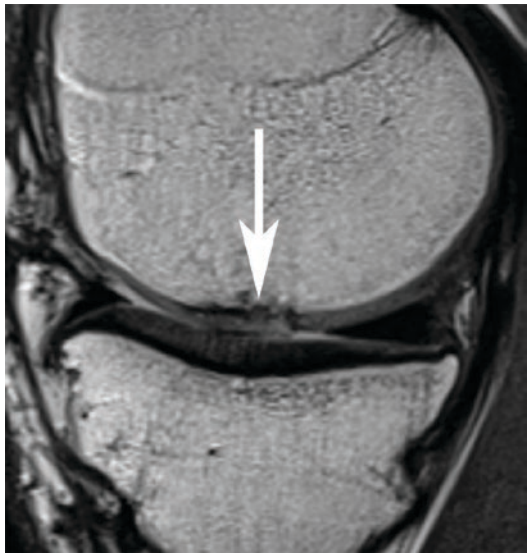

Fig. 25 Matrix-induced autologous chondrocyte implant. Sagittal 3D proton-density-weighted image shows complete filling of the cartilage defect with irregularity of both the surface of the repair tissue and the subchondral bone plate (arrow)

Fig. 26 Allogenic osteochondral graft in a 25-year-old dirt bike racer after extensive damage to the knee. Sagittal fat-suppressed intermediate-weighted image depicts a large graft in the medial femoral condyle with a small step off at the anterior side

placement into the defect, e.g. matrix-induced ACI (MACI).

Comparative clinical studies using matrix-induced cultured chondrocytes in autologous chondrocyte implantation (MACI) (Kon et al. 2009) have shown some superiority over conventional microfracturing under defined conditions, especially for medium or large defects and in long-term durability.

The latest evolution in this field is the addition of biochemical factors in the supportive scaffold of implanted chondrocytes in the hope of recreating the natural environment in which chondrogenesis occurs in the body (Vega et al. 2017).

If there is failure of the repair tissue, this occurs almost always in the first 2 years (Peterson 2002). In vivo, only hyaline-like repair tissue has been formed, without the structural or mechanical properties of mature cartilage (Redman et al. 2005).

A third subgroup includes the autologous or allogenous osteochondral transfers. These techniques are most often used for the repair of large osteochondral defects. Autologous osteochondral plug transfer is most effective in small- to medium-sized full-thickness defects. For larger lesions several osteochondral plugs can be fitted in the defect or a larger allograft can be used (Fig. 26). In mosaicplasty, the gaps between the plugs are filled with fibrocartilage, reducing the durability of the repair.

Other drawbacks of these autologous techniques are the inherent need to damage intact articular surface during prelevation of autologous osteochondral grafts (Bexkens et al. 2017) or the risks associated with implanting foreign tissue in a patient. These needs might be met by using costal osteochondral grafts (Sato et al. 2012).

2.4 Imaging Cartilage Repair

MR imaging is a good technique to evaluate cartilage repair by displaying thickness, edge integration, surface, subchondral bone plate and marrow.

The FSE sequence is more sensitive for assessment of the internal cartilage structure. In postoperative imaging, one advantage of FSE sequences is its low sensitivity to artefacts, which are suppressed by the 180° refocusing pulses of the FSE (Trattnig et al. 2011).

After surgical cartilage repair, the repair tissue should ideally have the same thickness and signal intensity as the surrounding cartilage. Furthermore, it should have a smooth surface and the margins should be continuous with the native cartilage. Ideally, the subchondral bone plate beneath the repair tissue should be smooth and continuous with the adjacent end plate although small differences are not clinically significant. There should be no abnormal signal in the underlying bone marrow. Other valuable information is location and size of the repair site as this is not always easy to assess particularly during arthroscopic procedures. Magnetic resonance imaging is ideally suited to evaluate these variables (Brittberg and Winalski 2003; Marlovits et al. 2004; Brittberg et al. 2005).

When evaluating the filling of a defect, the result is best recorded as a percentage of the thickness of the surrounding, native cartilage. This can exceed 100% if the repair tissue is hypertrophic, which is often noted in the first months (Winalski and Minas 2000; Alparslan et al. 2001; Brown et al. 2004). If the repaired lesion had an osseous component, separate evaluation of bone and cartilage repair should be done.

In a majority of patients, the interface between native and repair cartilage is visible and can be seen as an interface between two regions of different signal intensity or as a fluid-filled fissure. When a clear gap is seen between repair and native cartilage in ACI, thorough assessment of the integration with subchondral bone is needed, as failure of the repair occurs often in both locations.

MR arthrography is helpful in evaluating detachment of the graft (Brown et al. 2004).

T1ρ has been used for longitudinal evaluation of microfracture repair tissue suggesting an increase in proteoglycan over time, remaining significantly lower, however, than in native cartilage (Theologis et al. 2012).

Quantitative T2 mapping may be used to highlight differences between immature, disorganized, and more hyaline-like repair tissue (Fig. 27). Differences in the T2 value of repair tissue have been reported depending on the repair technique used (Domayer et al. 2008), the location of the procedure (Welsch et al. 2009b) and the time of follow-up (Crawford et al. 2009; Welsch et al. 2009a). Correlation of relative T2 values with clinical outcome measures has also been reported (Domayer et al. 2008).

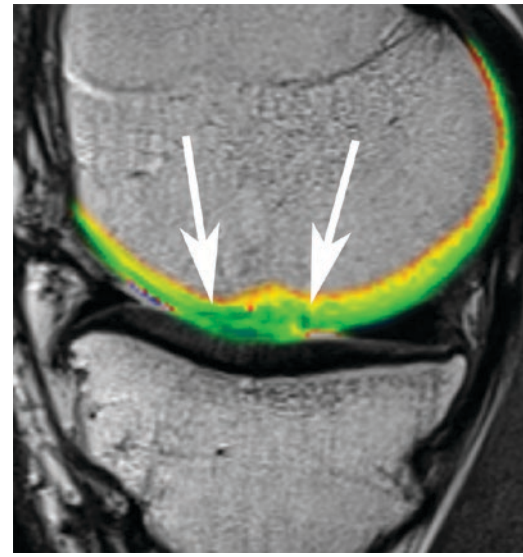

Fig. 27 Same patient as in Fig. 25. The T2 map colour overlay reveals immature repair tissue with low concentration or chaotic orientation of the collagen fibres (arrows)

Of note, T2 has a poor correlation with collagen content, showing no significant correlation in several repair models (Watanabe et al. 2009; Kim et al. 2010).

Similar to T2 mapping, differences in glycosaminoglycan concentration have been reported in the hyaline-like tissue using dGEMRIC depending on the repair technique used and the maturation of the tissue over time (Trattnig et al. 2011; Guermazi et al. 2015).

While T2 mapping is superior to dGEMRIC in discriminating repair tissue, the latter better differentiates between good and poor clinical outcomes in patients with talar osteochondral lesions (Rehnitz et al. 2017).

When osteochondral plug transfer is performed, integration and integrity of the osseous component should also be assessed.

The subchondral bone plate can display irregularities, subchondral cysts, especially located underneath the interface of native and repaired cartilage, and outright defects. In the early

postoperative period, bone marrow oedema is a common finding. This should resolve with progressive osseous incorporation, which takes between 6 and 14 weeks (Marlovits et al. 2004). Persistence of this abnormal signal after 6–12 months may indicate graft failure and is associated with pain complaints. The extent of this oedema should be compared to the size of the lesion. An overview of the most important criteria associated with graft failure is given in Table 4 (Marlovits et al. 2004; Plank et al. 2005; Trattnig et al. 2006).

Table 4 Signs of graft failure

Subchondral bone	• Persistent bone marrow oedema after 8–12 months • Subchondral cyst formation • Extensive subchondral sclerosis • Collapse of the bony end plate
Cartilage	• Thickness of repair tissue less than 50% of native cartilage • Delamination or dislocation of repair tissue • Extensive surface damage with loss of more than 50% of cartilage thickness

2.5 Scoring of Cartilage Repair

Two semiquantitative scoring systems for the knee have been published to date, although their use is currently limited to research purposes.

The Magnetic Resonance Observation of Cartilage Repair Tissue (MOCART) score was introduced in 2004 (Marlovits et al. 2004). It was based on nine pertinent variables and facilitated a standardized, reproducible, semiquantitative approach for the morphological assessment of cartilage repair. In 2009, the scoring system was updated and additional parameters were added based on the new information afforded by isotropic voxel MRI (Welsch et al. 2009d).

In 2019, a further update was introduced resulting in an almost perfect interrater and intrarater reliability in expert readers (Schreiner et al. 2019).

Inexperienced readers have poor interreader reliability. However, the use of an atlas depicting all variables, using a native MR image next to a colour-coded overlay would increase the comparability of results across studies.

An overview of the MOCART 2.0 score is given in Table 5.

Table 5 MOCART 2.0

MOCART 2.0 Knee Score: Cartilage repair tissue assessment: grading and Point Scale			
			Scoring
1	Volume fill of cartilage defect		
	1	Complete filling OR minor hypertrophy: 100–150% filling of total defect volume	20
	2	Major hypertrophy ≥105% (1-2a) OR 75–99% filing of total defect volume (1-2b)	15
	3	50–74% filling of total defect volume	10
	4	25–49% filling of total defect volume	5
	5	<25% filling of the total defect volume (1-5a) OR delamination in situ (1-5b)	0
2	Integration into adjacent cartilage		
	1	Complete integration	15
	2	Split-like defect at repair tissue and native cartilage interface ≤2 mm	10
	3	Defect at repair tissue and native cartilage interface >2 mm, but <50% of repair tissue circumference	5
	4	Defect at repair tissue and native cartilage interface ≥50% of repair tissue circumference	0
3	Surface of the repair tissue		
	1	Surface intact	10
	2	Surface irregular <50% of repair tissue diameter	5
	3	Surface irregular ≥50% of repair tissue diameter	0
4	Structure of the repair tissue		
	1	Homogeneous	10
	2	Inhomogeneous	0

Table 5 (continued)

MOCART 2.0 Knee Score: Cartilage repair tissue assessment: grading and Point Scale			
			Scoring
5	Signal intensity of the repair tissue		
	1	Normal	15
	2	Mildly abnormal—Mildly hyperintense (5-2a) OR mildly hypo-intense (5-2b)	10
	3	Severely abnormal—Almost fluid-like signal (5-3a) OR close to subchondral bone plate signal (5-3b)	0
6	Bony defect or bony overgrowth		
	1	No bony defect or bony overgrowth	10
	2	Bony defect: Depth < thickness of adjacent cartilage (6-2a) OR overgrowth <50% of adjacent cartilage (6-2b)	5
	3	Bony defect: Depth ≥ thickness of adjacent cartilage (6-3a) OR overgrowth ≥50% of adjacent cartilage (6-3b)	0
7	Subchondral changes		
	1	No major subchondral changes	20
	2	Minor oedema-like marrow signal—Maximum diameter < 50% of repair tissue diameter	15
	3	Severe oedema-like marrow signal—Maximum diameter ≥ 50% of repair tissue diameter	10
	4	Subchondral cyst ≥5 mm in longest diameter (7-4a) OR osteonecrosis-like signal (7-4b)	0

MOCART magnetic resonance observation of cartilage repair tissue

The cartilage repair OA knee score (CROAKS) is the second scoring system and combines features of original MOCART that have been left out in the latest version and the MR imaging OA knee score (MOAKS) (Hunter et al. 2011; Roemer et al. 2014). The specific features outside of the repair site, assessed for multiple joint subregions with the CROAKS, include bone marrow lesions beyond the repair site, subchondral cysts, non-operated cartilage status, osteophytes, synovitis, effusion, menisci, and anterior and posterior cruciate ligaments.

Things to Remember

1. Conventional radiographs show only late degenerative cartilage changes but are valuable in the detection of osteochondral lesions.
2. CT arthrography is excellent for detecting grade II, III and IV lesions
3. MR allows good evaluation of articular cartilage and is the only imaging technique that demonstrates bone marrow oedema.
4. MR arthrography and CT arthrography demonstrate the degree of separation of a fragment in osteochondritis dissecans.

3 Conclusion

For evaluating sports-related traumatic chondral and osteochondral lesions or assessing the quality of cartilage repair, MR imaging has long since become the most important diagnostic tool. In the future, this will become even more the case as experimental imaging sequences are integrated in routine clinical examinations. The only other imaging modality that can adequately depict the articular surface is CT arthrography. This technique is, however, unable to demonstrate bone marrow oedema, an imaging finding with high clinical significance.

Box 1 Standard Radiography and CT Arthrography

- Radiography is well suited for the evaluation of osteoarthritis and limb alignment but is unable to depict cartilage.
- Special views may be needed.
- CT arthrography is as accurate as MR but fails to demonstrate associated lesions and bone marrow oedema.

Box 2 MRI and MR arthrography

- MR is the gold standard for evaluation of cartilage injury.
- Excellent for depicting associated intra-articular derangement.
- Either 2D or 3D intermediate-weighted fast spine-echo (FSE) sequences with or without fat suppression are still the bedrock for MR imaging of cartilage.
- MR arthrography is more accurate for demonstrating cartilage lesions in small joints.
- Physiologic imaging of articular cartilage is available but still experimental.

References

Alizai H, Walter W, Khodarahmi I, Burke CJ (2019) Cartilage imaging in osteoarthritis. Semin Musculoskelet Radiol 23:569–578. https://doi.org/10.1055/s-0039-1695720

Alparslan L, Winalski CS, Boutin RD, Minas T (2001) Postoperative magnetic resonance imaging of articular cartilage repair. Semin Musculoskelet Radiol 5:345–363. https://doi.org/10.1055/s-2001-19044

An C, Chun YM, Kim S et al (2014) Dual-energy computed tomography arthrography of the shoulder joint using virtual monochromatic spectral imaging: optimal dose of contrast agent and monochromatic energy level. Korean J Radiol 15:746–756. https://doi.org/10.3348/kjr.2014.15.6.746

Arokoski J, Kiviranta I, Jurvelin J et al (1993) Long-distance running causes site-dependent decrease of cartilage glycosaminoglycan content in the knee joints of beagle dogs. Arthritis Rheum 36:1451–1459. https://doi.org/10.1002/art.1780361018

Bae WC, Dwek JR, Znamirowski R et al (2010) Ultrashort echo time MR imaging of osteochondral junction of the knee at 3 T: identification of anatomic structures contributing to signal intensity. Radiology 254:837–845. https://doi.org/10.1148/radiol.09081743

Baur A, Stäbler A, Brüning R et al (1998) Diffusion-weighted MR imaging of bone marrow: differentiation of benign versus pathologic compression fractures. Radiology 207:349–356. https://doi.org/10.1148/radiology.207.2.9577479

Bayliss MT, Ali SY (1978) Age-related changes in the composition and structure of human articular-cartilage proteoglycans. Biochem J 176:683–693. https://doi.org/10.1042/bj1760683

Becce F, Wettstein M, Guntern D et al (2010) Arthro-IRM directe en traction axiale [technique and value of direct MR arthrography applying articular distraction]. Rev Med Suisse 6:413–417

Beltran J, Shankman S (2001) MR imaging of bone lesions of the ankle and foot. Magn Reson Imaging Clin N Am 9(553–66):xi

Berndt AL, Harty M (1959) Transchondral fractures (osteochondritis dissecans) of the talus. J Bone Joint Surg Am 41-A:988–1020

Bexkens R, Ogink PT, Doornberg JN et al (2017) Donor-site morbidity after osteochondral autologous transplantation for osteochondritis dissecans of the capitellum: a systematic review and meta-analysis. Knee surgery. Sport Traumatol Arthrosc 25:2237–2246

Biswal S, Hastie T, Andriacchi TP et al (2002) Risk factors for progressive cartilage loss in the knee: a longitudinal magnetic resonance imaging study in forty-three patients. Arthritis Rheum 46:2884–2892. https://doi.org/10.1002/art.10573

Bittersohl B, Kircher J, Miese FR et al (2015) T2* mapping and delayed gadolinium-enhanced magnetic resonance imaging in cartilage (dGEMRIC) of humeral articular cartilage—a histologically controlled study. J Shoulder Elb Surg 24:1644–1652. https://doi.org/10.1016/j.jse.2015.03.016

Bloebaum RD, Radley KM (1995) Three-dimensional surface analysis of young adult human articular cartilage. J Anat 187(Pt 2):293–301

Boesen M, Ellegaard K, Henriksen M et al (2017) Osteoarthritis year in review 2016: imaging. Osteoarthr Cartil 25:216–226. https://doi.org/10.1016/j.joca.2016.12.009

Booz C, Nöske J, Lenga L et al (2020) Color-coded virtual non-calcium dual-energy CT for the depiction of bone marrow edema in patients with acute knee trauma: a multireader diagnostic accuracy study. Eur Radiol 30:141–150. https://doi.org/10.1007/s00330-019-06304-7

Braun HJ, Gold GE (2011) Advanced MRI of articular cartilage. Imaging Med 3:541–555. https://doi.org/10.2217/iim.11.43

Bredella MA, Tirman PFJ, Peterfy CG et al (1999) Accuracy of T2-weighted fast spin-echo MR imaging with fat saturation in detecting cartilage defects in the knee: comparison with arthroscopy in 130 patients. AJR Am J Roentgenol 172:1073–1080

Brittberg M, Winalski CS (2003) Evaluation of cartilage injuries and repair. J Bone Joint Surg Am 85-A:58–69

Brittberg M, Aglietti P, Gambardella R, et al (2000) ICRS cartilage injury evaluation package

Brittberg M, Sjögren-Jansson E, Thornemo M et al (2005) Clonal growth of human articular cartilage and the functional role of the periosteum in chondrogenesis. Osteoarthr Cartil 13:146–153. https://doi.org/10.1016/j.joca.2004.10.020

Broderick LS, Turner DA, Renfrew DL et al (1994) Severity of articular cartilage abnormality in patients with osteoarthritis: evaluation with fast spin-echo MR

vs arthroscopy. Am J Roentgenol 162:99–103. https://doi.org/10.2214/ajr.162.1.8273700

Brown WE, Potter HG, Marx RG et al (2004) Magnetic resonance imaging appearance of cartilage repair in the knee. Clin Orthop Relat Res 422:214–223. https://doi.org/10.1097/01.blo.0000129162.36302.4f

Bruce Moseley J, O'Malley K, Petersen NJ et al (2002) A controlled trial of arthroscopic surgery for osteoarthritis of the knee. N Engl J Med 347:81–88. https://doi.org/10.1056/NEJMoa013259

Buckwalter JA (2002) Articular cartilage injuries. Clin Orthop Relat Res (402):21–37

Burstein D, Gray ML, Hartman AL et al (1993) Diffusion of small solutes in cartilage as measured by nuclear magnetic resonance (NMR) spectroscopy and imaging. J Orthop Res 11:465–478. https://doi.org/10.1002/jor.1100110402

Cameron ML, Briggs KK, Steadman JR (2003) Reproducibility and reliability of the outerbridge classification for grading chondral lesions of the knee arthroscopically. Am J Sports Med 31:83–86. https://doi.org/10.1177/03635465030310012601

Cerezal L, Abascal F, García-Valtuille R, Canga A (2005a) Ankle MR arthrography: how, why, when. Radiol Clin N Am 43:693–707

Cerezal L, Abascal F, García-Valtuille R, Del Piñal F (2005b) Wrist MR arthrography: how, why, when. Radiol Clin N Am 43:709–731

Chang EY, Du J, Chung CB (2015) UTE imaging in the musculoskeletal system. J Magn Reson Imaging 41:870–883. https://doi.org/10.1002/jmri.24713

Chung CB, Isaza IL, Angulo M et al (2005) MR arthrography of the knee: how, why, when. Radiol Clin N Am 43:733–746. https://doi.org/10.1016/j.rcl.2005.02.003

Crawford DC, Heveran CM, Cannon WD et al (2009) An autologous cartilage tissue implant NeoCart for treatment of grade III chondral injury to the distal femur: prospective clinical safety trial at 2 years. Am J Sports Med 37:1334–1343. https://doi.org/10.1177/0363546509333011

Curl WW, Krome J, Gordon ES et al (1997) Cartilage injuries: a review of 31,516 knee arthroscopies. Arthroscopy 13:456–460. https://doi.org/10.1016/S0749-8063(97)90124-9

De Jonge MC, Vermeulen NP, Maas M (2020) Imaging of sports injuries of the elbow. Med Radiol. https://doi.org/10.1007/174_2020_251

De Smet AA, Fisher DR, Graf BK, Lange RH (1990) Osteochondritis dissecans of the knee: value of MR imaging in determining lesion stability and the presence of articular cartilage defects. Am J Roentgenol 155:549–553. https://doi.org/10.2214/ajr.155.3.2117355

De Smet E, Van Dyck P, Gielen J, Vanhoenacker FM (2020) Sports-related meniscal injury. Med Radiol. https://doi.org/10.1007/174_2020_244

Disler DG, McCauley TR, Kelman CG et al (1995) Detection of knee hyaline cartilage defects using fat-suppressed three-dimensional spoiled gradient-Echo MR imaging. Am J Roentgenol 165:377–382. https://doi.org/10.2214/ajr.167.1.8659356

Disler DG, McCauley TR, Kelman CG et al (1996) Fat-suppressed three-dimensional spoiled gradient-echo MR imaging of hyaline cartilage defects in the knee: comparison with standard MR imaging and arthroscopy. Am J Roentgenol 167:127–132. https://doi.org/10.2214/ajr.167.1.8659356

Domayer SE, Kutscha-Lissberg F, Welsch G et al (2008) T2 mapping in the knee after microfracture at 3.0 T: correlation of global T2 values and clinical outcome - preliminary results. Osteoarthr Cartil 16:903–908. https://doi.org/10.1016/j.joca.2007.11.014

Dupas B, Frampas E, Leaute F et al (2005) Complications of fluoroscopy-, ultrasound-, and CT-guided percutaneous interventional procedures. J Radiol 86:599–600. https://doi.org/10.1016/s0221-0363(05)81413-1

Farinelli L, Aquili A, Manzotti S et al (2019) Characterization of human costal cartilage: is it an adapt tissue as graft for articular cartilage repair? J Biol Regul Homeost Agents 33:69–77

Friedrich KM, Mamisch TC, Plank C et al (2010) Diffusion-weighted imaging for the follow-up of patients after matrix-associated autologous chondrocyte transplantation. Eur J Radiol 73:622–628. https://doi.org/10.1016/j.ejrad.2008.12.017

Fuller JA, Ghadially FN (1972) Ultrastructural observations on surgically produced partial-thickness defects in articular cartilage. Clin Orthop Relat Res 86:193–205. https://doi.org/10.1097/00003086-197207000-00031

Gao L, Goebel LKH, Orth P et al (2018) Subchondral drilling for articular cartilage repair: a systematic review of translational research. DMM Dis Model Mech 11:dmm034280. https://doi.org/10.1242/dmm.034280

Gatehouse PD, Thomas RW, Robson MD et al (2004) Magnetic resonance imaging of the knee with ultrashort TE pulse sequences. Magn Reson Imaging 22:1061–1067. https://doi.org/10.1016/j.mri.2004.08.018

Gatti AA (2018) NEURALSEG: state-of-the-art cartilage segmentation using deep learning—analyses of data from the osteoarthritis initiative. Osteoarthr Cartil 26:S47–S48. https://doi.org/10.1016/j.joca.2018.02.110

Ghadially FN, Thomas I, Oryschak AF, Lalonde JM (1977a) Long-term results of superficial defects in articular cartilage: a scanning electronmicroscope study. J Pathol 121:213–217. https://doi.org/10.1002/path.1711210404

Ghadially JA, Ghadially R, Ghadially FN et al (1977b) Long-term results of deep defects in articular cartilage. A scanning electron microscope study. Virchows arch B. Cell Pathol 25:125–136. https://doi.org/10.1007/bf02889427

Gold GE, Han E, Stainsby J et al (2004) Musculoskeletal MRI at 3.0 T: relaxation times and image contrast. Am J Roentgenol 183:343–351. https://doi.org/10.2214/ajr.183.2.1830343

Gray ML, Burstein D, Kim YJ, Maroudas A (2008) Magnetic resonance imaging of cartilage glycosami-

noglycan: basic principles, imaging technique, and clinical applications. J Orthop Res 26:281–291
Guermazi A, Roemer FW, Alizai H et al (2015) State of the art: MR imaging after knee cartilage repair surgery. Radiology 277:23–43. https://doi.org/10.1148/radiol.2015141146
Gurr E, Mohr W, Pallasch G (1985) Proteoglycans from human articular cartilage: the effect of joint location on the structure. Clin Chem Lab Med 23: 811–820. https://doi.org/10.1515/cclm.1985.23.12.811
Homminga GN, Bulstra SK, Bouwmeester PSM, Van der Linden AJ (1990) Perichondral grafting for cartilage lesions of the knee. J Bone Joint Surg Br 72:1003–1007. https://doi.org/10.1302/0301-620x.72b6.2246280
Huber M, Trattnig S, Lintner F (2000) Anatomy, biochemistry, and physiology of articular cartilage. Investig Radiol 35:573–580
Hunter DJ, Guermazi A, Lo GH et al (2011) Evolution of semi-quantitative whole joint assessment of knee OA: MOAKS (MRI osteoarthritis knee score). Osteoarthr Cartil 19:990–1002. https://doi.org/10.1016/j.joca.2011.05.004
Imhof H, Sulzbacher I, Grampp S et al (2000) Subchondral bone and cartilage disease: a rediscovered functional unit. Investig Radiol 35:581–588
Imhof H, Nöbauer-Huhmann IM, Krestan C et al (2002) MRI of the cartilage. Eur Radiol 12: 2781–2793
Jung JY, Yoon YC, Kwon JW et al (2009) Diagnosis of internal derangement. Radiology 253:780–787. https://doi.org/10.1148/radiol.2533090457/-/DC1
Kassarjian A, Fritz B, Afonso PD et al (2016) Guidelines for MR imaging of sports injuries. https://www.essr.org/subcommittees/sports/. Accessed 9 Sep 2020
Keats TE, Sistrom C (2001) Atlas of radiologic measurement, 7th edn. Mosby, St. Louis
Keeney JA, Peelle MW, Jackson J et al (2004) Magnetic resonance arthrography versus arthroscopy in the evaluation of articular hip pathology. Clin Orthop Relat Res 429:163–169
Kijowski R, De Smet AA (2005) MRI findings of osteochondritis dissecans of the capitellum with surgical correlation. Am J Roentgenol 185:1453–1459. https://doi.org/10.2214/AJR.04.1570
Kijowski R, Blankenbaker DG, Klaers JL et al (2009) Vastly undersampled isotropic projection steady-state free precession imaging of the knee: diagnostic performance compared with conventional MR. Radiology 251:185–194. https://doi.org/10.1148/radiol.2511081133
Kim M, Foo LF, Uggen C et al (2010) Evaluation of early osteochondral defect repair in a rabbit model utilizing Fourier transform-infrared imaging spectroscopy, magnetic resonance imaging, and quantitative T2 mapping. Tissue Eng Part C Methods 16:355–364. https://doi.org/10.1089/ten.tec.2009.0020
Kiviranta I, Tammi M, Jurvelin J et al (1992) Articular cartilage thickness and glycosaminoglycan distribution in the canine knee joint after strenuous running exercise. Clin Orthop Relat Res:302–308
Klaan B, Wuennemann F, Kintzelé L et al (2019) MR and CT arthrography in cartilage imaging: indications and implementation. Radiologe 59:710–721
Kolf A-K, Hesper T, Schleich C et al (2016) T2* mapping of ovine intervertebral discs: normative data for cervical and lumbar spine. J Orthop Res 34:717–724. https://doi.org/10.1002/jor.23071
Kon E, Verdonk P, Condello V et al (2009) Matrix-assisted autologous chondrocyte transplantation for the repair of cartilage defects of the knee. Am J Sports Med 37:156–166. https://doi.org/10.1177/0363546509351649
Krajewska-Włodarczyk M, Owczarczyk-Saczonek A, Placek W et al (2018) Articular cartilage aging-potential regenerative capacities of cell manipulation and stem cell therapy. Int J Mol Sci 19:623
Kramer J, Recht MP (2002) MR arthrography of the lower extremity. Radiol Clin N Am 40:1121–1132. https://doi.org/10.1016/S0033-8389(02)00057-X
Kramer J, Stiglbauer R, Engel A et al (1992) MR contrast arthrography (MRA) in osteochondrosis dissecans. J Comput Assist Tomogr 16:254–260. https://doi.org/10.1097/00004728-199203000-00014
Kramer J, Recht MP, Imhof H et al (1994) Postcontrast MR arthrography in assessment of cartilage lesions. J Comput Assist Tomogr 18:218–224. https://doi.org/10.1097/00004728-199403000-00009
Lang P, Noorbakhsh F, Yoshioka H (2005) MR imaging of articular cartilage: current state and recent developments. Radiol Clin N Am 43:629–639
Leardini A, Durante S, Belvedere C et al (2019) Weight-bearing CT Technology in Musculoskeletal Pathologies of the lower limbs: techniques, initial applications, and preliminary combinations with gait-analysis measurements at the Istituto Ortopedico Rizzoli. Semin Musculoskelet Radiol 23:643–656. https://doi.org/10.1055/s-0039-1697939
Li X, Benjamin Ma C, Link TM et al (2007) In vivo T1ρ and T2 mapping of articular cartilage in osteoarthritis of the knee using 3 T MRI. Osteoarthr Cartil 15:789–797. https://doi.org/10.1016/j.joca.2007.01.011
Link TM, Neumann J, Li X (2017) Prestructural cartilage assessment using MRI. J Magn Reson Imaging 45:949–965. https://doi.org/10.1002/jmri.25554
MacKay JW, Turmezei TD, Kaggie JD et al (2019) Cartilage imaging for experimental medicine studies: 6-month changes in morphology and composition can be detected by 3D cartilage surface mapping of knee magnetic resonance imaging data. Osteoarthr Cartil 27:S244–S245. https://doi.org/10.1016/j.joca.2019.02.609
Madelin G, Lee J-S, Regatte RR, Jerschow A (2014) Sodium MRI: methods and applications. Prog Nucl Magn Reson Spectrosc 79:14–47. https://doi.org/10.1016/j.pnmrs.2014.02.001
Mamisch TC, Menzel MI, Welsch GH et al (2008) Steady-state diffusion imaging for MR in-vivo evaluation of reparative cartilage after matrix-associated autologous chondrocyte transplantation at 3 tesla-

preliminary results. Eur J Radiol 65:72–79. https://doi.org/10.1016/j.ejrad.2007.09.015
Mankin HJ (1982) The response of articular cartilage to mechanical injury. J Bone Joint Surg Am 64:460–466. https://doi.org/10.1007/978-1-4471-5451-8_96
Mankin HJ, Dorfman H, Lippiello L, Zarins A (1971) Biochemical and metabolic abnormalities in articular cartilage from osteo-arthritic human hips. II Correlation of morphology with biochemical and metabolic data. J Bone Joint Surg Am 53:523–537. https://doi.org/10.2106/00004623-197153030-00009
Marlovits S, Striessnig G, Resinger CT et al (2004) Definition of pertinent parameters for the evaluation of articular cartilage repair tissue with high-resolution magnetic resonance imaging. Eur J Radiol 52:310–319. https://doi.org/10.1016/j.ejrad.2004.03.014
Martinek V (2003) Anatomie und pathophysiologie des hyalinen knorpels. Dtsch Z Sportmed 54:166–170
Mascarenhas VV, Castro MO, Diana Afonso P (2020) Hip, pelvis and sacro-iliac joints. Med Radiol. https://doi.org/10.1007/174_2020_256
McAdams TR, Mithoefer K, Scopp JM, Mandelbaum BR (2010) Articular cartilage injury in athletes. Cartilage 1:165–179
McDevitt CA, Webber RJ (1990) The ultrastructure and biochemistry of meniscal cartilage. Clin Orthop Relat Res (252):8–18
Meachim G (2001) Age changes in articular cartilage. Clin Orthop Relat Res 391:S6–S13
Minns RJ, Steven FS (1977) The collagen fibril organization in human articular cartilage. J Anat 123:437–457
Mosher TJ, Dardzinski BJ, Smith MB (2000) Human articular cartilage: influence of aging and early symptomatic degeneration on the spatial variation of T2-preliminary findings at 3T. Radiology 214:259–266. https://doi.org/10.1148/radiology.214.1.r00ja15259
Mosher TJ, Zhang Z, Reddy R et al (2011) Knee articular cartilage damage in osteoarthritis: analysis of MR image biomarker reproducibility in ACRIN-PA 4001 multicenter trial. Radiology 258:832–842. https://doi.org/10.1148/radiol.10101174
Nakagawa Y, Matsusue Y, Ikeda N et al (2001) Osteochondral grafting and arthroplasty for end-stage osteochondritis dissecans of the capitellum: a case report and review of the literature. Am J Sports Med 29:650–655. https://doi.org/10.1177/03635465010290052001
Newman AP (1998) Articular cartilage repair. Am J Sports Med 26:309–324
Nishii T, Tanaka H, Nakanishi K et al (2005) Arthrography of articular cartilage in patients with hip dysplasia. Am J Roentgenol 185:379–385
O'Driscoll SW, Keeley FW, Salter RB (1988) Durability of regenerated articular cartilage produced by free autogenous periosteal grafts in major full-thickness defects in joint surfaces under the influence of continuous passive motion. A follow-up report at one year. J Bone Joint Surg 70:595–606. https://doi.org/10.2106/00004623-198870040-00017
Oei EHG, Wick MC, Müller-Lutz A et al (2018) Cartilage imaging: techniques and developments. Semin Musculoskelet Radiol 22:245–260. https://doi.org/10.1055/s-0038-1639471
Ostergaard K, Petersen J, Andersen CB et al (1997) Histologic/histochemical grading system for osteoarthritic articular cartilage: reproducibility and validity. Arthritis Rheum 40:1766–1771. https://doi.org/10.1002/art.1780401007
Ostergaard K, Andersen CB, Petersen J et al (1999) Validity of histopathological grading of articular cartilage from osteoarthritic knee joints. Ann Rheum Dis 58:208–213. https://doi.org/10.1136/ard.58.4.208
Outerbridge RE, Caplan N, Kader DF (1961) The etiology of chondromalacia patellae. J Bone Joint Surg Br 43-B:752–757. https://doi.org/10.1007/978-1-4471-5451-8_45
Özmeriç A, Alemdaroğlu KB, Aydoğan NH (2014) Treatment for cartilage injuries of the knee with a new treatment algorith. World J Orthop 5:677–684
Parentis MA, Mohr KJ, ElAttrache NS (2002) Disorders of the superior labrum: review and treatment guidelines. Clin Orthop Relat Res (400):77–87
Pedoia V, Li X, Su F et al (2016) Fully automatic analysis of the knee articular cartilage T1ρ relaxation time using voxel-based relaxometry. J Magn Reson Imaging 43:970–980. https://doi.org/10.1002/jmri.25065
Peterfy CG (2000) Scratching the surface: articular cartilage disorders in the knee. Magn Reson Imaging Clin N Am 8:409–430
Peterson L (2002) Technique of autologous chondrocyte transplantation. Tech Knee Surg 1:2–12
Plank CM, Kubin K, Weber M et al (2005) Contrast-enhanced high-resolution magnetic resonance imaging of autologous cartilage implants of the knee joint. Magn Reson Imaging 23:739–744. https://doi.org/10.1016/j.mri.2005.05.004
Poole CA (1997) Articular cartilage chondrons: form, function and failure. J Anat 191:1–13
Poon CS, Henkelman RM (1992) Practical T2 quantitation for clinical applications. J Magn Reson Imaging 2:541–553. https://doi.org/10.1002/jmri.1880020512
Potter HG, Linklater JM, Allen AA et al (1998) Magnetic resonance imaging of articular cartilage in the knee. An evaluation with use of fast-spin-echo imaging. J Bone Joint Surg 80:1276–1284. https://doi.org/10.2106/00004623-199809000-00005
Rath E, Richmond JC (2000) The menisci: basic science and advances in treatment. Br J Sports Med 34:252–257
Recht MP, Kramer J (2002) MR imaging of the postoperative knee: a pictorial essay. Radiographics 22:765–774
Recht MP, Piraino DW, Paletta GA et al (1996) Accuracy of fat-suppressed three-dimensional spoiled gradient-Echo FLASH MR imaging in the detection. Radiology 198:209–2012

Redman SN, Oldfield SF, Archer CW et al (2005) Current strategies for articular cartilage repair. Eur Cell Mater 9:23–32

Regatte RR, Akella SVS, Borthakur A et al (2003) In vivo proton MR three-dimensional T1ρ mapping of human articular cartilage: initial experience. Radiology 229:269–274. https://doi.org/10.1148/radiol.2291021041

Rehnitz C, Kuni B, Wuennemann F et al (2017) Delayed gadolinium-enhanced MRI of cartilage (dGEMRIC) and T2 mapping of talar osteochondral lesions: indicators of clinical outcomes. J Magn Reson Imaging 46:1601–1610. https://doi.org/10.1002/jmri.25731

Resnick D (2002) Diagnosis of bone and joint disorders. Saunders, Philadelphia

Rijk PC (2004) Meniscal allograft transplantation-part i: background, results, graft selection and preservation, and surgical considerations. Arthroscopy 20:728–743. https://doi.org/10.1016/j.arthro.2004.06.015

Roemer FW, Frobell R, Hunter DJ et al (2009) MRI-detected subchondral bone marrow signal alterations of the knee joint: terminology, imaging appearance, relevance and radiological differential diagnosis. Osteoarthr Cartil 17:1115

Roemer FW, Guermazi A, Trattnig S et al (2014) Whole joint MRI assessment of surgical cartilage repair of the knee: cartilage repair OsteoArthritis knee score (CROAKS). Osteoarthr Cartil 22:779–799. https://doi.org/10.1016/j.joca.2014.03.014

Roos EM, Dahlberg L (2005) Positive effects of moderate exercise on glycosaminoglycan content in knee cartilage: a four-month, randomized, controlled trial in patients at risk of osteoarthritis. Arthritis Rheum 52:3507–3514. https://doi.org/10.1002/art.21415

Ruehm S, Zanetti M, Romero J, Hodler J (1998) MRI of patellar articular cartilage: evaluation of an optimized gradient-echo sequence (3D-DESS). J Magn Reson Imaging 8:1246–1251. https://doi.org/10.1002/jmri.1880080611

Sato K, Moy OJ, Peimer CA et al (2012) An experimental study on costal osteochondral graft. Osteoarthr Cartil 20:172–183. https://doi.org/10.1016/j.joca.2011.12.001

Schäffeler C (2020) Shoulder instability. Med Radiol. https://doi.org/10.1007/174_2020_245

Schreiner MM, Raudner M, Marlovits S et al (2019) The MOCART (Magnetic Resonance Observation of Cartilage Repair Tissue) 2.0 Knee Score and Atlas. Cartilage. epub ahead:1–17. https://doi.org/10.1177/1947603519865308

Shahriaree H (1985) Chondromalacia. Contemp Orthop 11:27–39

Shapiro F, Koide S, Glimcher MJ (1993) Cell origin and differentiation in the repair of full-thickness defects of articular cartilage. J Bone Joint Surg 75:532–553. https://doi.org/10.2106/00004623-199304000-00009

Singh A, Haris M, Cai K et al (2012) Chemical exchange saturation transfer magnetic resonance imaging of human knee cartilage at 3 T and 7 T. Magn Reson Med 68:588–594. https://doi.org/10.1002/mrm.23250

van der Sluijs JA, Geesink RG, van der Linden AJ et al (1992) The reliability of the Mankin score for osteoarthritis. J Orthop Res 10:58–61. https://doi.org/10.1002/jor.1100100107

Sonin AH, Pensy RA, Mulligan ME, Hatem S (2002) Grading articular cartilage of the knee using fast spin-echo proton density-weighted MR imaging without fat suppression. Am J Roentgenol 179:1159. https://doi.org/10.2214/ajr.179.5.1791159

Steadman JR, Rodkey WG, Singleton SB, Briggs KK (1997) Microfracture technique for full-thickness chondral defects: technique and clinical results. Oper Tech Orthop 7:300–304. https://doi.org/10.1016/S1048-6666(97)80033-X

Subhas N, Freire M, Primak AN et al (2010) CT arthrography: in vitro evaluation of single and dual energy for optimization of technique. Skelet Radiol 39:1025–1031. https://doi.org/10.1007/s00256-010-0932-2

Theologis AA, Schairer WW, Carballido-Gamio J et al (2012) Longitudinal analysis of T1ρ and T2 quantitative MRI of knee cartilage laminar organization following microfracture surgery. Knee 19:652–657. https://doi.org/10.1016/j.knee.2011.09.004

Trattnig S, Mlynárik V, Huber M et al (2000) Magnetic resonance imaging of articular cartilage and evaluation of cartilage disease. Investig Radiol 35:595–601. https://doi.org/10.1097/00004424-200010000-00006

Trattnig S, Pinker K, Krestan C et al (2006) Matrix-based autologous chondrocyte implantation for cartilage repair with Hyalograft®C: two-year follow-up by magnetic resonance imaging. Eur J Radiol 57:9–15. https://doi.org/10.1016/j.ejrad.2005.08.006

Trattnig S, Burstein D, Szomolanyi P et al (2009) T1(Gd) gives comparable information as Delta T1 relaxation rate in dGEMRIC evaluation of cartilage repair tissue. Investig Radiol 44:598–602. https://doi.org/10.1097/rli.0b013e3181b4c236

Trattnig S, Winalski CS, Marlovits S et al (2011) Magnetic resonance imaging of cartilage repair: a review. Cartilage 2:5–26

Vega SL, Kwon MY, Burdick JA (2017) Recent advances in hydrogels for cartilage tissue engineering. Eur Cell Mater 33:59–75. https://doi.org/10.22203/eCM.v033a05

Verstraete KL, Almqvist KF, Verdonk P et al (2004) Magnetic resonance imaging of cartilage and cartilage repair. Clin Radiol 59:674–689. https://doi.org/10.1016/j.crad.2004.01.012

Waldt S, Bruegel M, Ganter K et al (2005) Comparison of multislice CT arthrography and MR arthrography for the detection of articular cartilage lesions of the elbow. Eur Radiol 15:784–791. https://doi.org/10.1007/s00330-004-2585-9

Watanabe A, Boesch C, Anderson SE et al (2009) Ability of dGEMRIC and T2 mapping to evaluate cartilage repair after microfracture: a goat study. Osteoarthr

Cartil 17:1341–1349. https://doi.org/10.1016/j.joca.2009.03.022

Welsch GH, Mamisch TC, Marlovits S et al (2009a) Quantitative T2 mapping during follow-up after matrix-associated autologous chondrocyte transplantation (MACT): full-thickness and zonal evaluation to visualize the maturation of cartilage repair tissue. J Orthop Res 27:957–963. https://doi.org/10.1002/jor.20835

Welsch GH, Mamisch TC, Quirbach S et al (2009b) Evaluation and comparison of cartilage repair tissue of the patella and medial femoral condyle by using morphological MRI and biochemical zonal T2 mapping. Eur Radiol 19:1253–1262. https://doi.org/10.1007/s00330-008-1249-6

Welsch GH, Trattnig S, Domayer S et al (2009c) Multimodal approach in the use of clinical scoring, morphological MRI and biochemical T2-mapping and diffusion-weighted imaging in their ability to assess differences between cartilage repair tissue after microfracture therapy and matrix-associated autologous chondrocyte transplantation: a pilot study. Osteoarthr Cartil 17:1219–1227. https://doi.org/10.1016/j.joca.2009.03.018

Welsch GH, Zak L, Mamisch TC et al (2009d) Three-dimensional magnetic resonance observation of cartilage repair tissue (MOCART) score assessed with an isotropic three-dimensional true fast imaging with steady-state precession sequence at 3.0 tesla. Investig Radiol 44:603–612. https://doi.org/10.1097/rli.0b013e3181b5333c

Wheaton AJ, Casey FL, Gougoutas AJ et al (2004) Correlation of T1rho with fixed charge density in cartilage. J Magn Reson Imaging 20:519–525. https://doi.org/10.1002/jmri.20148

Winalski CS, Minas T (2000) Evaluation of chondral injuries by magnetic resonance imaging: repair assessments. Oper Tech Sport Med 8:108–119. https://doi.org/10.1053/otsm.2000.6577

Wolff SD, Chesnick S, Frank JA et al (1991) Magnetization transfer contrast: MR imaging of the knee. Radiology 179:623–628. https://doi.org/10.1148/radiology.179.3.2027963

Wong WD, Shah S, Murray N et al (2018) Advanced musculoskeletal applications of dual-energy computed tomography. Radiol Clin N Am 56:587–600. https://doi.org/10.1016/j.rcl.2018.03.003

Xia Y, Moody JB, Burton-Wurster N, Lust G (2001) Quantitative in situ correlation between microscopic MRI and polarized light microscopy studies of articular cartilage. Osteoarthr Cartil 9:393–406. https://doi.org/10.1053/joca.2000.0405

Yulish BS, Montanez J, Goodfellow DB et al (1987) Chondromalacia patellae: assessment with MR imaging. Radiology 164:763–766. https://doi.org/10.1148/radiology.164.3.3615877

Basic Imaging Principles of Tendons and Ligaments

R. Bakewell, E. L. Gerety, and A. J. Grainger

Contents

Abstract

Tendons and ligaments may be subject to acute or chronic sports-related injury. This chapter reviews the structural properties of tendons and ligaments that give rise to their unique imaging features and account for patterns of injury seen. The superb soft tissue contrast offered by ultrasound and MRI make them the most widely used imaging modalities for assessing tendons and ligaments, with the dynamic capabilities of ultrasound being particularly advantageous. We describe the important imaging features of normal tendons and ligaments and show examples of acute and chronic injuries. The chapter will also review the role radiographs and CT play in assessment of tendon and ligament injuries, particularly with reference to avulsion fractures and malalignment following ligament rupture. In some cases arthrography may better demonstrate the integrity of ligaments around a joint and this along with novel techniques such as elastography and dual energy CT are also discussed.

1 Introduction

Tendons and ligaments are vulnerable to sports-related injuries by both acute high-impact injury, due to traumatic incidents, and by chronic

R. Bakewell · E. L. Gerety
Department of Radiology, Cambridge University Hospitals NHS Foundation Trust, Cambridge, UK
e-mail: Robert.bakewell@addenbrookes.nhs.uk; Emma-louise.gerety@addenbrookes.nhs.uk

A. J. Grainger (✉)
Department of Radiology, Cambridge University Hospitals NHS Foundation Trust, Cambridge, UK

Department of Radiology, University of Cambridge, Cambridge Biomedical Campus, Cambridge, UK
e-mail: Andrewgrainger@nhs.net

Med Radiol Diagn Imaging (2020)
https://doi.org/10.1007/174_2020_249, © Springer Nature Switzerland AG
Published Online: 08 December 2020

low-impact repetitive strain injury. Depending on the sport, different tendons and ligaments will be affected, with lower limb, weight-bearing injuries prevalent in almost all sports and upper limb injuries more commonly in overarm sports such as racket and throwing sports and swimming. The structure of tendons and ligaments makes them well suited to distribute mechanical loads between bones (ligaments) or between bone and muscles (tendons) and these properties affect their appearance with different imaging modalities.

1.1 Tendons

Tendons connect muscle to bone and are of high tensile strength, transferring forces generated within the muscle to the bone. They comprise collagen molecules in a triple helix structure that is linked by hydrogen bonds (Ramachandran and Chandrasekharan 1968; Rich and Crick 1955, 1961). Collagen type I is the predominant collagen in tendons, with collagen type III being the second most abundant. Groups of five collagen molecules form pentafibrils/microfibrils which pack together to form fibrils. Collagen fibrils are hierarchically organized into fibres and fascicles that are arranged parallel to the long axis of the tendon (Kastelic et al. 1978). This structural arrangement leads to direction-dependency or 'anisotropy' of the mechanical characteristics of tendons and ligaments, which is reflected in their imaging appearances. The orientation of the fibres in tendons and ligaments is also affected by the direction of the forces to which they are submitted (Wang et al. 2012). Tendons are able to adapt to stresses to which they are subjected and have been shown to undergo fibrocartilaginous metaplasia at the point of stress (Wren et al. 2000).

The collagen fibres are interspersed with a ground matrix containing proteoglycans and glycoproteins, forming a fibre composite (McKee et al. 2019). Fascicles are surrounded by connective tissue, the interfascicular matrix or endotenon. Epitenon, which is continuous with the interfascicular matrix, covers the tendon surface. Tendons are further covered by loose connective tissue. Paratenon facilitates tendon movement in those tendons immediately deep to the skin, for example, the Achilles tendon. Tendons which pass over or around joints are surrounded by a synovial sheath to enable smooth gliding, for example, the peroneal tendons.

The tendon connects to the muscle at the myotendinous junction where the tendon collagen fibres interdigitate with the muscle cell membrane (sarcolemma). This increases the surface area of the attachment to distribute the forces generated by the muscle (Thorpe and Screen 2016). The connection between the tendon and the bone takes place at the enthesis, which may be fibrous or fibrocartilaginous (Thorpe and Screen 2016).

Mature tendons do not normally have internal vascularity, but receive vascular supply through the paratenon, vincula and via the osseotendinous and musculotendinous junctions. The vascular supply of a tendon may vary along its length making different areas more susceptible to injury; for example, the critical zone of the Achilles tendon is the most poorly vascularized zone, approximately 6 cm from the calcaneal insertion, and is particularly vulnerable to injury (Chen et al. 2009). Chronically damaged tendons undergo neovascularization, which may be imaged as indicator of tendinopathy (Jarvinen 2020).

Acute injuries may affect the myotendinous junction, the tendon itself or the enthesis. In children and adolescents, apophyseal avulsion injuries may occur where the weakest connection is at the ossification centre of the developing enthesis. In adults, myotendinous junction injuries are more common, while in older patients injuries to the ageing tendon become more common (Tadros et al. 2018). Nucleotide polymorphisms within the genes encoding the proteins that form tendons contribute to altered propensity to injury (Brazier et al. 2019). Age-related changes in tendons and ligaments also affect response to injury (McCarthy and Hannafin 2014). For example, experimental models have demonstrated increased straightness of collagen fibres in old tendons (Van Gulick et al. 2019) and decreased water content (Ishigaki and Kubo 2019). Tendons may also be affected by drugs; for example, there is an increased risk of tendon rupture in patients taking fluoroquinolone antibiotics (Arabyat et al. 2015) and statins (Deren et al. 2016; Marie et al. 2008).

Chronic, repetitive injury or training regimes may result in degenerative changes in the tendon (tendinosis) and/or inflammation in its paratenon (paratenonitis) or synovial sheath (tenosynovitis). The most common tendon injuries at the 2016 Olympics included the supraspinatus, Achilles and patella tendons (Jarraya et al. 2018); however, any tendon may be affected, depending on the sport. Many risk factors have been identified for chronic, repetitive tendon injury including type and volume of training, environmental factors, medications and intrinsic factors, such as age, biomechanics and adiposity (Scott et al. 2015). Bursae are frequently associated with tendons at risk of impingement and play a protective role. Where no bursa exists, chronic inflammation may lead to the development of adventitial bursae. Inflammation and irritation of these bursae leads to bursitis. Bursal inflammation may occur at sites of irritation, for example, retrocalcaneal bursitis between the calcaneus and the Achilles tendon insertion (Chang and Wu 2017).

1.2 Ligaments

Whereas tendons connect muscle to bone, ligaments connect different bones to provide stabilization and distribution of mechanical forces. They restrict and guide movement at joints. Infrequently ligaments are described that connect bone to another ligament, for instance the tibiospring ligament at the ankle and radial collateral ligament at the elbow. Ligaments have a higher proteoglycan and water content compared to tendons, with lower collagen content (reviewed by McKee et al. (McKee et al. 2019)). Ligaments may have different compositions depending on their mechanical properties, as recently demonstrated for ligaments of the ankle (Rein et al. 2015). The internal structure of ligaments is less ordered than in tendons, with an interlaced, weaving pattern. Like tendons, ligaments are covered by a thin layer of external connective tissue, the epiligament.

Ligaments range in size from the large cruciate and collateral ligaments in the knee to tiny ligaments of the hands and feet. Ligament sprain or rupture usually results from acute traumatic sports injuries. The most commonly injured ligaments are those of the ankle and knee; however upper limb ligament injuries are common in overhead throwing athletes. Interestingly a higher prevalence of tendon injuries was shown in athletes at the 2016 Summer Olympics compared to ligament injuries, although many pre-existing ligament injuries were demonstrated (Heiss et al. 2019).

2 Imaging of Tendons and Ligaments

Ultrasound and MRI are the main imaging modalities for tendons and ligaments (Hodgson et al. 2012). However, radiographs and CT also have a limited role for assessing tendon/ligament avulsion fractures and secondary effects of tendon or ligament injury.

2.1 Ultrasound Imaging

Ultrasound imaging plays a key role in the diagnosis and treatment of ligament and tendon injuries. The ability to perform point of care, real-time imaging with high resolution, as well as being able to guide intervention, means that ultrasound is well placed for the assessment of sports injuries (Hodgson et al. 2012; Allen 2018). The superficial location of the vast majority of ligaments and tendons means that high-frequency linear transducers (12–20 MHz) can be used to interrogate internal structure in superb detail. Lower frequency ultrasound has better depth penetration but results in lower resolution images. Brightness mode (B mode) ultrasound delineates anatomy and identifies disruption of normal architecture with high sensitivity. Colour Doppler modes are used to detect changes in blood flow that occur in inflamed and degenerative tissue. All these attributes, as well as widespread availability and relative low cost, mean that ultrasound imaging has become the first-line modality for the assessment of the majority of superficial ligament and tendon injuries in athletes (Baloch et al. 2018).

Due to the parallel fibre alignment in tendons, ultrasound appearances are of parallel echogenic

lines when imaging tendons longitudinally (Fig. 1a, c, e). When imaging in transverse, multiple tiny dots are demonstrated as the fibres are seen in cross section (Fig. 1b, d, f). Due to their uniform, parallel fascicular structure, both tendons and ligaments demonstrate anisotropy (Robinson 2009). When the ultrasound beam is perpendicular to the tendon or ligament, the structure appears brightest, but slight changes in insonation angle can produce hypoechoic areas within the tendon, and therefore careful positioning is necessary to avoid artefact. Ligaments tend to be less echo-

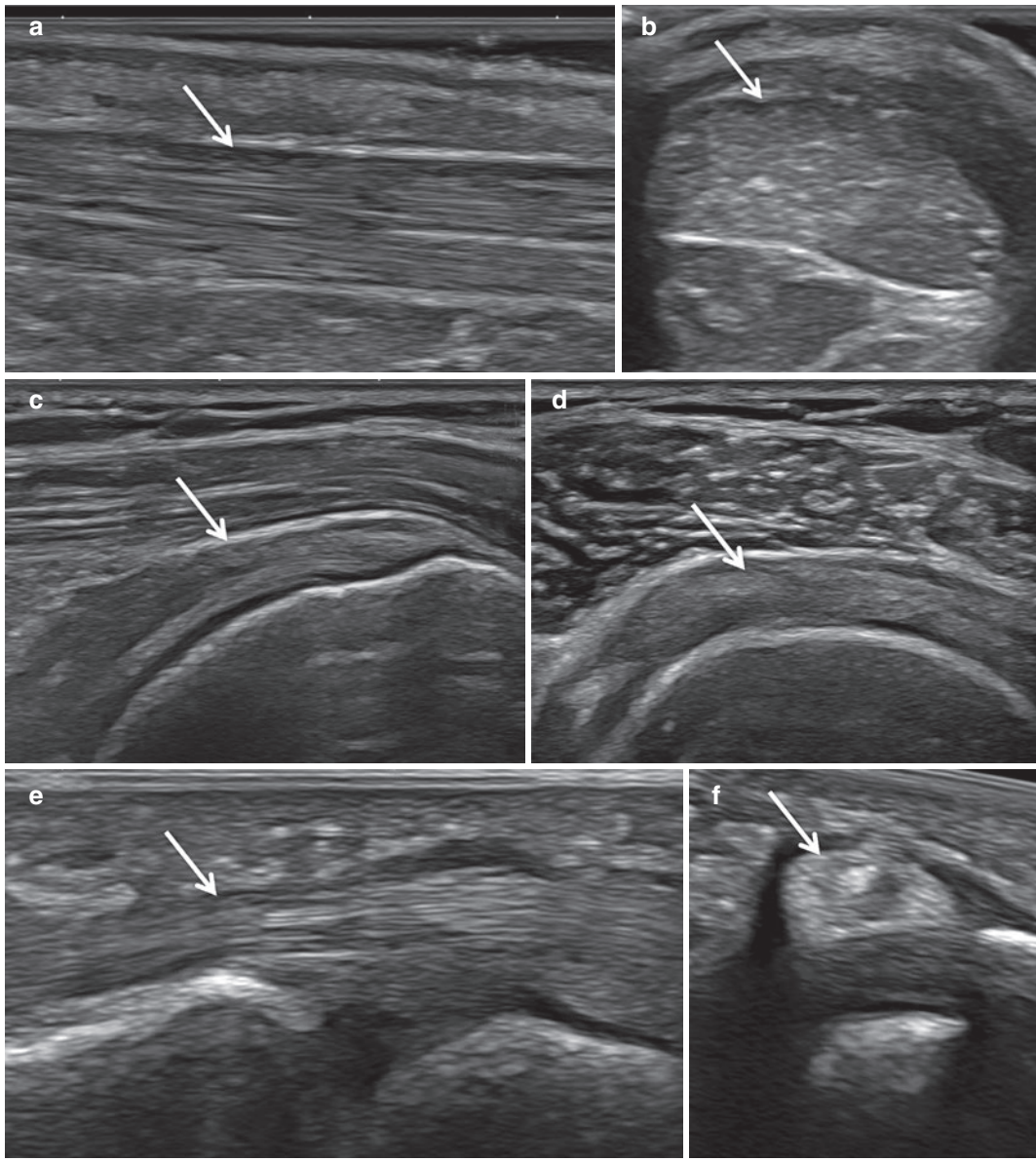

Fig. 1 Ultrasound images of normal tendons with appearance of parallel, hyperechoic lines when imaged longitudinally and hyperechoic dots when imaged transversely. (**a**) Achilles tendon imaged longitudinally (arrow). (**b**) Achilles tendon imaged transversely (arrow). (**c**) Supraspinatus insertion imaged longitudinally (arrow). (**d**) Supraspinatus tendon imaged transversely (arrow) and long head of biceps tendon anteriorly (to the left). (**e**) Little finger flexor at PIPJ imaged longitudinally (arrow). (**f**) Little finger flexor imagined transversely (arrow)

genic than tendons due their more complex fibrillar structure. However, when aligned to the collagen bundles, the parallel fibre alignment leads to a similar ultrasound appearance.

Doppler ultrasound utilizes the shift in frequency of returning echoes to detect movement, and therefore is a key sonographic tool to assess blood flow. Colour Doppler techniques are vital in the assessment of inflammation and neovascularization of tendons. Healthy tendons display a low level of vascularity (at least at a level detectable with current imaging techniques) and therefore detection of excess blood flow within a tendon is a useful marker of inflammation. Chronic injury may lead to neovascularization within the tendon, which can disrupt the usual structure, impair healing and contribute to degeneration (Tempfer and Traweger 2015).

Tendinosis results in tendon thickening, oedema (low echogenicity fluid within and surrounding the tendon), and high vascularity on Doppler imaging (Fig. 2). Fluid is anechoic (black) on B-mode ultrasound and its presence around a ligament or tendon should always be viewed with suspicion. Paratenonitis appears on ultrasound as a thickened and oedematous paratenon with increased vascularity. Tendon tears appear as hypoechoic areas within the parallel hyperechoic fibres, often with focal tendon thickening at the site of the tear and surrounding oedema. In a full-thickness tear discontinuity of the tendon is seen and there is usually significant surrounding fluid/haematoma (Fig. 3). The ends of the tendon are often separated due to retraction, but, in cases of minimal retraction or intervening haematoma, dynamic assessment of the tendon can help whether a tear is partial or full thickness.

As a caveat, recent research has shown that in certain athletes tendons may develop an abnormal sonographic appearance despite there being no symptoms or functional deficit. For instance, a recent study found the flexor hallucis longus of

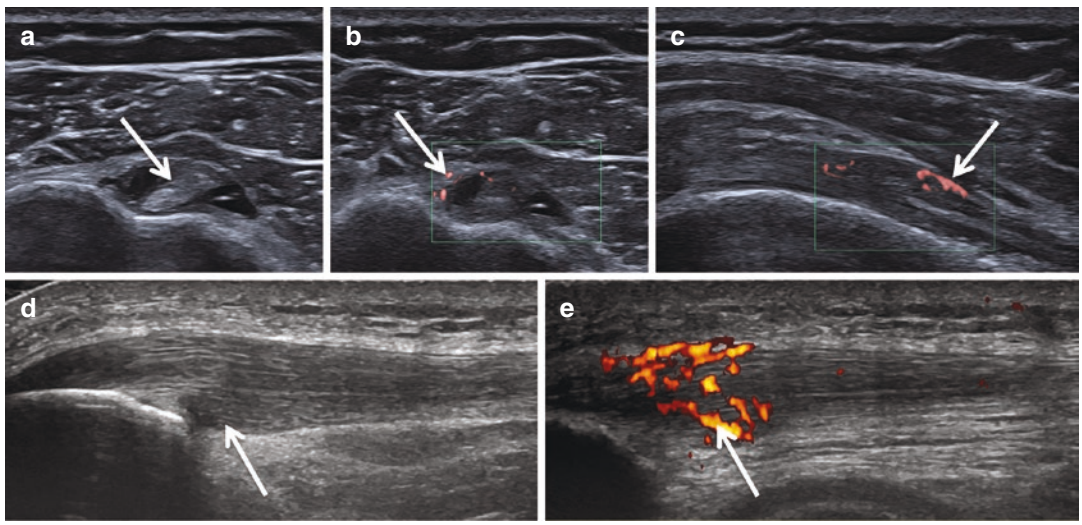

Fig. 2 Chronic tendinosis of the long head of biceps and proximal patella tendons. (**a**) Transverse image of the long head of biceps tendon (arrow) with surrounding peritendinous fluid (*). (**b**) Doppler image demonstrating tenosynovial hypervascularity (arrow). (**c**) Longitudinal Doppler image of the long head of biceps tendinosis and tenosynovitis (arrow). (**d**) Longitudinal image of a thickened proximal patellar tendon with reduced reflectivity (arrow) representing tendinosis. (**e**) Longitudinal Doppler image demonstrating proximal hypervascularity (arrow) in patellar tendinosis

asymptomatic ballet dancers to be thickened, despite normal appearance of the remainder of the tendons of the foot (Shih et al. 2019). This was found to be associated with vascular compromise to the great toe during forced active plantar flexion of the 'en pointe' position.

The Achilles tendon is one of the most commonly affected tendons in sports medicine, both acutely and chronically (Fig. 4). It is formed from the tendons of the gastrocnemius and soleus, and passes along the posterior aspect of the ankle to insert into the calcaneus. Anterior to the distal Achilles, between the tendon and calcaneus, lies the retrocalcaneal bursa which may become inflamed in bursitis (Fig. 4c). The retro-Achilles bursa is seen posterior to the tendon at the same level. Ultrasound demonstrates the healthy Achilles to be a tightly packed fibrillar tendon

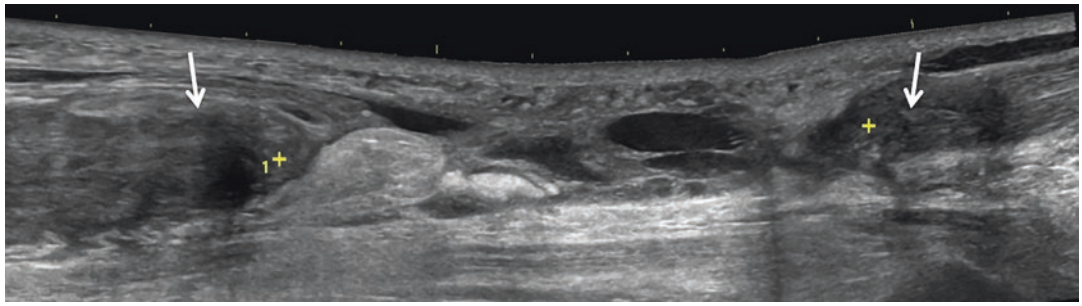

Fig. 3 Ultrasound images of acute Achilles tendon rupture. Achilles tendon rupture imaged longitudinally with proximal and distal stumps indicated by arrows and intervening haematoma (+ represent calipers to measure the tendon gap, in this case 6 cm)

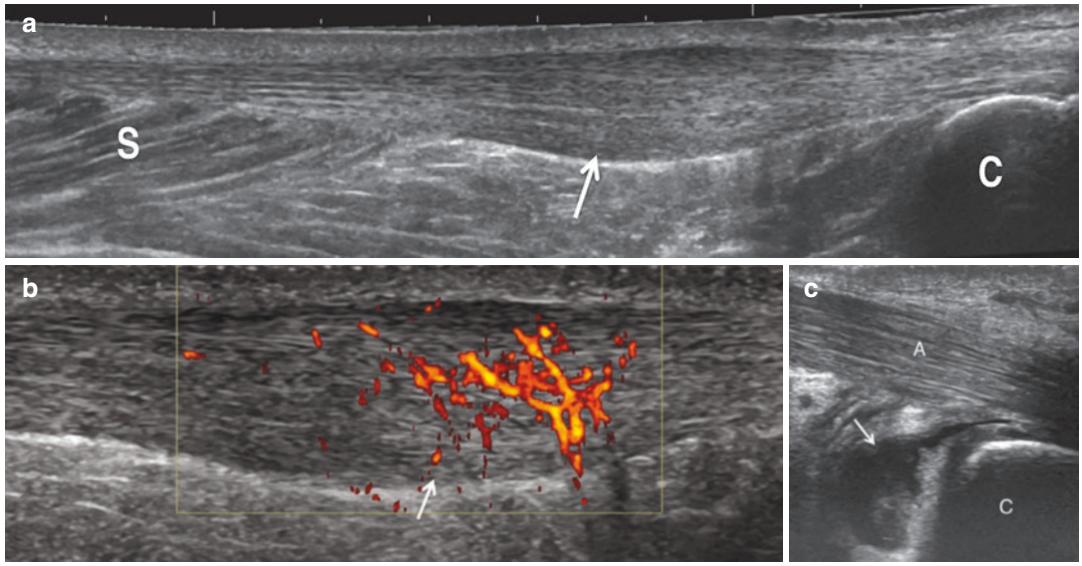

Fig. 4 Ultrasound images of chronic Achilles tendinosis. (**a**) Longitudinal image of the Achilles tendon with fusiform distal thickening (arrow, C = calcaneus, S = soleus muscle). (**b**) Doppler image demonstrating hypervascularity in the thickened region (arrow). (**c**) Retrocalcaneal bursitis deep to the Achilles tendon (arrow, A = Achilles tendon, C = calcaneus)

surrounded by a paratenon with no appreciable Doppler signal and a straight or concave anterior border. As this tendon is placed under considerable strain during exercise, injury due to chronic use or acute trauma is common in athletes. Imaging findings follow the same patterns as most other tendons, with thickening (loss of concavity of the anterior border), increased Doppler signal and hypoechoicity seen on ultrasound in cases of tendinopathy (Fig. 4a, b). Doppler ultrasound may be used to track healing of the injured Achilles tendon (Liu et al. 2017). Paratenonitis is also appreciated with ultrasound as thickening of the hypoechoic layer that surrounds the tendon. Tears may be partial or complete, and most commonly occur in a region approximately 5 cm from the calcaneus (Thevendran et al. 2013). In the case of a complete tear, ultrasound can be used to determine the site of the injury and length of separation of the tendon, both important in guiding management (Fig. 3a).

The real-time nature of ultrasound allows dynamic imaging of ligaments and tendons, enabling the assessment of function. Sonopalpation may be used to identify anatomical landmarks and abnormalities at the site of maximum pain, for example, in the assessment of intersection syndromes at the wrist (Draghi and Bortolotto 2014) and in assessment of greater trochanteric pain syndrome (Chowdhury et al. 2014). The patient may be asked to move into a position to optimize imaging of individual tendons, for example, the tendons of the four rotator cuff muscles are best imaged with the shoulder in specific positions to optimize their assessment (Lee et al. 2016). Features of subacromial impingement may be elicited during dynamic scanning of the supraspinatus tendon as it passes under the acromion. Ultrasound has been found to be of similar diagnostic accuracy to MRI and MRI arthrography for characterizing rotator cuff tears (Roy et al. 2015).

Dynamic imaging of tendon movement and glide with patient movements can also be examined using ultrasound, which is helpful where mechanical symptoms are to be evaluated, for example, in the assessment of the 'snapping hip' (Lungu et al. 2018; Yen et al. 2015). External hip snapping occurs when the iliotibial band or gluteus maximus transiently impinges on the greater trochanter on flexion of the hip and then, when released, produces a snapping sound as it passes over the lateral facet of the greater trochanter. This impingement and release can be seen on ultrasound. Iliopsoas snapping is most commonly due to flicking of the iliopsoas tendon around the iliacus muscle (Deslandes et al. 2008). Again, dynamic ultrasound with the patient flexing, externally rotating and then extending their hip in a circling motion may demonstrate the abnormal iliopsoas tendon motion.

Ultrasound is also a key tool for the dynamic assessment of ligaments, as mechanical integrity can be assessed by stressing the joint while imaging the ligament of interest. For example, the anterior talofibular ligament (ATFL) is one of the most commonly injured ankle ligaments, and damage is a leading cause of ankle instability. Ultrasound of the ligament with the foot placed in maximal inversion and plantarflexion allows a detailed assessment of the ligament structure as well as function (Doring et al. 2018; Kristen et al. 2019) (Fig. 5a). If the ligament does not tense with the foot placed in this position, ATFL injury can be suspected (Fig. 5b.).

Contrast-enhanced ultrasound imaging allows real-time assessment of blood flow by imaging the passage of intravenously administered microbubbles through tissues. Through the use of these contrast agents, tendon vascularity undetectable by conventional Doppler techniques has been more readily identified, for example, in the Achilles tendon (Genovese et al. 2011). Detection of tenosynovitis may also be improved through the use of microbubbles, which may allow earlier detection of inflammation in and around the tendon, to enable earlier treatments and quicker recovery for athletes (Klauser et al. 2010). Contrast-enhanced ultrasound imaging has also been investigated for evaluation of rotator cuff

tears by injection of microbubbles into the shoulder (Tang et al. 2019), for the investigation of impingement syndrome by injection of microbubbles into the subacromial bursa (Cheng et al. 2015) and for assessing vascularity of rotator cuff repairs (Adler et al. 2011). Contrast-enhanced ultrasound imaging in tendon/ligament injury has yet to be validated for clinical use; however it has widespread use in other areas of medical imaging and has been shown to have a good safety profile.

Ultrasound elastography is an advanced imaging technique that has recently shown clinical promise for the evaluation of tendon and ligament injuries (Domenichini et al. 2017). There are several differing methods, but the fundamental principle of the technique is to use ultrasound to quantify the stiffness of a tissue. Shear wave elastography produces a high-intensity pulse to generate shear waves that are transmitted perpendicular to those used for standard B mode imaging (Davis et al. 2019; Ryu and Jeong 2017; Taljanovic et al. 2017). Their transmission is detected and allows evaluation of the 'shear modulus', which is closely related to tissue stiffness. This technique has shown that the elasticity of the ruptured Achilles tendon is reduced and more heterogeneous compared to normal tendon (Chen et al. 2013). Similarly, in tendinopathy, the elasticity of the tendon reduces, which is readily detected using the shear wave method (Aubry et al. 2015; Dirrichs et al. 2016) (Fig. 6). Strain elastography utilizes freehand transducer compression to apply stress and generate a relative strain map of the tissue reflecting the relative stiffness within different areas of the tissue.

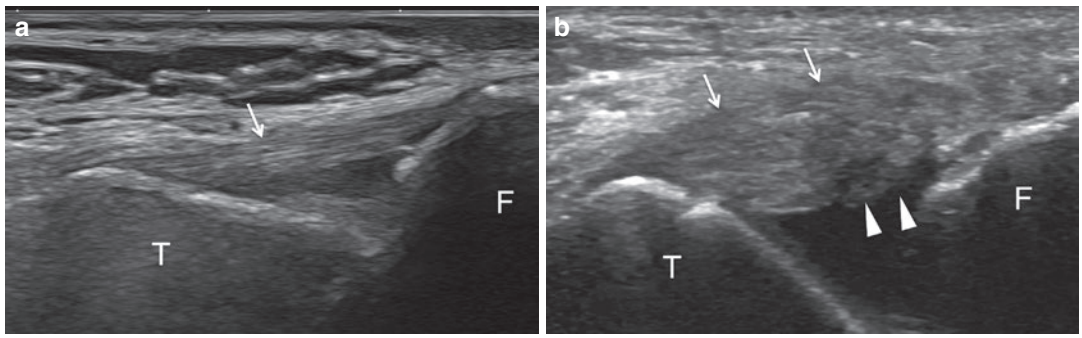

Fig. 5 Ultrasound images of normal and sprained anterior talofibular ligaments (T = talus, F = lateral malleolus of fibula). (**a**) Normal, organized appearance of the anterior talofibular ligament (arrow). (**b**) Thickened anterior talofibular ligament (arrows) with deep surface tearing (arrowheads) in keeping with partial-thickness disruption

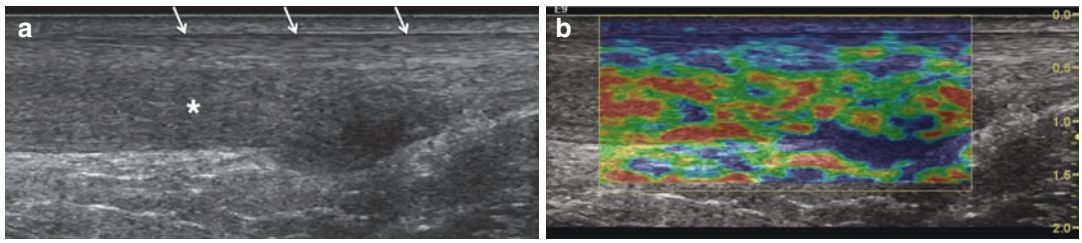

Fig. 6 Ultrasound elastography of Achilles tendinosis. (**a**) B-mode longitudinal image of the thickened Achilles tendon showing superficial normal fibres (arrows) and loss of the normal fibrillar architecture in the deeper fibres (*). (**b**) Elastography: blue represents firm tissue, red represents soft tissue. Observe that the more normal superficial fibres appear generally firm, while the deeper fibres showing tendinosis are of softer consistency

Strain elastography has shown promise in imaging of tendinosis with good correlation with histological evaluation of tendinosis in cadaveric tissue (Klauser et al. 2013) and has been investigated in evaluation of in vivo rotator cuff, patellar and Achilles tendinopathy (Brage et al. 2019; Ooi et al. 2016, 2015). While ultrasound elastography is not currently in widespread clinical use, the ability to objectively quantify changes in tendon stiffness may be a valuable tool in both diagnosis and follow-up of athletes with tendinopathy.

2.2 Magnetic Resonance Imaging (MRI)

MRI is a powerful tool for the imaging of tendons and ligaments, enabling high-resolution imaging of soft tissues with a wider field of view in a single image than for ultrasound imaging (Hodgson et al. 2012). Once appropriate imaging protocols have been established, MRI is less operator dependent than ultrasound imaging. However only static images are acquired and high-quality imaging relies on the patient remaining still during acquisition times of up to 4 min. Ultrasound allows the demonstration of the fine internal architecture of a tendon, showing its fibrillar structure, while conventional MRI shows the normal tendon to be void of signal with no internal architecture. However MRI is less influenced by the depth and orientation of the tendon and readily shows tendons such as the distal insertion of the biceps brachii or iliopsoas which can be challenging to show on ultrasound. In most cases, the choice of ultrasound imaging or MRI comes down to a question of local availability/expertise and clinician/radiologist preference.

MRI is of particular use in sports-related injuries of the hip, due to the deep location of the tendons and prevalence of tendon and myotendinous injuries in young athletes, particularly the hip flexors and hamstring tendons (Pesquer et al. 2016; Shabshin et al. 2005). Tears of the rectus femoris at the deep myotendinous junction may display the 'bull's-eye' sign on MRI (Gyftopoulos et al. 2008). MRI can well demonstrate the multiple tendons of the wrist simultaneously, which may be particularly affected in those participating in racket sports, golf, rowing and gymnastics, with the first extensor compartment and extensor carpi ulnaris tendons most commonly affected (Bancroft 2013; Llopis et al. 2019). However, the significance of abnormal MRI findings in tendons must be carefully considered and a recent paper reported finding features of tendinosis, partial- and full-thickness rotator cuff tears in asymptomatic individuals (Splittgerber and Ihm 2019).

While ultrasound has the ability to assess ligaments dynamically, MRI has advantages for ligaments where ultrasound visualization is prevented by overlying bone. The most frequently injured ligaments are those of the knee, the cruciate and collateral ligaments. Although the collateral ligaments may be imaged by ultrasound, the cruciate ligaments can only be reliably imaged by MRI due to their location in the intercondylar notch surrounded by bone. Many studies have demonstrated the good correlation between MRI and arthroscopy findings (Ruzbarsky et al. 2017). Ankle ligaments are well demonstrated by MRI as well as ultrasound (Perrich et al. 2009). Sports-related injuries of the wrist by either high- or low-impact sports may involve both the intrinsic and extrinsic ligaments and MRI arthrography may increase sensitivity for tears (Bancroft 2013).

Standard musculoskeletal imaging protocols acquire T1-weighted images, with high signal intensity for fat, proteinaceous fluid, melanin and haemorrhage, and water-sensitive T2-weighted or proton density (pd) images usually with fat suppression (fs). Normal tendons are of low signal on T2-weighted images (Fig. 7). Ligaments may be of low or intermediate signal intensity (Fig. 8). Acute and chronic trauma may result in a change of fibre orientation, hydration or vascularization of tendons and ligaments leading to change of signal intensity, size and/or shape. Water-sensitive sequences demonstrate fluid within a tendon or ligament tear and associated

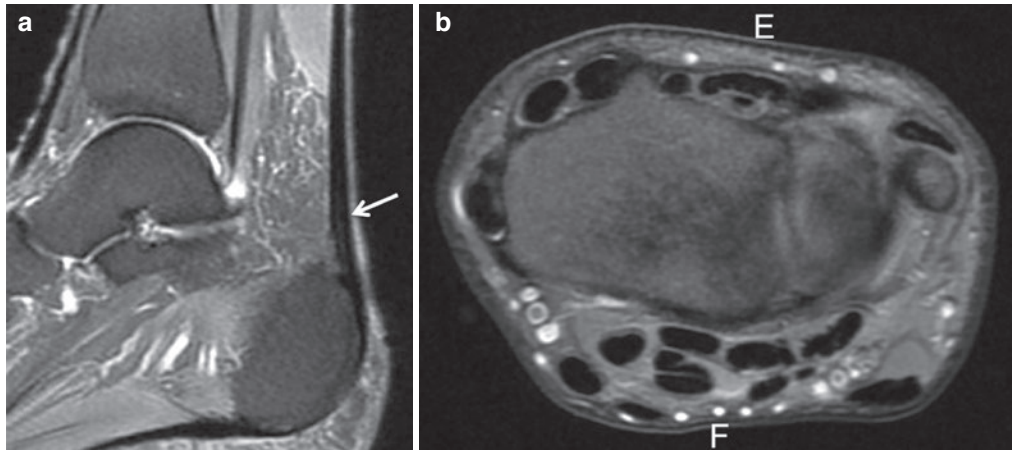

Fig. 7 MR images of normal tendons. (**a**) Achilles tendon (arrow) in longitudinal section in a sagittal proton density, fat-saturated pd fs image of the ankle. (**b**) Wrist tendons in transverse section in an axial pd fs image of the wrist. E = extensor compartments; F = flexor tendons

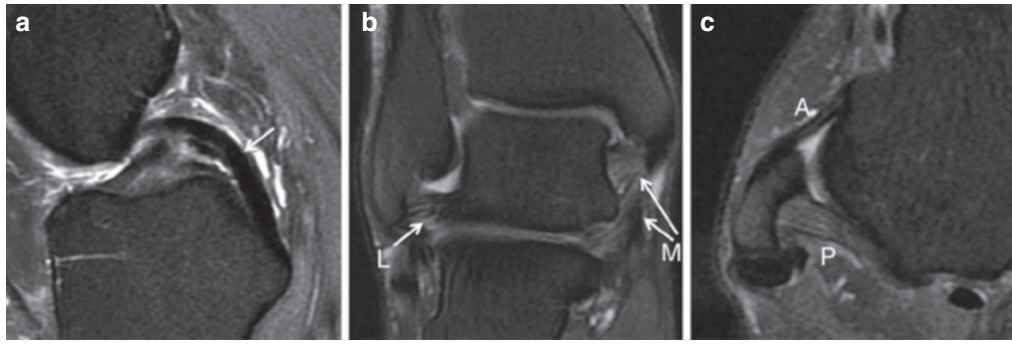

Fig. 8 MR images of normal ligaments. (**a**) Posterior cruciate ligament (arrow) in a sagittal pd fs image of the knee. (**b**) Coronal pd fs image of the medial (M) and lateral (L) ankle ligaments. (**c**) Axial pd fs image of the ankle showing anterior (A) and posterior (P) talofibular ligaments

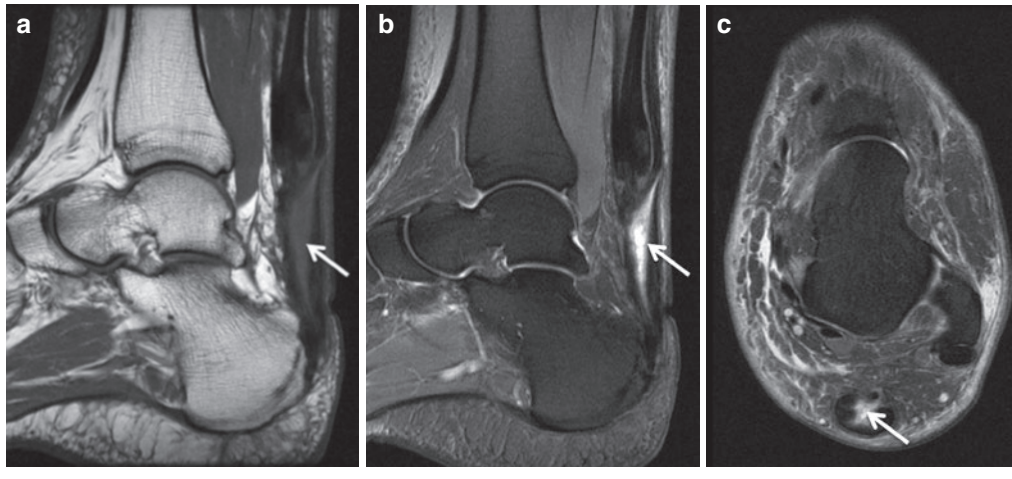

Fig. 9 MRI of acute Achilles tendon rupture (arrow). (**a**) Sagittal T1. (**b**) Sagittal pd fs image. (**c**) Axial pd fs image

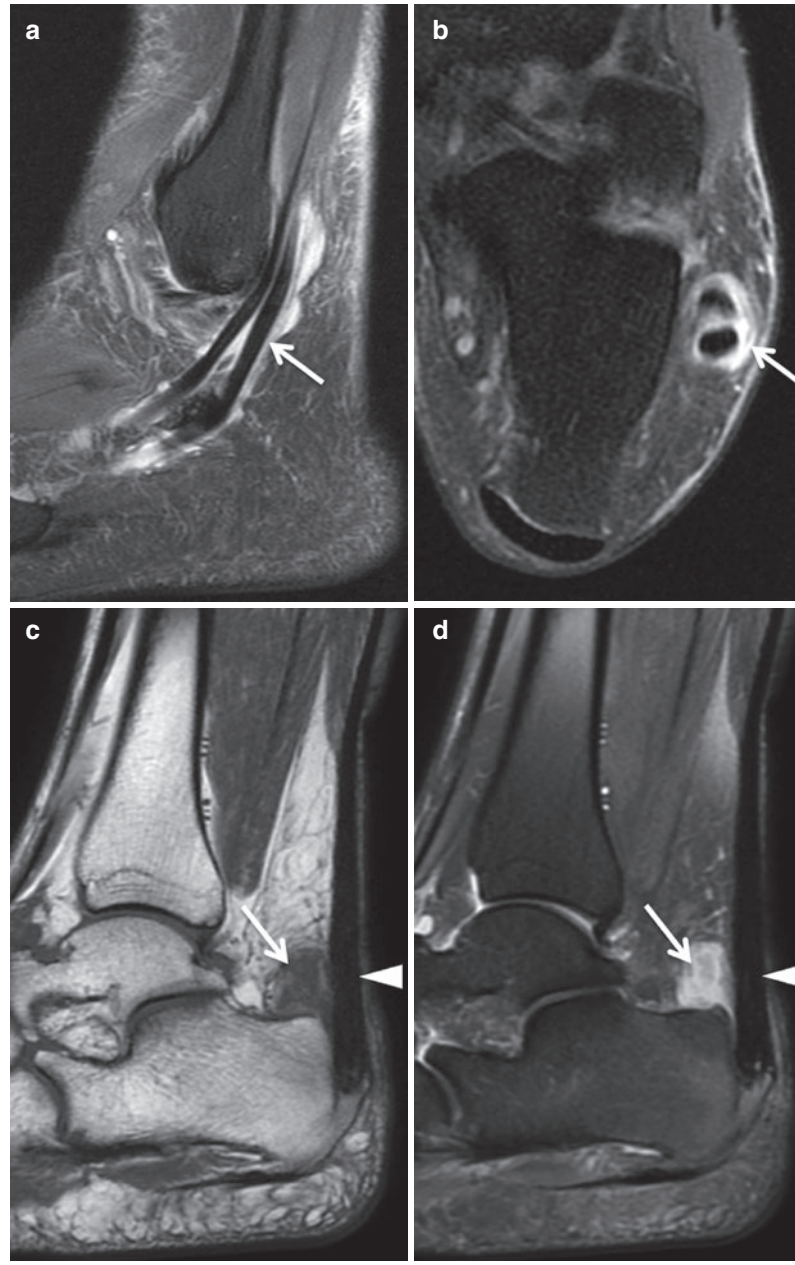

Fig. 10 MRI of chronic peroneal and Achilles tendinopathy. (**a** and **b**) Peroneal tenosynovitis. (**a**) Sagittal pd fs and (**b**) Axial pd fs image showing high T2 signal surrounding the peroneal tendons (arrows) representing fluid and synovitis in the tenosynovial sheath. (**c** and **d**) Achilles tendinosis (arrowhead) and retrocalcaneal bursitis (arrow) shown on (**c**) Sagittal T1-weighted and (**d**) Sagittal pd fs images

soft tissue oedema (Fig. 9). In chronic tendinosis tendons appear thickened and of increased signal on short and long TE imaging, for example, in the peroneal and Achilles tendons (Fig. 10).

Due to the nature of tendons and ligaments, with parallel alignment of collagen fibres and inter-molecular dipole-dipole proton coupling, ultrashort TE imaging (UTE) can be employed and will demonstrate signal from tendons. But the TE of conventional sequences is long compared to the normal T2 relaxation times seen in tendons and ligaments and they consequently

appear dark on conventional short and long TE sequences (Hodgson et al. 2012). However, the signal characteristics are also dependent on the angle at which the collagen fibres are oriented to the static magnetic field. At angles approaching 55° to Bo, tendons may appear artefactually bright on short TE imaging due to this so-called 'magic angle' effect (Fullerton et al. 1985; Fullerton and Rahal 2007). Magic angle effect may become problematic in tendons which change orientation along their course, such as the proximal posterior cruciate ligament in the knee, insertion of the patella tendon on the tibia, supraspinatus and the peroneal tendons as they pass around the lateral malleolus. Effects have recently been found to be underestimated by radiologists (Richardson et al. 2018). Imaging strategies to minimize magic angle effect include lengthening the echo time, incorporating T2w imaging rather than proton density imaging (Ieong et al. 2018) (Fig. 11) or optimizing positioning (Horn et al. 2015).

However, the magic angle effect may also be utilized to increase contrast in tendons by orienting the tendon appropriately to the static magnetic field (Bydder et al. 2007). When tendons are oriented at or near the magic angle, they may exhibit increased signal intensity and this may increase sensitivity for partial ligament tears. Due to difficulties in controlling the orientation of the fibres to the magnetic field, studies have mainly been of cadaveric material. For example, a sixfold variation in signal intensity was demonstrated for goat meniscus at different orientations within the magnetic field (Szeverenyi and Bydder 2011). Research work exploiting magic angle imaging enhancement in a 9.4 T small bore MRI scanner involved development of an MRI-conditional robotic angle positioning platform to optimize magic angle imaging of sheep tendon (Squires et al. 2016). Further studies have investigated tendon fibre orientation in cadaveric human iliotibial tract (Seidel et al. 2013) and animal knees (Chappell et al. 2019).

Higher magnetic field strengths result in greater image resolution and higher signal:noise ratios. Imaging at 3 T may therefore increase sensitivity and resolution compared to imaging at 1.5 T. In 2017, the EU and US approved 7 T MRI for neuroradiology and musculoskeletal radiology applications and recent publications have demonstrated superior resolution in traditionally chal-

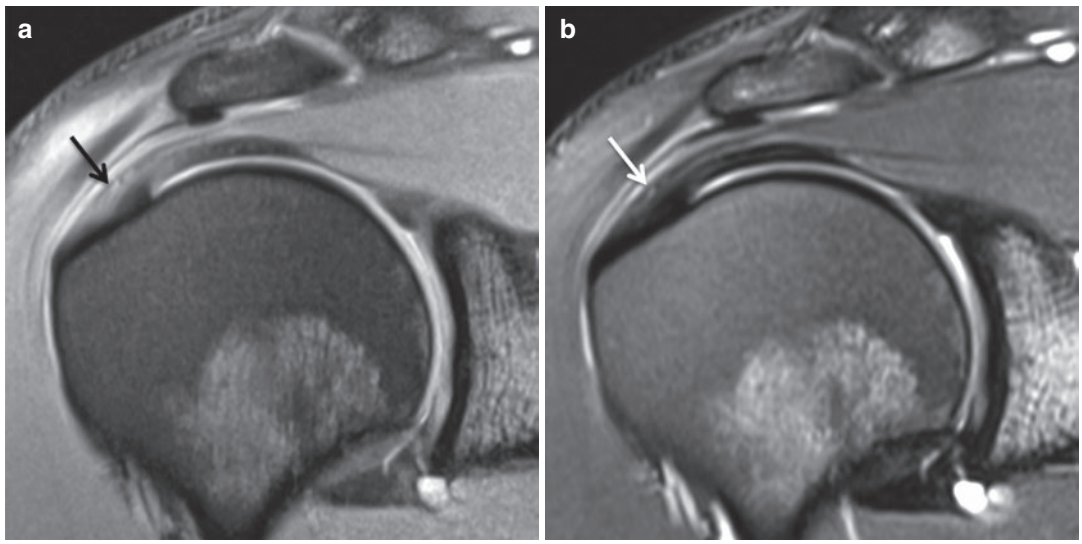

Fig. 11 MR images demonstrating magic angle effect in the supraspinatus tendon. (**a**) Coronal pd fs image of the shoulder. (**b**) T2 fs image of the shoulder. Artefactual high signal in the supraspinatus tendon (arrow) is due to magic angle effect on the proton density, fat-saturated image, improved on the T2 fs image

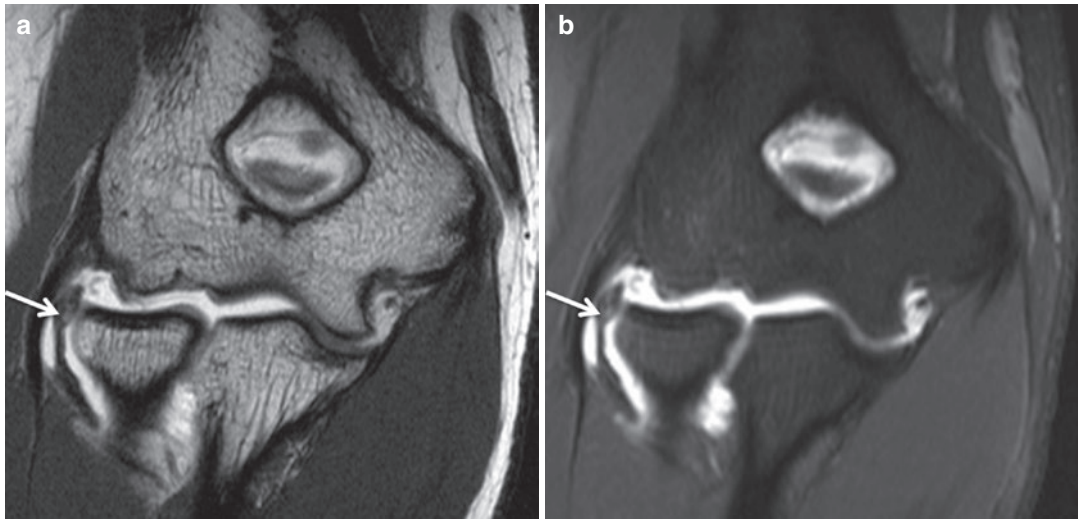

Fig. 12 MRI arthrogram demonstrating tear of the radial collateral ligament complex at elbow. (**a**) Coronal T1 image post intra-articular gadolinium. (**b**) Coronal pd fs image post intra-articular gadolinium

lenging areas such as the finger (Juras et al. 2019; Laistler et al. 2018). Ultra-high magnetic fields greater than 7 T are being used as research tools, for example, of rabbit tendons at 11.7 T (Guidetti et al. 2018) and detailed images have been acquired to further anatomical research of the flexor pulleys in cadaveric toes (Tafur et al. 2015).

MRI has long entailed a trade-off between resolution, signal-to-noise ratio and length of scanning time, with imaging in multiple different planes. However, new 3D volume sequences optimize acquisition of a single data set of isotropic voxels which can be reformatted into any plane and promising studies have been published, for example, imaging of the rotator cuff tendons (Kloth et al. 2014), ankle tendons and ligaments (Kalia et al. 2017) and wrist ligaments (Nozaki et al. 2017).

Gadolinium has minimal role in the imaging of tendons and ligaments although imaging post intra-venous gadolinium can be helpful in distinguishing active tenosynovitis from chronic, burnt out tenosynovitis. MRI arthrography may be helpful to demonstrate subtle injuries to small ligaments such as those at the wrist and elbow (LiMarzi et al. 2015; Magee 2015) (Fig. 12).

Functional MRI mapping the T2 and T2* relaxation times of tissues may be used to assess tissue extracellular fluid content, collagen content and organization. Originally used to assess cartilage, it has also been used to assess tendons, including the Achilles tendon and rotator cuff tendons (Anz et al. 2014; Juras et al. 2013; Krepkin et al. 2017).

Diffusion tensor imaging (DTI) is a specialist technique currently mainly used in research, which uses diffusion weighted imaging techniques (DWI) to evaluate anisotropic structures. The technique was first developed for imaging of white matter tracts in the brain but has recently been used to characterize fibre organization of skeletal muscle and tendons (Guidetti et al. 2018; Wengler et al. 2018). DTI combined with fibre tractography may be used to model 3D reconstructions of tendon and ligament fibres (Chianca et al. 2017).

As for ultrasound imaging, MRI may be used to assess tissue stiffness by MR elastography. A challenge for the development of MR elastography has been the design of MR-compatible vibration pads. Promising results have been published assessing stiffness of the rotator cuff muscles and this is another area of future development in imaging of tendons (Ito et al. 2019).

Fig. 13 Lisfranc ligament avulsion poorly demonstrated by (**a**) radiograph but well demonstrated by (**b** and **c**) CT (arrows) on multiplanar reformatted images in the (**b**) long axis and (**c**) short axis

2.3 Radiographs and CT

Although invaluable for demonstrating bone fractures, radiographs and CT are less useful for demonstrating tendon and ligament injuries. However radiographs should always be considered as first-line imaging in acute sports injuries to rule out a fracture.

Radiographs and CT may be useful in acute sports injuries if there has been a tendon or ligament avulsion. For example, avulsion of the tip of the proximal fibula by the conjoint tendon of the lateral collateral ligament and biceps femoris or avulsion of the tibial attachments of the cruciate ligaments (Gottsegen et al. 2008), or avulsion of the lateral corner of the medial cuneiform or medial aspect of the base of the second metatarsal by the Lisfranc ligament (Llopis et al. 2016) or other foot and ankle ligament avulsions (Fig. 13). Capsular ligament avulsion fracture or

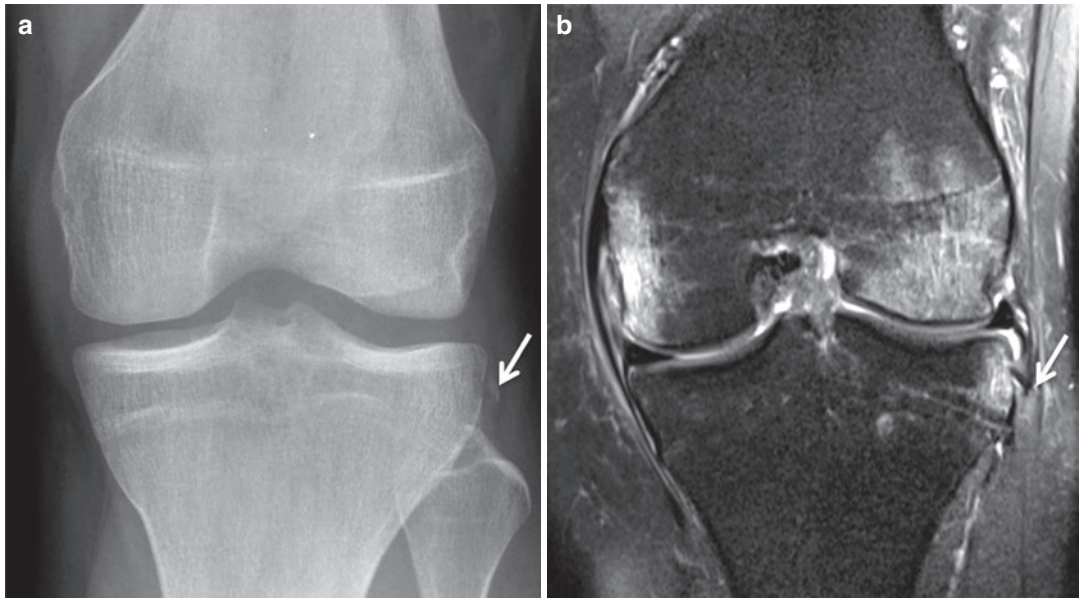

Fig. 14 Segond fracture of lateral aspect of the lateral tibial plateau. (**a**) Radiograph better demonstrates the fracture fragment (arrow) whereas (**b**) Coronal pd fs MRI better demonstrates the associated bone marrow oedema

Segond fracture may be demonstrated by radiograph (Fig. 14) and is usually associated with further significant ligamentous and meniscal injury. Phalangeal ligament and tendon avulsions are also well demonstrated (Fig. 15a–c) (Cockenpot et al. 2016).

In children and adolescents, there should be a high index of suspicion for apophyseal avulsions which may be demonstrated by radiographs (Schiller et al. 2017). For example, avulsion of the rectus femoris tendon from the anterior inferior iliac spine is a common athletic injury in children, typically occurring during sports involving kicking, such as football/soccer (Serbest et al. 2015) (Fig. 15d).

CT will frequently better demonstrate avulsion fractures compared to radiographs due to its cross-sectional multiplanar nature (Fig. 13). In the case of posterior tibial plateau avulsions, the posterior cruciate ligament may be demonstrated attached to the fracture fragment. Alternatively, in the absence of a fracture, radiographs and CT may demonstrate secondary effects of tendon or ligament injury such as malalignment, for example, in the wrist and ankle. Slender avulsion fragments may be poorly demonstrated by MRI making it much less sensitive than radiographs, CT and ultrasound for avulsion injuries (Figs. 14–16).

CT arthrography may be performed for visualization of ligaments at the wrist and elbow, for example, and has recently been found to be at least as sensitive as MR arthrography and less time consuming (Sonnow et al. 2019).

Dual energy CT utilizes images acquired from two different CT energy sources to enable separation of different tissues and is becoming a new tool in musculoskeletal radiology (Hickle et al. 2019; Wong et al. 2018). Dual energy CT may be used to reduce metal artefact to improve imaging in patients where MRI may not be possible. There is also potential for enhanced assessment of tendons and ligaments, the opportunities for which are just beginning to be explored, for example, in the assessment of tendon grafts following knee ligament reconstruction (Jeon et al. 2019).

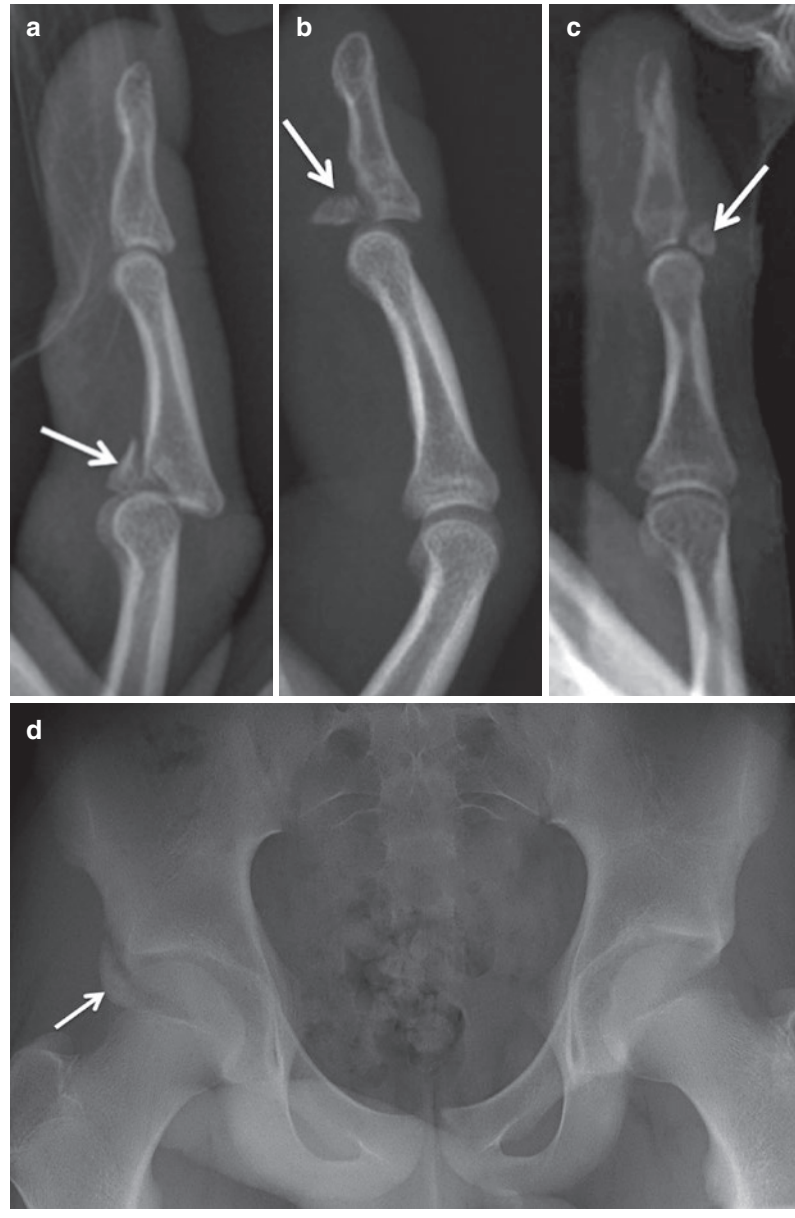

Fig. 15 Radiographs demonstrating tendon or ligament avulsion fractures. (**a**) Volar plate avulsion from the base of the proximal phalanx (arrow). (**b**) Flexor digitorum profundus avulsion at the base of the distal phalanx (arrow). (**c**) Extensor avulsion at the dorsal base of the distal phalanx (arrow). (**d**) Right anterior inferior iliac spine apophyseal avulsion (arrow) by the straight head of rectus femoris

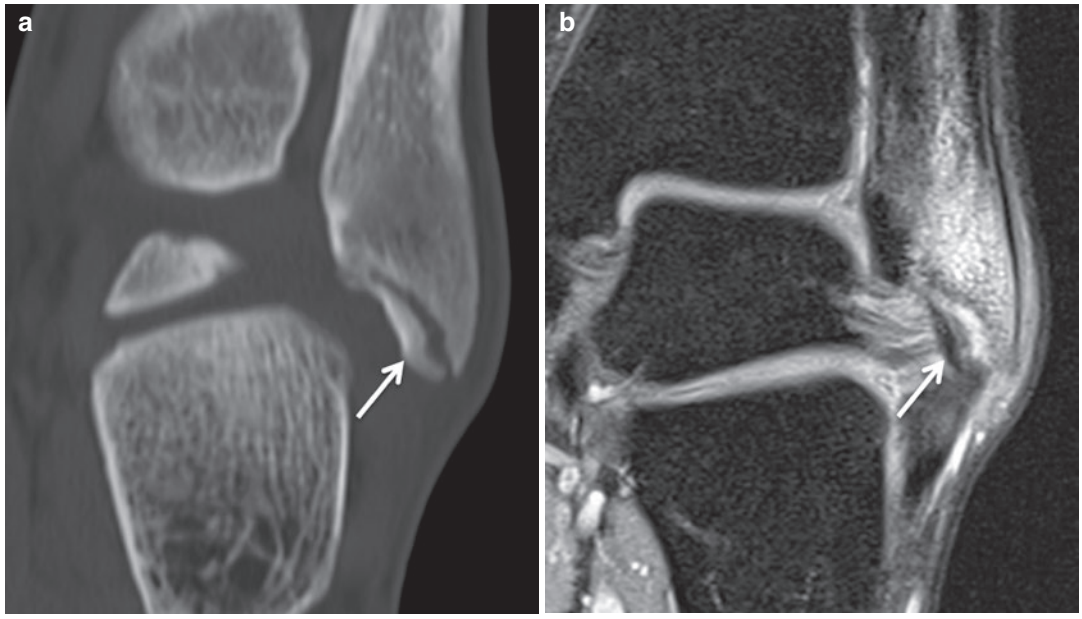

Fig. 16 PTFL avulsion fracture is better demonstrated by (**a**) CT than with (**b**) water-sensitive Coronal pd fs MRI demonstrating the associated bone marrow oedema but not well demonstrating the avulsion fracture fragment

3 Conclusion

The unique architecture of tendons and ligaments enables high-resolution imaging by both ultrasound and MRI with secondary effects of tendon and ligament injury frequently demonstrated by radiographs and CT. Many novel imaging techniques are being developed for tendon and ligament imaging and are already used in the research arena. In the future these may become more commonly used in routine clinical practice.

Things to Remember

1. The fibrillar structure of tendons and ligaments gives them unique imaging features, but also results in the specific imaging artefacts of magic angle effect on MRI and anisotropy on ultrasound.
2. Ultrasound is capable of high-resolution imaging of tendons and ligaments, with its dynamic capabilities being helpful in assessing ligament and tendon integrity.
3. MRI demonstrates ligaments and tendons well and has the advantage of imaging with a large field of view allowing assessment of adjacent structures and imaging bone.
4. Radiographs and CT may aid assessment of acute injury, bone alignment and tendon/ligament avulsion fractures and alignment.
5. The most commonly injured tendons in those participating in sports are the Achilles, patellar and supraspinatus tendons.
6. The most commonly injured ligaments in those participating in sports are those of the knee and ankle.

Box 1 Value of ultrasound in imaging tendons and ligaments

- High-resolution imaging of tendons and ligaments demonstrating their internal fibrillar architecture.
- Assess acute or chronic tendon or ligament injury.
- Dynamic scanning to assess structural integrity and abnormal movement.
- Assessment of neovascularization of chronically damaged tendons using Doppler ultrasound.
- Portable, on-site scanning.
- Be aware of disadvantages of anisotropy and difficulty in assessing deeper structures.

Box 2 Value of MRI in imaging tendons and ligaments

- Readily demonstrates deep and superficial tendons and ligaments.
- Larger field of view than ultrasound.
- Images internal joint and bone structure not visualized with ultrasound.
- Images optimized to detect tissues of different compositions.
- Imaging some ligamentous structures may be enhanced using MRI arthrography.
- Be aware of magic angle effect.

Box 3 Value of radiographs and CT in imaging tendons and ligaments

- Rule out fracture following acute injury.
- Increased sensitivity for small tendon or ligament avulsion or apophyseal fractures.
- Assess bone alignment following ligament injury.

References

Adler RS, Johnson KM, Fealy S et al (2011) Contrast-enhanced sonographic characterization of the vascularity of the repaired rotator cuff: utility of maximum intensity projection imaging. J Ultrasound Med 30:1103–1109

Allen GM (2018) The use of ultrasound in athletes. Eur J Radiol 109:136–141

Anz AW, Lucas EP, Fitzcharles EK et al (2014) MRI T2 mapping of the asymptomatic supraspinatus tendon by age and imaging plane using clinically relevant subregions. Eur J Radiol 83:801–805

Arabyat RM, Raisch DW, McKoy JM et al (2015) Fluoroquinolone-associated tendon-rupture: a summary of reports in the Food and Drug Administration's adverse event reporting system. Expert Opin Drug Saf 14:1653–1660

Aubry S, Nueffer JP, Tanter M et al (2015) Viscoelasticity in Achilles tendonopathy: quantitative assessment by using real-time shear-wave elastography. Radiology 274:821–829

Baloch N, Hasan OH, Jessar MM et al (2018) "Sports ultrasound", advantages, indications and limitations in upper and lower limbs musculoskeletal disorders. Review article. Int J Surg 54:333–340

Bancroft LW (2013) Wrist injuries: a comparison between high- and low-impact sports. Radiol Clin N Am 51:299–311

Brage K, Hjarbaek J, Kjaer P et al (2019) Ultrasonic strain elastography for detecting abnormalities in the supraspinatus tendon: an intra-and inter-rater reliability study. BMJ Open 9:e027725

Brazier J, Antrobus M, Stebbings GK et al (2019) Tendon and ligament injuries in elite rugby: the potential genetic influence. Sports 7:138

Bydder M, Rahal A, Fullerton GD et al (2007) The magic angle effect: a source of artifact, determinant of image contrast, and technique for imaging. J Magn Reson Imaging 25:290–300

Chang CD, Wu JS (2017) MR imaging findings in heel pain. Magn Reson Imaging Clin N Am 25: 79–93

Chappell KE, Brujic D, Van Der Straeten C et al (2019) Detection of maturity and ligament injury using magic angle directional imaging. Magn Reson Med 82:1041–1054

Chen TM, Rozen WM, Pan W et al (2009) The arterial anatomy of the Achilles tendon: anatomical study and clinical implications. Clin Anat 22:377–385

Chen XM, Cui LG, He P et al (2013) Shear wave elastographic characterization of normal and torn achilles tendons: a pilot study. J Ultrasound Med 32: 449–455

Cheng X, Lu M, Yang X et al (2015) The effect of percutaneous ultrasound-guided subacromial bursography using microbubbles in the assessment of subacromial impingement syndrome: initial experience. Eur Radiol 25:2412–2418

Chianca V, Albano D, Messina C et al (2017) Diffusion tensor imaging in the musculoskeletal and peripheral nerve systems: from experimental to clinical applications. Eur Radiol Exp 1:12

Chowdhury R, Naaseri S, Lee J et al (2014) Imaging and management of greater trochanteric pain syndrome. Postgrad Med J 90:576–581

Cockenpot E, Lefebvre G, Demondion X et al (2016) Imaging of sports-related hand and wrist injuries: sports imaging series. Radiology 279:674–692

Davis LC, Baumer TG, Bey MJ et al (2019) Clinical utilization of shear wave elastography in the musculoskeletal system. Ultrasonography 38:2–12

Deren ME, Klinge SA, Mukand NH et al (2016) Tendinopathy and tendon rupture associated with statins. JBJS Rev 4(5)

Deslandes M, Guillin R, Cardinal E et al (2008) The snapping iliopsoas tendon: new mechanisms using dynamic sonography. AJR Am J Roentgenol 190:576–581

Dirrichs T, Quack V, Gatz M et al (2016) Shear wave Elastography (SWE) for the evaluation of patients with tendinopathies. Acad Radiol 23:1204–1213

Domenichini R, Pialat J-B, Podda A et al (2017) Ultrasound elastography in tendon pathology: state of the art. Skelet Radiol 46:1643–1655

Doring S, Provyn S, Marcelis S et al (2018) Ankle and midfoot ligaments: ultrasound with anatomical correlation: a review. Eur J Radiol 107:216–226

Draghi F, Bortolotto C (2014) Intersection syndrome: ultrasound imaging. Skelet Radiol 43:283–287

Fullerton GD, Rahal A (2007) Collagen structure: the molecular source of the tendon magic angle effect. J Magn Reson Imaging 25:345–361

Fullerton GD, Cameron IL, Ord VA (1985) Orientation of tendons in the magnetic field and its effect on T2 relaxation times. Radiology 155:433–435

Genovese E, Ronga M, Recaldini C et al (2011) Analysis of achilles tendon vascularity with second-generation contrast-enhanced ultrasound. J Clin Ultrasound 39:141–145

Gottsegen CJ, Eyer BA, White EA et al (2008) Avulsion fractures of the knee: imaging findings and clinical significance. Radiographics 28:1755–1770

Guidetti M, Zampini MA, Gandini G et al (2018) Diffusion tensor imaging of tendons and ligaments at ultra-high magnetic fields. Crit Rev Biomed Eng 46:311–339

Gyftopoulos S, Rosenberg ZS, Schweitzer ME et al (2008) Normal anatomy and strains of the deep musculotendinous junction of the proximal rectus femoris: MRI features. AJR Am J Roentgenol 190:W182–W186

Heiss R, Guermazi A, Jarraya M et al (2019) Prevalence of MRI-detected ankle injuries in athletes in the Rio de Janeiro 2016 summer Olympics. Acad Radiol 26:1605

Hickle J, Walstra F, Duggan P et al (2019) Dual-energy CT characterization of winter sports injuries. Br J Radiol 93:20190620

Hodgson RJ, O'Connor PJ, Grainger AJ (2012) Tendon and ligament imaging. Br J Radiol 85:1157–1172

Horn DB, Meyers S, Astor W (2015) True pathologic abnormality versus artifact foot position and magic angle artifact in the peroneal tendons with 3T imaging. J Am Podiatr Med Assoc 105:443–450

Ieong E, Rafferty M, Khanna M et al (2018) Use of fat-suppressed T2-weighted MRI images to reduce the magic angle effect in peroneal tendons. Foot & Ankle Specialist:1938640018819783

Ishigaki T, Kubo K (2019) Mechanical properties and collagen fiber orientation of tendon in young and elderly. Clin Biomech (Bristol, Avon) 71:5–10

Ito D, Numano T, Takamoto K et al (2019) Simultaneous acquisition of magnetic resonance elastography of the supraspinatus and the trapezius muscles. Magn Reson Imaging 57:95–102

Jarraya M, Crema MD, Engebretsen L et al (2018) Epidemiology of imaging-detected tendon abnormalities in athletes participating in the Rio de Janeiro 2016 summer Olympics. Br J Sports Med 52:465–469

Jarvinen TA (2020) Neovascularisation in tendinopathy: from eradication to stabilisation? Br J Sports Med 54:1–2

Jeon JY, Lee SW, Jeong YM et al (2019) The utility of dual-energy CT collagen material decomposition technique for the visualization of tendon grafts after knee ligament reconstruction. Eur J Radiol 116:225–230

Juras V, Apprich S, Szomolanyi P et al (2013) Bi-exponential T2 analysis of healthy and diseased Achilles tendons: an in vivo preliminary magnetic resonance study and correlation with clinical score. Eur Radiol 23:2814–2822

Juras V, Mlynarik V, Szomolanyi P et al (2019) Magnetic resonance imaging of the musculoskeletal system at 7T: morphological imaging and beyond. Top Magn Reson Imaging 28:125–135

Kalia V, Fritz B, Johnson R et al (2017) CAIPIRINHA accelerated SPACE enables 10-min isotropic 3D TSE MRI of the ankle for optimized visualization of curved and oblique ligaments and tendons. Eur Radiol 27:3652–3661

Kastelic J, Galeski A, Baer E (1978) The multicomposite structure of tendon. Connect Tissue Res 6:11–23

Klauser AS, Franz M, Arora R et al (2010) Detection of vascularity in wrist tenosynovitis: power doppler ultrasound compared with contrast-enhanced grey-scale ultrasound. Arthritis Res Ther 12:R209

Klauser AS, Miyamoto H, Tamegger M et al (2013) Achilles tendon assessed with sonoelastography: histologic agreement. Radiology 267:837–842

Kloth JK, Winterstein M, Akbar M et al (2014) Comparison of 3D turbo spin-echo SPACE sequences with conventional 2D MRI sequences to assess the shoulder joint. Eur J Radiol 83:1843–1849

Krepkin K, Bruno M, Raya JG et al (2017) Quantitative assessment of the supraspinatus tendon on MRI using T2/T2* mapping and shear-wave ultrasound elastography: a pilot study. Skelet Radiol 46:191–199

Kristen K-H, Aspang JS, Wiedemann J et al (2019) Reliability of ultrasonography measurement of the anterior talofibular ligament (ATFL) length in healthy subjects (in vivo), based on examiner experience and patient positioning. J Exp Orthop 6:30

Laistler E, Dymerska B, Sieg J et al (2018) In vivo MRI of the human finger at 7 T. Magn Reson Med 79: 588–592

Lee MH, Sheehan SE, Orwin JF et al (2016) Comprehensive shoulder US examination: a standardized approach with multimodality correlation for common shoulder disease. Radiographics 36:1606–1627

LiMarzi GM, O'Dell MC, Scherer K et al (2015) Magnetic resonance arthrography of the wrist and elbow. Magn Reson Imaging Clin N Am 23:441–455

Liu W, Zhuang H, Shao D et al (2017) High-frequency color doppler ultrasound in diagnosis, treatment, and rehabilitation of Achilles tendon injury. Med Sci Monit 23:5752

Llopis E, Carrascoso J, Iriarte I et al (2016) Lisfranc injury imaging and surgical management. Semin Musculoskelet Radiol 20:139–153

Llopis E, Restrepo R, Kassarjian A et al (2019) Overuse injuries of the wrist. Radiol Clin N Am 57:957–976

Lungu E, Michaud J, Bureau NJ (2018) US assessment of sports-related hip injuries. Radiographics 38:867–889

Magee T (2015) Accuracy of 3-T MR arthrography versus conventional 3-T MRI of elbow tendons and ligaments compared with surgery. AJR Am J Roentgenol 204:W70–W75

Marie I, Delafenêtre H, Massy N et al (2008) Tendinous disorders attributed to statins: a study on ninety-six spontaneous reports in the period 1990–2005 and review of the literature. Arthritis Care Res 59:367–372

McCarthy MM, Hannafin JA (2014) The mature athlete: aging tendon and ligament. Sports health 6:41–48

McKee TJ, Perlman G, Morris M et al (2019) Extracellular matrix composition of connective tissues: a systematic review and meta-analysis. Sci Rep 9:1–15

Nozaki T, Wu W, Kaneko Y et al (2017) High-resolution MRI of the ulnar and radial collateral ligaments of the wrist. Acta Radiol 58:1493–1499

Ooi CC, Schneider ME, Malliaras P et al (2015) Diagnostic performance of axial-strain sonoelastography in confirming clinically diagnosed Achilles tendinopathy: comparison with B-mode ultrasound and color Doppler imaging. Ultrasound Med Biol 41:15–25

Ooi CC, Richards PJ, Maffulli N et al (2016) A soft patellar tendon on ultrasound elastography is associated with pain and functional deficit in volleyball players. J Sci Med Sport 19:373–378

Perrich KD, Goodwin DW, Hecht PJ et al (2009) Ankle ligaments on MRI: appearance of normal and injured ligaments. Am J Roentgenol 193:687–695

Pesquer L, Poussange N, Sonnery-Cottet B et al (2016) Imaging of rectus femoris proximal tendinopathies. Skelet Radiol 45:889–897

Ramachandran GN, Chandrasekharan R (1968) Interchain hydrogen bonds via bound water molecules in the collagen triple helix. Biopolymers 6:1 649–1658

Rein S, Hagert E, Schneiders W et al (2015) Histological analysis of the structural composition of ankle ligaments. Foot Ankle Int 36:211–224

Rich A, Crick FH (1955) The structure of collagen. Nature 176:915–916

Rich A, Crick FH (1961) The molecular structure of collagen. J Mol Biol 3:483–506

Richardson ML, Amini B, Richards TL (2018) Some new angles on the magic angle: what MSK radiologists know and don't know about this phenomenon. Skelet Radiol 47:1673–1681

Robinson P (2009) Sonography of common tendon injuries. AJR Am J Roentgenol 193:607–618

Roy JS, Braen C, Leblond J et al (2015) Diagnostic accuracy of ultrasonography, MRI and MR arthrography in the characterisation of rotator cuff disorders: a systematic review and meta-analysis. Br J Sports Med 49:1316–1328

Ruzbarsky JJ, Konin G, Mehta N et al (2017) MRI arthroscopy correlations: ligaments of the knee. Sports Med Arthrosc Rev 25:210–218

Ryu J, Jeong WK (2017) Current status of musculoskeletal application of shear wave elastography. Ultrasonography 36:185–197

Schiller J, DeFroda S, Blood T (2017) Lower extremity avulsion fractures in the pediatric and adolescent athlete. J Am Acad Orthop Surg 25:251–259

Scott A, Backman LJ, Speed C (2015) Tendinopathy: update on pathophysiology. J Orthop Sports Phys Ther 45:833–841

Seidel T, Hammer N, Garnov N et al (2013) An algorithm for the calculation of three-dimensional collagen fiber orientation in ligaments using angle-sensitive MRI. Magn Reson Med 69:1594–1602

Serbest S, Tosun HB, Tiftikci U et al (2015) Anterior inferior iliac spine avulsion fracture: a series of 5 cases. Medicine (Baltimore) 94:e562

Shabshin N, Rosenberg ZS, Cavalcanti CF (2005) MR imaging of iliopsoas musculotendinous injuries. Magn Reson Imaging Clin N Am 13:705–716

Shih WS, Wu CH, Wang TG (2019) How does ballet training alter ankle tendinous morphology and hemodynamics in asymptomatic pre-professional dancers? An ultrasonographic study. J Sci Med Sport 22:392–396

Sonnow L, Koennecker S, Luketina R et al (2019) High-resolution flat panel CT versus 3-T MR arthrography of the wrist: initial results in vivo. Eur Radiol 29:3233–3240

Splittgerber LE, Ihm JM (2019) Significance of asymptomatic tendon pathology in athletes. Curr Sports Med Rep 18:192–200

Squires A, Chan KC, Ho LC et al (2016) MAPS—a magic angle positioning system for enhanced imaging in high-field small-bore MRI. J Med Robot Res 1

Szeverenyi NM, Bydder GM (2011) Dipolar anisotropy fiber imaging in a goat knee meniscus. Magn Reson Med 65:463–470

Tadros AS, Huang BK, Pathria MN (2018) Muscle-tendon-Enthesis unit. Semin Musculoskelet Radiol 22:263–274

Tafur M, Iwasaki K, Statum S et al (2015) Magnetic resonance imaging of the pulleys of the flexor tendons of the toes at 11.7 T. Skelet Radiol 44:87–95

Taljanovic MS, Gimber LH, Becker GW et al (2017) Shear-wave Elastography: basic physics and musculoskeletal applications. Radiographics 37: 855–870

Tang YQ, Zeng C, Su XT et al (2019) The value of percutaneous shoulder puncture with contrast-enhanced ultrasound in differentiation of rotator cuff tear subtypes: a preliminary prospective study. Ultrasound Med Biol 45:660–671

Tempfer H, Traweger A (2015) Tendon vasculature in health and disease. Front Physiol 6:330

Thevendran G, Sarraf KM, Patel NK et al (2013) The ruptured Achilles tendon: a current overview from biology of rupture to treatment. Musculoskelet Surg 97:9–20

Thorpe CT, Screen HR (2016) Tendon structure and composition. Adv Exp Med Biol 920:3–10

Van Gulick L, Saby C, Morjani H et al (2019) Age-related changes in molecular organization of type I collagen in tendon as probed by polarized SHG and Raman microspectroscopy. Sci Rep 9:7280

Wang JH, Guo Q, Li B (2012) Tendon biomechanics and mechanobiology—a minireview of basic concepts and recent advancements. J Hand Ther 25:133–141

Wengler K, Tank D, Fukuda T et al (2018) Diffusion tensor imaging of human Achilles tendon by stimulated echo readout-segmented EPI (ste-RS-EPI). Magn Reson Med 80:2464–2474

Wong WD, Shah S, Murray N et al (2018) Advanced musculoskeletal applications of dual-energy computed tomography. Radiol Clin N Am 56:587–600

Wren TA, Beaupre GS, Carter DR (2000) Mechanobiology of tendon adaptation to compressive loading through fibrocartilaginous metaplasia. J Rehabil Res Dev 37:135–144

Yen YM, Lewis CL, Kim YJ (2015) Understanding and treating the snapping hip. Sports Med Arthrosc Rev 23:194–199

Bone Marrow Edema in Sports Injuries/General Concept

F. M. Vanhoenacker

Contents

Abstract

This chapter discusses the value of imaging in the detection and follow-up of bone marrow edema (BME) that may occur in sports.

The use of fluid-sensitive MR sequences is most helpful for detection of BME, whereas dual-energy CT with virtual non-calcium images may be used as an alternative in patients with contraindications for MRI.

The extent of bone marrow edema reflects the biomechanics of trauma. Compressive forces between two bony structures will result in extensive areas of BME, whereas distraction forces provoke more subtle areas of BME at the insertion of supporting structures of joints. Analysis of the distribution of BME around a joint can reveal the underlying mechanism of trauma and may help to analyze the supporting structures at risk.

Plain films have no role for depiction of BME, but may be useful to detect avulsion fractures such as a Segond fracture.

1 Introduction

Macroscopically, living bone consists of compact bone and cancellous bone.

Cancellous bone, also designated as trabecular or spongy bone, is a honeycomb of large cavities

F. M. Vanhoenacker (✉)
Department of Radiology, AZ Sint-Maarten Mechelen and Antwerp University Hospital, Faculty of Medicine and Health Sciences, University of Antwerp and Ghent University, Mechelen, Belgium
e-mail: filip.vanhoenacker@telenet.be

Med Radiol Diagn Imaging (2021)
https://doi.org/10.1007/174_2020_241, © Springer Nature Switzerland AG
Published Online: 23 February 2021

with an internal latticework of bars and plates (trabeculae).

Compact bone is usually limited to the cortices of mature bones (cortical bone) and is most important in providing the strength of bone.

Cancellous bone lies in the inner part of the bone, and particularly, in case of the long bones, within their expanded ends (metaphyses and epiphyses). Cancellous bone gives additional strength to cortical bone and supports the bone marrow (Standring 2016).

Before the advent of magnetic resonance imaging (MRI), trauma to the trabecular bone was difficult to assess on radiological examinations, because the overlying cortex is often intact (Mandalia et al. 2005). This chapter reviews bone marrow edema (BME) resulting from sports injuries, with special emphasis on the mechanisms of trauma, clinical significance, and natural evolution.

2 Definition and Classification

"Bone bruise" was described for the first time in the knee by *Yao* and *Lee* in 1988 (Yao and Lee 1988). The term "bruise" indicates the traumatic origin of these bone marrow changes. It was defined as an area of T2 hyperintensity in the absence of frank osseous fracture or subchondral cysts. MRI examination showed intraosseous hyperintense areas on fluid-sensitive sequences such as T2-weighted images (WI) or STIR and (to a lesser degree) hypo-intense on T1-WI, in acutely injured joints with no abnormalities on plain radiographs. The use of an intermediate TE in fat-suppressed (FS) T2-WI has an additional value in demonstrating underlying cartilage lesions. Since then the terms bone bruise, bone contusion, and occult fracture have been used interchangeably. The term "occult" is used when standard radiograph shows no osseous abnormalities in the presence of bone marrow edema (BME) on MRI. State-of-the-art multidetector CT with thin multiplanar reconstructions may however sometimes detect subtle fracture lines, which are not visible on plain radiographs.

In addition, recent advances in CT technology with the use of dual-energy computed tomography (DECT) virtual non-calcium (VNCa) images may even detect fractures that are not detectable on bone reconstruction CT images (Reddy et al. 2015). Although MRI remains the preferred technique for evaluation of BME, DECT virtual non-calcium (VNCa) reconstructions have an almost equivalent accuracy in depicting BME compared to MRI (Booz et al. 2019). In this regard, it may serve as an alternative to MRI in patients with contraindications for MRI. MRI, however, is better suited to evaluate concomitant soft-tissue damage.

Even in radiologically overt fracture lines, MRI is better suited to evaluate the precise extent of surrounding BME in the adjacent cancellous bone.

Several classification systems of BME have been proposed. Most authors agree on differentiation between reticular and geographic/demarcated pattern. Others stress the importance of the location (subchondral versus at distance of joint space). Costa-paz et al. (2001) proposed the following classification (Costa-Paz et al. 2001):

- Type I: diffuse, often reticular, alterations of the medullary component, distant from the subjacent articular surface
- Type II (a and b) localized/geographic signal (mostly convex margins towards normal marrow) with contiguity to articular surface
- Type III: (slight) disruption or depression of the normal contour of the cortical surface/subchondral lamella, often associated with type II lesion (small osteochondral compression fractures)

In a type II lesion compared to type I, the impact is more focally concentrated. Subchondral impaction fractures may present as marked hypointense area on T1-WI directly beneath the subchondral lamella, representing focal cancellous impaction (possible patterns are geographic, crescent, and linear). Those lesions can be designated as type IIb lesions.

Multidetector CT will of course pick up the focal depressions/osteochondral fractures (III) and probably also the subchondral impactions (IIb).

3 Pathogenesis of Bone Marrow Edema in Sports Injuries

Traumatic bone marrow edema (bruise) is most frequent and the underlying mechanism may be either acute or chronic.

Variable incidences have been published but BME is often encountered in acute trauma.

A minority of the studies of acute injuries of the knee and ankle will show isolated bruising without associated injuries.

3.1 Acute Traumatic Lesions

BME is frequently encountered on MRI after an injury to the musculoskeletal system (Sanders et al. 2000). These osseous injuries may result from several forces acting on the joint. In general, compressive forces versus traction forces will influence the extent of BME around the joint (Hayes et al. 1993).

3.1.1 Impaction Injuries

Focal bruise may result from direct trauma to the bone (Fig. 1), but often a specific pattern of bone marrow changes on adjacent bones occurs due to impaction of one bone on another.

Impaction type of BME is extensive and will involve a broad surface of the involved bony structures.

3.1.2 Avulsive Injuries

Distraction injuries are usually due to valgus, varus, or rotational stress on a joint, resulting in a small avulsion fracture related to a tendinous, ligamentous, or capsular attachment on the bone.

Because the cortical bone is involved rather than the trabecular bone, the resulting "avulsion BME pattern" is much less extensive than in impaction injuries.

Moreover, the avulsed bone fragment may be very difficult to detect on MRI (Fig. 2a). In most instances, a small avulsion is far better demonstrated on conventional radiographs (Fig. 2b) or CT.

3.1.3 Complex Patterns

In most clinical situations, this rigorous distinction between "*pure impaction-type injuries*" and "*avulsive type injuries*" is artificial, because both types will be seen in a single joint after acute traumatic injuries. Generally, the impaction

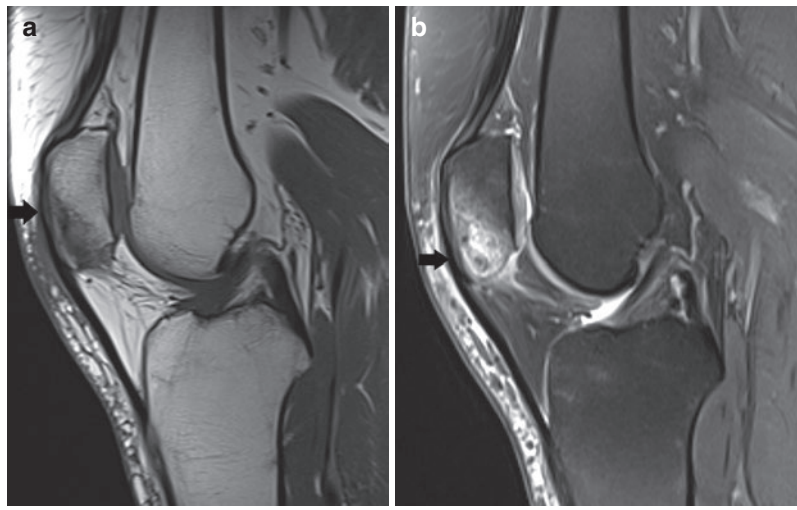

Fig. 1 (**a** and **b**) Bone marrow edema (BME) due to a direct blow (impaction type BME) on the patella. (**a**) Sagittal T1-weighted image (WI) of the knee shows BME as a hypointense signal compared to the normal fatty bone marrow at the inferior aspect of the patella (black arrow). (**b**) BME is more conspicuous on sagittal fat-suppressed (FS) T2-WI (black arrow). Note also subtle pre- and infrapatellar soft-tissue edema

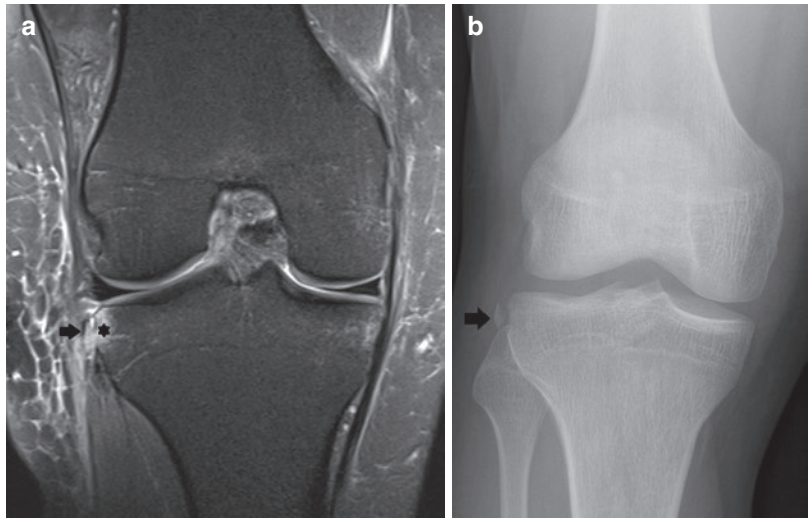

Fig. 2 (**a** and **b**) Typical example of an avulsion fracture and associated BME (avulsion-type BME). (**a**) Coronal FS T2-WI of the right knee shows only minor focal BME at the lateral aspect of the tibia (black asterisk). The bony avulsion fracture is difficult to distinguish from the adjacent ligamentous structures (black arrow). (**b**) Standard radiograph clearly shows an avulsion fracture (black arrow) at the insertion of the anterolateral ligament (Segond fracture)

type of bone marrow edema will be encountered on the *entry site* of the force acting on a joint, whereas a distraction type of bone marrow edema will be seen on the *exit site* of the force. Although avulsive type bone marrow edema is less extensive than the impaction type, the former is usually the witness of underlying ligamentous sprain.

These soft-tissue lesions are often less conspicuous than the bruises, though they are more important, at least in the short-term follow-up, for stability reasons.

Indeed, sprain of the supporting structures of the joint may cause instability, if not recognized and appropriately treated.

Moreover, BME around a joint is usually the result of a combination of multiple forces (and not of a single force), which all have a certain amplitude and direction. The impact of these forces may differ with the position of the joint at the moment of the trauma (e.g., degree of flexion, varus, valgus).

Certain combinations of forces are known to cause a specific injury.

Systematic analysis of the BME pattern, together with the associated soft-tissue changes, can often reveal the specific mechanism of injury.

In this regard, the pattern and distribution of BME represent a "footprint" of the mechanism of acute trauma (Sanders et al. 2000; Rios et al. 2011).

In the knee for example, classic patterns which are encountered in sports injuries are the pivot shift injury (Figs. 3 and 4) (Kijowski et al. 2014), hyperextension injury (Fig. 5), clip injury (Fig. 6), dashboard injury (Fig. 7), and (transient) lateral patellar dislocation (Fig. 8) (Vanhoenacker and Snoeckx 2007).

Pivot shift injury which occurs when valgus load is applied to the knee in various states of flexion, combined with external rotation of the tibia or internal rotation of the femur, will result in disruption of ACL. Resultant anterior subluxation of the tibia will cause impaction of the lateral femoral condyle against the posterolateral margin of the lateral tibial plateau. Therefore, BME will be present in the posterior aspect of the lateral tibial plateau and the middle portion of the

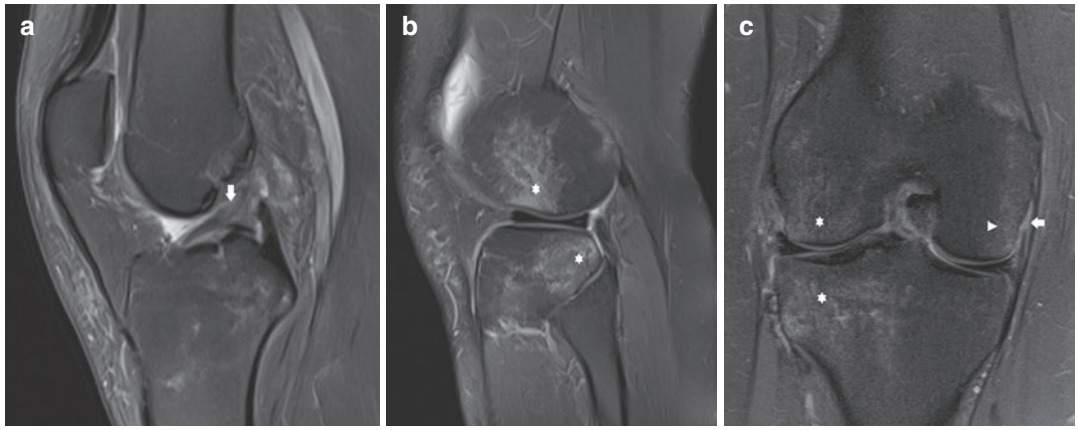

Fig. 3 (**a**–**c**) Pivot shift injury of the right knee due to a combination of external rotation of the tibia, valgus stress, and flexion. These maneuvers stress the anterior cruciate ligament (ACL), which is prone to rupture. (**a**) Midsagittal FS T2-WI shows disruption of the ACL (white arrow). (**b**) Sagittal FS T2-WI. Due to anterior subluxation of the tibia relative to the femur, impaction occurs between the posterolateral margin of the lateral tibial plateau and the lateral femoral condyle, resulting in extensive impaction-type BME (white asterisks). (**c**) Coronal FS T2-WI confirms the extensive BME at the lateral femur and tibia (white asterisks). On the medial femoral condyle, there is less extensive avulsive BME (white arrowhead) and disruption of the deep meniscofemoral layer of the medial collateral ligament (white arrow)

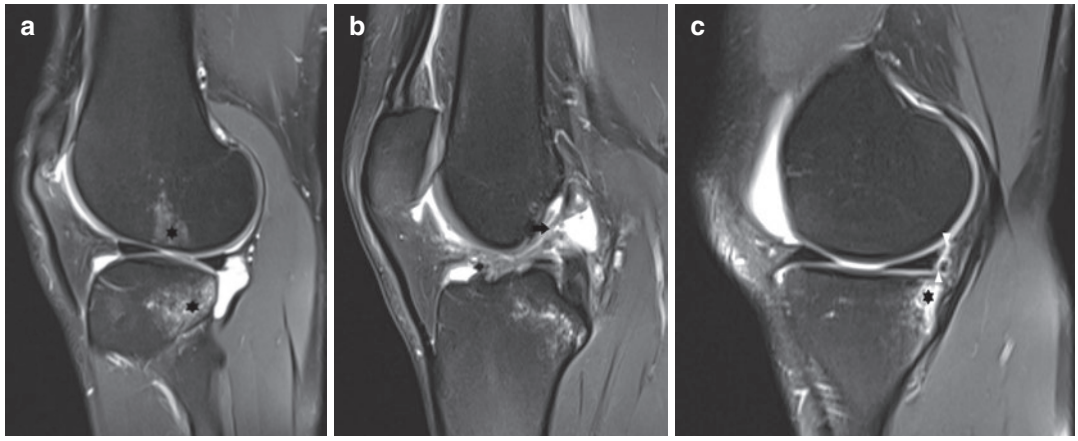

Fig. 4 (**a**–**c**) Another pivot shift injury in a soccer player with associated BME at the posteromedial corner of the knee. (**a**) Sagittal FS T2-WI of the lateral aspect of the knee. BME at the posterolateral aspect of the tibia and corresponding BME at the middle part of the lateral femoral condyle (black asterisks). (**b**) Midsagittal FS T2-WI of the right knee shows complete disruption of the ACL (black arrow). (**c**) Sagittal FS T2-WI of the medial aspect of the right knee. Note also BME at the posteromedial aspect of the tibia near the distal semimembranosus tendon (black asterisk). According to some authors, this lesion represents a contrecoup impaction lesion. According to others, however, this lesion represents a traction injury at the posteromedial corner of the knee due to external rotation of the knee. Note also a peripheral tear of the posterior horn of the medial meniscus (white arrowheads)

Fig. 5 Hyperextension-valgus trauma in a soccer player. FS T2-WI at the lateral aspect of the right knee. Severe hyperextension of the knee can result in the impaction of the anterior aspect of the femoral condyle against the anterior aspect of the tibial plateau, resulting in extensive BME (black asterisks). Because of valgus position of the knee at the moment of the trauma, BME in this case is located at the lateral part of the knee

Fig. 6 Clip injury in a soccer player. Coronal FS T2-WI of the left knee shows a large area of BME involving the lateral femoral condyle (black asterisk). There is complete disruption of the MCL at its femoral insertion (black arrow)

lateral femoral condyle. Associated bone bruising at the posterior lip of the medial tibial plateau may be the result of contrecoup forces due to valgus forces (Kaplan et al. 1999). According to others this medial sided bone bruise is attributed to avulsion at the semimembranosus attachment (Chan et al. 1999). Concomitant soft-tissue injuries of the pivot shift injury are medial collateral ligament (MCL) lesions, lesion of the posterior horn of the lateral and medial meniscus, or a tear at the posterior joint capsule.

Hyperextension injury results in a kissing contusion pattern in the anterior aspect of the distal femur and proximal tibia. Associated soft-tissue lesions may include ACL or PCL tears or meniscal lesions.

The classic bone contusion pattern seen after lateral patellar dislocation includes involvement of the anterolateral aspect of the lateral femoral condyle and the inferomedial aspect of the patella.

Associated soft-tissue injuries include sprain or disruption of the medial soft-tissue restraints (medial retinaculum, medial patellofemoral ligament, and medial patellotibial ligament). Associated (osteo)chondral lesions of the patella may be seen as well (Bosmans and Vanhoenacker 2019).

Clip injury occurs when pure valgus stress is applied to the knee while the knee is in mild flexion. BME is most prominent in the lateral femoral condyle due to impaction forces, whereas a second smaller area of BME may be present in the medial femoral condyle secondary to avulsive forces at the insertion of the MCL.

Dashboard injury occurs when a posteriorly directed force is applied to the anterior aspect of the proximal tibia while the knee is in a flexed position. This will result in BME at the anterior aspect of the tibia and occasionally at the posterior surface of the patella. Associated soft-tissue injuries are disruption of the posterior cruciate ligament and posterior joint capsule.

Failure of this pattern approach revealing the underlying mechanism of trauma may be due to several factors, including insufficient trauma, massive injury, or preexisting osteoarthritis associated with BME (Felson et al. 2001; Collins et al. 2016; Vanhoenacker et al. 2005; Vanhoenacker and Snoeckx 2007), usually encountered in older sporters. Moreover, accelerated osteoarthritis is more prevalent in sporters than in the general population, due to previous repetitive trauma.

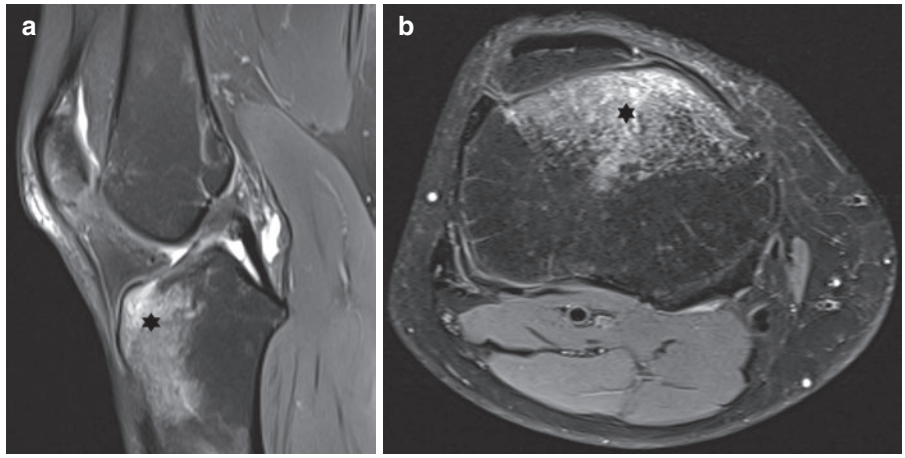

Fig. 7 (**a** and **b**) Dashboard injury. (**a**) Sagittal and (**b**) axial FS T2-WI showing BME at the proximal tibia (black asterisks)

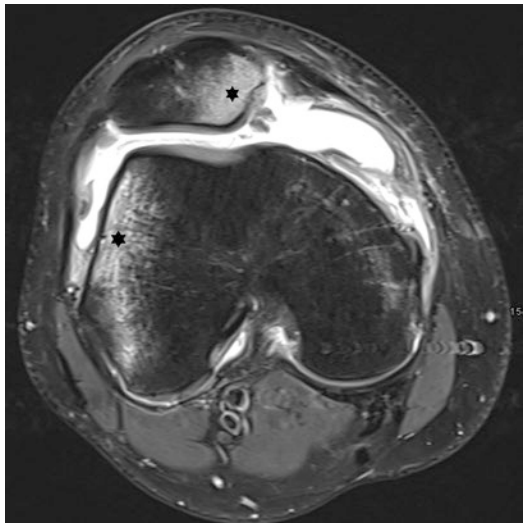

Fig. 8 Impaction-type bone marrow edema, associated with lateral patellar dislocation in a soccer player. An axial FS T2-WI of the right knee demonstrates BME involving the medial patellar facet and the lateral femoral condyle (black asterisks). Associated distraction at the medial patellar retinaculum will result in thickening and extensive hyperintensity due to partial disruption

3.2 Chronic Traumatic Lesions (Repetitive Trauma)

Besides pure acute traumatic causes of BME, BME may result from repetitive or chronic trauma in sports activities.

3.2.1 Fatigue Fractures

Chronic stress on a normally mineralized bone may result in a spectrum of MRI findings ranging from periosteal edema over severe marrow edema to a hypo-intense fracture line in cancellous or cortical bone. This item will be described more in detail in (Lefere et al. 2021).

3.2.2 Chronic Avulsive Injuries

Typical examples of chronic avulsive injuries include shin splints (traction periostitis of the calf muscles along the posteromedial tibia) (Franklyn and Oakes 2015; Winters 2020), thigh splints (distal adductor insertion avulsion syndrome) (Van De Perre et al. 2003; Hegazi et al. 2016), and "adductor/gracilis syndrome" (Schilders et al. 2017; Lee et al. 2017).

Apart from periosteal edema, MRI may also reveal BME and cortical signal abnormalities.

3.2.3 Altered Biomechanics and BME

Altered biomechanics due to certain sports activities (jogging, golf) may induce physiologic bone response to repeated stress. MRI may reveal BME in these cases, which may not necessarily correspond with severe trauma (Grampp et al. 1998; Yochum and Barry 1997).

The potential role of limb malalignment and BME was described by *Felson* et al. (Felson et al. 2003, 2013). Medial bone marrow lesions can be

seen in athletes with varus limb, whereas lateral lesions are associated with valgus limbs.

The importance of alignment has been experimentally demonstrated in an in vivo MRI demonstration of the Pond-Nuki animal model for the evaluation of osteoarthritis. In this experimental study, 24 beagle dogs underwent transection of the anterior cruciate ligament of the left leg (modified Pond-Nuki model). The first sign on MRI was the appearance of subchondral BME at the posteromedial aspect of the tibia followed by progressive cartilage degeneration, meniscus degeneration, and osteophytosis (Libicher et al. 2005).

3.3 Lesions of Unknown Pathogenesis

Bone marrow edema syndromes without any history of trauma are increasingly recognized on MRI (Mandalia et al. 2005).

Distinction between bone bruising and marrow edema syndromes is primarily based on the clinical history of the patient.

3.3.1 Bone Marrow Edema Syndrome

Transient bone marrow edema syndrome (BMES), also referred to as (transient) regional osteoporosis, is a distinct self-limiting syndrome located at the weight-bearing joints of the lower limbs (Toms et al. 2005). It usually affects middle-aged men (Cahir and Toms 2008) and women in the last trimester of pregnancy (Cano-Marquina et al. 2014), but association with sports activities has been reported (Miltner et al. 2003).

BMES usually affects only one bone, predominantly the proximal femur (Walgrave and Vanhoenacker 2019), but it may be bilateral as well (Cano-Marquina et al. 2014). In the hip, there is typical sparing of the medial aspect of the femoral head (Walgrave and Vanhoenacker 2019; Klontzas et al. 2015) and subchondral fractures are present in 48.7% of cases (Klontzas et al. 2015). The tarsal bones and the knee joint and acetabulum are involved less frequently (Feyen et al. 2008; Radke et al. 2001; Karantanas et al. 2008; Eyselbergs et al. 2011).

Three distinct clinical phases have been described (Schapira 1992). In the first phase, pain is rapidly aggravated, with functional disability lasting approximately 1 month. In the second phase, lasting 1 or 2 months, the pain reaches a plateau phase. The third phase is characterized by regression of symptoms. This period lasts approximately 4 months.

Imaging features consist of BME without associated findings on MRI (Hayes et al. 1993).

In the second phase of the disease, osteopenia may be present on the plain radiographs, whereas the third phase is characterized by reconstitution of bone density (Fig. 9).

Bone marrow edema syndrome may also migrate between the weight-bearing joints. The knee and hip are most frequently involved (Klontzas et al. 2015; Feyen et al. 2008; Karantanas et al. 2008).

3.3.2 Bone Marrow Edema in Long-Distance Runners

Bone marrow edema can be seen in recreational athletes 1–8 weeks after sports running (Krampla et al. 2001; Trappeniers et al. 2003). The affected bones included the knee and the tarsal and metatarsal bones. Fluid-sensitive sequences are most sensitive to detect these edema patterns. In well-trained runners, bone marrow edema is, however, not present (Schueller-Weidekamm et al. 2006).

3.3.3 Subchondral Insufficiency Fracture

A subchondral insufficiency fracture (SIF) with surrounding bone marrow edema may occur at the weight bearing of the (medial) femur condyle and tibial plateau in patients with meniscal injuries and after meniscal surgery. SIF has been described in the hip as well.

Altered biomechanics due to the subchondral fracture or resorption of the avascular segment may induce abnormal stress on the articular surfaces.

4 Histopathological Correlation

A variety of histologic studies of patients with BME have been described with different results. Some studies revealed necrosis of cellular element in the subchondral bone, trabecular

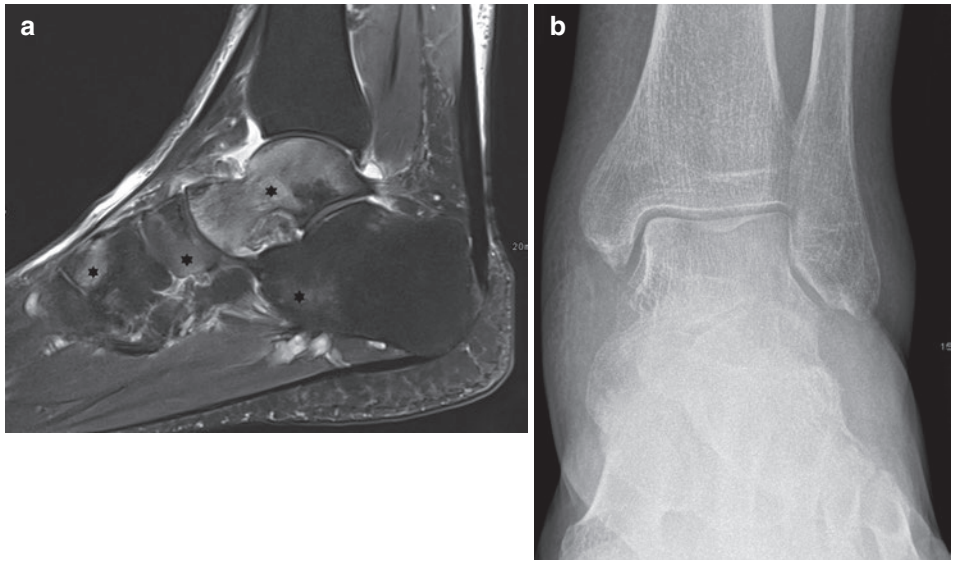

Fig. 9 (**a** and **b**) Bone marrow edema syndrome (BMES). (**a**) Sagittal fat-suppressed FSE T2-weighted image showing multifocal BME at the tarsal bones (black asterisks). (**b**) Plain radiograph of the ankle demonstrating the presence of osteopenia of the ankle with associated soft-tissue swelling

microfractures, and hemorrhage and edema (Johnson et al. 1998; Rangger et al. 1998; Ryu et al. 2000), whereas others demonstrated only edema with displacement of cellular element, but absence of necrosis (Escalas and Curell 1994).

Review of the different histologic studies suggests that differing degrees and severity of injury may determine the differing histological patterns. Relatively less severe trauma causes BME without obvious injury to the cellular element, whereas with increasing severity of trauma microfractures and hemorrhage are seen within the trabecular bone (Mandalia et al. 2005).

5 Clinical Significance

The clinical significance of bone marrow edema has been an issue of discussion ever since the first reports on bone bruise (Bonadio et al. 2017).

It is very difficult to identify clinical signs and symptoms directly attributable to the underlying bone bruising, because there are usually associated soft-tissue changes (Mandalia et al. 2005).

In a prospective study of 95 patients with inversion injuries of the ankle and no fracture on plain radiographs, Alanen et al. found an incidence of bone bruises of 27% (Alanen et al. 1998). Most of the bruises were located in the talus.

The authors found no statistical difference in the time to return to work, limitation in walking or physical activity, and clinical outcome at 3 months in two groups with and without BME. Also according to Zanetti et al., the presence of BME of the talar dome following sprain of the ankle did not significantly influence clinical outcome (Zanetti et al. 1997).

Vincken et al. (2006) evaluated the clinical consequences of bone bruise on MRI around the knee in 664 consecutive patients with subacute knee complaints. They evaluated the relation between bone bruise and (peri-)articular derangement and the impact of bone bruise at the time of MRI and 6 months thereafter.

Bone bruises were diagnosed in 18.7% of patients.

They concluded that bone bruise is no predictor for the presence of intra-articular pathology. Indeed, prevalence of bone bruise was not significantly different between patients with (21%) and those without (16%) intra-articular pathology. Bone bruise was particularly associated with tears in anterior cruciate ligaments, collateral ligaments, and lateral meniscus, whereas the medial meniscus tears (although representing the

most common knee lesion) were not associated with bone bruise.

On the other hand, patients presenting with bone bruise at the time of MRI had a significant higher level of symptoms, functional deficit, and decrease in activity.

Particularly, the presence of bone bruise and MCL tear has the most impact on function and symptoms at the time of MRI.

However, bone bruise did not have any effect on function, symptoms, and activity at 6 months.

6 Natural Evolution

6.1 Follow-Up of Acute Traumatic Bone Marrow Edema

The reported time for the resolution of bone bruising is variable, ranging from as early as 3 weeks to 2 years (Mandalia et al. 2005; Roemer and Bohndorf 2002). This variability may be attributed to several factors, such as the severity of injury, extent of bone bruising, and other associated internal knee derangement. Traumatic BME usually resolves with a median time interval ranging between 4 months and 8 months after acute knee trauma (Kijowski et al. 2014).

Two patterns of bruise resolution have been described (Davies et al. 2004). The *centripetal* pattern is the most frequent (Fig. 10), while other lesions (mostly type IIb and III) tend to resolve *towards the joint margin* (Karantanas 2021). The latter generally resolve slower and probably require longer rehabilitation because of higher risk of premature osteoarthritis.

The natural history of bruises is not well known as well as whether they predispose to premature osteoarthritis. Cartilage loss adjacent to bone marrow lesions has been reported several years after knee trauma (Kijowski et al. 2014; Potter et al. 2012; Faber et al. 1999).

Many studies have shown that bone bruising may have a deleterious effect on the overlying articular cartilage (Mandalia et al. 2005). The pathophysiological mechanisms by which the cartilage can undergo this degenerative process may be multifactorial. The initial blunt trauma might exceed a supraphysiological threshold and lead to progressive chondral damage (Charalambous 2014). In other words, injuries causing BME may alter the load-bearing properties of subchondral bone, which in turn allows for changes in the overlying cartilage (Faber et al. 1999). Additionally, the osseous lesion might heal into a stiffer construction than the previous normal bone. The decreased compliance might then generate greater loads in the articular cartilage, leading to a progressive cartilage degeneration.

6.2 Follow-Up of Chronic Traumatic Lesions

This item will be described more in detail in (Karantanas 2021).

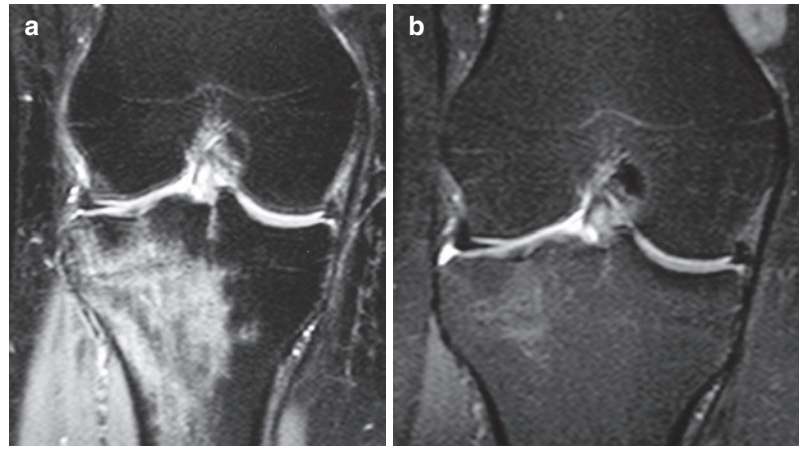

Fig. 10 (**a** and **b**) Resolution pattern of acute traumatic BME. Coronal FS T2-WI of the right knee at the moment of a direct trauma at the knee (**a**) and after 3-month follow-up (**b**). (**a**) Extensive impaction BME at the proximal tibia. (**b**) There is centripetal resolution of BME, with some residual BME at the center of the original lesion

6.3 Follow-Up of BMES

In BMES, the mean interval from the onset of symptoms until complete clinical resolution ranges from 4 to 24 months, with an average of 6 months (Fig. 11). All patients with BMES recover completely without intervention. Therefore, the term transient BMES can be used. However, it was demonstrated that in early stages of insufficient osseous blood flow iloprost can contribute to pain relief and improved joint function (Jäger et al. 2011; Meizer et al. 2009).

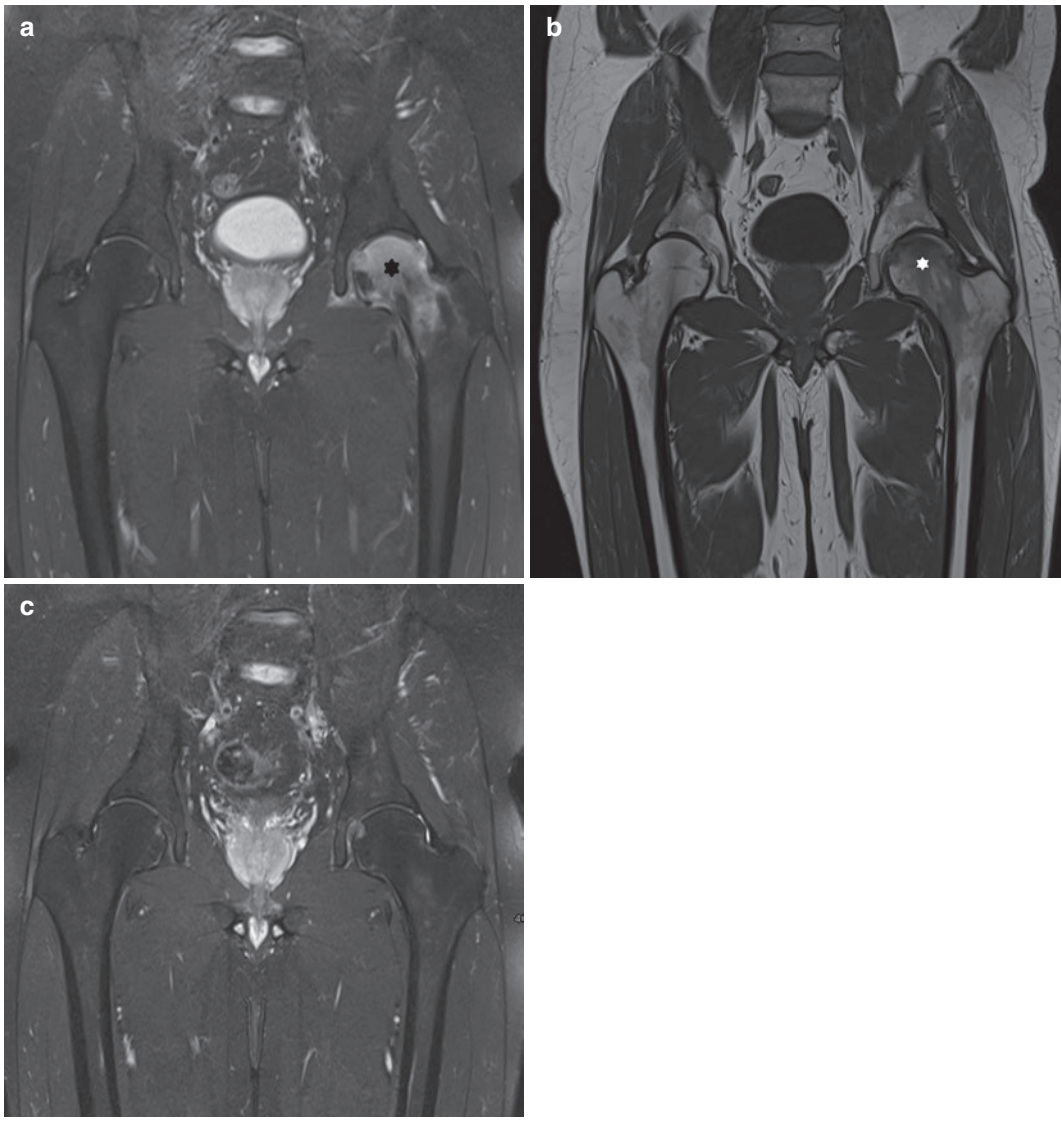

Fig. 11 (**a**–**c**) Resolution pattern of BMES of the hip. (**a**) Coronal FS T2-WI and (**b**) coronal T1 WI of the lateral aspect of the pelvis show BME in the left femoral head and neck (asterisk) with typical sparing of the medial aspect of the femoral head. (**c**) Follow-up after 3 months shows complete resolution of BME

7 Conclusion

BME is a relatively recently recognized entity. MRI has proved to be the most powerful tool to assess BME, as conventional imaging techniques are insensitive for detection of trabecular injuries.

The pathogenesis of BME is variable and may be due to acute or chronic trauma or may even occur in the absence of any history of obvious trauma.

Distinction between traumatic and nontraumatic bone marrow edema in sports injuries is primarily based on a clinical history of trauma, as imaging features are mostly indistinguishable.

In traumatic cases, the pattern of bone marrow edema, however, may reveal the mechanism of underlying trauma and is often a secondary sign for detecting associated abnormalities.

The clinical significance of BME is still a matter of debate, and long-term follow-up studies are required for further evaluation of this item.

Things to Remember

1. MRI is the imaging modality of choice to detect bone marrow lesions in sports injuries. Fluid-sensitive sequences such as FS T2-weighted images or (S)TIR sequences are the most sensitive ones.
2. Mostly BME in itself is benign/self-limiting. Longer follow-up studies are needed to determine the clinical importance of the (osteo) chondral sequelae and to evaluate the possible evolution towards premature degeneration. Isolated bruise can be the cause of pain.
3. A systematic analysis of the BME pattern often reveals a specific underlying trauma mechanism. This can help to detect the associated soft-tissue lesions, which are often less conspicuous.
4. Residual indications for conventional radiography (and/or CT) are (subtle) avulsion fractures and some stress fractures. DECT may be used for evaluation of BME in case of contraindications for MRI.

Box 1 MRI

- Gold standard for evaluation of traumatic bone marrow edema.
- May reveal associated soft-tissue lesions or intra-articular pathology.
- Fluid-sensitive sequences are most valuable for detection.

Box 2 Standard Radiography/CT

- Radiography has no role in the depiction of bone marrow edema.
- Dual-energy computed tomography (DECT) virtual non-calcium (VNCa) images may be an alternative for detection of BME if MRI is contraindicated.
- Main role is detection of (subtle) avulsion fractures.

References

Alanen V, Taimela S, Kinnunen J et al (1998) Incidence and clinical significance of bone bruises after supination injury of the ankle. A double-blind, prospective study. J Bone Joint Surg Br 80:513–515

Bonadio MB, Ormond Filho AG, Helito CP et al (2017) Bone marrow lesion: image, clinical presentation, and treatment. Magn Reson Insights:10.1178623X1770338

Booz C, Nöske J, Lenga L et al (2019) Color-coded virtual non-calcium dual-energy CT for the depiction of bone marrow edema in patients with acute knee trauma: a multireader diagnostic accuracy study. Eur Radiol 30:141. https://doi.org/10.1007/s00330-019-06304-7

Bosmans F, Vanhoenacker F (2019) Luxation latérale de la rotule avec lésion ostéochondrale sévère. Orthorhumato 17:36–38

Cahir JG, Toms AP (2008) Regional migratory osteoporosis. Eur J Radiol 67:2–10. https://doi.org/10.1016/j.ejrad.2008.01.051

Cano-Marquina A, Tarín JJ, García-Pérez MÁ, Cano A (2014) Transient regional osteoporosis. Maturitas 77:324–329

Chan KK, Resnick D, Goodwin D, Seeger LL (1999) Posteromedial tibial plateau injury including avulsion fracture of the semimembranosus tendon insertion site: ancillary sign of anterior cruciate ligament tear at MR imaging. Radiology 211:754–758. https://doi.org/10.1148/radiology.211.3.r99jn16754

Charalambous CP (2014) The response of articular cartilage to mechanical injury. In: Banaszkiewicz P, Kader DF (eds) Classic papers in orthopaedics. Springer, London, pp 381–383

Collins JA, Beutel BG, Strauss E et al (2016) Bone marrow edema chronic bone marrow lesions of the knee and the association with osteoarthritis. Bull Hosp Joint Dis 74:24–36

Costa-Paz M, Muscolo DL, Ayerza M et al (2001) Magnetic resonance imaging follow-up study of bone bruises associated with anterior cruciate ligament ruptures. Arthroscopy 17:445–449. https://doi.org/10.1053/jars.2001.23581

Davies NH, Niall D, King LJ et al (2004) Magnetic resonance imaging of bone bruising in the acutely injured knee—short-term outcome. Clin Radiol 59:439–445. https://doi.org/10.1016/j.crad.2003.11.012

Escalas F, Curell R (1994) Occult posttraumatic bone injury. Knee Surg Sports Traumatol Arthrosc 2:147–149. https://doi.org/10.1007/bf01467916

Eyselbergs M, Vanhoenacker FM, Boone P (2011) An unusual cause of bone marrow oedema in the acetabulum. Br J Radiol 84:1055–1058. https://doi.org/10.1259/bjr/64824020

Faber KJ, Dill JR, Amendola A et al (1999) Occult osteochondral lesions after anterior cruciate ligament rupture. Six-year magnetic resonance imaging follow-up study. Am J Sports Med 27:489–494. https://doi.org/10.1177/03635465990270041301

Felson DT, Chaisson CE, Hill CL et al (2001) The Association of Bone Marrow Lesions with pain in knee osteoarthritis. Ann Intern Med 134:541. https://doi.org/10.7326/0003-4819-134-7-200104030-00007

Felson DT, McLaughlin S, Goggins J et al (2003) Bone marrow edema and its relation to progression of knee osteoarthritis. Ann Intern Med 139:139. https://doi.org/10.7326/0003-4819-139-5_part_1-200309020-00008

Felson DT, Niu J, Gross KD et al (2013) Valgus malalignment is a risk factor for lateral knee osteoarthritis incidence and progression: findings from the multicenter osteoarthritis study and the osteoarthritis initiative. Arthritis Rheum 65:355–362. https://doi.org/10.1002/art.37726

Feyen H, Myncke J, Vanhoenacker FM (2008) Migratory symptomatic bone marrow oedema of the knee: a case report and literature review. Acta Orthop Belg 74:865–869

Franklyn M, Oakes B (2015) Aetiology and mechanisms of injury in medial tibial stress syndrome: current and future developments. World J Orthop 6:577–589

Grampp S, Henk CB, Mostbeck GH (1998) Overuse edema in the bone marrow of the hand: demonstration with MRI. J Comput Assist Tomogr 22:25–27. https://doi.org/10.1097/00004728-199801000-00004

Hayes CW, Conway WF, Daniel WW (1993) MR imaging of bone marrow edema pattern: transient osteoporosis, transient bone marrow edema syndrome, or osteonecrosis. Radiographics 13:1001–1011; discussion 1012

Hegazi TM, Belair JA, McCarthy EJ et al (2016) Sports injuries about the hip: what the radiologist should know. Radiographics 36:1717–1745. https://doi.org/10.1148/rg.2016160012

Jäger M, Zilkens C, Bittersohl B et al (2011) Efficiency of iloprost treatment for osseous malperfusion. Int Orthop 35:761–765. https://doi.org/10.1007/s00264-010-0998-4

Johnson DL, Urban WP, Caborn DNM et al (1998) Articular cartilage changes seen with magnetic resonance imaging-detected bone bruises associated with acute anterior cruciate ligament rupture. Am J Sports Med 26:409–414. https://doi.org/10.1177/03635465980260031101

Kaplan PA, Gehl RH, Dussault RG et al (1999) Bone contusions of the posterior lip of the medial tibial plateau (contrecoup injury) and associated internal derangements of the knee at MR imaging. Radiology 211:747–753. https://doi.org/10.1148/radiology.211.3.r99jn30747

Karantanas AH (2021) Natural history and monitoring of fractures and microfractures. Med Radiol. https://doi.org/10.1007/174_2020_271

Karantanas AH, Nikolakopoulos I, Korompilias AV et al (2008) Regional migratory osteoporosis in the knee: MRI findings in 22 patients and review of the literature. Eur J Radiol 67:34–41. https://doi.org/10.1016/j.ejrad.2008.01.054

Kijowski R, Roemer ZXF, Englund M et al (2014) Imaging following acute knee trauma. Osteoarthr Cartil 22:1429–1443. https://doi.org/10.1016/j.joca.2014.06.024

Klontzas ME, Vassalou EE, Zibis AH et al (2015) MR imaging of transient osteoporosis of the hip: an update on 155 hip joints. Eur J Radiol 84:431–436. https://doi.org/10.1016/j.ejrad.2014.11.022

Krampla W, Mayrhofer R, Malcher J et al (2001) MR imaging of the knee in marathon runners before and after competition. Skelet Radiol 30:72–76. https://doi.org/10.1007/s002560000296

Lee SC, Endo Y, Potter HG (2017) Imaging of groin pain: magnetic resonance and ultrasound imaging features. Sports Health 9:428–435. https://doi.org/10.1177/1941738117694841

Lefere M, Demeyere A, Vanhoenacker F (2021) Overuse bone trauma and stress fractures. Med Radiol. https://doi.org/10.1007/174_2020_240

Libicher M, Ivancic M, Hoffmann M et al (2005) Early changes in experimental osteoarthritis using the Pond-Nuki dog model: technical procedure and initial results of in vivo MR imaging. Eur Radiol 15:390–394. https://doi.org/10.1007/s00330-004-2486-y

Mandalia V, Fogg AJB, Chari R et al (2005) Bone bruising of the knee. Clin Radiol 60:627–636. https://doi.org/10.1016/j.crad.2005.01.014

Meizer R, Meraner D, Meizer E et al (2009) Outcome of painful bone marrow edema of the femoral head following treatment with parenteral iloprost. Indian J Orthop 43:36. https://doi.org/10.4103/0019-5413.45321

Miltner O, Niedhart C, Piroth W et al (2003) Transient osteoporosis of the navicular bone in a runner. Arch Orthop Trauma Surg 123:505–508. https://doi.org/10.1007/s00402-003-0532-x

Potter HG, Jain SK, Ma Y et al (2012) Cartilage injury after acute, isolated anterior cruciate ligament tear: immediate and longitudinal effect with clinical/MRI follow-up. Am J Sports Med 40:276–285. https://doi.org/10.1177/0363546511423380

Radke S, Vispo-Seara J, Walther M et al (2001) Transient bone marrow oedema of the foot. Int Orthop 25:263–267. https://doi.org/10.1007/s002640100253

Rangger C, Kathrein A, Freund MC et al (1998) Bone bruise of the knee: histology and cryosections in 5 cases. Acta Orthop Scand 69:291–294. https://doi.org/10.3109/17453679809000933

Reddy T, McLaughlin PD, Mallinson PI et al (2015) Detection of occult, undisplaced hip fractures with a dual-energy CT algorithm targeted to detection of bone marrow edema. Emerg Radiol 22:25–29. https://doi.org/10.1007/s10140-014-1249-6

Rios AM, Rosenberg ZS, Bencardino JT et al (2011) Bone marrow edema patterns in the ankle and hindfoot: distinguishing MRI features. Am J Roentgenol 197:W720

Roemer FW, Bohndorf K (2002) Long-term osseous sequelae after acute trauma of the knee joint evaluated by MRI. Skelet Radiol 31:615–623. https://doi.org/10.1007/s00256-002-0575-z

Ryu KN, Jin W, Ko YT et al (2000) Bone bruises: MR characteristics and histological correlation in the young pig. Clin Imaging 24:371–380. https://doi.org/10.1016/S0899-7071(00)00248-5

Sanders T, Medynski M, Feller J, Lawhorn K (2000) Bone contusion patterns of the knee at MR imaging: footprint of the mechanism of injury. Radiographics 20(Suppl 1):S135-51. https://doi.org/10.1148/radiographics.20.suppl_1.g00oc19s135

Schapira D (1992) Transient osteoporosis of the hip. Semin Arthritis Rheum 22:98–105. https://doi.org/10.1016/0049-0172(92)90003-V

Schilders E, Bharam S, Golan E et al (2017) The pyramidalis–anterior pubic ligament–adductor longus complex (PLAC) and its role with adductor injuries: a new anatomical concept. Knee Surg Sports Traumatol Arthrosc 25:3969–3977. https://doi.org/10.1007/s00167-017-4688-2

Schueller-Weidekamm C, Schueller G, Uffmann M, Bader TR (2006) Does marathon running cause acute lesions of the knee? Evaluation with magnetic resonance imaging. Eur Radiol 16:2179–2185. https://doi.org/10.1007/s00330-005-0132-y

Standring S (ed) (2016) Gray's Anatomy, 41st Edition. The Anatomical Basis of Clinical Practice. Elsevier Health Sciences UK, Philadelphia

Toms AP, Marshall TJ, Becker E et al (2005) Regional migratory osteoporosis: a review illustrated by five cases. Clin Radiol 60:425–438. https://doi.org/10.1016/j.crad.2004.07.002

Trappeniers L, De Maeseneer M, De Ridder F et al (2003) Can bone marrow edema be seen on STIR images of the ankle and foot after 1 week of running? Eur J Radiol 47:25–28. https://doi.org/10.1016/S0720-048X(02)00221-8

Van De Perre S, Vanhoenacker FM, De Schepper AM (2003) Thigh splints in a skeletally immature boy. RoFo Fortschritte auf dem Gebiet der Rontgenstrahlen und der Bildgeb Verfahren 175:1582–1584. https://doi.org/10.1055/s-2003-43413

Vanhoenacker FM, Snoeckx A (2007) Bone marrow edema in sports: general concepts. Eur J Radiol 62:6–15. https://doi.org/10.1016/j.ejrad.2007.01.013

Vanhoenacker FM, Snoeckx A, Vandaele L et al (2005) Bone marrow changes in sports injuries. JBR-BTR 88:332–335

Vincken PW, Ter Braak BP, van Erkel AR et al (2006) Clinical consequences of bone bruise around the knee. Eur Radiol 16(1):97–107. https://doi.org/10.1007/s00330-005-2735-8. Epub 2005 Apr 20. PMID: 15841383

Walgrave L, Vanhoenacker F (2019) Douleur aiguë de la hanche chez l'adulte : pensez à la moelle osseuse. Ortho-rhumato 17:32–34

Winters M (2020) The diagnosis and management of medial tibial stress syndrome: an evidence update. Unfallchirurg 123:15–19

Yao L, Lee JK (1988) Occult intraosseous fracture: detection with MR imaging. Radiology 167:749–751. https://doi.org/10.1148/radiology.167.3.3363134

Yochum TR, Barry MS (1997) Bone marrow edema caused by altered pedal biomechanics. J Manip Physiol Ther 20:56–59

Zanetti M, De Simoni C, Wetz HH et al (1997) Magnetic resonance imaging of injuries to the ankle joint: can it predict clinical outcome? Skelet Radiol 26:82–88. https://doi.org/10.1007/s002560050198

Overuse Bone Trauma and Stress Fractures

Mathieu Lefere, Annick Demeyere, and Filip Vanhoenacker

Contents

M. Lefere (✉) · A. Demeyere
Department of Radiology, Imelda Hospital, Bonheiden, Belgium
e-mail: mathieu.lefere@imelda.be

F. Vanhoenacker
Department of Radiology, AZ Sint-Maarten Mechelen, Mechelen, Belgium

Department of Radiology, University Hospital Antwerp and University Antwerp, Antwerp, Belgium

Faculty of Medicine and Health Sciences, Ghent University, Ghent, Belgium

Abstract

Stress-related bone injuries are common in athletes who are exposed to increased frequency, duration and intensity of activity. They are most common in the weight-bearing bones of the lower extremities, especially the posteromedial tibia. Under physiological circumstances, increasing the load on a bone will increase its strength through bone remodeling. When remodeling is unable to keep up with repetitive loading, a stress fracture will occur. The distinction between high-risk and low-risk stress fractures has prognostic and therapeutic consequences in athletes. Several extrinsic and intrinsic risk factors have been recognized. Overall, women are more sensitive to stress fractures than men. Conventional radiographs, despite having a low sensitivity, are used as a first-line test. Magnetic resonance imaging is the most sensitive and specific imaging modality for stress fractures. Computed tomography can be used as a problem solver in case of inconclusive MRI, and to better display fracture lines in a few specific locations.

1 Introduction

Stress-related bone injuries are common in athletes and account for up to 20% of cases in sports medicine practice (Abbott et al. 2019). The term

Med Radiol Diagn Imaging (2021)
https://doi.org/10.1007/174_2020_240, © Springer Nature Switzerland AG
Published Online: 23 February 2021

"stress fracture" is used when there is no single identifiable traumatic event, but rather an exposure to repetitive microtrauma. Two subtypes of stress fractures have been recognized. Fatigue fractures occur in individuals with presumed normal bone mineral density (BMD) who are exposed to increased frequency, duration, and intensity of activity. High-risk populations typically include military recruits and professional athletes. Insufficiency fractures occur in patients with decreased BMD or abnormally inelastic bone, in response to relatively normal activities. These lesions often occur in the setting of osteoporosis and metabolic bone disease and are not the main focus of this chapter. The distinction between the two types is not always clear, and certain subpopulations of athletes may also suffer from insufficiency fractures (Aicale et al. 2018). In the orthopedic literature, "stress fracture" and "fatigue fracture" are often used interchangeably. The term "stress reaction" is used when bone marrow edema (BME) is seen on magnetic resonance imaging (MRI) studies, without fracture line.

Although the reported incidence of stress fractures in the general athletic population is less than 1%, the incidence in runners may be as high as 20%. They are most common in the weight-bearing bones of the lower extremities. In terms of prevalence, the posteromedial distal tibia, the calcaneus, and the metatarsals constitute the "big three" (Mandell et al. 2017a). Specific anatomic sites for stress fractures may be associated with individual sports, such as the humerus in throwing sports, the ribs in golf and rowing, the spine in gymnastics, the lower extremities in running activities, and the foot in gymnastics (Bennell and Brukner 1997). Possible sites of stress injury are summarized in Table 1 (Resnick 1996).

The posteromedial tibial cortex is by far the most common location for stress fractures in active individuals. Pain in the lower leg brought on by exercise but relieved by rest is a common complaint. "Shin splints" is a nonspecific clinical term used in the setting of exertional lower leg pain (Mandell et al. 2017b).

Early diagnosis of a stress lesion is essential to enable specific treatment and to ensure the earliest possible return to sports.

2 Pathophysiology

2.1 Bone Anatomy

2.1.1 Macroscopic Anatomy

Bones provide a rigid support for muscles, allowing complex movements and locomotion. Most of the adult skeleton is composed of lamellar bone. The other major configuration is woven bone, which in physiological circumstances is found mainly in fetuses and during the healing phase of fractures. Woven bone is less organized, more flexible but weaker than lamellar bone. Lamellar bone exists in two major forms: cortical and trabecular (spongy, cancellous) bone.

Table 1 Possible sites of stress injuries

Upper extremity
– Phalangeal tufts
– Carpal bones: Hook of hamate
– Ulna: Coronoid, olecranon process, diaphysis
– Humerus: Distal diaphysis
– Scapula: Coracoid, inferior edge of glenoid fossa
Lower extremity
– Sesamoids
– Metatarsals
– Navicular
– Talus
– Calcaneus
– Tibia: Mid and distal diaphysis, proximal shaft, medial malleolus
– Fibula: Distal and proximal diaphysis
– Patella
– Femur: Diaphysis, neck
– Pelvis: Obturator ring, pubic rami, sacrum
Spine
– Lumbar vertebra: Pars interarticularis
– Lower cervical, upper thoracic spinous process
Thorax
– Ribs
– Clavicle
– Sternum

Cortical bone is dense and solid and surrounds the marrow space. Trabecular bone is much less compact; it consists of a meshwork of thin rods and plates called trabeculae (Fig. 1). In most sites, trabeculae are oriented along the axes of major compressive and tensile forces within that bone. In joints that are frequently compressed, trabeculae are often aligned perpendicularly to the subchondral bone plate. However, as has been observed in the femoral neck, trabecular organization is very complex and cannot always be predicted by the direction of principal stress (Pathria et al. 2016).

The proportion of cortical and trabecular bone varies between individuals and between types of bone: the ratio of cortical to trabecular bone is 50:50 in the femoral head and 95:5 in the radial diaphysis (Clarke 2008). The outer shafts of long bones are mainly cortical, with trabecular bone making up the ends of the bone and the central portion of the shaft. Short and flat bones such as the tarsals and pelvis have a higher amount of trabecular bone.

The outer surface of long bones is surrounded by a highly vascular outer coating called the periosteum. The periosteum is responsible for providing nutrition to the outer portion of the cortex and enlarges during remodeling to provide support to the cortex. Medullary canals allow the vascular passage for nutrients and blood vessels to the inner two-thirds of the cortex (Romani et al. 2002).

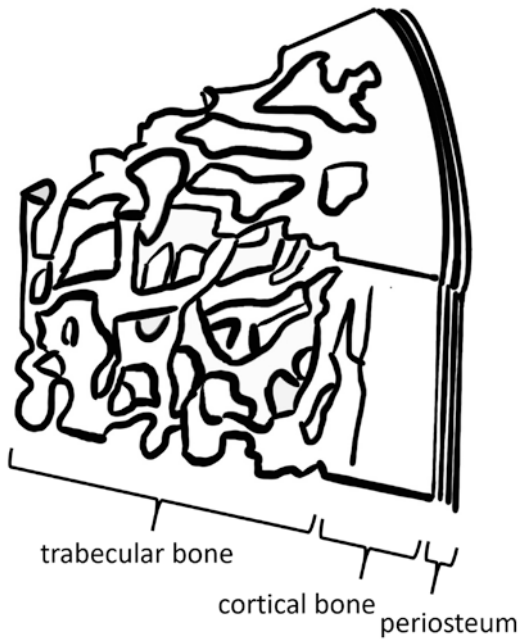

Fig. 1 Macroscopic bone anatomy

2.1.2 Microscopic Anatomy

The extracellular component of bone, also called the matrix, consists of collagen fibrils and ground substance. The orientation of the collagen fibrils and the integrity of their cross-links are important factors determining the force a bone can withstand before it breaks. The mineral component of the matrix is mostly composed of hydroxyapatite and is responsible for the strength, hardness, and rigidity of bone; however, it is also more brittle than the collagenous component (Pathria et al. 2016).

The fundamental unit of cortical bone is the osteon. In the osteon, concentric layers or lamellae of mineralized bone matrix surround small channels called haversian canals, with a diameter of around 100–400 μm. These canals house nerves and blood vessels. On the outside of the lamellae are small cavities, known as lacunae. Each lacuna contains a single bone cell, or osteocyte. Canaliculi form a transport system between the lacunae and the haversian canals which are responsible for the nutrition and metabolic transport within the bone.

2.2 Bone Remodeling

According to Wolff's law, if the loading on a particular bone increases, its strength will increase over time, and vice versa.

Bone remodeling involves three steps. Initially, microcrack formation occurs. Microcracks disrupt canaliculi and induce osteocyte apoptosis. In a second phase, osteoclasts create resorption cavities at the site of the microcracks, which temporarily weakens the bone. Finally, osteoblasts deposit new bone at the resorption cavities, thereby completing the remodeling cycle. In cortical bone, the adjacent periosteum may become inflamed during bone remodeling, providing

ancillary support. In trabecular bone, remodeling may trigger a reorientation of the struts to better withstand the applied force. The completion of bone remodeling is estimated to take 2–8 months. Because new bone deposition by osteoblasts lags behind the formation of resorption cavities by a period of 10–14 days, the bone is relatively weakened in these early stages of remodeling. When the process of skeletal remodeling is unable to keep up with repetitive loading, a stress fracture occurs (Mandell et al. 2017a; Marshall et al. 2018; Pathria et al. 2016).

3 Mechanisms of Injury

In general, the response of any material to a mechanical force is determined by its ability to absorb a load (stress) and the amount of deformation that can occur before failure (strain). The relationship between both is graphically depicted in a stress-strain curve, from which the stiffness (elastic modulus), yield, and failure points of a particular material can be deducted (Fig. 2). The term "brittle" is used when a substance is able to withstand a high load but is unable to deform (e.g., porcelain). Conversely, ductile material undergoes considerable deformation before failure. Bone, as a complex structure, behaves in an intermediate fashion.

A bone endures stress whenever a force is loaded upon it. Whether the stress comes from the pull of a muscle or the shock of a weight-bearing extremity contacting the ground, it is defined as the force applied per unit area of the load-bearing bone. The stress-strain response of bone depends on the direction of the load; the geometry, microarchitecture, and density of bone; and the influence of surrounding muscular contractions.

In most activities of daily living, when the force is removed, the bone elastically rebounds to its original position. The force that a bone can endure and still rebound back to its original state without damage is within the elastic range. If a bone is loaded beyond its yield point, it enters the plastic range where irreversible deformation will occur. This stage is characterized by microcrack formation. The amount of mechanical load required to cause a macroscopic bone fracture is determined by its failure point. As a living structure, bone is able to adapt its stress-strain curve to better withstand the loads under which it is placed, through the earlier described process of bone remodeling.

In vivo, forces are directly or indirectly applied to bone through a complex combination of compression, torsion, bending, and shear. Cortical bone has a higher modulus of elasticity than trabecular bone. Therefore, cortical bone is highly resistant to compressive forces but relatively sensitive to bending forces, and the inverse is true for trabecular bone. A bending force is thought to be the most important biomechanical factor leading to the development of a tibial stress fracture. It applies tension strain on the convex

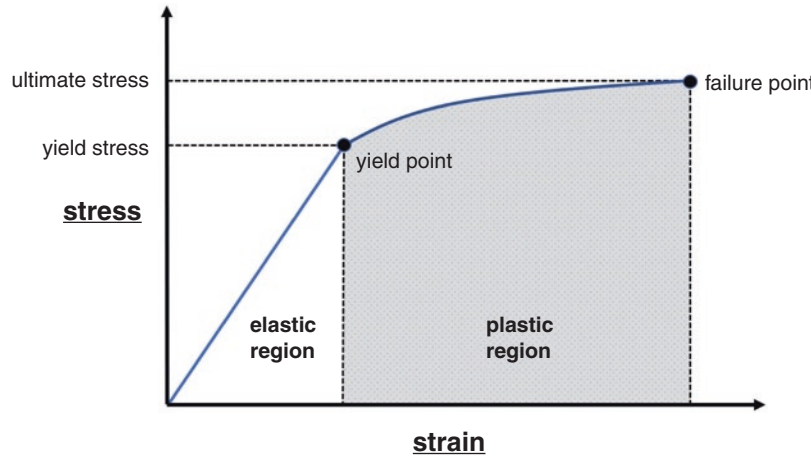

Fig. 2 Stress-strain curve. In the elastic region, a solid material (e.g., bone) will still regain its original shape when stress (load) is removed. If a bone is loaded beyond its yield point, it enters the plastic range where irreversible deformation will occur. The elastic modulus ε measures the stiffness of the material and is calculated from the slope of the curve

surface, and a compressive force on the concave aspect of the bone shaft (Pathria et al. 2016; Marshall et al. 2018).

3.1 High-Risk Versus Low-Risk Stress Fractures

The distinction between high-risk and low-risk stress fractures is of great importance since it affects the diagnostic and therapeutic pathways pursued by clinicians.

Stress fractures that arise under compressive forces are generally considered low risk. They can be managed with activity modification and continued weight bearing. High-risk stress fractures generally occur under tensile forces and often have a more unfavorable disease course (Marshall et al. 2018; Mandell et al. 2017b) (Table 2). Stress fractures at these sites are prone to recurrence, delayed union, and nonunion. Depending on the location, a more aggressive approach such as prolonged immobilization or surgery may be warranted (Diehl et al. 2006). Stress fractures of the anterior tibial diaphysis occur most frequently in jumpers and represent only 4.6% of tibial stress fractures. These lesions heal slowly, partly because of absent muscular support and relatively poor vascularization. Conservative treatment is prone to failure with progression to complete fracture. The hallmark sign on radiographs is a transverse fracture in the anterior tibial cortex, the so-called dreaded black line (Mandell et al. 2017b) (Fig. 3).

Table 2 High- and low-risk stress fracture locations in the lower extremities

High-risk stress fractures	Low-risk stress fractures
Anterior tibial cortex	Posteromedial tibial cortex
Medial malleolus	Second and third metatarsal
Base of second and fifth metatarsals	Calcaneus
Navicular	Distal fibula
Talus	Cuboid
Hallux sesamoids	Cuneiforms
Lateral femoral neck (tension side)	Medial femoral neck (compression side)
Patella	
Pars interarticularis	

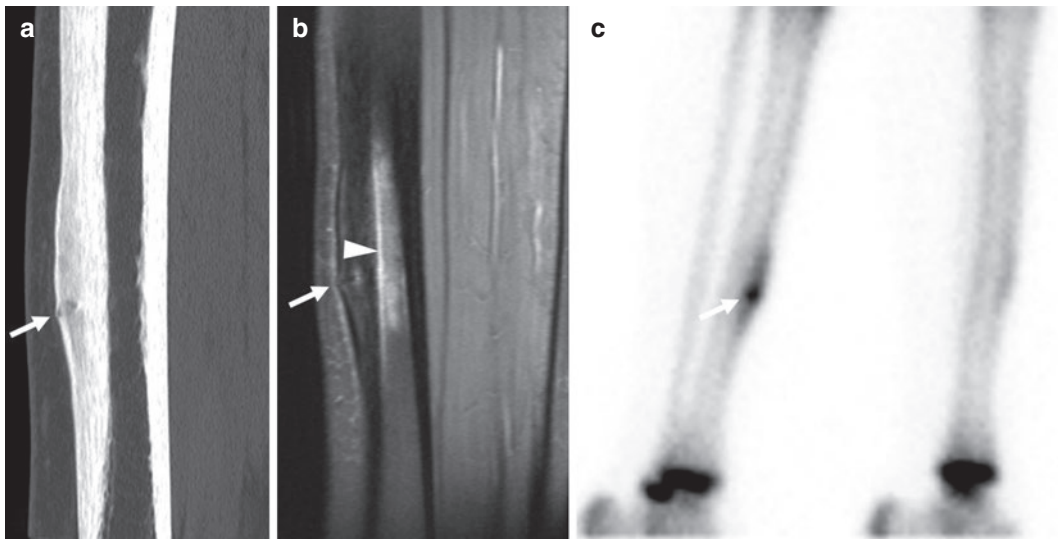

Fig. 3 (**a**–**c**) Anterior tibial stress fracture in a 16-year-old boy. (**a**) Sagittal CT image shows thickening of the anterior tibial cortex with a fracture through the anterior part (the equivalent of the "dreaded black line" on radiographs) (arrow). (**b**) Sagittal fat-suppressed (FS) T2-weighted image (WI) shows the fracture line (arrow) and adjacent bone marrow edema (arrowhead). (**c**) On planar bone scintigraphy, a corresponding hot spot is seen in the anterior tibial diaphysis (arrow)

4 Risk Factors

There are many highly interrelated risk factors contributing to the development of stress fractures, making it very difficult to study them independently. They are generally divided into intrinsic and extrinsic factors.

4.1 Intrinsic Risk Factors

Intrinsic risk factors refer to the physical characteristics of an individual that may contribute to the development of stress fractures.

4.1.1 Bone Mineral Density

The question whether low bone mineral density (BMD) is an independent risk factor has been the subject of research. Lauder et al. found a significantly higher risk of stress fractures in female soldiers with lower femoral neck BMD (Lauder et al. 2000). In their study however, the BMD at the lumbar spine level was not significantly related to the development of stress fractures. Davey et al. sought to investigate structural bone and BMD differences between military recruits with stress fractures and healthy controls, adjusted for confounders such as age, physical fitness level, height, and weight. They found a significant difference in BMD between both groups, both at the femoral neck and at the lumbar spine (Davey et al. 2015).

4.1.2 Female Sex

Stress fractures are known to occur at higher rates in female athletes. In a large study among student-athletes, the overall relative risk was 2.06 in women compared to men, all sports combined. There was a higher incidence in women for each injury site, except lower back, lumbar spine, and pelvis (Rizzone et al. 2017). Nearly one in seven female athletes are reported to have a history of either stress fracture or stress reaction. They are most prevalent in female endurance runners, track-and-field athletes, and dancers. Smaller tibial width in women is a known risk factor which may help to explain this difference in prevalence between women and men (Behrens et al. 2013).

A combination of mostly intrinsic risk factors can be found in the so called female athletic triad, i.e., the combination of low energy availability with or without eating disorder, menstrual abnormalities, and decreased bone mass. This concept has received considerable attention in the literature since its first description in 1992. The triad has been observed most commonly in athletes involved in sports where a slender physique and weight control are favored, such as gymnastics or ballet. A revised definition in 2007 no longer requires all three features to be present (Nattiv et al. 2007). At least one element of the triad was found to be present in 16–60% of women (Moreira and Bilezikian 2017). In a prospective cohort study on 259 female adolescent and young adult athletes, it was shown that the stress fracture risk progressively increases up to 50% when more triad-related risks are present (Barrack et al. 2014). A causal relationship between these risk factors has been shown: dietary restriction may lead to low BMD, which is also negatively influenced by an estrogen-deficient state.

4.1.3 Age

Young athletes seem to be more susceptible to stress fractures. 40–50% of bone stress injuries have been reported in athletes under 20 years of age. Increasing expectations, intensity of training, and physiological stress in 16- to 18-year-olds competing with older, more physically mature individuals may contribute to this phenomenon (Nussbaum et al. 2019).

4.1.4 Lower Extremity Biomechanics

Leg length discrepancy, pes planus or cavus deformity, and also hip adduction and rearfoot eversion angles have been associated with higher rates of lower extremity stress fractures (Behrens et al. 2013).

4.1.4.1 Pronated Foot

The pronated foot with a rearfoot valgus position produces increased stress on the lateral malleolus. When the foot pronates through the

midstance phase of gait into the toe-off phase, the first metatarsal is hypermobile and dorsiflexes, resulting in an increased pressure load on the second metatarsal. If the second metatarsal is short, then increased load is transferred to the third metatarsal.

4.1.4.2 Cavus Foot

The cavus foot is generally rigid in nature and its shock-absorptive properties are poor. The plantarflexed forefoot results in increased pressure on the metatarsals. A rigidly plantarflexed first metatarsal is placed under increased stress, which places the sesamoid complex at risk of stress fracture. A long or plantarflexed lesser metatarsal is exposed to a greater load and is subjected to fatigue failure. Limited subtalar joint motion produces increased pressure on the calcaneus and renders it susceptible to a stress fracture.

4.1.4.3 Varus Alignment

Varus alignment such as genu varum, tibia vara, subtalar varus, and forefoot varus is associated with lower extremity stress fractures, 49% of which are located at the tibia. The resulting excessive pronation increases the eccentric work that must be done by the medial aspect of the soleus muscle and enforces the strain on the posteromedial side of the tibia.

4.1.4.4 Limb Length Discrepancy

Limb length discrepancy is a relatively common skeletal malalignment with predispositon to stress fractures. It has been reported that runners with a leg length discrepancy experienced stress fractures more often than runners without. During running, the short leg rotates externally to increase stability and overstriding may occur. The foot on the short side is subjected to greater force over a short period of time (Haverstock 2001).

4.2 Extrinsic Risk Factors

Extrinsic factors include individual training regimen, footwear and other equipment, training surfaces, and dietary intake.

High training volume is nearly always present in healthy individuals with stress fractures. In addition to professional athletes, recreational runners who average above 25 miles a week are at increased risk (Moreira and Bilezikian 2017).

5 Diagnostic Imaging

Bone response to stress is evaluated on a dynamic continuum between early remodeling and periostitis to a cortical stress fracture. It is important to note that these bony changes reflect a wide spectrum of physical findings and radiographic presentations. Patients will therefore often undergo multiple exams before a final diagnosis is made. Early identification of stress fractures is essential to prevent long-term complications. Figure 4 shows a diagnostic algorithm for suspected stress fractures.

5.1 Conventional Radiography

Plain radiography is a readily available, low-cost modality, and is still widely used as the initial step in the imaging workup of a suspected stress fracture. Unfortunately, initial radiographs are often normal, which is not surprising given the degree of microscopic remodeling that occurs in the early stages of stress injury. Clinicians and patients should be aware that up to 85% of stress fractures are not detected on initial radiographs, and up to 50% are missed on follow-up radiographs (Wright et al. 2016). If it affects clinical management, more advanced imaging studies should be pursued in case of negative radiographs.

Imaging features of stress fractures are determined by two factors: the chronicity of injury and the proportion of cortical to trabecular bone involved. The earliest radiographic manifestation of cortical involvement is the “gray cortex” sign: a subtle ill definition of the cortex or faint intracortical radiolucent striations, which are presumably related to the osteoclastic tunneling found early in the remodeling process. These early radiographic changes only appear 2–3 weeks

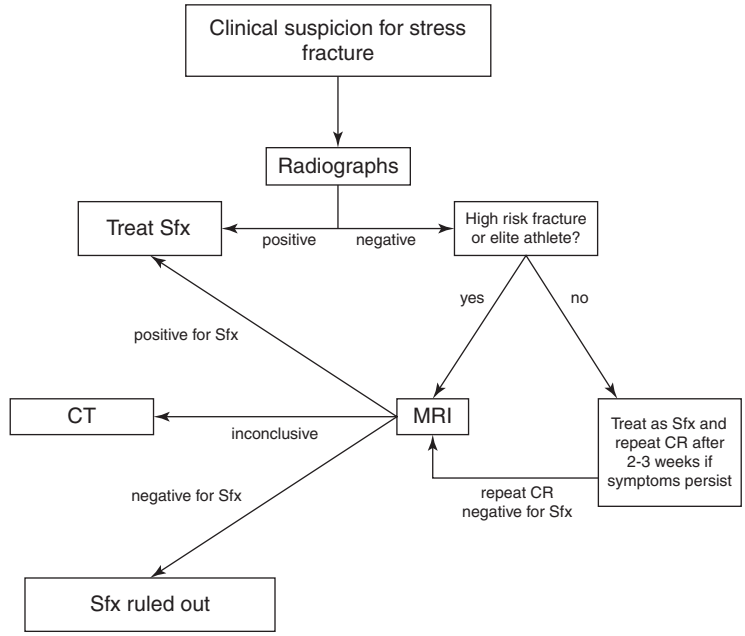

Fig. 4 Imaging algorithm for clinically suspected stress fracture. *Sfx* stress fracture, *CR* conventional radiograph

after onset of symptoms (Mandell et al. 2017a). They may be easily overlooked until periosteal new bone formation and/or endosteal thickening develops in an apparent attempt to buttress the temporarily weakened cortex. As damage increases, a true fracture line appears (Fig. 5). Radiographs can be used as an adjunct to MRI, to help elucidate more complex fracture patterns (Fig. 6).

Stress injuries in trabecular bone are notoriously difficult to detect. Subtle blurring of trabecular margins and faint sclerotic radiopaque areas may be seen secondary to peritrabecular callus (Fig. 7).

5.2 Bone Scintigraphy and SPECT-CT

Bone scintigraphy involves the intravenous injection of radiopharmaceuticals, most typically technetium 99m-labelled phosphates or diphosphonates. These agents bind to hydroxyapatite crystals in bone, in proportion to osteoblastic activity and blood flow, and can thus be considered markers of bone turnover and perfusion. In classic scintigraphy, mono-, bi-, or triphasic planar projection images are acquired with a gamma camera. Before the advent of MRI, three-phase planar scintigraphy was the gold standard imaging technique for the detection of stress fractures. It is generally considered a sensitive but not very specific exam (Wright et al. 2016). One of the earliest efforts to classify stress fractures was made by Roub and coworkers in 1979, who correlated scintigraphic abnormalities with clinical and radiographical data in 30 athletes with shin soreness (Roub et al. 1979). In 1987, two different four-grade scintigraphic classifications were published by Chisin et al. (1987) and Zwas et al. (1987), respectively. The latter is still in use (Pelletier-Galarneau et al. 2015); however, since MRI has become widely available, it has almost completely supplanted planar scintigraphy as the primary imaging modality for stress fractures.

Over the last decades, technical improvements have allowed for 3D reconstruction of scintigraphic images, with the introduction of single-photon emission computed tomography (SPECT). With this technique, cross-sectional scintigraphic images can be reconstructed in any desired plane. Hybrid SPECT-CT scanners have made their way into routine clinical practice. The

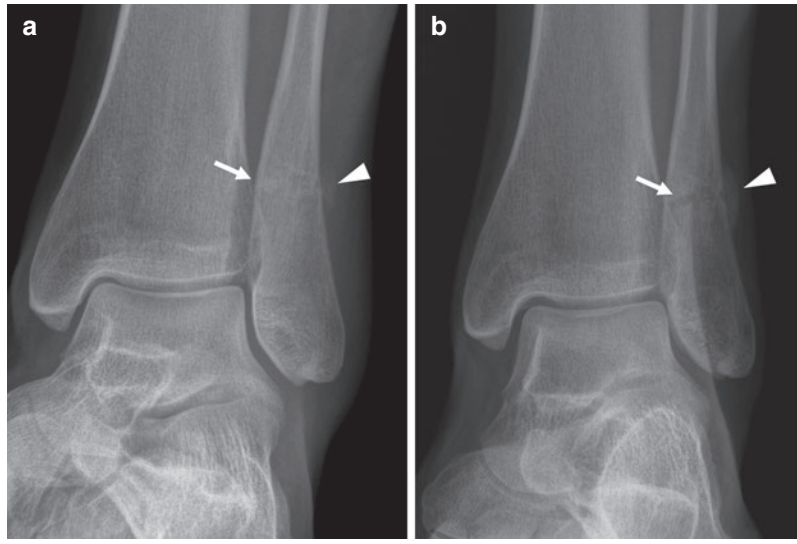

Fig. 5 (**a** and **b**) Radiographic evolution of a fibular stress fracture in a 45-year-old woman with exertional pain. (**a**) Mortise view of the ankle shows faint linear horizontal sclerosis in the distal fibular diaphysis (arrow) corresponding to microcallus formation, as well as indistinct periosteal bone deposition (arrowhead). (**b**) Follow-up radiograph shows progression to complete fracture (arrow) along with more mature periosteal bone apposition (arrowhead)

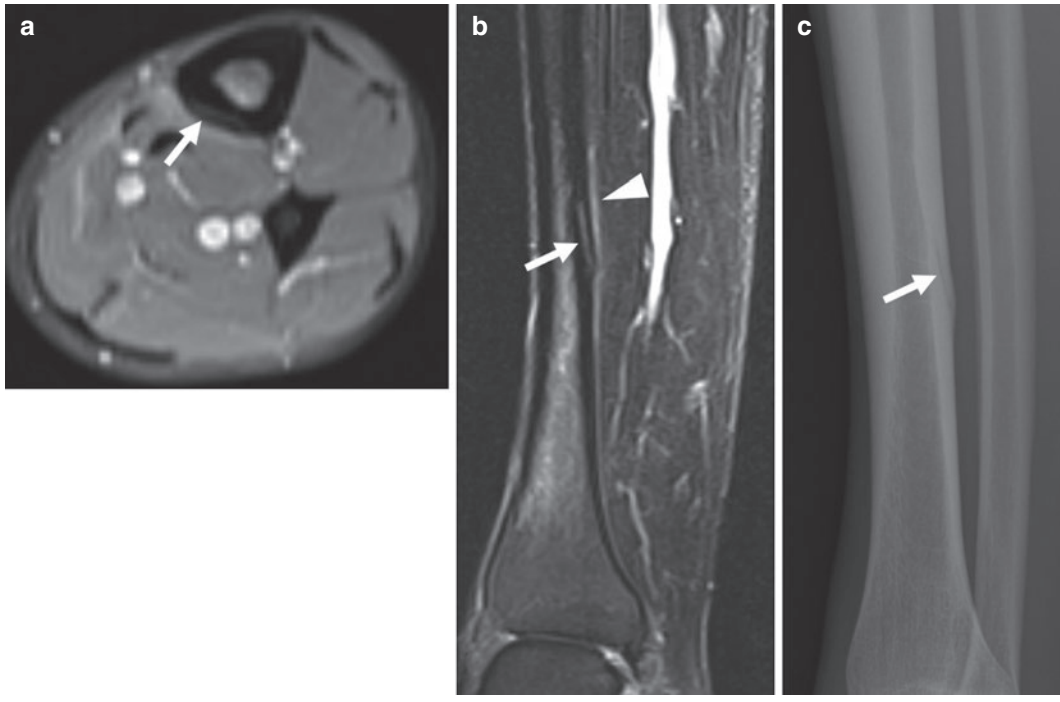

Fig. 6 (**a**–**c**) Longitudinal tibial stress fracture in a 46-year-old runner. (**a**) Axial FS T2-WI shows a cortical fracture line paralleling the cortical margin (arrow). (**b**) Sagittal FS T2-WI shows the longitudinal course of the stress fracture (arrow). Adjacent periosteal edema allows differentiation from a nutrient foramen (arrowhead). (**c**) Lateral radiograph shows the fracture line and associated slight cortical thickening (arrow)

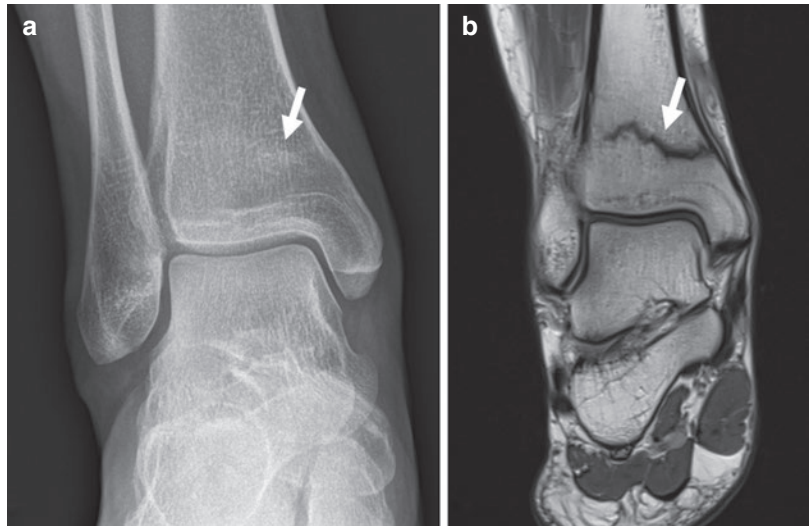

Fig. 7 (**a** and **b**) Trabecular stress fracture of the distal tibia in a 45-year-old woman. (**a**) On a frontal radiograph, only very subtle and blurry densification of the trabeculae is noticed, compatible with microcallus formation (arrow). (**b**) Coronal T1-WI taken 8 days later shows an incomplete horizontal fracture line in the metadiaphyseal region (arrow)

simultaneous acquisition of SPECT and CT images may help to improve the diagnostic accuracy by coupling functional and anatomical information (Ha et al. 2015).

At present, there seem to be no prospective studies on the accuracy of SPECT-CT versus MRI in the diagnosis of lower leg stress fractures (Glaudemans et al. 2015). In a retrospective study involving 50 patients, SPECT-CT was found to have comparable sensitivity and higher specificity than MRI in the detection of bone lesions in the ankle and foot; however, no stress fractures were mentioned (Ha et al. 2015).

5.3 Conventional CT and Dual-Energy CT

According to a recent systematic review, CT has a sensitivity of only 32–38% and a specificity of 88–98% for lower extremity stress fractures, resulting in a high number of false negatives. Therefore, CT has a small role in the diagnostic workup for most stress fractures (Wright et al. 2016). However, CT is particularly well suited for stress fractures of the tarsal bones, longitudinal stress fracture of the tibia, pars interarticularis stress fractures (spondylolysis), and stress fractures in the sacrum. CT may also detect fracture lines that are invisible on MRI, and serve as a problem-solving tool in cases of an inconclusive MRI (Glaudemans et al. 2015). For example, CT is often used as a secondary modality to detect partial or complete pars interarticularis stress fractures in young athletes with focal BME on MRI (Cheung et al. 2018) (Fig. 8). CT is also helpful in differentiating between stress fracture and osteoid osteoma, because both entities may be hot on bone scan, show BME at MR imaging, and demonstrate sclerosis on radiographs. The presence of a radiolucent nidus, however, is diagnostic for osteoid osteoma (Anderson and Greenspan 1996). CT has also proven its value in the diagnosis of pediatric stress fractures. Initial radiographs may demonstrate marked periosteal bone formation, which may mimic tumor. Demonstration of endosteal bone formation on CT often leads to the correct diagnosis.

In the past decade, dual-energy CT (DECT) has made its appearance into daily clinical practice. The basic principle of DECT is the simultaneous acquisition of images with low and high tube voltage (e.g., 80 and 140 kV). In the field of musculoskeletal radiology, DECT can provide additional information regarding tissue composition (e.g., urate detection in gout), metal artefact reduction, and image optimization. By using virtual non-calcium images, BME can be depicted on DECT images (Vanhoenacker 2021). This technique has shown promise for the detection of otherwise occult posttraumatic bone bruise in the

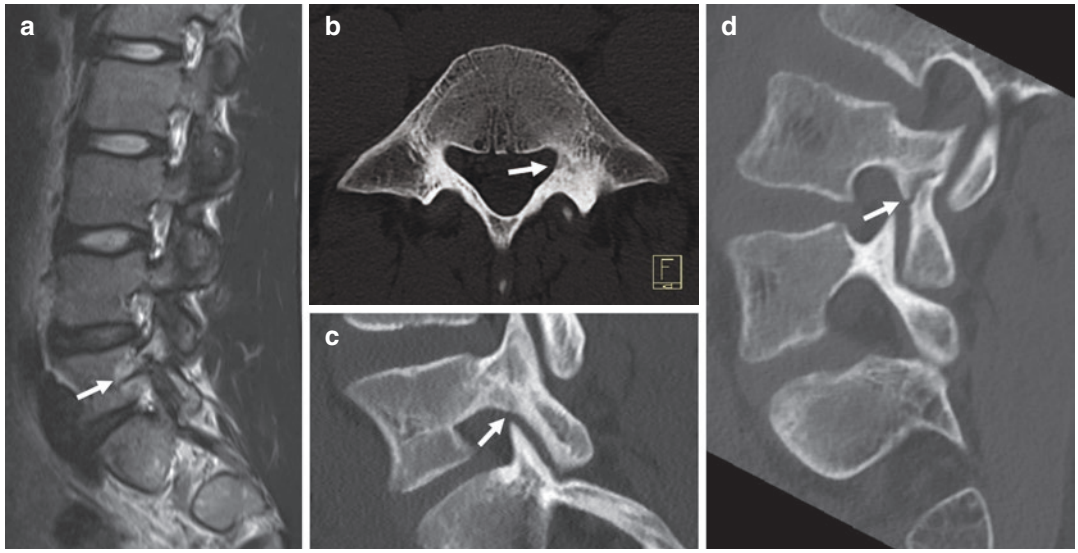

Fig. 8 (**a**–**d**) Pars interarticularis stress fractures in male adolescent athletes. (**a**) Sagittal T2-WI of the lumbar spine shows focal BME in the left pars interarticularis at L5. (**b**) Axial and (**c**) sagittal CT images show small incomplete stress fracture of the left pars, propagating in a predictable fashion from inferomedially to superolaterally. (**d**) Sagittal CT image in a different patient shows complete pars interarticularis stress fracture of the L4 vertebra. Unsharp fracture margins suggest recent injury, which was supported by the presence of BME on MRI (not shown)

emergency setting, and also for vertebral fractures and sacral insufficiency fractures in the elderly (Mallinson et al. 2016; Palm et al. 2019). At present however, there seem to be no studies regarding the performance of DECT in the diagnosis of lower extremity stress fractures in active individuals.

5.4 Ultrasound

US has a reported sensitivity of 43–99% and specificity of 13–79% for the detection of lower extremity stress fractures (Wright et al. 2016). US has the advantages of being a low-cost, radiation-free modality with point-of-care availability. Several sonographic signs in bone stress injuries have been described: periosteal thickening, cortical irregularities, calcified bone callus, subcutaneous edema, and hypervascular changes on color Doppler (Fig. 9). Newer techniques such as real-time sono-elastography have shown some promise in the diagnosis and follow-up of stress fractures. The inability to visualize structures beyond the cortical surface is perhaps the most important drawback of this modality (Fukushima et al. 2018).

5.5 MRI

Overall, MRI has a higher sensitivity and specificity than CT and scintigraphy for the detection of stress fractures (Wright et al. 2016). In addition to bony abnormalities, MRI also accurately displays associated soft-tissue injury. It is particularly useful during the first 3 weeks of symptoms, when BME can already be detected before new bone formation appears. This is especially true for cancellous bone stress lesions, in which BME is more abundantly present than bony changes. It should be noted that this early BME can be indistinguishable from posttraumatic bone bruise in the absence of ancillary findings (Glaudemans et al. 2015). MRI is routinely used to classify stress injuries and guide return-to-play decisions for athletes. A four-grade classification system for tibial

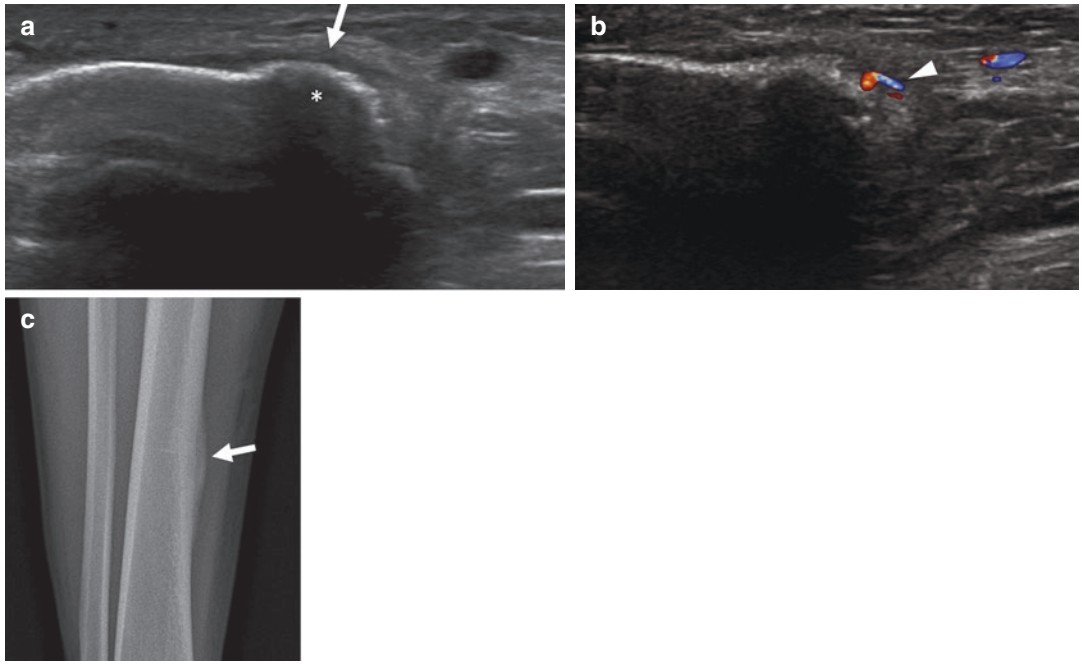

Fig. 9 (**a**–**c**) Tibial cortical stress fracture in a 31-year-old runner. (**a**) Axial US image shows focal thickening of the medial tibial cortex (asterisk) with adjacent periosteal thickening (arrow). (**b**) Color Doppler image at the same level shows focal increased vascularization (arrowhead). (**c**) Corresponding frontal radiograph confirms the presence of solid periosteal callus (arrow)

Table 3 Modified Fredericson MRI grading system for tibial stress injuries (Kijowski et al. 2012)

Modified Fredericson grade	MRI findings	Mean time before return to sports (days)
1	Periosteal edema with no other abnormalities	16
2	Periosteal edema and bone marrow edema, only visible on T2-weighted images	39–44
3	Periosteal edema and bone marrow edema, with signal abnormalities on both T1- and T2-weighted images	39–44
4a	Multifocal areas of cortical signal abnormalities, and bone marrow edema visible on both T1- and T2-weighted images	39–44
4b	Linear cortical lesion (fracture) and bone marrow edema on T1- and T2-weighted images	71

stress lesions on MRI was developed by Fredericson and coworkers in 1995, and was found to correlate well with the aforementioned Zwas et al. classification in the majority of examined lesions (Fredericson et al. 1995) (Table 3). In a 2012 validation study involving 138 patients, a modified Fredericson classification was used in which focal intracortical signal abnormalities without linear fracture were considered a separate category (grade 4a injury). These focal signal abnormalities are thought to represent a combination of osteopenia, cortical resorption cavities, and cortical striations, which are manifestations of accelerated intracortical remodeling and not necessarily a source of pain. Linear cortical signal abnormality was considered a grade 4b injury in the modified classification (Figs. 10–13). The authors found that grade 2, 3, and 4a injuries had a similar time to return to sports activity and made the

suggestion of grouping them together (Kijowski et al. 2012). One potential drawback of the Fredericson grading system is that the cortex seems to be involved only in grade 4a and 4b lesions. It is important to realize that microscopic cortical injury is already present in grade 1 lesions, but at this stage it is still beyond the resolution of MRI (Mandell et al. 2017b).

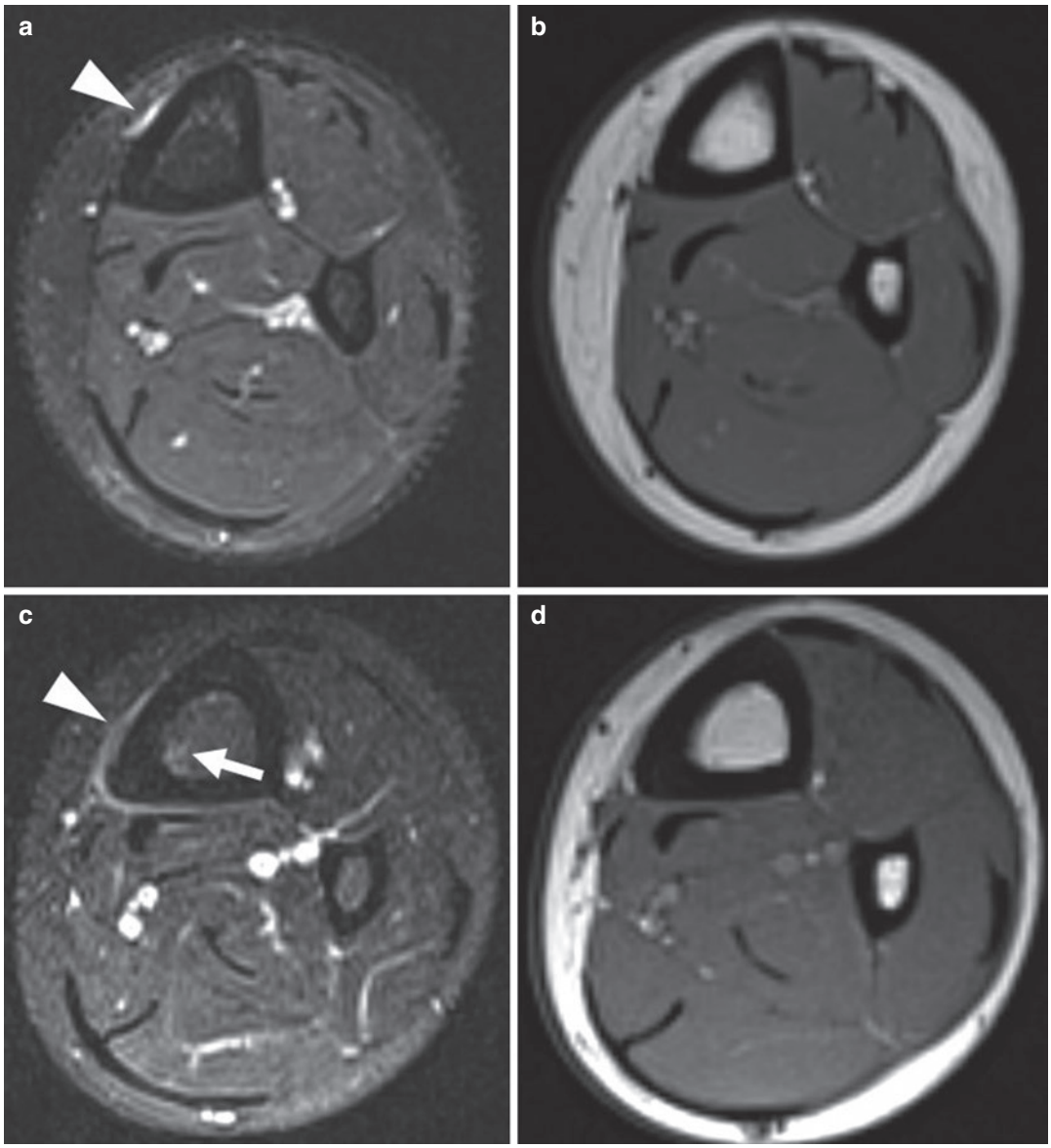

Fig. 10 (**a**–**d**) Low-grade tibial stress injuries. (**a**) Grade 1 lesion. Axial FS T2-WI in a 17-year-old girl shows focal periosteal edema (arrowhead) without further abnormalities. (**b**) T1-WI is normal. (**c**) Grade 2 lesion in a 29-year-old triathlete. Axial FS T2-WI shows periosteal edema (arrowhead) as well as faint BME (arrow). (**d**) No bone marrow abnormalities on T1-WI

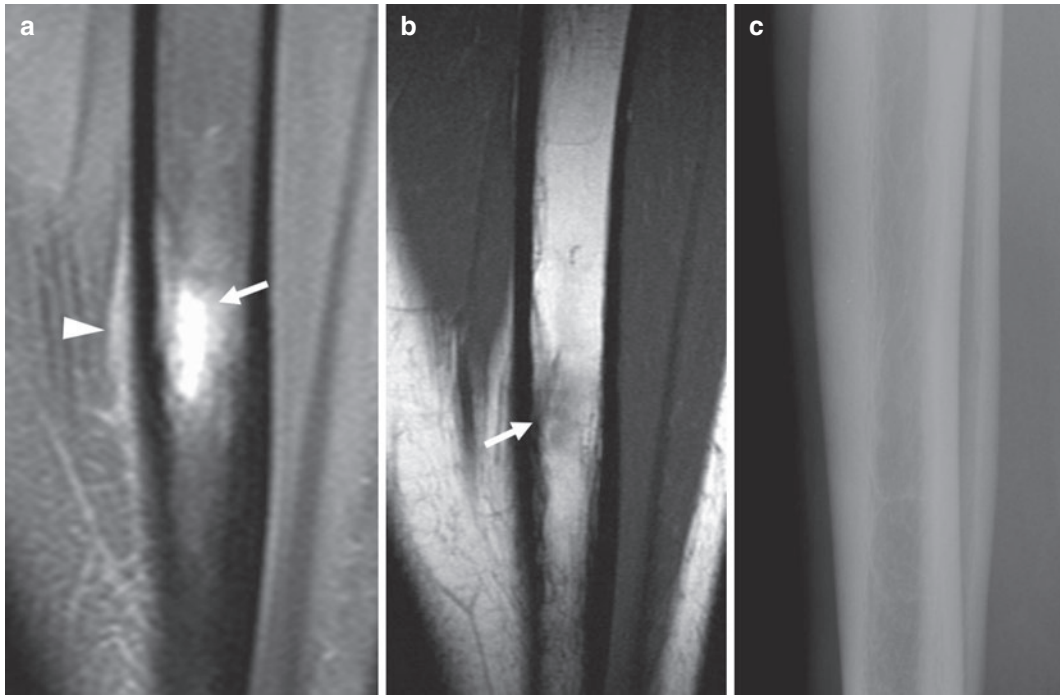

Fig. 11 (**a**–**c**) Fredericson grade 3 tibial diaphyseal stress injury in a 33-year-old woman. (**a**) Sagittal FS T2-WI shows fairly extensive BME (arrow) and periosteal edema (arrowhead). (**b**) Sagittal T1-WI shows focal moderately hypointense bone marrow (arrow). The intervening cortex appears normal on both sequences. (**c**) The corresponding lateral radiograph is normal; no fracture or bony periosteal apposition is seen

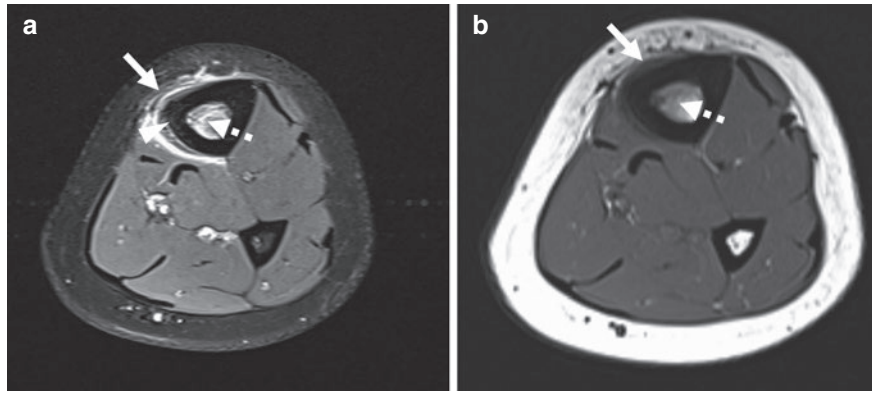

Fig. 12 (**a** and **b**) Grade 4a tibial stress injury in a 15-year-old female athlete. (**a**) Axial FS T2-WI shows severe periosteal edema (arrow), BME (dashed arrow), and multiple focal signal abnormalities in the cortex, not consistent with a fracture line (arrowhead). (**b**) Corresponding T1-WI shows bone marrow changes (dashed arrow) and periosteal thickening (arrow)

Things to Remember

1. Stress or fatigue fractures are caused by abnormal stress to normal bone. Insufficiency fractures are caused by normal stress to an abnormal bone.
2. Stress fractures occur in predictable locations, most often in the lower leg (tibia). The distinction between high-risk and low-risk stress fractures is important since it affects prognosis and management.
3. The radiological diagnosis of stress fractures always starts with conventional radiographs.
4. MRI is the most sensitive and specific imaging test for stress fractures, due to its ability to

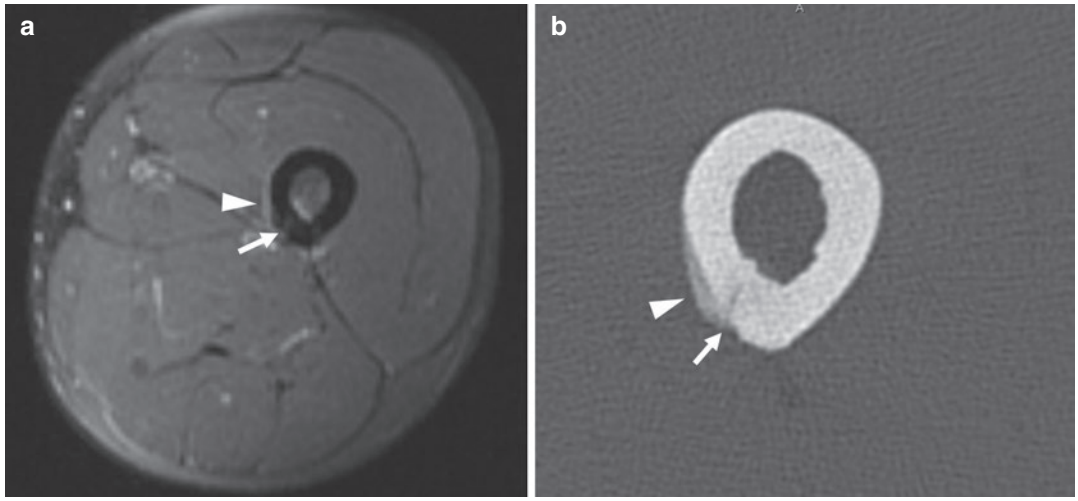

Fig. 13 (**a** and **b**) Femoral diaphyseal stress fracture in a male long-distance runner. (**a**) Axial FS T2-WI shows faint linear intracortical intermediate signal change suggesting a fracture (arrow), the equivalent of a modified Fredericson grade 4b stress lesion in the tibia. Periosteal edema is also noted (arrowhead). (**b**) Axial CT image reveals the incomplete nature of the cortical stress fracture (arrow) as well as solid periosteal bone deposition (arrowhead)

detect periosteal and bone marrow edema on fluid-sensitive sequences.

5. Stress fractures are classified with MRI according to severity, using a four-grade scale. The MR grade is correlated with the time before resumption of athletic activities.

Plain Films

1. Always the first imaging modality.
2. First signs of stress fractures in cortical bone are gray cortex sign, cortical striations, and periosteal new bone formation.
3. Early signs in cancellous bone are subtle and include blurring and faint sclerotic radiopaque areas.

Planar Scintigraphy and SPECT-CT

1. Planar scintigraphy is very sensitive but lacks specificity. It was the gold standard prior to the advent of MRI.
2. SPECT-CT is a hybrid technique coupling functional and anatomical information.
3. There are no prospective studies comparing the accuracy of SPECT-CT versus MRI for the diagnosis of stress fractures.

CT

1. Less sensitive than MRI.
2. Specific indications include complex anatomical sites, longitudinal stress fractures, and differential diagnosis with tumoral lesions.
3. Dual-energy CT allows the detection of bone edema; however, its accuracy for detecting stress fractures is currently unknown.

MRI

1. Currently the gold standard diagnostic exam for stress fractures.
2. Grading stress fractures with MRI allows predicting the time of recovery.
3. No radiation exposure.

References

Abbott A, Bird ML, Wild E et al (2019) Part I: epidemiology and risk factors for stress fractures in female athletes. Phys Sportsmed 11:1–8

Aicale R, Tarantino D, Maffulli N et al (2018) Overuse injuries in sport: a comprehensive overview. J Orthop Surg Res 13:1–11

Anderson MW, Greenspan A (1996) Stress fractures. Radiology 199:1–12
Barrack MT, Gibbs JC, De Souza MJ et al (2014) Higher incidence of bone stress injuries with increasing female athlete triad-related risk factors: a prospective multisite study of exercising girls and women. Am J Sports Med 42:949–958
Behrens SB, Deren ME, Matson A et al (2013) Stress fractures of the pelvis and legs in athletes: a review. Sports Health 5:164–174
Bennell KL, Brukner PD (1997) Epidemiology and site specificity of stress fractures. Clin Sports Med 16:179–196
Cheung KK, Dhawan RT, Wilson LF et al (2018) Pars interarticularis injury in elite athletes—the role of imaging in diagnosis and management. Eur J Radiol 108:28–42
Chisin R, Milgrom C, Giladi M et al (1987) Clinical significance of nonfocal scintigraphic findings in suspected tibial stress fractures. Clin Orthop Relat Res 220:200–205
Clarke B (2008) Normal bone anatomy and physiology. Clin J Am Soc Nephrol 3:131–139
Davey T, Lanham-New SA, Shaw AM et al (2015) Fundamental differences in axial and appendicular bone density in stress fractured and uninjured Royal Marine recruits—a matched case-control study. Bone 73:120–126
Diehl JJ, Best TM, Kaeding CC (2006) Classification and return-to-play considerations for stress fractures. Clin Sports Med 25:17–28
Fredericson M, Bergman AG, Hoffmann KL et al (1995) Tibial stress reaction in runners. Correlation of clinical symptoms and scintigraphy with a new magnetic resonance imaging grading system. Am J Sports Med 23:472–481
Fukushima Y, Ray J, Kraus E et al (2018) A review and proposed rationale for the use of ultrasonography as a diagnostic modality in the identification of bone stress injuries. J Ultrasound Med 37: 2297–2307
Glaudemans AW, Dierckx RA, Gielen LM et al (eds) (2015) Nuclear medicine and radiologic imaging in sports injuries. Springer, Heidelberg
Ha S, Hong SH, Paeng JC et al (2015) Comparison of SPECT/CT and MRI in diagnosing symptomatic lesions in ankle and foot pain patients: diagnostic performance and relation to lesion type. PLoS One 10(2):e0117583
Haverstock BD (2001) Stress fractures of the foot and ankle. Clin Podiatr Med Surg 18:273–284
Kijowski R, Choi J, Shinki K et al (2012) Validation of MRI classification system for tibial stress injuries. AJR Am J Roentgenol 198:898–884
Lauder TC, Dixit S, Pezzin LE et al (2000) The relation between stress fractures and bone mineral density: evidence from active-duty army women. Arch Phys Med Rehabil 81:73–79
Mallinson PI, Coupal TM, McLaughlin PD et al (2016) Dual-energy CT for the musculoskeletal system. Radiology 281:690–707
Mandell JC, Khurana B, Smith SE (2017a) Stress fractures of the foot and ankle, part 1: biomechanics of bone and principles of imaging and treatment. Skelet Radiol 46:1012–1029
Mandell JC, Khurana B, Smith SE (2017b) Stress fractures of the foot and ankle, part 2: site-specific etiology, imaging, and treatment, and differential diagnosis. Skelet Radiol 46:1165–1186
Marshall RA, Mandell JC, Weaver MJ (2018) Imaging features and management of stress, atypical and pathologic fractures. Radiographics 38:2173–2192
Moreira CA, Bilezikian JP (2017) Stress fractures: concepts and therapeutics. J Clin Endocrinol Metab 102:525–534
Nattiv A, Loucks AB, Manore MM (2007) American College of Sports Medicine position stand. The female athletic triad. Med Sci Sports Exerc 39: 1967–1882
Nussbaum ED, Bjornaraa J, Gatt CJ Jr (2019) Identifying factors that contribute to adolescent bony stress injury in secondary school athletes: a comparative analysis with a healthy athletic control group. Sports Health 11:375–379
Palm HG, Lang P, Hackenbroch C et al (2019) Dual-energy CT as an innovative method for diagnosing fragility fractures of the pelvic ring: a retrospective comparison with MRI as the gold standard. Arch Orthop Trauma Surg 140:473. https://doi.org/10.1007/s00402-019-03283-8
Pathria MN, Chung CB, Resnick DL (2016) Acute and stress-related injuries of bone and cartilage: pertinent anatomy, basic biomechanics, and imaging perspective. Radiology 280:21–38
Pelletier-Galarneau M, Martineau P, Goudreault M et al (2015) Review of running injuries of the foot and ankle: clinical presentation and SPECT-CT imaging patterns. Am J Nucl Med Mol Imaging 5: 305–316
Resnick D (1996) Bone and joint imaging, 2nd edn. WB Saunders, Philadelphia
Rizzone KH, Ackerman KE, Roos KG et al (2017) The epidemiology of stress fractures in collegiate student-athletes, 2004–2005 through 2013–2014 academic years. J Athl Train 52:966–975
Romani WA, Gieck JH, Perrin DH et al (2002) Mechanisms and management of stress fractures in physically active persons. J Athl Train 37:306–314
Roub LW, Gumerman LW, Hanley EN Jr et al (1979) Bone stress: a radionuclide imaging perspective. Radiology 132:431–438
Vanhoenacker FM (2021) Bone marrow edema in sports injuries/general concept. Med Radiol. https://doi.org/10.1007/174_2020_241
Wright AA, Hegedus EJ, Lenchik L et al (2016) Diagnostic accuracy of various imaging modalities for suspected lower extremity stress fractures: a systematic review with evidence-based recommendations for clinical practice. Am J Sports Med 44:255–263
Zwas ST, Elkanovitch R, Frank G (1987) Interpretation and classification of bone scintigraphic findings in stress fractures. J Nucl Med 28:452–457

Pseudotumors in Sports

Magdalena Lunkiewicz, A. Mark Davies,
and Suzanne E. Anderson

Contents

Abstract

Musculoskeletal pseudotumors on imaging are not a rarity and may be increasingly detected due to an increased use of diagnostic imaging and expanding subspecialized clinical referral basis. A large variety of pseudotumors exist. Although there have been technical advances and there is a diversity of imaging modalities, the diagnosis of a pseudotumor remains challenging and its morphologic features may be difficult to distinguish from those of a malignant neoplastic lesion. It requires a systematic approach with awareness of the common types of pseudotumors, its imaging appearances, regional anatomy, injury mechanisms, and carefully obtained clinical history. This chapter illustrates the most important pseudotumors on imaging, their imaging characteristics on different imaging modalities, and possible clinical settings with keys to differential diagnosis. Emphasis is placed on MRI.

M. Lunkiewicz
Kantonsspital Baden, Baden, Switzerland

A. M. Davies
The Royal Orthopedic Hospital NHS Trust, MRI Centre, Birmingham, UK

S. E. Anderson (✉)
Kantonsspital Baden, Baden, Switzerland

University of Notre Dame, Sydney School of Medicine, Sydney Darlinghurst, Australia
e-mail: suzanne.anderson1@bluewin.ch

Med Radiol Diagn Imaging (2021)
https://doi.org/10.1007/174_2020_270, © Springer Nature Switzerland AG
Published Online: 07 February 2021

1 Introduction

Although there have been technical advances and there is a diversity of imaging modalities, the diagnosis of a pseudotumor remains challenging and requires a systematic approach. The combination of clinical history, physical examination, and imaging appearance, including anatomical location, is crucial (Perdikakis et al. 2017). In many instances it will be evidently clear that an apparent clinical mass is a direct consequence of a specific sports injury, such as thigh hematoma after impaction during a football game. Commonly an athlete is fully aware of the injury and its relationship to the newly developed abnormality. Many sports activities are associated with specific injuries and findings.

Some sports injuries may be minor and forgotten and consecutively may not be immediately perceived as being related to the current clinical problem (e.g., only one-quarter of children with a fat necrosis on MRI imaging recalled a history of trauma, Tsai et al. 1997). The minor repetitive trauma with no inciting event is one of the more challenging constellations in the diagnostic process. Also acute trauma associated with unusual radiological findings may confuse the diagnosis (e.g., complicated by secondary infection).

Contributory features include the presence of normal variants with possible overuse syndromes, specific body habitus, or patient's history suggesting inappropriate training or equipment predisposing to overuse injuries. Some characteristic locations and patient age may be suggestive of the diagnosis, e.g., elastofibroma dorsi of the infra-scapular posterior thoracic wall.

Musculoskeletal pseudotumors on MRI are not a rarity and may be increasingly detected due to an increased availability of MRI and expanding subspecialized clinical referral basis. The growing sports activity especially in older children and adolescents predisposes to more injuries and overuse. A unique group in this context is female athletes, affected by the "female athlete triad" (osteoporosis, eating disorder, and amenorrhea).

A large variety of MRI pseudotumors exist. Some pseudotumors are clinically apparent as a mass or swelling. Some are only evident on imaging with morphologic features which may be mistaken for a neoplastic lesion. However pseudotumors are far more common than neoplasms. They can be classified either anatomically or by etiology. All anatomical structures may be involved.

2 General Imaging Principles

All modalities are involved in pseudotumor imaging. Often the radiologist is confronted with already performed imaging and may not be able to influence the initial choice of the imaging modality or protocol. Otherwise remaining with basic principles is prudent. Radiographs in two planes may show calcifications, zoning phenomena, fractures, presence of normal variants, or signs of overuse such as advanced degenerative joint disease not corresponding to patient's age. Correlation with conventional radiographs is extremely important as many masses or focal abnormalities on MRI simulating neoplasms may have characteristic radiographic appearances and be easily diagnosed (Jelinek and Kransdorf 1995; Kransdorf and Murphey 1997). Examples include the peripheral calcific rim of myositis ossificans, retained radio-opaque foreign bodies, stress fractures, and hydroxyapatite deposition within tendons (see also Sects. 4.4, 5.1, 8, and 10).

Computed tomography can help with demonstrating the above characteristics; however analogue to the general musculoskeletal tumor diagnostic MRI is a mainstay with sports pseudotumors given its multiplanar capability, regional anatomic review, and a superior soft-tissue contrast resolution. Depending on the primary goal of the imaging the field of view may be adapted accordingly. If the main aim of the examination is to establish the presence of mass, visualization of the contralateral side may be helpful to detect the asymmetry, using a larger field of view. A smaller field of view with higher spatial resolution may be useful for detailed assessment of the lesion.

Due to technical advances high-field MRI scanners (1.5 T or higher) in connection with dedicated multichannel coils provide superior image quality. Analogue to the diagnosis of musculoskeletal tumor, there are standardized algorithms based on consensus guidelines of the European Society of the Musculoskeletal Radiology (Nöbauer-Huhmann 2019). Routine sequences in three planes are important, including T1-weighted and STIR sequences (short tau inversion recovery) in at least one plane.

Skin markers may also help in the detection of the lesion, as the absence of a true mass on imaging may be challenging.

Gradient echo sequences may be useful to enhance a "blooming" artifact associated with hemosiderin deposition, metallic foreign bodies, and gas. Though contrast administration may not necessarily change the diagnosis, it may increase the conspicuity of the findings (e.g., unique cases of muscle strains in professional athletes with negative findings on the T2-weighted imaging).

If a true mass is absent on MRI, the finding is associated with a large reactive soft-tissue component or an extensive hemorrhage and whether there has been a history of sports injury, trauma, or overuse with a possible pseudotumor should be included in the differential diagnosis.

The morphologic appearance on imaging (preferably both radiographs and MRI) in association with a detailed clinical history may help avoid an unnecessary biopsy with also sometimes inconclusive histopathological diagnosis (e.g., false-positive histopathological diagnosis of a soft-tissue osteosarcoma in case of a myositis ossificans, Ragunanthan and Sugavanam 2006). It is crucial to perform clinical and imaging follow-up examinations after suspecting a pseudotumor diagnosis, particularly with less experienced readers, in order to avoid a false-negative diagnosis regarding a neoplastic lesion.

As the pseudotumor diagnosis may be challenging, increased awareness of the common types of pseudotumors, its imaging appearances, regional anatomy, injury mechanisms, and carefully obtained clinical history (e.g., precise questionnaire) may significantly increase the specificity of the MRI diagnosis, which may often be a surprise to the referring clinician.

3 Keys to Differential Diagnosis and True Tumors

Typically true musculoskeletal tumors of either bone or soft-tissue origin present with an increasing mass effect and relatively minor pain compared to the size of the mass, unless there has been a history of bleeding, biopsy, or trauma. Neoplastic lesions tend to displace or invade the local anatomy. Pseudotumors may often only show a subtle distortion of the regional anatomy, so that the comparison with the contralateral side may be very helpful and sometimes essential in the diagnostic process.

Pseudotumors are commonly associated with a marked adjacent soft-tissue reaction, as classically seen with myositis ossificans (Walczak et al. 2015). Adjacent marked reactive soft-tissue changes or hemorrhage is unusual with a neoplastic lesion unless there has been a history of a direct trauma, bleeding, or biopsy.

4 Soft Tissue-Related Pseudotumors

4.1 Muscle Tear, Morel-Lavallée Syndrome, and Rhabdomyolysis

Muscle strains and tears, soft-tissue hematomas, but also less common injuries like Morel-Lavallée syndrome or calcific myonecrosis may mimic true soft-tissue tumors on imaging.

Muscle tears often occur in professional athletes. The correct diagnosis and grading of the muscle injury may be relevant especially in elite athletes (Thierfelder et al. 2019). Most muscle injuries (around 96%) occur due to an indirect mechanism of accident and result in muscle tear (Mueller-Wohlfahrt et al. 2013). Some muscle injuries occur more often in particular sporting activities (Fig. 1). For instance muscle injuries of

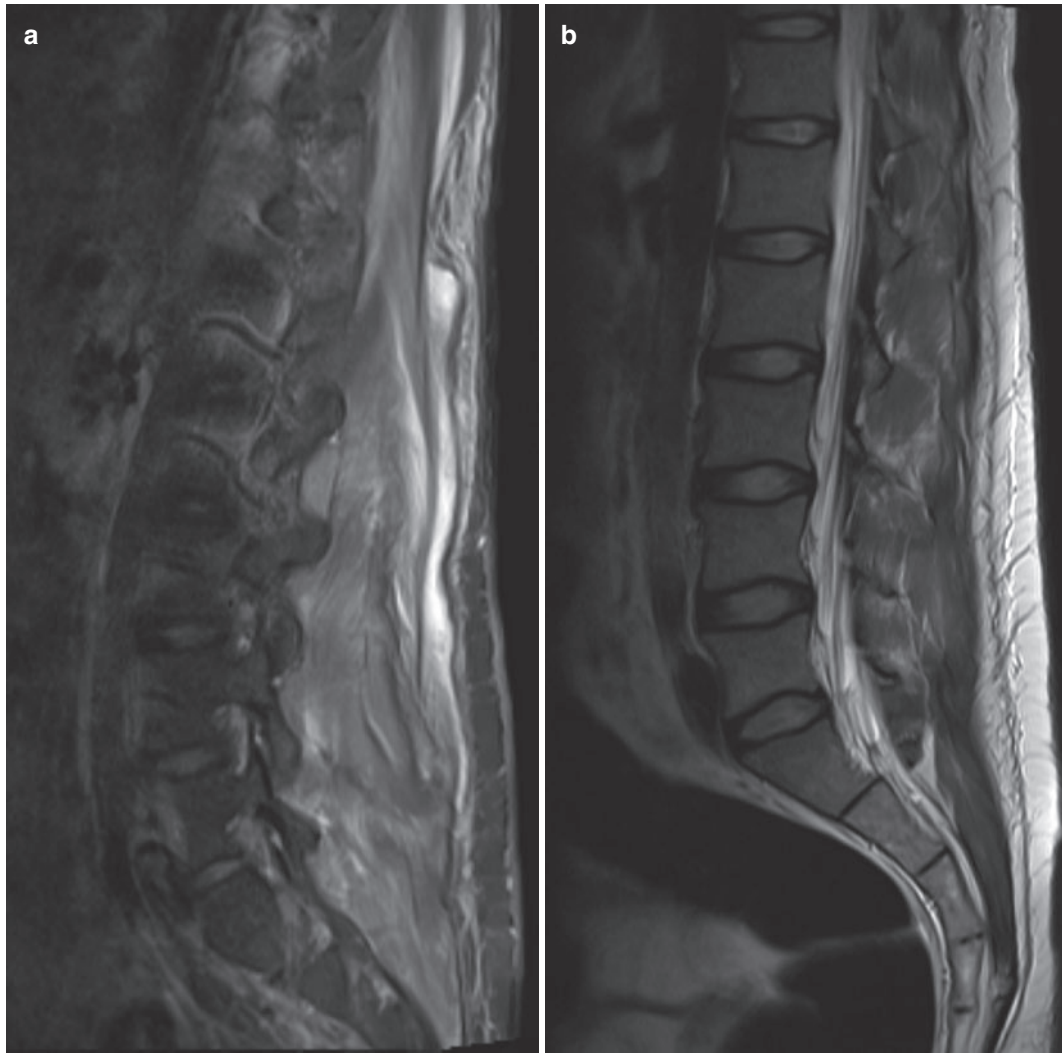

Fig. 1 (**a**, **b**) Muscle injury and rhabdomyolysis. 23-Year-old male Swiss wakeboarder with unilateral lower back soft-tissue swelling with side asymmetry. (**a**) STIR parasagittal image shows extensive muscle signal change and partial tear. (**b**) Sagittal T1-weighted image (WI) shows absence of fracture. Hematological results showed extensively increased muscle enzymes. After further review a clinical history of acute trauma was obtained. Surgical fasciotomy was performed. Follow-up MRI demonstrated marked fatty replacement of unilateral paravertebral posterior muscles consistent with posttraumatic compartment syndrome

hip and thigh (hamstrings, adductors, and quadriceps strains) are frequent among soccer players, and rotator cuff tears occur frequently in tennis and baseball players (Ekstrand et al. 2013). The correct interpretation of the radiological findings including the type and grading of the injury may be relevant for the therapy options and prognosis. Apart from the clinical grading systems, which consider bulge size and loss of strength, one most commonly used MRI-based grading system distinguishes four different muscle injury grades (Mueller-Wohlfahrt et al. 2013). Grade 0 stands for normal muscle, grade 1 stands for intramuscular edema with no fiber discontinuity, grade 2 stands for partial muscle tear, and grade 3 stands for complete muscle tear (Ekstrand et al. 2013). In case of a grade 3 injury, which may frequently require a surgical therapy, the exact extension of the tear should be reported. Another predictive factor in muscle tears is the longitudinal exten-

sion of the injury, which is considered to have the highest predictive value as it correlates with the amount of the muscle units separated from the aponeurosis (Connell et al. 2004). Morel-Lavallée syndrome, muscle hernia, and calcific myonecrosis are possible complications of a muscle injury, which are treated in a separate paragraph.

4.1.1 Hematoma

Superficial soft-tissue hematomas may be associated with minimal and often forgotten trauma. Deep-muscle hematomas are more frequently associated with more obvious trauma, coagulation disorders (e.g., hemophilia), or derailed anticoagulation therapy. Often the MRI appearances of hematomas are complex due to the different stages of blood content as there may be a repeated hemorrhage within movement. The MRI appearance of hematoma depends on the state of the hemoglobin molecule, whether it is intra- or extracellular in nature (Kransdorf and Murphey 1997; Dooms et al. 1985; Gomori et al. 1985; Rubin et al. 1987). In the hyperacute phase blood is isointense on T1 weighting and decreased on T2 weighting, reflecting the earliest phase of oxygenated hemoglobin to deoxyhemoglobin. Due to cell lysis in the subacute phase (1 week to 3 months old) hemoglobin molecules are released into the extracellular space and become methemoglobin, which is characteristically increased in signal intensity on T1 and T2 weighting. Weeks to months later the methemoglobin breaks down into hemosiderin (Fig. 8) with decreased signal intensity on T1 and T2 weighting. Breakdown of blood products in a hematoma is not a uniform process. The accelerated peripheral breakdown will show a low-signal rim whereas the central region may show higher, inhomogeneous signal intensity. It may sometimes be difficult to distinguish a simple hematoma from a large hemorrhagic neoplastic lesion (Jelinek and Kransdorf 1995). A solid, enhancing nodularity or rim may be helpful in distinguishing between these lesions (Jelinek and Kransdorf 1995). However an organizing hematoma may show some internal enhancement due to enhancing fibrovascular tissue and should be followed up to resolution, especially in an atraumatic clinical setting. Secondarily infected hematomas may present a more complex MRI appearance with peripheral and surrounding soft-tissue reaction.

4.1.2 Morel-Lavallée Syndrome

Soft-tissue injuries like the muscle strains and tears stated above may present months or even years after a trauma, which makes the diagnosis more difficult. A posttraumatic cystic lesion, known as Morel Lavallée syndrome, occurs after a severe trauma to pelvis or thigh in an abrupt shearing force mechanism (De Coninck et al. 2017). It is a degloving injury where soft tissue is sheared from the underlying fascia which is accompanied by a repeated hemorrhage. Morel-Lavallée lesion presents as a subcutaneous cystic mass surrounded by a postinflammatory, fibrous capsule situated in the peritrochanteric region in between the iliotibial band and fascia lata (McLean and Popovic 2017). The contents of the lesion may accumulate slowly over a longer period of time, due to the anatomical predisposition of this region. The subcutaneous localization of the bone, the increased mobility of the soft tissues, as well as the rich vascular supply of the dermis on this anatomical site may result in continuous drainage of blood into the lesion. The lesion presents with fluid-equivalent signal, but it may also be homogeneously hyperintense on T1- and T2-weighted images with no signal dropout after fat saturation due to chronic hemorrhagic contents. After gadolinium administration there is no or minimal peripheral enhancement (due to granulation tissue), seen on subtracted images due to hyperintense appearance on native T1-weighted images. The peritrochanteric region is the most frequent site; however Morel-Lavallée lesions have also been reported in the suprapatellar region, abdominal wall, buttocks, and lower lumbar spine (M. erector spinae). The nonspecific signal intensity may be challenging in the diagnostic process; however the typical localization abutting a fascial plane in the peritrochanteric region should be suggestive. A differential diagnosis of a fat necrosis (typically less homogeneous signal intensity), abscess (typically locules of air and strong rim enhancement), and a soft-tissue hematoma (different localizations) should be considered.

4.1.3 Myocele/Hernia

Muscle hypertrophy, which is commonly found in sporty individuals, may lead to a myocele, which is a muscle protrusion through an acquired or congenital fascial or myofascial defect, mimicking a mass lesion. It is a rare and painful lesion, which may occur in athletes due to exertional fatigue and muscle hypertrophy (Sanders et al. 2011). It occurs most frequently in lower extremities and may be undetectable during rest periods which requires dynamic visualization during muscle contraction (Thierfelder et al. 2019). Less frequent localization is the lateral abdominal wall, which may be acutely or chronically injured in a variety of athletic endeavors and may result in a lumbar hernia formation (Stensby and Baker 2016). Regarding dynamic examination ultrasound may be here advantageous (Karantanas 2019).

4.1.4 Rhabdomyolysis

Rhabdomyolysis may occur due to endurance exercise and weight lifting in athletes or sudden increase in physical activity in less trained individuals (Furman 2015). Its clinical presentation may be very subtle in early phase, which makes the diagnosis challenging. Muscular pain or swelling, limited range of motion, and excretion of dark urine in young males with a history of extensive physical activity should raise concern for this condition. Undiagnosed and untreated rhabdomyolysis may lead to severe complications such as renal failure, compartment syndrome, and dysrhythmias (Furman 2015). On MRI imaging there is a diffuse T2 hyperintensity of the affected muscle group due to edema, sometimes occurring bilaterally. Together with the laboratory testing results (increased creatinine kinase level) it may be consistent with rhabdomyolysis. MRI imaging may be helpful to detect the exact distribution and extent of the affected muscle group.

4.1.5 Calcific Myonecrosis

Calcific myonecrosis is a rare entity, which occurs as a late complication of a lower limb trauma, often as a late sequel to compartment syndrome and injury of the common peroneal nerve (Fig. 2) . It is a fusiform mass with peripheral calcification and central liquefaction or cyst formation. Since there may be a long delay (up to few decades) between the injury and the presentation with a soft-tissue mass, the association with a traumatic event initially may not be considered in the diagnostic process, which may be challenging to differentiate from a neoplastic lesion. The common site of the calcific myonecrosis is the calf. On radiographs calcific myonecrosis presents as a well-defined lesion with distinct, plaque-like, peripheral calcification replacing the leg musculature. Due to the very slow development process the lesion may erode the outer cortex of the adjacent bone, sometimes leading to a complete destruction of a diaphyseal segment (in particular in thin tubular bones like the fibula). On MRI the lesion presents on both T1- and T2-weighted sequences as a heterogeneous mass formation with some T2 hyperintense components due to the cystic changes. The chronic masses may increase in size over a period of months, several years, or even many decades due to the repeated intralesional hemorrhage. The lesion may show fluid-fluid levels, possibly due to precipitation of calcium salts and layering out of the old hemorrhage. The differential diagnosis of this rare condition includes malignant soft-tissue tumors with calcifications, e.g., synovial sarcoma and soft-tissue osteosarcoma. In contrary to the calcific myonecrosis the mineralization in synovial sarcomas commonly shows diffuse distribution throughout the lesion. Synovial sarcomas are frequently localized in a periarticular way within 5 cm of the joint. While synovial sarcomas may show some contrast enhancement, calcific myonecrosis typically shows no enhancement after gadolinium administration. Other conditions like dermatomyositis, polymyositis, and diabetic myonecrosis may also demonstrate calcifications; however they commonly show systemic manifestations with no history of a trauma.

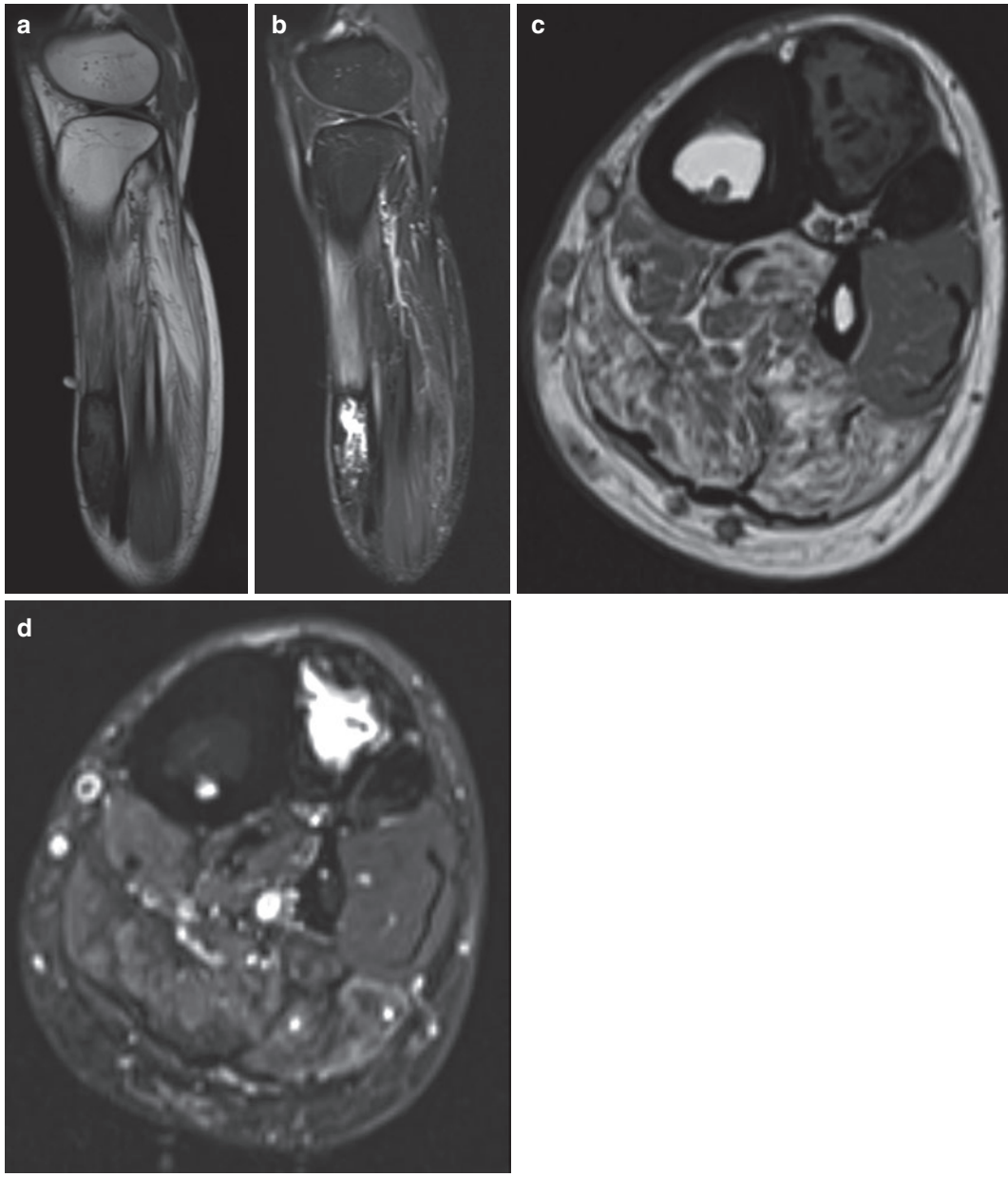

Fig. 2 (**a**–**d**) Calcific myonecrosis. 45-Year-old male, Swiss yachtsman, who continues with cross-training which includes 100 km bike riding, presents with a fluctuating lower limb mass. History of a prior trauma 30 years ago at a Sydney Harbour New Year's Eve party was obtained, with lower limb boat crush injury and compartment syndrome, which at the time had resulted in near amputation. (**a**) Sagittal T1-WI, anterior compartment muscle altered signal with peripheral decreased signal, mass-like effect, and posterior compartment extensive muscle fatty replacement. (**b**) Sagittal STIR sequence, marked peripheral decreased signal with central variable increased fluid signal. (**c**) Axial T1-WI, mass-like expansion of two anterior compartment muscles and absence of normal muscle structure compared to normal muscle adjacent to proximal fibula and extensive fatty atrophy of the posterior compartment muscles. Extensive fasciotomy scar is not demonstrated here. (**d**) Axial STIR sequence shows the equivalent of anterior muscle replacement by peripheral calcified margin, central fluid collection, and dense calcification of the adjacent muscle

4.2 Overuse and Tear of Ligaments and Tendons

Tears and overuse of ligaments, tendons, and muscles, both acute and chronic, may mimic neoplastic lesions on imaging. The exact localization of the tear often depends on patient's age. The typical site in young athletes is the non-fused apophysis (Fig. 3). In older patients the tear is commonly localized in the tendon, due to degenerative changes as a predisposing factor. In adult athletic patients the tears occur most commonly in the myotendinous junction, which is the weakest anatomic site (Thierfelder et al. 2019).

Acute and chronic avulsion injuries which commonly affect immature bone structure may be mistaken for a soft tissue or bone tumor due to reactive bone overgrowth and fragmentation, associated tendinopathy, and peritendinitis (Perdikakis et al. 2017). In acute phase, when the MRI appearance may be suggestive for an aggressive lesion, plain radiographs may be helpful to detect the avulsed bone fragment and thus to narrow the differential diagnosis. Partial avulsion of the adductor muscles from the femoral diaphysis in children due to sports injuries or overuse may simulate a malignant sarcoma on MRI (Anderson et al. 2001). There is typical widespread intramedullary edema but absence of stress fracture lines as well as bone or soft-tissue mass. This condition has been studied using bone scans in adults during army training and was called "adductor insertion avulsion syndrome" or "thigh splints." The cause is thought to be due to excessive adductor contraction with stripping of the femoral periosteum anteromedially. Knowledge, particularly of the MRI findings with an appropriate clinical setting, can help physicians to make the correct diagnosis and avoid unnecessary biopsy. Proximal adductor avulsions near the symphysis pubis (Schneider et al. 1976) and intramuscular strains (Yoshioka et al. 1994) have been described in adults. Chronic muscle avulsion injuries in a variety of lower limb sites in children have been described (Anderson et al. 2004a, b). Overuse with excessive prolonged carrying of large babies may rarely lead to masses of the wrist, found to be due to de Quervain's tenosynovitis.

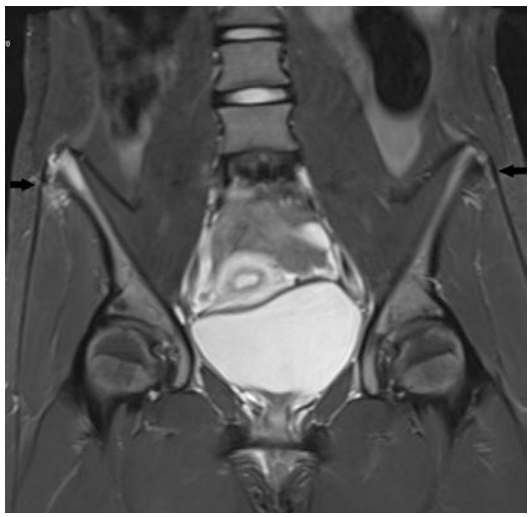

Fig. 3 Avulsion anterior superior iliac crest and tensor fascia lata tear. 16-Year-old female gymnast who presents with bilateral flank pain and possible right-sided mass for review. Coronal STIR image demonstrates iliac crest avulsion fracture fragment on the right with focal tear of tensor fascia lata. Less marked left-sided focal tear is also noted (arrows)

Posttraumatic tendon tears of certain muscles may result in compensatory hypertrophy of other muscle groups due to changed weight load of the affected region (Sutter et al. 2013). The hypertrophic region may mimic a mass lesion. An example of this phenomenon is the hypertrophy of the ipsilateral tensor fasciae latae muscle due to tears of the gluteus medius or minimus tendon.

4.3 Nodular Fasciitis (Pseudosarcomatous Fasciitis)

Though quite rare nodular fasciitis is the most common pseudosarcomatous lesion, first described by Konwaler in 1955, most often occurring in young, athletic patients (20- to 35-year-olds) (Rani and Gupta 2019). It is a

benign, mass-forming, proliferative fibrous lesion considered to be reactive after trauma or infection. However the exact etiology is unknown. The lesions may grow rapidly and show spontaneous regression. The most common clinical presentation is a painful subcutaneous nodule. There is a predilection for the upper limb (especially forearms), followed by trunk and abdominal wall; however it may occur anywhere in the body (Rani and Gupta 2019). There are three forms of nodular fasciitis based on its localization: subcutaneous, fascial, and intramuscular. The most common is the subcutaneous form, presenting as named above subcutaneous nodules. The intramuscular form commonly appears as a focal round or ovoid mass attached to the fascia with sometimes infiltrative borders, which may be challenging to distinguish from a sarcoma. The fascial form usually spreads along superficial fascial planes with no circumscribed margins and may sometimes show stellate growth pattern. Early lesions typically have a high T2 signal intensity reflecting the myxoid histology (Jelinek and Kransdorf 1995; Kransdorf and Murphey 1997). Older lesions may have decreased signal intensity on T2 weighting reflecting the predominantly fibrous histology (Jelinek and Kransdorf 1995). On T1-weighted images nodular fasciitis shows a homogeneous low signal intensity with slightly inhomogeneous enhancement after contrast media administration. There may also be some subtle soft-tissue edema and the lesion may show some aggressive features like transcompartmental growth, osseous, or articular involvement which make the diagnosis even more challenging (Coyle et al. 2013). The lesions are mostly smaller than 4 cm; 72% of them are smaller than 2 cm. Overall the MRI appearance is nonspecific.

Not only the radiological diagnosis may be challenging but also the pathological diagnosis based on the cytology (fine-needle biopsy) may be demanding due to the hypercellular and polymorphic cell population. The awareness of the possible cytological misdiagnosis (false positive for sarcoma) is an important component of the diagnostic process and may require a tight collaboration between the radiologist and pathologist (Rani and Gupta 2019). A suspected nodular fasciitis diagnosis should be followed up for the expected spontaneous regression.

4.4 Myositis Ossificans and Nora Lesion (BPOP)

4.4.1 Myositis Ossificans

Myositis ossificans is a common pseudotumor on MRI mostly related to a skeletal muscle with the highest prevalence for the flexor muscles of the arm and extensor muscles of the thigh (Boutin et al. 2002; Walczak et al. 2015). It may occur in association with other structures such as tendons and fascia.

Myositis ossificans is a solitary, self-limiting, abnormal ossifying soft-tissue mass mostly associated with trauma, typically occurring in young, active males (Walczak et al. 2015; Wang et al. 2018). The pathophysiology of MO is not completely understood. It is assumed to be caused by an inappropriate differentiation of fibroblasts into osteogenic cells induced by a skeletal muscle injury (Walczak et al. 2015; Wang et al. 2018). The history of trauma is often not initially apparent, which can make the diagnosis difficult (Kwee and Kwee 2019). Thus carefully obtained detailed clinical history may play an important role in the diagnostic process.

The variability in appearance depending on the stage of the disease may also be challenging in the diagnostic process. Three stages are described in the evolution of myositis ossificans: early stage (<4 weeks), intermediate stage (4–8 weeks), and mature stage (>8 weeks) (Walczak et al. 2015). The awareness of the possible clinical presentation and the radiological appearance during all stages of the disease may be the key to diagnosis. The morphologic features of the early stage of myositis ossificans may often be mistaken for a soft-tissue sarcoma due to the lack of typical ossification pattern. This may

lead to an unnecessary biopsy which may predispose to even more extensive ossification and a worse outcome (Kransdorf and Murphey 1997).

In the initial phase of myositis ossificans (<4 weeks) the calcifications are frequently inapparent as the lesion includes mainly fibroblasts and myoblasts with only a small amount of osteoid formation (Wang et al. 2018). The progression of the calcification process may only partially be defined by the stage of the disease, as the maturation process of the bones strongly depends on the age of the patient, similar to the callus formation (Kwee and Kwee 2019). During the initial, active phase the mass-like region may be clinically warm, painful, and woody in consistency. Biopsy during the early phase of development may give a false osteosarcoma diagnosis, as there is a florid osteoblastic activity. Serial radiographs are useful to demonstrate the initial development of amorphous bone, which may mimic the osteoid matrix on imaging and may be difficult to differentiate from an extraskeletal osteosarcoma.

During the intermediate phase (4–8 weeks) the amorphous bone progresses to a peripheral rim of calcification with a lucent center. In the mature phase (>8 weeks) the dense calcification is separate from bone, frequently running parallel to the long axis of the bone in a zonal pattern. The parosteal localization with distribution along the cortex may mimic melorheostosis. Characteristic sclerotome distribution in melorheostosis and lack of zonal ossification pattern should be helpful in the differentiation between these (Greenspan and Azouz 1999).

The presence of a cleft between the mass and the adjacent bone in myositis ossificans may be helpful in the differentiation from parosteal osteosarcoma. Also the localization of the lesion may be helpful in the diagnosis. Lesions located in MO-specific anatomical regions like the anterior femoral cortex together with other characteristics are suggestive of myositis ossificans (Walczak et al. 2015). Lesions in atypical localizations such as hands, feet, ribs, head, and neck should raise concern for malignancy (Walczak et al. 2015). Recurrent giant-cell tumor of bone in the soft tissue is a rare differential diagnosis of myositis ossificans with almost identical appearance on imaging (eggshell peripheral calcifications) (Walczak et al. 2015). One rare variant of myositis ossificans occurring in the fingers and less commonly in the toes is a fibro-osseous pseudotumor of the digits. Florid reactive periostitis and Nora lesion (Fig. 4) (bizarre parosteal osteochondromatous proliferation/

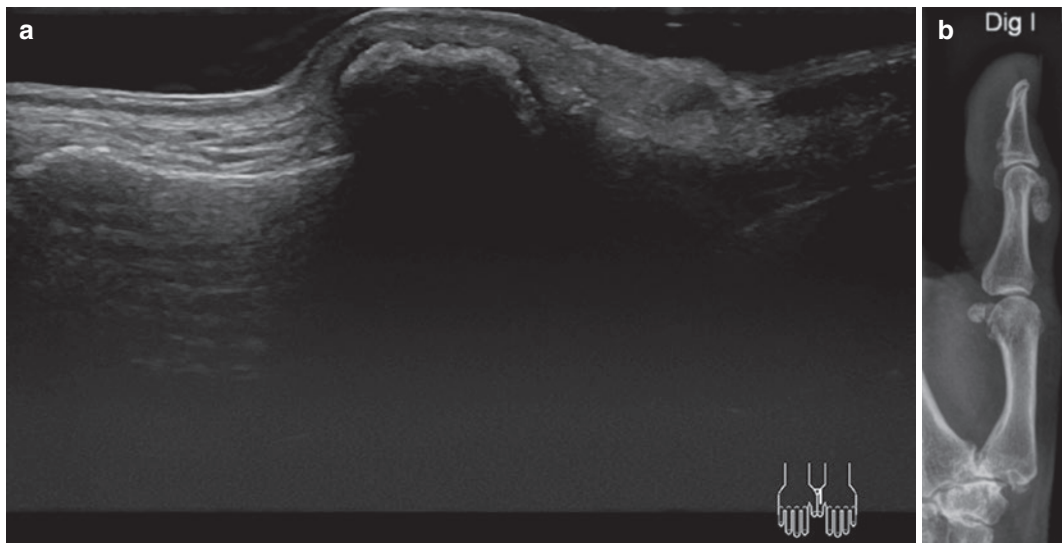

Fig. 4 (**a**, **b**) Nora lesion. 50-Year-old female after sports injury. (**a**) Ultrasound shows hyperechogenic rimmed lesion with posterior shadowing, at the site of previous trauma, with a history of decreasing mass size and soft-tissue swelling. (**b**) Lateral thumb radiograph confirms calcification (image courtesy of Dr. G. Stuckmann, Kantonsspital Baden, Switzerland)

BPOP) are considered to be a part of the same spectrum of lesions and may occur as a continuum (Dorfman and Czerniak 1998) (see separate paragraph).

CT is the best modality for detecting the typical zonal calcification pattern of myositis ossificans even before it becomes apparent radiographically. Mature calcification pattern is typical for MO; however on radiographs alone it may not be diagnostic (differential diagnosis parosteal sarcoma), which makes the intermodal approach crucial.

MRI is the best modality for imaging of soft-tissue masses; however due to limitations in the detection of calcifications it should be interpreted together with recent radiographs.

On ultrasound myositis ossificans may appear as an infiltrative muscle lesion with peripheral hyperechogenic calcifications and no detectable blood flow on Doppler study (Fonseca et al. 2019).

If the trauma involves deep-muscle injury in some cases there may be an associated periosteal reaction of the adjacent bone, referred to as periostitis ossificans. The appearances of myositis ossificans on MRI reflect the phase of development and the zonal phenomenon of the histology. In the early phase before ossification the lesion is usually isointense to muscle on T1-weighted images with no distinct borders. It is centrally hyperintense on T2-weighted images with marked adjacent soft-tissue edema (De Smet et al. 1992). The marked perilesional muscle edema (more than the double size of the central lesion) is specific but not pathognomonic for myositis ossificans in early/intermediate stage and may help to differentiate from malignant soft-tissue lesions (Zubler et al. 2020).

Since hematomas often occur in the initial phase, MO may show a heterogeneous signal intensity with high-signal areas on T1-weighted images due to the blood products. T2 hypointensity may represent hemosiderin deposition or calcifications (Walczak et al. 2015). At the initial stage there may be a subtle peripheral rim. In subacute lesions with early peripheral calcification there is a low-signal-intensity rim, like a tidemark on the beach when the wave is residing, reflecting this calcification. The center of the lesion may be isointense to muscle or slightly increased in signal intensity on T1-weighted images.

The T2 hyperintensity of the central portion may delineate the decreased signal of the peripheral rim more clearly (Jelinek and Kransdorf 1995; De Smet et al. 1992). At the acute and subacute stages the adjacent soft-tissue edema may be very prominent, which is unusual in malignant tumors, unless they have undergone a biopsy or an intralesional hemorrhage (Jelinek and Kransdorf 1995). In the chronic phase, the central portion of the lesion is slowly ossifying, so that the signal intensity on T1- and T2-weighted images is analogous to yellow bone marrow (De Smet et al. 1992). Marked intralesional enhancement should raise concern for sarcoma.

4.4.2 Nora Lesion (Bizarre Parosteal Osteochondromatous Proliferation/BPOP)

BPOP is an uncommon mineralized lesion of mesenchymal origin, usually affecting the proximal and middle phalanx of hand and feet, metacarpals, and metatarsals with commonly parosteal localization adjacent to bone surfaces. Hands are four times more often affected than feet (Torreggiani et al. 2001). Less common documented localizations are long bones, skull, and maxilla. The lesion presents commonly as a rounded calcified mass attached to the adjacent bone with no alteration of the underlying cortex. It consists of bone, cartilage, and fibrous tissue (Gruber et al. 2008). BPOP affects most commonly patients in the third and fourth decades; there is no sex predilection. The exact etiology of the lesion is unclear. It may occur within a reparative process due to trauma (Mahajan et al. 2012). However in many affected patients no trauma has been recorded in the clinical history. According to its remarkably high recurrence rate (29–55%) and aggressive appearance it may be difficult to distinguish from a malignant tumor (Gruber et al. 2008; Dhondt et al. 2006).

4.5 Inflammatory Myopathies

As a heterogeneous group of muscle diseases, inflammatory myopathies may mimic other pathologies (Maurer and Walker 2015). Early diagnosis may be important for the outcome due to the amenability of the immunosuppressive therapy (Maurer and Walker 2015). Inflammatory myopathies are most usually diffuse in nature, commonly bilateral in the thighs or calves, associated with weakness or tiredness and elevated blood enzyme levels (Fujimoto et al. 2002). Muscle edema, fatty replacement, and muscle atrophy may be visualized on MRI imaging (STIR and T1-weighted images). A rare entity of pseudosarcomatous myofibroblastic proliferations (proliferative myositis, proliferative fasciitis, nodular fasciitis) may mimic soft-tissue sarcomas both clinically and on imaging (Jarraya et al. 2014). Proliferative myositis may present as a rapidly growing nodule, localized around the neck, head, or upper extremities. Due to the rapid growth the definite diagnosis mostly requires a biopsy. The MRI appearance may include some interspersed muscle fascicles within the mass, which may suggest the correct diagnosis and help to distinguish from nodular fasciitis (Jarraya et al. 2014). Inflammatory myopathies may occur in sporting individuals.

4.6 Muscle Denervation

Muscle denervation may mimic a tumor due to edema and swelling on MRI imaging in the acute phase. There are predisposing sporting activities leading to specific neural compression syndromes. Not uncommonly, labral tear associated with suprascapular notch ganglion may be associated with acute to chronic supraspinatus and infraspinatus muscle denervation. Quadrilateral space syndrome is a relatively rare condition with symptoms caused by a mechanical compression (e.g., labral tear with paralabral cyst) of the axillary nerve inferoposterior to the glenohumeral joint in the quadrilateral space leading to the atrophy of teres minor muscle and less commonly deltoid muscle (Robinson et al. 2000). It is associated with overhead sports like baseball, volleyball, swimming, yoga, or triathlon (Brown et al. 2015). Repeated arm abduction and external rotation may also lead to compression of the posterior circumflex humeral artery (PCHA), resulting in a vascular quadrilateral space syndrome (vQSS) due to thrombosis, aneurysm formation, and distal emboli (Brown et al. 2015). Quadrilateral space syndrome may present with neurogenic symptoms (weakness, paresthesia, pain). It is commonly underdiagnosed, which may lead to a permanent disability of overhead athletes and threaten their career (Brown et al. 2015). Repetitive traction and microtrauma within overhead motion in athletes may lead to the injury of the suprascapular nerve in the suprascapular notch with consecutive denervation of both supraspinatus and infraspinatus muscle. Inflammatory, infectious, or idiopathic conditions are the cause of suprascapular neuropathy in Parsonage-Turner syndrome (Ahlawat et al. 2015).

Iatrogenic nerve injuries, e.g., common peroneal nerve injury within knee surgery after minor sports-related trauma, may also lead to muscle denervation mimicking a tumor in the acute phase with muscle edema.

4.7 Stress Reactions in Soft Tissue

Superficial fat impingement, which mimics a mass lesion, is a relatively rare condition due to repetitive pressure with abnormal positioning or equipment over a longer period of time. Fortunately, this is infrequent; however, occasionally obvious clinical histories may have been forgotten.

Chronic compression of the metatarsal region may lead to formation of a subcutaneous synovial lined intermetatarsal bursa. This is a painful fluid collection in between the metatarsal heads, deep to the transverse metatarsal ligament (Van Hul et al. 2011) with fluid-equivalent signal intensity and possible subtle enhancement in the periphery after gadolinium administration. If the fluid collection measures more than 3 mm in transverse diameter it is perceived as a cutoff

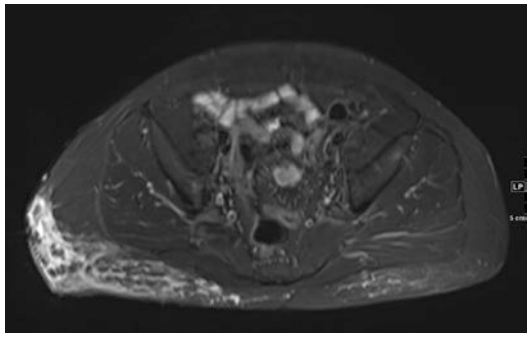

Fig. 5 Fat impingement. 45-Year-old starting back to weekend sports activities. Gluteal fat impingement due to hard wear. Vasculitis and systemic disorders were excluded. Fat apron resection was performed and tumor excluded

suggesting intermetatarsal bursitis. The diagnosis should be correlated with the clinical symptoms.

Another similar entity in the metatarsal region developed due to chronic stress and friction is an adventitious bursa. In contrary to the native named above, permanent bursa, this fluid collection is not lined with mesothelium, but with synovium-like columnar cells, being gradually formed within the process of chronic friction in the subcutaneous soft tissues. Due to the fluid content the lesion also shows low signal intensity in T1-weighted sequences and high signal intensity on T2-weighted sequences, often with some intralesional band-like low-intensity structures (Van Hul et al. 2011).

Fortunately, rarely chronic fat impingement may occur due to shoe equipment wear and repetitive fat impingement (Fig. 5).

5 Bone-Related Pseudotumors

5.1 Fractures, Occult Fractures, and Stress Reactions

Posttraumatic bony abnormalities such as occult fracture, stress reactions, and stress fractures may mimic bone tumors. Rarely high-end sports individuals may present after forgotten sports trauma, and imaging appearances may initially be alarming, but with careful review for fracture lines and specific clinical questioning on trauma the diagnosis can be made (Figs. 6 and 7). Stress reactions and fractures may be mistaken for sarcomas among other trauma-related lesions on imaging. Due to increased athletic activity and advances in imaging technology stress fractures may be a common finding in athletes and military recruits (Breer et al. 2012; Behrens et al. 2013). Stress fractures may be subdivided due to their etiology into fatigue and insufficiency fractures (Breer et al. 2012). Fatigue fractures occur due to abnormal or repetitive stress on a normal bone structure and are typical for athletes (Fig. 5). Insufficiency fractures mostly affect weakened bone structure (e.g., due to osteoporosis, vitamin D insufficiency, steroid use, anorexia, bisphosphonate therapy) and are often seen in postmenopausal women (Fig. 8). Female athletes with eating disorder and lower bone density are often affected by stress fractures (e.g., female athlete triad) (Behrens et al. 2013).

The most common sites of stress fractures in athletes are metatarsals, tibia, fibula, and tarsal navicular (Behrens et al. 2013). Dancers and runners are commonly affected athletes (Fig. 9).

Many sporting activities are associated with some specific sites and injury patterns (Pavlov 1995) such as junction of pelvis and ischium in long-distance runners, and hook of hamate in golf and tennis players. Some localizations of stress fractures are practically pathognomonic for specific athletic activities such as spinal pars defects of the thoracic and lower lumbar spine in cricketers and unilateral defects often involving the side opposite to the bowling arm in fast-spin bowlers (Hardcastle et al. 1992). Some sites of stress fractures may predispose to delayed union, e.g., anterior tibial diaphysis, lateral femoral neck, patella, medial malleolus, navicular, fifth metatarsal bone, and talus (Behrens et al. 2013). Fracture sites with lower risk for delayed union are posteromedial tibia, metatarsals, calcaneus, cuboid, cuneiform, fibula, medial femoral neck, and femoral shaft (Behrens et al. 2013).

The patient's age predisposes to specific fracture types. Both acute and chronic but also acute-on-chronic avulsion injuries in the immature

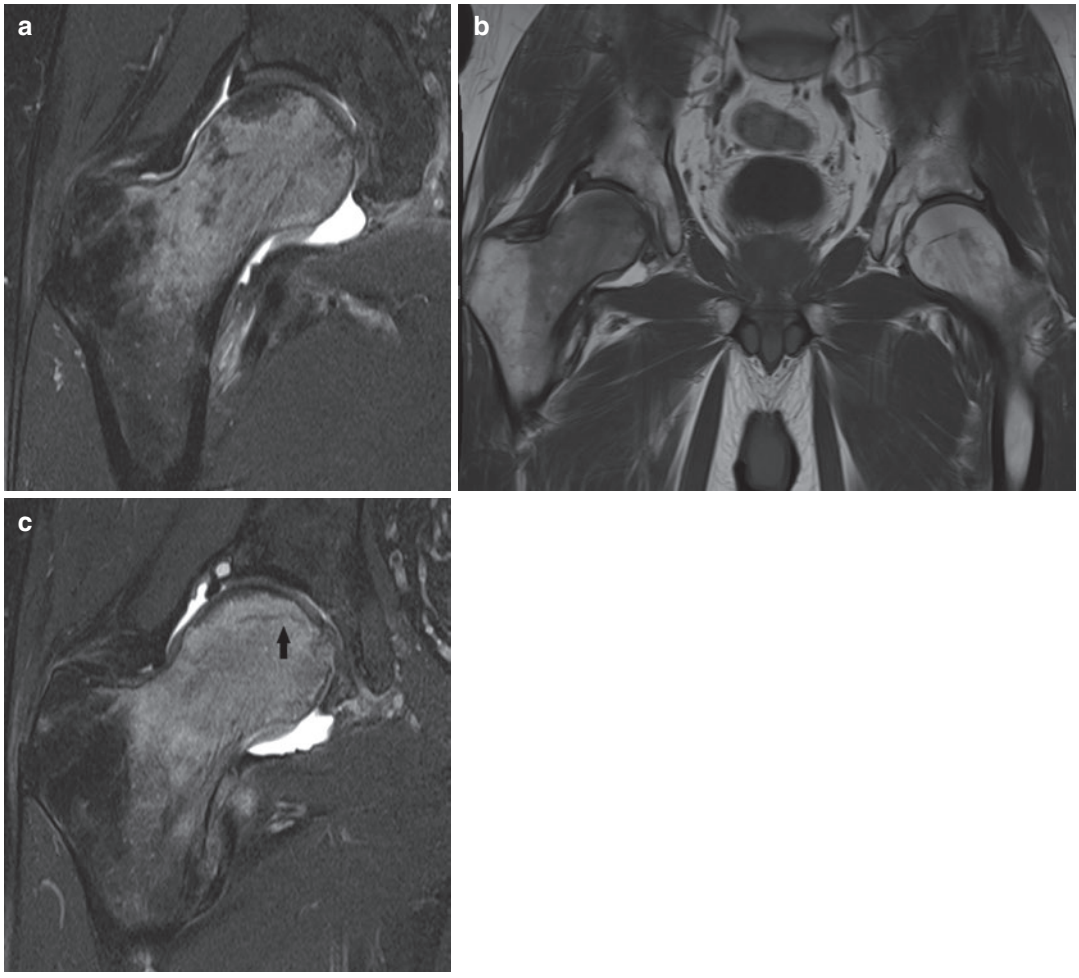

Fig. 6 (**a**–**c**) Occult posttraumatic fracture. A 38-year-old male with clinical concern for mass lesion, impingement, or labral tear. Additional history by radiology team elicited heavy sports tackle injury. (**a**) Coronal STIR of the right hip shows bone marrow edema extending from femoral head to intertrochanteric region. (**b**) Coronal T1-WI of the pelvis shows decreased signal right proximal femur, contralateral left intact. (**c**) Coronal T1-WI with fat suppression after gadolinium contrast administration of the right hip outlines femoral head fracture line (arrow). Small ganglion is noted as well. There was no osteopenia or osteoporosis on bone density review. Orthopedic follow-up confirmed normal return to function

skeleton may simulate bone-forming surface tumors or intraosseous sarcomas. Stress fractures in the immature skeleton are frequently mistaken for sarcomas on imaging (particularly localized in the proximal tibia and distal femur) (Shimal et al. 2010).

MRI is the imaging modality with the highest sensitivity and specificity for stress fractures (Behrens et al. 2013). Any linear low signal intensity on T1-weighed sequence associated with increased signal intensity of T2-weighted sequence which becomes more obvious after contrast administration and with fat suppression should prompt a diagnosis of a stress fracture.

Radiographs should always be performed as it may provide the correct diagnosis in many cases (e.g., stress fracture of the metatarsals). Along with attentive review of the clinical history (e.g., altered or excessive training, changed equipment)

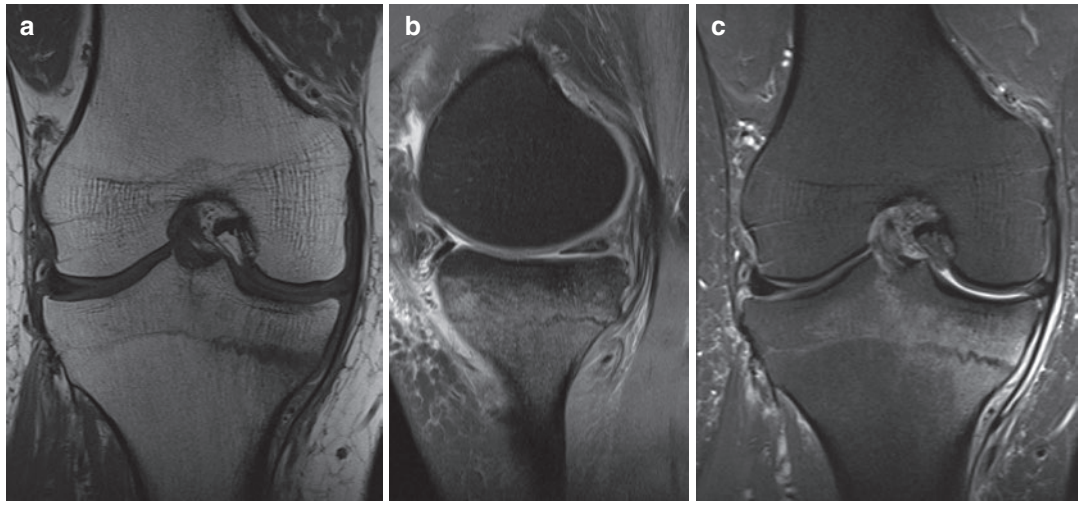

Fig. 7 (**a**–**c**) Tibial stress fracture. 57-Year-old-patient with knee pain and swelling. Additional clinical history revealed short-term period of heavy weight lifting. (**a**) Coronal T1-WI reveals medial tibial stress fracture. (**b**) Sagittal STIR shows reactive marrow changes, posterior medial tibial stress fracture line, and prominent soft-tissue reaction. (**c**) Coronal STIR stress fracture at the same level as in (**a**)

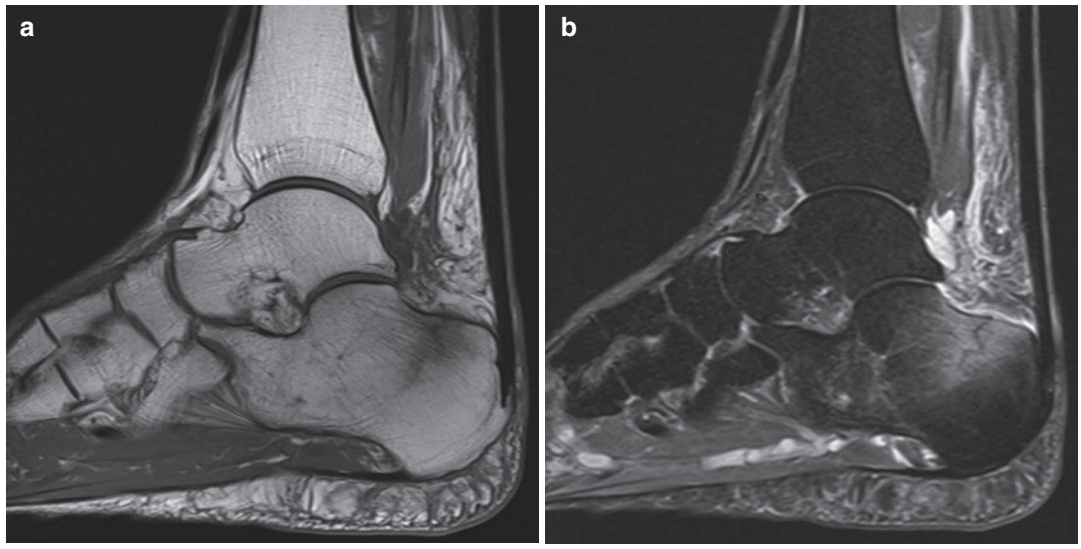

Fig. 8 (**a**, **b**) Insufficiency fracture of calcaneus. 50-Year-old female presents with soft-tissue swelling of ankle and Achilles tendon dysfunction, with concern for mass, after increase in walking activity. (**a**) Sagittal T1-WI reveals a fracture line at the posterosuperior calcaneus and small Achilles tendon enthesophyte. (**b**) Coronal STIR shows the fracture line, marrow change, and minor imbibition of pre-Achilles Kager's fat pad

the awareness of the typical sites may suggest the correct diagnosis.

Furthermore some subtle findings like a specific pattern of the accompanying soft-tissue edema may also suggest the diagnosis (e.g., soft-tissue edema localized next to the MCL in a subchondral insufficiency fracture of the knee) (Wilmot et al. 2016). Any periosteal reaction associated with muscle hypertrophy in an athlete should prompt a review of the type of training and accurate pain characteristics, as the MRI findings may be due to overuse.

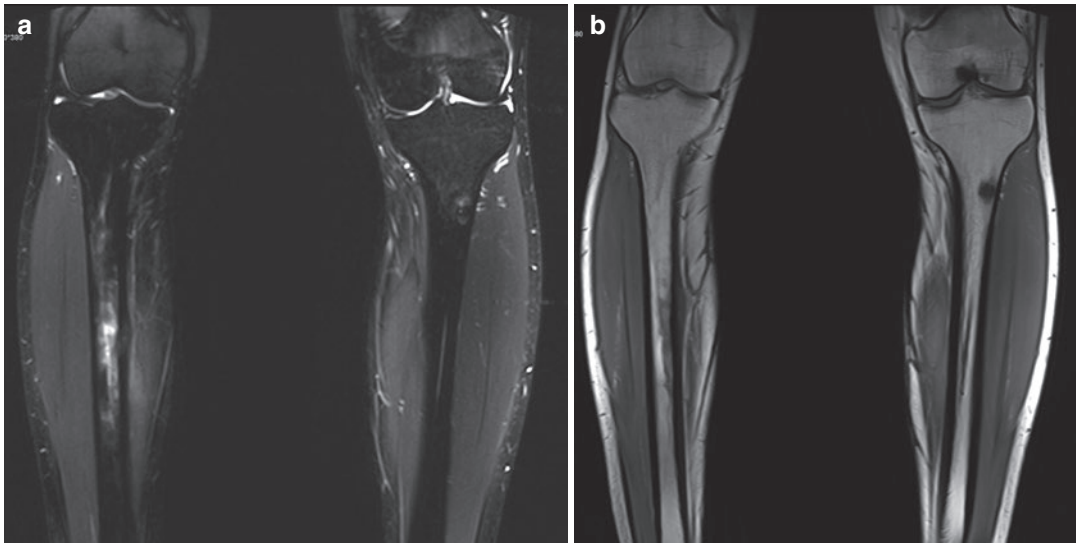

Fig. 9 (**a**, **b**) Bilateral tibial stress fractures. 18-Year-old male marathon runner, including mountain running. Presents after 14-km mountain run with concern for tumor and osteoid osteoma. Coronal STIR bilateral tibia demonstrates right-sided incomplete stress fracture at the proximal to mid-third junction with adjacent soft-tissue reaction and left proximal tibial stress reaction. (**b**) Coronal T1-WI with right diaphyseal cortical periosteal and intramedullary stress reaction and more diffuse region of stress reaction at the left proximal tibia

5.2 Avascular Necrosis

Avascular necrosis may occasionally mimic a cartilage lesion on radiographs, but the presence of the classical double-geographic line sign should make this diagnosis obvious on MRI. Young children practicing overhead sports like baseball may present with humeral capitellum avascular necrosis (Panner's disease) (Sakata et al. 2015).

Long-term use of steroids may be a predisposing factor in the development of avascular necrosis (Min et al. 2008).

5.3 Rheumatological or Degenerative Joint Disease

Young athletes may also first present with a monoarticular joint disease which should be differentiated from overuse within advanced degenerative joint disease. Laboratory screens are helpful here.

6 Normal Variants

Normal variants and their overuse may present as MRI pseudotumors. Normal bone marrow may occasionally cause concern for tumors; however use of T1/T2-weighted and STIR sequences usually excludes real pathology. The bone marrow composition may be assessed using chemical shift encoding-based water-fat MRI (Baum et al. 2015).

Supernumerary bones (styloid bone, accessory ossification centers for scaphoid tuberosity) (Capelastegui et al. 1999), tarsal coalition, and accessory muscles (e.g., soleus muscle and extensor digitorum brevis manus muscle) (Capelastegui et al. 1999) are some targets. Normal variants like accessory muscles are usually asymptomatic. However, sometimes they may cause symptoms due to the mass effect of the supernumerary muscle on adjacent structures like nerves, vessels, or tendons, especially in trained athletes with hypertrophic muscles (Perdikakis et al. 2017). Visible swelling may mimic a soft-tissue tumor (Fig. 10)

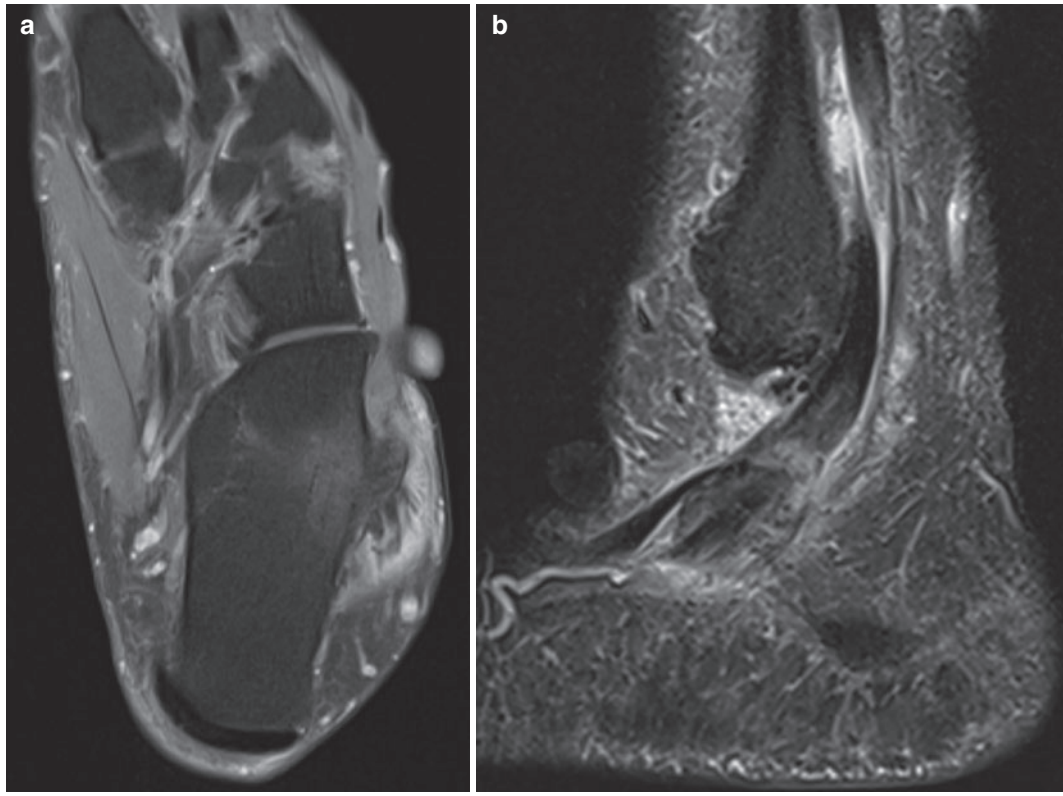

Fig. 10 (**a**, **b**) Bony anatomic variant (prominent tuberculum peroneum) associated with tendon partial tear and inflammatory reaction of soft tissues. 50-Year-old weekend sportsman with clinical concern for overuse or tumor mass. (**a**) Axial fat-suppressed T1-WI after administration of gadolinium contrast shows lateral calcaneal tubercle prominence associated with peroneal tendinosis, adjacent tenosynovitis, and skin contour deformity. (**b**) Sagittal STIR, peroneal tendon partial longitudinal split tear, and soft-tissue reactive change

(Desimpel et al. 2017). The awareness of the regional anatomy and normal variants together with MRI imaging may help in differentiation between both conditions.

Occasionally tarsal coalition and calcaneal spurs associated with peroneal tendon inflammation and partial tear may be associated with a marked synovial reaction and tenosynovitis, mimicking a pseudotumor.

Awareness of these syndromes and review of the radiographs usually allow correct diagnosis. A frequent finding among the normal variants is a periosteal desmoid presenting with an avulsive cortical irregularity of the distal femur often misinterpreted as a suspicious finding by less experienced readers.

7 Infection

Pyomyositis may occur in healthy sporty individuals; however the clinical presentation prior to MRI strongly suggests infection with reddened skin, pain, and often systemic features such as fever. Patients with immunosuppression may present with less signs of inflammation, which may be confusing both clinically and radiologically. MRI features (Soler et al. 1996, 2000; Ogilvie et al. 2001; Abdelwahab et al. 2003) suggesting an abscess include a thickened peripheral rim on T1 and T2 weighting, which may have increased signal intensity on T1 weighting and demonstrate marked contrast enhancement. Immunosuppressed patients com-

monly have an absence of marked adjacent soft-tissue and subcutaneous edema. Fortunately, atypical organisms such as cysticercosis, *Echinococcus granulosus* in hydatid disease, and *Coccidioides immitis* in coccidioidomycosis may rarely cause abscess formations with a mass-like appearance on MRI (Jelinek and Kransdorf 1995). HIV-positive patients may rarely present with a highly vascularized, angiomatosis-focal infection in soft tissues, which may erode and involve adjacent bone, mimicking a sarcoma, due to infection with *Bartonella henselae*, a gram-negative bacillus (Biviji et al. 2002). This organism may also be involved in "cat scratch disease" (Dong et al. 1995), as the carrier is usually a cat and is usually associated with single lymph node enlargement.

8 Calcium Deposition Disorders

Calcium deposition disorders—hydroxyapatite, gout, and calcium pyrophosphate dihydrate crystal deposition disorders with calcium deposition in tendons, ligaments, and bursae—may create MRI pseudotumors. Patients with a provisional clinical diagnosis of tumor associated with ligament calcification may be referred for MRI (Anderson et al. 2003a, b). The MRI appearance may include a focal thickening of the lateral collateral ligament associated with adjacent marked soft-tissue reaction and intravenous gadolinium contrast enhancement, which may correlate on radiographs with soft-tissue calcifications. In the resorptive phase the calcifications may migrate inside the tendon, which may cause severe pain due to the inflammatory process (Bianchi and Becciolini 2019). Extratendinous and intramuscular migration of hydroxyapatite crystals has also been documented, which due to muscle edema and inflammation may be misdiagnosed as neoplasm on MRI (Pereira et al. 2016) (Figs. 11 and 12). With its acute clinical onset and dissipation on follow-up radiographs, this entity is presumed to occur due to hydroxyapatite deposition.

Awareness of this entity is critical for a correct MRI diagnosis of a pseudotumor.

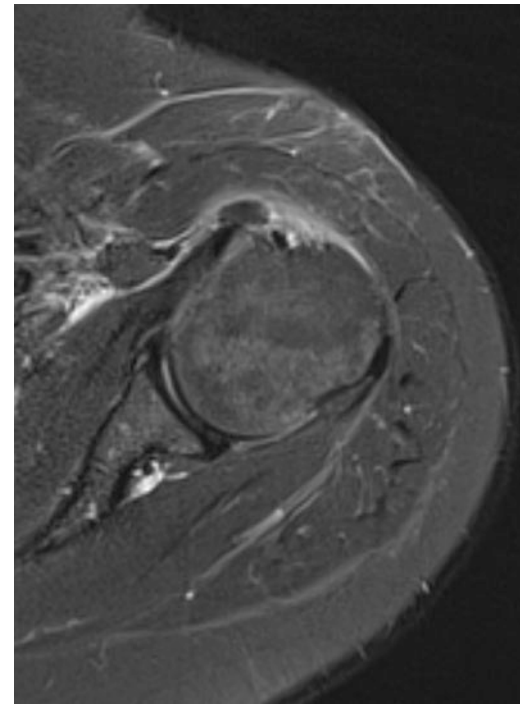

Fig. 11 Calcific tendinosis. 40-Year-old female, weekend tennis player. Axial STIR sequence shows calcification of subscapularis tendon, extratendinous subdeltoid extension, and reactive muscle changes. Additional history was obtained by the radiologist for sudden marked pain increase. Radiograph confirmed calcific tendinosis

Review of radiographs at the time of MRI may be helpful in detecting calcifications. This condition is more characteristic within the rotator cuff tendons of the shoulder.

9 Metabolic Disorders

Metabolic disorders may be associated with MRI pseudotumors such as amyloid deposition and hyperparathyroidism, though they are most unusual in sporting individuals. Secondary amyloidosis is the most common of this unusual group, often seen in association with chronic renal failure. This condition occurs due to the deposition of beta-2 microglobulins within joint capsules and tendon sheaths. It may rarely be associated with pseudotumors near joints. Characteristically there is a decreased signal intensity on T2 weighting, which appears to reflect the collagen-like

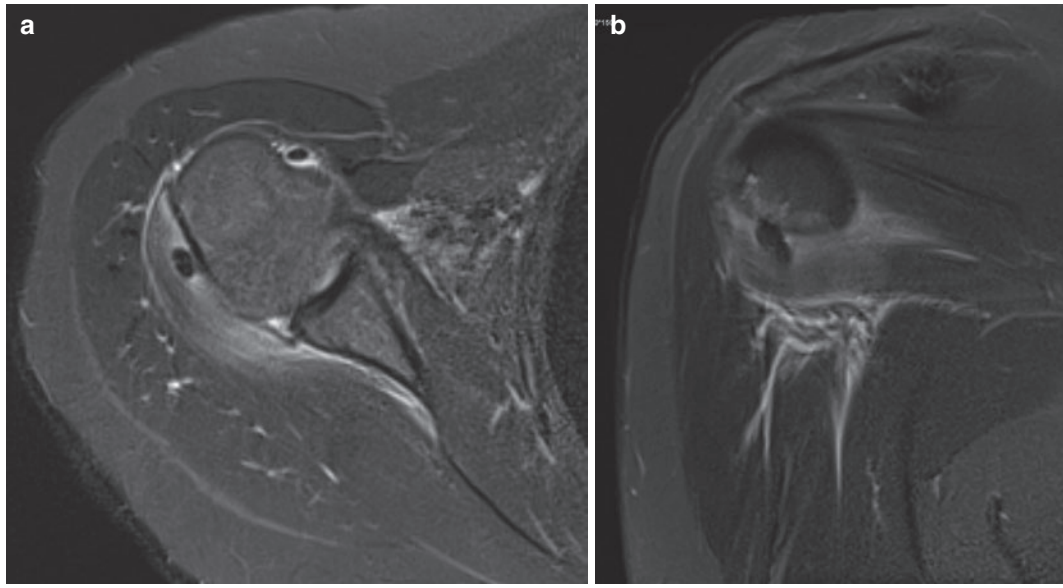

Fig. 12 (**a**, **b**) Calcific tendinosis. 35-Year-old female, weekend sports, presents with a pseudopalsy of upper limb and concern for tumor. (**a**) Axial STIR sequence shows calcific tendinosis, calcification rupture, and adjacent reactive signal change in the teres minor muscle. (**b**) Coronal STIR shows soft-tissue reactive changes adjacent to the focal calcification

nature of the amyloid (Kransdorf and Murphey 1997). The hypointense appearance on T2-weighted imaging may already narrow the differential diagnosis as it is less common. Besides amyloidosis, hypointense signal may occur more typically with hyperacute hemorrhage or chronic hemosiderin deposition, cartilaginous loose bodies, tenosynovial giant-cell tumor, rheumatoid arthritis, hemochromatosis, gout, calcium pyrophosphate arthropathy (CPPD), hydroxyapatite deposition disease (HADD), tumoral calcinosis (Steinbach et al. 1995), arthrofibrosis, and iatrogenic lesions with fibrosis (Wadhwa et al. 2016).

Unusual in athletes, though mentioned for completeness sake, secondary hyperparathyroidism may be associated with brown tumors of bone which are nonspecific on MRI. The most common clinical setting is chronic renal failure with high serum calcium, low serum phosphorus, and high parathormone level. Idiopathic tumoral calcinosis may present as an MRI pseudotumor with large septated regions of variable signal intensity in periarticular regions on both T1 and T2 weighting; however review of the radiographs allows for this diagnosis.

10 Foreign-Body Reactions

Foreign-body reactions due to trauma or as a consequence of trauma such as retained surgical swabs ("cottonballoma") (Kalbermatten et al. 2001) fortunately are less common, though they should be considered in the appropriate clinical setting. Close inspection for traces of intramedullary screws, subtle metallic artifacts, or direct evidence of retained foreign bodies, such as glass, should be sought for.

Surfers may be rarely exposed to foreign-body reactions, as described in a case report presenting a "Surfinoma" (Squire et al. 2010). A fragment of a fiberglass surfboard, located in M. latissimus dorsi, has been left after a surgical closing procedure, forming a sinus to the axillary region. A year after the injury the patient presented with a mass in the left axillary region, redness of skin, and a small fluid collection consistent with an abscess formation inferior to the foreign bodies (Squire et al. 2010). This rare case may help to raise awareness for any foreign-body reaction and its possible appearance in athletes.

11 Vascular Pseudoaneurysms

Less common MRI pseudotumors include pseudoaneurysms of the hand arteries, which may present as soft-tissue masses without further symptoms (Anderson et al. 2003a, b). Due to their superficial location and proximity to the bones, the arteries of the hand are frequently exposed to minor or repetitive trauma, which may lead to a pseudoaneurysm formation (Gardiner Jr. and Tan 2017; Conn Jr. et al. 1970).

The most common location of the arterial injury due to blunt trauma is the hypothenar region, where the superficial branch of the ulnar artery passes directly over the hook of hamate within the Guyon's canal (Gardiner and Tan 2017). This condition has been described as the hypothenar hammer syndrome and is associated with ischemia of the hand and fingers. The damage of the endothelial cells results in platelet aggregation and thrombus formation with a further cascade of a traumatic insult of the vessel wall, which may eventually lead to an aneurysm formation (Gardiner and Tan 2017; Glichenstein et al. 1988). The compression of the sensory branch of the ulnar nerve may also occur (Glichenstein et al. 1988). The hypothenar hammer syndrome has been usually described in adult men with industrial occupations involving repetitive blunt trauma to the hands (Newmeyer 1993; Little and Ferguson 1972). It has also been described in sports-related injuries in handball players and baseball catchers (Glichenstein et al. 1988; Newmeyer 1993; Little and Ferguson 1972).

The thenar hammer syndrome (Janevski 1979) involves an acute or chronic compression of the radial artery between the first and second metacarpal, due to its superficial location being covered only by the muscle of flexor pollicis brevis and subcutaneous fat.

The commonest pseudoaneurysms involve the popliteal artery, which in up to 75% of cases may occur bilaterally if due to arteriosclerosis (Kransdorf and Murphey 1997). Additional MR angiography sequence may give the diagnosis here.

12 Posttreatment/Intervention (Steroid-Induced Osteoporosis, Insufficiency Fracture)

Though rare in sporting individuals, post-therapeutic appearance on MRI, including postradiation changes, may be associated with an MRI pseudotumor. Due to increasing popularity of physical activity among the elderly population with possible oncologic background, these conditions may gain in significance. Postradiation findings on MRI with signal alterations in soft tissue and bone marrow may initially raise concern for a true neoplasm; however on close review of the imaging characteristics, there is usually no real mass. The attentive review of the patient's history (e.g., radiotherapy) usually allows a correct diagnosis (Richardson et al. 1996).

Things to Remember

1. Check for the history of trauma—think myositis ossificans.
   Review the history for specific sport and repetitive activity—think overuse/tears of ligaments, muscles, and stress reactions or fractures.
2. Ascertain whether there is true focal mass present. Consider larger FOV to look for asymmetries and compare to the contralateral side.
3. Always correlate MRI with radiographs and/or CT.
4. 4. In case of superficial lesion—think hematoma/fat necrosis; in case of intramuscular lesion—think hematoma/infection/myositis ossificans (tidemark sign).
5. Remember age-specific lesions:
   Adolescents: Stress reactions and chronic avulsion fractures may mimic neoplastic lesion.
   Aging population with more sporting activity.
   Aging population—more osteoporosis and insufficiency fractures.
   Check risk factors for AVN.
6. Joint lesions: Remember that systemic disorders may first present in one joint.

7. Marked irregular synovitis—think of rheumatologic disorder or infection.
   Abscess wall sign—increased signal on T1 weighting within thickened wall.
8. Ensure T1 weighting to review for normal marrow signal.
9. Exclude normal variants with overuse—check radiographs.

Imaging Boxes

Plain Radiography/CT

Radiopaque or radiolucent foreign bodies.
Evaluation of acute or chronic avulsion fractures.
(Mature) myositis ossificans.
Calcifications.

Ultrasound

Foreign bodies (wood, glass, …).
Muscle/tendon trauma and Morel-Lavallée lesions.
Early detection and characterization of myositis ossificans.
Myocele/muscle hernia: muscle contraction aids in confident diagnosis.

MR Imaging

Imaging in three planes required.
Imaging protocol should include at least T1-WI and STIR or fat-suppressed T2-WI.
Gradient echo imaging: useful to detect hemosiderin, metallic foreign bodies, and gas.
Should always be correlated with clinical history and plain films/CT.

References

Abdelwahab IF, Klein MJ, Hermann G (2003) Solitary cysticercosis of the biceps brachii in a vegetarian: a rare and unusual pseudotumor. Skelet Radiol 32:424–428

Ahlawat S, Wadhwa V, Belzberg AJ, Batra K, Chhabra A (2015) Spectrum of suprascapular nerve lesions: normal and abnormal neuromuscular imaging appearances on 3-T MR neurography. AJR Am J Roentgenol 204:589–601

Anderson SE, Johnston JO, ODonnel R et al (2001) MR imaging of Sports related pseudotumor in Children: mid femoral diaphyseal periostitis at insertion site of adductor musculature. AJR Am J Roentgenol 176:1227–1231

Anderson SE, Bosshard C, Steinbach LS et al (2003a) Calcification of the lateral collateral ligament of the knee: a rare pathology and cause of lateral knee pain shown by MR imaging. AJR Am J Roentgenol 181(1):199–202

Anderson SE, De Monaco D, Buechler U et al (2003b) Imaging Features of Pseudoaneurysms of the Hand in Children and Adults. AJR Am J Roentgenol 180:659–664

Anderson SE, Steinbach LS, De Monaco D et al (2004a) The baby wrist: MRI of an overuse syndrome of mothers. AJR Am J Roentgenol 182:719–724

Anderson SE, Weber M, Steinbach LS et al (2004b) Shoe rim and shoe buckle pseudotumor of the ankle in elite and professional ice figure skaters and snow boarders: MR imaging findings. Skelet Radiol 33: 325–329

Baum T, Yap SP, Dieckmeyer M et al (2015) Assessment of whole spine vertebral bone marrow fat using chemical shift-encoding based water-fat MRI. J Magn Res Imag 42:1018–1023

Behrens SB, Deren ME, Matson A, Fadale PD, Monchik KO (2013) Stress fractures of the pelvis and legs in athletes: a review. Sports Health 5:165–174

Bianchi S, Becciolini M (2019) Ultrasound appearance of the migration of tendon calcifications. J Ultrasound Med 38:2493–2506

Biviji AA, Paiement GD, Steinbach LS (2002) Musculoskeletal manifestations of the human immunodeficiency virus infection. J Am Acad Orthop Surg 10:312–320

Boutin RD, Fritz RC, Steinbach LS (2002) MRI of muscle injury. Radiol Clin N Am 40:333–362

Breer S, Krause M, Marshall RP, Oheim R, Amling M, Barvencik F (2012) Stress fractures in elderly patients. Int Orthop 36:2581–2587

Brown S-AN, Doolittle DA, Bohanon CJ et al (2015) Quadrilateral space syndrome: the mayo clinic experience with a new classification system and case series. Mayo Clin Proc 90:382–394

Capelastegui A, Astigarraga E, Fernandez-Canton G et al (1999) Masses and pseudomasses of the hand and wrist: MR findings in 134 cases. Skelet Radiol 28:498–507

Conn J Jr, Bergan JJ, Bell J (1970) Hypothenar hammer syndrome: posttraumatic digital ischaemia. Surgery 68:1122–1128

Connell DA, Schneider-Kolsky ME, Hoving JL et al (2004) Longitudinal study comparing sonographic and MRI assessments of acute and healing hamstring injuries. AJR Am J Roentgenol 183:975–984

Coyle J, White LM, Dickson B, Ferguson P, Wunder J, Naraghi A (2013) MRI characteristics of nodular

fasciitis of the musculoskeletal system. Skelet Radiol 42:975–982
De Coninck T, Vanhoenacker F, Verstraete K (2017) Imaging features of Morel-Lavallée lesions. J Belg Soc Radiol 101(Suppl 2):15. https://doi.org/10.5334/jbr-btr.1401
De Smet AA, Noris MA, Fisher DR (1992) Magnetic resonance imaging of myositis ossificans: analysis of seven cases. Skelet Radiol 21:503–507
Desimpel J, Posadzy M, Vanhoenacker F (2017) Imaging features of symptomatic hypertrophic tuberculum peroneum. J Belg Soc Radiol 101(Suppl 2):7. https://doi.org/10.5334/jbr-btr.1376
Dhondt E, Oudenhoven L, Khan S et al (2006) Nora's lesion, a distinct radiological entity? Skelet Radiol 35:497–502
Dong PR, Seeger LL, Yao L et al (1995) Uncomplicated cat-scratch disease: findings at CT, MR imaging, and radiography. Radiology 195:837–839
Dooms GC, Fisher MR, Hricak H et al (1985) MR imaging of intra-muscular hemorrhage. J Comput Assist Tomogr 9:908–913
Dorfman HD, Czerniak B (1998) Benign osteoblastic tumors. In: Bone tumors. 1st ed. Mosby, St Louis, MO, pp 85–127
Ekstrand J, Askling C, Magnusson H, Mithoefer K (2013) Return to play after thigh muscle injury in elite football players: implementation and validation of the Munich muscle injury classification. Br J Sports Med 47:769–774
Fonseca E, Castro A, Kubo RS, Miranda FC, Taneja AK, Santos D, Rosemberg LA (2019) Musculoskeletal "don't touch" lesions: pictorial essay. Radiol Bras 52(1):48–53
Fujimoto H, Ikeda M, Shimofusa R et al (2002) Sarcoidosis breaching the fascia and mimicking a sarcoma. Skelet Radiol 31:706–708
Furman J (2015) When exercise causes exertional rhabdomyolysis. J Am Acad Phys Assist 28:38–43
Gardiner GA Jr, Tan A (2017) Repetitive blunt trauma and arterial injury in the hand. Cardiovasc Intervent Radiol 40:1659–1668
Glichenstein J, Ohana J, Leclercq C (1988) Tumors of the hand. Springer, Berlin, pp 147–150
Gomori JM, Grossman RI, Golberg HI et al (1985) High field magnetic resonance imaging of intracranial hematomas. Radiology 157:87–93
Greenspan A, Azouz EM (1999) Bone dysplasia series. Melorheostosis: review and update. Can Assoc Radiol J 50:32
Gruber G, Giessauf C, Leithner A et al (2008) Bizarre parosteal osteochondromatous proliferation (Nora lesion): a report of 3 cases and a review of the literature. Can J Surg 51:486–489
Hardcastle P, Annear P, Foster DH et al (1992) Spinal abnormalities in young fast bowlers. J Bone Joint Surg (Br) 74-B:421–425
Janevski BK (1979) Angiography of the upper extremity. In: Greep JN et al (eds) Pain in the shoulder and arm. Nijhoff M, The Hague-Boston-London, pp 25–48
Jarraya M, Parva P, Stone M, Klein MJ, Guermazi A (2014) Atypical proliferative myositis: original MR description with pathologic correlation: case report. Skelet Radiol 43:1155–1159
Jelinek J, Kransdorf MJ (1995) MR imaging of soft-tissue masses. Mass-like lesions that simulate neoplasms. Magn Reson Imaging Clin N Am 4:727–741
Kalbermatten DF, Kabermatten NT, Hertel R (2001) Cotton-induced pseudotumor of the femur. Skelet Radiol 30:415–417
Karantanas A (2019) Imaging of motion and performance, sports overuse and injury. Muscle Injuries Chapter 3(2):35
Kransdorf M, Murphey M (1997) Masses that may mimic soft tissue tumors. In: Kransdorf M (ed) Imaging of soft tissue tumors. WB Saunders Company, Philadelphia, pp 373–420
Kwee RM, Kwee TC (2019) Calcified or ossified benign soft tissue lesions that may simulate malignancy. Skelet Radiol 48:1875–1890
Little JM, Ferguson DA (1972) The incidence of hypothenar hammer syndrome. Arch Surg 105:684–685
Mahajan S, Chandra R, Mohan LY (2012) "Nora lesion"—Bizarre parosteal osteochondromatous proliferation. J Clin Orthopaed Trauma 3(2):119–121. https://doi.org/10.1016/j.jcot.2012.07.001
Maurer B, Walker UA (2015) Role of MRI in diagnosis and management of idiopathic inflammatory myopathies. Curr Rheumatol Rep 17:67–67
McLean K, Popovic S (2017) Morel-Lavallee lesion: airp best cases in radiologic-pathologic correlation. Radiographics 37:190–196
Min B-W, Song K-S, Cho C-H, Lee S-M, Lee K-J (2008) Untreated asymptomatic hips in patients with osteonecrosis of the femoral head. Clin Orthop Relat Res 466:1087–1092
Mueller-Wohlfahrt HW, Haensel L, Mithoefer K et al (2013) Terminology and classification of muscle injuries in sport: the Munich consensus statement. Br J Sports Med 47(6):342–350. https://doi.org/10.1136/bjsports-2012-091448
Newmeyer W (1993) Vascular disorders. In: Green D (ed) Operative hand surgery, 3rd edn. Churchill Livingstone, New York, pp 2251–2299
Nöbauer-Huhmann (2019) Imaging of motion and performance. Bone Tumours Chapter 24:231
Ogilvie CM, Kasten P, Rovinsky D et al (2001) Cysticercosis of the triceps—an unusual pseudotumor. Clin Orthop Relat Res 382:217–221
Pavlov H (1995) Physical injuries: sports related abnormalities. In: Resnick D (ed) Diagnosis of bone and joint disorders, 3rd edn. WB Saunders, Philadelphia, pp 3229–3263
Perdikakis E, Tsifountoudis I, Kalaitzoglou I, Rountas C, Malliaropoulos N, Maffulli N (2017) Soft tissue pseudotumours: a pictorial review with emphasis on MRI. Muscles Ligaments Tendons J 7: 353–375
Pereira BPG, Chang EY, Resnick DL, Pathria MN (2016) Intramuscular migration of calcium hydroxyapatite

crystal deposits involving the rotator cuff tendons of the shoulder: report of 11 patients. Skelet Radiol 45:97–103
Ragunanthan N, Sugavanam C (2006) Pseudomalignant myositis ossificans mimicking osteosarcoma: a case report. J Orthop Surg (Hong Kong) 14: 219–221
Rani D, Gupta A (2019) Cytological diagnosis and misdiagnosis of nodular fasciitis. J Cytol 36:196–199
Richardson ML, Zink-Brody GC, Patten RM et al (1996) MR characterization of post-irradiation soft tissue edema. Skelet Radiol 25:537–543
Robinson P, White LM, Lax M, Salonen D, Bell RS (2000) Quadrilateral space syndrome caused by glenoid labral cyst. AJR Am J Roentgenol 175:1103–1105
Rubin JI, Gomori JM, Grossman RI et al (1987) High-field MR imaging of extracranial hematomas. AJR Am J Roentgenol 148:813–817
Sakata R, Fujioka H, Tomatsuri M et al (2015) Treatment and diagnosis of Panner's disease. A report of three cases. Kobe J Med Sci 61:E36–E39
Sanders BS, Bruce J, Robertson J (2011) Treatment of a symptomatic forearm muscle herniation with a mesh graft. Sports Health 3:179–181
Schneider R, Kaye JJ, Ghelman B (1976) Adductor avulsive injuries near the symphysis pubis. Radiology 120:567–569
Shimal A, Davies AM, James SL, Grimer RJ (2010) Fatigue-type stress fractures of the lower limb associated with fibrous cortical defects/non-ossifying fibromas in the skeletally immature. Clin Radiol 65:382–386
Soler R, Castro JM, Rodriguez E (1996) Value of MR findings in predicting the nature of soft tissue lesions: benign, malignant or undetermined lesion? Comput Med Imaging Graph 20:163–169
Soler R, Rodriguez E, Aguilera C et al (2000) Magnetic resonance imaging of pyomyositis in 43 cases. Eur J Radiol 35:59–64
Squire T, Sherlock M, Wilson P, Tan B, Hope N, Anderson SE (2010) Surfinoma: a case report on a pseudotumor developing after a surfing sports injury. Skelet Radiol 39:1239–1243
Steinbach LS, Johnston JO, Tepper EF et al (1995) Tumoral calcinosis: radiologic-pathologic correlation. Skelet Radiol 24:573–578
Stensby JD, Baker JC, Fox MG (2016) Athletic injuries of the lateral abdominal wall: review of anatomy and MR imaging appearance. Skelet Radiol 45:155–162
Sutter R, Kalberer F, Binkert CA, Graf N, Pfirrmann CWA, Gutzeit A (2013) Abductor tendon tears are associated with hypertrophy of the tensor fasciae latae muscle. Skelet Radiol 42:627–633
Thierfelder KM, Gerhardt JS, Gemescu IN et al (2019) Imaging of hip and thigh muscle injury: a pictorial review. Insights Imaging 10:20. https://doi.org/10.1186/s13244-019-0702-1
Torreggiani WC, Munk PL, Al-Ismail K et al (2001) MR imaging features of bizarre parosteal osteochondromatous proliferation of bone (Nora's lesion). Eur J Radiol 40:224–231
Tsai TS, Evans HA, Donnelly LF et al (1997) Fat necrosis after trauma: a benign cause of palpable lumps in children. AJR Am J Roentgenol 169:1623–1626
Van Hul E, Vanhoenacker F, Van Dyck P, De Schepper A, Parizel PM (2011) Pseudotumoural soft tissue lesions of the foot and ankle: a pictorial review. Insight Imaging 2:439–452
Wadhwa V, Cho G, Moore D, Pezeshk P, Coyner K, Chhabra A (2016) T2 black lesions on routine knee MRI: differential considerations. Eur Radiol 26:2387–2399
Walczak BE, Johnson CN, Howe BM (2015) Myositis Ossificans. J Am Acad Orthop Surg 23:612–622
Wang H, Nie P, Li Y et al (2018) MRI findings of early myositis ossificans without calcification or ossification. Biomed Res Int 2018:4186324
Wilmot AS, Ruutiainen AT, Bakhru PT, Schweitzer ME, Shabshin N (2016) Subchondral insufficiency fracture of the knee: a recognizable associated soft tissue edema pattern and a similar distribution among men and women. Eur J Radiol 85:2096–2103
Yoshioka H, Anno I, Niitsu M et al (1994) MRI of muscle strain injuries. J Comput Assist Tomogr 18: 454–460
Zubler V, Muhlemann M, Sutter R et al (2020) Diagnostic utility of perilesional muscle edema in myositis ossificans. Skelet Radiol 49(6):929–936. https://doi.org/10.1007/s00256-019-03351-5

Part II

Topographic Discussion

Shoulder Instability

Christoph Schäffeler

Contents

Abstract

The shoulder is the most common dislocated joint of the body with traumatic anterior instability accounting for >90% of all dislocations. Sufficient interaction between static and dynamic stabilizers is important to prevent instability. Knowledge of the imaging anatomy and the variations of the labrum and the glenohumeral ligaments is crucial to identify pathology related to shoulder instability. Particularly traumatic injury to the anteroinferior labroligamentous complex (LLC) and the biceps-labral-complex (BLC) can be detected on cross-sectional imaging. Osseous injury and wear of the anterior glenoid are common as well as impaction fracture at the posterosuperior humeral head. Quantification of glenoid bone loss is important for therapeutic decisions and should be related to the extension of the Hill-Sachs lesion by applying the on-track/off-track concept.

Microinstability is a typical phenomenon in overhead athletes in whom osseous and soft-tissue adjustments may lead to pathologic glenohumeral internal rotational deficit and/or posterosuperior impingent with a complex of certain imaging findings.

Atraumatic instability has to be clinically differentiated from non-pathologic hyperlaxity and is described to be related to shoulder complaints. The task of imaging is to rule out structural pathology in the glenohumeral joint and may allow for the documentation of redundancy of the anteroinferior LLC.

C. Schäffeler (✉)
Musculoskeletal and Trauma Imaging, Cantonal Hospital Grisons, Chur, Switzerland
e-mail: christoph.schaeffeler@ksgr.ch

Med Radiol Diagn Imaging (2020)
https://doi.org/10.1007/174_2020_245, © Springer Nature Switzerland AG
Published Online: 19 December 2020

1 Introduction: Epidemiology—Classification

The shoulder joint requires a high range of motion to meet the tasks of everyday life and in particular to reach full athletic performance. Regarding the osseous articulation, the shoulder is the most inherently unstable joint of the body. Therefore a complex system of dynamic and static soft-tissue stabilizers is required in order to maintain joint congruence in any kind of movement and sports activity. However, the wide range of motion makes the glenohumeral joint susceptible to subluxation and dislocation due to acute traumatic events with injury to the stabilizing structures (Sheehan et al. 2013). Traumatic anteroinferior dislocation of the shoulder joint accounts for more than 90% of shoulder pathologies associated with glenohumeral instability (Smith 2006).

In addition, there are a number of sporting activities that require high mobility or even drive the glenohumeral range of motion to an extreme level in order to achieve maximum performance. This may result in repetitive microtraumatic damage, which in turn may lead to secondary complaints, structural adjustments, and injury and can thus significantly limit athletic performance (Reinold and Curtis 2013).

In the general population of the United States, the incidence of traumatic shoulder dislocation has been reported as 8–24/100,000 persons per year. This would increase drastically in a male, young, and athletic risk group with 30/100,000 shoulder dislocations per year (Galvin et al. 2017). Particularly in contact sports like American football there is a high incidence of shoulder dislocation with 51/100,000 cases per year and it has been documented that about 10% of the participants in the National Football League (NFL) combine report a previous history of shoulder instability (Galvin et al. 2017; Gibbs et al. 2015).

Both traumatic and microtraumatic instabilities can occur or be promoted together with a preexisting bilateral hyperlaxity of the joint capsule and the ligaments, which in itself should not be considered pathological, but which additionally may complicate diagnosis and therapy (Longo et al. 2015).

Due to the overlap of these phenomena, existing classification systems are usually not sufficiently comprehensive. Most classification systems divide instability subgroups by either by etiology or direction of dislocation or by a combination of both.

A common classification approach for shoulder instability is that developed by Thomas and Matsen (Thomas and Matsen 1989). The acronym TUBS (traumatic-unidirectional-Bankart lesion-surgery required) summarizes patients with acute traumatic anteroinferior shoulder dislocations. The AMBRI group (atraumatic-multidirectional-bilateral-rehabilitation-inferior capsular shift) was considered separate, comprising patients with atraumatic multidirectional instability. In addition, a further patient group AIOS (acquired-instability-overhead-surgery) was added later, which covers overhead athletes with signs of microinstability (Burkhart et al. 2000).

Another classification system is that of Stanmore and co-workers, which is based on a triangular pole theory (Jaggi and Alexander 2017). The traumatic structural pole I comprises the same patients like the TUBS subgroup. At pole II there are patients with structural atraumatic instability and pole III includes patients with nonstructural habitual instability with abnormal muscle patterning. No strict separation of these three poles is needed as patients may have various signs of each pole and may represent an individual point within the area of this triangle.

In 2002, Gerber and colleagues introduced a classification that incorporates the combination of unidirectional or multidirectional post-traumatic instability with or without hyperlaxity (Gerber and Nyffeler 2002). According to the classification particular treatment strategies can be applied. In addition to dynamic instabilities, static instabilities are also included; however the latter are usually based on rotator cuff disease or degeneration and cannot be considered a sports injury.

Most recently a classification system has been introduced that covers the frequency, etiology, primary direction, and severity of the dislocation (subluxation vs. dislocation) and is therefore named the FEDS system (Kuhn 2010).

For the radiologist, the precise assignment of a patient to a category of a particular classification system of shoulder instability is not of primary importance. However, knowledge of the various causes of glenohumeral instability, their patterns on imaging, and different treatment strategies is important for the detection of relevant imaging findings in the spectrum of this disease.

2 Relevant Anatomy: Variants—Biomechanics

The glenohumeral articulation consists of the humeral head and the glenoid of the scapula, whereby the osseous contact of the two joint partners contains only about 25% of the humeral joint surface (Murray et al. 2013). The osseous articulation is part of the static stabilization of the shoulder, with the depth of the glenoid fossa having the greatest effect on reducing glenohumeral translation. The glenoid labrum, composed of fibrous connective tissue, increases the humeral contact area with the scapula by 50% and is also the attachment site for further static stabilizers, the glenohumeral ligaments that are considered to be reinforcements of the joint capsule (Burkart and Debski 2002; Howell and Galinat 1989). The superior (SGHL), the middle (MGHL), and the inferior glenohumeral ligament (IGHL) can be distinguished, whereby the latter can be divided into an anterior and posterior band forming the axillary recess in between (Fig. 1) (Motamedi et al. 2014). Primarily the rotator cuff but also the deltoid muscle, the scapular rotatory muscles, and the long head of the biceps tendon function as dynamic stabilizers (Murray et al. 2013). Essentially, the glenohumeral stability is ensured by two mechanisms: the compression of the humeral head into the glenoid cavity and scapulohumeral muscular balance.

The contribution of the glenohumeral ligaments to the stability of the shoulder joint depends on joint position. The glenohumeral ligaments play a particularly important role in the extreme positions of shoulder movement. Abduction and external rotation (ABER) of the humerus is the joint position that is particularly prone to anteroinferior dislocation. The anteroinferior labroligamentous complex (LLC) is of crucial importance in this joint position (Burkart and Debski 2002). It can be described as a continuous unit from the bone of the glenoid over the anteroinferior labrum as the attachment point of the anterior band of the IGHL to its insertion at the humeral head (Fig. 2a). Normally folded and redundant in neutral position, the LLC becomes stretched in the overhead position in ABER and forms a stabilizing sling for the humeral head to resist anteroinferior dislocation

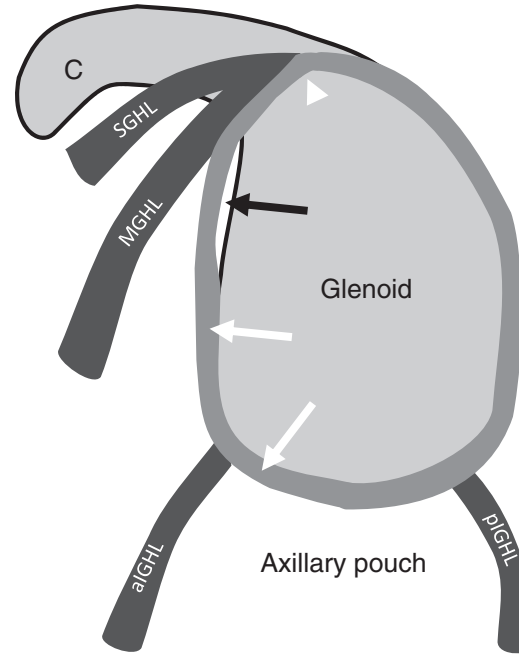

Fig. 1 Schematic en face view of the glenoid with glenohumeral ligaments. The SHGL and the MGHL usually origin at the supraglenoid tubercle (arrowhead). Anteroinferiorly the aIGHL and posteroinferiorly the pIGHL can be found with the axillary pouch or recess in between. White arrows indicate the labrum with the sublabral foramen (black arrow) at the anterosuperior glenoid (*SGHL* superior glenohumeral ligament, *MGHL* middle glenohumeral ligament, *aIGHL* anterior band of inferior glenohumeral ligament, *pIGHL* posterior band of inferior glenohumeral ligament, *C* coracoid process)

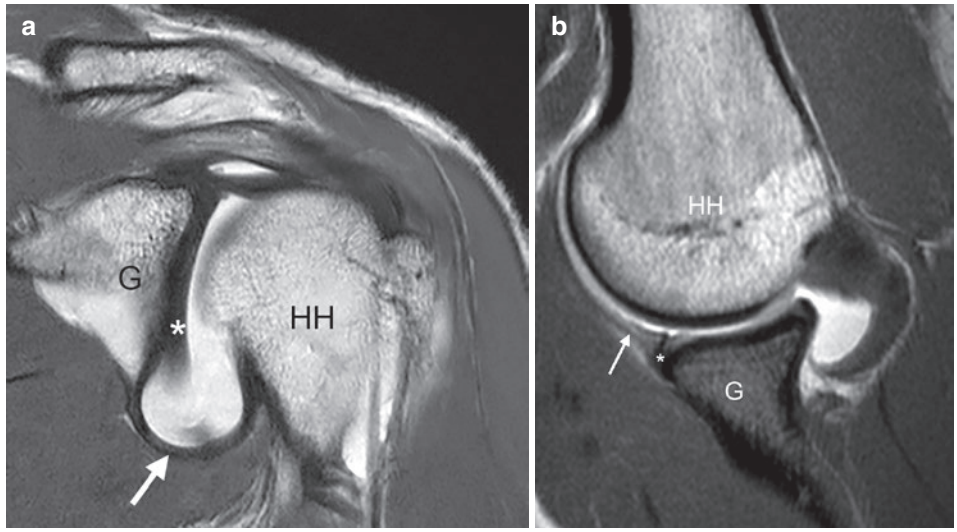

Fig. 2 (**a** and **b**) T1-weighted MR arthrograms showing the normal appearance of the anteroinferior labroligamentous complex (LLC) (arrow) from the labrum at the glenoid (G) to the humeral head (HH). (**a**) Standard paracoronal plane in neutral position with folded LLC. (**b**) Abduction and external rotation (ABER) position demonstrating functional tightness of the LLC stabilizing the HH

(Fig. 2b) (Murray et al. 2013). The posterior band of the IGHL provides posterior stability with the humerus in flexion and internal rotation (Murray et al. 2013).

Variations of the labrum and the glenohumeral ligaments are common and must not be mistaken for pathology. The labrum is most of the time firmly attached to the glenoid rim and usually shows a triangular or rounded appearance on cross-sectional imaging (De Maeseneer et al. 2000). However, the superior labrum at the supraglenoid tubercle of the glenoid shows a variable attachment (Fig. 3). A sublabral recess or sulcus is the most common variation and can be seen in up to 73% of individuals and has to be differentiated from injury to the bicipital-labral-complex (BLC) which is referred to as a superior labral anterior to posterior (SLAP) lesion (Smith et al. 1996).

In about 12–18.5% of the cases, a sublabral foramen or hole can be found between the anterosuperior labrum and glenoid and must not be confused with a Bankart injury, which would be located more anteroinferiorly (Fig. 4) (Williams and Snyder 1994; Ilahi et al. 2002; Pfahler et al. 2003). In the appearance of a sublabral foramen 75% of the cases show a thickened, so-called

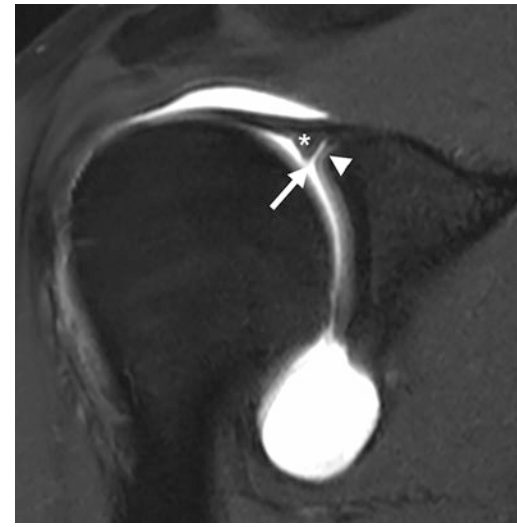

Fig. 3 Normal appearance of the sublabral recess (arrow) on a T1-weighted fat-suppressed MR image in the paracoronal plane. The recess can be found between the superior labrum (asterisk) and the supraglenoid tubercle (arrowhead), which is covered with cartilage

cord-like MGHL. If the anterosuperior labrum is completely absent in the presence of a cord-like MGHL, this is referred to as a Buford complex, a rare variation (1.5–6% of cases) with no pathologic value (Fig. 5a,b) (Williams et al. 1994; Ilahi

et al. 2002; Ide et al. 2004). Of all glenohumeral ligaments MGHL is the one with the most variations. In the studies by Morgan et al. the variations of the glenohumeral ligaments are described (Snyder 1994). In approximately 2/3 of the cases, all three bands can be identified separately. The "cord-like" MGHL can be found in 19% and a fusion of IGHL and MGHL can be distinguished in 7% of the cases. This has been described as just as common as a complete absence of all glenohumeral ligaments (8%). Complete absence or poor definition of the MGHL alone is described in up to 30% of cases (Fig. 6) (Wall and O'Brien 1995; DePalma 1983).

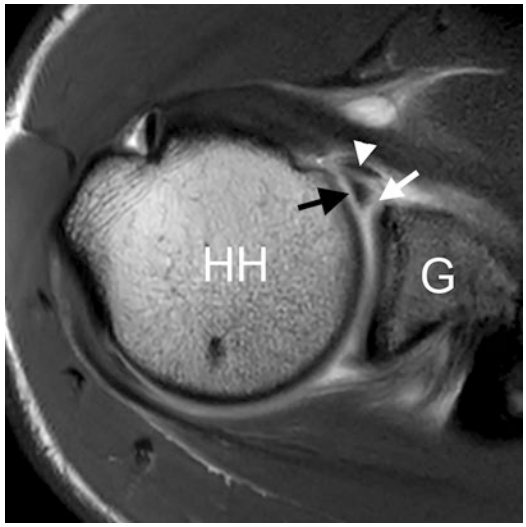

Fig. 4 Transverse T1-weighted MR arthrogram. Anterosuperior labrum (black arrow) and the MGHL (arrowhead) are shown as two structures at the anterosuperior joint with the sublabral foramen (white arrow) between the labrum and the glenoid. *HH* humeral head

It is important to acknowledge that these variations of the labrum and the glenohumeral ligaments are almost exclusively located in the superior and anterosuperior region of the shoulder joint, essentially above the equator of the glenoid. On the other hand, injury to the LLC in the context of traumatic anteroinferior shoulder dislocation can be found below.

In the presence of a hypoplastic anterior labrum with concomitant hypertrophy of the anterior band of the IGHL, the ligament may overlap the labrum at the glenoid rim forming a small sulcus seen on transverse MR images in neutral shoulder position, which may not be mistaken for labral detachment (Fig. 7).

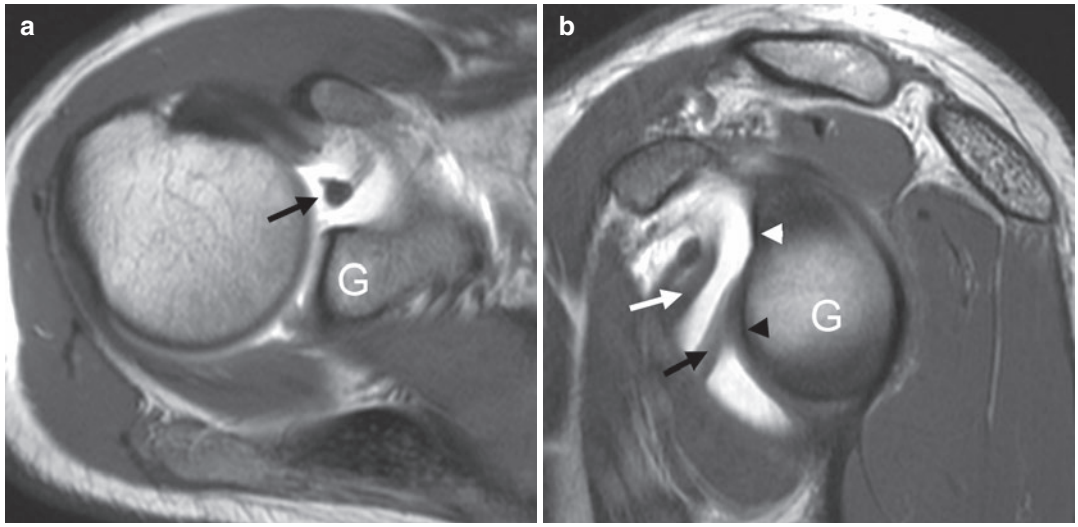

Fig. 5 (**a** and **b**) Buford complex. (**a**) Transverse T1-weighted MR arthrogram at the level of the superior shoulder joint showing absence of the anterosuperior labrum but a cord-like MGHL (black arrow). (**b**) On the corresponding sagittal T1-weighted MR arthrogram the absence of the anterosuperior labrum can be depicted as well as the appearance of the anteroinferior labrum (black arrowhead). Note the course of the MGHL (white arrow) to the joint capsule and the anterior band of the IGHL (black arrow). *G* glenoid

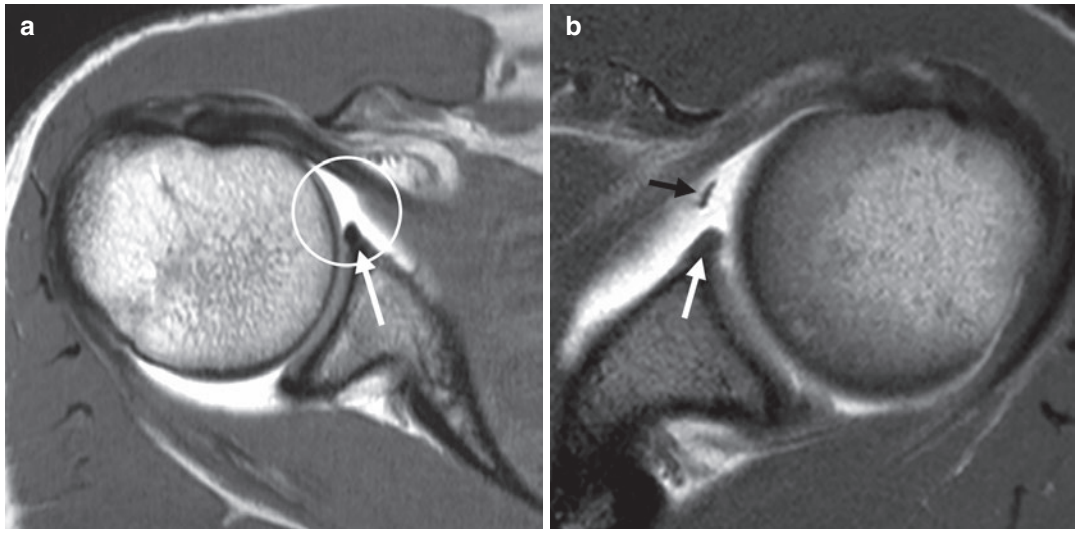

Fig. 6 (**a** and **b**) Anatomic variation of normal MGHL anatomy on T1-weighted transverse MR arthrograms. (**a**) Complete absence of the MGHL (circle) with firm attachment of the anterosuperior labrum (white arrow) to the glenoid. (**b**) Hypoplasia of the MGHL (black arrow) with firm attachment of the anterosuperior labrum

3 Traumatic Anterior Instability

With about 90% of cases traumatic anterior dislocation of the shoulder is by far the most common form of instability (Smith 2006). If any external force exceeds the resistance forces of the anteroinferior LLC, the humeral head may dislocate anteroinferiorly. It is evident that the LLC has to be injured and interrupted at least at one point on the stabilizing chain during the event of dislocation. During a first-time dislocation this may be soft-tissue injury with traumatic detachment of the labral insertion from the glenoid bone (Bankart lesion and variants) (Fig. 8a–f), disruption or extensive stretching of the anterior band of the IGHL, or avulsion of the IGHL at the humeral insertion (HAGL). Disruption of the stabilizing sling may also occur as bony avulsion of the LLC at the anteroinferior glenoid rim or more rarely at the humeral insertion. In acute first-time dislocation anterior or anteroinferior glenoid defects may be small (bony Bankart lesion) but larger glenoid fractures may also be present. The impact of the humeral head into the glenoid rim during the event of shoulder dislocation often leads to a characteristic posterosuperior impression at the humeral head (Hill-Sachs lesion) or even a shear fracture of the whole greater tuberosity. Chronic instability with recurrence of shoulder dislocation is very common and may lead to additional soft-tissue injury and progressive wear of the glenoid rim, attrition of a bony Bankart fragment, and increase of the Hill-Sachs impression.

3.1 Imaging in Shoulder Instability

Initially, radiographs of the shoulder should be obtained with a true anteroposterior and scapular Y-view to determine joint position and to search for fractures pre- and post-reduction (Ruiz Santiago et al. 2017). Due to immobility and apprehension in acute dislocation axial views of the shoulder may not be possible; however, these views should be included in the evaluation of recurrent and chronic shoulder instability (Box 1). Further imaging would be needed to determine the amount of soft-tissue and osseous injury. If radiographs show signs of a large glenoid fracture subsequent computed tomography (CT) may be indicated in the preoperative evaluation of the shoulder (Fig. 9a, b). Particularly blurring of the anterior glenoid contour on

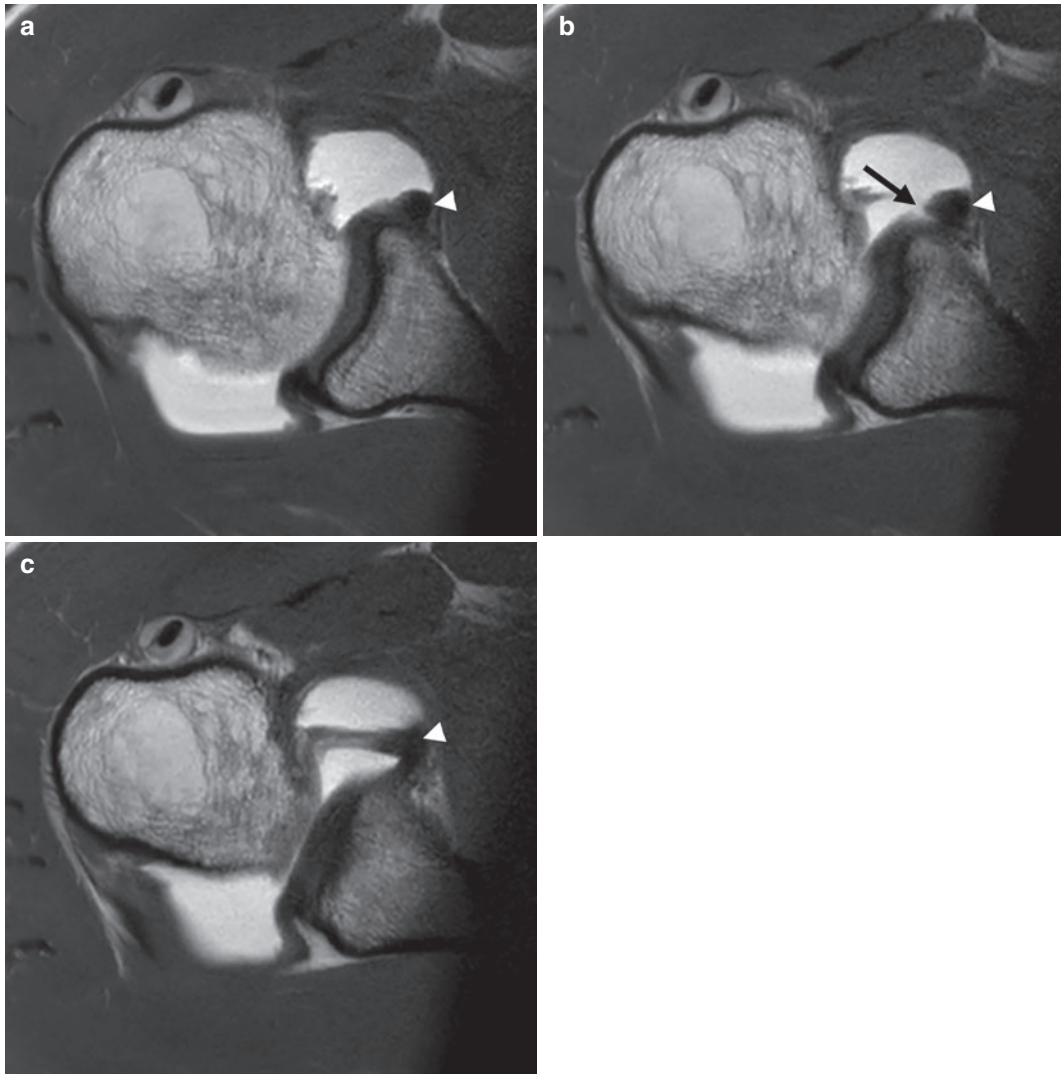

Fig. 7 (**a**–**c**) Pseudolesion of the anteroinferior labroligamentous complex on consecutive transverse T1-weighted MR arthrograms. (**a**) Origin of the anterior band of the IGHL (aIGHL) (arrowhead) from the anteroinferior labrum. (**b**) The prominent and folded aIGHL (arrowhead) builds a small pouch with the labrum, which may not be mistaken for a labral tear. (**c**) Note the further course of the aIGHL (arrowhead) to the humerus

anteroposterior radiographs suggests an osseous Bankart lesion (Ruiz Santiago et al. 2017). MR arthrography has proven to allow for safe detection and classification of lesions of the anteroinferior LLC, the BLC, and also the rotator cuff (Waldt et al. 2005, 2004, 2007, 2006). Furthermore, bipolar osseous lesions can be depicted and quantified (Gyftopoulos et al. 2015) (Fig. 10a). Due to the presence of intra-articular hemorrhage MR imaging may be performed without intraarticular contrast in the first 7 days after initial trauma. High soft-tissue contrast and lack of radiation exposure are the advantages of MR imaging over CT (Box 2). However, CT arthrography has shown to also have the possibility to detect labral lesions and rotator cuff injury but primarily benefits from the excellent presentation of osseous structures (Fig. 10b) (Chandnani et al. 1993; Acid et al. 2012) (Box 3). Standard CT without intra-articular contrast application may be sufficient for the assessment of glenoid bone loss (GBL) alone (Lo et al. 2004).

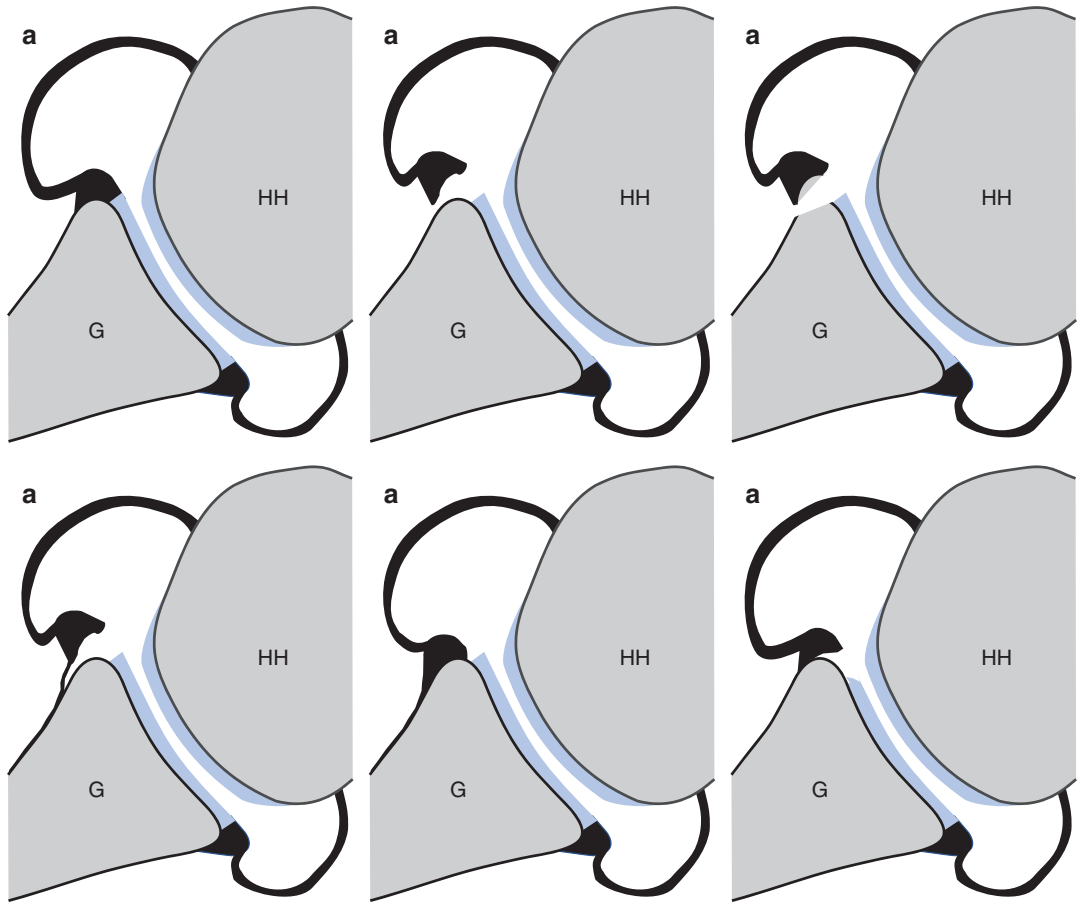

Fig. 8 (**a**–**f**) Bankart lesion and variants. (**a**) Normal labrum; (**b**) Bankart lesion with complete detachment of the labrum form the glenoid; (**c**) bony Bankart lesion; (**d**) Perthes lesion: Detachment of the labrum with intact periosteum which is stripped medially; (**e**) anterior labrum posterior sleeve avulsion (ALPSA): medially dislocated rounded labrum with triangular cleft between the cartilage and the dislocated labrum; (**f**) glenolabral articular disruption (GLAD): Anteroinferior cartilage defect with adjacent incomplete labral tear

Box 1 Radiography

- First-line imaging modality in the evaluation of shoulder pathology.
- True anteroposterior, Neer view, and axial view should be obtained.
- To determine joint position and rule out fracture.
- Subtle imaging signs may reveal posterior dislocation.

3.2 Soft-Tissue Lesions

Approximately 2/3 of the patients suffering from a first-time anteroinferior shoulder dislocation show soft-tissue injury at the anteroinferior LLC. This is more common in younger individuals <25 years of age as the strength of the labral attachment to the glenoid increases with age and osseous injuries become more likely. The classic form of injury is the Bankart lesion whereby different variations may occur.

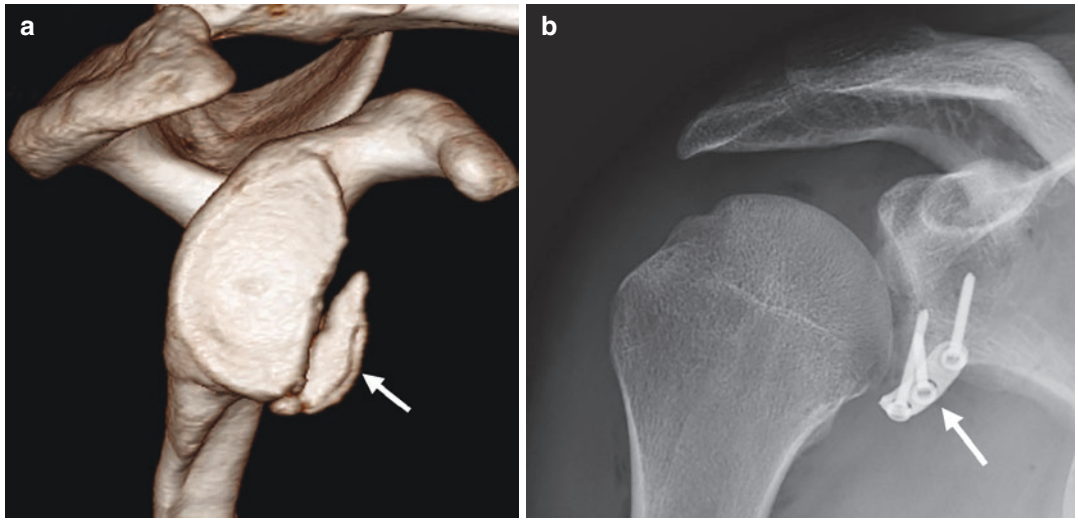

Fig. 9 (**a** and **b**) 25-Year-old patient after anteroinferior shoulder dislocation: (**a**) Computed tomography with volume-rendering reconstruction showing large glenoid fracture (arrow) for preoperative planning. (**b**) Anteroposterior radiograph after open reduction and direct internal fixation

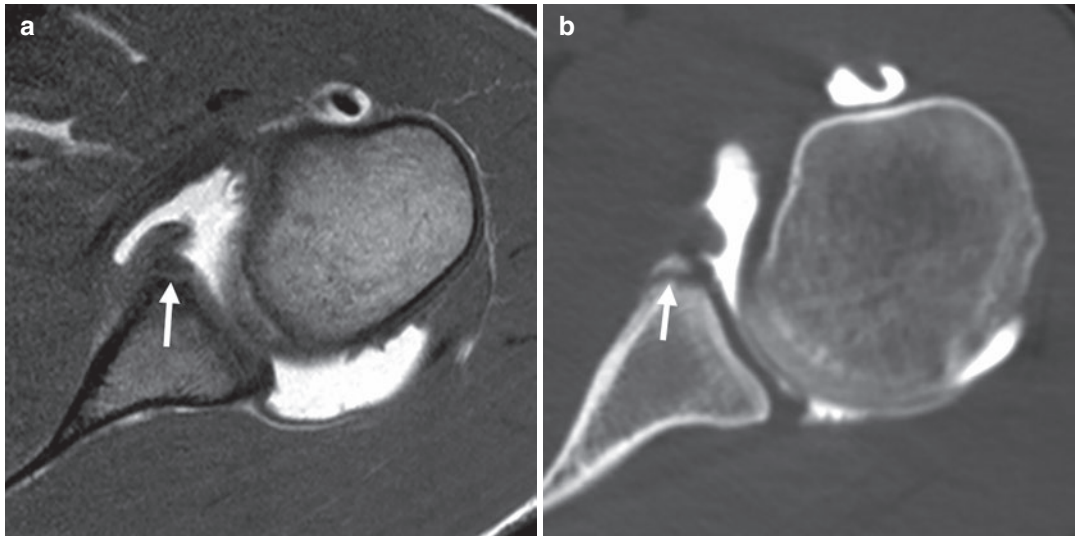

Fig. 10 (**a** and **b**) Bony Bankart lesion. (**a**) T1-weighted MR arthrogram in the transverse plane. The arrow points to the hypointense osseous fragment at the anterior glenoid within the hypointense labrum. (**b**) Transverse reconstruction of a CT arthrogram in the same patient. On CT the osseous injury (arrow) can easily be depicted

Box 2 MRI and MR Arthrography

- MR arthrography is the gold standard in the detection of labral tears, partial rotator cuff tears, and biceps pulley lesions.
- Additional imaging in abduction and external rotation (ABER) increases the detection of the Perthes lesion, and may be of additional value in imaging after Bankart repair and evaluation of redundancy of the anterior labroligamentous complex. ABER MR imaging must not be forced if the patient reports signs of apprehension.
- Due to hemarthrosis after acute shoulder dislocation standard MR imaging is sufficient in the first 7 days after trauma.
- MR arthrography allows for the determination of glenoid bone loss and relevance of bipolar bone loss according to the on-track/off-track concept.

Box 3 CT and CT Arthrography

- Standard CT is sufficient in the determination of the size of a glenoid fracture and glenoid bone loss on 2D and 3D images; however radiation exposure must be considered. Comparison with contralateral glenoid is helpful.
- CT arthrography may show additional labral and rotator cuff tears but creating 3D images for determination of glenoid bone loss is not possible due to density of intra-articular contrast.
- CT arthrography is the best imaging tool for the evaluation of the shoulder after coracoid transfer.

However, about 1/5 of the lesions cannot be clearly classified into these categories either on MR imaging or with arthroscopy, although it is described in the literature that most of these lesions show features of a chronic ALPSA lesion (Waldt et al. 2005).

3.2.1 Bankart Lesion

The Bankart lesion is defined as a complete detachment of the IGHL and the anteroinferior labrum from the glenoid below the equator with additional disruption of the scapular periosteum (Fig. 11a, b) (Bankart 1938). In acute anteroinferior instability 86% of the patients show a classic Bankart lesion (Waldt et al. 2005).

3.2.2 Perthes Lesion

The Perthes lesion is a variant of the Bankart lesion, which occurs in about 17.9% of the cases (Waldt et al. 2005). It also shows an avulsion of the LLC from the glenoid below the equator. However, the detached labrum remains partially attached to the glenoid by the intact periosteum, which is stripped medially (Fig. 12). Therefore, the labrum may remain in its anatomical position on MR imaging with the shoulder in neutral position, which can make the diagnosis more difficult (Waldt et al. 2005). In this particular type of lesion functional MR imaging in the ABER position may be beneficial in order to better recognize the defect (Fig. 13a, b) (Wischer et al. 2002; Tian et al. 2013).

3.2.3 ALPSA Lesion

ALPSA is an acronym for anterior labrum periosteal sleeve avulsion and is another Bankart variant with an avulsed LLC but intact periosteal sleeve. The detached labrum is allowed to rotate medially at the scapular neck and has the tendency to heal insufficiently with rounded scar formation at the anteroinferior glenoid (Neviaser 1993a). The incidence of the ALPSA lesion increases with recurrent instability of the shoulder and therefore may also be considered a chronic variant of an initially existing Perthes lesion (Waldt et al. 2005). The typical sign of the ALPSA lesion on cross-sectional imaging is medial displacement of the rounded and scarred anteroinferior labrum with respect to the plane of the glenoid articular surface on coronal images (Fig. 14a). Furthermore a triangular cleft between the glenoid cartilage and the displaced labrum can be found on transverse images (Fig. 14b).

3.2.4 HAGL Lesion

Failure of the LLC may occur at the humeral insertion and result in humeral avulsion of the

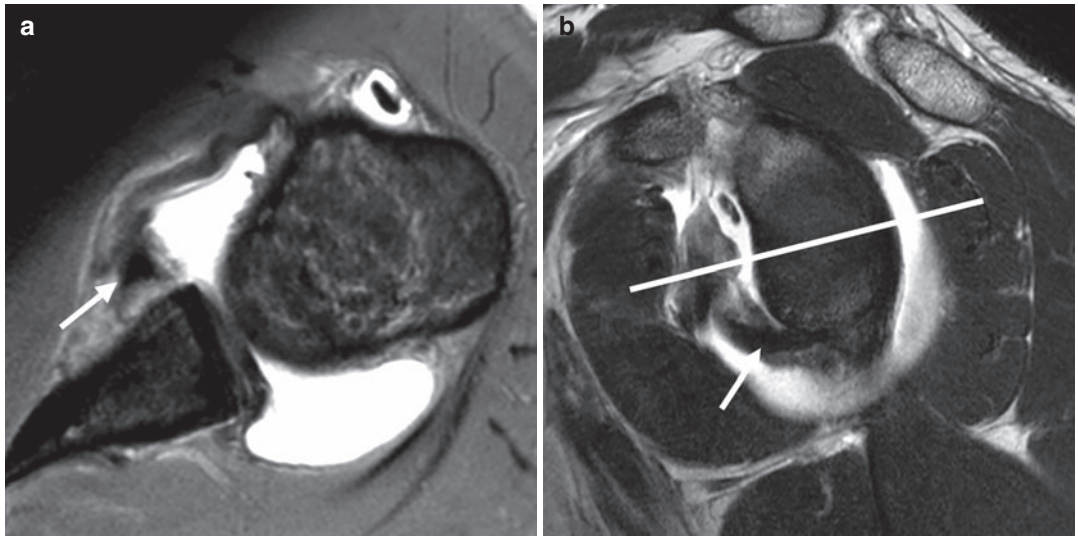

Fig. 11 (**a** and **b**) Acute Bankart lesion. (**a**) Transverse intermediate-weighted MR arthrogram with fat suppression in the transverse plane showing complete detachment of the anteroinferior labrum (arrow). (**b**) Corresponding sagittal T1-weighted MR arthrogram: The Bankart lesion (arrow) can be found anteroinferiorly below the equator of the glenoid (white line)

Fig. 12 Perthes lesion on a T1-weighted MR arthrogram in the transverse plane. Anteroinferior labral detachment (arrow) with continuity of the medially stripped periosteum (arrowhead)

glenohumeral ligament (HAGL) (Fig. 15a). This is a rare variation of injury to the LLC found in 9.3% of patients who underwent surgery for anterior shoulder instability (Wolf et al. 1995). The pathomechanism is described as shoulder dislocation in extreme adduction and external rotation and is related to contact sports. On coronal MR images the configuration of the distally detached IGHL appears like the letter "J"; that is why this finding is referred to as the "J-sign" (Fig. 15b) (Carlson 2004). Occasionally, the IGHL may be avulsed with a small cortical fragment (bony HAGL or BHAGL) and if additionally associated with a Bankart lesion the injury is described as "floating IGHL" (Oberlander et al. 1996). Reporting the HAGL lesion is crucial as the surgical approach may be different in the treatment of this lesion. It is assumed that early MR arthrography (within 7 days after trauma) shows a higher rate in the detection of a HAGL lesion as scar formation may impair the detection of the humeral sided defect later on (Liavaag et al. 2011).

3.2.5 GLAD Lesion

In a glenolabral articular disruption (GLAD) lesion there is a small anteroinferior labral tear with an adjacent chondral injury at the glenoid (Fig. 16) (Neviaser 1993b). Due to the fact that the fibers of the anterior IGHL and the distal labrum remain attached patients with a GLAD lesion do usually not suffer from clinically reproducible instability but anterior shoulder pain.

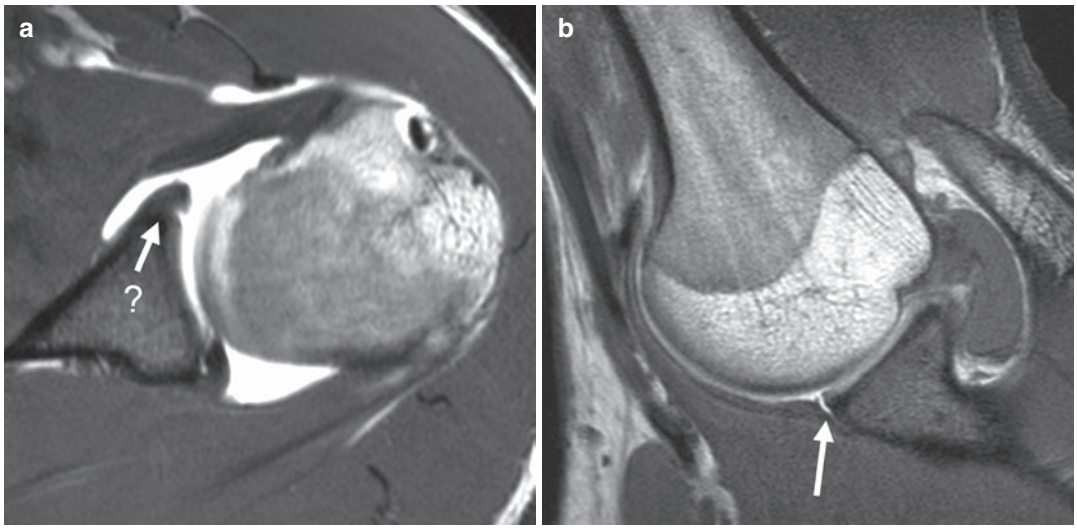

Fig. 13 (**a**) Transverse T1-weighted MR arthrogram in a patient with anterior shoulder instability. At the anteroinferior labrum (arrow) no injury can be detected. (**b**) T1-weighted MR arthrogram in abduction and external rotation (ABER) tightens the labroligamentous complex and allows the intra-articular contrast agent to fill the defect in this Perthes lesion (arrow)

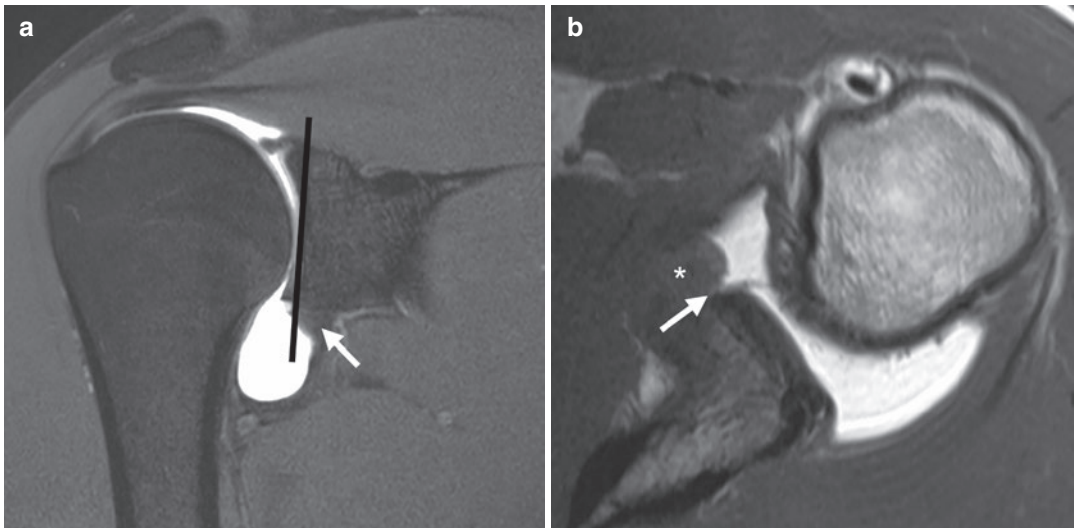

Fig. 14 (**a**) Coronal T1-weighted MR arthrogram with fat suppression: The black line corresponds to the glenoid plane. The white arrow points on the medially dislocated and scarred anteroinferior labrum in an anterior labrum periosteal sleeve avulsion (ALPSA). (**b**) Corresponding T1-weighted MR arthrogram in the transverse plane showing the typical triangular cleft (arrowhead) between the cartilage of the glenoid and the injured labrum (asterisk)

3.2.6 SLAP Lesion

A superior anterior to posterior lesion (SLAP) tear originates at the attachment of the BLC at the supraglenoid tubercle of the glenoid and may extend in the adjacent anterior and posterior labrum as well as into the biceps tendon or glenohumeral ligaments (Modarresi et al. 2011). Basically Snyder and co-workers have described

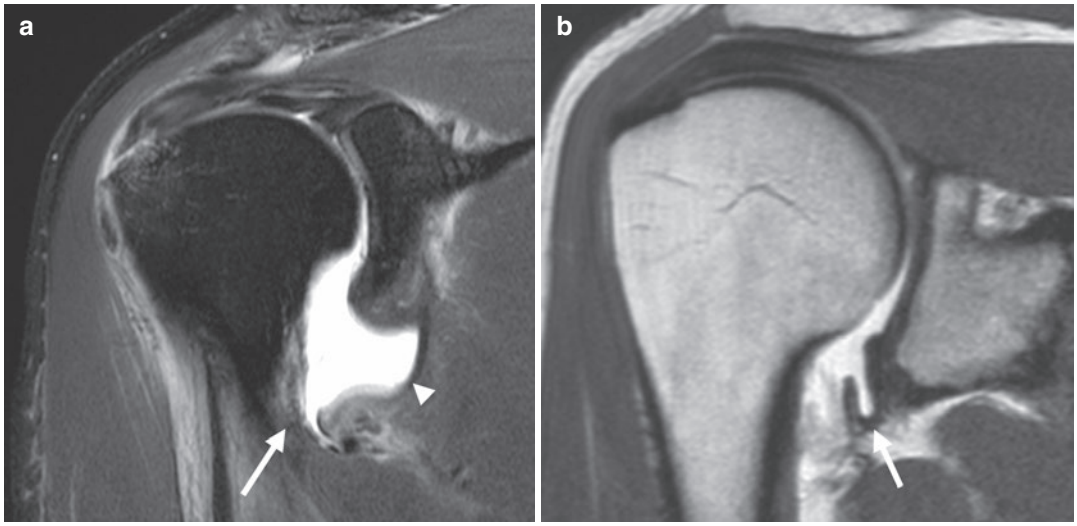

Fig. 15 (**a** and **b**) Humeral avulsion of the glenohumeral ligament (HAGL). (**a**) Acute HAGL lesion in a coronal T2-weighted MR arthrogram with fat suppression. Note the humeral-sided defect (arrow) of the IGHL (arrowhead). (**a** and **b**) J-sign in a chronic HAGL lesion on a coronal intermediate-weighted MR arthrogram

Fig. 16 Transverse T1-weighted MR arthrogram: Anteroinferior cartilage defect (arrow) with adjacent partial labral tear also referred to as glenolabral articular disruption (GLAD) lesion

four types of SLAP lesions (Snyder et al. 1990). A SLAP type I lesion describes an incidental finding with fraying of the superior labrum with intact biceps anchor and is of no clinical relevance. Type II is the most common form of SLAP tears with an unstable tear of the BLC and most often associated with repetitive overhead motions and the peel-back phenomenon (Fig. 17) (Burkhart and Morgan 2001). Type III is defined as a bucket-handle tear of the superior labrum including the biceps anchor, considered a stable lesion (Fig. 17b). Type IV describes a bucket-handle tear with extension into the biceps tendon (Fig. 17c). Maffet et al. extended the classification by types V–VII, which are SLAP II lesion with injury to additional structures (Maffet et al. 1995). SLAP VI shows additional unstable flap tear of the superior labrum. Types V and VII are considered to be associated with traumatic instability as type V shows additional Bankart lesion and type VII extension of the SLAP II lesion into the MGHL (Kandeel 2020). Mohana-Borges described a type VIII lesion as a SLAP tear extending into the posterior labrum (Mohana-Borges et al. 2003). Type IX has been described as a complete circumferential tear of the glenoid labrum. A superior labral lesion with extension into the rotator interval has been classified as SLAP X lesion.

The differentiation between a SLAP II lesion and the common sublabral recess can be challenging; however several criteria, which can be applied to CT and MR arthrography, have shown to aid with the diagnosis (Waldt et al. 2006; Modarresi et al. 2011). Contrast-filled defects on

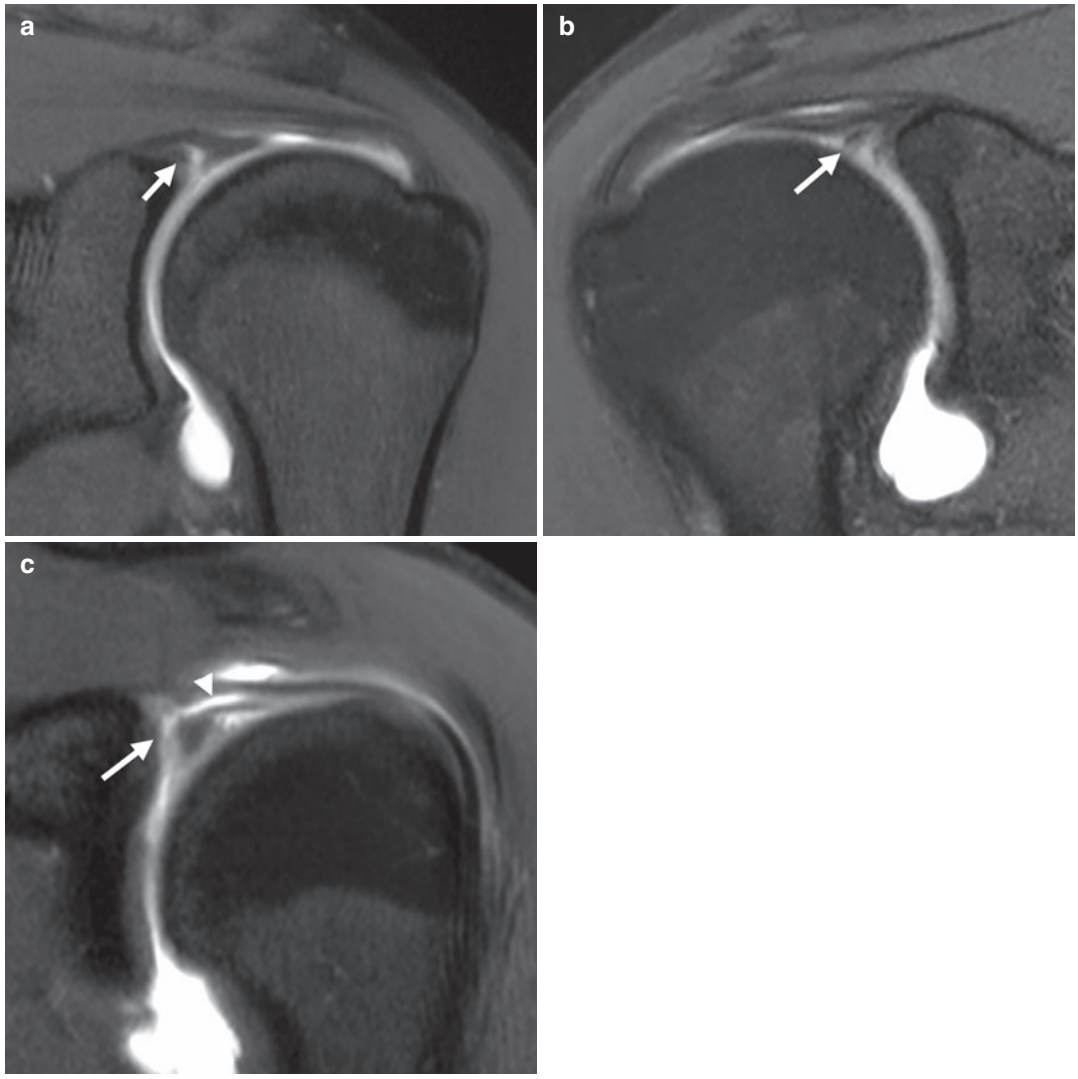

Fig. 17 (**a**–**c**) Basic superior anterior to posterior (SLAP) lesions on coronal T1-weighted MR arthrograms with fat suppression: (**a**) SLAP II lesion with contrast-filled defect at the superior biceps-labral complex (arrow). (**b**) Bucket-handle tear (arrow) of the superior labrum (SLAP III). (**c**) SLAP IV tear (arrow) with extension of the defect along the fibers of the biceps tendon (arrowhead)

coronal images in the superior labrum that are widened and show irregular margins are not seen in an anatomic variant as well as lateral extension of the defect or medial extension into the insertion of the biceps tendon (Fig. 18a–f).

MR arthrography allows for safe classification of the basic four types of SLAP lesions; however it is not so important to accurately classify lesions SLAP V–X but to correctly describe extension into additional anatomic structures (Holzapfel et al. 2010).

3.3 Osseous Lesions

3.3.1 Glenoid Bone Loss (GBL)

Detection of osseous glenohumeral injury is important as this may have influence on the treatment strategy. To restore shoulder stability and function the decision between an arthroscopic Bankart repair, which means an anatomic refixation of the labrum to the glenoid, or an extra-anatomic stabilization procedure such as a

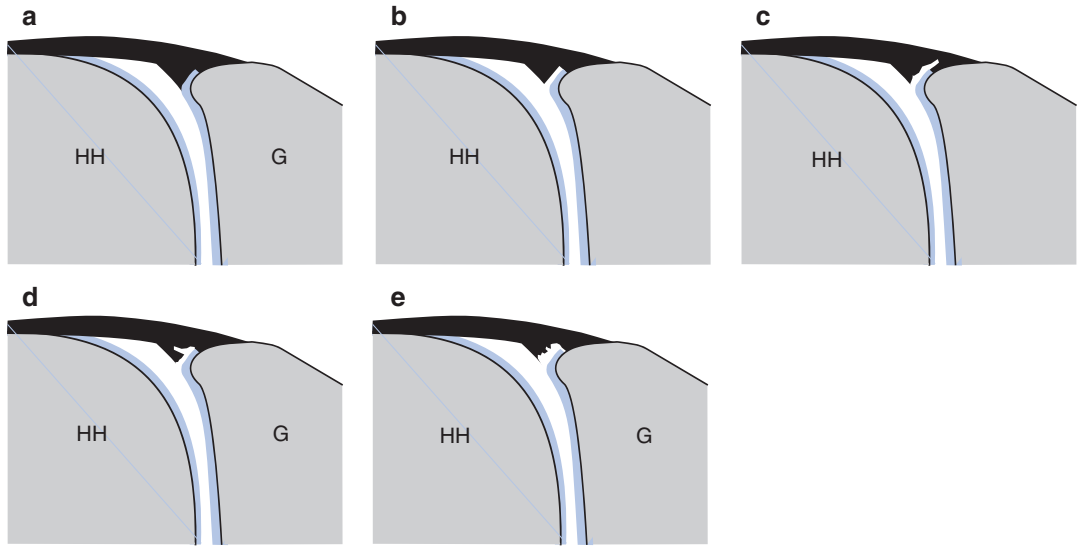

Fig. 18 (**a**–**e**) Differentiation between normal labrum, sublabral recess, and SLAP II tear at the biceps-labral complex: (**a**) Normal labrum with firm attachment; (**b**) sublabral recess with sharp and smooth margins, not extending over the cartilage at the supraglenoid tubercle; (**c**) SLAP II tear: Medial extension of the effect into the biceps anchor; (**d**) SLAP II tear: Lateral extension of the defect, which cannot be found in a sublabral recess; (**e**) SLAP II tear: widening and irregular margins of the defect without media or lateral extension

coracoid transfer (e.g., Latarjet or Bristow procedure) or other bone augmentation techniques has to be made. In the acute setting large glenoid fractures may be fixed directly. Apart from the clinical and imaging findings the decision for arthroscopic Bankart repair may also be influenced by local preferences of the surgical team. Anterior or anteroinferior GBL is common after first-time dislocation with about 22% of cases. It is present in >90% of cases of recurrent anterior instability as glenoid wear and attrition of osseous fragments are linked to the number of dislocations (Sugaya et al. 2003; Taylor and Arciero 1997; McNeil et al. 2017; Dickens et al. 2019; Nakagawa et al. 2014). Since the early 2000s there is an ongoing evolution in the literature which amount of GBL is tolerable and allows for successful performance of arthroscopic Bankart repair, particularly in recurrent shoulder instability. In severe GBL the glenoid loses its normal pear shape and takes the form of an inverted pear representing GBL of more than 25%, which has been shown to severely limit the success of an anatomic LLC reconstruction (Fig. 19a, b) (Burkhart et al. 2002; Lo et al. 2004). However, other studies have shown that loss of more than 20% of the osseous glenoid should be treated with an extra-anatomic procedure and detection and quantification of GBL in preoperative imaging are extremely important (Shin et al. 2017; Gottschalk et al. 2017; Shaha et al. 2015). Quantification of glenoid bone loss can be performed on either 2D or 3D CT and MR imaging with more or less equal results; in the optimal case there is the possibility to compare the measurements with the contralateral healthy shoulder (Walter et al. 2019; Moroder et al. 2013; Souza et al. 2014; Stillwater et al. 2017). A number of different measurements have been described, but ultimately two measurements, both using the best-fit circle method, have prevailed: the Pico method (Fig. 20a), which can determine the area of GBL or the representation of GBL as a percentage of the glenoid width (Fig. 20b) (Gottschalk et al. 2017).

3.3.2 Hill-Sachs Impression

Another osseous lesion resulting from shoulder dislocation is named the Hill-Sachs impression, which arises from the impact of the humerus

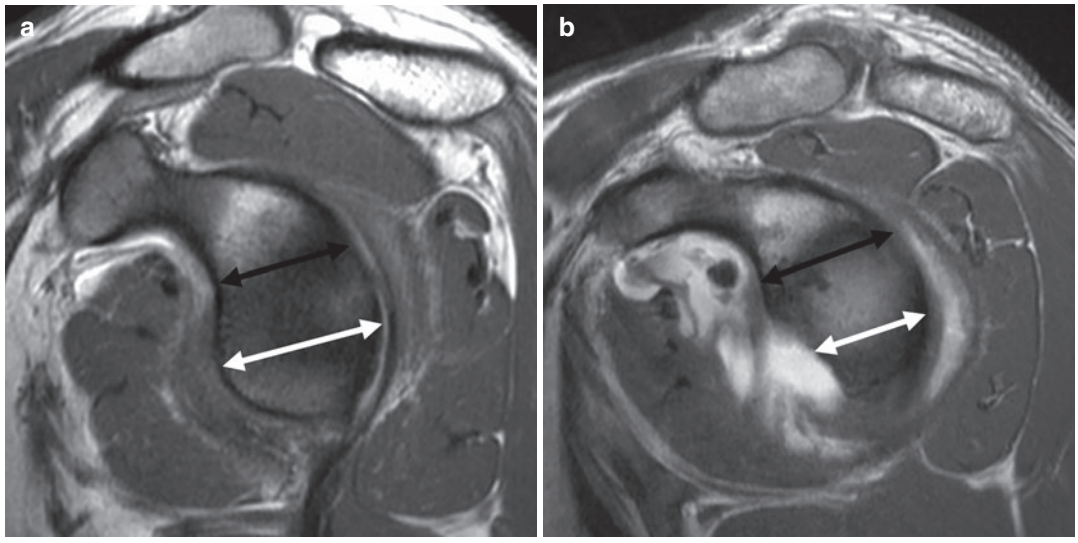

Fig. 19 (**a** and **b**) Sagittal en face views of the glenoid on T1-weighted MR arthrograms: (**a**) Normal pear shape of the glenoid. The superior diameter (black arrow) is shorter than the inferior diameter (white arrow). (**b**) Inverted pear shape of the glenoid with substantial glenoid wear in a patient with recurrent shoulder instability. The inferior diameter (white arrow) becomes smaller than the superior diameter (black arrow)

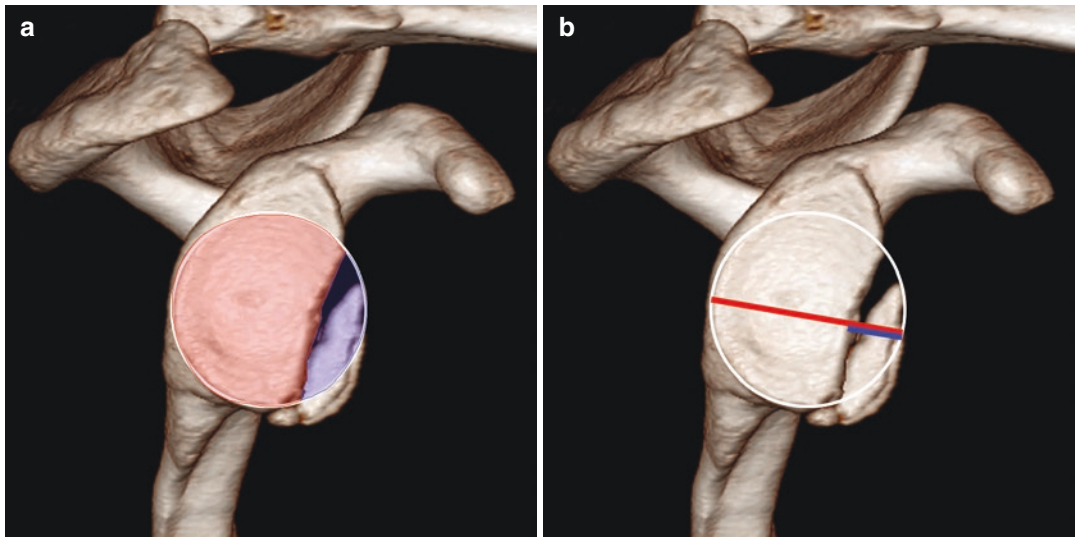

Fig. 20 (**a** and **b**) Measurement of glenoid bone loss on reconstructed 3D computed tomography images: (**a**) Pico method: After drawing a best-fit circle over the inferior glenoid the area of the glenoid bone loss (blue) can be determined and related to the area of the intact glenoid (red). (**b**) Glenoid width: A best-fit circle is drawn over the inferior glenoid and the width of the intact glenoid can be determined at the equator of the circle (red line). Percentage of the glenoid defect (blue) of the glenoid width can be calculated

against the anteroinferior glenoid during the event of dislocation. The lesion is very common and can be observed in up to 90% of patients with anterior shoulder instability (Yiannakopoulos et al. 2007). Accordingly, the impression is found on the posteroinferior humeral head (Fig. 21a). As a rule of thumb, the level of the coracoid process should be used as a reference on transverse

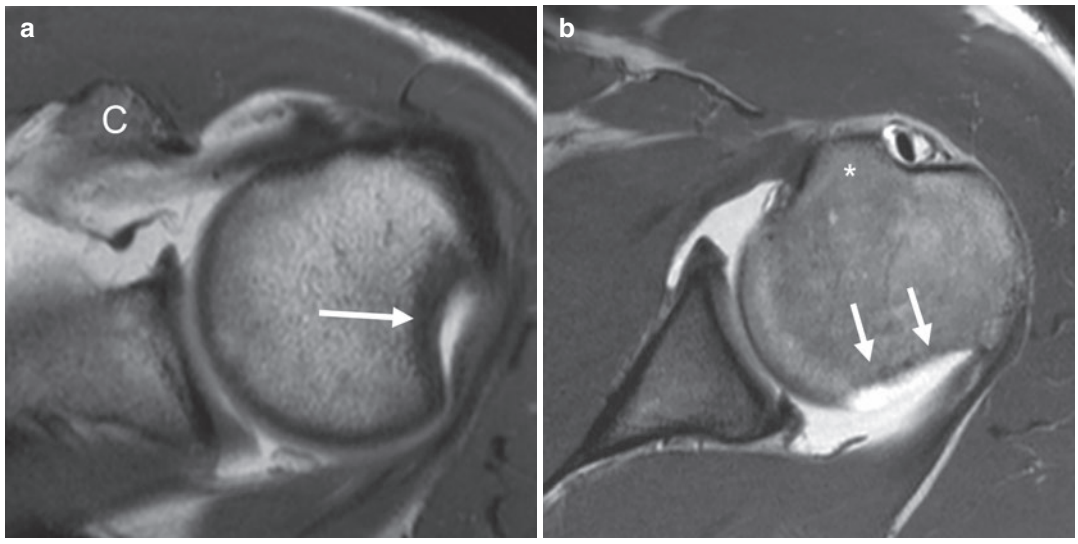

Fig. 21 (**a** and **b**) Transverse T1-weighted MR arthrograms: (**a**) Typical location of the Hill-Sachs impression fracture (arrow) at the posterosuperior humeral head, which can be found at the level of the coracoid process (C). (**b**) Normal posterior humeral groove (arrows) at the level of the lesser tuberosity (asterisk)

CT or MR images so that it may not be confused with the normal posterior humeral groove, which is located somewhat more distal (Fig. 21b) (Richards et al. 1994). A large defect, an oblique orientation, and medial location of the Hill-Sachs impression have been considered to be risk factors for engagement of the defect with the anterior glenoid rim during abduction and external rotation predisposing to recurrent shoulder dislocation (Di Giacomo et al. 2016). Several measurements determining the amount of an osseous humeral defect have been described on either 2D/3D CT or MR imaging (Gowd et al. 2019). However, recent literature suggests evaluating Hill-Sachs lesions under the concept of bipolar bone loss with measurement of the glenoid track and Hill-Sachs interval (HSI) (Gowd et al. 2019; Di Giacomo et al. 2014).

3.3.3 On-Track/Off-Track Concept in Bipolar Bone Lesions

Engagement of the Hill-Sachs impression at the anterior glenoid depends on the sliding movement of the humerus over the articular surface of the glenoid and its width. Therefore, the size of a Hill-Sachs lesion and the width of the glenoid must be related. Scientific observations have shown that the humerus glides from the neutral position to the position in abduction and external rotation on a defined path over the glenoid. This is called the glenoid track (GT) and it has a width of approximately 83% of the glenoid width (Fig. 22a) (Omori et al. 2014). If the medial border of the Hill-Sachs impression lies within the GT there is no risk of engagement and the Hill-Sachs lesion can be described as "on-track" (Fig. 22b). In contrast, an "off-track" lesion describes a Hill-Sachs lesion that is wider than the GT and may engage in a certain shoulder position, predominantly ABER (Fig. 22c) (Di Giacomo et al. 2014). Transferred to imaging, the GT can be determined by measuring the glenoid width using the best-fit circle method and multiplying it by 0.83. In order to determine the width of the Hill-Sachs lesion, the distance from the medial border of the Hill-Sachs impression on transverse CT or MR images to the articular sided insertion of the rotator cuff has to be determined. This distance is called the Hill-Sachs interval (HSI) because it consists of the width of the Hill-Sachs impression plus a potential osseous bridge between the lateral border of the impression and the attachment of the rotator cuff (Di Giacomo et al. 2014). In the presence of GBL the

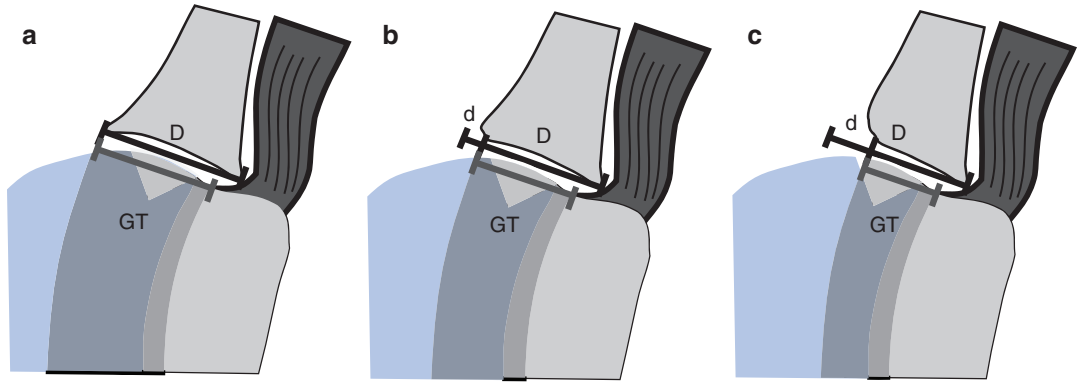

Fig. 22 (**a**–**c**) On-track/Off-track concept: Schematic drawings with the shoulder in abduction and external rotation. (**a**) The triangular Hill-Sachs impression lies within the glenoid track (GT) which is about 83% of the glenoid width (D) without glenoid bone loss ("on-track"). (**b**) Small amount of glenoid bone loss (d) leads to slight narrowing of the glenoid track that the triangular Hill-Sachs impression still is within the glenoid track ("on-track") during shoulder movement. (**c**) In substantial glenoid bone loss (d) the GT is narrowed so much that the Hill-Sachs impression may engage with the anterior glenoid rim during abduction and external rotation and is therefore "off-track"

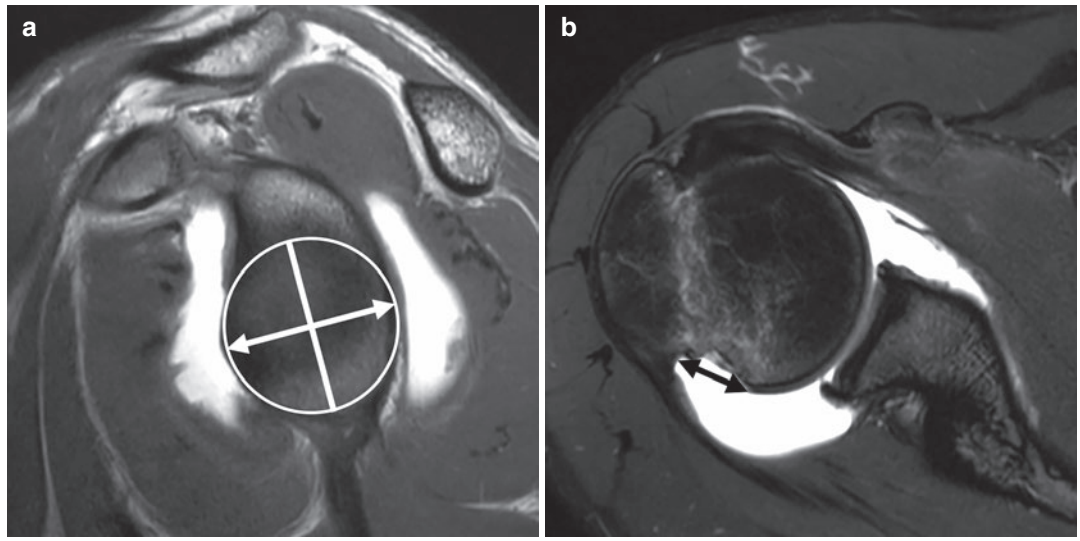

Fig. 23 (**a** and **b**) MR arthrograms in a patient after first-time shoulder dislocation: (**a**) Sagittal T1-weighted images showing no glenoid bone loss. Glenoid width is determined with the best-fit circle method (22 cm). Width of glenoid track: GT = 22 cm × 0.83 = 18.3 cm. (**b**) Width of Hill-Sachs interval (HSI) is 10 mm documenting an "on-track" Hill-Sachs impression (GT > HSI)

width of the GT decreases and the distance of the GBL has to be subtracted from the GT of the original glenoid width. Therefore the risk of engagement of a Hill-Sachs impression can be determined with the relation between the GT and the HSI (Fig. 23a, b). Increasing GBL narrows the glenoid track and consecutively smaller and more laterally located Hill-Sachs impressions may be at risk for engagement and are indicated to be addressed with surgical techniques such as remplissage or bone augmentation (Hartzler et al. 2016; Locher et al. 2016).

Fig. 24 Fragmentation of the labrum (black arrow) after Bankart repair in a patient with recurrent anterior shoulder instability. The position of a suture anchor can be depicted (white arrow) in the glenoid

Fig. 25 Transverse T1-weighted MR arthrogram in a patient after Bankart repair for anterior shoulder instability. Note the loss of articular cartilage at the anterior glenoid (arrowhead) and osteophyte formation at the humeral head in dislocation arthropathy

3.4 Postoperative Imaging

Nonoperative treatment of shoulder instability leads to a high rate of recurrent shoulder instability (55%) (Bliven and Parr 2018). After previous stabilization procedures the recurrence rate drops to 7.5–23.2% with the Latarjet procedure being the more stable operation technique than Bankart repair (Donohue et al. 2017; Bliven and Parr 2018; Longo et al. 2014). Return to full sports activity after Bankart repair may lead to another trauma, consecutive dislocation, and recurrent injury. However, postoperative instability or microinstability may also be present with failure of the procedure. In arthroscopic Bankart repair the injured labrum is fixed to the anterior glenoid rim with the use of bioabsorbable suture anchors often combined with an anterior capsular shift. MR arthrography is the method of choice in the evaluation of the postoperative labrum (Probyn et al. 2007). If abduction and external rotation can be actively performed by the patient without signs of apprehension ABER MR imaging may be of additional diagnostic value. The reattached labrum may be plump, rounded, or irregular in configuration; however, there should be objective continuity from the labrum to the glenoid bone (Woertler 2007). Imbibition of contrast agent into the labrum and contrast agent separating the labrum from the glenoid are signs of detachment and fragmentation of the labrum (Probyn et al. 2007; Sugimoto et al. 2002; Beltran et al. 2018) (Fig. 24). Dislocation of suture anchors or foreign-body reaction has also been described as a complication of Bankart surgery (Burkhart 2000; Woertler 2007). Mid- and long-term results show that arthropathy with osteoarthritis is a common phenomenon in nonoperative treated patients as well as after surgical stabilization (Bliven and Parr 2018; Franceschi et al. 2011; Harris et al. 2013) (Fig. 25). Furthermore, determination of bipolar bone loss is as important as preoperatively (Fig. 26).

Coracoid transfer, Bristow, or Latarjet procedures have been shown to present the lowest recurrence rate of shoulder instability and are therefore the preferred first-line treatment in many countries even with minor glenoid bone loss. The tip of the coracoid process with the conjoined tendon is transferred to the anterior glenoid through a split of the subscapularis muscle belly. This can be performed either

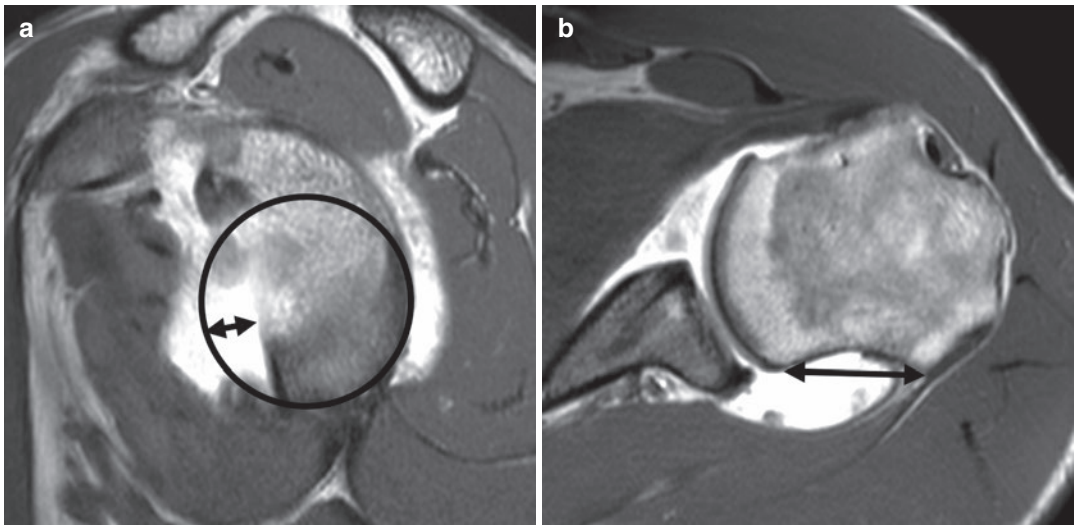

Fig. 26 (**a**) Progressive glenoid wear (black arrow) and (**b**) increase of the Hill-Sachs impression (black arrow) resulting in substantial glenoid bone loss (>25%) and an "off-track" Hill-Sachs defect in a patient with chronic anterior shoulder instability after Bankart repair

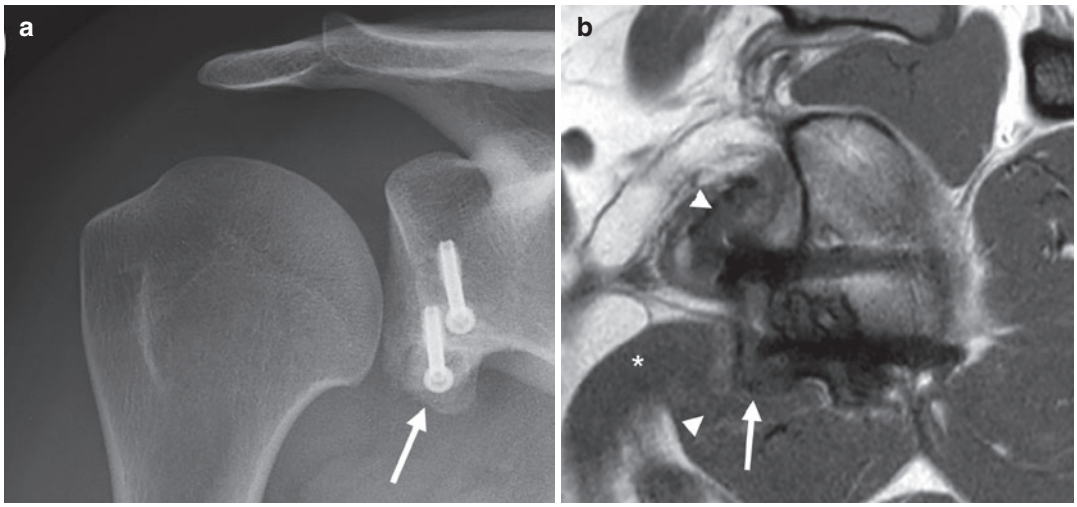

Fig. 27 (**a**) Anteroposterior radiograph after Latarjet procedure. The distal coracoid process (arrow) including the conjoined tendon is transferred to the anteroinferior glenoid. (**b**) T1-weighted MR arthrogram in the sagittal plane through the glenoid showing the attached coracoid process (arrow) with the conjoined tendon (asterisk). Note the split of the subscapularis muscles (arrowheads)

arthroscopically or with open surgery (Fig. 27a, b). Often seen complications of the Latarjet procedure are nonunion, and loosening or fracture of screws as well as bone resorption of the transferred coracoid process with possible soft-tissue irritation (Willemot et al. 2019; Ho et al. 2016). CT or CT arthrography should preferably be used to evaluate patients after coracoid transfer (Fig. 28a, b). Other complications of the Bristow and Latarjet procedures include coracoid fracture, fatty degeneration of the subscapularis muscle, infection, and secondary osteoarthritis of the glenohumeral joint (Woertler 2007).

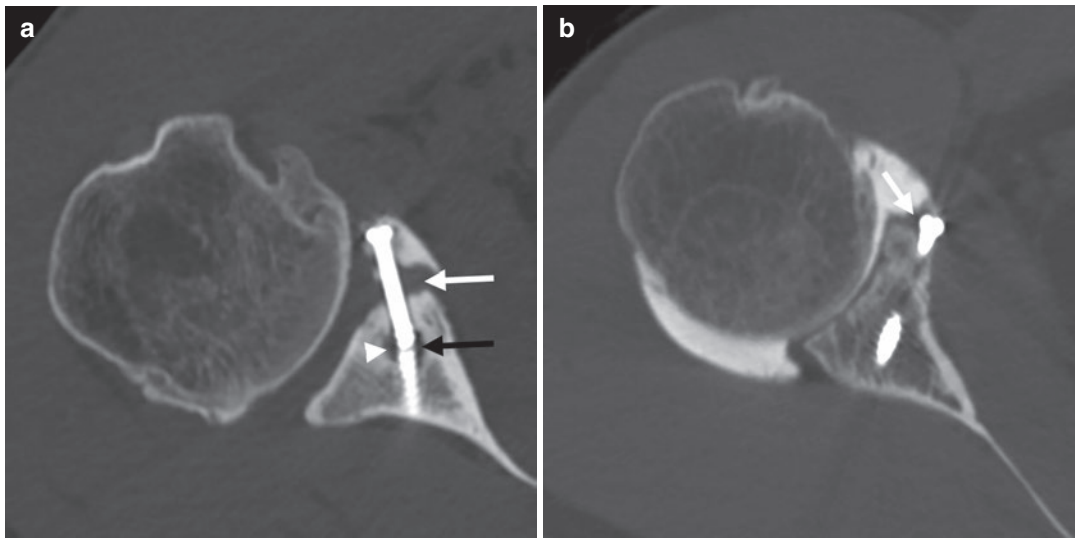

Fig. 28 (**a** and **b**) Transverse computed tomograms with typical findings of failure after shoulder stabilization according to Latarjet. (**a**) Screw fracture (black arrow) and surrounding signs of loosening (arrowhead) and concomitant nonunion of the coracoid transfer (white arrow). (**b**) Partial bone resorption of the coracoid transfer with exposure of the fixation screw (arrow), which may lead to mechanical irritation of the adjacent subscapularis tendon

4 Traumatic Posterior Instability

Traumatic posterior shoulder dislocation occurs in approximately 2% of all shoulder dislocations (Millett et al. 2006). Especially in an active, young patient population, traumatic posterior dislocation may be present in up to 10% of cases with shoulder instability (Owens et al. 2013). This is particularly true in American football players who are 15 times more prone to experience a posterior shoulder dislocation than the general population (Escobedo et al. 2007). In general, posterior instability also refers to more common posterior subluxation phenomena through repetitive microtrauma that can ultimately lead to frank posterior dislocation. In addition to classic causes of posterior shoulder dislocation such as violent muscle contraction in electric shock or convulsive seizures, direct anterior or axial force applied to the adducted, internally rotated humeral head with 90° of elevation in contact sports or through recoil during shooting maneuvers can lead to posterior dislocation (Murray et al. 2013; Backer et al. 2018).

On initial radiographs the findings of posterior shoulder dislocation may be subtle (Fig. 30). First the joint space appears widened but the medial humeral contour overlaps the glenoid, although the true anteroposterior view is correctly tangential to the glenoid surface (Cisternino et al. 1978). Second, the humerus may be trapped in internal rotation (Cisternino et al. 1978) (Fig. 29a). Third, the reverse Hill-Sachs impression forms an abnormal double line at the medial circumference of the humeral head, the so-called trough line sign which is pathognomonic for posterior shoulder dislocation (Gor 2002; Cisternino et al. 1978) (Fig. 29a). Fourth, on Neer views the posterior decentering of the humeral head with respect to the center of the glenoid can be identified (Fig. 29b). On MR imaging a reverse Hill-Sachs lesion, also named McLaughlin lesion, can be detected in 86% of the cases. Rarely, adjacent fractures of the tuberosities or the humeral shaft may be found (Saupe et al. 2008; McLaughlin 1952). The presence of a reverse Hill-Sachs impression may predispose to recurrent posterior shoulder dislocation with engagement in internal rotation. The reverse Hill-Sachs defect can be quantified with the gamma angle, which is considered critical in values over 90° (Moroder et al. 2015). To determine the gamma angle a best-fit circle is placed over the humeral head contour at

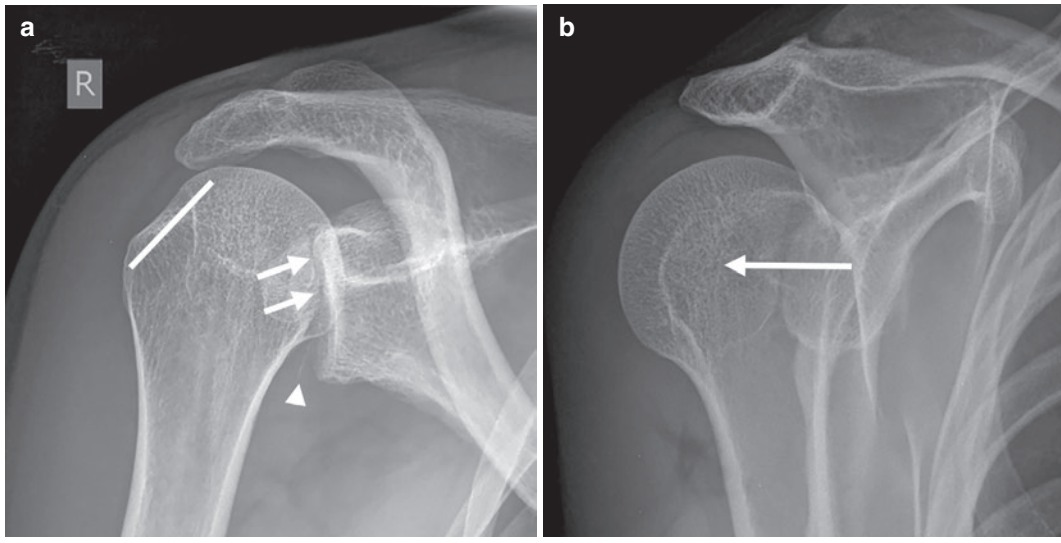

Fig. 29 (**a** and **b**) Radiographs of posterior shoulder dislocation. (**a**) Anteroposterior radiograph with trapped internal rotation of the humerus indicated by the oblique appearance of the greater tubercle contour (white line). The trough line sign can be seen with a double contour at the medial humeral head (arrows) representing an impaction fracture. Although the image is taken tangential to the glenoid, the joint space cannot be identified. Bone fragment indicating reverse Bankart fracture (arrowhead). (**b**) Neer view radiograph clearly demonstrating posterior dislocation of the humeral head with respect to the center of the glenoid (white arrow)

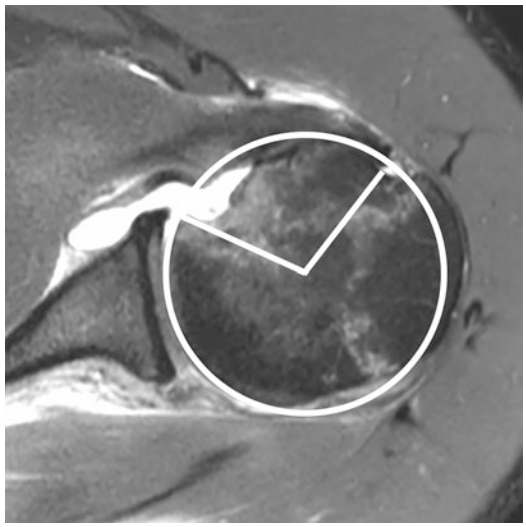

Fig. 30 Evaluation of the significance of the reversed Hill-Sachs defect. A best-fit circle is drawn over the humeral head contour. The gamma angle represents the angle between the medial edge of the reversed Hill-Sachs impression and the center of the intertubercular groove

the site of the largest extent of the reverse Hill-Sachs defect (Fig. 30). After that an angle is drawn from the center of the circle to the bicipital groove and the medial defect margin.

About 1/3 of the patients show a reversed osseous Bankart lesion and approximately 2/3 present with a posterior capsulolabral defect (Saupe et al. 2008) (Fig. 31). The soft-tissue lesion may be complete avulsion of the posterior labrum (reverse Bankart lesion) or posterior labrum periosteal sleeve avulsion (POLPSA) in which the periosteum remains intact (Fig. 32). A specific finding described in the literature is Kim's lesion, a concealed partial avulsion of the posteroinferior labrum, which is important to detect on MR imaging as it may be easily overlooked on arthroscopy (Kim et al. 2004) (Fig. 33).

In contrast to the anterior labrum, the posterior labrum shows no significant normal variation, although a small posterior cleft between the labrum and the glenoid can be normal. However, a posterior chondrolabral cleft has been described to be associated with increased retroversion of the glenoid and posteroinferior glenoid dysplasia (Campbell et al. 2014). Slight retroversion of the glenoid is normal and reported with a mean of 1.23° (range 9.5° anteversion–10.5° retroversion) (Churchill et al. 2001). However, in the presence of a posterior labral tear retroversion of >5° can lead to increased posterior translation of the

Fig. 31 Transverse intermediate-weighted MR image with fat suppression after acute posterior shoulder dislocation showing a reversed osseous Bankart lesion (arrow). Additionally, retroversion of the glenoid can be appreciated (white line)

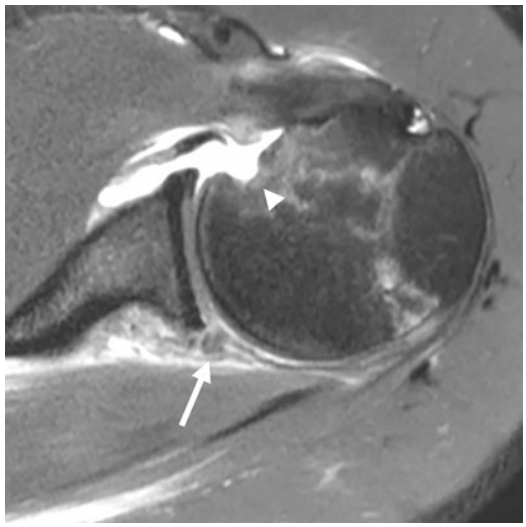

Fig. 32 Completely detached posterior labrum representing a reversed Bankart lesion on a transverse intermediated MR image with fat suppression. Arrow indicates a large reversed Hill-Sachs impression at the anteromedial humeral head

humeral head. In the absence of labral pathology isolated retroversion of >10° leads to increased posterior translation forces and in values >15° surgical correction is suggested (Imhoff et al. 2019). A study by Owens et al. showed that for

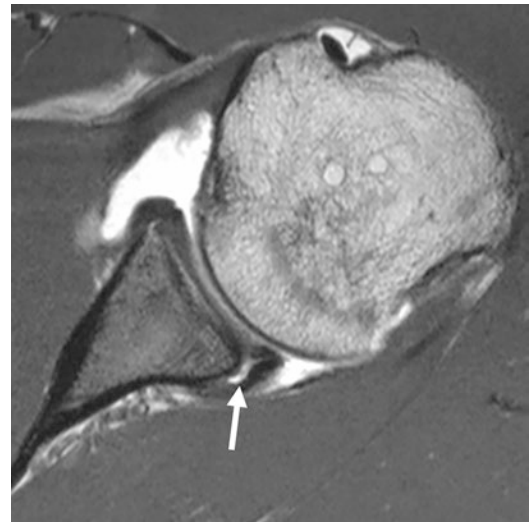

Fig. 33 Kim's lesion on a transverse T1-weighted MR arthrogram. Note the concealed detachment of the labrum filled with contrast agent (arrow)

every 1° of increased retroversion the odds of developing posterior instability increase by 17% (Owens et al. 2013) (Fig. 34).

Localized hypoplasia of the posteroinferior glenoid has been found in about 15–20% of the population (Edelson 1995; Harper et al. 2005). Typical forms are the rounded posteroinferior edge of the glenoid, the so-called lazy J form, or a triangular bony deficiency, the "delta form" (Weishaupt et al. 2000). The deficiency of bone is usually compensated by hypertrophy of cartilage and labrum (Harper et al. 2005). Glenoid dysplasia is associated with posterior labral tears as well as posterior and atraumatic multidirectional instability (Harper et al. 2005) (Fig. 35).

Particularly in recurrent posterior shoulder dislocation osseous wear of the posterior glenoid rim may also occur. It has been indicated that an osseous restoration procedure, such as a bone block procedure, may be necessary in shoulders with a posterior glenoid defect ≥20% of glenoid width (Nacca et al. 2018). In addition it has been described that posterior glenoid bone loss (pGBL) may lead to engagement of smaller reverse Hill-Sachs lesions during internal rotation. To determine critical reverse Hill-Sachs lesion in pGBL 2° should be added to the value of the gamma angle for every millimeter of posterior GBL (Moroder et al. 2017).

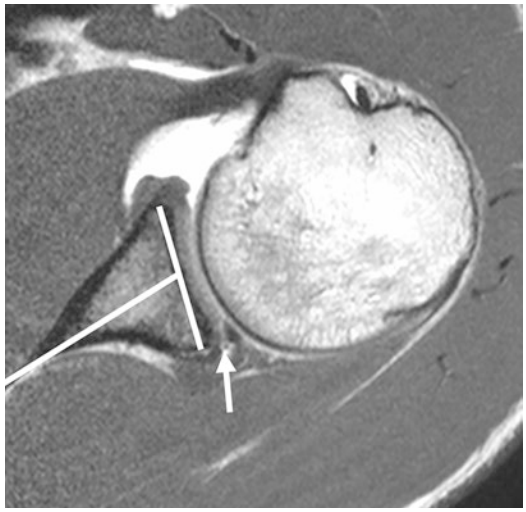

Fig. 34 T1-weighted MR arthrogram in the transverse plane in a patient without a history of posterior shoulder dislocation. Retroversion of the glenoid can be appreciated (white lines) and the white arrow indicates posterior labral defect suggesting posterior stress and recurrent subluxation

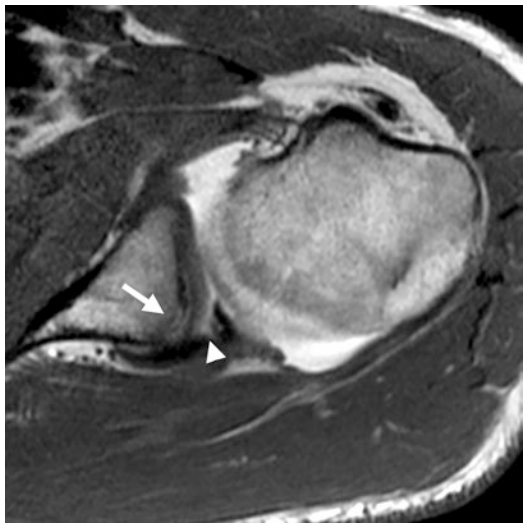

Fig. 35 Glenoid dysplasia on a T1-weighted MR arthrogram in the transverse plane. There is a rounded contour of the hypoplastic posteroinferior glenoid (arrow) with hypertrophy of the labrum showing additional tearing (arrowhead)

5 Microtraumatic Instability and Internal Impingement

There is no uniform classification of microtraumatic instability; however, the condition is often defined as any rotational or directional pathologic laxity that leads to abnormal biomechanics of the glenohumeral joint without dislocation. Furthermore it is unclear whether microinstability and posterosuperior impingement in overhead athletes refer to the same pathologic condition or actually are two closely related but different entities (Lin et al. 2018).

Overhead athletes require a high degree of mobility in the dominant shoulder in order to achieve maximum performance. The prototype of the overhead athlete is the baseball pitcher who passes through defined phases during throwing movement: windup, early cocking, late cocking, acceleration, deceleration, and follow-through (Weber et al. 2014). Particularly at the transition from the cocking phase to the acceleration phase, high loads occur on the shoulder joint and humeral internal rotation angular velocity exceeds 7000°/s (Lintner et al. 2008). To achieve maximum speed in ball acceleration, the degree of external rotation of the shoulder is of crucial importance. This means to achieve maximum performance the overhead-throwing athlete has to maximize external rotation of the shoulder. Over time, the athlete develops increased mobility in abduction and external rotation, which go hand in hand with certain adjustments of soft tissue and osseous structures.

On one side overhead athletes are particularly susceptible to injury in extreme abduction and external rotation. On the other side repetitive throwing movements also result in adaptations of soft tissue and osseous structures of the shoulder joint. The term “thrower’s paradox” describes the fine line between achieving maximum external rotation through structural changes in order to achieve maximum performance and the potential injuries that may result from these changes and concomitant repetitive microtrauma (Wilk et al. 2002).

Osseous adaptation in overhead throwers includes humeral retrotorsion and glenoid retroversion, both of which allow for a greater osseous clearance and therefore increased external rotation of the arm (Kay et al. 2018). The latter is assumed to appear as a reaction on posterior compression forces during the late cocking phase. Humeral retrotorsion may develop through extreme external torsional forces on the arm

while throwing during childhood and adolescence (Lin et al. 2018).

5.1 Glenohumeral Internal Rotational Deficit (GIRD)

In the healthy throwing shoulder an increase in external rotation comes with a natural decrease in internal rotation. Normally, the full range of motion of the throwing shoulder should be the same as in the nondominant arm. During deceleration and particularly the follow-through phase of the throwing movement microtrauma to the posterior joint capsule, including the posterior band of the IGHL, occurs. This leads to scarring, contractures, and thickening of the posterior joint capsule with consecutive posterosuperior shift of the humeral head position allowing excessive external rotation (Burkhart et al. 2003a). However, posterior capsular contracture also decreases internal rotation and is considered clinically relevant when the internal rotational deficit of the throwing arm exceeds 25° relative to the nondominant shoulder (Braun et al. 2009). Tuite and co-workers described findings of a thickened posterior joint capsule, reduced posterior capsular recess, and thickened posterior labrum on MR arthrography in throwers with GIRD compared to normal shoulders (Tuite et al. 2007). However, these findings have never been approved in further studies.

The stress applied to the posterior band of the IGHL leads to osseous proliferation at the posterior glenoid rim, which is referred to as the Bennett lesion (Fig. 36) (Ferrari et al. 1994; Park et al. 2016). This finding is described to be present in 22% of baseball pitchers and is usually asymptomatic (Wright and Paletta 2004). However, the Bennett lesion may become symptomatic through compression of the axillary nerve, impingement on the labrum and capsule, or avulsion.

Excessive external rotation is described to apply torsional and tensional forces on the biceps anchor and to "peel back" the biceps from the supraglenoid tubercle resulting in SLAP 2 lesions, which may extend into the posterosuperior labrum (Burkhart et al. 2003b) (Figs. 17 and 18).

Posterosuperior shifting of the humerus with respect to the glenoid also reduces the cam effect of the anterior humeral circumference resulting in secondary pseudolaxity of the anterior joint

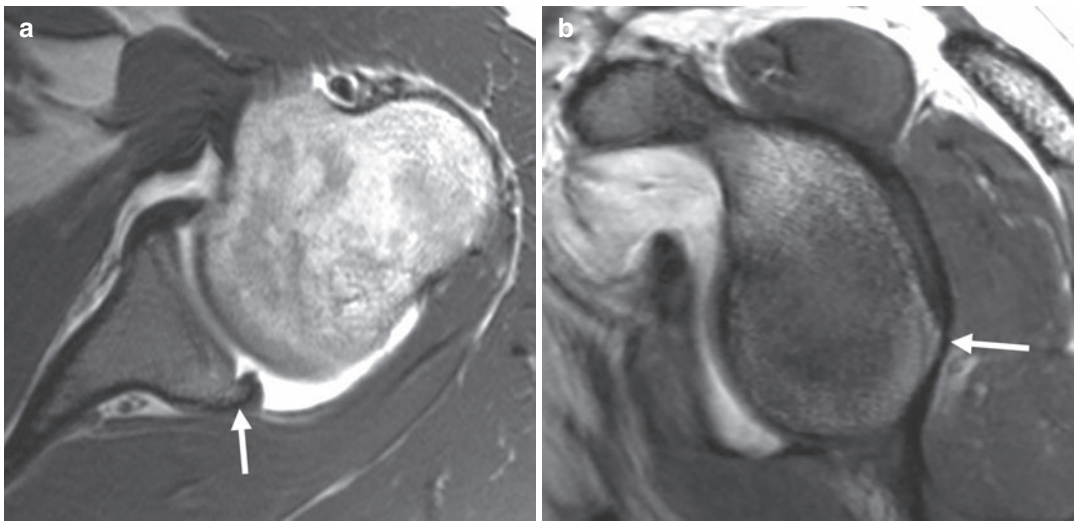

Fig. 36 (**a** and **b**) Bennett lesion on T1-weighted MR arthrograms of the dominant arm in a 26-year-old volleyball player: (**a**) On the transverse image bony apposition at the posterior glenoid rim can be detected (arrow). (**b**) Corresponding sagittal image demonstrating the inferior location of the typical Bennett lesion (arrow)

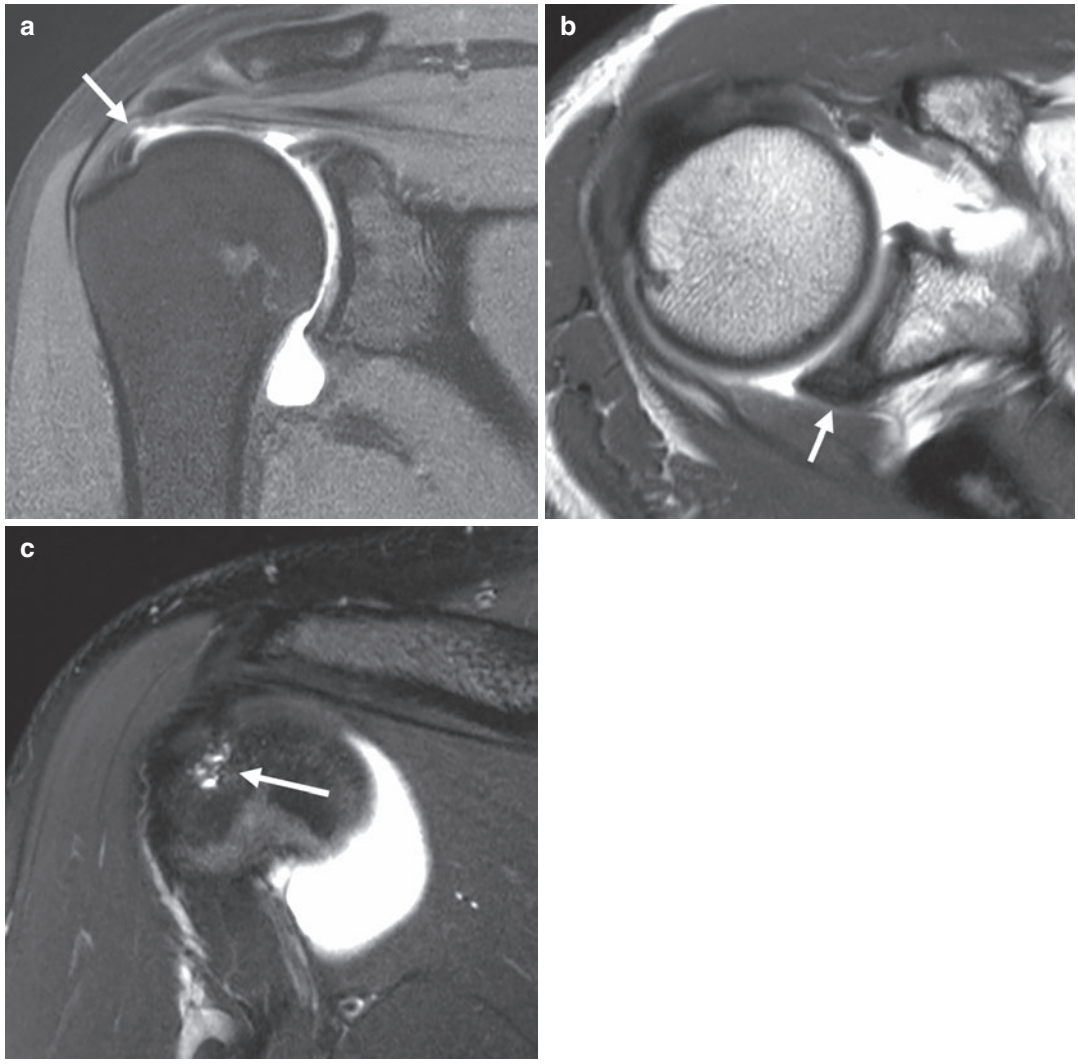

Fig. 37 (**a**–**c**) Tennis player with posterosuperior impingement. (**a**) T1-weighted MR arthrogram with fat suppression in the coronal plane showing posterior articular sided tear of the supraspinatus tendon (arrow). (**b**) On the transverse T1-weighted MR arthrogram bony remodeling of the glenoid and ossification of the posterosuperior labrum can be detected (arrow). (**c**) T2-weighted MR arthrogram with fat suppression in the coronal plane through the posterior greater tuberosity revealing intraosseous cyst formation

capsule (Burkhart and Lo 2007). This is described to worsen microinstability and increases the risk of developing posterosuperior impingement in the thrower's shoulder. MR imaging in ABER position has the possibility to demonstrate posterosuperior decentering of the humerus as well as redundancy of the anterior joint capsule (Waldt et al. 2014).

5.2 Posterosuperior Impingement (PSI)

PSI is described as the contact of the articular surface of the rotator cuff with the posterosuperior labrum and glenoid rim during extreme abduction and external rotation. This contact is physiologic; however repetitive forced abduc-

tion and external rotation can lead to pathologic impingement with damage of the impinged structures. As described above certain soft-tissue changes related to GIRD might aggravate symptoms in PSI (Mihata et al. 2015). Furthermore it is described that pathologic impingement can be worsened by muscular fatigue and concomitant scapular dyskinesia in the athlete's shoulder girdle (Laudner et al. 2006; Mihata et al. 2009).

A combination of findings is described in athletes with PSI, which can be found on MR imaging and more accurately MR arthrography (Fessa et al. 2015). The abnormal contact between the cuff and the labrum leads to articular sided partial tears of the posterior supraspinatus tendon and/or the anterior infraspinatus tendon (Walch et al. 1992) (Fig. 37). Additionally fraying or tearing of the posterosuperior labrum can be found as well as ossification of the posterosuperior glenoid (Fig. 37b) (Walch et al. 1992). Bone remodeling and cyst formation at the posterior humerus have been described to be more frequent in dominant shoulder of overhead athletes (Fig. 37c). MR arthrography in ABER position allows for demonstration of the corresponding defects and may be of additional value in the diagnosis of small articular sided rotator cuff tears.

5.3 Anterosuperior Impingement

Anterosuperior impingement (ASI) is a condition that particularly occurs in overhead athletes, although significantly less common than PSI (Kirchhoff and Imhoff 2010). In horizontal adduction and internal rotation of the arm, like in the follow-through phase of throwing or hitting a forehand strike in tennis the biceps pulley and the adjacent subscapularis tendon may be impinged against the anterosuperior glenoid rim. The long head of the biceps tendon (LHBT), the superior SSC tendon, and the biceps pulley may be injured through repetitive microtrauma (Elser et al. 2011). Biceps pulley lesions can be isolated tears of the SGHL or occur with additional superior SSC or anterior SSP tendon tearing. Isolated pulley lesion can be detected on parasagittal MR arthrography if there is non-visibility of the SGHL and direct contact of the LHBT with the superior SSC (Fig. 38a, b) (Schaeffeler et al. 2012). Progressive wear through the biceps

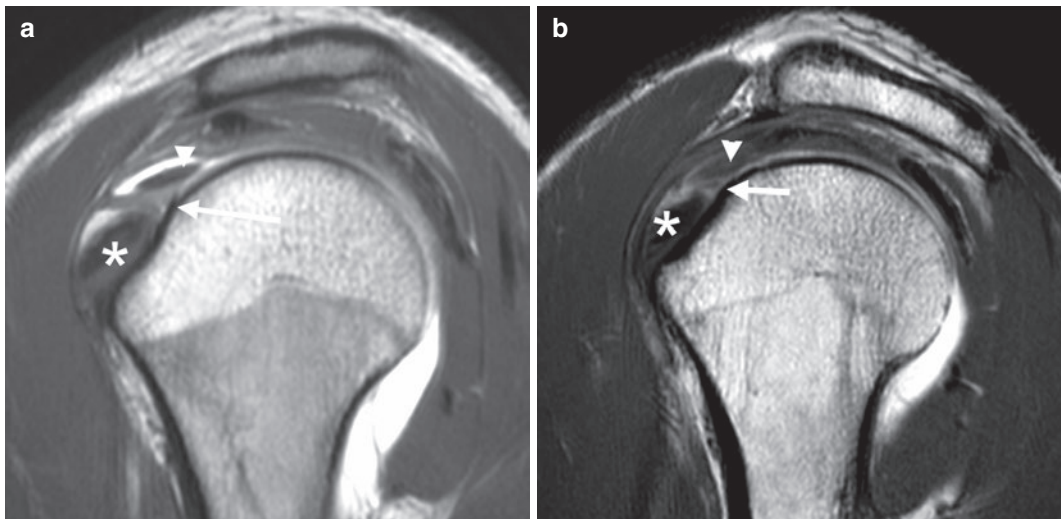

Fig. 38 (**a** and **b**) T1-weighted MR arthrograms in the sagittal plane through the lesser tuberosity. (**a**) Normal appearance of the reflection pulley (arrow) of the long head of the biceps tendon (LHBT) and the relation to the subscapularis tendon (SSC) (asterisk). (**b**) Isolated tear of the biceps pulley (arrow) and concomitant tendinopathy of the LHBT. The SSC tendon (asterisk) is intact

tendon may lead to superior SSC tearing with displacement of the biceps tendon into the defect (Fig. 39). Tendinopathy of the LHBT is a common finding associated with pulley lesions. A combined lesion of the biceps pulley and the SSC tendon may allow the LHBT to subluxate or dislocate medially with respect to the intertubercular groove (Braun et al. 2010).

Fig. 39 T1-weighted MR arthrogram in the sagittal plane in a patient with a pulley lesion and an additional superior subscapularis tendon tear (arrow). Note the displacement of the biceps tendon (arrow) into the rotator cuff defect with signs of tendinopathy

6 Hyperlaxity: Atraumatic Instability

Atraumatic instability is often described as multidirectional instability (MDI) as instability occurs in more than one direction (Warby et al. 2017). However, multidirectional instability may also exist on the basis of an initial traumatic event or through microtraumatic adaptations. Generally atraumatic instability has to be differentiated from non-pathologic hyperlaxity of the joints (Longo et al. 2015). There may also be some overlap with microtraumatic instability in overhead throwing athletes and swimmers where increased range of motion in the shoulder is important to maximize athletic performance. Primarily, MR imaging has to rule out structural pathology of

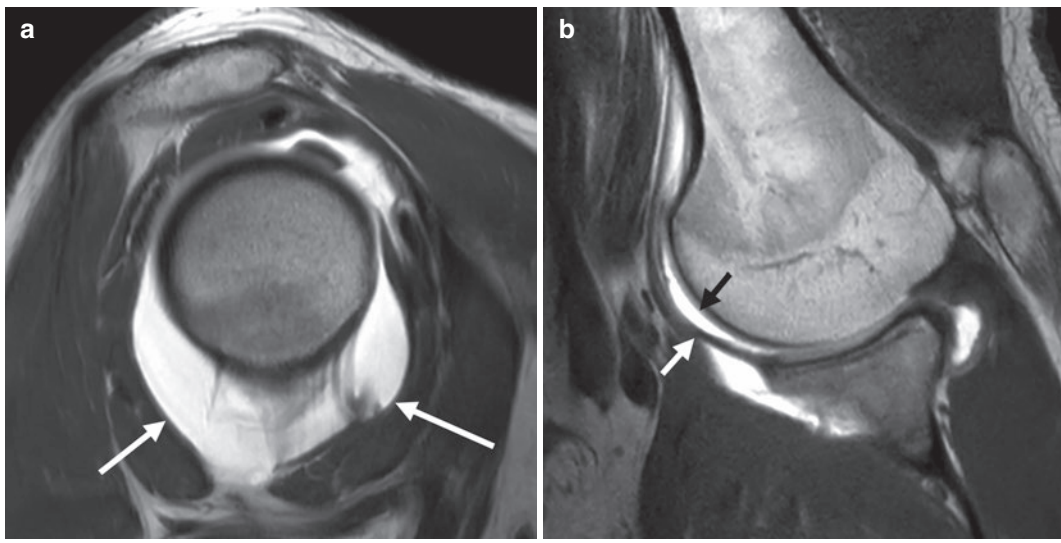

Fig. 40 (**a** and **b**) T1-weighted MR arthrograms in a 21-year-old swimmer with clinical signs of multidirectional instability without a history of trauma. (**a**) The sagittal image shows a large axillary recess (arrow). (**b**) Image in abduction and external rotation revealing redundancy of the labroligamentous complex (LLC) (white arrow). In this extreme joint position the LLC is not taut and a contrast-filled crescent-shaped space can be appreciated (black arrow)

the shoulder joint. Furthermore it is described that patients with atraumatic instability show a high joint volume with a widened capsule in the rotator interval or the axillary pouch (Lee et al. 2013; Hsu et al. 2010). MR arthrography in ABER position has the ability to demonstrate redundancy of the anterior capsular structures compared to stable shoulders with the crescent sign (Fig. 40a, b) (Waldt et al. 2014).

Things to Remember

1. The determination of glenoid bone loss is crucial for the decision between an anatomical or an extra-anatomical stabilization technique in the treatment of acute and chronic anterior shoulder instability.
2. The relevance of the Hill-Sachs impression is evaluated using the on-track/off-track concept, in which the size of the Hill-Sachs interval is compared to the glenoid track.
3. Defined image criteria allow the often subtle diagnosis of posterior shoulder dislocation on radiography.
4. Glenoid retroversion and glenoid dysplasia affect the occurrence of posterior shoulder instability.
5. Adjustments of the shoulder to the requirements of overhead sports lead to a glenohumeral internal rotational deficit and pathological posterosuperior impingement.
6. Typical imaging findings in overhead athletes are SLAP II lesion, posterior articular sided rotator cuff tear, posterosuperior labral lesion, intraosseous cysts at the posterior greater tuberosity, and Bennett lesion.
7. Pulley lesions and superior subscapularis tear occur in anterosuperior impingement and can be best evaluated on T1-weighted parasagittal MR arthrograms.

References

Acid S, Le Corroller T, Aswad R, Pauly V, Champsaur P (2012) Preoperative imaging of anterior shoulder instability: diagnostic effectiveness of MDCT arthrography and comparison with MR arthrography and arthroscopy. AJR Am J Roentgenol 198(3):661–667. https://doi.org/10.2214/AJR.11.7251

Backer HC, Galle SE, Maniglio M, Rosenwasser MP (2018) Biomechanics of posterior shoulder instability—current knowledge and literature review. World J Orthop 9(11):245–254. https://doi.org/10.5312/wjo.v9.i11.245

Bankart A (1938) The pathology and treatment of recurrent dislocation of the shoulder joint. Br J Surg 26:23–29

Beltran LS, Duarte A, Bencardino JT (2018) Postoperative imaging in anterior glenohumeral instability. AJR Am J Roentgenol 211(3):528–537. https://doi.org/10.2214/AJR.17.19304

Bliven KCH, Parr GP (2018) Outcomes of the Latarjet procedure compared with Bankart repair for recurrent traumatic anterior shoulder instability. J Athl Train 53(2):181–183. https://doi.org/10.4085/1062-6050-232-16

Braun S, Kokmeyer D, Millett PJ (2009) Shoulder injuries in the throwing athlete. J Bone Joint Surg Am 91(4):966–978. https://doi.org/10.2106/JBJS.H.01341

Braun S, Millett PJ, Yongpravat C, Pault JD, Anstett T, Torry MR, Giphart JE (2010) Biomechanical evaluation of shear force vectors leading to injury of the biceps reflection pulley: a biplane fluoroscopy study on cadaveric shoulders. Am J Sports Med 38(5):1015–1024. https://doi.org/10.1177/0363546509355142

Burkart AC, Debski RE (2002) Anatomy and function of the glenohumeral ligaments in anterior shoulder instability. Clin Orthop Relat Res 400:32–39. https://doi.org/10.1097/00003086-200207000-00005

Burkhart SS (2000) The evolution of clinical applications of biodegradable implants in arthroscopic surgery. Biomaterials 21(24):2631–2634. https://doi.org/10.1016/s0142-9612(00)00131-9

Burkhart SS, Lo IK (2007) The cam effect of the proximal humerus: its role in the production of relative capsular redundancy of the shoulder. Arthroscopy 23(3):241–246. https://doi.org/10.1016/j.arthro.2006.11.018

Burkhart SS, Morgan C (2001) SLAP lesions in the overhead athlete. Orthop Clin North Am 32(3):431–441, viii. https://doi.org/10.1016/s0030-5898(05)70212-1

Burkhart SS, Morgan CD, Kibler WB (2000) Shoulder injuries in overhead athletes. The "dead arm" revisited. Clin Sports Med 19(1):125–158. https://doi.org/10.1016/s0278-5919(05)70300-8

Burkhart SS, Debeer JF, Tehrany AM, Parten PM (2002) Quantifying glenoid bone loss arthroscopically in shoulder instability. Arthroscopy 18(5):488–491. https://doi.org/10.1053/jars.2002.32212

Burkhart SS, Morgan CD, Kibler WB (2003a) The disabled throwing shoulder: spectrum of pathology part I: pathoanatomy and biomechanics. Arthroscopy 19(4):404–420. https://doi.org/10.1053/jars.2003.50128

Burkhart SS, Morgan CD, Kibler WB (2003b) The disabled throwing shoulder: spectrum of pathology. Part II: evaluation and treatment of SLAP lesions in throwers. Arthroscopy 19(5):531–539. https://doi.org/10.1053/jars.2003.50139

Campbell SE, Dewitt RM, Cameron KL, Thompson AK, Owens BD (2014) Posterior chondrolabral cleft: clinical significance and associations with shoulder instability. HSS J 10(3):208–212. https://doi.org/10.1007/s11420-014-9404-x

Carlson CL (2004) The "J" sign. Radiology 232(3):725–726. https://doi.org/10.1148/radiol.2323021239

Chandnani VP, Yeager TD, DeBerardino T, Christensen K, Gagliardi JA, Heitz DR, Baird DE, Hansen MF (1993) Glenoid labral tears: prospective evaluation with MRI imaging, MR arthrography, and CT arthrography. AJR Am J Roentgenol 161(6):1229–1235. https://doi.org/10.2214/ajr.161.6.8249731

Churchill RS, Brems JJ, Kotschi H (2001) Glenoid size, inclination, and version: an anatomic study. J Shoulder Elb Surg 10(4):327–332. https://doi.org/10.1067/mse.2001.115269

Cisternino SJ, Rogers LF, Stufflebam BC, Kruglik GD (1978) The trough line: a radiographic sign of posterior shoulder dislocation. AJR Am J Roentgenol 130(5):951–954. https://doi.org/10.2214/ajr.130.5.951

De Maeseneer M, Van Roy F, Lenchik L, Shahabpour M, Jacobson J, Ryu KN, Handelberg F, Osteaux M (2000) CT and MR arthrography of the normal and pathologic anterosuperior labrum and labral-bicipital complex. Radiographics 20(Suppl 1):S67-81. https://doi.org/10.1148/radiographics.20.suppl_1.g00oc03s67

DePalma AF (1983) Surgery of the shoulder, 3rd edn. Lippincott, Philadelphia

Di Giacomo G, Itoi E, Burkhart SS (2014) Evolving concept of bipolar bone loss and the hill-Sachs lesion: from “engaging/non-engaging” lesion to "on-track/off-track" lesion. Arthroscopy 30(1):90–98. https://doi.org/10.1016/j.arthro.2013.10.004

Di Giacomo G, Golijanin P, Sanchez G, Provencher MT (2016) Radiographic analysis of the Hill-Sachs lesion in anteroinferior shoulder instability after first-time dislocations. Arthroscopy 32(8):1509–1514. https://doi.org/10.1016/j.arthro.2016.01.022

Dickens JF, Slaven SE, Cameron KL, Pickett AM, Posner M, Campbell SE, Owens BD (2019) Prospective evaluation of glenoid bone loss after first-time and recurrent anterior glenohumeral instability events. Am J Sports Med 47(5):1082–1089. https://doi.org/10.1177/0363546519831286

Donohue MA, Mauntel TC, Dickens JF (2017) Recurrent shoulder instability after primary Bankart repair. Sports Med Arthrosc Rev 25(3):123–130. https://doi.org/10.1097/JSA.0000000000000159

Edelson JG (1995) Localized glenoid hypoplasia. An anatomic variation of possible clinical significance. Clin Orthop Relat Res (321):189–195

Elser F, Braun S, Dewing CB, Giphart JE, Millett PJ (2011) Anatomy, function, injuries, and treatment of the long head of the biceps brachii tendon. Arthroscopy 27(4):581–592. https://doi.org/10.1016/j.arthro.2010.10.014

Escobedo EM, Richardson ML, Schulz YB, Hunter JC, Green JR 3rd, Messick KJ (2007) Increased risk of posterior glenoid labrum tears in football players. AJR Am J Roentgenol 188(1):193–197. https://doi.org/10.2214/AJR.05.0277

Ferrari JD, Ferrari DA, Coumas J, Pappas AM (1994) Posterior ossification of the shoulder: the Bennett lesion. Etiology, diagnosis, and treatment. Am J Sports Med 22(2):171–175; discussion 175–176. https://doi.org/10.1177/036354659402200204

Fessa CK, Peduto A, Linklater J, Tirman P (2015) Posterosuperior glenoid internal impingement of the shoulder in the overhead athlete: pathogenesis, clinical features and MR imaging findings. J Med Imaging Radiat Oncol 59(2):182–187. https://doi.org/10.1111/1754-9485.12276

Franceschi F, Papalia R, Del Buono A, Vasta S, Maffulli N, Denaro V (2011) Glenohumeral osteoarthritis after arthroscopic Bankart repair for anterior instability. Am J Sports Med 39(8):1653–1659. https://doi.org/10.1177/0363546511404207

Galvin JW, Ernat JJ, Waterman BR, Stadecker MJ, Parada SA (2017) The epidemiology and natural history of anterior shoulder instability. Curr Rev Musculoskelet Med 10(4):411–424. https://doi.org/10.1007/s12178-017-9432-5

Gerber C, Nyffeler RW (2002) Classification of glenohumeral joint instability. Clin Orthop Relat Res 400:65–76. https://doi.org/10.1097/00003086-200207000-00009

Gibbs DB, Lynch TS, Nuber ED, Nuber GW (2015) Common shoulder injuries in American football athletes. Curr Sports Med Rep 14(5):413–419. https://doi.org/10.1249/JSR.0000000000000190

Gor DM (2002) The trough line sign. Radiology 224(2):485–486. https://doi.org/10.1148/radiol.2242010352

Gottschalk LJ, Bois AJ, Shelby MA, Miniaci A, Jones MH (2017) Mean glenoid defect size and location associated with anterior shoulder instability: a systematic review. Orthop J Sports Med 5(1):2325967116676269. https://doi.org/10.1177/2325967116676269

Gowd AK, Liu JN, Cabarcas BC, Garcia GH, Cvetanovich GL, Provencher MT, Verma NN (2019) Management of recurrent anterior shoulder instability with bipolar bone loss: a systematic review to assess critical bone loss amounts. Am J Sports Med 47(10):2484–2493. https://doi.org/10.1177/0363546518791555

Gyftopoulos S, Beltran LS, Bookman J, Rokito A (2015) MRI evaluation of bipolar bone loss using the on-track off-track method: a feasibility study. AJR Am J Roentgenol 205(4):848–852. https://doi.org/10.2214/AJR.14.14266

Harper KW, Helms CA, Haystead CM, Higgins LD (2005) Glenoid dysplasia: incidence and association with posterior labral tears as evaluated on MRI. AJR Am J Roentgenol 184(3):984–988. https://doi.org/10.2214/ajr.184.3.01840984

Harris JD, Gupta AK, Mall NA, Abrams GD, McCormick FM, Cole BJ, Bach BR Jr, Romeo AA, Verma NN (2013) Long-term outcomes after Bankart shoulder stabilization. Arthroscopy 29(5):920–933. https://doi.org/10.1016/j.arthro.2012.11.010

Hartzler RU, Bui CN, Jeong WK, Akeda M, Peterson A, McGarry M, Denard PJ, Burkhart SS, Lee TQ (2016) Remplissage of an off-track Hill-Sachs lesion is necessary to restore biomechanical glenohumeral joint stability in a bipolar bone loss model. Arthroscopy 32(12):2466–2476. https://doi.org/10.1016/j.arthro.2016.04.030

Ho AG, Gowda AL, Michael Wiater J (2016) Evaluation and treatment of failed shoulder instability procedures. J Orthop Traumatol 17(3):187–197. https://doi.org/10.1007/s10195-016-0409-8

Holzapfel K, Waldt S, Bruegel M, Paul J, Heinrich P, Imhoff AB, Rummeny EJ, Woertler K (2010) Inter- and intraobserver variability of MR arthrography in the detection and classification of superior labral anterior posterior (SLAP) lesions: evaluation in 78 cases with arthroscopic correlation. Eur Radiol 20(3):666–673. https://doi.org/10.1007/s00330-009-1593-1

Howell SM, Galinat BJ (1989) The glenoid-labral socket. A constrained articular surface. Clin Orthop Relat Res (243):122–125

Hsu YC, Pan RY, Shih YY, Lee MS, Huang GS (2010) Superior-capsular elongation and its significance in atraumatic posteroinferior multidirectional shoulder instability in magnetic resonance arthrography. Acta Radiol 51(3):302–308. https://doi.org/10.3109/02841850903524421

Ide J, Maeda S, Takagi K (2004) Normal variations of the glenohumeral ligament complex: an anatomic study for arthroscopic Bankart repair. Arthroscopy 20(2):164–168. https://doi.org/10.1016/j.arthro.2003.11.005

Ilahi OA, Labbe MR, Cosculluela P (2002) Variants of the anterosuperior glenoid labrum and associated pathology. Arthroscopy 18(8):882–886. https://doi.org/10.1053/jars.2002.36119

Imhoff FB, Camenzind RS, Obopilwe E, Cote MP, Mehl J, Beitzel K, Imhoff AB, Mazzocca AD, Arciero RA, Dyrna FGE (2019) Glenoid retroversion is an important factor for humeral head centration and the biomechanics of posterior shoulder stability. Knee Surg Sports Traumatol Arthrosc 27(12):3952–3961. https://doi.org/10.1007/s00167-019-05573-5

Jaggi A, Alexander S (2017) Rehabilitation for shoulder instability—current approaches. Open Orthop J 11:957–971. https://doi.org/10.2174/1874325001711010957

Kandeel AA (2020) Type V superior labral anterior-posterior (SLAP) lesion in recurrent anterior glenohumeral instability. J Shoulder Elb Surg 29(1):95–103. https://doi.org/10.1016/j.jse.2019.05.038

Kay J, Kirsch JM, Bakshi N, Ekhtiari S, Horner N, Gichuru M, Alolabi B, Khan M, Bedi A (2018) Humeral retroversion and capsule thickening in the overhead throwing athlete: a systematic review. Arthroscopy 34(4):1308–1318. https://doi.org/10.1016/j.arthro.2017.10.049

Kim SH, Ha KI, Yoo JC, Noh KC (2004) Kim's lesion: an incomplete and concealed avulsion of the posteroinferior labrum in posterior or multidirectional posteroinferior instability of the shoulder. Arthroscopy 20(7):712–720. https://doi.org/10.1016/j.arthro.2004.06.012

Kirchhoff C, Imhoff AB (2010) Posterosuperior and anterosuperior impingement of the shoulder in overhead athletes-evolving concepts. Int Orthop 34(7):1049–1058. https://doi.org/10.1007/s00264-010-1038-0

Kuhn JE (2010) A new classification system for shoulder instability. Br J Sports Med 44(5):341–346. https://doi.org/10.1136/bjsm.2009.071183

Laudner KG, Myers JB, Pasquale MR, Bradley JP, Lephart SM (2006) Scapular dysfunction in throwers with pathologic internal impingement. J Orthop Sports Phys Ther 36(7):485–494. https://doi.org/10.2519/jospt.2006.2146

Lee HJ, Kim NR, Moon SG, Ko SM, Park JY (2013) Multidirectional instability of the shoulder: rotator interval dimension and capsular laxity evaluation using MR arthrography. Skelet Radiol 42(2):231–238. https://doi.org/10.1007/s00256-012-1441-2

Liavaag S, Stiris MG, Svenningsen S, Enger M, Pripp AH, Brox JI (2011) Capsular lesions with glenohumeral ligament injuries in patients with primary shoulder dislocation: magnetic resonance imaging and magnetic resonance arthrography evaluation. Scand J Med Sci Sports 21(6):e291–e297. https://doi.org/10.1111/j.1600-0838.2010.01282.x

Lin DJ, Wong TT, Kazam JK (2018) Shoulder injuries in the overhead-throwing athlete: epidemiology, mechanisms of injury, and imaging findings. Radiology 286(2):370–387. https://doi.org/10.1148/radiol.2017170481

Lintner D, Noonan TJ, Kibler WB (2008) Injury patterns and biomechanics of the athlete's shoulder. Clin Sports Med 27(4):527–551. https://doi.org/10.1016/j.csm.2008.07.007

Lo IK, Parten PM, Burkhart SS (2004) The inverted pear glenoid: an indicator of significant glenoid bone loss. Arthroscopy 20(2):169–174. https://doi.org/10.1016/j.arthro.2003.11.036

Locher J, Wilken F, Beitzel K, Buchmann S, Longo UG, Denaro V, Imhoff AB (2016) Hill-Sachs off-track lesions as risk factor for recurrence of instability after arthroscopic Bankart repair. Arthroscopy 32(10):1993–1999. https://doi.org/10.1016/j.arthro.2016.03.005

Longo UG, Loppini M, Rizzello G, Ciuffreda M, Maffulli N, Denaro V (2014) Latarjet, Bristow, and Eden-Hybinette procedures for anterior shoulder dislocation: systematic review and quantitative synthesis of the literature. Arthroscopy 30(9):1184–1211. https://doi.org/10.1016/j.arthro.2014.04.005

Longo UG, Rizzello G, Loppini M, Locher J, Buchmann S, Maffulli N, Denaro V (2015) Multidirectional instability of the shoulder: a systematic review. Arthroscopy 31(12):2431–2443. https://doi.org/10.1016/j.arthro.2015.06.006

Maffet MW, Gartsman GM, Moseley B (1995) Superior labrum-biceps tendon complex lesions of the shoulder. Am J Sports Med 23(1):93–98. https://doi.org/10.1177/036354659502300116

McLaughlin HL (1952) Posterior dislocation of the shoulder. J Bone Joint Surg Am 24 A(3):584–590

McNeil JW, Beaulieu-Jones BR, Bernhardson AS, LeClere LE, Dewing CB, Lynch JR, Golijanin P, Sanchez G, Provencher MT (2017) Classification and analysis of attritional glenoid bone loss in recurrent anterior shoulder instability. Am J Sports Med 45(4):767–774. https://doi.org/10.1177/0363546516677736

Mihata T, Gates J, McGarry MH, Lee J, Kinoshita M, Lee TQ (2009) Effect of rotator cuff muscle imbalance on forceful internal impingement and peel-back of the superior labrum: a cadaveric study. Am J Sports Med 37(11):2222–2227. https://doi.org/10.1177/0363546509337450

Mihata T, Gates J, McGarry MH, Neo M, Lee TQ (2015) Effect of posterior shoulder tightness on internal impingement in a cadaveric model of throwing. Knee Surg Sports Traumatol Arthrosc 23(2):548–554. https://doi.org/10.1007/s00167-013-2381-7

Millett PJ, Clavert P, Hatch GF 3rd, Warner JJ (2006) Recurrent posterior shoulder instability. J Am Acad Orthop Surg 14(8):464–476. https://doi.org/10.5435/00124635-200608000-00004

Modarresi S, Motamedi D, Jude CM (2011) Superior labral anteroposterior lesions of the shoulder: part 1, anatomy and anatomic variants. AJR Am J Roentgenol 197(3):596–603. https://doi.org/10.2214/AJR.10.7236

Mohana-Borges AV, Chung CB, Resnick D (2003) Superior labral anteroposterior tear: classification and diagnosis on MRI and MR arthrography. AJR Am J Roentgenol 181(6):1449–1462. https://doi.org/10.2214/ajr.181.6.1811449

Moroder P, Resch H, Schnaitmann S, Hoffelner T, Tauber M (2013) The importance of CT for the pre-operative surgical planning in recurrent anterior shoulder instability. Arch Orthop Trauma Surg 133(2):219–226. https://doi.org/10.1007/s00402-012-1656-7

Moroder P, Runer A, Kraemer M, Fierlbeck J, Niederberger A, Cotofana S, Vasvari I, Hettegger B, Tauber M, Hurschler C, Resch H (2015) Influence of defect size and localization on the engagement of reverse Hill-Sachs lesions. Am J Sports Med 43(3):542–548. https://doi.org/10.1177/0363546514561747

Moroder P, Plachel F, Tauber M, Habermeyer P, Imhoff A, Liem D, Lill H, Resch H, Gerhardt C, Scheibel M (2017) Risk of engagement of bipolar bone defects in posterior shoulder instability. Am J Sports Med 45(12):2835–2839. https://doi.org/10.1177/0363546517714456

Motamedi D, Everist BM, Mahanty SR, Steinbach LS (2014) Pitfalls in shoulder MRI: part 1—normal anatomy and anatomic variants. AJR Am J Roentgenol 203(3):501–507. https://doi.org/10.2214/AJR.14.12848

Murray IR, Goudie EB, Petrigliano FA, Robinson CM (2013) Functional anatomy and biomechanics of shoulder stability in the athlete. Clin Sports Med 32(4):607–624. https://doi.org/10.1016/j.csm.2013.07.001

Nacca C, Gil JA, Badida R, Crisco JJ, Owens BD (2018) Critical glenoid bone loss in posterior shoulder instability. Am J Sports Med 46(5):1058–1063. https://doi.org/10.1177/0363546518758015

Nakagawa S, Ozaki R, Take Y, Mizuno N, Mae T (2014) Enlargement of glenoid defects in traumatic anterior shoulder instability: influence of the number of recurrences and type of sport. Orthop J Sports Med 2(4):2325967114529920. https://doi.org/10.1177/2325967114529920

Neviaser TJ (1993a) The anterior labroligamentous periosteal sleeve avulsion lesion: a cause of anterior instability of the shoulder. Arthroscopy 9(1):17–21. https://doi.org/10.1016/s0749-8063(05)80338-x

Neviaser TJ (1993b) The GLAD lesion: another cause of anterior shoulder pain. Arthroscopy 9(1):22–23. https://doi.org/10.1016/s0749-8063(05)80339-1

Oberlander MA, Morgan BE, Visotsky JL (1996) The BHAGL lesion: a new variant of anterior shoulder instability. Arthroscopy 12(5):627–633. https://doi.org/10.1016/s0749-8063(96)90205-4

Omori Y, Yamamoto N, Koishi H, Futai K, Goto A, Sugamoto K, Itoi E (2014) Measurement of the glenoid track in vivo as investigated by 3-dimensional motion analysis using open MRI. Am J Sports Med 42(6):1290–1295. https://doi.org/10.1177/0363546514527406

Owens BD, Campbell SE, Cameron KL (2013) Risk factors for posterior shoulder instability in young athletes. Am J Sports Med 41(11):2645–2649. https://doi.org/10.1177/0363546513501508

Park JY, Noh YM, Chung SW, Moon SG, Ha DH, Lee KS, Chung SW (2016) Bennett lesions in baseball players detected by magnetic resonance imaging: assessment of association factors. J Shoulder Elb Surg 25(5):730–738. https://doi.org/10.1016/j.jse.2015.11.062

Pfahler M, Haraida S, Schulz C, Anetzberger H, Refior HJ, Bauer GS, Bigliani LU (2003) Age-related changes of the glenoid labrum in normal shoulders. J Shoulder Elb Surg 12(1):40–52. https://doi.org/10.1067/mse.2003.3

Probyn LJ, White LM, Salonen DC, Tomlinson G, Boynton EL (2007) Recurrent symptoms after shoulder instability repair: direct MR arthrographic assessment--correlation with second-look surgical evaluation. Radiology 245(3):814–823. https://doi.org/10.1148/radiol.2453061329

Reinold MM, Curtis AS (2013) Microinstability of the shoulder in the overhead athlete. Int J Sports Phys Ther 8(5):601–616

Richards RD, Sartoris DJ, Pathria MN, Resnick D (1994) Hill-Sachs lesion and normal humeral groove: MR imaging features allowing their differentiation. Radiology 190(3):665–668. https://doi.org/10.1148/radiology.190.3.8115607

Ruiz Santiago F, Martinez Martinez A, Tomas Munoz P, Pozo Sanchez J, Zarza Perez A (2017) Imaging of shoulder instability. Quant Imaging Med Surg 7(4):422–433. https://doi.org/10.21037/qims.2017.08.05

Saupe N, White LM, Bleakney R, Schweitzer ME, Recht MP, Jost B, Zanetti M (2008) Acute traumatic posterior shoulder dislocation: MR findings.

Radiology 248(1):185–193. https://doi.org/10.1148/radiol.2481071003

Schaeffeler C, Waldt S, Holzapfel K, Kirchhoff C, Jungmann PM, Wolf P, Stat D, Schroder M, Rummeny EJ, Imhoff AB, Woertler K (2012) Lesions of the biceps pulley: diagnostic accuracy of MR arthrography of the shoulder and evaluation of previously described and new diagnostic signs. Radiology 264(2):504–513. https://doi.org/10.1148/radiol.12112007

Schaeffeler C, Waldt S, Bauer JS, Kirchhoff C, Haller B, Schroder M, Rummeny EJ, Imhoff AB, Woertler K (2014) MR arthrography including abduction and external rotation images in the assessment of atraumatic multidirectional instability of the shoulder. Eur Radiol 24(6):1376–1385. https://doi.org/10.1007/s00330-014-3133-x

Shaha JS, Cook JB, Song DJ, Rowles DJ, Bottoni CR, Shaha SH, Tokish JM (2015) Redefining "critical" bone loss in shoulder instability: functional outcomes worsen with "subcritical" bone loss. Am J Sports Med 43(7):1719–1725. https://doi.org/10.1177/0363546515578250

Sheehan SE, Gaviola G, Gordon R, Sacks A, Shi LL, Smith SE (2013) Traumatic shoulder injuries: a force mechanism analysis-glenohumeral dislocation and instability. AJR Am J Roentgenol 201(2):378–393. https://doi.org/10.2214/AJR.12.9986

Shin SJ, Kim RG, Jeon YS, Kwon TH (2017) Critical value of anterior glenoid bone loss that leads to recurrent glenohumeral instability after arthroscopic Bankart repair. Am J Sports Med 45(9):1975–1981. https://doi.org/10.1177/0363546517697963

Smith TO (2006) Immobilisation following traumatic anterior glenohumeral joint dislocation: a literature review. Injury 37(3):228–237. https://doi.org/10.1016/j.injury.2005.06.005

Smith DK, Chopp TM, Aufdemorte TB, Witkowski EG, Jones RC (1996) Sublabral recess of the superior glenoid labrum: study of cadavers with conventional nonenhanced MR imaging, MR arthrography, anatomic dissection, and limited histologic examination. Radiology 201(1):251–256. https://doi.org/10.1148/radiology.201.1.8816553

Snyder SJ (1994) Shoulder arthroscopy. McGraw-Hill, Health Professions Division, New York

Snyder SJ, Karzel RP, Del Pizzo W, Ferkel RD, Friedman MJ (1990) SLAP lesions of the shoulder. Arthroscopy 6(4):274–279. https://doi.org/10.1016/0749-8063(90)90056-j

e Souza PM, Brandao BL, Brown E, Motta G, Monteiro M, Marchiori E (2014) Recurrent anterior glenohumeral instability: the quantification of glenoid bone loss using magnetic resonance imaging. Skelet Radiol 43 (8):1085–1092. doi:https://doi.org/10.1007/s00256-014-1894-6

Stillwater L, Koenig J, Maycher B, Davidson M (2017) 3D-MR vs. 3D-CT of the shoulder in patients with glenohumeral instability. Skelet Radiol 46(3):325–331. https://doi.org/10.1007/s00256-016-2559-4

Sugaya H, Moriishi J, Dohi M, Kon Y, Tsuchiya A (2003) Glenoid rim morphology in recurrent anterior glenohumeral instability. J Bone Joint Surg Am 85(5):878–884. https://doi.org/10.2106/00004623-200305000-00016

Sugimoto H, Suzuki K, Mihara K, Kubota H, Tsutsui H (2002) MR arthrography of shoulders after suture-anchor Bankart repair. Radiology 224(1):105–111. https://doi.org/10.1148/radiol.2241011128

Taylor DC, Arciero RA (1997) Pathologic changes associated with shoulder dislocations. Arthroscopic and physical examination findings in first-time, traumatic anterior dislocations. Am J Sports Med 25(3):306–311. https://doi.org/10.1177/036354659702500306

Thomas SC, Matsen FA 3rd (1989) An approach to the repair of avulsion of the glenohumeral ligaments in the management of traumatic anterior glenohumeral instability. J Bone Joint Surg Am 71(4):506–513

Tian CY, Cui GQ, Zheng ZZ, Ren AH (2013) The added value of ABER position for the detection and classification of anteroinferior labroligamentous lesions in MR arthrography of the shoulder. Eur J Radiol 82(4):651–657. https://doi.org/10.1016/j.ejrad.2012.11.038

Tuite MJ, Petersen BD, Wise SM, Fine JP, Kaplan LD, Orwin JF (2007) Shoulder MR arthrography of the posterior labrocapsular complex in overhead throwers with pathologic internal impingement and internal rotation deficit. Skelet Radiol 36(6):495–502. https://doi.org/10.1007/s00256-007-0278-6

Walch G, Boileau P, Noel E, Donell ST (1992) Impingement of the deep surface of the supraspinatus tendon on the posterosuperior glenoid rim: an arthroscopic study. J Shoulder Elb Surg 1(5):238–245. https://doi.org/10.1016/S1058-2746(09)80065-7

Waldt S, Burkart A, Lange P, Imhoff AB, Rummeny EJ, Woertler K (2004) Diagnostic performance of MR arthrography in the assessment of superior labral anteroposterior lesions of the shoulder. AJR Am J Roentgenol 182(5):1271–1278. https://doi.org/10.2214/ajr.182.5.1821271

Waldt S, Burkart A, Imhoff AB, Bruegel M, Rummeny EJ, Woertler K (2005) Anterior shoulder instability: accuracy of MR arthrography in the classification of anteroinferior labroligamentous injuries. Radiology 237(2):578–583. https://doi.org/10.1148/radiol.2372041429

Waldt S, Metz S, Burkart A, Mueller D, Bruegel M, Rummeny EJ, Woertler K (2006) Variants of the superior labrum and labro-bicipital complex: a comparative study of shoulder specimens using MR arthrography, multi-slice CT arthrography and anatomical dissection. Eur Radiol 16(2):451–458. https://doi.org/10.1007/s00330-005-2864-0

Waldt S, Bruegel M, Mueller D, Holzapfel K, Imhoff AB, Rummeny EJ, Woertler K (2007) Rotator cuff tears: assessment with MR arthrography in 275 patients with arthroscopic correlation. Eur Radiol 17(2):491–498. https://doi.org/10.1007/s00330-006-0370-7

Wall MS, O'Brien SJ (1995) Arthroscopic evaluation of the unstable shoulder. Clin Sports Med 14(4):817–839

Walter WR, Samim M, LaPolla FWZ, Gyftopoulos S (2019) Imaging quantification of glenoid bone loss in patients with glenohumeral instability: a systematic review. AJR Am J Roentgenol 212:1–10. https://doi.org/10.2214/AJR.18.20504

Warby SA, Watson L, Ford JJ, Hahne AJ, Pizzari T (2017) Multidirectional instability of the glenohumeral joint: etiology, classification, assessment, and management. J Hand Ther 30(2):175–181. https://doi.org/10.1016/j.jht.2017.03.005

Weber AE, Kontaxis A, O'Brien SJ, Bedi A (2014) The biomechanics of throwing: simplified and cogent. Sports Med Arthrosc Rev 22(2):72–79. https://doi.org/10.1097/JSA.0000000000000019

Weishaupt D, Zanetti M, Nyffeler RW, Gerber C, Hodler J (2000) Posterior glenoid rim deficiency in recurrent (atraumatic) posterior shoulder instability. Skelet Radiol 29(4):204–210. https://doi.org/10.1007/s002560050594

Wilk KE, Meister K, Andrews JR (2002) Current concepts in the rehabilitation of the overhead throwing athlete. Am J Sports Med 30(1):136–151. https://doi.org/10.1177/03635465020300011201

Willemot L, De Boey S, Van Tongel A, Declercq G, De Wilde L, Verborgt O (2019) Analysis of failures after the Bristow-Latarjet procedure for recurrent shoulder instability. Int Orthop 43(8):1899–1907. https://doi.org/10.1007/s00264-018-4105-6

Williams MM, Snyder SJ (1994) A sublabral foramen must not be confused with a Bankart lesion. Arthroscopy 10(5):586. https://doi.org/10.1016/s0749-8063(05)80022-2

Williams MM, Snyder SJ, Buford D Jr (1994) The Buford complex—the "cord-like" middle glenohumeral ligament and absent anterosuperior labrum complex: a normal anatomic capsulolabral variant. Arthroscopy 10(3):241–247. https://doi.org/10.1016/s0749-8063(05)80105-7

Wischer TK, Bredella MA, Genant HK, Stoller DW, Bost FW, Tirman PF (2002) Perthes lesion (a variant of the Bankart lesion): MR imaging and MR arthrographic findings with surgical correlation. AJR Am J Roentgenol 178(1):233–237. https://doi.org/10.2214/ajr.178.1.1780233

Woertler K (2007) Multimodality imaging of the postoperative shoulder. Eur Radiol 17(12):3038–3055. https://doi.org/10.1007/s00330-007-0649-3

Wolf EM, Cheng JC, Dickson K (1995) Humeral avulsion of glenohumeral ligaments as a cause of anterior shoulder instability. Arthroscopy 11(5):600–607. https://doi.org/10.1016/0749-8063(95)90139-6

Wright RW, Paletta GA Jr (2004) Prevalence of the Bennett lesion of the shoulder in major league pitchers. Am J Sports Med 32(1):121–124. https://doi.org/10.1177/0363546503260712

Yiannakopoulos CK, Mataragas E, Antonogiannakis E (2007) A comparison of the spectrum of intraarticular lesions in acute and chronic anterior shoulder instability. Arthroscopy 23(9):985–990. https://doi.org/10.1016/j.arthro.2007.05.009

Rotator Cuff and Impingement Symptoms

Henk-Jan Van der Woude and Derek van Deurzen

Contents

Abstract

Shoulder pain is a common sports-related complaint that may be caused by rotator cuff-related abnormalities. Accurate imaging plays a pivotal role in direct timing and type of treatment and subsequential outcome.

Native MR imaging and ultrasonography are equally accurate and optimal and complementary tools to discriminate different forms of impingement symptoms and to localize and classify rotator cuff injuries. Currently, considering accuracy, safety, and cost, US is the preferred imaging modality to start with, when rotator cuff pathology is expected.

Partial-thickness rotator cuff tears are most commonly encountered in (overhead throwing) athletes, particularly on the articular side, which are best appreciated using MR arthrography including abduction-exorotation views. MR arthrography is also the preferred tool to rule out concurrent labral-ligamentous lesions and depict abnormalities related to posterosuperior (internal) impingement.

H.-J. Van der Woude (✉)
Department of Radiology, Onze Lieve Vrouwe Gasthuis, Amsterdam, The Netherlands
e-mail: H.J.vanderWoude@olvg.nl

D. van Deurzen
Department of Orthopedic Surgery, Onze Lieve Vrouwe Gasthuis, Amsterdam, The Netherlands

1 Introduction

Shoulder pain is a common sports-related clinical complaint, both in the recreational and professional setting, that may be accompanied by many disorders including abnormalities of the rotator

Med Radiol Diagn Imaging (2021)
https://doi.org/10.1007/174_2020_252, © Springer Nature Switzerland AG
Published Online: 12 March 2021

cuff and osseous acromial outlet and the biceps-labrum complex, and various other pathologic conditions, based on repetitive stress but also on torsional forces (Fritz 2002). One should be aware that rotator cuff and biceps-labral lesions secondary to trauma or overuse may coexist, posing challenges to physical examination (Van Kampen et al. 2014). The role of accurate (preoperative) imaging is thus pivotal, particularly when uncertainty exists regarding the primary cause of the pain (Helms 2002; Sanders and Miller 2005; Tirman et al. 2004). In professional sports the income interests are enormous, and athletes may return to sports activities earlier than medically justified. Insight into the right diagnosis thus has important consequences for timing and type of treatment with subsequential outcome.

Because magnetic resonance (MR) imaging and ultrasonography (US) are noninvasive examinations, both imaging tools are touted for establishing rotator cuff disease and cuff-related abnormalities.

Ultrasonography has substantial privileges for shoulder examination because of its noninvasive and nonionizing capabilities. Moreover, it is highly available and non-expensive, and the painful shoulder can be easily compared with the asymptomatic side (Box 1).

Box 1: Ultrasonography in Rotator Cuff Imaging: Privileges

- Noninvasive, nonionizing and highly available
- Non-expensive and fast
- Interaction with patient and comparison with contralateral shoulder
- Dynamic examination capabilities
- Highly accurate for depiction of (partial) cuff tears

Another advantage of US is the dynamic evaluation capability, which can be helpful in the assessment of dislocated tendons. Nowadays, the spatial resolution of US with high-frequency transducers is higher than routine MR imaging (Fig. 1).

Besides diagnostic imaging, US can also be used as a guidance for interventional procedures,

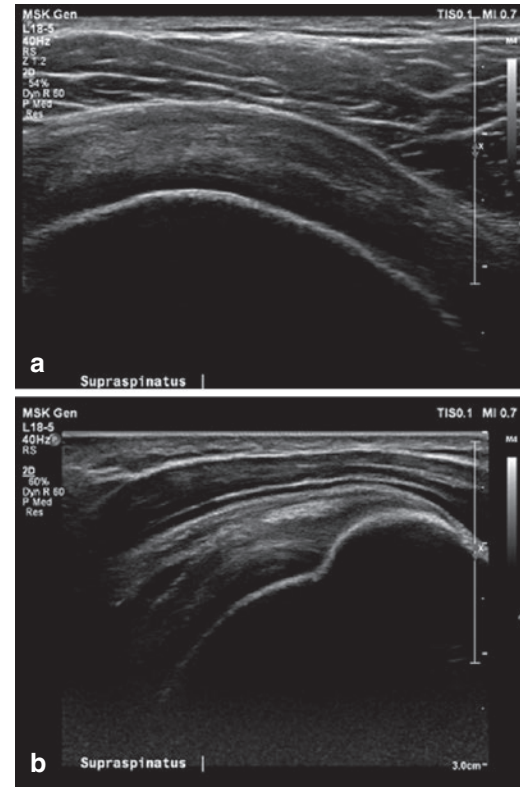

Fig. 1 (**a**, **b**) Normal appearance of rotator cuff. Transverse (**a**) and longitudinal (**b**) ultrasound images show normal insertion of supraspinatus fibers at the footplate of major tubercle. In between tendon and deltoid muscle, hyperechoic subacromial/subdeltoid bursa is seen. The cortical bone is hyperechoic, cartilage beneath the tendon is hypoechoic

including aspiration of fluid or needle aspiration of calcific deposits, and biopsies, or injections for therapeutic reasons and differentiation in case of coexisting pathology, such as related to AC joint or biceps tendon. The agreement between examiners with different levels of experience is very good with regard to the detection of rotator cuff tears and therefore US is a strong noninvasive tool in the initial examination of shoulder pain (Brenneke and Morgan 1992; Hodler et al. 1988; O'Connor et al. 2005; Teefey et al. 2000, 2004; Van Holsbeeck et al. 1995; Wiener and Seitz 1993; Rutten et al. 2010; Middleton et al. 2004). Considering accuracy, safety, and cost, US is the preferred imaging modality to start with, when rotator cuff pathology is expected (Roy et al. 2015; Nazarian et al. 2013; Wengert et al. 2019).

US, MR imaging, and MR arthrography all have high accuracy and any of these tests may be equally used for detection of full-thickness rotator cuff tears (Lenza et al. 2013; De Jesus et al. 2009; Roy et al. 2015; Nazarian et al. 2013; Lee et al. 2016).

MR imaging, and MR arthrography in particular, is frequently the preoperative imaging tool of choice for many sports medicine surgeons (Fritz 2002; Helms 2002; Magee et al. 2004; Palmer et al. 1993). MR imaging is superior for the visualization of even delicate intra- and extra-articular soft-tissue structures involved in the clinical syndrome of impingement. Due to the multiplanar capabilities, MRI is also favored for the detection of anatomical variations of the osseous outlet that may be involved with impingement symptoms (Fritz 2002; Sanders and Miller 2005) (Box 2). MR arthrography, performed after intra-articular injection of diluted contrast medium, improves the diagnostic accuracy in individuals with shoulder pain with regard to the detection of partial rotator cuff lesions and lesions of the glenoid labrum, capsule, and glenohumeral ligaments. Sensitivity of MRI and US is less than MR arthrography for the detection of partial tears (Lenza et al. 2013; Roy et al. 2015). Therefore, young athletes with chronic injuries or instability seem to benefit most from direct MR arthrography because they tend to have smaller labral tears and in addition partial rotator cuff pathology tends to occur more frequently and in atypical locations (Jbara et al. 2005; Magee et al. 2004; Tuite 2003; De Jesus et al. 2009; Wengert et al. 2019) (Box 3).

Box 2: MRI in Rotator Cuff Imaging: Privileges

- Noninvasive, nonionizing and multidimensional
- High soft-tissue contrast
- Optimal visualization of both normal bone and soft-tissue anatomy and rotator cuff pathology
- Highly accurate for depiction of (partial) cuff tears
- Depiction of anatomical variants of (osseous) outlet

Box 3: MR Arthrography in Rotator Cuff Imaging: Privileges

- Particularly useful in athletes to rule out or depict small partial-thickness tears
- Optimal for detection of (concurrent) labral-ligamentous lesions

The mainstay of treatment of high-level athletes suffering from rotator cuff pathology is nonsurgical. Initial treatment usually consists of exercises focusing on range of motion, flexibility, strengthening, and advanced strengthening/proprioception. The rehabilitation may be combined with the judicious use of NSAIDs and corticosteroid injections. However, caution must be exercised with repeated corticosteroid injections due to the reported risk of tendon weakening and rupture. Although there is limited evidence to support one surgical treatment over the other, most operations are performed with arthroscopic technique. In most cases debridement of partial-thickness lesions will lead to decrease in pain and increase in function. However, return of pre-injury level of sports cannot be guaranteed, especially for the elite-level overhead athletes (Weiss et al. 2018).

2 MR Imaging Technique

Imaging of the shoulder can be performed on 1.5 or 3 T MR systems. Low-field systems are adequate for evaluation of rotator cuff and osseous structures, but are less sufficient for assessment of the labroligamentous structures. In any system, a dedicated multichannel shoulder coil or flexible body phased array coil is essential for acquiring optimal details. Patients should be placed in a comfortable supine position with the arm at the side in neutral or slight external rotation. Field of views chosen should be kept as small as possible, still enclosing the entire shoulder. Slice thickness should be in the range of 3–4 mm (Sanders and Miller 2005). In the literature, different imaging protocols are recommended (Fritz 2002; Jbara et al. 2005; Jost et al. 2005; Meister et al. 2003; Miniaci et al. 2002). A

standard conventional MR protocol typically includes sequences in the axial, oblique coronal, and oblique sagittal plane (Box 4). The axial images extend from the (complete) acromion through the axillary pouch. The oblique coronal images are prescribed from the axial images and should be directed parallel to the supraspinatus tendon. The oblique sagittal images are also prescribed from the axial series and aligned perpendicular to the coronal images. Sagittal images extend from the scapular neck and distal clavicle through the lateral aspect of the greater tuberosity. T2- and proton density-weighted images with or without fat suppression in the axial, oblique coronal, and sagittal planes are the working horses for evaluation of the painful shoulder (Fig. 2). These sequences in all dimensions optimally reflect the pathology of bones, rotator cuff, capsule, and labrum, by identifying fluid and edema related to bursae, muscles and tendons, joints, and paralabral cysts (Jbara et al. 2005; Sanders and Miller 2005).

Box 4: Shoulder MR Imaging Protocol

- Combination of axial, oblique coronal, and oblique sagittal sequences
- Axial from above A-C joint to below axillary pouch
- Oblique coronal parallel to supraspinatus tendon or scapula body, including the entire humeral head
- Oblique sagittal perpendicular to oblique coronal plane
- Combination of T1- and/or proton density- and T2-weighted TSE sequences with and without fat saturation
- MR arthrography: axial, oblique coronal, and oblique sagittal T1-weighted fat-saturated sequences; oblique coronal T2-weighted fat-saturated series; and separate sequence in abduction-exorotation (ABER) position

Intermediate-weighted sequences offer higher signal-to-noise ratio, whereas T2-weighed sequences with longer echo times minimize

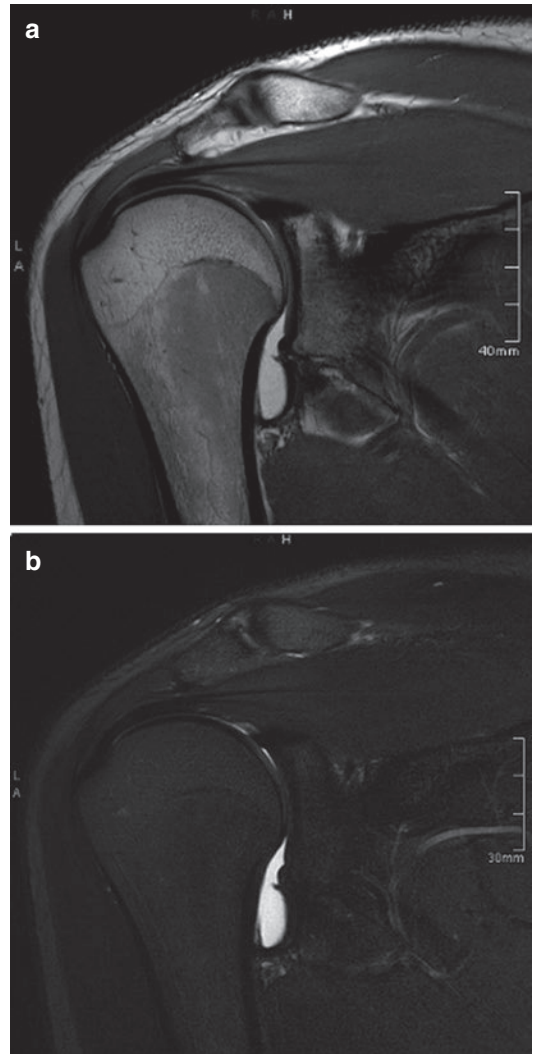

Fig. 2 (**a**, **b**) Normal MR imaging appearance of supraspinatus tendon. Distal supraspinatus tendon is not enlarged and hypointense on coronal PD-weighted (**a**) and T2-weighted fat-suppressed (**b**) Dixon MR images with intra-articular contrast. There is no bursal reaction or bone marrow edema

magic angle effect present in curved structures such as at the distal supraspinatus insertion. Nonfat-suppressed sequences can be included for further anatomical information of the rotator cuff and osseous structures and to determine signs of fatty atrophy of the cuff (Jbara et al. 2005; Jost et al. 2005; Miniaci et al. 2002; Sanders and Miller 2005; Lin et al. 2018).

Patients with clinical symptoms of impingement and/or suspected rotator cuff abnormalities

can be assessed with non-enhanced MR imaging study in three directions and will accurately demonstrate full-thickness tears (Fig. 3). In the young athletic individuals, partial-thickness tears that may cause symptoms and hamper sports activities can be encountered more frequently (Fig. 4) (Tirman et al. 1994a, b; Tuite 2003). Although specificity is high, the sensitivity for the detection of those tears using non-contrast MRI is more susceptible to variation (Roy et al. 2015).

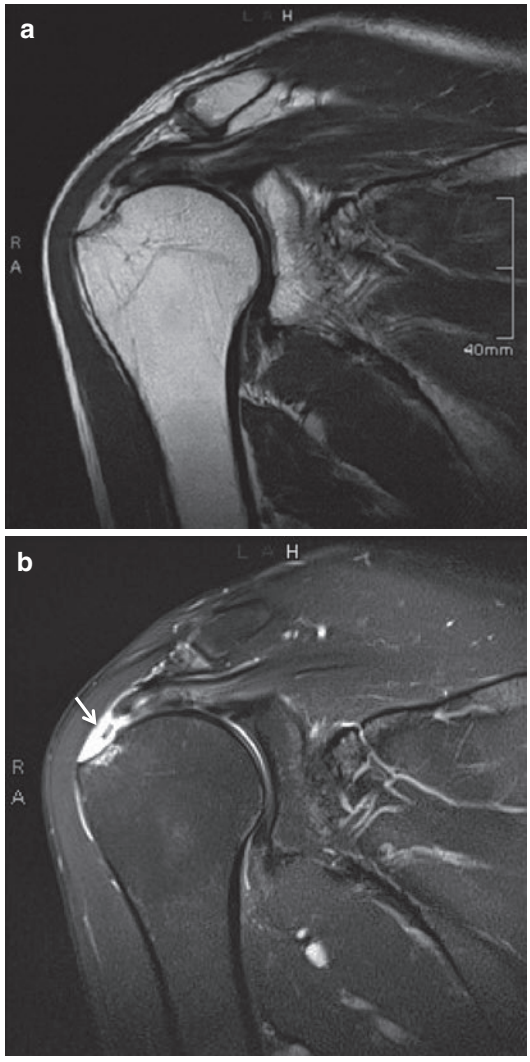

Fig. 3 (**a**, **b**) Incomplete full-thickness tear of supraspinatus tendon. Coronal PD-weighted (**a**) and T2-weighted fat-suppressed (**b**) MR images show fluid-filled gap (*arrow*) with retraction of the tendon halfway the humeral head

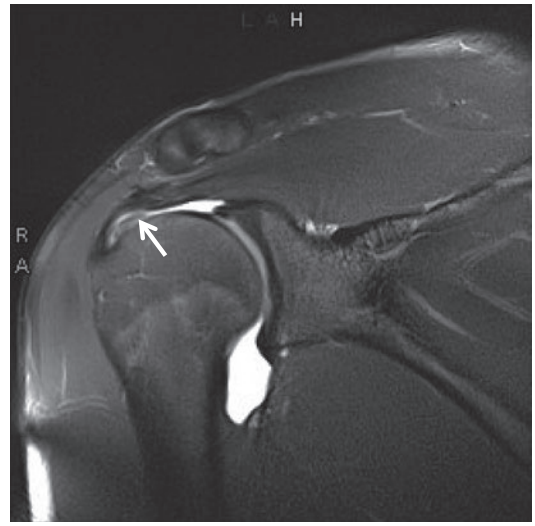

Fig. 4 Partial-thickness articular sided tear of supraspinatus tendon (PASTA lesion). Coronal PD-weighted fat-suppressed MR arthrogram shows increased signal at articular side (*arrow*) of anterior distal tendon whereas other fibers are normally attached to the footplate

Particularly articular sided surface tears can be detected more accurately when intra-articular dilute gadolinium is administered. Using MR arthrography, T1-weighted fast spin-echo sequences are performed with fat suppression in the axial, oblique coronal, and oblique sagittal direction after intra-articular injection of approximately 12–15 ml of a 0.1 mmol/kg solution of gadopentetate dimeglumine (Vanhoenacker et al. 2000). Adding abduction and exorotation stress imaging (ABER) to this protocol is also very useful for detecting small partial tears on the articular side, besides the improved appreciation of (non-displaced) anterior-inferior labral tears (Fig. 5) (Jbara et al. 2005; Meister et al. 2003; Sanders and Miller 2005; Schreinemachers et al. 2009). As an alternative, delayed indirect MR arthrography after intravenous administration of gadolinium allows visualization of synovial tissue lining the bursae, joint capsule, and tendon sheaths in the early phase and may enhance (partial) rotator cuff tears in the later phase after diffusion of the contrast medium into the joint space (Fig. 6).

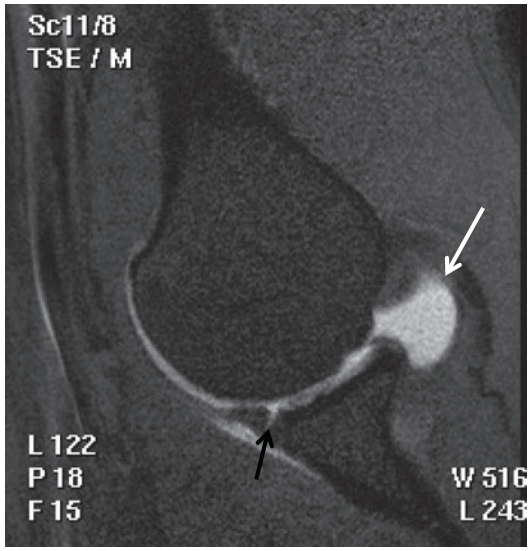

Fig. 5 Anteroinferior labral tear with intact spinatus tendons. T1-weighted fat-saturated MR arthrogram in ABER view. Articular undersurface of supraspinatus tendon is completely normal (*white arrow*). Inferior glenohumeral ligament is under stress in this view accentuating subtle anteroinferior labral tear (*black arrow*)

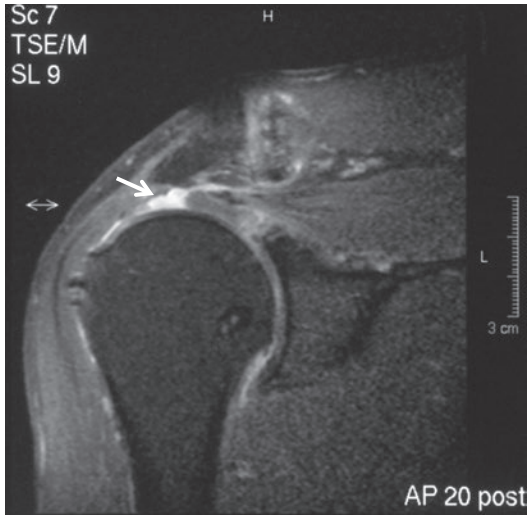

Fig. 6 Full-thickness supraspinatus tear. Coronal T1-weighted fat-saturated TSE MR image after delayed i.v. contrast administration (indirect arthrogram). Gap representing tear (*arrow*) is filled with contrast medium after transsynovial diffusion into the joint

3 Ultrasonography: Normal Appearance of the Shoulder

Over the last decennia, significant improvements of shoulder US have been achieved with the introduction of linear-array, high-frequency transducers. Nowadays, 9–18 MHz linear broadband-array transducers are used, allowing a section thicknesses of 0.5–1 mm and in-plane spatial resolution in the range of 200–400 μm. Using these high frequencies, the spatial resolution with US is higher than acquired with MR imaging.

Assessment of clinical symptoms and plain radiographs should ideally be performed prior to US examination. Real-time diagnostic US of the shoulder should be conducted in a logical and systematic fashion. Performance of the shoulder US investigation has been eminently reported by Teefey et al. (1999), and can be subdivided into different anatomical regions (anterior, anterolateral, superior, and posterior) (Lee et al. 2016).

Most imagers prefer a seated position of the patient with the examiner facing the patient or in a standing position behind the patient. The rotator cuff tendons must always be carefully evaluated in both coronal (longitudinal) and transversal dimensions to verify its continuity and quality (Fig. 1). Moreover, extending the examination dynamically with passive motion is a prerequisite. The tendon must be strained during the investigation by rotating and extending the arm in the direction that is contrary to the function of that muscle. Hypoechoic appearance and a non-stretched buckled tendon can erroneously be mistaken for a teared tendon.

From inside out, cortical bone, hyaline cartilage, rotator cuff tendons and muscles, subacromial/subdeltoid bursa, peribursal fat, deltoid muscle, and subcutaneous tissue are normally appreciated with US (Fig. 1). The appearance of the cortical bone is hyperechoic with posterior acoustic shadowing. Hyaline cartilage is hypoechoic in contrast with the echogenicity of bone. Hodler et al. established an average depth of cartilage of 1.23 mm with MR imaging (Hodler

et al. 1995) confirmed by Seibold et al. (1999) based on US. At the bare area, the posterolateral part of the humeral head, lack of hyaline cartilage is detected as a normal finding. The echogenicity of the tendons is substantially dependent on probe position. When the ingoing ultrasonic beam is not perpendicular to the tendon, the appearance of the tendon can modify from hyperechoic and hypoechoic to even anechoic, referred to as anisotropy (Crass et al. 1988b). Perpendicular direction of the beam will result in a hyperechoic appearance of the tendon with an echogenic fibrillar echotexture (Martinoli et al. 1993). Rotator cuff muscle texture appears isoechoic. The subacromial-subdeltoid bursa, which is interposed between the rotator cuff and the acromion and deltoid muscle, is a two-layered hyperechoic compartment in which very little fluid can be seen. This fluid visually disappears by compression. The deltoid muscle itself has a less echogenic appearance compared with the rotator cuff tendons. The supraspinatus tendon consistently courses laterally from the supraspinatus fossa, blends with the infraspinatus tendon (coursing superolaterally from the infraspinatus fossa), and gets inserted on the anteromedial aspect of the superior facet of the greater tuberosity.

One advantage of US over other imaging modalities is its ability to examine dynamically, indicating possible subacromial impingement. The transducer is placed over the anterolateral region of the shoulder and free gliding of the supraspinatus tendon and subacromial-subdeltoid bursa beneath the acromion can be assessed while the patient is abducting the arm slowly (Lee et al. 2016).

4 Shoulder Impingement Syndrome

Impingement reflects a clinical condition in which the subacromial soft tissues (supraspinatus tendon, biceps tendon, bursa) are compressed between the humeral head and (components of) the coracoacromial arch. Mechanical impingement may lead to a compromise of tensile integrity and eventually rotator cuff tears. Several types of impingement can be distinguished when discussing sports trauma to the rotator cuff: primary (extrinsic) impingement, secondary impingement from instability, and posterosuperior (internal) impingement, particularly in throwing athletes. Another rare form of impingement is coracohumeral impingement, which involves anterior soft tissues, particularly the subscapularis muscle and tendon.

MR imaging and MR arthrography are important tools in establishing the form of impingement with significant relevance for subsequent therapy.

4.1 Primary Extrinsic Impingement

The arch that surrounds the rotator cuff is composed of the acromion, the acromioclavicular joint, the coracoid process, and the coracoacromial ligament. Anatomical variants and reactive degenerative irregularities of this osseous outlet may result in primary extrinsic impingement of the underlying cuff tendons and adjacent bursa with subsequent clinical impingement (Fritz 2002). Although rotator cuff degeneration and tearing may be due to intrinsic factors, such as diminished vascularity and overuse, it has been proposed that the vast majority of rotator cuff tears may be secondary to chronic impingement between the humeral head and coracoacromial arch. It should be noticed, however, that primary impingement is fairly uncommon in young (athletic) individuals (Tuite 2003). The pain is believed to be caused primarily by compression of the well-innervated subacromial bursa between rotator cuff and arch. In this respect, the shape and aspect of the anterior acromion, assessed on the oblique sagittal and coronal MR images, have been suggested to be of critical importance (Peh

et al. 1995). The shape of the under surface of the anterolateral acromion can be classified as flat (I), curved (II), anteriorly hooked (III), or convex (IV); however, variability among observers can be significant. Types II and III in particular are associated with higher incidence of impingement and rotator cuff abnormalities (Farley et al. 1994; Peh et al. 1995) (Fig. 7). Downsloping of the acromion, either anteriorly (determined on sagittal images, immediately lateral to the A-C joint) or laterally (on coronal images), may result in narrowing of the outlet and impingement of the distal part of the supraspinatus tendon (Fritz 2002) (Fig. 8). Another causing factor of impingement may be the presence of bony spurs on the inferior surface of the acromion (Farley et al. 1994). Incidentally, a non-fused os acromiale may lead to osteophytic lipping at the acromial gap and as such impingement of the rotator cuff, tendinopathy, and tearing of the supraspinatus (Park et al. 1994). The non-fused ossification center of the acromion is best appreciated on axial MR images. The subsequent effects on the rotator cuff are best visible on the oblique coronal and sagittal images.

Osteoarthritic changes of the A-C joint are frequently encountered after the age of 40. This may result in spur formation and synovial and capsular hypertrophy with scarring. Although these factors may influence the rotator cuff, it is usually less critical compared with the changes of the anterior acromion (Sanders and Miller 2005). Separation or instability of the A-C joint may result in a low-lying acromion that may contribute to impingement (Tirman et al. 1994a, b, 2004).

In the young athlete, posttraumatic A-C separation and/or lysis of the distal clavicle is not uncommon. This may occur after acute moderate trauma or secondary to repetitive microtrauma caused by repetitive stress to the joint. In the early phase marrow edema of the distal clavicle can be seen on T2-weighted fat-suppressed images with some effusion, mild synovial hypertrophy, and soft-tissue edema. Later on joint widening can be found with irregularity of the cortex and subchondral sclerosis (Tirman et al. 1994a, b, 2004). Bone marrow edema in the acromion and/or distal clavicle can be found in a clinical picture of impingement without rotator cuff abnormalities, but may also be appreciated in asymptomatic subjects (Fig. 9).

The coracoacromial ligament (CAL) is another component of the osseous outlet. This ligament is best appreciated on the oblique sagittal MR images, as it extends from the coracoid process anteriorly to the acromion more posteriorly, covering the anterior fibers of the supraspinatus tendon and the rotator interval. The thickness of the normal ligament measures about 2–3 mm. The CAL can be congenitally thickened and incidentally be a source of primary impingement (Tuite 2003), or thickening can be reactive due to chronic pressure exerted by subacromial structures during arm abduction. Incidentally, and almost exclusively in athletes, hypertrophy of the supraspinatus may cause

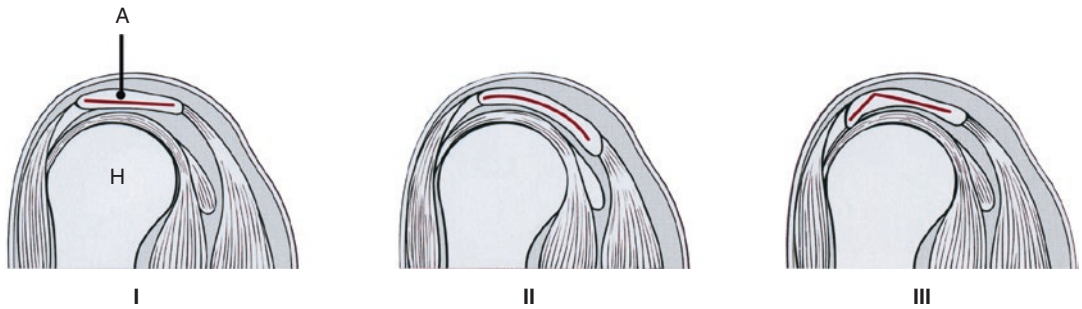

Fig. 7 Schematic drawing of most common anterolateral acromion types. Type I: flat undersurface, type II: smoothly curved undersurface, type III: anteriorly hooked acromion (*A*, acromion, *H*, humerus). Type IV (not shown) represents convex undersurface of acromion

Fig. 8 Downsloping of acromion. Coronal T2-weighted fat-suppressed MR image shows lateral downsloping of acromion (*white line*) with subacromial bursal reaction and intratendinous high signal based on tendinopathy and bone marrow reaction

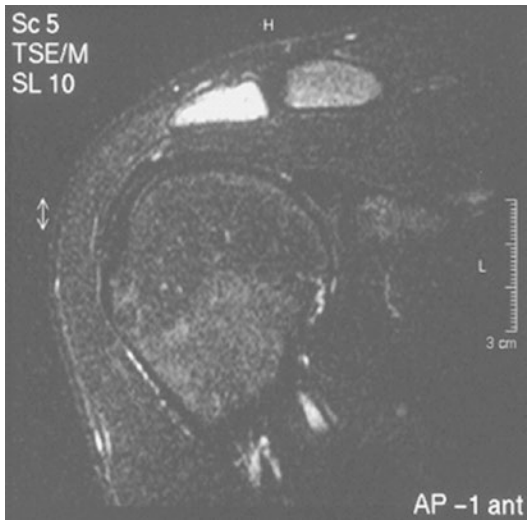

Fig. 9 Young table tennis player with complaints of impingement, no trauma. Coronal T2-weighted fat-saturated TSE image shows diffuse high signal intensity of acromion and a completely normal underlying cuff

clinical symptoms. In this case, the enlargement of the soft tissues is the cause of impingement rather than (osseous) narrowing of the acromiohumeral space.

4.2 Secondary Extrinsic Impingement

Secondary extrinsic impingement refers to instability of the glenohumeral joint resulting in dynamic narrowing of the coracoacromial outlet (Fritz 2002). The outlet itself can be morphologically normal. This secondary impingement is considered the most common cause of impingement pain in the athlete (Tirman et al. 2004). Usually, stability of the shoulder joint is provided by the static effects of the capsule, ligaments, and labrum on the one hand and by dynamic stabilizers including rotator cuff muscles and biceps tendon on the other hand. Repetitive microtrauma and weakening of the anterior capsule are quite commonly seen in overhead-throwing athletes. The instability itself is usually minor and by itself asymptomatic and may result from an asymmetric capsular tightness secondary to repetitive throwing with a loose anterior capsule and a tight and shortened posterior capsule (Lin et al. 2018). This injury of the static stabilizers may influence and overload the dynamic stabilizers (cuff muscles). Due to superior translation of the humeral head in these throwers, there is dynamic impingement of the rotator cuff in the coracoacromial outlet, resulting in tendinosis and (partial) tearing (Tirman et al. 1994a, b, 2004) (Fig. 10).

Accurate assessment of the cause of impingement has critical consequences for further treatment: in the primary form of extrinsic impingement, open or arthroscopic surgery is warranted to remove osseous irregularities, whereas secondary impingement may be best treated by physical therapy aiming at balancing rotator cuff and avoidance of activities causing instability. Various surgical procedures are available to decrease the many factors that contribute to mechanical impingement of the rotator cuff, particularly the supraspinatus tendon: these include resection of a thickened coracoacromial ligament, anterior acromioplasty, resection of the distal clavicle, and resection of subacromial osteophytes. Small partial-thickness tears may be treated by arthroscopic debridement, whereas full-thickness tears are indicated for repair.

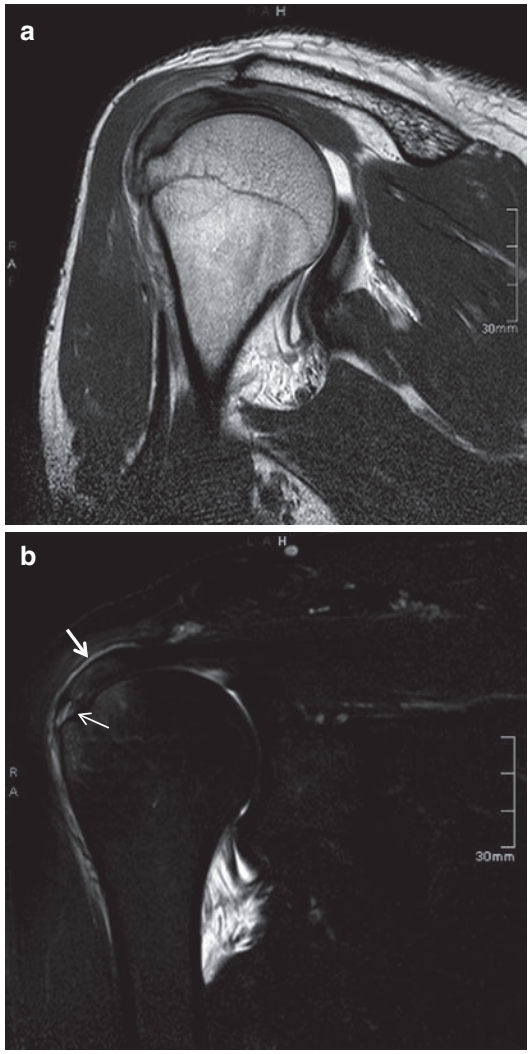

Fig. 10 (**a**, **b**) Tendinosis and partial tearing of supraspinatus tendon. Double-oblique PD-weighted TSE (**a**) and T2-weighted fat-suppressed (**b**) MR arthrogram images. Distal supraspinatus tendon is thickened and there is a rim of fluid in the subdeltoid bursa (*arrow*) and also small partial tear (*thin arrow*) distally and some edema of humeral head

4.3 Internal Impingement

Internal impingement, also referred to as posterosuperior glenoid impingement, is a condition that is frequently encountered in athletes performing repetitive overhead throwing. Impingement occurs due to contact of the undersurface of the posterior rotator cuff between the humeral head and the posterosuperior labrum and osseous glenoid (Fritz 2002; Jobe et al. 1989; Walch et al. 1992; Lin et al. 2018). This position occurs during the late cocking phase of throwing with the arm in extreme abduction and exorotation (ABER). This may typically result in degeneration and partial cuff tears, particularly infraspinatus and posterior supraspinatus, fraying of the posterosuperior labrum, and quite large subcortical cystic changes and edema of the humeral head in the posterior greater tuberosity, due to repetitive impaction (Figs. 11 and 12). Moreover, posterior capsular thickening and ossification (Bennett lesion) may occur under these circumstances (Ferrari et al. 1994; Lin et al. 2018).

The thickening of the posteroinferior capsule leads to limited internal rotation and is typically described as GIRD: glenohumeral internal rotation deficit. In the overhead-throwing athlete this is frequently associated with an increased exorotation as well, caused by the repetitive throwing motion (Rose and Noonan 2018).

These changes at this particular site are optimally appreciated on MR arthrograms in ABER position (Fritz 2002; Tirman et al. 1994a, b, 2004; Tuite 2003; Lin et al. 2018) and are crucial in making the diagnosis prior to arthroscopy.

4.4 Coracohumeral Impingement

An unusual form of impingement is coracohumeral or coracoid impingement, in which the coracohumeral distance is narrowed (less than the normal 11 mm) on axial images, for instance due to developmental enlargement of the coracoid process or posttraumatic changes of the coracoid process or lesser tuberosity. This may result in entrapment of the subscapularis tendon between the humeral head and coracoid process comparable to the classic impingement syndrome of the supraspinatus tendon (Sanders and Miller 2005).

The syndrome is most common after a history of chronic overuse with multiple episodes of microtrauma. Patients with this syndrome typically present with a history of dull pain in the anterior aspect of the shoulder that is exacerbated by activities performed when the shoulder is in a forward flexed, adducted, and internally rotated position (Okoro et al. 2009).

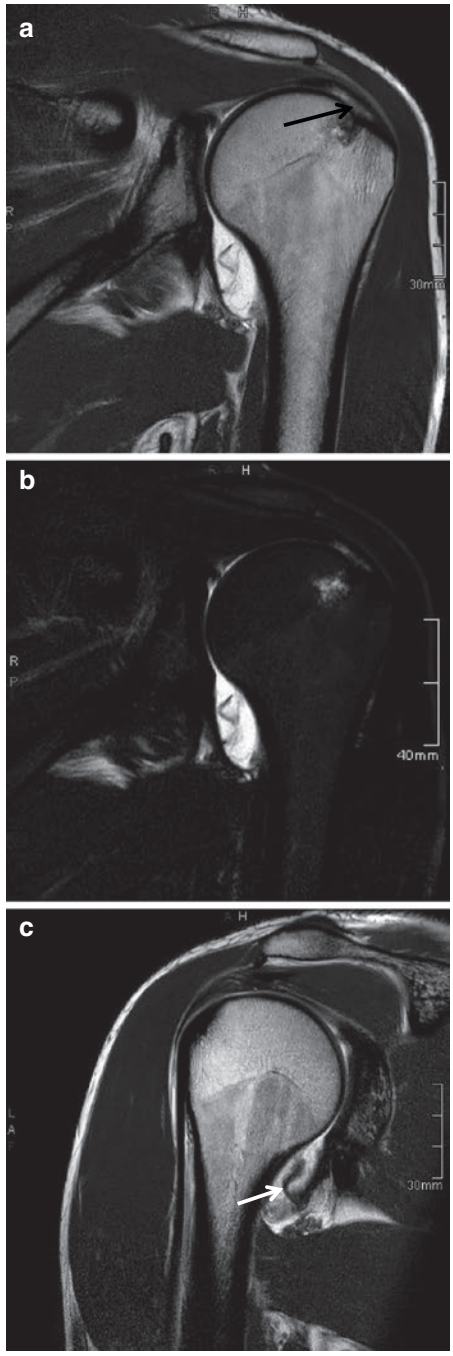

Fig. 11 (**a**–**c**) Internal or posterosuperior impingement. Coronal PD-weighted TSE (**a**, **c**) and T2-weighted fat-saturated (**b**) MR arthrogram. There is a focus of bone marrow edema in the humeral head and articular sided partial-thickness tear (*black arrow*) of posterior supraspinatus tendon (**a**, **b**) There is also suspicion of a subtle SLAP lesion (**a**, **b**) and HAGL lesion (**c**) (*white arrow*)

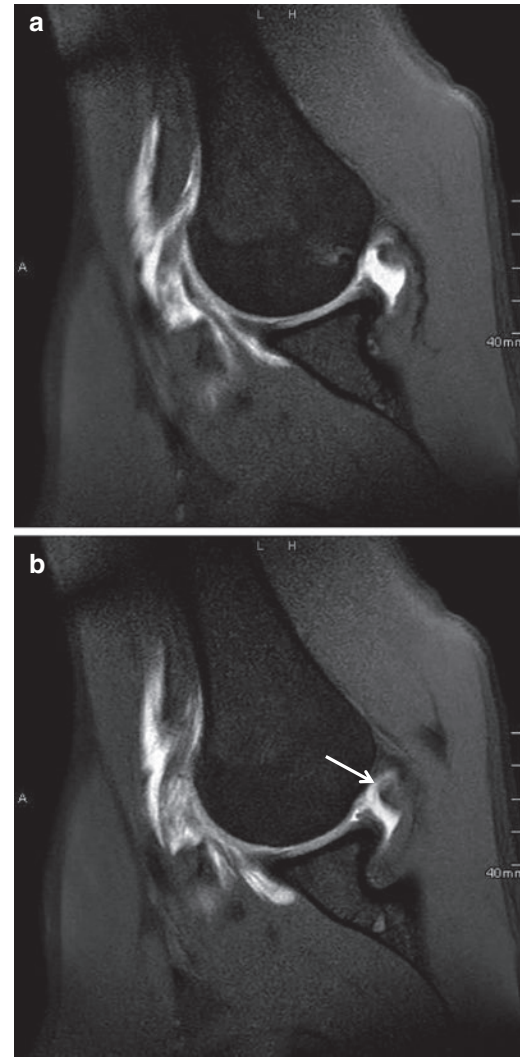

Fig. 12 (**a**, **b**) Internal or posterosuperior impingement. MR arthrogram slices in ABER view. There is a focus of edema of humeral head and partial-thickness tear (*arrow*) at articular side of posterior supraspinatus tendon (**a**) and fraying of posterosuperior labrum (**b**)

Moreover, tears of the subscapularis tendon may occur in overhead-throwing athletes, particularly within the inferior half at the myotendinous junction. These patients present with axillary pain and loss of internal rotation and on MR increased fluid signal can be seen within the inferior subscapularis muscle with associated discontinuity of the myotendinous junction (Lin et al. 2018).

5 MR Imaging and Rotator Cuff Injuries

Repetitive supraphysiological strains combined with internal impingement make overhead athletes prone to rotator cuff pathology. Nonoperative management remains the main treatment option for most overhead athletes. Although techniques in imaging and surgical procedures in rotator cuff pathology have markedly improved over the years, not all patients will return to their pre-injury level of sports. The most common MR finding in the athlete with complaints of mild impingement pain is a normal cuff (Tuite 2003). In contrast, abnormal MR imaging findings are frequently encountered in shoulders of throwing athletes, due to highly repetitive stress and loads of the joints; however these findings do not necessarily indicate pathologic symptoms (Aoyama et al. 2019). In a study among professional handball players abnormal findings were encountered in 93%, and only 37% were symptomatic (Jost et al. 2005). Only players with simultaneous MRI abnormalities of all three cuff tendons were more frequently symptomatic.

Partial rotator cuff lesions, posterosuperior glenoid impingement, and superolateral osteochondral defects with cyst formation and edema were most frequently identified in those throwing shoulders (Connor et al. 2003; Jost et al. 2005; Miniaci et al. 2002). Knowledge of these signal changes of the rotator cuff in athletes may assist in differentiation between pathologic and non-pathologic findings, but correlation with physical examination is always pivotal (Connor et al. 2003; Jost et al. 2005). In another study, no significant signal differences were found in supra- and infraspinatus tendons between throwing and non-throwing athletes (Miniaci et al. 2002). Moreover, abnormal MRI signals can also be found in asymptomatic nonathletic shoulders in up to 30%, with an increase of incidence with age (Miniaci et al. 2002; Sanders and Miller 2005).

In the spectrum of cuff abnormalities, tendinopathy or tendinosis is defined as the presence of intermediate-to-high signal intensity on intermediate- or T2-weighted sequences not equal to water within the otherwise low SI substance of the tendon, frequently but not always accompanied with mild-to-moderate thickening of the tendon (Fritz 2002) (Fig. 13). Degeneration of the rotator cuff becomes more common with age and may be primarily caused by intrinsic factors, such as diminished vascularity, overuse, and failure of the normal healing response within the tendon. Tendinosis is common in the supraspinatus tendon near the humeral attachment of the tendon. When the tendon is morphologically normal, it may not be possible to differentiate

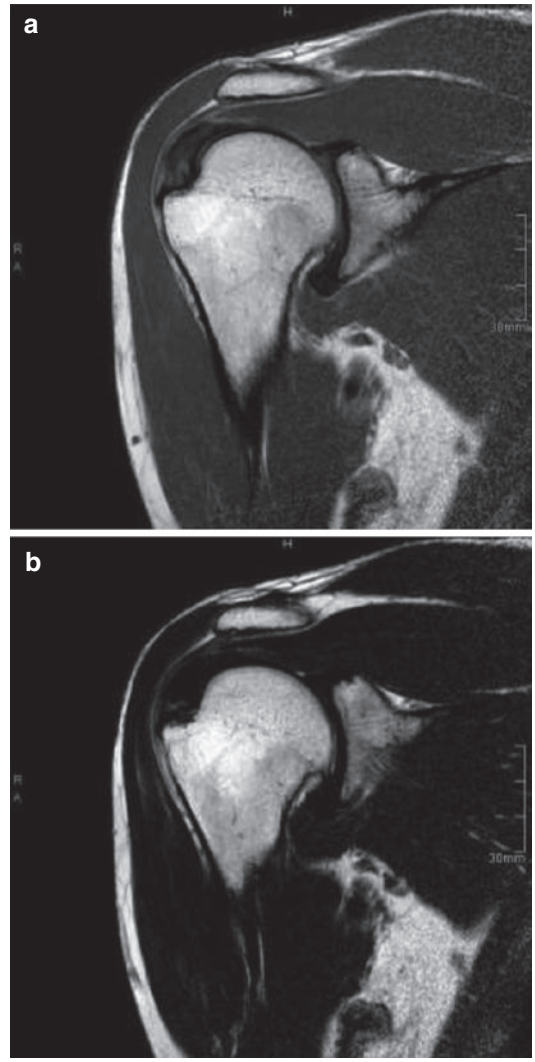

Fig. 13 (**a**, **b**) Tendinosis of supraspinatus tendon. Coronal PD-weighted TSE (**a**) and T2-weighted TSE (**b**) MR images. There is increased thickness of the tendon with focal increased signal intensity not equal to water

tendinosis from signal alterations due to magic angle effect or partial volume averaging of signal from adjacent soft tissues on short echo time (TE) images. Persistence of abnormal signal on long TE images is a stronger indicator for tendinosis (Fritz 2002). In the more severe cases, fissures, edema, and myxoid changes may develop within the tendon substance with associated MR findings including fluid-signal fissures, intrinsic high signal intensity not equal to water within the cuff, and/or swelling of the cuff (Fig. 10).

In calcifying tendinosis calcific deposits can be appreciated either within the rotator cuff or in the bursa or periarticular ligaments. These calcifications are best seen either on plain radiographs or by US (Fig. 14). On MR imaging, the calcific deposits demonstrate as foci of low SI on both T1- and T2-weighted sequences, and are most conspicuous on gradient-echo T2*-weighted images (Fig. 15). Calcifying tendinosis most commonly affects the supraspinatus tendon. Commonly, there is associated thickening of the tendon and reactive inflammation of the bursal soft tissues. It should be noticed that increased signal intensity changes on T2-weighted images of the peribursal fat plane may also be present in the normal asymptomatic population. Superimposed tears of the rotator cuff are not typically encountered.

In general, sensitivity and specificity numbers of MR imaging in the detection of rotator cuff tears are in the range of 88–100% (Hodler et al. 1992; Meister et al. 2003; Quinn et al. 1995). Correct identification of rotator cuff tearing in the young athletic individual by conventional MRI can be difficult since these tears are usually small and shallow and may not appear as the classic fluid-filled high SI defects on T2-weighted images. Moreover, tears can be found in more atypical locations (Tuite 2003).

Partial-thickness tears extend by definition partially through the thickness of the tendon in the superior-inferior direction, either on the articular or on the bursal surface. Moreover, interstitial partial tears can be encountered. Irregularity

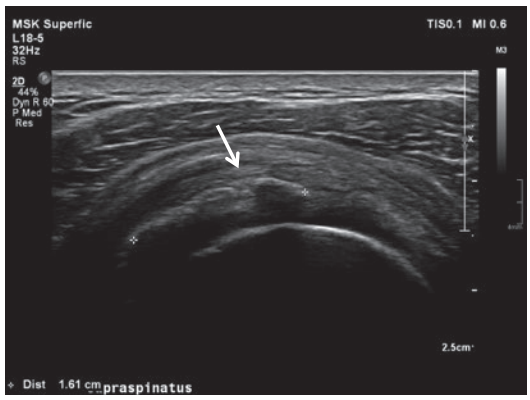

Fig. 14 Calcifying tendinosis. Ultrasound image reveals calcium deposits (*arrow*) in more posterior part of supraspinatus tendon

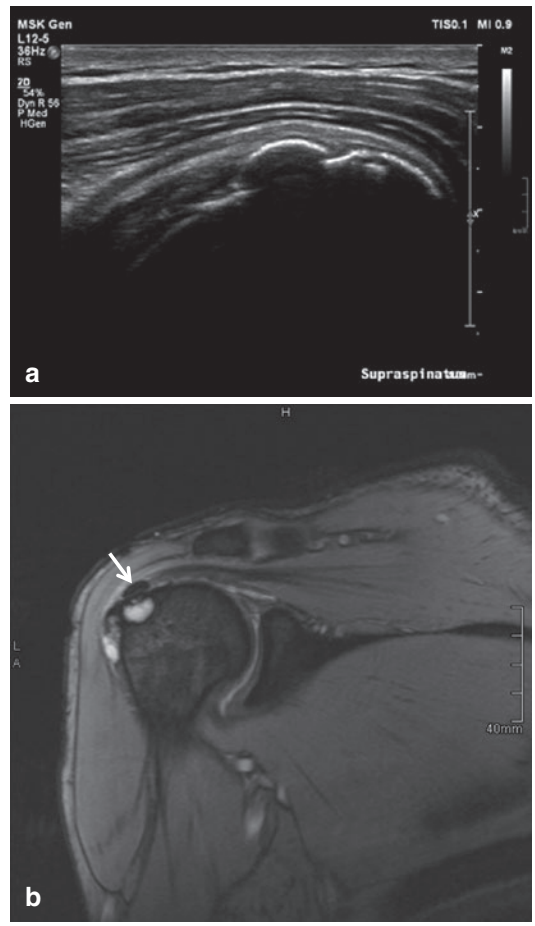

Fig. 15 (**a**, **b**) Calcifying tendinosis. Ultrasound image (**a**) reveals calcium deposit in the distal supraspinatus tendon, confirmed by low-signal-intensity focus (*arrow*) on coronal gradient-echo MR image (**b**), accompanied by high-signal-intensity humeral head cyst

and thinning or thickening of the tendon are other findings suggestive of a partial-thickness tear (Box 5). In the group of athletes, these types of tears are most frequently encountered (Tirman et al. 2004; Lin et al. 2018).

Box 5: MR Spectrum of Rotator Cuff Abnormalities

- Tendinosis: intermediate or high SI on PD or T2-weighted images, not equal to water with mild-to-moderate tendon thickening
- Partial-thickness tear: Partial defect with SI equal to water on fluid-sensitive sequences on articular side or bursal side, with or without thinning or thickening of tendon
- Full-thickness tears: Fluid-filled gap through the entire thickness of tendon from articular side to bursal side, with or without retraction of tendon, with or without muscle atrophy and/or fatty infiltration

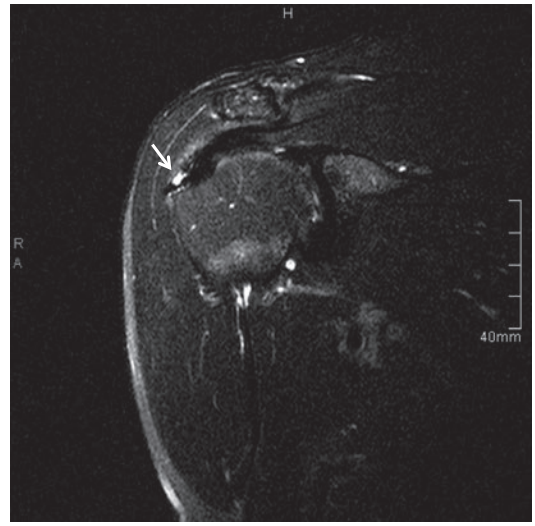

Fig. 16 Partial-thickness tear, bursal side of supraspinatus tendon. Coronal T2-weighted fat-saturated MR image displays small gap (*arrow*) with fluid intensity at bursal side, increased thickness of tendon, and some bursal reaction

The high tensile strength of the tendons in young athletes makes the cuff resistant to extensive tearing. On T2-weighted images, a partial-thickness tear is represented by high SI, equal to water, which is the hallmark of a rotator cuff tear. Fluid that extends in a discrete defect of the bursal surface is found in bursal surface partial tears (Fig. 16). However, the most frequent locations of rotator cuff tears in athletes are the critical zone in the anterior half of the supraspinatus tendon at 0.5–1 cm from the insertion, the undersurface area of the cuff attachment to the humerus (referred to as rim-rent tears), and posterosuperior supraspinatus and anterior infraspinatus tears at 0.5–1 cm from the insertion site, particularly in overhead-throwing athletes (Tirman et al. 2004; Tuite 2003; Lin et al. 2018). The higher incidence of articular surface tears compared with bursal side tears is related to the eccentric forces on the cuff that are greater on the articular side in athletes. Moreover, the articular side fibers are weaker and healing after injury is diminished due to less vascularization. On native MR images, partial tears are best demonstrated on oblique coronal images, in particular on combined proton density- and T2-weighted images with and without fat suppression (Fig. 17).

MR arthrography with fat suppression including coronal sequence (Fig. 18) and images in the abduction-exorotation stress position (ABER) allows detection of even small partial tears and delamination on the articular surface of the spinatus tendons and is strongly advocated by many authors (Hodler et al. 1992; Magee et al. 2004; Meister et al. 2003; Palmer et al. 1993; Sanders and Miller 2005; Tirman et al. 1994a, b; Tuite 2003; Schreinemachers et al. 2009; Lin et al. 2018). In the ABER position, the posterosuperior cuff is relaxed whereas simultaneously the anteroinferior labroligamentous complex is stressed. Analysis of the ABER images in (throwing) athletes should be focused on the posterosuperior articular surface side, which is a predilection site for small partial-thickness tears (Fig. 12). Both the vertical and horizontal (interstitial) components of a tear can be evaluated (Lee and Lee 2002). Folds that may appear when the cuff is not under tension

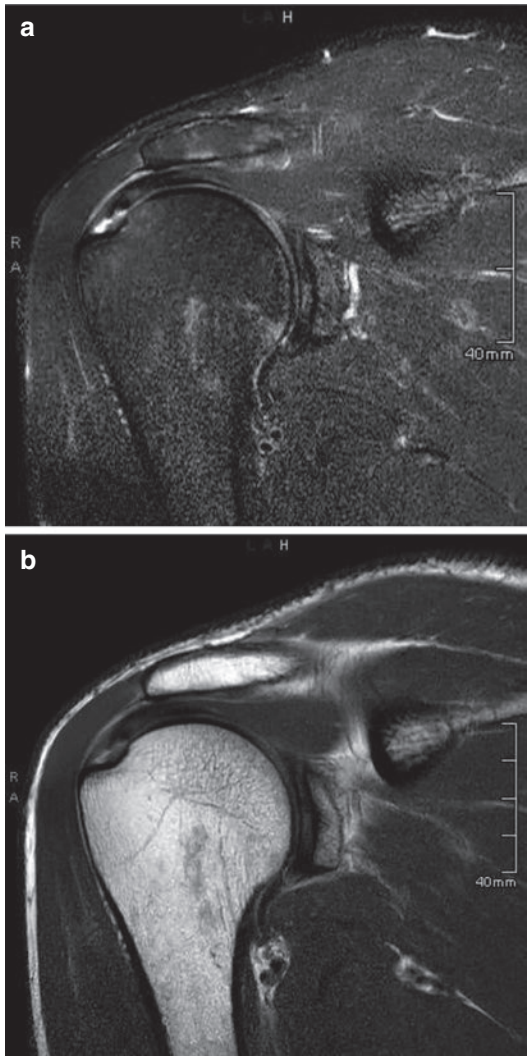

Fig. 17 (**a**, **b**) Partial-thickness tear supraspinatus tendon. Coronal T2-weighted fat-suppressed (**a**) and PD-weighted (**b**) MR images show increased signal intensity at articular side of distal tendon but no complete discontinuity

should not be misinterpreted as tears (Fig. 19). Tears of the posterosuperior glenoid labrum are not uncommonly demonstrated in association with articular surface partial tears at the junction of the supra- and infraspinatus tendon.

Partial-thickness tears, if untreated, can evolve to full-thickness tears (Fig. 18) and finally to complete tears. Therefore, although treatment of impingement pain usually starts with physical therapy, athletes with small partial tears may

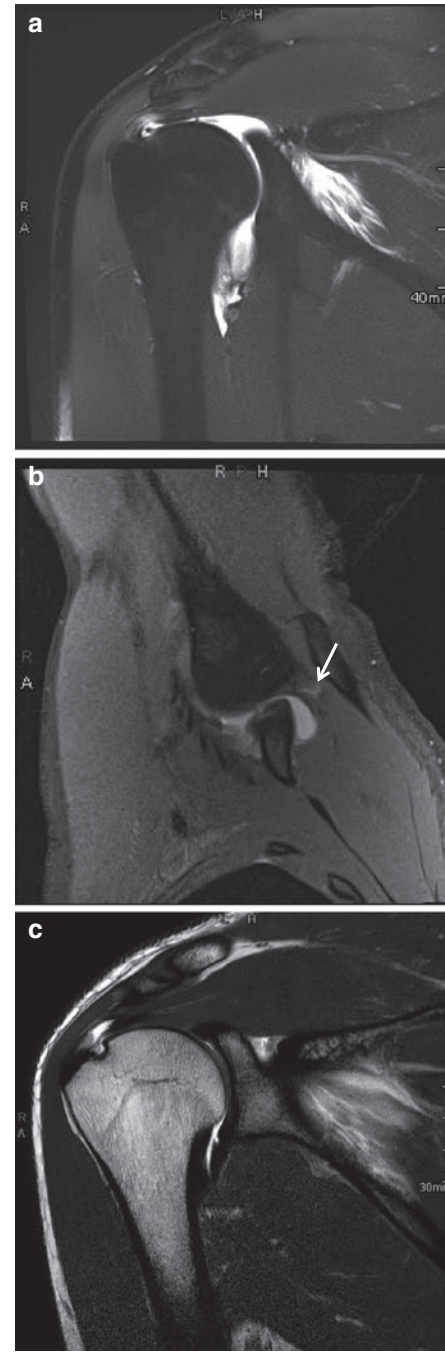

Fig. 18 (**a**–**c**) Partial-thickness tear of supraspinatus tendon in elite handball player. Coronal T1-weighted fat-saturated (**a**) MR arthrography and ABER view (**b**) show small articular sided defect at the distal tendon (*white arrow*). Coronal PD-weighted MR arthrogram after 3 years (**c**) demonstrates extension to small full-thickness tear

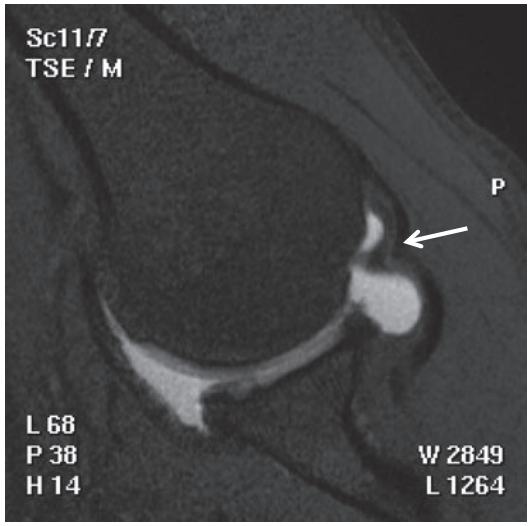

Fig. 19 Relaxation of supraspinatus tendon. T1-weighted fat-suppressed MR arthrogram, ABER view, shows relaxation of posterosuperior supraspinatus tendon (*arrow*), which should not be misinterpreted as a partial tear

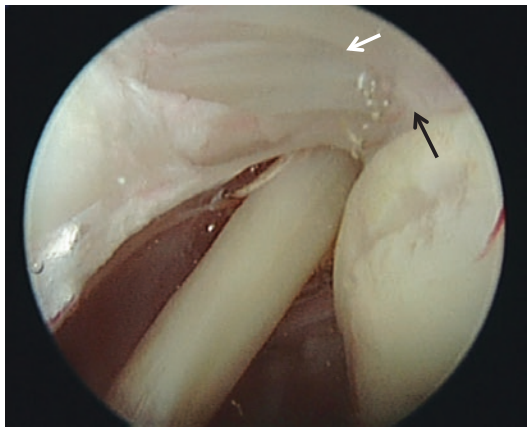

Fig. 20 Partial-thickness rotator cuff tear. Arthroscopic image of right shoulder demonstrates partial thickness under surface tear (*white arrow*) of supraspinatus, posterior to biceps tendon, leaving a small area of the footprint uncovered (*black arrow*)

benefit from arthroscopic debridement to become pain free (Fig. 20) (Payne et al. 1997). Although arthroscopic debridement in the general population has been reported to be successful, widely ranging outcome may be expected in overhead athletes. Return to sport may be possible, but return to pre-injury level is mostly not more than 50% of cases (Reynolds et al. 2008; Brockmeijer et al. 2008). Reporting on the extent of the tendon involvement is important as in patients demonstrating partial-thickness tears with >50% of tendon involvement a repair should be considered as opposed to debridement (when extensive nonsurgical management has failed) (Shaffer and Huttman 2014; Lin et al. 2018). Due to the risk of overconstraining the joint, some surgeons prefer repair in >75% of tendon involvement. The eventual decision to operate is influenced by the patient's age and coexisting pathology.

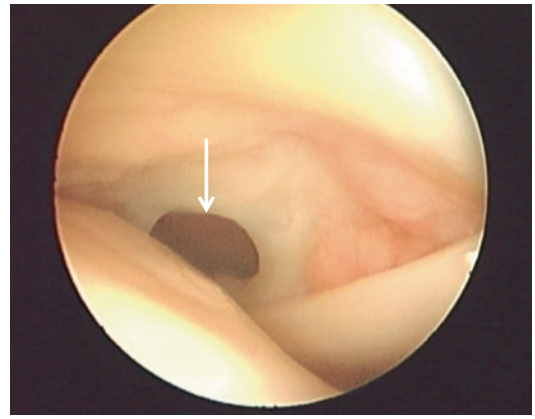

Fig. 21 Full-thickness rotator cuff tear. Arthroscopic image of left shoulder displays small full-thickness tear of supraspinatus tendon (*arrow*), adjacent to biceps tendon. On the left side humeral head is appreciated

Full-thickness tears are lesions that extend through the entire thickness of the tendon in superior-inferior direction (Fig. 21). In case of a complete tear, there is also full extension in the anterior-posterior direction. Oblique coronal T2-weighted images may reveal a gap filled with high SI of fluid and there may be attraction of the involved tendon (Fig. 3) (Box 5). Some tears do not show fluid signal intensity due to tendon debris or granulation tissue. In equivocal cases, when a typical fluid-filled gap is not present, additional MR arthrography can be useful (Fig. 22). Full-thickness tears can be characterized on the basis of location and size. The latter

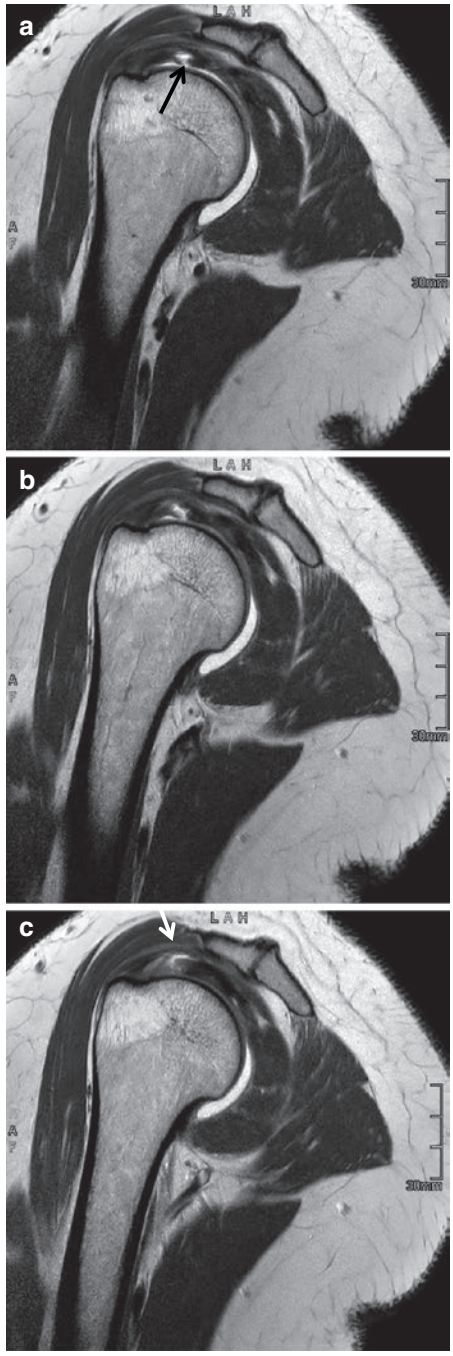

Fig. 22 (**a**–**c**) Combined partial- and full-thickness tear of supraspinatus tendon. Double-oblique coronal PD-weighted MR images with intra-articular contrast (**a**, **b**) demonstrate partial tear at articular side (*black arrow*), focally full thickness (*white arrow*) extending to subacromial space (**c**)

factor, expressed in both the anteroposterior and mediolateral dimensions, appears to have the highest clinical significance regarding outcome and prognosis (Gartsman and Milne 1995). MR reports should thus ideally include the exact site and extension of the tear, estimated size of the gap, involvement of different tendons and rotator interval, and secondary characteristics such as retraction of the tendon, muscle atrophy, and fatty infiltration (Morag et al. 2006). The rate of fatty atrophy of the rotator cuff muscles can be scored on sagittal images and graded using a modified classification based on CT (Goutallier et al. 1994; Fuchs et al. 1999): minor: streaks of fat within the muscle, moderate: more remnant muscle tissue than fat, and marked: more fat than muscle. Rotator cuff repair should be performed before the appearance of fatty infiltration and atrophy, especially when the tear involves more than one tendon (Melis et al. 2010) (Fig. 23).

Full-thickness tears are most commonly appreciated in the distal anterior part of the supraspinatus tendon. Larger tears may extend posteriorly to involve the entire attachment of the supraspinatus and further extension may involve the infraspinatus tendon posteriorly or the rotator interval capsule with the long head of the biceps tendon and subscapularis tendon anteriorly. Isolated tears of the infraspinatus tendon are unusual, but may be encountered in young overhead-throwing athletes (Tirman et al. 1994a, b, 2004) or in view of a posterosuperior impingement syndrome. The teres minor is typically spared in an otherwise complete ruptured rotator cuff. Incidentally, teres minor tears can be shown after posterior dislocation with injury of the posterior capsule. Isolated tears of the subscapularis are also uncommon, but can be seen after acute abduction and exorotation trauma (Fig. 24) (Deutsch et al. 1997). Axial and oblique sagittal MR images are optimal to assess partial and complete subscapularis tears, and also to determine or exclude injury or (sub)luxation of the biceps tendon, which is quite often seen in association with subscapularis tears (Fig. 25). Young patients with isolated traumatic tears of the subscapularis

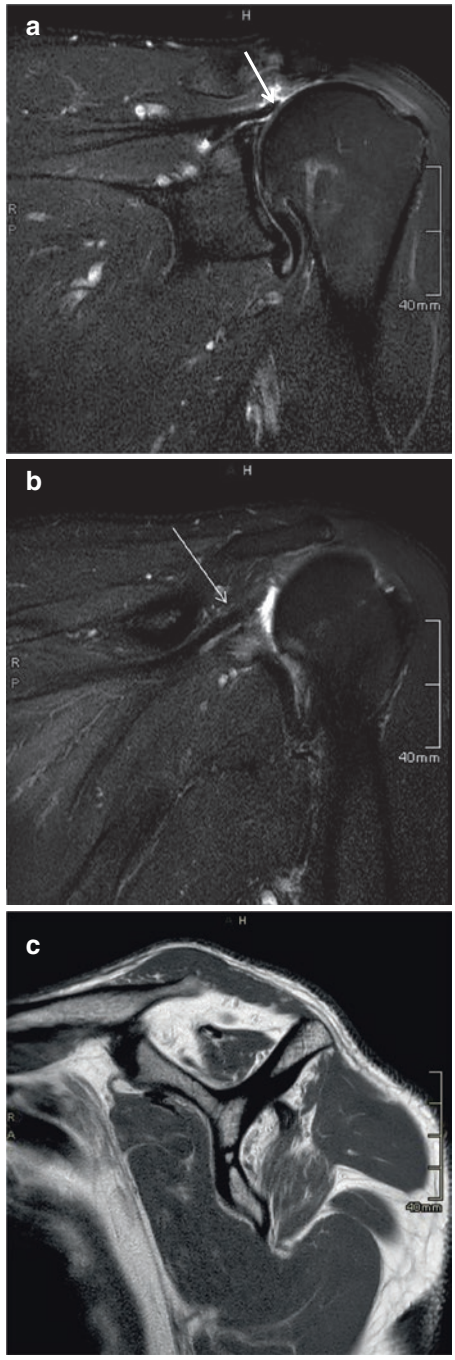

Fig. 23 (**a**–**c**) Complete full-thickness tear of supra- and infraspinatus tendon. Coronal T2-weighted fat-suppressed MR images display retracted tendons of supraspinatus (*arrow*) (**a**) and infraspinatus (*thin arrow*) (**b**). The subacromial space is decreased. Oblique sagittal PD-weighted image (**c**) shows atrophy of both supra- and infraspinatus muscles

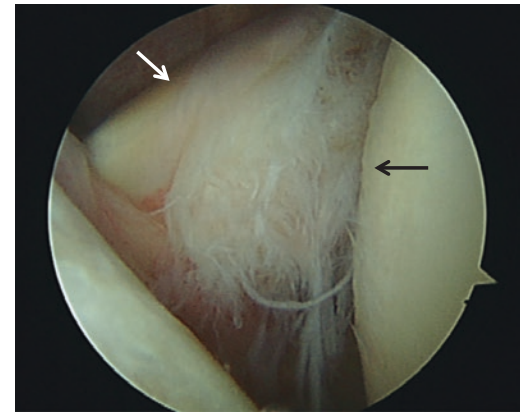

Fig. 24 Partial tear of subscapularis tendon. Arthroscopic image of right shoulder demonstrates intra-articular part of subscapularis tendon (*white arrow*), which is partly detached from insertion at humeral head (*black arrow*). On the left, the glenoid surface is appreciated

tendon and immediate repair have the best prognostic factors for treatment (Kreuz et al. 2006; Liem et al. 2008).

Involvement of both the supra- and infraspinatus as well as (portions of) the subscapularis may eventually lead to a high-riding humeral head within the glenohumeral joint, in close relation to the undersurface of the acromion.

6 Ultrasonography and Rotator Cuff Injuries

The ultrasonographic appearance of tendinosis is a focal or diffuse heterogeneous, ill-defined hypoechoic (sometimes hyperechoic) tendon with increased size (Fig. 26) (Bachmann et al. 1997; Jacobson et al. 2004). Sometimes in tendinosis the size of the tendon may be unaltered, but will show increased signal on T2-weigted MR images, which makes MR more sensitive for assessment of tendinosis.

In calcifying tendinitis, hydroxyapatite crystal depositions can be appreciated as hyperechoic foci within the rotator cuff, most commonly in the supraspinatus tendon (Fig. 14). It is a common finding in patients with shoulder pain, usually affecting people aged between 30 and

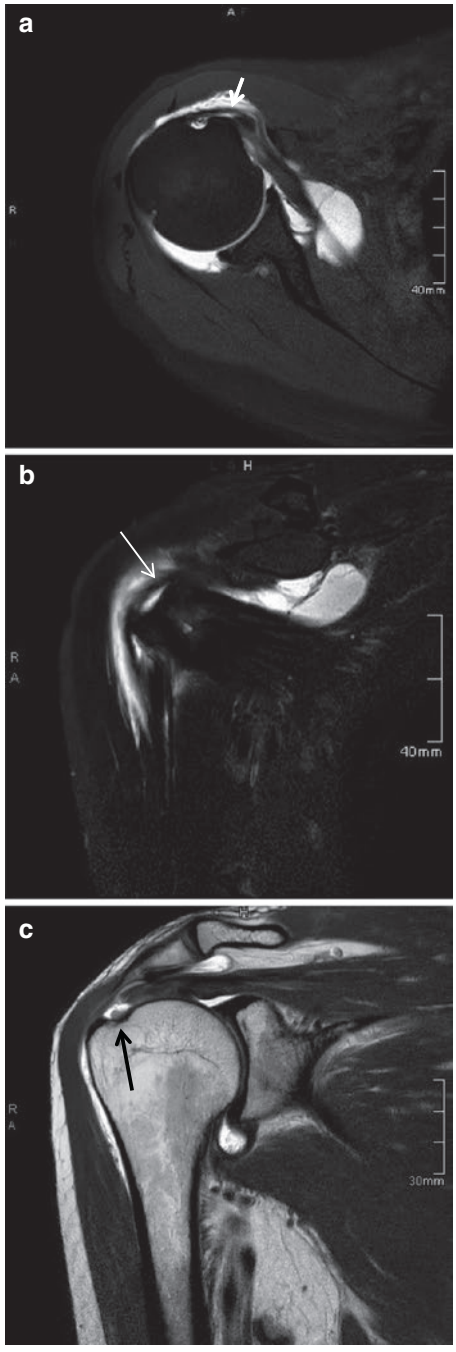

Fig. 25 (**a**–**c**) Partial-thickness tear of subscapularis with full-thickness tear of supraspinatus tendon. MR arthrography with axial T1-weighted fat-suppressed (**a**) and coronal T2-weighted fat-suppressed (**b**) and PD-weighted (**c**) TSE MR images. There is a partial lesion of subscapularis tendon (*thin arrow*) with medial dislocation of biceps tendon (*arrow*) within subscapularis tendon and fluid-filled gap (*black arrow*) at distal insertion of supraspinatus tendon and contrast extending into subdeltoid space

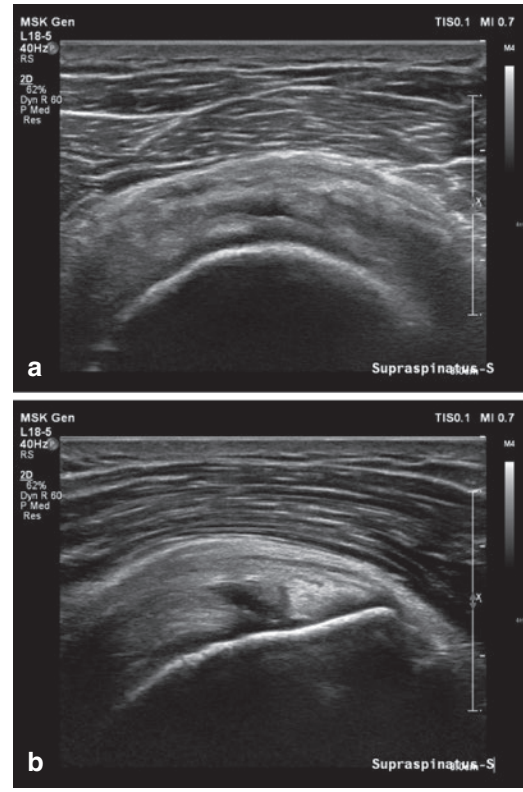

Fig. 26 (**a**, **b**) Tendinosis with partial-thickness tear of supraspinatus tendon. Transverse (**a**) and longitudinal (**b**) ultrasound images show inhomogeneous thickened supraspinatus tendon with articular sided hypoechoic defect

50 years. Although it appears to be a self-limiting disease, symptoms can be severe and long-lasting. Ultrasound-guided barbotage, combined with subacromial infiltration with corticosteroids, is the preferred treatment in patients who do not respond to more conservative treatment (De Witte et al. 2013; Louwerens et al. 2016).

The established criteria of a partial-thickness tear using US are a hypoechoic, anechoic, or a mixed hypo- and hyperechoic area and/or discontinuity of the fibrillar pattern (Rutten et al. 2006) (Figs. 26 and 27) (Box 6). The hypoechogenicity of the tear is based upon filling of the tear with fluid or edema. Some larger partial-thickness tears of the bursal surface may demonstrate flattening under compression. Tiny tears can be easily overlooked, whereas on the other hand an extensive partial-thickness tear can be mistaken for a complete full-thickness tear without

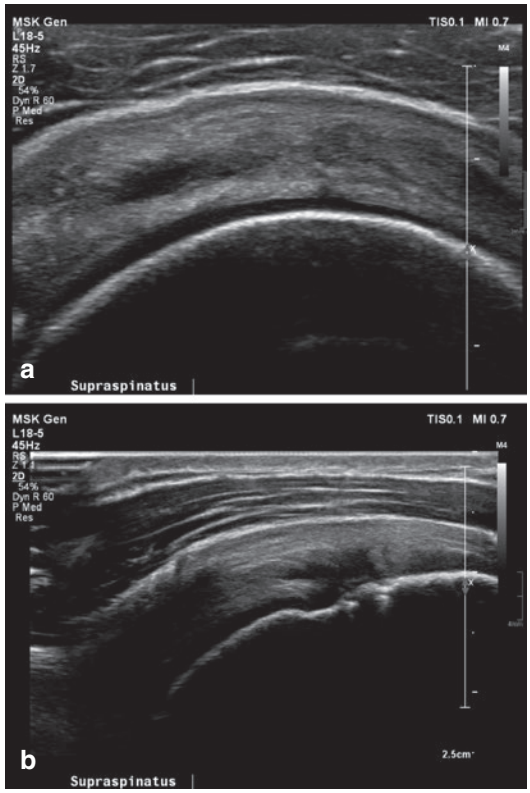

Fig. 27 (**a**, **b**) Partial-thickness tear of supraspinatus tendon. Transverse (**a**) and longitudinal (**b**) ultrasound images demonstrate some irregularity of cortical bone near the insertion of the tendon with hypoechoic defect at articular side

Box 6: Ultrasonographic Criteria for Rotator Cuff Abnormalities

- Tendinosis: Ill-defined heterogeneous hypo- and sometimes hyperechoic area within tendon, with or without increased tendon size, with or without irregularity of osseous footprint
- Partial-thickness tear: Hypoechoic, anechoic, or a mixed hypo- and hyperechoic tendon area and/or partial discontinuity of the fibrillar pattern
- Full-thickness tear: Non-visualization of tendon substance, fluid-filled (hypoechoic) gap, abnormal tendon echogenicity, tendon flattening with or without fluid in joint and/or bursa

retraction. The combination of tendinosis and anisotropy appears to be the most common cause of a false-positive diagnosis of a partial-thickness cuff tear (Rutten et al. 2006). Moreover, the filling of a partial defect by granulation or synovial tissue on the articular or bursal side may hamper the assessment of a partial-thickness tear (Rutten et al. 2006).

The sensitivity and specificity figures for detection of partial tears using US are operator dependent and vary from, respectively, 41% to 93% and from 76% to 94% (Brenneke and Morgan 1992; Farin and Jaroma 1995; Read and Perko 1998; Teefey et al. 2000; Van Holsbeeck et al. 1995; Wiener and Seitz 1993; Smith et al. 2011). The highest accuracy rates for detection of partial cuff tears, although dependent on tear size, were obtained in studies with experienced examiners (Teefey et al. 2004, 2005; Van Holsbeeck et al. 1995; Winter et al. 2001).

Secondary findings that may be encountered with partial-thickness tears include arthritic signs in up to 50–71% of patients, joint effusion in 13–19% but reserved to articular sided partial-thickness tears, and subacromial-subdeltoid bursal effusion in 20% of patients (established as an amount of fluid greater than 2 mm) (Arslan et al. 1999; Hollister et al. 1995; Jacobson et al. 2004; Van Holsbeeck and Strouse 1993; Van Holsbeeck et al. 1995). Moreover, Jacobson et al. established subacromial-subdeltoid bursal effusion in more symptomatic patients without presence of a tear than with a partial-thickness tear (Jacobson et al. 2004).

The highest sensitivity and positive predictive values were observed for focal hypoechoic abnormalities within the tendon. The highest specificity, negative predictive values, and accuracy were established for non-visualization of the tendon since this finding is exclusively correlated with full-thickness tears.

US has been reported to have high accuracy for the detection of full-thickness tears, even in non-experienced hands (Moosmayer and Smith 2005; Smith et al. 2011; Rutten et al. 2006) with sensitivity and specificity values ranging from 57% to 100% and 76% to 100%, respectively (Bachmann et al. 1997; Brenneke and Morgan 1992; Crass et al. 1988a; Hodler et al. 1988; Miller et al. 1989;

Paavolainen and Ahovuo 1994; Read and Perko 1998; Teefey et al. 2004; Vick and Bell 1990; Wiener and Seitz 1993; Smith et al. 2011; De Jesus et al. 2009; Roy et al. 2015; Nazarian et al. 2013; Lenza et al. 2013). The appearance of such tears can be variable: non-visualization of tendon substance based on full retraction in 24–50%, abnormal tendon echogenicity in 25–56% of patients, and tendon flattening in 71% of patients (Bachmann et al. 1997; Jacobson et al. 2004; Teefey et al. 1999, 2005; Wiener and Seitz 1993). To increase the efficacy of US, the transducer should be compressed on the shoulder structures. The deltoid muscle or the peribursal fat may be compressed within the defect or flatten the supraspinatus. Both ends of the teared but non-retracted tendon will separate and this facilitates visualization of the tear. Fully retracted tendon and the cartilage interface sign (seen as a small linear hyperechoic part lying over the hypoechoic cartilage) are findings exclusively observed in full-thickness tear (Jacobson et al. 2004).

In general, secondary findings that are frequently observed in full-thickness tears include arthritic signs in 86% of patients, joint effusion in 65% of patients, and subacromial-subdeltoid bursal effusion in 68% of patients (Arslan et al. 1999; Farin and Jaroma 1995; Jacobson et al. 2004; Teefey et al. 1999; Van Holsbeeck and Strouse 1993; Van Holsbeeck et al. 1994). Combined fluid in joint and subacromial-subdeltoid bursa raises the probability of a rotator cuff tear up to 95% (Hollister et al. 1995) (Box 6). Finding of a normal greater tuberosity was associated with absence of a rotator cuff tear in 96% (Wohlwend et al. 1998). The highest sensitivity, negative predictive value, and accuracy values were, respectively, observed for cortex irregularity (86%), bursal to articular surface abnormality (82%), and joint fluid (80%).

In patients in seated position, joint fluid will surround the long head of the biceps brachii tendon, since this is the lowest part of the articular joint. Effusion in the biceps sheath is probably closely related to the (limited) range of motion in patients with painful shoulders but is not a specific finding for a teared tendon or biceps tendovaginitis, as this may also be observed in patients with synovitis and adhesive capsulitis (Park et al. 2015). Dislocation or subluxation of the long head of the biceps brachii may return to normal position and therefore be undetected by MR imaging in contrast to dynamic US imaging. Disruption of the transverse humeral ligament may lead to subluxation or complete dislocation of the biceps tendon medially, even slide outside the biceps groove, and shift beneath the subscapularis tendon. The latter condition can only exist in case of complete subscapularis tendon disruption. Subscapularis tears may occur due to direct trauma (Fig. 28), forced exorotation, and

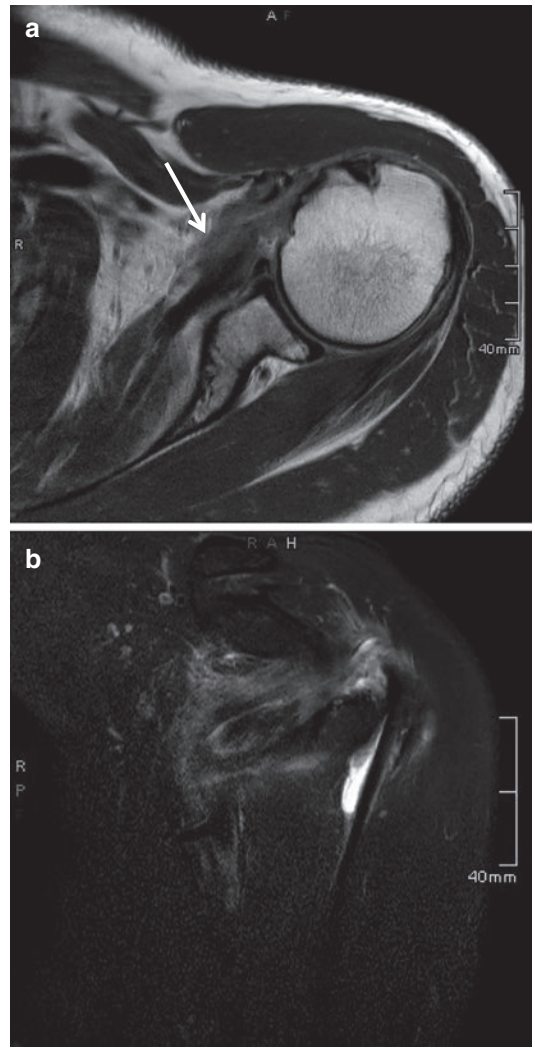

Fig. 28 (**a**, **b**) Subscapularis tear after direct trauma. Axial PD-weighted (**a**) TSE and coronal T2-weighted (**b**) fat-suppressed MR images. There is retraction of subscapularis tendon (arrow) anteriorly with peritendinous edema

abduction or in patients with recurrent anterior shoulder luxation but the incidence is significantly lower compared with supraspinatus tears. Small circumference subscapularis tears (less than 5 mm) or limited external rotation of the shoulder during examination may contribute to failure of interpretation. Diagnosis of a subscapularis tear is important because of the altered surgical approach (Teefey et al. 2005).

7 Rotator Interval and Biceps Tendon Injuries

The rotator interval is the anatomic space along the anterosuperior aspect of the shoulder between the supraspinatus and subscapularis prior to their fusion. Oblique sagittal MR images are the most important in analyzing the interval (Ho 1999). The interval is bridged by the rotator interval capsule, comprising the coracohumeral ligament (CHL), which extends from the coracoid posteriorly and laterally and merges with the capsule. The fused capsule and CHL further merge with the anterior margin and superficial and deep fascial fibers of the supraspinatus. The capsule and ligament together serve as a roof over the intra-articular course of the biceps tendon (Fig. 29). As

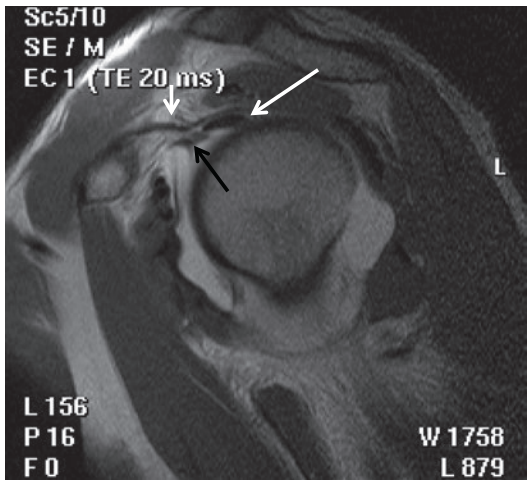

Fig. 29 Rotator cuff interval. Oblique sagittal T2-weighted TSE MR arthrogram showing the relationship of the CHL (*short white arrow*) to the intra-articular course of the biceps tendon (*long white arrow*), rotator interval capsule, and SGHL (*black arrow*)

such, the CHL together with the superior glenohumeral ligament, which is a focal thickening of the glenohumeral capsule, contributes to the stability of the long biceps tendon within the sulcus.

The many structures that are involved with and course through the rotator interval can be injured together. The interval and biceps tendon are stressed in the athlete who uses repetitive and/or forceful overhead motions. Also a fall on the outstretched hand may sprain or tear the rotator interval. The normal CHL should present as thin and smooth with low SI on oblique sagittal images. As a result of acute injuries such as traumatic tearing, the rotator interval and CHL may show thickening and irregularity with heterogeneous higher SI. With more chronic derangement, such as in repetitive overuse situations, irregular scarring of the rotator interval capsule and CHL may be seen (Ho 1999).

Prominent scarring of the CHL has also been thought to play a role in the clinical picture of an adhesive capsulitis. Besides thickening on the oblique sagittal images, one should be aware of synovitis within the rotator interval. Frequently, however, no specific MR abnormalities are noticed in patients with clinical symptoms of adhesive capsulitis (Sanders and Miller 2005).

The long tendon of the biceps extends from the superior glenoid tubercle or superior labrum, through the glenohumeral joint and rotator interval, and exits the joint anteriorly. Extra-articularly, the tendon is located within the intertubercular sulcus. The long head biceps tendon, together with the superior labrum, contributes to the prevention of superior displacement of the humeral head.

The spectrum of biceps tendon injuries includes tendinopathy, partial-thickness tear, complete disruption, and subluxation or dislocation of the extra-articular portion of the tendon (Sanders and Miller 2005). The extra-articular appearance of the biceps tendon is best evaluated on axial MR images. Tears of the long head of the biceps tendon are usually associated with supraspinatus pathology. Clinically, it can be difficult to differentiate partial biceps tendon tears from partial-thickness anterior supraspina-

tus tendon tears or tendinosis. In partial-thickness biceps tendon tears, fluid signal is appreciated within the tendon substance on fluid-sensitive MR sequences. Presence of two rather than one tendon slips, which is a normal variant, should not be misinterpreted as partial tearing. In complete tears of the long head biceps tendon, the tendon is absent or there is complete discontinuity.

Tearing most frequently occurs in the lateral intra-articular portion. In complete tears, the tendon is no longer visualized within the bicipital groove due to distal retraction of the muscle. A small proximal remnant at the biceps-labral anchor is frequently seen. Severe degeneration with thinning of the long biceps tendon may give rise to an apparently empty interval. An empty sulcus on the other hand can also exist without complete tear of the tendon, in case of medial dislocation. Intra-articular biceps tendon dislocation is usually associated with a full-thickness tear of the subscapularis tendon or rotator cuff interval injury, whereas extra-articular dislocation is associated with a partial-thickness tear of the subscapularis or tear of the transverse ligament (Sanders and Miller 2005).

8 Miscellaneous Conditions That May Mimic Rotator Cuff Pathology

MR imaging is also very useful to identify abnormalities that may mimic cuff lesions or labroligamentous lesions, including, among others, Parsonage-Turner syndrome, quadrilateral space syndrome, and spinoglenoid notch cyst (Helms 2002; Helms et al. 1998). Parsonage-Turner syndrome (acute brachial neuritis) is a self-limiting disorder, which presents with sudden onset of shoulder pain, sometimes bilateral, and accompanying weakness. MR imaging usually shows characteristic intramuscular denervating edema of rotator cuff muscles, most commonly supra- and infraspinatus (Fig. 30), and deltoid muscle (Scalf et al. 2007). In quadrilateral space syndrome, patients present with pain that may simulate cuff pathology, presumably due to (posttraumatic) scar tissue and fibrous band in the quadrilateral space that may cause impingement on the axillary nerve. Again, MR is rather typical demonstrating fatty atrophy of the teres minor muscle. A cyst in the spinoglenoid notch is usually associated with tearing of the posterior labrum (Fritz et al. 1992). The cyst or ganglion cannot be detected with arthroscopy, which stresses the role of MRI or US (Fig. 31). Due to

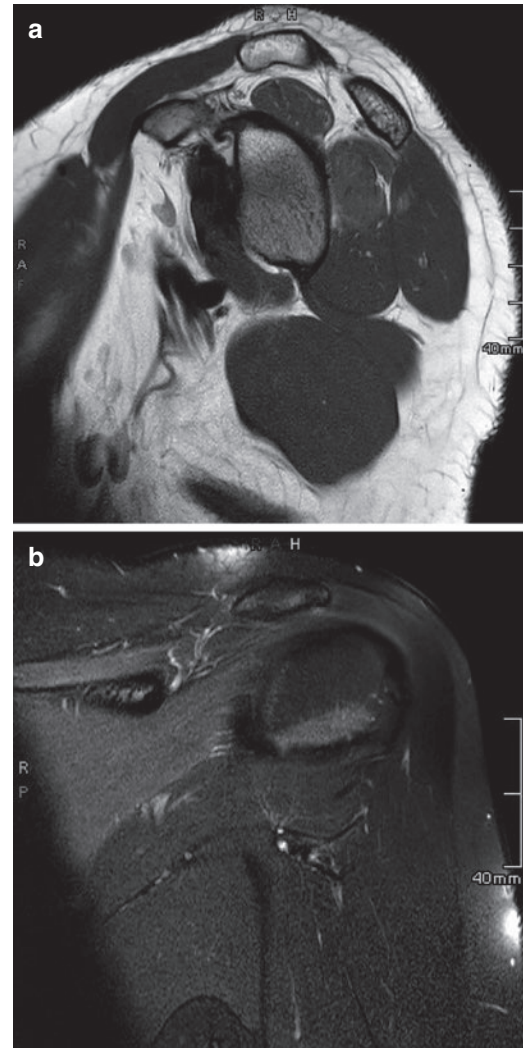

Fig. 30 (**a**, **b**) Parsonage-Turner syndrome. Oblique sagittal PD (**a**) and coronal T2-weighted fat-suppressed (**b**) images reveal mild atrophy and increased signal intensity of supra- and infraspinatus muscles

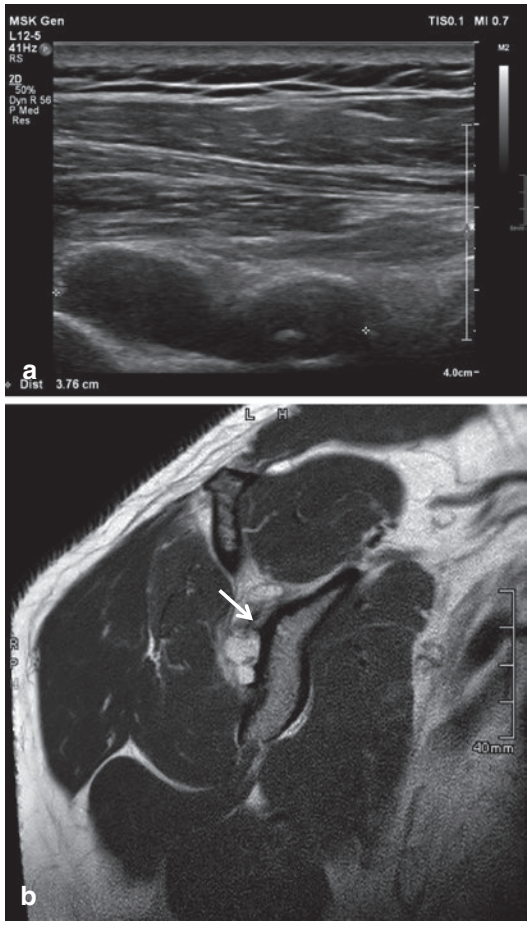

Fig. 31 (**a**, **b**) Spinoglenoidal notch cyst. Posterior US image (**a**) and oblique sagittal PD-weighted MR image (**b**) demonstrate lobulated cystic structure and relation to suprascapular nerve (*white arrow*)

compression on the suprascapular nerve, edema and atrophy of the infraspinatus muscle can be appreciated in fat-saturated T2-weighted MR images or US (Brys and Geusens 2020).

9 Conclusion

Shoulder pain due to trauma or overuse is a common complaint in the populations of athletes in general, with a variety of causes that are frequently difficult to differentiate by physical examination alone.

MR imaging and ultrasonography are optimal and complementary tools to discriminate different forms of impingement and to localize and classify rotator cuff injuries. Currently, considering accuracy, safety, and cost, US is the preferred imaging modality to start with, when rotator cuff pathology is expected.

A native MR imaging protocol including axial, oblique sagittal, and oblique coronal sequences is in general suitable for patients presenting with symptoms of impingement, and to assess full-thickness tears.

Partial-thickness rotator cuff tears are most commonly encountered in (overhead throwing) athletes, particularly on the articular side, which are best appreciated using MR arthrography including abduction-exorotation views.

Things to Remember

1. Rotator cuff and biceps-labral lesions secondary to trauma or overuse may be encountered simultaneously in athletes.
2. ABER views in an MR arthrography protocol are very helpful to detect small partial cuff tears on the articular side, besides the identification of non-displaced labroligamentous tears.
3. Most frequent locations of rotator cuff tears in athletes are the anterior half of the supraspinatus tendon at 0.5–1 cm from the insertion, undersurface area of the cuff attachment to the humerus, and posterosuperior tears at 0.5–1 cm from the insertion site.
4. Secondary extrinsic impingement is frequently encountered in throwing athletes. Usually, instability is minor and the coracoacromial outlet is morphologically normal.

References

Aoyama JT, Maier P, Servaes S et al (2019) MR imaging of the shoulder in youth baseball players: anatomy, pathophysiology and treatment. Clin Imaging 57:99–109

Arslan G, Apaydin A, Kabaalioglu A et al (1999) Sonographically detected subacromial/subdeltoid bursal effusion and biceps tendon sheath fluid: reliable signs of rotator cuff tear? J Clin Ultrasound 27:335–339

Bachmann GF, Melzer C, Heinrichs CM et al (1997) Diagnosis of rotator cuff lesions: comparison of

US and MRI on 38 joint specimens. Eur Radiol 7(2):192–197
Brenneke SL, Morgan CJ (1992) Evaluation of ultrasonography as a diagnostic technique in the assessment of rotator cuff tendon tears. Am J Sports Med 20:287–289
Brockmeijer SF, Dodson CC, Gamradt SC, Coleman S, Altchek DW (2008) Arthroscopic intratendinous repair of the delaminated partial-thickness rotator cuff tear in overhead athletes. Arthroscopy 24:961–965
Brys P, Geusens E (2020) Scapular, clavicular, acromioclavicular and sternoclavicular joint injuries. Med Radiol https://doi.org/10.1007/174_2020_250
Connor PM, Banks DM, Tyson AB et al (2003) Magnetic resonance imaging of the asymptomatic shoulder of overhead athletes: a 5-year follow-up study. Am J Sports Med 31:724–727
Crass JR, Craig EV, Feinberg SB (1988a) Ultrasonography of rotator cuff tears: a review of 500 diagnostic studies. J Clin Ultrasound 16(5):313–327
Crass JR, van de Vegte GL, Harkavy LA (1988b) Tendon echogenicity: ex vivo study. Radiology 167(2):499–501
De Jesus JO, Nazarian LN, Frangos AJ, Parker L (2009) Accuracy of MRI, MR arthrography and ultrasound in the diagnosis of rotator cuff tears: a meta-analysis. AJR Am J Roentgenol 192(6):1701–1707
De Witte P, Selten J, Navas A et al (2013) Calcific tendinitis of the rotator cuff. A randomized controlled trial of ultrasound-guided needling and lavage versus subacromial corticosteroids. Am J Sports Med 41: 1665–1673
Deutsch A, Altchek DW, Veltri DM et al (1997) Traumatic tears of the subscapularis tendon: clinical diagnosis, magnetic resonance imaging findings, and operative treatment. Am J Sports Med 25:13–22
Farin PU, Jaroma H (1995) Acute traumatic tears of the rotator cuff: value of sonography. Radiology 197(1):269–273
Farley F, Neumann C, Steinbach L et al (1994) The coracoacromial arch: MR evaluation and correlation with rotator cuff pathology. Skelet Radiol 23:641–645
Ferrari JD, Ferrari DA, Courmas J et al (1994) Posterior ossification of the shoulder: the Bennett lesion. Etiology, diagnosis and treatment. Am J Sports Med 22:171–176
Fritz RC (2002) Magnetic resonance imaging of sports-related injuries to the shoulder: impingement and rotator cuff. Radiol Clin N Am 40:217–234
Fritz RC, Helms CA, Steinbach LS et al (1992) Suprascapular nerve entrapment: evaluation with MR imaging. Radiology 182:437
Fuchs B, Weishaupt D, Zanetti M, Hodler J, Gerber C (1999) Fatty degeneration of the muscles of the rotator cuff: assessment by computed tomography versus magnetic resonance imaging. J Shoulder Elbow Surg 8:599–605
Gartsman GM, Milne JC (1995) Articular surface partial thickness tears of the rotator cuff. J Shoulder Elbow Surg 4:409–415
Goutallier D, Postel J, Bernageau J et al (1994) Fatty muscle degeneration in cuff ruptures: pre- and postoperative evaluation by CT scan. Clin Orthop Relat Res 304:78–83
Helms CA (2002) The impact of MR imaging in sports medicine. Radiology 224:631
Helms CA, Martinez S, Speer KP (1998) Acute brachial neuritis (Parsonage-Turner syndrome): MR imaging appearance-report of three cases. Radiology 207:255
Ho CP (1999) MR imaging of rotator interval, long biceps, and associated injuries in the overhead-throwing athlete. Magn Reson Imaging Clin N Am 7:23–37
Hodler J, Fretz CJ, Terrier F et al (1988) Rotator cuff tears: correlation of sonographic and surgical findings. Radiology 169:791–794
Hodler J, Kursunoglu-Brahme S, Snyder S et al (1992) Rotator cuff disease: assessment with MR arthrography versus standard MR imaging in 36 patients with arthroscopic confirmation. Radiology 182: 431–436
Hodler J, Loredo RA, Longo C et al (1995) Assessment of articular cartilage thickness of the humeral head: MR-anatomic correlation in cadavers. AJR Am J Roentgenol 165(3):615–620
Hollister MS, Mack LA, Patten RM et al (1995) Association of sonographically detected subacromial/subdeltoid bursal effusion and intraarticular fluid with rotator cuff tear. AJR Am J Roentgenol 165(3):605–608
Jacobson JA, Lancaster S, Prasad A et al (2004) Full-thickness and partial-thickness supraspinatus tendon tears: value of US signs in diagnosis. Radiology 230(1):234–242
Jbara M, Chen Q, Marten P et al (2005) Shoulder MR arthrography: how, why, when. Radiol Clin N Am 43(4):693–709
Jobe FW, Kvitne RS, Giangarra CE (1989) Shoulder pain in the overhand or throwing athlete: the relationship of anterior instability and rotator cuff impingement. Orthop Rev 18:963–975
Jost B, Zumstein M, Pfirrmann CW et al (2005) MRI findings in throwing shoulders—abnormalities in professional handball players. Clin Orthop Relat Res 434:130–137
Kreuz P, Remiger A, Erggelet C et al (2006) Isolated and combined tears of the subscapularis tendon. Am J Sports Med 33:1831–1837
Lee SY, Lee JK (2002) Horizontal component of partial-thickness tears of rotator cuff: imaging characteristics and comparison of ABER view with oblique coronal view at MR arthrography. Radiology 224:470–476
Lee MH, Sheehan SE, Orwin JF, Lee KS (2016) Comprehensive shoulder US examination: a standardized approach with multimodality correlation for common shoulder disease. Radiographics 36:1606–1627
Lenza M, Buchbinder R, Takwing Y et al (2013) Magnetic resonance imaging, magnetic resonance arthrography and ultrasonography for assessing rotator cuff tears in people with shoulder pain for whom surgery is being

considered (review). Cochrane Database Syst Rev 2013(9):CD009020
Liem D, Lichtenberg S, Magosch P, Habermeyer P (2008) Arthroscopic rotator cuff repair in overhead-throwing athletes. Am J Sports Med 36:1317–1322
Lin DJ, Wong TT, Kazan JK (2018) Shoulder injuries in the overhead-throwing athlete: epidemiology, mechanisms of injury and imaging findings. Radiology 286:370
Louwerens JK, Veltman ES, Van Noort A, Van den Bekerom MP (2016) The effectiveness of high-energy extracorporeal shockwave therapy versus ultrasound-guided needling versus arthroscopic surgery in the management of chronic calcific rotator cuff tendinopathy: a systematic review. Arthroscopy 32:165–175
Magee T, Williams D, Mani N (2004) Shoulder MR arthrography: which patient group benefits most? AJR Am J Roentgenol 183:969–974
Martinoli C, Derchi LE, Pastorino C et al (1993) Analysis of echotexture of tendons with US. Radiology 186(3):839–843
Meister K, Thesing J, Montgomery W et al (2003) MR arthrography of partial thickness tears of the undersurface of the rotator cuff: an arthroscopic correlation. Skelet Radiol 33:136–141
Melis B, DeFranco M, Chuinard C, Walch G (2010) Natural history of fatty infiltration and atrophy of the supraspinatus muscle in rotator cuff tears. Clin Orthop Relat Res 468:1498–1505
Middleton WD, Teefey SA, Yamaguchi K (2004) Sonography of the rotator cuff: analysis of interobserver variability. AJR Am J Roentgenol 183:1465–1468
Miller CL, Karasick D, Kurtz AB et al (1989) Limited sensitivity of ultrasound for the detection of rotator cuff tears. Skelet Radiol 18(3):179–183
Miniaci A, Mascia AT, Salonen DC et al (2002) Magnetic resonance imaging of the shoulder in asymptomatic professional baseball pitchers. Am J Sports Med 30:66–73
Moosmayer S, Smith HJ (2005) Diagnostic ultrasound of the shoulder-a method for experts only? Results from an orthopedic surgeon with relative inexpensive compared to operative findings. Acta Orthop 76:503–508
Morag Y, Jacobson J, Miller B (2006) Rotator cuff injury: what the clinician needs to know. Radiographics 26:1045–1065
Nazarian LN, Jacobson JA, Brenson CB et al (2013) Imaging algorithms for evaluating suspected rotator cuff disease: society of radiologists in ultrasound conference statement. Radiology 267:589–595
O'Connor PJ, Rankine J, Gibbon WW et al (2005) Interobserver variation in sonography of the painful shoulder. J Clin Ultrasound 33:53–56
Okoro T, Reddy V, Pimpelnarkar A (2009) Coracoid impingement syndrome: a literature review. Curr Rev Musculoskelet Med 2:51–55
Paavolainen P, Ahovuo J (1994) Ultrasonography and arthrography in the diagnosis of tears of the rotator cuff. J Bone Joint Surg Am 76:335–340
Palmer WE, Brown JH, Rosenthal DI (1993) Rotator cuff: evaluation with fat-suppressed MR arthrography. Radiology 188:683–687
Park JG, Lee JK, Phelps CT (1994) Os acromiale associated with rotator cuff impingement: MR imaging of the shoulder. Radiology 193:255–257
Park I, Lee H, Kim S (2015) Evaluation of the effusion within biceps long head tendon sheath using ultrasonography. Clin Orthop Surg 7:351–358
Payne LZ, Altcheck DW, Craig EV et al (1997) Arthroscopic treatment of partial rotator cuff tears in young athletes. Am J Sports Med 25: 299–305
Peh W, Farmer T, Totty W (1995) Acromial arch shape: assessment with MR imaging. Radiology 195: 501–505
Quinn SF, Sheley RC, Demlow TA et al (1995) Rotator cuff tendon tears: evaluation with fat-suppressed MR imaging with arthroscopic correlation in 100 patients. Radiology 195:497–500
Read JW, Perko M (1998) Shoulder ultrasound: diagnostic accuracy for impingement syndrome, rotator cuff tear, and biceps tendon pathology. J Shoulder Elbow Surg 7(3):264–271
Reynolds SB, Dugas JR, Cain EL, McMichael CS, Andrews JR (2008) Debridement of small partial thickness rotator cuff tears in elite overhead throwers. Clin Orthop Relat Res 466:614–621
Rose MB, Noonan T (2018) Glenohumeral internal rotation deficit in throwing athletes: current perspectives. Open Access J Sports Med 19:69–78
Roy J-S, Braën C, Leblond J et al (2015) Diagnostic accuracy of ultrasonography, MRI and MR arthrography in the characterisation of rotator cuff disorders: a systematic review and meta-analysis. Br J Sports Med 49:1316–1328
Rutten MJ, Jager GJ, Blickman JG (2006) US of the rotator cuff: pitfalls, limitations and artifacts. Radiographics 26:589–604
Rutten MJ, Jager GJ, Kiemeney LM (2010) Ultrasound detection of rotator cuff tears: observer agreement related to increasing experience. AJR Am J Roentgenol 195:440–446
Sanders TG, Miller MD (2005) A systematic approach to magnetic resonance imaging interpretation of sports medicine injuries of the shoulder. Am J Sports Med 33:1088–1105
Scalf RE, Wenger DE, Frick MA, Mandrekar JN, Adkins MC (2007) MRI findings of 26 patients with Parsonage-Turner syndrome. AJR Am J Roentgenol 189:39–44
Schreinemachers SA, van der Hulst VP, Willems WJ, Bipat S, Van der Woude HJ (2009) Detection of partial-thickness supraspinatus tendon tears: is a single direct MR arthrography series in ABER position as accurate as conventional MR arthrography? Skelet Radiol 38:967
Seibold CJ, Mallisee TA, Erickson SJ et al (1999) Rotator cuff: evaluation with US and MR imaging. Radiographics 19(3):685–705

Shaffer B, Huttman D (2014) Rotator cuff tears in the throwing athlete. Sports Med Arthrosc Rev 22:101–109

Smith T, Back T, Hing C (2011) Diagnostic accuracy of ultrasound for rotator cuff tears in adults: a systematic review and meta-analysis. Clin Radiol 66:1036–1048

Teefey SA, Middleton WD, Yamaguchi K (1999) Shoulder sonography. State of the art. Radiol Clin N Am 37(4):767–785

Teefey SA, Hasan SA, Middleton WD et al (2000) Ultrasonography of the rotator cuff. A comparison of ultrasonographic and arthroscopic findings in one hundred consecutive cases. J Bone Joint Surg Am 82:498–504

Teefey SA, Rubin DA, Middleton WD et al (2004) Detection and quantification of rotator cuff tears. Comparison of ultrasonographic, magnetic resonance imaging, and arthroscopic findings in seventy-one consecutive cases. J Bone Joint Surg Am 86(4):708–716

Teefey SA, Middleton WD, Payne WT (2005) Detection and measurement of rotator cuff tears with sonography: analysis of diagnostic errors. AJR Am J Roentgenol 184(6):1768–1773

Tirman PF, Bost FW, Garvin GJ et al (1994a) Posterosuperior glenoid impingement of the shoulder: findings at MR imaging and MR arthrography with arthroscopic correlation. Radiology 193: 431–436

Tirman PF, Bost FW, Steinbach LS et al (1994b) MR arthrographic depiction of tears of the rotator cuff: benefit of abduction and external rotation of the arm. Radiology 192:851–856

Tirman PF, Smith ED, Stoller DW et al (2004) Shoulder imaging in athletes. Semin Musculoskelet Radiol 8:29–40

Tuite MJ (2003) MR imaging of sports injuries to the rotator cuff. Magn Reson Imaging Clin N Am 11: 207–219

van Holsbeeck M, Strouse PJ (1993) Sonography of the shoulder: evaluation of the subacromial-subdeltoid bursa. AJR Am J Roentgenol 160(1):561–564

van Holsbeeck M, Introcaso JH, Kolowich PA (1994) Sonography of tendons: patterns of disease. Instr Course Lect 43:475–481

van Holsbeeck MT, Kolowich PA, Eyler WR et al (1995) US depiction of partial-thickness tear of the rotator cuff. Radiology 197:443–446

Van Kampen DA, Van den Berg T, Van der Woude HJ et al (2014) The diagnostic value of the combination of patient characteristics, history and clinical shoulder tests for the diagnosis of rotator cuff tear. J Orthop Surg Res 9:70

Vanhoenacker FM et al (2000) MR imaging of the shoulder: imaging techniques and anatomy. JBR-BTR 83:309–312

Vick CW, Bell SA (1990) Rotator cuff tears: diagnosis with sonography. AJR Am J Roentgenol 154(1): 121–123

Walch G, Boileau P, Noel E et al (1992) Impingement of the deep surface of the supraspinatus tendon on the posterosuperior glenoid rim: an arthroscopic study. J Shoulder Elbow Surg 1:238–245

Weiss LJ, Wang D, Hendel M, Buzzerio P, Rodeo SA (2018) Management of rotator cuff injuries in the elite athlete. Curr Rev Musculoskelet Med 11: 102–112

Wengert GJ, Schmutzer M, Bickel H et al (2019) Reliability of high-resolution ultrasound and magnetic resonance arthrography of the shoulder in patients with sports-related shoulder injuries. PLoS One 14(9):e0222783

Wiener SN, Seitz WHJ (1993) Sonography of the shoulder in patients with tears of the rotator cuff: accuracy and value for selecting surgical options. AJR Am J Roentgenol 160:103–107

Winter TC III, Teefey SA, Middleton WD (2001) Musculoskeletal ultrasound: an update. Radiol Clin N Am 39:465–483

Wohlwend JR, van Holsbeeck M, Craig J et al (1998) The association between irregular greater tuberosities and rotator cuff tears: a sonographic study. AJR Am J Roentgenol 171(1):229–233

Scapular, Clavicular, Acromioclavicular, and Sternoclavicular Joint Injuries

Peter Brys and Eric Geusens

Contents

Abstract

The chapter starts with a short overview of the relevant anatomy of bones and surrounding soft tissues. Most of an imaging part is focused on plain radiography discussing routine views as well as relevant special views, followed by the role of ultrasound, CT, MRI, bone scintigraphy, and SPECT-CT. The main part of the chapter is dedicated to specific overuse trauma, including typical overuse lesions of the immature skeleton. Discussed bony lesions are fractures, the rare stress fractures of scapula and clavicle, stress-related growth plate injury of the coracoid process and medial clavicle, lateral acromial apophysitis, and distal clavicular osteolysis. Joint pathology comprises acromioclavicular and sternoclavicular sprain or dislocation and AC joint osteoarthritis. Typical nerve pathologies of this anatomical area are the suprascapular nerve entrapment and the long thoracic neuropathy.

1 Introduction

1.1 Scapula

The scapula is a flat bone with three prominences, the spine and acromion, the glenoid, and the coracoid process. Medial to the base of the coracoid process is the *scapular notch* arched by the superior transverse scapular ligament. The

P. Brys (✉) · E. Geusens
Department of Radiology, University Hospitals Leuven, Leuven, Belgium
e-mail: peter.brys@uzleuven.be

Med Radiol Diagn Imaging (2020)
https://doi.org/10.1007/174_2020_250, © Springer Nature Switzerland AG
Published Online: 08 December 2020

spinoglenoid notch arched by the inferior transverse scapular ligament is situated between the lateral margin of the base of the scapular spine and the dorsal side of the glenoid. Both notches are important fixation points along the course of the *suprascapular nerve*.

1.2 Clavicle

The growth plates of the medial and lateral clavicular epiphyses do not fuse until the age of 25 years. The deltoid, trapezius, and pectoralis major muscles have important attachments to the clavicle. The deltoid muscle inserts onto the anterior surface of the lateral third of the clavicle, and the trapezius muscle onto the posterior aspect. The pectoralis major muscle inserts onto the anterior surface of the medial two thirds.

1.3 Acromioclavicular Joint

The synovium-lined AC joint has interposed between its fibrocartilaginous joint surfaces a fibrocartilaginous disc of variable size which is frequently completely absent (Wickiewicz 1983). The joint has a thin capsule, reinforced by the *AC ligaments* of which the superior one is continuous with the deltoid and trapezius aponeuroses. The lateral clavicle is anchored to the coracoid process by the *coracoclavicular ligament*, composed of the lateral *trapezoid* and medial *conoid* parts (Fig. 1). The static joint stabilizers are the AC ligaments, controlling the horizontal stability, and the CC ligament, controlling the vertical stability. The dynamic stabilizers are the deltoid and trapezius muscles. The trapezius muscle attaches at the dorsal aspect of the acromion, part of the anterior deltoid muscle inserts on the clavicle medial to the AC joint. Their force vectors prevent excessive superior migration of the distal clavicle after disruption of the AC and CC ligaments alone (Wulker 1998).

1.4 Sternoclavicular Joint

The synovium-lined SC joint is formed by the medial clavicle, the clavicular notch of the manubrium, and the cartilage of the first rib (Fig. 2). Interposed between the fibrocartilaginous joint surfaces is a usually complete fibrocartilaginous *disc*, which acts to reduce the incongruities between the articulating joint surfaces, and as a shock absorber against medial translation of the clavicle. The *anterior and posterior SC ligaments* are thickenings of the joint capsule. The *interclavicular ligament* connects the clavicles with the capsular ligaments and the upper sternum. The *costoclavicular or rhomboid ligament*

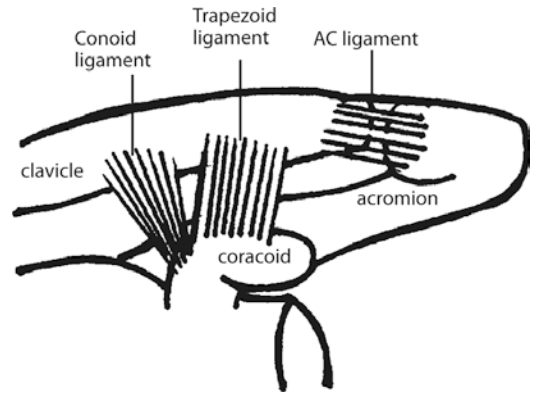

Fig. 1 Normal anatomy: the acromioclavicular and coracoclavicular ligament, the latter with its medial conoid and lateral trapezoid parts

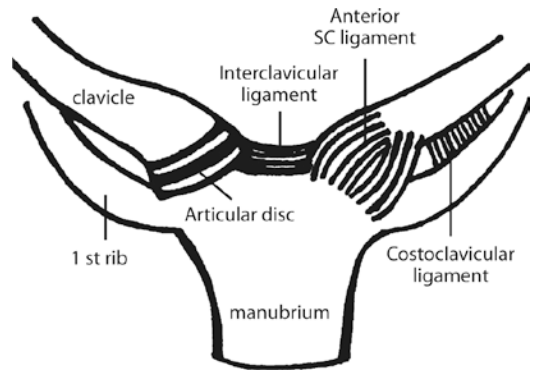

Fig. 2 Normal anatomy: the sternoclavicular joint

runs from the first rib to the rhomboid fossa at the inferior side of the medial clavicular metaphysis. This fossa should not be mistaken for a tumor when seen on radiographs. The SC joint is freely movable and functions almost like a ball-and-socket joint with motion in almost all planes, including rotation (Lucas 1973). The ligamentous support is so strong that it is one of the least commonly dislocated joints in the body (Wirth and Rockwood 1996).

2 Imaging

2.1 Plain Radiography

Diagnostic plain films are tailored to the clinical findings and should be of impeccable quality.

2.1.1 Scapula

Routine views of the scapula include the *AP view* abducting the arm 90° and the *lateral view or scapular Y.* The *axillary view*, which requires abduction of the arm, gives an excellent view on the anterior acromion, the glenoid, and the coracoid process. In case of a fractured coracoid process, the patient's pain usually precludes abduction. The fracture may be demonstrated with the so-called *modified axillary view* (Wallace and Hellier 1983).

2.1.2 Clavicle

The *Zanca view*, an anteroposterior projection with 15° of cephalic angulation, projects the lateral and most of the middle third of the clavicle free of overlying adjacent bones (Zanca 1971). Although not required on a routine base, visualization of the medial third of the clavicle is accomplished with 40° cephalic angulation (Wirth and Rockwood 1996).

2.1.3 AC Joint

The best view of the AC joint is the *Zanca view*. Imaging in case of an AC sprain will be discussed in its specific part 3.3.1.

2.1.4 SC Joint

Standard radiographic views of the SC joint include *posteroanterior and oblique views*. However, they are *often inadequate* due to overlap of the medial clavicle with the sternum, the first rib, and the spine. Special projections have been described to aid in the evaluation. Unless done by an experienced technologist these special views can be technically difficult to perform and interpret, limiting their utility and reproducibility (Brossmann et al. 1996).

- The *Rockwood projection*, also called the "serendipity view," is an anteroposterior projection obtained with 40° cephalic tilt, centered on the manubrium. The cassette is placed under the upper part of the shoulders and neck so that the clavicle is projected in the middle of the film. In an anterior dislocation, the affected clavicle is projected superior to the normal clavicle, and with posterior dislocation it is projected inferior to it (Rockwood and Wirth 1996). Other special views are currently replaced by CT.
- For first-line imaging special views might be replaced by *digital tomography* with a reduced radiation dose of 0.5 milliSievert (mSv), compared to 6.0 mSv for standard tomograms and 6.6 mSv for CT (Thyterleigh-Strong et al. 2019).
- *Stress manoeuver*: A reducible or intermittent SC dislocation can look misleadingly normal on a routine radiograph. A stress manoeuver helps to avoid this problem. This manoeuver is performed by bringing the ipsilateral arm across the chest and pulling against the contralateral elbow (Cope 1993).

2.2 Ultrasound

2.2.1 AC Joint

In a trauma setting, US can be used to confirm a grade 1 sprain, or in the assessment of the status of the surrounding musculature. In chronic disease, US allows the evaluation of capsular

distension and presence of soft tissue lesions like arthrosynovial cysts.

2.2.2 SC Joint

The role of US of the SC joint is limited. It can be used for the assessment of capsular bulging or the position of the joint surfaces in suspected dislocation, the latter if CT is not readily available.

2.3 CT

2.3.1 Scapula and Clavicle

With its excellent bony detail and its multiplanar and 3D reconstruction capabilities, modern multi-detector CT equipment is the imaging technique of choice in the evaluation of fractures and stress fractures.

2.3.2 SC Joint

CT is particularly valuable if a SC joint dislocation is suspected. It is recommended to *image both sides*, as comparison is often helpful in assessing the degree of abnormality. CT can be acquired in a neutral position alone or with the stress maneuver as described in the plain film section, which increases the sensitivity (Burnstein and Pozniak 1990; Cope 1993). If there is suspicion of secondary vascular compromise or impingement by a posterior dislocation, the study can be performed with IV contrast to allow optimal visualization of the adjacent vessels.

2.4 MRI

2.4.1 AC Joint

The role of MRI in isolated AC pathology is *not well established*. In addition to the findings visible on standard radiographs, soft tissue abnormalities (capsular hypertrophy, joint effusion, CC ligaments, muscular attachments) and subchondral bone marrow edema may be demonstrated. The coronal oblique plane best demonstrates the AC joint. The parasagittal plane roughly corresponds to the radiographic supraspinatus outlet view.

2.4.2 SC Joint

MRI is far superior to CT in its ability to define bone marrow abnormalities, disc- and cartilage injury, joint effusion, and to evaluate the extra-articular soft tissues. To allow appropriate evaluation of all involved structures, imaging in three orthogonal planes is recommended (Klein et al. 1997; Brossmann et al. 1996). There may be difficulty in obtaining good quality MR images of the SC joint: the small joint is poorly imaged with the body coil. In surface coil imaging both the applied coil and the SC joint move with patient breathing, causing severe artifact. Vascular pulsations and swallow also cause artifacts. This *difficulty in imaging*, combined with *most radiologist's limited experience* with SC joint imaging, and the availability of CT has prevented the emergence of MRI of the SC joint (Klein et al. 1997).

2.5 Scintigraphy

Bone scintigraphy is a very sensitive technique for detection of early changes related to osseous injuries. In the workup of patients with posttraumatic pain due to sports injuries, which is suspected to be of *osseous origin*, it is a *useful next diagnostic step when plain films are negative*. Examples of injury in which bone scintigraphy may be helpful are occult fractures, stress fractures or other stress-related injury, distal clavicular osteolysis, and symptomatic AC or SC osteoarthritis. SPECT-CT *increases the specificity,* providing better anatomical resolution of the images and exact localization of osteoarticular lesions. However, the key drawback of SPECT-CT is the exposure to *ionizing radiation*. Therefore the use of MRI is recommended in almost all cases that require advanced imaging, especially in a young athletic population.

3 Specific Overuse Trauma

3.1 Scapula

3.1.1 Fractures

Scapular fractures are usually the result of a direct blow to the scapular area. Fractures of the

scapular body are rare in athletes. *Glenoid* fractures are associated with glenohumeral dislocations although an avulsion fracture of the infraglenoid tubercle may occur due to forceful contraction of the triceps (Vansevenant et al. 2014) (Fig. 3). Fractures of the *acromion* most frequently are caused by a direct blow. An avulsion of the anterior acromion may result from deltoid muscle forces. *Coracoid process* fractures result from direct trauma or avulsion. Avulsion is possible with contraction of the short head of the biceps or the coracobrachialis muscle, or as a result of traction from the coracoclavicular ligament in association with a sprain of the AC joint. The latter may be seen as an apophyseal avulsion in adolescents before closure of the growth plate between 15 and 18 years of age, since the ligament is often stronger than the growth plate (Salter and Harris 1963).

3.1.2 Lateral Acromial Apophysitis

Repetitive contraction of muscles attaching on an apophysis can produce microfractures or apophyseal irritation, also called traction apophysitis, typically seen in athletically active children between 12 and 17 years old. When apophyses begin to ossify, they are susceptible to overstress injuries. In *throwing movements* the deltoid muscle undergoes repeated vigorous contraction. The acromial apophysis is the weakest part in the wide origin of the deltoid muscle and the central portion, the strongest belly attaches at this region (Morisawa et al. 1996). An apophysitis at the tip of the coracoid process from the pull of the short head of the biceps and the coracobrachialis is also described (Gregg and Torg 1988). Plain radiography typically shows fragmentation, irregularity, and sclerosis of the ossification center (Fig. 4). MR shows bone marrow edema across the two largest acromial apophyses, the meta-acromion and the meso-acromion (Fig. 5), in one third of cases associated with a fluid signal (pseudarthrosis) between them (Roedl et al. 2015a). The process resolves without complication.

3.1.3 Stress-Related Growth Plate Injury of the Coracoid Process

Injuries of the coracoid process physis are rare and commonly associated with AC joint sprain.

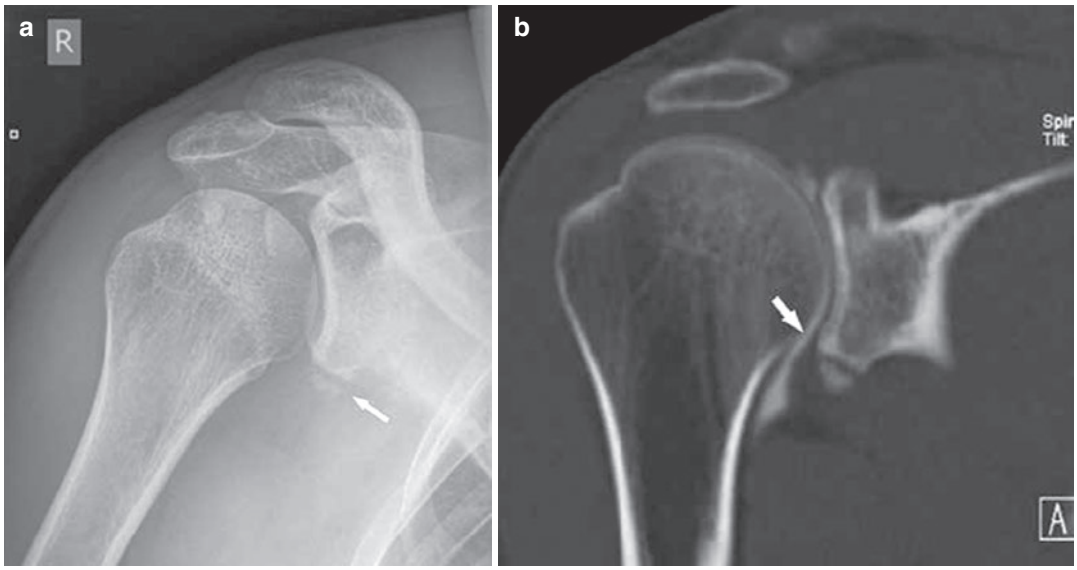

Fig. 3 (**a** and **b**) Proximal avulsion fracture of the long head of the triceps brachii muscle in an indoor soccer goalkeeper. (**a**) Plain radiograph showing a bony fragment at the inferior rim of the glenoid (white arrow). (**b**) Coronal CT arthrogram showing the sclerotic delineated bony fragment without concomitant lesion of the inferior labrum (white arrow). (Reprinted with permission from Vansevenant et al. JBR-BTR 2014, 97(5):316)

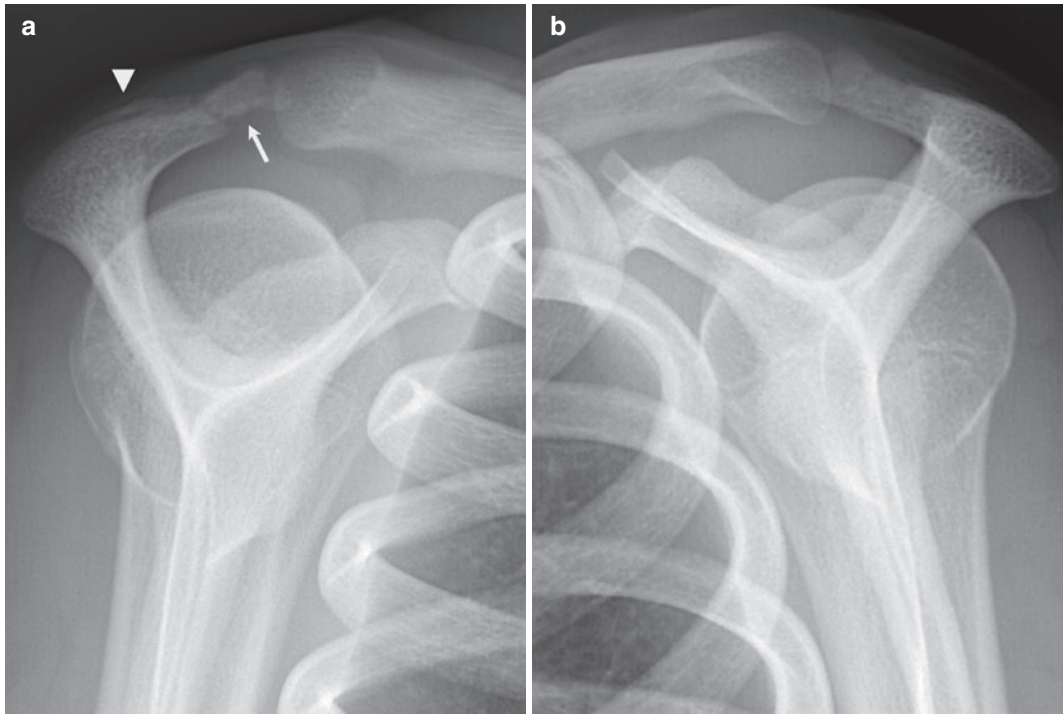

Fig. 4 (**a** and **b**) Lateral acromial apophysitis in a 15-year-old gymnast. Plain radiographs, bilateral supraspinatus outlet view. (**a**) Symptomatic right side showing slight hypertrophy and irregular lining of the meso-acromion (arrow) including the junction with the meta-acromion, as well as a unilamellated periosteal reaction (arrowhead) along the superior margin of the meta- and baso-acromion. (**b**) Asymptomatic left side showing no abnormalities. (Courtesy of F.M. Vanhoenacker)

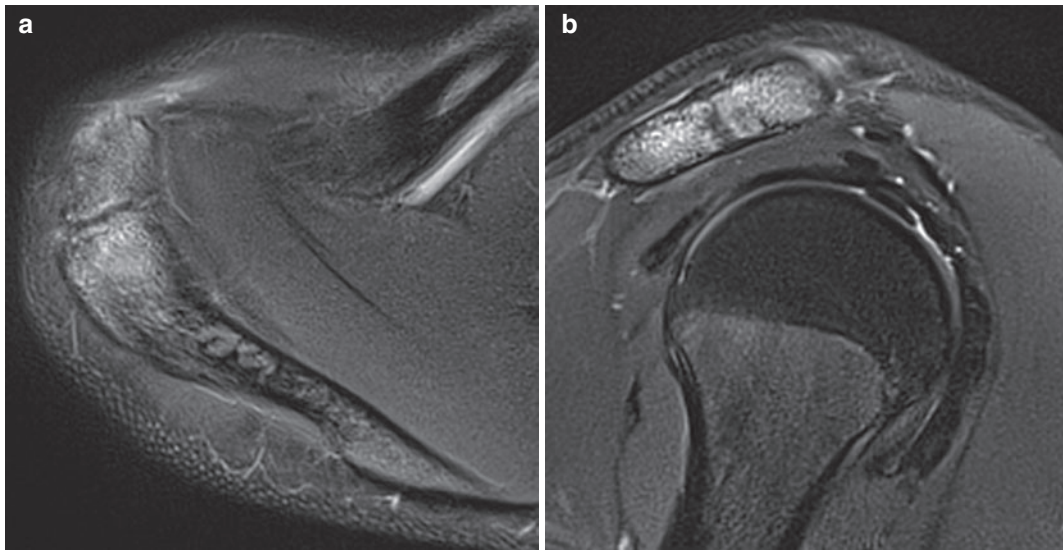

Fig. 5 (**a** and **b**) Lateral acromial apophysitis in an 18-year-old gymnast. (**a**) Axial and (**b**) sagittal fat-suppressed T2-weighted MR images, both showing bone marrow edema in the meso-acromion and the adjacent meta-acromion without a fluid signal in between them

Increased muscular pull on the coracoid process may result in a stress-related injury to its physis. In a series of 8 cases 5 were seen in athletes: football, archery, basketball, swimming, and rugby. MR showed widening, irregularity, and increased signal of the physis, apposing bone marrow edema and hypertrophy, as well as soft tissue edema (Alaia et al. 2017). Previously another case had been reported in archery (Naraen et al. 1999).

3.1.4 Stress Fractures

Sports-related stress fractures of the scapula and clavicle are *rare*. Consequently, the *index of suspicion for these lesions is low*, which may delay diagnosis and appropriate treatment. Low suspicion of a stress fracture in these bones may lead to an *erroneous diagnosis of a tumoral or infectious lesion*. A detailed occupational history may overcome the problem. These stress fractures can occur either as a result of *repetitive loading at the point of muscular attachments to bone* or as a result of *impact loading* (Brukner 1998).

About 14 cases of a scapular stress fracture were reported:

- In five cases the fracture was located in the acromion. Three occurred in the base, of which two in amateur golf players (Hall and Calvert 1995; Taneja et al. 2013) and one in American football (Ward et al. 1994). One case between the ventral and middle third of the acromion was reported in an elite tennis player (Rupp et al. 1998), and one at the medial aspect in American football (Schils et al. 1990).
- Three cases were reported in the base of the coracoid process: Two reports of probably the same trapshooter (Boyer 1975; Sandrock 1975), one in a beginner golfer (Lee et al. 2018), and one extending from the coracoid base to the glenoid in a cricket bowler (Chammaa et al. 2010).
- In two cases the lateral margin of the scapula was the fracture site: in a cricket fast bowler (de Villiers et al. 2005) and in a baseball pitcher (Herickhoff et al. 2007).
- Four additional cases occurred in various other sites: at the medial side of the supraspinatus fossa in jogging with hand-held weights (Veluvolu et al. 1988), at the superior margin in a water polo player (Donaldson 2012), at the junction of the scapular neck and body in a baseball pitcher (Levine and Resnick 2013), and at the spine in a soft ball player (Marcano et al. 2014).

Plain radiography continues to be the primary method for diagnosis, but its limitations in the early detection of these injuries are well known. *MRI* has a comparative sensitivity to bone scan with the additional advantage of depicting the lesion, especially the surrounding bone marrow and soft tissue edema (Fig. 6). *MDCT* is excellent in depicting the presence and extension of the fracture line and callus formation (Fig. 6).

3.1.5 Suprascapular Nerve Entrapment (SSNE)

The suprascapular nerve is a mixed motor and sensory nerve providing *motor supply to the supraspinatus and infraspinatus muscle*. Causes of suprascapular nerve injury are anatomical variants of the suprascapular or spinoglenoid notch, compressive mass lesions, which most frequently are paralabral cysts at the level of the spinoglenoid notch (Ticker et al. 1998), direct trauma such as a fracture of the scapula, direct blow to the shoulder, or traction on the nerve through a pull on the upper extremity, and dynamic entrapment.

Dynamic nerve entrapment occurs at the suprascapular or spinoglenoid notch, where mobility is already limited, during violent or repeated scapular motion. In *athletes*, this appears *more frequently at the spinoglenoid notch*, whereas in the general population it occurs mainly at the suprascapular notch (Montagna and Colonna 1993; Ferretti et al. 1998). In the majority of cases sports-related dynamic entrapment occurs in *overhead sports* such as baseball, tennis, and weightlifting. *Most frequently* affected by entrapment at the spinoglenoid notch are

Fig. 6 (**a**–**c**) Stress fracture of the left scapula in an 18-year-old elite gymnast. (**a**) Sagittal fat-suppressed T2-weighted MR image showing bone marrow edema in the area of the supraspinatus fossa. There is extensive soft tissue edema along the anterior half of the fossa in the deep part of the supraspinatus and subscapularis muscles (arrows), and to a lesser extent in the posterior half at the infraspinatus and teres minor muscles (arrowhead). (**b**) Sagittal and (**c**) coronal CT arthrogram revealing a slightly displaced fracture (white arrow) at the anterior half of the supraspinatus fossa. A rather extensive and immature calcified periosteal reaction (black arrows) is seen at the level of the on MR visualized soft tissue edema

professional volleyball players. Several mechanisms have been proposed but excessive traction or microtrauma of the nerve is the most plausible mechanism of trauma.

The diagnosis is based primarily on clinical findings, confirmed by EMG. Imaging studies may demonstrate an etiological diagnosis. US and MRI may identify a *paralabral cyst*. In addition, MRI is able to identify *signs of muscular denervation*, including edema in an early stage, and fatty infiltration and atrophy in later stages (Ludig et al. 2001). Entrapment at the suprascapular notch will result in denervation of both supra- and infraspinatus muscles, entrapment at the spinoglenoid notch in isolated infraspinatus denervation. CT may be useful to demonstrate variant notch anatomy (Polguj et al. 2013) or fragment displacement after a fracture.

3.1.6 Long Thoracic Neuropathy

The long thoracic nerve, the sole *innervation to the serratus anterior muscle*, courses downward and laterally along the mid-axillary line along the outer surface of the muscle which arises from the first 8–9 ribs and inserts on the costal surface of the scapula along its medial border. It serves to protract the scapula and maintain the medial border of the scapula against the thorax. *Isolated paralysis of the serratus anterior* is a well-recognized clinical entity accounting for the *characteristic scapular winging* seen with weakness of this muscle, most pronounced at

the inferior margin of the scapula. Many traumatic and nontraumatic causes have been reported. This injury has been reported to occur in almost every sport. However, the *most common sport* reported to cause the injury is *tennis*, especially the act of serving. The common theme in sports-related cases is that the injury occurred when the ipsilateral arm was in an outstretched an unusually overhead position, suggesting the nerve was subjected to traction (Gregg et al. 1979). This paralysis is usually apparent on clinical examination and confirmed by EMG. CT and MRI usually are not necessary unless other disease such as cervical disc herniation is suspected. However, imaging of the nerve itself is feasible with 3 T MR (Deshmukh et al. 2017) and ultrasound (Chang et al. 2019), although with MR no abnormalities were visualized along the course of the nerve in a series of 20 patients with clinical suspicion of LTN neuropathy (Deshmukh et al. 2017). Imaging of the serratus anterior muscle may show signs of denervation.

3.2 Clavicle

3.2.1 Fractures

Fractures of the clavicle are common. 90% occur as the result of a fall directly on the shoulder, a small number after direct blow, and rarely a fall on an outstretched hand. The middle third is involved in 65–80%, the lateral in 15–30%, and the medial in 5%.

3.2.2 Distal Clavicular Osteolysis (DCO)

DCO is an uncommon, *self-limiting* condition characterized by progressive resorption of the distal end of the clavicle (Cahill 1982; Matthews et al. 1993). *Two types* are described with the same radiological imaging and pathologic features:

– *Posttraumatic*: after a single or repeated episodes of local trauma which can be a fracture or AC dislocation. However, usually the trauma is relatively minor. The osteolytic process begins as early as 2–3 weeks and as late as several years after the injury.
– *Stress-induced*: overuse injury caused by repetitive microtrauma, most commonly seen in adult *weightlifters* (Scavenius and Iversen 1992) and athletes who are engaged in strenuous physical exercise involving use of the upper extremities. It is caused by repetitive compression of the distal clavicle at the AC joint encountered during lifting activities, particularly the high intensity, high frequency bench press, requiring the AC joint to assume the role of a weight-bearing joint (Haupt 2001; Nevalainen et al. 2016). A higher incidence of bilateral involvement is noted in this type.

The pathogenesis of DCO has often been debated. Of all proposed etiologies, Cahill's is the most accepted. He found microfractures in the subchondral bone in 50% of the surgical specimens and proposed that repetitive microtrauma caused subchondral stress fractures and remodeling (Cahill 1982).

Plain radiographs are not sensitive to the early stage of the disease. *Initial findings often are subtle*, including osteopenia of the distal clavicle, and loss of the clavicular subarticular cortex (Levine et al. 1976; Kaplan and Resnick 1986). However, *early recognition and treatment with immobilization can shorten the course of the process*. The condition progresses into a *lytic phase* in which cystic areas, irregularity of the articular cortex, periarticular erosions, osteolysis, and soft tissue swelling can be seen. It may be associated with osteopenia and erosion of the acromion (Levine et al. 1976). If untreated this lytic phase may last 12–18 months and osteolysis may progress to include the distal 0.5–3 cm of the clavicle, resulting in an increased AC joint space (Kaplan and Resnick 1986).

Once the lytic phase has stabilized, *reparative changes* occur over a period of 4–6 months, resulting in either complete reconstitution or partial reformation with a permanently widened AC joint space (Fig. 7) (Kaplan and Resnick 1986).

Beside findings comparable to those seen on plain films, typical MR features include capsular distention, joint effusion, distal clavicular bone

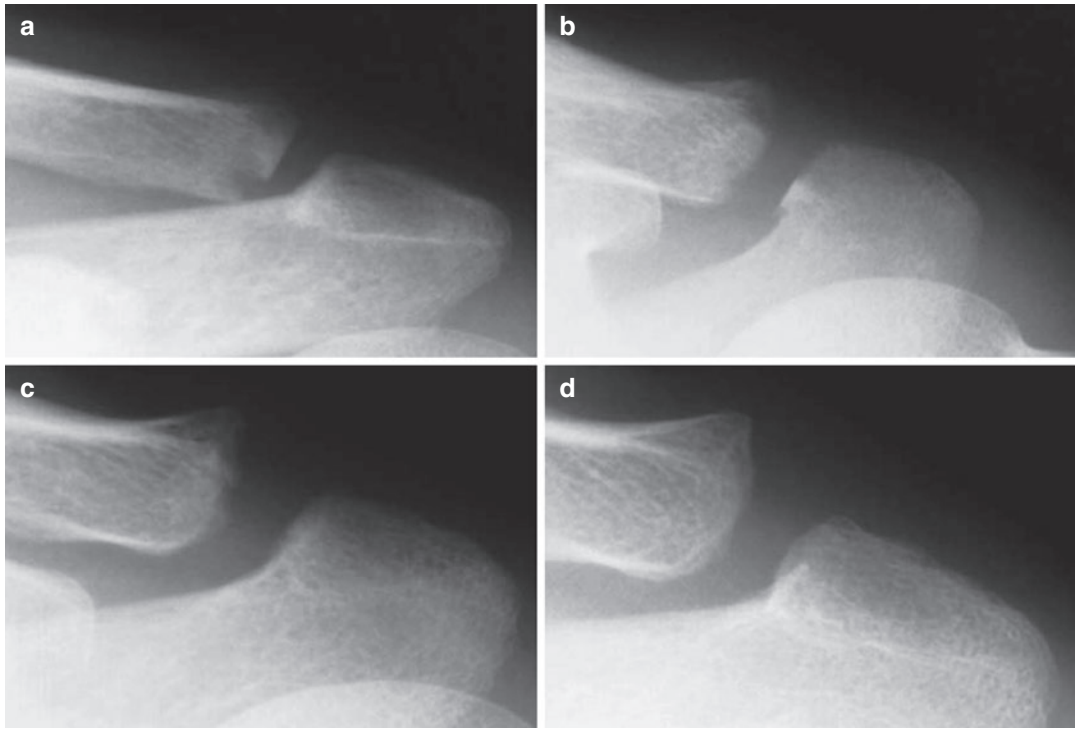

Fig. 7 (**a**–**d**) Lateral clavicular osteolysis in a judo athlete. (**a**) Unsharply marginated subchondral erosion at the inferior margin of the lateral end of the clavicle. Normal width of the AC joint space. (**b**) 8 weeks later: widening of the AC joint space with ill-defined resorption of the lateral clavicle, and loss of the subchondral bone plate in the proximal part at the acromial side. (**c**) 8 months later: further resorption of the lateral clavicle and increased width of the joint space. The margins are less ill-defined. (**d**) Follow-up after 15 months: partial reconstitution of the joint space width and now sharply marginated lateral end of the clavicle

marrow edema out of proportion to edema at the acromion, and in advanced cases periostitis at the distal clavicle (Roedl et al. 2015b). Consistent with Cahill's microfracture theory, on MR a subchondral fracture line was seen within the clavicular bone marrow edema in 74% to 86% of cases (Kassarjian et al. 2007; Roedl et al. 2015b) (Fig. 8). Some have suggested that in the right clinical setting, bone marrow edema alone may represent an early form of DCO (Fiorella et al. 2000).

3.2.3 Stress Fractures

Sports-related stress fractures of the clavicle are *rare*. From a biomechanical point of view the clavicle may be considered a lever with is axis of rotation close to the sternoclavicular joint. It is pulled down by the pectoralis major muscle, subclavius muscle, and deltoid musculature, counterbalanced by the cranial pull of the sternocleidomastoideus and trapezius muscles. The point of maximum stress is immediately lateral to the strongly anchoring costoclavicular and sternoclavicular attachments (Calvo et al. 1995).

About 10 cases of a clavicular stress fracture were reported:

Five cases in the *medial* third

- Baseball: in a professional third baseman with high demands on his throwing shoulder (Wu and Chen 1998).
- Gymnastics: in a 10-year-old gymnast through a deep rhomboid fossa, possibly caused by the pull of sternocleidomastoideus and pectoralis major (Fallon and Fricker 2001).
- Rowing: in a lightweight sculler, most likely resulting from cyclic scapular protraction and retraction (Abbot and Hannafin 2001).

Fig. 8 A recreational cyclist sustained a fall on his shoulder 5 weeks ago. Coronal fat-suppressed T2-weighted MR image showing a fluid-distended AC joint, bone marrow edema at the distal clavicle with a hypointense fracture line in the subchondral zone as well as about 1 cm more proximally (white arrows). In the superior part of the clavicular subchondral bone a small erosion is seen (black arrow). The image is suspect of an early posttraumatic DCO with associated (occult) fractures. (Courtesy of F.M. Vanhoenacker)

- Human tower construction: in this traditional Catalan sport the medial clavicle is pushed down by the weight of other athletes while the surrounding muscles are pulled upon (Roset-Llobet and Salo-Orfila 1998).
- Gymnastics: a bilateral stress fracture is reported in a 17-year-old gymnast caused by muscle imbalance during static poses on ring height (Fujioka et al. 2014).
  Three cases in the *middle* third
- Javelin throwing: in an elite athlete, caused by repeated stress from the contraction of the clavicular portion of the deltoid and pectoralis major muscles (Adolfsson and Lysholm 1990).
- Springboard diving: in a male diver, resulting from transmission of stress from his hands to the clavicle on entry in the water (Waninger 1997).
- Weight lifting: in a recreational weight lifter due to accelerated weight training (Constantinou and Kastanos 2008).
  Two cases in the *lateral* third
- Weight lifting: in an athlete at 1 cm from the AC joint due to structural fatigue (Shellhaas et al. 2004).
- Cricket: in a fast bowler caused by muscle imbalance around the shoulder girdle (Read and Bell 2008).

3.2.4 Stress-Related Growth Plate Injury of the Proximal Clavicle

One case of a bilateral physeal stress-related lesion of the proximal clavicular growth plate has been reported in a 13-year-old male gymnast caused by a maneuver at the parallel bars requiring him to catch his full body weight after swinging on the bars with both hands. On plain film the growth plate showed widening and irregularity similar to the well-known changes seen in the so-called gymnast wrist (Carson et al. 2012).

3.3 AC Joint

3.3.1 Sprain/Dislocation

AC sprains are common during athletic activities, *most frequently* occurring *directly* by a blow to the acromion (a fall or other contact) with an adducted humerus driving the acromion medially and inferiorly, or *indirectly* by a fall on the outstretched hand or elbow with a superiorly directed force.

Initially injuries to the AC joint were graded I to III as proposed by *TOSSY* according only to the degree of injury to the AC and CC ligaments (Tossy et al. 1963). *ROCKWOOD* added three additional types, all subsets of Tossy type III (Rockwood 1984) (Fig. 9) (Table 1).

The grading of AC injuries is typically based on plain film analysis:

- In *type 1* plain films are normal.
- A *type 2* is characterized by *widening* of the joint space and *slight upward displacement* of

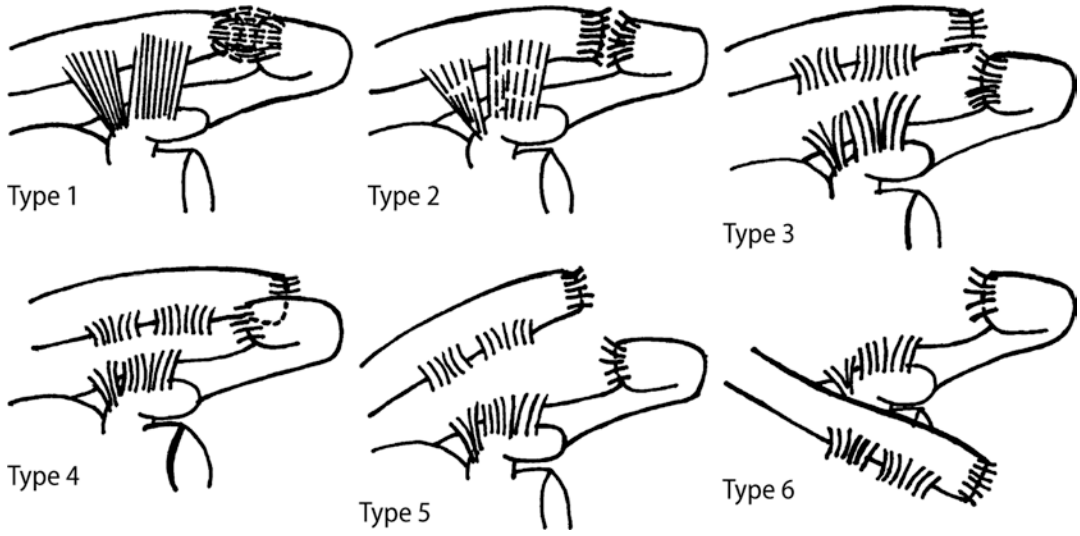

Fig. 9 Rockwood classification of acromioclavicular joint injuries

Table 1 Rockwood classification of AC injuries

Type 1	*Sprain* AC ligaments and intact CC ligament
Type 2	*Subluxation* with rupture AC ligaments and sprain CC ligament
Type 3	*Dislocation* with rupture AC ligaments and CC ligament
Type 4	*Dislocation* with posterior dislocation of the clavicle
Type 5	*Dislocation* with severe upward displacement of clavicle into the subcutis
Type 6	*Dislocation* of the clavicle inferiorly, locked under the coracoid process

the lateral clavicle, less than the width of the acromion. The width of the joint space is pathologic if more than 7 mm in men, more than 6 mm in women, or with a difference of more than 2 mm compared to the uninjured side (Petersson and Redlund-Johnell 1983). The assessment of upward displacement of the clavicle relative to the acromion should be *based on the alignment of the inferior margins*.

– In *type 3* there is an *upward dislocation* of the clavicle, more than the width of the acromion, with an increased CC distance from 25% to 100%. Rupture of the CC ligament is very likely if there is a difference of 5 mm or more between the two sides (Neer and Rockwood 1975). The normal coracoclavicular distance is 11–13 mm. In type 4 the clavicle is posteriorly dislocated.
– A severely upward displaced clavicle, more than 100% of the CC distance, is the hallmark of a *type 5* injury.

While in adults dislocation of the AC joint accounts for 12% of all dislocations of the shoulder (Rowe 1968), a *true AC dislocation is very rare before the age of 16*. Usually the trauma results in a physeal separation of the lateral clavicle. While the clavicular epiphysis remains intact in the periosteal tube, the lateral clavicle shows upward displacement through a tear in the thick periosteal tube, also called a *pseudodislocation* (Kocher et al. 2000).

3.3.1.1 Plain Film Analysis

Zanca View Unilateral Versus *Bilateral*

In case of an AC trauma it is recommended to obtain an upright view without the patient allowed to support his elbow with the opposite hand, which might reduce any dislocation (Neer and Rockwood 1975). ACJ injuries cannot be accurately classified by estimation of clavicular elevation on a unilateral AP radiograph. Bilateral comparison views with the measurement of the

increase in CC distance are necessary (Ibrahim et al. 2015). To minimize variation in the angle of the X-ray beam and the distance to the patient, a single large image of both sides should be taken (Nguyen et al. 1990).

Weighted Views Unilateral Versus *Bilateral*

The traditionally held belief of weighted views is that they should be used to differentiate grade 2 from 3 lesions. Over the last two decades, the use of weighted radiographs has fallen out of favor because of the shift towards nonsurgical management of grade 3 injuries. However, the true value of bilateral weighted films is to "unmask" a grade 5 injury which should be offered surgery (Ibrahim et al. 2015).

Type 4 Lesion

Traditionally an axillary or modified axillary view is taken to detect a posterior dislocation of the clavicle. The disadvantages of the axillary view are the variability in the patient's position and that a dynamic posterior translation is masked with this static view (Rahm et al. 2013). To reveal a dynamic horizontal instability dynamic axillary views (Tauber et al. 2010) and the modified Alexander view (Minkus et al. 2017) were developed, the latter being easy to reproduce.

The role of *ultrasound* in AC sprains is not well established. US is sensitive in the detection of type 1 sprains: findings are distension of the joint space and stripping of the periosteum from the medial clavicular head. Since treatment for type 3 injuries is controversial (Phillips et al. 1998), US may be valuable in differentiation between type 3 lesions based on the presence or absence of detachment of muscle insertions, the dynamic joint stabilizers (Heers and Hedtmann 2005). In the same way, *MRI* might be a valuable tool to decide between conservative and operative treatment based on the associated soft tissue damage.

3.3.2 Osteoarthritis (OA)

OA occurs early and frequently because the adult AC joint (ACJ) cannot compensate for the incongruity of the joint surfaces (Petersson 1987). OA is the most common cause of AC-related pain (Shaffer 1999). Causes of *OA related to sports activity* are *AC sprains* and *chronic repetitive loading*. With ruptured AC ligaments, the CC ligament is unable to control adequately anteroposterior translation, or rotation of the distal clavicle (Debski et al. 2001). Chronic repetitive loading typically is seen in overhead athletes, weight lifters, and golf players.

On routine radiography the ACJ is not loaded in compression. Consequently, the joint space does not depict the thickness of the cartilage. A *loaded view*, obtained by forced adduction of the humerus by pulling the elbow with the opposite hand, may demonstrate an additional 27% of OA (Stenlund et al. 1992). However, the role of this view is not well established. OA may also be present on plain films in patients without symptoms (Zanca 1971; Bonsell et al. 2000). The prevalence of OA on MRIs of asymptomatic subjects has been reported to be as high as 48% and 82% (Needell et al. 1996; Shubin Stein et al. 2001).

Although some authors found bone marrow edema specific for symptomatic OA (Shubin Stein et al. 2006; Veen et al. 2018), others found it neither a sensitive (Singh et al. 2018) nor a specific (Singh et al. 2018; Frigg et al. 2019) sign of symptomatic OA. In conclusion, clinical symptoms are not associated with radiological imaging features of OA, and therefore should only be used as an adjunct in decision-making.

3.4 SC Joint

3.4.1 Sprain/Dislocation

No more than 2–3% of all dislocations involving the pectoral girdle occur at the SC joint. SC dislocations are classified as either *anterior or posterior*, the *anterior* one being *far more common*. In nearly 150 traumatic SC dislocations a sports-related injury accounted for 21% (Wirth and Rockwood 1996). *Two types of injury* may result in a SC dislocation: The most common is an *indirect blow to the shoulder*, which may be seen in contact athletes. Subsequently the clavicle acts as a lever through the fulcrum of the costoclavicular ligament (Rogers 1983). An *anterolateral blow* results in *anterior*, a *posterolateral blow* in

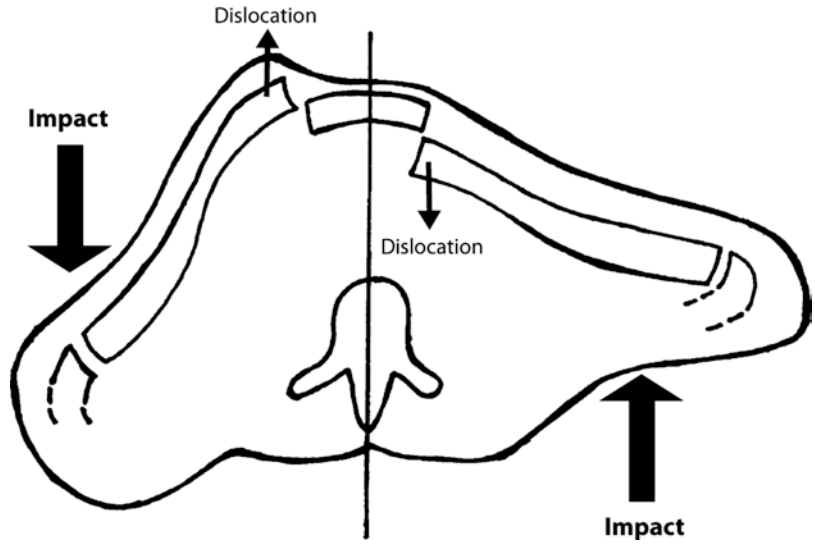

Fig. 10 Mechanism of sternoclavicular dislocations caused by an indirect blow to the shoulder. Right: anterolateral blow resulting in an anterior sternoclavicular dislocation. Left: posterolateral blow resulting in a posterior sternoclavicular dislocation

posterior dislocation (Fig. 10). Contact sports (especially martial arts, American football, and rugby) and motorcycle injuries are the commonest causes of posterior dislocation. A posterior dislocation may also result from a *direct blow to the anterior medial portion of the clavicle.*

Approximately *25% of posterior dislocations* are associated with some form of *complication* as the medial clavicle can impinge on vital mediastinal structures (Neer and Rockwood 1975). They consist of pneumothorax, laceration of the superior vena cava, compression of the venous structures of the neck, compression or rupture of the trachea, rupture of the esophagus, occlusion or compression of the subclavian or carotid artery, and changes in voice caused by compression of the recurrent laryngeal nerve. *A high index of suspicion is required* to determine the presence of these serious complications, which may manifest insidiously.

The center of ossification of the medial end of the clavicle appears at the age of 18–20 years, and its growth plate fuses at the age of 20–25 years. Therefore many presupposed SC dislocations in patients younger than 25 years old are actually fractures through the physeal plate. Although the epiphysis usually stays attached via the sternoclavicular ligaments, a displaced epiphysis can block reduction of the sternoclavicular joint. In two large series of posterior dislocation in patients under 25 years, the reported frequency of physeal separation was 57% and 55% (Laffosse et al. 2010; Lee et al. 2014).

Table 2 Allmann classification of SC injuries

Type 1	Mild sprain with intact ligaments and a stable joint
Type 2	Moderate sprain with subluxation and possible partial rupture of the ligaments
Type 3	Dislocation with complete disruption of the supporting ligaments

Injuries to the SC joint are graded I to III according to *ALLMANN* (Allmann 1967) (Table 2).

Dislocations of the SC joint are notoriously difficult to characterize on plain radiography. The diagnosis is usually evident on CT scan, and one should directly proceed to CT instead of focusing on special plain film projections (Fig. 11). US can be used to make the diagnosis if CT is not readily available (Bengtzen and Petring 2017; Hellwinkel et al. 2019). MR may be more useful than CT in athletes under 20 years of age to differentiate between an epiphyseal disruption and a true dislocation and to demonstrate a displaced unossified epiphysis or epiphyseal fracture component (Beckmann and Crawford 2016; Laffosse et al. 2010). On MRI of 41 patients imaged with complaints related to a SC trauma, the most common sites of SC joint soft tissue injury were the

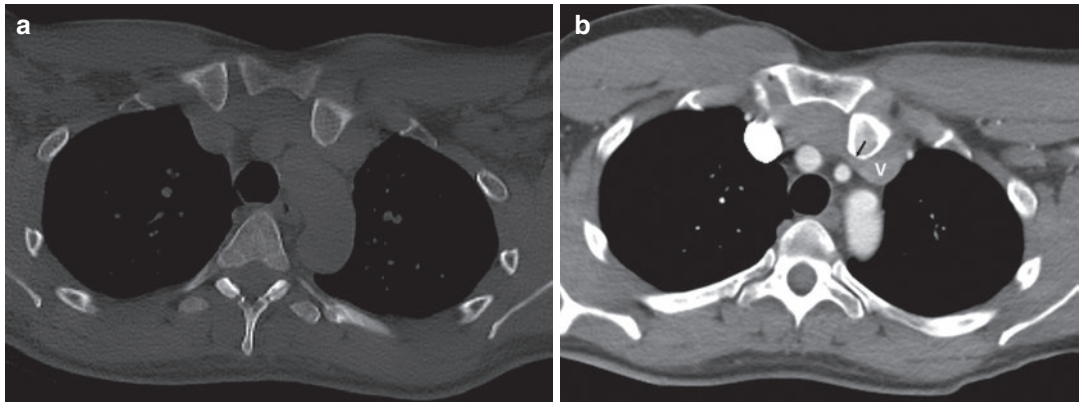

Fig. 11 (**a** and **b**) Impact trauma at the level of the left sternoclavicular joint during a martial art training session. Axial CT images at the same level in (**a**) bone and (**b**) soft tissue window showing a posterior luxation of the left sternoclavicular joint causing an impression (arrow) on the left brachiocephalic vein (v)

articular disc (80%), the anterior SC ligament (73%), and the posterior SC ligament (39%). Injuries to the interclavicular and costoclavicular ligaments were rare (Benitez et al. 2004).

Things to Remember

- In sports lesions plain films tailored to the clinical findings and of impeccable quality will significantly increase diagnostic performance.
- Because of their low prevalence and low index of suspicion, sports-related stress fractures of the scapula and clavicle may be mistaken for a tumoral or infectious lesion unless a detailed occupational history is taken.
- In sports-related AC joint or posterior shoulder pain, radiologists, respectively, should also consider a possible lateral clavicular osteolysis or a suprascapular nerve entrapment syndrome.
- In sternoclavicular joint dislocation one should immediately proceed to CT instead of focusing on special plain film projections.
- Complications of a posterior sternoclavicular dislocation may be serious and eventually life threatening.
- In order to limit the exposure to ionizing radiation, especially with SPECT-CT, the use of MRI is recommended in almost all cases that require advanced imaging, especially in a young athletic population.

Referral Criteria

Plain Radiography

- Initial modality in osseous or articular disease
  - Tailored approach and good quality essential
  - Only AC stress views when therapeutical consequences
  - No special SC views when CT available
  - Low sensitivity for early stress fracture or DCO

CT

- Second stage evaluation of fractures or SC dislocation
  - If plain radiography negative and bone scan positive

Ultrasound

- Limited role in AC joint:
  - AC sprain: type 1 or muscular status.
  - AC joint: joint distension? arthrosynovial cyst?
  - Limited role in SC joint: distension?
  - Posterior shoulder pain/weakness: paralabral cyst?
  - Soft tissue trauma

MRI

- No clear role in sprain or isolated disease of AC joint
- Limited role in SC sprain
- Soft tissue trauma
- Posterior shoulder pain: muscle denervation? paralabral cyst?

Scintigraphy—SPECT-CT

- When plain radiography is negative
- Suspected active osseous disease
  - Occult fracture
  - Stress fracture
  - Growth plate injury or apophysitis
  - Arthritis or osteoarthritis
  - Distal clavicular osteolysis

References

Abbot AE, Hannafin JA (2001) Stress fracture of the clavicle in a female lightweight rower. Am J Sports Med 29:370–372

Adolfsson L, Lysholm J (1990) Case report: clavicular stress fracture in a javelin thrower. Clin Sports Med 2:41–45

Alaia EF, Rosenberg ZS, Rossi I et al (2017) Growth plate injury at the base of the coracoid: MR features. Skeletal Radiol 46:1507–1512

Allmann FI (1967) Fractures and ligamentous injuries of the clavicle and its articulations. J Bone Joint Surg Am 49:774–784

Beckmann N, Crawford L (2016) Posterior sternoclavicular Salter-Harris fracture-dislocation in a patient with unossified medial clavicle epiphysis. Skeletal Radiol 45:1123–1,127

Bengtzen RR, Petring RC (2017) Point-of-care ultrasound diagnosis of posterior sternoclavicular joint dislocation. J Emerg Med 52:513–515

Benitez CL, Mintz DN, Potter HG (2004) Magnetic resonance imaging of the sternoclavicular joint following trauma. J Clin Imag 28:59–63

Bonsell S, Persall AW, Heitman RJ et al (2000) The relationship of age, gender, and degenerative changes observed on radiographs of the shoulder in asymptomatic individuals. J Bone Joint Surg Br 82: 1135–1139

Boyer D Jr (1975) Trapshooter's shoulder: stress fracture of the coracoid process. J Bone Joint Surg Am 57:862

Brossmann J, Stabler A, Preidler KW et al (1996) Sternoclavicular joint; MR imaging-anatomic correlation. Radiology 198:193–198

Brukner P (1998) Stress fractures of the upper limb. Sports Med 26:415–424

Burnstein MI, Pozniak MA (1990) Computed tomography with stress maneuver to demonstrate sternoclavicular joint dislocation. J Comput Assist Tomogr 14(1):159–160

Cahill B (1982) Osteolysis of the distal part of the clavicle in male athletes. J Bone Joint Surg Am 64A:1053–1058

Calvo E, Fernandez-Yruegas D, Alvarez L et al (1995) Bilateral stress fracture of the clavicle. Skeletal Radiol 24:613–616

Carson JT, McCambridge TM, Carrino TA et al (2012) Bilateral proximal epiphyseal clavicular stress-related lesion in a male gymnast. Clin Orthop Relat Res 470:307–311

Chammaa R, Miller D, Datta P et al (2010) Coracoid stress fracture with late instability. Am J Sports Med 38:2328–2330

Chang K, Wu W, Mezian K et al (2019) Sonoanatomy revisited: the long thoracic nerve. Med Ultrason 21:349–352

Constantinou D, Kastanos K (2008) Sport related stress fracture of the clavicle with non-union: case report and literature review. Int J Shoulder Surg 21:22–24

Cope R (1993) Dislocations of the sternoclavicular joint. Skelet Radiol 22:233–238

Debski RE, Parsons IM, Woo SL-Y et al (2001) Effects of capsular injury on the acromioclavicular joint mechanics. J Bone Joint Surg Am 83:1344–1351

Deshmukh S, Fayad LM, Ahlawat S (2017) MR neurography (MRN) of the long thoracic nerve: retrospective review of clinical findings and imaging results at our institution over 4 years. Skeletal Radiol 46:1531–1540

de Villiers R, Pritchard M, de Beer J et al (2005) Scapular stress fracture in a professional cricketer and a review of the literature. S Afr Med J 95(5):312–317

Donaldson LD (2012) Scapular stress fracture in water polo: a case report. Sports Health 4:502–503

Fallon KE, Fricker PA (2001) Stress fracture of the clavicle in a young female gymnast. Br J Sports Med 35:448–449

Ferretti A, de Carli A, Fontana M (1998) Injury of the suprascapular nerve at the spinoglenoid notch. The natural history of infraspinatus atrophy in volleyball players. Am J Sports Med 26:759–763

Fiorella D, Helms CA, Speer KP (2000) Increased T2 signal intensity in the distal clavicle: incidence and clinical implications. Skeletal Radiol 36:17–22

Frigg A, Song D, Willi J et al (2019) Seven-year course of asymptomatic acromioclavicular osteoarthritis diagnosed by MRI. J Shoulder Elbow Surg 28:344–251

Fujioka H, Nishikawa T, Koyama S et al (2014) Stress fractures of bilateral clavicles in an adolescent gymnast. J Shoulder Elbow Surg 23:e88–e90

Gregg J, Torg E (1988) Upper extremity injuries in adolescent tennis players. Clin Sports Med 7:371–385

Gregg JR, Labosky D, Harty M et al (1979) Serratus anterior paralysis in the young athlete. J Bone Joint Surg Am 61:825–832

Hall R, Calvert P (1995) Stress fracture of the acromion: an unusual mechanism and review of the literature. J Bone Joint Surg Br 77:153–154

Haupt HA (2001) Upper extremity injuries associated with strength training. Clin Sports Med 20:481–490

Heers G, Hedtmann A (2005) Correlation of ultrasonographic findings to Tossy's and Rockwood's classification of acromioclavicular joint injuries. Ultrasound Med Biol 31(6):725–732

Hellwinkel JE, McCarty EC, Khodaee M (2019) Sports-related sternoclavicular joint injuries. Phys Sports Med 47:253–261

Herickhoff PK, Keyurapan E, Fayad LM et al (2007) Scapular stress fracture in a professional baseball player. Am J Sports Med 35:1193–1196

Ibrahim EF, Forrest MP, Forester A (2015) Bilateral weighted radiographs are required for accurate classification of acromioclavicular separation: an observational study of 59 cases. Injury. Int J Care Injured 46:1900–1905

Kaplan P, Resnick D (1986) Stress-induced osteolysis of the clavicle. Radiology 158:139–140

Kassarjian A, Llopis E, Palmer WE (2007) Distal clavicular osteolysis: MR evidence for subchondral fracture. Skeletal Radiol 36:17–22

Klein MA, Spreitzer AM, Miro PA et al (1997) MR imaging of the abnormal sternoclavicular joint—a pictorial essay. Clin Imaging 21:138–143

Kocher MS, Waters PM, Micheli LJ (2000) Upper extremity injuries in the paediatric athlete. Sports Med 30(2):117–135

Laffosse J, Espié A, Bonnevialle N et al (2010) Posterior dislocation of the sternoclavicular joint and epiphyseal disruption of the medial clavicle with posterior displacement in sports participants. J Bone Joint Surg (Br) 92:103–109

Lee JT, Nasreddine AY, Black AM et al (2014) Posterior sternoclavicular joint injuries in skeletally immature patients. J Pediatr Orthop 34:369–375

Lee JH, Kim JR, Wang SI (2018) An unusual mechanism of coracoid fracture in a beginner golfer. Knee Surg Sports Traumatol Arthrosc 26:76–78

Levine AH, Pais MJ, Schwartz EE (1976) Posttraumatic osteolysis of the distal clavicle with emphasis on early radiologic changes. Am J Roentgenol 127:781–784

Levine BD, Resnick DL (2013) Stress fracture of the scapula in a professional baseball pitcher: case report and review of the literature. J Comput Assist Tomogr 37:317–319

Lucas DB (1973) Biomechanics of the shoulder joint. Arch Surg 107:425–432

Ludig T, Walter F, Chapuis D et al (2001) MR imaging evaluation of suprascapular nerve entrapment. Eur Radiol 11:2161–2169

Marcano AI, Samitier G, Wright TW et al (2014) Stress fracture of second rib and scapular spine in a female softball player. Curr Sports Med Rep 13:314–318

Matthews LS, Simonson BG, Wolock BS (1993) Osteolysis in the distal clavicle in a female body builder. Am J Sports Med 21:150–152

Minkus M, Hann C, Scheibel M et al (2017) Quantification of dynamic posterior translation in modified bilateral Alexander views and correlation with clinical and radiological parameters in patients with acute acromioclavicular joint instability. Arch Orthop Trauma Surg 137:845–852

Montagna P, Colonna S (1993) Suprascapular neuropathy restricted to the infraspinatus muscle in volleyball players. Acta Neurol Scand 87:248–250

Morisawa K, Umemura A, Kitamura T et al (1996) Apophysitis of the acromion. J Shoulder Elbow Surg 5:153–156

Naraen A, Giannikas K, Livesley P (1999) Overuse epiphyseal injury of the coracoid process as a result of archery. Int J Sports Med 20:53–55

Needell SD, Zlatkin MB, Sher JS et al (1996) MR imaging of the rotator cuff**:** peritendinous and bone abnormalities in an asymptomatic population. Am J Roentgenol 166:863–867

Neer CS, Rockwood CA Jr (1975) Fractures and dislocations of the shoulder. In: Rockwood CA Jr, Green DP (eds) Fractures. Lippincott Co, Philadelphia, p 585

Nevalainen MT, Ciccotti MG, Morrison WB et al (2016) Distal clavicular osteolysis in adults: association with bench pressing intensity. Skeletal Radiol 45:1473–1479

Nguyen V, Williams G, Rockwood C (1990) Radiography of acromioclavicular dislocation and associated injuries. Crit Rev Diagn Imaging 32:191–228

Petersson CJ (1987) The acromioclavicular joint in rheumatoid arthritis. Clin Orthop 223:86–93

Petersson CJ, Redlund-Johnell I (1983) Radiographic joint space in normal acromioclavicular joints. Acta Orthop Scand 54:431–433

Phillips AM, Smart C, Gromm AFG (1998) Acromioclavicular dislocation. Conservative or operative therapy. Clin Orthop 353:10–17

Polguj M, Sibinski M, Grzegorzewski A et al (2013) Variation in morphology of suprascapular notch as factor of suprascapular nerve entrapment. Int Orthop 37:2185–2195

Rahm S, Wieser K, Spross C et al (2013) Standard axillary radiographs of the shoulder may mimic posterior subluxation of the lateral end of the clavicle. J Orthop Trauma 27:622–626

Read JA, Bell P (2008) Clavicular stress fracture in a cricket fast bowler: a case report. J Med Case Rep 2:306

Rockwood CA Jr (1984) Subluxations and dislocations about the shoulder. In: Rockwood CA Jr (ed) Fractures in adults. J.B. Lippincott, Philadelphia, p 722

Rockwood CA Jr, Wirth MA (1996) Injuries to the sternoclavicular joint. In: Rockwood CA Jr, Green DP, Bucholz RW et al (eds) Rockwood and Green's fractures in adults. Lippincott-Raven, Philadelphia, pp 1415–1471

Roedl JB, Morrison WB, Ciccotti MG et al (2015a) Acromial Apophysiolysis: superior shoulder pain and acromial nonfusion in the young throwing athlete. Radiology 274:201–209

Roedl JB, Nevalainen M, Gonzalez FM et al (2015b) Frequency, imaging findings, risk factors, and long-term sequelae of distal clavicular osteolysis in young patients. Skeletal Radiol 44:659–666

Rogers LF (1983) The radiology of sports injuries. Curr Probl Diagn Radiol 12:1

Roset-Llobet J, Salo-Orfila JM (1998) Sports-related stress fracture of the clavicle: a case report. Int Orthop 22:266–268

Rowe CR (1968) An atlas of anatomy and treatment of midclavicular fractures. Clin Orthop Relat Res 58:29–42

Rupp S, Seil R, Kohn D (1998) Surgical reconstruction of a stress fracture of the acromion after arthroscopic subacromial decompression in an elite tennis player. Arthroscopy 14:106–108

Salter RB, Harris WR (1963) Injuries involving the epiphyseal plate. J Bone Joint Surg Am 45:587–622

Sandrock A (1975) Another sports fatigue fracture. Stress fracture of the coracoid process of the scapula. Radiology 117:274

Scavenius M, Iversen BF (1992) Nontraumatic clavicular osteolysis in weight lifters. Am J Sports Med 20:463–467

Schils JP, Freed HA, Richmond BJ et al (1990) Stress fracture of the acromion. Am J Roentgenol 155(5):1140–1141

Shaffer BS (1999) Painful conditions of the acromioclavicular joint. J Am Acad Orthop Surg 7:176–188

Shellhaas JS, Glaser DL, Drezner JA (2004) Distal clavicular stress fracture in a female weight lifter. Am J Sports Med 32(7):1755–1758

Shubin Stein BE, Wiater M, Pfaff C et al (2001) Detection of acromioclavicular joint pathology in asymptomatic shoulders with magnetic resonance imaging. J Shoulder Elbow Surg 10(3):204–208

Shubin Stein BE, Ahmad CS, Pfaff CH et al (2006) A comparison of magnetic resonance imaging findings of the acromioclavicular joint in symptomatic versus asymptomatic patients. J Shoulder Elbow Surg 15:57–59

Singh B, Gulihar A, Bilagi P et al (2018) Magnetic resonance imaging scans are not a reliable tool for predicting symptomatic acromioclavicular arthritis. Shoulder Elbow 10:250–254

Stenlund B, Goldie I, Marions O (1992) Diminished space in the acromioclavicular joint in forced arm adduction as a radiographic sign of degeneration and osteoarthrosis. Skelet Radiol 21:529–533

Taneja AK, Negromonte FP, Skaf A (2013) Stress injury of the acromion: case report and literature review. Eur J Orthop Surg Traumatol 23:S189–S192

Tauber M, Koller H, Hitzl W et al (2010) Dynamic radiologic evaluation of horizontal instability in acute acromioclavicular joint dislocations. Am J Sports Med 38:1188–1195

Thyterleigh-Strong G, Mulligan A, Babu S et al (2019) Digital tomography is an effective investigation for sternoclavicular joint pathology. Eur J Orthop Surg Tramatol 29:1217–1221

Ticker JB, Djurasovic M, Strauch RJ et al (1998) The incidence of ganglion cysts and other variations in anatomy along the course of the suprascapular nerve. J. Shoulder Elbow Surg 7:472–478

Tossy JD, Mead NC, Sigmond HM (1963) Acromioclavicular separations: useful and practical classification for treatment. Clin Orthop 28:111–119

Vansevenant M, Vanhoenacker FM, Wauters T (2014) Proximal avulsion fracture of the long head of the triceps brachii muscle. JBR-BTR 97(5):316

Veen EJ, Donders CM, Westerbeek RE (2018) Predictive findings on magnetic resonance imaging in patients with symptomatic acromioclavicular osteoarthritis. J Shoulder Elbow Surg 27:e252–e258

Veluvolu P, Kohn HS, Guten GN et al (1988) Unusual stress fracture of the scapula in a jogger. Clin Nucl Med 13(7):531–532

Wallace WA, Hellier M (1983) Improving radiographs of the injured shoulder. Radiography 49:229–233

Waninger KN (1997) Stress fracture of the clavicle in a collegiate diver. Clin J Sport Med 7:66–68

Ward WG, Bergfeld JA, Carson WG (1994) Stress fracture of the base of the acromial process. Am J Sports Med 22(1):146–147

Wickiewicz TL (1983) Acromioclavicular and sternoclavicular joint injuries. Clin Sports Med 2(2):429–438

Wirth MA, Rockwood CA Jr (1996) Acute and chronic traumatic injuries of the sternoclavicular joint. J Am Acad Orthop Surg 4:268–278

Wu CD, Chen YC (1998) Stress fracture of the clavicle in a professional baseball player. J Shoulder Elbow Surg 7:164–167

Wulker N (1998) Applied biomechanics. In: Fu FH, Ticker JB, Imhoff AB (eds) Atlas of shoulder surgery. Appleton and Lange, Stanford (CT), pp 30–52

Zanca P (1971) Shoulder pain: involvement of the acromioclavicular joint—analysis of 1,000 cases. Am J Roentgenol 112:493–506

Imaging of Sports Injuries of the Elbow

Milko C. de Jonge, Niels P. Vermeulen, and Mario Maas

Contents

M. C. de Jonge (✉)
Department of Radiology, St Antonius Hospital Midden Nederland, Nieuwegein, The Netherlands
e-mail: m.dejonge@antoniusziekenhuis.nl

N. P. Vermeulen · M. Maas
Department of Radiology, Amsterdam UMC, Location AMC, Amsterdam, The Netherlands

Abstract

The elbow, compared to the lower extremity and shoulder, is much less involved in sports injuries in general; however in specific sports it is nevertheless quite common (e.g., gymnastics). Acute injuries are relatively rare and most injuries are the result of overuse. From a biomechanical standpoint two major mechanisms are responsible for this. The first is the athlete who is involved in sports that require a large number of the same repetitive movements like in baseball, specifically in pitchers. The second mechanism is seen in athletes who basically use their arm as a weight-bearing limb like in gymnastics or weightlifting. All known imaging modalities are useful in elbow imaging each with their own merit. Plain films is almost always the first imaging modality used. The clinical situation and the findings on plain films direct the next step of imaging (if necessary). For the evaluation of the soft tissues ultrasound will usually suffice but if more information is needed, especially for the evaluation of the joint, MRI and CT both play important roles. It has to be emphasized that both have their own merits and that they often are complementary to each other.

Med Radiol Diagn Imaging (2020)
https://doi.org/10.1007/174_2020_251, © Springer Nature Switzerland AG
Published Online: 08 December 2020

1 Introduction

Elbow injuries in athletes are relatively uncommon. Compared to overuse injuries, acute injuries are less common. Acute injuries are most likely the result of direct trauma or a fall on the outstretched arm and can lead to a variety of injuries which are summarized in Table 1 (Fig. 1). Overuse injuries are chronic and are the result of repetitive motions which generate chronic stress on anatomical structures in and around the elbow joint, especially ligaments, tendons, and cartilage. Sports activities that are prone to overuse elbow injuries involve those with extensive use of the arm in throwing (e.g., baseball pitching, javelin), those in which the arm is used as a lever with swinging and/or hitting (e.g., golf, tennis, racquetball), and those in which the arm is turned into a weight-bearing joint (e.g., gymnastics, weightlifting). In addition, sports activities in which the arm is used to block goal fired shots are prone to elbow injuries (e.g., goalkeepers in handball and soccer).

There are several factors that contribute to injuries of the elbow in sports activities. They can basically be divided into intrinsic and extrinsic factors (Wilder and Sethi 2004; Gissane et al. 2001). Intrinsic factors are athlete related, such as joint stability, muscle strength, skeletal maturity, and history of previous injuries. Extrinsic factors are sports related such as biomechanics of the game, equipment used, training hours, and coaching. Particularly game biomechanics seems to be the most important extrinsic factor. In overhead throwing athletes the amount of valgus stress at the elbow is significant even in adequately trained, non-injured, professional athletes with proper throwing techniques (Fleisig et al. 1995; Loftice et al. 2004; Werner et al. 2002). These forces are inherent to the movements the arm makes to accelerate balls. Knowledge of specific game dynamics is a prerequisite for a thorough understanding of specific sports related elbow lesions.

This chapter aims to give an overview of the dynamics of the most frequent sports related injuries of the elbow (Table 2). The merits of the different imaging modalities (standard radiography, ultrasound, computed tomography and magnetic resonance imaging) in the diagnostic algorithm will be emphasized and are summarized in different boxes.

Table 1 Classic traumatologic injuries of the elbow

Adult	Child/adolescent
Fracture/dislocation	Fracture/dislocation

– Radial head/neck fracture
– Olecranon fracture
– Elbow dislocation
  – Posterior
  – Anterior (less common)
– Supracondylar humerus fracture
– Coronoid process fracture
– Epicondyle fracture (rare)
– Galleazzi/Monteggia Fracture-dislocation (rare)
	– Radial head dislocation ('Pulled elbow')
	– Supracondylar humerus fracture
	– Elbow dislocation
	  – Posterior
	  – Anterior (rare)
	– Epicondyle fracture
	– Galleazzi/Monteggia Fracture-dislocation
	– Radial head and olecranon Fractures (rare)

Soft tissue injury	**Soft tissue injury**
– Distal biceps tendon rupture – Triceps tendon rupture	Rare

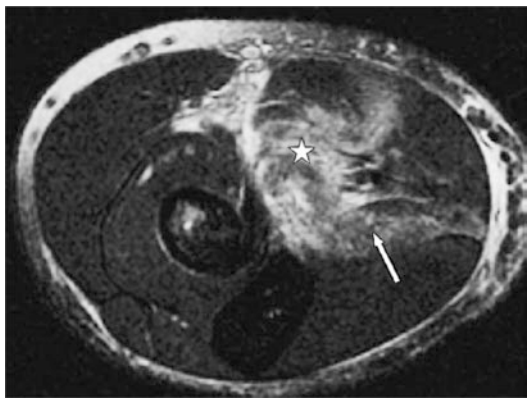

Fig. 1 A 23-year-old female gymnast sustained a fall on the left elbow while training on the balance beam. Axial T2-WI FS image of the left elbow at the level of the tuberositas radii. Extensive muscle edema and partial rupture of the pronator teres muscle (asterisk), muscle edema in the superficial flexor digitorum muscle (arrow) and extensive fluid in the fascial planes and subcutaneously

Table 2 Common injuries in selected sports

Sport	Injury	Common name
Baseball	Ulnar collateral ligament	"Pitchers elbow"
Baseball—child/adolescent	Medial epicondyle apophysitis	"Little League elbow"
Tennis	Lateral epicondylitis	"Tennis elbow"
Golf	Medial epicondylitis	"Golfers elbow"
Handball and soccer	Intra-articular loose bodies	"Goalkeepers elbow"
Gymnastics	Osteochondral lesions	–

2 Anatomy

The elbow has a central position in the shoulder-hand kinetic chain. It consists of three articulations joined in a common synovial compartment known as the humero-ulnar, the capitello-radial, and the (proximal) radio-ulnar joint. To allow a combination of flexion-extension (humero-ulnar), pro-supination (radio-ulnar), and stability of the elbow joint, a specific congruent design of the humero-ulnar articular surfaces is needed. A triangular shaped fortification of the medial capsular structures is the medial or ulnar collateral ligament (UCL), the origin or top of the broad based triangle is located at the medial epicondyle and the insertion is located at the ulna (anterior to the processus coronoideus and posterior to the olecranon). On the lateral side a capsular fortification arises from the lateral epicondyle and forms the radial ligamentous complex (RLC) (Alcid et al. 2004; Kijowski et al. 2004; Bryce and Armstrong 2008; Karbach and Elfar 2017). The UCL consists of three separate structures, the anterior bundle, the posterior bundle, and the transverse bundle (Fig. 2). The anterior bundle is the most important valgus stress stabilizer of the elbow joint, and can be further divided into anterior and posterior bands that alternate in tautness in extended and flexed position, respectively. Since the transverse bundle does not cross the elbow joint itself it does not contribute much to the stability (Alcid et al. 2004; Chung and Kim 2003; Kijowski et al. 2004; Thornton et al. 2003; Bryce and Armstrong 2008; Karbach and Elfar 2017). The RLC is composed of four different ligaments and protects the elbow against varus stress and posterolateral instability. It is much less prone to injury than the UCL (Alcid et al. 2004; Chung and Kim 2003; Kijowski et al. 2004; Thornton et al. 2003; Bryce and Armstrong 2008; Karbach and Elfar 2017). The most important osseous landmarks are the medial and lateral epicondyle of the humerus, the olecranon, the coronoid process of the anterior ulna and the radial head. The most important musculotendinous structures are, arising from the lateral epicondyle, the common extensor tendon including the lower arm, hand and wrist extensors, and the common flexor tendon or pronator-flexor complex which arises from the medial epicondyle (Alcid et al. 2004). The ulnar nerve, which is the most often compromised nerve around the elbow in athletes, runs in a fibro-osseous groove at the medial humeral epicondyle, close to the origin of the UCL.

Fig. 2 Normal anatomy of the ulnar collateral ligament. It consists of three separate bundles: the anterior bundle (black arrow), the posterior bundle (white arrow), and the transverse bundle (arrowhead). (Reprinted with permission from Kijowski R, Tuite M, Sanford M. 2004 Magnetic resonance imaging of the elbow. Part I: Normal anatomy, imaging technique and osseous abnormalities. Skeletal Radiology 33: 685–697)

3 Biomechanics

3.1 Introduction

Biomechanically the elbow joint acts as a combination of a hinge joint (ulno-humeral and radio-humeral) and a more pivot joint (radio-humeral and proximal radio-ulnar) allowing not only flexion-extension but also pronation-supination movements. The main stability of the elbow results from the highly congruent ulno-humeral joint surfaces and the collateral ligaments, preventing hyperextension and hyperflexion and varus and valgus, respectively (Bryce and Armstrong 2008; Karbach and Elfar 2017).

3.2 Baseball (and Other Overhead Throwing Sports)

In baseball, elbow injuries most commonly originate due to pitching, and hence the term "pitcher's elbow" which actually most often refers to an injury of the UCL. The pitch, a very complicated movement, is commonly divided into six phases: windup, stride, cocking, acceleration, deceleration, and follow through (Alcid et al. 2004; Fleisig et al. 1995; Loftice et al. 2004; Werner et al. 1993, 2002; Escamilla et al. 2017). These different phases are well described in the literature and apply more or less to other overhead throwing movements performed by other athletes. Essentially, the elbow moves during these phases from a flexed to an extended position; the greatest forces occur during the cocking and acceleration phases when maximum valgus and extension forces are applied to the UCL that acts as the primary valgus stabilizer (Loftice et al. 2004; Werner et al. 1993; Chen et al. 2001). This can result in acute and chronic injuries of the UCL and/or the pronator-flexor complex that acts as the secondary medial stabilizing structure (Alcid et al. 2004; Cain et al. 2003; Chen et al. 2001). With this knowledge, studies have shifted their focus to identifying kinematic differences between different pitch types. The first results of these studies suggest lower amounts of force and torque in the changeup compared to fastballs, curveballs, and sliders (Escamilla et al. 2017). The stability of the osteochondral structures itself, more specifically the olecranon in the fossa olecrani and the radio-capitellar joint, increases when the elbow moves towards extension leading to torque forces and shearing of the olecranon in its fossa and to posterior osteophyte formation resulting in what is called "valgus extension overload syndrome" (VEO) (Ahmad and Elattrache 2004). The compressive forces that are generated in the lateral elbow can lead to cartilage damage or bone lesions of the radial head and/or capitellum (e.g., osteochondral lesions) (Bojanic et al. 2006; Cain et al. 2003; Gerbino 2003; Loftice et al. 2004; Kijowski et al. 2004).

The term "little league elbow" usually refers to athletic injuries in the immature skeleton, probably due to improper throwing techniques. Originally described as a medial epicondyle fracture (Brogdon and Crow 1960), the term is actually reserved to describe medial epicondyle traction apophysitis or medial apophyseal avulsion.

Although javelin and American football involve overhead throwing similar to the baseball pitch, injuries to the elbow are much less frequent. It is suggested that in football this is probably due to lower forces and less torque in the elbow during the throw (Loftice et al. 2004). Although several studies are published on the specific biomechanics of the throw in javelin which also involves powerful flexion from maximal extended position (Bartlett and Best 1988; Morris and Bartlett 1996), there is lack of large studies on elbow injuries in this sports discipline.

3.3 Golf

For a non-throwing sport, golf places enormous strains on the different components of the kinetic shoulder-elbow-wrist chain. The swing can be divided into the takeaway, forward swing, acceleration, early follow through, and late follow through (Zouzias et al. 2018). An injury to the elbow in golfers is almost always swing related or due to improper technique. The medial epicondylitis or so-called "golfer's elbow" is an overuse injury of the common pronator-flexor origin and occurs typically in the elbow of the dominant arm

(the right arm in a right-handed golf player). Forceful overuse of the common extensor muscles leading to lateral epicondylitis is more frequent when the grip of the golf club is to tight (Zouzias et al. 2018). Not only improper technique contributes biomechanically but also abrupt trauma when the player hits the ground in front of or behind the ball. It is the violent deceleration on impact that strains the medial compartment and that raises forceful contractions at the medial and lateral lower arm musculature to stabilize the elbow and the club that lead to the condition (McCarroll 2001; Thériault and Lachance 1998; Zouzias et al. 2018). Therefore, lateral epicondylitis is also a common problem at the nondominant arm or lead arm in golf players (Loftice et al. 2004; McCarroll 1996, 2001; Thériault and Lachance 1998; Zouzias et al. 2018). The frequency of medial and lateral injuries is more or less equal in golf players (McCarroll 1996).

3.4 Tennis

"Tennis elbow" or lateral epicondylitis is associated with excessive overuse of the hand and wrist extensors. The tendon most commonly involved is the extensor carpi radialis brevis (ECRB) (Levin et al. 2005; Miller et al. 2002; Roetert et al. 1995; Walz et al. 2010). Injuries seem to be predominantly associated with improper backhand use, leading to excessive forces at the level of the common extensor origin. This may explain the higher incidence of lateral epicondylitis in nonprofessional tennis players compared to professional tennis players (Walz et al. 2010). Despite the fact that studies have shown that in all major strokes at tennis the wrist extensors are highly involved, only improper backhand use is predominantly associated with tendinosis and paratenonitis of the origin of the ECRB (Loftice et al. 2004; Roetert et al. 1995). Other factors that have been incriminated consist of improper hand/wrist positioning (over-pronation and hyperflexion), eccentric location of impact of the ball on the racket, and the amount of force impact/transfer from the ball to the racket (Roetert et al. 1995). In addition to these factors, the deep parts of the tendon tend to lack vascularity which can also contribute to degeneration and tendinosis (Walz et al. 2010).

3.5 Handball and Soccer (European Football)

Although biomechanically there is a large difference between handball and soccer players, with regard to elbow injuries the goalkeepers in both sports share a common injury pattern of the elbow, which is called the "goalkeeper's elbow." Two mechanisms are involved: the first is the injury pattern as seen in many overhead throwing athletes. Therefore, similar elbow lesions as in overhead throwing athletes are found (Popovic and Lemaire 2002; Popovic et al. 2001). The second (which is more typical for goalkeepers) is repeated combined high valgus stress load and hyperextension of the elbow due to the blockage of shots fired at the goal (Akgun et al. 2007). This trauma leads to medial elbow instability and repetitive abutment of the olecranon in its fossa and can lead to cartilage damage, osteophyte formation, and intra-articular loose bodies.

3.6 Gymnastics

Participants in gymnastics are traditionally and increasingly younger in age. This puts them at a particular risk for injuries to the growing skeleton which are different compared to injury patterns encountered in adults. Osteochondral lesions are frequently seen in gymnasts, because they use their elbow as a weight-bearing joint (Bojanic et al. 2006; Jackson et al. 1989). It is predominantly an overuse injury caused by repetitive microtrauma to the immature cartilage. A similar pattern is seen in weightlifters.

4 Imaging the Elbow

4.1 Introduction

In the authors' opinion standard radiography should be the first imaging modality of choice. Apart from a so-called reversed axial projection

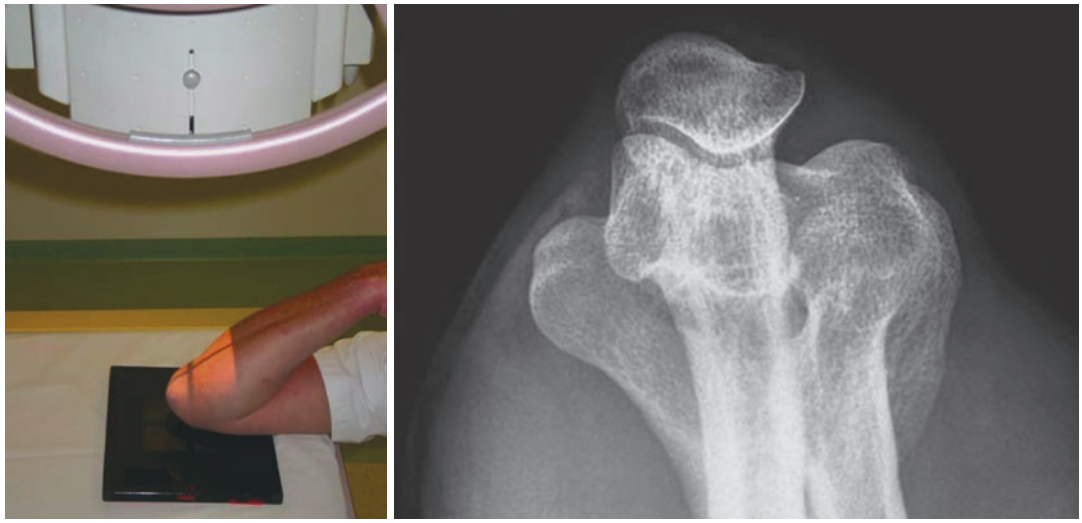

Fig. 3 Reversed axial projection of the right elbow allows better visualization of the posterior elbow, in particular the olecranon and the posterior part of the humero-ulnar joint

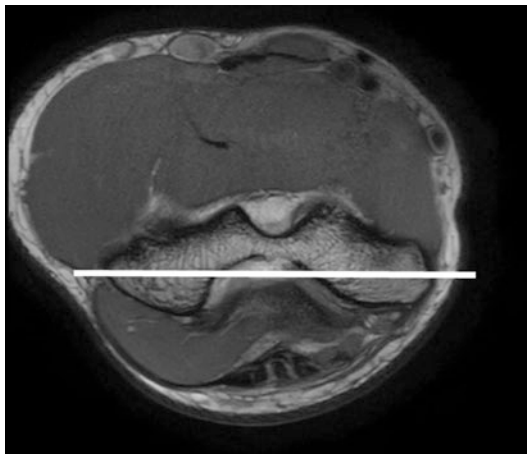

Fig. 4 A coronal MRI plane (or a coronal MPR on a CT) is planned on an axial image and runs parallel to the condyles of the distal humerus (white line)

which allows better visualization of the olecranon and the trochlea (Fig. 3), additional views in many different directions are usually not helpful. The value of stress radiographs is discussed elsewhere (see Sect. 4.2.1).

Ultrasound is a fast and cheap way to evaluate the elbow. To evaluate the anterior recess, the arm is partially flexed and supinated while the posterior recess is best evaluated in elbow extension. Lateral and medial visualization is most optimal in extension or 90° flexion semi-pronated or a slightly flexed elbow in exorotation, respectively. The posterior elbow soft tissues are most easily examined in flexion with the palm of the hand flat on the table (fingers directed towards patient) (Ferrara and Marcelis 1997).

The positioning of the elbow on MRI is considered to be one of the most important factors which can be either fully supinated and extended (besides supine body) or in an overhead pronated and extended position (body prone) ("Superman's position") in which case the elbow is more in the center of the magnet which improves image quality. All imaging planes can be useful but one has to make sure that the coronal plane is parallel to the middle of both humeral condyles (Fig. 4), although a coronal oblique plane is also proposed, especially for the collateral ligaments (Cotten et al. 1997). The role of MR arthrography is controversial, but there is no evidence that routinely MR arthrography is more accurate than conventional MR.

Helical high-resolution CT (HRCT) with 0.6 or 0.5 mm slice thickness can have its advantages over MRI due to the superior spatial resolution in which the osseous structures are visualized. Examining the elbow with HRCT takes a considerable shorter time compared to a MRI investigation which can be of significant importance in a painful patient.

Fig. 5 A 20-year-old baseball player with pain in the region of the UCL for several months. AP radiograph of the left arm. A faint calcification is seen at the region of the proximal attachment of the UCL (arrow)

Fig. 6 Longitudinal ultrasound view of a normal UCL (arrowheads). The normal UCL is hyperechoic and has a fanlike shape proximally. Distally its insertion is at the sublime tubercle of the proximal ulna (arrow)

The role of bone scintigraphy is declining since the introduction of MRI. It is not the high sensitivity of scintigraphy for bony abnormalities but the low specificity and blindness to soft tissue lesions that limits its use (Van der Wall et al. 2001).

4.2 Baseball and Overhead Throwing Sports

4.2.1 Standard Radiographs

Before the widespread use of ultrasound, which is described in Sect. 4.2.2, to assess UCL injury, standard radiography was the primary diagnostic tool of choice. In case of suspicion of UCL injury, standard radiography and CT (see Sect. 4.2.4) aims to exclude or visualize small avulsions at its proximal attachment at the medial epicondyle of the humerus (Figs. 5 and 6) or at its distal insertion at the sublime tubercle, which is the medial aspect of the coronoid process of the ulna. Osteophytes are more difficult to appreciate, for these are most common at the posteromedial olecranon in case of chronic UCL injury or "valgus extension overload syndrome." There are several studies that describe the value of stress radiography of the elbow in which AP views of the elbow are made while valgus stress is applied to the elbow (Lee et al. 1998; Rijke et al. 1994; Eygendaal et al. 2000). Rijke et al. (1994) differentiates partial (grade 2) from complete (grade 3) UCL tears using this technique. Lee et al. (1998) recognized the value of stress radiography in valgus instability, with comparative views of the uninjured elbow to differentiate instability from nontraumatic joint laxity. However, evaluating the UCL with US or MRI has almost completely taken over the role of these stress radiographs. Medial apophysitis, in skeletally immature throwers, may produce subtle abnormalities on plain films. Slight widening of the apophysis or fragmentation of the ossification center can be seen (Chen et al. 2005; Hang et al. 2004; Klingele and Kocher 2002; Wei et al. 2010).

4.2.2 Ultrasound

Ultrasonography is a convenient, noninvasive, and cheap method to detect several morphologic changes in the ligaments and tendons of the elbow in injured athletes. It has several other advantages compared to other means of radio-

logical evaluation. It offers the possibility to examine the elbow dynamically and evaluation of the contralateral side for comparison can be performed simultaneously in the same setting.

Ultrasound can provide a good and reliable evaluation of the UCL (Fig. 7). The anterior band of the UCL is most commonly associated with chronic traumatic changes in throwing athletes as it is the major stabilizer of valgus stress in the elbow. On normal ultrasound the anterior band should appear as a hyperechoic, thin, and compact fibrillar band under the common flexor tendon (Konin et al. 2013). Several studies have been performed on both injured and non-injured professional and amateur baseball players to assess changes in the UCL and medial joint laxity as a result of UCL trauma. These studies showed a significant increase in thickness of the anterior band of the UCL and more hypoechoic foci and calcifications in the dominant elbow compared to the nondominant one (Ciccotti et al. 2017; Nagamoto et al. 2014; Tajika et al. 2016; Sasaki et al. 2002).

Fig. 7 Coronal CT MPR of the same patient as in Fig. 5. A small avulsion at the origin of the UCL is very well appreciated on CT (arrow)

As a result of UCL trauma with partial or complete tears of the ligament, the medial joint space can widen when valgus stress is applied. As mentioned above, this widening can also be measured with ultrasound as dynamic assessment is possible. Several studies found a significantly larger increase in medial joint space when applying valgus stress in the dominant elbow compared to the nondominant elbow (Sasaki et al. 2002; Ciccotti et al. 2017) when comparing overhead throwing athletes with healthy volunteers.

Osteochondritis dissecans of the capitellum is thought to be caused by repetitive compressive forces during pitching and has a reported prevalence in young baseball players between 1.3 and 3.4% (Matsuura et al. 2014; Otoshi et al. 2017; Kida et al. 2014; Harada et al. 2006). Although US is in general not used to evaluate OCD lesions, several subchondral characteristics of OCD can be identified using ultrasonography. These consist of cortical irregularities of the subchondral bone, cystic lesions, a double floor line, or discontinuities of the capitellum (Matsuura et al. 2014; Yang et al. 2017).

In a study performed by Lee et al. ultrasound had a positive predictive value of 88% for detecting medial epicondylar lesions in young baseball players when compared to MRI (Lee et al. 2019). Ultrasonography showed irregularities or fragmentation of the medial epicondyle in 9.4% of their study population which consisted of 7 (junior) high school baseball teams, including UCL injuries which are more often seen in skeletally mature pitchers.

Though ultrasonography can be used to identify several injuries in the adolescent and professional baseball player, all results should be interpreted with caution as all morphologic changes have also been reported in uninjured players and asymptomatic elbows.

4.2.3 MRI

The anterior bundle of the UCL is the most important structure to visualize in an overhead throwing athlete with medial elbow pain. It is the only part of the medial complex that is reliably seen in the coronal plane in which it should appear as a thin continuous linear structure with a low signal intensity on all sequences (Kijowski

Fig. 8 Normal UCL. Coronal T2-fatsat image on which the ulnar collateral ligament is displayed as a thin, smooth edged appearance and of overall low signal intensity (white arrowheads). There is a relative broad insertion below the undersurface of the medial epicondyle which is normal. The discrete hyperintensity at this level of the insertion is also normal

Fig. 9 An 18-year-old baseball pitcher with chronic ulnar-sided elbow pain. Coronal T2*-weighted image. There is a complete disruption of the origin of the UCL at the level of the medial epicondyle (arrow) with fluid surrounding the ligament that is slackened, somewhat irregular and blurred

et al. 2005; Ciccotti et al. 2017) (Fig. 8). A small amount of fat can be seen deep and/or superficial to the ligament (Jacobson et al. 2003). Complete rupture is demonstrated through non-visualization of the ligament or focal complete disruption at the ulnar or humeral attachment (Fig. 9). Other signs of rupture, either partial or complete, include laxity, thickening, irregularities, and poor definition of the ligament as well as abnormal signal intensity in or around the ligament (Kijowski et al. 2005; Nakanishi et al. 1996; Sonin and Fitzgerald 1996; Thornton et al. 2003). Ossification and osteophyte formation can be seen (Fig. 10). In case of injury of the UCL around the sublime tubercle, a T-sign can be seen on MRI (Ciccotti et al. 2017; Nocerino et al. 2018). A T-sign is described as contrast between the attachment of the UCL and the sublime tubercle and can be indicative of a partial tear. A very recent study by Lin et al. demonstrated that the T-sign is most likely not an anatomical variation but that it is a poor predictor of symptoms or need for surgery (Lin et al. 2019). Complete ruptures are easier to diagnose than partial ruptures. A sensitivity and specificity of as high as 100% has been described for complete ruptures, for partial rupture a sensitivity of only 57% is reported (Timmerman et al. 1994). Partial ruptures are more easily seen if surrounded by fluid. This explains the preference of some radiologists to perform MR arthrography in which there is extravasation of fluid or gadolinium extra-articular into or beyond the ligament (Munshi et al. 2004; Nakanishi et al. 1996; Timmerman et al. 1994; Thornton et al. 2003; Nocerino et al. 2018). Whatever technique used, we have to be careful in diagnosing partial tears since several studies showed that the UCL can have a variable appearance not only at its distal insertion at the sublime tubercle but also at its proximal attachment at the humeral epicondyle (Jacobson et al. 2003; Munshi et al. 2004).

In "valgus extension overload syndrome" MRI is used to evaluate the UCL, the joint cartilage, and the olecranon to look for osteophytes and loose bodies. The UCL is expected to be

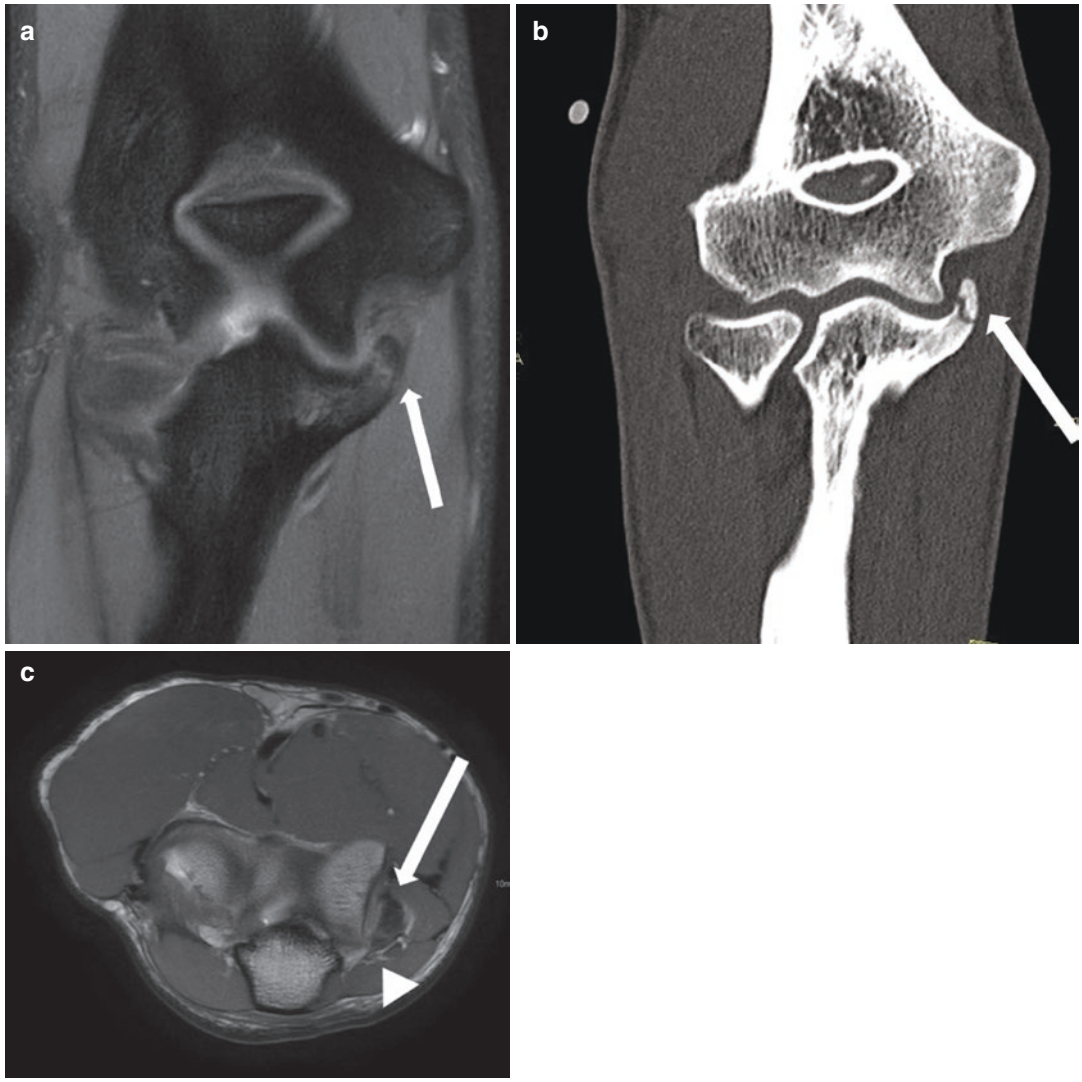

Fig. 10 A 26-year-old baseball player with acute on chronic medial elbow pain. (**a**) Coronal PD FS demonstrating extensive bone formation at the level of the ulnar origin of the UCL with bone marrow edema (arrow). There is no clearly recognizable ulnar collateral ligament. (**b**) The coronal CT MPR confirmed these findings and showed strong suggestion of a possible recent fracture of the tip of the bone formation causing the acute component (arrow). (**c**) Axial T1 displays the proximity of the ulnar nerve (arrowhead).

thickened and irregular and predominantly hypointense on T1-weighted and T2-weighted sequences reflecting fibrosis as part of repair of microtears. Bone marrow edema can be seen in the olecranon representing repetitive bony stress. Particular attention has to be paid to the ulnar nerve since ulnar neuropathy can accompany VEO syndrome (Fig. 11). The ulnar nerve may be thickened with high signal intensity on PD or T2-weighted images and/or can be subluxed from the ulnar groove (Cain et al. 2003; Field and Savoie 1998; Gerbino 2003; Kijowski et al. 2005; Thornton et al. 2003).

In the immature skeleton the apophysis of the medial epicondyle is particularly vulnerable to repetitive valgus stress (Klingele and Kocher 2002; Chauvin and Gustas-French 2019). This recurrent stress results in medial epiphysitis (which is of course a misnomer) which can demonstrate sclerosis, trabecular thickening, and a

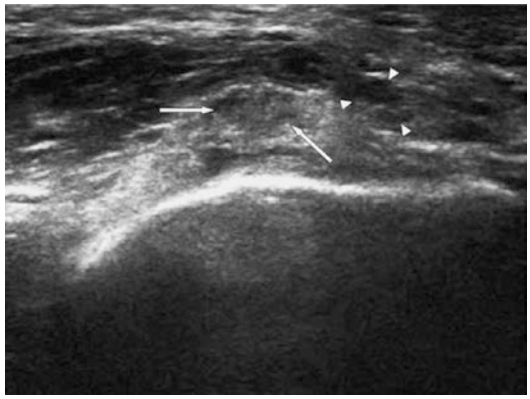

Fig. 11 Transverse US image of the elbow showing the UCL (arrows). Note the close proximity of the ulnar nerve (arrowheads) which is often compromised in cases of UCL injuries

widening of the physis with an increased fluid-sensitive signal on either side of the physis in young players with an open physis (Chauvin and Gustas-French 2019). In severe cases fragments of the medial apophysis, or the complete medial apophysis, might avulse as a result of the recurrent valgus stress. The same valgus stress can also lead to capitellar osteochondritis dissecans which will be described in further detail in Sect. 4.6.3 as it is common in both young baseball players and gymnasts.

A study performed by Hurd et al. (2011) in uninjured high school baseball players showed abnormal MRI findings in 87% of the 23 participants. The most common finding being thickening of the UCL in the dominant elbow in 65% of the participants. Other identified soft tissue abnormalities were joint effusion in 17% of cases and one case of increased T2-weighted signal intensity at the insertion of the triceps in the dominant arm. Several osteoarticular changes were also observed and included subchondral sclerosis in the ulnotrochlear articulation (61%), osteophytes at the olecranon (35%), ulnotrochlear chondromalacia (17%), and bone marrow edema in one case. Ten individuals (43%) were identified with multiple abnormalities (Hurd et al. 2011).

The findings of abnormalities in uninjured players lead to the question whether these findings can predict future injuries and several performed studies have found conflicting results. Similar studies were performed by Gutierrez et al. (2017) and Garcia et al. (2019) that retrospectively analyzed routine MRIs in Major League Baseball pitchers and the correlation of these scans with future placement on disabled lists found conflicting results. The study performed by Garcia et al. (2019) reviewed scans of 41 pitchers of a single organization from 2005 to 2017 and found a significantly higher amount of uninjured pitchers to be placed on the disabled list when an MRI found UCL heterogeneity, partial UCL tears, and posteromedial impingement compared to pitchers whose MRI did not show these changes (Garcia et al. 2019). Gutierrez et al. (2017) however found no statistically significant prediction of placement on the disabled list following any abnormalities on MRI with a total of 26 MRIs examined.

4.2.4 CT

The use of CT as a secondary imaging modality (after standard radiography) to evaluate elbow injuries in overhead throwing athletes is almost exclusively reserved for acute bony trauma (fractures). Chronic osseous injuries like stress fractures of the olecranon are relatively uncommon in overhead throwers but have been described in baseball players and javelin throwers and can be visualized with CT, especially the type III and IV fractures (classification by Arendt/Griffiths) (Iwamoto and Takeda 2003; Arendt and Griffiths 1997). If, on standard radiographs, a bony avulsion is suspected in case of an UCL injury, CT will yield better results than MRI in describing the exact size and location of the fragment (Fig. 6). In case of "valgus extension overload syndrome," CT can depict the exact size and location of the osteophytes at the posterior olecranon better than standard radiography. An additional advantage of CT is that in case of absence of intra-articular fluid an intra-articular osseous loose fragment will be picked up more easily than with MRI.

4.3 Golf

4.3.1 Standard Radiography

Standard radiography is of little value in golfer's elbow. Nonspecific findings such as soft tissue swelling, loss of normal fat planes adjacent to the

Fig. 12 Two patients with chronic lateral and medial epicondylitis. Calcifications are seen at the level of the common extensor tendon on the left image and on the right image of the common flexor tendon (white arrows)

medial epicondyle, small calcifications, or subtle cortical irregularities at the origin of the common flexor tendon can be seen (Chen et al. 2003; Kijowski et al. 2005; Kani et al. 2017) (Fig. 12). A bony avulsed fragment at the common flexor tendon origin or the UCL is another possible finding.

4.3.2 Ultrasound

Ultrasound is the imaging modality of choice in medial epicondylitis. A clinical study by Park et al. showed high sensitivity, specificity, positive predictive value, and negative predictive value of 95.2%, 92%, 90.9%, and 95.8%, respectively (Park et al. 2008) This study showed the common flexor pronator tendon (CFPT) can show various abnormalities of which a focal hypoechoic area was most commonly seen. The CFPT can also show thickening, outward bowing, a decreased or heterogeneous architecture, or hyperemia. Other abnormalities consist of intratendinous calcifications and epicondylar irregularities or erosions (Kani et al. 2017). Interindividual variability with a short common flexor tendon makes ultrasonographic evaluation more difficult. In these cases, comparison with the uninjured arm is useful.

4.3.3 MRI

With medial epicondylitis being a clinical diagnosis in most cases and ultrasonography being a good diagnostic tool, MRI should only be reserved for cases with high concern for concomitant pathology or when the source of medial elbow pain is unclear (Walz et al. 2010; Amin et al. 2015).

In healthy individuals, the common flexor tendon is seen as a structure with low signal intensity on all sequences (Kani et al. 2017). In medial epicondylitis MRI can reveal a spectrum of abnormalities depending upon the duration and severity of the symptoms. The more acute phase of tendinosis with paratenonitis is characterized by increased signal respectively in and around the tendon on any sequence (Kijowski et al. 2005; Walz et al. 2010; Kani et al. 2017). This increased signal can vary between faint hyperintensity on fluid-sensitive sequences to areas with frank fluid signal although the latter

most likely represents partial tearing. Thickening of the tendon can be seen in more chronic cases, which will most often be referred to as tendinosis. Although tendinosis and tendinitis are confusingly interchangeably used in the literature to describe overuse and degenerative pathology, the correct terminology from the histopathological point of view is tendinosis. Intratendinous inflammation is not predominantly present on pathological specimens. Inflammatory infiltration may be present at the tendon sheath or paratenon and thus is referred to as tenovaginitis and paratenonitis, respectively. It is obvious that only the "-itis" disorders respond to anti-inflammatory drugs (Khan et al. 1999; Puddu et al. 1976). In case of a rupture of the common flexor tendon, thinning or disruption with a fluid-filled gap at the level of the tear is seen (Thornton et al. 2003; Walz et al. 2010). Abnormalities are most frequent at the flexor carpi radialis and pronator teres part of the common flexor tendon (Kijowski et al. 2005; Thornton et al. 2003). Other structures most frequently described with abnormalities in medial epicondylitis are bone marrow, the medial collateral ligament (MCL), and the ulnar nerve. Bone marrow edema in the medial epicondyle and in the surrounding muscles has been described (Thornton et al. 2003). Damage to the MCL has been described as varying between increased signal intensity on proton density-weighted fat-saturated SE images to full thickness tears (Kani et al. 2017). The ulnar nerve is compromised in up to 60% of patients (Jobe and Cicotti 1994); neuritis will show thickening of the ulnar nerve within or distal to the cubital tunnel with an increased signal on T2-weighted or proton density-weighted fat-saturated fast SE images in the nerve and the surrounding tissues (Walz et al. 2010).

4.4 Tennis

4.4.1 Standard Radiography

The most common finding in standard radiology is calcifications at the lateral epicondyle which is seen in 16–47% of cases (Pomerance et al. 2002; Shillito et al. 2017) (Fig. 12). Though this supports the diagnosis of "tennis elbow," it does not alter treatment in patients with a clinical diagnosis. Standard radiography is therefore found to be not cost-effective and should not be used routinely (Keijsers et al. 2019).

4.4.2 Ultrasound

The ultrasound appearance of the common extensor tendinosis (Fig. 13) is basically similar to the findings in common flexor tendon overuse. They include linear intrasubstance tears, thickening of the tendon, calcifications as well as enthesophytes, bone irregularities, focal hypoechoic areas, peritendinous fluid, and diffuse tendon heterogeneity (Connell et al. 2001; Levin et al. 2005; Miller et al. 2002) (Fig. 14). Compared to MRI, studies by Levin et al. (2005), Miller et al. (2002), and Bachta et al. (2017) showed a good US sensitivity for lateral epicondylitis ranging from 64% to 88% with MRI sensitivity ranging from 90% to 100%. A large discrepancy was found in outcomes for specificity ranging from 67–100% (Miller et al. 2002; Bachta et al. 2017) to 36–48% (Levin et al. 2005). A possible explanation for these outcomes could be the used criteria for diagnosing lateral epicondylitis.

A study by Arslan et al. (2018) comparing diagnostic performance of different sonographic modalities showed optimal diagnostic properties when combining B-mode sonography with SMI (Superb Microvascular Imaging). This reported a sensitivity, specificity, positive predictive value, and negative predictive value of 94%, 98%, 97.7%, and 94.2% and was superior

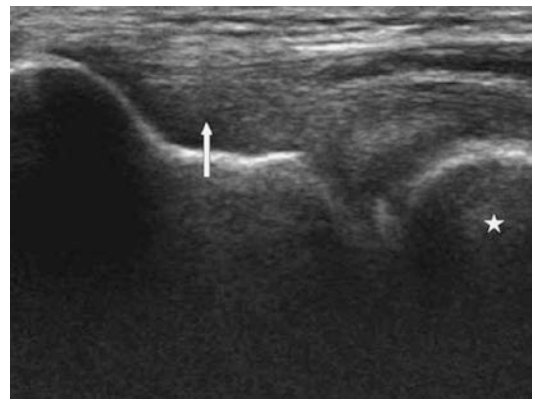

Fig. 13 Longitudinal US view of the normal common extensor tendon origin (arrow). Radial head (asterisk)

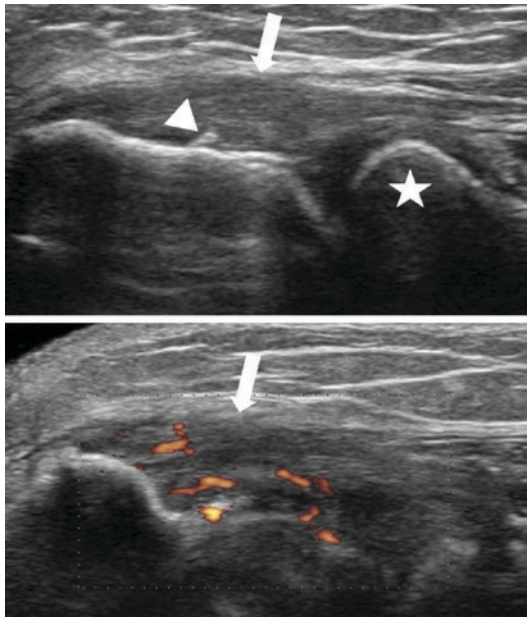

Fig. 14 A 38-year-old avid tennis player with chronic lateral elbow pain. Longitudinal US images on which the common extensor tendon is shown (white arrow). There is small calcification (arrowhead upper image), distortion of the normal fibrillar architecture of the tendon with hypoechoic areas, and intratendinous increased signal on power Doppler (lower image)

compared to other combinations including power Doppler, color Doppler, and strain elastography.

4.4.3 MRI

A very high sensitivity is repeatedly reported for MRI in the evaluation of lateral epicondylitis, although a meta-analysis in 2001 concluded that the assessment of MR findings in epicondylitis is questionable due to small sample sizes and methodological shortcomings (Pasternack et al. 2001). Fluid-sensitive sequences are mandatory (STIR or T2-Fat Sat); the axial and coronal planes are the most helpful in the evaluation of the common extensor tendon which should demonstrate low signal intensity on all sequences (Walz et al. 2010) in normal individuals. The ECRB is most often involved, not rarely with secondary involvement of the extensor digitorum communis (EDC) (Nirschl 1992; Walz et al. 2010). Findings depend upon chronicity of the condition and are thickening or thinning of the tendon and increased signal on the fluid-sensitive sequences and/or the T1-weighted sequences (Fig. 15). These findings can however also be found in non-symptomatic high-performance athletes (Martin and Schweitzer 1998). Furthermore, the radiologist has to be informed if any treatment has been applied (e.g., local corticosteroid injection, shock wave therapy) prior to MRI. In the coronal plane the LUCL is assessed because injuries to this ligament are not uncommon in patients with lateral epicondylitis (Bredella et al. 1999; Walz et al. 2010). Bone marrow edema at the lateral humeral epicondyle can occur (Martin and Schweitzer 1998) as well as T2-weigthed hyperintense signal in the surrounding soft tissues (e.g., anconeus muscle) (Coel et al. 1993).

4.5 Handball and Soccer

4.5.1 Standard Radiography

A radiographic study of handball goalkeepers found several minor abnormalities in the elbow with conventional radiography (Fig. 16). Of the investigated symptomatic elbows 21% showed either radiologic signs of medial instability with manual valgus force, arthritic changes, loose bodies, or a spur at the insertion of the MCL. All these changes were however not statistically significant when compared to the uninjured elbows of the same players (Tyrdal and Finnanger 1999).

A different study described osteophyte formation in 67% of radiographs and were usually located at the olecranon process. The same study also found that stress radiography usually reveals laxity of the medial elbow structures (as in baseball players) demonstrated as increase in ulno-humeral distance if valgus stress is applied to the elbow. This study did find a statistically significant increase in ulno-humeral distance when comparing with a healthy control group from the general population (Popovic and Lemaire 2002; Popovic et al. 2001).

Also reported in handball and baseball players is a generalized bony hypertrophy of the humerus of the dominant arm. This is manifested by an increased humeral diameter and cortical hypertrophy of the humeral shaft, regardless of any

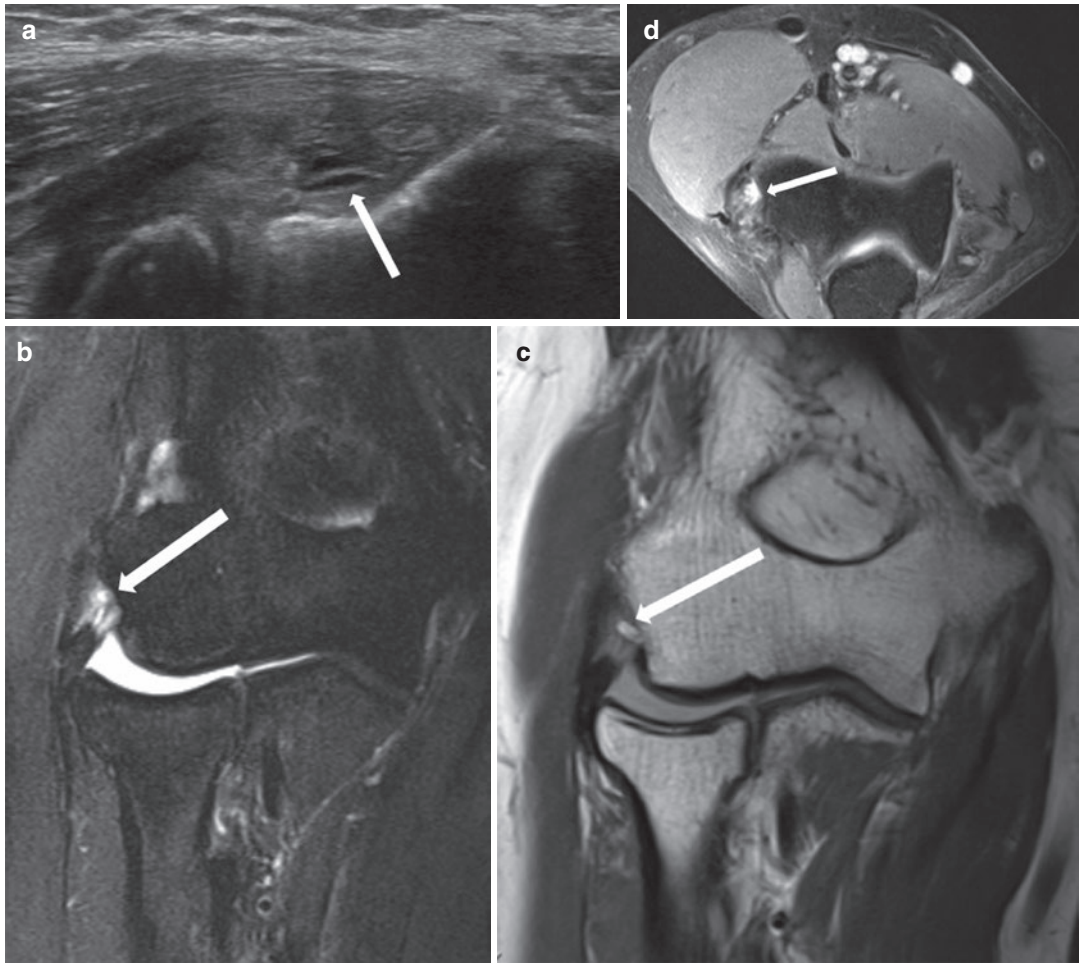

Fig. 15 (**a**–**d**) A 40-year-old recreational tennis player with chronic lateral elbow pain. (**a**) Longitudinal US image shows thickening and distortion of the common extensor tendon with a small tear (white arrow). MRI images after 6 months conservative treatment but ongoing pain. (**b**) coronal STIR, (**c**) Coronal PD, and (**d**) axial PD FS demonstrate persistent epicondylitis with an abnormal common extensor insertion with subtotal tear of the central and deep fibers (white arrows)

complaints (Popovic et al. 2001; Gore et al. 1980).

4.5.2 Ultrasound

US can be useful in the detection (but not exclusion) of loose bodies in the elbow joint (Popovic and Lemaire 2002; Popovic et al. 2001; Ferrara and Marcelis 1997). This is especially true if there is an associated joint effusion which is often present due to secondary synovitis. Calcified loose intra-articular bodies present as focal echogenic structures separate from cortical bone, the larger one's with posterior shadowing. Loose bodies as small as 1 mm can be detected especially in the presence of joint effusion (Marcelis et al. 1996). The most common locations include the olecranon fossa and the coronoid fossa (O'Driscoll 1992).

Physiologic and pathologic thickening of the various tendons surrounding the elbow joint is described in handball goalkeepers (Popovic et al. 2001).

4.5.3 MRI

MRI can be used to detect intra-articular loose bodies especially when there is an associated effusion (Quinn et al. 1994). This is also demonstrated in a study performed on baseball pitchers

Fig. 16 Professional 28-year-old soccer goalkeeper with recurrent right elbow pain. Lateral radiograph of the right elbow. A small ossicle is seen in the fossa olecrani (arrow) which can represent an accessory ossicle or intra-articular loose body. No other loose bodies are identified

who underwent surgery for posteromedial elbow impingement. In three patients loose bodies were found during surgery which were all identified during a prior MRI study (Cohen et al. 2011). The signal intensity is variable depending upon the amount of calcification and bone marrow if ossification is present. Particularly T2-weighted and gradient echo sequences are useful to detect loose bodies; the latter sequence can also be particularly helpful to evaluate a potential donor site, e.g., chondral defects. In the absence of an effusion the accuracy of MRI is far less with a sensitivity of 50% and a specificity of 60% (Miller 1999). In these cases injection of saline or gadolinium into the joint improves accuracy but one has to be careful not to inject air bubbles into the joint for these can easily be mistaken for loose bodies. Osteophytes and synovial proliferations can be mistaken for loose bodies.

4.5.4 CT

In the authors' opinion CT of the elbow is superior to MRI and US in the detection of calcified loose bodies but also for the detection of osteophytes. Our high-resolution CT (HRCT) protocol includes axial plane imaging with 0.5 or 0.6 mm slice thickness with two-dimensional Multi Planar Reformatting in the coronal and sagittal plane. The position of the elbow is relatively unimportant and can range from fully supine to fully prone. Even in the absence of fluid, the small calcifications can be detected in any part of the joint (Fig. 17). The cartilage layer itself cannot be evaluated without intra-articular iodine contrast, but for the detection of osteochondral lesions CT probably has an accuracy as high as MRI, as is demonstrated in the ankle joint (Verhagen et al. 2005). A potential pitfall is the pseudodefect of the capitellum (see Sect. 4.6.3).

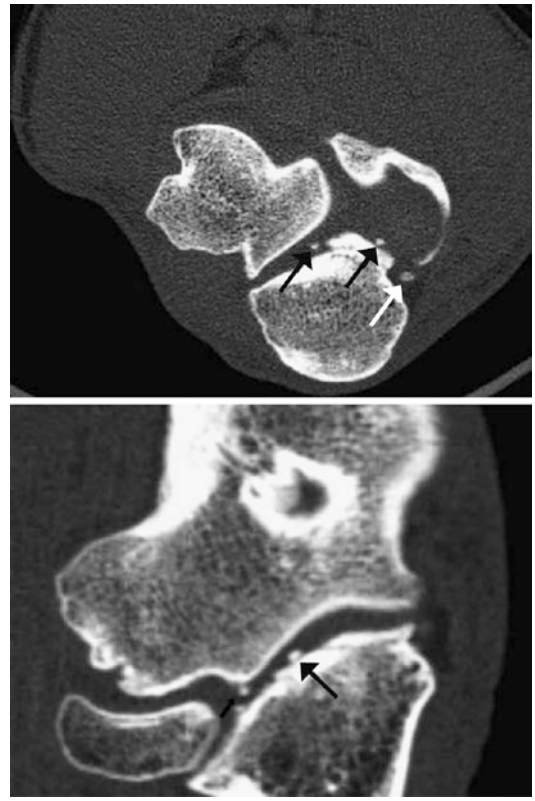

Fig. 17 Same patient as in Fig. 16. MDCT MRP reconstructions in the axial and coronal plane demonstrating multiple small intra-articular loose bodies (arrows) in the right elbow joint which are not appreciated on plain films

4.6 Gymnastics

4.6.1 Standard Radiography

Osteochondral lesions in the elbow are for the most part located at the capitellum most often

anterior to central. The second most frequent location is the radial head. Several studies have shown that standard radiography has a sensitivity for diagnosing OCD of around 45%. This is significantly lower than CT scan and MRI. This is partly because of the location of the osteochondral lesions. Therefore, it has been recommended to perform not only a standard anteroposterior and lateral radiograph, but an anteroposterior radiograph with the elbow flexed 45° as well (Takahara et al. 2008) although this is not routinely performed. Usually a radiolucent area is seen surrounded by more or less sclerosis depending upon the age of the lesion (Figs. 18 and 19a, b). Subtle irregularities of the subchondral bone lamella may precede flattening of the contour of the involved bone. A "displaced fat pad" sign results from joint effusion; loose bodies may be identified (Takahara et al. 2000). A distinction has to be made between osteochondral lesions (osteochondritis dissecans—OD) and Panner's disease, which is not always easy. The latter is considered to be an osteochondrosis of the capitellum. It is most common in young prepubescent males. On radiographs the entire capitellum can be involved with sclerosis, irregularities, and lucencies. It is, however, a benign self-limiting disorder in which the capitellum will regain a normal appearance.

Fig. 18 A 15-year-old gymnast with right elbow pain. AP and lateral radiographs of the right elbow. On the lateral view the lucency in the capitellum (black arrowheads) is compatible with an osteochondral defect. The lesion is much more difficult to appreciate on the AP view; it is discriminated because of the surrounding faint sclerosis (black arrows)

4.6.2 Ultrasound

In recent years several studies have been performed to evaluate the use of ultrasound to examine possible osteochondral lesions in the elbow. Most of these studies have been performed in young baseball players and their results have been described in Sect. 4.2.2.

4.6.3 MRI

A recently performed MRI study found OCD of the capitellum in 7 out of 30 young high-performing gymnasts (Dexel et al. 2014). Grading these osteochondral lesions is important for choosing the optimal treatment. The grading of osteochondral lesions was primarily done during arthroscopy and was originally described in the knee by Outerbridge in 1961. In 2003, the International Cartilage Repair Society (ICRS) suggested a classification system where stable lesions with a continuous but softened area covered by intact cartilage were classified as class I lesions. Stable lesions with a partial discontinuity were classified as class II, lesions with complete discontinuity that have not been dislocated were classified as class III, and dislocated or loose

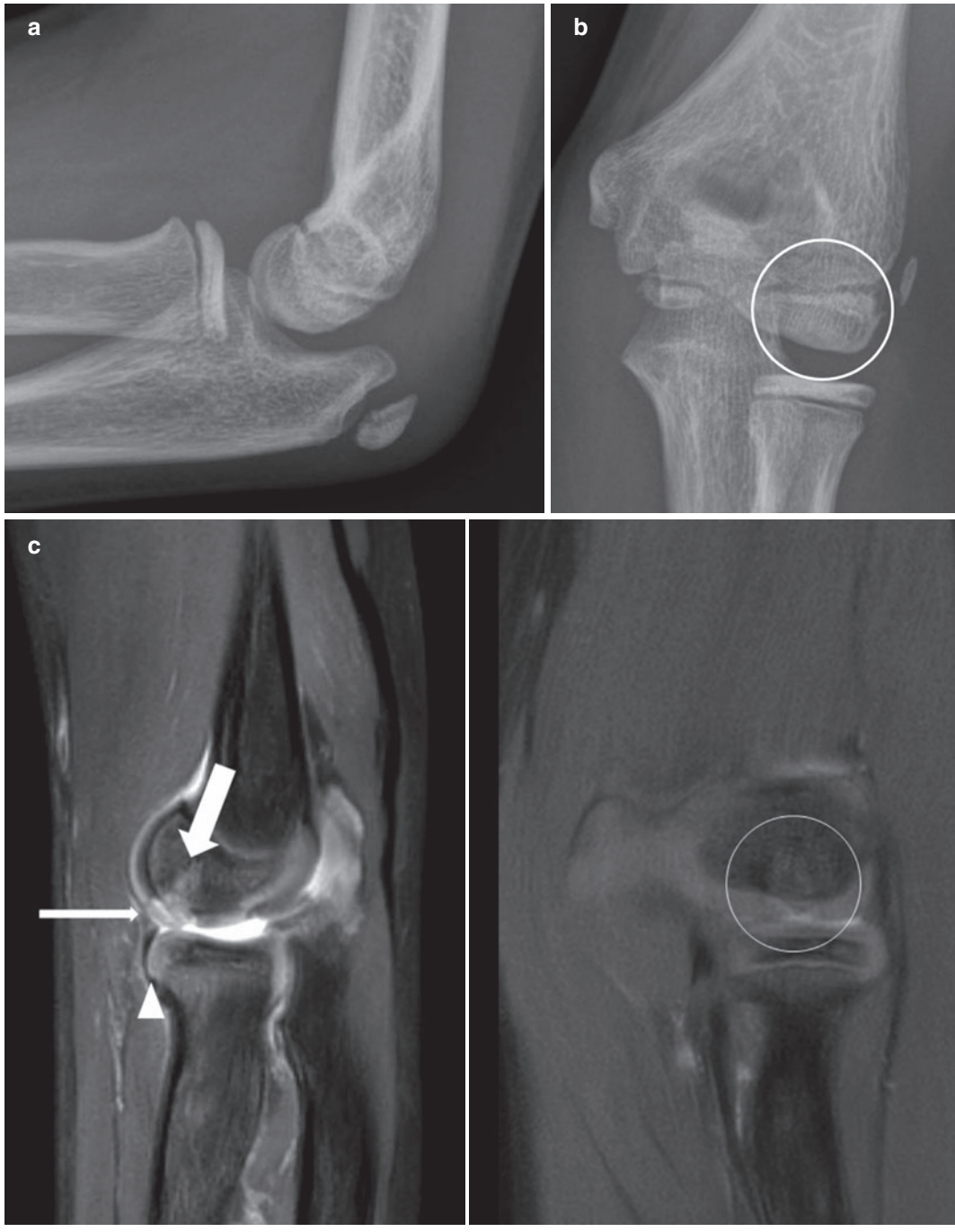

Fig. 19 (**a**–**e**) A 9-year-old professional gymnast with chronic lateral elbow pain. (**a** and **b**) The conventional radiographs demonstrate only minimal distortion of the trabecular architecture of the capitellum with minimal sclerosis; (**c**) the sagittal and coronal PD FS images show extensive osteochondral pathology of the capitellum with bone marrow edema (thick arrow and circle), cartilage defect, and partial detached cartilage flap (thin arrow). In addition, there is a small amount of bone marrow edema in the anterior radial head (arrowhead); (**d**) a slightly more medial image shows an intra-articular loose body in the olecranon fossa (arrow). (**e**) The coronal and sagittal MPR CT images show the irregularity of the capitellum and the small osteochondral defect of the radial head. The loose body was not seen on CT

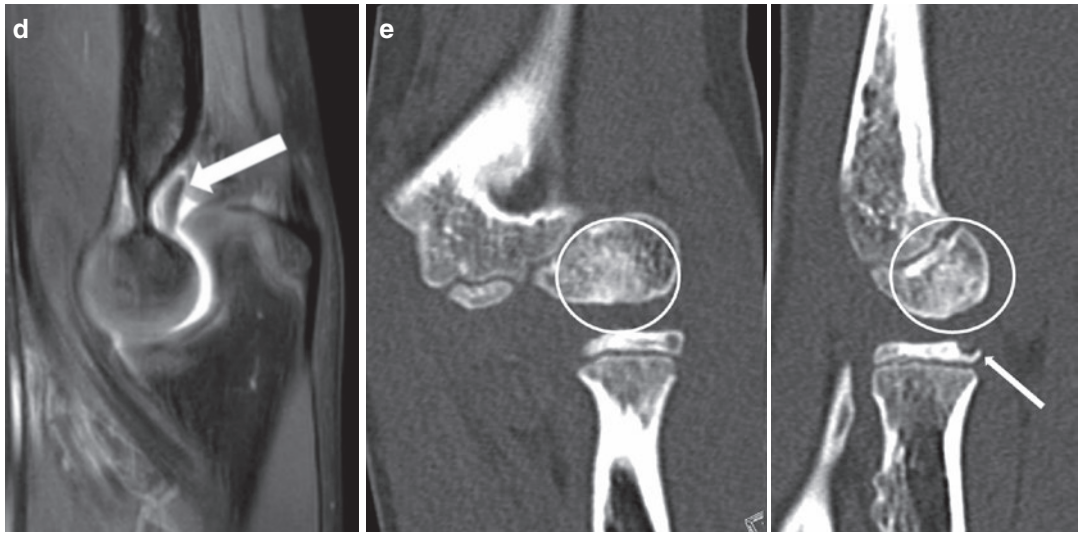

Fig. 19 (continued)

fragments as well as empty defects were classified as class IV. In the same article they recommended an MRI protocol to evaluate the articular cartilage. This protocol consisted of Proton-density-weighted FSE with and without fat saturation, T2-weighted FSE with or without fat suppression, T1-weighted gradient echo with chemical fat suppression, and T1-weighted gradient echo with water excitation (Brittberg and Winalski 2003). Since this publication several studies have been performed to optimize the assessment of OD lesions.

A study performed by Satake et al. (2013) found a specificity higher than 80% to detect an unstable lesion with articular irregularities and defects, a T2 high intensity interface and a high signal intensity line through the articular cartilage (Satake et al. 2013). Kohyama et al. (2018) suggested a slightly different classification which focused on the outline of the capitellum and the articular cartilage. They classified their lesions as: stage 1, normal (circular)-shaped capitellum with no change in the intensity of the articular cartilage, corresponding to ICRS class I. Stage 2, normal (circular)-shaped capitellum with a change in the intensity of the articular cartilage, corresponding to ICRS class II. Stage 3, irregular-shaped capitellum with an observable discontinuity or displacement of the articular cartilage as well as the subchondral bone, corresponding to ICRS class III, and stage 4, a completely dislocated OCD lesion with an articular cartilage defect, corresponding to ICRS class IV (Figs. 19 and 20). The MRI protocol used consisted of sagittal PDW images with 1.5 mm thick slices with a 0.3 mm gap between slices, and T2-weighted and T2-weighted Fast Spin images 1.5 mm thick slices with a 0.3 mm gap between slices. When comparing their classification with intraoperative evaluation, the researchers found a sensitivity of 98.4% and specificity of 84.2%, with a PPV and NPV of 95.3% and 94.1% to detect unstable lesions (Kohyama et al. 2018).

A pitfall in diagnosing OD lesions is the so-called "pseudodefect" of the capitellum. This is found at the junction of the inferior capitellum with the posterior nonarticular surface of the lateral epicondyle (Rosenberg et al. 1994) (Fig. 21).

4.6.4 CT

Imaging of osteochondral lesions in the elbow is most often performed with MRI. Very few studies have been performed to compare CT and MRI in the detection of OD in the capitellum. While MRI provides better visualization of the cartilage compared to CT, it has been suggested CT scans might provide better visualization of loose bodies (van den Ende et al. 2011). A recent study by van

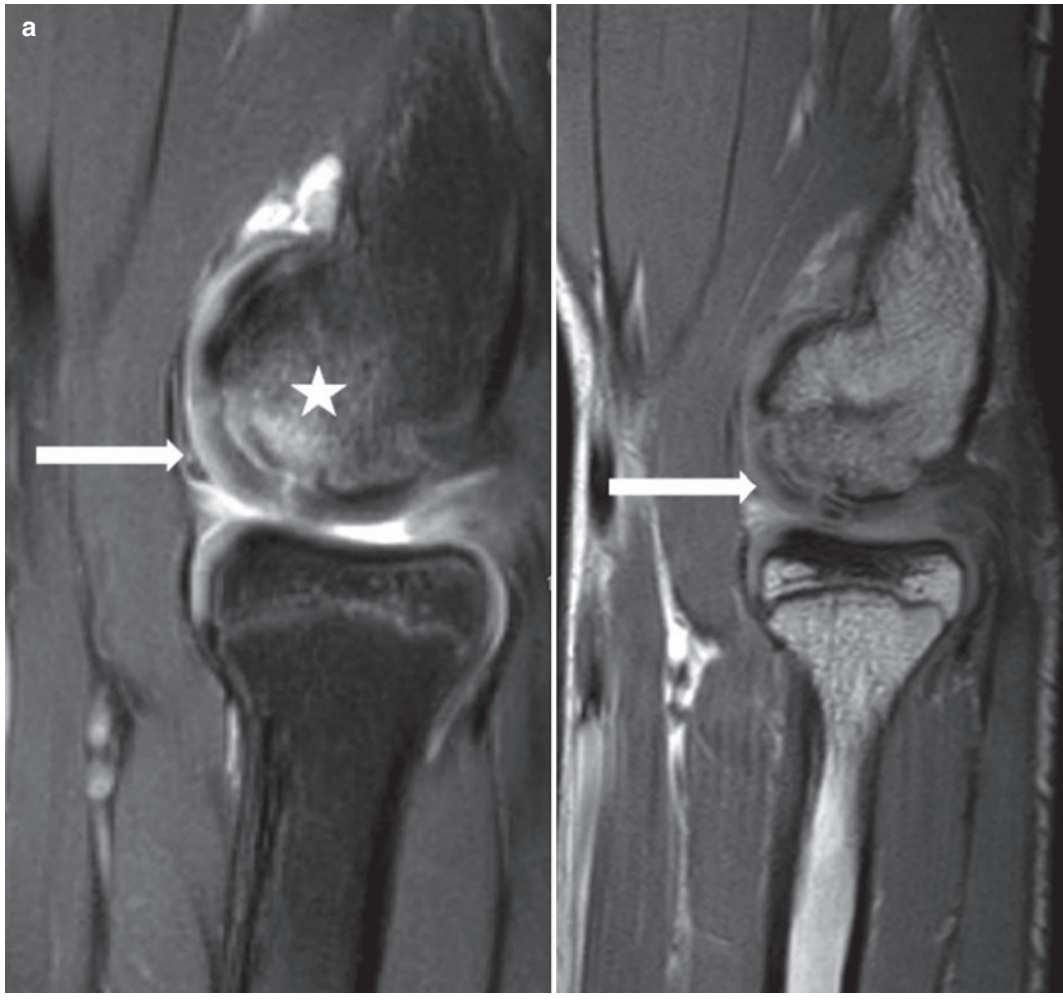

Fig. 20 (**a** and **b**) A 16-year-old professional gymnast with elbow pain. (**a**) On sagittal PD FS and PD images focal bone marrow edema is seen on MRI (asterisk) in the capitellum with extensive signal changes in the cartilage (white arrows) which appears to be detached over a large area. (**b**) Sagittal and coronal MRP CT images demonstrate the fragmentation of the subchondral bone which is somewhat less appreciated on the MRI. There are no intra-articular loose bodies

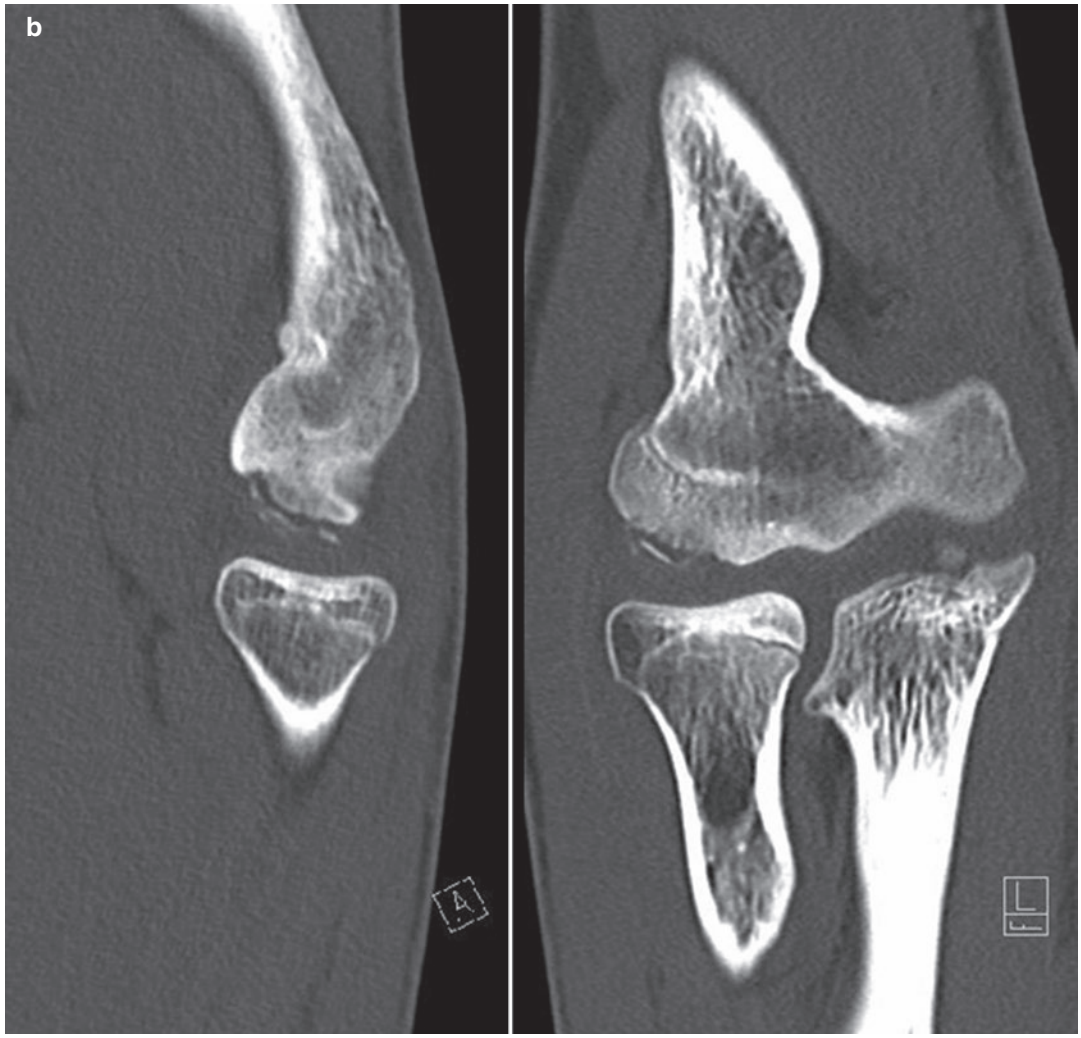

Fig. 20 (continued)

den Ende et al. (2019) in 25 elbows even found CT to be superior to MRI to identify and localize OD lesions (van den Ende et al. 2019).

Osteochondral lesions will present as (subtle) subchondral bone lamellar irregularities, subchondral cystic changes, subchondral density changes, and/or defects at the subchondral lamella (Fig. 22). The joint space width will usually be normal. The cartilage itself cannot be assessed without intra-articular contrast.

Fig. 21 Sagittal PD image of the elbow demonstrating the area of a pseudodefect (arrow). These can be quite prominent and in this case with some cystic lesions but should not be mistaken for osteochondral lesions

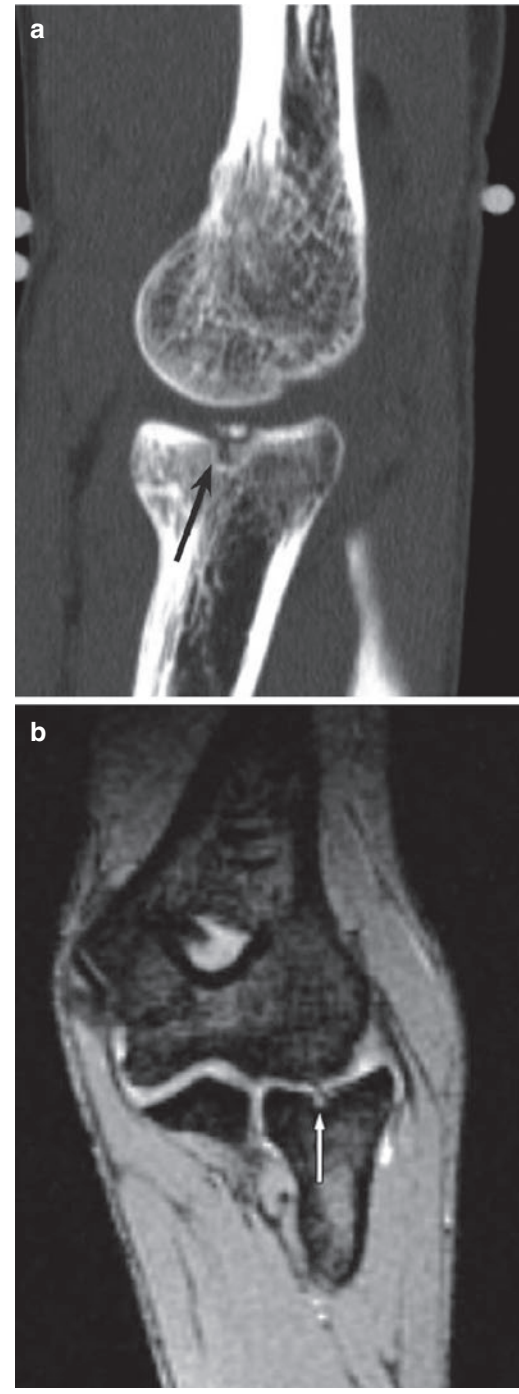

Fig. 22 A 16-year-old female gymnast with an osteochondral (OC) lesion of the radial head. (**a**) Sagittal CT and (**b**) coronal gradient-echo T2* WI MR image of the elbow. The OC lesion with the cortical defect (black arrow) (**a**), white arrow (**b**) and the small loose fragments are better appreciated on the CT than on the MR

5 Conclusions

Elbow injuries in athletes are relatively uncommon compared to shoulder injuries and lower extremity injuries, especially acute injuries. There is however a specific group of athletes in which it is not uncommon but it depends upon the sports involved. Most injuries are contributed to overuse. Throwing, using the arm as a lever or as a weight-bearing joint and stopping goal fired shots are the mechanisms in which injuries most often occur. Ulnar collateral ligament injuries, lateral and medial epicondylitis, medial epicondylar apophysitis, osteochondral lesions, and intra-articular loose bodies are the most common encountered injuries. Standard radiography should be the initial imaging modality but in general MRI is the most useful imaging modality to use. In certain selected cases however US and CT can replace MRI or add valuable information.

Things to Remember

1. AP and lateral radiographs of the elbow are usually sufficient to evaluate the osseous structures of the elbow. In selected cases (Valgus Extension Overload) a reversed axial projection can be helpful.
2. Ultrasound has a very high sensitivity and specificity to diagnose lateral and medial epicondylitis and usually confirms the diagnosis.
3. In medial epicondylitis and ulnar collateral ligament injuries particular attention has to be paid to the ulnar nerve which is often compromised in these conditions.
4. Ulnar collateral ligament injuries are best assessed using MRI. There is no evidence to support that MR arthrography is superior to non-enhanced MRI.
5. CT has a better sensitivity compared to MRI for intra-articular loose bodies especially in the absence of joint effusion.
6. CT and MRI are comparable for demonstrating osteochondral lesions.

Imaging Boxes

Standard Radiography
- Initial survey, especially in acute injuries.
- Evaluation of osseous structures, avulsion injuries and calcifications.
- Cheap and fast.
- AP and lateral views will usually suffice.
- Reversed axial projection and stress views can be helpful.

Ultrasound
- Evaluation of soft tissues.
- Higher sensitivity for avulsions and calcifications compared to MRI.
- Very high spatial resolution compared to MRI.
- Easily available and cheap.
- Detection of loose intra-articular bodies best with joint effusion.

MRI
- Evaluation of soft tissues and osseous structures.
- Superior contrast resolution compared to US.
- Low sensitivity for small avulsions and calcifications.
- Difficult especially in painful lesions.
- Low sensitivity for intra-articular loose bodies in the absence of joint effusion.

CT
- Evaluation of predominantly osseous structures.
- High sensitivity for avulsions, calcifications, and intra-articular loose bodies.
- Available and short examination time.
- Radiation.
- Often complementary to MRI.

References

Ahmad CS, ElAttrache NS (2004) Valgus extension overload syndrome and stress injury of the olecranon. Clin Sports Med 23:665–676

Akgun U, Karahan M, Tiryaki C, Erol B, Engebretsen L (2007) Direction of the load on the elbow of the ball blocking handball goalie. Knee Surg Sports Traumatol Arthrosc 16:522–530

Alcid JG, Ahmad CS, Lee TQ (2004) Elbow anatomy and structural biomechanics. Clin Sports Med 23: 503–517

Amin NH, Kumar NS, Schickendantz MS (2015) Medial epicondylitis: evaluation and management. J Am Acad Orthop Surg 23(6):348–355

Arendt EA, Griffiths HJ (1997) The use of MR imaging in the assessment and clinical management of stress reactions of bone in high-performance athletes. Clin Sports Med 16:291–306

Arslan S, Karahan AY, Oncu F, Bakdik S, Durmaz MS, Tolu I (2018) Diagnostic performance of superb microvacular imaging and other sonographic modalities in the assessment of lateral epicondylosis. J Ultrasound Med 37(3):585–593

Bachta A, Rowicki K, Kisiel B, Zabicka M, Elert-Kopec S, Plominski J, Tlustochowicz W, Maliborski A (2017) Ultrasonography versus magnetic resonance imaging in detecting and grading common extensor tendon tear in chronic lateral epicondylitis. PLoS 12(7):e0181828

Bartlett RM, Rent RJ (1988) The biomechanics of javelin throwing. J Sports Sci 6:1–38

Bojanic I, Ivkovic A, Boric I (2006) Arthroscopy and micro fracture technique in the treatment of osteochondritis dissecans of the humeral capitellum: report of three adolescent gymnasts. Knee Surg Sports Traumatol Arthrosc 14(5):491–496

Bredella MA, Tirman PF, Fritz RC et al (1999) MR imaging findings of lateral ulnar collateral ligament abnormalities in patients with lateral epicondylitis. Am J Roentgenol 193:1379–1382

Brittberg M, Winalski CS (2003) Evaluation of cartilage injuries and repair. J Bone Joint Surg Am 85-A Suppl 2:58–69

Brogdon BG, Crow NE (1960) Little leaguer's elbow. Am J Roentgenol 83:671–675

Bryce CD, Armstrong AD (2008) Anatomy and biomechanics of the elbow. Orthop Clin N Am 39:141–154

Cain EL Jr, Dugas JR, Wolf RS et al (2003) Elbow injuries in throwing athletes: a current concepts review. Am J Sports Med 31:621–635

Chauvin NA, Gustas-French CN (2019) Magnetic resonance imaging of elbow injuries in children. Pediatr Radiol 49:1629–1642

Chen FS, Diaz VA, Loebenberg M et al (2005) Shoulder and elbow injuries in the skeletally immature athlete. J Am Acad Orthop Surg 13:172–185

Chen FS, Rokito AS, Jobe FW (2001) Medial elbow problems in the overhead-throwing athlete. J Am Acad Orthop Surg 9:99–113

Chen AL, Youm T, Ong BC et al (2003) Imaging of the elbow in the overhead throwing athlete. Am J Sports Med 31:466–473

Chung CB, Kim HJ (2003) Sports injuries of the elbow. Magn Reson Imaging Clin N Am 11:239–253

Ciccotti MC, Stull JD, Buckley PS, Cohen SB (2017) Correlation of MRI to arthroscopy in the elbow: thrower's elbow and ulnar collateral ligament injury. Sports Med Arthrosc Rev 25:191–198

Coel M, Yamada CY, Ko J (1993) MR imaging of patients with lateral epicondylitis of the elbow (tennis elbow): importance of increased signal of the anconeus muscle. Am J Roentgenol 161:1019–1021

Cohen SB, Valko C, Zoga A, Dodson CC, Cicotti MG (2011) Posteromedial elbow impingement: magnetic resonance imaging findings in overhead throwing athletes and results of arthroscopic treatment. Arthroscopy 27:1364–1370

Connell D, Burke F, Coombes P et al (2001) Sonographic examination of lateral epicondylitis. Am J Roentgenol 176:777–782

Cotten A, Jacobson J, Brossmann J et al (1997) Collateral ligaments of the elbow: conventional MR imaging and MR arthrography with coronal oblique plane and elbow flexion. Radiology 204:806–812

Dexel J, Marschner K, Beck H, Platzek I, Wasnik S, Schuler M, Nasreddin A, Kasten P (2014) Comparitive study of elbow disorders in young high-performance gymnasts. Int J Sports Med 35(11):960–965

Escamilla RF, Fleisig GS, Groeschner D, Akizuki K (2017) Biomechanical comparisons among fastball, slider, curveball and changeup pitch types and between balls and strikes in professional baseball pitchers. Am J Sports Med 45:3358–3367

Eygendaal D, Heijboer MP, Obermann WR et al (2000) Medial instability of the elbow. Findings on valgus load radiography and MRI in 16 athletes. Acta Orthop Scand 71:480–483

Ferrara MA, Marcelis S (1997) Continuing education—ultrasound of the elbow. JBR-BTR 80:122–123

Field LD, Savoie FH (1998) Common elbow injuries in sport. Sports Med 26:193–205

Fleisig GS, Andrews JR, Dillman CJ et al (1995) Kinetics of baseball pitching with implications about injury mechanisms. Am J Sports Med 23:233–239

Garcia GH, Gowd AK, Cabarcas BC, Liu JN, Meyer JR, White GM, Romeo AA, Verma NN (2019) Magnetic resonance imaging findings of the asymptomatic elbow predict injuries and surgery in major league baseball pitchers. Orthop J Sports Med 29:2325967118818413

Gerbino PG (2003) Elbow disorders in throwing athletes. Orthop Clin North Am 34:417–426

Gissane C, White J, Kerr K et al (2001) An operational model to investigate contact sports injuries. Med Sci Sports Exerc 33:1999–2003

Gore RM, Rogers LF, Bowerman J et al (1980) Osseous manifestations of elbow stress associated with sports activities. Am J Roentgenol 134:971–977

Gutierrez NM, Granville C, Kaplan L, Baraga M, Jose J (2017) Elbow MRI findings do not correlate with future placement on the disabled list in asymptomatic professional baseball pitchers. Sports Health 9:222–229

Hang DW, Chao CM, Hang YS (2004) A clinical and roentgenographic study of little league elbow. Am J Sports Med 32:79–84

Harada M, Takahara M, Sasaki J, Mura N, Ito T, Igino T (2006) Using sonography for the early detection of elbow injuries among young baseball players. AJR 187:1436–1441

Hurd WJ, Kaufman KR, Murthy NS (2011) Magnetic resonance imaging of the throwing elbow in the uninjured, high school–aged baseball pitcher. Am J Sports Med 39:722–728

Iwamoto J, Takeda T (2003) Stress fractures in athletes; review of 196 cases. J Orthop Sci 8:273–278

Jackson DW, Silvino N, Reiman P (1989) Osteochondritis dissecans in the female gymnast's elbow. Arthroscopy 5:129–136

Jacobson JA, Propeck T, Jamadar DA et al (2003) US of the anterior bundle of the ulnar collateral ligament: findings in five cadaver elbows with MR arthrographic and anatomic comparison—initial observations. Radiology 227:561–566

Jobe FW, Cicotti MG (1994) Lateral and medial epicondylitis of the elbow. J Am Acad Orthop Surg 2:1–8

Kani K, Porrino J, Dahiya N, Taljanovic M, Mulcahy H, Chew F (2017) Visualization of the soft tissues at the lateral and medial epicondyles of the elbow. PM&R 9:533–539

Karbach LE, Elfar J (2017) Elbow instability: anatomy, biomechanics, diagnostic maneuvers and testing. J Hand Surg Am 42:118–126

Keijsers R, de Ros RJ, Kuijer PPF, van den Bekerom MP, van der Woude HJ, Eygendaal D (2019) Tennis elbow. Shoulder Elbow 11:384–392

Khan KM, Cook JL, Bonar F, Harcourt P, Astrom M (1999) Histopathology of common tendinopathies. Update and implications for clinical management. Sports Med 27:393–408

Kida Y, Morihara T, Kotoura Y, Hojo T, Tachiiri H, Sukenari T, Iwata Y, Furukawa R, Oda R, Arai Y, Fujiwara H, Kubo T (2014) Prevalence and clinical characteristics of osteochondritis dissecans of the humeral capitellum among adolescent baseball players. Am J Sports Med 42:1963–1971

Kijowski R, Tuite M, Sanford M (2004) Magnetic resonance imaging of the elbow. Part I: normal anatomy, imaging technique, and osseous abnormalities. Skelet Radiol 33:685–697

Kijowski R, Tuite M, Sanford M (2005) Magnetic resonance imaging of the elbow. Part II: abnormalities of the ligaments, tendons, and nerves. Skelet Radiol 34:1–18

Klingele KE, Kocher MS (2002) Little league elbow. Valgus overload injury in the pediatric athlete. Sports Med 32:1005–1015

Kohyama S, Ogawa T, Mamizuka N, Hara Y, Yamazaki M (2018) A magnetic resonance imaging-based staging system for osteochondritis dissecans of the elbow. A validation study against the international cartilage repair society classification. Orthop J Sports Med 6:2325967118794620

Konin GP, Nazarian LN, Walz DM (2013) US of the elbow: indications, technique, normal anatomy and pathologic conditions. Radiographics 33:E125–E147

Lee GA, Katz SD, Lazarus MD (1998) Elbow valgus stress radiography in an uninjured population. Am J Sports Med 26:425–427

Lee YY, Yang TH, Huang CC, Huang YC, Chen PC, Hsu CH, Wang LY, Chou WY (2019) Ultrasonography has high positive predictive value for medial epicondyle lesions among adolescent baseball players. Knee Surg Sports Traumatol Arthrosc 27:3261–3268

Levin D, Nazarian LN, Miller TT et al (2005) Lateral epicondylitis of the elbow: US findings. Radiology 237:230–234

Lin DJ, Kazam JK, Ahmed FS, Wong TT (2019) Ulnar collateral ligament insertional injuries in pediatric overhead athletes: are MRI findings predictive of symptoms or need for surgery? AJR 212: 867–873

Loftice J, Fleisig GS, Zheng N et al (2004) Biomechanics of the elbow in sports. Clin Sports Med 23:519–530

McCarroll JR (1996) The frequency of golf injuries. Clin Sports Med 15:1–7

McCarroll JR (2001) Overuse injuries of the upper extremity in golf. Clin Sports Med 20:469–479

Marcelis S, Daenen B, Ferrara MA (1996) Peripheral musculoskeletal ultrasound atlas. Thieme, Stuttgart, pp 79–89

Martin CE, Schweitzer ME (1998) MR imaging of epicondylitis. Skelet Radiol 27:133–138

Matsuura T, Suzue N, Iwame T, Nishio S, Sairyo K (2014) Prevalence of osteochondritis dissecans of the capitellum in young baseball players: results based on ultrasonographic findings. Orthop J Sports Med 2:2325967114545298

Miller TT (1999) Imaging of elbow disorders. Orthop Clin North Am 30:21–36

Miller TT, Shapiro MA, Schultz E et al (2002) Comparison of sonography and MRI for diagnosing epicondylitis. J Clin Ultrasound 30:193–202

Morris C, Bartlett RM (1996) Biomechanical factors critical for performance in the men's javelin throw. Sports Med 21:438–446

Munshi M, Pretterklieber ML, Chung CB et al (2004) Anterior bundle of ulnar collateral ligament: evaluation of anatomic relationships by using MR imaging, MR arthrography, and gross anatomic and histologic analysis. Radiology 231:797–803

Nagamoto H, Yamamoto N, Kurokawa D, Takahashi H, Muraki T, Tanaka M, Koike Y, Sano H, Itoi E (2014) Evaluation of the thickness of the medial ulnar collateral ligament in junior high and high school baseball players. J Med Ultrason 42:395–400

Nakanishi K, Masatomi T, Ochi T et al (1996) MR arthrography of elbow: evaluation of the ulnar collateral ligament of elbow. Skelet Radiol 25:629–634
Nirschl RP (1992) Elbow tendinosis/tennis elbow. Clin Sports Med 11:851–870
Nocerino EA, Cucchi D, Arrigoni P, Brioschi M, Fusi C, Genovese EA, Messina C, Randelli P, Masciocchi C, Aliprandi A (2018) Acute and overuse elbow trauma: radio-orthopedics overview. Acta Biomed 89:124–137
O'Driscoll SW (1992) Elbow arthroscopy for loose bodies. Orthopedics 15(7):855–859
Otoshi K, Kikuchi S, Kato K, Sato R, Igari T, Kaga T, Konno S (2017) Age-specific prevalence and clinical characteristics of humeral medial epicondyle apophysitis and osteochondritis dissecans: ultrasonographic assessment of 4249 players. Orthop J Sports Med 5:2325967117707703
Park GY, Lee SM, Lee MY (2008) Diagnostic value of ultrasonography for clinical medial epicondylitis. Arch Phys Med Rehabil 89:738–742
Pasternack I, Tuovinen EM, Lohman M et al (2001) MR findings in humeral epicondylitis. Acta Radiol 42:434–440
Pomerance J (2002) Radiographic analysis of lateral epicondylitis. J Shoulder Elbow Surg 11(2):156–157
Popovic N, Ferrara MA, Daenen B et al (2001) Imaging overuse injury of the elbow in professional team handball players: a bilateral comparison using plain films, stress radiography, ultrasound and magnetic resonance imaging. Int J Sports Med 22:60–67
Popovic N, Lemaire R (2002) Hyperextension trauma to the elbow; radiological and ultrasonographic evaluation in handball goalkeepers. Br J Sports Med 36:452–456
Puddu G, Ippolito E, Postacchini F (1976) A classification of Achilles tendon disease. Am J Sports Med 4:145–150
Quinn SF, Haberman JJ, Fitzgerald SW et al (1994) Evaluation of loose bodies in the elbow with MR imaging. J Magn Reson Imaging 4:169–172
Rijke AM, Goitz HT, McCue FC (1994) Stress radiography of the medial elbow ligaments. Radiology 191:213–216
Roetert EP, Brody H, Dillman CJ et al (1995) The biomechanics of tennis elbow. Clin Sports Med 14:47–57
Rosenberg ZS, Beltran J, Cheung YY (1994) Pseudodefect of the capitellum: potential MR imaging pitfall. Radiology 191:821–823
Sasaki J, Takahara M, Ogino T, Kashiwa H, Ishigaki D, Kanauchi Y (2002) Ultrasonographic assessment of the ulnar collateral ligament and medial elbow laxity in college baseball players. J Bone Joint Surg Am 84:525–531
Satake H, Takahara M, Harada M, Maruyama M (2013) Preoperative imaging criteria for unstable osteochondritis dissecans of the capitellum. Clin Orthop Relat Res 471:1137–1143
Shillito M, Soong M, Martin N (2017) Radiographic and clinical analysis of lateral epicondylitis. J Hand Surg [Am] 42:436–442
Sonin AH, Fitzgerald SW (1996) MR imaging of sports injuries in the adult elbow: a tailored approach. Am J Roentgenol 167:325–331
Tajika T, Yamamoto A, Oya N, Ichinose T, Shimoyama D, Sasaki T, Shitara H, Kitigawa T, Saito K, Osawa T, Takagishi K (2016) The morphologic change of the ulnar collateral ligament of elbow in high school baseball pitchers, with and without symptoms, by sonography. J Shoulder Elb Surg 25:1223–1228
Takahara M, Ogino T, Tsuchida H, Tagaki M, Kashiwa H, Nambu T (2000) Sonographic assessment of osteochondritis dissecans of the humeral capitellum. AJR 174:411–415
Thériault G, Lachance P (1998) Golf injuries. An overview. Sports Med 26:43–57
Thornton R, Riley GM, Steinbach LS (2003) Magnetic resonance imaging of sports injuries of the elbow. Top Magn Reson Imaging 14:69–86
Timmerman LA, Schwartz ML, Andrews JR (1994) Preoperative evaluation of the ulnar collateral ligament by magnetic resonance imaging and computed tomography arthrography. Am J Sports Med 22:26–32
Tyrdal S, Finnanger AM (1999) Osseous manifestations of 'handball goalie's elbow'. Scand J Med Sci Sports 9(2):92–97
Van den Ende KI, McIntosh AL, Adams JE, Steinmann SP (2011) Osteochondritis dissecans of the capitellum: a review of the literature and a distal ulnar portal. Shoulder Elbow 11:129–136
Van den Ende KIM, Keijsers R, van den Bekerom MPJ, Eygendaal D (2019) Imaging and classification of osteochondritis dissecans of the capitellum: X-ray, magnetic resonance imaging or computed tomography? Shoulder Elbow 11:129–136
Van der Wall H, Storey G, Frater C et al (2001) Importance of positioning and technical factors in anatomic localization of sporting injuries in scintigraphic imaging. Semin Nucl Med 31:17–27
Verhagen RA, Maas M, Dijkgraaf MG et al (2005) Prospective study on diagnostic strategies in osteochondral lesions of the talus. Is MRI superior to helical CT ? J Bone Joint Surg Br 87-B:41–46
Walz DM, Newman JF, Konin GP, Ross G (2010) Epicondylitis: pathogenesis, imaging and treatment. Radiographics 30:167–184
Ward SI, Teefey SA, Paletta GA Jr et al (2003) Sonography of the medial collateral ligament of the elbow: a study of cadavers and healthy adult male volunteers. Am J Roentgenol 180:389–394
Wei AS, Khana S, Limpisvasti O, Crues J, Podesta L, Yocum LA (2010) Clinical and MR findings associated with little league elbow. J Pediatr Orthop 30:715–719
Werner SL, Fleisig GS, Dillman CJ et al (1993) Biomechanics of the elbow during baseball pitching. J Orthop Sports Phys Ther 17:274–278
Werner SL, Murray TA, Hawkins RJ et al (2002) Relationship between throwing mechanics and elbow valgus in professional baseball pitchers. J Shoulder Elb Surg 11:151–155

Wilder RP, Sethi S (2004) Overuse injuries: tendinopathies, stress fractures, compartment syndrome, and shin splints. Clin Sports Med 23(55–81):vi

Yang TH, Lee YY, Huang CC, Huang YC, Chen PC, Hsu CH, Wang LY, Chou WY (2017) Effectiveness of US screening and risk factor analysis of capitellar OCD in adolescent baseball players. J Shoulder Elb Surg 27:2038–2044

Zouzias IC, Hendra J, Stodelle J, Limpisvasti O (2018) Golf injuries: epidemiology, pathophysiology and treatment. J Am Acad Orthop Surg 26:116–123

Imaging of Wrist Injuries

Teck Yew Chin, Wilfred C. G. Peh,
and Howard R. Galloway

Contents

Abstract

Wrist injuries are commonly encountered in both the amateur and professional sports communities. They can occur through a single traumatic event or from repetitive episodes leading to overuse injuries. As the wrist is a complex structure encompassing many bones, joints, and ligaments, early recognition and diagnosis of these injuries play a vital role in directing treatment and preserving wrist function. A sound understanding of the anatomy and biomechanics of the wrist is required for this. Specific injury patterns are also associated with specific sports activities and knowledge of this will enable the diagnostician to arrive at an accurate diagnosis. This chapter aims to review the patterns of injuries encountered in the wrist among the more popular and emerging sports, along with the biomechanics and pathophysiology of these injuries that help to explain the imaging findings.

1 Introduction

The benefits of sports are well recognized but many sports-related activities carry a specific injury risk. Injuries to the wrist and hand occur with a frequency of between 3 and 9% (Geissler 2001). This injury incidence will obviously be higher in those sports utilizing the hand and wrist, and where the potential for trauma during

T. Y. Chin · W. C. G. Peh (✉)
Department of Diagnostic Radiology, Khoo Teck Puat Hospital, Singapore, Republic of Singapore
e-mail: chin.teck.yew@ktph.com.sg; wilfred.peh@gmail.com

H. R. Galloway
Musculoskeletal Radiologist, Southeast Radiology, Canberra, Australia
e-mail: galloway.howard@gmail.com

Med Radiol Diagn Imaging (2020)
https://doi.org/10.1007/174_2020_242, © Springer Nature Switzerland AG
Published Online: 07 December 2020

sporting activity is present. Trauma to the wrist may cause bone or soft-tissue injury, which may sometimes be difficult to diagnose. Symptoms vary, according to the structure involved or nature of injury, but pain and limited joint function are the usual complaints. Physical examination may be difficult due to the proximity of many small bony and soft-tissue structures, as well as small articulations.

The wide spectrum of sporting activities places demands of different magnitudes, orientations, and degrees of repetitions on the wrist. These injuries may result from a single debilitating episode or repetitive traumatic episodes. Proper diagnosis of injuries in this region therefore requires a basic knowledge of the anatomy and biomechanics of the wrist (Halikis and Taleisnik 1996). Many sporting activities are associated with a specific injury pattern related to the actions and stresses associated with that particular activity. Knowledge of the sport or recreational activity therefore aids in the diagnosis of these injuries. Early diagnosis of the injury and proper referral of these patients can help prevent complications, including prolonged pain and discomfort, surgery, and lost time from sports participation. Failure to diagnose sports injuries may lead to permanent disability (Pulos and Kakar 2018).

It is important for athletes to be educated about how to recognize wrist injuries promptly. Seeking early medical attention for wrist injuries should be emphasized to athletes. Specific care to wrist-supporting ligaments and muscles is necessary to prevent overuse injuries during the recovery period and return of function. For preadolescent and adolescent athletes, injury to a growing wrist requires a more gradual return to full sporting activity than a nongrowing wrist. Wrist injuries may potentially be prevented by implementing proper technique, maintaining good strength and flexibility, and, if the particular sports permit, using wrist guards. The use of wrist guards may help protect from fractures and skin scrapes if one falls or slides in sports such as rollerblading or hockey. Proper stretching is especially useful for sports that involve a lot of upper extremity bodywork, such as racquet sports.

2 Sports Injuries in Children

Hand and wrist injuries are more common in preadolescent and adolescent athletes than in adults (Geissler 2001). It is particularly important to recognize wrist injuries that occur in the immature skeleton, particularly those that involve the epiphyseal growth plates like Salter-Harris fractures (Fig. 1). Continued sports participation in these affected children may result in growth arrest and other long-term problems. Injured children should therefore abstain from the sport until the symptoms disappear and the wrist has healed completely (Morgan and Slowman 2001). Worldwide, an increasing number of children are involved in competitive and organized sports. The frequency and severity of both acute and overuse injuries are continuing to rise (Flynn et al. 2002).

Sprains (34%), contusions (30%), and fractures (25%) are the most common injury types (Damore et al. 2003). The six most common sports causing injuries in children are basketball (19.5%), football (17.1%), baseball/softball (14.9%), soccer (14.2%), rollerblading/skating (5.7%), and hockey (4.6%). Sprains/strains (32.0%), fractures (29.4%), contusions/abrasions (19.3%), and lacerations (9.7%) account for 90% of injury types. The most common injury location is the wrist/hand (28%). Contact with another person or object is the mechanism for more than 50% of the sports-related injuries (Taylor and Attia 2000).

Most ball-related injuries occur during soccer and rugby (86%), while the majority of fractures occurring during wheel sports are in cycling (63%). The radius/ulna is the most frequent fracture location (36%) (Lyons et al. 1999). Hassan and Dorani (2001) found that soccer, rollerblading, cycling, and netball injuries are the most frequent causes of the fractures. Soccer and rollerblading are the commonest causes of fractures among boys, while rollerblading and netball injuries are most frequent causes among girls. Brudvik and Hove (2003) found that scaphoid fracture, an infrequent fracture in children, is seen in 9% of all fractures due to rollerblading/skating, with a doubled risk of fracture in boys aged 13–15 years, compared with girls.

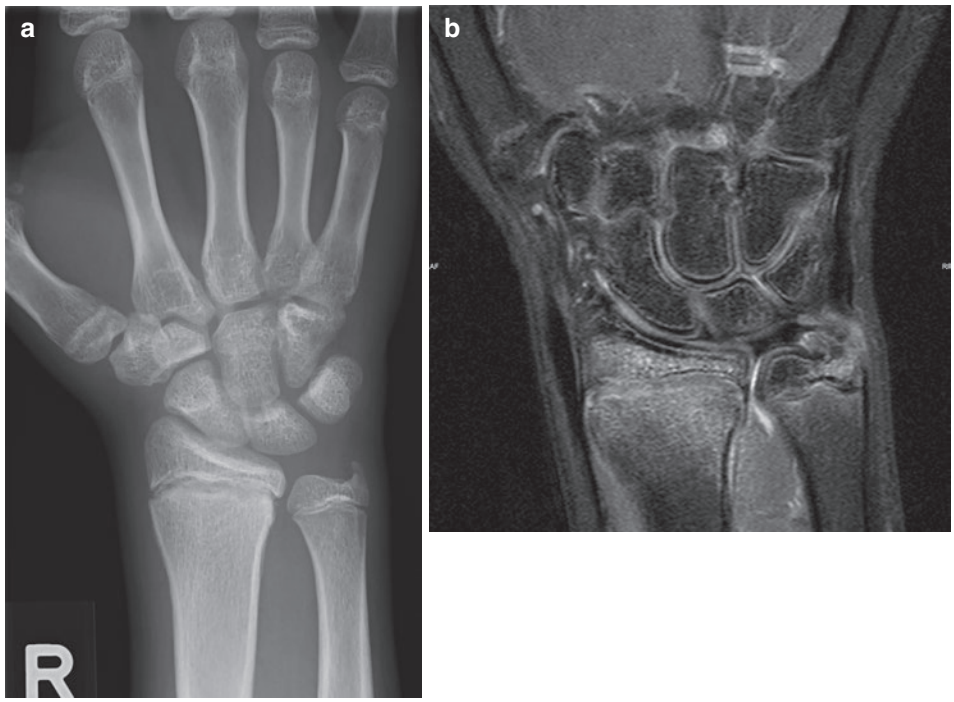

Fig. 1 (**a** and **b**) Male recreational skateboarder who fell during a maneuver. (**a**) PA radiograph shows stress changes of the distal radius, with mild sclerosis adjacent to the slight irregularly marginated growth plates. (**b**) Coronal fat-suppressed proton density MR image shows a subacute Salter-Harris type 1 fracture of the distal radius with surrounding marrow edema. Note also injuries to the TFCC ulnar styloid attachment accompanied with bone bruising of the ulnar styloid process and a small DRUJ effusion

3 Anatomy

The wrist is a complex joint that is comprised of bones and soft-tissue structures. The bones consist of the distal radius and ulna, eight carpal bones, and proximal metacarpal bones. The eight carpal bones are arranged in two rows to form a compact unit. The proximal carpal row is formed by the scaphoid, lunate, triquetrum, and pisiform, and articulates with the distal end of the radius and the triangular fibrocartilaginous complex (TFCC). The distal carpal row is formed by the trapezium, trapezoid, capitate, and hamate, and articulates with the proximal surfaces of the metacarpal bones. The ulna does not articulate directly with the carpus. The wrist is composed of a series of articulations that are separated into several major joint compartments, including the radiocarpal, distal radioulnar, pisiform-triquetral, midcarpal, first carpometacarpal, and intermetacarpal joints.

The carpal bones are held together by a complex set of ligaments, including the intrinsic (or interosseous) and extrinsic ligaments. These strong ligamentous attachments help stabilize the wrist. The dorsal ligaments are weaker than the volar ligaments, resulting in dorsal dislocation being more common. Intrinsic (or interosseous) ligaments connect pairs of carpal bones. In the proximal carpal row, the intrinsic scapholunate and lunotriquetral ligaments join the proximal, dorsal, and volar margins of these carpal bones, and separate the radiocarpal from the midcarpal compartments. The extrinsic ligaments are formed by thickenings of the inner surface of the joint capsule, and are located dorsally and volarly. The main dorsal extrinsic ligaments are the dorsal intercarpal, dorsal radiotriquetral, and dorsal radioulnar ligaments. The main volar extrinsic ligaments are the volar radioscaphocapitate, volar radiotriquetral, volar ulnolunate, volar ulnotriquetral, and volar radioulnar (Bateni et al. 2013).

The TFCC is an important stabilizer of the wrist. Its main component is the triangular fibrocartilage (TFC) articular disc, which separates the radiocarpal compartment from the distal radioulnar joint (DRUJ). The TFC disc is anchored to the articular cartilage at the sigmoid notch and lunate facet of the distal radius, and attaches to the ulnar styloid and fovea of the ulnar head (Fig. 2). The central and radial aspects of the TFC disc are avascular, while the peripheral and ulnar aspects have a blood supply. The latter regions hence have the potential to heal, either spontaneously or after surgical repair, following injury (Saito et al. 2017). Other components of the TFCC are the dorsal and volar radioulnar ligaments, the meniscal homologue (a fibrostyloid

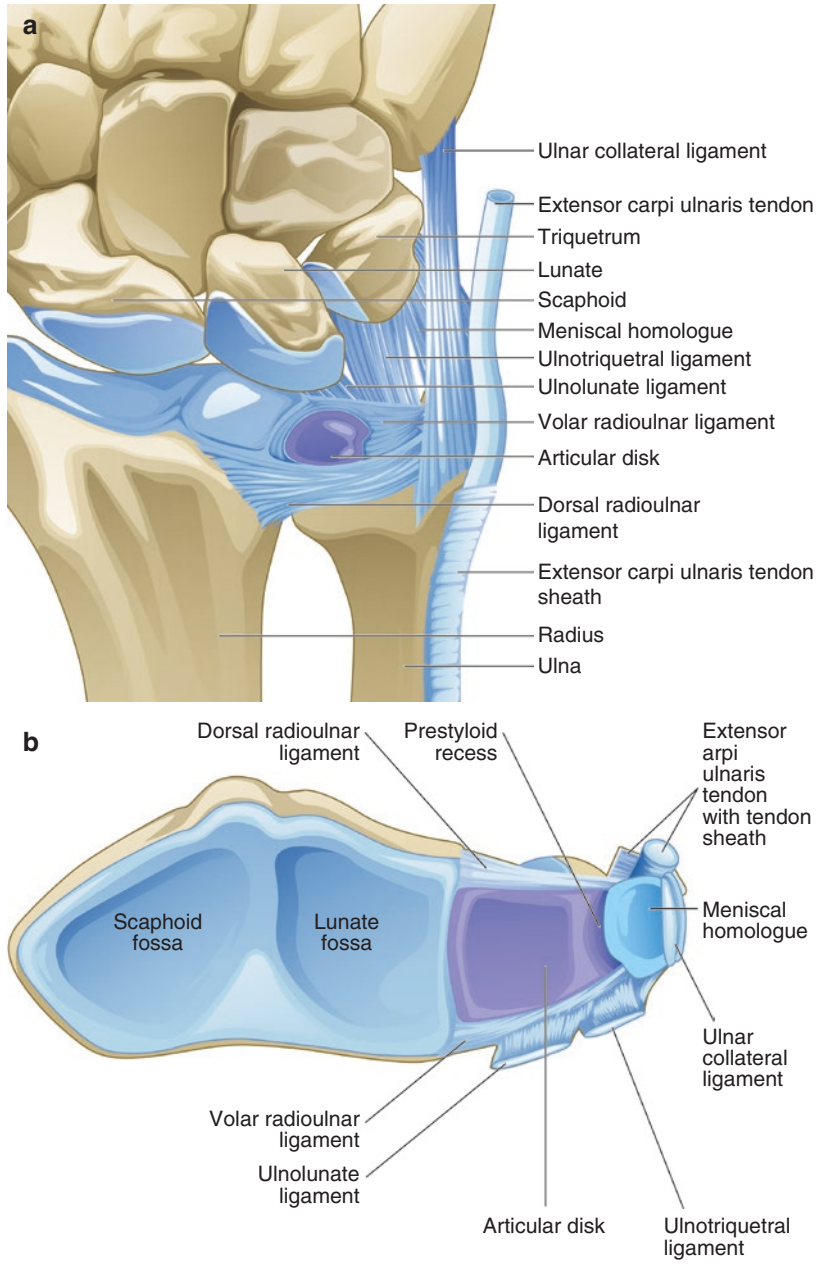

Fig. 2 (**a**) Coronal and (**b**) axial diagrams show the anatomy of the TFCC complex

fold that extends into the prestyloid recess), ulnar collateral ligament, ulnolunate/ulnotriquetral ligaments, subsynovial sheath of the extensor carpi ulnaris tendon sheath, and volar ulnotriquetral and ulnolunate ligaments.

The DRUJ consists of an articular surface that covers two-thirds of the circumference of the distal ulna, which in turn articulates with the sigmoid notch of the distal radius. This joint configuration allows supination and pronation of the forearm. The DRUJ is stabilized intrinsically by the TFCC and extrinsically by the interosseous membrane, extensor carpi radialis, flexor carpi ulnaris, and pronator quadratus. The fovea attachment of the TFCC stabilizes the DRUJ, with avulsion injuries often leading to DRUJ instability (Saito et al. 2017).

The muscles of the hand originate primarily in the forearm and pass over the wrist. The flexor carpi ulnaris, which inserts into the pisiform bone, is the only muscle that inserts into one of the wrist bones. The dorsal aspect of the wrist consists of six compartments, each containing one or more extensor tendons within a synovial sheath (Fig. 3a). The two compartments in the volar aspect of the wrist are the carpal tunnel and

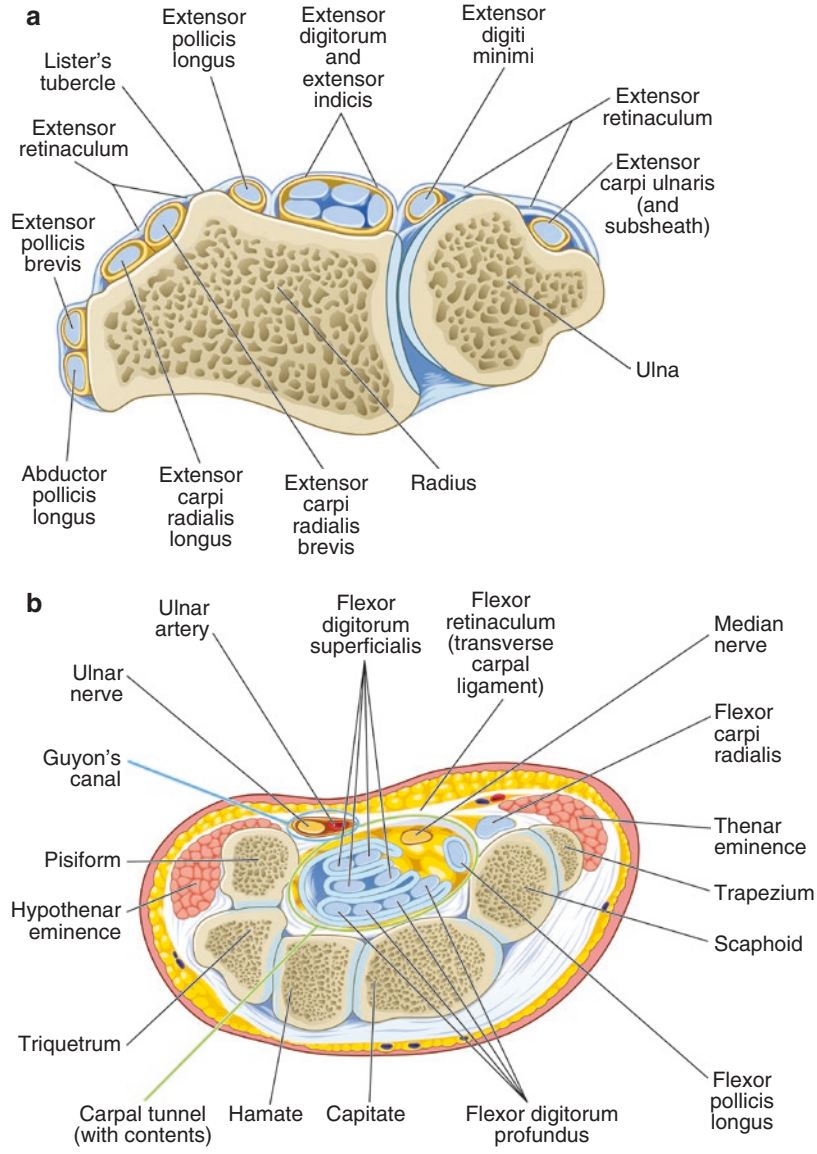

Fig. 3 Diagrams show anatomy of the (**a**) extensor compartment in relation to Lister's tubercle and (**b**) flexor compartment showing the carpal tunnel and Guyon's canal

Guyon's canal. The carpal tunnel is bounded superficially by the transverse carpal ligament (also known as the flexor retinaculum), and contains nine flexor tendons and median nerve (Fig. 3b). The median nerve lies between the flexor carpi radialis and palmaris longus tendons within the carpal tunnel. Guyon's canal lies superficial and radial to the hook of hamate, and contains the ulnar nerve and artery. The ulnar nerve runs deep to the flexor carpi ulnaris tendon in Guyon's canal. Blood supply is via the radial and ulnar arteries which form the dorsal palmar arch. The scaphoid bone receives its blood supply from the distal part of this arch.

4 Biomechanics of Sports Injuries

4.1 Overview

The wrist is a complex joint that biomechanically transmits forces generated at the hand through to the forearm. The carpal bones serve as a link between the hands and the upper body, with much of the motion at the wrist joint occurring between the radius and carpal bones. Its size, position, and relation to the radius and surrounding carpal bones make the wrist joint vulnerable to injury. A great deal of force is transmitted through these structures for certain types of sports. The radial side of the wrist carries 80% of the axial load, and the ulnar side the remaining 20%. Wrist injuries can be divided into four categories, namely traumatic, overuse, neurovascular, and weight-bearing injuries (Howse 1994).

Traumatic injuries are the most common. They are due to either a fall onto the hand, a direct blow to the wrist, or a combination of a rotatory and torsional force (Howse 1994). These acute wrist injuries are often caused by accident and are hard to prevent (Fig. 4). Fractures, dislocations, strains (injury to muscle near the musculotendinous junction due to forceful contraction of the muscle), contusions, hematomas, and sprains (ligamentous injuries) are types of these injuries. Examples of common acute traumatic injuries are distal radius fracture (often intra-articular in athletes), scaphoid fracture, wrist joint sprain, and intercarpal ligament sprain or tear. Less common injuries include fracture of the hook of hamate, TFCC tear, DRUJ instability, and scapholunate dissociation. Important acute injuries that should not be missed are lunate dislocation, perilunate dislocation, any type of carpal dislocation, and traumatic arterial thrombosis.

Fig. 4 Male adolescent gymnast who fell from the gymnastic apparatus. PA radiograph shows a transverse fracture of the distal ulnar shaft. Note stress changes of the distal radius and, to a lesser extent, of the distal ulna, adjacent to the growth plates

Overuse injuries are common in sports involving the hand and wrist, such as racquet sports, netball, and volleyball (Howse 1994). In this form of injury, pain usually develops gradually. They are the result of repetitive application of submaximal stresses to otherwise normal tissues. This causes sufficient structural disruption to overcome the tissue's adaptive ability, and thus produces injuries without necessarily causing complete loss of function (Fig. 5). The common pathway is most likely to be microdamage to tissue collagen, combined with a direct or indirect

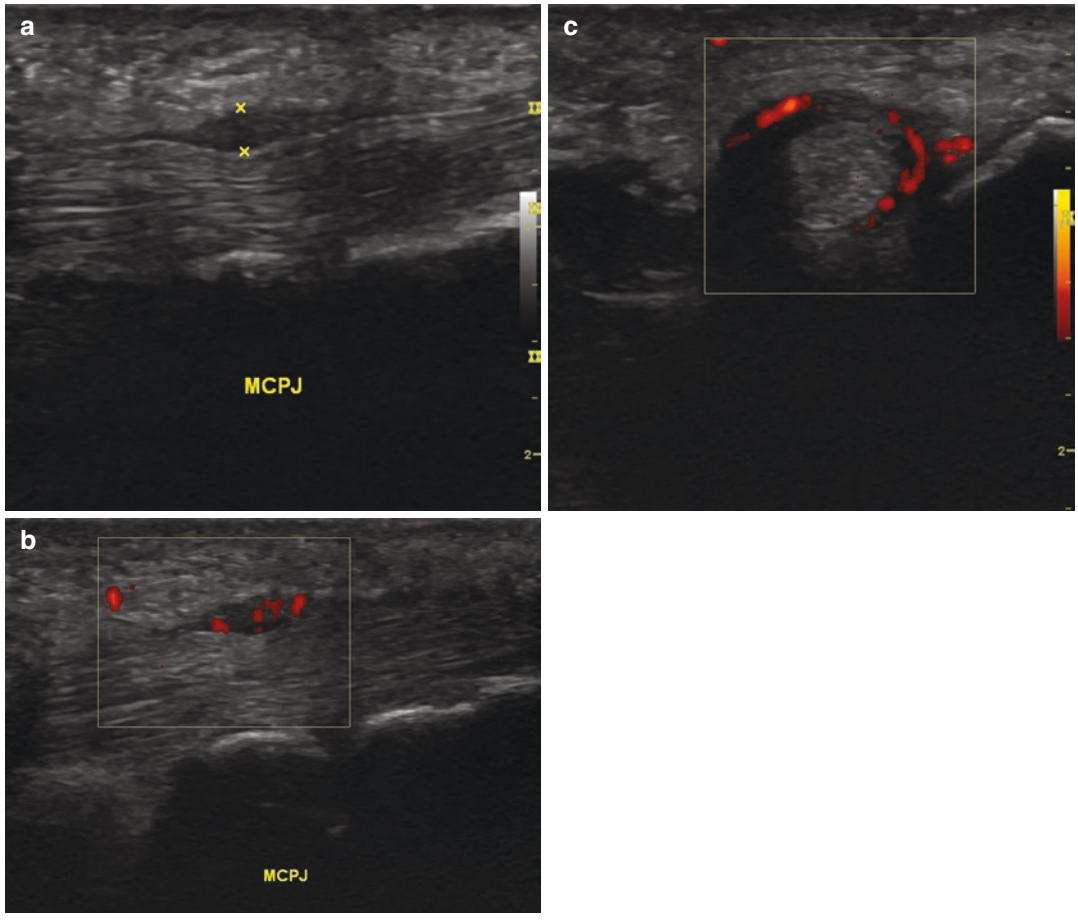

Fig. 5 (**a**–**c**) Rock climber with painful MCP joint and triggering. (**a** and **b**) Longitudinal US images show marked thickening of the A1 pulley at the level of the third MCP joint with increased vascularity. (**c**) There is subsequent flexor tenosynovitis with thickening of the flexor tendon sheath and circumferential neovascularity

effect on the microvasculature, with subsequent oxygen deprivation (Aicale et al. 2018). Stress fractures, periostitis, tendinitis, and growth plate injuries in children are examples of overuse injuries. Common overuse injuries of the tendon include de Quervain's syndrome, extensor and flexor carpi ulnaris tendinopathy, and intersection syndrome (Cockenpot et al. 2016). Other overuse injuries in athletes include Kienbock's syndrome, pisotriquetral syndrome, ligamentous injuries such as scapholunate, lunotriquetral and midcarpal instability injuries, and injuries to the DRUJ and TFCC (Rettig 1998).

Nerve injuries in athletes are more commonly compressive neuropathies. Carpal tunnel syndrome which occurs from median nerve compression in the carpal tunnel can develop from repeated flexion activities in athletes, e.g., bowlers. Wheelchair athletes and cyclists on the other hand are more prone to Guyon's canal syndrome, whereby the ulnar nerve is compressed from prolonged hyperextension while gripping the handlebars (Cockenpot et al. 2016). Isolated *vascular injuries* are uncommon in the wrist but can occur in association with other injuries like fractures and dislocations.

Sports-specific biomechanical injury depends on the unique characteristics that place a particular structure at risk for injury during a sporting activity. In carpal bone injury for example, a fall on outstretched hand during rollerblading or skating or a hand plant during a gymnastics move

may directly result in a fracture. The chronic use and movements in racquet sports, golf, and baseball require the carpus to resist torque stress. Depending on the strength of the weakest link, the hyperpronation-supination activity in the modern golf swing can result in either an acute or a chronic injury.

4.2 Fractures

Wrist fractures are common in sports, usually occurring during a fall on the outstretched hand. Depending on the patient's age, bone density, and reaction time, this type of fall can result in different injuries, such as fractured scaphoid, scapholunate dislocation, or distal radius fracture. Fractures may also be caused by direct trauma, e.g., impact with a helmet during American football. The angle at which the wrist hits the ground may also determine the type of injury. The more dorsiflexed the wrist is, the more likely the scaphoid bone will break. With less wrist dorsiflexion, it is more likely that the radius will break.

4.2.1 Radial Fractures

Fractures to the distal end of radius are typically caused by a fall on the pronated dorsiflexed hand. On striking a hard surface, the hand becomes fixed while the momentum of the body produces two forces, namely a twisting force causing excessive supination of the forearm, and a compression force which acts vertically through the carpus to the radius. The type of fracture is also dependent on whether the hand is in radial or ulnar flexion at the moment of impact (Masciocchi et al. 2001). Distal radial fractures are often associated with ulnar fractures. Distal radial fractures may be extra- or intra-articular, and displaced or undisplaced (Fig. 6).

4.2.2 Scaphoid Fractures

Stress fractures of the scaphoid have been reported to be due to repetitive loading of the wrist in dorsiflexion, occurring to sportsmen such as gymnasts and shot-putters (Yamagiwa et al. 2009). On magnetic resonance (MR) imaging, the presence of bone marrow edema may mask an underlying fracture line; in such cases, T1-weighted sequences reveal the occult fractures better (Fig. 7).

4.2.3 Hamate Fractures

Hamate fractures are relatively common in athletes. They may be either isolated or associated with more widespread injury such as carpometacarpal dislocation or pisiform fracture. These fractures are most commonly classified into hook or body of hamate fractures. Isolated fracture to the body of the hamate is less common. It is due to a direct force such as a punch-press injury, falling on a hyperdorsiflexed and ulnar-deviated wrist, or posterior dislocation or subluxation of the fourth and/or fifth metacarpal.

A fractured hook of hamate is less common compared to the scaphoid fracture. It is often not diagnosed because it is not apparent on standard radiographic views. This is commonly an isolated injury and is the most common type of hamate fracture. It is encountered in racquet sports, golf, and baseball where the palm contacts the implement directly during the swing-through. The dominant hand is involved in tennis players, and the nondominant hand in baseball, hockey, and golf (Rettig 2003). Another mechanism is via the avulsion of the flexor retinaculum which can occur during a fall on an outstretched hand or during power grips, e.g., weight lifting (Cockenpot et al. 2016).

4.2.4 Lunate Fracture

The lunate, being the fulcrum of the proximal carpal row, is frequently exposed to traumatic forces to the wrist. Kienbock's syndrome or osteonecrosis of the lunate is thought to be due to repetitive microtrauma and is associated with negative ulnar variance. Lunate fractures are uncommon. When occurring through the body, they are caused by compressive action between the radius and capitate. When occurring through one of the horns, they are due to ligamentous avulsion (Masciocchi et al. 2001).

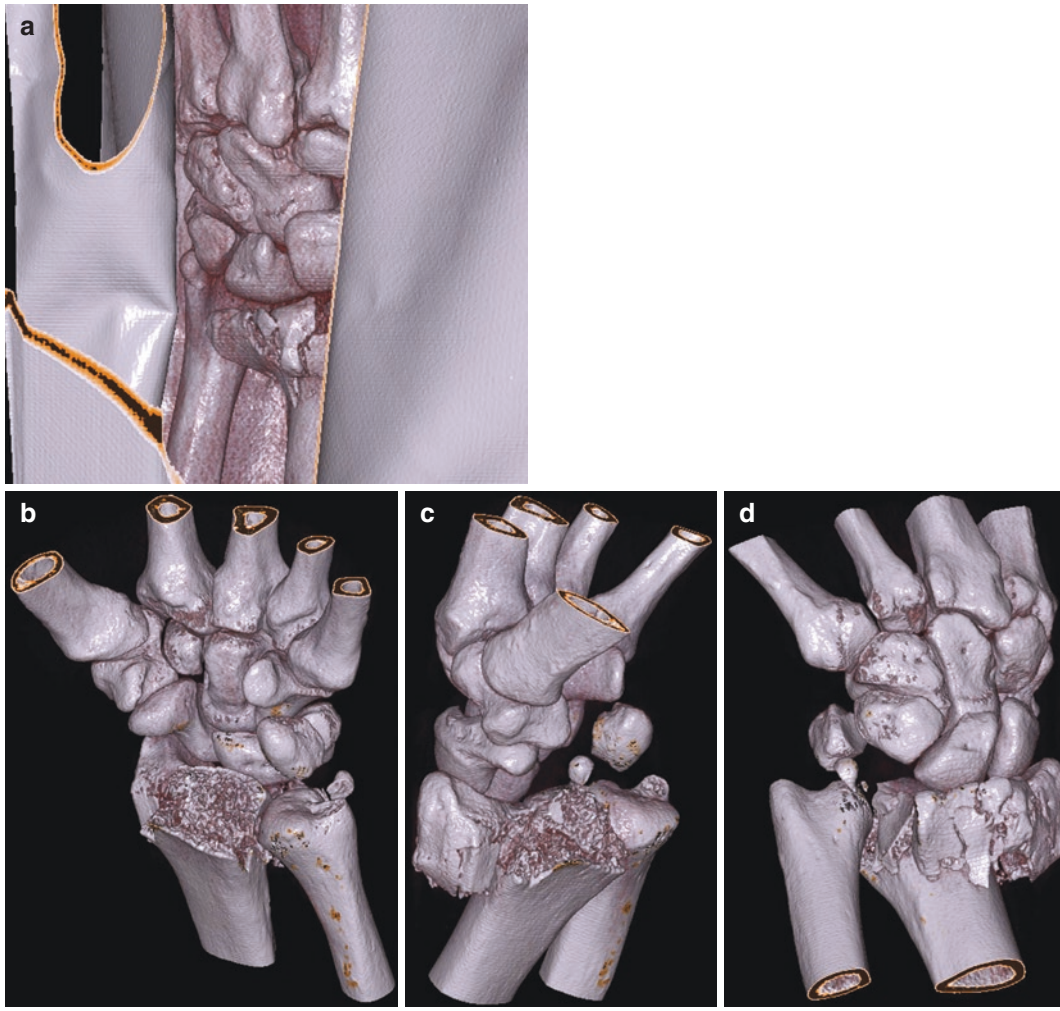

Fig. 6 (**a**–**d**) Displaced intra-articular fractures of the distal radius and ulnar styloid process. (**a**) 3D CT image shows immobilization of the fractures with a plaster cast. (**b** and **c**) CT image manipulation allowed virtual removal of the cast and rotation of images to better show the fracture (courtesy of Professor Jan Gielen, University Hospital, Antwerp, Belgium)

4.3 Wrist Instability

Injuries to the ligaments can alter the wrist kinematics, leading to instability and early post-traumatic degenerative arthritis. These injuries are usually the result of a single traumatic event. Physical findings are often equivocal. Imaging is important as diagnosis of a significant ligamentous injury will dictate treatment. Partial ligamentous injury is treated by cast immobilization, while complete disruptions may require early surgery to prevent long-term degenerative arthritis (Schlegel et al. 1999).

Wrist instability most commonly results from ligamentous disruption between bones of the proximal carpal row. Scapholunate (SL) and lunotriquetral (LT) dissociations are forms of this instability pattern, with SL instability being the most common. Patients with these injuries have a high degree of pain, even though the initial

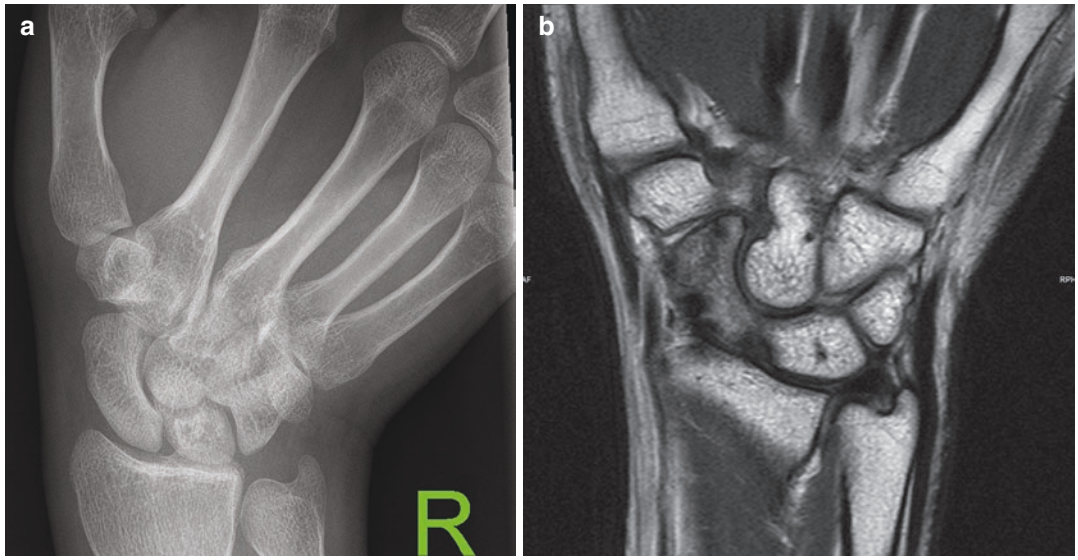

Fig. 7 (**a** and **b**) Soccer player who fell onto his outstretched hand and had persistent wrist pain. (**a**) PA angled scaphoid series radiograph shows a normal scaphoid. (**b**) Coronal T1-W MR image shows diffuse hypointensity of the scaphoid bone from underlying marrow edema along with a more distinct hypointense band in the distal pole to the waist of the scaphoid, corresponding to an occult fracture

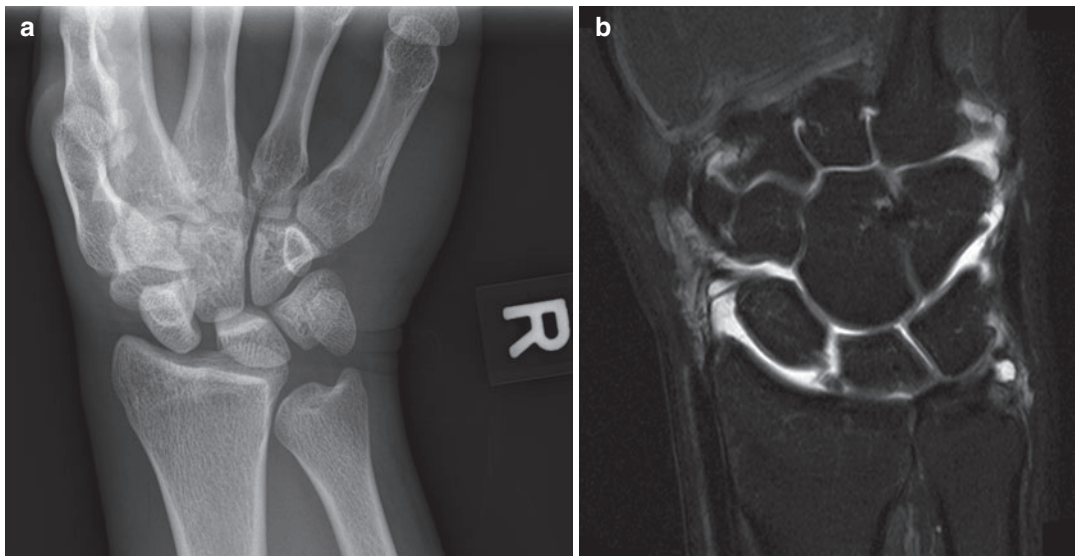

Fig. 8 (**a** and **b**) Female collegiate volleyball player with wrist injury sustained during a match. (**a**) Frontal radiograph with clenched fist shows scapholunate diastasis. Incidental negative ulnar variance is also present. (**b**) MR arthrographic coronal fat-suppressed proton density image shows a complete tear of all components of the scapholunate ligament, confirmed during surgical exploration and subsequently repaired

radiographs may appear normal. A gap exceeding 3 mm in the scapholunate joint is considered abnormal and typically associated with scapholunate ligament injury (Fig. 8). This should be suspected in patients with wrist effusion and pain that is seemingly out of proportion to the injury (Gilula and Yin 1996). Untreated scapholunate instability can eventually lead to secondary

Fig. 9 Conventional arthrogram using a single radiocarpal injection shows a class 1A TFCC tear as well as a LT tear, with contrast leakage into the midcarpal compartment

osteoarthritis of the radiocarpal and midcarpal joints, termed scapholunate advanced collapse (SLAC) wrist (Tischler et al. 2014).

Patients with LT injuries typically present with ulnar-sided wrist pain after high-energy impaction to the wrist (Fig. 9). LT stability is most dependent on the following structures: palmar portion of the LT interosseous ligament, dorsal radiocarpal ligament, and dorsal intercarpal ligament. LT injuries without instability respond well to immobilization. Acute LT injuries with instability and chronic LT injuries can be treated arthroscopically (Weiss et al. 2000). Carpal instability can also occur due to loss of the normal ligamentous restraints between the carpal row, for example, ulnar midcarpal instability. Treatment depends on the specific type and degree of carpal disruption and the presence or absence of degenerative changes (Cohen 1998).

4.4 Post-traumatic Deformity Patterns

Post-traumatic deformity patterns cause the lunate to lose its linear relationship with the capitate and to tilt dorsally or volarly, resulting in a collapse deformity. The most common collapse deformity is caused by the lunate dorsiflexing on the radius. This is compensated by the capitate flexing volarly, and is known as dorsiflexed intercalated segment instability pattern (DISI). DISI normally occurs in unrecognized scaphoid subluxations or scaphoid fractures. Volar intercalated segment instability pattern (VISI) can be seen in healthy patients with lax ligaments but post-traumatically; it is due to the lunate flexing volarly on the radius as the capitate tilts dorsally (Linscheid et al. 1972; Lichtman and Alexander 1997). VISI is a sign of midcarpal instability or lunotriquetral injury.

4.5 TFCC Injuries

TFCC injuries are quite common in athletes because of the high loads placed on the ulnar side of the wrist, especially in patients with ulnar-neutral and ulnar-positive variance. Lesions of the TFCC may be confined to the articular disc, or involve one or more components of the TFCC. There may also be associated DRUJ instability. Injuries to the TFCC can occur during acute trauma or repetitive stress. Acute tears may be due to axial loading of the distal radius, such as a fall onto the outstretched hand, leading to proximal radial shift and tearing of the TFCC over the ulnar head. Sudden excessive pronation or supination may also cause TFCC disruption.

TFCC tears should be suspected in patients with ulnar-sided wrist pain and tenderness (Fig. 10). On physical examination, there may be localized tenderness over the TFCC, with pain on pronation and supination. With rotation of the forearm, a palpable or audible click may be present. The Palmer classification of TFCC tears divides TFCC tears into traumatic (classes 1A–D) and degenerative (classes 2A–E) types (Palmer 1989). Traumatic tears are usually linear and occur at the edges of the TFCC at either the soft tissue attachments or the attachment to the distal radius. Degenerative tears generally occur in ulnar impaction syndrome, in older people, and in the midportion of the TFC disc.

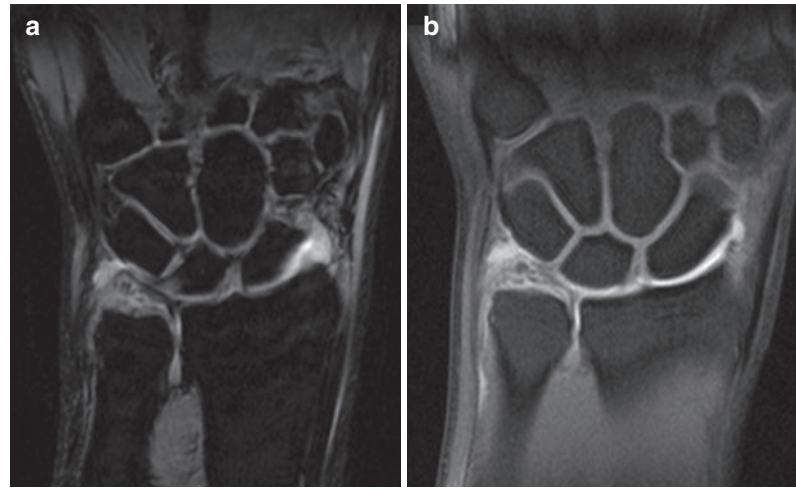

Fig. 10 (**a** and **b**) Recreational squash player with ulnar-sided wrist pain. (**a**) Coronal GRE MR and (**b**) T1-W FS MR direct MR arthrographic sequences show extensive complex tears of the ulnar styloid and fovea attachments of the TFCC. Note the contrast extravasation into the DRUJ

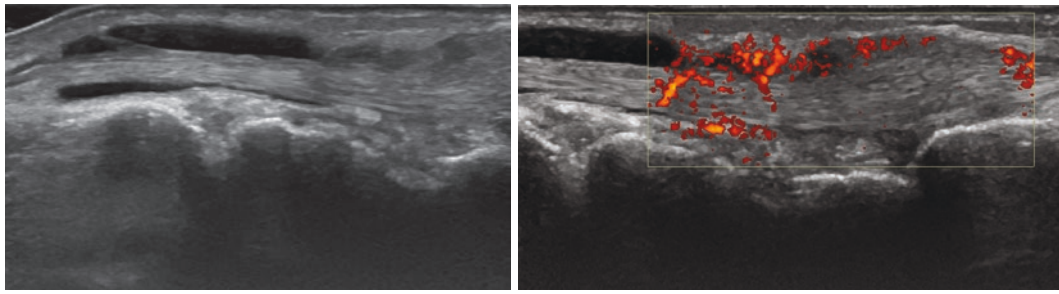

Fig. 11 Male basketball player with pain over the dorsal aspect of his wrist on extension. Longitudinal US image shows tendon sheath effusion with synovial thickening and increased vascularity of the extensor digitorum tendon consistent with tendinosis and tenosynovitis

4.6 Tendon Injuries

De Quervain's tenosynovitis (or De Quervain's disease) is a common injury in racquet sport and in athletes who use a lot of wrist motion, especially repetitive rotating and gripping. Overuse of the hand in these sports may eventually result in irritation or swelling of the tendons found along the thumb side (first dorsal compartment) of the wrist, with resultant tenosynovitis. Releasing an object with a sudden twist-and-snap action will trigger tendinitis, e.g., in bowling, weight lifting, and rowing. Most closed tendon injuries, if seen acutely, can be treated successfully with nonoperative management. Those that are undiagnosed and untreated may result in permanent instability (Aronowitz and Leddy 1998). Extensor carpi ulnaris tendinosis is the second most common type of sports-related closed tendon injury. Extensor carpi ulnaris tendinosis is most commonly seen in basketball players and those playing racquet sports. Inflammation of tendons is the most frequent abnormality found on US of the wrist. Tenosynovitis involves mainly the peritendinous synovial sheath covering the tendons. Hypertrophic-exudative tenosynovitis is seen as thickening of the tendon sheath that is distended by a hypoechoic effusion (Fig. 11). Tendon rupture and its severity can also be detected on US.

4.7 Neurovascular Injuries

Neurovascular syndromes in the wrist are uncommon occurrences in athletes (Rettig 1990). Most sports-related peripheral neuropathies in the distal upper limb are compressive in nature. These result from overuse or overload superimposed on normal or variant anatomy. Nerve damage is

often caused by external pressure from handles of racquets, sticks, and bats, or by pressure from leaning on bicycle handlebars. Neurologic syndromes are usually incomplete, and patients typically have subjective complaints of pain or vague sensory disturbances (Weinstein and Herring 1992). Carpal tunnel syndrome is a neuropathy that is encountered in sports and is caused by median nerve compression in the carpal tunnel. Paralysis of the ulnar nerve at the wrist is seen among cyclists, usually as a result of poor bicycle setup, causing weakness of grip and numbness of the ulnar 1.5 digits (Lorei and Hershman 1993). Hypothenar hammer syndrome leads to ulnar arterial wall damage from blunt-repetitive or acute severe injuries and may be associated with aneurysm formation. This is more commonly associated with racquet/batting sports, martial arts, and break dancing (Blum et al. 2006). Timely recognition, diagnosis, and appropriate treatment of neurovascular injuries are vital in order to avoid the potential risk of permanent injury (Nuber et al. 1998).

5 Specific Types of Sports Injuries

Many sporting activities produce a specific injury pattern related to the actions and stresses peculiar to that particular activity. Knowledge of the sport or recreational activity can therefore aid in the diagnosis and management of injury patterns. We have highlighted some popular and emerging sports, and attempted to group sports injuries of the wrist according to their common mechanisms of injury. Knowledge of the biomechanics behind a particular sporting activity is useful for understanding the pathophysiology of wrist injury and helps explain the findings seen at imaging (Jacobson et al. 2005).

5.1 Golf, Baseball, and Racquet Sports

Wrist injuries that are common to golf, baseball, and racquet sports include hook of hamate fractures, ulnar neuropathies, and tendon injuries. All these sports entail gripping an implement such as a bat, club, or racquet to strike a ball. When a bat hits a ball, a racquet makes contact with a ball or hard surface, or a golf club catches the ground, the hypothenar eminence of the palm is forcefully struck. This may result in a hook of hamate fracture (Fig. 12). In baseball and golf, the hamate fractures usually occur in the nondominant hand, while fractures to the dominant hand tend to occur in racquet sports such as tennis and squash.

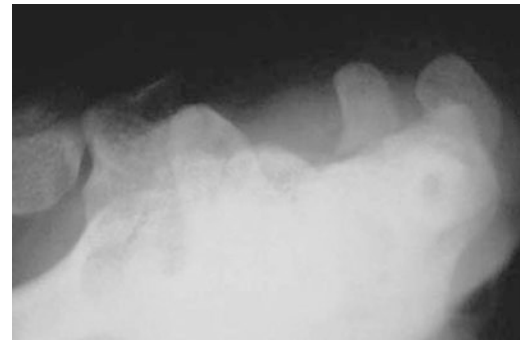

Fig. 12 Carpal tunnel radiographic projection shows a transverse fracture of the hook of hamate

Among golfers, the wrist is one of the most commonly injured anatomic locations and can affect average golfers as well as high-level professionals. A study of 225 professional golfers showed a 34% incidence of wrist and hand injuries involving the soft tissue, cartilage, bone, nerve, and vascular structures (McCarroll 1986). Hand and wrist injuries are more common among professionals, compared to amateurs, and are frequent in both male and female professional golfers (Batt 1992, 1993; McCarroll 1996; Gosheger et al. 2003; Wiesler and Lumsden 2005).

When they occur, wrist injuries can be devastating for the avid golfer, as the hand and wrist are integral to this game. Most golf injuries are overuse injuries of the wrist flexor or extensor tendons. The golf swing phase involves both components of wrist extension/pronation and wrist flexion/supination which specifically predisposes to extensor carpi ulnaris tendon instability (Ek et al. 2013). The left wrist in the right-handed golfer is the most common location. Excessive motion of the left wrist, along with a catapulting action, accounts for the vulnerability of the left wrist to injury. Hyperextension and

radial deviation of the right wrist may cause an impingement syndrome. Injury may also be sustained during the impact of the swing phase (Murray and Cooney 1996).

Professional and weekend golfers, although showing a similar overall anatomic distribution of injuries by body segment, tend to have differences in the ranking of injury occurrence by anatomic site. These differences can be explained by their playing habits and the biomechanical characteristics of their golf swings (Theriault and Lachance 1998). Golfing injuries are usually the result of overuse due to excessive practice, poor conditioning, excessive play, or poor swing mechanics that put the wrist at risk. Increased risk factors include previous injury, advancing age, and anatomic abnormalities. In addition to producing new injuries, golf may also reignite old injuries and exacerbate preexisting degenerative disease (Batt 1992, 1993; Wiesler and Lumsden 2005). TFCC injuries may also be seen in golfers. Increased motion of the wrist that occurs in golfers makes this structure prone to tearing.

Soft-tissue injuries in racquet sports include those due to direct impact of the handle, as well as repetitive stretching that occurs as the wrist is forcefully whipped into extremes of position. Although all the tendons can be affected, tendinosis is most common in the first dorsal compartment, flexor carpi ulnaris, flexor carpi radialis, and extensor carpi ulnaris. Ligamentous tears can result in instability patterns which if untreated may become chronic. Neurovascular structures may be compromised by repetitive blunt trauma to these structures or by entrapment by surrounding structures (Osterman et al. 1988). Thrombosis and vascular aneurysms may form, more often on the ulnar side in hypothenar hammer syndrome (De Mooij et al. 2015).

Tennis is a popular racquet sport, with players frequently beginning playing in childhood and continuing into late adulthood. Most wrist injuries in tennis are due to chronic overuse rather than acute direct trauma (Rettig 1994). The most common types of injury in tennis players of all ages are muscle sprains and ligament sprains secondary to overuse. These are a particular problem in the adolescent age group because these athletes generally play at a lower level of physical conditioning (Fig. 13). Fortunately, injuries in younger players are usually not long-standing

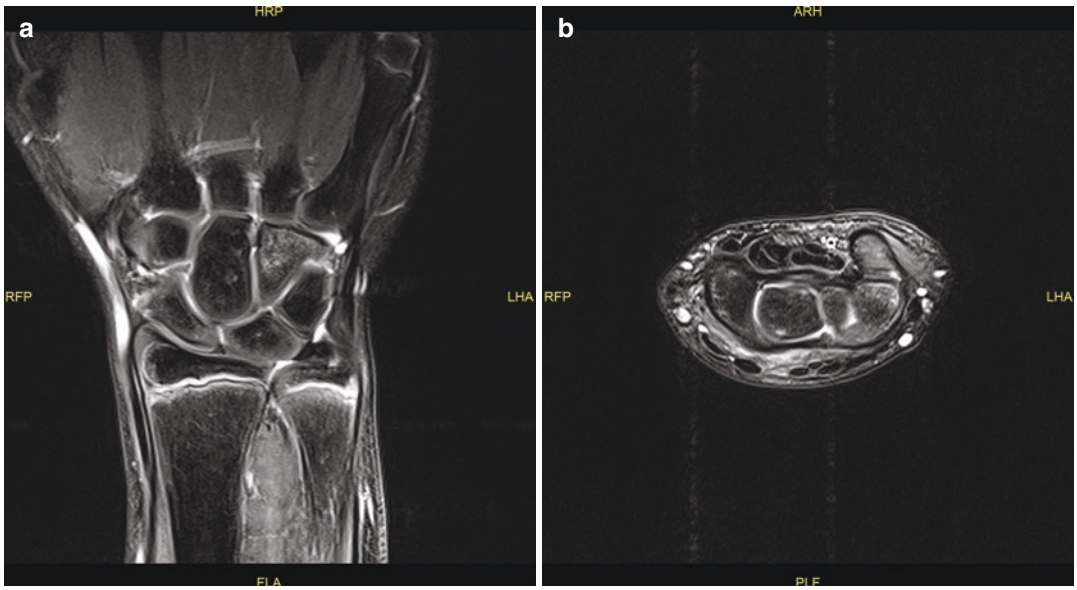

Fig. 13 (**a** and **b**) Tennis player with ulnar-sided wrist pain from bone bruising. (**a**) Coronal PD FS image shows edema in the hamate. (**b**) Axial PD FS MR image shows further edema in the pisiform and triquetrum. These are likely related to pisotriquetral and pisohamate impaction (courtesy of Professor Jan Gielen, University Hospital, Antwerp, Belgium)

and the chronic overuse problems seen in older players are less common in younger players (Bylak and Hutchinson 1998).

Young tennis players should aim at prevention of overuse injuries. Principles of a gradual, progressive increase in the intensity of tennis practice, the slow introduction of new court surfaces, and a staged progression in the teaching of tennis skills can help to reduce the incidence of injury in young tennis players (Bylak and Hutchinson 1998; Fernandez-Fernandez et al. 2013). The goal of early recognition and treatment of wrist injuries is to restore the wrist to a pain-free stable unit with a normal range of motion, so as to allow early return to athletic activity and prevent development of chronic discomfort or permanent disability (Osterman et al. 1988; Rettig 1994).

Ulnar-side wrist pain can be disabling in sports such as golf and tennis due to limitation of pronation-supination. Erosion of the floor of the sixth dorsal space should be considered as a possible cause of unresponsive ulnar-side wrist pain and should be suspected when severe ulnar-sided pain persists in athletes after the usual methods of treatment (Carneiro et al. 2005).

5.2 Gymnastics

Gymnastics places high demands on the upper extremity and is unique in that it requires the athlete to repetitively use the upper extremities as weight-bearing structures, such that high-impact loads are distributed through the elbow and wrist joints. The forces exerted on the wrist can approach as much as 16 times of the athlete's body weight (Difiori et al. 2006). Since most gymnasts begin training from an early age, it is common for injuries to occur in the physis of skeletally immature gymnasts (Wolf et al. 2017). In gymnasts, the wrist is a frequent site of symptoms and injury, both acute and chronic. A systematic review encompassing 12 studies has shown that the incidence and prevalence of wrist-overuse injuries were highest in gymnasts, when compared with other wrist-loading sports (Kox et al. 2015). The gymnast may present with wrist pain secondary to repetitive hyperextension and overuse (Fig. 14). The gymnast wrist pain syndrome can present as a difficult diagnostic and therapeutic challenge. It is debilitating, resulting in a reduction in training and performance, and may be due to a response to repetitive trauma during the period of growth and development. Many variables contribute to the risk of gymnastic injuries. It is generally proportional to the competitive level of the athlete and the increased training and exposure time required, with a 25-fold increase in injury rates between the highest and lowest levels of competition in the United States Gymnastics Federation (Webb and Rettig 2008). There is also evidence that the

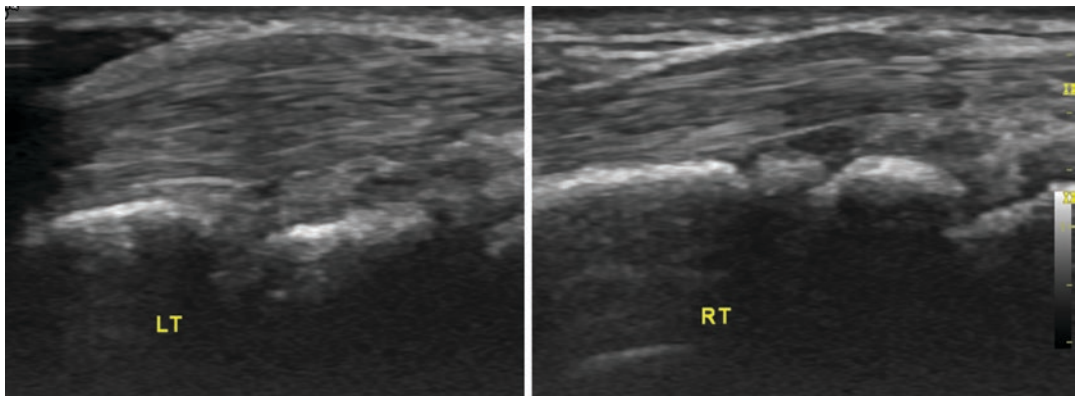

Fig. 14 Overuse injury in a female recreational gymnast with left wrist pain. Transverse US image shows relative thickening of the common sheath of the extensor digitorum tendon in the left wrist, when compared to the right, from chronic tendinopathy

specific type of gymnastic routine performed influences the incidence of injuries with nonartistic Team Gymnastics having an incidence of 50.3 per 1000-h exposure (Lund and Myklebust 2011) versus an incidence between 9.22 and 22.7 per 1000-h exposure for collegiate artistic gymnastics (Hart et al. 2018).

An extensive review of the literature of gymnastic injury in the pediatric population revealed that the incidence and severity of injuries are relatively high, particularly among advanced-level female gymnasts. Overuse and nonspecific pain conditions of the wrist occurred frequently among these gymnasts. Factors associated with an increased injury risk among female gymnasts included greater body size and body fat, periods of rapid growth, and increased life stress (Caine and Nassar 2005). A cross-sectional survey of 52 nonelite gymnasts (32 girls, 20 boys; average age 11.8 years) showed that wrist pain was common, occurring in 73% of gymnasts. Gymnasts with wrist pain were older, trained more hours per week, trained at a higher skill level, and began training at an older age (Difiori et al. 1996) (Fig. 15).

A recent 10-year observational epidemiology study of male and female gymnastic teams in a Division 1 collegiate association revealed a more similar injury incidence between sexes, with reported injuries of 8.78 per 1000 male gymnasts and 9.37 per 1000 female gymnasts. Wrist and hand injuries were the most commonly injured anatomic part in males, whereas in females, this was ranked sixth, with foot and ankle injuries accounting for the majority (Westermann et al. 2015). The differences for this are likely accounted for the biomechanical demands imposed on the athletes from their differing routines and apparatus; in male athletes, the upper extremity is almost exclusively used for support in the high bar, rings, and parallel bars. The "missed move" is also cited as an injury mechanism, with somersaults and handsprings accounting for the most frequent injury-producing moves (Fig. 16). There was an increased chance of injury when the gymnast had been on the apparatus for an extended period; hence loss of concentration was regarded as a major source of injury (Lindner and Caine 1990).

Fig. 15 Elite gymnast with ulnar-sided wrist pain. PA radiograph shows a well-corticated bony fragment at the tip of the ulnar styloid process due to previous trauma. There is bony overgrowth, causing ulnar-sided mechanical problems

Fig. 16 Male gymnast who missed his landing and developed soreness over the radial aspect of his wrist. Radiographs were normal (not shown). Coronal T2-W MR image shows diffuse hyperintense signal in the scaphoid but no fracture line is seen, consistent with a bone bruise

To determine the frequency and characteristics of wrist pain in young, non-elite gymnasts and to describe the effects of chronic wrist upon gymnastics training, a prospective cohort study of 47 non-elite female and male gymnasts between 5 and 16 years of age was performed. Wrist pain was reported by 57% (27/47) of subjects at the study onset. 89% (24/27) reported wrist pain both at the study onset and 1 year later. The floor exercise, the pommel horse, and the balance beam were most frequently associated with wrist pain symptoms. 42% of subjects with wrist pain at each survey reported that the symptoms interfered with training. Adolescent gymnasts between 10 and 14 years of age training at non-elite level were found to be more likely to have wrist pain (Difiori et al. 2002a). This age group has been reiterated and confirmed as one of the major predisposing risk factors for wrist pain in young gymnasts, with the other being high-intensity training and earlier onset of training (Kox et al. 2015).

Gymnast's wrist results from repetitive and excessive loading on the joint, leading to premature closure of the growth plates and other growth disturbances. Repeated stresses affect the distal radial growth plate, causing undergrowth or even physeal arrest of the radius, with resultant positive ulnar variance which may become symptomatic (Fig. 17). Radiographs show physeal irregularities and bony sclerosis. If untreated, radial deformity and shortening may occur, leading to permanent deformity. De Smet et al. (1993) presented six new cases, all of whom had an ulnar-positive variance and an increased sagittal angle of the distal radial epiphysis. Five of the gymnasts elected to stop their sports careers, while one was successfully treated with an arthroscopic TFCC debridement. Epiphysiodesis of the distal radial and ulnar growth plates has been used to surgically treat a skeletally immature gymnast in order to prevent Madelung's deformity (Bak and Boeckstyns 1997).

The radiographic appearances of chronic stress injury to the wrist joint consist of bilateral, asymmetrical widening and irregularity of the distal radial growth plates, with ill-defined cystic areas, sclerosis, and flaring of the metaphyses. Similar but less marked changes are seen in the distal ulnar growth plates (Fig. 18). The etiology is thought to be a Salter-Harris type I stress fracture of the growth plate due to chronic repetitive shear forces applied to the hyperextended wrist joint. Rapid healing of the stress fracture occurs with cessation of the sporting activity but continued strenuous use of the wrist results in further widening and irregularity of the growth plate (Carter et al. 1988). On MR imaging, fractures

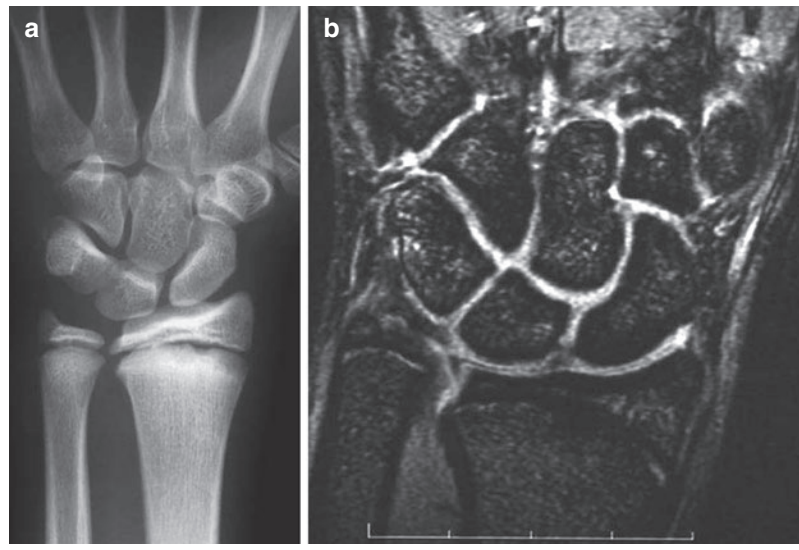

Fig. 17 (**a** and **b**) Female gymnast with left wrist pain and tenderness at the DRUJ on dorsiflexion. (**a**) PA radiograph shows stress changes adjacent to the distal radial and ulnar growth plates. (**b**) Coronal GRE MR image shows a central perforation of the TFCC. Positive ulnar variance is better seen on the MR image

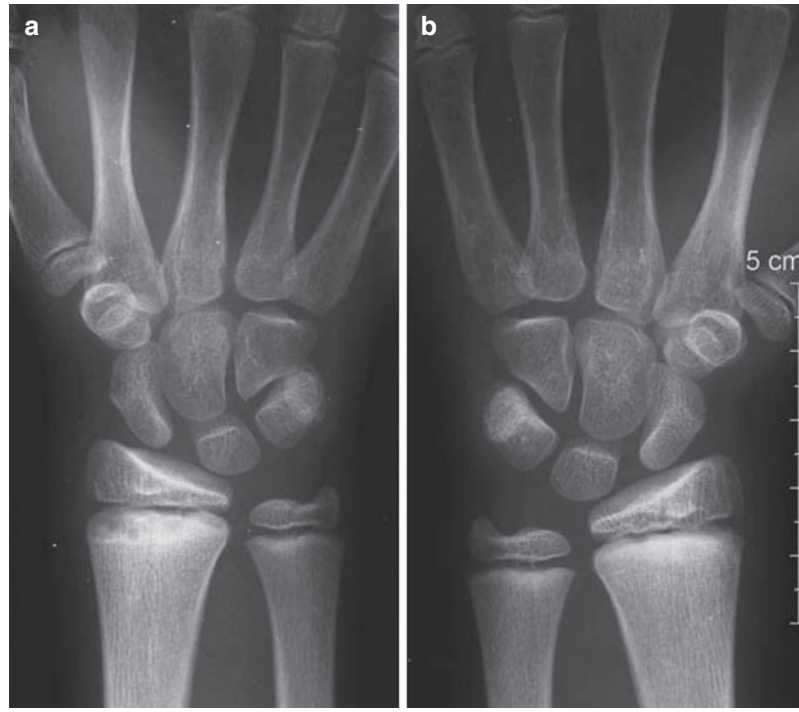

Fig. 18 (**a** and **b**) Female adolescent gymnast with stress changes to both distal forearm bones. (**a**) PA radiographs of the right and (**b**) left wrists show sclerosis and patchy cystic areas adjacent to the distal radial growth plates. Similar but milder changes are present in the distal ulna

and stress fractures are identified as hypointense fracture lines, surrounded by patchy areas of T1 hypointensity and T2 hyperintensity representing edema (Peh et al. 1996; Breitenseher et al. 1997). The presence of edema without a visible fracture line may represent a bone bruise or a stress reaction. Stress injuries related to growth plates of the distal radius and ulna may be seen in adolescent gymnasts (Shih et al. 1995). Fraying, irregularity, and widening of the physis on MRI were consistent indicators of a physeal injury in 3 out of 10 female gymnasts in a study examining gymnastic wrist injuries (Dwek et al. 2009). There is recent provisional evidence that volumetric measurements of the physis can indicate early physeal stress changes in a group of 45 symptomatic and asymptomatic gymnasts when compared to the 24 non-gymnast cohort (Kraan et al. 2019). The gymnast population had median physeal volumes of 971 (symptomatic) and 951 (asymptomatic) mm^3, versus the non-gymnastic population who had median volumes of 646 mm^3.

In a follow-up study of 21 young, high-performance gymnasts with stress changes related to the distal radial epiphysis, 11 of the gymnasts who presented with radiographic changes of the distal radial epiphysis took at least 3 months to recover. In comparison, ten gymnasts who had similar symptoms but no radiographic changes recovered within an average of 4 weeks. The radiographic changes were considered to represent stress changes, possibly stress fractures, of the distal radial epiphysis (Roy et al. 1985).

A radiographic survey to determine skeletal age and nature and prevalence of stress-related changes affecting the distal radial growth plate in 60 young competitive gymnasts (39 females, 21 males) revealed a significant delay in maturation for girls. It was found that the widening and irregularities of the distal radial physis appear to be the first in a spectrum of abnormal changes secondary to overuse, and probably represented a stress fracture of the distal radial growth plate. The authors concluded that the radiographic changes associated with this injury were not the normal adaptive changes seen in young, competitive gymnasts. More serious long-term abnormality may result even though the injury may initially resemble a Salter-Harris type I or II

stress fracture. Long-term complications may include symmetrical or asymmetrical retardation or halted growth at the affected site, positive ulnar variance, and associated pathoanatomic sequelae (Caine et al. 1992).

A cross-sectional study of 59 gymnasts (28 girls and 31 boys; average age 9.3 years) revealed that wrist pain was reported by 56% (33/59) of the gymnasts, with 45% (15/33) describing pain of at least 6-month duration. Factors significantly associated with wrist pain included higher skill level, older age, and more years of training. 51% (30/59) of the gymnasts had findings of stress injury to the distal radial physis, and 7% had frank widening of the growth plate. Wrist pain prevalence was significantly related to the grade of radiographic injury. Mean ulnar variance was significantly more positive than established norms. Ulnar variance was not associated with wrist pain or radiographic injury of the distal radial physis. The authors concluded that radiographic findings of distal radial physeal injury are associated with wrist pain among young non-elite gymnasts (Difiori et al. 2002b).

In a study undertaken to define and characterize factors contributing to the causes and development of gymnast wrist pain and to establish an effective means of systematic and comprehensive evaluation and treatment, 75% of 38 collegiate gymnasts were found to have wrist pain for at least 4 months. The males averaged 2.82 ± 1.94 mm positive ulnar variance and the females averaged 1.44 ± 1.88 mm positive ulnar variance, with all of the gymnasts having significantly greater variance than the controls, who averaged −0.52 mm. The pommel horse routine was consistently responsible for wrist pain among the males. Anatomic and histologic correlation of cryosections with MR imaging performed to establish the usefulness of MR imaging in the diagnosis of wrist pain showed that MR imaging was able to differentiate the complex transitions between cortical and trabecular bone, articular surfaces, ligaments, and TFCC of the wrist joint (Figs. 16 and 17). Arthroscopic findings correlated well with those of MR imaging and arthrography, with arthroscopic surgery being a successful mode of treatment (Mandelbaum et al. 1989).

To assess the prevalence of stress injury to the distal radial growth plate and of positive ulnar variance in a non-elite gymnast population, a radiographic survey was performed in 44 skeletally immature non-elite gymnasts consisting of 27 girls and 17 boys. Radiographic findings consistent with stress injury of the distal radial physis were found in 25% (11/44) of participants. Ulnar variance was found to be more positive in the gymnasts when compared with age-predicted norms, with an average side-to-side difference in ulnar variance of 0.9 mm. Radiographic findings of stress injury to the growth plate and the amount of ulnar variance were not associated with age, sex, training intensity, wrist pain, height, or weight. There was also no significant relationship between ulnar variance and radiographic findings. It also appears that ulnar variance is more positive than would otherwise be predicted, suggesting growth inhibition of the distal radius, a growth stimulation of the ulna, or a combination of both (Difiori et al. 1997). Tolat et al. (1992) described five teenage female gymnasts who had symptomatic acquired positive ulnar variance occurring due to premature physeal closure of the growth plate. All cases demonstrated ulnocarpal impingement, and arthroscopic assessment of the wrist allowed assessment of the integrity of the TFCC and helped decide on the most appropriate surgery such as distal ulna recession and shaving for a TFCC perforation.

The ulnar variance in female gymnasts attending the 1987 Artistic Gymnastics World Championship was measured, showing a marked increase in the ulnar length in adult as well as immature gymnasts, compared with nonathletes. The changes in relative ulnar length were correlated to weight, height, and skeletal age of the athletes. In 10% of the gymnasts' wrists, stress-related changes of the distal physis of the radius were noted. The authors concluded that repetitive injury and compression of the wrist lead to a premature closure of the distal radial growth plate resulting in secondary ulnar overgrowth (De Smet et al. 1994). Interestingly, contradictory results appeared in another study using the PA radiographs of 201 female participants of the 1987 Artistic Gymnastics World Championships.

This study showed that female gymnasts who demonstrated ulnar overgrowth were skeletally more advanced in maturity status of the entire hand-wrist compared with gymnasts who did not show ulnar overgrowth. The authors concluded that ulnar overgrowth was not associated with advanced maturity of the distal radial epiphysis as defined in protocols for assessing skeletal maturity and did not lead to premature epiphyseal closure of the distal radius (Beunen et al. 1999).

5.3 Rowing/Canoeing, Volleyball, and Basketball

Overuse of the hand in sports such as rowing, volleyball, and basketball may eventually result in irritation or swelling of the tendons of the wrist, with resultant tenosynovitis.

Rowing has gained considerable popularity in recent years. Rowers hail from a wide spectrum of age groups. Rowing is an endurance activity with no sudden accelerations or ballistic impact forces. It is associated with several injuries that are so typical that they are easily recognized and in many cases do not require imaging. Injuries of the forearm and wrist are common in rowing, with incidence between 5.3 and 22% (Smoljanovic et al. 2018; Baugh and Kerr 2016). These include De Quervain's tenosynovitis and proximal intersection syndrome (also known as the "Oarsman's wrist") which involves the extensor carpi radialis longus and brevis (Fig. 19). Proximal intersection syndrome is an overuse tenosynovitis from repetitive wrist flexion and extension, leading to predominantly second extensor compartment tenosynovitis at the point where it crosses over the first extensor compartment at about 4 cm proximal to Lister's tubercle. Distal intersection syndrome is another similar overuse tenosynovitis but is much less common, occurring just distal to Lister's tubercle and involving the extensor pollicis longus tendon (third extensor compartment) as it crosses over extensor carpi radialis longus and brevis tendons (second extensor compartment) (Fig. 20). Chronic exertional compartment syndrome can afflict the volar muscles of the forearm typically when the drive phase is initiated by the elbow and not the shoulder girdle. The increased blood flow, metabolic products, muscle size, and tension on the surrounding fascia can lead to pain and neurological symptoms mimicking a neuropathy (Cole et al. 2017). Knowledge of the basic rowing physiology and equipment, mechanics of the rowing stroke, and training habits will make those involved in patient management better equipped to diagnose, treat, and prevent injuries in rowers (Rumball et al. 2005; Thornton et al. 2017).

Du Toit et al. (1999) investigated the incidence and causes of acute tenosynovitis in long-distance canoeists, and found that an average of 23% of competitors in each race developed this

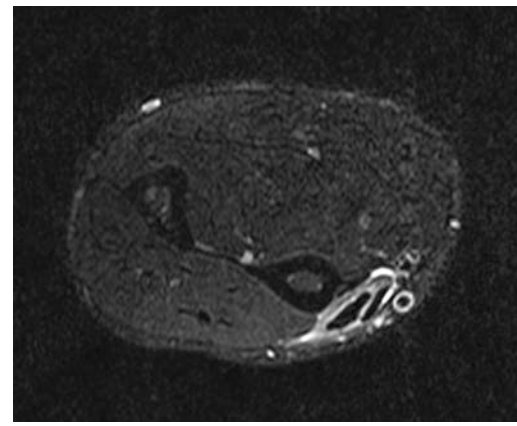

Fig. 19 Axial T2-W FS image shows proximal intersection syndrome with tenosynovitis of the extensor carpi radialis longus and brevis (courtesy of Professor Jan Gielen, University Hospital, Antwerp, Belgium)

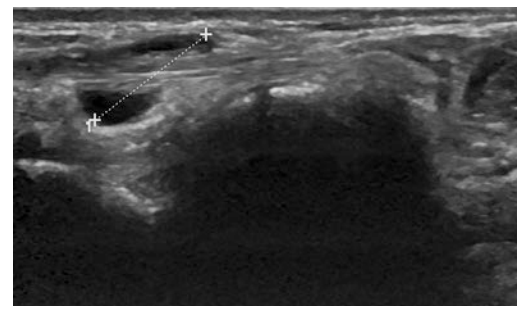

Fig. 20 Longitudinal US images shows a localized effusion in the extensor pollicis longus tendon sheath from distal intersection syndrome (courtesy of Professor Jan Gielen, University Hospital, Antwerp, Belgium)

condition. The incidence was significantly higher in the dominant than in the nondominant hand but was unrelated to the type of canoe and the angle of the paddle blades. Canoeists who covered more than 100 km a week for 8 weeks preceding the race had a significantly lower incidence of tenosynovitis than those who trained less. Environmental conditions during racing, including fast-flowing water, high winds, and choppy waters, and the paddling techniques, especially hyperextension of the wrist during the pushing phase of the stroke, were both related to the incidence of tenosynovitis. The study suggested that development of tenosynovitis is not related to the equipment used, but is probably caused by difficult paddling conditions, in particular uneven surface conditions, which may cause an altered paddling style. The athlete's level of fitness and the ability to balance a less stable canoe, thereby maintaining optimum paddling style without repeated eccentric loading of the forearm tendons to limit hyperextension of the wrist, appear to be important factors (Du Toit et al. 1999).

Volleyball players are subjected to application of limited multiple trauma to the dorsal radial portion of the wrist. Rossi et al. (2005) studied 45 volleyball players with the diagnosis of de Quervain's stenosing tenosynovitis and showed that increased training time and consequent microtrauma may increase the likelihood of this injury. Volleyball players commonly complain of pain in the hypothenar area. Fatigue fracture of the pisiform bone has been suggested as a cause of this incapacity (Israeli et al. 1982). Although this can be demonstrated on oblique and carpal tunnel view radiographs of the wrist, this is no longer recommended as CT is ultimately superior in all instances for detection and diagnosis and is widely available. MR imaging is also able to detect occult impaction and stress-induced marrow edema (Moraux et al. 2014).

Acute basketball injuries often involve the hand and wrist. Extensor carpi ulnaris tendinosis, along with TFCC and DRUJ injuries, is commonly encountered in basketball players (Cohen and Metzl 2000; Pang and Yao 2017). Scapholunate interosseous ligament disruption occurs more commonly in the dominant hand and can lead to scapholunate dissociation, if not surgically repaired (Melone Jr et al. 2012). Tehranzadeh and Labosky (1984) reported using double-contrast wrist arthrography to detect loose intra-articular osteochondral fracture fragments caused by basketball injury. These were subsequently removed surgically.

5.4 Cycling/Wheelchair Athletes

Distal peripheral neuropathies have been identified in cyclists because of prolonged grip pressures on handlebars. The so-called cyclist palsy has been postulated to be an entrapment neuropathy of the ulnar nerve in Guyon's canal of the wrist. Wheelchair athletes are also prone to developing hand pain and numbness, due to extremity peripheral nerve entrapment related to prolonged gripping of the wheelchair wheels. Ulnar neuropathy, characterized by tingling, numbness, and weakness in the hands, is common in serious cyclists, especially following several days of riding (Mellion 1991; Richmond 1994).

Chan et al. (1991) studied the 14 national level competitive cyclists and found that the prevalence of median nerve lesions at the wrist, although usually mild, was substantially higher than expected. Electrodiagnosis was recommended as a sensitive detector for neuropathy, even at a subclinical stage. Fracture of the trapezium is a rare injury associated with cycling and may need a special radiographic projection (Bett's oblique view) for visualization (Lilley et al. 2000).

Wheelchair athletes commonly experience hand pain and numbness, due to extremity peripheral nerve entrapment. The most common electrodiagnostic dysfunction was of the median nerve at the carpal tunnel (46%), and the portion of the nerve within the proximal carpal tunnel was most frequently affected. Ulnar neuropathy was the second most common entrapment electrodiagnostically (39%) (Burnham and Steadward 1994). Body mass index and total time of wheelchair usage during training and competition are also established contributing factors to the development of carpal tunnel syndrome (Kim et al. 2017).

5.5 American Football, Horse Riding/Rodeo, Roller-Skating/Rollerblading/Skateboarding/Hoverboarding

Sporting activities that involve hand contact with a fast-moving heavy ball have the potential for injury to athletes. Examples include soccer (as goalkeeper), basketball, netball, volleyball, cricket, and rugby (MacGregor 2003). Ball games have been found to account for the largest number of sports injuries among children in Hong Kong (Maffuli et al. 1996). Fractures and dislocations to the wrist may result from direct blow to hand-wrist (e.g., American football, boxing, rugby) or falls (e.g., horse riding, motocross, soccer, skating, snowboarding, track and field) (Fig. 21).

5.5.1 American Football

An analysis of injuries from American football clubs in Colorado revealed an incidence of upper extremity injuries that range from 15 to 25%.

Fig. 21 Male track athlete who sustained a fall. Oblique PA radiograph shows a minimally displaced fracture of the tuberosity of the scaphoid

There were both traumatic and overuse injuries, with involvement of the distal forearm and carpus being common in this contact sports. Injuries encountered include distal radial and scaphoid fractures, ligamentous injuries, and TFCC tears (Schlegel et al. 1999). Ellsasser and Stein (1979) reviewed hand injuries in a professional American football team over a 15-year period. 38 players from one professional football team suffered 46 major hand and wrist injuries. The injuries included fractures, dislocations, fracture dislocations, and soft-tissue injuries of the phalanges, metacarpals, carpals (particularly the scaphoid), and distal radius/ulna, including intra-articular injuries. 12 surgical procedures were performed, allowing the players to return to active participation with a minimum loss of practice time. Carlisle et al. (2008) analyzed elbow, forearm, and wrist injuries involving National Football League players over a 10-year period. They found that ligamentous sprain and instability injuries of the wrist were most frequently encountered, comprising 19% of reported incidents (n = 160/859). When considering other injuries such as fractures, dislocations, and tenosynovitis, the wrist accounted for 30% of total injuries.

In a retrospective study of lunate and perilunate carpal dislocations in professional football players in the US National Football League over a 5-year period, Raab et al. (1994) reported seven lunate and three perilunate dislocations in ten players. The mechanism of injury was hyperextension in nine of ten players. The study demonstrated that lunate and perilunate carpal dislocations were not career-ending injuries in professional football, although a minimum loss of 4 weeks of playing time was expected. Treatments varied but none was clearly superior or detrimental, although four of the five players who returned to play in the same season were treated by closed reduction with percutaneous pinning.

5.5.2 Horse Riding/Rodeo

Moss et al. (2002) found that upper limb injuries accounted for 29.2% of all horse riding injuries, the majority (85.5%) of whom sustained the injury falling from the horse. The commonest

upper limb fractures were distal radial fractures, with scaphoid fractures also being reported. The authors noted that the incidence of upper limb injuries among horse riders appears to be increasing.

Rodeo is regarded as a nontraditional sporting activity that is high collision in nature. In a radiographic study of 25 male rodeo riders, also known as roughstock athletes, 82 upper limb abnormalities were found. This comprised 24 fractures of the hand and wrist, including 5 nonunions, involving bones such as the scaphoid. There were 14 cases of degenerative joint disease (e.g., radioscaphoid, scapholunate, and TFCC), joint calcification, dorsal instability, and scapholunate dissociation (Meyer et al. 2003). Inexperienced competitors have a greater rate of injury to areas such as the hand and wrist (Butterwick and Meeuwisse 2002).

5.5.3 Roller-Skating/Rollerblading/Skateboarding/Hoverboarding

Roller-skating, rollerblading (also known as wheels-in-line skating), skateboarding, and scooter riding are popular recreational and sporting activities among children and adolescents, but have attendant risks and can be associated with skeletal injury. Similarly, the recent advent and increasing popularity of hoverboarding (also known as self-balancing electric scooters) have also contributed to the increasing spectrum of injuries. All these activities, being conducted on wheels moving along hard surfaces, involve movement at high speeds and potential for attempts at extreme maneuvers. Most of these injuries result from falls, with fractures to the distal radius and ulna being common.

Zalavras et al. (2005), in a study of patients who presented to the pediatric fracture clinic of the level I trauma center over a 1-year period after sustaining fractures due to skateboarding, roller-skating, and scooter riding, identified 325 fractures (13.7%) among a total of 2371 fractures. Mean age of patients ranged from 9.7 to 13 years, with a male predominance. The forearm was fractured most often, composing 48.2% of skateboarding fractures, 63.1% of roller-skating fractures, and 50.7% of fractures due to scooter-riding. 94% of forearm fractures were located in the distal third. Schieber et al. (1994) found that of approximately 30,863 persons treated for rollerblading injuries, for every rollerblading injury, approximately 3.3 roller-skating and 1.2 skateboarding injuries occurred. The median ages of those injured in these three sports were 15, 12, and 13 years, respectively, with wrist fractures and/or dislocations being a common injury.

Orenstein (1996) prospectively studied the types of injuries sustained during the use of rollerblades and compared them with injuries sustained during the use of roller skates and skateboards. Minor injuries (sprains, bruises, lacerations) were more common than fractures, and there was no statistical difference in the types of injury between the skate groups. The most common serious injury was fracture of the distal arm, which occurred in each of the three skater groups (43%). Injuries occurred more commonly because the skater was going too fast (35%), because the skater struck an object in the pavement (20%), or because the skater was unable to brake (19%). The authors concluded that injuries sustained by rollerbladers were similar to those sustained by roller skaters and skateboarders, and that the risk of wrist or elbow fracture was greater when wrist guards were not worn.

The most common injury in the increasingly popular recreational activity of rollerblading is a fracture of the distal radius, which comprises 50% of all fractures. Reasons for the increasing number of serious injuries in rollerblading include the following: majority of skaters do not wear proper protective equipment and many users cannot handle their in-line skates in dangerous situations (Ellis et al. 1995; Jerosch and Heck 2005). Studies on rollerblading injuries from Europe, Australia, and the USA produced similar findings in that majority of victims were male aged 10–14 years, had fallen, and sustained wrist injuries (Young et al. 1998; Nguyen and Letts 2001; Mulder and Hutten 2002).

Skateboarding has experienced intermittent periods of popularity since the 1960s. Skateboarding injuries have increased with the rise in popularity of the sport, and the changes to the injury pattern could be expected with the development of both skateboard tricks and materials used for skateboard construction. Most

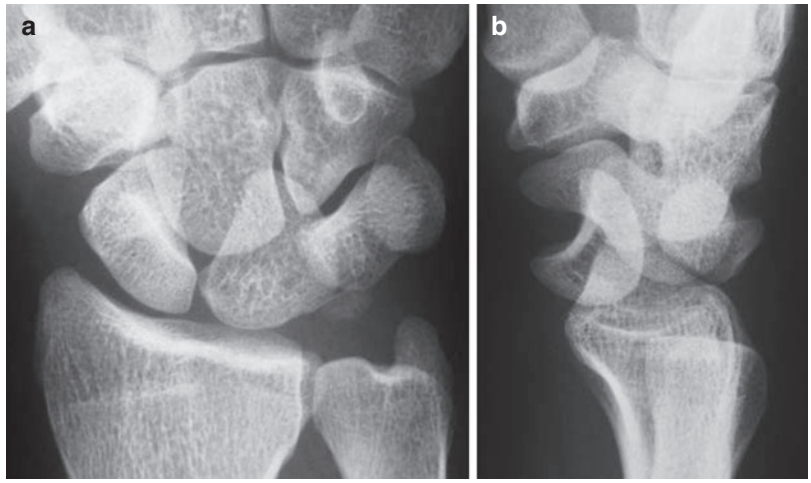

Fig. 22 (**a** and **b**) Male adult snowboarder who fell while snowboarding. (**a**) PA radiograph shows disruption of all the carpal arcs. The lunate has an abnormal triangular shape, with overlapping of the LT and capitolunate articular surfaces. (**b**) Lateral radiographs show that the lunate is dislocated volarly and is rotated such that its distal articular surface faces volarly. Appearances are typical of a lunate dislocation (courtesy of Professor Shigeru Ehara, Iwate University, Morioka, Japan)

documented cases occur in boys aged from 10 to 14 years, with injuries ranging from minor cuts and abrasions to multiple fractures and, in some cases, even death (Fountain and Meyers 1996). Forsman and Eriksson (2001) studied 139 people injured in skateboarding accidents, and found that most were children with a mean age of 16 years, with the most common fractures involving the ankle and wrist. Kyle et al. (2002) also found that the most frequent injuries in skateboarding were ankle strain/sprain, followed by wrist fracture.

A recent study of 47 pediatric patients who presented to the emergency department following a hoverboard injury over an 8-month period revealed a total of 42 fractures in 32 of the patients (Schapiro et al. 2017). Of these, 74% (31/42) of the fractures involved the upper extremity with the most commonly fractured bone being the distal radius (38% [16/42]), followed by the distal ulna (17% [7/42]).

Wrist fractures are the most common type of injury in roller-skating, rollerblading, skateboarding, and hoverboarding. Use of industrially tested equipment and wearing of protective gear, particularly wrist and forearm guards, are needed. If skaters do not protect themselves adequately, injuries are expected to increase with a rise in the sport's popularity (Schieber et al. 1994; Ellis et al. 1995). The American Academy of Pediatrics recommends that children under 5 years of age should not be allowed to ride skateboards. At an early age, injuries may occur due to reasons such as high center of mass, immature skeletal development, an undeveloped neuromuscular system, and simply poor judgement (Fountain and Meyers 1996).

5.6 Snowboarding and Skiing

Alpine skiing and snowboarding are two of the most popular winter sports in the world, and both have a reputation for an inherently high risk of injury. Snowboarding involves riding a single board down a ski slope or on a half-pipe snow ramp. The injury profile in snowboarding differs from that of traditional alpine skiing. Compared with injuries resulting from skiing, snowboarding injuries occur more frequently in the upper extremities and ankles, and less frequently in the knees. Snowboarders typically sustain wrist injuries (Bladin et al. 2004; Boutin and Fritz 2005) (Fig. 22).

In a comparative study of snowboarders and skiers, Matsumoto et al. (2002) found that upper

extremity injuries were much more common in snowboarders than in skiers, with upper extremity fractures being three times more common in snowboarders. Wrist fractures were the most common fractures among snowboarders, comprising 62% of all fractures, and were found to have a different underlying cause compared with other upper extremity fractures. Matsumoto et al. (2004) found that the most common events leading to injury were falling (59.6%) and jumping (36.1%).

Different types of snowboard equipment, rider stance, and snowboarding activity result in different types of injury. The risk of injury may be lowered by using protective equipment, such as wrist guards, particularly for beginners. Wrist guards have been found to decrease the incidence of wrist injuries in snowboarding (Matsumoto et al. 2002; O'Neill 2003; Made and Elmqvist 2004). O'Neill (2003) tested the protective value during snowboarding of an off-the-shelf wrist guard originally designed for rollerblading, and found it to be effective.

6 Conclusion

Many sporting activities produce a specific injury pattern related to the risks, actions, and stresses peculiar to that particular activity. Knowledge of the sport or recreational activity aids in the diagnosis and management of injury patterns (Fig. 23). This chapter highlights some popular and emerging sports, and attempts to group sports injuries of the wrist according to their common mechanisms of injury. Imaging has an important role in the evaluation and diagnosis of the range of bone and soft-tissue injuries due to various sports. Knowledge of the biomechanics behind a particular sporting activity is useful for understanding the pathophysiology of wrist injury and helps explain the findings seen at imaging.

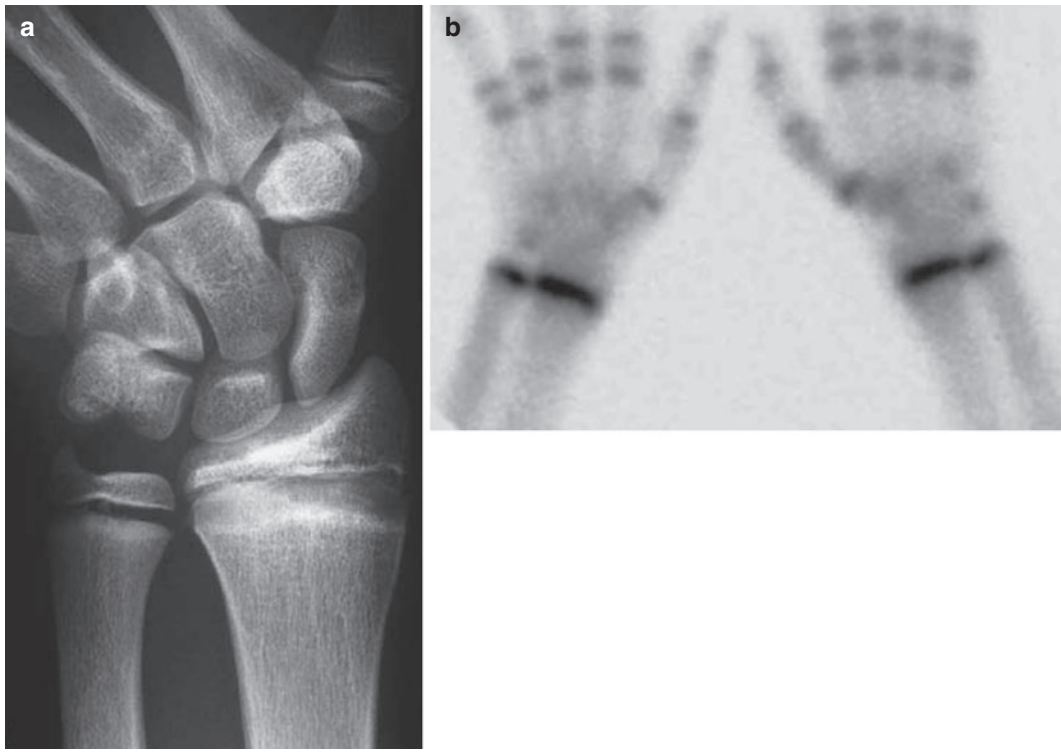

Fig. 23 (**a** and **b**) Male gymnast with stress changes of the distal radius and ulna bilaterally. (**a**) PA radiograph of the left wrist shows mild growth plate widening and adjacent sclerotic changes. (**b**) Bone scintiscan shows increased linear uptake at the distal ends of the radius and ulna bilaterally

Things to Remember

1. Many anatomic structures in the wrist may be injured in a wide variety of ways during participation in sports.
2. Many of these sporting activities, whether competitive or recreational, are associated with specific injury patterns related to the actions and stresses associated with that particular sport.
3. Knowledge of the sport biomechanics and imaging features aids in the early diagnosis, identification and prevention of potential complications, management, and follow-up of these injuries.
4. It is particularly important to recognize wrist injuries in the immature skeleton of preadolescent and adolescent athletes, as continued sporting activity may result in growth arrest and other long-term problems.

Imaging Technique Boxes

Radiography

- Standard frontal and lateral radiographs are the initial imaging investigation for detection of fractures and malalignment.
- Classification of distal radial fractures is made on radiographs.
- Special projections may be needed for scaphoid, hamate hook, and other carpal fractures.
- Stress radiographs or video fluoroscopy may be required to show dynamic carpal instability.

Computed Tomography

- Useful in supplementing normal or equivocal radiographs in clinically suspected injury.
- Accurate for diagnosis of hook of hamate fractures and DRUJ subluxation/dislocation.
- Helpful in the assessment of preoperative planning, healing, and post-traumatic deformity.

Bone Scintigraphy

- Useful only while bone is still remodeling.
- Helpful in radiographically occult trauma.

Arthrography

- Useful for diagnosis of ligament and TFCC tears.
- Single- versus triple-compartment injection technique.
- Single radiocarpal injection followed by either CT or MR imaging is commonly practised.

Ultrasonography

- Provides answers to very specific diagnostic questions for superficial lesions such as tendon abnormalities.
- Cheaper and time saving compared to MR imaging.
- Highly operator dependent with long learning curve.
- Availability of high-frequency transducer is essential.

Magnetic Resonance Imaging

- Provides a comprehensive overview of injuries to both bone and soft-tissue structures such as muscle, tendon, tendon sheath, nerve, and vessels.
- May be performed following arthrography.
- MR arthrography is useful for TFCC and SL and LT tears.
- 3 T MR imaging offers increased signal-to-noise ratio and resolution and can compete with MR arthrography studies in .terms of sensitivity and specificity.

Further information on imaging techniques: Gilula (1979); Egawa and Asai (1983); Wechsler et al. (1987); Desser et al. (1990); Peh and Gilula (1996); Peh et al. (1996); Breitenseher et al. (1997); Potter et al. (1997); Jacobsen (1999); Scheck et al. (1997); Bottinelli and Campani (2001); Bencardino (2004); Zlatkin and Rosner (2004); Kumar et al. (2005); Schmid et al. (2005); Boer et al. (2018).

References

Aicale R, Tarantino D, Maffulli N (2018) Overuse injuries in sport: a comprehensive overview. J Orthop Surg Res 13:309

Aronowitz ER, Leddy JP (1998) Closed tendon injuries of the hand and wrist in athletes. Clin Sports Med 17:449–467

Bak K, Boeckstyns M (1997) Epiphysiodesis for bilateral irregular closure of the distal radial physis in a gymnast. Scand J Med Sci Sports 7:363–366

Bateni CP, Bartolotta RJ, Richardson ML et al (2013) Imaging key wrist ligaments: what the surgeon needs the radiologist to know. Am J Roentgenol 200:1089–1095

Batt ME (1992) A survey of golf injuries in amateur golfers. Br J Sports Med 26:63–65

Batt ME (1993) Golfing injuries. An overview. Sports Med 16:64–71

Baugh CM, Kerr ZY (2016) High school rowing injuries: National Athletic Treatment, Injury and Outcomes Network (NATION). J Athl Train 51:317–320

Bencardino JT (2004) MR imaging of tendon lesions of the hand and wrist. Magn Reson Imaging Clin N Am 12:333–347

Beunen G, Malina RM, Claessens AL et al (1999) Ulnar variance and skeletal maturity of radius and ulna in female gymnasts. Med Sci Sports Exerc 31:653–657

Bladin C, McCrory P, Pogorzelski A (2004) Snowboarding injuries: current trends and future directions. Sports Med 34:133–139

Blum AG, Zabel JP, Kohlmann R et al (2006) Pathologic conditions of the hypothenar eminence: evaluation with multidetector CT and MR imaging. Radiographics 26:1021–1044

Boer BC, Vestering M, van Raak SM et al (2018) MR arthrography is slightly more accurate than conventional MRI in detecting TFCC lesions of the wrist. Eur J Orthop Surg Traumatol 28:1549–1553

Bottinelli O, Campani R (2001) Ultrasound of the hand. In: Guglielmi G, Van Kuijk C, Genant HK (eds) Fundamentals of hand and wrist imaging. Springer, Berlin Heidelberg New York, pp 63–74

Boutin RD, Fritz RC (2005) MRI of snow skiing and snowboarding injuries. Semin Musculoskelet Radiol 9:360–378

Breitenseher MJ, Metz VM, Gilula LA et al (1997) Radiographically occult scaphoid fractures: value of MR imaging in detection. Radiology 203: 245–250

Brudvik C, Hove LM (2003) Childhood fractures in Bergen, Norway: identifying high-risk groups and activities. J Pediatr Orthop 23:629–634

Burnham RS, Steadward RD (1994) Upper extremity peripheral nerve entrapments among wheelchair athletes: prevalence, location, and risk factors. Arch Phys Med Rehabil 75:519–524

Butterwick DJ, Meeuwisse WH (2002) Effect of experience on rodeo injury. Clin J Sport Med 12:30–35

Bylak J, Hutchinson MR (1998) Common sports injuries in young tennis players. Sports Med 26:119–132

Caine DJ, Nassar L (2005) Gymnastics injuries. Med Sport Sci 48:18–58

Caine D, Roy S, Singer KM et al (1992) Stress changes of the distal radial growth plate. A radiographic survey and review of the literature. Am J Sports Med 20:290–298

Carlisle JC, Goldfarb CA, Mall N et al (2008) Upper extremity injuries in the national football league: part II: elbow, forearm, and wrist injuries. Am J Sports Med 36:1945–1952

Carneiro RS, Fontana R, Mazzer N (2005) Ulnar wrist pain in athletes caused by erosion of the floor of the sixth dorsal compartment: a case series. Am J Sports Med 33:1910–1913

Carter SR, Aldridge MJ, Fitzgerald R et al (1988) Stress changes of the wrists in adolescent gymnasts. Br J Radiol 61:109–112

Chan RC, Chiu JW, Chou CL et al (1991) Median nerve lesions at wrist in cyclists. Zhonghua Yi Xue Za Zhi (Taipei) 48:121–124

Cockenpot E, Lefebvre G, Demondion X et al (2016) Imaging of sports-related hand and wrist injuries: sports imaging series. Radiology 279:674–692

Cohen MS (1998) Ligamentous injuries of the wrist in the athlete. Clin Sports Med 17:533–552

Cohen AR, Metzl JD (2000) Sports-specific concerns in the young athlete: basketball. Pediatr Emerg Care 16:462–468

Cole A, Hiatt JL, Arnold C et al (2017) Chronic exertional compartment syndrome in the forearm of a collegiate softball pitcher. Sports Med Open 3:11

Damore DT, Metzl JD, Ramundo M et al (2003) Patterns in childhood sports injury. Pediatr Emerg Care 19: 65–67

De Mooij T, Duncan AA, Kakar S (2015) Vascular injuries in the upper extremity in athletes. Hand Clin 31:39–52

De Smet L, Clasessens A, Fabry G (1993) Gymnast wrist. Acta Orthop Belg 59:377–380

De Smet L, Claessens A, Lefevre J et al (1994) Gymnast wrist: an epidemiologic survey of ulnar variance and stress changes of the radial physis in elite female gymnasts. Am J Sports Med 22:846–850

Desser TS, McCarthy S, Trumble T (1990) Scaphoid fracture and Kienbock's disease of the lunate: MR imaging with histopathologic correlation. Magn Reson Imaging 8:357–361

DiFiori JP, Puffer JC, Mandelbaum BR et al (1996) Factors associated with wrist pain in the young gymnast. Am J Sports Med 24:9–14

DiFiori JP, Puffer JC, Mandelbaum BR et al (1997) Distal radial growth plate injury and positive ulnar variance in nonelite gymnasts. Am J Sports Med 25:763–768

DiFiori JP, Puffer JC, Aish B et al (2002a) Wrist pain in young gymnasts: frequency and effects upon training over 1 year. Clin J Sport Med 12:348–353

DiFiori JP, Puffer JC, Aish B et al (2002b) Wrist pain, distal radial physeal injury, and ulnar variance in young gymnasts: does a relationship exist? Am J Sports Med 30:879–885

DiFiori JP, Caine DJ, Malina RM (2006) Wrist pain, distal radial physeal injury, and ulnar variance in the young gymnast. Am J Sports Med 34:840–849

Du Toit P, Sole G, Bowerbank P et al (1999) Incidence and causes of tenosynovitis of the wrist extensors in long distance canoeists. Br J Sports Med 33:105–109

Dwek JR, Cardoso F, Chung CB (2009) MR imaging of overuse injuries in the skeletally immature gymnast: a spectrum of soft-tissue and osseous lesions in the hand and wrist. Pediatr Radiol 39:1310–1316

Egawa M, Asai T (1983) Fractures of the hook of the hamate: report of six cases and the suitability of computerised tomography. J Hand Surg Am 8:393

Ek ET, Suh N, Weiland AJ (2013) Hand wrist injuries in golf. J Hand Surg Am 38:2029–2033

Ellis JA, Kierulf JC, Klassen TP (1995) Injuries associated with in-line skating from the Canadian hospitals injury reporting and prevention program database. Can J Public Health 86:133–136

Ellsasser JC, Stein AH (1979) Management of hand injuries in a professional football team. Review of 15 years of experience with one team. Am J Sports Med 7:178–182

Fernandez-Fernandez J, Ellenbecker T, Sanz-Rivas D et al (2013) Effects of a 6-week junior tennis conditioning program on service velocity. J Sports Sci Med 12:232–239

Flynn JM, Lou JE, Ganley TJ (2002) Prevention of sports injuries in children. Curr Opin Pediatr 14: 719–722

Forsman L, Eriksson A (2001) Skateboarding injuries of today. Br J Sports Med 35:325–328

Fountain JL, Meyers MC (1996) Skateboarding injuries. Sports Med 22:360–366

Geissler WB (2001) Carpal fractures in athletes. Clin Sports Med 20:167–188

Gilula LA (1979) Carpal injuries: analytic approach and case exercises. AJR 133:503–517

Gilula LA, Yin Y (1996) Imaging of the wrist. WB Saunders, Philadelphia London Toronto

Gosheger G, Liem D, Ludwig K et al (2003) Injuries and overuse syndromes in golf. Am J Sports Med 31:438–443

Halikis MN, Taleisnik J (1996) Soft-tissue injuries of the wrist. Clin Sports Med 15:235–259

Hart E, Meehan WP 3rd, Bae DS et al (2018) The young injured gymnast: a literature review and discussion. Curr Sports Med Rep 17:366–375

Hassan I, Dorani BJ (2001) Sports related fractures in children in north East England. Emerg Med J 18:167–171

Howse C (1994) Wrist injuries in sport. Sports Med 17:163–175

Israeli A, Engel J, Ganel A (1982) Possible fatigue fracture of the pisiform bone in volleyball players. Int J Sports Med 3:56–57

Jacobsen JA (1999) Musculoskeletal sonography and MR imaging. A role for both imaging methods. Radiol Clin N Am 37:713–735

Jacobson JA, Miller BS, Morag Y (2005) Golf and racquet sports injuries. Semin Musculoskeletal Radiol 9:346–359

Jerosch J, Heck C (2005) Injury patterns and prophylaxis in inline skating. Orthopade 34:441–447

Kim DK, Kim BS, Kim MJ et al (2017) Electrophysiologic and ultrasonographic assessment of carpal tunnel syndrome in wheelchair basketball athletes. Ann Rehabil Med 41:58–65

Kox LS, Kuijer PP, Kerkhoffs GM et al (2015) Prevalence, incidence and risk factors for overuse injuries of the wrist in young athletes: a systematic review. Br J Sports Med 49:1189–1196

Kraan RBJ, Kox LS, Mens MA et al (2019) Damage of the distal radial physis in young gymnasts: can three-dimensional assessment of physeal volume on MRI serve as a biomarker? Eur Radiol 29:6364–6371

Kumar S, O'Coonor A, Despois M, Galloway H (2005) Use of early magnetic resonance imaging in the diagnosis of occult scaphoid fractures: the CAST study (Canberra Area Scaphoid Trial). N Z Med J 118:U1296

Kyle SB, Nance ML, Rutherford GW Jr et al (2002) Skateboard-associated injuries: participation-based estimates and injury characteristics. J Trauma 53:686–690

Lichtman DM, Alexander AH (1997) The wrist and its disorders. WB Saunders, Philadelphia

Lilley J, Halikis M, Taleisnik J (2000) Fractures of the carpal bones. In: Weinzweig J (ed) Hand and wrist surgery secrets. Hanley and Blefus, Philadelphia, pp 197–203

Lindner KJ, Caine DJ (1990) Injury patterns of female competitive club gymnasts. Can J Sport Sci 15:254–261

Linscheid RL, Dobyns JH, Beabout JW (1972) Traumatic instability of the wrist. Diagnosis, classification, and pathomechanics. J Bone Joint Surg Am 54: 1612–1632

Lorei MP, Hershman EB (1993) Peripheral nerve injuries in athletes. Treatment and prevention. Sports Med 16:130–147

Lund SS, Myklebust G (2011) High incidence in TeamGym competition: a prospective cohort study. Scand J Med Sci Sports 21:439–444

Lyons RA, Delahunty AM, Kraus D et al (1999) Children's fractures: a population based study. Inj Prev 5:129–132

MacGregor DM (2003) Don't save the ball! Br J Sports Med 37:351–353

Made C, Elmqvist LG (2004) A 10-year study of snowboard injuries in Lapland Sweden. Scand J Med Sci Sports 14:128–133

Maffuli N, Bundoc RC, Chan KM et al (1996) Paediatric sports injuries in Hong Kong: a seven year survey. Br J Sports Med 30:218–221

Mandelbaum BR, Bartolozzi AR, Davis CA et al (1989) Wrist pain syndrome in the gymnast. Pathogenetic, diagnostic, and therapeutic considerations. Am J Sports Med 17:305–317

Masciocchi C, Catalucci A, Barile A et al (2001) Trauma of the hand and wrist. In: Guglielmi G, Van Kuijk C, Genant HK (eds) Fundamentals of hand and wrist imaging. Springer, Berlin Heidelberg New York, pp 97–421

Matsumoto K, Miyamoto K, Sumi H et al (2002) Upper extremity injuries in snowboarding and skiing: a comparative study. Clin J Sport Med 12:354–359

Matsumoto K, Sumi H, Sumi Y et al (2004) Wrist fractures from snowboarding: a prospective study for 3 seasons from 1998 to 2001. Clin J Sport Med 14:64–71

McCarroll JR (1986) Golf: common injuries from a supposedly benign activity. J Musculoskelet Med 3:9–16

McCarroll JR (1996) The frequency of golf injuries. Clin Sports Med 15:1–7

Mellion MB (1991) Common cycling injuries. Management and prevention. Sports Med 11:52–70

Melone CP Jr, Polatsch DB, Flink G et al (2012) Scapholunate interosseous ligament disruption in professional basketball players: treatment by direct repair and dorsal ligamentoplasty. Hand Clin 28:253–260

Meyer MC, Sterling JC, Souryal TO (2003) Radiographic findings of the upper extremity in collegiate rodeo athletes. Med Sci Sports Exerc 35:543–547

Moraux A, Lefebvre G, Pansini V et al (2014) Pisotriquetral joint disorders: an underrecognized cause of ulnar side wrist pain. Skelet Radiol 43:761–773

Morgan WJ, Slowman LS (2001) Acute hand and wrist injuries in the athlete require individualized management, depending on athlete's age, sport, and level of competition. J Am Acad Orthop Surg 9:389–400

Moss PS, Wan A, Whitlock MR (2002) A changing pattern of injuries to horse riders. Emerg Med J 19:412–414

Mulder S, Hutten A (2002) Injuries associated with inline skating in the European region. Accid Anal Prev 34:65–70

Murray PM, Cooney WP (1996) Golf-induced injuries of the wrist. Clin Sports Med 15:85–109

Nguyen D, Letts M (2001) In-line skating injuries in children: a 10-year review. J Pediatr Orthop 21:613–618

Nuber GW, Assenmacher J, Bowen MK (1998) Neurovascular problems in the forearm, wrist, and hand. Clin Sports Med 17:585–610

O'Neill DF (2003) Wrist injuries in guarded versus unguarded first time snowboarders. Clin Orthop Relat Res 409:91–95

Orenstein JB (1996) Injuries and small-wheel skates. Ann Emerg Med 27:204–209

Osterman AL, Moskow L, Low DW (1988) Soft-tissue injuries of the hand and wrist in racquet sports. Clin Sports Med 7:329–348

Palmer AK (1989) Triangular fibrocartilage lesions: a classification. J Hand Surg Am 14:594–606

Pang EQ, Yao J (2017) Ulnar-sided wrist pain in the athlete (TFCC/DRUJ/ECU). Curr Rev Musculoskelet Med 19:53–61

Peh WCG, Gilula LA (1996) Normal disruption of carpal arcs. J Hand Surg Am 21:561–566

Peh WCG, Gilula LA, Wilson AJ (1996) Detection of occult wrist fractures by magnetic resonance imaging. Clin Radiol 51:285–292

Potter HG, Asnis-Ernberg L, Weiland AJ et al (1997) The utility of high-resolution magnetic resonance imaging in the evaluation of the triangular fibrocartilage complex of the wrist. J Bone Joint Surg Am 79: 1675–1684

Pulos N, Kakar S (2018) Hand and wrist injuries: common problems and solutions. Clin Sports Med 37:217–243

Raab DJ, Fischer DA, Quick DC (1994) Lunate and perilunate dislocations in professional football players. A five-year retrospective analysis. Am J Sports Med 22:841–845

Rettig AC (1990) Neurovascular injuries in the wrists and hands of athletes. Clin Sports Med 9:389–417

Rettig AC (1994) Wrist problems in the tennis player. Med Sci Sports Exerc 26:1207–1212

Rettig AC (1998) Elbow, forearm and wrist injuries in the athlete. Sports Med 25:115–130
Rettig AC (2003) Athletic injuries of the wrist and hand: part 1—traumatic injuries of the wrist. Am J Sports Med 31:1038–1048
Richmond DR (1994) Handlebar problems in bicycling. Clin Sports Med 13:165–173
Rossi C, Cellocco P, Margaritondo E et al (2005) De Quervain's disease in volleyball players. Am J Sports Med 33:424–427
Roy S, Caine D, Singer KM (1985) Stress changes of the distal radial epiphysis in young gymnasts. A report of twenty-one cases and a review of the literature. Am J Sports Med 13:301–308
Rumball JS, Lebrun CM, Di Ciacca SR et al (2005) Rowing injuries. Sports Med 35:537–555
Saito T, Sterbenz JM, Chung KC (2017) Chronological and geographic trends of TFCC repair. Hand Clin 33:593–605
Schapiro AH, Lall NU, Anton CG et al (2017) Hoverboards: spectrum of injury and association with an uncommon fracture. Pediatr Radiol 47:437–441
Scheck RJ, Kubitzek C, Hierner R et al (1997) The scapholunate interosseous ligament in MR arthrography of the wrist: correlation with nonenhanced MRI and wrist arthroscopy. Skelet Radiol 26:263–271
Schieber RA, Branche-Dorsey CM, Ryan GW (1994) Comparison of in-line skating injuries with roller-skating and skateboarding injuries. JAMA 15:1856–1858
Schlegel TF, Boublik M, Ho CP et al (1999) Role of MR imaging in the management of injuries in professional football players. Magn Reson Imaging Clin N Am 7:175–190
Schmid MR, Schertler T, Pfirrmann CW et al (2005) Interosseous ligament tears of the wrist: comparison of multi-detector row CT arthrography and MR imaging. Radiology 237:1008–1013
Shih C, Chang CY, Penn IW et al (1995) Chronically stressed wrists in adolescent gymnasts: MR imaging appearance. Radiology 195:855–859
Smoljanovic T, Bohacek I, Hannafin J et al (2018) Sports injuries in international masters rowers: a cross sectional study. Croat Med J 59:258–266
Taylor BL, Attia MW (2000) Sports-related injuries in children. Acad Emerg Med 7:1376–1382
Tehranzadeh J, Labosky DA (1984) Detection of intraarticular loose osteochondral fragments by double-contrast wrist arthrography. A case report of a basketball injury. Am J Sports Med 12:77–79
Theriault G, Lachance P (1998) Golf injuries. An overview. Sports Med 26:43–57
Thornton JS, Vinther A, Wilson F et al (2017) Rowing injuries: an updated review. Sports Med 47:641–661
Tischler BT, Diaz LE, Murakami AM et al (2014) Scapholunate advanced collapse: a pictorial review. Insights Imaging 5:407–417
Tolat AR, Sanderson PL, De Smet L et al (1992) The gymnast's wrist: acquired positive ulnar variance following chronic epiphyseal injury. J Hand Surg Br 17:678–681
Webb BG, Rettig LA (2008) Gymnastic wrist injuries. Curr Sports Med Rep 7:289–295
Wechsler RJ, Wehbe MA, Rifkin MD et al (1987) Computed tomography diagnosis of distal radioulnar subluxation. Skelet Radiol 25:1–5
Weinstein SM, Herring SA (1992) Nerve problems and compartment syndromes in the hand, wrists, and forearm. Clin Sports Med 11:161–188
Weiss LE, Taras JS, Sweet S et al (2000) Lunotriquetral injuries in the athlete. Hand Clin 16:433–438
Westermann RW, Giblin M, Vaske A et al (2015) Evaluation of men's and women's gymnastics injuries: a 10-year observational study. Sports Health 7:161–165
Wiesler ER, Lumsden B (2005) Golf injuries of the upper extremity. J Surg Orthop Adv 14:1–7
Wolf MR, Avery D, Wolf JM (2017) Upper extremity injuries in gymnasts. Hand Clin 33:187–197
Yamagiwa T, Fuijoka H, Okuno H et al (2009) Surgical treatment of stress fracture of the scaphoid of an adolescent gymnast. J Sports Sci Med 8:702–704
Young CC, Seth A, Mark DH (1998) In-line skating: use of protective equipment, falling patterns, and injuries. Clin J Sport Med 8:111–114
Zalavras C, Nikolopoulou G, Essin D et al (2005) Pediatric fractures during skateboarding, roller skating, and scooter riding. Am J Sports Med 33:568–573
Zlatkin MB, Rosner J (2004) MR imaging of ligaments and triangular fibrocartilage complex of the wrist. Magn Reson Imaging Clin N Am 12:301–331

Finger and Hand

Arn Van Royen, Maryam Shahabpour,
and Michel De Maeseneer

Contents

Abstract

In this chapter we discuss injuries of the fingers. The dorsal hood centers the extensor tendons over the MCP joint and with injuries the tendon may become displaced. Flexor tendon ruptures may occur in the different hand zones but typically in the finger. Retraction may be a very severe complicating surgery. The extensor mechanism is very complex. Ruptures of the central slip may lead to boutonniere deformity and distal slip mallet finger. The palmar pulleys keep the tendons close to the bone and prevent bowstringing. The palmar plates typically tear in association with collateral ligaments due to their intimate connection. The most common tendinopathy involves the first extensor compartment and is designated De Quervain disease.

1 Introduction and Technical Considerations

With technical advances in imaging systems, injuries of hand and fingers can be accurately evaluated with ultrasound and magnetic resonance. Although such injuries can be assessed by expert clinical examination, additional information obtained from imaging can help in optimizing treatment planning.

For ultrasound, linear or dedicated hand transducers can be used. High resolution is essential.

A. Van Royen
Vrije Universiteit Brussel, Brussels, Belgium

M. Shahabpour
Radiology, Universitair Ziekenhuis Brussel, Brussels, Belgium

M. De Maeseneer (✉)
Vrije Universiteit Brussel, Brussels, Belgium

Radiology, Universitair Ziekenhuis Brussel, Brussels, Belgium
e-mail: Michel.demaeseneer@uzbrussel.be

Med Radiol Diagn Imaging (2020)
https://doi.org/10.1007/174_2020_253, © Springer Nature Switzerland AG
Published Online: 01 January 2021

As a rough guideline, transducers of 14 MHz or higher are ideal.

For magnetic resonance, high-resolution images can be obtained with dedicated finger coils. A drawback of these coils is the small field of view offered. Wrist coils also give excellent results. Meticulous attention to patient immobilization, choice of the smallest field of view obtainable, and optimizing signal-to-noise ratio by carefully selecting imaging parameters will yield the best results. Choice of imaging parameters may vary among systems. The same is true for the imaging sequences, although these should include "anatomical" and "fluid-sensitive" sequences. Anatomical images will consist of either spin-echo T1-weighted images or spin-echo proton density-weighted images. These sequences offer high details; however, excellent knowledge of normal anatomy is essential to assess pathological changes. "Fluid-sensitive" sequences will consist of STIR-weighted images or T2 fat-saturated images and will emphasize high signal intensity changes. These sequences offer less imaging details in the fingers due to the small field of view. Gradient-echo sequences are an alternative to spin-echo sequences, but susceptibility artifacts related to bone-soft tissue interfaces, and chemical shift artifact related to muscle-fat interfaces, adversely affect image quality.

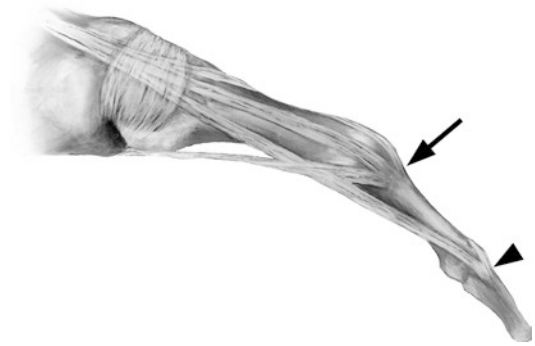

Fig. 1 Extensor system. Line drawing shows the lateral aspect of finger. Extensor tendon combines with interosseus tendons to terminate in central insertion (*arrow*), and distal insertion (*arrowhead*)

Fig. 2 Extensor tendon. Sagittal fat-saturated proton density-weighted MR image. Termination of the central insertion (*arrow*) and distal insertion is shown (*arrowhead*)

2 Extensor Tendon Rupture

The extensor tendon system has a distal insertion terminating on the base of the distal phalanx and a proximal insertion terminating on the base of the middle phalanx (Figs. 1 and 2). The extensor system receives contributions from the interosseus muscles as well as from the lumbrical muscles (Landsmeer 1949). A rupture of the distal insertion is designated "mallet finger" or "baseball finger" and typically results in pain and swelling, and inability to extend the distal phalanx (Kleinbaum et al. 2005). Flexion deformity is present at the DIP joint. The diagnosis is usually made clinically. Ultrasound may be performed to establish the degree of retraction, and diagnose associated collections or tiny avulsion fractures which may be underestimated clinically (Fig. 3). Ruptures of the central insertion are more commonly recognized in the setting of inflammatory conditions but may also relate to trauma. A rupture of the central slip insertion typically leads to boutonniere deformity. This usually results from sudden DIP extension, and leads to hyperextension at the MCP, flexion at the PIP, and hyperextension at the DIP joints. Diagnosis of tendon rupture is straightforward with ultrasound. Ultrasound can show the tendon rupture dynamically, as well as demonstrate the conjoint tendons that slide to the side of the PIP joint (Fig. 4). The conjoint tendons are normally held in place by the transverse retinacular

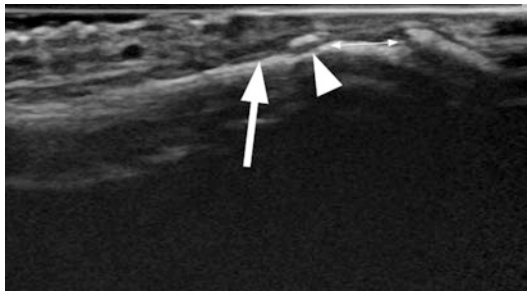

Fig. 3 Mallet finger. Sagittal ultrasound image. Note complete tear of distal insertion (mallet finger) with a hyperechoic bony avulsion (*arrowhead*) and retracted tendon end (*arrow*). There is a gap between the bony avulsion and the insertion (*double arrow*)

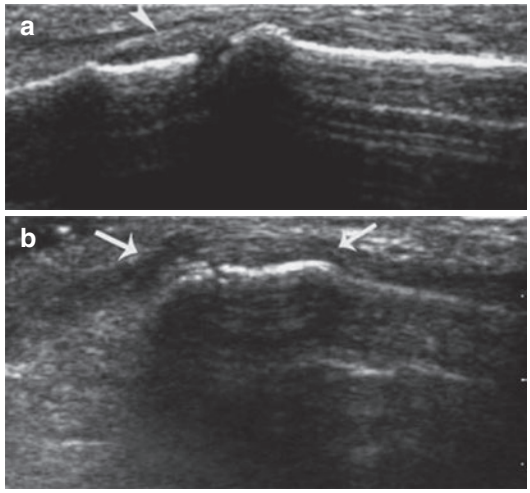

Fig. 4 (**a**, **b**) Boutonniere deformity. (**a**) Sagittal ultrasound image. Note the avulsion of fibers at the insertion of central slip (arrowhead). (**b**) Coronal ultrasound image at the lateral aspect of finger shows laterally located components (arrows) of extensor system that are thickened and scarred down adjacent to the bone

ligament at the PIP joint. More proximal ruptures of the extensor system over the midhand can also occur (Fig. 5). MR may also be employed to diagnose extensor rupture, but lacks the dynamic capability of ultrasound.

3 Dorsal Hood Rupture

At the level of the metacarpophalangeal joint the extensor tendon is kept in place by dorsal reinforcements designated dorsal hood (Fig. 6). The dorsal hood consists of sagittal bands attaching to and covering the extensor tendons at the metacarpal head level. Ruptures of the sagittal bands lead to displacement of the extensor tendons from their central positions over the metacarpal heads. Usually the second and third digits are involved secondary to direct trauma such as in boxing. On ultrasound the tendon can be shown dynamically to displace from its normal central position. A hypoechoic cleft may also be apparent in the normal location of the sagittal bands. At MR disruption of the sagittal bands may be depicted as a hyperintense signal intensity area adjacent to the tendons.

4 Flexor Tendon Rupture

At midhand level the flexor tendons are easily depicted. The flexor superficialis tendon is located more ventrally (Fig. 7). The lumbrical muscle bellies are located at the radial side of the flexor system in the hand (Figs. 8 and 9). The

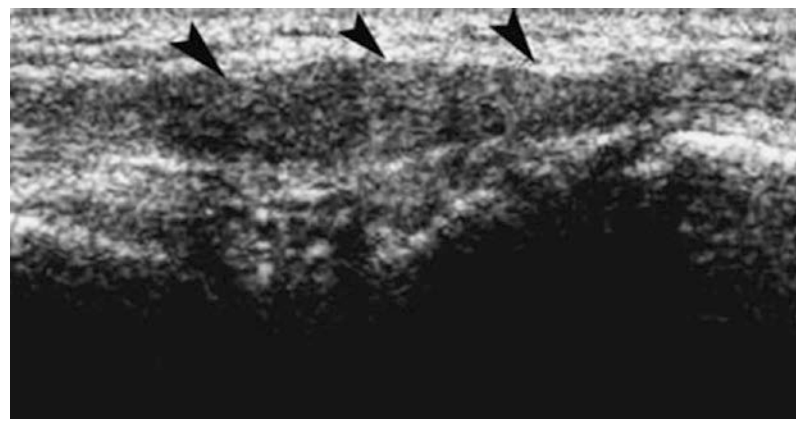

Fig. 5 Extensor rupture. Sagittal ultrasound image shows proximal rupture of extensor tendon over midhand (arrowheads)

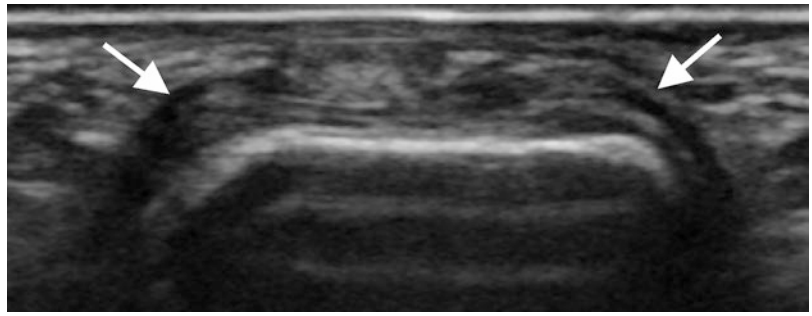

Fig. 6 Dorsal hood. Transverse ultrasound image shows triangular sagittal bands (arrows) at both sides of extensor tendon

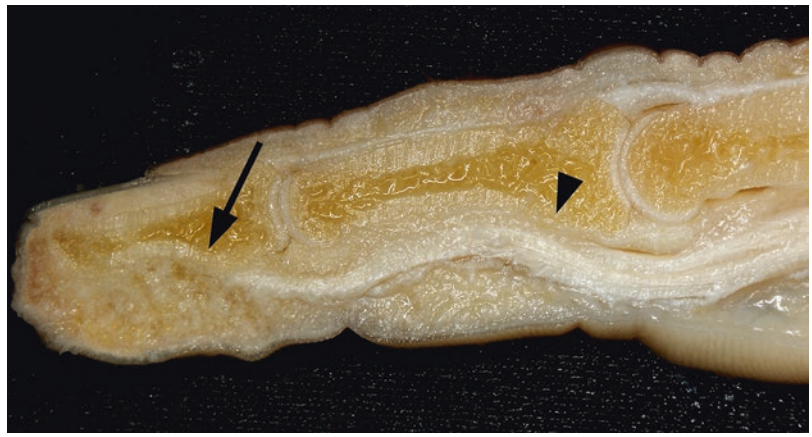

Fig. 7 Flexor tendons. Sagittal anatomical slice shows insertion of flexor profundus (arrow) and of flexor superficialis (arrowhead)

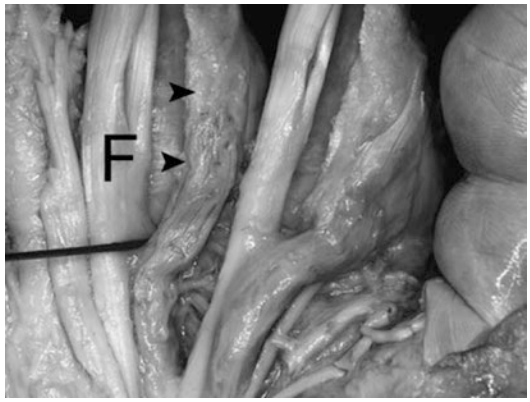

Fig. 8 Lumbricals. Anatomical dissection shows lumbrical muscle (arrowheads) adjacent to the radial side of flexor tendons (*F*)

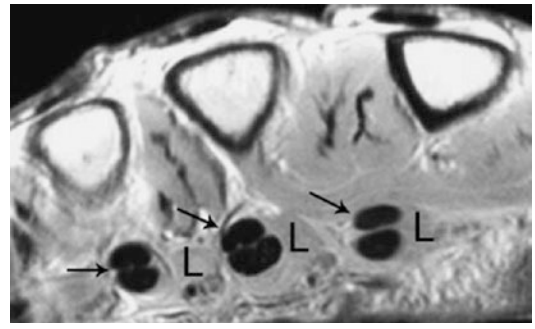

Fig. 9 Lumbricals. Transverse proton density MR image shows lumbricals (*L*) at the radial aspect of flexor tendons (arrows)

lumbricals are located on the radial side of the flexor system. Their tendons move from ventrally in a dorsal direction to attach to the extensor system. Tears of the lumbricals have been described in rock climbers leading to rupture and hematoma in the muscle belly (Schweizer 2003). Such muscle tears are most easily demonstrated with ultrasound (Fig. 10). "Fluid-sensitive" magnetic resonance sequences may also show muscle tears as hyperintense areas.

The relationship of the flexor superficialis tendon and the flexor profundus tendon varies

considerably throughout the finger. The flexor profundus tendon passes through an opening in the flexor superficialis tendon and continues to insert onto the base of the distal phalanx. The flexor superficialis tendon inserts at the level of the midaspect of the middle phalanx (Fig. 11). Flexor tendon disruption may be related to transection. Avulsive injuries in blunt trauma typically involve the distal insertion (flexor profundus) and this condition is also designated rugger jersey finger (Figs. 12 and 13) (Cohen et al. 2004). Tendon ruptures can be demonstrated both by ultrasound and magnetic resonance.

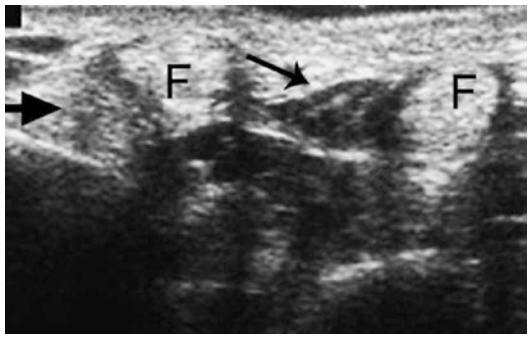

Fig. 10 Lumbrical tear. Transverse ultrasound image. Normal flexor tendons are seen (*F*). Normal hypoechoic lumbrical (thin arrow) is seen, as well as hyperechoic lumbrical (thick arrow) corresponding to recent tear

5 Annular Pulley Rupture

The flexor tendons are covered by fibrous reinforcements that are termed annular and cruciform pulleys (Fig. 14) (Parellada et al. 1996; Kovacs 2002). The cruciform reinforcements are less important and are even difficult to recognize on anatomic dissection. The annular reinforcements are strong bands easily recognizable at dissection. They are classified as five different bands, termed the A1 to the A5 pulleys. The A1, A3, and A5 are located at the level of the joints. Usually, when an injury occurs, it extends from proximal to distal involving the A1 pulley first, and then continuing

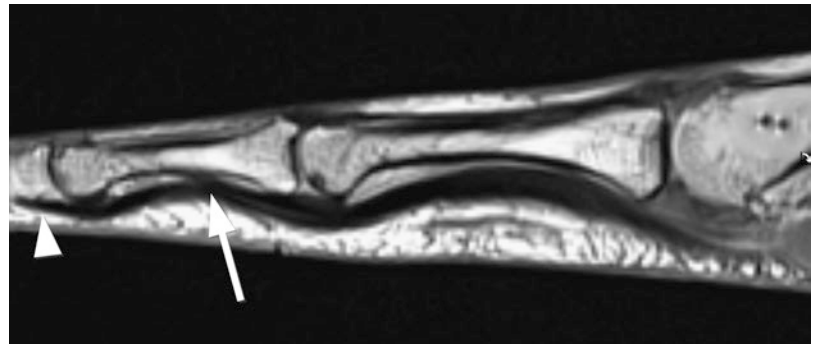

Fig. 11 Flexor tendons. Sagittal proton density-weighted MR image. Insertion of flexor profundus (*arrowhead*) and of flexor superficialis (*arrow*)

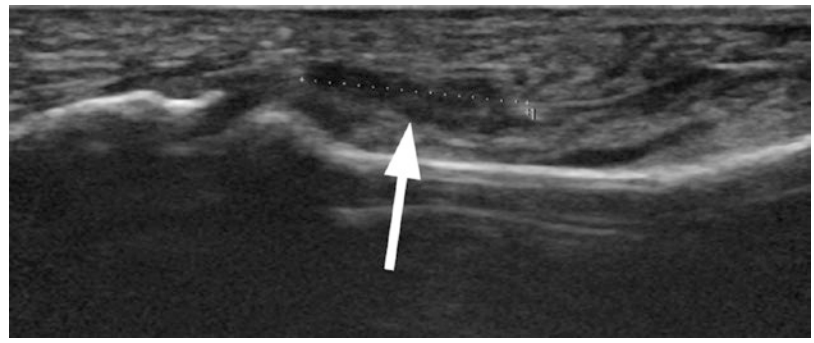

Fig. 12 Flexor rupture. Flexor rupture. Sagittal ultrasound image shows proximal rupture of flexor tendon over midhand (*arrow*)

Fig. 13 Flexor rupture. Coronal proton density-weighted MR image shows proximal rupture of flexor tendon of the fourth digit at the level of the metacarpal bone (*arrow*)

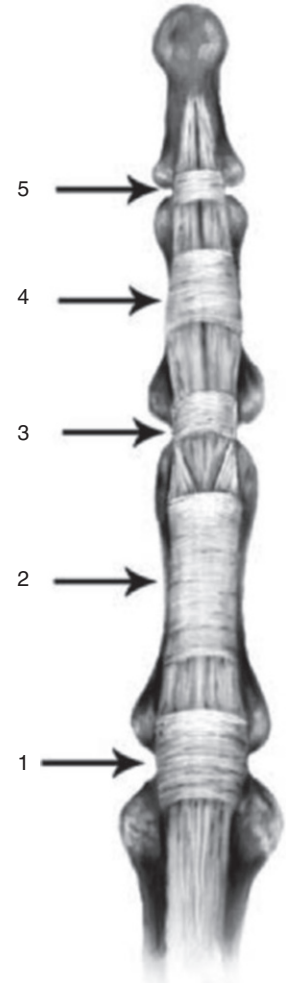

Fig. 14 Annular pulleys. Line drawing shows ventrally located annular pulleys A1 to A5 (arrows)

distally involving the A2 pulley. The A3 pulley is located in regard to the proximal interphalangeal joint. The A4 pulley is located at the middle aspect of the middle phalanx, and the A5 pulley is located in regard to the distal interphalangeal joint. The purpose of the annular pulleys is to keep the tendon in close contact with the bone during flexion of the finger. The pulleys cannot be seen consistently using US, but may occasionally be evident as hypoechoic interfaces at the superficial aspect of the tendons (Fig. 15). Annular pulley rupture has typically been described in rock climbers. Dynamic ultrasound shows the increased distance of the tendon to the bone in comparison to the normal side (Fig. 16). This displacement, also designated "bowstring deformity," may also be shown using magnetic resonance.

6 Volar Plate and Collateral Ligament Injury

At the level of the joints the flexor tendons are at a slight distance from the bone. This is related to the shape of the head of a phalanx, but also to the presence of thick volar plates at the level of the interphalangeal and metacarpophalangeal joints (Figs. 15 and 17). The volar plates are fibrous structures attached to the distal phalanx and extending proximally (Nance et al. 1979). The accessory bands of the collateral ligaments of the joint connect to the volar plates. Hence, volar plate injuries are often associated with injuries of the collateral ligaments. Volar plate injuries can occur as a consequence of hyperextension but also medial or lateral deviation. Ultrasound can show the disrupted volar plate, bony avulsion, or

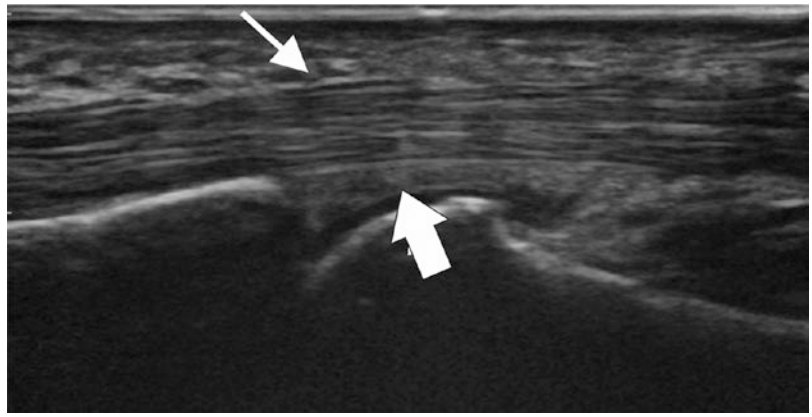

Fig. 15 Pulley and volar plate. Sagittal ultrasound image of a normal A1 pulley at the level of the MCP joint. Flexor system in close proximity to bone, the pulley appears as a thin hypoechoic band overlying the flexor tendons (*arrow*). Deep to the flexor tendons is a normal volar plate (*bold arrow*)

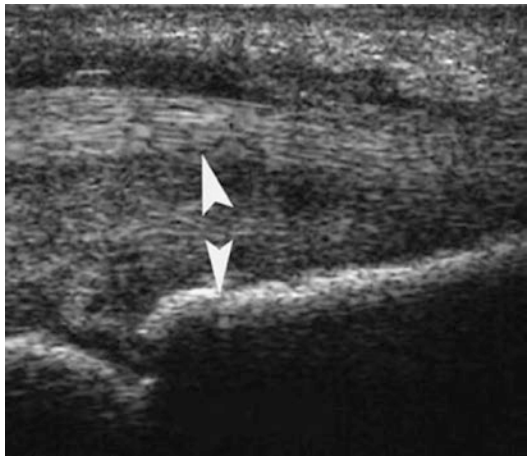

Fig. 16 Pulley rupture. Sagittal ultrasound image of an A1 pulley rupture with bowstring appearance; in contrast to Fig. 15 flexor system is displaced from adjacent bone (*arrowheads*)

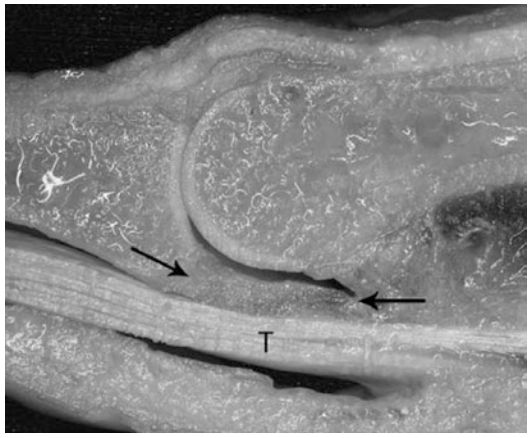

Fig. 17 Volar plate. Sagittal anatomic slice shows flexor tendons (T), superficial to volar plate (arrows)

Fig. 18 Volar plate avulsion. Lateral radiographs show avulsion (arrowhead) of ventral aspect of base of phalanx, typical of volar plate avulsive injury

associated small collections (Figs. 18 and 19). Magnetic resonance may show thickening of the volar plates and collateral ligaments.

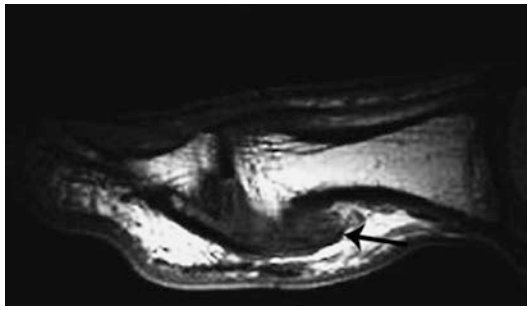

Fig. 19 Volar plate injury. Sagittal proton MR image shows thickened volar plate (arrow)

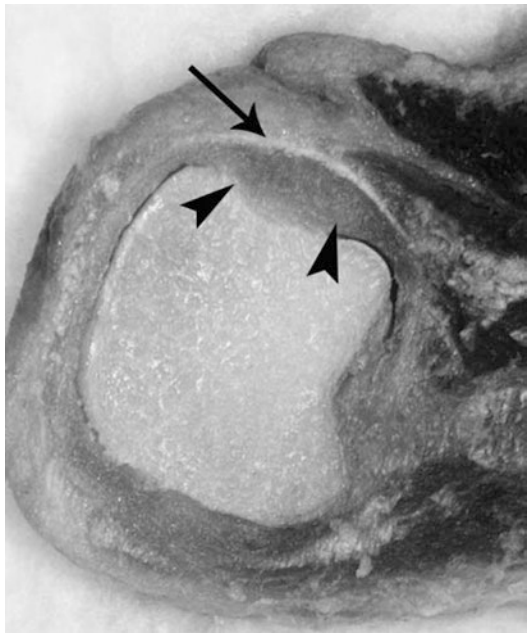

Fig. 20 Ulnar collateral ligament of thumb. Transverse anatomical slice shows adductor aponeurosis (arrow) overlying ulnar collateral ligament of thumb (arrowheads)

Fig. 21 Ulnar collateral ligament of thumb. Coronal MR image shows hypointense adductor aponeurosis and deeper ulnar collateral ligament (arrow)

7 Ulnar Collateral Ligament of the Thumb

The metacarpophalangeal area of the thumb is vulnerable to a spectrum of injuries, sometimes designated ski thumb, or gamekeeper's thumb. Such an injury may occur by thumb hyperextension or radial deviation. Injuries of the ligament may result in loss of grasp function between thumb and index finger (Figs. 20 and 21). The ulnar collateral ligament may show partial or complete tears (Fig. 22). Plain radiographs may show an avulsion fracture at the base of the proximal phalanx (Fig. 23). A specific complication occurs when the ulnar collateral ligament retracts and becomes

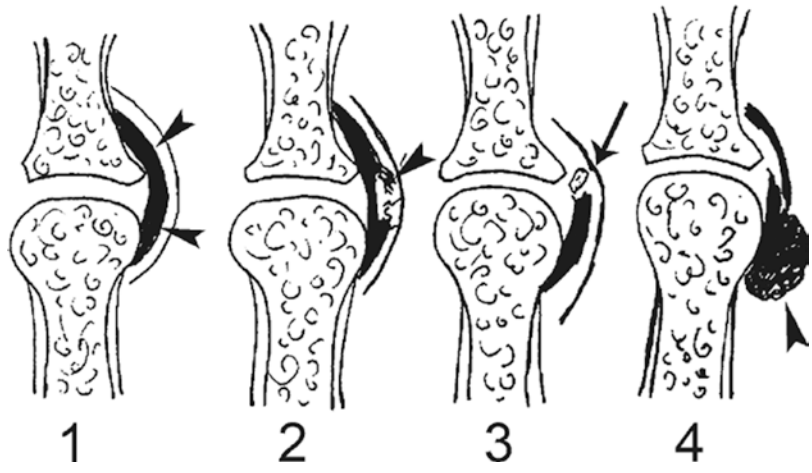

Fig. 22 Ulnar collateral ligament of thumb injury. Line drawing shows the spectrum of injury. In 1, sprain of the ligament is seen (arrowheads). In 2, a partial tear (arrowhead) is illustrated. In 3, a complete tear and a small bony avulsion are seen (arrow). In 4, proximal retraction and displacement superficial to the adductor aponeurosis, corresponding to Stener lesion, are shown (arrowhead)

Fig. 23 Gamekeeper's thumb. AP radiograph shows avulsion (arrow) at the base of proximal phalanx corresponding to gamekeeper's thumb

located superficially to the adductor pollicis aponeurosis. This complication is designated "Stener lesion" (O'Callaghan et al. 1994).

Diagnosis of different stages of UCL tear and Stener lesion can be accomplished by ultrasound (Fig. 24). Magnetic resonance can also differentiate between ulnar collateral ligament tear and Stener lesion. In Stener lesion a proximally located soft-tissue nodule is apparently located superficial to the adductor aponeurosis which has been designated the "jojo" sign (Fig. 25).

8 De Quervain Tendons

The De Quervain tendons consist of the abductor pollicis longus and the extensor pollicis brevis (De Quervain 2005). Inflammation results in tendon thickening, synovial sheath effusion, and retinaculum thickening. It may be caused by overuse such as in racquet sports, or sports requiring repetitive rotating of the wrist. Diagnosis can be made either by ultrasound or by magnetic resonance (Fig. 26).

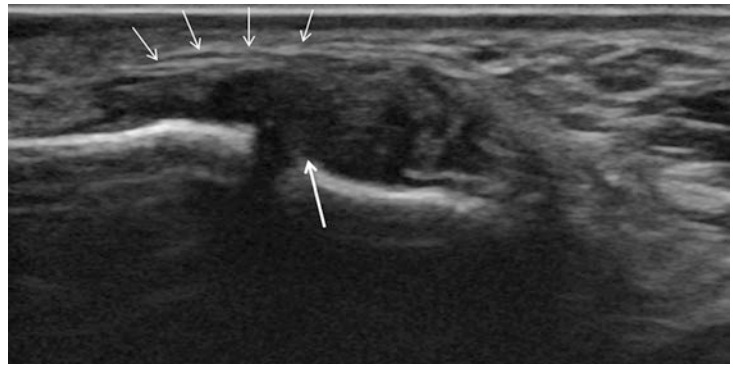

Fig. 24 UCL tear. Coronal ultrasound image shows a thickened and hypoechoic UCL (white arrow); the adductor aponeurosis (short arrows) is still positioned superficially to the ligament

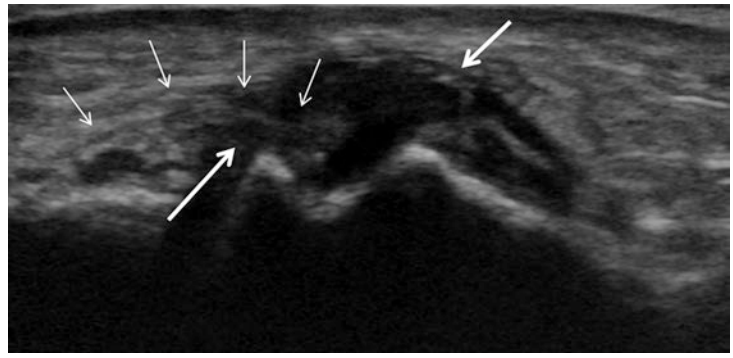

Fig. 25 Stener lesion. Coronal ultrasound image shows a thickened UCL (arrows) and interposition of the adductor aponeurosis (short arrows) between the torn UCL and the MCP joint

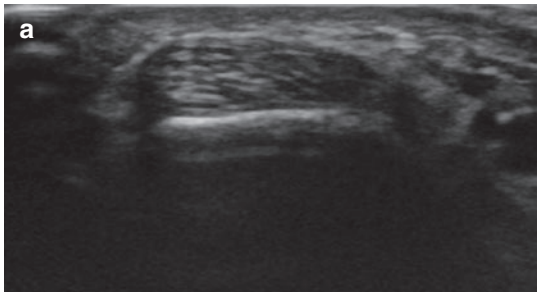

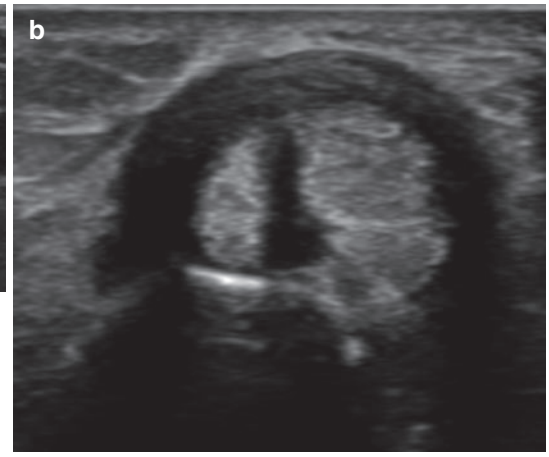

Fig. 26 (**a**, **b**) De Quervain tenosynovitis. (**a**) Transverse ultrasound image of a normal first extensor group. (**b**) Transverse ultrasound image of De Quervain tenosynovitis. Note the thickened aspect of tendons, synovium, and retinaculum

9 Other Sport-Related Injuries of the Hand

In a study of 100 consecutive hand injuries in boxing, Noble (1987) found that 35% of the injuries occurred at the base of the second to fifth metacarpals, including the wrist joint. Mechanism of injury was forced flexion of the wrist. Other boxing injuries affecting the hand occurred in the thumb area (39%) and the phalanges and the rest of the metacarpals (Fig. 27), excluding the bases (26%). Other soft-tissue structures of the wrist may also be traumatized.

Fig. 27 Spiral fracture of the third metacarpal shaft in a boxer, as seen on a PA radiograph of the hand. (Courtesy of W. Peh)

10 Conclusion

Ultrasound and MRI are important tools for diagnosing sports-related injuries of the ligaments and tendons of the hand. Important injuries may involve the flexor and extensor tendons, collateral ligaments, annular pulleys, volar plate, and dorsal hood.

Radiography

Of value if bony injury or change in bony alignment

Normal if bone changes are absent

Ultrasound

Excellent for fine hand soft-tissue structures

Quick, and inexpensive

Requires excellent knowledge of anatomy and ultrasound approach

Dynamic examination possible

Competitive with MRI for hand soft-tissue injury

MRI

Excellent for soft-tissue and bone marrow changes

Good system and technique mandatory for hand imaging

May be time consuming and expensive

Things to Remember

1. Rupture of central extensor insertion can lead to "boutonniere," and distal insertion to "mallet" finger.
2. With dorsal hood injury extensor tendons can be displaced from their central position over the MCP heads.
3. Flexor avulsion typically involves the flexor profundus and is designated rugger jersey finger.
4. With rupture of the pulleys, bowstring deformity can occur.
5. Volar plate and collateral ligament injuries are often associated.
6. When the proximal portion of the UCL of the thumb becomes located superficial to the adductor aponeurosis, Stener lesion is diagnosed.
7. Racquet sports may be a risk factor for developing De Quervain tenosynovitis.

References

Cohen SB, Chabra AB, Anderson MW et al (2004) Use of ultrasound in determining treatment for avulsion of the flexor digitorum profundus (rugger jersey finger): a case report. Am J Orthop 33:546–549

De Quervain F (2005) On the nature and treatment of stenosing tendovaginitis on the styloid process of the radius. (Translated article: Muenchener Medizinische Wochenschrift 1912, 59, 5–6). J Hand Surg 30:392–394

Kleinbaum Y, Heyman Z, Ganel A et al (2005) Sonographic imaging of mallet finger. Ultraschall Med 26:223–226

Kovacs BG (2002) High resolution ultrasound diagnosis of the annular tendon system of the hand. Orthopade 31:284–287

Landsmeer JM (1949) The anatomy of the dorsal aponeurosis of the human finger and the functional significance. Anat Rec 104:31–44

Nance EP Jr, Kaye JJ, Milek MA (1979) Volar plate fractures. Radiology 133:61–64

Noble C (1987) Hand injuries in boxing. Am J Sports Med 15(4):342–6. (PMID: 3661815. https://doi.org/10.1177/036354658701500408)

O'Callaghan BI, Kohut G, Hoogewoud HM (1994) Gamekeeper thumb: identification of the Stener lesion with US. Radiology 192:477–480

Parellada JA, Balkisson AR, Hayes CW et al (1996) Conway WF. Bowstring injury of the flexor tendon pulley system: MR imaging. AJR Am J Roentgenol 167:347–349

Schweizer A (2003) Lumbrical tears in rock climbers. J Hand Surg 28:187–189

Athletic Groin Pain

Radhika Prasad, Omar Abdulla,
and Philip Robinson

Contents

R. Prasad · O. Abdulla
Musculoskeletal Centre X-Ray Department, Leeds Teaching Hospitals Trust, Chapel Allerton Hospital, Leeds, UK
e-mail: radhika.prasad@nhs.net; omar.abdulla@doctors.org.uk

P. Robinson (✉)
Musculoskeletal Centre X-Ray Department, Leeds Teaching Hospitals Trust, Chapel Allerton Hospital, Leeds, UK

Leeds Musculoskeletal Biomedical Research Centre, University of Leeds, Leeds, UK
e-mail: philip.robinson10@nhs.net

Abstract

Groin injury and pain account for a significant proportion of all athletic injuries particularly in sports involving kicking and sudden change of direction. Acute adductor and hip flexor muscle injuries are only second in incidence to hamstring injury. Non-acute or long-standing groin pain is also a complex clinical and radiological area with confusing terminology often being used. Research has largely focused on long-standing groin pain but increasing studies are now appearing on acute injury and prevention.

This chapter reviews the anatomy of the anterior pelvis and groin and illustrates the normal anatomy and normal variation seen in athletes. Imaging strategies will be discussed emphasising the use of MRI to evaluate the symphysis pubis and surrounding rectus abdominis-adductor longus aponeurosis. Clinical and imaging findings in athletes with acute and long-standing groin pain are described and illustrated. The evidence for the specificity of imaging findings in the context of asymptomatic athletes is also presented.

Med Radiol Diagn Imaging (2021)
https://doi.org/10.1007/174_2020_254, © Springer Nature Switzerland AG
Published Online: 23 February 2021

1 Introduction

In sports which stress the pelvic girdle and lower limbs, such as football, groin pain accounts for 4–19% of all athletic sports injuries (Waldén et al. 2015; Werner et al. 2009). In the past this type of injury has led to career-altering or career-terminating outcomes for many athletes (Morelli and Weaver 2005). Groin pain is the third most common cause of time out of training and play, after fractures and anterior cruciate ligament reconstruction (Robinson et al. 2011). Studies in football have shown an incidence of about 0.21% hour of play for groin injury constituting 7–13% of all injuries in men's and women's senior football, with a more than twofold increase in incidence for male players compared to females (Waldén et al. 2015; Giza 2005).

Groin pain can be categorised into acute and long-standing groin pain. Acute groin pain is a sudden onset and is usually due to acute muscular, tendinous, or bony injury. Long-standing groin pain can be defined as a pain that persists for longer than 3 months in the general population, and persists longer than 3 weeks in elite athletes, typically with insidious onset (Robinson et al. 2011).

The most prevalent clinical groin injury in sports is adductor strain (Sedaghati et al. 2013). Combined acute and chronic adductor muscle injuries are the second most commonly injured muscle group (23%) after the hamstrings (37%) (Ekstrand et al. 2011). In football and in subelite male football players, these account for 51% of overall groin pain (Kiel and Kaiser 2018). Groin injuries also account for 10% of all injuries in elite Swedish ice hockey players (Kluin et al. 2004), and 43% of all muscle strains in elite Finnish ice hockey players.

2 Overview of Regional Anatomy

Knowledge of the complex anatomical structures in the groin is key to understanding groin injury. There are no distinct anatomical boundaries delineating the groin; however it is widely referred to as centred on the pubic symphysis, and including the bilateral lower abdominal wall, proximal adductor and inguinal compartments.

2.1 Pubic Symphysis

The pubic symphysis is a non-synovial amphiarthrodial joint with a shock-absorbing intervening central fibrocartilaginous disc. A normal central 'primary cleft' often develops in this disc by late teens due to increased mechanical forces running through the pubic symphysis (Chopra and Robinson 2016; Omar et al. 2008).

In the normal gait cycle, the pubic symphysis is prone to vertical plane shear stress, as each lower limb transmits the weight of the body onto the contralateral lower limb via the pelvis (Koulouris 2008). The articular surfaces are irregular to protect the joint from shear forces and are covered by hyaline cartilage. The pubic body apophyses are on the anteromedial aspect of each bone and fuse in a player's early 20s (Fig. 1) (Madani and Robinson 2019).

The joint capsule is supported by four pubic ligaments: superior, inferior (also known as arcuate ligament), anterior and posterior. The superior and inferior are felt to be the most structurally important as they resist shear forces.

2.2 Muscles/Aponeurosis

There are multiple overlapping muscle attachments around the pubic symphysis that also contribute to stability. These include the anterolateral abdominal muscles: rectus abdominis, pyramidalis, external oblique, internal oblique, transversus abdominis and thigh adductors. The short thigh adductors are adductor longus, brevis and pectineus. The long thigh adductors are adductor magnus and gracilis. Rectus abdominis and adductor longus are thought to be particularly important contributors to stability.

The rectus abdominis is a paired midline abdominal wall muscle which has a narrow origin at the anterior pubis, formed by medial and lateral heads. Inferiorly, the medial head blends with the

contralateral rectus abdominis, and superiorly the medial heads diverge and are separated by the linea alba (Madani and Robinson 2019).

The adductor longus is the most anterior of the adductors. It is a characteristically triangular shaped muscle, originating just below the anterior pubis (below the crest), and gets inserted onto the middle third of the femur (Fig. 2).

Cadaveric dissection has shown that the distal rectus abdominis and pyramidalis insertional fibres are in continuity distally with the proximal origin fibres of the adductor longus, across the pubic crest and joint capsule. The joint capsule, capsular ligaments and fibrocartilaginous disc receive contributions from pyramidalis, adductor longus and rectus abdominis tendons merging as anterior aponeurosis (Figs. 3, 4 and 5) (Robinson et al. 2007). This is a common site for injury and there have been several terms attributed to this anatomical area, including enthesis, 'aponeurotic plate' and 'pyramidalis-anterior pubic ligament-adductor longus complex (PLAC)'. The PLAC theory suggests that the anterior abdominal wall muscle pyramidalis is in continuation with the anterior pubic capsular ligament rather than the rectus abdominis. We choose to use the term the 'rectus abdominis-adductor longus aponeurosis' to describe this anatomical area as it is the most widely used term and includes all of the above structures (Zajick et al. 2008; Robinson et al. 2007; Schilders et al. 2007).

2.3 Inguinal Canal

The inguinal canal is an oblique fascial tunnel containing the spermatic cord in males and round ligament in females. The walls of the inguinal canal are continuous with the anterior abdominal wall.

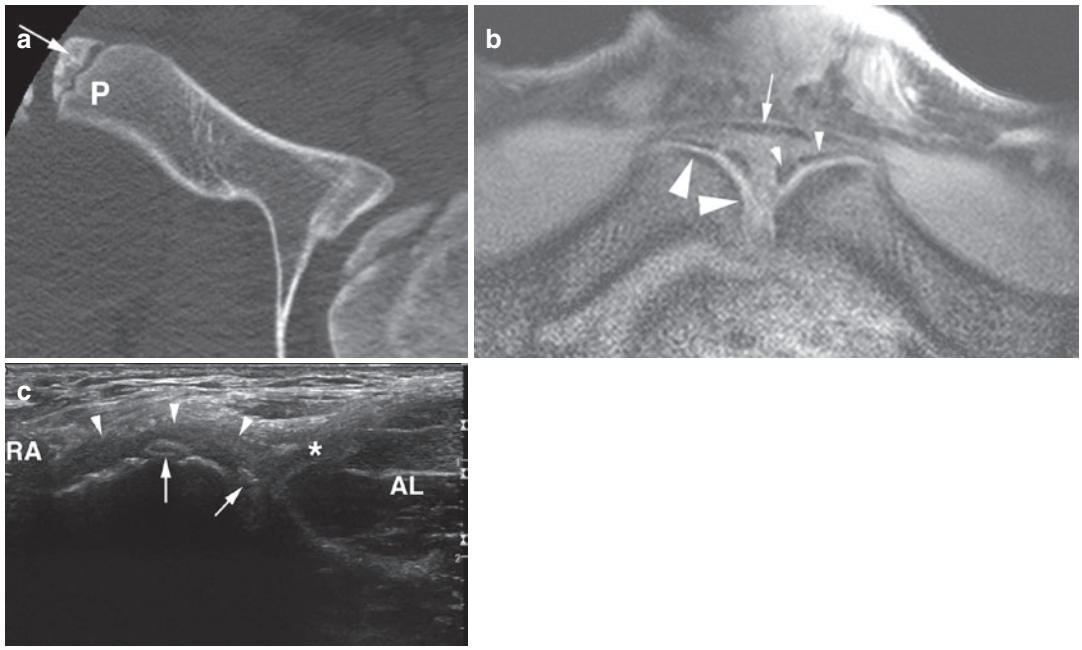

Fig. 1 (**a**–**c**) Normal apophysis, 17-year-old asymptomatic males. (**a**) Axial CT image shows the left pubis (P), intervening apophyseal cartilage and ossified apophysis (arrow). (Reproduced with permission from Robinson et al. 2011). (**b**) Axial T1-weighted FFE spectral inversion recovery fat suppression MR image shows low-signal subchondral pubic cortex (large arrowheads), intervening high-signal apophyseal cartilage and areas of endochondral ossification (small arrowheads) merging with capsular tissues and rectus abdominis tendon (arrow). (Reproduced with permission from Robinson et al. 2007). (**c**) Sagittal ultrasound image shows irregular apophyseal ossification (arrow) and merging of the anterior capsular tissues (arrowheads), rectus abdominis (RA), adductor longus (AL) and its tendon (*). (Reproduced with permission from Robinson et al. 2011)

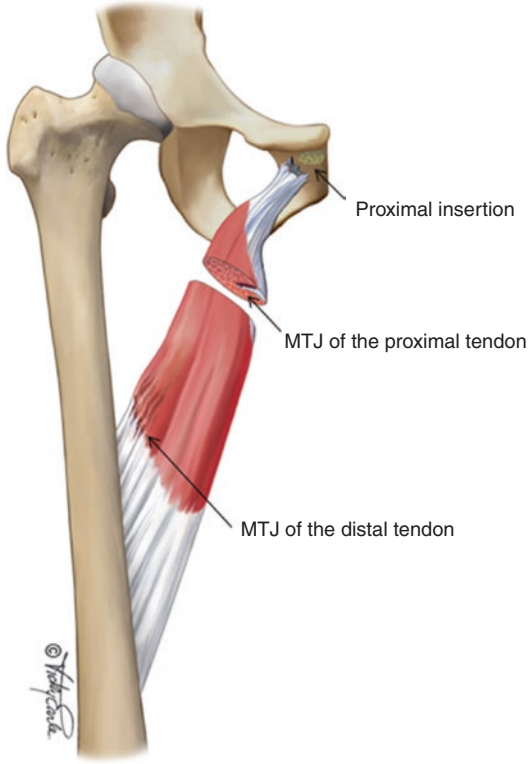

Fig. 2 Anatomical illustration of the three most common adductor longus injury locations. *MTJ* musculotendinous junction. (Reproduced with permission from Serner et al. 2018a)

The floor is made up of the rolled edge of the inferior margin of the external oblique aponeurosis, i.e. the inguinal ligament. The medial fibres of the external oblique form the anterior wall, splitting into two fascicles at its insertion at the pubic tubercle to form the superficial inguinal ring. The posterior wall is formed by the transversalis fascia, in which there is a defect to form the deep inguinal ring. The roof is formed by the transversalis fascia, internal oblique and transversus abdominis (Omar et al. 2008; Chopra and Robinson 2016).

2.4 Iliopsoas Muscle

The iliopsoas muscle mainly functions as a hip flexor, with a lesser role in hip external rotation. The iliopsoas muscle is formed by the combination of psoas major and iliacus muscles. The psoas muscle originates from the transverse processes and the lateral aspect of the vertebral bodies of T12-L5. The iliacus muscle originates from the internal aspect of the iliac fossa. Both muscles combine at the level of the inguinal canal and cross anterior to the hip joint to get inserted onto the lesser trochanter (Fig. 6). Separate tendon insertions have been described with the psoas major tendon located medially and the iliacus muscle laterally. At the proximal myotendinous junction of the iliacus muscle, the tendon is divided into posteromedial and anterolateral portions (Guillin et al. 2009; Chopra and Robinson 2016).

Deep to the musculotendinous portion of the iliopsoas muscle is the iliopsoas bursa, which is the largest in the body, and communicates with hip joint in approximately 15% of individuals (Chopra and Robinson 2016).

3 Overview of Imaging in Groin Pain

Conventional X-rays and computed tomography (CT) may rarely help to evaluate hip and lower lumbar spine bony pathology which can mimic groin injury, but are largely superseded by the soft tissue detail provided by ultrasound and magnetic resonance imaging (MRI) in the investigation of athletic groin pain (Branci and Robinson 2014).

Ultrasound can exclude an inguinal hernia and iliopsoas bursitis as well as allow dynamic assessment of the groin including iliopsoas tendon snapping (Vasileff et al. 2017). This modality also allows diagnostic intervention with anaesthetic infiltration which may help define the underlying cause of symptoms.

However, MRI is typically preferred because it provides assessment of low-grade soft-tissue oedema, bone marrow oedema and joint pathology not readily accessed by ultrasound.

3.1 Ultrasound Protocol

The patient is scanned supine with hips abducted and externally rotated. A high-frequency

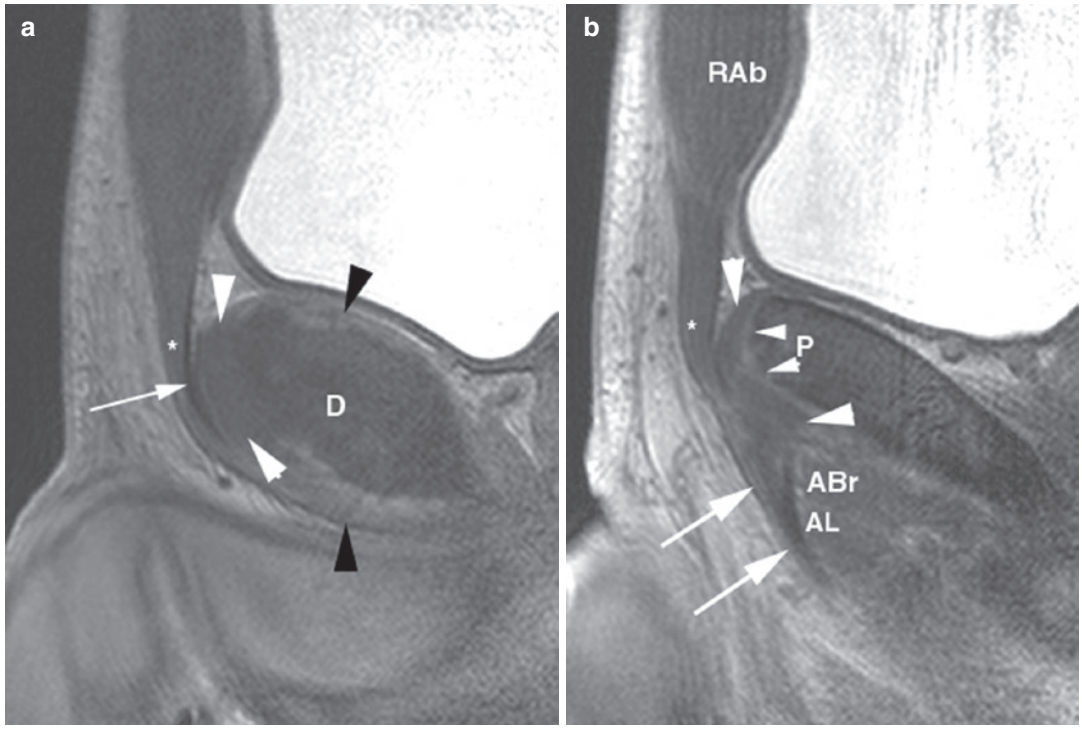

Fig. 3 (**a**, **b**) Normal sagittal MRI anatomy of a 29-year-old male athlete (experienced previous pubalgia). (**a**) Sagittal T1-weighted FFE MR image shows the edge of fibrocartilaginous disc (D), interdigitating hyaline cartilage and pubic bone (black arrowheads). Anteriorly, the capsular tissues (white arrowheads) merge with the disc (D) and rectus abdominis tendon (white arrow). Pyramidalis present anteriorly (asterisk). (**b**) Lateral to image (**a**) pubic marrow and cortex (P) with thin layer of intermediate-signal hyaline cartilage (small arrowheads) closely applied to the anterior capsular tissues (between large white arrowheads). Merging with this tissue are the rectus abdominis tendon (RAb), pyramidalis (asterisk), superficial adductor longus tendon (arrows), deeper adductor longus muscle (AL) and adductor brevis (ABr) muscle. (Reproduced with permission from Robinson et al. 2007)

(>14 MHz) linear array transducer is used to assess the pubic symphysis and rectus abdominis-adductor longus aponeurosis in both longitudinal and transverse planes (Figs. 1 and 5). The inguinal canal is also assessed with dynamic Valsalva manoeuvre (Robinson et al. 2006) (Boxes 1 and 2).

Box 1: Ultrasound
Ultrasound is useful in studies requiring a dynamic component, e.g. Valsalva manoeuvre for functionally assessing hernias, conditions where colour or power Doppler imaging may be helpful, e.g. hip synovitis, and for guiding a range of percutaneous diagnostic and therapeutic procedures.

Box 2: Radiography/Computed Tomography
The indications for CT in athletes with pelvic, hip and groin pain are limited but include bony abnormalities at the symphysis pubis (stress fracture or apophyseal abnormality) when MRI is inconclusive.

3.2 MRI Protocol

A dedicated MR protocol is advised in athletic groin pain investigation which should include both large and small field-of-view sequences.

Small field-of-view high-resolution imaging is preferred to assess the intricate structures of

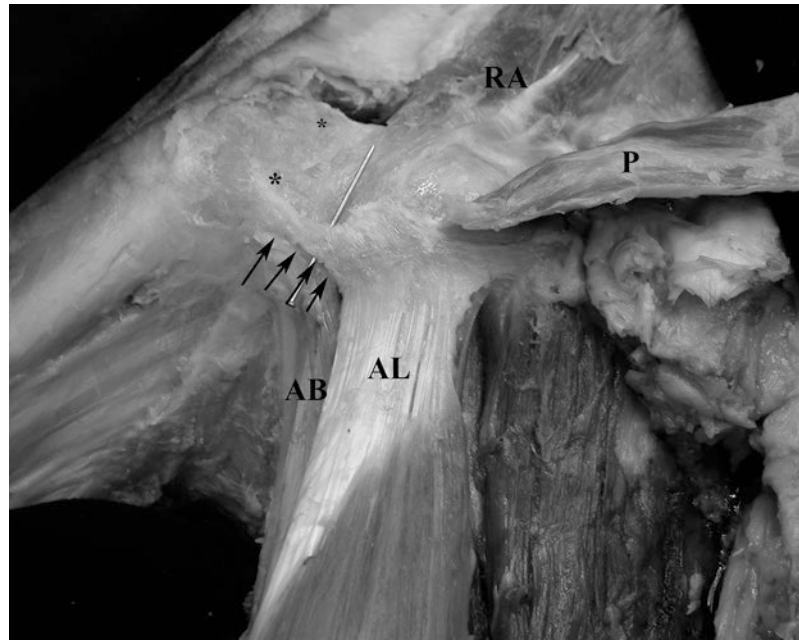

Fig. 4 Male cadaver dissection, normal anatomy, anterolateral view. Asterisks mark the centre of the symphysis pubis. The tendinous attachment of adductor longus (AL) to tissue overlying the anterior symphysis pubis is elevated by a pin and inferiorly outlined with arrows. Pyramidalis (P) is reflected to reveal rectus abdominis (RA). The medial margin of adductor brevis (AB) can be seen medial to adductor longus (AL). (Reproduced with permission from Robinson et al. 2007)

the groin. An anterior surface coil is suggested with a slice thickness of 2 or 3 mm. As well as the usual conventional planes (coronal, sagittal, axial), oblique axial imaging in a plane parallel to the pelvic brim anterior tilt is recommended (Fig. 5). Larger field-of-view imaging of the pelvis can be performed to exclude other causes of pain in this region. With the advancements in MRI resolution, contrast is no longer considered necessary (Robinson et al. 2011; Lee et al. 2017).

Our institution athletic groin protocol consists of six sequences: large field-of-view (400 × 400) coronal T1 and STIR sequences, axial T2 fat-saturated sequence followed by small field-of-view (using an anterior surface coil) sagittal T2 fat-saturated and axial oblique T1 and proton density fat-saturated sequences (Fig. 5).

Zajick et al. describe similar protocols but add a small field-of-view axial oblique fat-saturated T2 sequence (Zajick et al. 2008). The Copenhagen MRI protocol consists of an eight-sequence protocol including STIR and T1 axial and axial oblique as well as T2 fat-saturated and proton density fat-saturated axial oblique sequences (Branci et al. 2015b) (Box 3).

Box 3: Magnetic Resonance Imaging

In athletes this is the first-line imaging investigation for most causes of pelvic, hip and groin pain due to its high anatomical detail and ability to demonstrate a wide range of osseous and soft-tissue pathologies.

Pubic body bone marrow oedema and soft-tissue aponeurotic oedema (±tearing) are the most frequent findings in long-standing pain with more severe features correlating with symptoms. However milder features are a common finding in asymptomatic athletes due to chronic stress or previous healing following resolution of symptoms.

4 Acute Groin Pain

4.1 Overview

The literature on acute groin injuries is often limited to case studies and general data that does not specify the individual structures involved. Most

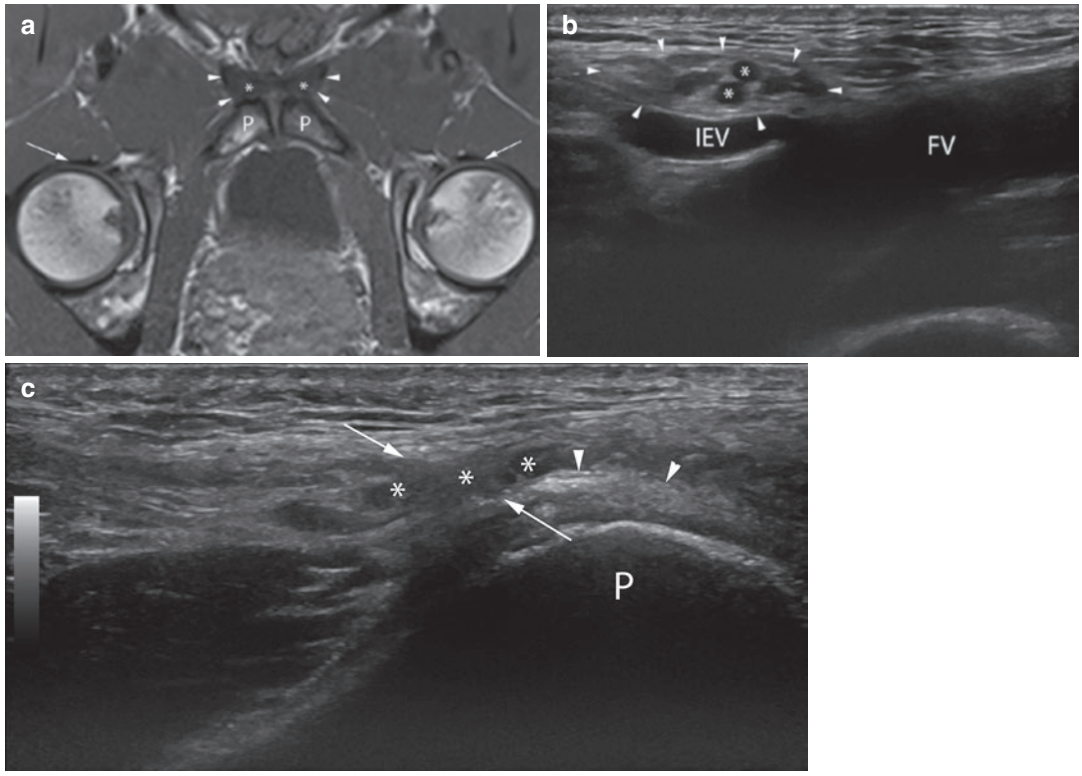

Fig. 5 (**a**–**c**) Normal anatomy, imaging. (**a**) Axial oblique T1w MR image shows pubic bodies (P) and the adductor group tendons (arrowheads) beginning to separate from the aponeurotic tissues (*). Normal iliopsoas tendons (small arrows). (**b**) Sagittal (short-axis) ultrasound image shows the inguinal canal (arrowheads) and contents (*) just medial to the deep ring at the level of inferior epigastric vein (IEV). *FV* femoral vein. (**c**) Axial oblique ultrasound image shows the inguinal canal contents (*) at the level of the superficial ring (arrows) with adjacent pubic body (P) and capsular/aponeurotic tissues (arrowheads). (Reproduced with permission from Hardi and Robinson 2019)

literature covering the topic of groin injuries focuses on long-standing groin pain.

Understanding the mechanism of injury is essential in the clinical assessment of acute groin injury as certain muscle groups are more likely to be injured from a specific mechanism; for example, rapid change in body direction is more likely to cause injury to the iliopsoas muscle while sudden kicking or sprinting is associated with higher rates of rectus femoris injury.

Despite the importance of clinical assessment and physical examination, imaging plays an important role in the management of acute groin injuries. With imaging, the exact site of injury can be determined. MRI is the gold standard imaging modality with good inter-observer and intra-observer reproducibility and the ability to detect pathology elsewhere in the pelvis. Plain radiography, computed tomography and ultrasound have a relatively limited role in the context of acute groin injury sports imaging.

Acute groin injuries can be divided into:

1. Acute muscle-related injuries
   (a) Acute hip adductor injuries
   (b) Acute hip flexor and rotator muscle injuries
2. Acute bone-related injuries
   (a) Pubic apophyseal injury
   (b) Pubic stress fracture

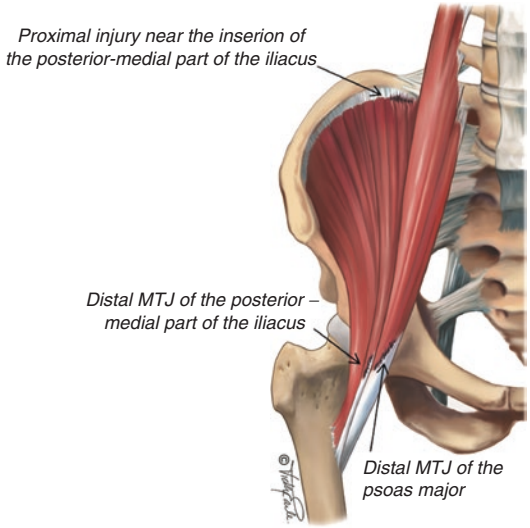

Fig. 6 Anatomical illustration of acute injury locations of the iliacus and psoas major. *MTJ* musculotendinous junction. (Reproduced with permission from Serner et al. 2018b)

4.2 Acute Groin Injury: Muscle-Related Injuries

For acute muscle injuries, assessment with MRI is the imaging gold standard due to its superior spatial and contrast resolution, and ability to assess deep injuries and multiplanar image acquisition.

Imaging of the injured site is performed using a dedicated surface coil with a small field of view (FOV). T1-weighted imaging has a smaller role to play in the context of acute injuries; it can detect high-signal acute or subacute haematoma as well as established fatty infiltration and atrophy in chronic injuries.

The traditional acute muscle injury grading system categorises injuries on a scale from 1 to 3 (Peetrons 2002). Injury severity ranges from only interstitial oedema at the myotendinous junction (grade I) with no architectural disruption or functional loss to the most severe form with complete muscle fibre disruption at the myotendinous junction, or complete tendon avulsion from its bony attachment site, and complete functional loss clinically.

There are inherent problems associated with this grading system. It does not include grade 0 injury where there is a clinical syndrome of acute muscle injury with negative imaging findings. The latter injury category is relevant as it is associated with a quicker return to sport. Another problem of this grading system is the lack of precise prognostic information, which is necessary for enhanced decision-making in the management of muscle injuries. Prognostic factors validated in the literature are predominantly for acute hamstring injuries and include injury distance from the muscle origin, length of muscle tear on MRI, cross-sectional area of oedema, tendon involvement and MR-negative injuries (Pollock et al. 2014).

Alternative muscle injury grading systems have been proposed, which attempt to provide better prognostic evidence to assist in classification.

The modified Peetrons (Ekstrand et al. 2012) classification is based on an original ultrasound (US) classification (Peetrons 2002) in footballers which has shown fair correlation with return to sport. This classification is widely used; however, its precise prognostic relevance is debatable in the literature (Ekstrand et al. 2012).

An alternative MR classification system was proposed by Chan et al. (2012) but there is also no inclusion of MR-negative muscle injuries in this classification.

The British Athletics Muscle Injury Classification (BAMIC) (Pollock et al. 2014) was developed to address the deficiencies of the above grading systems by having a more complex but clear anatomically focused diagnostic framework which utilises the available prognostic evidence to assist in classification. It includes grade 0 injury, with 5 injury grades overall, 0–4. For grades 1–4, there is subdivision into a, b or c categories depending on the site of injury and degree of tendon involvement.

A prospective study (Wangensteen et al. 2018) evaluated the prognostic value of these three grading systems in acute hamstring injuries finding moderate agreement for severity grading in MRI-positive injuries.

4.2.1 Acute Hip Adductor Muscle Injury

4.2.1.1 Anatomy and Mechanism of Acute Adductor Longus Injuries

The hip adductor muscles are made up of the short adductors, i.e. adductor longus, adductor brevis and pectineus, and the long adductors, i.e. adductor magnus and gracilis.

All the adductor muscles originate from the pubic and ischial bones and get inserted onto the femoral shaft posteromedially, except for gracilis which gets inserted onto the medial tibial plateau. The adductor longus muscle has a triangular muscle belly (Fig. 2). The proximal tendon, the most anterior of the adductor muscle group, blends with the contralateral adductor longus tendon across the midline and continues with the inferior fibres of the rectus abdominis muscle and pyramidalis at the pubic symphysis capsular attachment (Figs. 3, 4 and 5) (see anatomy section previously). The adductor muscles play a major role when there is fast leg movement against resistance (e.g. kicking a ball) or sudden change in direction.

Clinically, adductor injury manifests as tenderness at the pubic bone and adductor origin with medial sided thigh pain and pain on both passive and active thigh adduction. Of all the adductor muscles, adductor longus is by far the commonest muscle to sustain injury.

Therefore, detailed analysis of the mechanism of injury, injury pattern and prevention programmes is of paramount importance in the context of acute muscular groin injuries' preventive strategies.

Football player actions have been categorised (Serner et al. 2019) into closed- and open-chain movements with triplanar hip movements. Closed-chain movements include change in direction and reaching, which involve hip extension and abduction while the hip is externally rotated. Kicking and jumping are classed as open-chain movements with hip flexion and adduction while the hip is externally rotated.

The combination of rapid muscle activation and increase in muscle tendon unit length is believed to be the major factor in the mechanism of injury. Accordingly, increasing muscle capacity to withstand rapid loading at a lengthened state is key in the injury prevention (Serner et al. 2019).

4.2.1.2 Acute Adductor Muscle Injury Pattern

A detailed classification system of acute adductor injuries is lacking in the literature. Serner et al. (2018a) studied 111 acute adductor injuries in 71 athletes and concluded that acute adductor injury usually involves a single muscle but can also involve multiple adductor muscles. However, the combination of adductor muscle injury and injury in another muscle group in the groin is rare. Of the adductor muscle group injuries, the adductor longus is the most frequently affected muscle in isolation. When it is part of a combined adductor injury, adductor longus injury tends to be the most severely affected.

The adductor longus injury pattern can be divided into three main categories (Serner et al. 2018a):

1. At the proximal tendon inserting into the capsule and anterior pubic body
2. At the proximal myotendinous junction
3. At the distal myotendinous junction

At the Proximal Insertion into the Capsule and Anterior Pubic Body

The proximal tendinous origin of the adductor longus is small (measuring about 2–4 cm), narrow and flat originating from the anterior aspect of the pubic bone in the angle between the pubic crest and symphysis pubis (Tuite et al. 1998). The distance between the medial border of both right and left adductor muscles is greater in women than men, secondary to the inherent difference in pelvic anatomy.

Injuries at this site are often of high severity (grade 3) representing complete tendon avulsion from its insertion (Figs. 7 and 8). Complete intrasubstance tendon tear can also be seen. These injuries are often associated with tendon retraction and a gap clinically. Sometimes, minimal

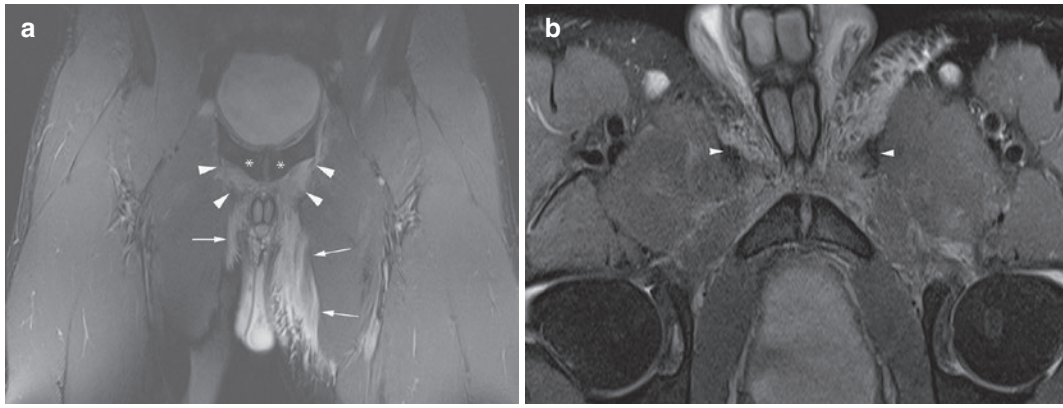

Fig. 7 (**a**, **b**) Complete bilateral adductor avulsion. (**a**) Coronal T2w FS and (**b**) axial oblique PDw MR images show normal pubic bone marrow signal (*) with inferior haematoma, avulsed pectineus, adductor tendons (arrowheads) and haemorrhage tracking inferiorly into the thighs (arrows)

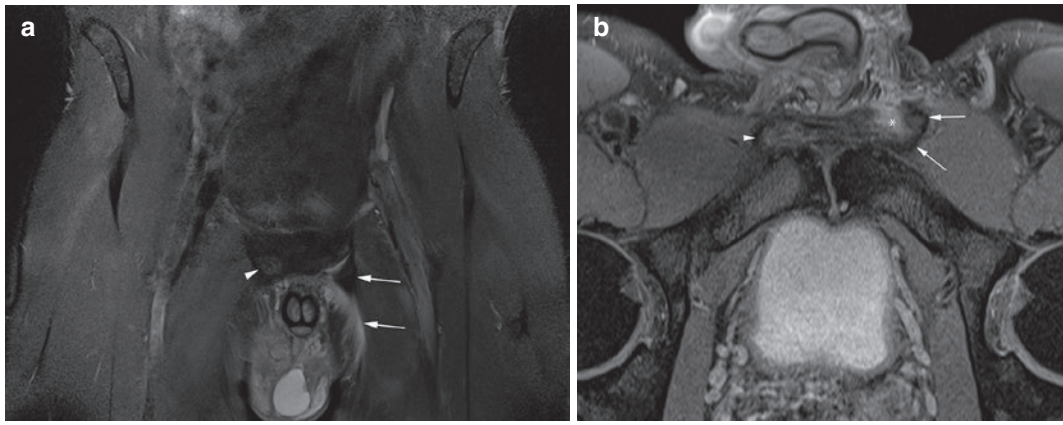

Fig. 8 (**a**, **b**) Partial left adductor avulsion. (**a**) Coronal T2w FS MR image shows normal pubic bone marrow signal and partial adductor longus tendon tear and haemorrhage tracking inferiorly into the thigh (arrows). Normal right side (arrowhead). (**b**) Axial oblique PDw MR image shows the haematoma (*) and displaced left adductor tendon (arrows). Oedematous but intact right side (arrowhead)

residual fibres result in minor retraction and no gap can be felt clinically, posing a clinical dilemma (Fig. 9).

This is where imaging can differentiate between a severe injury which needs longer rehabilitation and a minor one. Often extensive haematoma of the groin, thigh, and external genitalia will be present (Fig. 7). An uncommon variant of adductor tendon avulsion has been described as complete avulsion of the adductor sleeve complex, which includes adductor longus, pectineus and rectus abdominis (Tansey et al. 2015) which can be treated surgically and non-surgically (Fig. 7).

At the Proximal Myotendinous Junction

The adductor longus proximal myotendinous junction shows a sharp oblique line anteriorly. However, the posterior origin of the proximal muscle often consists of muscle fibres with no definite tendinous component. MRI studies of acute groin injuries showed that for proximal adductor longus myotendinous injuries, soft-tissue changes are noted anteriorly where the

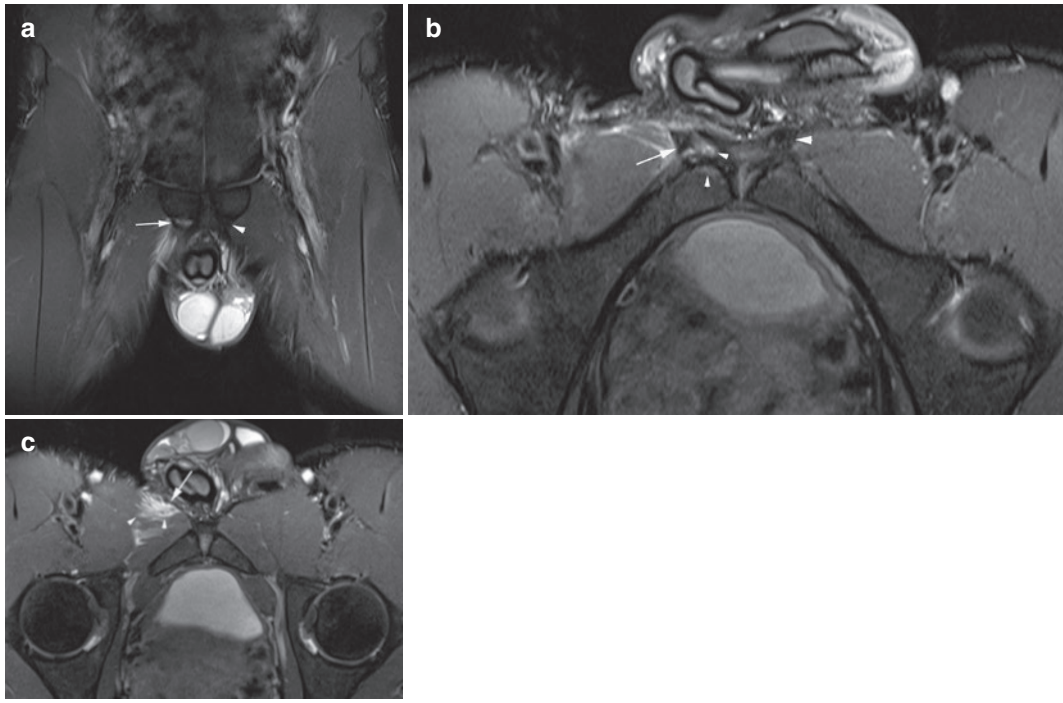

Fig. 9 (**a**–**c**) Partial right adductor longus tendon and proximal myotendinous tear. (**a**) Coronal T2w FS and (**b**) axial oblique PDw MR images show partial adductor longus tendon tear (arrows). Haematoma and minor reactive bone marrow oedema (small arrowheads). Normal left side (large arrowhead). (**c**) Axial oblique PDw MR image inferior to (**b**) shows the proximal myotendinous injury with low-signal tendon (arrow) and muscle haematoma (arrowheads)

myotendinous junction is more well defined (Serner et al. 2018a).

The injury usually affects the attachment of the muscle fibres onto the intramuscular tendon giving a high signal "feathery appearance" on MRI as the blood products track along the edges of the torn muscle fibres (Fig. 9). Occasionally, the intramuscular tendon itself can be part of the injury often inferring a more severe injury (see classification summary above).

In the case of the adductor longus, this injury can affect the superficial tendon, where the proximal tendon first becomes intramuscular, approximately 1–2.5 cm from the insertion, and the intramuscular tendon, where it becomes entirely intramuscular 5.5–8 cm from the insertion (Fig. 9) (Serner et al. 2018a). Additional injury of the tendon itself is relatively rare and is suggested by waviness/redundancy to the contour of the tendon. In general, the myotendinous junction injuries of the proximal tendon are located at the anterior aspect of the intramuscular tendon (Serner et al. 2018a).

At the Distal Myotendinous Junction

The anatomy of the distal adductor longus tendon and its distal myotendinous junction is poorly defined in the literature. The fleshy muscle belly inserts as an aponeurosis into the linea aspera. However, MR imaging using the current protocols does not clearly delineate the boundaries of the tendon at the distal myotendinous junction. When injury happens at this site, oedema is often seen at the proximal part of the distal myotendinous junction (Fig. 10) (Serner et al. 2018a).

There is a possible overlap between the clinical presentation of the proximal and distal myotendinous junction injuries because of the expansion of the muscle oedema proximally from a distal injury and vice versa. The injury can also occur midway between the proximal and distal

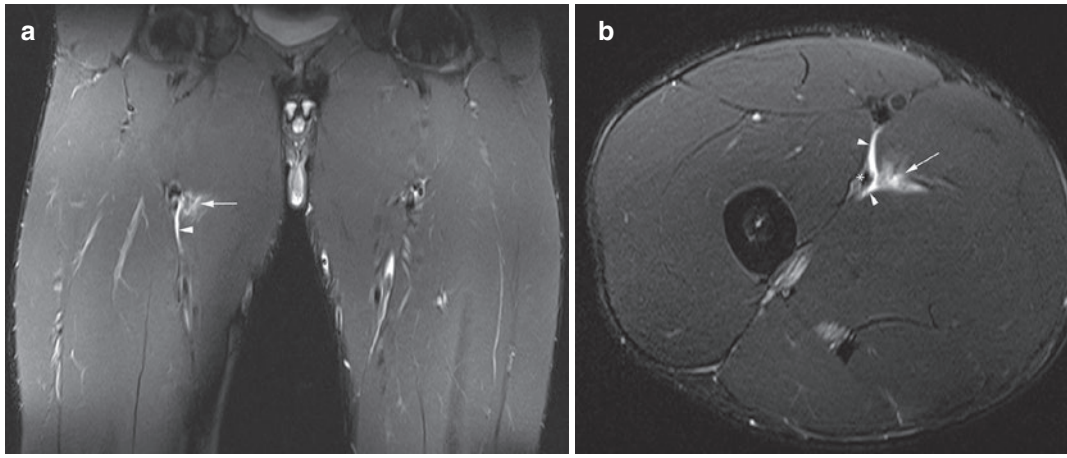

Fig. 10 (**a**, **b**) Distal right adductor longus myotendinous tear. (**a**) Coronal T2w FS and (**b**) axial oblique PDw MR images show distal muscle haematoma (arrow) with haemorrhage decompressing into the muscle fascia (arrowheads) and adjacent normal blood vessels (*)

parts of the muscle. All these factors can lead to confusion about the site of injury on clinical examination with implications on treatment and recovery.

4.2.1.3 Other Adductor Muscle Injuries

Involvement of other adductor muscles is less common than adductor longus injury.

Gracilis injury tends to be in combination with adductor longus muscle; however, when it happens in isolation it usually involves the distal myotendinous junction causing posterior thigh pain. A similar injury pattern is observed for adductor magnus.

Injury to the pectineus muscle tends to involve its distal part in the vicinity of the iliopsoas muscle, making differentiation between injuries of these two different muscle groups rather difficult clinically (Fig. 7).

4.2.2 Acute Hip Flexor and Rotator Muscle Injury

One-third of acute groin injuries in athletes affect the hip flexors (Serner et al. 2018b). A detailed description of rectus femoris injury is dealt with in chapter on muscle injuries covering acute muscle injury. Other small hip rotator muscle injuries including the obturator muscles can present with acute groin pain (Fig. 11).

4.2.2.1 Iliacus and Iliopsoas Injury

Acute psoas injuries usually occur in combination with iliacus injuries. The majority of injuries occur at the myotendinous junction, with the iliacus muscle injury occurring slightly more distally (Fig. 12). Tendon injuries, unlike with rectus femoris injuries, occur less frequently.

There is conflicting evidence in the literature on the incidence of combination muscle group injuries in the groin. A combination of adductor and iliopsoas injury is considered the most common by one study (13%) (Serner et al. 2015a) whereas another study (Serner et al. 2018b) found that such a combination is unlikely to occur. However, in our experience iliopsoas muscle injuries usually occur in isolation.

4.3 Correlation Between Clinical Examination and MR Findings in Acute Muscle Injuries

Physical examination plays a big part in the assessment of acute groin injury. Exacerbation of pain upon passive adductor stretching or resistive thigh adduction is highly suspicious for adductor injury whereas iliopsoas-related pain is usually associated with aggravated pain by rising from squatting or sitting positions.

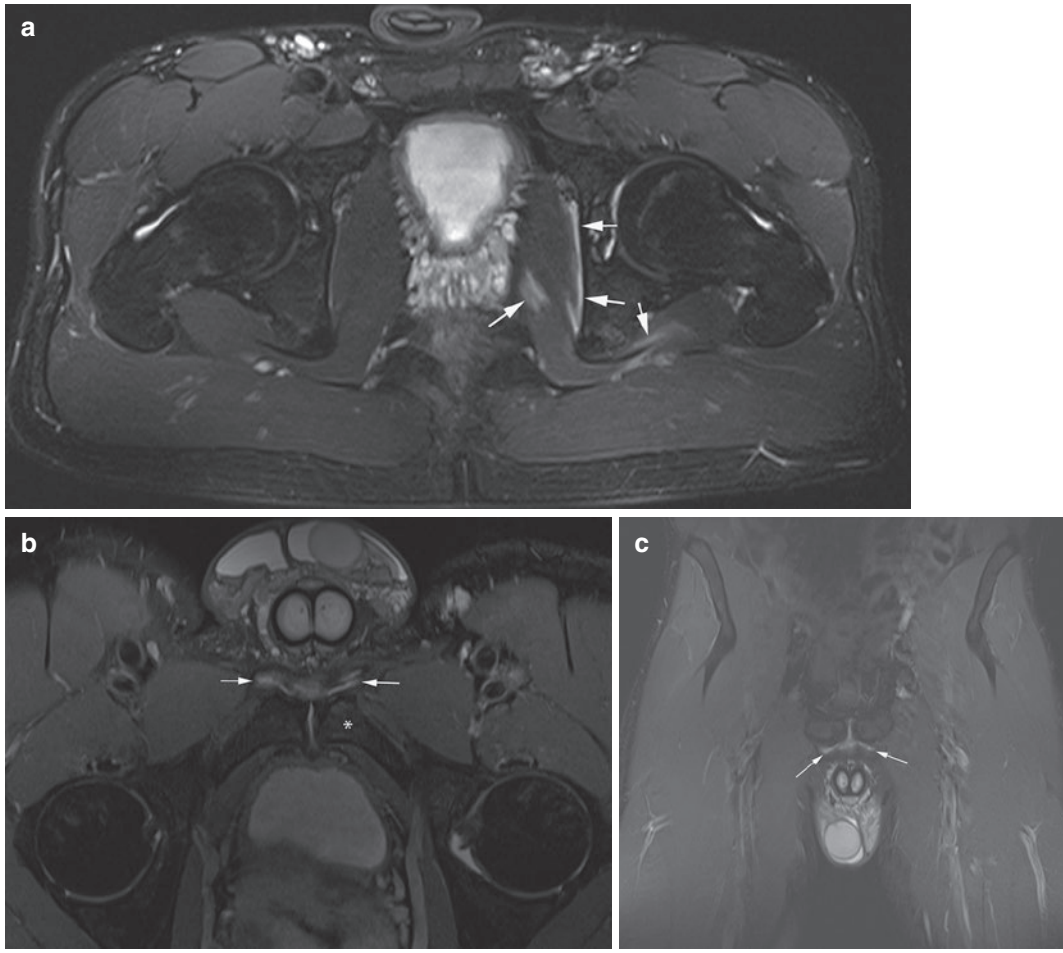

Fig. 11 (**a**–**c**) Acute left obturator internus muscle tear and asymptomatic bilateral symphysis pubis and capsule/aponeurosis change. (**a**) Axial T2w FS MR image shows low-grade left obturator internus muscle oedema (arrows). (**b**) Axial oblique PDw and (**c**) coronal T2w FS MR images show chronic oedema in the capsule/aponeurosis (arrows) and low-grade left pubic bone marrow oedema (*)

Combination of multiple muscle injuries within the same group, or from different groups, is not uncommon. Only imaging can accurately delineate the affected muscles in these situations. Imaging can also reveal stress-related pubic bone marrow oedema, widening or avulsion of the pubic apophysis. This information can dictate the type of treatment, duration of rehabilitation and prognosis.

Diagnostic terminology in acute groin injuries is less heterogeneous than in chronic injuries. Serner et al. (2016) examined the correlation between clinical examination findings and presence and location of MR findings in three muscle groups around the hip: hip adductors, hip flexors and abdominal muscles. No valid data was obtained for abdominal muscle group due to the small sample size. Three types of pain provocation tests were used: palpation, muscle resistance and stretch tests.

When all tests are negative, there is a very low probability to find an acute lesion on MRI (0% for hip adductors and 7% for hip flexors). It is harder to predict a negative MR when some tests are positive, and some are negative, in which case the results of individual test should

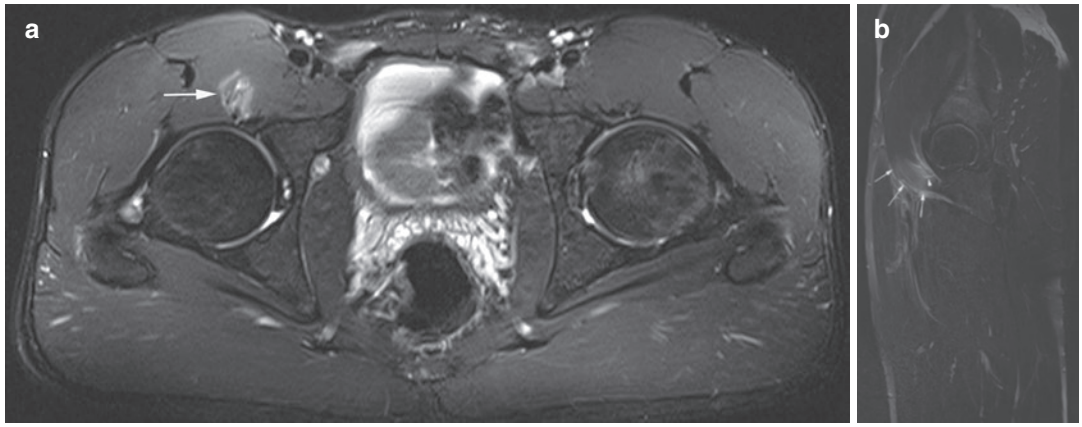

Fig. 12 (**a**, **b**) Acute iliopsoas myotendinous tears. Two different athletes. (**a**) Axial T2w FS MR image shows right iliopsoas myotendinous oedema (arrow). (**b**) Sagittal T2w FS MR image shows left iliopsoas myotendinous oedema (arrows) with some focal areas of fibre separation (arrowhead)

be considered. Palpation showed the highest probability of a negative MR finding when the examination is negative (negative predictive value of 91% for hip adductors and 96% for hip flexors). Based on the above, it is highly unlikely to have positive MR findings when all examinations are negative, or if there is no pain on palpation of the hip adductor and flexor muscle examination.

When all clinical examination tests are positive, there is a high probability of a positive MR finding (positive predictive value of 83% for hip adductors and 86% for hip flexors). The best tests are resisted outer range adduction, adductor stretch and squeeze test in hip-neutral position.

In predicting injury location in MRI-positive cases, the highest positive predictive value (100%) for a positive MR finding in hip adductors was obtained when all hip adductor tests were positive.

Lower positive predictive values are noted for hip flexors (71% and 43% for iliopsoas and rectus femoris muscles, respectively). This means that even when all test results are positive, clinicians cannot be completely confident of the localisation of injury to the hip flexor group. Therefore, imaging may be needed if more confidence is required to aid treatment and rehabilitation.

4.4 Acute Groin Injury: Bone-Related Injuries

4.4.1 Pubic Apophysitis and Avulsion Fractures

Pubic apophysitis is a subacute stress reaction at the secondary growth centre of the pubic bone. Apophyseal avulsion is an acute injury caused by extreme, unbalanced and often eccentric muscle contraction. These injuries usually develop at any age before closure of the growth plate.

4.4.1.1 Apophyseal Anatomy

The pubic symphysis is the last component of the human skeleton to achieve maturation. Its secondary ossification centres appear during puberty and physeal closure is achieved in the third decade of life. Following the physeal closure, continuous remodelling happens until full maturity around the age of 45 years. Studying the maturation of the pubic apophysis is used in both physical and forensic anthropology to determine age-at-death of skeletal remains (Meindl et al. 1985).

Cadaveric (Robinson et al. 2007) and imaging studies have described the anatomy of pubic apophysis as extending from the antero-medial pubis to the lateral limit of the capsular tissues

closely applied to the fibrocartilaginous disc, capsular tissues and deeper subchondral bone (Fig. 1). The medial aspect of the physeal plate is intra-articular and the symphyseal articular cortex is undulating and ill defined in appearance. The normal physeal plate is uniform in thickness and MR signal, and often symmetrical on both sides (Fig. 1).

A staging system has been proposed in the literature to describe the maturation status of the pubic apophysis, with four developmental groups depicted (Sailly et al. 2015):

Stage 1: Open apophyseal plate without secondary ossification centre
Stage 2: Open apophyseal plate with secondary ossification centre
Stage 3a: Closed apophyseal plate without secondary ossification centre
Stage 3b: Closed apophyseal plate with remaining secondary ossification centre

Generally speaking, physeal maturation starts at the age of 16 years and is complete at the age of 21 years (Sailly et al. 2015). Typically, between these years athletes may develop pubic apophyseal injuries.

Chronic pubic stress from sports may delay the age of the physeal plate closure by compromising the blood supply at the metaphysis and preventing the development of the provisional zone of calcification. This results in widening of the metaphyseal plate which could be uniform, focal or mixed. The widened physeal plate is more prone to additional injury, including separation and avulsion. Sometimes, persistent non-closure can happen and separate ossicles can be seen at the inferomedial aspect of the symphysis pubis normally in adults.

Acute avulsion injuries are not common and result from sudden, forceful and unbalanced contraction of the attached muscle group resulting in severe pain and loss of function while engaged in a sport activity. It has been described in footballers during kicking the ball and tackling with forced hip abduction, and in other sports like sprinters, baseball and track athletes.

Chronic or stress-related avulsion injuries are the result of repetitive microtrauma or overuse causing repetitive traction on the developing apophysis. Avulsion injuries can be associated with chronic non-union.

4.4.1.2 Diagnosis

Apophyseal fractures can pose a diagnostic difficulty due to their relatively low incidence, constituting about 4% of all pelvic fractures (Pogliacomi et al. 2014), and 1.4% of all fractures in young athletes (Calderazzi et al. 2018). When cited in the literature, pelvic avulsion fractures are limited to five principal sites: anterior superior iliac spine, anterior inferior iliac spine, ischial tuberosity, iliac crest and lesser trochanter. Pubic apophyseal injuries are only sporadically mentioned in the literature.

Pubic apophysitis is a combined clinico-radiological diagnosis. Pain in the pubic area in athletes can be vague and due to many causes. Furthermore, coexisting adductor tendinopathy can be present. Imaging alone is not useful either, as low-grade stress changes in the pubic bone are not uncommon in asymptomatic individuals. Therefore, the combination of relevant clinical history, examination and suggestive imaging findings of active stress changes, metaphyseal widening, separation or avulsion is required to make the diagnosis. Physical findings include tenderness over the symphysis pubis and proximal adductor origin, pain with adductor stretching and resisted hip adduction.

Some authors (Sailly et al. 2015) believe that CT provides the best depiction of the symphysis pubis both on axial and coronal views, allowing assessment of stress-related signs such as unilateral physeal plate widening, asymmetric irregularities and subchondral cysts. Avulsion fractures can also be seen clearly on CT (Fig. 13). However due to the radiation dose in this young age group, the use of CT is restricted for equivocal cases with non-conclusive MRI findings.

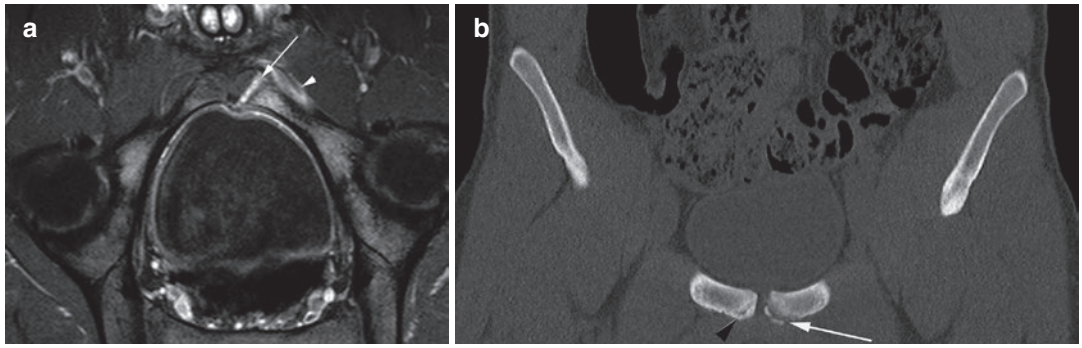

Fig. 13 (**a**, **b**) Apophyseal injury. (**a**) Axial oblique T2FS MR image and (**b**) coronal reformatted CT image of a 16-year-old soccer player with severe left-sided pain show severe left pubic body and ramus bone marrow oedema with adjacent soft-tissue oedema (small white arrowhead MRI). The apophyseal junction is ill defined and widened (large arrow, CT) and of high signal (small arrow, MRI). (Reproduced with permission from Hardi and Robinson 2019)

MRI is the best modality to examine the symphysis pubis. It can demonstrate widening of the physeal plate with hyperintensity on fluid-sensitive sequences, which could be diffuse or focal, unilateral or bilateral. Subchondral marrow oedema along the metaphyseal side can also be seen (Fig. 13). When there is physeal separation, a partial or complete thin longitudinal hyperintense line along the physeal plate is seen in keeping with non-displacement. Chronic avulsions on the other hand can show remodelling changes with aggressive appearance on imaging like lysis and rarefaction and can therefore be confused with infection or a neoplastic process (Stevens et al. 1999).

4.4.1.3 Management

Due to the relative rarity of pelvic apophyseal fractures in general, and pubic apophyseal fractures in particular, evidence-based guidelines on best treatment do not exist (Sailly et al. 2015); conservative antalgic management was followed successfully without any early recurrence, based on reduction of the mechanical loading on the adductor muscles.

4.4.2 Pubic Stress Fractures

A stress fracture is a fatigue fracture of bone when exposed to repetitive stress, which is not sufficient to cause a fracture in a single loading (Vanhoenacker 2021).

Fig. 14 Right pubic body stress fracture. Axial oblique T2FS MR image shows severe right pubic body with small intrasubstance trabecular fracture (arrow). Note that the left pubic body has no bone marrow oedema

Pelvic stress fractures are rare, representing 1.6–7.1% of all stress fractures (Behrens et al. 2013). Common sites for injury include sacrum, inferior pubic ramus and femoral neck (Liong and Whitehouse 2012). A rare fracture of the iliac bone has been described (Vitale et al. 2019). Pubic rami fractures can cause pain in the inguinal, perineal and adductor regions.

MRI is the gold standard for the diagnosis of stress fractures. On T1, a low-to-intermediate signal intensity fracture line can be seen. Along the fracture line, bone marrow oedema shows on T2 sequences as high signal (Fig. 14). MRI severity grading is described in Table 1.

Table 1 MR grading of stress fractures (Arendt and Griffiths 1997)

Grade of injury	MRI findings
I	STIR positive
II	STIR and T2-weighted positive
III	T1- and T2-weighted positive without a fracture line
IV	T1- and T2-weighted positive with a fracture line

4.5 Management and Prevention of Acute Groin Injuries

Multiple studies have evaluated the efficacy of different treatment strategies for groin injuries. The majority of these studies investigated long-standing groin pain and very little information is known about acute groin injuries.

A systematic review examined the available best evidence on the treatment of groin pain in athletes (Serner et al. 2015b). After exclusions, 72 studies were reviewed. Only 4 (6%) of these studies were of high quality and were examined in detail. In these studies, there were multiple treatment strategies with no strong evidence to support any particular strategy.

Serner et al. (2019) have proposed strategies to prevent adductor muscle injuries. One of these is the adoption of eccentric training which is believed to cause remodelling to the extracellular matrix and addition of sarcomeres in series within the muscle. This leads to the increase of muscle fascicle length, and shift in the angle of peak torque to longer muscle lengths resulting in a reduction in total passive tension.

A second strategy is to focus on strengthening the myotendinous junction of the adductor longus as this is the commonest site of injury. Animal models showed that high-intensity load increases branching at the myotendinous junction with better force distribution capacity in high-load exercises.

The role of the synergistic muscle groups around the adductor longus muscle has also been found to play a part in injury mechanism by reducing the load on the latter. These muscle groups include the anterior and posterior chain muscles assisting in the open- and closed-chain movements, respectively. Among the many synergistic groups are the hip flexors, hip extensors, knee extensors, trunk rotators and trunk lateral flexors.

5 Long-Standing Groin Pain

5.1 Overview

The complex anatomy, overlapping similar clinical presentations as well as the varied terminology used by radiologists and clinicians, has often led to diagnostic confusion around the common presentation of long-standing groin pain. Some of the terms used previously include sports hernia, sportsman's hernia, pubalgia, Gilmore's groin, adductor dysfunction and osteitis pubis (Omar et al. 2008; Weir et al. 2017).

Unfortunately, terminology for radiological signs can also be confusing and overlapping (Weir et al. 2017).

To streamline and standardise the terminology related to groin pain, an expert panel termed the 2014 Doha consensus produced recommendations that long-standing (non-acute) athletic groin pain should be clinically categorised into the following (Weir et al. 2015):

1. Adductor related
2. Pubic related
3. Inguinal related
4. Iliopsoas related
5. Other including hip related (Mascarenhas et al. 2020)

Long-standing groin pain is widely thought to propagate after an initial low-grade injury which alters the complex biomechanical stresses on the pelvis (Madani and Robinson 2019). The literature shows that the most common imaging findings are abnormalities in the pubic bone marrow, adductor/rectus aponeurosis and pubic symphysis capsular attachment sites, and therefore we will focus on these areas.

5.2 Adductor-Related Groin Pain

The most common clinical cause of groin injury found in larger series involves the adductor longus muscle (Koulouris 2008).

5.2.1 Pathophysiology

As described, the rectus abdominis-adductor longus aponeurosis is key to the biomechanics of the pubic symphysis (Koulouris 2008). The two muscles are antagonists to each other; contraction of the rectus abdominis and pyramidalis muscles places a posterior and superior force on the pubis and elevates the pubic region. In contrast, the adductor longus muscle has an anterior-inferior force vector (Omar et al. 2008).

Any disorder of either the common adductor-rectus abdominis origin or the pubic symphysis predisposes the other to failure. More commonly, the adductor longus fails and this leads to an increased load on the rectus abdominis muscle, which is smaller. Subsequently when both the adductor longus and rectus abdominis fail, the pubic symphysis can become relatively unbalanced (Koulouris 2008).

Failure of the common adductor-rectus abdominis aponeurosis can also disrupt the attachment of the inguinal canal posterior wall onto the anterior rectus sheath, resulting in posterior inguinal wall deficiency and rarely a direct inguinal hernia (Koulouris 2008; Robinson et al. 2011).

The most commonly injured area of the adductor longus is the proximal tendon myotendinous junction. Studies using cadaveric dissection have shown that the posterior part of the proximal myotendinous junction is less developed than the anterior part, and posteriorly the muscle attaches directly to bone and capsule (Omar et al. 2008).

5.2.2 Clinical Findings

As described by the 2014 Doha consensus, adductor tenderness (medial thigh) and pain on passive adductor stretching or resisted adduction testing should be elicited on examination (Weir et al. 2015; Madani and Robinson 2019).

5.2.3 Imaging Findings

Many described imaging findings in adductor- and pubic-related groin pain overlap.

A systematic review by Branci et al. found that the most commonly identified imaging findings in adductor and symphyseal groin pain are pathological changes at the adductor muscle origin, presence of a 'secondary cleft' sign, degenerative changes at or around the pubic symphysis joint and pubic bone marrow oedema. However other studies have shown that a number of these findings can occur in asymptomatic athletes and in the right clinical context are incidental. Adductor longus tendon thickening and 'degenerative changes' in particular are non-specific. We have simplified and combined the findings as there is much overlap:

Imaging features of long-standing adductor-related groin pain:

1. Pathological changes at the common adductor-capsule-rectus abdominis aponeurosis (including features described radiologically as 'secondary cleft' sign, PLAC, plate, enthesis and aponeurotic injuries)
2. Pubic bone marrow oedema

5.2.3.1 Pathological Changes at the Common Adductor-Capsule-Rectus Abdominis Aponeurosis

The adductor origin does not just involve the tendon but its junction with symphysis pubis, joint capsule and aponeurosis of the other converging soft-tissue structures (e.g. pyramidalis, rectus abdominis and inguinal canals). Tendinopathy is poorly demonstrated on ultrasound by a hypoechoic and thickened tendon. It is much better visualised on MRI by high signal at the adductor enthesis. Partial tears will be identified by focal anechoic areas on ultrasound and by focal high signal on MRI. Full-thickness tears may be diagnosed if tendon/muscle retraction is identified but are rare in long-standing pain. Enhancement/oedema of the adductor enthesis and abnormal anterior pubis has been shown to correlate with athlete's symptoms (Koulouris 2008; Robinson et al. 2004).

The physiological cleft in the symphysis pubis is referred to as the primary cleft. Brennan et al. first described the 'secondary cleft' as a fluoroscopy finding with a contrast-outlined cleft

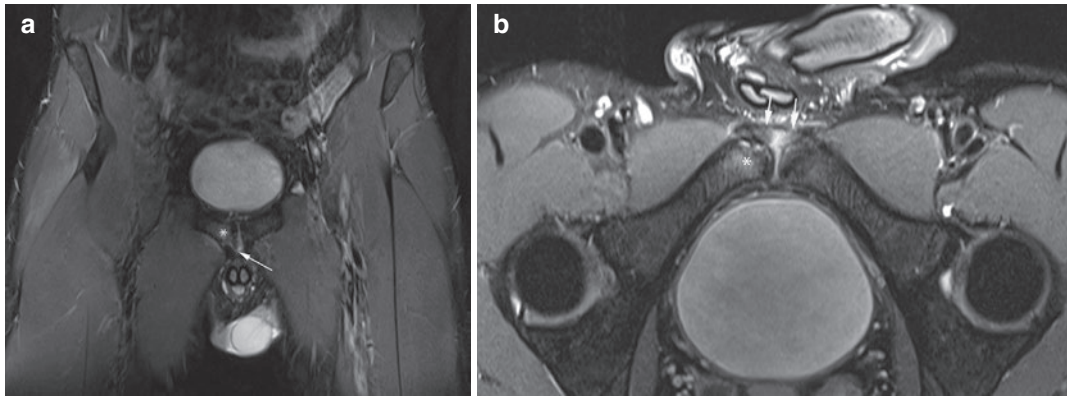

Fig. 15 (**a**, **b**) Long-standing right groin pain. (**a**) Coronal T2w FS and (**b**) axial oblique PDw MR images show moderate right pubic bone marrow oedema (*) and partial capsule/aponeurosis tear with moderate oedema (arrow) which extends across the anterior capsule to the left side on the axial oblique image (arrows)

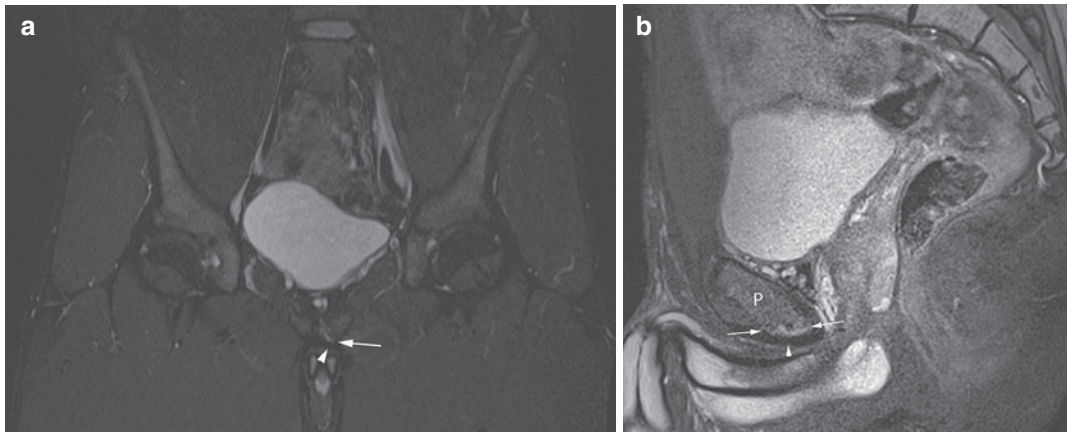

Fig. 16 (**a**, **b**) Long-standing left groin pain. (**a**) Coronal T2w FS and (**b**) axial oblique PDw MR images show no pubic bone marrow oedema and low-grade partial capsule/aponeurosis tear with oedema (arrow) between the pubic cortex (P) and low-signal aponeurosis of adductor longus and gracilis (arrowheads)

extending from the primary cleft into the adductor enthesis. The same finding is identified on MRI as linear T2 high signal adjacent to the pubic body, best seen on coronal sequences (Figs. 15, 16 and 17). This high signal is due to tearing of the unilateral rectus abdominis/adductor aponeurosis capsular attachment. It is thought to occur because of chronic distraction forces on the pubic rami and on the rectus abdominis/adductor longus aponeurosis (Brennan et al. 2005; Cunningham et al. 2007). Tearing or oedema at this same junctional area has been described as PLAC, plate, enthesis and aponeurotic injuries/defects and highlights the need for a common terminology (Figs. 16, 17 and 18) (Shortt et al. 2008; Schilders et al. 2007; Weir et al. 2017).

5.2.3.2 Pubic Bone Marrow Oedema

Pubic marrow oedema and degenerative changes have been demonstrated in both clinical adductor- and pubic-related groin pain and it is therefore not a completely reliable localising MRI sign (Chopra and Robinson 2016; Branci et al. 2015a). Pubic marrow oedema can also be frequently seen in asymptomatic elite athletes (Fig. 11) (Robinson et al. 2016). This finding, as well as apparent tearing of the rectus abdominis/adductor longus aponeurosis (Fig. 11) and persistent adjacent soft-tissue oedema, can also be seen

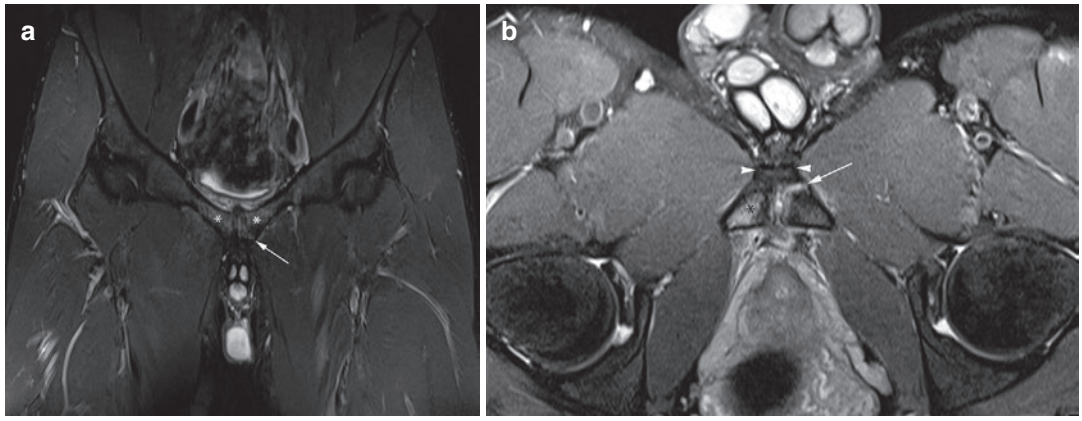

Fig. 17 (**a**, **b**) Bilateral long-standing groin pain (left > right). (**a**) Coronal T2w FS shows moderate bilateral pubic bone marrow oedema (white asterisk) and low-grade adductor capsule/aponeurosis oedema (arrow). (**b**) Axial oblique PDw MR image at an inferior level shows more marked right pubic bone marrow oedema (black asterisk), low-signal intact gracilis origin/aponeurosis (arrowheads) but marked oedema (arrow) on the left at the junction with the left pubic cortex with loss of cortical definition

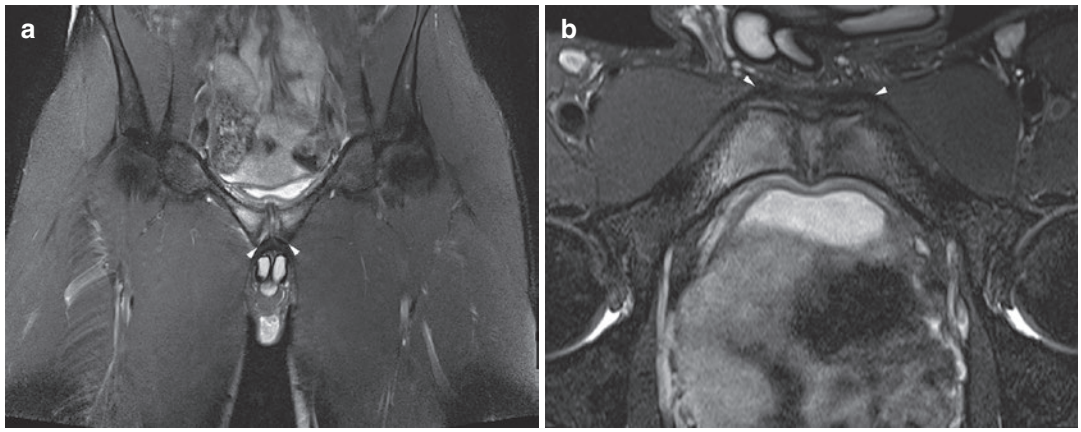

Fig. 18 (**a**, **b**) Bilateral long-standing groin pain (right > left). (**a**) Coronal T2w FS and (**b**) axial oblique PDw MR images show marked bilateral pubic bone marrow oedema (right > left) and low-grade oedema between the pubic cortices and low-signal aponeurosis of adductor longus and gracilis (arrowheads)

in post-surgical patients which may mimic true pathology. Therefore, careful correlation with the history and examination has to be undertaken prior to coming to a diagnosis with implications for treatment.

5.3 Pubic-Related Groin Pain

5.3.1 Pathophysiology

Particularly in sports in which there are repeated torsional shearing forces, the pubic symphysis is susceptible to overuse injury and degeneration (Chopra and Robinson 2016). The term 'osteitis pubis' has been phased out of use in recent times as it is a purely descriptive term which can be due to many varied causes.

5.3.2 Clinical Findings

The 2014 Doha consensus agreed that there should be local tenderness of the pubic symphysis and the immediately adjacent bone. The group felt that there was no particular resistance test that specifically provoked symptoms related to pubic-related groin pain that could be used in conjunction with palpation (Weir et al. 2015).

5.3.3 Imaging Findings

Ultrasound has limited use because only the anterior surfaces of the pubic joint are visualised, and these can have normal physiological or degenerative remodelling (Fig. 1) (Madani and Robinson 2019; Kunduracioglu et al. 2007).

Pubic bone oedema is thought to be due to mechanical overload of the pubic symphysis. As mentioned, the clinical symptoms should correlate as mild-to-moderate pubic bone oedema can be seen in non-symptomatic athletes who undergo repetitive loading of this area in training (Figs. 18 and 19). Studies have shown that increased/more severe degrees of marrow oedema correlate with increased symptoms (Figs. 18 and 19) (Verrall et al. 2001). Stress fractures should be considered and excluded when bone marrow oedema is severe and predominantly unilateral (Fig. 14). In symptomatic adolescent elite athletes apophyseal injury should be considered (Fig. 13) (Sailly et al. 2015) (see "Acute Injury" Sect. 4.4).

5.4 Inguinal Related Groin Pain

5.4.1 Pathophysiology

There are multiple confusing clinical terms and syndromes described for inguinal pain. Koulouris describes both anterior and posterior acquired inguinal canal functional weakness or 'deficiency' which occurs in around 15% of athletes with groin pain (Koulouris 2008). The Manchester

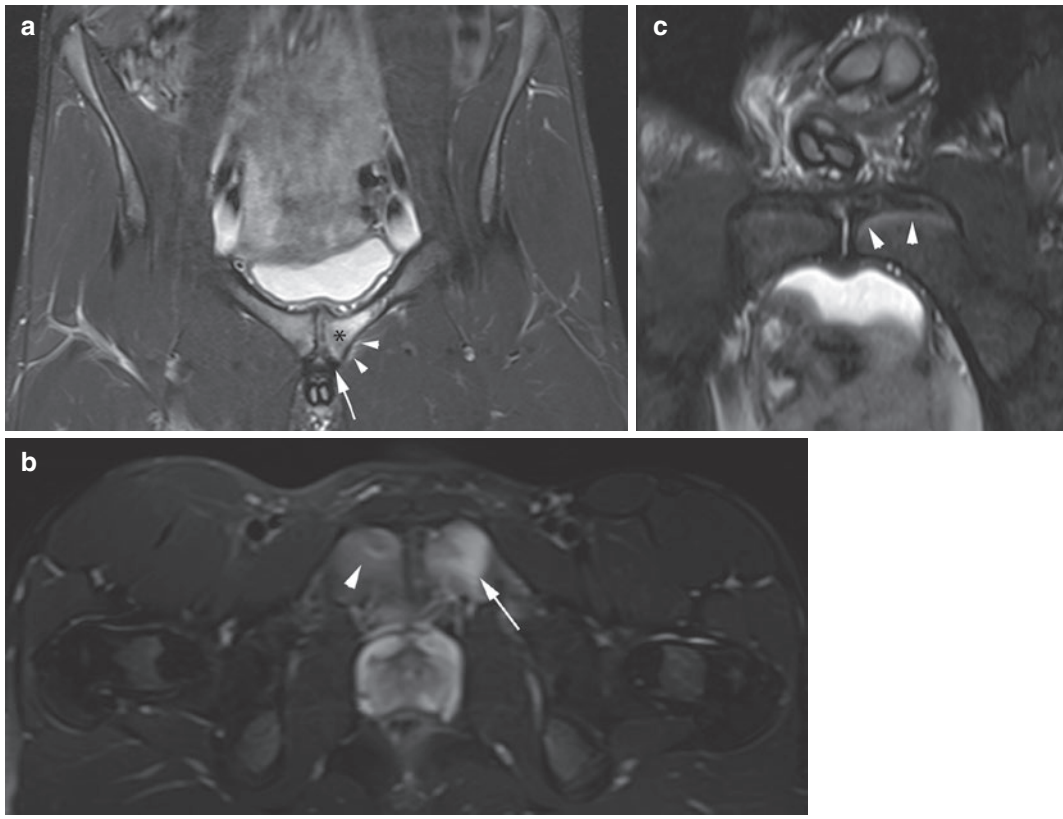

Fig. 19 (**a**–**c**) Pubic bone marrow oedema. (**a**) 25-Year-old professional soccer player with left-sided symptoms. Coronal T2FS MR image shows marked left pubic oedema (*), intact capsule/aponeurosis (arrow) and minimal soft-tissue oedema (arrowheads). (**b**) 18-Year-old professional soccer player with bilateral symptoms. Axial T2FS MR image shows moderate-to-severe left pubic oedema (arrow) and mild-to-moderate right pubic oedema (arrowhead). (**c**) 17-Year-old professional soccer player with no symptoms. Axial oblique T2FS MR image shows mild left subchondral pubis oedema (arrowheads) and normal right pubis. (Reproduced with permission from Hardi and Robinson 2019)

Consensus Conference expert panel coined the term 'inguinal disruption' to describe this 'pre-hernial' entity (Sheen et al. 2014).

5.4.1.1 Anterior Inguinal Wall Deficiency

This is a result of degeneration and partial tearing of the external oblique aponeurosis, leading to dehiscence between the inguinal ligament and causing superficial inguinal ring dilatation. Tenderness is elicited at the superficial inguinal ring, and pain is reproduced when kicking, sprinting, externally rotating the hip and increasing intra-abdominal pressure.

Positive diagnostic imaging findings are rarely seen, and therefore anterior inguinal wall deficiency is a clinical diagnosis and a radiologic diagnosis of exclusion (Koulouris 2008; Chopra and Robinson 2016).

5.4.1.2 Posterior Inguinal Wall Deficiency

This is a result of degeneration and weakness of the transversus abdominis and internal oblique muscles. Medially, split tears just lateral to the rectus abdominis muscle occur, and further micro-injury and poor healing cause the posterior inguinal wall to weaken. This can cause mass effect on the spermatic cord during straining. Subsequently, this can lead to a direct inguinal hernia, but actual herniation is rare in athletes. Rectus abdominis abnormalities are often seen in association with posterior inguinal wall deficiency as the posterior inguinal wall attaches onto the anterior sheath of the rectus abdominis muscle. This can be assessed by dynamic ultrasound as described below.

5.4.2 Clinical Findings

The Doha 2014 consensus agreed that inguinal related groin pain could be identified if the pain was located in the inguinal canal region and there was tenderness of the inguinal canal elicited. No palpable inguinal hernia should be present. The group agreed that inguinal related groin pain is more likely if the pain is aggravated with resistance testing of the abdominal muscles or on Valsalva/cough/sneeze (Weir et al. 2015).

5.4.3 Imaging Findings

Imaging in this patient group is controversial as studies have shown no reproducible results for certain clinical or imaging findings. In theory ultrasound should be the best modality to dynamically visualise the inguinal and femoral canals. As discussed, true femoral or inguinal hernias are rare in athletes, and it is posterior wall deficiency that is more pertinent to identify. This is demonstrated by posterior inguinal wall excessive movement, or laxity which correlates with the side of symptoms and is asymmetrical with the opposite side. However, these findings remain non-specific as they have been found in asymptomatic athletes, necessitating thorough clinical assessment (Sheen et al. 2014; Robinson et al. 2016).

MRI has less of a role in imaging for inguinal canal-related pain and is used to assess the symphysis pubis and the common adductor-capsule-rectus abdominis.

5.5 Iliopsoas-Related Groin Pain

This is the least common cause of groin pain. Chronic injury related to the iliopsoas is most likely to occur in sports in which there is repeated hip flexion and external rotation of the thigh (Chopra and Robinson 2016).

5.5.1 Clinical Findings

The 2014 Doha consensus agreed that iliopsoas-related groin pain is more likely if there is pain on resisted hip flexion and/or pain on stretching the hip flexors (Weir et al. 2015).

5.5.2 Imaging Findings

Ultrasound and MRI both provide information about the iliopsoas tendon and bursa.

Iliopsoas bursitis, due to overuse and friction of the iliopsoas tendon as it slides over the iliopectineal eminence of the pubis, can be identified as a well-defined, fluid-filled acute bursa or thick-walled complex chronic bursa (Fig. 20). This may or may not be in continuation with the joint space (Wunderbaldinger et al. 2002). Ultrasound

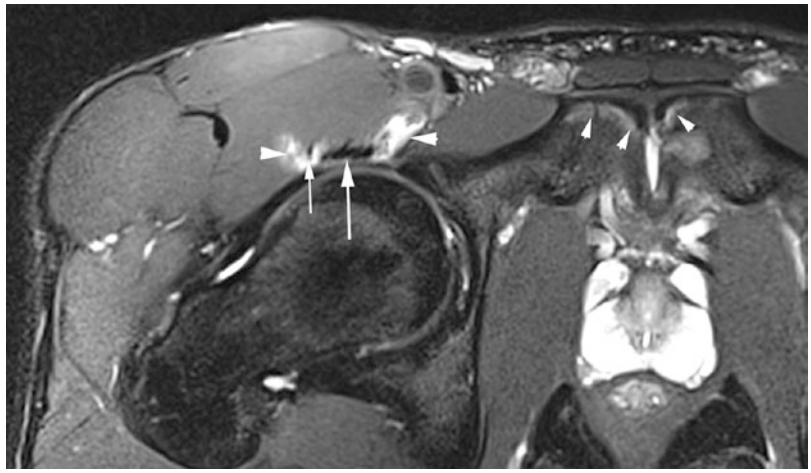

Fig. 20 Iliopsoas bursitis. 23-Year-old soccer player with right-sided pain. Axial T2FS MR image shows marked oedema and bursitis (arrowheads) surrounding both the psoas (large arrow) and iliacus (small arrow) components of the iliopsoas tendon anterior to a normal hip joint. Note the normal pubic apophyses (small white arrowheads). (Reproduced with permission from Hardi and Robinson 2019)

can also assess for iliopsoas snapping tendon (Chopra and Robinson 2016).

5.6 Overview of Treatment of Long-Standing Groin Pain

Surgery was traditionally the first-line treatment for athletes with long-standing groin pain. Research has now shown that a dedicated multidisciplinary approach with rehabilitation, anti-inflammatory treatment and physiotherapy should be the focus of management (Sheen et al. 2014; Elattar et al. 2016; Hölmich et al. 1999).

Ultrasound-guided injections of local anaesthetic, steroid or PRP into the adductor origin and pubic symphysis can provide short- to mid-term symptom relief, which may allow more effective rehabilitation (Schilders et al. 2009).

5.6.1 Adductor Strengthening in Groin Injury Prevention Programme

Adductor injures are the major part of the overall groin injuries, accounting for 69% (Hölmich 2007), and the adductor longus is injured in 90% of these cases (Werner et al. 2009; Harøy et al. 2017a).

Studies have found that reduced strength of hip adductors is an important modifiable risk factor for subsequent groin injury (Engebretsen et al. 2010). Players with groin pain demonstrated a reduced eccentric strength of the hip adductors by about 20% (Thorborg et al. 2014). Previous groin injuries with poor rehabilitation are found to be a risk factor for further injuries (Arnason et al. 2004).

Various hip adductor exercises have been examined in the literature. The Copenhagen Adduction (CA) exercise has been shown to contribute to high activation of the adductor longus muscle (Serner et al. 2014) and eccentric adductor strength gains (Harøy et al. 2017b). An 8-week intensive CA programme resulted in a 36% eccentric hip adduction strength (Ishøi et al. 2016), compared to 8% increase for a less intensive 8-week programme (Harøy et al. 2017b). It is possible that a higher intensity protocol would further reduce groin injury risk but this needs further exploration.

Based on the above, CA or the modified CA programme is potentially classed among the best exercises for the prevention of adductor-related groin injuries in football.

6 Summary

Athletic groin injury can be a common yet challenging clinical entity to diagnose given the similar clinical presentations, complex intricate anatomy and confusing terminology used to describe this entity. Imaging strategies evaluate the symphysis pubis and surrounding rectus abdominis-adductor longus aponeurosis focusing on oedema and tearing. However milder or isolated changes in these areas can be seen in asymptomatic athletes normally. Imaging findings appear to be more specific when severe and involving both bone and soft tissue structures.

Things to Remember

1. Groin injuries are the commonest cause of acute and chronic injuries in a wide range of sports, especially those involving kicking and sudden changes of direction. Great diagnostic difficulties exist reflecting the fact that previous clinical causes of groin pain have used confusing terminology, possibly reflecting clinical prejudice.
2. In imaging terms MRI is the most effective tool being sensitive to bone and soft-tissue oedema involved in acute and long-standing injury. However milder bone and soft-tissue oedema are a common finding in asymptomatic athletes due to chronic stress or previous healing following resolution of symptoms.
3. Acute soft-tissue injury typically involves the adductor longus tendon and myotendinous junctions.
4. For more long-standing groin pain the concept of an anatomical and functional relationship between the rectus abdominis-adductor longus aponeurosis and the symphysis pubis and its capsule provides a unifying concept for groin injuries in athletes. The inguinal ligament is inseparable from the superolateral attachment of the aponeurosis; however positive imaging findings are typically confined to the symphysis pubis and aponeurosis with no reliable primary imaging abnormality of the inguinal canal itself.

References

Arendt EA, Griffiths HJ (1997) The use of MR imaging in the assessment and clinical management of stress reactions of bone in high-performance athletes. Clin Sports Med 16:291–306

Arnason A, Sigurdsson SB, Gudmundsson A et al (2004) Risk factors for injuries in football. Am J Sports Med 32:5–16

Behrens SB, Deren ME, Matson A et al (2013) Stress fractures of the pelvis and legs in athletes: a review. Sports Health 5:165–174

Branci S, Robinson P (2014) Imaging in long-standing groin pain in athletes. Aspetar Sports Med J 3:316–324

Branci S, Thorborg K, Bech BH et al (2015a) MRI findings in soccer players with long-standing adductor-related groin pain and asymptomatic controls. Br J Sports Med 49:681

Branci S, Thorborg K, Bech BH et al (2015b) The Copenhagen standardised MRI protocol to assess the pubic symphysis and adductor regions of athletes: outline and intratester and intertester reliability. Br J Sports Med 49:692

Brennan D, O'Connell MJ, Ryan M et al (2005) Secondary cleft sign as a marker of injury in athletes with groin pain: MR image appearance and interpretation. Radiology 235:162–167

Calderazzi F, Nosenzo A, Galavotti C et al (2018) Apophyseal avulsion fractures of the pelvis. A review. Acta Biomed 89:470–476

Chan O, Del Buono A, Best TM, Maffulli N (2012) Acute muscle strain injuries: a proposed new classification system. Knee Surg Sports Traumatol Arthrosc 20:2356–2362

Chopra A, Robinson P (2016) Imaging athletic groin pain. Radiol Clin N Am 54(5):865–873

Cunningham PM, Brennan D, O'Connell M et al (2007) Patterns of bone and soft-tissue injury at the symphysis pubis in soccer players: observations at MRI. AJR Am J Roentgenol 188:291–296

Ekstrand J, Hägglund M, Waldén M (2011) Epidemiology of muscle injuries in professional football (soccer). Am J Sports Med 39:1226–1232

Ekstrand J, Healy JC, Waldén M et al (2012) Hamstring muscle injuries in professional football: the correlation of MRI findings with return to play. Br J Sports Med 46:112–117

Elattar O, Choi H, Dills VD, Busconi B (2016) Groin injuries (athletic pubalgia) and return to play. Sports Health 8:313–323

Engebretsen AH, Myklebust G, Holme I et al (2010) Intrinsic risk factors for groin injuries among male soccer players: a prospective cohort study. Am J Sports Med 38:2051–2057

Giza E, Mithöfer K, Farrell L et al (2005) Injuries in women's professional soccer. Br J Sports Med 39:212–216

Guillin R, Cardinal É, Bureau NJ (2009) Sonographic anatomy and dynamic study of the normal iliopsoas musculotendinous junction. Eur Radiol 19:995–1001

Hardi M, Robinson P (2019) Top-Ten Tips for Imaging Groin Injury in Athletes. Semin Musculoskelet Radiol 23(4):361–75.

Harøy J, Clarsen B, Thorborg K et al (2017a) Groin problems in male soccer players are more common than previously reported. Am J Sports Med 45: 1304–1308

Harøy J, Thorborg K, Serner A et al (2017b) Including the Copenhagen adduction exercise in the FIFA 11+ provides missing eccentric hip adduction strength effect in male soccer players: a randomized controlled trial. Am J Sports Med 45:3052–3059

Hölmich P (2007) Long-standing groin pain in sports people falls into three primary patterns, a 'clinical entity' approach: a prospective study of 207 patients. Br J Sports Med 41:247–252

Hölmich P, Uhrskou P, Ulnits L et al (1999) Effectiveness of active physical training as treatment for long-standing adductor-related groin pain in athletes: randomised trial. Lancet 353:439–443

Ishøi L, Sørensen CN, Kaae NM et al (2016) Large eccentric strength increase using the Copenhagen Adduction exercise in football: a randomized controlled trial. Scand J Med Sci Sports 26:1334–1342

Kiel J, Kaiser K (2018) Adductor strain. StatPearls Publishing. Available via DIALOG. https://www.ncbi.nlm.nih.gov/books/NBK493166/. Accessed 19 Jan 2020

Kluin J, Den Hoed PT, Van Linschoten R et al (2004) Endoscopic evaluation and treatment of groin pain in the athlete. Am J Sports Med 32:944–949

Koulouris G (2008) Imaging review of groin pain in elite athletes: an anatomic approach to imaging findings. AJR Am J Roentgenol 191:962–972

Kunduracioglu B, Yilmaz C, Yorubulut M, Kudas S (2007) Magnetic resonance findings of osteitis pubis. J Magn Reson Imaging 25:535–539

Lee SC, Endo Y, Potter HG (2017) Imaging of groin pain: magnetic resonance and ultrasound imaging features. Sports Health 9:428–435

Liong SY, Whitehouse RW (2012) Lower extremity and pelvic stress fractures in athletes. Br J Radiol 85:1148–1156

Mascarenhas VV, Castro MO, Diana Afonso P (2020) Hip, pelvis and sacro-iliac joints. Med Radiol. https://doi.org/10.1007/174_2020_256

Madani H, Robinson P (2019) Top-ten tips for imaging groin injury in athletes. Semin Musculoskelet Radiol 23:361–375

Meindl RS, Lovejoy CO, Mensforth RP, Walker RA (1985) A revised method of age determination using the os pubis, with a review and tests of accuracy of other current methods of pubic symphyseal aging. Am J Phys Anthropol 68:29–45

Morelli V, Weaver V (2005) Groin injuries and groin pain in athletes: part 1. Prim Care 32:163–183

Omar IM, Zoga AC, Kavanagh EC et al (2008) Athletic pubalgia and "Sports Hernia": optimal MR imaging technique and findings. Radiographics 28:1415–1438

Peetrons P (2002) Ultrasound of muscles. Eur Radiol 12:35–43

Pogliacomi F, Calderazzi F, Paterlini M, Ceccarelli F (2014) Surgical treatment of anterior iliac spines fractures: our experience. Acta Biomed 85:52–58

Pollock N, James S, Lee J, Chakraverty R (2014) British athletics muscle injury classification: a new grading system. Br J Sports Med 48:1347–1351

Robinson P, Barron D, Parsons W et al (2004) Adductor-related groin pain in athletes: correlation of MR imaging with clinical findings. Skelet Radiol 33:451–457

Robinson P, Hensor E, Lansdown M et al (2006) Inguinofemoral hernia: accuracy of sonography in patients with indeterminate clinical features. AJR Am J Roentgenol 187:1168–1178

Robinson P, Salehi F, Grainger A et al (2007) Cadaveric and MRI study of the musculotendinous contributions to the capsule of the symphysis pubis. AJR Am J Roentgenol 188:440–445

Robinson P, Bhat V, English B (2011) Imaging in the assessment and management of athletic pubalgia. Semin Musculoskelet Radiol 15:14–26

Robinson P, Grainger AJ, Hensor EMA (2016) Do MRI and ultrasound of the anterior pelvis correlate with, or predict, young football players' clinical findings? A 4-year prospective study of elite academy soccer players. Br J Sports Med 49:176–182

Sailly M, Whiteley R, Read JW (2015) Pubic apophysitis: a previously undescribed clinical entity of groin pain in athletes. Br J Sports Med 49:828–834

Schilders E, Bharam S, Golan E et al (2007) The pyramidalis-anterior pubic ligament-adductor longus complex (PLAC) and its role with adductor injuries: a new anatomical concept. Knee Surg Sports Traumatol Arthrosc 25:3969–3977

Schilders E, Talbot J, Robinson P (2009) Adductor-related groin pain in recreational athletes: role of the adductor enthesis, magnetic resonance imaging, and entheseal pubic cleft injections. J Bone Joint Surg Am 91:2455–2460

Sedaghati P, Alizadeh M, Shirzad E, Ardjmand A (2013) Review of sport-induced groin injuries. Trauma Mon 18:107–112

Serner A, Jakobsen MD, Andersen LL et al (2014) EMG evaluation of hip adduction exercises for soccer players: implications for exercise selection in prevention and treatment of groin injuries. Br J Sports Med 48:1108–11014

Serner A, Tol JL, Jomaah N et al (2015a) Diagnosis of acute groin injuries: a prospective study of 110 athletes. Am J Sports Med 43:1857–1864

Serner A, Van Eijck C, Beumer BR et al (2015b) Study quality on groin injury management remains low: a systematic review on treatment of groin pain in athletes. Br J Sports Med 49:813

Serner A, Weir A, Tol JL et al (2016) Can standardised clinical examination of athletes with acute groin injuries predict the presence and location of MRI findings? Br J Sports Med 50:1541–1547

Serner A, Weir A, Tol JL et al (2018a) Characteristics of acute groin injuries in the adductor muscles: a detailed MRI study in athletes. Scand J Med Sci Sports 28:667–676

Serner A, Weir A, Tol JL et al (2018b) Characteristics of acute groin injuries in the hip flexor muscles—a detailed MRI study in athletes. Scand J Med Sci Sports 28:677–685

Serner A, Mosler AB, Tol JL et al (2019) Mechanisms of acute adductor longus injuries in male football players: a systematic visual video analysis. Br J Sports Med 53:158–164

Sheen AJ, Stephenson BM, Lloyd DM et al (2014) "Treatment of the sportsman's groin": British Hernia Society's 2014 position statement based on the Manchester Consensus Conference. Br J Sports Med 48:1079–1087

Shortt CP, Zoga AC, Kavanagh EC, Meyers WC (2008) Anatomy, pathology, and MRI findings in the sports hernia. Semin Musculoskelet Radiol 12:54–61

Stevens MA, El-Khoury G, KATHOL MH et al (1999) Imaging features of avulsion injuries. Radiographics 19:655–672

Tansey RJ, Benjamin-Laing H, Jassim S et al (2015) Successful return to high-level sports following early surgical repair of combined adductor complex and rectus abdominis avulsion. Bone Joint J 97-B:1488–1492

Thorborg K, Branci S, Nielsen MP et al (2014) Eccentric and isometric hip adduction strength in male soccer players with and without adductor-related groin pain: an assessor-blinded comparison. Orthop J Sports Med 2:2325967114521778

Tuite DJ, Finegan PJ, Saliaris AP et al (1998) Anatomy of the proximal musculotendinous junction of the adductor longus muscle. Knee Surg Sports Traumatol Arthrosc 6:134–137

Vanhoenacker FM (2021) Bone marrow edema in sports injuries/general concept. Med Radiol. https://doi.org/10.1007/174_2020_241

Vasileff WK, Nekhline M, Kolowich PA et al (2017) Inguinal hernia in athletes: role of dynamic ultrasound. Sports Health 9:414–421

Verrall GM, Slavotinek JP, Fon GT (2001) Incidence of pubic bone marrow oedema in Australian rules football players: relation to groin pain. Br J Sports Med 35:28–33

Vitale K, Smitaman E, Huang BK (2019) Medial iliac stress fractures in athletes: report of two rare cases: review of literature and clinical recommendations. Skelet Radiol 48:1119–1123

Waldén M, Hägglund M, Ekstrand J (2015) The epidemiology of groin injury in senior football: a systematic review of prospective studies. Br J Sports Med 49:792–797

Wangensteen A, Guermazi A, TOL JL et al (2018) New MRI muscle classification systems and associations with return to sport after acute hamstring injuries: a prospective study. Eur Radiol 28:3532–3541

Weir A, Brukner P, Delahunt E (2015) Doha agreement meeting on terminology and definitions in groin pain in athletes. Br J Sports Med 49:768–774

Weir A, Robinson P, Hogan B, Franklyn-Miller A (2017) MRI investigation for groin pain in athletes: is radiological terminology clarifying or confusing? Br J Sports Med 51:1185–1186

Werner J, Hägglund M, Waldén NM, Ekstrand J (2009) UEFA injury study: a prospective study of hip and groin injuries in professional football over seven consecutive seasons. Br J Sports Med 43:1036–1040

Wunderbaldinger P, Bremer C, Schellenberger E (2002) Imaging features of iliopsoas bursitis. Eur Radiol 12:409–415

Zajick D, Zoga A, Omar I, Meyers W (2008) Spectrum of MRI findings in clinical athletic pubalgia. Semin Musculoskelet Radiol 12:3–12

Hip, Pelvis and Sacro-Iliac Joints

V. V. Mascarenhas, M. O. Castro,
and P. Diana Afonso

Contents

V. V. Mascarenhas (✉) · P. D. Afonso
Imaging Center, MSK Imaging Unit (UIME),
Hospital da Luz Lisboa, Luz Saúde, Lisbon, Portugal
e-mail: mascarenhas.vasco@gmail.com;
p.diana.a@gmail.com

M. O. Castro
Radiology Department, Centro Hospitalar
Universitário do Algarve, Portimão, Portugal
e-mail: migkastro@yahoo.com

Abstract

Hip and groin pain in athletes is common and clinical presentation is often non-specific. Causal pathology represents a complex scenario in athletes, with improper diagnosis serving as a cause of delayed return to sports.

Radiologists play an essential role in guiding the work-up of athletes with hip pain. This chapter provides an overview on hip and pelvis anatomy and biomechanics and discusses strategies for imaging assessment. Magnetic resonance imaging (MRI) is often the modality of choice for evaluating many of the injuries observed, although preliminary evaluation with conventional radiography and use of other imaging modalities such as ultrasonography (US), computed tomography (CT) and bone scintigraphy may be supplementary or important in some situations.

With the main focus on MRI, the authors present abnormalities of the pelvis and hip joint and the surrounding soft tissues that can occur in athletes: intra- and extra-articular hip impingement syndromes, labral and cartilage disease, microinstability of the hip, bone and myotendinous injuries of the pelvis and sacroiliac dysfunction.

Muscle injuries, stress fractures, thigh splints and apophyseal injuries are particularly important to consider in young athletes and may be acute or related to chronic repetitive microtrauma. The authors highlight current concepts of femoroacetabular impinge-

Med Radiol Diagn Imaging (2020)
https://doi.org/10.1007/174_2020_256, © Springer Nature Switzerland AG
Published Online: 01 January 2021

ment (FAI), labral tears and cartilage abnormalities. Tear of the *ligamentum teres* is now recognized as a potential cause of hip pain and instability, best evaluated with MR arthrography (MRA).

Greater trochanteric pain syndrome encompasses a group of conditions leading to lateral hip pain, with US playing an increasingly important role for both evaluation and image-guided treatment. Snapping hip syndrome and sacroiliac joint pathology are also important considerations.

Innovation has been the catalyst for the transformation of hip imaging, as the arrival of new modalities and the widespread introduction of MRI resulted in a paradigm shift from bone morphology analysis to integrated soft tissue, joint and cartilage assessment. Understanding the pathophysiology through the visualization of osseous structures and detailed depiction of soft tissues has become part of routine imaging and has had a major impact on therapeutic decision-making.

1 Introduction

Imaging of the hip, pelvis and sacroiliac joints (SIJ) is presently in the spotlight, boosted by both new technical developments and novel clinical conditions discovered in the past decade, such as the recognition of femoroacetabular impingement syndrome (FAIS) as a cause of early-onset osteoarthritis (Ganz et al. 2003; Lynch et al. 2016).

Clinically, hip and groin pain lists in the top 6 most common athletic injuries (up to 23% of athletes during a 1-year period) (Jónasson et al. 2011), mainly affecting activities that involve accelerations/decelerations, rapid direction changes and kicking (Table 1). The most common hip/groin injuries in soccer players are adductor injuries (63%; not counting hamstring injuries), followed by hip flexor/iliopsoas injury (8%) (Werner et al. 2019). In professional soccer players, overuse hip injuries are up to three times more common compared with acute injuries (73% vs. 27%) (Agten et al. 2016). Intra-articular hip injuries in athletes are less frequent (6.2% in soccer and 5% in American football) (Makovicka et al. 2019; Werner et al. 2019; Cruz et al. 2019).

Hip and groin injuries constitute a considerable proportion of all time-loss injuries in men's professional football. Interestingly, athletes with hip pain typically consult a large number of different medical specialists, with time to return to sport (RTS) often being the main question asked by every stakeholder (Cruz and Mascarenhas 2018). Mean number of days lost before RTS in hip/groin injuries largely varies by injury type (Table 2). Although there was a promising slight

Table 1 Frequencies and most common sports-related hip/groin injuries in professional athletes by type of sport (as a percentage of all injuries)

Sports	Frequency of injuries affecting the hip/groin	Most common injury type in the hip/groin
Soccer (Ekstrand et al. 2011; Werner et al. 2019)	11–17%	Adductor (63%)/ hamstring injuries
American football(Makovicka et al. 2019)	3.1%	Adductor (38%)/ Hip flexor injury (28%)
Basketball (Zuckerman et al. 2018)	2.1–7.8%	Hamstring injury
Ice hockey (McKay et al. 2014)	4–13.1%	Muscle-tendon injury

Table 2 Days lost before return to sports per hip/groin injury (Werner et al. 2019)

Injury type	Mean no. of days lost
Adductor injury	14 (20)
Hip flexor/iliopsoas injury	11 (10)
Symphysitis/pelvic stress fracture	40 (34)
Chondral lesion	46 (53)
Labral tear	56 (61)
FAI	64 (60)
Fracture	99

Note: Numbers are mean days lost before full return to sports for soccer (Union of European Football Associations), with SD in parentheses
FAI femoroacetabular impingement

decreasing trend in the rates of hip and groin injury (as a category) and adductor-related injury (as a specific diagnosis), the injury burden at a consistent level over the last 15 years (Werner et al. 2019). Accordingly, imaging has a pivotal role in the athlete's clinical management.

Sports-related injuries mainly depend on (1) sex, (2) age, (3) type of sport and (4) activity level.

1. **Sex**: Men have a higher risk of hip/groin injury than women when playing the same sport (Orchard 2015). Additionally it has been reported that hip pathology is more common in white males with a family history of hip surgery (Cruz et al. 2019).
2. **Age**: Sports injuries in children differ by age diagnosis, type and body area. In children and adolescents, up to 24% of injuries affect the hip as opposed to only 5–6% in adults (Stracciolini et al. 2013). Older children sustain a greater proportion of overuse injuries.
3. **Type of sport:** An increased incidence of hip injuries in specific sports is reported, including soccer, basketball, martial arts and ice hockey. By category these most frequently occur in impingement sports, followed by contact sports, and cutting sports (Cruz et al. 2019) (Table 3).
4. **Activity level:** When compared with recreational athletes undergoing arthroscopic treatment for FAI, high-level athletes are more likely to be younger, male, and to undergo bilateral surgery. When high-level athletes are grouped by the mechanical demands placed on the hip by their sport, athletes participating in cutting sports are more likely to be younger than those in the other groups (Nawabi et al. 2014).

2 Aetiology, Diagnosis and Prognosis of Hip and Groin Pain

Aetiology*:* Hip pain is a common but non-specific symptom that has many aetiologies. These include multiple pathologies, most of which have been extensively studied (Blankenbaker and al 2006). Interestingly, with the development of newer imaging modalities several additional causes of hip pain have become apparent, namely FAIS, labral tears and snapping hip (Mascarenhas et al. 2016) (Table 4).

Table 3 Sports Categories for Athletes according to Nawabi et al. (Nawabi et al. 2014) and rates of hip/groin injury (per 100,000 Athletic Exposures)

Sport category	Impingement	Contact	Cutting	Flexibility	Asymmetric overhead	Endurance
Examples	• Ice hockey • Baseball • Crew/ rowing • Equestrian polo, water polo	• American football • Rugby • Wrestling	• Soccer • Basketball • Lacrosse • Field hockey	• Dance • Gymnastics • Yoga • Figure skating • Martial arts	• Tennis • Golf • Volleyball • Baseball • Softball • Field events: javelin, discus, hammer throw	• Track, cross-country, other running • Cycling • Swimming (not breaststroke)
Rate of injury per 100,000 AE	96.90	60.33	57.92	37.51	31.26	27.93

Data from National Collegiate Athletic Association (NCAA) athletes across 25 collegiate sports during the 2009/10 to 2013/14 academic years (Cruz et al. 2019)
AE Athletic exposure

Table 4 Differential diagnosis of hip and groin-related pain: an overview of possible causes of intra-articular and extra-articular causes

Intra-articular	Peri-articular	Mimickers
FAI **Instability** **Microinstability**	**Muscle and Tendon-related pathology** – Iliopsoas-related pathology – Iliotibial band pathology – *Rectus femoris* pathology – Gluteal pathology – Hamstring pathology	**Axial skeletal pathology** – Lumbar spine pathology – Sacroiliac joints pathology
Osteoarthritis	**Stress fracture** – Femoral neck or acetabulum – Pubic ramus	**Pubic-related pathology**
Non-FAI related – Chondrolabral injuries – Loose bodies – *Ligamentum teres* pathology – Capsular laxity	**Greater trochanteric pain syndrome** – Gluteus medius or minimus pathology – Trochanteric bursitis	**Neurological** disorders and nerve entrapment – Obturator – Ilioinguinal – Genitofemoral – Iliohypogastric
Developmental disorders – Acetabular dysplasia – Slipped capital femoral epiphysis – Perthes disease	**Apophysitis or avulsion fracture** – Anterior superior iliac spine – Anterior inferior iliac spine – Iliac crest – Ischial tuberosity – Lesser trochanter	**Hernia** – Femoral or inguinal – Posthernioplasty
Avascular necrosis and **Acute bone marrow oedema syndrome**	**Extra-articular impingement** – External/internal snapping hip – Trochanteric-pelvic impingement – Pectineo-foveal impingement – Ischiofemoral impingement – Subspine impingement	**Intra-abdominal/pelvic abnormality** – Gynaecological conditions – Prostatitis/urinary tract infections/kidney stone – Appendicitis/diverticulitis
Arthritis (autoimmune, reactive or infectious) and **synovial disorders** (PVNS, chondromatosis)	**Deep gluteal syndrome**	**Tumours** and pseudo tumours of the hip and pelvis

PVNS pigmented villonodular synovitis. *FAI* femoroacetabular impingement

A recent practical classification system (Weir et al. 2015) described three major subheadings of hip/groin pain in athletes: (1) Defined clinical entities for ***groin pain***: Adductor-related, iliopsoas-related, inguinal-related and pubic-related groin pain; (2) ***Hip-related*** groin pain and (3) ***other causes*** of groin pain in athletes.

Diagnosis: The complex anatomy of the hip/pelvis region and the high prevalence of "pathologic" findings in asymptomatic athletes are likely the main reasons why making a clear diagnosis is often challenging. Accordingly, a myriad of intra- and extra-articular lesions can contribute to symptoms. After a thorough clinical examination and close communication between radiologists/referring colleagues, the **imaging work-up** should: (1) begin with a **dedicated radiographic series**, including an anteroposterior (AP) view of the pelvis and views tailored to the region of interest (if appropriate); (2) **Comprehensive imaging** is often crucial to assess intra- and extra-articular disease (Mascarenhas et al. 2018a) as well as for treatment planning. Considering that several conditions can mimic and/or frequently coexist when assessing an athlete, if other potential causes are not considered, patients may fail to improve after conservative treatment or surgery (Tibor and Sekiya 2008; Krishnamoorthy et al. 2019a, b) (further discussed under Imaging Techniques).

Treatment: Although beyond the scope of this chapter, treatment strategies for hip and groin pain include conservative care/rehabilitation, surgery and post-surgery care. Each of these may

have a role in different injuries, type and level of activity, but there is little evidence to compare their effectiveness, namely for FAI (Griffin et al. 2018). This is best done in a shared decision-making process, supporting the individual athlete to make an informed decision on the best treatment option (Alonso-Coello et al. 2016).

Prognosis: Accurately predicting an individual's RTS using current strategies is challenging because of the complexity/heterogeneity of lesions. In many ways, sports physicians and radiologists still cannot satisfy these high expectations from an evidence-based point of view (Cruz and Mascarenhas 2018). In the setting of FAI and hip preservation surgery (HPS), there is emerging evidence on the prognostic value of age and hip intra-articular lesions detected on MRI, namely (1) femoral and acetabular subchondral cysts are associated with increased rates of clinical failure at short and long term (Krych et al. 2016; Hartigan et al. 2017), (2) cartilage damage exceeding 2 o'clock/60° on the acetabular clockface and (3) central acetabular osteophytes are poor prognostic factors and are associated with higher rates of clinical failure 10 years after HPS (Hanke et al. 2016).

3 Anatomy

3.1 Hip and Pelvis Morphology

Presently there is no detailed knowledge about the combined function of the pelvic/abdominal muscle girdle and the mobility of the hip, but there is a clear relationship between these two anatomical regions (Rivière et al. 2017a). The pelvic ring is formed by the 2 innominate bones and the sacrum, united by the SI joints posteriorly and the pubic symphysis anteriorly. Stability of this ring is provided mainly by the strong SI ligaments, sacrospinous and sacrotuberous ligaments. Classically, the hip has been described as one morphologically simple loading joint, although the recent description of some anatomical features has enriched this simplicity. The functional interpretation of anatomical structures by "layers", with specific and complementary function levels, more closely parallels clinical significance (Ranawat and Kelly 2005; Rivière et al. 2017a, b; Grammatopoulos et al. 2018).

The basic anatomy around the hip consists of the superficial surface anatomy (and palpable bony prominences) and deep bony, muscular and neurovascular anatomy. The anterior landmarks consist of the prominent anterior superior iliac spine (ASIS) and anterior inferior iliac spine (AIIS), which serve as insertion points for the *sartorius* and direct head of the *rectus femoris*, respectively. The greater trochanter (GT) and posterior superior iliac spine (PSIS) are also easily identifiable. They are important landmarks for clinical/imaging diagnosis and incision planning.

3.1.1 Structural Layer

This layer consists of the proximal femur, the acetabulum, the hyaline cartilage and the acetabular labrum. The hip is a diarthrodial joint and is defined by the constrained bony articulation of the proximal femur and acetabulum. Labrum and cartilage will be discussed in the appropriate sections.

Femur: The femoral head (FH) has a spherical shape in continuity with the femoral neck, which usually has a cylindrical shape flattened from front to back. Although this is the normal anatomy classically described, we now know that in up to 7–100% of humans there are variants of this morphology, with the presence of a non-spherical sector at the FHN junction (Anwander et al. 2018). Usually, the articular cartilage covers about 2/3 of the FH and presents a variable thickness (higher in its central region and in the loading zone). The *fovea capitis* is a small area devoid of cartilage, located slightly posterior and inferior to the centre of the FH cartilage (Fig. 1).

Acetabulum: The acetabular cavity has a concave hemispherical shape (Seldes et al. 2001) that results from the contributions of the 3 pelvic bones, the ilium, ischium and pubis. It is orientated approximately 45° caudally (abduction) and 15° anteriorly (anteversion) (Philippon et al. 2014). Its hemispherical shape covers 170° of the FH (Seldes et al. 2001; Philippon et al. 2014). The acetabular fossa (non-articular surface of the acetabulum, covered by synovia) is located in the inferior region of the acetabulum and is sur-

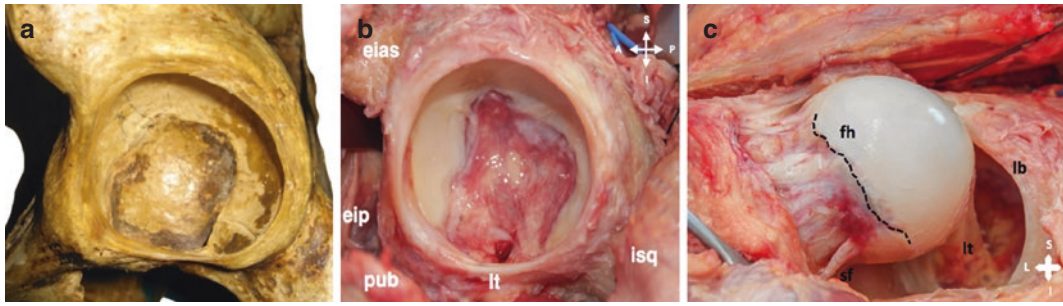

Fig. 1 (**a–c**) (**a**) Bony pelvis cadaveric specimen, representing the acetabulum anatomy. (**b**) Soft tissue cadaveric specimen of the acetabulum. *(eias)* anterosuperior iliac spine, *(eip)* eminence iliopectineus, *(pub)* pubis, *lt* transverse ligament, *isq* ischion. *S* superior, *I* inferior, *A* anterior, *P* posterior. Dissection photography of the hip. (**c**) Femoral head with the typical spherical shape of a *coxa rotunda* and the hyaline articular cartilage lining slightly lateral to the equatorial region and with an irregular border (dashed line). *fh* femoral head, *lb* labrum, *lt ligamentum teres*, *sf* synovial fold, *S* superior, *I* inferior, *M* medial, *L* lateral

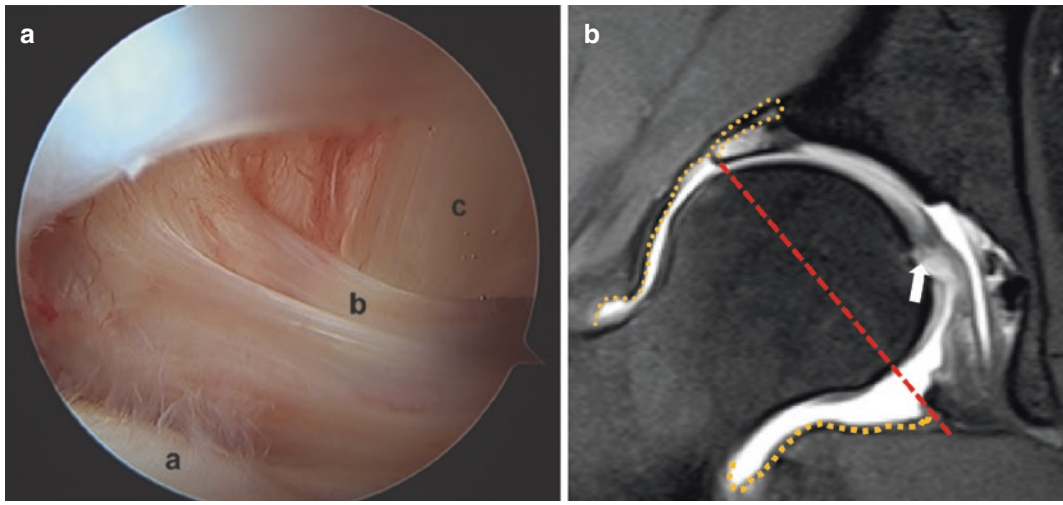

Fig. 2 (**a–b**) (**a**) Arthroscopic image of the peripheral compartment of a right hip with an articular communication with the iliopsoas tendon. The femoral head (**a**), the anterior capsule (**b**) and the iliopsoas tendon (**c**). (**b**) Arthrography magnetic resonance image of the hip, coronal proton-density with fat-sat. *Fovea capitis* with *ligamentum teres* insertions are shown (arrow). Dashed red line represents virtual separation between the peripheral and central compartments. Dashed orange curved line represents capsular contour

rounded by the horseshoe-shaped lunate articular surface. The transverse ligament limits the inferior margin of the fossa (Dienst 2005).

3.1.2 Capsulo-ligamentous Layer (Fig. 2)

The anatomical structure that most influences the peripheral space is the joint capsule. It is a thick and tense fibrous sleeve extending from the outer neck to the acetabular rim. The spiral orientation of the capsular ligaments provides a "screw" effect in full extension. Some portions of the capsule have an increased thickness or are reinforced. Namely, (1) the superolateral part is reinforced by the reflected **tendon of the *rectus femoris***, (2) the anterolateral part by the **iliofemoral ligament** (y-shaped ligament of Bigelow), (3) the anteromedial part by the **pubofemoral ligament**, (4) the posterior capsule by the **ischio-femoral ligament** (Ranawat and Kelly 2005) and (5) circumferentially by the ***zona orbicularis* (ZO)** or femoral arcuate ligament form-

ing a ring around the femoral head-neck (FHN) (a major hip stabilizer). The *iliopsoas bursa* is located beneath the myotendinous portion of the iliopsoas muscle, anterior to the hip joint capsule. It may directly communicate with the peripheral compartment in 15–20% of cases (clinical relevance: can increase the risk of fluid extravasation during hip arthroscopy) (Dienst 2005). *Ligamentum teres* (LT) will be discussed in the appropriate section.

3.1.3 Muscular Layer

The muscular attachments surrounding the hip and pelvis are extensive, with a total of 27 muscles crossing the hip joint. A detailed understanding of the muscular attachments and innervations is critical (Aprato et al. 2016). They can be broadly broken down by their main function (Ranawat and Kelly 2005; Dienst 2005):

1. **Primary flexors**: iliac, psoas, *iliocapsularis*, *pectineus*, *rectus femoris* (direct and indirect heads) and *sartorius*.
2. **Extensors**: *gluteus maximus*, *semimembranosus*, *semitendinosus*, *biceps femoris* (long and short heads) and *adductor magnus* (ischiocondyle part).
3. **Abductors**: *gluteus medius*, *gluteus minimus*, *tensor fascia lata* and iliotibial band.
4. **Adductors**: *adductor brevis*, *adductor longus*, *gracilis* and the anterior part of the *adductor magnus*.
5. **External rotators**: *piriformis*, *quadratus femoris*, *inferior gemellus*, *superior gemellus*, *obturator externus* and *obturator internus*.

3.1.4 Neuromechanical Layer

This is a theoretical concept that integrates multiple interlinked anatomical structures, physiological events and kinematic changes that depend on the proprioception and pain sensitivity of the periarticular structures. This layer is formed by the neurovascular structures, mechanoreceptors and nociceptors present in LT, capsule, labrum and tendons. On a broader view, this level refers to the principle of "reciprocal interaction" which explains the difficulty to set threshold values for morphologic parameters predisposing to impingement, with only extreme values being strongly predictive for the development of impingement or instability (Rivière et al. 2017a).

3.1.5 Vascular Anatomy of the Hip

Detailed knowledge of the vascularization of the proximal femur and iliac allowed the development of HPS techniques (Ganz et al. 2001). The primary vascular pathways are extensions from the internal and external iliac vessels. From the internal iliac system, the superior and inferior gluteal arteries and obturator artery supply most of the surrounding hip musculature (laterally and medially respectively) and periacetabular region (Kalhor et al. 2010). From the external iliac system, the medial and lateral femoral circumflex arteries anastomose around the proximal femur. The main blood supply to the femoral head arises from the medial circumflex femoral artery (Rego et al. 2017). The femoral, obturator and superior gluteal nerves all supply innervation to the hip (Fig. 3).

4 Imaging Techniques

Radiographs (CR) remain the standard imaging modality to assess the hip and pelvis despite US and modern three-dimensional CT, or MRI being increasingly used. For most clinical scenarios US, MRI and MRA remain the decisive imaging tools in sports and prearthritic patients, although their application mainly depends on the specific clinical indication. In this setting, MRI protocols combining hip dedicated sequences as well as sequences covering the pelvis offer the best chance of identifying all potential sources of symptoms. In MRA, the anaesthetic arthrogram combined with the increased diagnostic accuracy provided by the intra-articular contrast can both be extremely useful diagnostic features (Agten et al. 2016). Although very promising, quantitative MRI cartilage imaging still needs to be further validated. Whenever appropriate diagnostic injections may prove useful to confirm the source of symptoms (namely for deep gluteal pain syndrome, ischiofemoral impingement and in certain FAI cases) (Khan et al. 2015).

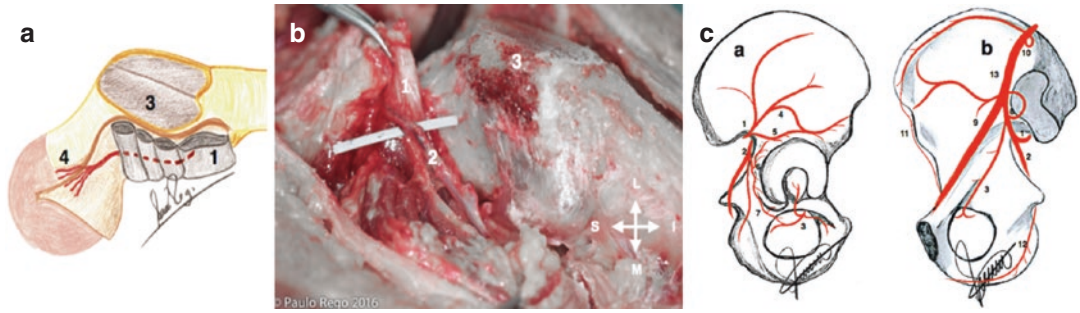

Fig. 3 (**a–c**) (**a**) Schematic drawing of the external rotators' flap containing the deep branch of the posterior circumflex artery (posterior view), the most important branch for femoral vascularization. (**b**) Representative cadaveric photograph of the same anatomy. (1) External rotators; (2) deep branch of the posterior circumflex artery; (3) great trochanter; *S* superior; *I* inferior; *L* lateral; *M* medial. (**c**) Illustration of the lateral (**a**) and medial (**b**) facets of the iliac with the respective arterial anastomotic network of the peri-acetabular region. (1) Upper gluteal artery; (2) gluteal inferior artery; (3) obturator a.; (4) supra-acetabular a.; (5) acetabular a.; (6) acetabular branch of gluteal inferior a.; (7) anastomosis between inferior gluteal a. and obturator a.; (8) iliolumbar a.; (9) nourishing branch of iliolumbar a.; (10) fourth lumbar a.; (11) deep iliac circumflex a.; (12) medial pudendal a.; (13) common iliac a. (Adaptation from Prof. Dr. Paulo Rego's illustration, with permission)

4.1 Radiographs

For hip-related pain, nearly all patients will be initially evaluated with radiographs per the American College of Radiology (ACR) Appropriateness Criteria (Agten et al. 2016). However, in clinical practice, not every injury requires a radiographic examination, particularly for clinically suspected soft-tissue non-articular injuries.

Hip morphology is assessed using angles and lines that are usually visible on an AP radiograph with standardized acquisition of the entire pelvis with additional views according to each specific clinical situation (Siebenrock et al. 2003; Pedersen et al. 2004; Kalberer et al. 2008; van der Bom et al. 2011; Tannenbaum et al. 2014; Hellman et al. 2016). In contrast to CT or MRI, CR is a two-dimensional projection of a 3D reality. Given the enormous individual variability and overlap, it is difficult to precisely define the thresholds between what is normal and pathological regarding hip shape (Tönnis 1976; Tönnis 1987).

4.1.1 General Technical Considerations

For the pelvis AP radiograph, the legs must be 15° internally rotated to compensate for femoral antetorsion. The central beam is centred to the midpoint between the upper border of the symphysis and a line connecting the two ASIS.

Main technical factors to consider include (1) ***Conical projection*** (Tannast et al. 2014) (the closer an object is located to the X-ray source, the more lateral it will be projected), (2) ***Film-tube distance*** (Tannast et al. 2007; Clohisy 2008): should be around 120 cm (increasing film-tube distance the apparent acetabular anteversion increases), (3) ***Centring and direction of the x-ray beam*** (Tannast et al. 2007) (the sacrococcygeal joint should be located 1–3 cm from the superior aspect of the pubic symphysis) and (4) ***pelvic orientation*** (Siebenrock et al. 2003; Tannast et al. 2014) (orientation can vary in three dimensions: obliqueness, rotation and tilt).

4.1.2 Views and Basic Technique (Table 5)

Supine pelvic radiographs are preferred by some authors because they can be directly compared to CR performed intraoperatively or at follow-up during early rehabilitation and restricted weight bearing (Tannast et al. 2007). On the other hand, in clinical entities where acetabular evaluation is of paramount importance (such as Pincer FAI and developmental hip dysplasia (DDH)),

Table 5 Summary of technical details and imaging purposes of several radiographic projections of the hip and pelvis

	Position	Hip flexion	Knee flexion	Foot position	X-ray beam	Usefulness
AP pelvis	Supine/standing	0°	0°	15°–20° internal rotation	Centred to midpoint between: upper border of PS and a line connecting both ASIS	Basic radiographic evaluation for HPS, total hip arthroplasty or trauma; assessment of NSA, acetabular coverage/depth/inclination, head sphericity, JSW
Lauenstein	Supine	45–70° flexion + 45° abduction	45°	Parallel to the table	Hip-centred: vertically to the FH	Assessment of the anterosuperior coverage of the FH, assessment of the anterosuperior FHN junction
Lauenstein (variant)	Supine + 45° lateral rotation to the side of interest	45–70° flexion, no abduction	45°	Parallel to the table	Hip-centred: vertically to the FH	Assessment of the anterosuperior coverage of the FH, and of the anterosuperior FHN junction
Frog-leg lateral	Supine	45° External Rotation	30°-40°	United plantar soles (if bilateral)	Pelvis-centred	Evaluation of the anterior and posterior FHN contour, sphericity of the femoral head, joint congruency
Cross table lateral view	Supine	0°	0°	15°–20° internal rotation	Parallel to the table + oriented at 45° to the limb	Evaluation of the anterior and posterior FHN contour
False profile (Lequesne)	Standing + back tilted 65° to the "wall"	0°	0°	Parallel to the detector	Hip-centred	Assessment of the anterior coverage of the FH, quantification of posteroinferior JSW
Ducroquet	Supine	90° flexion + 45° abduction	90°	45° abduction	Hip-centred	Assessment of the anterosuperior FHN junction
Dunn 45°	Supine	45° + 20° abduction	90°	Neutral	Perpendicular and centred midway to the PS and the ASIS	Assessment of the anterosuperior FHN junction
Dunn-rippstein	Supine	90° flexion + 20° abduction	90°	Neutral	Perpendicular and centred midway to the PS and the ASIS	Assessment of the anterosuperior FHN junction, femoral antetorsion, anterior and posterior FHN contour

AP anteroposterior, *ASIS* anterior superior iliac spines, *FHN* femoral head-neck, *PS* pubic symphysis, *α* alpha, *HPS* hip preserving surgery, *NSA* neck-shaft angle, *JSW* joint space width, *FH* femoral head

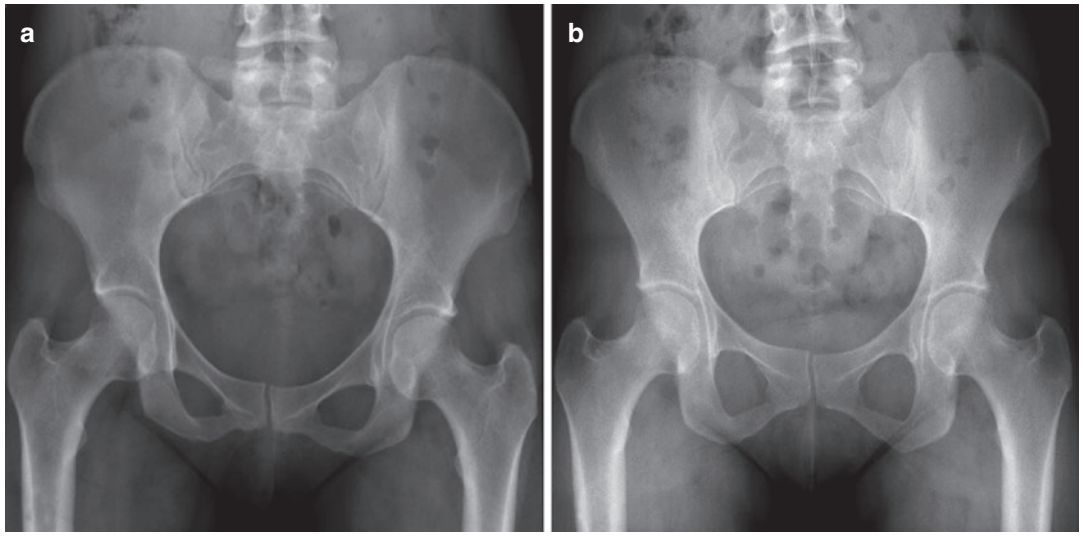

Fig. 4 (**a**, **b**) AP radiographs of the pelvis obtained in the (**a**) supine and (**b**) weight-bearing positions in the same patient. In B the sacrum becomes more vertical and anterior acetabular coverage is reduced. Proper positioning on an AP pelvic radiograph is recognized when: (1) femur—the greater trochanter is seen laterally and the lesser trochanter is partially superimposed on the femoral neck, (2) the obturator rings and acetabular teardrops are symmetric and (3) midsacral line aligns with the pubic symphysis

Table 6 Advantages of obtaining AP radiographs of the pelvis in the supine and standing positions

Supine radiographs	Standing radiographs
• Technically easier to obtain • Easier to perform in obese and older patients • Reproducible in the operating room • Feasible in recent postoperative setting • Most outcome studies derive from supine radiographs	• Accurate JSW and JSN measurement • Allow functional assessment of acetabular morphology, version and coverage

JSN joint space narrowing, *JSW* joint space width

Table 7 Influence of pelvic positioning (rotation and pelvic tilt) on radiographic hip parameters

No significant change with pelvic rotation and tilt	Relevant change with pelvic rotation and tilt
• LCEA • Acetabular index • Extrusion index • Sharp angle • Craniocaudal coverage	• Anterior acetabular coverage • Posterior acetabular coverage • Cross-over sign • Posterior wall sign • Retroversion index

LCEA lateral centre-edge angle

weight-bearing AP pelvic radiographs should be obtained given that they reflect functional anatomical positioning (Jackson et al. 2016) and also account for the differences in pelvic flexion-extension and acetabular version variations (Fig. 4 and Tables 6 and 7).

Axial/lateral view of the hip: Different techniques have been described (Mascarenhas et al. 2019), which are performed to answer specific questions (Table 5 and Fig. 5). The single optimal lateral radiograph for cam morphology assessment is the Dunn 45° view as the femoral head-neck asphericity is most often localized in the anterosuperior region. An AP pelvis radiograph and a Dunn 45° view are the best choice for the initial radiographic assessment of the FHN junction, as further radial imaging is usually performed when FAI is clinically suspected.

Lumbar imaging: There is no current evidence to support additional lumbar imaging when approaching hip and groin-pain, although assessment of spinopelvic (SP) parameters and lumbar pathology is increasingly recognized as important in this setting. Sagittal pelvic kinematics along with SP parameters have recently been

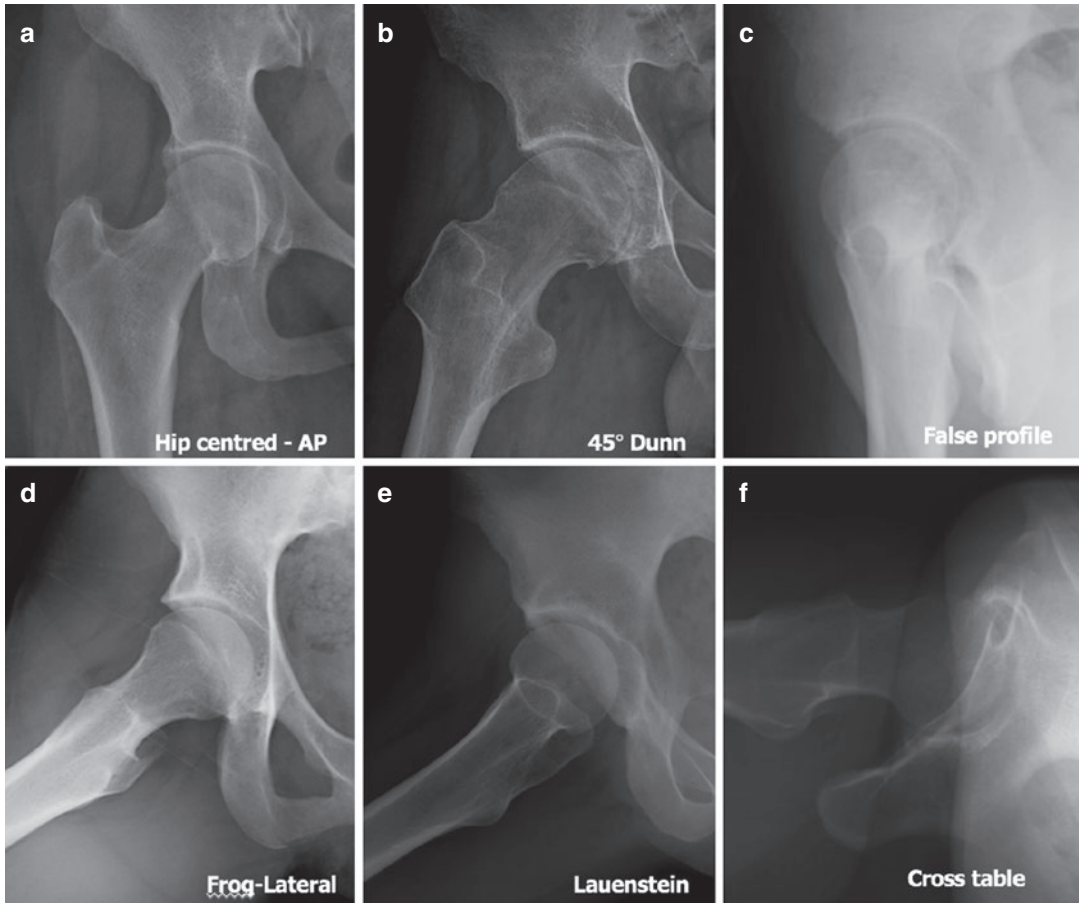

Fig. 5 (**a–f**) Most commonly used radiographic hip views: (**a**) Anteroposterior hip centred. (**b**) Dunn 45; this is the recommended lateral view as a first-line evaluation of proximal femoral morphologies, in combination with an AP view of the pelvis. It is obtained with the hip in 45° of flexion, 20° of abduction and neutral rotation. (**c**) False profile, (**d**) Frog-leg lateral, (**e**) Lauenstein and (**f**) cross-table lateral view

studied for their effect on hip function, FAI (Grammatopoulos et al. 2018; Ng et al. 2018; Mascarenhas et al. 2018a), and hip replacement (Rivière et al. 2017b). Variability in sagittal pelvic function may substantially influence impingement phenomena (Rivière et al. 2017b; Grammatopoulos et al. 2018; Ng et al. 2018; Mascarenhas et al. 2018a), but many of the spine-hip relations are still unexplored. When clinically deemed important, imaging evaluation may include a review of SP parameters and assessment for lumbar disease as a hip pain mimicker, either with a lateral lumbosacral radiograph, or by CT/MRI of the entire pelvis with multiplanar reconstructions, instead of imaging only the hip of interest (Grammatopoulos et al. 2018; Ng et al. 2018; Mascarenhas et al. 2018a).

4.1.3 Parameters

Femoral side: The most commonly described parameters to evaluate femoral morphology can be divided according to the main features that they assess: joint congruency, FH sphericity and other important parameters, such as neck orientation in the coronal (neck-shaft angle) and axial (torsion) planes (Fig. 6 and Table 8).

Acetabular side and spinopelvic parameters: Overall, the most commonly described parameters to assess acetabular morphology can be divided according to the main features that

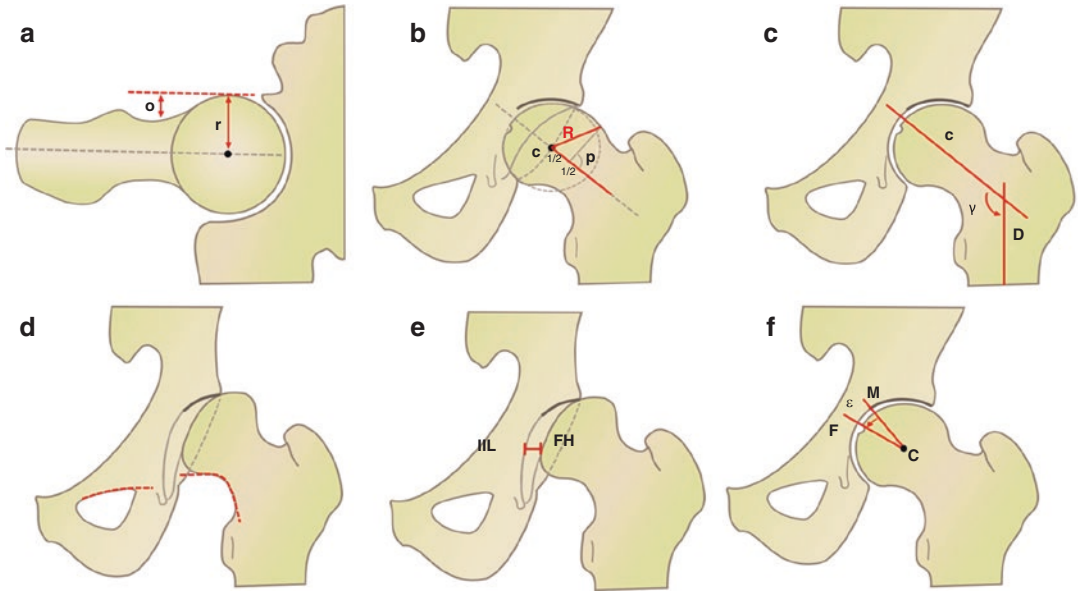

Fig. 6 (**a–f**) Imaging parameters to describe proximal femoral morphology. See Table 8 for definitions. (**a**) offset and offset ratio, (**b**) triangular index, (**c**) cervicodiaphyseal (CCD) angle, (**d**) Shenton's line, (**e**) lateralization of femoral head, (**f**) fovea angle delta

Table 8 Imaging parameters to describe femoral morphology (see Fig. 6 for corresponding illustration)

Femur and joint	Parameter	Unit	Imaging technique	Definition
Femur sphericity	Alpha angle	(°)	Axial and AP pelvis CT and MRI	Angle formed by the FHN axis and line through the centre of the femoral head and the point where the anterior (posterior) FHN contour exceeds head radius
	Pistol-grip Deformity	Qualitative	Axial and AP pelvis	Seen as bump at the FHN junction other than osteophytes from seronegative arthritis and osteoarthritis
	Asphericity and Flattening of the lateral aspect of the FH	Qualitative	Axial and AP pelvis CT and MRI	Flattening of the normal concavity of the FHN junction The head is said to be aspherical if the femoral epiphysis extended more than 2 mm outside the reference circle corresponding to a spherical head
	Offset Offset ratio	[mm] NA	Axial and AP pelvis CT and MRI	Difference (o) between the FH radius (r) and the neck radius Ratio of offset (o) to the FH radius (r)
	Femoral distance	[mm]	Axial and AP pelvis CT and MRI	The perpendicular distance between a tangent along the cortex of the FN and the point of the largest osseous deformity at the FHN junction is measured
	Triangular index	NA	AP pelvis	A perpendicular line (p) is drawn at half the head radius (r). Distance (R) is measured from the FH centre (C) to the point where p intersects the anterior FHN contour. The triangular index is positive if R > r + 2 mm
	Omega angle	(°)	Radial imaging and 3D MRI/CT	Quantifies the extent of abnormally elevated α angles, providing information on cam magnitude (defined by the radial extension of the FHN deformity)

Table 8 (continued)

Femur and joint	Parameter	Unit	Imaging technique	Definition
Joint congruency	Shenton's line	(intact/ interrupted)	AP pelvis	Interrupted if the caudal FHN contour and the superior border of the obturator foramen do not form an harmonic arc
	Lateralization of femoral head or position of the hip centre	(mm)	AP pelvis	Shortest distance between the medial aspect of the femoral head (FH) and the ilioischial line (IIL) Lateralized if greater than 10 mm
Additional findings	Cervicodiaphyseal angle or NSA	(°)	AP pelvis CT/MRI	Angle formed by FHN axis and femoral shaft axis
	Femoral torsion	(°)	Axial images over proximal/ distal femur (CT, MRI or Dunn 90°)	Angle between the longitudinal axis of the FN and the tangent at the condyles of the distal femur
	Joint space width Minimum JSW	(mm)	AP pelvis standing	JSW should be measured in the superior region of the hip joint (distance between the superior FH cortex and the acetabular sourcil). mJSW: inter-bone distance at the point of maximal narrowing
	Fovea angle delta	(°)	AP pelvis	Angle formed by a line through the medial edge of the acetabular roof (M) and the FH centre (C) and a line through the lateral border of the fovea capitis (F) and the FH centre (C). Angle ≤ 10° associated with DDH (fovea alta)
	FEAR index	(+/−)	AP pelvis	Angle formed by: (a) the central straight section of the femoral physis and (b) the most medial and lateral points of the sourcil sclerosis. Positive FEAR index if a laterally directed angle results. Painful hip with a LCEA ≤25° and FEAR index <5° is likely to be stable

AP anteroposterior, *CT* computed tomography, *DDH* developmental dysplasia of the hip, *FEAR* Femoro-Epiphyseal Acetabular Roof, *IIL* ilioischial line, *FH* femoral head, *FHN* femoral head-neck, *FN* femoral neck, *MRI* magnetic resonance imaging, *NA* not applicable

they measure: depth, coverage or orientation (Fig. 7 and Table 9). Spinopelvic parameters have been increasingly recognized as paramount on the hip-spine relationship (Table 10).

4.2 Ultrasound

Although highly dependent on operator experience, US is a valuable tool in the work-up of an athlete with hip pain and particularly for muscle and tendon disease, for both diagnostic purposes and therapeutic interventions (Hegazi et al. 2016). Physicians must have pertinent knowledge of the normal anatomy and should make judicious use of surface anatomy landmarks while using a systematic diagnostic approach. Main advantages are (1) accessibility on site at sporting events, (2) relatively low cost, (3) real-time dynamic imaging capability, as well as (4) radiation-free examination and (5) guidance of interventions such as fluid aspiration and/or substance injection (Boric et al. 2019), improving the accuracy of medication delivery (Sconfienza et al. 2019) and reported satisfaction compared to fluoroscopy-guided injections (Byrd et al. 2014).

Accurate diagnosis of hip injuries is often challenging, given the complex soft-tissue anatomy and the wide spectrum of injuries that can occur (Lungu et al. 2018). Commonly assessed structures are the iliopsoas tendon, iliopsoas bursa, iliotibial tract and joint effusion. Evaluation

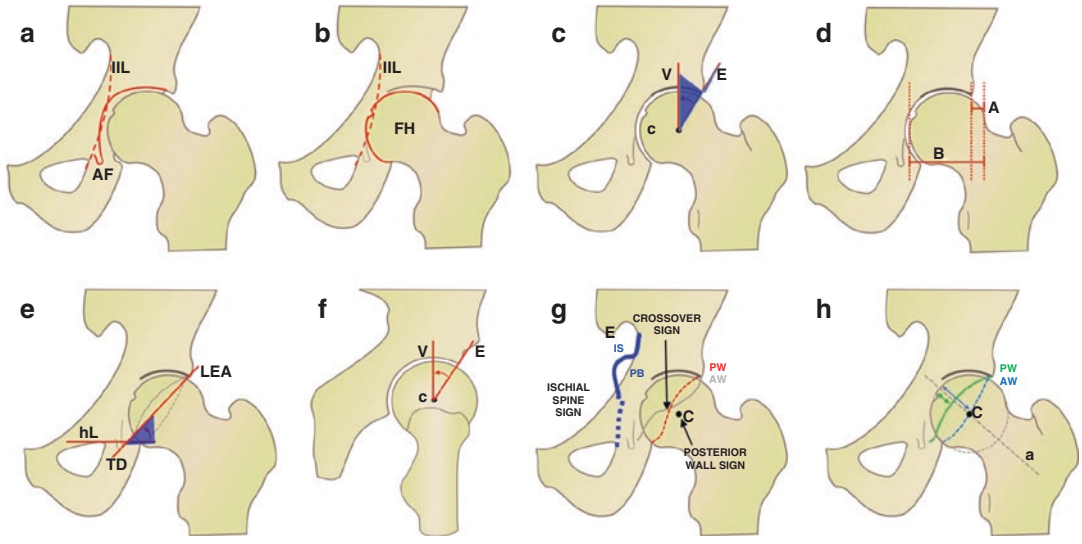

Fig. 7 (**a–i**) Imaging parameters to describe acetabular morphology. See Table 9 for definitions. (**a**) *Coxa profunda*, (**b**) *protrusio*, (**c**) lateral centre-edge angle, (**d**) extrusion index, (**e**) Sharp angle, (**f**) anterior centre-edge angle, (**g**) posterior wall sign, ischial spine sign and crossover sign, (**h**) anterior and posterior acetabular wall index

Table 9 Imaging parameters to describe acetabular morphology (see Fig. 7 for corresponding illustration)

Acetabulum	Parameter	Values	Imaging technique	Definition
Depth	*Coxa profunda*	Positive/ negative	AP pelvis	Acetabular fossa (AF) touches or crosses the ilioischial line (IIL)
	Protrusio acetabuli	Positive/ negative	AP pelvis	Femoral head (FH) touches or crosses the ilioischial line (IIL)
	Acetabular depth	mm	CT/MRI-transverse oblique image of the FN long axis	Distance between the FH centre and the line connecting the anterior/posterior acetabular rim
Coverage	Lateral centre-edge, LCEA	(°)	AP pelvis CT/MRI	Angle formed by a vertical line (v), which is perpendicular to a line connecting the teardrops, and a line through the centre of the FH (C) and the lateral bony rim of the acetabulum
	Centre-edge angle of Wiberg, W-CEA	(°)	AP pelvis	Same as previous, but using the lateral end of the sourcil, i.e. the weight-bearing area of the acetabulum, rather than the lateral rim of the acetabulum
	Acetabular inclination or Sourcil angle	(°)	AP pelvis CT/MRI	Angle formed by a horizontal line and a line through the medial and lateral edge of the acetabular roof
	Extrusion index	(%)	AP pelvis	Percentage of the FH width which is not covered by the acetabulum
	Sharp angle	(°)	AP pelvis	Angle between a horizontal line (hL) and a line connecting the acetabular teardrop (TD) and lateral edge of the acetabulum (LEA)
	Acetabular depth-width ratio (ADR)	NA	AP pelvis	The depth of the acetabulum divided by the width of the acetabulum, multiplied by 1000, presented as a ratio: (A/B)*1000
	Anterior centre-edge	(°)	False profile CT/MRI	Angle formed by a vertical line (V) and a line through the centre of the femoral head (C) and the anterior edge of the acetabulum (E)

Table 9 (continued)

Acetabulum	Parameter	Values	Imaging technique	Definition
	Coverage	(%)	CT/MRI	Technique to measure the % cover of the FH by the weight-bearing zone (pelvic position standardized relative to a specific anatomical plane)
	AASA PASA	(°)	CT/MRI	Lines through the FH centre and contralateral femoral head and tangential to the anterior (AASA) or posterior (PASA) lip of the acetabulum
Orientation	Posterior wall sign	Positive/ negative	AP pelvis	Positive if the posterior wall (PW) runs medially to centre of FH (C)
	Anterior (AWI) and posterior acetabular wall index (PWI)	–	AP pelvis	Ratio of the width of the anterior (AW)/ posterior acetabular walls (PW) measured along the FN axis (a) divided by the FH radius (r)
	Crossover sign	Positive/ negative	AP pelvis	Anterior wall (AW) crosses the posterior wall (PW)
	Retroversion index	(%)	AP pelvis	% of retroverted acetabular opening divided by entire opening
	Ischial spine sign	Positive/ negative	AP pelvis	Positive if ischial spine (IS) is projected medially to pelvic brim (PB)
	Acetabular version (1, 2 and 3 o'clock)	(°)	CT/MRI	Intersection of a perpendicular to the line between the posterior pelvic margins and a line connecting the anterior/posterior acetabular rims
Others	McKibbin index	–	CT/MRI	Sum of femoral version and the acetabular version (at 3 o'clock)

FN femoral neck, *FH* femoral head, *NA* not applicable, *MRI* magnetic resonance imaging, *CT* computed tomography, *AP* anteroposterior, *AASA* anterior sector angle, *PASA* posterior sector angle

Table 10 Spinopelvic parameters. Definition of pelvic incidence, sacral slope and pelvic tilt

Spinopelvic parameters	Parameter	Values	Imaging	Definition
	Pelvic incidence	(°)	Standing sagittal lumbosacral 3D CT or MRI	Angle between a line perpendicular to the sacral plate at its midpoint and a line from the mid-point between the axis of the two femoral heads to the centre of the sacral plate. PI = SS + PT
	Sacral slope	(°)	Standing sagittal lumbosacral	Angle formed by a line drawn parallel to the sacral plate and a horizontal reference line
	Pelvic tilt	(°)	Standing sagittal lumbosacral	Angle formed by a line from the midpoint of the sacral plate to the centre of the femoral heads and a vertical plumb line

of the acetabular labrum with US has been described. However, only the anterior part of the labrum is consistently seen, and other techniques such as MRA are far superior for detection of labral tears.

Ultrasound in FAI: Although level 2 evidence exists supporting a limited role of US in FAI, currently its use cannot be recommended as a diagnostic tool. Labral tears in patients with FAI have been found at US in 63.6% of cases (Orellana et al. 2018), with highly variable diagnostic performance (sensitivity 58–75%, specificity 25–67%, accuracy 61–75%) when compared to arthroscopy (Jung et al. 2013).

4.3 Computed Tomography

Although volumetric CT is excellent at depicting osseous morphologies, assessing osteoarthritic changes (Samim et al. 2019; Mascarenhas et al. 2019) and in virtual range of motion (ROM) 3D simulation studies (Mascarenhas and Caetano 2018; Samim et al. 2019; Mascarenhas et al. 2019), it is (1) unable to detect chondrolabral changes, (2) is associated with radiation exposure and (3) has limited value in evaluation of sports injuries. Mainly it is reserved for (1) detecting subtle fractures not visible on CR, (2) for preoperative evaluation of complex fractures and dislocations, and for the (3) diagnosis of intra-articular ossified bodies or extra-articular ossifications.

Protocol: Patient is positioned supine in the scanner with the legs in slight internal rotation. CT of the hip and pelvis should cover from the iliac crests through the lesser trochanters in thin-section acquisition/reformats (0.5–1 mm), using both bone and soft-tissue algorithm kernels (axial, sagittal and coronal planes). 3D volume-rendered reformations may also be useful.

CT arthrography (hip): Usually reserved for patients in whom MRI is contra-indicated, to appreciate the labrum and cartilage. It is performed after direct intra-articular injection of an iodinated contrast agent. Single-contrast studies are often sufficient and preferred. It involves the injection into the joint space of 10–14 mL of a low-osmolar contrast agent. Usually, no dilution is generally needed if a low to medium concentration preparation (i.e., 180–240 mg of iodine per millilitre) is used, to prevent streak artifacts observed at higher concentrations.

4.4 Magnetic Resonance Imaging

MRI is useful to evaluate intra- and extra-articular disease being the preferred imaging modality for assessment of bone and soft-tissue structures. According to the ACR, in patients with chronic hip pain, MRI should be the next imaging modality of choice when radiographs are normal (Zoga et al. 2016). Because hip/groin pain in athletes can have multiple origins, a problem-oriented imaging protocol is paramount (refer to https://www.essr.org/subcommittees/sports/ for detailed hip/groin area protocols).

Unenhanced MRI and direct MRA (dMRA) are the techniques of choice for detection of hip chondral-labral lesions, although dMRA is the best technique to study intra-articular pathology (Smith et al. 2012; Sutter et al. 2014; Saied et al. 2017). 3T MRI was reportedly equivalent to 1.5T dMRA for diagnosing labral tears and cartilage delamination, but superior for acetabular cartilage defects. Additionally, 3T MRI demonstrated similar sensitivity to 3T dMRA in the detection of acetabular labral tears, although the latter is more sensitive for the detection of acetabular chondral lesions (Smith et al. 2010; Smith et al. 2012; Saied et al. 2017; Crespo-Rodríguez et al. 2017). Indirect MRA is generally not indicated (shows overall less accuracy when compared to dMRA) (Smith et al. 2012; Saied et al. 2017).

Protocol: While evidence is lacking regarding the ideal hip MRI protocol, sequence details or comparison between protocols, the following is recommended for the assessment of a young patient with hip/groin pain (Fig. 8):

1. A fluid-sensitive sequence with a large FOV covering the whole pelvis, in the axial or coronal planes, to screen for soft-tissue and bone marrow oedema and other possible differential diagnosis
2. Unilateral hip, small FOV: should be centred in the magnetic field, high-resolution sequences of the symptomatic hip/area of interest
3. If assessing FAI: use radial imaging (either direct acquisition or 3D reformats) and fast axial sequence of the femoral condyles and femoral neck, to assess femoral torsion

MRA: When intra-articular disease is suspected, dMRA is the imaging study of choice, as both a **diagnostic** arthrography and **anaesthetic** injection can be combined into a single procedure. The main goals are (1) to achieve joint distension hence greater lesion conspicuity and (2) confirm the intra-articular origin of the athlete's pain. dMRA is superior to standard MRI for detection of labral lesions (compared sensitivity: 69–81% vs. 50%). dMRA also improves detection of ace-

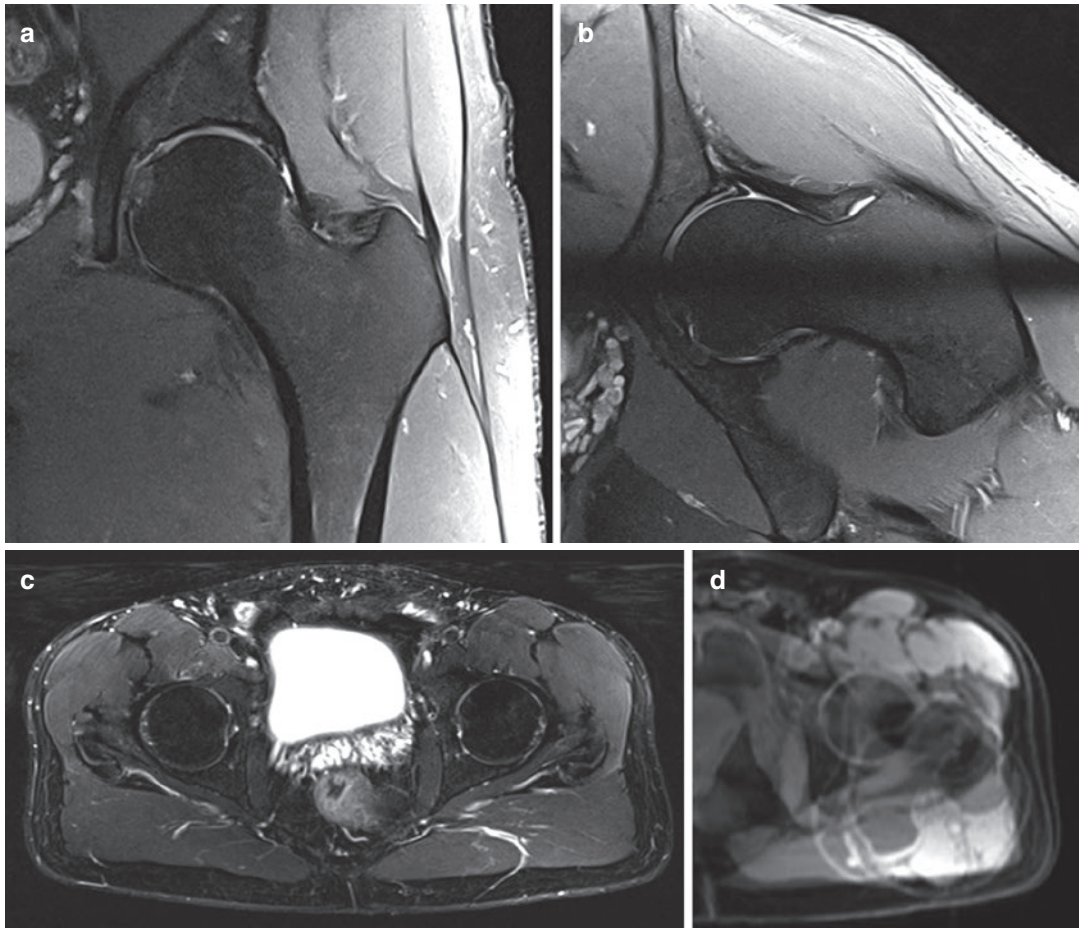

Fig. 8 (**a–d**) Sequences that should be included on the proposed routine MRI protocol for the assessment of hip and groin pain, comprise a pelvic fluid-sensitive sequence and unilateral 2D sequences (coronal, axial and sagittal are most useful). If FAI is suspected, femoral torsion assessment and radial imaging should be performed. (**a**) Unilateral FOV coronal fat-suppressed proton-density and (**b**) radial sequences might be used for hip detailed assessment. (**c**) A 2D large-FOV axial sequence of the pelvis is used to screen for other possible differential diagnosis. (**d**) Assessment of femoral torsion: different slices may be superimposed on a single image with post-processing software, making it easy to measure

tabular cartilage defects, while no advantage was found for cartilage defects on the femoral head in comparison with conventional MRI.

Technique basics: 8–14 mL of diluted gadolinium-based contrast agent (2.5 mmol/L solution or a 1:200–400 dilution in saline, depending on the contrast agent) mixed with 3 mL of anaesthetic (e.g. ropivacaine). The target zone for the needle is the centre of the femoral neck or the superolateral quadrant of the FH (preferred in a previous arthroscopy setting, because of possible adhesions between the joint capsule and the femoral neck).

Traction MRA: The main goal is to achieve joint distension and distraction, hence greater lesion conspicuity. There is evidence that dMRA with hip traction aids in the detection of cartilage delamination both at 1.5T and at 3T, by uncovering cartilage flaps that are usually less visible on the reduced FH (Llopis et al. 2008; Schmaranzer et al. 2014). It is still unclear whether traction at hip MRI should be used routinely and, if so, whether images should be obtained without and with traction or only with traction.

Technique basics: The combination of dMRA and leg traction (Llopis et al. 2008) may be

achieved by using orthopaedic traction devices (weight used for traction varies from 6 kg (Llopis et al. 2008), 8–10 kg (Suter et al. 2015) and 15–23 kg (Schmaranzer et al. 2014) and varying injected volumes of 10–14 ml to 18–27 ml.

5 Pathology

5.1 Hip Intra-articular

A combination of abnormal bony morphology, which is seen in a high percentage of athletes, and specific hip load may be related to the development of specific intra-articular hip pathologies in athletes (Heerey et al. 2019). Morphological hip shapes give rise to a continuous spectrum ranging from isolated instability to impingement with decreased mobility. Located at one end of this spectrum is DDH, and at the other is FAI. In many situations, however, there is a combination of several morphologies that may have greater or lesser clinical expression and determine the predominance of a mechanism of chondral and labral injury: instability or impingement (Tibor et al. 2013).

5.1.1 Acetabular Dysplasia and Instability (Fig. 9)

DDH is regarded as an insufficiency of contact between the articular surfaces (Wilkin et al. 2017). The surrounding soft tissues such as the labrum, joint capsule, ligaments and muscles are important static and dynamic hip stabilizers in sports. This combination usually results in a **static overload** of the acetabular roof and an instability or inability to maintain the centre of rotation of the joint fixed, resulting in lateral, superior and anterior migration of the FH. Clinically, DDH may be quite symptomatic (Wilkin et al. 2017) and has been reported as a risk factor for early-onset OA (Morvan et al. 2013). Recent advances in imaging of the dysplastic hip with CT scans have demonstrated that DDH is, in fact, a 3D deformity of the acetabulum and that multiple patterns of acetabular instability exist that may not be completely assessed on 2D imaging (Kraeutler et al. 2016).

The concept of **microinstability** is based on symptomatic hip laxity without marked subluxation. Aetiology may be either (1) traumatic (single or repetitive trauma) or (2) atraumatic (generalized laxity or DDH). Patients may feel hip unsteadiness, snapping, and/or pain during sports (Cerezal et al. 2012). Diagnosis is problematic, due to no established criteria.

Imaging:

Radiographs (AP pelvis), characterized by increased (1) inclination of the acetabular roof (acetabular inclination>13°) and/or (2) decrease in lateral and/or anterior coverage (established DDH: LCEA<20° or *borderline* DDH: 20<LCEA<25°). Additionally, (3) aspherical FH (usually "pear-shaped"), (4) *coxa valga*, (5) anteversion of the femoral neck and (6) retroversion of the acetabulum (Tibor et al. 2013) may be present.

MRI: most characteristic findings include (1) labrum hypertrophy, (2) "inside-out" acetabular cartilage lesions, (3) increased iliocapsularis-to-rectus-femoris ratio in hips with DDH (i.e. if the cross-sectional area of the iliocapsularis, measured in an axial slice through the centre of the FH, exceeds the cross-sectional area of the rectus femoris muscle, a DDH is said to be present in 89% of patients (Haefeli et al. 2015)).

– *Microinstability* suspected patients might have (1) a thickened iliofemoral ligament (anterior joint capsule) with irregularities on the undersurface of the anterior capsule, (2) an increased capsular volume, detectable during MRA and (3) larger or easier widening/distraction of a hip joint during traction MRA, suggesting hip laxity. Other findings associated with positive joint distraction were higher alpha angles, higher neck-shaft angles, smaller acetabular depths and hypertrophy of the LT (Cerezal et al. 2012).

5.1.2 Ligamentum Teres Pathology

Anatomy: The *LT* (Fig. 9) is a strong intra-articular ligament that is anatomically and biochemically similar to the anterior cruciate ligament of the knee (with an anterior and

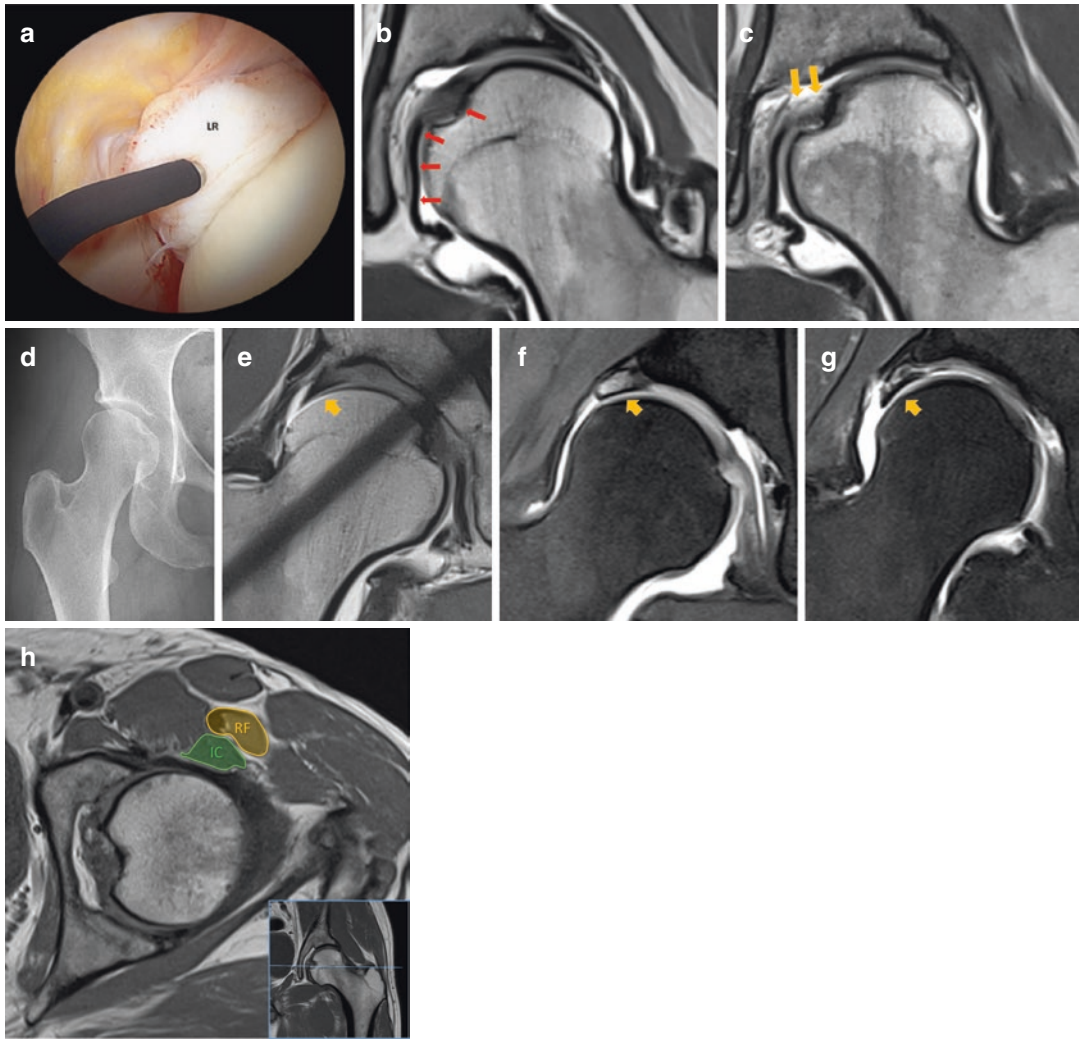

Fig. 9 (**a–h**) (**a**) Hip arthroscopic and (**b**, **c**) coronal MRA proton-density images of *ligamentum teres (LT)*. (**a**) Hypertrophic degenerated ligament (LR). (**b**) Normal hypointense LT (red arrows). (**c**) Degeneration and fraying (partial rupture) of the LT at the foveal insertion. Note the shallow acetabulum, highly located fovea, pear-shaped FH and labrum degeneration all characteristic of DDH in a 25-year-old ballet dancer. (**d**) Right hip AP radiograph on a 29-year-old ballet dancer shows characteristic DDH, with a shallow acetabulum, *coxa valga*, pear-shaped FH, decreased LCEA and increased acetabular inclination. (**e–g**) showing different stages of labral disease in DDH and microinstability, ranging from (**e**) labrum hypertrophy, (**f**) labrum hypertrophy and degeneration and ultimately leading to (**g**) tear of the capsular labral surface. (**h**) T1w axial MR image of the left hip at the level of the femoral head centre, in a 48-year-old patient with complaints of lumbar pain radiating to the hip. The contours of the rectus femoris (RF) and iliocapsularis (IC) are outlined. In this case, the cross-sectional area of the IC does not exceed that of the RF

posterior bundle). It arises from the transverse ligament and the ischial and pubic margins of the acetabular fossa. The ligament is trapezoidal at its base and runs to the FH, where it becomes progressively round or oval shaped and inserts into the *fovea capitis*. The **functions** of the LT might include: (1) intrinsic stabilizer that resists joint subluxation forces, (2) may play a role in nociception and coordination of movements, (3) provides blood supply to the developing FH and (4) helps to distribute synovial fluid within the hip joint via a "windshield wiper effect".

Why is it important?: Athletes with LT tears may develop pain and hip microinstability. When combined with sporting activities, this results in damage to the labrum and cartilage (explaining the high association rate between tears of the LT, labral tears and cartilage lesions) (Chahla et al. 2016). In symptomatic ballet dancers and mixed athletes, it was reported a prevalence of 44% LT tears per hip (compared to 21% in asymptomatic mixed athletes' population), reflecting the demands during sporting activity, particularly those sports requiring large ranges of hip motion.

Imaging: LT lesions are categorized arthroscopically as rupture (partial or complete) or degeneration. Complete rupture occurs after hip dislocation or after sudden external rotation episodes and are most commonly located near the fovea (showing a discontinuity of the ligament with lax contours).

On MRI, the normal LT is best visualized in the coronal/axial planes and has smooth borders and a homogeneous, hypointense structure on all sequences. Ligament degeneration is similar to tendons, ranging from mucoid degeneration to complete tear. MRA revealed better diagnostic performance compared with MRI regarding partial tears (increased intrasubstance signal intensity abnormality visualized on fluid-sensitive images as well as focal partial loss of continuity). For the detection of complete tears MRI and MRA imaging (67% sensitivity, 99–100% specificity) show similar good results.

5.1.3 Femoroacetabular Impingement

Concept: FAI is a motion-related clinical disorder associated with a triad of insidious onset of groin/hip pain, signs of limited motion and characteristic imaging findings (Ganz et al. 2003; Nepple et al. 2013), which results from a conflicting contact between the proximal femur and the acetabular rim (Ganz et al. 2003). This abnormal contact may ultimately lead to premature OA (Agricola et al. 2013a; Glyn-Jones et al. 2015; Mascarenhas et al. 2020a) (Table 11). FAI remains controversial in terms of true incidence, diagnosis, prognosis and management (Jung et al. 2011; Mascarenhas et al. 2016; Griffin et al. 2016). With the implementation of this concept, concerns have been raised about overdiagnosis and overtreatment.

Table 11 Summarizing table of the clinical, epidemiological and joint damage characteristics of femoroacetabular impingement

	Patient characteristics					**Intra-articular damage**	
	Sex	Age	Activity	Deformity	Mechanism	Early damage	Late damage
Cam FAI	Mainly male	Young	High-level athletes; high-impact sports	"Cam-type morphology": Eccentric femoral head with laterally increasing radius	Sheering forces inside the joint and damage to the acetabular cartilage; "inclusion injury"	Acetabular cartilage delamination "Outside-in" acetabular cartilage lesions	Large, full-thickness anterosuperior acetabular cartilage defects; Labral damage with undersurface tears; femoral head cartilage lesions
Pincer FAI	Mainly female	Middle aged	Recreational athletic activity	"Overcoverage" of the femoral head: *protrusio acetabuli*, acetabular retroversion	Linear impact between acetabular rim and FHN junction; "impaction injury"	Labral damage ranging from subtle shortening and rounding to extensive labral damage	Ossified bony rim with partially ossified labrum; cartilage damage at acetabular rim; "contrecoup" posteroinferior acetabular damage

5.1.3.1 Cam Mechanism

Cam impingement is caused by extra bone formation—a cam morphology—in the anterolateral FHN junction (Ito et al. 2001) (resulting in flattening or convexity). This morphology may cause impingement against the acetabular rim, especially during flexion and internal hip rotation (Matheney et al. 2013). The abnormal contact results in shear forces at the acetabular rim (Bowman et al. 2010) and is typically accompanied by labral tears (Bedi et al. 2008) and detachment of the acetabular cartilage from the subchondral bone (Bittersohl et al. 2009; Matheney et al. 2013). Acetabular cartilage delamination (Anderson et al. 2009) has characteristically been found in the anterosuperior quadrant of the joint, corresponding to the site where the deformity is forced into the acetabulum. Clinically it is associated with limited internal hip rotation (Nötzli et al. 2002) as well as hip pain (Allen et al. 2009) and OA (Agricola et al. 2013c) (Fig. 10).

Interestingly, a cam morphology might develop during skeletal maturation as a result of high-impact sporting activities, which would be a promising preventative opportunity to avoid the formation of this morphology and subsequent hip OA (Agricola et al. 2014; Mascarenhas et al. 2017).

5.1.3.2 Pincer Mechanism

Pincer impingement is caused by overcoverage of the acetabulum relative to the FH (either global or focal overcoverage). The hypothesis proposed by Ganz et al. (2003) states that the femoral neck causes an abnormal linear contact against the acetabulum during terminal motion of the hip. Initially, labral damage is the main characteristic as it might be crushed between the acetabular rim and the femoral neck (Fig. 11). When there are repetitive episodes of impingement, chondral damage might gradually develop throughout the acetabulum in a small, thin marginal strip (Beck et al. 2005). The relationship between pincer FAI and OA (Giori and Trousdale 2003; Bardakos and Villar 2009; Anderson et al. 2009; Gosvig et al. 2010; Nicholls et al. 2011; Agricola et al. 2013b) is still not clear, as even when overcoverage is symptomatic it seems to be protective in relation to advanced chondral aggression (Agricola et al. 2013b).

5.1.3.3 Diagnosis (Fig. 12)

Definition: There is no consensus regarding FAI preoperative diagnostic assessment and FAI case definition. The clinical concept of FAIS has been recently defined as a triad of: (1) symptoms, (2) physical signs and (3) imaging findings (Ganz et al. 2003; Sankar et al. 2013b; Griffin et al. 2016). This term and its definition build on the definitions of FAI from Ganz et al. (2003) and Sankar et al. (2013a) to ensure that there is a distinction between patients with FAIS and those with cam or pincer morphology but no symptoms.

Symptoms: The primary symptom of FAIS is motion-related or position-related pain in the hip or groin (Ganz et al. 2003), although it may also be felt in the back, buttock or thigh. In addition to pain, patients may also describe clicking, catching, locking, restricted ROM or giving way (Philippon et al. 2007; Ayeni et al. 2012; Nepple et al. 2014).

Signs: There is often a limited ROM, typically restricted internal rotation in flexion (Freke et al. 2016). Hip impingement tests usually reproduce the patient's typical pain, although the most commonly used test, flexion adduction internal rotation (FADIR), is sensitive but not specific (Reiman et al. 2015). With further and gradual internal rotation, hip pain is usually elicited (Shanmugaraj et al. 2018). When FAIS is suspected, it is important to examine gait, leg control, muscle tenderness and the FABER distance (flexion abduction external rotation).

Imaging (Mascarenhas et al. 2020a): Although paramount to diagnose FAIS, imaging assessment remains non-standardized with no consensus on which imaging modalities and parameters should be routinely assessed (Kassarjian 2019; Mascarenhas et al. 2019). Assessment should be based on radiographs (minimum required are AP pelvis and a Dunn 45°) and MRI in selected cases (Fig. 12). **Imaging goals** are: (1) to diagnose associated soft-tissue damage, (2) to detect early or focally advanced OA and (3) to assess patho-

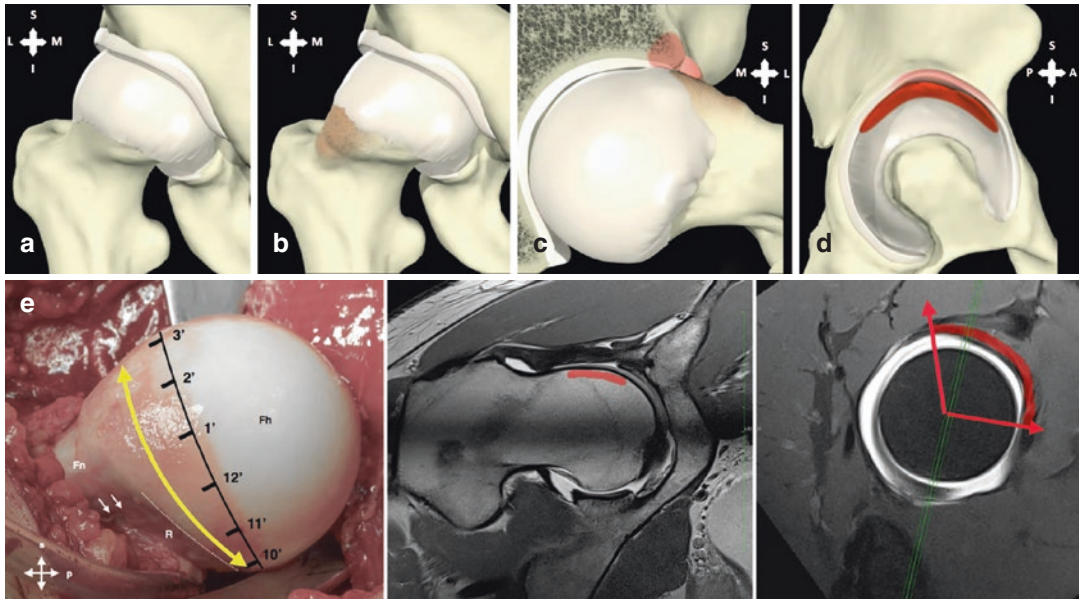

Fig. 10 (**a–e**) A schematic representation of the hypothesized mechanism of cam FAI. (**a**) Normal spherical femoral head and acetabulum, which is congruent with the femoral head, provides the hip a wide range of motion. (**b**) cam morphology can cause (**c**) Cam impingement against the acetabular rim, especially during flexion and internal rotation of the hip leading to a typical pattern of (**d**) acetabular chondrolabral damage anterosuperiorly. (**e**) dMRA examination and corresponding surgical hip dislocation procedure in a former 35-year-old elite soccer athlete. Sagittal fat-suppressed proton-density sequence (right image), corresponding radial proton-density-weighted sequence (middle image) and surgical hip dislocation caption (left image). Red curved line represents cam morphology assessed on the radial image at 1:00 o'clock and corresponding deformity in the sagittal plane extending from 11:30 to 3:00, later confirmed by direct observation. *dMRA* direct arthro-magnetic resonance, *FAI* femoroacetabular impingement

logic FAI hip morphologies. The differentiation or quantification of cam (femoral side), pincer (acetabular side) and their frequent combination is done on the basis of a predominance of either a femoral or an acetabular abnormality (Ganz et al. 2003; Pfirrmann et al. 2006; Mascarenhas et al. 2016; Griffin et al. 2016) (Table 12).

The radiologist should not state that abnormal signs and parameters are indicative of FAI/FAIS in an asymptomatic patient (as a substantial proportion of the general population have FAI-related morphology (Frank et al. 2015). Although these may be mentioned in the radiological report, interpretation should be undertaken in conjunction with the clinical history and physical examination (Frank et al. 2015; Mascarenhas et al. 2016; Mascarenhas et al. 2018b) (Fig. 12).

Diagnostic injections: A common clinical problem lies in determining whether pain (or surrogate symptoms) is really arising from the hip or from other structures in the groin and hip region. Frequently, image-guided local anaesthetic injections are useful in helping to resolve this situation (Kivlan et al. 2011; Khan et al. 2015), as they have both diagnostic and therapeutic value. Pain relief following a local anaesthetic injection would support a FAIS diagnosis, when the other diagnostic criteria are met (Griffin et al. 2016). Relief with an intra-articular injection was 90% accurate for predicting the presence of intra-articular findings during arthroscopy (Byrd and Jones 2004) (no relief is a negative predictor of short-term outcome following FAI surgery (Ayeni et al. 2014)).

Final conclusions (Mascarenhas et al. 2020a): Considering previously mentioned parameters and ongoing questions, some authors try to define what is normal and what is abnormal, also suggesting possible combinations of morphology

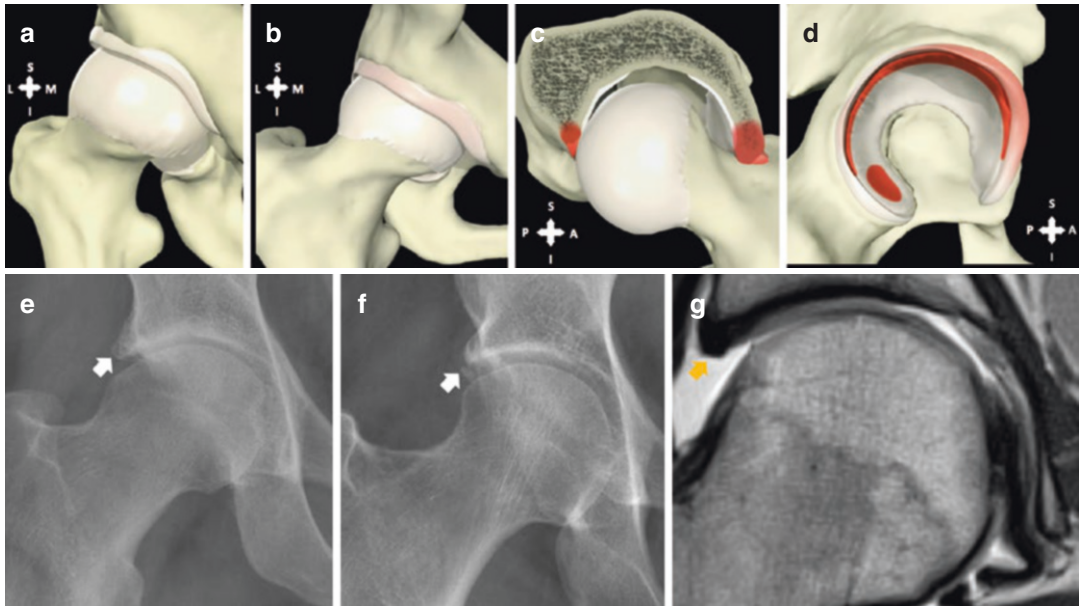

Fig. 11 (**a–g**) Schematic representation of the hypothesized mechanism of pincer FAI. (**a**) Normal spherical femoral head and acetabulum, which is congruent with the femoral head, provides the hip a wide range of motion. (**b**) A pincer deformity can cause pincer impingement against the femoral neck, (**c**) especially during terminal flexion of the hip leading to (**d**) a typical pattern of circumferential acetabular cartilage damage. (**e**) Acetabular rim ossification and (**f**) labral ossification associated with acetabular overcoverage, findings usually seen in Pincer FAI. (**g**) MRA of the right hip of a female 26-year-old field hockey player, same athlete as in (**f**), revealing (1) a small sized globular labrum with (2) peripheral cartilage thinning and (3) overcoverage of the acetabulum

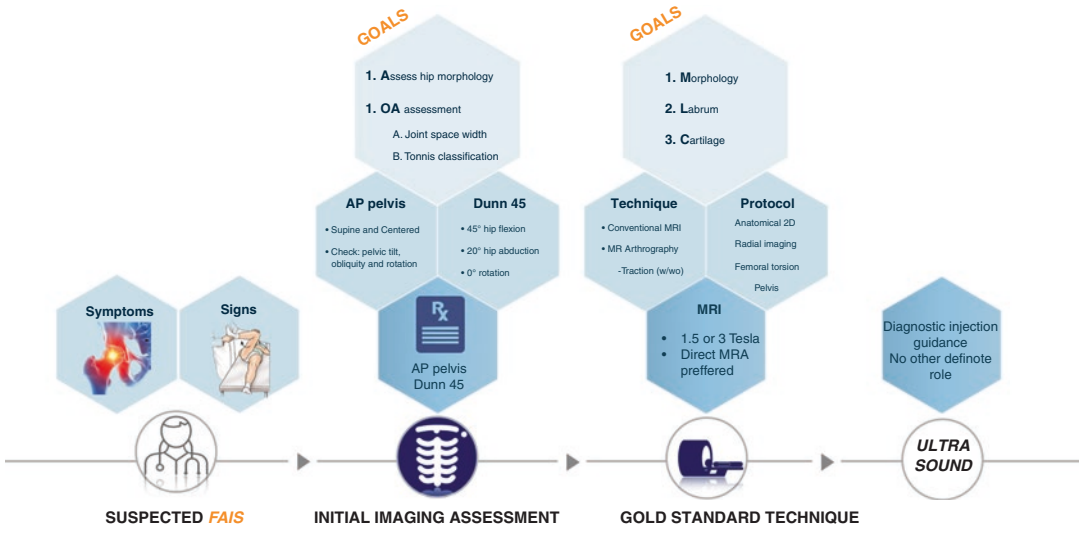

Fig. 12 Diagnostic pathway assessment for FAIS (Mascarenhas et al. 2020a, b)

that characterize classically and recently described pathological entities (Sutter and Pfirrmann 2017) (Tables 13 and 14).

5.1.3.4 Association Between FAIS and Sport Activities

Genetics, sex and physical activity influence

Table 12 Criteria proposed for classifying pincer and cam morphology in a research/clinical trial setting (regardless of the symptomatic state) (Mascarenhas et al. 2020a, b)

Imaging classification criteria for hip morphology			
Cam morphology *(1 or more)*		**Values**	**Technique**
Osseous convexity of the FHN junction		+	Radiography *(preferably AP pelvis and Dunn 45°)* CT or MRI *(with radial imaging)*
Alpha angle		*≥60°*	
FHN offset[a] *FHN offset ratio*[a]		<8 mm *≤0.15*	*Radiography (cross-table view)* CT or MRI *(with radial imaging)*
Pincer morphology		**Values**	**Technique**
Global pincer *(1 or more)*	*Protrusio acetabuli*	+	Radiographs *(standardized AP pelvis)*
	W-CEA	≥40°	
	W-CEA[a] Acetabular index[a]	≥35° <0°	
Global retroversion *(all criteria)*	Cross-over sign	+	Radiographs *(standardized AP pelvis)*
	Posterior wall sign	+	
	Ischial spine sign	+	
Focal pincer[b] *(1 or more)*	Cross-over sign	+	Radiographs *(standardized AP pelvis)* *Confirmation with CT or MRI recommended*
	Acetabular version	<0°	CT or MRI (*corrected for tilt on coronal plane and rotation on the axial plane)*

FHN femoral head-neck, *W-CEA* Wiberg centre-edge angle, *COS* cross-over sign, *CT* computed tomography, *MRI* magnetic resonance imaging

[a]Both measurements necessary to satisfy this criterion

[b]Corresponding to cranial retroversion in non-dysplastic hips

whether or not a cam morphology develops (Nepple et al. 2015). Accordingly, a strong association between sports and the development of FAIS exists, with high-level male athletes having 2–8 times more likelihood in developing a cam-type morphology (Nepple et al. 2015). Specifically, the prevalence of cam morphology is as high as 89% in athletes participating in activities that result in impact loading of the hip as compared to only 9% in non-athletic controls (Sutter and Pfirrmann 2017).

1. **Activity Type**:
   (a) Weight-bearing impact sports: High-level athletes participating in activities that require high flexion together with rotational movements of the hip (hockey, basketball, and possibly soccer) are at an increased risk of physeal abnormalities that result in a cam morphology at skeletal maturity (e.g. ice hockey players are 4.5 times more at risk than skiers).
   (b) Extreme and supraphysiologic hip motion: High-level athletes requiring beyond physiologic hip joint range of motion may not exhibit the typical hallmarks of FAIS but rather develop a type of atypical hip impingement (resembling that of Pincer-type) that is associated with ballet dancing, ice skating or martial arts.
2. **Activity Level**: A dose–response relationship exists; elite soccer players who practiced more than three times a week before the age of 12 years were 2.6 times more likely to have a cam morphology than players that practiced three times or less.
3. **Window of "increased-**risk**":** particularly between the age of 12 years and the closure of the growth plate, athletes with previously normal hips may develop a cam-type morphology of the proximal femur, as this morphology mainly develops when the proximal femoral growth plate is open. Prevention of potentially serious conditions such as cam morphology is a major sports medicine priority, although currently there is no recommendation on how and when to adjust athletic activities (Sutter and Pfirrmann 2017).

Table 13 Possible combinations of morphology and angular parameters that characterize pathological entities

	Normal	Dysplasia	*Cam* FAI	*Pincer* FAI
Acetabular inclination	0–10°	>10°	Variable	<0°
Lateral centre-edge	25–30°	<20°	Variable	>35°
Alpha angle	<55°	Variable	>60°	Variable
Retroverted acetabulum	Absent	Up to 1/3 of patients	Variable	Frequent
Femoral version	15–20°	Mostly anteverted	Variable	Variable

Table 14 Overview of most relevant femoral and acetabular parameters, notes and recommendations for research and clinical practice

Parameter	Measurement values to consider	Preferred measurement method	Notes and recommendations
Alpha angle	• >60° indicates cam morphology (at any location around the anterosuperior FHN junction)	• Radial imaging • AP pelvic radiograph and Dunn 45° view	• State measurement location • Measure and report where maximal deformity is noted around the FHN junction
Neck-shaft angle	• AP Pelvic radiograph: 120–135° • CT: 120–140°	• AP pelvic radiograph • CT and/or MRI in the coronal femoral neck plane	• Hip rotation and femoral torsion influence assessment • Vary with sex and age
Femoral torsion	• 13 ± 10° (Reikeras method)	• CT or MRI	• Clearly define measurement method
W-CEA	• <20°: undercoverage • 20–25°: *borderline* undercoverage • 25–39°: normal coverage • ≥40°: overcoverage	• AP pelvic radiograph	• Clearly define whether W-CEA or LCEA is measured • Represents superior and lateral coverage
Acetabular index	• >13°: undercoverage • <0°: overcoverage	• AP pelvic radiograph	• Represents acetabular inclination
Protrusio acetabuli	• Present or absent	• AP pelvic radiograph	• Represent a qualitative sign of global overcoverage • Always pathological
Cross-over sign **Posterior wall sign** **Ischial spine sign**	• Present or absent	• AP pelvic radiograph	• Represent qualitative signs of version • COS indicative of Focal Pincer (acetabular retroversion) • When all signs are present indicative of Global Pincer (global retroversion)
Acetabular version	• Cranial version < 0°: Focal retroversion	• CT or MRI	• Clearly define measurement method • Indicative of Focal Pincer (acetabular retroversion)

COS cross-over sign, *CT* computed tomography, *FHN* femoral head-neck junction, *LCEA* lateral centre-edge angle, *MRI* magnetic resonance imaging, *W-CEA* Wiberg centre-edge angle

5.1.4 Labrum Pathology

5.1.4.1 Anatomy and Imaging Description

The labrum (Fig. 13) is a fibrocartilaginous structure, usually with a triangular cross section (morphology can vary widely) inserted in the osseous acetabular rim (Seldes et al. 2001). The articular or internal surface is in continuity with the acetabular cartilage and the capsular or external surface is attached to the articular capsule. Inferiorly, the labrum is in continuity with the transverse ligament. The labral vascular supply arises from a periacetabular vascular ring with radial branches that course over the capsular surface of the labrum. As it has its own inner-

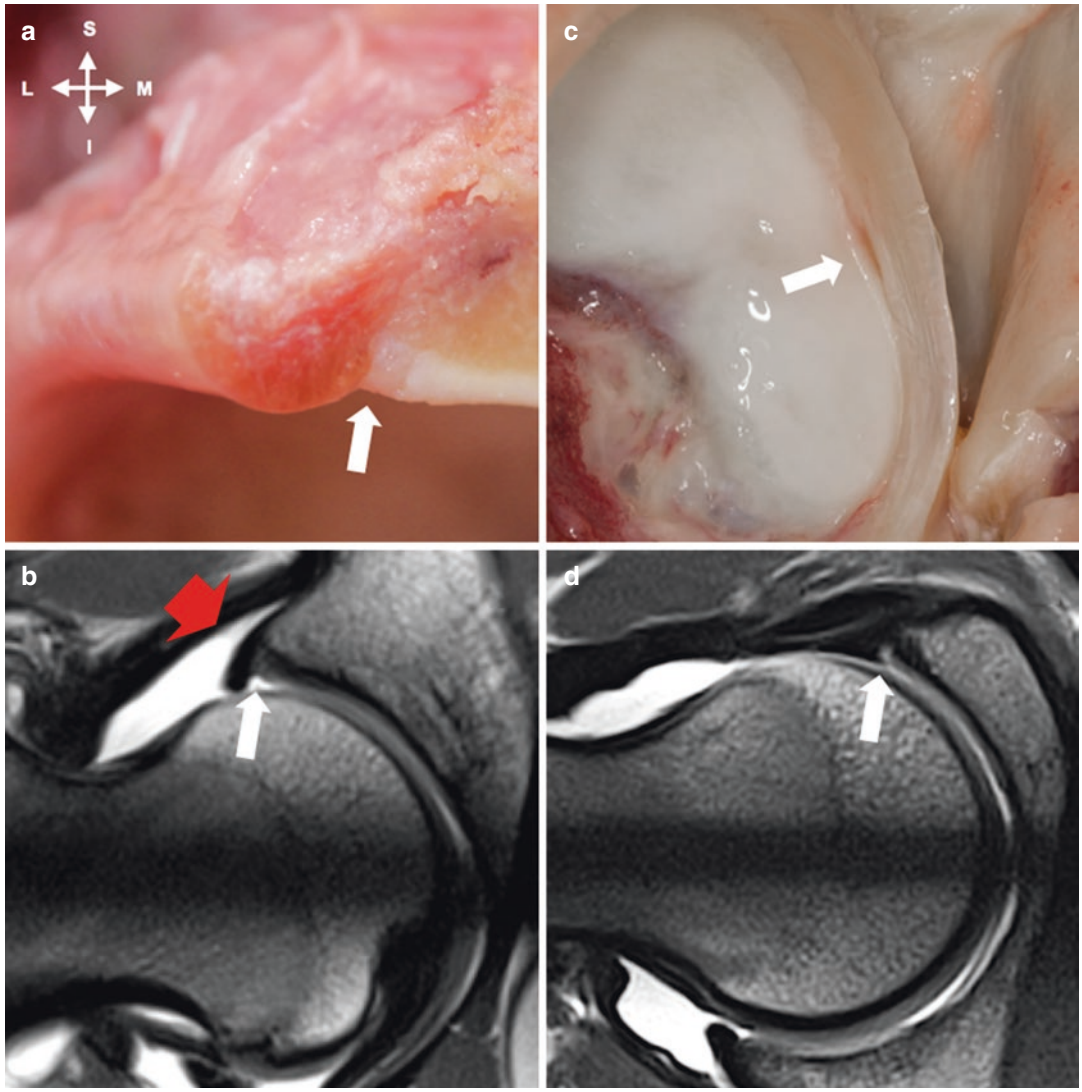

Fig. 13 (**a–d**) (**a**) Macrophotography of the acetabular labrum section. There is a normal depression in the chondrolabral transition and the continuity of the labral tissue with the bone and cartilage surface (arrow). (**b**) Radial proton-density MRA image of the same groove as in (**a**) (arrow) at the postero-superior quadrant. A peri-labral recess is also shown (red arrow). This variant should not be confused with labrum rupture. (**c**) Detail of the anterior articular surface where we frequently observe a more pronounced depression in the chondrolabral continuity (arrow). (**d**) Radial proton-density MRA image of the same recess as in (**c**) (arrow) at an anterior position. *S* superior; *I* Inferior; *M* medial; *L* lateral, *MRA* arthrography magnetic resonance imaging

vation (coming from the obturator nerve; both proprioceptors and nociceptors), when injured the labrum can be an important source of pain (Seldes et al. 2001) and also might explain the decreased proprioception and pain in an athlete with a torn labrum. Like the knee meniscus, the labrum may have the greatest healing potential at the peripheral capsulo-labral junction (Seldes et al. 2001).

Localization: Use either (1) the clock-face method, where 3 o'clock corresponds to anterior and 12 o'clock to a superior position, regardless of laterality of the hip (Blankenbaker et al. 2007), or the (2) a geographic zone classification system

modified from the acetabular zone method described by Ilizaliturri Jr. et al. (2008).

5.1.4.2 Normal Variants (Fig. 13)

Reflect variations of the normal anatomy with no clinical consequences, found in up to 25% of patients at arthroscopy. **Types:** (1) *Perilabral recess*: at the capsular surface of the labrum, between the joint capsule and the labrum. It is present circumferentially with variable depths and usually easily distinguishable from a labral tear. (2) *Sublabral recesses*: found arthroscopically (18–22%) at any location (Saddik et al. 2006), although typically found at the 4 o'clock position or most frequently (48%) at a posteroinferior location at the insertion of the transverse ligament. It is a well-defined cleft between the labrum and the acetabular hyaline cartilage with smooth edges, no signs of inflammation and no labral instability on probing.

5.1.4.3 Labral Tears (Fig. 14)

General considerations: Known causes are direct trauma, capsular laxity, FAI and instability. A combination of the dynamic movements performed in sport and the high prevalence of altered bony hip morphology, in particular cam morphology, is believed to place athletes at greater risk (Agten et al. 2016). Isolated labral tears at an anterior position have been associated with iliopsoas impingement (Blankenbaker et al. 2007). About half of all labral tears are full-thickness tears.

In individuals without pain, a labral tear prevalence per person of 56% was reported while in persons with pain prevalence was 64% (Heerey et al. 2019). Specifically, in sports (such as football, golf and tennis), it appears that athletes do not have a higher prevalence of labral tears than non-athletic individuals regardless of pain status, highlighting a potential discordant relationship between tears and pain (hence only to be consid-

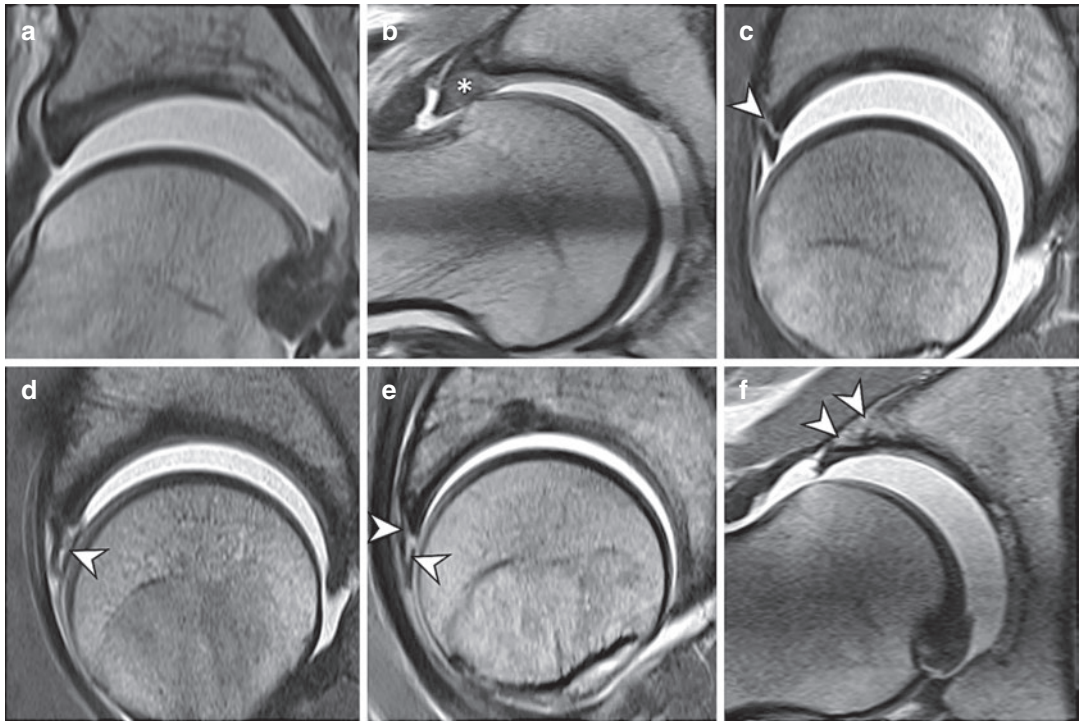

Fig. 14 (**a–f**) Classification of labrum damage patterns (traction MRA). (**a**) Normal labrum; (**b**) intrasubstance labrum degeneration (*); (**c**) labral-chondral separation (=labral detachment) (arrowhead); (**d**) intrasubstance labrum tear (arrowhead); (**e**) complex labrum tear (labral-chondral separation and intrasubstance labrum tear) (arrowheads); (**f**) labral ossification (arrowheads). *MRA* arthrography magnetic resonance imaging

ered relevant with an adequate patient history and suggestive clinical examination).

Localization: anterosuperior quadrant (84–86%; lower compressive elastic and lower tensile modulus compared with other parts of the labrum, favour tears in this location), posterosuperior (16%), anteroinferior and posteroinferior tears (rare) (Sutter et al. 2014).

Differential diagnosis: A recess (1) is located at the base of the labrum, (2) is linear in shape (labral tears may extend into the labral substance), (3) has smooth edges (unlike labral tears, that often have irregular borders), (4) do not extend through the full-thickness of the labrum and (5) are not associated with paralabral cysts.

Imaging and Classification (Fig. 14): Typically, in pincer-type FAI the labrum shows thinning, intrasubstance fissuring, and fraying, while in cam-type FAI there is usually a chondrolabral avulsion. Superior labral tears are best identified on dedicated coronal images, whereas anterosuperior labral tears are best seen on sagittal and/or axial oblique images. Posterior or anterior tears are typically most conspicuous on axial oblique images. Several surgical and MRI-based classifications for description of labrum lesions have been proposed (Czerny et al. 1996; Seldes et al. 2001; Beck et al. 2005). Due to the weak agreement between these classifications, imaging assessment of the acetabular labrum may instead focus on an accurate descriptive report (Schmaranzer et al. 2017; Mascarenhas et al. 2020a) (Table 15).

5.1.5 Cartilage Pathology

5.1.5.1 Anatomy and Imaging Description

Hyaline cartilage consists of four discrete layers: superficial, transitional, deep and calcified. The volume of chondrocytes is highest in the transitional and deep layers, and the orientation of collagen changes at each level. A tidemark between the deep and calcified layers acts as a barrier to vascular penetration.

5.1.5.2 Normal Variants (Fig. 15)

- *Supraacetabular fossa* (10% of individuals): anatomic variant located in the acetabular roof (12 o'clock), probably representing an age-related developmental morphologic variation. Type 1: defect in the subchondral bone and cartilage, filled with joint fluid; Type 2: defect only in the subchondral bone, filled with cartilage (Dietrich et al. 2012).
- *Superior acetabular roof notch* (17% of men and 22% of women on radiographs): sharply delineated, more longitudinally, fluid- or fat-filled pit in the medial aspect of the acetabular roof (Agten et al. 2016).
- *Stellate lesion* (or stellate crease): area of the acetabular roof without cartilage coverage, located more medially than a supraacetabular fossa. Some authors believe it is a residuum of a healed supraacetabular fossa or a healed roof notch (Philippon et al. 2014).

Table 15 Recommended descriptors of labral injury (Mascarenhas et al. 2020a, b), based on inferential evidence (Schmaranzer et al. 2014; Saied et al. 2017; Crespo-Rodríguez et al. 2017)

Parameters	Description	MRI findings
Location/extent	Quadrant description	**Primary findings:** • Increased intra-substance signal intensity • Surface irregularity, truncation, or diminutive appearance • Linearly increased signal intensity traversing the substance of the labrum or at the chondrolabral junction • Contrast material extending into the tear defect (MRA) **Secondary findings:** • Adjacent cartilage abnormalities • Paralabral cyst formation • Adjacent bone oedema
Shape and width	Triangular/round; mm	
Calcifications and ossifications	Location and Size	
Lesion patterns	1. Intrasubstance labrum degeneration	
	2. Intrasubstance labral tear	
	3. Labral-chondral separation (= labral detachment)	
	4. Complex labral tear (both intrasubstance tear and labral-chondral separation)	
	5. Labral ossification	

MRI magnetic resonance imaging, *MRA* arthrography magnetic resonance imaging

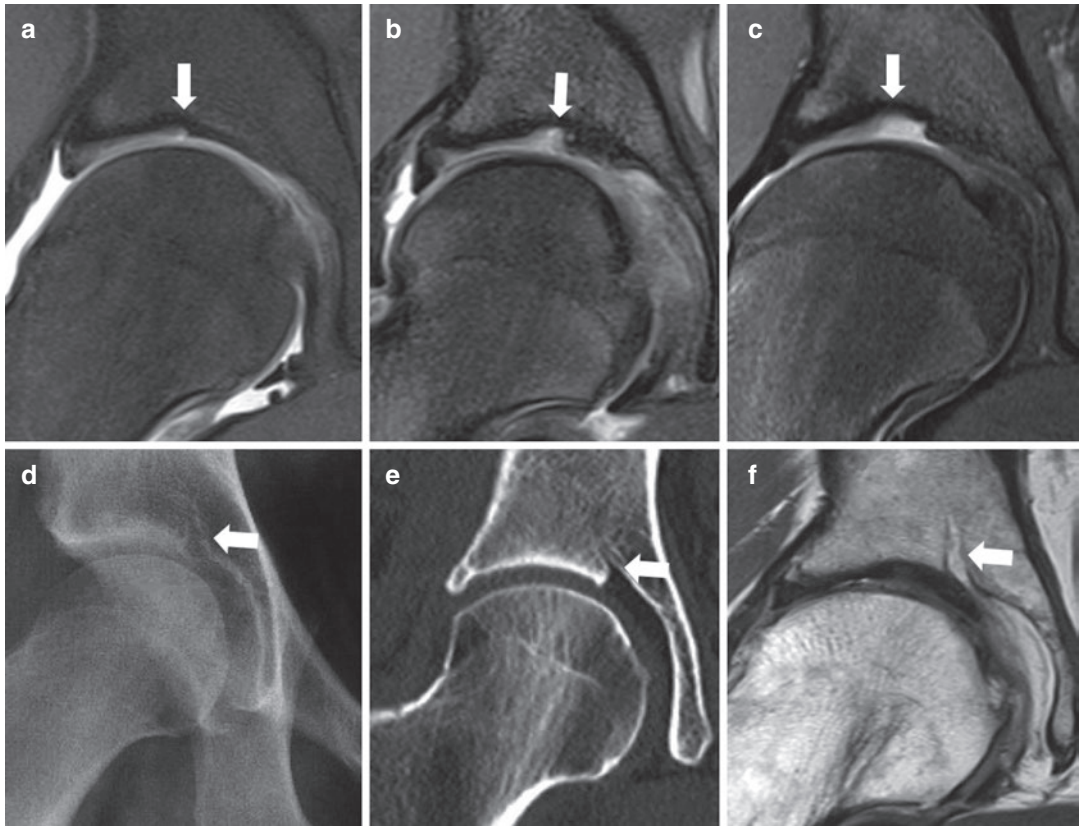

Fig. 15 (**a-f**) (**a–c**) Coronal proton density fat-supressed images with supraacetabular fossa examples with varying degrees and depth. (**d–f**) Superior acetabular roof notch seen on (**d**) radiograph, (**e**) CT and (**f**) MRI (fat-filled superior acetabular roof notch)

5.1.5.3 Cartilage Injury

General considerations: Cartilage defects are commonly seen in athletes, both symptomatic (25–40% of athletes, as opposed to 64% of all symptomatic populations) and asymptomatic (10% of athletes and 12% of all asymptomatic populations) (Heerey et al. 2019). Thus, it could be considered that cartilage defects might contribute to hip-related symptoms and reduction in function, with a trend highlighting a greater prevalence of acetabular chondral lesions observed in symptomatic individuals. Paradoxically, articular cartilage is deficient of neural and vascular supply, rendering it unable to produce pain, reflecting the variable relationship seen between cartilage defects and pain. Conceptually, injury to the articular cartilage affects joint homeostasis, in addition to biomechanical and neuromuscular function. This alteration in joint function combined with athletic activity may accelerate hip joint degenerative change, which is known to occur more frequently in retired athletes.

In athletes, cartilage damage can either result from (1) direct impact injury or (2) underlying bone deformities (Kaya et al. 2016). Cam morphologies lead to cartilage delamination (in 44–52% of FAI cam cases), most often located anterosuperiorly adjacent to labral tears (Anderson et al. 2009). Conversely, acetabular overcoverage may have some protective effect against cartilage delamination, although cartilage lesions are found in the posteroinferior quadrant of Pincer-type FAI patients. Parafoveal cartilage defects posterosuperiorly on the FH have been described in active patients with cam-type FAI participating in activities requiring repetitive, fast and forceful hip flex-

ion (American football, soccer, hurdles and martial arts) (Zaltz and Leunig 2012).

Imaging: Cartilage assessment can be performed with multiple imaging modalities.

- *Radiographs* demonstrate secondary signs of cartilage loss, such as decreased JSW, subchondral sclerosis and marginal osteophyte formation.
- *MRI*: imaging technique of choice. Given the high signal-to-noise ratio and contrast, 2D or 3D gradient-echo or FSE proton density-weighted sequences are the basic imaging techniques used in clinical practice. Additionally, 3D imaging is useful for cartilage volume and thickness measurements.
- *dMRA:* for detecting cartilage disease the sensitivity/specificity may be as high as 79%/94%, respectively (Crespo-Rodríguez et al. 2017). Chondral abnormalities are recognized as (1) focal signal intensity abnormality, (2) contour defects, (3) thinning compared with normal adjacent cartilage, and/or (4) gadolinium contrast material outlining the articular margins and filling surface irregularities or cartilage defects. On fat-supressed proton density and T1w MR images, low-signal intensity within the normally intermediate intensity acetabular cartilage is a helpful sign with high specificity (90–95%; although with low sensitivity, 22–74%) for cartilage delamination detection.
- *Advanced biochemically sensitive MRI techniques*—such as dGEMRIC, T2, T2* and T1ρ mapping, can distinguish subtle early cartilage matrix alterations, thereby acting as tools for early disease detection and monitoring. Despite mapping variations that mirror anatomical differences in various zones and regions of hip joint, there are still many unanswered questions including the standardized application of these techniques and cut-off values to provide an algorithmic cartilage damage-based approach to managing injury. Further evidence that address protocol issues regarding reproducible, objective, and meaningful evaluation of articular hip joint cartilage are necessary (Hemke et al. 2018).

Classification: Description of the location, surface and pattern/grade is recommended (Mascarenhas et al. 2020b) (Table 16 and Fig. 16).

Table 16 Recommended descriptors of cartilage lesions on a hip MRI study (Mascarenhas et al. 2020a, b)

Parameters	Description	Importance
Location[a]	Quadrant description	Diagnostic and surgical planning implications (Zaltz et al. 2014): • location supports a cam/pincer FAI mechanism • posterior lesions are difficult to access by arthroscopy
Surface side[a]	Acetabular or femoral	Surgical planning and prognostic implications as femoral cartilage damage is: • A poor prognostic factor • Easier to treat with open surgery than with arthroscopy
Extent[b]	Any MRI cartilage damage extending <2/>2 "hours" on the clock-face	Long-term outcome of FAIS surgery is worse if cartilage damage is greater than 60° around the clock face (Hanke et al. 2016)
Pattern[a]	*Grades:* 1. no damage 2. any cartilage damage 3. complete cartilage loss *Other descriptors:* 1. peripheral (chondrolabral junction) vs. central 2. any cartilage damage: if possible add details, such as "superficial cartilage damage" or "cartilage delamination"	Surgical planning implications: • Complete cartilage loss in the chondral-labral junction: acetabular rim trimming • Cartilage damage centrally located: cartilage repair procedure

MRI magnetic resonance imaging, *FAI* femoroacetabular impingement, *FAIS* femoroacetabular impingement syndrome
[a]Recommendations based on inferential evidence
[b]Recommendations based on outcome evidence

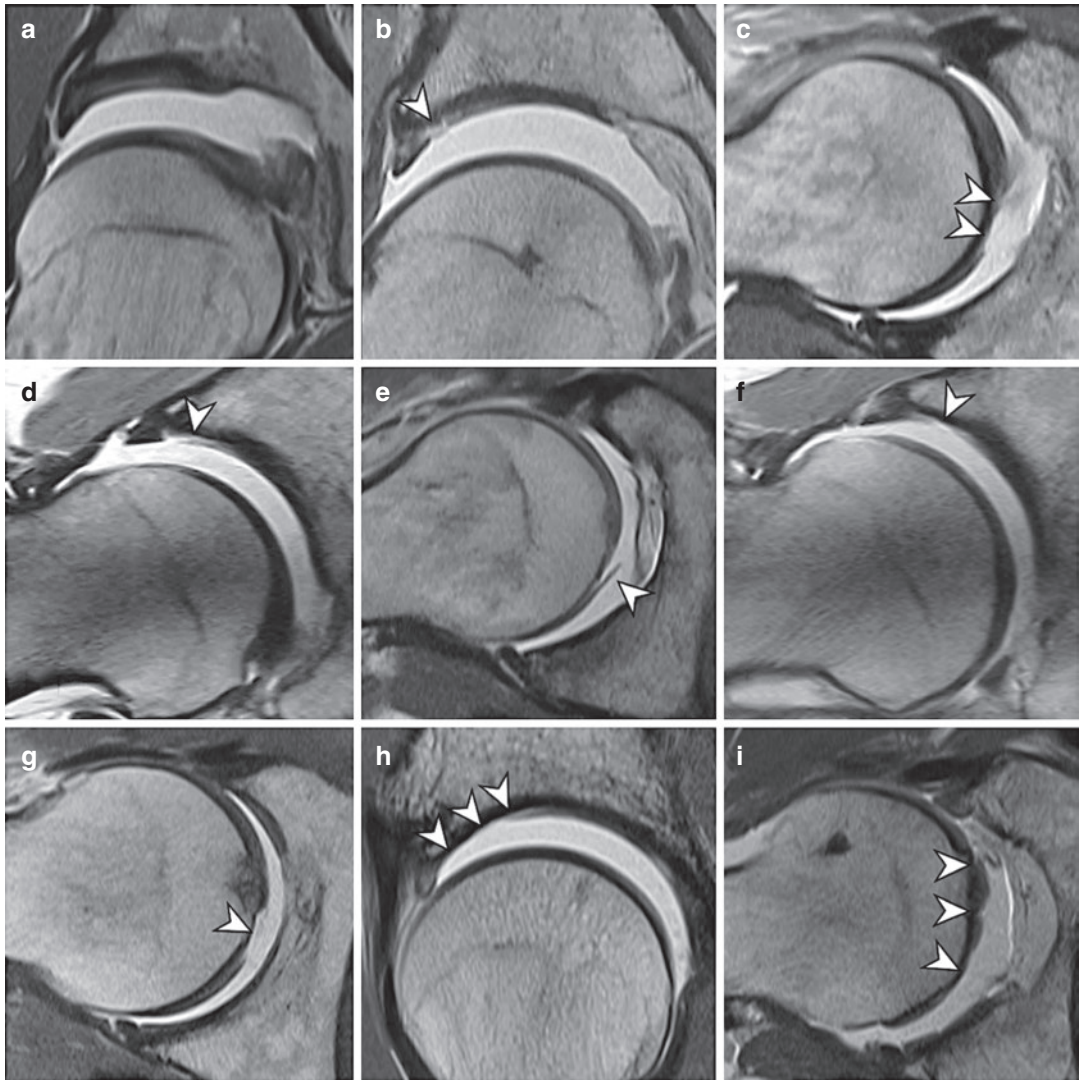

Fig. 16 (**a–i**) Classification of femoroacetabular cartilage damage patterns (traction MRA). (**a**) **Grade 1**: no damage (normal cartilage thickness). **Grade 2**: any cartilage damage, (**b**) focal acetabular and (**c**) femoral partial-thickness cartilage lesion (arrowheads). **Grade 2**: any cartilage damage, (**d**) acetabular cartilage delamination involving the chondral-labral junction and (**e**) femoral cartilage delamination (arrowheads). **Grade 3**: complete cartilage loss, focal full-thickness (**f**) acetabular and (**g**) femoral cartilage lesion (arrowheads). **Grade 3**: complete cartilage loss, diffuse full-thickness (**h**) acetabular and (**i**) femoral cartilage lesion (arrowheads). *MRA* arthrography magnetic resonance imaging

5.1.6 Hip Osteoarthritis

General considerations: Hip OA is not commonly seen in athletes who are currently active at an elite/professional level, even if they have hip and groin pain. The prevalence of hip OA in asymptomatic senior athletes appears similar to that of older non-athletic populations (17% vs. 15%). However, after retirement elite male athletes have a greater prevalence of OA and likelihood of undergoing hip arthroplasty (odds ratio = 2.5) (Gouttebarge et al. 2015). Interestingly, radiographic early hip OA may be seen in younger athletes regardless of the presence or absence of pain, highlighting a discordant relationship between radiographic features observed in early hip OA and pain in active athletes.

What is OA?—It is the most frequently occurring chronic joint disease worldwide (Hawker and Stanaitis 2014). Clinically it is characterized by pain, stiffness and loss of function (Hawker and Stanaitis 2014), and on a tissue level by loss of cartilage, osteophyte formation, subchondral sclerosis and cyst formation (Wang et al. 2016). OA has a detrimental impact on quality of life and represents an increasing economic burden to health systems (Turkiewicz et al. 2014) (both direct and indirect costs).

The lack of a precise definition of the disease has made it difficult to determine the prevalence of OA. There is often a discrepancy between the clinical presentation and the radiographic evidence of OA. In research, the commonly used definitions of hip OA include (1) "symptomatic OA" (ACR criteria) (Hunter et al. 2011), (2) "radiographic OA" (quantified by the Tonnis or Kellgren and Lawrence scale (Kellgren et al. 1963)) or (3) total joint replacement as a result of OA (Hunter et al. 2011).

How to assess?—An AP pelvic radiograph with a standardized technique should be preferably used for measuring joint space width (JSW) and joint space narrowing (JSN) (Fig. 17). Radiographic measurements of JSW and JSN are currently the best way to assess structural progression and disease severity. (Lane et al. 2015). Alternative projections (e.g. false profile) can evaluate JSW/JSN in locations other than the superior aspect of the joint and, when combined with an AP view, may increase sensitivity to detect structural alterations (Maheu et al. 2005). Tönnis classification represents current practice in HPS, although evidence supports that the "minimum JSW" may be preferable compared to the other classification systems (Table 17).

However, considering that several studies used radiographs and these are insensitive to early cartilage damage, the real disease prevalence in athletes may be underestimated. The use of imaging methods with greater sensitivity to early features of OA may be important for identifying athletes at risk of progression to hip OA.

5.2 Hip Peri-articular Pathology

5.2.1 Greater Trochanteric Pain Syndrome

What is it?—Greater trochanteric pain syndrome (GTPS) refers to the clinical manifestation of dis-

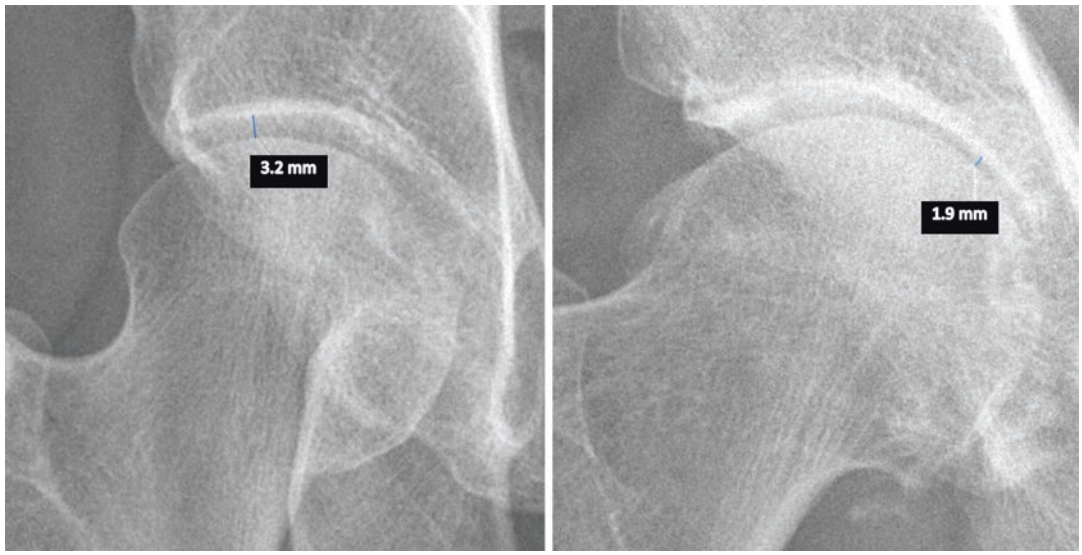

Fig. 17 Examples of measurement of minimum joint space width. This measurement should be carried out in an AP pelvic or hip-centred radiographs. Joint space width should be measured where maximal joint space narrowing is observed, preferably at the weight-bearing region of the hip joint

Table 17 The Tönnis and the Kellgren and Lawrence classifications of osteoarthritis (Busse et al. 1972; Schiphof et al. 2008)

	Tönnis	Kellgren and Lawrence
Grade 0	No signs	No features
Grade 1	Slight narrowing of joint space, slight lipping at joint margin, slight sclerosis of femoral head or acetabulum	Doubtful narrowing of joint space and possible osteophytic lipping
Grade 2	Small cysts, increased narrowing of joint space, moderate loss of femoral head sphericity	Definite osteophytes and possible narrowing of joint space
Grade 3	Large cysts, severe narrowing or obliteration of joint space, severe deformity of femoral head, avascular necrosis	Moderate multiple osteophytes, definite narrowing of joint space, some sclerosis and possible deformity of bone ends
Grade 4	–	Large osteophytes, marked narrowing of joint space, severe sclerosis and definite deformity of bone ends

ease about the GT, presenting with lateral hip pain and focal tenderness on palpation. Abnormalities of the hip abductor tendons (namely *gluteus minimus* (Gmin) and *gluteus medius* (Gmed) tendon) and the GT bursa are the most common aetiologies. It is a common cause for lateral hip pain in active middle-aged women and an increasingly recognized entity in athletes, mainly runners and ballet dancers (Nawabi et al. 2014; Cruz et al. 2019).

What causes it?—The main cause is usually a tendinopathy resulting from chronic repetitive microtrauma of the abductors followed by iliotibial band (ITB) hypertrophy, and, to a lesser extent, abductor tendon tears and degeneration (especially the Gmed and Gmin). GTPS also includes (1) trochanteric bursitis, (2) calcific tendinosis and (3) *coxa saltans*. Two or more of these findings may be found jointly. Paratendinopathy is the earliest manifestation (fluid-like signal intensity superficial to the tendons on MR) (Boric et al. 2019).

Anatomy (Hirschmann et al. 2017)**:** The *GT* has four facets: the anterior, lateral, posterior and superoposterior facets. The Gmin tendon inserts on the anterior facet. The Gmed tendon has two attachments: the anterior (attaches broadly on the lateral facet) and the posterior portions (narrower attachment on the superoposterior facet). *Bursae*: (1) subgluteus minimus bursa (between the Gmin tendon/anterior facet), (2) the subgluteus medius bursa (between the Gmed tendon/lateral facet) and (3) trochanteric bursa (superficial to the posterior facet and deep to the gluteus maximus muscle).

Imaging (Boric et al. 2019):

- *Radiographs:* usually normal, although calcifications adjacent to the GT may be seen.
- *US*: Sonopalpation is useful for reproducing pain. *Tendinopathy* is defined by tendon thickening and heterogeneous hypoechogenicity. *Peritendinous hyperaemia* may be demonstrated at Doppler. *Enthesopathy* is manifested by bony irregularity at the GT facet insertion. Anechoic defects within the tendon are consistent with tendon tears (partial or full-thickness).
- *MRI:* gluteal *tendinopathy* is characterized by tendon thickening and increased intrasubstance signal intensity on T2-weighted images, with peritendinous oedema representing *paratendinopathy*. A focal defect in tendon fibres suggests a partial-thickness *tear*. In the setting of complete tendon tear, there is often (1) retraction of torn fibres with fluid and/or granulation tissue filling the tear defect, (2) a "bald" GT facet sign when there is complete absence of the Gmed or Gmin tendon insertions, similar to the shoulder rotator cuff.

5.2.2 Snapping Hip

What is it?—It is characterized by sudden painful, audible snapping around the hip, typically seen in young athletic adults. Painful symptoms are reproduced with specific

movements, most frequently moving the hip from a frog-leg position to a neutral position (Boric et al. 2019).

What causes it?—Two forms: (1) intra-articular (due to intra-articular disease) and (2) extra-articular causes (these are further divided into external and internal types) (Boric et al. 2019).

1. **Internal snapping hip syndrome** (or iliopsoas snapping) (Agten et al. 2016; Hegazi et al. 2016):
   (a) Caused by sudden movements of the iliopsoas tendon over either (1) the iliopectineus eminence, (2) the FH, (3) a paralabral cyst or (4) the medial aspect of the iliac muscle. It can be accompanied by an iliopsoas tendinopathy and/or bursitis. When the leg is brought into extension, the tendon moves smoothly into a position in contact with the pubic bone.
   (b) Can be asymptomatic. Symptomatic cases most commonly occur with activities or sports that require significant hip ROM, such as dance, soccer, hockey and football.
   (c) **Imaging**: dynamic US can show in real time the sudden displacement of the referred tendons over the underlying structure or pathological structure. US and MRI can reveal iliopsoas tendinopathy and iliopsoas bursitis.
2. **External snapping hip syndrome** (including iliotibial band snapping) (Agten et al. 2016; Boric et al. 2019):
   (a) Involves lateral structures such as the ITB and the *gluteus maximus* muscle. Snapping occurs as these structures move over the GT during hip flexion and extension. The underlying cause could be a thickening of the posterior part of the ITB and the anterior part of the *gluteus maximus*.
   (b) Athletes, particularly runners, dancers, soccer players and weight lifters, may experience popping movements of the ITB or the *gluteus maximus* muscle over the GT during full hip extension.
   (c) **Imaging**: It is usually a clinical diagnosis and seldom requires imaging. US can show in real time the sudden displacement of the ITB or the *gluteus maximus* muscle over the GT and fluid in the trochanteric bursa. Other US findings are a hypoechoic and thickened ITB at the level of the GT. MRI can also reveal reactive fluid within the trochanteric bursa from repetitive mechanical snapping, between the Gmed tendon and the *gluteus maximus* muscle/iliotibial band, sometimes extending posteriorly around the GT.

5.2.3 Extra-articular Hip Impingement Syndromes

5.2.3.1 Deep Gluteal Pain Syndrome (and Piriformis Syndrome)

What is it (Hernando et al. 2015; Kizaki et al. 2020)**?—**The deep gluteal pain syndrome (DGPS) definition comprises three characteristics: (1) non-discogenic, (2) sciatic nerve pain and (3) entrapment in deep gluteal space (DGS). Common and underdiagnosed causes are fibrovascular bands and entrapment related to the external rotator muscles. Piriformis syndrome can be classified as a subgroup of DGPS (Fig. 18).

Anatomy (Hernando et al. 2015)**:** The DGS is the cellular and fatty tissue located between the middle and deep gluteal aponeurosis, not clearly visible on MR, limited by (1) *posteriorly*: *Gluteus maximus* muscle, (2) *inferiorly*, continues into and with the posterior thigh, (3) *laterally* it is demarcated by the *linea aspera* and the lateral fusion of the middle and deep gluteal aponeurosis layers extending up to the *tensor fasciae lata* muscle via the iliotibial tract, (4) *anteriorly* by the posterior face of the femoral neck and the GT and (5) *medially* comprised of the greater and minor sciatic foramina.

Diagnosis (Kizaki et al. 2020): The general diagnostic pathway for DGPS is composed of (1) clinical history (posterior hip pain, radicular pain, and difficulty sitting for 30 min), (2) physical examination (tenderness in deep gluteal space, positive seated piriformis test, and positive Pace sign), (3) imaging tests (pelvic radiographs,

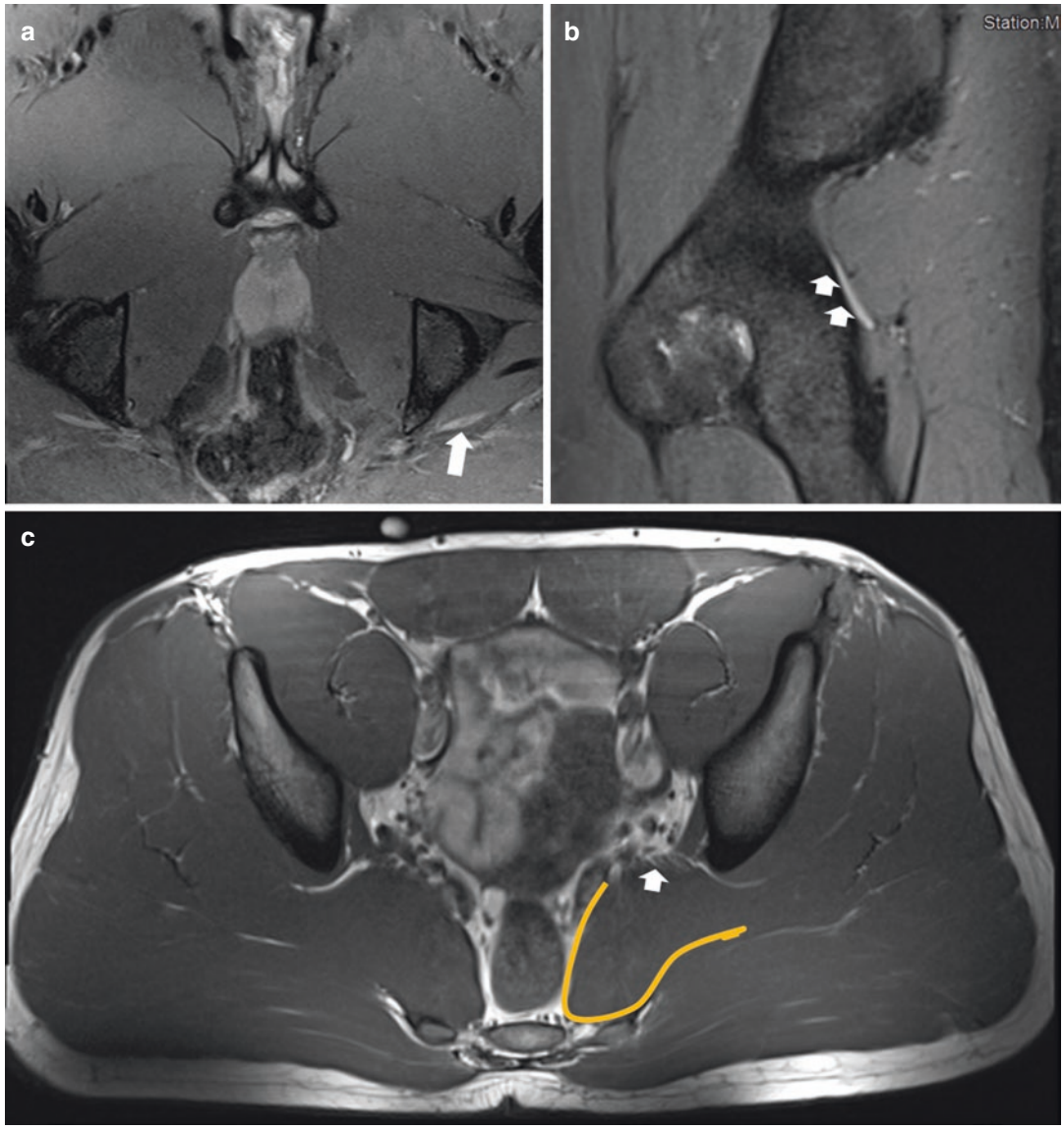

Fig. 18 Male soccer player, 28 years old. Bilateral piriformis hypertrophy (piriformis syndrome), symptomatic on the left. (**a**) Axial oblique PD Fat-Sat and (**b**) sagittal PD Fat-Sat show oedema and enlargement of the left sciatic nerve (white arrows), entrapped beneath an enlarged piriformis muscle. (**c**) Pelvis T1w shows bilateral hypertrophic piriformis muscle (orange curved line) with the enlarged sciatic nerve (white arrow)

pelvic MRI, and spine MRI) and (4) local imaging guided injections (perineural injections with corticosteroid and local anaesthetic have both a diagnostic and therapeutic function).

Imaging: The sciatic nerve/subgluteal space is not routinely scoped during hip arthroscopy, and therefore a preoperative diagnosis of sciatic nerve entrapment on MRI is necessary. *MRI* is the diagnostic procedure of choice and may substantially influence management of these patients. MRI may identify (1) anatomical muscle or tendons variations and (2) sciatic nerve abnormalities, such as signal changes. The normal sciatic nerve is a well-defined oval structure, isointense to adjacent muscle tissue (T1w). On T2-weighted or short tau inversion recovery images, the normal sciatic nerve is isointense or mildly hyperintense to muscle and hypointense to regional

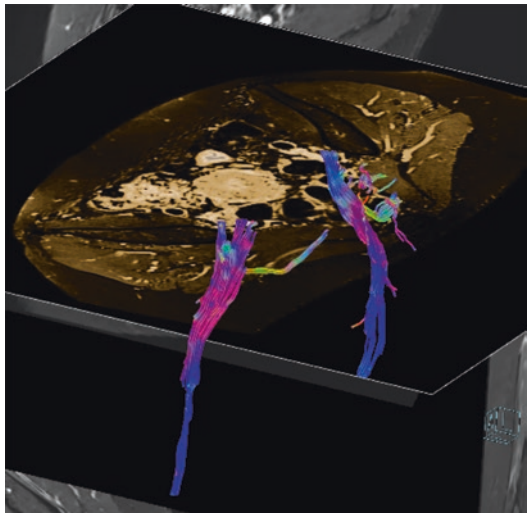

Fig. 19 Female non-athlete, 48 years old. MR tractography showing altered parameters and enlarged right sciatic nerve in the deep gluteal space (middle and distal segments)

vessels, with clearly defined fascicles separated by interposed lower signal connective tissue (Hernando et al. 2015).

MR neurography: The use of high resolution and high field strength equipment revealed excellent anatomic capability to demonstrate sciatic neuritis and entrapment. *Diffusion tensor imaging and diffusion tensor tractography* of the sciatic nerve (Fig. 19) have shown promising capabilities in patients with suspected entrapment (Hernando et al. 2015; Nakano et al. 2017; Kizaki et al. 2020).

5.2.3.2 Ischiofemoral Impingement

What is it?—It is a form of atypical, extra-articular hip impingement defined by hip pain related to narrowing of the space between the ischial tuberosity and the femur (Singer et al. 2015). In asymptomatic elite gymnasts, however, a narrowed ischiofemoral space (IFS) and oedema in the *quadratus femoris* (QF) muscle are frequent findings, often bilaterally.

What causes it?—The aetiology is multifactorial including (1) anatomical variants (of the proximal femur or pelvis; e.g. *coxa valga*), (2) hip or pelvic/spinal instability, (3) muscle imbalance (e.g. abductor/adductor), (4) overuse or extreme hip movements, (5) ischial tuberosity/hamstring enthesopathies, (6) trauma, (7) iatrogenic conditions and (8) tumours (Singer et al. 2015).

Anatomy: The IFS lies between the ischial tuberosity and the lesser trochanter. The quadratus femoris space (QFS) lies between hamstring tendons and lesser trochanter.

Diagnosis (Singer et al. 2015): based in suggestive clinical presentation and MRI findings (Table 18 and Fig. 20). MRI signal abnormalities are present within the IFS in 9.1% of asymptomatic patients.

- *Clinical presentation* (Hernando et al. 2016): Pain in the DGS, often on dynamic movement, radiating to the groin, buttock and hip region. Clicking and locking is also described. Physical examination is imprecise and often difficult to interpret.
- *Imaging* (Hernando et al. 2016): MRI is the diagnostic procedure of choice as it may substantially influence clinical management (best assessed on axial views). Dynamic MRI utilizing a full range of rotation will help to confirm impingement (see Table 18 for characteristic findings).
- *Injection test of the IFS*: paramount in many cases as it has both a diagnostic and therapeutic function.

5.2.3.3 Subspine Impingement

What is it?—It is an osseous and/or soft-tissue impingement due to a mechanical conflict following an altered position or morphology of the AIIS which impacts the distal femoral neck and FHN junction particularly during hip flexion (clinical-radiologic diagnosis) (Nakano et al. 2017).

Anatomy: The AIIS (origin of the direct tendon of the *rectus femoris* muscle and the tendon of the *iliocapsularis* muscle) may have a variable morphology (based on the relations between the AIIS and the anterosuperior acetabular rim). *Types* described: (1) type I (normal)—a smooth ilium wall between the AIIS and the acetabular rim; (2) type II—AIIS extends to the level of the rim; (3) type III—AIIS extends distally to the

Table 18 Peri- and extra-articular hip impingement syndromes

	Clinical characteristics	Physiopathology	Radiologic findings
Deep Gluteal Pain Syndrome	• Men = women, typically >40 years • Cx confused with lumbar and intra- or extra-articular hip diseases • Sitting pain with the absence of lumbar spine pathology on imaging • Active piriformis test and seated piriformis test stretch	• Multifactorial aetiology of sciatic nerve entrapment through its subgluteal path. • **Causes**: iatrogenic (30%; previous injection/intervention), piriformis syndrome (26%), trauma (15%), non-piriformis (hamstring, obturator internus) muscle pathology (14%), skeletal injury and entrapment (7%), endometriosis (6%), and vascular compression (2%) • First-line therapy includes injection and physiotherapy	• Image-guided injections(US or CT/MRI guided) are a useful tool to diagnose and treat this syndrome. • MRI, MRN and MR tractography. • Typically morphological muscle/tendons anomalies (namely piriformis syndrome), fibrovascular bands and sciatic neuritis. • Neural alterations: (1) Neural enlargement, (2) loss of the normal fascicular appearance, (3) increased perifascicular and endoneural signal intensity on fluid sensitive sequences
Ischiofemoral impingement	• ↑ Women, 50–55 y.o. (range 11–77) • Pain in the deep gluteal region, ↑ ER-EX-AD • Positive ischiofemoral impingement test, and long stride walking test	• Multifactorial aetiology • Reduced IFS or QFS with quadratus femoris muscle impingement • Quadratus femoris muscle injury with variable severity	• QF muscle: oedema ± fatty atrophy ± tear • Narrowed IFS (cut-off of ≤15 mm, a sensitivity/specificity/accuracy of 76.9%/81.0%/78.3%, respectively) • Narrowed QFS (cut-off of ≤10.0 mm results in sensitivity/specificity/accuracy of 78.7%/74.1%/77.1%, respectively) • Sciatic neuritis
Subspine AIIS impingement	• ↑ Men, 15–30 y.o., sports active ≈ FAI • Groin/anterior pain ↑ Forced FL • Positive impingement test	• Acute or chronic pain due to repeated microtrauma to the RF insertion in the AIIS → apophysis, osseous or tendinous avulsion **Aetiology**: • Extra articular (AIIS hypertrophy or elongation; primary or, secondary to trauma, acetabular retroversion or post-PAO) • Intra-articular (morphological alteration in the subspinal space)	• Osseous abnormality of the AIIS or subspinal space (deformity or excessive elongation, with caudal extension at or below the acetabular rim level) • Heterotopic ossifications in the path of the *rectus femoris* muscle • Ganglion cysts in the femoral neck in a more distal location than seen in FAI. • Fracture of the acetabular rim, focal chondrolabral damage
Iliopsoas impingement	• 25–35 y.o. • Groin/anterior pain, ↑ FL and prolonged sitting	• Excessive contact of the iliopsoas tendon over the labrum, particularly with EX movements • Signs of FAI may be absent	• MRI/MRA • Lesion of anterior labrum (3 o'clock position)
Trochanteric-pelvic impingement	• Men = women, 15–40 y.o. • Posterolateral pain, ↑ EX and ABD • Positive "gear stick" sign	• Morphological alteration of the femoral proximal epiphysis of multifactorial aetiology → abnormally high position of the GT with respect to the femoral head, *coxa vara* • Hypermobility or hyperlax (without morphological alterations)	• Radiographs: AP pelvis and hip • Typical morphological alterations; (1) *coxa vara*, *magna*, *brevis* or *plana*, (2) high position of GT ± DDH

Cx clinical features, *FL* flexion, *EX* extension, *ABD* abduction, *AD* adduction, *ER* external rotation, *IFS* ischiofemoral space, *QFS* quadratus femoris space, *GT* greater trochanter, *PAO* periacetabular osteotomy, *AIIS* anteroinferior iliac spine, *MRN* MR neurography, *DDH* developmental hip dysplasia, *MRI* magnetic resonance imaging, *MRA* magnetic resonance arthrography, *yo* years old, *RF* rectus femoris, *AIIS* antero-inferior iliac spine, *AIIS* antero-superior iliac spine, *FAI* femoracetubular impingement

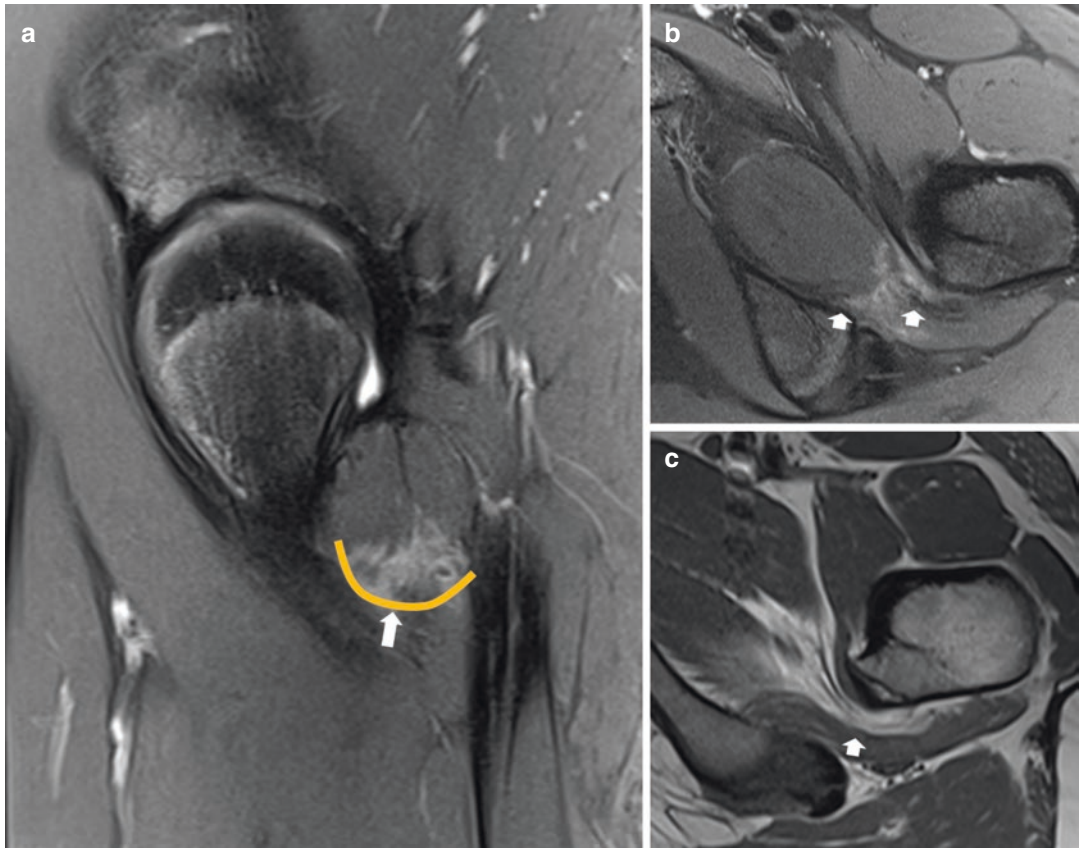

Fig. 20 (**a**–**c**) Ballet male dancer, 32 years old. Symptomatic ischiofemoral impingement. (**a**) Sagittal PD Fat-Sat. Moderate oedema (orange line and white arrow) with fatty atrophy of the *Quadratus femoris* muscle. (**b**) Axial PD Fat-Sat and (**c**) T1w show narrowed IFS (around 14 mm) and borderline QFS (10 mm) (white arrows). No sciatic neuritis or hamstring changes were depicted

acetabular rim. Type II and III variants are associated with a decrease in hip flexion and internal rotation, although they may be asymptomatic (Hetsroni et al. 2013).

Diagnosis (Fig. 21): Conjunction of characteristic clinical and imaging findings (Galeano et al. 2018).

– *Clinical Presentation*: anterior hip or groin pain aggravated with certain sporting activities such as the ball-kicking/speed-running when playing soccer. Sometimes it unilaterally affects the dominant leg.

Imaging

- Radiographs: AP pelvis radiograph, hip Lequesne's false profile and three-dimensional CT play important roles since they allow the orthopaedic surgeon to perform an adequate preoperative evaluation.
- MRI/MRA role is detecting associated intra-articular pathology as fractures of the acetabular rim and focal chondrolabral lesions are similar to the ones visible in the pincer type of FAI (see Table 18 for characteristic findings).

5.3 Pelvis

5.3.1 Stress Fractures

General considerations: Stress fractures (SF) are caused by mechanical overload of bone and comprise a spectrum of bone strain, stress reaction and true stress fractures. They occur when

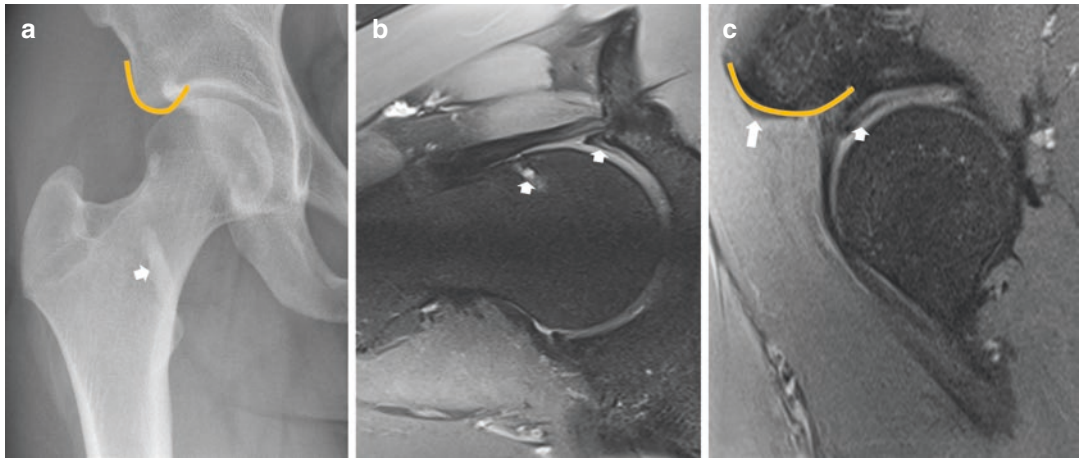

Fig. 21 (**a–c**) Male soccer player, 25 years old. Right subspine impingement. (**a**) Right AP hip radiograph showing a prominent AIIS (orange line) with caudal extension below the acetabular rim level (type 3). Also, heterotopic ossifications are seen in the path of the *rectus femoris* muscle (white arrow). (**b**) Radial fat-supressed proton density at 2 o'clock. Associated ganglion cysts in the femoral neck and acetabular chondral delamination is seen (white arrows). (**c**) Sagittal fat-supressed proton density. Osseous abnormality of the AIIS, deformed and with excessive elongation (orange curved line) with acetabular cartilage delamination (small white arrow)

repetitive mechanical stresses are applied to bone, none of which intense enough to cause an acute fracture. Although in reality both mechanisms often coexist in athletes (e.g. young females with osteopenia) (Marshall et al. 2018), conceptually SF can be divided in

1. *Fatigue fractures*: mainly seen in young, active individuals, when supraphysiologic repeated stress is applied to a bone with normal elastic resistance.
2. *Insufficiency fractures*: more commonly seen in the elderly population, caused by repeated mechanical stress, within the normal physiologic range, applied to a bone with diminished elastic resistance (most commonly due to osteoporosis).

Stress fractures are more common in women, athletes and military recruits, and usually occur in weight-bearing bones. SF of the femur and pelvis account for approximately 4.2–48.0% and 1.3–5.6% of SF in athletes, respectively (Liong and Whitehouse 2012). They may occur anywhere in the pelvic region and femur, but predominate in the proximal femur, sacrum and inferior pubic ramus (Table 19). Certain activities, such as running, are associated with a high incidence of these lesions. Furthermore, osteoporosis, previous irradiation of the pelvis, the "female athlete triad" (low energy availability, with or without disordered eating, menstrual dysfunction and low bone mineral density), corticoid therapy, total hip replacement and spinal instrumentation are factors associated with pelvic SF (Peh et al. 1996; Vavken et al. 2008; Miller et al. 2015).

Femoral neck stress fractures (predominantly of the fatigue type) (Fig. 22) are particularly worrisome, as they can progress to complete fractures with dislocation and result in avascular necrosis of the FH. When these fractures involve the tension (lateral) side of the femoral neck the risk is higher, as opposed to compression (medial) side fractures (Marshall et al. 2018). Some of these lesions are uncommon and require a high level of suspicion for adequate diagnosis (e.g. sacral fractures in young female runners (Major and Helms 2000)). In older patients, stress fractures (predominantly of the insufficiency type) commonly involve the sacrum and pubic rami, in one or both sides of the pelvis (Figs. 23 and 24). The supraacetabular region, ilium and pubic rami are other occasional locations of stress fractures.

Imaging Assessment

- *Radiographs:* useful in first-line assessment and for differential diagnosis, although they are inaccurate in the initial demonstration of stress lesions. Radiographic findings may not appear in every patient, and, even if they do, it may take weeks to months after the onset of symptoms (Greaney et al. 1983). Findings include: (1) focal osteopenia or blurring of bone contours, followed by (2) focal periosteal reaction and linear sclerosis or a (3) frank fracture line, usually perpendicular to the cortex and trabeculae.
  - *MRI*: gold standard technique in the assessment of stress lesions. It is both sensitive and specific to evaluate the continuum of stress response and is able to differentiate stress reactions (bone marrow oedema on fluid-sensitive sequences, associated with periosteal, endosteal and peri-osseous oedema, but no fracture line) from a stress fracture (when a fracture line becomes evident).
  - *CT* can show bony detail to a better degree and is frequently used in the evaluation of the bony pelvis and as a problem-solving tool when other techniques are equivocal. Sclerotic bands or fracture lines can easily be demonstrated with CT (Fig. 23) but it cannot show the early stages of stress lesions.
  - *Bone scintigraphy* is a very sensitive technique that can show early stress lesions, but it lacks specificity and has limited spatial resolution.

Table 19 Topographic distribution and associated sports in pelvic and proximal femoral stress injuries (Kiuru et al. 2003; Liong and Whitehouse 2012)

Location	% of cases	Associated activities
Sacrum	16,1%	Long-distance running, hockey, basketball, tennis and volleyball
Inferior pubic ramus	19,5%	Long-distance running
Superior pubic ramus	1,7%	Football
Iliac bone/ Acetabulum	2,3%	Running
Femoral neck	40,2%	Long-distance running, jumping and ballet dancing
Femoral proximal shaft	19,5%	
Femoral head	0,6%	

5.3.2 Muscles, tendons and enthesis

5.3.2.1 Apophyseal Injuries

General considerations: Apophysis are normal bony outgrowths that serve as insertion points for tendons and ligaments. They arise from a separate ossification centre, fusing to the remaining bone later in life (Table 20). Mechanical stress applied to the muscle-tendon-bone unit in the adult athlete may result in tendon tear or myotendinous lesions. In the child or adolescent, the weakest structure in this unit is the cartilaginous growth plate of the unfused apophysis, which may tear and displace as a result of traction stress, resulting in bony or cartilage avulsion.

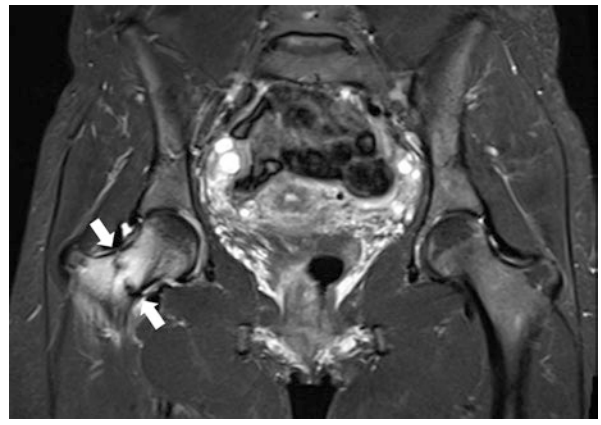

Fig. 22 Incomplete stress fracture involving the tension and compression sides of the femoral neck in a 29-year-old female trail runner. Coronal STIR image of the pelvis shows extensive bone marrow oedema in the right femoral neck, associated with cortical discontinuity and a transverse hypointense trabecular fracture line (arrows)

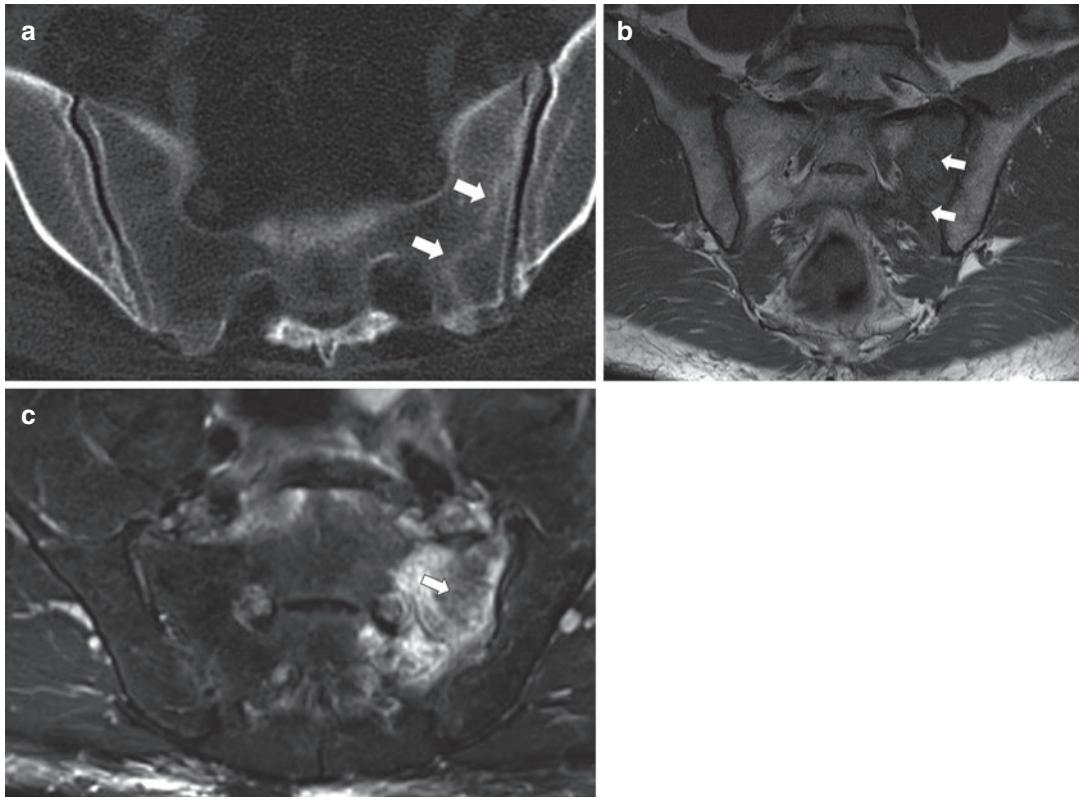

Fig. 23 (**a–c**) Stress fracture of the sacrum in a 61-year-old woman with spinal arthrodesis (not shown). (**a**) Axial oblique CT scan image reveals linear hyperdensity on the left sacral wing (arrows), paralleling the sacroiliac joint space. Arthrodesis-related abnormal distribution of loads may be a factor contributing stress. (**b** and **c**) 35-year-old non-professional athlete. (**b**) Coronal oblique T1w and (**c**) axial oblique fat-suppressed T2-weighted images show a similar stress fracture (arrows), surrounded by extensive bone marrow oedema

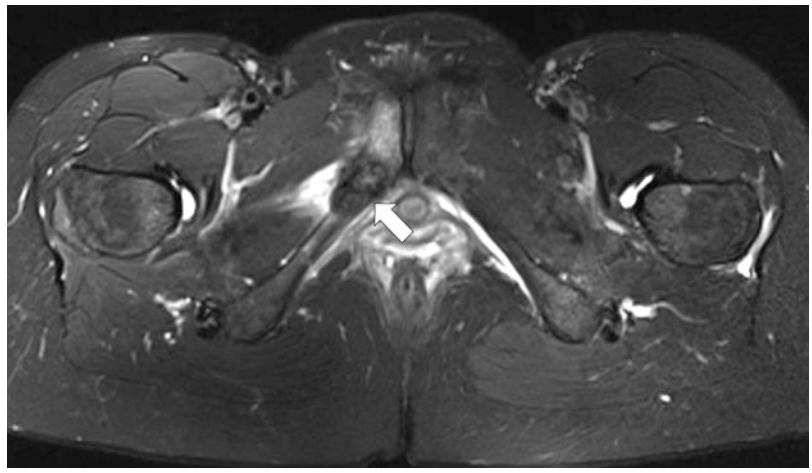

Fig. 24 Pubic ramus stress fracture in a 45-year-old non-professional athlete (long-distance runner). Axial fat-supressed T2-weighted image of the pelvis depicts a right inferior pubic ramus fracture (arrow) with surrounding bone and soft tissue oedema

Table 20 Appearance and fusion of pelvic apophyseal ossification centres (Boyd et al. 1997)

Ossification centre	Appearance	Fusion
Iliac crest	13–15y	15–17y
Anterior-superior iliac spine	13–15y	21–25y
Anterior-inferior iliac spine	13–15y	16–18y
Ischial tuberosity	16–18y	19–25y
Greater trochanter	2–5y	16–18y
Lesser trochanter	8–12y	16–18y

Apophyseal avulsion fractures are typically seen in the developing skeleton, being more prevalent in male adolescents. They usually occur after a strong sudden pull exerted on the apophysis by muscle contraction, although they may also be caused by chronic repetitive microtrauma. Intensive training further aggravates the structural imbalance at the muscle-tendon-bone unit in the young athlete, due to the combined effect of increased repetitive traction stresses and training-induced hypertrophic muscles (which place increased traction forces across the growth plate) (Boric et al. 2019). Sports that involve kicking, jumping and sudden velocity changes, such as football, rugby and sprinting, are frequently implicated.

Apophyseal avulsions are unusual in the mature skeleton and should prompt a search for an underlying cause. Avulsion of the lesser trochanter in an adult patient, in particular, should be considered a sign of metastatic disease until proven otherwise (Sanders and Zlatkin 2008).

The pelvis is a frequent location of apophyseal injury (Fig. 25). Although any pelvic enthesis can be affected, the (1) ASIS, (2) AIIS and (3) ischial tuberosities are more commonly injured (Table 21).

Diagnosis: While (1) **clinical presentation** is often diagnostic (onset is typically sudden, after the inciting event, with focal pain, swelling and gait impairment), (2) ***AP and oblique radiographs*** with contralateral comparison views are important to assess the size and degree of displacement of the avulsed fragment (Fig. 26). They may be inconspicuous however, if the apophysis is non-displaced or non-ossified, in which case US or MRI can be very helpful (Figs. 27, 28, 29, and 30). (3) ***MRI*** may show discontinuity of the apophysis, along with bone, physeal and soft tissue oedema and associated muscle and tendon injuries. (4) **CT** may have a role to better delineate bone detail in equivocal cases. Occasionally, exuberant callus formation can have an aggressive imaging appearance and be misinterpreted as neoplasm or infection (Sanders and Zlatkin 2008). A high degree of suspicion, along with a detailed clinical history and thorough anatomic knowledge should help avoid this pitfall.

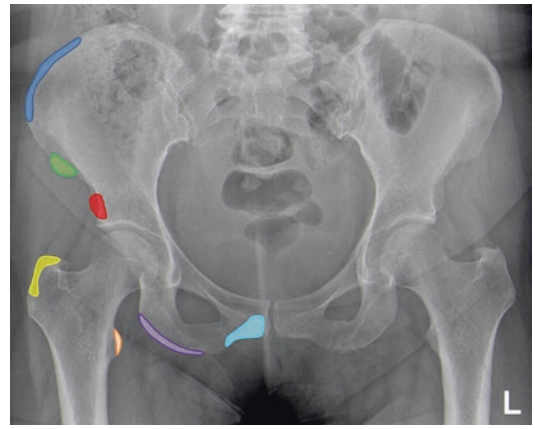

Fig. 25 AP radiograph of the pelvis depicting common and uncommon sites of apophyseal avulsion fractures: insertion of the abdominal wall muscles at the iliac crest (dark blue), insertion of the tensor fascia lata and sartorius tendons at the anterior superior iliac spine (green), insertion of the direct head of the rectus femoris tendon at the anterior inferior iliac spine (red), insertion of the gluteus medius and minimus tendons at the greater trochanter (yellow), insertion of the iliopsoas tendon at the lesser trochanter (orange), insertion of the hamstrings at the ischial tuberosity (purple) and insertion of the adductors and gracilis at the symphysis pubis (light blue)

Table 21 Prevalence and sports distribution of pelvic apophyseal avulsion injuries (Eberbach et al. 2017)

Location	Prevalence	Main associated activities
Ischial tuberosity	11–54%	Gymnastics and football
Anterior-inferior iliac spine	22–49%	Football, athletics and tennis
Anterior-superior iliac spine	19–30%	Football, athletics and gymnastics
Iliac crest	2–10%	Football, gymnastics and tennis
Pubic symphysis	0–3%	Football and fencing
Lesser trochanter	0–2%	Ball sports

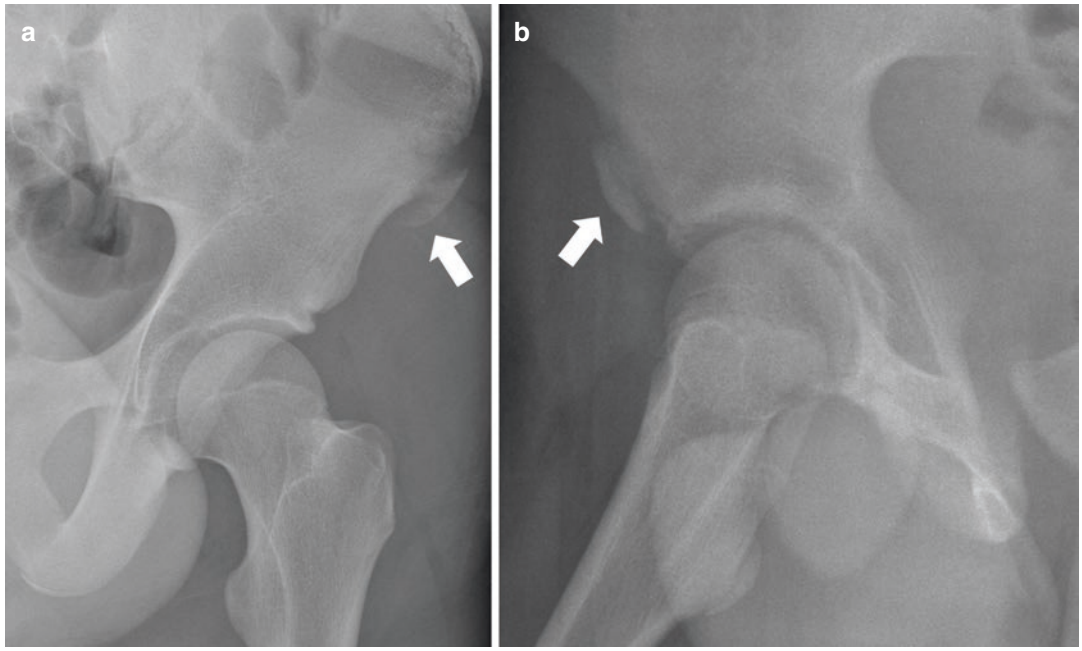

Fig. 26 (**a**, **b**) Iliac spine avulsion injuries. Oblique hip radiographs in adolescent males after (**a**) sprinting and (**b**) football injuries, depicting apophyseal avulsion fractures (arrows) of the (**a**) ASIS and (**b**) AIIS. *AIIS* anterior inferior iliac spine, *ASIS* anterior superior iliac spine

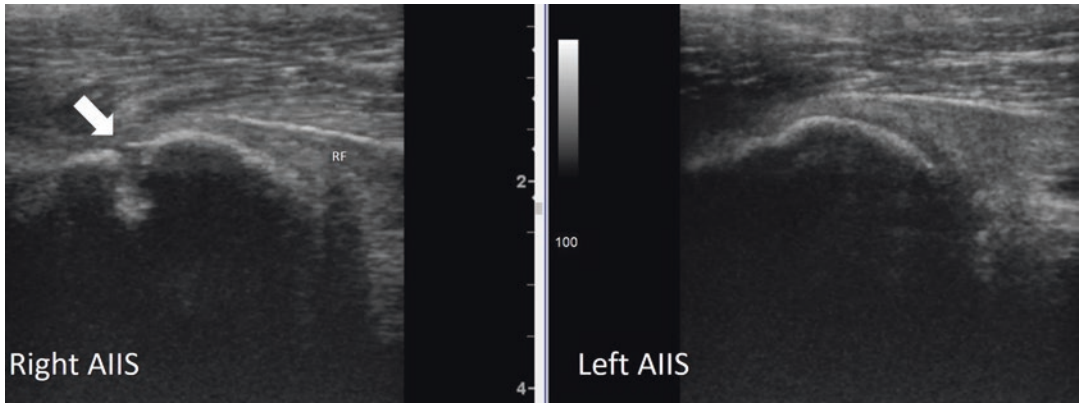

Fig. 27 14-year-old boy with anterior right hip pain after a football injury ("kicking in the air"). Longitudinal US scan of the insertion of the direct tendon of the rectus femoris (RF) on the right AIIS, evidencing apophyseal separation (arrow). The left asymptomatic side is shown for comparison. *AIIS* anterior inferior iliac spine, *US* ultrasound

Treatment is usually conservative, but when significant displacement occurs (more than 1.5–2 cm), surgery may be beneficial. Residual post-traumatic apophyseal deformity or non-union (Fig. 31) at specific locations may cause soft tissue impingement (e.g. subspine or ischiofemoral) (Calderazzi et al. 2018).

5.3.2.2 Muscle and Tendon Injuries

General considerations: Muscle lesions are the most common pelvic injuries in sports (Boyd et al. 1997; Brittenden and Robinson 2005). They can be caused by indirect (stretch-induced) or direct (contusion or laceration) trauma.

In the adult athlete, the myotendinous junction (MTJ) is a particularly vulnerable region from

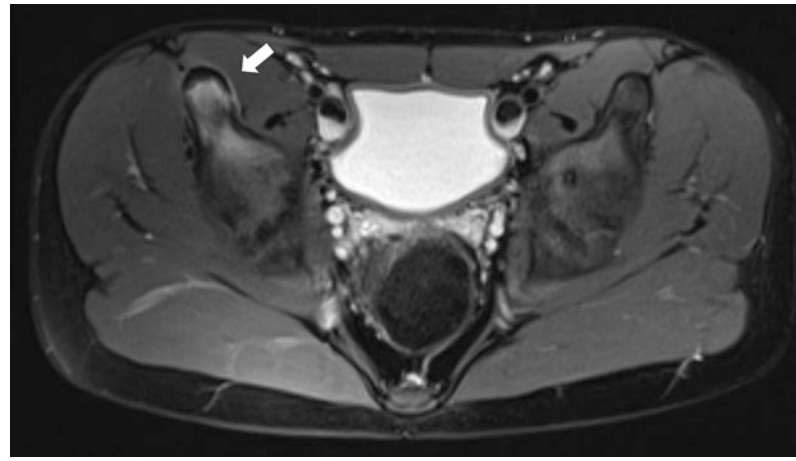

Fig. 28 15-year-old boy with anterior hip pain after a football injury. Axial fat-supressed T2w image of the pelvis shows bone and soft tissue oedema involving the right anterior inferior iliac spine (arrow), consistent with non-dislocated apophyseal avulsion

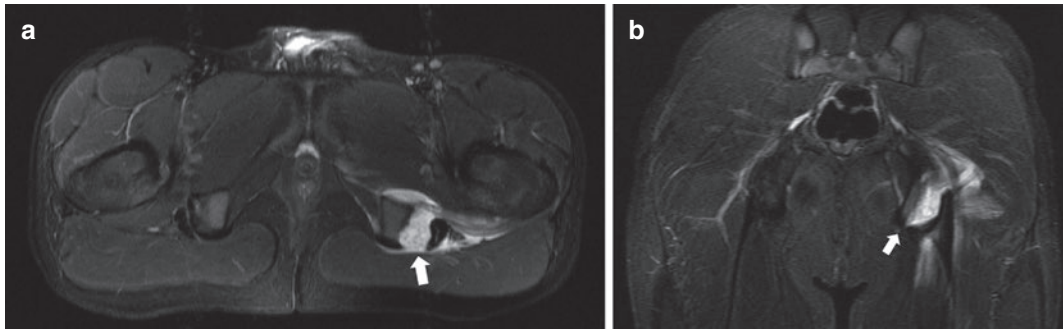

Fig. 29 (**a**, **b**) 14-year-old football player complaining of pain after a sudden pull during a match. (**a**) Axial and (**b**) coronal fat-supressed T2w images show left ischial tuberosity avulsion (arrow), with moderate dislocation of the avulsed fragment

the biomechanical standpoint, which accounts for its usual involvement in **indirect trauma**, typically after a violent contraction or an abrupt motion block. The *rectus femoris*, *biceps femoris* and *adductor longus* are most commonly involved in this type of injury (Crema et al. 2015; Agten et al. 2016). Soft tissue contusions are common in collision and contact sports. These **direct-type** injuries may occasionally result in muscle hematoma and, less commonly, compartment syndrome or myositis ossificans. In the hip and thigh region, the most frequently affected muscle by direct injuries is the *vastus intermedius*.

Delayed-onset muscle soreness (DOMS) is another common condition in sports that results from strenuous exercise of a muscle or muscle group, and presents on MRI as muscle oedema that can mimic a low-grade muscle injury. Clinical presentation is distinct and allows differentiation between the two, since pain associated with DOMS reaches a peak from 24–72 h after the inciting activity, while in muscle injury it has an immediate onset (Guermazi et al. 2017).

In contradistinction to muscle injuries, which are typically the result of a single major traumatic event, tendon lesions can present either as an overuse or as an acute injury.

Imaging: While MRI is the most sensitive and comprehensive technique to evaluate muscle injuries, US can be very useful as an adjunct, when access to MRI is limited or a fast screening is desired.

US: Muscle fibre and tendon discontinuity can be detected, along with hyperechoic hematic

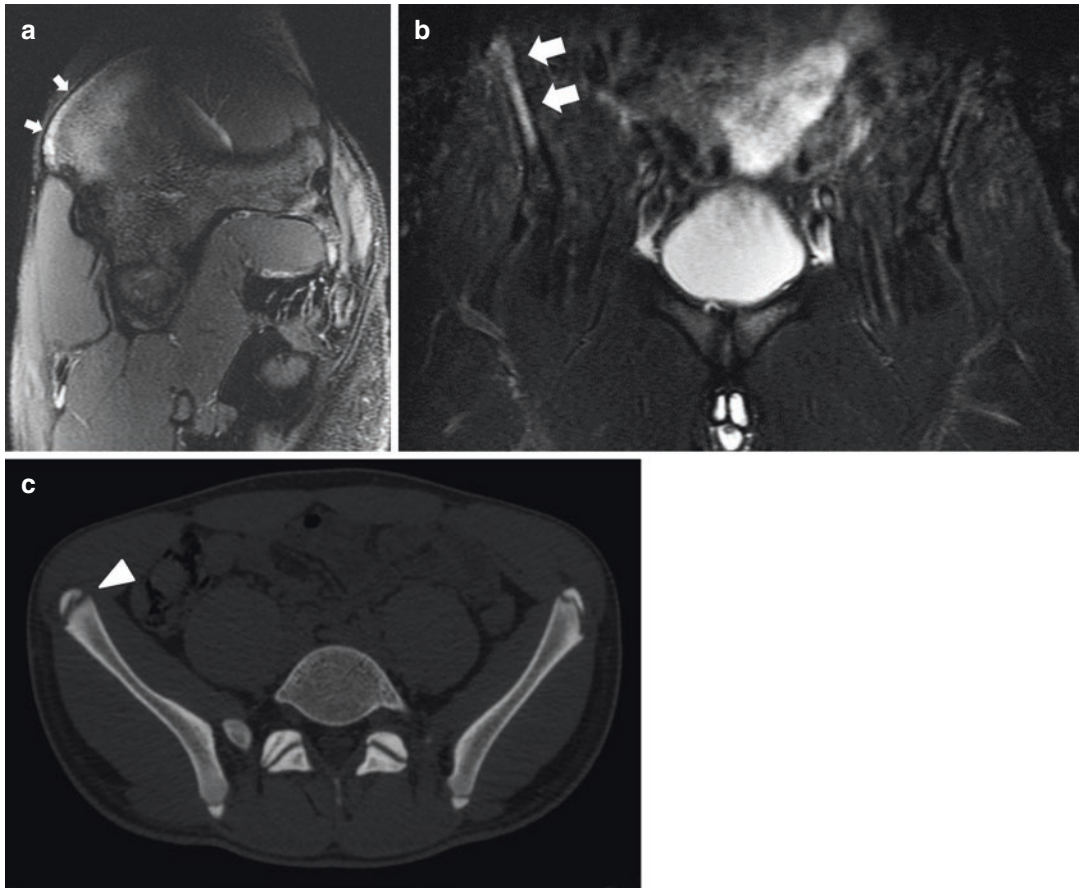

Fig. 30 (**a–c**) 16-year-old male football player boy with pain over the right anterior iliac crest. (**a**) Sagittal and (**b**) coronal fat-suppressed T2w MR images of the pelvis show bone oedema of the iliac crest apophysis and adjacent iliac bone (arrows). (**c**) Axial CT scan image confirms the diagnosis of right iliac crest apophyseal injury (arrowhead). (Case courtesy of Dr. Armando de Abreu, Porto Alegre, Brazil)

muscle infiltration, fluid collections, perifascial fluid and fascial disruption. This technique also allows comparative and dynamic assessment (active muscle contraction may help demonstrate subtle tears), and can be used to guide interventional procedures in real time.

MRI: Currently, MRI may be of value for confirming the clinical diagnosis and determining the extent of muscle injury, but so far MRI findings have not demonstrated superiority over clinical features in determining time to RTS. A combination of T1w and fluid-sensitive (fat-suppressed PD/T2 or STIR) sequences should be used. Oedema and/or fibre discontinuity should be noted, as well as the amount of fibre retraction when present.

Classification: Several systems have been developed (Cruz and Mascarenhas 2018). The most commonly used are (1) the classic three-grade system described by Takebayashi, and the more recently developed (2) Munich Consensus, (3) British Athletics Muscle Injury and (4) MLG-R classifications. Despite the continued endeavours to establish more comprehensive classification systems, the prognostic value of MRI in muscle injury is limited. The overlap in recovery times between different anatomic types of injury may be explained by a multitude of other relevant factors, such as the type of sport, the player's role in the team, his/her mental characteristics and the timing of the injury in the season (Reurink et al. 2014).

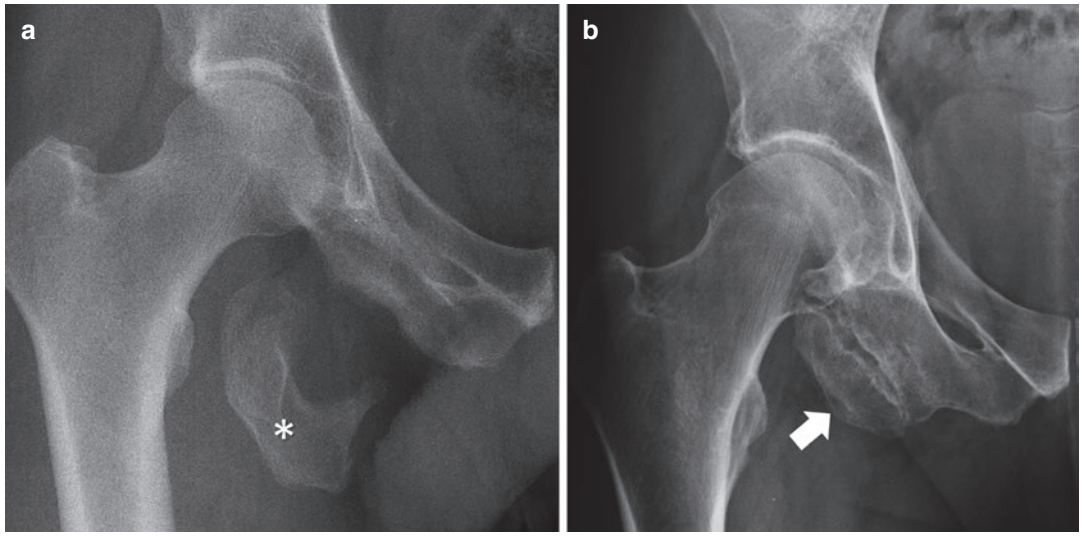

Fig. 31 (**a**, **b**) Acute and chronic ischial tuberosity avulsion injuries. (**a**) Hip AP radiograph of a male 23-year-old soccer player shows a large acutely displaced right ischial tuberosity avulsion fracture (asterisk). (**b**) Hip AP radiograph of a 58-year-old male with non-union of the ischial tuberosity (arrow), due to an old apophyseal avulsion injury

What to report: (a) the involved structure(s), (b) the location of the lesion (proximal, central or distal), (c) the anatomical site of injury (myofascial, musculo-tendinous, or intratendinous) and (d) the injury extent (percentage of cross-sectional area and longitudinal length).

How to report: As a general rule, for both MRI and US, the axial plane should be used primarily to assess muscle injuries and determine the maximum percentage cross-sectional area of fibre discontinuity, while imaging in the sagittal and coronal planes helps to evaluate the longitudinal extent and degree of retraction (Cruz and Mascarenhas 2018).

In the following paragraphs, the more typical pelvic muscle and tendon injuries in athletes are briefly reviewed, except for adductor injuries, which are discussed elsewhere in this book.

Hamstring Injuries

Anatomy: The hamstrings comprise the biceps femoris (BF), semitendinosus (ST) and semimembranosus (SM), which originate at the ischial tuberosity as a common BF-ST tendon and a separate SM tendon. Each component possesses long proximal and distal tendons and long MTJs, which, in addition to features like the high proportion of type II ("fast twitch") muscle fibres and the crossing of two joints, makes this muscle complex particularly susceptible to injury (Bencardino and Mellado 2005).

Hamstring acute lesions are very prevalent in sports (Fig. 32). They are the most common muscle injury in professional football players (37% of all muscle injuries (Ekstrand et al. 2011)), but are also frequent in other sports that involve kicking, sprinting and jumping, as well as in dancing, skiing, water skiing, and contact sports such as martial arts (Ekstrand et al. 2011; Kuske et al. 2016). Forced flexion of the hip with hyperextension of the knee is the commonly implicated mechanism.

The main injuries observed in young athletes are (1) proximal tendon avulsions (including apophyseal avulsions before skeletal maturation; Fig. 29), (2) tendon lesions, and (3) proximal MTJ injuries (Fig. 32), with or without concomitant tendon involvement. The proximal MTJ of the BF is the most frequent hamstring injury location in football (26.7%) (Crema et al. 2015). Purely muscular and myofascial injuries are less common (De Smet and Best 2000).

MRI shows similar appearance as muscle injuries in other anatomical sites. It is advocated

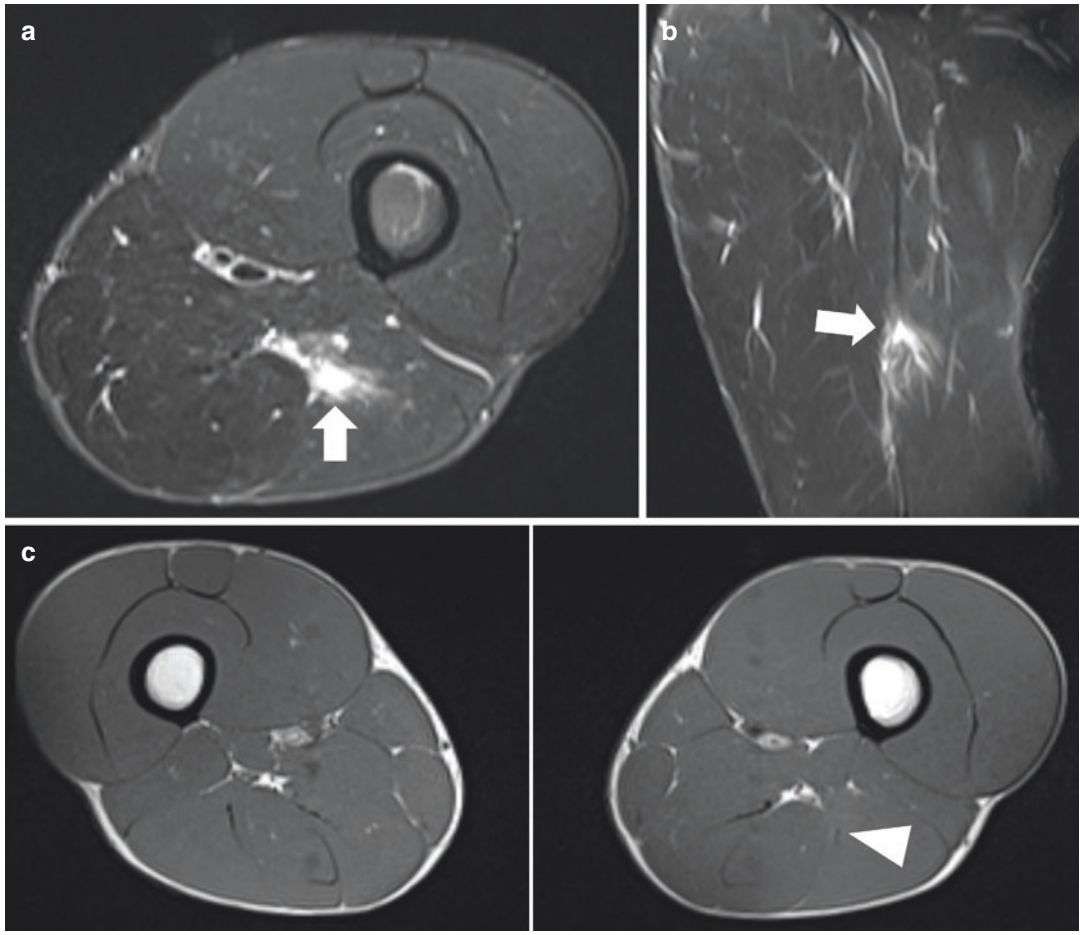

Fig. 32 (**a–c**) 27-year-old professional football player with acute posterior thigh pain during sprinting. (**a**) Axial and (**b**) coronal STIR images demonstrate a small partial myotendinous junction tear of the long head of the biceps femoris, located at the middle third of the thigh, as a fluid-like hyperintense focus (arrows) associated with muscle fascicle disruption, mild fibre retraction and fascial disruption. (**c**) Notice the involvement of the intramuscular proximal tendon (arrowhead), which appears attenuated compared with the asymptomatic contralateral side on a T1w axial MR image

ideal for detection of subtle injury, for central intramuscular tendon tears of the biceps femoris and for follow-up imaging. Due to its close anatomic location adjacent to the hamstring muscle complex, sciatic nerve entrapment is a possible complication of hamstring injuries.

Hamstring chronic tendinopathy is a frequent finding in the elderly. It manifests as tendon thickening and increased signal and peritendinous and ischial tuberosity oedema, but these appearances are also found in asymptomatic individuals (De Smet et al. 2012). In partial tears a fluid-filled defect at the tendon insertion is observed, while complete tears display detachment from the ischial tuberosity and retraction (Fig. 33).

Ischial bursitis in sports usually have a direct traumatic origin. It is visible as a fluid collection between the hamstrings insertion in the ischial tuberosity and the gluteus maximus muscle.

Proximal *Rectus Femoris* Injuries

Anatomy: RF has a complex architecture, displaying a muscle-within-a-muscle configuration (Fig. 34). It possesses two proximal tendons, a

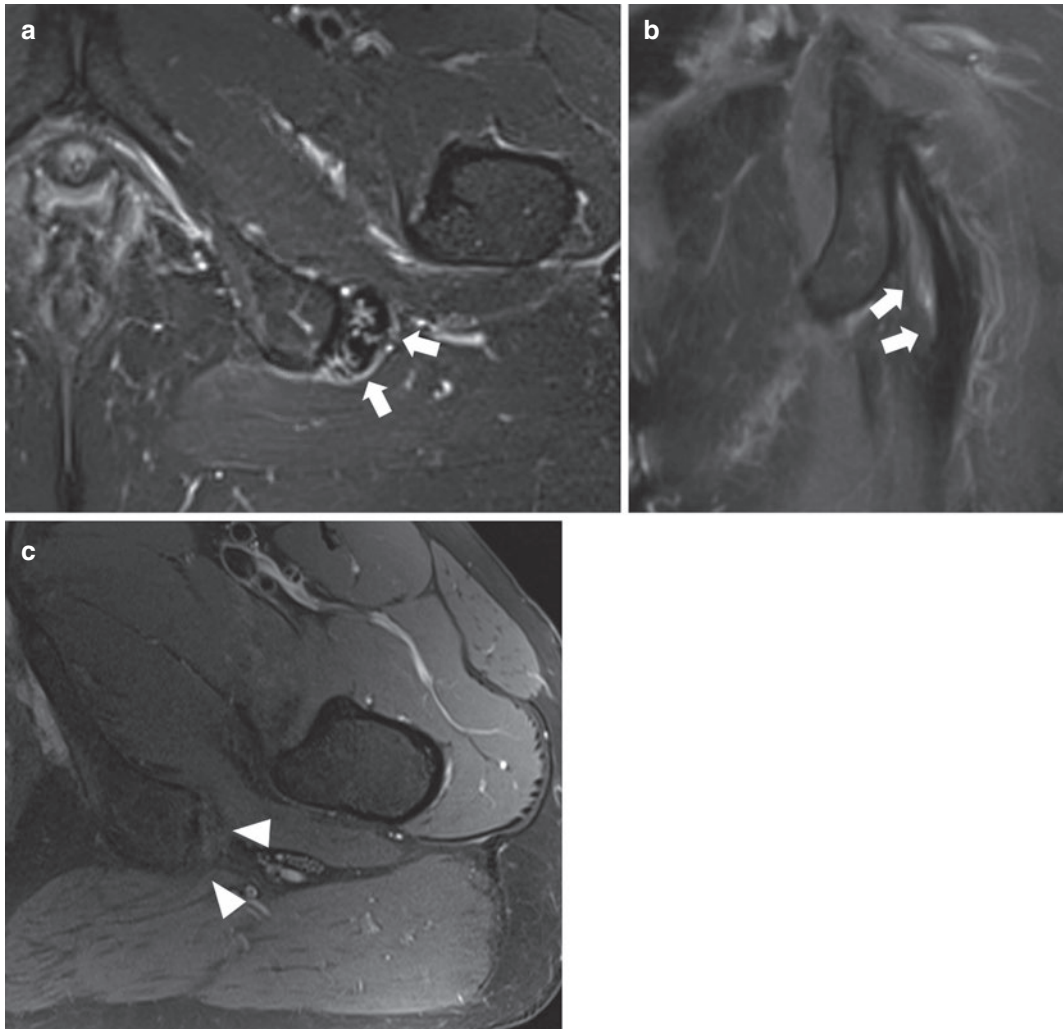

Fig. 33 (**a–c**) (**a**, **b**) 37-year-old former professional tennis player with hamstring tendinopathy. (**a**) Axial and (**b**) coronal fat-supressed T2w MR images demonstrate proximal hamstring thickening and increased tendon signal (arrows) associated with mild peritendinous oedema, representing tendinosis. (**c**) In another former athlete, axial fat-suppressed T2w MR image shows absence of the tendinous hamstring origins, consistent with hamstring avulsion. No fluid is appreciated, implying a chronic nature for this finding

direct and an indirect one. The direct tendon originates at the AIIS, while the indirect tendon originates laterally at the acetabulum. They form a conjoint tendon for a short segment, a few centimetres distal to their origin, diverging thereafter (Kassarjian et al. 2014). The direct tendon continues distally as a superficial anterior tendon that covers the proximal third of the muscle and fuses with the anterior fascia, giving rise to a peripheral unipennate muscle belly. The indirect tendon gives rise to a long intramuscular central tendon and a bipennate central muscle belly.

General considerations: RF injuries have been reported as the second or third most common muscle lesion in the lower extremity, after hamstring injuries, occurring frequently in sports such as football, rugby, basketball and other activities that involve kicking and sprinting (Ekstrand et al. 2011).

Several factors account for the high frequency and variety of RF injuries, namely (1) its structural complexity, (2) the crossing of two joints

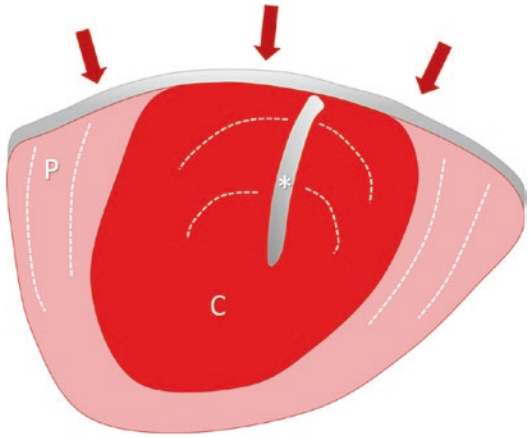

Fig. 34 Diagram illustrating the cross-sectional structure of the rectus femoris muscle in the upper third of the thigh. The muscle-within-a-muscle architecture is demonstrated. The intramuscular central tendon (*) and the bipennate central muscle belly (C) derive from the indirect tendon. The direct tendon gives rise to the peripheral unipennate muscle belly (P) and to the superficial anterior tendon (arrows) that blends with the anterior fascia. The white interrupted lines illustrate the orientation of the muscle fibres in each component of the muscle

and (3) the high proportion of type II fibres, and (4) specific biomechanical vulnerabilities associated with certain movements (e.g. running, kicking) (Kassarjian et al. 2012).

The most common injuries involve the proximal tendons (Fig. 35) and myotendinous and myofascial junctions, either of the direct head, indirect head, or both (Figs. 36, and 37).

Imaging: MRI and US features of these injuries are similar to those of other muscles and tendons. The intramuscular degloving pattern of injury, however, is unique to the RF (Fig. 38), consisting of a circumferential tear at the junction of the direct and indirect muscle bellies, partially or completely dissociating and separating the two (Kassarjian et al. 2014).

Iliopsoas Injuries

Iliopsoas tendinous and myotendinous injuries are a cause of acute and chronic groin pain in sports, typically after a forceful thigh extension

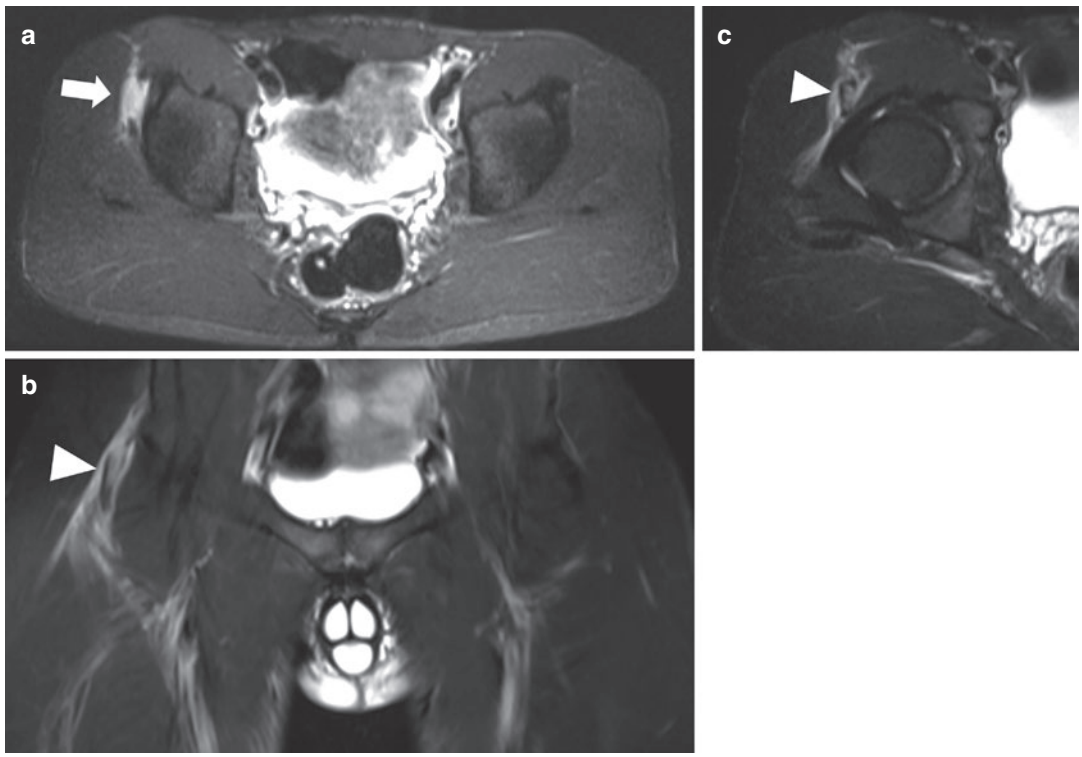

Fig. 35 (**a–c**) 20-year-old professional football player with acute injury during training. (**a**, **c**) Axial and (**b**) coronal fat-supressed T2w images show a complete tear of the indirect tendon (arrow in **a**) and a partial tear of the conjoint/direct tendon (arrowheads in (**b** and **c**) of the right rectus femoris muscle

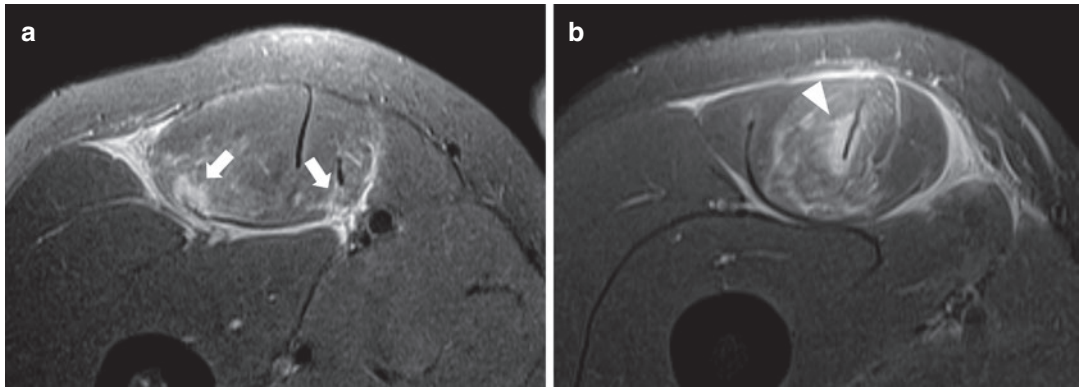

Fig. 36 (**a**, **b**) 35-year-old amateur football player with acute injury during a match. (**a**) Axial fat-supressed T2w MR image in the upper third of the thigh show myofascial posterior tears at the peripheral portion (direct head) of the rectus femoris muscle (arrows), with peripheral muscle oedema. (**b**) Axial fat-supressed T2w image in the middle third of the thigh depicts a myotendinous junction central tear (arrowhead), with central (indirect head) muscle oedema, but no tendon disruption. Abundant associated perifascial fluid is visible in both images

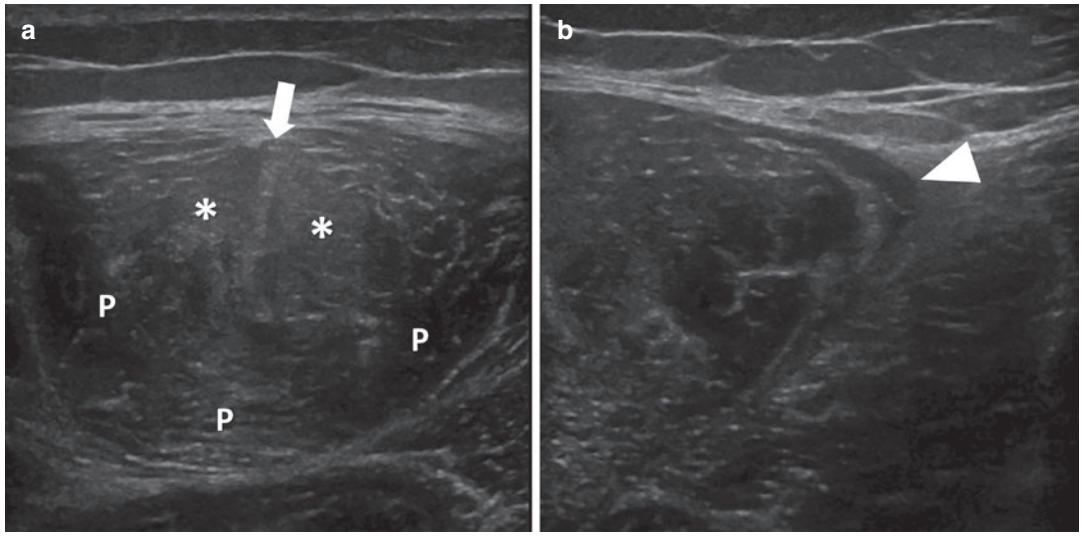

Fig. 37 (**a**, **b**) US transverse images of the anterior thigh of the patient in Fig. 36. (**a**) An ill-defined central tendon (arrow) and faint central muscle hyperechogenicity (*) are evident, consistent with injury of the central myotendinous junction. The peripheral muscle belly appears normal (P). (**b**) Perifascial fluid is demonstrated (arrowhead)

or block during flexion. They have been associated with several activities including football, basketball, tennis, hockey, running and dancing (Domb et al. 2011). Ballet dancers seem to be particularly affected, with symptomatic snapping observed in up to 58% of elite ballet dancers.

Findings of tendinopathy on MRI include thickening and increased tendon signal on T1 and T2WI. Paratendinopathy manifests as fluid tracking along the tendon (Fig. 39), and sometimes associated bursitis is observed as a distension of the iliopsoas bursa (Fig. 40). Fluid in this bursa is not always pathological, since the bursa may communicate with the hip joint. Partial tearing may manifest as focal fluid-filled tendon discontinuity or as focal oedema at the myotendinous junction or fascia (Fig. 41). Complete tears of the tendon are rarely seen in the athlete.

Iliopsoas bursitis, paratendinopathy or tendinopathy are sometimes associated with internal

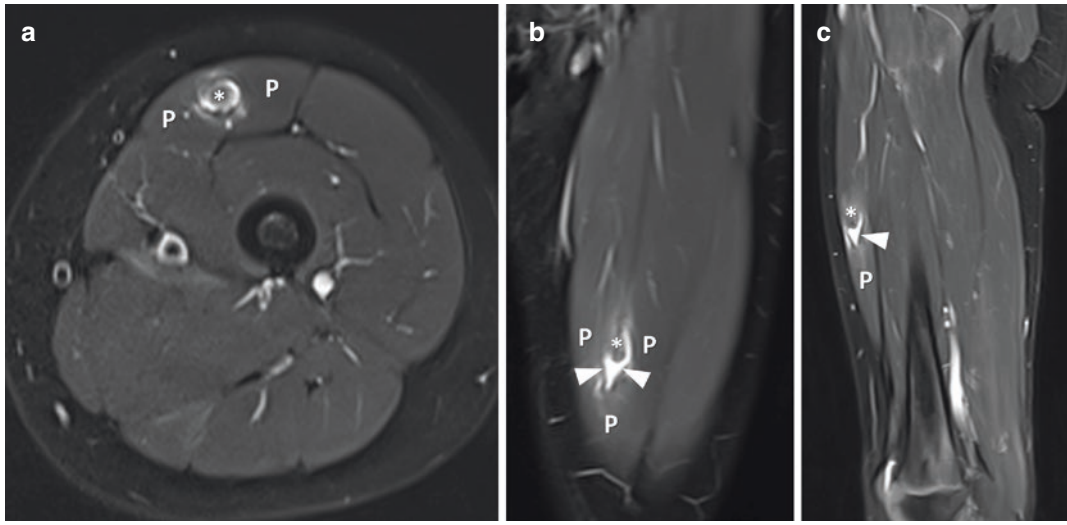

Fig. 38 (**a–c**) Intramuscular rectus femoris degloving injury. (**a**) Axial fat-suppressed T2w image shows a circumferential fluid-filled tear between the central (*) and peripheral (P) bellies of the rectus femoris muscle. (**b**) Coronal and (**c**) sagittal fat-suppressed T2w images demonstrate mild proximal retraction of the central muscle belly (*), which is separated from the peripheral belly (P) by a small amount of fluid (arrowheads)

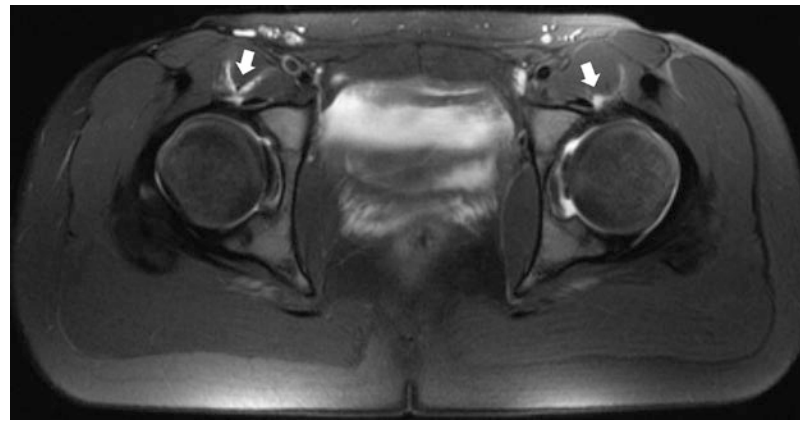

Fig. 39 Iliopsoas paratendinitis. Axial fat-supressed T2-weighted MR image shows peritendinous and perimuscular oedema (arrow). No signal changes are appreciated in the muscle or tendon

snapping hip (previously described). *Iliopsoas impingement syndrome* is another related condition, caused by chronic friction or traction of the iliopsoas tendon on the capsulolabral complex at the acetabular rim. It is more common in young adult female athletes and is associated with a distinct pattern of labral lesion in a direct anterior location, at the 3 o'clock position (Domb et al. 2011).

Proximal Iliotibial Band Syndrome

The proximal insertion of the ITB at the iliac tubercle is the location of an overuse syndrome known as the proximal ITB syndrome, which mainly involves young female long-distance runners, but may also be found in older overweight women (Sher et al. 2011).

US shows hypoechoic asymmetric thickening of the ITB enthesis, with pain elicited by local probe compression. *MRI* will show thickening and high-signal intensity on fluid-sensitive sequences at the fascial insertion on the iliac tubercle. Associated insertional bone marrow oedema and partial and complete tears may also be found (Fig. 42). The fact that hip-focused MRI frequently excludes the iliac tubercle from the

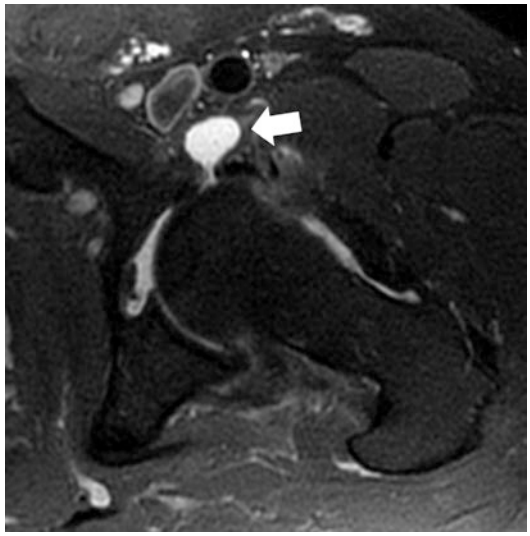

Fig. 40 Iliopsoas bursitis. Axial fat-supressed T2w image shows a distended iliopsoas bursa (arrow)

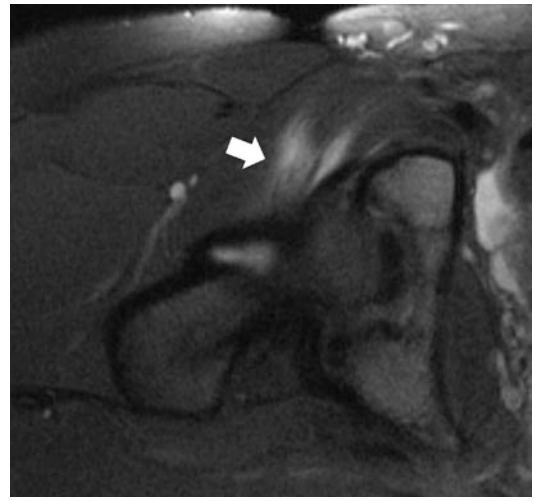

Fig. 41 Myotendinous iliopsoas partial tear. Axial fat-supressed T2w MR image shows a feathery oedema pattern at the myotendinous junction (arrow)

field of view underlines the usefulness of acquiring one large-FOV fluid-sensitive sequence of the pelvis to detect pathology beyond the hip, which may be clinically unsuspected.

Adductor Insertion Avulsion Syndrome

The adductor insertion avulsion syndrome, also known as "thigh splints", belongs to the spectrum of stress lesions of the bone. It represents a painful overuse traction periostitis at the distal insertion of the adductors in the thigh, similar to "shin splints" at the tibia (Anderson et al. 2001).

Periostitis may be present radiographically. MRI will show hyperintense linear signal in fluid-sensitive sequences at the medial femoral cortex, representing periostitis, which may evolve into a stress fracture if left untreated (Fig. 43). US may show cortical irregularity with adjacent hypoechoic soft-tissue thickening, painful to transducer pressure, in a suggestive location in the posteromedial aspect of the femur.

5.3.2.3 Nerves and Nerve Entrapment Syndromes

***General considerations*:** Several acute and chronic nerve entrapment syndromes were described in the pelvic region in athletes, involving the sciatic, obturator, femoral, posterior femoral cutaneous, lateral femoral cutaneous, pudendal, iliohypogastric, ilioinguinal and genitofemoral nerves. They may present with an unclear clinical picture, simulating or coexisting with lumbar radiculopathy, which accounts for their frequent underdiagnosis. These compressive neuropathies have been attributed to (1) fascial thickening, (2) mass effect from hernias and ganglion cysts, (3) adjacent fractures, (4) muscle hypertrophy, while (5) scarring from previous surgery or (6) trauma is also pointed out as a possible cause (Omar et al. 2008; Petchprapa et al. 2010).

Imaging *US and MR imaging* are frequently used in the work-up of peripheral neuropathies, as an adjunct to clinical examination and electrophysiologic studies. Image-guided nerve blocks are a helpful tool when a neuropathic origin of the symptoms is suspected, and are used with both diagnostic and therapeutic purposes.

US is a popular and accurate technique for the evaluation of medium and small sized pelvic nerves along their extra pelvic course, allowing dynamic studies and contralateral comparison. Proximal hypoechoic swelling of the involved nerve, fascicle enlargement and loss of fascicular pattern may be observed in entrapment neuropathies (Fig. 44).

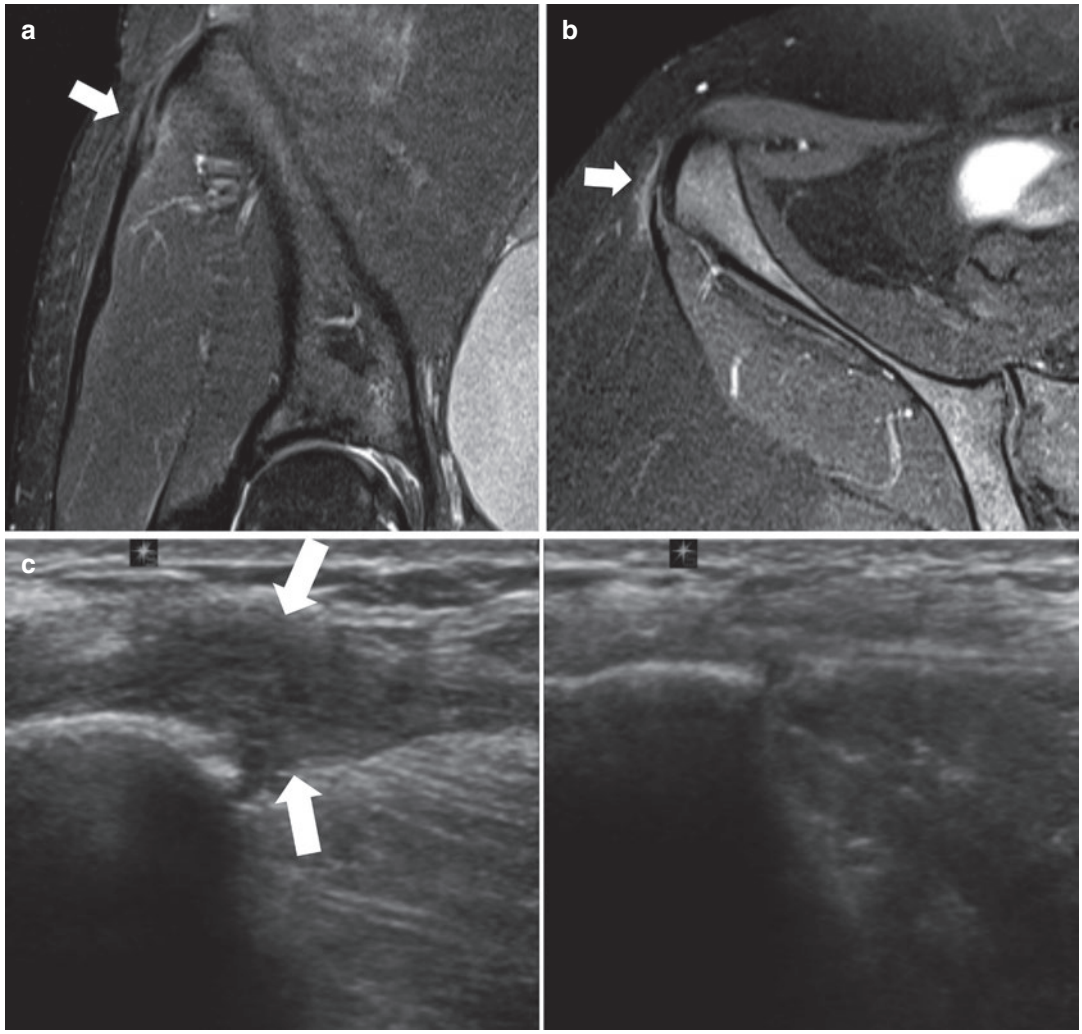

Fig. 42 (**a–c**) Proximal iliotibial band (ITB) syndrome. (**a**) Coronal fat-supressed T2-weighted MR image depicting a partial tear of the proximal ITB (arrow) in a 34-year-old female long distance runner. (**b**) Axial T2w fat-suppressed T2-weighted MR image showing a low-grade injury of the proximal ITB in an overweight non-athlete 29-year-old female, with fascial attenuation and perifascial oedema. (**c**) Longitudinal US scan of the iliac tubercle region demonstrating a marked hypoechoic thickening of the ITB insertion (arrows), which was painful to sonopalpation, in a 37-year-old female runner. The contralateral normal side is shown in the right

3-T MR neurography, in particular, is able to provide high-resolution and high-contrast anatomic images of peripheral nerves, allowing accurate assessment of size, signal and fascicular pattern, even for small nerves. Abnormal MRI features are (1) nerve enlargement (larger than the adjacent artery), (2) hyperintensity on fluid-sensitive images (Fig. 45), (3) loss of fascicular pattern, (4) fascicle swelling, (5) abnormal nerve course, (6) obliteration of perineural fat, along with (7) regional muscle denervation changes if motor or mixed nerves are affected (Soldatos et al. 2013).

Diffusion-weighted imaging and Diffusion Tensor Imaging have shown good results in the functional and quantitative evaluation of peripheral nerve pathologies, but the widespread use of these advanced techniques in clinical practice is currently limited by technical and hardware requirements (Naraghi et al. 2015) (Fig. 19).

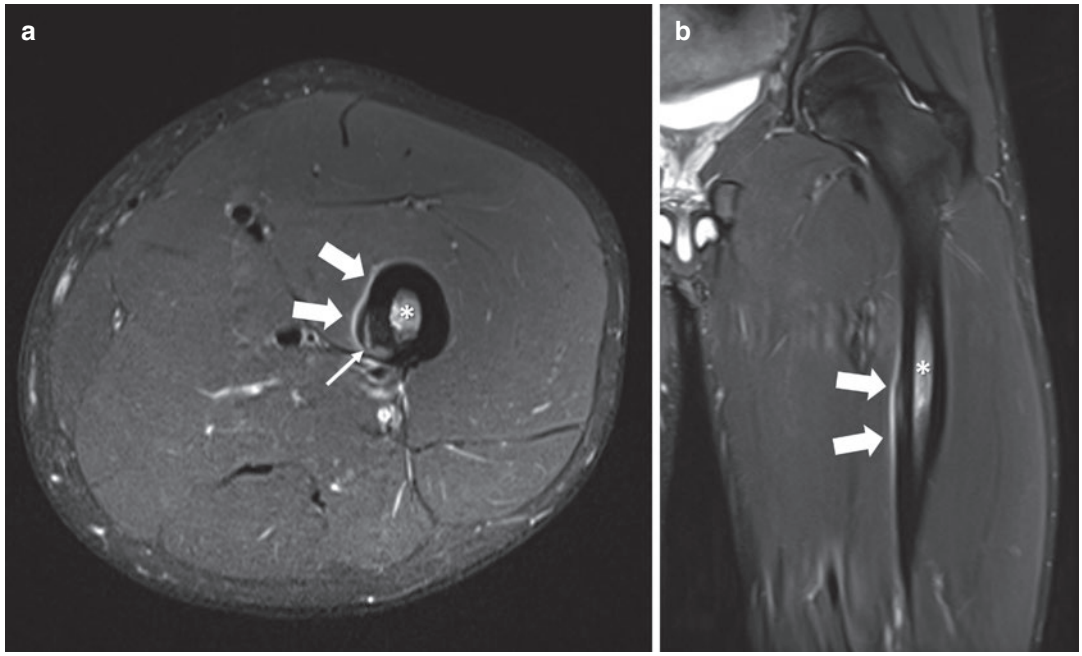

Fig. 43 (**a**, **b**) Thigh splints in a 25-year-old long-distance runner. (**a**) Axial and (**b**) coronal T2w fat-suppressed images demonstrate linear increased signal (thick arrows) at the medial cortex of the femoral diaphysis, representing periostitis. Marrow oedema (*) and increased intracortical signal (thin arrow) represent advanced stress-related changes and impending stress fracture

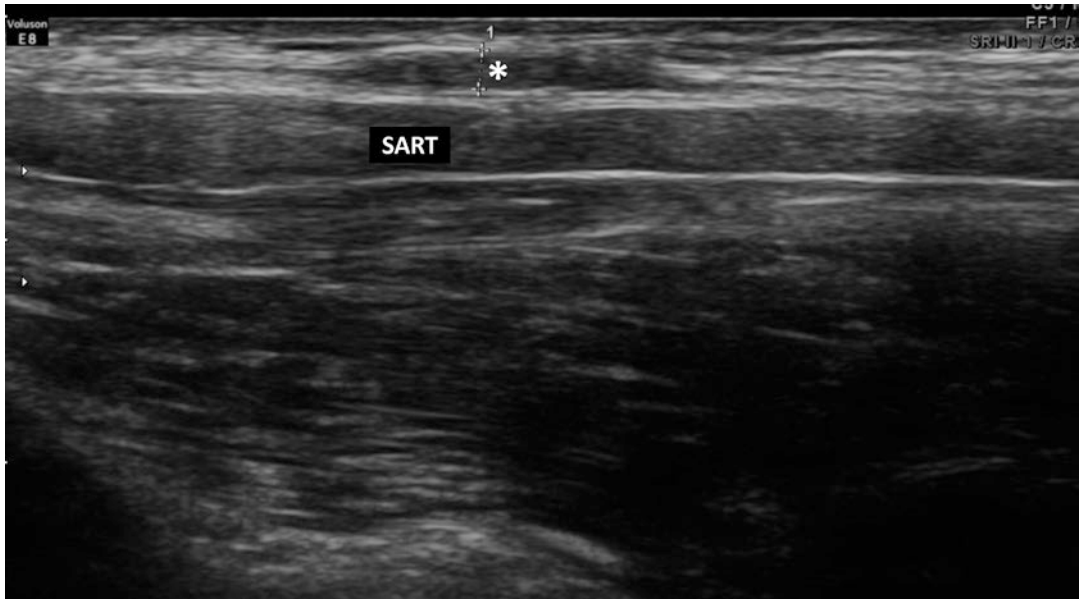

Fig. 44 Lateral femoral cutaneous neuropathy in a 37-year-old man with symptoms of meralgia paresthetica. Longitudinal proximal anterior thigh US scan shows focal hypoechoic swelling of the lateral femoral cutaneous nerve (*) below the inguinal ligament. *SART* sartorius

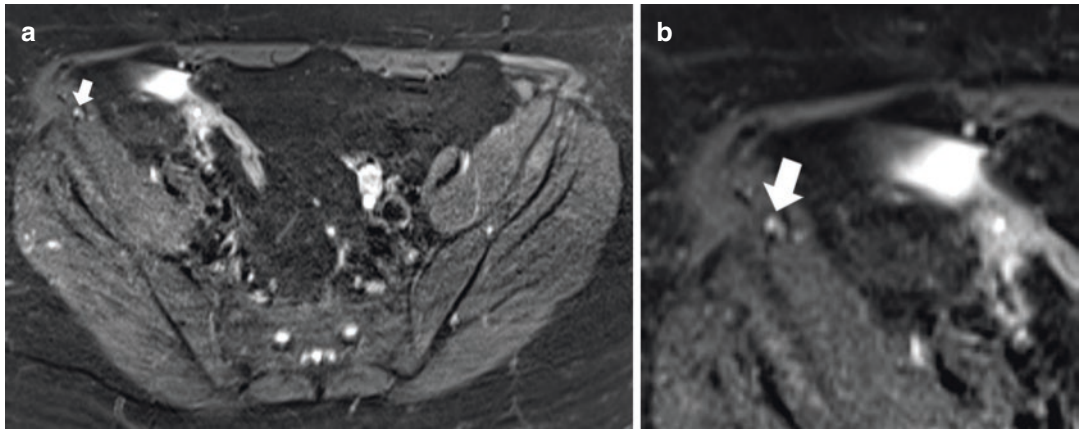

Fig. 45 (**a**, **b**) Lateral femoral cutaneous neuropathy in a 53-year-old woman with symptoms of meralgia paresthetica. (**a**, **b**) Axial fat-suppressed T2-weighted image shows thickening and increased signal of the lateral femoral cutaneous nerve (arrow) near the right anterior superior iliac spine

5.4 Sacroiliac Joints

5.4.1 General Considerations

Anatomy: The sacroiliac joints (SIJ) are the largest axial joints in the human body, linking the spine to the pelvis, with a mobility of 3° to 8° of nutation. SIJ have a central location, between the sacrum and the iliac bones. Obliquely orientated undulating joint facets provide stability to the SIJ, additionally empowered by strong ligaments (interosseous, iliolumbar, sacrotuberous, sacrospinous) and muscles, that interconnect with the lumbosacropelvic sling (Brolinson et al. 2003; Campos-Correia et al. 2019). The stability of this region is dependent upon these muscle-ligamentous relationships, and their breakdown can lead to chronic pain.

SIJ are composed of two main compartments (Fig. 46): (1) an inferior-anteriorly located C-shaped *cartilaginous compartment*, which resembles a symphysis, with hyaline cartilage firmly attached to the bone by fibrous tissue. It was formerly called "synovial portion" but, in fact, only a small part (its lower third) has a true synovial-lined joint capsule, and (2) a *ligamentous compartment (syndesmosis),* located superior-posteriorly, which contains strong interosseous ligaments (Campos-Correia et al. 2019).

Normal variants (iliosacral complex, bipartite iliac bony plate, semi-circular defect, crescent-like iliac bony plates, accessory SIJ), **intra-articular ossified nuclei** and **normal small vessels** should not be mistaken for pathology**.** Accessory SIJ (Fig. 47) are the most frequent variant (8–40%), often found between the iliac and the sacral articular sides at the posterior portion of the SIJ, from the level of the first to the second sacral foramina (Faflia et al. 1998; Campos-Correia et al. 2019).

Clinical presentation: SIJ disorders may present as low back pain or sciatica-like symptoms. For a long time, SIJ pain have been mostly assigned to spondyloarthropathies (SpA), but nowadays it is well recognized that SIJ dysfunction includes a broad differential, including (1) age- and stress-related changes, (2) fractures, (3) infection, (4) other inflammatory sacroiliitis, (5) metabolic, (6) tumours (primary or secondary), and other less common causes. It is also well established that changes on SIJ are commonly found in athletes and/or asymptomatic healthy patients and should be kept in mind. Additionally, the differential diagnosis should always include other pelvic and extra pelvic sites of pain, including the spine, hip and pubic symphysis (Brolinson et al. 2003; Campos-Correia et al. 2019).

Imaging: Interpretation of MRI findings in daily practice is dependent on the clinical context. Age, sex, clinical picture/features and laboratory data help shorten the imaging differential

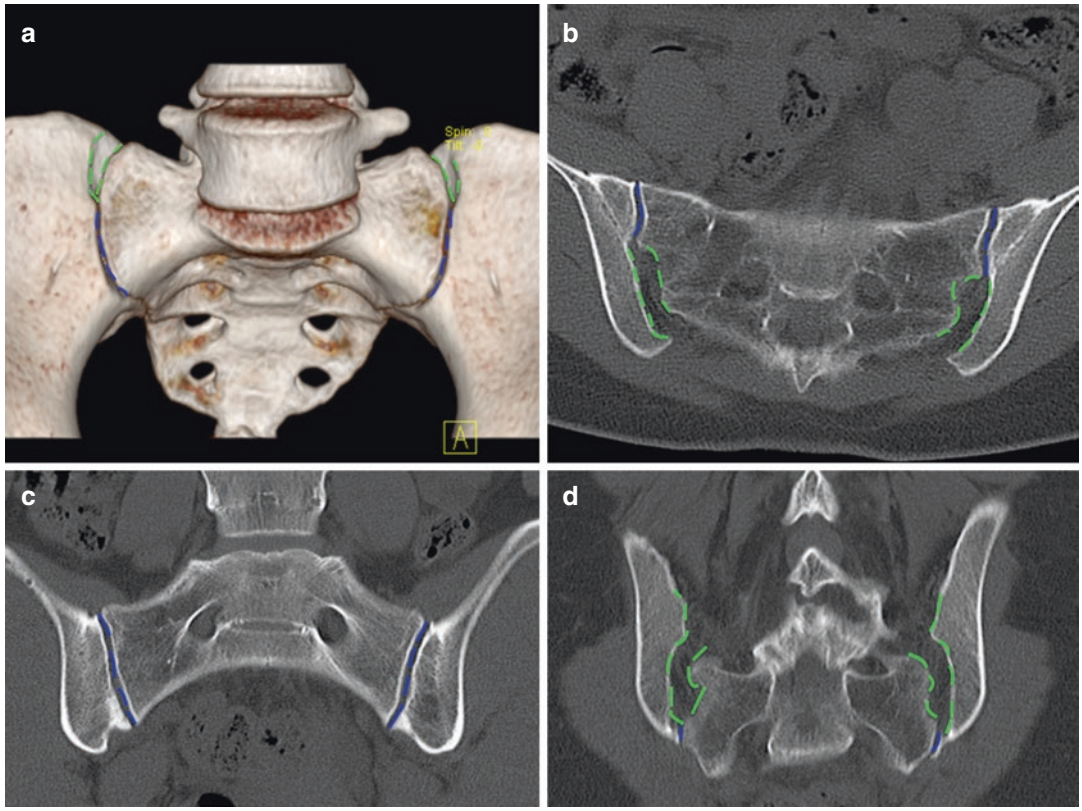

Fig. 46 (**a–d**) 33-year-old female, basketball player. (**a**) 3D volume CT image depicting the cartilaginous (blue) and ligamentous (green) components. (**b**) Axial CT image and (**c**, **d**) coronal CT images at different levels (**c**, anterior; **d** posterior) depicting the same SIJ components (cartilaginous (blue) and ligamentous (green)). Notice on (**c**) the subtle subchondral sclerosis in the lower ilium bilaterally, more conspicuous on the right side, with minor osteophytes due to mild mechanical changes

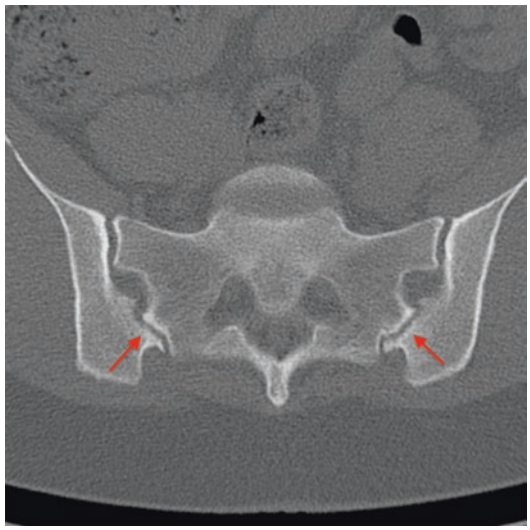

Fig. 47 Axial CT image shows bilateral accessory SIJ (red arrows), a common normal variant, which occasionally may become symptomatic

diagnosis. Prior imaging studies should always be used for comparison, when available (Campos-Correia et al. 2019).

5.4.2 Mechanical/Degenerative Changes of the SIJ: Athletes

The concept of the SIJ as a pain generator is well recognized but controversy exists due to several factors, namely: the complex anatomy and biomechanics of the SIJ and the absence of any specific clinical sign or symptom that is both sensitive and specific for the diagnosis of SIJ dysfunction (Brolinson et al. 2003).

Mechanical changes of the SIJ may account for as much as 20% of low back pain cases in the general population. The prevalence of SIJ pain among athletes is unknown and, likely, underreported because pain referral patterns are nonspecific, and often similar to spinal disease.

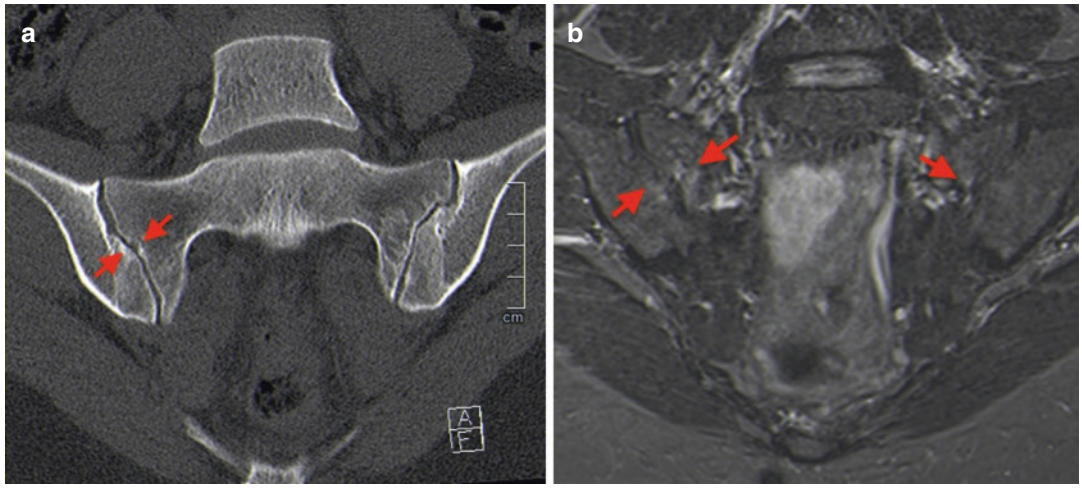

Fig. 48 (**a**, **b**) 25-year-old female, gymnast and contemporary dancer. (**a**) coronal CT image with cortical irregularity/minor erosions, subtle space joint changes and mild sclerosis more evident on the right SIJ (red arrows). (**b**) Coronal fat-suppressed T2-weighted image on the same level, depicts mild oedema foci (red arrows) surrounding these structural changes, related to mechanical, repetitive stress over the SIJ. Another focus of oedema, very subtle, is seen on the left side, probably preceding structural changes

Furthermore, 39% of individuals with SIJ dysfunction have concomitant spinal pathology. In this age range, it is also mandatory to exclude inflammatory sacroiliitis as a cause for the low back pain.

Because of the unique nature of sports' demands on the spine and pelvis, SIJ dysfunction is acknowledged in athletes. Risk factors include:

1. **Type of activity**: sports that involve (1) frequent direct or torsional impact on the axial skeleton, (2) repetitive or asymmetric loading (kicking, swinging, throwing and single leg stance) and (3) repetitive traumatic falls onto the buttocks. Hence, sports with the highest pain prevalence include football, powerlifting, basketball, gymnastics, golfing, cross country skiing, rowing, step aerobics and those that use elliptical and stair stepper machines (Figs. 48 and 49). Furthermore, runners, ice hockey or football players with cumulative repetitive torsional strain of the pelvic ring are also at risk. Rowers are at risk for SIJ dysfunction secondary to their biomechanical demands (prevalence of SIJ dysfunction in 54.1% of USA Senior National Rowing Team members reported (Brolinson et al. 2003)).
2. **Associated conditions:** inflammatory conditions, leg length discrepancy, hypermobility, scoliosis, direct trauma, pregnancy/postpartum and other biomechanical abnormalities (Saunders et al. 2018).

Imaging: Mechanical and degenerative SIJ changes can be seen on imaging, namely (1) **bone marrow oedema** (BME), not only anteriorly in the symphysis pubis, but also potentially dorsally in the SIJ (via propagation of biomechanical strain along the pelvic skeleton), (2) **erosions,** which are less common in athletes, but some studies show scarce, minor erosions in this population, (3) **fat metaplasia,** also relatively scarce in published series while ankylosis of the SIJ was not reported (Weber et al. 2019).

Low-grade BME surrounding the SIJ is present in up to 25% of asymptomatic healthy adults (Ritchlin 2018), most often (but not exclusively) located in the lower iliac bone. Potential triggers of low-grade BME in healthy individuals are mechanical or degenerative stress injury to the spine, overweight or peri/postpartum changes. To date, imaging studies cannot distinguish asymptomatic from symptomatic individuals (Weber et al. 2019).

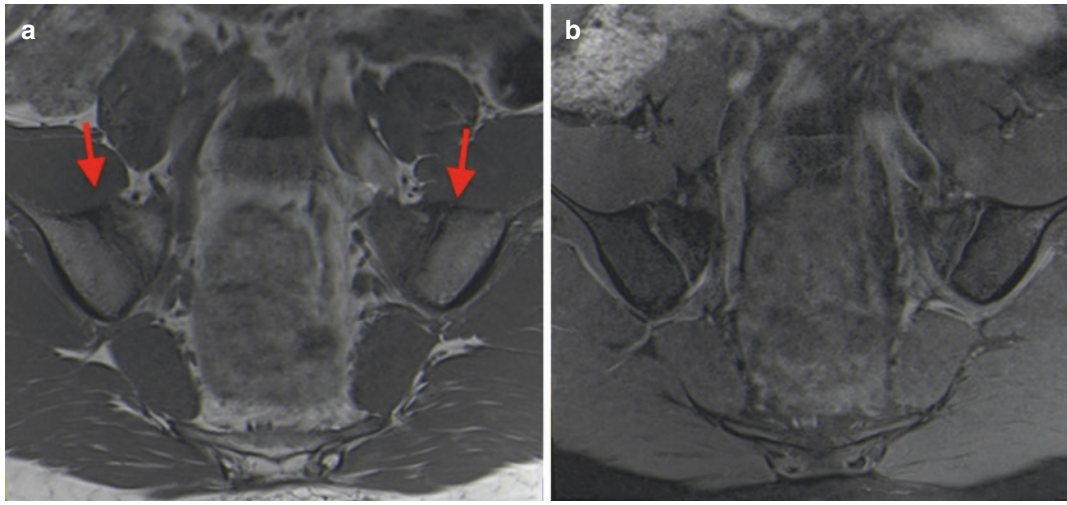

Fig. 49 (**a**, **b**) 17-year-old male, table tennis player with 3-months low back pain. (**a**) Coronal T1w image shows sclerosis, cortical irregularity and minor osteophytes in the anterosuperior part of both SIJ (red arrows). (**b**) Coronal fat-suppressed proton-density-weighted image shows scarce and very subtle oedema on the left side

Athletes may show BME fulfilling ASAS criteria (Assessment of Spondyloarthritis International Society) for active sacroiliitis, which has been reported in 30–35% of recreational runners and 41% of elite ice hockey players (mean age of 27.2 and 25.9 years, respectively) De Smet (2000). The posterior lower ilium quadrant was the single most affected for BME lesions, followed by the anterior upper sacrum. Potential mechanisms for non-specific SIJ BME in athletes are (1) partial-volume effects of presacral vascular plexus or from the deep iliac ligament insertion, (2) local axial strain or (3) anatomic SIJ joint variation encompassing lumbosacral transitional vertebral.

5.4.3 Mechanical/Degenerative Changes of the SIJs: Non-athletes

Osteoarthritis of the SIJ is a common finding in CT (appearing in 65.1% of adults and increasing with age) (Faflia et al. 1998). Moderate adaptive changes begin to occur on the iliac side as early as the third decade, especially in men. Age-related imaging features include (1) space narrowing (often mild), (2) marginal osteophytes, (3) subchondral sclerosis (more well defined and narrower than in SpA), cysts and joint vacuum phenomena (Fig. 50).

While the prevalence of degenerative changes increases with age, they can be seen in young patients, particularly if sport's active. Osteoarthritis tends to affect the iliac side more due to increased load bearing and thinner articular cartilage (Schueller-Weidekamm et al. 2014). Small erosions can also occur within the spectrum of degenerative changes in the SIJ, especially in elderly overweight women, confounding the clinical picture. BME due to osteoarthritis also occurs, particularly surrounding sclerotic areas. It tends to be mild and often is limited to the immediate subchondral area, commonly in the antero-superior part of the SIJs (Weber et al. 2019). Fat deposition is a non-specific finding, but may sometimes be seen in the degenerative setting and even in older healthy individuals. Bridging osteophytosis in osteoarthritis leads to para-articular bony ankyloses (not to be mistaken for the true intra-articular bony ankylosis seen in SpA).

5.4.4 Differential Diagnosis

The list of SIJ differential diagnosis in SIJ disorders is broad, and beyond the scope of this chapter. These are some of the most important differential diagnosis in clinical practice:

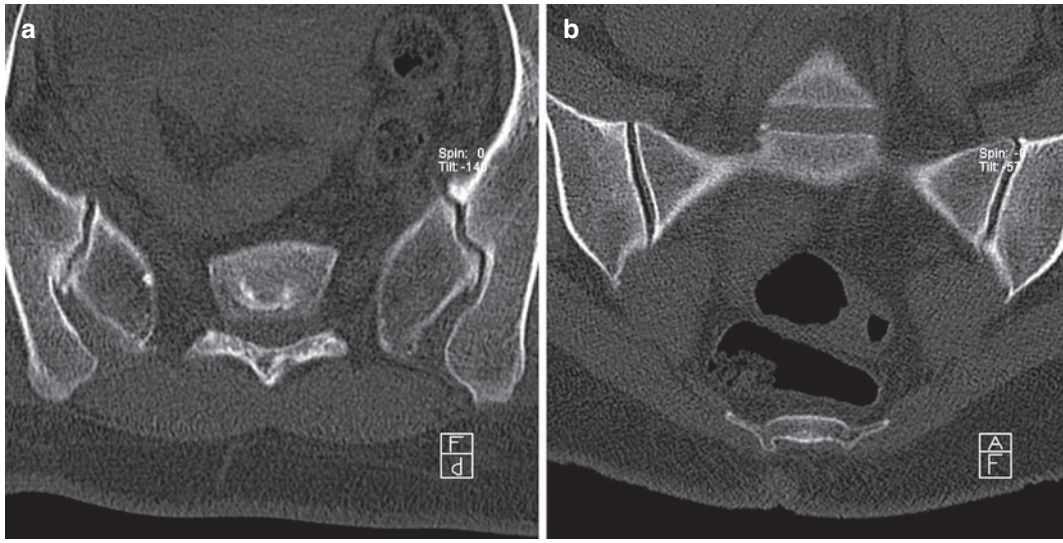

Fig. 50 (**a**, **b**) 49-year-old male with SIJs osteoarthritis. (**a**) axial and (**b**) coronal CT images show bilateral vacuum phenomenon, mild subchondral sclerosis and anterior marginal osteophytosis, with subtle cortical irregularity

Spondyloarthropathies (inflammatory sacroiliitis) (Fig. 51): SpA are a group of inflammatory entities which share overlapping clinical, imaging, genetic and therapeutic features, that are often associated with human leukocyte antigen (HLA) B27 positivity and seronegativity for rheumatoid factor (Rudwaleit et al. 2009). Based on the dominant clinical features, they can be divided into two main groups: (1) **axial SpA** (where sacroiliitis is the cornerstone) and (2) **peripheral SpA**.

A consensus organized by ASAS culminated in the definition of SIJ imaging criteria for the diagnosis of SpA (ASAS imaging arm). Sacroiliitis on imaging is defined as "definite radiographic sacroiliitis according to modified New York criteria" and/or as active sacroiliitis on MRI ("positive" MRI defined by the unequivocal presence of subchondral BME). According to ASAS criteria, the diagnosis of SpA in an adult is based on the presence of active inflammatory lesions (positive MRI "sacroiliitis" ± structural post inflammatory changes (Lambert et al. 2016)) and of at least one clinical feature of SpA (Table 22).

Even with well-established criteria, it is crucial to be aware that a wide range of conditions can pose diagnostic challenges on MRI. Even in patients with inflammatory low-back pain, it is important to consider non-inflammatory disease. It has been documented that 23–33% of patients referred for MRI due to clinical suspicion of SpA had alternative non-inflammatory conditions, and that 41–50% had normal SIJs on MRI.

Other diagnosis: Stress fractures (fatigue and insufficiency), infectious sacroiliitis, osteitis condensans ilii, diffuse idiopathic skeletal hyperostosis (DISH), hyperparathyroidism, chronic recurrent multifocal osteomyelitis (CRMO)/synovitis, acne, pustulosis, hyperostosis and osteitis (SAPHO) and gout.

6 Future Trends in Hip Imaging

The future of hip imaging will include comprehensive 3D joint imaging, performed within fractions of the time currently spent and multiparametric in nature, allowing for (1) high resolution 3D MRI acquisitions with potential for replacing MRA; (2) automated biochemical cartilage and quantitative imaging biomarkers analysis in clinical routine imaging; (3) fully automated diagnostic examinations with algorithms to diagnose and automatically quantify

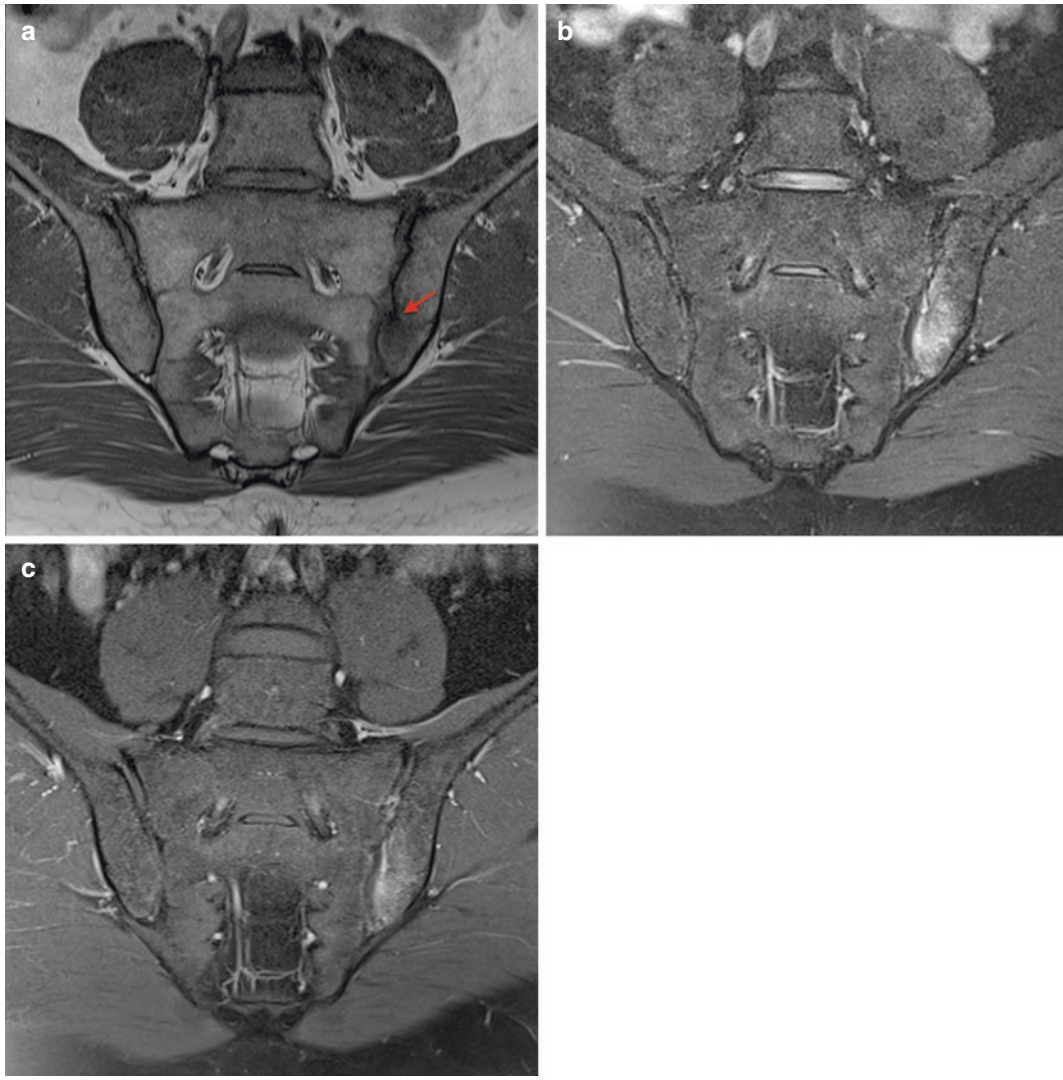

Fig. 51 (**a–c**) 33-year-old male with psoriatic arthritis. (**a**) Coronal T1 (**b**) coronal fat-suppressed proton-density and (**c**) coronal fat-suppressed post-contrast, T1w MR images depict extensive BME adjacent to the left SIJ, on the iliac side, fulfilling ASAS criteria for "positive MRI". Notice cortical irregularity and minor erosions (red arrow) seen on (**a**)

Table 22 Types of MRI lesions in the SIJ

Active inflammatory lesions	Chronic (structural) postinflammatory lesions
BME/osteitis (primary criterion)	Subchondral sclerosis
Capsulitis	Erosions
Enthesitis	Backfill
Joint space enhancement (formerly called synovitis)	Fat metaplasia
Active erosion	Bone ankylosis
Joint space fluid	Bone bud

specific biomarkers (Mascarenhas and Caetano 2018) (Fig. 52).

6.1 Artificial Intelligence

Clinical large databases in the era of value-based health care are paramount. The implementation of standardized national sports registries in conjunction with programmes tailored to radiologists

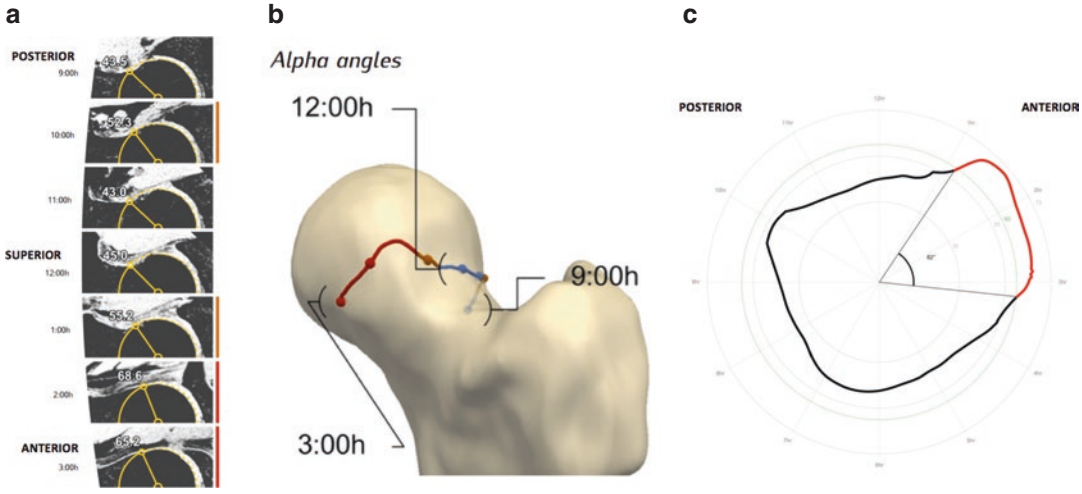

Fig. 52 (**a–c**) Automated segmentation and quantification of femoral parameters based on a 3D MRI dataset of a 25-year-old elite soccer player. (**a**) Volumetric 3D MRI alpha-angle (α°) automated measurements made at different points around the femoral head/neck junction. α° measured at 9 o'clock (posterior); 10, 11 and 12 o'clock (superior); and 1, 2 and 3 o'clock (anterior). (**b**) 3D generated model representing the radial extension of the cam deformity (orange and red line representing increased alpha angles). (**c**) Polar plot (2D) of the automated 360° α° measurements around the FHN, representing the Ω° angle and corresponding perimeter (red line) for a given α° threshold (60°). Red lines represent increased α°s for a given threshold. The Ω° is formed by two lines intersecting the centre of the femoral neck at the level of the head-neck junction. The most posterior line posteriorly intersects the point at which the α° angle begins to be abnormal beyond a best-fitting circle and the anterior line at the point where the α° angle returns to normal

and sports medicine practisers will ultimately improve patient outcomes while minimizing the economic burden.

Artificial intelligence in the sports medicine field will certainly set the new standard by automatically detecting patterns in injury data, and then using those patterns to predict RTS or enable decision making under uncertain conditions. Applications include (1) automatic image segmentation and registration; (2) computer-aided detection and diagnosis; (3) integration with healthcare big data and (4) defining "personalized" RTS prediction and treatment strategies (Syed and Zoga 2018).

6.2 Personalized Medicine and Biobanks

The original concept of precision sports medicine involves the implementation of treatment and prevention strategies that consider individual variability by assessing large sets of data, including patient information, medical imaging, and genomic sequences. Patient-based imaging data will be implemented and cross-linked to population-based data already acquired in biobanks, allowing a "tailored" decision to a specific athlete (Kooijman et al. 2016).

7 Conclusion

Innovation has been the catalyst for the transformation of hip imaging, as the arrival of new modalities and the introduction of MRI resulted in a paradigm shift from bone morphology analysis to integrated soft tissue, joint and cartilage assessment. Understanding the pathophysiology through the visualization of osseous structures and detailed depiction of soft tissues has become part of routine imaging and has had a major impact on therapeutic decision-making.

With increasing sports medicine specialization and also rising rates of overuse injuries,

major questions have still to be answered when it comes to sports injuries, namely RTS specific predictors and the role played by intense athletic activity in FAIS development. The delicate balance between early preventive measures, conservative treatment and surgical intervention has yet to be clearly defined. It is time to refine the diagnostic and therapeutical algorithm by incorporating both clinical and imaging data into the medical equation. Looking ahead, imaging and sports will continue to evolve hand-in-hand, with new problems and greater challenges.

Box 1: Standard Radiography

- Radiography is the first-line imaging modality to assess the bony hip and pelvis; it is not well suited, however, to evaluate soft tissue injuries.
- Radiographs are two-dimensional projections of three-dimensional structures, which limit their value in particular clinical settings (e.g. morphological assessment in FAI).
- Specific radiographic views may be warranted, depending on a particular clinical problem.

Box 2: Ultrasound (US)

- US is an established technique in the work-up of an athlete with hip/groin pain, particularly for suspected muscle and tendon disease.
- US is a fast, low-cost, radiation-free, widely available technique which easily allows dynamic imaging and contralateral comparison.
- US-guided injections may prove very useful in both the diagnostic (confirm the source of symptoms) and therapeutic settings.

Box 3: Computed Tomography

- CT is an excellent imaging method to assess osseous morphologies, hence useful in the evaluation of fractures and calcification/ossification although very limited in depicting soft tissues injuries.
- In athletes, CT should be used mainly as a problem-solving tool, whenever radiographic occult fractures are suspected or in pre-operative planning.
- Hip CT arthrography can be used to assess hip chondrolabral injuries particularly if MRI is contra-indicated.

Box 4: Magnetic Resonance Imaging

- MRI is a comprehensive radiation-free technique considered the gold standard imaging approach in sports, to assess both bony and soft tissue structures in the pelvis/hip region.
- MRI protocols combining hip dedicated sequences as well as sequences covering the pelvis offer the best chance of identifying all potential sources of symptoms; tailoring the MRI protocol to the specific clinical scenario is crucial to achieve the best results.
- When intra-articular disease is suspected, dMRA is the imaging study of choice, as both a **diagnostic** arthrography and an **anaesthetic** injection can be combined into a single procedure.

Things to Remember (Hip)

1. Knowledge of hip biomechanics helps in the understanding of sports-related hip disease.
2. In athletes with hip-groin pain, periarticular structures need to be imaged because many abnormalities occur outside the hip joint.
3. If radiographs are normal and clinical suspicion for stress fracture remains high, fur-

ther investigation with MRI should be sought.
4. Imaging findings described in cam-type FAI include an increased α angle, anterosuperior labral tears and anterosuperior chondral abnormalities at the chondrolabral junction.
5. Labral tears are common in athletes (both symptomatic and asymptomatic), and usually best identified on small FOV images.
6. The most common underlying cause of GTPS is *gluteus minimus* and *medius* insertional tendon disease resulting from chronic repetitive microtrauma, including tendinosis, tendon tearing and peritendinitis.

Things to Remember (Pelvis)

1. MRI is the gold standard technique to assess the continuum of stress response of bone.
2. Mechanical stress applied to the muscle-tendon-bone unit may result in tendon tears or myotendinous lesions in the adult athlete and in apophyseal avulsion the child or adolescent. This is due to the intrinsic fragility of the apophyseal growth plate in the immature skeleton, which may tear in response to traction stress.
3. Pelvic apophyseal avulsions are unusual in the mature skeleton and should prompt a search for an underlying cause (e.g. metastasis).
4. The *rectus femoris*, *biceps femoris* and *adductor longus* are the most commonly injured muscles in the pelvis and thigh.
5. MRI is useful to confirm the clinical diagnosis and determine the extent of muscle injury, but has limited prognostic value in determining recovery times.

Things to Remember (SIJ)

1. SIJ dysfunction is a well-known clinical entity in sports, with repetitive, asymmetric mechanical loading and microtrauma, leading to imaging changes, including low-grade BME and occasionally minor erosions in the SIJ in athletes.
2. BME is present in up to 25% of SIJ of healthy adults, usually low-grade and non-extensive even though a substantial proportion will fulfil ASAS criteria for a positive MRI of inflammatory sacroiliitis. Clinical correlation, including sports history, is warranted.
3. There is a broad differential diagnosis for SIJ dysfunction. When assessing active athletes, sacral fractures and SpA-related sacroiliitis must be sought. Deep (extensive) BME lesions are almost exclusively found in axial SpA patients. Other sites of pelvic (e.g.: pubic symphysis and hip) and extra pelvic (e.g.: spine) pain must be excluded.

References

Agricola R, Heijboer MP, Bierma-Zeinstra SMA et al (2013a) Cam impingement causes osteoarthritis of the hip: a nationwide prospective cohort study (CHECK). Ann Rheum Dis 72:918–923. https://doi.org/10.1136/annrheumdis-2012-201643

Agricola R, Heijboer MP, Ginai AZ et al (2014) A cam deformity is gradually acquired during skeletal maturation in adolescent and young male soccer players: a prospective study with minimum 2-year follow-up. Am J Sports Med 42:798–806. https://doi.org/10.1177/0363546514524364

Agricola R, Heijboer MP, Roze RH et al (2013b) Pincer deformity does not lead to osteoarthritis of the hip whereas acetabular dysplasia does: acetabular coverage and development of osteoarthritis in a nationwide prospective cohort study (CHECK). Osteoarthr Cartil 21:1514–1521. https://doi.org/10.1016/j.joca.2013.07.004

Agricola R, Waarsing JH, Arden NK et al (2013c) Cam impingement of the hip: a risk factor for hip osteoarthritis. Nat Rev Rheumatol 9:630–634. https://doi.org/10.1038/nrrheum.2013.114

Agten CA, Sutter R, Buck FM, Pfirrmann CWA (2016) Hip imaging in athletes: sports imaging series. Radiology 280:351–369. https://doi.org/10.1148/radiol.2016151348

Allen D, Beaulé PE, Ramadan O, Doucette S (2009) Prevalence of associated deformities and hip pain in patients with cam-type femoroacetabular impingement. J Bone Joint Surg Br 91:589–594. https://doi.org/10.1302/0301-620X.91B5.22028

Alonso-Coello P, Schünemann HJ, Moberg J et al (2016) GRADE Evidence to Decision (EtD) frameworks: a systematic and transparent approach to making well informed healthcare choices. 1: Introduction. BMJ 353:i2016. https://doi.org/10.1136/bmj.i2016

Anderson LA, Peters CL, Park BB et al (2009) Acetabular cartilage delamination in femoroacetabular impingement. Risk factors and magnetic resonance imaging

diagnosis. J Bone Joint Surg 91:305–313. https://doi.org/10.2106/JBJS.G.01198

Anderson MW, Kaplan PA, Dussault RG (2001) Adductor insertion avulsion syndrome (thigh splints): spectrum of MR imaging features. Am J Roentgenol 177:673–675. https://doi.org/10.2214/ajr.177.3.1770673

Anwander H, Beck M, Büchler L (2018) The influence of evolution on cam deformity and its impact on biomechanics of the human hip joint. J Orthop Res. https://doi.org/10.1002/jor.23863

Aprato A, Giachino M, Massè A (2016) Arthroscopic approach and anatomy of the hip. Muscles Ligaments Tendons J 6:309–316. https://doi.org/10.11138/mltj/2016.6.3.309

Ayeni OR, Farrokhyar F, Crouch S et al (2014) Preoperative intra-articular hip injection as a predictor of short-term outcome following arthroscopic management of femoroacetabular impingement. Knee Surg Sports Traumatol Arthrosc 22:801–805. https://doi.org/10.1007/s00167-014-2883-y

Ayeni OR, Wong I, Chien T et al (2012) Surgical indications for arthroscopic management of femoroacetabular impingement. Arthrosc J Arthrosc Related Surg 28:1170–1179. https://doi.org/10.1016/j.arthro.2012.01.010

Bardakos NV, Villar RN (2009) Predictors of progression of osteoarthritis in femoroacetabular impingement a radiological study with a minimum of ten years follow-up. J Bone Joint Surg 91:162–169. https://doi.org/10.1302/0301-620X.91B2

Beck M, Kalhor M, Leunig M, Ganz R (2005) Hip morphology influences the pattern of damage to the acetabular cartilage. J Bone Joint Surg 87:1012–1018. https://doi.org/10.1302/0301-620X.87B7

Bedi A, Chen N, Robertson W, Kelly BT (2008) The management of labral tears and femoroacetabular impingement of the hip in the young, active patient. Arthrosc J Arthrosc Related Surg 24:1135–1145

Bencardino JT, Mellado JM (2005) Hamstring Injuries of the Hip. Magn Reson Imaging Clin N Am 13:677–690. https://doi.org/10.1016/j.mric.2005.08.002

Bittersohl B, Steppacher S, Haamberg T et al (2009) Cartilage damage in femoroacetabular impingement (FAI): preliminary results on comparison of standard diagnostic vs delayed gadolinium-enhanced magnetic resonance imaging of cartilage (dGEMRIC). Osteoarthr Cartil 17:1297–1306. https://doi.org/10.1016/j.joca.2009.04.016

Blankenbaker DG, al E (2006) The painful hip: new concepts

Blankenbaker DG, De Smet AA, Keene JS, Fine JP (2007) Classification and localization of acetabular labral tears. Skelet Radiol 36:391–397. https://doi.org/10.1007/s00256-006-0240-z

Boric I, Isaac A, Dalili D et al (2019) Imaging of articular and extra-articular sports injuries of the hip. Semin Musculoskelet Radiol 23:e17–e36. https://doi.org/10.1055/s-0039-1688696

Bowman KF, Fox J, Sekiya JK (2010) A clinically relevant review of hip biomechanics. Arthroscopy 26:1118–1129. https://doi.org/10.1016/j.arthro.2010.01.027

Boyd KT, Peirce NS, Batt ME (1997) Common hip injuries in sport. Sports Med 24:273–288. https://doi.org/10.2165/00007256-199724040-00005

Brittenden J, Robinson P (2005) Imaging of pelvic injuries in athletes. Br J Radiol 78:457–468. https://doi.org/10.1177/036354659502300515

Brolinson PG, Kozar AJ, Cibor G (2003) Sacroiliac joint dysfunction in athletes. Curr Sports Med Rep 2:47–56. https://doi.org/10.1249/00149619-200302000-00009

Busse J, Gasteiger W, Tönnis D (1972) Eine neue Methode zur röntgenologischen Beurteilung eines Hüftgelenkes--Der Hüftwert [A new method for roentgenologic evaluation of the hip joint--the hip factor]. Arch Orthop Unfallchir 72(1):1–9. German. https://doi.org/10.1007/BF00415854. PMID: 5020681

Byrd JWT, Jones KS (2004) Diagnostic accuracy of clinical assessment, magnetic resonance imaging, magnetic resonance arthrography, and intra-articular injection in hip arthroscopy patients. Am J Sports Med 32:1668–1674. https://doi.org/10.1177/0363546504266480

Byrd JWT, Potts EA, Allison RK, Jones KS (2014) Ultrasound-guided hip injections: a comparative study with fluoroscopy-guided injections. YJARS 30:42–46. https://doi.org/10.1016/j.arthro.2013.09.083

Calderazzi F, Nosenzo A, Galavotti C et al (2018) Apophyseal avulsion fractures of the pelvis. A review. Acta Biomed 89:470–476. https://doi.org/10.23750/abm.v89i4.7632

Campos-Correia D, Sudoł-Szopińska I, Diana Afonso P (2019) Are we overcalling sacroillitis on MRI? Differential diagnosis that every rheumatologist should know—Part II. Acta Reumatol Port 44:42–56

Cerezal L, Arnaiz J, Canga A et al (2012) Emerging topics on the hip: Ligamentum teres and hip microinstability. Eur J Radiol 81:3745–3754. https://doi.org/10.1016/j.ejrad.2011.04.001

Chahla J, Soares EAM, Devitt BM et al (2016) Ligamentum teres tears and femoroacetabular impingement: prevalence and preoperative findings. Arthroscopy 32:1293–1297. https://doi.org/10.1016/j.arthro.2016.01.045

Clohisy JC (2008) A systematic approach to the plain radiographic evaluation of the young adult hip. J Bone Joint Surg 90:47. https://doi.org/10.2106/JBJS.H.00756

Crema MD, Guermazi A, Tol JL et al (2015) Acute hamstring injury in football players: Association between anatomical location and extent of injury—a large single-center MRI report. J Sci Med Sport 19(4):317–322. https://doi.org/10.1016/j.jsams.2015.04.005

Crespo-Rodríguez AM, De Lucas-Villarrubia JC, Pastrana-Ledesma M et al (2017) The diagnostic performance of non-contrast 3-Tesla magnetic resonance imaging (3-T MRI) versus 1.5-Tesla magnetic resonance arthrography (1.5-T MRA) in femoroacetabular impingement. Eur J Radiol 88:109–116. https://doi.org/10.1016/j.ejrad.2016.12.031

Cruz CA, Kerbel Y, Smith CM et al (2019) A sport-specific analysis of the epidemiology of hip injuries in National Collegiate Athletic Association Athletes from 2009 to 2014. Arthroscopy 35:2724–2732. https://doi.org/10.1016/j.arthro.2019.03.044

Cruz J, Mascarenhas V (2018) Adult thigh muscle injuries-from diagnosis to treatment: what the radiologist should know. Skelet Radiol. https://doi.org/10.1007/s00256-018-2929-1

Czerny C, Hofmann S, Neuhold A et al (1996) Lesions of the acetabular labrum: accuracy of MR imaging and MR arthrography in detection and staging. Radiology 200:225–230. https://doi.org/10.1148/radiology.200.1.8657916

De Smet AA, Best TM (2000) MR imaging of the distribution and location of acute hamstring injuries in athletes. Am J Roentgenol 174:393–399. https://doi.org/10.2214/ajr.174.2.1740393

De Smet AA, Blankenbaker DG, Alsheik NH, Lindstrom MJ (2012) MRI appearance of the proximal hamstring tendons in patients with and without symptomatic proximal hamstring tendinopathy. AJR Am J Roentgenol 198:418–422. https://doi.org/10.2214/AJR.11.6590

Dienst M (2005) Hip arthroscopy: technique and anatomy. Operat Tech Sports Med 13:13–23. https://doi.org/10.1053/j.otsm.2004.09.009

Dietrich TJ, Suter A, Pfirrmann C, Dora C (2012) Supraacetabular Fossa (Pseudodefect of Acetabular Cartilage): frequency at MR arthrography and comparison of findings at MR arthrography and arthroscopy

Domb BG, Shindle MK, McArthur B et al (2011) Iliopsoas impingement: a newly identified cause of labral pathology in the hip. HSS JRNL 7:145–150. https://doi.org/10.1007/s11420-011-9198-z

Eberbach H, Hohloch L, Feucht MJ, Konstantinidis L, Südkamp NP, Zwingmann J (2017) Operative versus conservative treatment of apophyseal avulsion fractures of the pelvis in the adolescents: a systematical review with meta-analysis of clinical outcome and return to sports. BMC Musculoskelet Disord 18(1):162. https://doi.org/10.1186/s12891-017-1527-z. PMID: 28420360; PMCID: PMC5395880

Ekstrand J, Hägglund M, Waldén M (2011) Epidemiology of muscle injuries in professional football (soccer). Am J Sports Med 39:1226–1232. https://doi.org/10.1136/bjsm.2004.014571

Faflia CP, Prassopoulos PK, Daskalogiannaki ME, Gourtsoyiannis NC (1998) Variation in the appearance of the normal sacroiliac joint on pelvic CT. Clin Radiol 53:742–746. https://doi.org/10.1016/s0009-9260(98)80316-4

Frank JM, Harris JD, Erickson BJ et al (2015) Prevalence of femoroacetabular impingement imaging findings in asymptomatic volunteers: a systematic review. Arthroscopy 31:1199–1204. https://doi.org/10.1016/j.arthro.2014.11.042

Freke MD, Kemp J, Svege I et al (2016) Physical impairments in symptomatic femoroacetabular impingement: a systematic review of the evidence. Br J Sports Med 50:1180–1180. https://doi.org/10.1136/bjsports-2016-096152

Galeano NA, Guinea NS, Molinero JG, Bárez MG (2018) Extra-articular hip impingement: a review of the literature. Radiología (English Edition) 60:105–118. https://doi.org/10.1016/j.rxeng.2018.02.002

Ganz R, Gill TJ, Gautier E et al (2001) Surgical dislocation of the adult hip a technique with full access to the femoral head and acetabulum without the risk of avascular necrosis. J Bone Joint Surg 83:1119–1124

Ganz R, Parvizi J, Beck M et al (2003) Femoroacetabular impingement: a cause for osteoarthritis of the hip. Clin Orthop Relat Res:112–120. https://doi.org/10.1097/01.blo.0000096804.78689.c2

Giori NJ, Trousdale RT (2003) Acetabular retroversion is associated with osteoarthritis of the hip. Clin Orthop Relat Res:263–269. https://doi.org/10.1097/01.blo.0000093014.90435.64

Glyn-Jones S, Palmer AJR, Agricola R et al (2015) Osteoarthritis. Lancet:1–12. https://doi.org/10.1016/S0140-6736(14)60802-3

Gosvig KK, Jacobsen S, Sonne-Holm S et al (2010) Prevalence of malformations of the hip joint and their relationship to sex, groin pain, and risk of osteoarthritis: a population-based survey. J Bone Joint Surg Am 92:1162–1169. https://doi.org/10.2106/JBJS.H.01674

Gouttebarge V, Inklaar H, Backx F, Kerkhoffs G (2015) Prevalence of osteoarthritis in former elite athletes: a systematic overview of the recent literature. Rheumatol Int 35:405–418. https://doi.org/10.1007/s00296-014-3093-0

Grammatopoulos G, Speirs AD, Ng KCG et al (2018) Acetabular and spino-pelvic morphologies are different in subjects with symptomatic cam femoroacetabular impingement. J Orthop Res 36:1840–1848. https://doi.org/10.1002/jor.22375

Greaney RB, Gerber FH, Laughlin RL et al (1983) Distribution and natural history of stress fractures in U.S. Marine recruits. Radiology 146:339–346. https://doi.org/10.1148/radiology.146.2.6217486

Griffin DR, Dickenson EJ, O'Donnell J et al (2016) The Warwick Agreement on femoroacetabular impingement syndrome (FAI syndrome): an international consensus statement. Br J Sports Med 50:1169–1176. https://doi.org/10.1136/bjsports-2016-096743

Griffin DR, Dickenson EJ, Wall PDH et al (2018) Hip arthroscopy versus best conservative care for the treatment of femoroacetabular impingement syndrome (UK FASHIoN): a multicentre randomised controlled trial. Lancet 391:2225–2235. https://doi.org/10.1016/S0140-6736(18)31202-9

Guermazi A, Roemer FW, Robinson P et al (2017) Imaging of muscle injuries in sports medicine: sports imaging series. Radiology 282:646–663. https://doi.org/10.1148/radiol.2017160267

Haefeli PC, Steppacher SD, Babst D et al (2015) An increased iliocapsularis-to-rectus-femoris ratio is suggestive for instability in borderline hips. Clin Orthop Relat Res 473:3725–3734. https://doi.org/10.1007/s11999-015-4382-y

Hanke MS, Steppacher SD, Anwander H et al (2016) What MRI findings predict failure 10 years after surgery for femoroacetabular impingement? Clin Orthop Relat Res:1–16. https://doi.org/10.1007/s11999-016-5040-8

Hartigan DE, Perets I, Yuen LC, Domb BG (2017) Results of hip arthroscopy in patients with MRI diagnosis of subchondral cysts—a case series. J Hip Preserv Surg 4:324–331. https://doi.org/10.1016/j.arth.2014.03.054

Hawker GA, Stanaitis I (2014) Osteoarthritis year in review 2014: clinical. Osteoarthr Cartil 22:1953–1957. https://doi.org/10.1016/j.joca.2014.06.018

Heerey JJ, Kemp JL, Mosler AB et al (2019) What is the prevalence of hip intra-articular pathologies and osteoarthritis in active athletes with hip and groin pain compared with those without? a systematic review and meta-analysis. Sports Med:1–22. https://doi.org/10.1007/s40279-019-01092-y

Hegazi TM, Belair JA, McCarthy EJ et al (2016) Sports injuries about the hip: what the radiologist should know. Radiographics 36:1717–1745. https://doi.org/10.1148/rg.2016160012

Hellman MD, Gross CE, Hart M et al (2016) Radiographic comparison of anterior acetabular rim morphology between pincer femoroacetabular impingement and control. Arthroscopy 32:468–472. https://doi.org/10.1016/j.arthro.2015.08.035

Hemke R, Mascarenhas V, Maas M (2018) Novel imaging techniques in rheumatic diseases. Semin Musculoskelet Radiol 22:237–244. https://doi.org/10.1055/s-0038-1641160

Hernando MF, Cerezal L, Pérez-Carro L et al (2015) Deep gluteal syndrome: anatomy, imaging, and management of sciatic nerve entrapments in the subgluteal space. Skelet Radiol 44:919–934. https://doi.org/10.1007/s00256-015-2124-6

Hernando MF, Cerezal L, Pérez-Carro L et al (2016) Evaluation and management of ischiofemoral impingement: a pathophysiologic, radiologic, and therapeutic approach to a complex diagnosis. Skelet Radiol 45:771–787. https://doi.org/10.1007/s00256-016-2354-2

Hetsroni I, Poultsides L, Bedi A et al (2013) Anterior inferior iliac spine morphology correlates with hip range of motion: a classification system and dynamic model. Clin Orthop Relat Res 471:2497–2503. https://doi.org/10.1007/s11999-013-2847-4

Hirschmann A, Falkowski AL, Kovacs B (2017) Greater trochanteric pain syndrome: abductors, external rotators. Semin Musculoskelet Radiol 21:539–546. https://doi.org/10.1055/s-0037-1606139

Hunter DJ, Arden N, Conaghan PG et al (2011) Nition of osteoarthritis on MRI: results of a Delphi exercise. Osteoarthr Cartil 19:963–969. https://doi.org/10.1016/j.joca.2011.04.017

Ilizaliturri VM Jr, Byrd JWT, Sampson TG et al (2008) A geographic zone method to describe intra-articular pathology in hip arthroscopy: cadaveric study and preliminary report. Arthrosc J Arthrosc Related Surg 24:534–539. https://doi.org/10.1016/j.arthro.2007.11.019

Ito K, Minka-II MA, Leunig M et al (2001) Femoroacetabular impingement and the cam-effect. J Bone Joint Surg 83:171–176. https://doi.org/10.1302/0301-620X.83B2.11092

Jackson TJ, Estess AA, Adamson GJ (2016) Supine and standing AP pelvis radiographs in the evaluation of pincer femoroacetabular impingement. Clin Orthop Relat Res 474:1692–1696. https://doi.org/10.1007/s11999-016-4766-7

Jónasson P, Halldin K, Karlsson J et al (2011) Prevalence of joint-related pain in the extremities and spine in five groups of top athletes. Knee Surg Sports Traumatol Arthrosc 19:1540–1546. https://doi.org/10.1007/s00167-011-1539-4

Jung JY, Kim G-U, Lee H-J et al (2013) Diagnostic value of ultrasound and computed tomographic arthrography in diagnosing anterosuperior acetabular labral tears. Arthroscopy 29:1769–1776. https://doi.org/10.1016/j.arthro.2013.07.274

Jung KA, Restrepo C, Hellman M et al (2011) The prevalence of cam-type femoroacetabular deformity in asymptomatic adults. J Bone Joint Surg 93:1303. https://doi.org/10.1302/0301-620X.93B10

Kalberer F, Sierra RJ, Madan SS et al (2008) Ischial spine projection into the pelvis: a new sign for acetabular retroversion. Clin Orthop Relat Res 466:677–683. https://doi.org/10.1007/s11999-007-0058-6

Kalhor M, Horowitz K, Beck M et al (2010) Vascular supply to the acetabular labrum. J Bone Joint Surg Am 92:2570–2575. https://doi.org/10.2106/JBJS.I.01719

Kassarjian A (2019) Hip hype: FAI syndrome, amara's law, and the hype cycle. Semin Musculoskelet Radiol. https://doi.org/10.1055/s-0039-1677695

Kassarjian A, Rodrigo RM, Santisteban JM (2012) Current concepts in MRI of rectus femoris musculotendinous (myotendinous) and myofascial injuries in elite athletes. Eur J Radiol 81:3763–3771. https://doi.org/10.1016/j.ejrad.2011.04.002

Kassarjian A, Rodrigo RM, Santisteban JM (2014) Intramuscular degloving injuries to the rectus femoris: findings at MRI. AJR Am J Roentgenol 202:W475–W480. https://doi.org/10.2214/AJR.13.10931

Kaya M, Suzuki T, Emori M, Yamashita T (2016) Hip morphology in uences the pattern of articular cartilage damage. Knee Surg Sports Traumatol Arthrosc 24:2016–2023. https://doi.org/10.1007/s00167-014-3297-6

Kellgren JH, Jeffrey MR, Ball J (1963) The epidemiology of chronic rheumatism: a symposium

Khan W, Khan M, Alradwan H et al (2015) Utility of intra-articular hip injections for femoroacetabular impingement: a systematic review. Orthop J Sports Med. https://doi.org/10.1177/2325967115601030

Kiuru MJ, Pihlajamaki HK, Ahovuo JA (2003) Fatigue stress injuries of the pelvic bones and proximal femur: evaluation with MR imaging. Eur Radiol 13(3):605–11. https://doi.org/10.1007/s00330-002-1562-4. Epub 2002 Aug 16. PMID: 12594565

Kivlan BR, Martin RL, Sekiya JK (2011) Response to diagnostic injection in patients with femoroacetabular

impingement, labral tears, chondral lesions, and extra-articular pathology. Arthroscopy 27:619–627. https://doi.org/10.1016/j.arthro.2010.12.009

Kizaki K, Uchida S, Shanmugaraj A et al (2020) Deep gluteal syndrome is defined as a non-discogenic sciatic nerve disorder with entrapment in the deep gluteal space: a systematic review. Knee Surg Sports Traumatol Arthrosc:1–11. https://doi.org/10.1007/s00167-020-05966-x

Kooijman MN, Kruithof CJ, van Duijn CM et al (2016) The generation R study: design and cohort update 2017. Eur J Epidemiol 31:1243–1264. https://doi.org/10.1007/s10654-016-0224-9

Kraeutler MJ, Garabekyan T, Pascual-Garrido C, Mei-Dan O (2016) Hip instability: a review of hip dysplasia and other contributing factors. Muscles Ligaments Tendons J 6:343–353. https://doi.org/10.11138/mltj/2016.6.3.343

Krishnamoorthy VP, Beck EC, Kunze KN et al (2019a) Radiographic prevalence of sacroiliac joint abnormalities and clinical outcomes in patients with femoroacetabular impingement syndrome. Arthroscopy 35:2598–2605.e1. https://doi.org/10.1016/j.arthro.2019.03.030

Krishnamoorthy VP, Kunze KN, Beck EC et al (2019b) Radiographic prevalence of symphysis pubis abnormalities and clinical outcomes in patients with femoroacetabular impingement syndrome. Am J Sports Med 47:1467–1472. https://doi.org/10.1177/0363546519837203

Krych AJ, King AH, Berardelli RL et al (2016) Is subchondral acetabular edema or cystic change on MRI a contraindication for hip arthroscopy in patients with femoroacetabular impingement? Am J Sports Med 44:454–459. https://doi.org/10.1177/0363546515612448

Kuske B, Hamilton DF, Pattle SB, Simpson AHRW (2016) Patterns of hamstring muscle tears in the general population: a systematic review. PLoS One 11:e0152855. https://doi.org/10.1371/journal.pone.0152855.s003

Lambert RGW, Bakker PAC, van der Heijde D et al (2016) Defining active sacroiliitis on MRI for classification of axial spondyloarthritis: update by the ASAS MRI working group. Ann Rheum Dis. https://doi.org/10.1136/annrheumdis-2015-208642

Lane NE, Hochberg MC, Nevitt MC et al (2015) OARSI clinical trials recommendations: design and conduct of clinical trials for hip osteoarthritis. Osteoarthr Cartil 23:761–771. https://doi.org/10.1016/j.joca.2015.03.006

Liong SY, Whitehouse RW (2012) Lower extremity and pelvic stress fractures in athletes. Br J Radiol 85:1148–1156. https://doi.org/10.1259/bjr/78510315

Llopis E, Cerezal L, Kassarjian A et al (2008) Direct MR arthrography of the hip with leg traction: feasibility for assessing articular cartilage. AJR Am J Roentgenol 190:1124–1128. https://doi.org/10.2214/AJR.07.2559

Lungu E, Michaud J, Bureau NJ (2018) US assessment of sports-related hip injuries. Radiographics 38:867–889. https://doi.org/10.1148/rg.2018170104

Lynch TS, Steinhaus ME, Popkin CA et al (2016) Outcomes after diagnostic hip injection. Arthroscopy 32:1702–1711. https://doi.org/10.1016/j.arthro.2016.02.027

Maheu E, Cadet C, Marty M et al (2005) Reproducibility and sensitivity to change of various methods to measure joint space width in osteoarthritis of the hip: a double reading of three different radiographic views taken with a three-year interval. Arthritis Res Ther 7:R1375–R1385. https://doi.org/10.1186/ar1831

Major NM, Helms CA (2000) Sacral stress fractures in long-distance runners. Am J Roentgenol 174:727–729. https://doi.org/10.2214/ajr.174.3.1740727

Makovicka JL, Chhabra A, Patel KA et al (2019) A decade of hip injuries in National Collegiate Athletic Association football players: an epidemiologic study using National Collegiate Athletic Association surveillance data. J Athl Train 54:483–488. https://doi.org/10.4085/1062-6050-59-18

Marshall RA, Mandell JC, Weaver MJ et al (2018) Imaging features and management of stress, atypical, and pathologic fractures. Radiographics 38:2173–2192. https://doi.org/10.1148/rg.2018180073

Mascarenhas VV, Ayeni OR, Egund N et al (2019) Imaging methodology for hip preservation: techniques, parameters, and thresholds. Semin Musculoskelet Radiol 23:197–226. https://doi.org/10.1055/s-0039-1688714

Mascarenhas VV, Caetano A (2018) Imaging the young adult hip in the future. Ann Joint 3:47–47. https://doi.org/10.21037/aoj.2018.04.10

Mascarenhas VV, Castro M, Rego PA, et al (2020a) The Lisbon Agreement on Femoroacetabular impingement imaging—Part 2: general issues, parameters and reporting

Mascarenhas VV, Castro MO, Rego PA et al. (2020) The Lisbon Agreement on Femoroacetabular Impingement Imaging-part 1: overview. Eur Radiol 30(10):5281–5297. https://doi.org/10.1007/s00330-020-06822-9. Epub 2020 Jul 17. Erratum in: Eur Radiol. PMID: 32405754

Mascarenhas VV, Rego P, Dantas P et al (2017) Cam deformity and the omega angle, a novel quantitative measurement of femoral head-neck morphology: a 3D CT gender analysis in asymptomatic subjects. Eur Radiol 27:2011–2023. https://doi.org/10.1007/s00330-016-4530-0

Mascarenhas VV, Rego PA, Dantas P et al (2018a) Can we discriminate symptomatic hip patients from asymptomatic volunteers based on anatomic predictors? a 3-dimensional magnetic resonance study on cam, pincer, and spinopelvic parameters. Am J Sports Med 46:3097–3110. https://doi.org/10.1177/0363546518800825

Mascarenhas VV, Rego PA, Dantas P et al (2018b) Hip shape is symmetric, non-dependent on limb dominance and gender-specific: implications for femoroacetabular impingement. A 3D CT analysis in asymptomatic subjects. Eur Radiol 28:1609–1624. https://doi.org/10.1007/s00330-017-5072-9

Mascarenhas VV, Rego PA, Dantas P et al (2016) Imaging prevalence of femoroacetabular impingement in symptomatic patients, athletes, and asymptomatic individuals: a systematic review. Eur J Radiol 85:73–95. https://doi.org/10.1016/j.ejrad.2015.10.016

Matheney T, Sandell L, Foucher K et al (2013) Motion analysis, cartilage mechanics, and biology in femoroacetabular impingement: current understanding and areas of future research. J Am Acad Orthop Surg 21(Suppl 1):S27–S32. https://doi.org/10.5435/JAAOS-21-07-S27

McKay CD, Tufts RJ, Shaffer B, Meeuwisse WH (2014) The epidemiology of professional ice hockey injuries: a prospective report of six NHL seasons. Br J Sports Med 48(1):57–62. https://doi.org/10.1136/bjsports-2013-092860. PMID: 24334505

Miller, Christopher C. Kaeding (eds.) (2015) Stress Fractures in Athletes_ Diagnosis and Management-Springer International Publishing 4–7

Morvan J, Bouttier R, Mazieres B et al (2013) Relationship between hip dysplasia, pain, and osteoarthritis in a cohort of patients with hip symptoms. J Rheumatol 40:1583–1589. https://doi.org/10.3899/jrheum.121544

Nakano N, Yip G, Khanduja V (2017) Current concepts in the diagnosis and management of extra-articular hip impingement syndromes. 1–8. https://doi.org/10.1007/s00264-017-3431-4

Naraghi A, Awdeh H, Wadhwa V et al (2015) Diffusion tensor imaging of peripheral nerves. Semin Musculoskelet Radiol 19:191–200. https://doi.org/10.1055/s-0035-1546824

Nawabi DH, Bedi A, Tibor LM et al (2014) The demographic characteristics of high-level and recreational athletes undergoing hip arthroscopy for femoroacetabular impingement: a sports-specific analysis. Arthroscopy 30:398–405. https://doi.org/10.1016/j.arthro.2013.12.010

Nepple JJ, Prather H, Trousdale RT et al (2013) Clinical diagnosis of femoroacetabular impingement. J Am Acad Orthop Surg 21(Suppl 1):S16–S19. https://doi.org/10.5435/JAAOS-21-07-S16

Nepple JJ, Riggs CN, Ross JR, Clohisy JC (2014) Clinical presentation and disease characteristics of femoroacetabular impingement are sex-dependent. J Bone Joint Surg 96:1683–1689. https://doi.org/10.2106/JBJS.M.01320

Nepple JJ, Vigdorchik JM, Clohisy JC (2015) What is the association between sports participation and the development of proximal femoral cam deformity?: a systematic review and meta-analysis. Am J Sports Med 43:2833–2840. https://doi.org/10.1177/0363546514563909

Ng KCG, Lamontagne M, Jeffers JRT et al (2018) Anatomic predictors of sagittal hip and pelvic motions in patients with a cam deformity. Am J Sports Med 2014:036354651875515. https://doi.org/10.1016/j.arthro.2016.01.011

Nicholls AS, Kiran A, Pollard TCB et al (2011) The association between hip morphology parameters and nineteen-year risk of end-stage osteoarthritis of the hip: a nested case-control study. Arthritis Rheum 63:3392–3400. https://doi.org/10.1002/art.30523

Nötzli HP, Wyss TF, Stoecklin CH et al (2002) The contour of the femoral head-neck junction as a predictor for the risk of anterior impingement. J Bone Joint Surg 84:556–560

Omar IM, Zoga AC, Kavanagh EC et al (2008) Athletic pubalgia and "sports hernia": optimal MR imaging technique and findings. Radiographics 28:1415–1438. https://doi.org/10.1148/rg.285075217

Orchard JW (2015) Men at higher risk of groin injuries in elite team sports: a systematic review. Br J Sports Med 49:798–802. https://doi.org/10.1136/bjsports-2014-094272

Orellana C, Moreno M, Calvet J et al (2018) Ultrasound findings in patients with femoracetabular impingement without radiographic osteoarthritis: a pilot study. J Ultrasound Med 38:895–901. https://doi.org/10.1038/nrrheum.2013.114

Pedersen DR, Lamb CA, Dolan LA et al (2004) Radiographic measurements in developmental dysplasia of the hip: reliability and validity of a digitizing program. J Pediatr Orthop 24:156–160

Peh WC, Khong PL, Yin Y, Ho WY, Evans NS, Gilula LA, Yeung HW, Davies AM (1996) Imaging of pelvic insufficiency fractures. Radiographics 16(2):335–48

Petchprapa CN, Rosenberg ZS, Sconfienza LM et al (2010) MR imaging of entrapment neuropathies of the lower extremity. Part 1. The pelvis and hip. Radiographics 30:983–1000. https://doi.org/10.1148/rg.304095135

Pfirrmann CWA, Mengiardi B, Dora C et al (2006) Cam and pincer femoroacetabular impingement: characteristic MR arthrographic findings in 50 patients. Radiology 240:778–785. https://doi.org/10.1148/radiol.2403050767

Philippon MJ, Maxwell RB, Johnston TL et al (2007) Clinical presentation of femoroacetabular impingement. Knee Surg Sports Traumatol Arthrosc 15:1041–1047. https://doi.org/10.1007/s00167-007-0348-2

Philippon MJ, Michalski MP, Campbell KJ et al (2014) An anatomical study of the acetabulum with clinical applications to hip arthroscopy. J Bone Joint Surg 96:1673–1682. https://doi.org/10.2106/JBJS.M.01502

Ranawat AS, Kelly BT (2005) Anatomy of the hip: open and arthroscopic structure and function. Oper Tech Orthop 15:160–174. https://doi.org/10.1053/j.oto.2005.06.010

Rego PA, Mascarenhas V, Collado D et al (2017) Arterial topographic anatomy near the femoral head-neck perforation with surgical relevance. J Bone Joint Surg Am 99:1213–1221. https://doi.org/10.2106/JBJS.16.01386

Reiman MP, Goode AP, Cook CE et al (2015) Diagnostic accuracy of clinical tests for the diagnosis of hip femoroacetabular impingement/labral tear: a systematic review with meta-analysis. Br J Sports Med 49:811. https://doi.org/10.1136/bjsports-2014-094302

Reurink G, Brilman EG, de Vos R-J et al (2014) Magnetic resonance imaging in acute hamstring injury: can we provide a return to play prognosis? Sports Med 45:133–146. https://doi.org/10.1136/bjsm.37.5.384

Ritchlin C (2018) Editorial: magnetic resonance imaging signals in the sacroiliac joints of healthy athletes: refining disease thresholds and treatment strategies in axial spondyloarthritis. Arthrit Rheumatol 70:629–632. https://doi.org/10.1002/art.39298

Rivière C, Hardijzer A, Lazennec JY et al (2017a) Spine-hip relations add understandings to the pathophysiology of femoro-acetabular impingement: a systematic review. Orthop Traumatol Surg Res 103:549–557. https://doi.org/10.1016/j.otsr.2017.03.010

Rivière C, Lazennec JY, Van Der Straeten C et al (2017b) The influence of spine-hip relations on total hip replacement: a systematic review. Orthop Traumatol Surg Res 103:559–568. https://doi.org/10.1016/j.otsr.2017.02.014

Rudwaleit M, Landewe R, van der Heijde D et al (2009) The development of Assessment of SpondyloArthritis international Society classification criteria for axial spondyloarthritis (part I): classification of paper patients by expert opinion including uncertainty appraisal. Ann Rheum Dis 68:770–776. https://doi.org/10.1136/ard.2009.108217

Saddik D, Troupis J, Tirman P et al (2006) Prevalence and Location of Acetabular Sublabral Sulci at Hip Arthroscopy with Retrospective MRI Review. Am J Roentgenol 187:W507–W511. https://doi.org/10.2214/AJR.05.1465

Saied AM, Redant C, El-Batouty M et al (2017) Accuracy of magnetic resonance studies in the detection of chondral and labral lesions in femoroacetabular impingement: systematic review and meta-analysis. BMC Musculoskelet Disord 18:83. https://doi.org/10.1186/s12891-017-1443-2

Samim M, Eftekhary N, Vigdorchik JM et al (2019) 3D-MRI versus 3D-CT in the evaluation of osseous anatomy in femoroacetabular impingement using Dixon 3D FLASH sequence. Skelet Radiol 48:429–436. https://doi.org/10.1007/s00256-018-3049-7

Sanders T, Zlatkin M (2008) Avulsion injuries of the pelvis. Semin Musculoskelet Radiol 12:042–053. https://doi.org/10.1055/s-2008-1067936

Sankar WN, Matheney TH, Zaltz I (2013a) Femoroacetabular impingement: current concepts and controversies. Orthop Clin North Am 44:575–589. https://doi.org/10.1016/j.ocl.2013.07.003

Sankar WN, Nevitt M, Parvizi J et al (2013b) Femoroacetabular impingement: defining the condition and its role in the pathophysiology of osteoarthritis. J Am Acad Orthop Surg 21:S7–S15. https://doi.org/10.5435/JAAOS-21-07-S7

Saunders J, Cusi M, Robinson D, Van der Wall H (2018) Sacroiliac joint dysfunction in the athlete: diagnosis and management. Curr Sports Med Rep 17:73–74. https://doi.org/10.1249/JSR.0000000000000456

Schiphof D, Boers M, Bierma-Zeinstra SM (2008) Differences in descriptions of Kellgren and Lawrence grades of knee osteoarthritis. Ann Rheum Dis 67(7):1034–6. https://doi.org/10.1136/ard.2007.079020. Epub 2008 Jan 15. PMID: 18198197

Schmaranzer F, Klauser A, Kogler M et al (2014) Diagnostic performance of direct traction MR arthrography of the hip: detection of chondral and labral lesions with arthroscopic comparison. Eur Radiol. https://doi.org/10.1007/s00330-014-3534-x

Schmaranzer F, Todorski IAS, Lerch TD et al (2017) Intra-articular lesions: imaging and surgical correlation. Semin Musculoskelet Radiol 21:487–506. https://doi.org/10.1055/s-0037-1606133

Schueller-Weidekamm C, Mascarenhas V, Sudol-Szopinska I et al (2014) Imaging and interpretation of axial spondylarthritis: the radiologist's perspective—consensus of the arthritis subcommittee of the ESSR. Semin Musculoskelet Radiol 18:265–279. https://doi.org/10.1055/s-0034-1375569

Sconfienza LM, Adriaensen M, Albano D, et al (2019) Clinical indications for image-guided interventional procedures in the musculoskeletal system: a Delphi-based consensus paper from the European Society of Musculoskeletal Radiology (ESSR)—part I, shoulder. 1–11. https://doi.org/10.1007/s00330-019-06419-x

Seldes RM, Tan V, Hunt J et al (2001) Anatomy, histologic features, and vascularity of the adult acetabular labrum. Clin Orthop Relat Res:232–240

Shanmugaraj A, Shell JR, Horner NS, et al (2018) How useful is the flexion–adduction–internal rotation test for diagnosing femoroacetabular impingement. Clin J Sport Med 1. https://doi.org/10.1097/JSM.0000000000000575

Sher I, Umans H, Downie SA et al (2011) Proximal iliotibial band syndrome: what is it and where is it? Skelet Radiol 40:1553–1556. https://doi.org/10.1016/j.clinbiomech.2008.07.011

Siebenrock KA, Kalbermatten DF, Ganz R (2003) Effect of pelvic tilt on acetabular retroversion: a study of pelves from cadavers. Clin Orthop Relat Res:241–248. https://doi.org/10.1097/01.blo.0000030508.43495.79

Singer AD, Subhawong TK, Jose J et al (2015) Ischiofemoral impingement syndrome: a meta-analysis. Skelet Radiol 44:831–837. https://doi.org/10.1007/s00256-015-2111-y

Smith TO, Hilton G, Toms AP et al (2010) The diagnostic accuracy of acetabular labral tears using magnetic resonance imaging and magnetic resonance arthrography: a meta-analysis. Eur Radiol. https://doi.org/10.1007/s00330-010-1956-7

Smith TO, Simpson M, Ejindu V, Hing CB (2012) The diagnostic test accuracy of magnetic resonance imaging, magnetic resonance arthrography and computer tomography in the detection of chondral lesions of the hip. Eur J Orthop Surg Traumatol 23:335–344. https://doi.org/10.1007/s00590-012-0972-5

Soldatos T, Andreisek G, Thawait GK et al (2013) High-resolution 3-T MR neurography of the lumbosacral plexus. Radiographics 33:967–987. https://doi.org/10.1148/rg.334115761

Stracciolini A, Casciano R, Levey Friedman H et al (2013) Pediatric sports injuries: an age comparison of children versus adolescents. Am J Sports Med 41:1922–1929. https://doi.org/10.1177/0363546513490644

Suter A, Dietrich TJ, Maier M et al (2015) MR findings associated with positive distraction of the hip joint achieved by axial traction. Skelet Radiol 44:787–795. https://doi.org/10.1016/j.arthro.2012.04.057

Sutter R, Pfirrmann CWA (2017) Update on femoroacetabular impingement: what is new, and how should we assess it? Semin Musculoskelet Radiol 21:518–528. https://doi.org/10.1055/s-0037-1606141

Sutter R, Zubler V, Hoffmann A et al (2014) Hip MRI: how useful is intraarticular contrast material for evaluating surgically proven lesions of the labrum and articular cartilage? AJR Am J Roentgenol 202:160–169. https://doi.org/10.2214/AJR.12.10266

Syed AB, Zoga AC (2018) Artificial intelligence in radiology: current technology and future directions. Semin Musculoskelet Radiol 22:540–545. https://doi.org/10.1055/s-0038-1673383

Tannast M, Fritsch S, Zheng G, et al (2014) Which radiographic hip parameters do not have to be corrected for pelvic rotation and tilt? Clin Orthop Relat Res https://doi.org/10.1007/s11999-014-3936-8

Tannast M, Siebenrock KA, Anderson SE (2007) Femoroacetabular impingement: radiographic diagnosis—what the radiologist should know. AJR Am J Roentgenol 188:1540–1552. https://doi.org/10.2214/AJR.06.0921

Tannenbaum E, Kopydlowski N, Smith M et al (2014) Gender and racial differences in focal and global acetabular version. J Arthroplast 29:373–376. https://doi.org/10.1016/j.arth.2013.05.015

Tibor LM, Liebert G, Sutter R et al (2013) Two or more impingement and/or instability deformities are often present in patients with hip pain. Clin Orthop Relat Res 471:3762–3773. https://doi.org/10.1007/s11999-013-2918-6

Tibor LM, Sekiya JK (2008) Differential diagnosis of pain around the hip joint. Arthroscopy 24:1407–1421. https://doi.org/10.1016/j.arthro.2008.06.019

Tönnis D (1987) Congenital dysplasia and dislocation of the hip in children and adults. Springer, Berlin

Tönnis D (1976) Normal values of the hip joint for the evaluation of X-rays in children and adults. Clin Orthop Relat Res:39–47. https://doi.org/10.1097/00003086-197609000-00007

Turkiewicz A, Petersson IF, Björk J et al (2014) Current and future impact of osteoarthritis on health care: a population-based study with projections to year 2032. Osteoarthr Cartil 22:1826–1832. https://doi.org/10.1016/j.joca.2014.07.015

van der Bom MJ, Groote ME, Vincken KL et al (2011) Pelvic rotation and tilt can cause misinterpretation of the acetabular index measured on radiographs. Clin Orthop Relat Res 469:1743–1749. https://doi.org/10.1007/s11999-011-1781-6

Vavken P, Krepler P (2008) Sacral fractures after multisegmental lumbosacral fusion: a series of four cases and systematic review of literature. Eur Spine J 17(Suppl 2):285–290.

Wang Y, Teichtahl AJ, Cicuttini FM (2016) Osteoarthritis year in review 2015: imaging. Osteoarthr Cartil 24:49–57. https://doi.org/10.1016/j.joca.2015.07.027

Weber U, Jurik AG, Zejden A, et al (2019) MRI of the sacroiliac joints in athletes: recognition of non-specific bone marrow oedema by semi-axial added to standard semi-coronal scans. Rheumatology (Oxford). https://doi.org/10.1093/rheumatology/kez458

Weir A, Brukner P, Delahunt E, et al (2015) Doha agreement meeting on terminology and definitions in groin pain in athletes. pp 768–774

Werner J, Hägglund M, Ekstrand J, Waldén M (2019) Hip and groin time-loss injuries decreased slightly but injury burden remained constant in men's professional football: the 15-year prospective UEFA Elite Club Injury Study. Br J Sports Med 53(9):539–546. https://doi.org/10.1136/bjsports-2017-097796. Epub 2018 Apr 24. PMID: 29691289

Wilkin GP, Ibrahim MM, Smit KM, Beaulé PE (2017) A contemporary definition of hip dysplasia and structural instability: toward a comprehensive classification for acetabular dysplasia. J Arthroplasty 32:S20–S27. https://doi.org/10.1016/j.arth.2017.02.067

Zaltz I, Kelly BT, Larson CM, Leunig M, Bedi A (2014) Surgical treatment of femoroacetabular impingement: what are the limits of hip arthroscopy? Arthroscopy 30(1):99–110. https://doi.org/10.1016/j.arthro.2013.10.005. PMID: 24384276

Zaltz I, Leunig M (2012) Parafoveal chondral defects associated with femoroacetabular impingement. Clin Orthop Relat Res 470:3383–3389. https://doi.org/10.1007/s11999-012-2453-x

Zoga AC, Hegazi TM, Roedl JB (2016) Algorithm for imaging the hip in adolescents and young adults. Radiol Clin N Am 54:913–930. https://doi.org/10.1016/j.rcl.2016.05.016

Zuckerman SL, Wegner AM, Roos KG, Djoko A, Dompier TP, Kerr ZY (2018) Injuries sustained in National Collegiate Athletic Association men's and women's basketball, 2009/2010–2014/2015. Br J Sports Med 52(4):261–268. https://doi.org/10.1136/bjsports-2016-096005. Epub 2016 Jun 30. PMID: 27364907

Sports-Related Meniscal Injury

E. De Smet, P. Van Dyck, J. Gielen,
and F. M. Vanhoenacker

Contents

Abstract

Meniscal lesions are frequent in both the general and the athletic population and may cause severe functional impairment. In this chapter, the (micro)anatomy, vascularization and function of the menisci are described. In the event of a suspected meniscal injury, conventional radiography and arthrography are no longer recommended. Conventional MRI has become the preferred imaging modality, if necessary followed by MR (or CT) arthrography in the postoperative meniscus. Correct description of tears seen on MRI is essential, as it may guide treatment. The major classifications of meniscal lesions are described as well as some more rare lesions that can be seen in athletes. It must however be stressed that correlation with clinical information is of utmost importance, as some meniscal lesions may be asymptomatic and do not require treatment.

E. De Smet (✉) · P. Van Dyck · J. Gielen
Department of Radiology, University Hospital Antwerp, Edegem, Belgium
e-mail: eline.desmet2@uza.be

F. M. Vanhoenacker
Department of Radiology, University Hospital Antwerp, Edegem, Belgium

Department of Radiology, AZ Sint-Maarten, Mechelen, Belgium

Department of Radiology, Ghent University Hospital and Ghent University, Ghent, Belgium

Med Radiol Diagn Imaging (2020)
https://doi.org/10.1007/174_2020_244, © Springer Nature Switzerland AG
Published Online: 07 December 2020

1 Introduction

Meniscal injuries are very common among professional and amateur athletes and are a major cause of functional impairment of the knee. It is the most common indication for arthroscopic surgery of the knee. For athletes, unnecessary treatment or intervention may be as damaging to a competitive future as failure to diagnose a clinically significant injury. Therefore, rapid and accurate evaluation of possible injuries in this group is crucial (Ludman et al. 1999).

Acquisition of a precise history of the injury mechanism may be difficult, as is performance of an accurate physical examination in the setting of an acute injury (Karachalios et al. 2005).

Magnetic resonance imaging (MRI) is performed more commonly on the knee than on any other joint, and it is an excellent diagnostic tool that can aid in the evaluation of a host of sports-related injuries involving the ligaments, tendons, menisci, osseous structures, and articular surfaces. It has currently become the most widely used non-invasive imaging method for detecting meniscal injuries, with a reported diagnostic accuracy of as high as 98%, compared to arthroscopy, remaining the gold standard for confirming the diagnosis of meniscal tear. MRI is a valuable, cost-effective tool for the preoperative evaluation of the menisci, and proved useful, on the basis of its high negative predictive value, to exclude patients from unnecessary arthroscopy, and, thus, avoiding unnecessary hospitalization, morbidity and waste of limited financial and manpower resources (Karachalios et al. 2005; Elvenes et al. 2000).

However, radiologists must be aware of numerous imaging pitfalls and artefacts simulating a tear and leading to an erroneous diagnosis. Moreover, it must be kept in mind that "silent" meniscal abnormalities in athletes exist and knowledge of these MR appearances is important in order to avoid attributing greater significance to these than is clinically justified.

For many years, the meniscus was treated with disrespect as an unnecessary appendage that could be sacrificed with the first hint of malfunction. As long-term results after major meniscectomy were disappointing, a conservative approach to the management of meniscal tears has developed, with emphasis on meniscal preservation (Rath and Richmond 2000).

2 Anatomy and Function

To adequately evaluate and treat meniscal injuries, understanding of meniscal anatomy and function is necessary. From a gross anatomic perspective, the menisci are C-shaped fibrocartilaginous structures, firmly attached to the anterior and posterior aspects of the tibial plateau by the so-called root ligaments. Conventionally, they are described as having three segments: anterior horn, body and posterior horn. Each meniscus measures approximately 5 mm in height along its periphery and tapers to a thin inner edge such that it demonstrates a triangular shape in cross section. The outer rims of the menisci are convex and attached to the fibrous joint capsule and through it to the edges of the articular surfaces of the tibia. The inner edges are concave, thin and free. Their superior surfaces are slightly concave for reception of the femoral condyles, whereas their inferior surfaces that rest on the tibial condyles are flatter. The anterior horns of the medial and lateral menisci are attached to each other through the (anterior) transverse ligament (Fig. 1).

The *medial meniscus* is C-shaped and occupies 50–60% of the articular contact area of the medial compartment (Arnoczky et al. 1987; Thompson et al. 1991) (Fig. 1). Its posterior horn is wider than the anterior horn. Although anatomic variations in meniscal morphology and attachments exist, the anterior horn of the medial meniscus has a firm bony attachment to the tibia anterior to the anterior cruciate ligament (ACL). The posterior horn is attached immediately in front of the attachment of the posterior cruciate ligament (PCL) (McKeon et al. 2009; Palastanga and Soames 2011). The outer border of the medial meniscus is firmly attached to the knee joint capsule. The meniscotibial and meniscofemoral ligaments attach the meniscus to the tibia and femur, respectively, and are referred to as the deep medial collateral ligaments (Fig. 2).

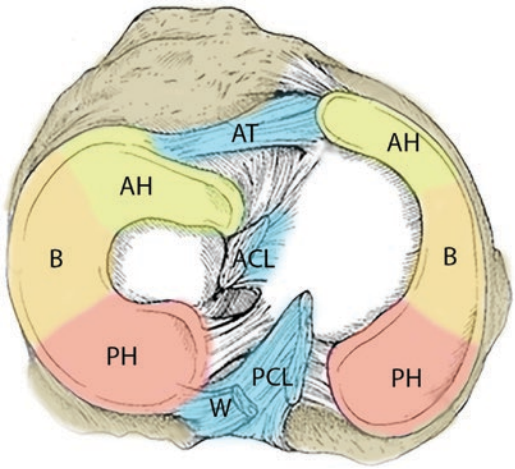

Fig. 1 Schematic drawing of meniscal anatomy. Both menisci are divided into an anterior horn (AH) and posterior horn (PH) with the body (B) in between. The anterior transverse (AT) ligament connects the anterior horns. Wrisberg ligament (W) starts at the posterior horn of the lateral meniscus and follows the posterior cruciate ligament (PCL). *ACL* anterior cruciate ligament

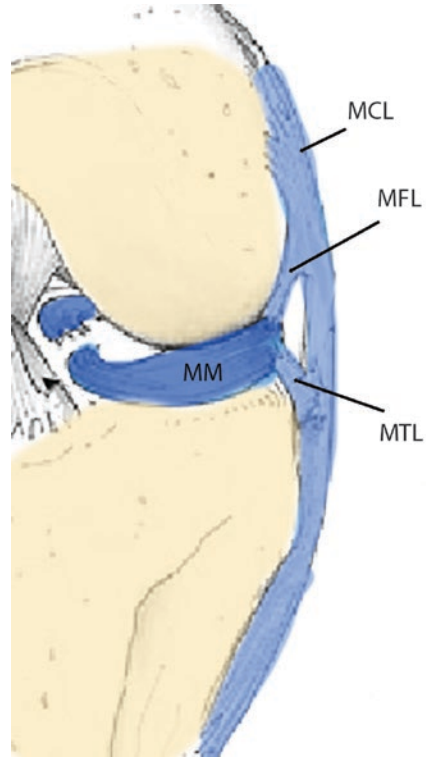

Fig. 2 Schematic drawing of the relation between the medial meniscus (MM) and the medial collateral ligament (MCL). The deep layer of the MCL consists of the meniscotibial (MTL) and meniscofemoral (MFL) ligaments, which are connected to the body of the MM

The *lateral meniscus* is more uniform in width and semicircular, covering 70–80% of the lateral tibial plateau (Arnoczky et al. 1987; Thompson et al. 1991) (Fig. 1). The anterior horn attaches to the inter-condylar fossa, next to the attachment of the ACL. The posterior horn of the lateral meniscus is attached to the medial femoral condyle through the posterior meniscal-femoral (Wrisberg) and anterior meniscal-femoral (Humphrey) ligament. Therefore, during rotation, the motion of the lateral meniscus is coupled with that of the femoral condyle. The lateral meniscus has loose attachments to the joint capsule and is separated from it by the popliteus tendon posterolaterally where it courses through a meniscocapsular tunnel. In this region, the superior and inferior popliteal meniscal fascicles are seen, running from the peripheral margin of the meniscus, around the popliteus tendon, to the joint capsule (Fig. 3). The lateral meniscus is more mobile and is not anchored to the lateral collateral ligament. In flexion and internal rotation, the popliteal tendon retracts the posterior horn, thus reducing entrapment of the lateral meniscus between the femur and the tibia. It is therefore less likely to be injured than the relatively immobile medial meniscus (Rath and Richmond 2000).

The *composition of the menisci* varies with age and may also be altered by injury (Sweigart and Athanasiou 2001). The main component is water (>70%), followed by collagen (±20%, primarily collagen type I with small amounts of types II–VI), glycosaminoglycans, DNA, glycoproteins and elastin (Makris et al. 2011). Within the menisci, a small cell population is present, consisting of fibrochondrocytes, fibroblast-like cells and cells in the superficial meniscus (Verdonk et al. 2005; Van der Bracht et al. 2007).

The *microanatomy of the menisci* may explain injury patterns (Fig. 4). A network of type I collagen fibres arranged in a circumferential direction is the dominant morphological pattern, allowing dispersion of compressive loads and development of “hoop stresses”. Radial oriented

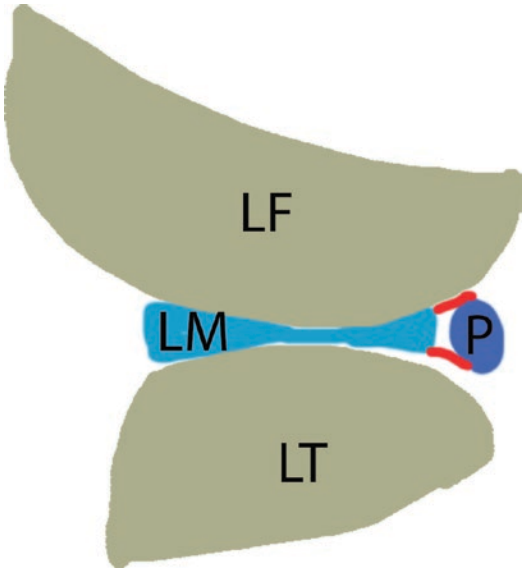

Fig. 3 Schematic drawing of the relation between the lateral meniscus (LM) and the meniscopopliteal fascicles (red). The anteroinferior and posterosuperior fascicles extend from the LM to engulf the popliteal tendon and blend into the capsule

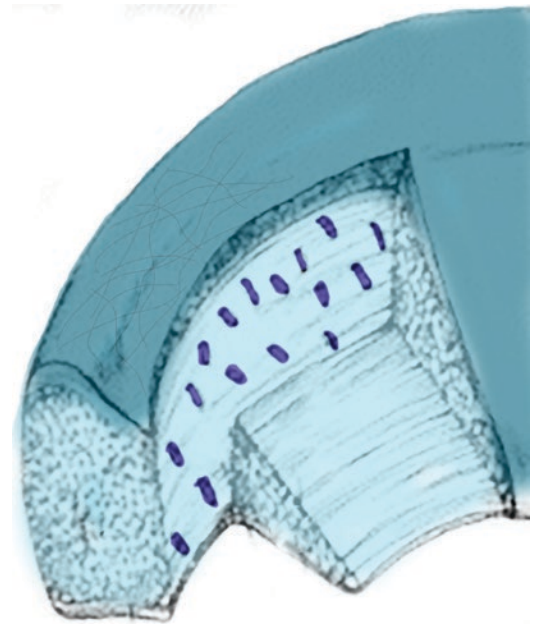

Fig. 4 Microstructure of the meniscus. The majority of the fibres are longitudinal or "hoop" fibres (light blue), following the long axis of the meniscus. These fibres are responsible for the distribution of axial loads. A minority of radial or "tie" fibres run perpendicular to the long axis, from the inner to the outer rim (purple), to withstand longitudinal splitting. The most superficial fibres (dark blue zone) follow a random course

fibres ("tie fibres") may function to restrain motion between circumferential fibres and resist longitudinal splitting. At the surface of the meniscus, fibre orientation is more of a random configuration (Greis et al. 2002).

The *blood supply to the menisci* originates from the lateral and medial superior and inferior genicular arteries. These vessels reach the periphery of the meniscus through the synovial covering of the anterior and posterior horn attachments. Vessels are present throughout the substance of the foetal menisci. Beginning at birth, there is a progressive decrease in vascularity proceeding from the inner to the outer regions of the meniscus. The adult meniscus is avascular in the inner two-thirds ("*white zone*") and vessels are most prominent in the peripheral one-third of the menisci and in the adjacent coronary and capsular ligaments ("*red zone*"). In younger persons, an intermediate vascularized "*red-white zone*" is located between the vascular red and avascular white zone (Rath and Richmond 2000) (Fig. 5).

The menisci are important in many aspects of knee function, with the main functions being tibiofemoral load transmission and shock absorption. The menisci compensate for significant incongruity between the femoral and tibial articulating surfaces and increase tibiofemoral contact area, with subsequent reduction in joint contact stresses. The menisci transmit at least 50–70% of the load when the knee is in extension. This increases to 85–90% with 90° of knee flexion. These loads are well distributed when the menisci are intact (Greis et al. 2002). After meniscectomy, tibiofemoral contact area may decrease by 40–70%, leading to a proportional increase in contact and shear stresses across the joint. These changes will lead eventually to joint degeneration. Furthermore, several studies have demonstrated that meniscal tissue is approximately one half as stiff as articular cartilage. The shock absorption capacity of the normal knee is reduced by 20% after meniscectomy (Voloshin and Wosk 1983).

It is important to remember that the menisci are not stationary structures. With flexion and extension of the knee, the medial meniscus translates about 2–5 mm on the tibia, and the lateral meniscus translates about 9–11 mm (Greis et al. 2002).

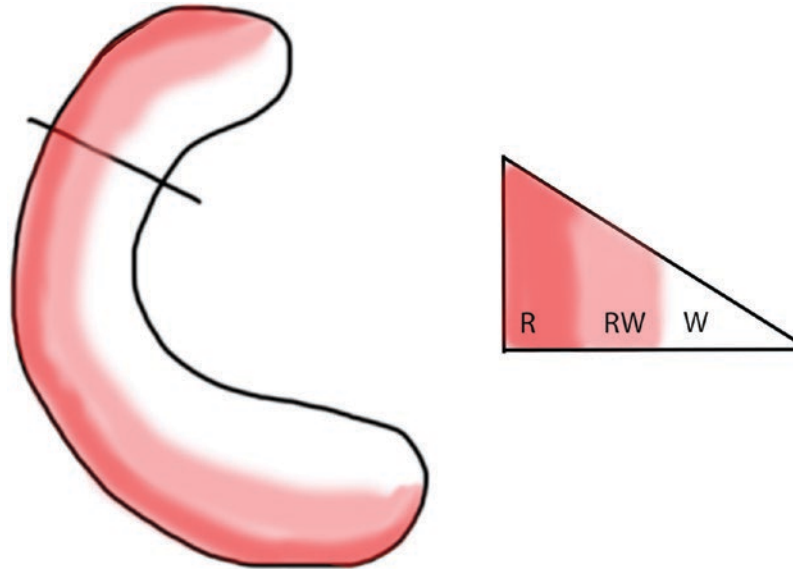

Fig. 5 Vascularization of the menisci. The most peripheral part of the meniscus (red zone, R) is well vascularized. The innermost part or white zone (W) has no vascularization and therefore no healing potential. The red-white zone (RW) is an intermediate vascularized zone, present in young people

Additionally, the menisci play a key role in enhancing joint stability, largely as secondary soft-tissue restraints which prevent anterior tibial displacement (Rath and Richmond 2000). The body of the meniscus prevents the femur from gliding too far off the tibia. Shoemaker and Markolf (1986) demonstrated that the posterior horn of the medial meniscus is the most important structure resisting an applied anterior tibial force in an ACL-deficient knee. Patients who tear the posterior meniscal horn may feel instability—even if their ACL is intact—because this stabilizing effect is lost.

Finally, the menisci contribute significantly to joint lubrication, probably by fluid exudation across their surfaces. Compression squeezes the liquid out into the joint space, to allow smoother gliding of the joint surfaces. This also helps to distribute synovial fluid throughout the joint and aids nutrition of the articular cartilage (Rath and Richmond 2000).

3 Epidemiology of Meniscal Injuries

Meniscal lesions are the most common encountered knee injuries and meniscal tear surgery is one of the most frequent orthopaedic procedures. Therefore, these lesions have a high cost in both morbidity and healthcare expenses.

Meniscal tears have a bimodal age distribution and are most frequently seen in both young sports(wo)men and the elderly population.

Reported risk factors (Snoeker et al. 2013) for degenerative tears include age >60, male gender, squatting, work-related kneeling and stair climbing (>30 flights). Acute traumatic tears were more often seen in rugby and soccer players and patients with delay between ACL rupture and reconstruction greater than 12 months.

Meniscal tears are more frequently seen in the medial meniscus and in the posterior horns of the menisci (Metcalf and Barrett 2004).

4 Imaging of the Meniscus

Although meniscal injuries are extremely common, the clinical history and mechanism of injury are usually non-specific, and are often of little value in determining the diagnosis. Mechanical symptoms of popping, catching, locking or buckling along with joint-line pain are suggestive, but not conclusive, of meniscal pathology, and other types of intra- and extra-articular pathology may confound the clinical picture.

Numerous specialized tests have been described that may aid in making the diagnosis of

meniscal tear. These include joint-line palpation, McMurray test, the Apley grind test and many others. Although conflicting results regarding the diagnostic accuracy of the various meniscal tests have been reported, no specific examination manoeuvre has impressive test performance characteristics, with the exception of the joint-line tenderness test, which showed an acceptable diagnostic accuracy (Karachalios et al. 2005).

4.1 Plain Radiography and Conventional Arthrography

Nowadays, plain radiography is not regarded as a suitable examination for the detection of isolated meniscal injury. Depending on patient history and clinical examination, radiographs may however be useful in the detection or exclusion of associated skeletal injury or fracture, presence of loose bodies or degenerative changes.

For decades, conventional fluoroscopic arthrography (after sterile preparation and injection of intra-articular contrast medium) was the radiological technique for investigating meniscal injury. After the development of cross-sectional imaging techniques, conventional radiography only has a place as part of these techniques, i.e. in the context of CT or MR arthrography.

4.2 Ultrasound

Ultrasound is not the preferred method to evaluate meniscal pathology but occasionally meniscal tears or parameniscal cysts may be seen on an ultrasound of the knee performed for other indications (Fig. 6).

4.3 Magnetic Resonance Imaging

Because of its exquisite contrast resolution and ability to simultaneously display the osseous and soft-tissue structures of the knee in virtually any plane, MRI has become the most widely used non-invasive imaging method that can aid in the evaluation of the entire spectrum of internal derangements of the knee.

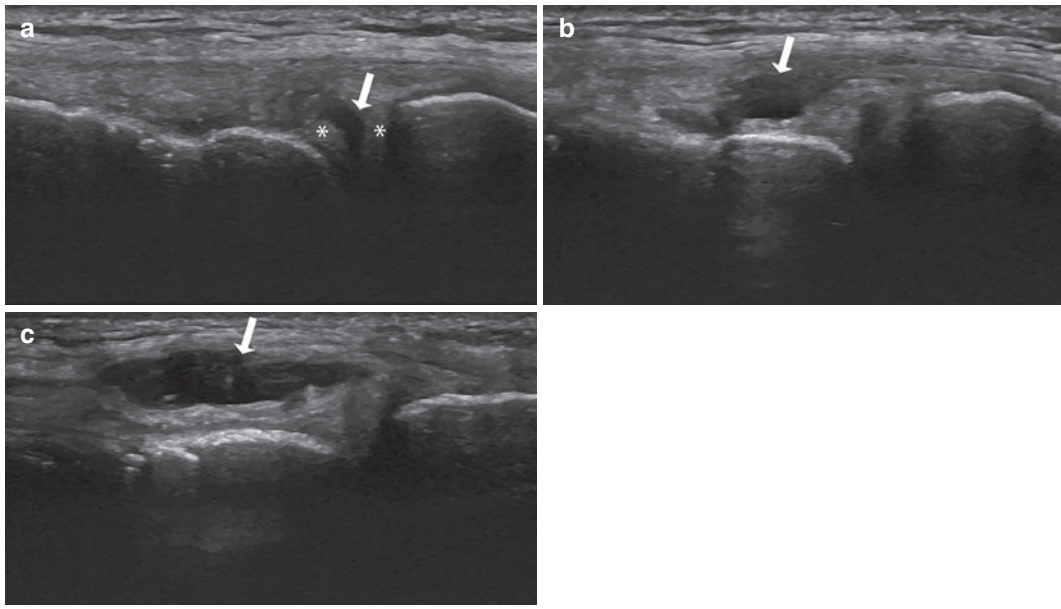

Fig. 6 (**a**–**c**) Ultrasound of the medial aspect of the knee in a 45-year-old long-distance runner. (**a**) An anechogenic fluid cleft (arrow) represents a horizontal tear, which divides two parts of the meniscus (asterisk). (**b** and **c**) Extension of the fluid collection (parameniscal cyst) in the superficial soft tissues anteromedial to the knee (arrows)

4.3.1 Technique

MRI of the knee is performed with the patient in supine position and the knee extended or slightly flexed. An extremity coil is positioned around the knee to optimize signal-to-noise ratio (SNR). Nowadays, the standard field strengths in clinical practice are 1.5 or 3 Tesla (T).

To obtain a full overview of the knee, images in the axial, coronal and sagittal plane are acquired, ideally with a slice thickness of 3 mm or less. The field of view is preferably 160 mm or smaller and imaging matrix 140 × 256 (Tuite et al. 2012).

For routine imaging, proton density (PD)- or T2-weighted 2D turbo spin echo (TSE) sequences and T1-weighted 3D gradient echo (GRE) sequences are used (Recht et al. 2005, Kijowski 2010). The addition of fat suppression techniques to the PD- or T2-weighted sequences allows better identification of bone marrow or soft-tissue oedema. Spectral, inversion recovery and Dixon techniques are available to perform FS. In a study by Fleckenstein et al. (1991), spectral FS proved to have better spatial resolution and SNR than other techniques.

3D TSE sequences have become available in the last decade on almost every vendor platform, allowing for reduced partial volume effect compared to 2D sequences. Additionally, the volumetric source data acquired by these 3D sequences may be rendered in every direction.

3D GRE sequences have also been developed. Despite higher spatial and contrast resolution, these sequences suffer from longer acquisition times, high susceptibility to metallic artefacts and poor visualization of bone marrow, menisci and ligaments (Kijowski and Gold 2011).

During the last decade, (semi)quantitative sequences have been studied for their ability to identify meniscal pathology.

Diffusion-weighted imaging (DWI) is able to detect meniscal tears through ADC mapping (preferably with b-values of 400 s/mm^2), although the sensitivity of DWI does not surplus that of conventional sequences and spatial resolution is lower (Kizilgöz et al. 2013; Aydin et al. 2011).

T1ρ, T2 and T2* mapping sequences have demonstrated alterations in meniscal values after trauma without clinical evidence of subsurface abnormalities, suggestive of subclinical trauma (Williams et al. 2012). Other authors found a correlation between meniscal T1ρ and T2 values and clinical findings of osteoarthritis (Rauscher et al. 2008). Further research is warranted on the possibility to predict long-term meniscal lesions and subsequent (early) osteoarthritis after knee trauma.

4.3.2 MRA

MR arthrography can be performed by direct injection of diluted gadolinium contrast in the knee (direct MR arthrography) or by administering gadolinium contrast intravenously and allowing diffusion from the bloodstream into the joint. Direct nor indirect MRA should be performed in the native (non-operated) meniscus.

4.3.3 Normal MR Anatomy

Menisci must be evaluated on both the sagittal and coronal images. Axial images have proven to be useful in the detection of peripheral meniscal tears as well as small radial tears of the free edge of the meniscus (Tarhan et al. 2004).

The normal menisci demonstrate diffusely low signal intensity on all MRI pulse sequences because of their fibrocartilaginous structure. The most peripheral images of the sagittal plane demonstrate a "bow-tie" appearance of the meniscus. The normal meniscus should have 1.5–2 bow ties (5–13 mm) on 4–5 mm thick images. Broad and disc-shaped menisci (>13 mm) with 3–4 or more bow ties are called "discoid" and are more prone to meniscal tears. The normal meniscus measures 3–5 mm in height. The medial meniscus varies in width from 6 mm at the anterior horn to 12 mm at the posterior horn. The lateral meniscus is approximately 10 mm in width throughout its length.

More centrally, the normal meniscus becomes triangular in appearance. The anterior and posterior horns of the lateral meniscus are nearly equal in size, whereas the posterior horn of the medial meniscus is nearly twice the size of the anterior horn.

4.3.4 Diagnosis of Meniscal Tears

To understand the significance of increased signal intensity in meniscal abnormalities, an MR grading system has been developed and correlated with a histopathologic model (Stoller et al.

1987): ***grade 1***, intrasubstance globular appearing signal not extending to the articular surface; ***grade 2***, linear increased signal patterns not extending to the articular surface (Fig. 7a); and ***grade 3***, the abnormal signal extends to the articular surface (Fig. 7b). The clinical importance of grade 2 signal abnormality in the meniscus, as seen on MRI and not visualized arthroscopically, is still not well understood. Grades 1 and 2 represent intrasubstance mucinous degeneration in an adult or prominent vascularity in a child and have no surgical significance. Grade 3 is visible by arthroscopy and represents a meniscal tear.

In addition to observing increased signal intensity within tears, the morphology of the meniscus should be assessed when evaluating meniscal lesions.

The "*direct*" signs (De Smet et al. 2001) associated with meniscal tears on MRI include

1. Unequivocal grade 3 signal (Fig. 7b)
2. Abnormal meniscal morphology with displaced or missing meniscal tissue:
   (a) Absent bow-tie sign (1 or fewer): either postsurgical or displaced tear (Fig. 8)
   (b) Double-PCL sign: displaced bucket-handle tear of the medial meniscus (Fig. 9)
   (c) Large anterior horn sign: displaced bucket-handle tear of the meniscus with flipped fragment
3. Meniscocapsular separation (Fig. 10)

The "*indirect*" signs (Costa et al. 2004) associated with meniscal tears on MRI include

1. Abnormal superior popliteomeniscal fascicle and posterior pericapsular, oedema: lateral meniscal tear, most commonly posterior horn.
2. Posterior bone bruise of the medial tibial plateau: peripheral tears of the posterior horn of the medial meniscus or tears of the posterior root ligament of the medial meniscus. Tears of this ligament can be associated with ganglion cysts at the posterior aspect of the tibia as well.
3. Extrusion (>3 mm) of the medial meniscus: degeneration, complex or large radial tear, tear involving the meniscal root.

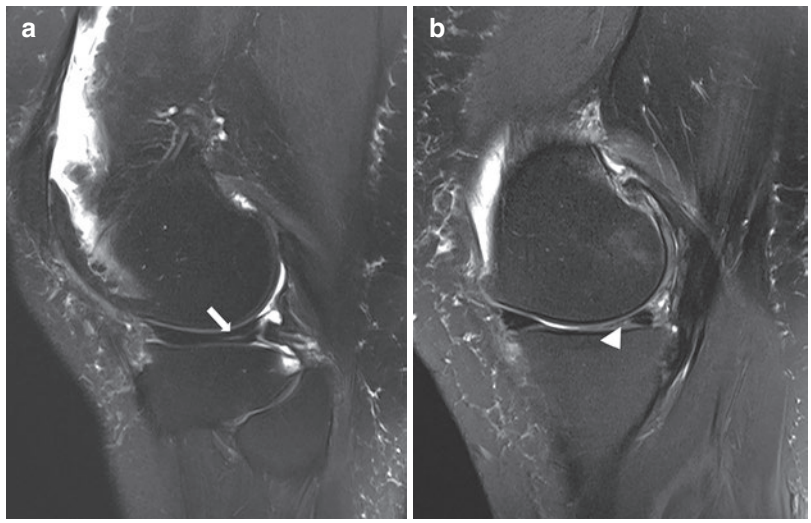

Fig. 7 (**a** and **b**) Sagittal TSE T2 WI with FS through the (**a**) lateral and (**b**) medial femorotibial joint in a 43-year-old footballer with medial knee pain. (**a**) Linear high signal intensity in the lateral meniscus (arrow) without contact with the meniscal surface. This grade II signal represents intrasubstance degeneration and is not clinically relevant in this patient. (**b**) Linear high signal intensity in the medial meniscus (arrow), in contact with the meniscal surface. This is consistent with a grade III signal and proved to be a tear on arthroscopy

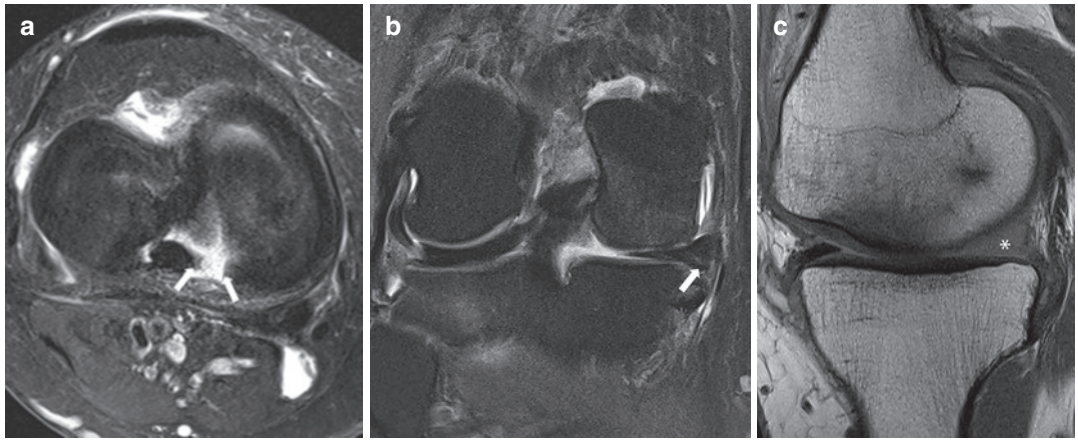

Fig. 8 (**a**–**c**) Tear in the posterior root of the medial meniscus with displacement. Axial (**a**) and coronal (**b**) TSE PD WI with FS reveals a defect in the posterior root of the medial meniscus (arrows in **a**). There is extrusion of the body of the medial meniscus due to the displaced tear (arrow in **b**). (**c**) Sagittal PD WI at the location of the defect reveals an absent bow-tie sign (asterisk)

4.3.5 Classification of Meniscal Tears

A plethora of meniscal classification systems are available, for example based on aetiology or tear pattern. However, findings or descriptions of meniscal tears on MRI do not always correlate with arthroscopic results and may become the cause of confusion between radiologist and orthopaedic surgeon.

In 2011, the International Society of Arthroscopy, Knee Surgery and Orthopaedic Sports Medicine (ISAKOS) knee committee proposed a concise and reliable classification pattern for meniscal tears on arthroscopy (Anderson et al. 2011). The inter-observer reliability of this ISAKOS classification amongst orthopaedic surgeons proved sufficient to use this system for pooling of international trial data for comparison. Studies on the use of the ISAKOS classification on MRI also showed acceptable agreement between radiologists when describing meniscal tears, both on 2D and 3D MRI (Chhabra et al. 2019).

The ISAKOS system describes meniscal tears based on seven characteristics: *tear pattern, tear depth, tear length, rim width, radial location, central to popliteus hiatus and quality of tissue.*

Tear pattern: Meniscal tears can be classified into two primary tear planes: vertical and horizontal (Fig. 11). Vertical tears are often of a traumatic origin and occur in younger individuals, whereas horizontal tears are usually secondary to meniscal (mucoid) degeneration and occur at later age.

Vertical tears are further subdivided into *radial* (perpendicular to the surface of the meniscus) and *longitudinal* (parallel to the long axis of the meniscus) varieties.

Radial tears are relatively uncommon meniscal tears and most commonly occur at the junction of the anterior horn and body of the lateral meniscus and at the meniscotibial attachment of the posterior horn of the medial meniscus. They are often seen as blunting of the free edge on coronal (MR) images. On sagittal images, the only evidence of a radial tear may be increased signal intensity on one or two peripheral sections.

Longitudinal vertical tears run perpendicular to the tibial plateau, parallel to the long axis of the meniscus. The meniscus is divided into a central and a peripheral part (Fig. 12).

Horizontal tears extend through the meniscus along a plane parallel to the tibial plateau, dividing the meniscus into inferior and superior segments. A horizontal cleavage tear is the most common type of tear to be associated with a meniscal cyst (Figs. 13 and 14). These cysts occur as a result of fluid extruding through the

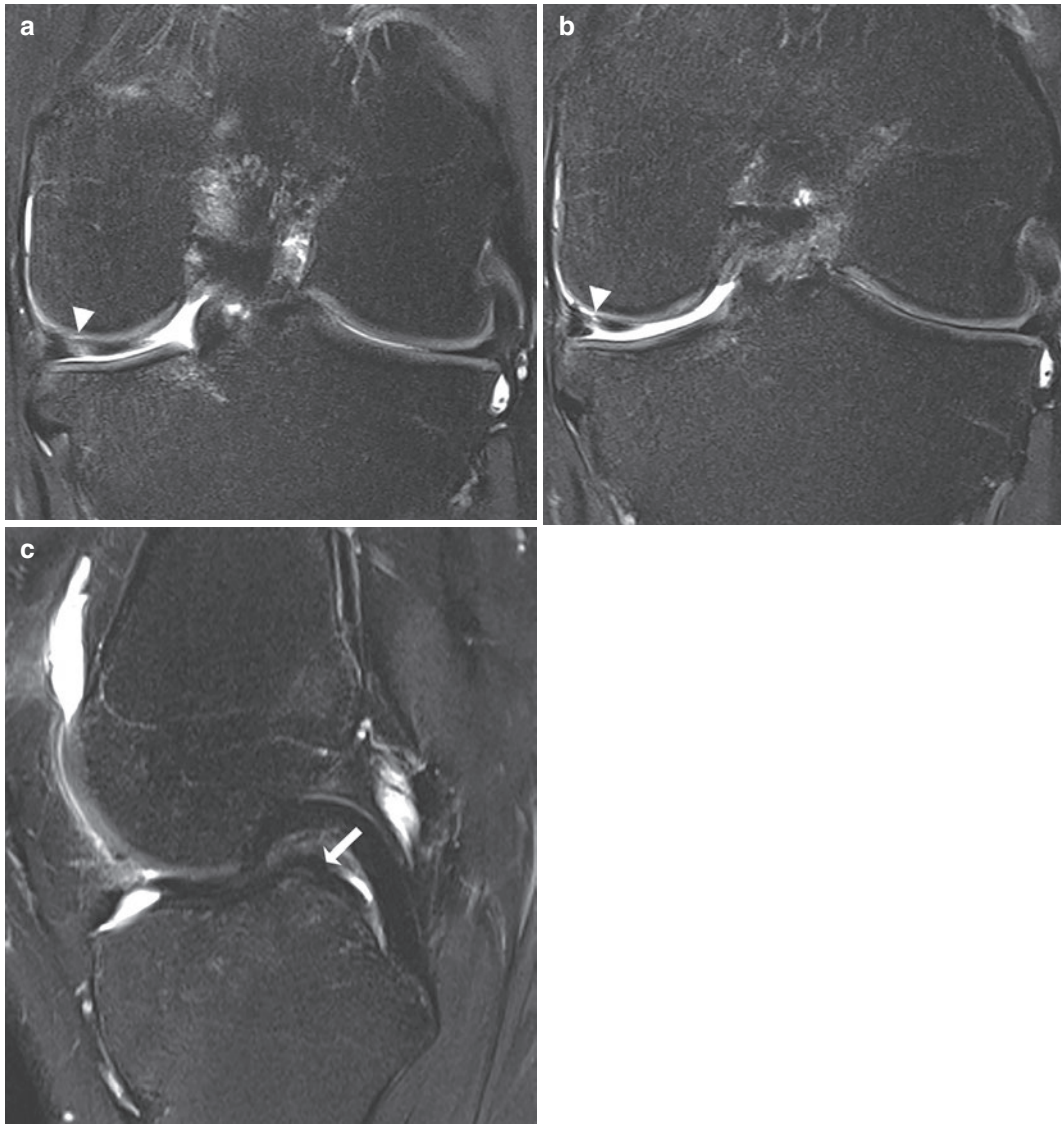

Fig. 9 (**a**–**c**) Bucket-handle tear of the medial meniscus. (**a** and **b**) Coronal TSE PD WI with FS shows a displaced tear in the body of the medial meniscus (arrows). (**c**) Sagittal TSE T2 WI with FS reveals a hypo-intense structure inferior to the PCL ("double-PCL sign", arrow), consistent with the displaced flap ("bucket-handle")

tear by a ball valve effect, and collecting either in the meniscus (intrameniscal cyst) or at the meniscocapsular junction (parameniscal cyst). These cysts tend to recur after resection if the underlying meniscal cyst is not repaired.

Horizontal flap tears are predominantly horizontal tears, where a portion of the meniscus may flip into the adjacent synovial gutter along the margin of the joint. These fragments may be missed easily at arthroscopy, when they are not identified on MRI.

A bucket-handle tear is an important and not infrequent type of meniscal injury, occurring in about 10% of meniscal tears in most series. It typically consists of a vertical or an oblique tear in the posterior horn that extends longitudinally through the body segment and anterior horn, usually occurring acutely with a sudden impact

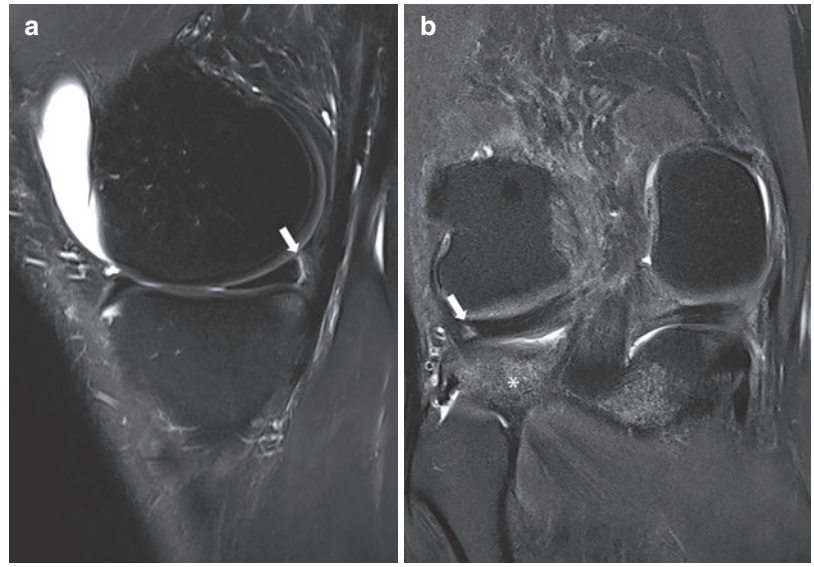

Fig. 10 (**a** and **b**) Meniscocapsular separation in 26-year-old rugby player with lateral knee pain after tackle. (**a**) Sagittal TSE T2 WI with FS and (**b**) coronal TSE PD WI with FS reveal a distinctive cleft (arrow) between the posterior horn of the lateral meniscus and joint capsule, compatible with meniscocapsular avulsion/separation. The coronal image also shows extensive bone marrow oedema in the later tibial plateau (asterisk)

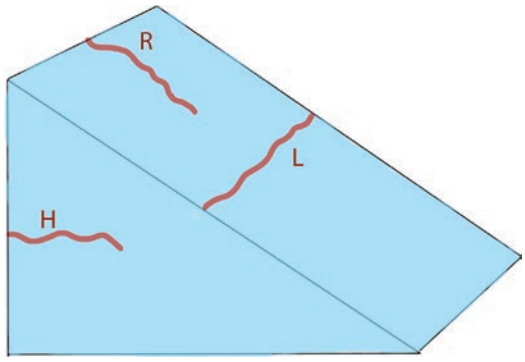

Fig. 11 Drawing of meniscal tear types. Horizontal tears (H) run parallel and vertical tears (R, L) perpendicular to the tibial plateau. Vertical-longitudinal tears (L) follow the long axis of the meniscus. Radial (R) tears transect the longitudinal collagen fibres

splitting the meniscus longitudinally. Coronal and sagittal MR images demonstrate blunting of the meniscus donor with the remaining meniscus being smaller than normal. The inner meniscal fragment is often displaced in the intercondylar notch, creating a "handle". Reported MRI signs for bucket-handle tears include absent bow-tie sign, double-PCL sign, disproportional posterior horn sign, anterior flipped fragment sign and double-anterior horn sign (Aydingöz et al. 2003) (Fig. 9).

Complex meniscal tears display combinations of vertical and horizontal tear patterns (Fig. 15).

Tear depth: extension of tear through one or (partial) or two (complete) meniscal surfaces.

Tear length: length of extension within meniscus (in mm).

Rim width: describes location of the tear in relation to the meniscal rim. Zone 1: 0–3 mm from the inner border; zone 2: 3–5 mm from the inner border; zone 3: >5 mm from the inner border (outer part of the meniscus).

Radial location: anterior, mid body or posterior.

Central to popliteus hiatus: describes extension of the tear in front of the popliteal hiatus.

Quality of the tissue: degenerative tissue exhibits diffusely increased signal, fraying and/or multiple tear patterns.

Chhabra et al. (2019) found fair-to-excellent interrater correlation for these characteristics in both the medial and lateral meniscus. There was moderate-to-excellent inter-method correlation for tear pattern and radial location and moderate correlation for the categorization central or not to popliteus hiatus. The other characteristics showed fair-to-good and moderate-to-good correlation.

The disadvantage of this classification is the absence of several types of meniscal tear patterns

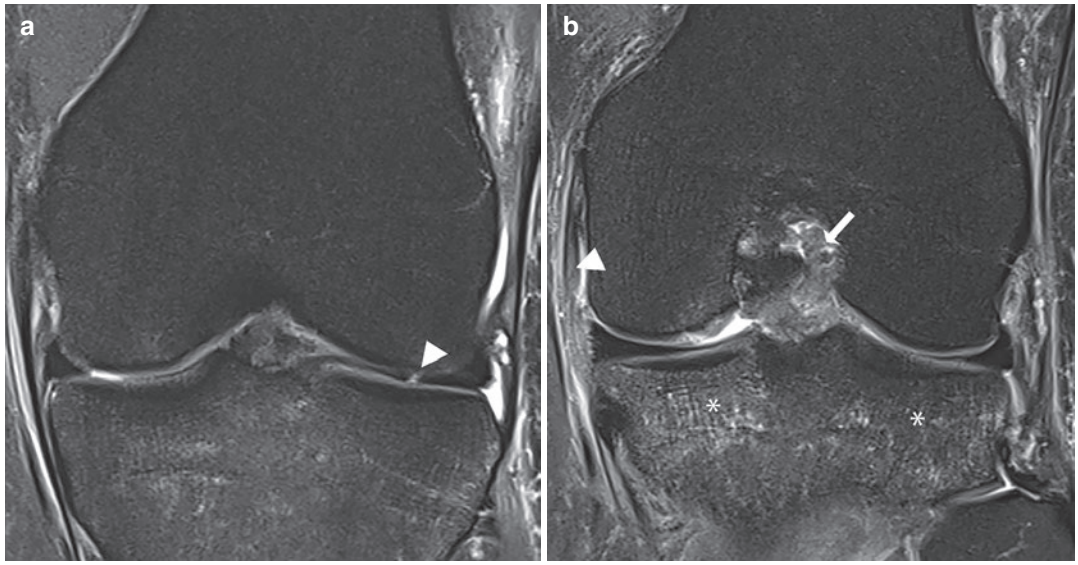

Fig. 12 (**a** and **b**) Coronal TSE PD WI with FS in a 38-year-old snowboarder. A longitudinal-vertical tear in the lateral meniscus (arrowhead in **a**) is noted, without significant displacement. Additionally, extensive bone marrow oedema in the medial and lateral tibial plateau (asterisks) is present, as well as a rupture of the ACL (arrow) and sprain grades 2–3 of the MCL (arrowhead in **b**)

(oblique, meniscocapsular separation, root ligament injuries), meniscal variants (discoid meniscus) and post-operative menisci.

Meniscocapsular separation (Fig. 10) is a subtype of meniscal tear, occurring most commonly along the medial meniscus, but the lateral meniscus may be affected also. Typically, the posterior meniscal horn is separated from the capsule with displacement of the posterior meniscal margin from the posterior tibial border by more than 8–10 mm.

An *oblique tear* (Fig. 16) is the most common meniscal tear type and demonstrates both radial and longitudinal components, as it courses obliquely across the meniscus, resulting in a flap of unstable meniscus. They most commonly affect the posterior horn and are seen as predominantly horizontal on sagittal MR images originating along the inferior surface at the free edge.

4.3.6 Accuracy and Limitations of MRI

Although arthroscopy still remains the gold standard in the diagnosis of meniscal injuries, the accuracy of MRI has made it a useful screening tool to avoid diagnostic interventional procedures (Elvenes et al. 2000). The pooled weighted sensitivity and specificity for medial meniscal lesions are 93.3% and 88.4%, respectively. For the lateral meniscus, these are 79.3% and 95.7%, respectively (Oei et al. 2003).

However, MR findings do not always agree with surgical findings. A study by Van Dyck et al. (2007) of 200 menisci analysed the various causes of incorrect MR diagnoses. They found 27 cases of discrepancy between MRI and arthroscopic findings. 44% of discrepancies between MRI and arthroscopy were determined as unavoidable, 37% as equivocal (or "borderline") and 19% as interpretation errors.

4.3.6.1 Unavoidable Errors

Unavoidable errors are defined as those in which the diagnosed anomalies on MRI do not correlate with those on arthroscopy, even when multiple observers agree on the MRI diagnosis.

Unavoidable false-positive results are rare (1%) (Van Dyck et al. 2007). They may be the result of a healing or healed meniscal tear (Deutsch et al. 1990). A healing tear (e.g. after meniscal repair) may be seen as hyperintense signal intensity in meniscal substance owing to the

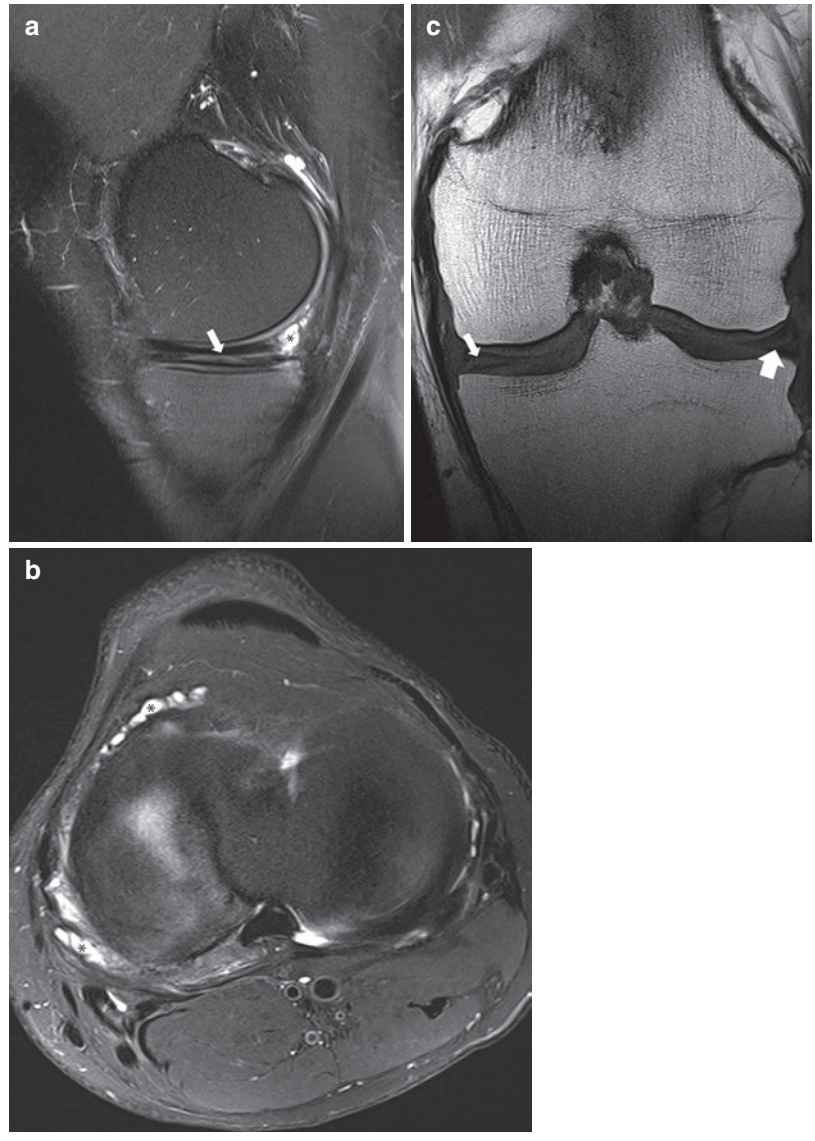

Fig. 13 (**a**–**c**) MRI in the 45-year-old long-distance runner in Fig. 6. (**a**) Sagittal T2 WI with FS shows a horizontal tear (arrow) in the body of the medial meniscus with parameniscal cyst (asterisk). (**b**) Axial TSE PD WI with FS reveals the true extent of the parameniscal cyst(s). (**c**) On TSE T1 WI, there is also abnormal signal intensity in the body of the lateral meniscus, consistent with a horizontal tear (thick arrow)

presence of granulation tissue (Farley et al. 1991). Also, they may be related to incomplete arthroscopic evaluation of the meniscus (Quinn and Brown 1991). Blind spots for the arthroscopist include the anterior horn of each meniscus, the extreme inner portion of the posterior horn of the medial meniscus and the undersurface of both menisci. Therefore, it is important to describe any tear in these areas clearly, because they may be easily missed during arthroscopy. Confusion between what represents fraying and what represents a tear may be another source of erroneous MR diagnosis.

Unavoidable false-negative errors are due to limitations of the MR sequences and imaging planes and do not represent observer errors. Small meniscal tears may not be discernible because the edges of small tears may be very closely apposed. The largest percentage of these false-negative results are found in the lateral meniscus. In the aforementioned study by Van Dyck et al. (2007), 23% of lateral meniscal

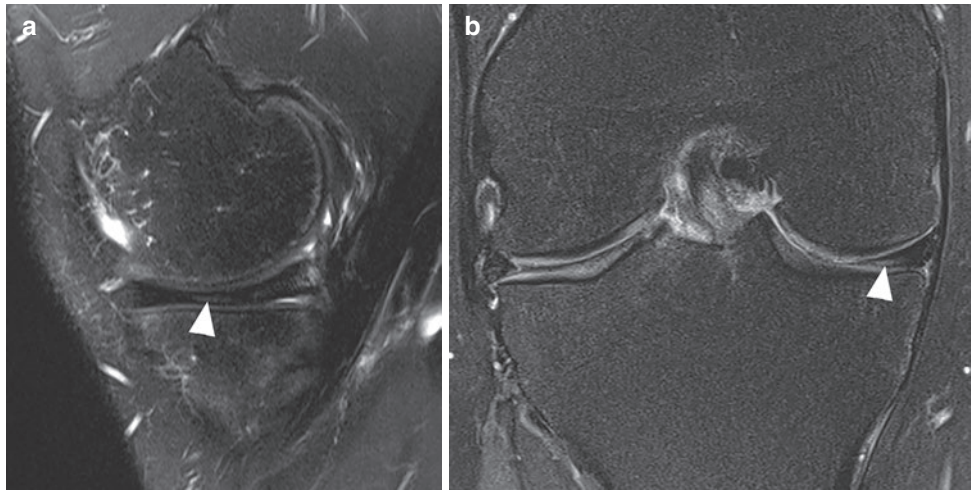

Fig. 14 (**a** and **b**) Horizontal tear (arrowheads) in the body and posterior horn of the medial meniscus on (**a**) sagittal TSE T2 WI with FS and (**b**) coronal TSE PD WI with FS

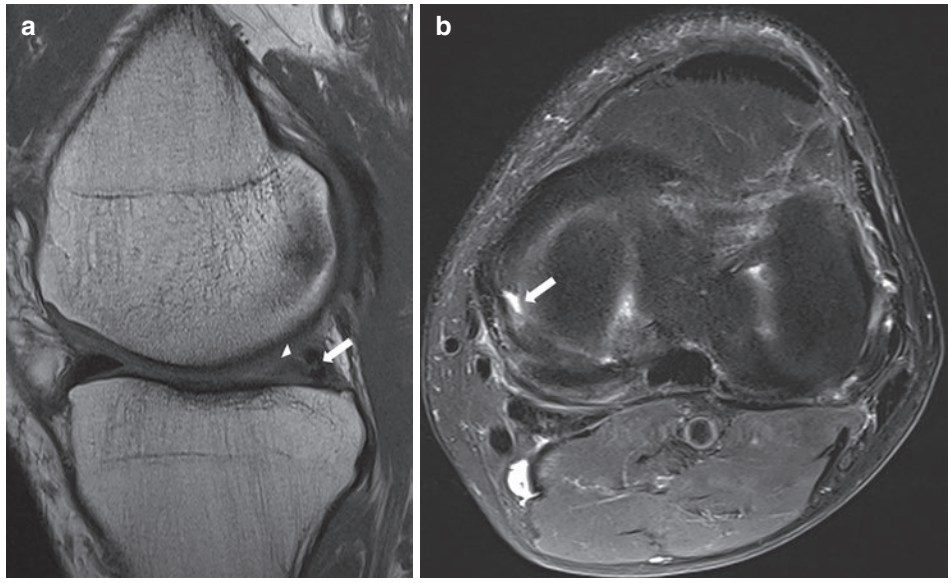

Fig. 15 (**a** and **b**) Complex tear in the posterior horn of the medial meniscus. (**a**) On the sagittal TSE PD WI, vertical (arrowhead) and horizontal (arrow) tears are revealed. (**b**) The axial TSE PD WI with FS shows a small defect in the posterior horn and body of the medial meniscus (arrow)

lesions were missed by MRI. Another study by De Smet et al. (1994) reported a lower yet also significant 11% of lateral meniscus lesions that were not detected on MRI. Furthermore, if a tear of the ACL is present, meniscal tears are more likely to be missed on MR images. Presumably, the biomechanical forces that result in an ACL tear cause meniscal tears that are difficult to diagnose on MR, namely in the posterior and peripheral parts of the lateral meniscus (De Smet and Graf 1994).

4.3.6.2 Equivocal Errors

It is not always possible to neatly categorize meniscal signal and determine if it is confined to the substance of the meniscus or extends

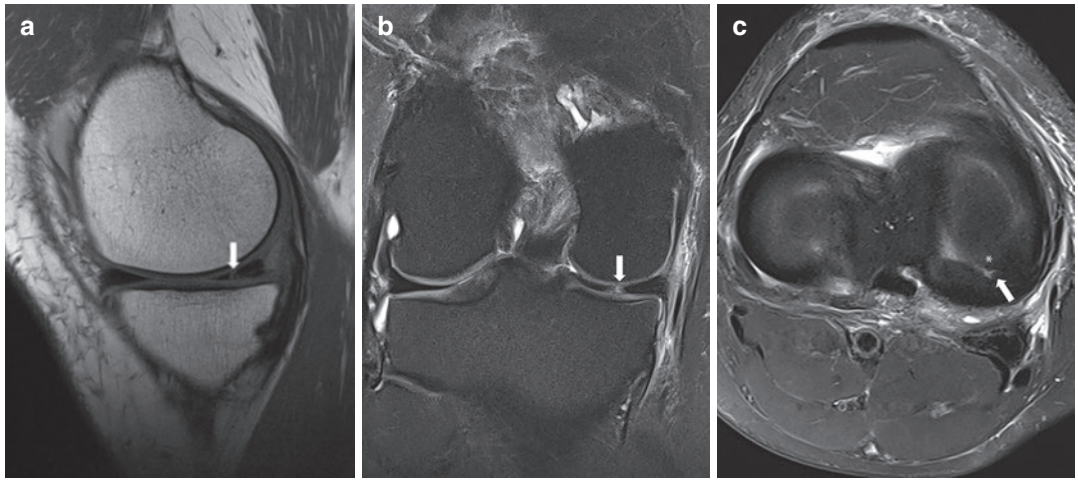

Fig. 16 (**a**–**c**) Oblique ("parrot beak") tear in the posterior horn of the medial meniscus of a 42-year-old footballer. Grade 3 signal (arrow) is seen on the (**a**) sagittal TSE PD WI and (**b**) coronal TSE PD WI with FS, consistent with a radial orientated tear. (**c**) The axial image reveals a slight oblique course of the tear (arrow) which creates a small, non-displaced flap (asterisk)

through the surface (Kelly et al. 1991). These equivocal MR imaging findings may lead to both false-positive and false-negative results compared to arthroscopy. De Smet et al. (1993) found that menisci with signal possibly contacting the surface had the same frequency of tears as menisci without signal contacting the surface. Furthermore, only 55% of medial and 30% of lateral menisci with signal contacting the surface on only one image were torn. Therefore, we suggest when linear signal closely approximates, but does not convincingly violate an articular surface, it is best to be descriptive rather than overcall a questionable finding. If surface contact is seen on only one image, the diagnosis should be qualified as a possible tear. Menisci with internal signal that only possibly contacts the surface should be considered intact.

Interestingly, it is not clear whether improved image quality leads to decrease of these equivocal errors (Van Dyck et al. 2010).

4.3.6.3 Interpretation Errors

This type of error may occur due to normal variants (Fig. 14). Radiologists must be aware of numerous pitfalls simulating a meniscal tear, including normal anatomical structures in close proximity to the meniscus (anterior transverse ligament, oblique meniscomeniscal ligament, meniscofemoral ligament, popliteal tendon, Wrisberg variant of discoid lateral meniscus), MR artefacts (volume averaging of adjacent bright structures, e.g. fat or fluid, truncation and motion-blurring artefacts, magic-angle phenomenon) and pathologic conditions (gas within the joint-vacuum phenomenon or iatrogenic, chondrocalcinosis, cartilage defects, meniscal ossicle) (Vanhoenacker et al. 2016).

4.4 CT Arthrography

The major indication of CT arthrography in meniscal evaluation is the detection of meniscal tears in the post-operative meniscus (see the following paragraph). Additionally, CTA is an alternative in patients with relative or absolute contraindications for MRI, including claustrophobia or implants such as defibrillators, or when MRI is not readily available.

Limitations inherent to the performance of this technique include invasiveness, possible allergic reaction, use of ionizing radiation and limited value for detection of associated ligamentous and/or soft-tissue disorders.

Multidetector CT arthrography (CTA) of the knee is an accurate and reproducible method for detecting meniscal abnormalities. Vande Berg et al. (2000) found a sensitivity and specificity for the detection of meniscal abnormalities of 98% and 94%, respectively, equivalent to those in most studies with MR imaging. More recent studies found a significantly lower accuracy (Fox et al. 2016), although this may be attributed to a delay between contrast injection and CT scan (≥60 min). Furthermore, CTA proved to be an accurate technique for detection of unstable meniscal tears with a sensitivity and specificity of 97% and 90%, respectively. Poor performance of MR imaging in the recognition of displaced meniscal fragments smaller than one-third of the meniscus has been reported (Wright et al. 1995).

5 Therapeutic Management in Athletes

When faced with a meniscal tear, the orthopaedic surgeon has three options: (1) leave the tear alone, (2) attempt a primary meniscal repair or (3) perform a partial or complete meniscectomy. When clinical symptoms persist after complete meniscectomy, meniscal replacement may be considered.

The treatment goal is to preserve as much functional meniscal tissue as possible to lessen the probability of developing osteoarthritis while addressing the clinical symptoms caused by meniscal tears.

Evaluation of the clinical situation is essential for optimal treatment planning, as well as meniscal tear location, extent and stability (Weiss et al. 1989).

Although MRI provides valuable information by displaying the location and extent of the tear, it is often impossible to determine with certainty whether or not a tear is stable using MRI (unless a displaced fragment is present). Meniscal tear stability is best determined with direct depiction and palpation at arthroscopy (Dandy 1990).

However, on MRI, tears that are considered stable include (1) a partial-thickness tear (less than half the height of the meniscus), (2) a full-thickness oblique or vertical tear measuring less than 7–10 mm in length and (3) a radial tear measuring less than 5 mm (Matava et al. 1999).

5.1 Conservative Treatment

In older or less active patients with minor symptoms, a more conservative approach is often employed. The mere presence of a meniscal tear in the degenerative knee is not an indication for arthroscopy. Research demonstrated that meniscal tears were a very common magnetic resonance imaging finding in asymptomatic patients and that there was no difference in pain or function between osteoarthritic patients with and without meniscal tears (Miller 2004). Other studies suggested that horizontal (degenerative) tears should be treated non-operatively in the presence of cartilage damage (Katz et al. 2013). However, in athletes, non-operative treatment is usually inadequate for a patient with high physical demands associated with sport, as the reduction in activity necessitated by the symptoms is not acceptable (Ludman et al. 1999).

5.2 Surgical Interventions

Based on MR images, it is important to classify the location of the tear relative to the blood supply of the meniscus. This allows repair potential of the lesion to be predicted. A red-red tear is located at the meniscal periphery within the vascularised zone or represents capsular detachment. It has the best prognosis for healing, as the blood supply persists in this region (Fig. 17). The red-white tear has no blood supply from the inner surface of the lesion; however the remaining vascularity is usually sufficient for the healing process. A red-red and red-white tear may spontaneously heal or may be repaired. White-white tears need to be resected, as they are located in the avascular zone and have no healing potential.

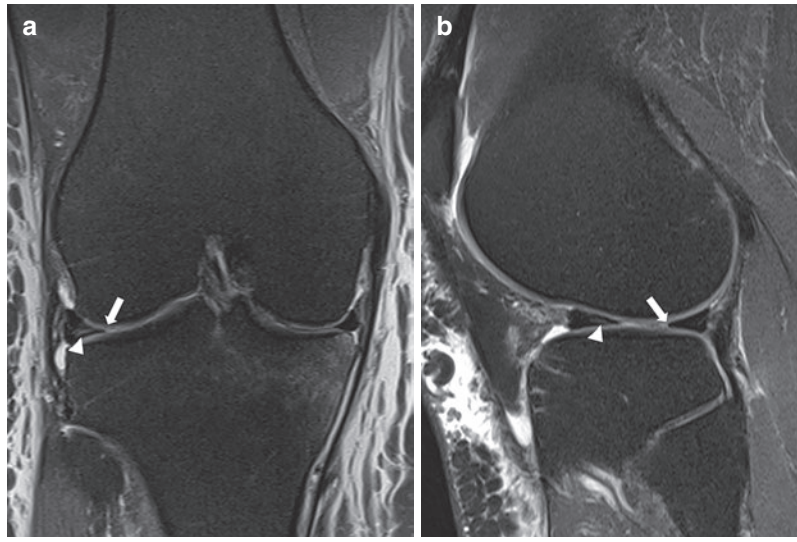

Fig. 17 (**a** and **b**) Potential retear after previous partial lateral meniscectomy on (**a**) coronal TSE PD WI with FS and (**b**) sagittal TSE T2 WI with FS. Discrete blunted aspect of the body of the lateral meniscus suggests previous partial lateral meniscectomy (arrows). There is linear high signal intensity in contact with the resection surface, suggestive of retear. However, clinical information stated the presence of a stable residual tear that was left by the surgeon in order to minimize meniscal volume loss. The patient was pain free

5.2.1 Meniscectomy (Partial-Complete)

Partial meniscectomy is often the treatment of choice in symptomatic horizontal tears persistent to conservative treatment, unstable flap tears, radial tears, longitudinal-vertical tears in the white-white zone and complex tears. Associated parameniscal cysts are preferably debrided to reduce symptoms (Tafur et al. 2018). Other indications include irreparable root tears or vertical tear or failed meniscal repair.

Short-term clinical results were demonstrated for this type of surgery, but long-term follow-up revealed a high rate of progression to osteoarthritis (Fauno and Nielsen 1992).

5.2.2 Meniscus Repair

The main indication for meniscal repair is acute, traumatic longitudinal-vertical tears within the red-red zone (Vaquero and Forriol 2016). Extended indications for meniscal repair surgery include tears red-white zone in younger patients, radial tears, root avulsions and meniscocapsular avulsions/meniscal ramp lesions (Kurzweil et al. 2014; Thaunat et al. 2016). Contraindications are extensive degenerative changes or ligamentary instability without concomitant ligament repair.

A recent meta-analysis concluded that reoperation rates were higher for meniscal repair than those for meniscectomy but it leads to better long-term function outcome and better activity level (Xu and Zhao 2015).

5.2.3 Meniscus Reconstruction

Persistent joint-line pain and swelling after complete or partial meniscectomy are possible indications for meniscal replacement. Meniscal allograft transplantation is mostly reserved for patients under 50 years of age. For older patients with chronic meniscal problems, synthetic (polycarbonate urethane (PCU) or collagen) implants are available.

Prophylaxis for further advancement of osteoarthrosis is not the main goal in these patients. Rather, the main aims are to restore normal knee mechanics, improve joint function and relieve pain (Doral et al. 2018).

6 Imaging of the Post-operative Meniscus

Because meniscal surgery is so common in the young, athletic population, many patients who have undergone meniscal surgery present with recurrent knee injury or pain. For the radiologist, imaging the post-operative meniscus remains a challenge. Contour abnormalities and diffuse signal changes may be present in both normal post-operative menisci and recurrent meniscal tears. As in preoperative patients, MR imaging is the most valuable imaging method for post-operative evaluation of the knee (McCauley 2005). Standard MR imaging protocols, however, are less reliable in imaging post-operative knees than in unoperated knees, especially for the diagnosis of meniscal tears, with accuracies ranging from less than 50% to 80%.

6.1 MR Appearance After (Partial) Meniscectomy

Following partial meniscectomy, the meniscus has a smaller aspect, possibly with some degree of deformity. Intermediate signal intensity on a proton density/intermediate-weighted sequence-weighted image extending to the meniscal surface ("grade 3 signal") may represent fibrovascular or fibrocartilaginous repair tissue, pre-existing degenerative signal abnormalities abutting the post-operative surface or a new tear (Figs. 17 and 18).

Increased signal on a T2-weighted image extending into the meniscus is a stricter criterion for recurrent or residual tear, providing higher specificity (73% versus 53%) but lower sensitivity (72% versus 76%) (White et al. 2002).

6.2 MR Appearance After Meniscus Repair

Following meniscal repair, the fibrovascular repair tissue and later fibrocartilaginous scar tissue may present as abnormal signal intensity contacting the meniscal surface on intermediate-weighted sequences (Toms et al. 2005) (Fig. 19). Differentiating these normal post-operative findings from recurrent tear remains challenging. The presence of high signal on T2-weighted images has a higher specificity and accuracy (90–99% and 83–91%, respectively) than PD- and T1-weighted sequences (Miao et al. 2009, 2011). Additional signs suggestive for retear include diastasis of the suture edges >1 mm or displaced meniscal flaps (Recht and Kramer 2002).

6.3 MR Appearance After Meniscal Replacement

Meniscal allograft transplants often develop diffuse signal abnormalities, even shortly after transplantation. These grade 3 alterations may remain stable or progress, most frequently in the lateral knee compartment (Buma et al. 2004). It was suggested by Verdonk et al. (2006) that these changes were alterations in the extracellular matrix composition and water content rather than real tears.

Often, radial displacement of the body of the transplant meniscus is seen. This phenomenon was more frequently observed in the medial than lateral meniscus. The relevance of this finding remains debated, as some authors believe this to be a sign of subsequent degeneration (Costa et al. 2004; Gale et al. 1999) while other studies did not find a correlation with clinical outcome (Verdonk et al. 2006; Lee et al. 2015).

Only few studies examined the MR findings of artificial meniscal implants. Both PCU and collagen implants show higher signal intensity on T2-weighted sequences. In PCU implants, defects in the posterior horn have been described (Huysse et al. 2008). Radial displacement may also be seen in PCU implants but, as in allograft transplantation, has no significant effect on clinical outcome (De Coninck et al. 2013).

6.4 Conventional MR Versus MRA Versus CTA in the Post-operative Meniscus

The discussion on which imaging modality is the most accurate for diagnosing recurrent tear after

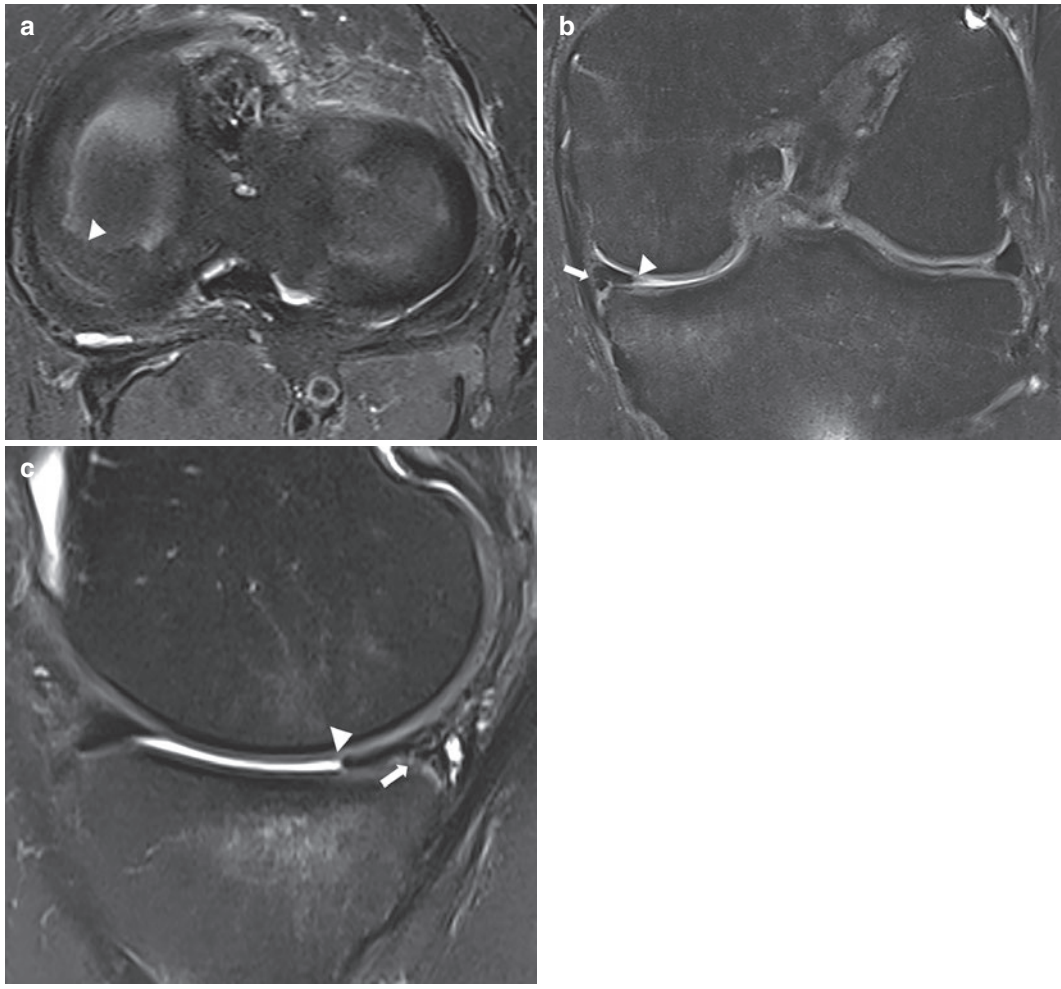

Fig. 18 (**a**–**c**) New meniscal tear after partial meniscectomy. (**a**) On axial TSE PD WI with FS, irregularity of the inner rim of the medial meniscus is noted (arrowhead), consistent with previous partial medial meniscectomy. (**b**) Coronal TSE PD WI with FS and (**c**) sagittal TSE T2 WI with FS confirm partial volume of the medial meniscus (arrowheads). High signal intensity is seen at a distance of the surgery site (arrows), compatible with a new oblique tear

meniscal surgery has been the subject of many studies.

Most authors report a higher accuracy for direct and indirect MR arthrography than MRI. In a recent meta-analysis, reported accuracies for recurrent tear for both partial meniscectomy and meniscal repair are 57–80% for MRI, 81–93% for indirect MRA and 85–93% for direct MRA (Baker et al. 2018). In CTA, the reported sensitivity and specificity after partial meniscectomy are 93% and 89%, respectively (Mutschler et al. 2003).

In partial meniscectomy, the accuracy of the different techniques varies according to the amount of meniscus that was resected. When less than 25% of the meniscus was resected, the accuracy of conventional MRI was 89%. In larger resection volumes (greater than 25%), the accuracy of conventional MRI dropped to 69%, significantly less than that of direct MRA (89%) (Applegate et al. 1993, Magee et al. 2003).

CT arthrography or direct MR arthrography may reveal contrast extravasation within (partial-thickness recurrent tear or partial-healed repair)

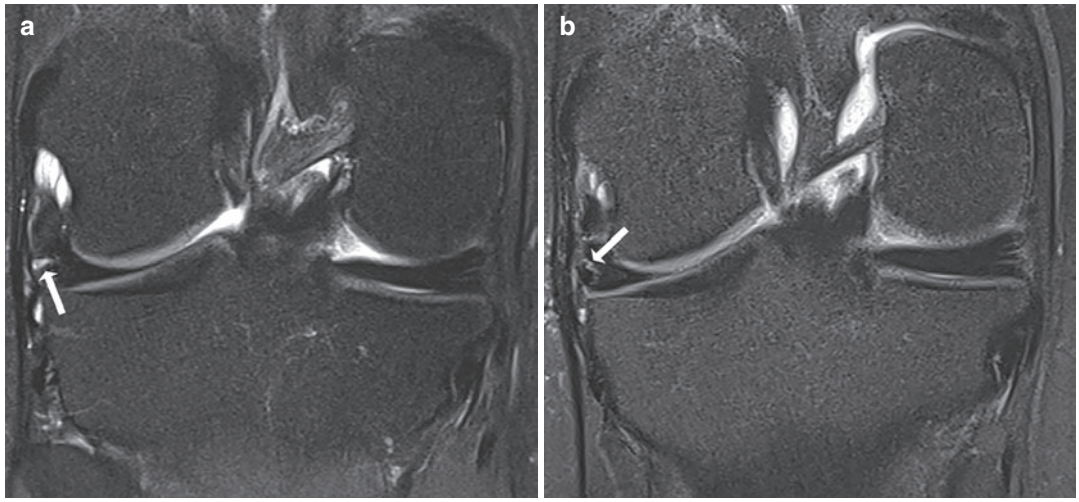

Fig. 19 (**a**) Preoperative and (**b**) post-operative coronal TSE PD WI with FS. The preoperative image (**a**) reveals a grade 3 signal/horizontal tear (arrow) in the red zone of the body of the lateral meniscus. 3 months after repair surgery (**b**), persistent high signal (arrow) is noted at the surgery site. This represents fibrovascular repair tissue and not a new tear

or through the meniscus (full-thickness recurrent tear or failed repair). However, these findings are not present in every retear, possibly due to mechanical obstruction (e.g. scar tissue) (De Smet et al. 2006; Magee 2014).

6.4.1 Imaging Pathway in the Post-operative Meniscus

In general, most patients do not need to undergo MR arthrography and conventional MRI should be considered as the first-line investigation (38) (Fig. 16). We look for unequivocal sites of fluid intensity signal within the meniscal remnant, displaced fragments or tears in a new location, as the only reliable criteria for a recurrent or residual tear. Standard criteria can be used to interpret areas of the menisci known to be separated from the site of prior surgery. Investigation with MRA (or CTA) could then be considered if conventional MRI is normal (no severe degenerative arthrosis, avascular necrosis, chondral injuries, native joint fluid extending into a meniscus or a tear in a new area), if the clinical suspicion of recurrent tear is high, or if conventional MRI is inconclusive. In particular, MRA may be useful when there is prior knowledge of significant meniscal resection (more than 25%) or meniscal repair with new symptoms in the same area as the initial symptoms. Furthermore, MR arthrography is of additional value in assessing the articular cartilage, deteriorating more rapidly after meniscectomy.

7 Specific Sports and Overuse Trauma of the Meniscus

7.1 Injury Mechanisms in Sports Injury

Sports-related meniscal tears may result from excessive application of force to a normal meniscus (in the young athlete) or normal forces acting on a degenerative meniscus (in older patients). Meniscal injury, particularly sports-related injuries, usually involves damage due to twisting motions, which are common in sports, with a varus or valgus force directed to a flexed knee. Contact with another player typically does not occur, nor does lunging or landing awkwardly. A single "wrong" step is sufficient.

The most common traumatic mechanism, accounting for nearly half of all injuries, combines valgus force directed to a flexed knee with the tibia in exorotation (Hayes et al. 2000). Therefore, compression with impaction injury usually occurs in the lateral compartment, whereas

tension with distraction injury occurs in the medial compartment. Thus, the medial meniscus is at risk for peripheral avulsion injury at the capsular attachment site resulting in peripheral meniscal tear (and/or meniscocapsular injury) whereas the lateral meniscus gets entrapped by compressive force, splays and splits (because of its more circular shape and decreased radius of curvature) the free margin resulting in a radial tear.

In contact sports, tackles are often directed towards the lateral side of the knee, resulting in the same injury mechanism and type of (meniscal) lesions.

Injury to the medial meniscus is about five times more common than injury to the lateral meniscus. Compared to the lateral meniscus, the medial meniscus is relatively immobile because of its firm attachment to the medial capsule along its peripheral border. The lateral meniscus, loosely applied to the joint capsule, moves freely with the condyle and usually can escape entrapment (Muller 1983).

The trauma-related medial meniscal tear typically demonstrates a vertical orientation extending across the full thickness of the meniscus. It may redirect itself obliquely towards the free margin of the meniscus, creating a flap configuration.

Radial tears are rare in the medial meniscus and appear to follow more severe forms of athletic trauma. Kidron and Thein (2002) described the presence of a small radial root tear in the posterior horn of the medial meniscus in 11 of the 1270 operated knees (0.86%). Each of these 11 patients, all active in demanding sports, including handball, judo and gymnastics, had a history of acute flexion injury and medial joint-line pain. Arthroscopic trimming of the edges of the tear revealed a developing cleavage plane tear extending to the body of the meniscus, resulting in partial meniscectomy.

Moreover, according to a study by Magee et al. (2004), the prevalence of meniscal radial tears may be increased in the post-operative knee due to the altered hoop mechanism of the meniscus and decreased ability to transmit loads. These authors found a prevalence of meniscal radial tears of 32% in the post-operative knee as opposed to a reported prevalence of 14% in the non-operated knee.

There are significant regional differences in sports-related meniscal injuries depending upon the popularity of specific sports. In a study by Baker et al. (1985), meniscectomies performed in Syracuse, New York, from 1973 to 1982 were reviewed. Medial versus lateral meniscus injury was 81 versus 19%. Football had a 75% predominance of medial meniscectomy; basketball, 75%; wrestling, 55%; skiing, 78%; and baseball, 90%. These data indicate that there are differences in the ratio of medial versus lateral meniscal disruption associated with specific sports activities. Medial meniscal injuries were consistently more common in all sports categories, except wrestling, where the frequency of lateral meniscal tear is nearly equal to that of a medial meniscal tear.

7.2 Symptomatic and Asymptomatic Meniscal Lesions in Athletes

Asymptomatic or “silent” grade 3 intrameniscal signal abnormalities have been described in both athletes and less active patients (Ludman et al. 1999). The incidence of asymptomatic meniscal tears increases with age, with 5.6–13% of those less than 45 years old and 36% of those more than 45 years old (Greis et al. 2002). Some studies have suggested that athletic groups, including American football players and marathon runners, show an increased incidence of meniscal abnormalities (Shellock et al. 1991). In a study by LUDMAN et al. (1), the overall incidence of grade 3 changes (13%) in gymnasts was not significantly different from the incidence in the controls. However, when compared with the control group, the group of gymnasts had a significantly different distribution of grade 3 intrameniscal changes, preferentially involving the lateral meniscus (evenly divided between the anterior and posterior horns), whereas in the control group, grade 3 changes were mostly found in the medial meniscus (only posterior horn). The reason why the lateral meniscus of gymnasts is preferentially affected is unclear. Nevertheless, knowledge of these MR appearances is important when evaluating the lateral menisci within this group of athletes to prevent unnecessary

treatment or intervention. This is particularly important when the imaging findings do not closely correlate with the site of symptoms.

On the other hand, symptomatic grade 2 intrameniscal signal has been described in athletes (Biedert 1993). In 35 of 43 patients (77.7%) with clinical features of a possible meniscus lesion, a pure intrasubstance tear with linear grade 2 signal was identified on MRI. This type of lesion in the posterior horn represents a frequent cause of false-negative result on arthroscopy. All patients were free of symptoms after conservative treatment or partial meniscectomy. In this study, the highest rates of intrasubstance tears were found in soccer, running and ice hockey.

Although not specifically described in any sports branch, a potential source for false-positive interpretation for meniscal tear in the MR evaluation of the post-traumatic knee is the so-called *meniscal contusion*. Cothran et al. (2001) described focal signal abnormalities in the knees of six patients who had a history of acute knee trauma, associated with tears of the ACL and bone contusions. This signal reached the articular surface of the meniscus, but did not meet the criteria for a meniscal tear or degeneration. The meniscus gets trapped between the femur and tibia during a traumatic event. The adjacent bone contusion should alert one to the possible presence of a contusion rather than a meniscal tear.

Meniscocapsular separation ("ramp lesions") has been partially discussed previously in this chapter. They are most commonly seen along the medial meniscus, which is more tightly adherent to the joint capsule. Small avulsed corners of the medial meniscus may be difficult to identify unless a directed search is made for them.

George et al. (2000) have found that anterolateral meniscocapsular separations of the lateral aspect of the knee were frequently missed on MRI reporting in a group of athletes presenting with lateral joint-line pain suggestive of meniscal injury. During arthroscopy, in all patients meniscocapsular separation was confirmed and no meniscal tears were found. Meniscocapsular tears can also occur along the posterolateral corner of the joint, with disruption of the meniscopopliteal fascicles.

Another entity, recently described in severe acute (sports) injury of the knee by Bikkina et al. (2005) is the so-called *floating meniscus*, corresponding to a meniscal avulsion or detachment from the tibial plateau with an associated disruption of the meniscotibial coronary ligaments, which attach the meniscus to the tibia, allowing fluid to encompass the meniscus. It is usually seen as a sequela of high-impact (sports) injury or trauma. The presence of a "floating meniscus" on MRI is often associated with significant ligamentous injury without evidence of a tear within the substance of the meniscus. Alerting the surgeon to the presence of a meniscal avulsion facilitates appropriate surgical planning with meniscal reattachment to the tibial plateau.

8 Conclusion

Meniscal injuries are very common among professional and amateur athletes and are a major cause of functional impairment of the knee. For athletes, unnecessary treatment or intervention may be as damaging to a competitive future as failure to diagnose a clinically significant injury. Therefore, rapid and accurate evaluation of possible meniscal injuries is crucial in these patients.

For detection of meniscal pathology, MRI is an excellent diagnostic imaging tool, with accuracy of as high as 98%, compared to arthroscopy, remaining the gold standard. Furthermore, MRI proved useful, on the basis of its high negative predictive value, to avoid unnecessary arthroscopy and hospitalization, morbidity and waste of limited financial and manpower resources.

However, radiologists must be aware of numerous pitfalls simulating a meniscal tear. Furthermore, MRI pictures contain many details with an uncertain clinical relevance, delineating the need to correlate MR with clinical findings in order to plan treatment optimally.

Things to Remember

1. Meniscal tears are the most common cause of knee pain and instability in athletes.

2. Symptoms and clinical findings are usually non-specific and must be regarded as of little value in making the correct diagnosis.
3. MRI has replaced other imaging techniques for diagnosis of meniscal tears.
   MR criteria for classifying meniscal tears have been clearly described. In addition to diagnosing meniscal tears, the radiologist should describe the features of each meniscal tear that may affect treatment.
4. As the long-term protective effect of the menisci on the joint surfaces has been well documented, meniscal preservation should be the goal of treatment. Stability, location and type of meniscal tear are essential in deciding whether to repair, resect or leave alone a meniscal lesion. Allograft replacement is an evolving technique.

9 Imaging Boxes

Box 1

Plain radiography and standard arthrography

Have been replaced by other (cross-sectional) imaging techniques for the evaluation of meniscal injury.

Ultrasound

No significant role for the detection of meniscal tears, although meniscus extrusion and parameniscal cysts are suggestive of tear.

Box 2

MR arthrography and CT arthrography

High accuracy for the evaluation of meniscal injury.

Invasive.

Useful for the evaluation of the post-operative meniscus.

Standard MRI

Non-invasive.

The dominant imaging technique for the assessment of meniscal lesions.

Box 3

Because both asymptomatic grade 3 and symptomatic grade 2 lesions exist, MRI findings need to be correlated with clinical symptoms in order to plan treatment optimally.

References

Anderson AF, Irrgang JJ, Dunn W, Beaufils P, Cohen M, Cole BJ, Kowalchuk DA (2011) Interobserver reliability of the International Society of Arthroscopy, Knee Surgery and Orthopaedic Sports Medicine (ISAKOS) classification of meniscal tears. Am J Sports Med 39:926–932

Applegate GR, Flannigan BD, Tolin BS et al (1993) MR diagnosis of recurrent tears in the knee: value of intra-articular contrast material. AJR Am J Roentgenol 161:821–825

Arnoczky SP, Adams ME, DeHaven KE et al (1987) The meniscus. In: Woo SL, Buckwalter J (eds) Injury and repair of musculoskeletal soft tissues. Park Ridge, IL, American Academy of Orthopaedic Surgeons, pp 487–537

Aydin H, Kizilgöz V, Hekimoğlu B (2011) Is the quantitative diffusion-weighted MR imaging and ADC mapping with b-values of 50, 400, and 800 sec/mm2 a reliable method for evaluation of meniscal tears in the knee? Pol J Radiol 76(1):30–40

Aydingöz Ü, Firat AK, Atay ÖA et al (2003) MR imaging of meniscal bucket-handle tears: a review of signs and their relation to arthroscopic classification. Eur Radiol 13:618–625

Baker BE, Peckham AC, Pupparo F et al (1985) Review of meniscal injury and associated sports. Am J Sports Med 13:1–4

Baker JC, Friedman MV, Rubin DA (2018) Imaging the postoperative knee meniscus: an evidence-based review. AJR Am J Roentgenol 211:519–527

Biedert RM (1993) Intrasubstance meniscal tears. Arch Orthop Trauma Surg 112:142–147

Bikkina RS, Tujo CA, Schraner AB et al (2005) The "floating" meniscus: MRI in knee trauma and implications for surgery. AJR Am J Roentgenol 184:200–204

Buma P, Ramrattan NN, van Tienen TG, Veth TP (2004) Tissue engineering of the meniscus. Biomaterials 25:1523–1532

Chhabra A, Ashikyan O, Hlis R, Cai A, Planchard K, Xi Y, McCrum C, Shah J (2019) The International Society of Arthroscopy, Knee Surgery and Orthopaedic Sports Medicine classification of knee meniscus tears: three-dimensional MRI and arthroscopy correlation. Eur Radiol 29:6372–6384

Costa CR, Morrison WB, Carrino JA (2004) Medial meniscus extrusion on knee MRI: is extent associated with severity of degeneration or type of tear? AJR Am J Roentgenol 183:17–23

Cothran RL, Major NM, Helms CA et al (2001) MR imaging of meniscal contusion in the knee. AJR Am J Roentgenol 177:1189–1192

Dandy DJ (1990) The arthroscopic anatomy of symptomatic meniscal lesions. J Bone Joint Surg Br 72: 628–633

De Coninck T, Huysse W, Verdonk R, Verstraete K, Verdonk P (2013) Open versus arthroscopic meniscus allograft transplantation: magnetic resonance imaging study of meniscal radial displacement. Arthroscopy 29:514–521

De Smet AA, Graf BK (1994) Meniscal tears missed on MR imaging: relationship to meniscal tear patterns and anterior cruciate ligament tear. AJR Am J Roentgenol 162:905–911

De Smet AA, Norris MA, Yandow DR et al (1993) MR diagnosis of meniscal tears of the knee: importance of high signal in the meniscus that extends to the surface. AJR Am J Roentgenol 161:101–107

De Smet AA, Tuite MJ, Norris MA et al (1994) MR diagnosis of meniscal tears: analysis of causes of errors. AJR Am J Roentgenol 163:1419–1423

De Smet AA, Asinger DA, Johnson RL (2001) Abnormal superior popliteomeniscal fascicle and posterior pericapsular edema: indirect MR imaging signs of a lateral meniscal tear. AJR Am J Roentgenol 176:63–66

De Smet AA, Horak D, Davis KW, Choi JJ (2006) Intensity of signal contacting meniscal surface in recurrent tears on MR arthrography compared to that of contrast material. AJR Am J Roentgenol 187:635–641

Deutsch A, Mink JH, Fox JM, Arnoczky SP, Rothman BJ, Stoller DW, Cannon WD (1990) Peripheral meniscal tears: MR findings after conservative treatment or arthroscopic repair. Radiology 176:485–488

Doral M, Bilge O, Huri G, Turhan E, Verdonk R (2018) Modern treatment of meniscal tears. EFORT Open Reviews 3:260–268

Elvenes J, Jerome CP, Reikeras O et al (2000) Magnetic resonance imaging as a screening procedure to avoid arthroscopy for meniscal tears. Arch Orthop Trauma Surg 120:14–16

Farley TE, Howell SM, Love KF et al (1991) Meniscal tears: MR and arthrographic findings after arthroscopic repair. Radiology 180:517–522

Fauno P, Nielsen AB (1992) Arthroscopic partial meniscectomy: a long-term follow up. Arthroscopy 8:345–349

Fleckenstein JL, Archer BT, Barker BA et al (1991) Fast short-tau inversion recovery MRI. Radiology 179:499–504

Fox MG, Graham JA, Skelton BW, Blount KJ, Alford BA, Patrie JT, Gaskin CM (2016) Prospective evaluation of agreement and accuracy in the diagnosis of meniscal tears: MR arthrography a short time after injection versus CT arthrography after a moderate delay. Am J Roentgenol 207:142–149

Gale DR, Chaisson CE, Totterman SM, Schwartz RK, Gale ME, Felson D (1999) Meniscal subluxation: association with osteoarthritis and joint space narrowing. Osteoarthr Cartil 7:526–532

George J, Saw KY, Ramlan AA et al (2000) Radiological classification of meniscocapsular tears of the anterolateral portion of the lateral meniscus in the knee. Australas Radiol 44:19–22

Greis PE, Bardana DD, Holmstrom MC et al (2002) Meniscal injury: basic science and evaluation. J Am Acad Orthop Surg 10:168–176

Hayes CW, Brigido MK, Jamadar DA et al (2000) Mechanism-based pattern approach to classification of complex injuries of the knee depicted at MR imaging. Radiographics 20:121–134

Huysse W, Verstraete KL, Verdonk PC, Verdonk R (2008) Meniscus imaging. Semin Musculoskelet Radiol 12:318–333

Karachalios T, Hantes M, Zibis AH et al (2005) Diagnostic accuracy of a new clinical test (the Thessaly test) for early detection of meniscal tears. J Bone Joint Surg 87:955–962

Katz J, Brophy R, Chaisson C (2013) Surgery versus physical therapy for a meniscal tear and osteoarthritis. N Engl J Med 368:1675–1684

Kelly MA, Flock TJ, Kimmel JA et al (1991) MR imaging of the knee: clarification of its role. Arthroscopy 7:78–85

Kidron A, Thein R (2002) Radial tears associated with cleavage tears of the medial meniscus in athletes. Arthroscopy 3:254–256

Kijowski R (2010) Clinical cartilage imaging of the knee and hip joints. AJR Am J Roentenol 195: 61–628

Kijowski R, Gold GE (2011) Routine three-dimensional magnetic resonance imaging of joints. J Magn Reson Imaging 33:758–771

Kizilgöz V, Aydin H, Hekimoğlu B (2013) The efficacy of diffusion weighted imaging and apparent diffusion coefficient mapping for meniscal tears in the knee. Sci J Clin Med 2(6):171–175

Kurzweil P, Lynch N, Coleman S, Kearney B (2014) Repair of horizontal meniscus tears: a systematic review. Arthroscopy 30:1513–1519

Lee D, Lee C, Jeon J, Kim K, Bin S (2015) Graft extrusion in both the coronal and sagittal planes is greater after medial compared with lateral meniscus allograft transplantation but is unrelated to early clinical outcomes. Am J Sports Med 43:213–219

Ludman CN, Hough DO, Cooper TG et al (1999) Silent meniscal abnormalities in athletes: magnetic resonance imaging of asymptomatic competitive gymnasts. Br J Sports Med 33:414–416

Magee Y (2014) Accuracy of 3-Tesla MR and MR arthrography in diagnosis of meniscal retear in the post-operative knee. Skelet Radiol 43: 1057–1064

Magee T, Shapiro M, Rodriguez J, Williams D (2003) MR arthrography of postoperative knee: for which patients is it useful? Radiology 229:159–163

Magee T, Shapiro M, Williams D (2004) Prevalence of meniscal radial tears of the knee revealed by MRI after surgery. AJR 182:931–936

Makris EA, Hadidi P, Athanasiou KA (2011) The knee meniscus: structure, function, pathophysiology, current repair techniques, and prospects for regeneration. Biomaterials 32:7411–7431

Matava MJ, Eck K, Totty W et al (1999) Magnetic resonance imaging as a tool to predict meniscal reparability. Am J Sports Med 27:436–443

McCauley TR (2005) MR imaging evaluation of the postoperative knee. Radiology 234:53–61

McKeon BP, Bono JV, Richmond JC (2009) Knee arthroscopy. Springer Science and Business Media, New York, NY

Metcalf MH, Barrett GR (2004) Prospective evaluation of 1485 meniscal tear patterns in patients with stable knees. Am J Sports Med 32(3):675–680

Miao Y, Yu J, Zheng Z et al (2009) MRI signal changes in completely healed meniscus confirmed by second-look arthroscopy after meniscal repair with bioabsorbable arrows. Knee Surg Sports Traumatol Arthrosc 17:622–630

Miao Y, Yu JK, Ao YF, Zheng ZZ, Gong X, Leung KKM (2011) Diagnostic values of 3 methods for evaluating meniscal healing status after meniscal repair: comparison among second-look arthroscopy, clinical assessment, and magnetic resonance imaging. Am J Sports Med 39:735–742

Miller MD (2004) What's new in sports medicine? J Bone Joint Surg Am 86:653–661

Muller W (1983) The knee. Springer, New York

Mutschler C, Vande Berg BC, Lecouvet FE, Poilvache P, Dubuc JE, Maldague B, Malghem J (2003) Postoperative meniscus: assessment at dual-detector row spiral CT arthrography of the knee. Radiology 228:635–641

Oei EHG, Nikken JJ, Verstijnen ACM, Ginai AZ, Hunink MGM (2003) MR imaging of the menisci and cruciate ligaments: a systematic review. Radiology 226:837–848

Palastanga N, Soames R (2011) Anatomy and human movement, structure and function. Elsevier Health Sciences, Philadelphia, PA

Quinn SF, Brown TF (1991) Meniscal tears diagnosed with MR imaging versus arthroscopy: how reliable a standard is arthroscopy? Radiology 181: 843–847

Rath E, Richmond JC (2000) The menisci: basic science and advances in treatment. Br J Sports Med 34:252–257

Rauscher I, Stahl R, Cheng J et al (2008) Meniscal measurements of T1rho and T2 at MR imaging in healthy subjects and patients with osteoarthritis. Radiology 249(2):591–600

Recht M, Kramer J (2002) MR imaging of the postoperative knee: a pictorial essay. Radiographics 22: 765–774

Recht MP, Goodwin DW, Winalski CS, White LM (2005) MRI of articular cartilage: revisiting current status and future directions. AJR Am J Roentgenol 185: 899–914

Shellock FG, Deutsch AL, Mink JH et al (1991) Do asymptomatic marathon runners have an increased prevalence of meniscal abnormalities? An MR study of the knee in 23 volunteers. AJR Am J Roentgenol 157:1239–1244

Shoemaker SC, Markolf KL (1986) The role of the meniscus in the anterior-posterior stability of the loaded anterior cruciate deficient knee: effects of partial versus total excision. J Bone Joint Surg Am 68: 71–79

Snoeker BA, Bakker EW, Kegel CA, Lucas C (2013) Risk factors for meniscal tears: a systematic review including meta-analysis. J Orthop Sports Phys Ther 43:352–367

Stoller DW et al (1987) Meniscal tears: pathological correlation with MR imaging. Radiology 163: 731–735

Sweigart MA, Athanasiou KA (2001) Toward tissue engineering of the knee meniscus. Tissue Eng 7:111–129

Tafur M, Probyn L, Chahal J, White LM (2018) Diagnosing meniscal pathology and understanding how to evaluate a postoperative meniscus based on the operative procedure. J Knee Surg 31:166–183

Tarhan NC, Chung CB, Mohana-Borges AV et al (2004) Meniscal tears: role of axial MRI alone and in combination with other imaging planes. AJR Am J Roentgenol 183:9–15

Thaunat M, Fayard JM, Tales Guimaraes M, Jan N, Murphy CG, Sonnery-Cottet B (2016) Classification and surgical repair of ramp lesions of the medial meniscus. Arthrosc Tech 5:871–875

Thompson WO, Thaete FL, Fu FH et al (1991) Tibial meniscal dynamics using three-dimensional reconstruction of magnetic resonance images. Am J Sports Med 19:210–215

Toms AP, White LM, Marshall TJ, Donnell ST (2005) Imaging the postoperative meniscus. Eur J Radiol 54:189–198

Tuite MJ, Daffner RH, Weissman BN et al (2012) ACR appropriateness criteria of the knee® acute trauma to the knee. J Am Coll Radiol 9:96–103

Van der Bracht H, Verdonk R, Verbruggen G et al (2007) Cell based meniscus tissue engineering. In: Ashammakhi N, Reis RL, Chiellini E (eds) Topics in tissue engineering. Biomaterials and Tissue Engineering Group (BTE), London, UK

Van Dyck P, Gielen J, D'Anvers J, Vanhoenacker F, Dossche L, Van Gestel J, Parizel PM (2007) MR diagnosis of meniscal tears of the knee: analysis of error patterns. Arch Orthop Trauma Surg 127:849–854

Van Dyck P, Vanhoenacker FM, Gielen JL, Dossche L, Weyler J, Parizel PM (2010) Three-tesla magnetic resonance imaging of the meniscus of the knee: what about equivocal errors? Acta Radiol 51:296–301

Vande Berg BC, Lecouvet FE, Poilvache P et al (2000) Dual-detector spiral CT arthrography of the knee: accuracy for detection of meniscal abnormalities and unstable meniscal tears. Radiology 216:851–857

Vanhoenacker FM, De Vos N, Van Dyck P (2016) Common mistakes and pitfalls in magnetic resonance imaging of the knee. J Belg Soc Radiol 100(1):99. https://doi.org/10.5334/jbr-btr.1206

Vaquero J, Forriol F (2016) Meniscus tear surgery and meniscus replacement. Muscles Ligaments Tendons J 19:71–89

Verdonk PC, Forsyth RG, Wang J et al (2005) Characterisation of human knee meniscus cell phenotype. Osteoarthr Cartil 13:548–560

Verdonk PC, Verstraete KL, Almqvist KF, De Cuyper K, Veys EM, Verbruggen G, Verdonk R (2006) Meniscal allograft transplantation: long-term clinical results with radiological and magnetic resonance imaging correlations. Knee Surg Sports Traumatol Arthrosc 14:694–706

Voloshin AS, Wosk J (1983) Shock absorption of menisectomized and painful knees: a comparative in-vivo study. J Biomed Eng 5:157–161

Weiss CB, Lundberg M, Hamberg P et al (1989) Non-operative treatment of meniscal tears. J Bone Joint Surg Am 71:811–822

White LM, Schweitzer ME, Weishaupt D, Kramer J, Davis A, Marks PH (2002) Diagnosis of recurrent meniscal tears: prospective evaluation of conventional MR imaging, indirect MR arthrography, and direct MR arthrography. Radiology 229(1):159–163

Williams A, Qian Y, Golla S et al (2012) UTE-T2∗ mapping detects sub-clinical meniscus injury after anterior cruciate ligament tear. Osteoarthr Cartil 20(6):486–494

Wright DH, De Smet AA, Norris M (1995) Bucket-handle tears of the medial and lateral menisci of the knee: value of MR imaging in detecting displaced fragments. AJR Am J Roentgenol 165:621–625

Xu C, Zhao J (2015) A meta-analysis comparing meniscal repair with meniscectomy in the treatment of meniscal tears: the more meniscus, the better outcome? Knee Surg Sports Traumatol Arthrosc 23:164–170

Knee: Ligaments and Tendons

Eugene McNally and Graeme Thompson

Contents

Abstract

The knee has no intrinsic osseous stability and relies primarily on strong intra- and extra-articular ligaments to perform this task, aided by dynamic muscular forces. The cruciate and collateral ligaments are the most important of these and knowledge of the patterns of injury leading to their disruption is vital when interpreting MRI studies following trauma, either direct or indirect. Studies of the outcomes of ligament repair and reconstruction have highlighted the ligaments of the posterolateral and more recently the posteromedial corners, although their importance is yet to be firmly established. These ligaments are often small, but improving MRI resolution and reliable indirect signs make assessment possible in most studies. For comprehensive descriptions of anatomy with illustrations, please see the many excellent articles referenced.

1 Introduction

This chapter is divided into two main parts, the intra-articular ligaments and extra-articular ligaments of the knee. This division is important as the extra-articular ligaments are not visible on routine arthroscopic procedures and consequently MR plays a most important role in their evaluation.

E. McNally (✉) · G. Thompson
Oxford Musculoskeletal Radiology, Oxford, UK
e-mail: eugene.mcnally@gmail.com; graemevthompson@gmail.com

Med Radiol Diagn Imaging (2020)
https://doi.org/10.1007/174_2020_255, © Springer Nature Switzerland AG
Published Online: 01 January 2021

2 Intra-articular Ligaments

The principle intra-articular ligaments are the anterior cruciate and posterior cruciate ligaments. Minor ligaments include the anterior intermeniscal ligament, the posterior intermeniscal ligament, the meniscofemoral ligament, the oblique intermeniscal ligament and the infrapatellar plica.

2.1 The Anterior Cruciate

2.1.1 Anatomy

The anterior cruciate ligament (ACL) runs from a semicircular origin on the medial aspect of the lateral femoral condyle, in a spiral course forwards, and laterally to a fan-shaped insertion on the anterior tibial eminence. In its proximal portion it runs parallel to the intercondylar roof. It is composed of a number of collagen fibre bundles which are organised into two principle bundles. The largest of these, the anteromedial bundle, comprises densely packed fibres compared with the more loosely packed posterolateral bundle. The anteromedial bundle becomes taut in flexion, when most of the ligament is relaxed. In extension, the larger, posterolateral portion is under tension (Remer et al. 1992). The attachment sites are like other entheses, with a transitional zone of fibrous and mineralised cartilage. The ligament is intra-articular but extrasynovial and is enclosed in a fibrous connective tissue sheath which also contains a little fluid. The size of the ACL averages 4 cm long and 1 cm thick, but differs between the sexes, being slightly smaller in women. The femoral notch is also correspondingly smaller and these findings may account for the differences between the sexes in the incidence of ACL injury (Charlton et al. 2002). Neurovascular supply to the ACL is from the lateral geniculate artery and tibial nerve branches, respectively.

2.1.2 Imaging

On most sequences the anterior cruciate ligament is easily identified as a structure of low signal intensity (Fig. 1). The anteromedial bundle is best depicted on sagittal sections, where the taut

Fig. 1 Normal ACL. Sagittal fat-suppressed proton density MR image. Note the hypointense line representing the anteromedial bundle (arrow). The fibres spread out as they approach the tibial insertion (arrowhead)

ACL shows as a hypointense line which can be traced from origin to close to the insertion on the tibia. In the insertional area, the fibres of the anteromedial bundle spread out and may therefore become poorly defined as the space between them is filled with fluid, fat or connective tissue. This apparent loss of conspicuity of the ligament should not be misinterpreted as an insertional tear. The posterolateral bundle is more poorly defined but can be identified as a number of strands separated by fluid and connective tissue. A number of variants in the normal appearance can be identified. Occasionally linear confluence of fluid can be seen separating the fibre bundles (Fig. 2). This is particularly evident on gradient echo. In children the lower third of the ligament in particular can be poorly defined. Indeed in very young children the anteromedial bundle in its entirety may be poorly demarcated making interpretation of anterior cruciate ligament rupture more difficult. Fortunately, in children it is a

Fig. 2 Normal ACL. Sagittal coronal fat-suppressed proton density MR image showing prominent fluid lines between fibres (arrow)

Fig. 3 Normal ACL. Coronal fat-suppressed proton density MR image demonstrating the origin of the ACL from the medial aspect of the lateral condyle (arrow)

rare injury and when it occurs it is usually an avulsion injury from the tibial insertion.

A maximum slice thickness of 4 mm is recommended to ensure that the ligament is properly seen. Orientation of images along the axis of the ACL can be helpful. The anterolateral margin of the lateral femoral condyle can be used as a guide. In practice, with 3–4 mm slices on modern imaging equipment, angulation is rarely necessary, though it is useful to show the anterior cruciate in a single slice. Sagittal images can be supported by coronal and axial sections and all three planes are often needed for accurate diagnosis. These can be particularly helpful in providing alternative visualisation of the femoral origin which can sometimes be difficult to depict on sagittal images (Fig. 3).

2.1.3 Injuries to the Anterior Cruciate

Sports injuries account for a high proportion of injuries to the ACL. The injury can occur in a variety of mechanisms, but most frequently occurs with tibial internal rotation and valgus. It is an especially common skiing injury, where two main mechanisms cause ACL rupture: valgus-external rotation and flexion-internal rotation. The latter is more common in women and older skiers (Jarvinen et al. 1994). Valgus results in distraction of the medial joint compartment and impaction of the lateral femoral condyle with the lateral tibia plateau. There is a 6% 5-year incidence in professional soccer players (Pereira et al. 2003), 4% of Australian rules football (Gabbe and Finch 2001) and 2% of American footballers in the NFL (Bradley et al. 2002). The rate is likely to be higher in semi-professional and amateur players.

Typically the patient will describe an instantaneous moment of injury, where indeed an audible 'pop' may be heard. This is followed by slow-onset haemarthrosis occurring 2–3 h after the event. The delay is due to a slow drip from the investing blood vessels. Signs of injury are divided into primary (those that directly depict the tear) and secondary signs. Subsequent sections will describe the primary imaging findings in complete ACL rupture, changes that might suggest partial rupture, secondary signs of ACL rupture and their usefulness and associated injuries.

Fig. 4 Acute ACL rupture. Sagittal fat-suppressed proton density MR image. The ACL is torn proximally (arrow) and assumes a lax wavy configuration (arrowhead)

2.1.3.1 Primary Signs of ACL Rupture

The principal finding in acute anterior cruciate ligament rupture on sagittal orientated MR images is failure to identify the normal hypointense low-signal line of the anteromedial bundle (Fig. 4) taut between its two bony attachments. After injury, the ligament fibres are grossly disrupted and separated by haemorrhage and oedema such that it is often difficult to identify whether the injury involves the proximal, distal or midsubstance of the ligament. Less commonly the anterior cruciate ligament may displace anteriorly within the notch and present as an inability to fully extend the knee. This locked-knee presentation may mimic a bucket handle tear of the meniscus clinically. Huang et al. (2002) have described the appearance of the entrapped ACL stump as being of two types. The more common type 1 stump appeared as a nodular mass located in the anterior recess of the joint (Fig. 5). Type 2 stumps had a tongue-like fold of ACL displacing

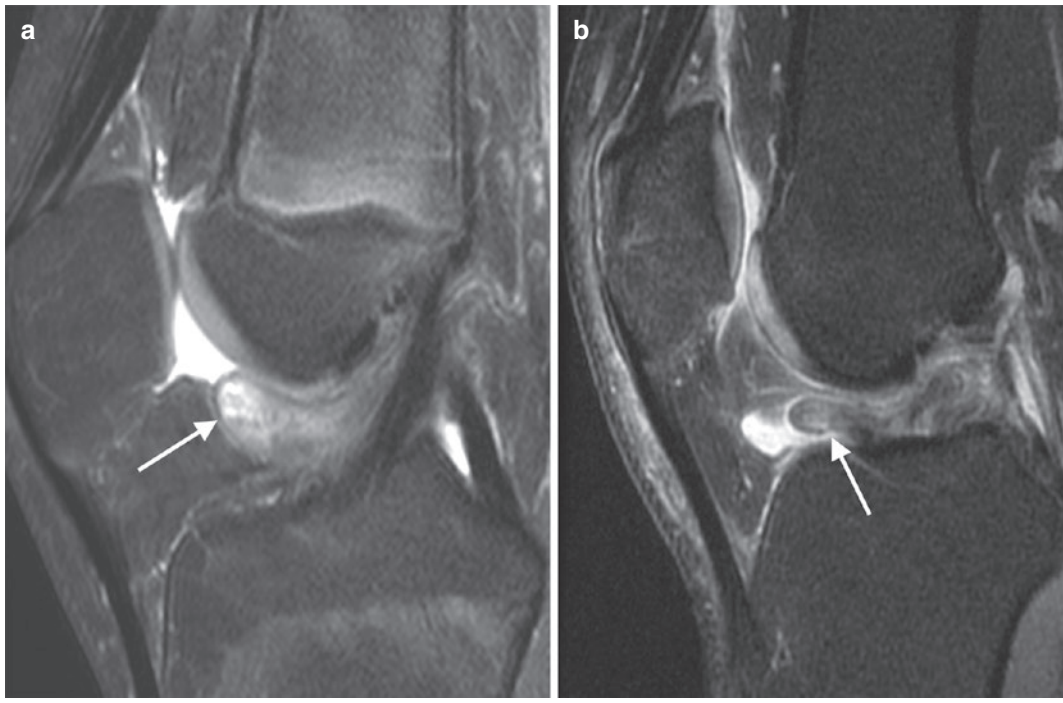

Fig. 5 ACL stump entrapment. (**a**, **b**) Sagittal fat-suppressed proton density MR images show (**a**) a nodular mass-like stump (arrow), and (**b**) a tongue-like folded stump (arrow)

out of the intercondylar notch into the anterior joint recess (Huang et al. 2002). Most often, it is often difficult to identify a displaced anterior cruciate ligament stump as the cause of impingement and should be considered in cases of knee locking where a displaced meniscal tear is not identified. The differential diagnosis on the locked knee in the absence of a displaced bucket handle tear also includes injury to other ligaments, particularly a tear of the medial collateral ligament, leading to muscle spasm and pseudo-locking. Osteochondral fragment impingement should also be considered particularly if there is a suspicion of reduced patellar dislocation. Care should be taken not to confuse a prominent oblique intermeniscal ligament for a torn anterior cruciate ligament.

The tibial attachment of the ACL may avulse with a fragment of bone which itself may be variably elevated and rotated. Such fragments can be subtle on X-ray (Fig. 6). This type of avulsion tear can be managed conservatively or undergo primary repair depending on the degree of fragment elevation and displacement.

In more chronic stages, the torn anterior cruciate ligament can undergo complete atrophy such that no remnant of the ligament is visible. In other cases, as the oedema and haemorrhage settle the torn ligament may reappear having fallen to the floor of the intercondylar groove (Fig. 7).

2.1.3.2 Secondary Signs

The primary signs described above carry strong predictive values for ACL rupture. When the primary signs of non-visualisation of fibre bundles or focal disruption and intrinsic oedema are also applied to coronal and axial images, the diagnosis can usually be firmly established (Fig. 8). A variety of secondary signs of anterior cruciate ligament disruption have been described. In the majority of cases, the primary signs have a reliability such that the secondary signs are rarely if ever of practical value. They may however be helpful in differentiating a partial or low-grade tear from a complete or high-grade injury. Secondary signs of anterior cruciate ligament rupture can be divided into three groups: (1)

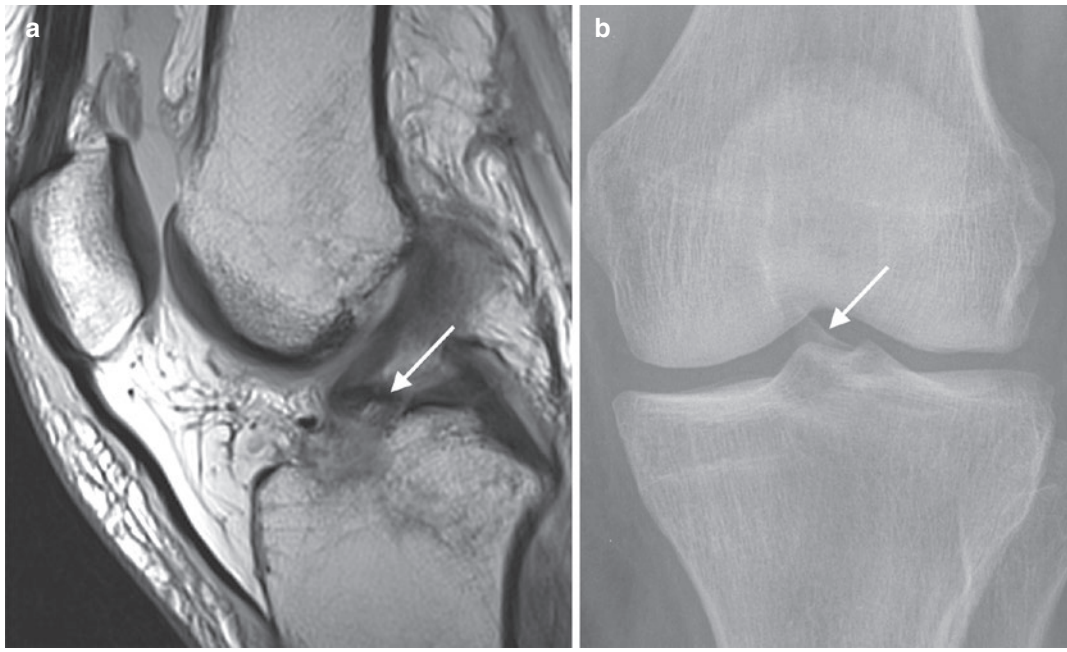

Fig. 6 (**a**, **b**) ACL avulsion. (**a**) Sagittal proton density MR image showing ACL avulsion with a displaced tibial fragment (arrow). (**b**) AP X-ray showing the subtle fragment (arrow)

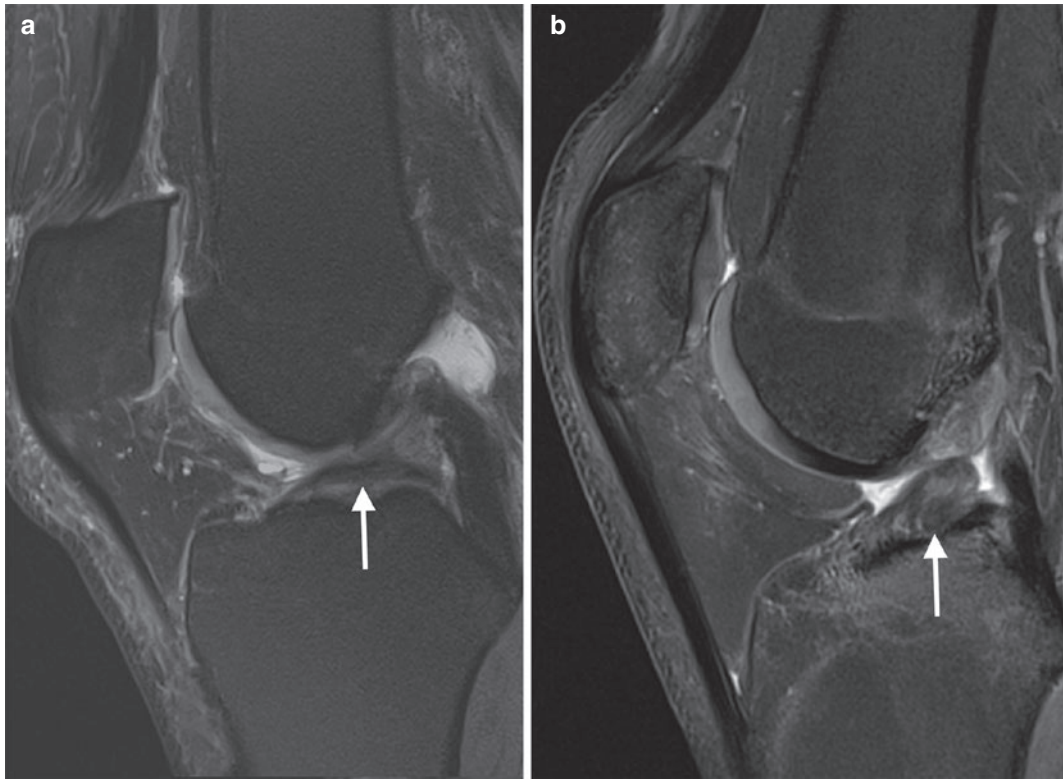

Fig. 7 Chronic ACL rupture. (**a**, **b**) Sagittal fat-suppressed proton density MR images. (**a**) The torn ACL has a horizontal configuration along the floor of the joint (arrow). (**b**) The ACL is coiled (arrow)

Fig. 8 ACL rupture. Coronal fat-suppressed proton density MR image. There is a bare area at the femoral origin of the ACL (arrows) compared with Fig. 3

those that involve a bony injury, (2) those reflecting soft-tissue injury and (3) those that reflect anterior tibial translation.

Secondary Signs: Bone Injury

Three separate bony injuries are associated with ACL rupture. The most common of these is microfracture of the posterior and lateral margin of the tibial plateau (Fig. 9). Indeed if this typical pattern of microfracture is identified, the patient should be regarded as having a torn anterior cruciate ligament until this can be firmly proven otherwise. It should be remembered that microfracture is more usually encountered in the acute phase following injury, although the finding can persist for many months. Posterolateral tibial microfracture may be associated with lateral femoral condylar microfracture in a proportion of patients. In a series reported by Kaplan

Fig. 9 Secondary bone bruise associated with ACL rupture. Coronal fat-suppressed proton density MR image. Typical location of tibial microfracture posterolaterally (arrow). There is also a feature of varus compression injury with medial microfracture (arrowhead)

et al. (1992) occult fractures were isolated in 43% of ACL ruptures and were present in combination with the lateral femoral condyle microfracture in 46%. Less common patterns were fractures in the posterior aspect of the medial tibial plateau in 7% and fractures involving all three areas in 2% (Kaplan et al. 1992). In a study of 32 patients, Murphy et al. found this pattern of posterolateral microfracture in 94% and an associated 'kissing' femoral lesion in 91% (Murphy et al. 1992). The combined pattern relates to the 'pivot shift' mechanism of injury. The femoral compression fracture is easily seen in water-sensitive MR images (Fig. 10). There is also a plain radiographic correlate to this injury; deepening of the femoral notch by more than 1.5 mm on a lateral plain film is strongly associated with ACL rupture (Cobby et al. 1992).

Fig. 10 Secondary bone bruise associated with ACL rupture. Sagittal fat-suppressed proton density MR image. Lateral condylar and tibial microfractures (arrows)

Less common are bony injuries to the posteromedial tibia (Chan et al. 1999) with avulsion of the central slip of semimembranosus from the infraglenoid tubercle. Whether this is a true avulsion due to external rotation (Yao and Lee 1989) or impaction as a result of anterior subluxation of the medial tibia during varus and external rotation (Vanek 1994) is debated. The latter has been shown to occur experimentally, but the telltale impaction injury that might be expected in the medial femoral condyle is not always present.

The Segond fracture (Fig. 11) is an avulsion fracture of the anterolateral margin of the proximal tibial plateau, originally described by a French surgeon Paul Ferdinand Segond (1879). This is a tiny avulsion flake vertically orientated on the anterolateral aspect of the tibia at the site of attachment of the anterolateral ligament. The Segond fracture results from internal rotation and varus stress on the ligament resulting in avulsion. Although uncommon, there is a very high association with ACL rupture.

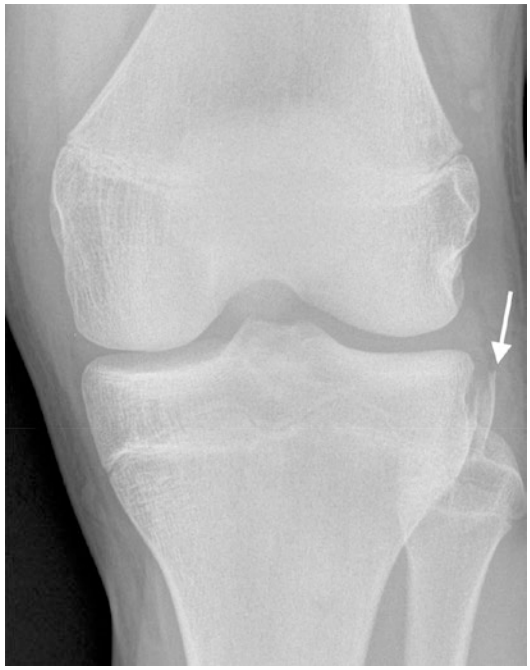

Fig. 11 Segond fracture. Plain radiograph demonstrating a vertically oriented avulsion flake fracture at the lateral proximal tibia (arrow)

Secondary Signs: Soft Tissue

In the acute phase of injury, haemorrhage and oedema result in non-visualisation of the ligament, the typical primary sign. In more chronic injuries, the torn ligament reappears as the acute haemorrhage and oedema settle. In many cases it lies in a clearly abnormal position along the floor of the joint; in others it can reattach to the femur or PCL and simulate a normal ligament. In these cases, evaluation of the ACL or Blumensaat's angle can help diagnose a tear.

ACL Angle The ACL angle is the angle formed by the intersection of the anterior aspect of the distal portion of the ACL and the most anterior aspect of the intercondylar eminence on a mid-sagittal MRI image. The normal angle lies between 53° and 56° (Gentili et al. 1994; Murao et al. 1998; Mellado et al. 2004). An angle of less than 45° is regarded as abnormal and indicative of a torn ACL. Sensitivity and specificity increase with decreasing angle, reaching 100% at angles less than 25° (Mellado et al. 2004).

Blumensaat's Angle The Blumensaat's angle is formed by the anterior aspect of the distal portion of the ACL and the intercondylar roof. By convention angles with proximal vortices are considered negative and those with distal vortices positive. As the ACL usually parallels Blumensaat's line, the angle is normally zero or up to 8° negative (Gentili et al. 1994; Lee et al. 1999; Mellado et al. 2004). An angle over 21° positive is strongly associated with ACL rupture.

Secondary Signs: Anterior Tibial Translation

An intact anterior cruciate ligament prevents forward displacement of the tibia with respect to the femur. When disrupted, tibial translation is free to occur, though it is not seen in all patients. It is less likely to occur in sporting injuries, where there is good muscle tone and particularly when the posterior portions of the menisci remain intact. In these cases, the meniscus abuts the posterior aspect of the femoral condyle and prevents anterior translation. When the tibia translates anteriorly the configuration of other structures changes, and it is these changes that are used as secondary signs. Signs of anterior tibial translation include the PCL line sign, PCL angle sign, PCL curvature ratio, femoral line sign, straight FCL sign and lateral condylar tangent.

The PCL Line Sign On sagittal images, the posterior cruciate ligament assumes a sigmoid appearance caused by forward movement of its tibial insertion with respect to the femoral origin. This is readily apparent on visual inspection, but several measures of this PCL laxity have been described. A line drawn connecting two points outlining a linear region in the distal portion of the PCL when traced proximally should intersect the medullary cavity within 5 cm of its distal aspect (Schweitzer et al. 1992). The linear area is defined by 2 points, the more distal within 3–4 mm of the PCL insertion. The sign is positive when the proximally extended line does not intersect the medullary cavity of the femur (Fig. 12). The reason for this becomes obvious when the line is drawn along the buckled PCL.

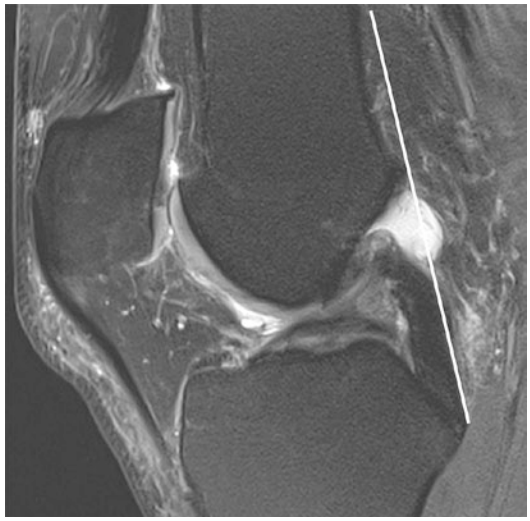

Fig. 12 Anterior tibial translation as secondary sign of ACL rupture. Sagittal fat-suppressed proton density MR image. A line drawn along the posterior margin of the PCL does not intersect the femoral medulla within 5 cm

The PCL Angle Sign As the PCL buckles during anterior tibial translation, the angle between the proximal and distal portion becomes more acute. Under normal circumstances the angle is greater than 115° and usually greater than 125°. This angle becomes more acute when the tibia has translated anteriorly (Fig. 13). Maximum angles between 96° and 111° have been described in ACL rupture. The variation in these findings probably reflects the variation in anterior tibial translation that will be present in the study populations (Gentili et al. 1994; Mccauley et al. 1994; Lee et al. 1999).

Lateral Condyle Tangent A further useful method of assessing for anterior tibial translation is to measure it directly. A tangent is drawn at the most posterior cortical margin of the lateral femoral condyle to form the baseline from which the tibial position will be measured (Chan et al. 1994). The section midway between the cortex adjacent to the posterior cruciate ligament and the most lateral section containing the femoral condyle is used. Under normal circumstances the posterior margin of the tibial plateau passes within 5 mm of this line (Fig. 14). A distance of greater than 5 mm separating the posterior margin of the tibial plateau from this line indicates anterior tibial translation.

Fig. 13 Anterior tibial translation as a secondary sign of ACL rupture. Sagittal proton density MR image in a patient with a ruptured ACL graft. The angle between the proximal and distal limbs of the PCL becomes more acute when there is tibial translation

Posterior Femoral Line The sign is positive when a line drawn at 45° from the posterosuperior corner of the Blumensaat's line fails to intersect the flat portion of the proximal tibial surface or within 5 mm of its posterior margin (Robertson et al. 1994).

Straight LCL The lateral collateral ligament runs posteroinferiorly in an oblique coronal plane from its origin on the lateral femoral condyle to the head of the fibula. On orthogonal coronal slices, the course of the ligament has to be traced to a series of adjacent slices, reflecting its oblique course. As the tibia translates anteriorly, the ligament is brought into a true coronal plane and can therefore be visualised on a single coronal slice.

PCL Curvature The bowstringing that occurs as the PCL buckles has also been quantified by (Siwinski and Ziemianski 1998; and Tung et al. 1993). The longest perpendicular is dropped from the PCL to a line drawn from the origin to

Fig. 14 Anterior tibial translation as a secondary sign of ACL rupture. Sagittal fat-suppressed proton density MR image. A line drawn tangential to the lateral femoral condyle passes more than 5 mm from the posterior tibial margin

insertion (the string of the bow). The ratio of the perpendicular to the 'string' is calculated. The more the PCL is buckled, the larger this ratio becomes, and values over 0.39 have a high specificity for ACL rupture.

Other signs that have been described include the posterior synovial bulge sign irregular anterior margin of the ACL, rupture of the iliotibial band, severe buckling of the patellar tendon, shearing injury of Hoffa's fat pad and posterior displacement of lateral meniscus (Lee et al. 1988; Weber et al. 1991; Remer et al. 1992; Schweitzer et al. 1993; Robertson et al. 1994).

2.1.3.3 Partial ACL Rupture

In the majority of cases the presence of an intact anteromedial bundle confirms an intact anterior cruciate ligament and its absence is a reliable sign of rupture. The diagnosis of partial anterior cruciate ligament rupture can be more problematic. The reported signs are neither as sensitive nor as specific as those indicating complete rupture. Focal areas of loss of signal and poor fibre definition, other than close to the insertion, kinks, buckles or loss of parallelism between the ligament and the intercondylar roof, should all be regarded with suspicion (Fig. 15).

In a study of 13 patients with arthroscopically proven partial ACL tear and using criteria which included abnormal intrasubstance signal, bowing of the ACL, or non-visualisation of the ACL on one MR imaging sequence with visualisation of intact fibres on other, in the absence of findings of complete ACL tear, the sensitivity of MR ranged from 0.40 to 0.75, and the specificity ranged from 0.62 to 0.89 (Umans et al. 1995). Lawrance et al. (1996) in a retrospective review proposed four features which helped to differentiate partial ACL tears from either complete ACL tears or normal ligaments. These were the appearance of some intact fibres, thinning of the ligament, a wavy or curved ligament and the presence of an inhomogeneous mass posterolateral to the ACL (Lawrance et al. 1996). These have not been tested prospectively. Partial tears involving only the posterolateral bundle may be identified as loss of signal at the more inferior femoral attachment with preservation of the straight anterior margin of the ACL, representing the anteromedial bundle, in the sagittal plane (Fig. 16).

In the presence of such findings, it is important to seek the secondary signs, both those of bony injury and anterior tibial translation. If secondary signs are present they are likely to indicate a high-grade tear. In the absence of secondary signs the diagnosis is more circumspect. Clinical correlation, particularly the presence of an anterior draw sign, can be helpful in identifying a significant ACL injury. Many clinicians regard a partial anterior cruciate ligament with less clinical concern if the knee is stable clinically. It is therefore more helpful for the radiologist to attempt to differentiate stable from unstable tears, rather than partial from normal/complete tears. Signs of anterior tibial translation as outlined above are likely to be indicators of an

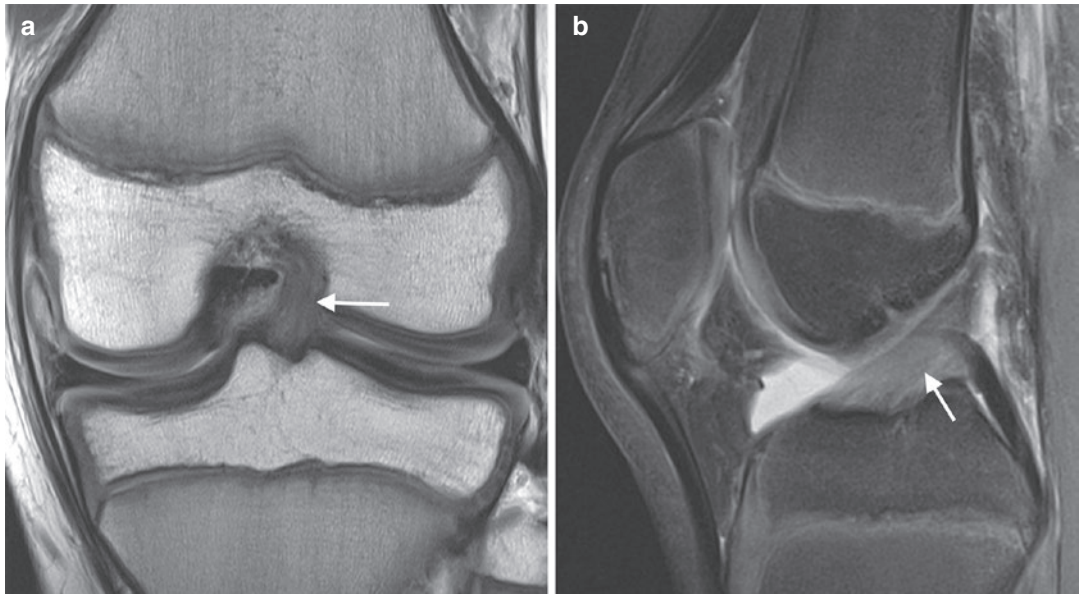

Fig. 15 (**a**, **b**) ACL partial tear. (**a**) Coronal and (**b**) sagittal proton density MR images without and with fat saturation. The ligament fibres are poorly defined (arrows), but continuous

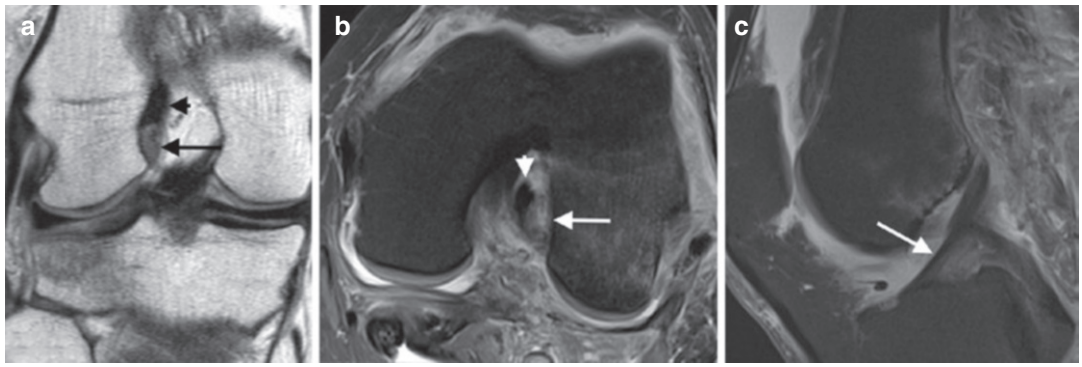

Fig. 16 (**a**) Coronal, (**b**) axial and (**c**) sagittal proton density MR images (a without fat saturation) show a tear of the posterolateral bundle (arrow) with an intact anteromedial bundle (arrowhead)

unstable tear. Roychowdhury et al. (1997) used axial images to try to differentiate stable from unstable knees. Stable ACLs were described as elliptical, attenuated or showing areas of increased intrasubstance signal intensity. Unstable ligaments showed an isolated ACL bundle, non-visualisation of the ligament or a cloud-like mass in place of the ACL. The latter are more typical of primary signs. Despite these difficulties, a combination of clinical and MRI findings is usually sufficient to allow the correct choice of management.

2.1.4 Associated Injuries

Rupture of the anterior cruciate ligament is commonly associated with injuries to other structures of the knee. The associated bony contusions have been outlined above, and the pattern and prevalence of associated soft-tissue injuries vary, dependent on the nature of the injury (e.g. type of sport) and the age of the patient. Particular care should be taken to exclude an associated meniscal tear, which will be present in up to 70% of cases. Overall lateral meniscal tears are more common; Duncan et al. (1995) found a signifi-

cantly greater preponderance of lateral meniscal tears in patients undergoing ACL reconstruction following alpine skiing injuries, where the lateral meniscus was affected in 83% of cases. Conversely, in children Prince et al. (2005) found meniscal tears occurring in 37% of patients with ACL rupture, two-thirds of which were medial. Meniscal tear patterns that are typically associated with ACL rupture include a vertical tear of the meniscal periphery (ramp lesion) and a radial tear involving the posterior portion or meniscal attachment (posterior root tear). Particular attention should therefore be paid to the posterior thirds of the menisci, especially the lateral (De Smet and Graf 1994).

From the nature of the injury anterior cruciate ligament ruptures also are associated with valgus sprain; hence tears of the medial collateral ligament are not infrequently associated. The combination of anterior cruciate ligament rupture, medial meniscal tear and medial collateral ligament injury is sometimes referred to as the 'O'Donoghue' or 'Sorry' triad. A tetrad has also been described, with the additional finding of trabecular microfracture. Although well known among radiologists, the triad is relatively uncommon. Shelbourne divided patients with ACL rupture and MCL tear according to the grade of MCL injury. Patients with grade 2 MCL injury had more medial meniscus tears than grade 3 or completely rupture MCL. Lateral meniscal tears were more common in both groups, and in the grade 2 MCL group, medial meniscal injuries were always associated with lateral meniscal injury (Shelbourne and Nitz 1991). The MCL was injured in 22% in Prince's paediatric study group (Prince et al. 2005).

Injuries to the posterolateral corner are well recognised in anterior cruciate ligament injury though there is disagreement on both their incidence and importance. It has been suggested that failure to identify a lax posterolateral corner is the commonest cause of anterior cruciate ligament graft failure, though studies to support this are lacking. Others argue that only patients who re-present with graft failure undergo detailed assessment of their posterolateral corner and the prevalence of posterolateral deficient knees in successful ACL-reconstructed patients remains unknown.

When the radiologist encounters an anterior cruciate ligament rupture, a careful checklist to look for a vertical tear, particularly of the medial meniscus, a radial tear, particularly of the posterior portion of the lateral meniscus and the posterolateral corner, should be undertaken.

2.1.5 Ganglion Cyst of the Cruciate Ligament

The ability of MRI to depict the internal anatomy of the knee with great detail has led to increased recognition of intra-articular ganglionic cysts (Vanhoenacker et al. 2003; McCarthy and McNally 2004). These are most commonly associated with Hoffa's fat pad, where they may arise from the intermeniscal ligament. Ganglion cysts are also recognised as arising from the cruciate ligaments. Bui-Mansfield identified cruciate ganglia in 1.3% of a retrospective review of over 1700 knee MRI (Bui Mansfield and Youngberg 1997). The majority were not associated with any other internal derangement. Pain was described as the most common complaint, worse on activity and sport, but medial joint line tenderness was also described. One-quarter gave a history of trauma. Only 5 (20%) of the patients in this group underwent arthroscopic debridement, and 4 had improved symptoms. On this basis, it is difficult to apply a pattern of symptoms to ACL ganglia or to comment on aetiology, though improved symptoms have been described in other studies following arthroscopic or CT aspiration (Nokes et al. 1994) (Box 1).

Box 1: Plain Radiography/CT

- Plain radiographs have little role in most sporting injuries.
- They are indicated if there has been a significant impact injury.
- Occasionally positive findings can be demonstrated in anterior cruciate ligament disruption, with depression of the lateral femoral notch, tibial translation and the Segond fracture.

- The arcuate fracture is an avulsion of a portion of the fibular head and indicates significant PLC injury.
- Lipohaemarthrosis implies a fracture in most cases; however occasionally significant synovial disruption can cause this finding.
- CT is generally required to categorise fractures of the tibia plateau.
- CT angiography is required in bicruciate injuries and where three or more ligaments are disrupted. Care should be taken to exclude subtle intimal injuries.

ACL ganglia typically have two patterns. One is where the ganglion is interspaced between the fibres of the ACL, distending its sheath with posterior bulging. The fibres of the ACL are easily seen within the sheath, though their course may be deviated by the mucinous material. This is also known as myxoid degeneration (Fig. 17).

Fig. 17 ACL myxoid degeneration. Sagittal fat-suppressed proton density MR image. The fibres of the ACL are distended and separated by mucoid material (arrow)

The second pattern is more cyst-like, where the ganglion extends from the ACL sheath, most commonly near its femoral attachment.

2.2 Posterior Cruciate Ligament

2.2.1 Anatomy

The function of the anterior cruciate ligament is balanced by its counterpart, the posterior cruciate ligament (PCL). The PCL courses from the lateral aspect of the medial femoral condyle to its insertion in a depression in the posterior aspect of the intra-articular tibia, approximately 1 cm below the articular surface. The PCL is between 32 and 38 mm in length from origin to insertion and thicker (mean 31 mm^2) and stronger than the ACL. Its main function is to prevent posterior translation of the tibia. Like the ACL, the PCL is made up of spirally arranged collagen fibre bundles. Functionally there are two fibre bundles, an anterolateral (AL) and posteromedial (PM) bundle, named for the anatomical location of the femoral insertion to the tibial insertion (Girgis et al. 1975; Vanhoenacker et al. 2001; Wind et al. 2004). Like the ACL, the two main bundles are taut at different stages in the flexion/extension cycle. The AL bundle tightens in knee flexion and loosens in knee extension. The PM bundle tightens in knee extension and is lax in knee flexion (Girgis et al. 1975). The PCL is also intracapsular but extrasynovial. It appears darker and more uniform than the ACL due to the presence of a tighter stronger investing sheath (Fig. 18). The anterolateral and posteromedial bundles are less well separated and more difficult to make out on routine MR sequences. It takes considerably more force to rupture the posterior cruciate ligaments than it does the anterior. It has a more abundant blood supply than ACL.

2.2.2 Imaging

Once again sagittal images are the mainstay for diagnosis. Spin echo provides the most homogenous depiction. T2-weighted or proton density images, preferably with fat saturation, are the best. Internal signal changes on T1-weighted images only are non-specific and may not indicate

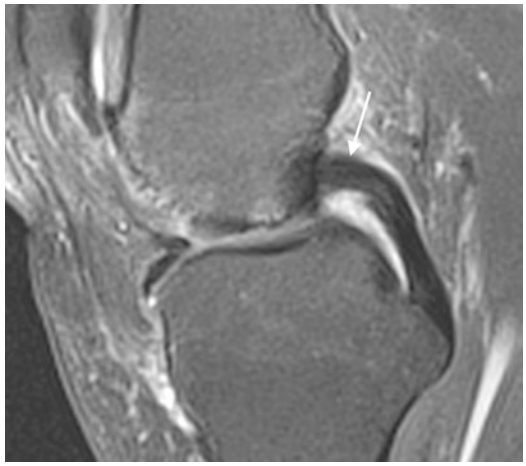

Fig. 18 Normal PCL. Sagittal fat-suppressed proton density MR image. Note the slight heterogeneity at the femoral insertion which may relate to magic angle (arrow)

Fig. 19 Gross disruption of the PCL (arrow) following anterior impact injury on a sagittal proton density image

a tear (Grover et al. 1990). Some variation in signal can be encountered in the proximal third especially on gradient echo sequences. A variety of explanations have been offered for this appearance; most likely it represents a form of magic angle phenomenon. A number of apparent focal thickenings may be identified in the region of the middle third of the ligament. This is usually due to section through prominent meniscofemoral ligaments which will be discussed later in this section.

2.2.3 Posterior Cruciate Ligament Injury

The force required to disrupt the PCL is larger than the ACL; consequently knee injuries resulting in PCL tears are most often in combination with other ligamentous injuries. The incidence of these combined injuries varies between 80% and 95% of PCL injuries, which themselves vary from 1% to 44% of all acute knee injuries (Shelbourne et al. 1999). 37% of all patients with knee haemarthrosis have an associated PCL injury (Fanelli 1993). Injuries occur more frequently in contact sports and those involving high-contact forces. Not all are symptomatic; Parolie found a 2% incidence of PCL injury among asymptomatic college football players at the NFL predraft examinations (Parolie and Bergfeld 1986). The mechanism of PCL injury in the athlete is most commonly a fall on the flexed knee with a plantar flexed foot and hyperflexion of the knee (Wind et al. 2004). Dashboard injuries account for another high proportion of PCL injuries, where the flexed knee is impacted and the tibia forced posteriorly. When this force is combined with a varus or rotational component, the lateral or posterolateral structures may also be injured. Hyperextension injuries also occur; these are associated with a higher incidence of avulsion injuries.

MRI plays an important role in the assessment of PCL injuries. This is because not all are apparent on clinical examination; even under general anaesthesia (Grover et al. 1990) and at arthroscopy the PCL can be difficult to identify in the presence of an intact ACL (Grover et al. 1990) or meniscofemoral ligament. Furthermore, untreated lesions may predispose to early-onset osteoarthritis (Cross and Powell 1984) and extensor mechanism failure.

Signs of a complete PCL tear include non-visualisation of the ligament with or without a haemorrhagic or oedematous mass (Fig. 19). Discrete tears are identified more commonly than with ACL rupture. This is thought to be due to the tighter synovial sheath within which the ligament

is invested. Tears are most commonly intrasubstance (Grover et al. 1990; Sonin et al. 1994; Mair et al. 2004). The incidence of distal versus proximal injuries is more variably reported. In Sonins group of 71 patients, 27% were proximal and only 3% distal. In contrast, Grover found distal avulsions three times more common than proximal, though the number of patients was much smaller in this study group (Grover et al. 1990). In a more recent study of 35 high-grade PCL tears, MAIR also found tibial avulsions to be more common than femoral (Mair et al. 2004). These may involve osseous avulsion (Fig. 20). The criteria for partial tear are less well defined; Sonin suggests the presence of abnormal signal intensity within the substance of the PCL or a combination of intact and disrupted fibres as signs of a partial tear (Sonin et al. 1995).

PCL injuries are isolated in about a quarter of cases (Sonin et al. 1994) with associated meniscal tears in 25–50%, medial slightly more than lateral and ligamentous injuries in 40%, most commonly ACL in a quarter and MCL in a fifth. Posterolateral corner injuries are present in approximately half of PCL injuries, but two-thirds of these will be minor with oedema around the capsule, no discernible structural abnormality and a stable knee to examination (Mair et al. 2004).

The incidence of bony injury has also been variously reported, with more recent studies identifying a higher incidence, possibly reflecting improved detection. Sonin identified microfracture in 35% (Sonin et al. 1994), whereas the incidence in MAIRS group was 83% (Mair et al. 2004). Of these 29 patients with microfracture, 16 were in the lateral tibial plateau, 10 lateral femoral condyle, 14 medial tibial plateau, 5 medial femoral condyle and 4 patella. Patients with medial bone bruises were more likely to have posterolateral ligamentous injuries and patients with lateral bone bruises were more likely to have MCL injuries.

2.3 Minor Intracapsular Ligaments

There is a large number of minor ligaments that lie within the joint. Although the function of

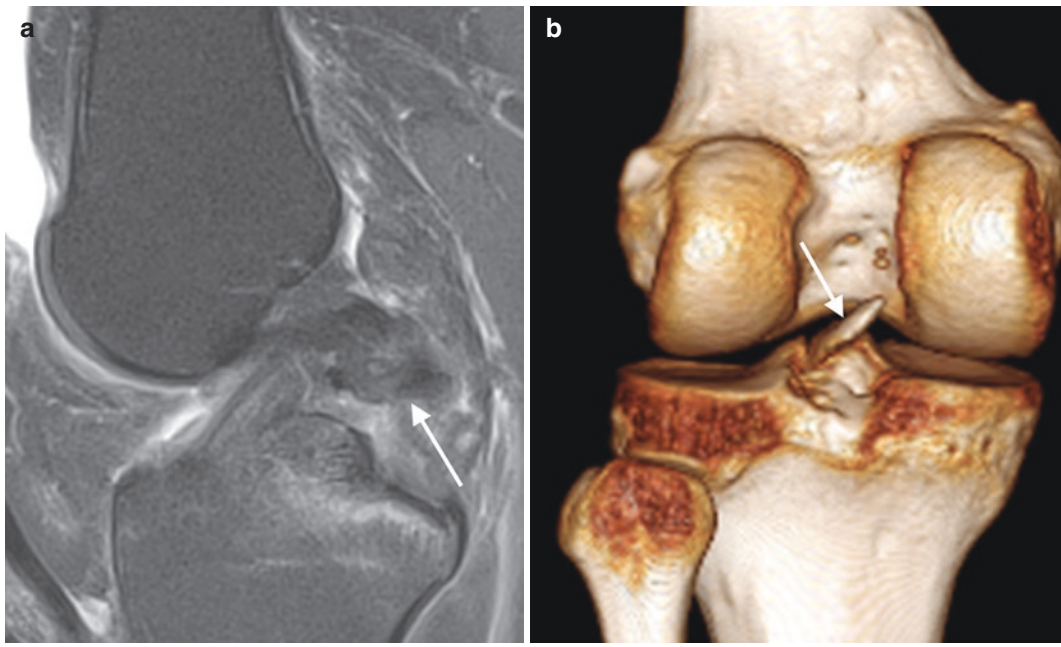

Fig. 20 (**a**, **b**) PCL avulsion fracture. (**a**) Sagittal proton density fat saturation MR image and (**b**) CT volume-rendered image. The PCL has avulsed a fragment from the tibial attachment (arrows)

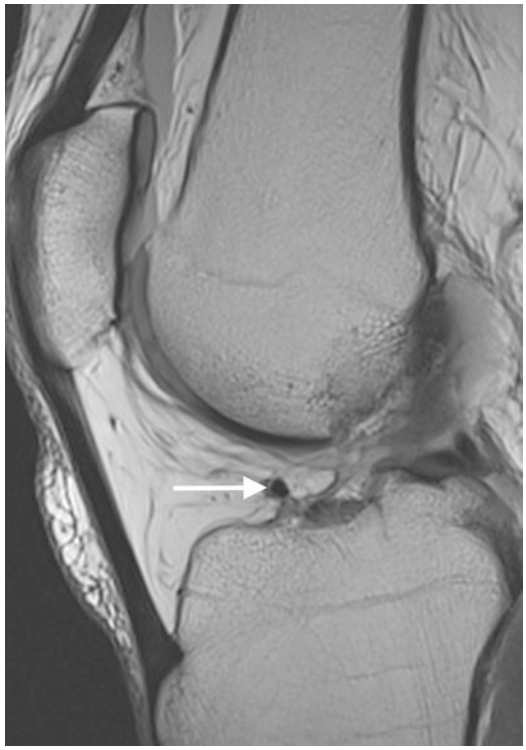

Fig. 21 The anterior intermeniscal ligament. Sagittal proton density MR image. The ligament is darker and more rounded (arrow) than the adjacent anterior horn of the lateral meniscus. It can be followed on serial sagittal images

these ligaments is incompletely understood, from a radiological perspective disruption rarely imparts clinically significant instability. Their impact on imaging therefore is mainly that they mimic other pathology when enlarged or prominent and can thus lead to difficulties in interpretation.

2.3.1 Intermeniscal Ligaments

There are three intermeniscal ligaments, anterior, posterior and oblique. The anterior ligament runs between the two anterior meniscal horns. Also called the transverse geniculate ligament or anterior transverse ligament, it is 33 mm long and its average midsubstance width is 3.3 mm (Nelson and LaPrade 2000) (Fig. 21). Whilst the attachments were most commonly to the substance of the menisci themselves, some variation is seen and in some cases the ligament attaches to the capsule anterior to the meniscus (Nelson and LaPrade 2000). On MRI, a cord-like structure representing the anterior intermeniscal ligament can be identified in most studies. The ligament is generally round or oval shaped and can be quite prominent. The ligament attaches to the anterior portion of the menisci some distance external to the tip of the horn (Fig. 22). As a consequence, a small slither of fluid can gather between the ligament and the meniscus. When the ligament is prominent this can mimic a meniscal tear. The anterior intermeniscal ligament runs at the posterior tip of Hoffa's fat pad, either through the fat or just below it. Hoffa's ganglia, which are multiloculated fluid-filled structures, are most commonly found in this location; indeed the ganglia may arise from degenerative or possibly post-traumatic changes to the anterior intermeniscal ligament.

There is also a posterior intermeniscal ligament although this is less prominent than the anterior and is less commonly visualised in its entirety. A further ligament runs in the transverse plane from the anterior horn of the medial meniscus to the posterior horn of the lateral meniscus (Fig. 23) or vice versa. This is called the medial or lateral oblique intermeniscal ligament depending on the anterior meniscal origin and has a prevalence of 2–4% (Tyler et al. 2010). It separates the posterior cruciate ligament from the anterior cruciate ligament. When it is prominent it can give the impression of additional tissue lying within the notch (Sanders et al. 1999). It therefore lies in a differential diagnosis which includes rupture of the anterior cruciate ligament with the torn ligament lying along the floor of the notch, a displaced meniscal fragment or an osteochondral loose body. Usually these can easily be differentiated. The intact anterior cruciate ligament should be readily apparent, no microfracture or fluid-blood levels are apparent to suggest an osteochondral fragment and the location of the

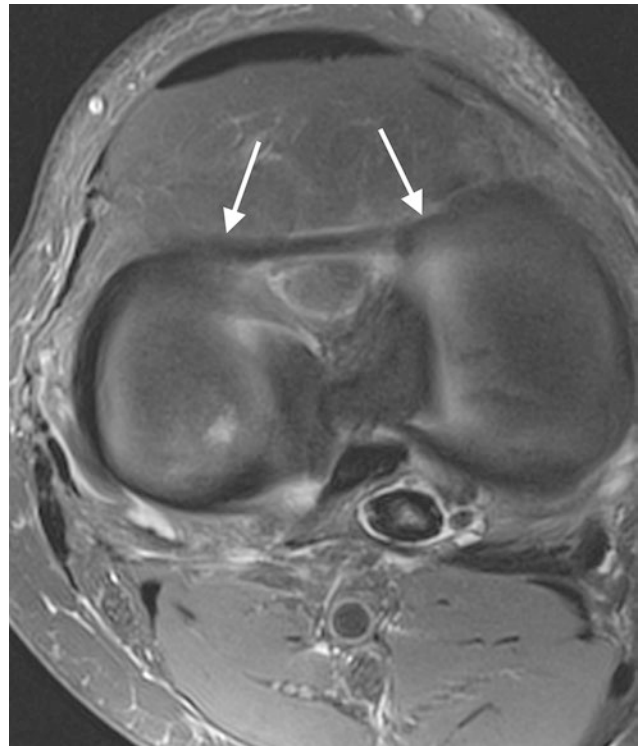

Fig. 22 The anterior intermeniscal ligament. Axial fat-suppressed proton density MR image. The ligament attaches external to the tips of the anterior horns (arrows)

structure between the two cruciates should provide useful clues. Once the diagnosis is considered, the structure can be traced on the workstation on sequential images between the two meniscal horns.

2.3.2 The Meniscofemoral Ligament

Close to the attachment of the posterior intermeniscal ligament to the lateral meniscus is a further ligament which runs superiorly and obliquely to the lateral aspect of the medial femoral condyle. The meniscofemoral ligament (MFL) is a prominent intra-articular structure. It has two components, either one of which can be dominant. One component runs posterior to the posterior cruciate ligament when it is given the name 'ligament of Wrisberg'. A second component runs anterior to the PCL whence it is called the 'ligament of Humphrey' (Vanhoenacker et al. 2001). There is considerable variation in the size of the MFL. Care must be taken not to mistake an often separated bunch of PCL fibres, which has been termed the oblique PCL (Fig. 24), from the MFL (Gupte et al. 2002). They are believed to play a role in protecting the lateral meniscus from femorotibial compression by pulling it forward when the knee is flexed (Heller and Langman 1964).

One or other of the MFL will be visualised on over 80% of MR examinations (Lee et al. 2000; Grover et al. 1990). Like the intermeniscal ligaments, the principal impact of the MFL is to mimic a tear of the posterior horn of the lateral meniscus. Fluid can gather between a prominent MFL and the meniscus simulating a tear (Fig. 25). This is more obvious when the MFL is enlarged. In these cases, it should be appreciated that the posterior horn of the lateral meniscus is approximately the same size as the anterior horn. The normal meniscofemoral ligament inserts onto the posterior horn of the lateral meniscus 14 mm lateral to the lateral margin of the PCL or less than

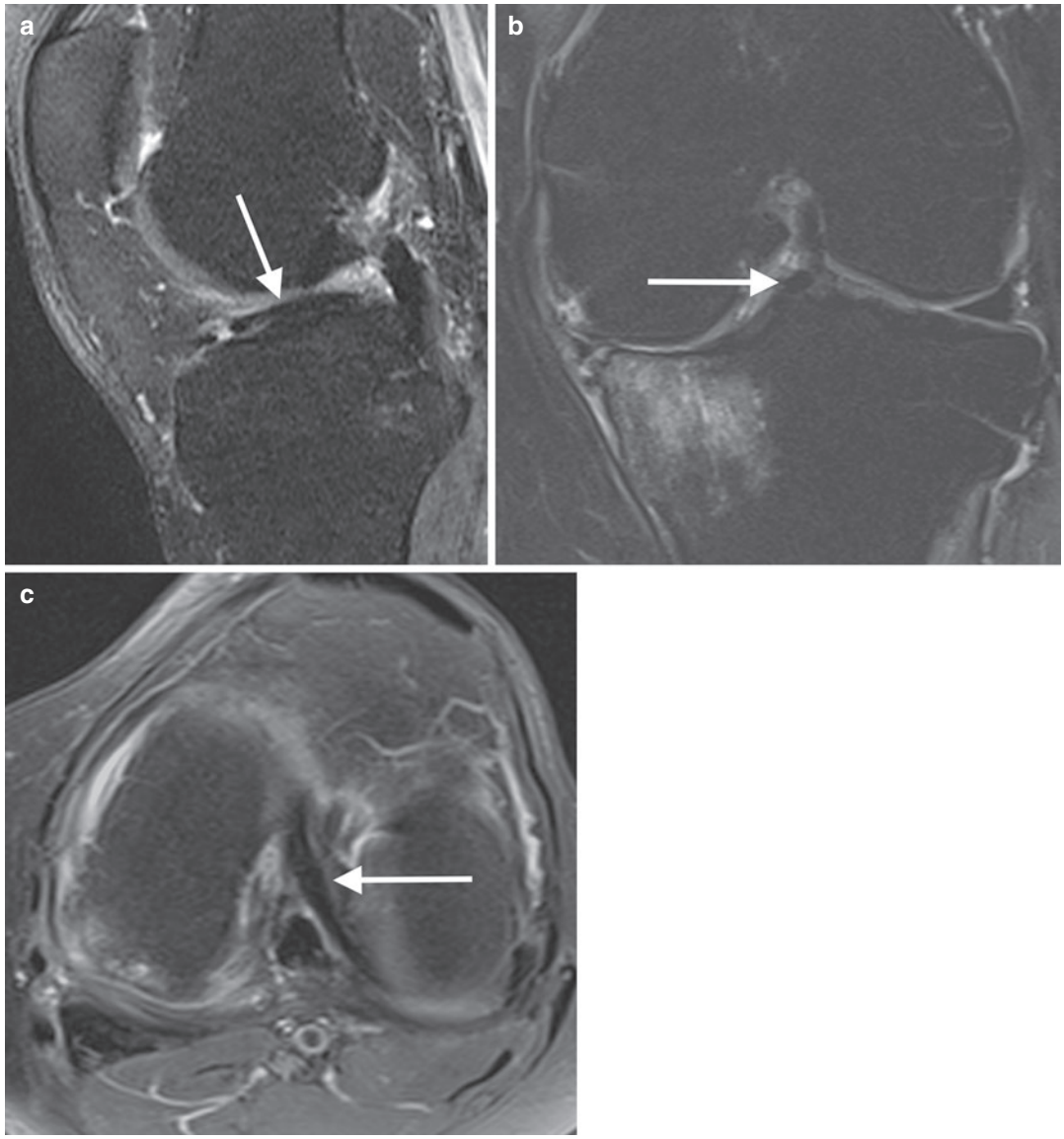

Fig. 23 (**a**–**c**) A prominent oblique intermeniscal ligament. (**a**) Sagittal, (**b**) coronal and (**c**) axial fat-suppressed proton density MR images. The ligament (arrow) can mimic a torn ACL, displaced meniscal fragment or an osteochondral loose body lying in the notch

four sagittal slices (3 mm thickness and 0.5 mm gap). If the vertical cleft between ligament and meniscus persists for four or more slices then a peripheral meniscal tear known as a Wrisberg rip should be considered (Fig. 25). These are thought to occur in association with ACL tears because of traction of the ligament on the meniscus (Park et al. 2007). As for the intermeniscal ligaments, tracing the ligament medially to its insertion also confirms its true nature. Comment on the MFL is important in patients with posterior root tears as they may help to stabilise the meniscus.

Fig. 24 The false MFL or oblique PCL. Coronal fat-suppressed proton density MR image. This ligamentous structure (arrow) does not arise from the lateral meniscus and in fact is a bundle of PCL fibres rather than another intra-articular ligament. The meniscofemoral ligament (arrowhead) is also shown

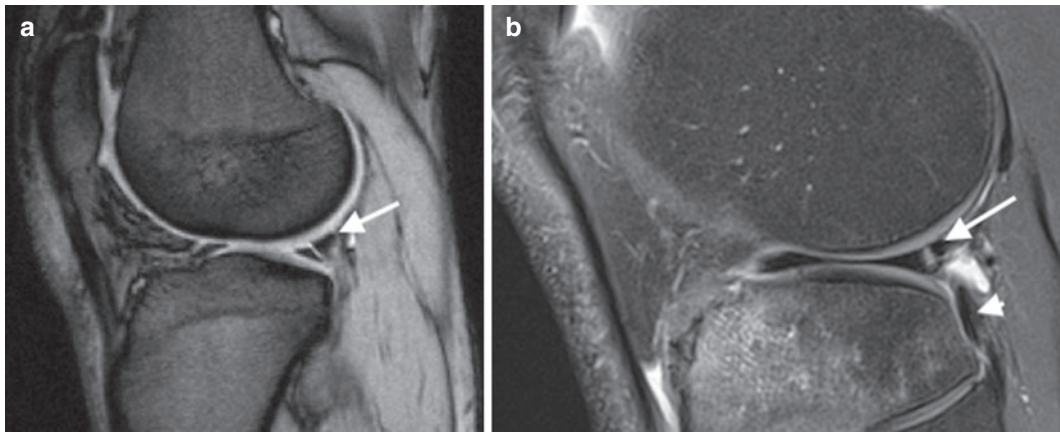

Fig. 25 (**a**, **b**) Pseudotear of the meniscus due to MFL. (**a**) Sagittal gradient-echo MR image. MFL (arrow) attachment to the posterior third of lateral meniscus simulating a tear. (**b**) Sagittal proton density fat-saturated image. Cleft persists too far laterally (arrow) indicating a Wrisberg rip. Note the popliteus tendon (arrowhead)

2.3.3 Miscellaneous Intra-articular Minor Ligaments

A number of other rarer variants of meniscofemoral attachments have been described. The infrapatellar plica or ligamentum mucosum runs an arcuate course from its posterior femoral attachment just anterior to the ACL, anteriorly and inferiorly to the tip of Hoffa's fat pad, before turning superiorly to approach the lower pole of the patella (Fig. 26). When prominent, this ligament has been reported to be misinterpreted as

Fig. 26 Ligamentum mucosum. Sagittal proton density MR image showing the ligament extending to the apex of Hoffa's fat pad

the ACL resulting in a false-negative diagnosis for ACL rupture. Anderson identified the rare anteromedial meniscofemoral ligament (Anderson et al. 2004) whose course matches the posterior portion of infrapatellar plica except for its insertion on the anterior horn of the medial meniscus or inter meniscal ligament, rather than Hoffa's fat pad (Fig. 27). A normal infrapatellar plica was found to coexist with the anteromedial meniscofemoral ligament in all cases and the attachment of the latter into the medial meniscus was clearly shown to be separate from the infrapatellar plica. An anterior meniscofemoral ligament running from the lateral meniscus to the condylar notch has also been described (Wan and Felle 1995).

3 Extra-articular Ligaments and Tendons

The stability of the knee joint to valgus or varus strain is preserved by the presence of strong ligaments on the medial and lateral aspect of the joint. They also act as secondary stabilisers to the cruciates, preventing anterior and posterior translation during the early phase of flexion (Rosas 2016).

3.1 The Lateral Stabilisers

On the lateral side ligamentous stability is maintained by two separate components: anteriorly, the iliotibial band and posteriorly, the fibular collateral ligament/biceps/popliteus complex.

3.1.1 The Iliotibial Band

The iliotibial band or tract (ITB) is a condensation of fibrous tissue which extends from the tensor fascia lata at the hip along the entire length of the lateral aspect of the thigh to insert on Gerdy's tubercle on the anterolateral aspect of the tibia.

The principal bundle passes close to the lateral femoral condyle, separated from it by a little connective tissue, fat and two layers of synovium lining the knee joint. In this position, it can impinge

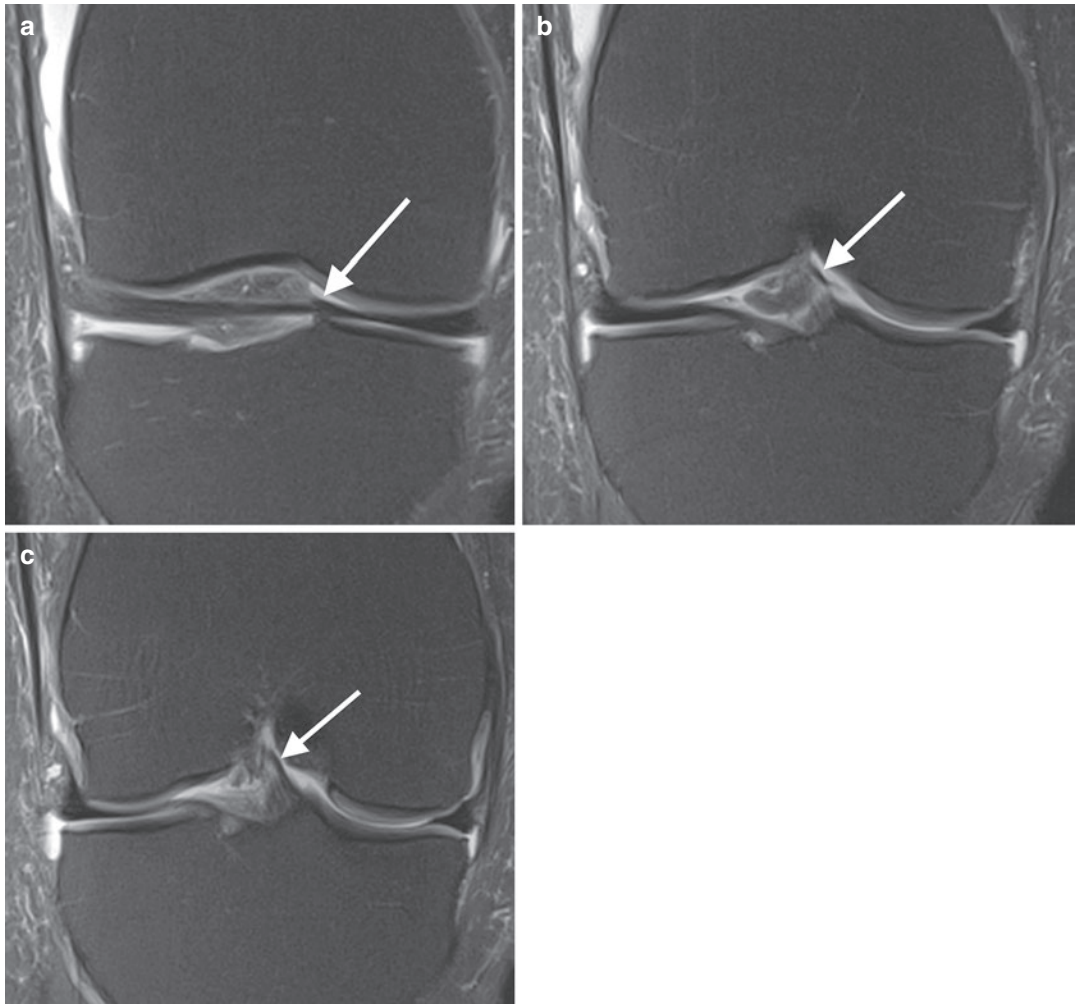

Fig. 27 Anteromedial meniscofemoral ligament. (**a**–**c**) Serial sagittal fat-saturated proton density MR images demonstrating the meniscofemoral ligament extending from the anterior horn of the medial meniscus (**a**) to the ACL (**c**)

against the lateral femoral condyle resulting in iliotibial tract friction syndrome which is also referred to as 'runner's knee'. Although classically associated with runners, step aerobics and cycling are other reported sporting associations (Holmes et al. 1993). Clinically this presents as an area of tenderness overlying the tract 2–3 cm above the knee joint. Radiologically it is best appreciated on coronal fat-suppressed images. The usual MRI finding is hyperintensity and thickening of the vascularised fat pad between the ITB and the condyle (Flato et al. 2017) (Fig. 28). Thickening of the ITB itself is less common. Care should be taken in ensuring that high signal changes are differentiated from normal joint fluid or knee effusion. Treatment by corticosteroid injection has been reported to be effective (Gunter et al. 2004) and modification of training or adjustment to cycling equipment. Rupture of the iliotibial band can occur but is uncommon. These are most commonly seen at the level of the knee joint rather than where friction syndrome occurs. Occasionally the ligament may be avulsed with a fragment of Gerdy's tubercle, usually associated with injury to the cruciates (Fig. 29). Insertional tendinosis is uncommon, but manifests as focal tenderness at the attachment with characteristic ultrasound findings (Fig. 30) (Box 2).

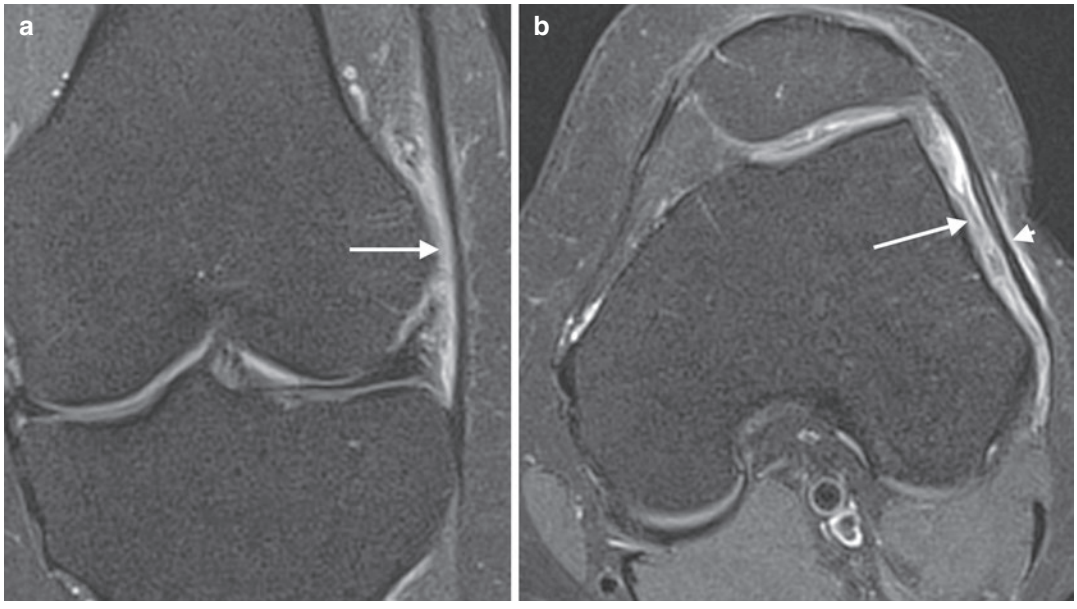

Fig. 28 (**a**, **b**) Iliotibial band friction syndrome (runner's knee). (**a**) Coronal and (**b**) axial fat-suppressed proton density MR images. Increased signal within the fat pad (arrow) deep to the ITB (arrowhead)

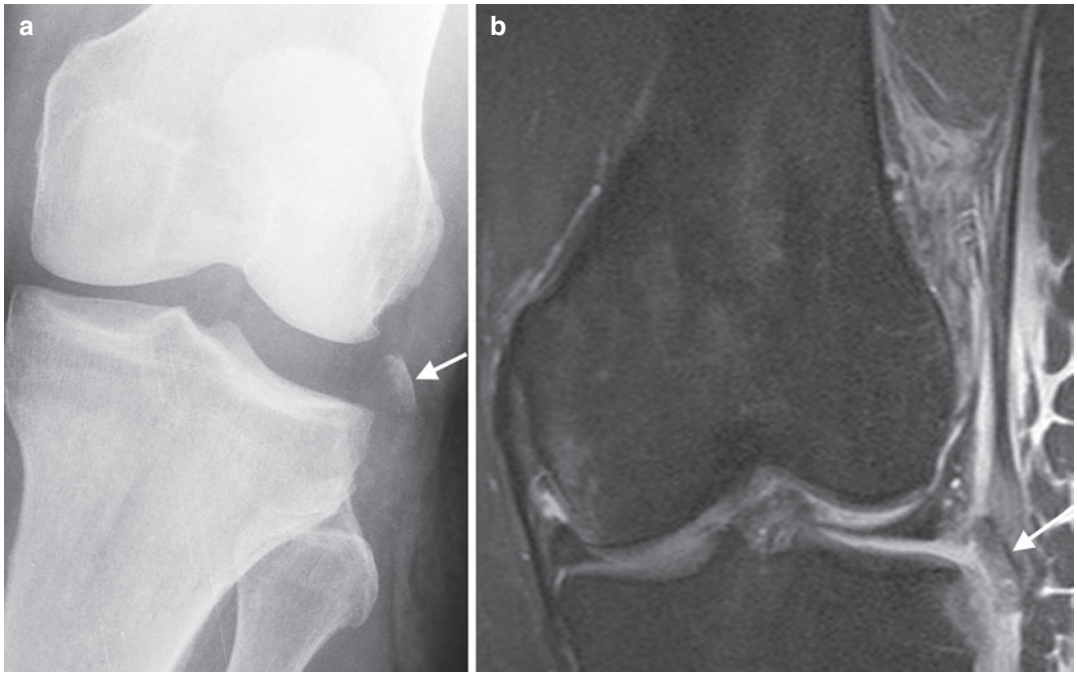

Fig. 29 (**a**, **b**) Iliotibial band avulsion. (**a**) X-ray and (**b**) coronal fat-suppressed proton density MR image demonstrating avulsion of the ITB with a fragment of bone (arrow)

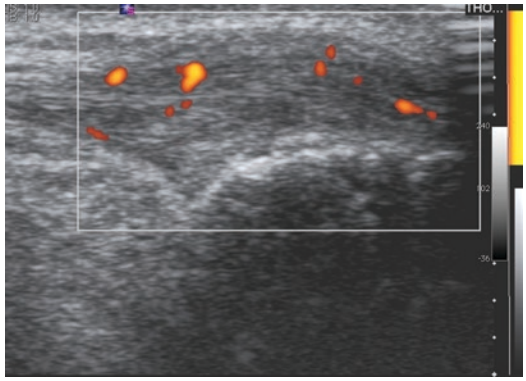

Fig. 30 Sagittal US image showing neovascularity secondary to tendinosis in the ITB insertion

Box 2: Ultrasound

- Ultrasound plays a subsidiary role to magnetic resonance imaging in many knee injuries. If the patient's symptoms are located in the anterior joint, and are focal, then ultrasound can reliably assess the quadriceps and patellar tendons.
- The collateral ligaments are also easy to see using ultrasound; however injuries to these structures are frequently associated with internal derangement and consequently MRI is necessary to demonstrate the full spectrum of injury.

3.1.2 Posterolateral Corner

The posterolateral corner is supported by the biceps femoris tendon, the fibular collateral ligament and the popliteus complex as well as a number of other smaller ligamentous structures which are condensations of the posterolateral capsule (LaPrade et al. 2000). The main one to consider is the popliteofibular ligament.

The biceps femoris tendon arises from the ischial tuberosity and descends in the posterolateral compartment to insert on the fibular head. The tendon of the long head of the biceps femoris attaches to the anterior and posterolateral aspects of the fibular head (Fig. 31), and the short head to the more anteromedial aspect of the fibular head, with a component attaching along the superolateral edge of the lateral tibia (Vinson et al. 2008).

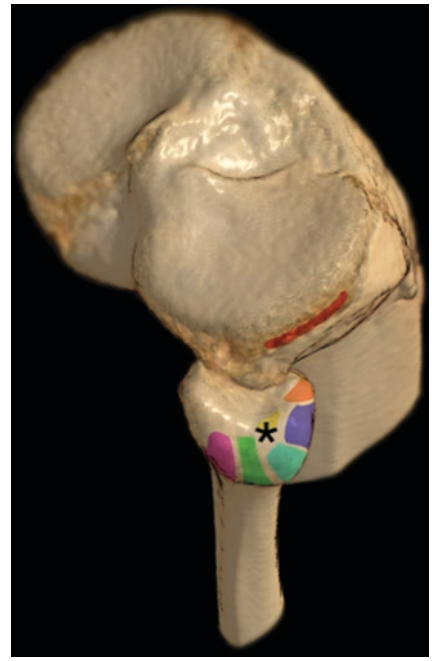

Fig. 31 3D VR CT image with colour-coded fibular and tibial insertions for the LCL/BF complex. Short-head biceps: anterior arm. Short-head biceps: direct arm. Long-head biceps: anterior arm. Long-head biceps: Direct arm. Arcuate ligament. Popliteofibular ligament. Asterisk: LCL

The fibular collateral ligament averages 67 mm in length and 3.4 mm in thickness (Fig. 32). Its femoral attachment is 3 mm posterior to the ridge of the lateral femoral epicondyle (Meister et al. 2000), above and a little anterior to the popliteus tendon. It inserts on a V-shaped bony depression that extends to the distal one-third of the lateral aspect of the fibular head, anterior and distal to the styloid, with some fibres extending along the peroneus longus fascia (LaPrade et al. 2003). The insertion can be either on its own or as a conjoint tendon with the biceps tendon. If they are separated, the insertion of the fibular collateral ligament is more anterior and medial than biceps femoris. The distal FCL is partially enveloped by the distal biceps tendon and there is an inverted J-shaped bursa between them which is not visualised when normal (McCarthy 2004).

The popliteus complex includes the muscular origin from the tibia, a fibular origin referred to as the popliteofibular ligament, the tendinous

Fig. 32 Fibular collateral ligament. Coronal proton density MR image showing the FCL in one section (arrow). This is unusual for this oblique ligament and should prompt evaluation for anterior tibial translation

insertion into the popliteus fossa, superior and inferior popliteomeniscal ligaments which form the popliteal hiatus and soft-tissue attachments to the lateral meniscus and posterior tibia (Shahane et al. 1999). The complex is important in preventing external rotation. The popliteus muscle runs from its origin on the dorsal aspect of the proximal tibia to insert into the popliteus fossa on the lateral femoral condyle.

The popliteofibular ligament is a frequently identified short, strong tendinous band (Fig. 33) measuring 47 mm long and 9 mm^2 in cross section which acts as a sling centred at the musculotendinous junction (LaPrade et al. 2003). Two divisions, anterior and posterior, are described which descend from the popliteal tendon between the hiatus and MTJ to the medial aspect of the fibular styloid (McKean et al. 2015). Its contribution to posterolateral stability is debated (Shahane et al. 1999; Maynard et al. 1996; LaPrade et al. 2003; Sugita and Amis 2001). The final component of the posterolateral corner is the posterior capsule with specifically named ligamentous condensations. These minor ligaments can be divided into the long and short ligaments. The long ligament is the fabellofibular ligament if a fabella is present and an arcuate ligament if it is not. The fabellofibular and arcuate ligaments attach to the apex of the fibular styloid. The short ligament is the popliteofibular ligament. These ligaments are variously identified on MR imaging (De Maeseneer et al. 2001). Coronal oblique imaging orientated to the posterior limb of the posterior cruciate is said to improve visualisation but this still remains less than 50% of cases. Non-visualisation therefore is difficult to interpret and tears of these specific ligaments are difficult to identify on MRI. Coronal images have also been advocated for visualising the fabellofibular ligament (Recondo et al. 2000).

Injuries to the posterolateral corner are most commonly caused by a combination of rotation and varus stress, particularly in the hyperextended knee. They are less common than medial collateral ligament injuries but are more disabling. They are associated with up to 20% of full-thickness ruptures of the anterior cruciate ligament (Temponi et al. 2017) and a high percentage of PCL ruptures when, on occasion, the clinical signs of cruciate rupture can mask the

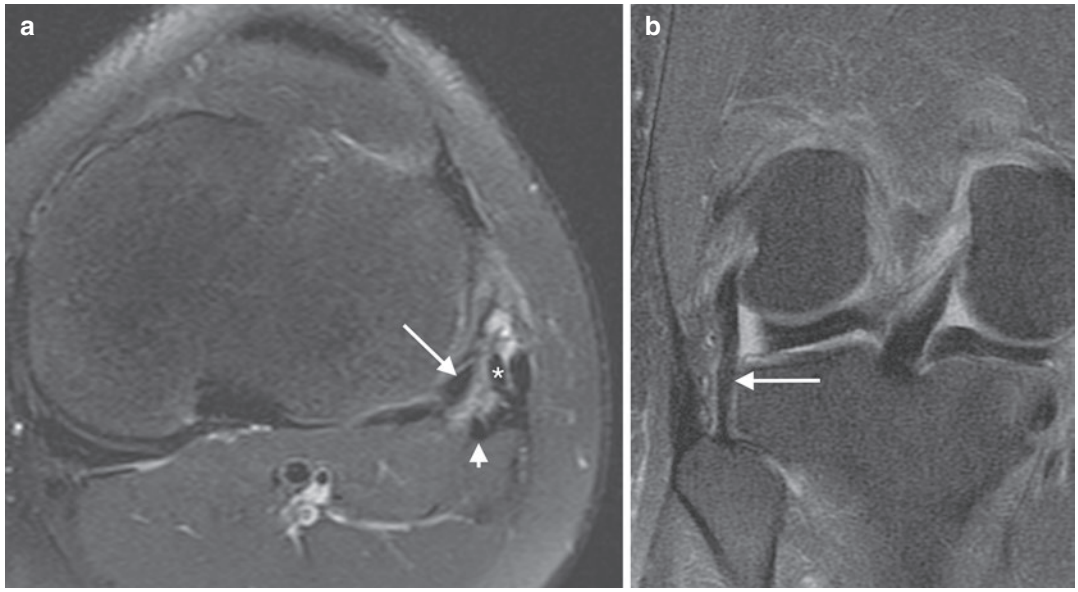

Fig. 33 (**a**, **b**) Popliteofibular ligament. (**a**) Axial and (**b**) coronal fat-saturated proton density images. The PFL is thick, possibly related to previous injury (arrow in **a** and **b**). The axial also shows the fabellofibular ligament (arrowhead) and the FCL (asterisk) with the biceps tendon lateral to it

presence of posterolateral instability. It has been said that an overlooked posterolateral corner injury is the commonest cause of anterior cruciate ligament graft failure, but not all authors agree (Box 3).

Box 3: MRI

- Magnetic resonance imaging is indicated early in the diagnosis and management of athletes with internal derangement of the knee.
- In the acutely locked knee, MRI can distinguish between mechanical and nonmechanical causes of locking. Nonmechanical causes are present in between 40% and 50% of patients, and are usually due to a significant injury to the medial collateral ligament.
- Mechanical causes include bucket handle tears of the menisci, loose bodies and impinging anterior cruciate ligament stumps.

3.1.2.1 Fibular Collateral Ligament Injury

Tears of the fibular collateral ligament are most commonly midsubstance or fibular avulsions though more proximal tears can also occur (Fig. 34). They are usually combined with other lateral injuries, though isolated injuries have been reported (Shahane et al. 1999). Lesions of the fibular collateral ligament are divided into sprains, partial tears or complete tears. Like the iliotibial tract, the external anatomical relationship of the collateral ligaments is fat. Consequently, the most subtle change of injury is fluid within subcutaneous fat abutting the ligament. Injuries are therefore best appreciated on coronal orientated images with fat suppression. The presence of oedema surrounding the ligament with an otherwise normal ligament is termed a grade 1 injury or sprain. These are largely treated conservatively. When the ligament itself becomes disorganised with increased intrasubstance signal, but remains continuous from origin to insertion, a partial tear or grade 2 injury is diagnosed (Fig. 35). Complete interruption of the normal low signal constitutes a complete rupture and is often associated with loss of axial or longitudinal tension. Occasionally fibular

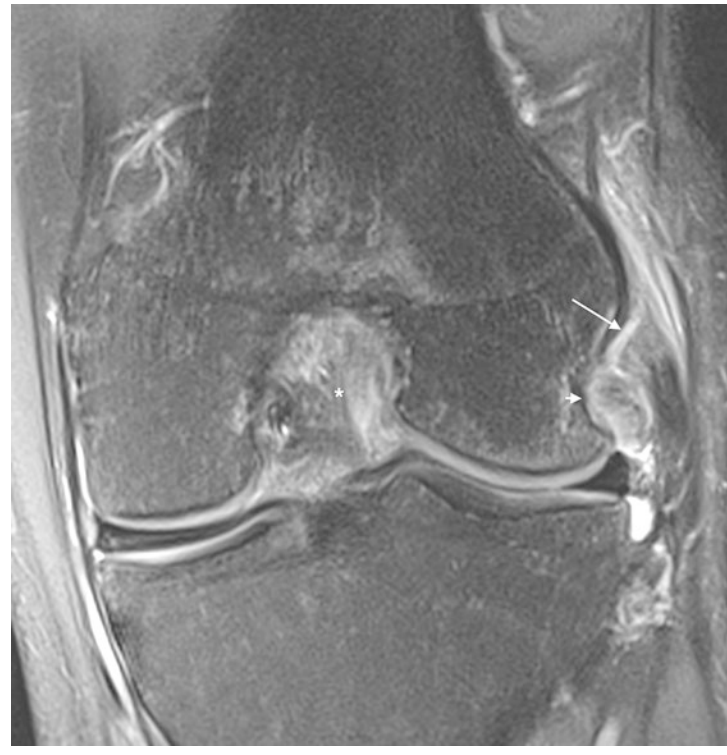

Fig. 34 Rupture of the FCL (arrow) on coronal fat-saturated proton density MR image. Note the associated tear of popliteus tendon (arrowhead) and cruciate (asterisk)

Fig. 35 Grade 2 injury of the FCL (arrow) on a coronal fat-suppressed proton density MR image

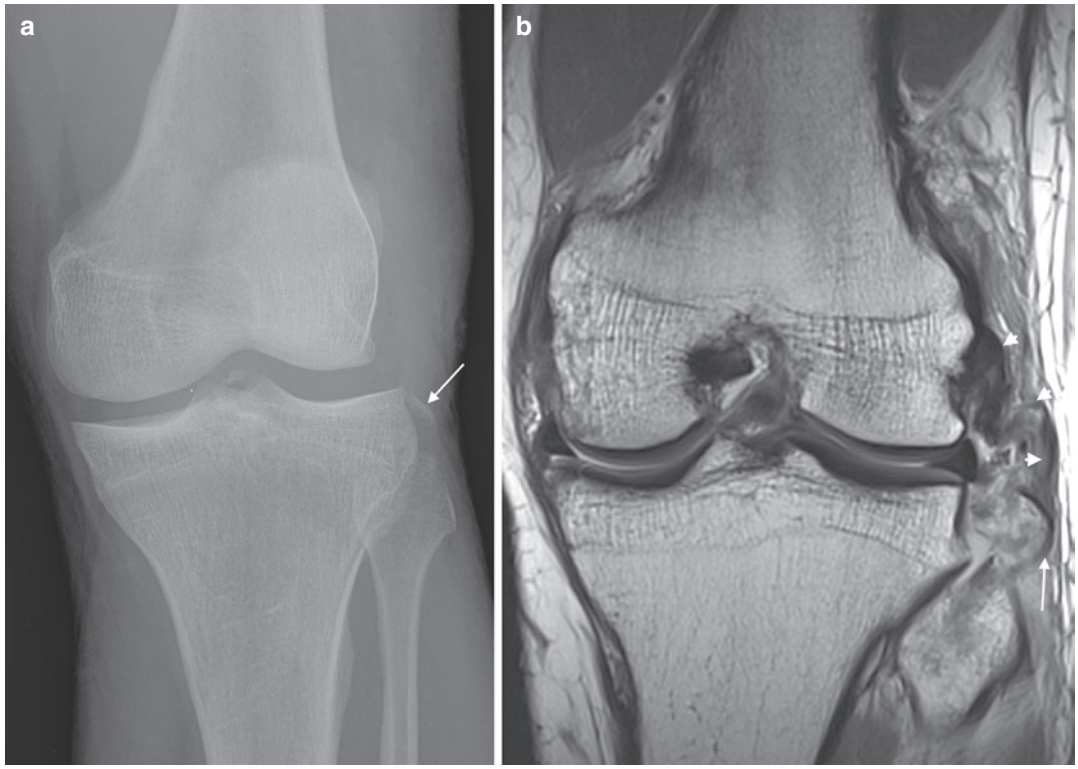

Fig. 36 (**a**, **b**) Avulsion fracture of FCL insertion. (**a**) X-ray and (**b**) coronal proton density MR image showing avulsed arcuate fragment (arrows). Arrowheads in (**b**) indicate the recoiled FCL

avulsion fractures can occur, often referred to as arcuate fractures. The PFL and arcuate ligament may avulse the tip of the styloid, with biceps/FCL avulsions involving a larger or more lateral fragment (Fig. 36). A further clue to the presence of a lateral ligament injury is microfracture in the medial femoral condyle. This occurs during varus strain with impaction of the tibial plateau against the medial femoral condyle. Complete tear or avulsion of the FCL is the most significant predictor of posterolateral instability in the presence of ACL tears (Filli et al. 2018).

3.1.2.2 Biceps Femoris Injuries

Biceps femoris injuries are less common than FCL injuries. Most often they are seen as overuse tendinopathy with thickening of the tendon just proximal to its insertion or bursitis, but when the injury is more acute a tendon tear can occur (Fig. 37). This is most commonly an avulsion fracture. Like avulsion injuries elsewhere, the degree of microfracture associated with them is less than is normally expected for fracture. The posterolateral corner is no exception and avulsion of the biceps femoris tendon can be difficult to appreciate if not specifically sought. Tracing the cortical margin of the fibula is a helpful way of assessing this. An interruption due to avulsion of a small component of the cortex is a clue to rupture and is termed the arcuate sign (Huang et al. 2003). Occasionally biceps femoris injuries can occur in conjunction with injuries to the iliotibial tract due to shared fibres (Terry and LaPrade 1996a, b). Other biceps injuries include subluxation or snapping (Bach and Minihane 2001), when the long tendon is displaced over the fibular head during knee extension from a flexed position. There may be an association with a prominent fibular head or anomalous insertions of the tendon. Subluxation may also occur in the asymptomatic population (Bach and Minihane 2001).

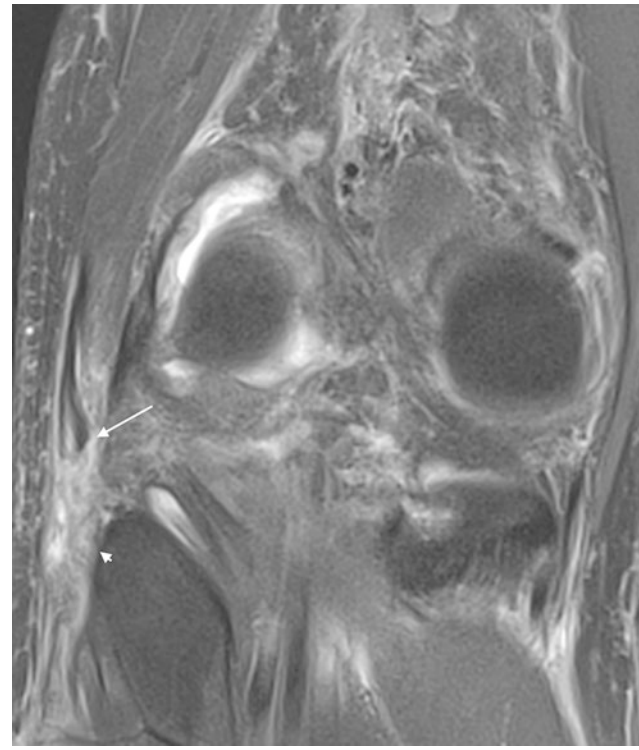

Fig. 37 Biceps tendon avulsion. Coronal fat-saturated proton density MR image. The biceps tendon (arrow) is avulsed and retracted from the lateral portion of the fibular head (arrowhead)

3.1.2.3 Popliteus Complex Injuries

Injuries to the popliteus muscle tendon complex also occur during posterolateral corner strain. The commonest site is at the musculotendinous junction (Fig. 38), but tendon tears or avulsions are also reported. An acute haemarthrosis, lateral or posterolateral tenderness and pain on resisted internal tibial rotation have been described as clinical signs (Guha et al. 2003). Anatomically, the muscle can be difficult to depict due to the oblique course it follows from origin on the posterior margin of the tibia to insertion in the popliteus fossa. Both sagittal and coronal images should therefore be perused for increased signal particularly at the musculotendinous junction. Acute findings include oedema at the musculotendinous junction or avulsion of the tendon insertion in the popliteus fossa. The popliteal recess is an extra-articular continuation of the knee synovium from the hiatus along the tendon and muscle. Fluid distension of the joint can distend the tendon sheath. On occasion, effusion in the sheath can rupture into the popliteus muscle and the finding should not be confused with muscle injury (Jadhav 2014). Loose bodies and even meniscal fragments may also displace into the bursa. Chronic injuries have been described with late-onset muscle atrophy.

Popliteus tenosynovitis has been correlated with downhill walking or skiing. Popliteus tendon snapping is a differential diagnosis for iliotibial friction and snapping. The tendon subluxes from its groove proximal to the lateral meniscus, and may be bilateral (Cooper 1999; McAllister and Parker 1999). This area cannot be appreciated at arthroscopy. The dynamic capabilities of US offer a distinct advantage over MR in depicting this entity.

3.1.2.4 Capsule and Capsular Ligaments

Tears of the individual small ligaments of the posterolateral corner are difficult to appreciate. The popliteofibular ligament is best visualised in the coronal plane above the fibular head, deep to the paired lateral geniculate vessels. On parasagittal images at the level of the popliteal hiatus, the arcuate ligament/joint capsule is deep to the lateral geniculate vessels and the fabellofibular ligament superficial. Popliteofibular ligament injuries may be directly observed in the coronal plane (Fig. 39). More useful than identifying

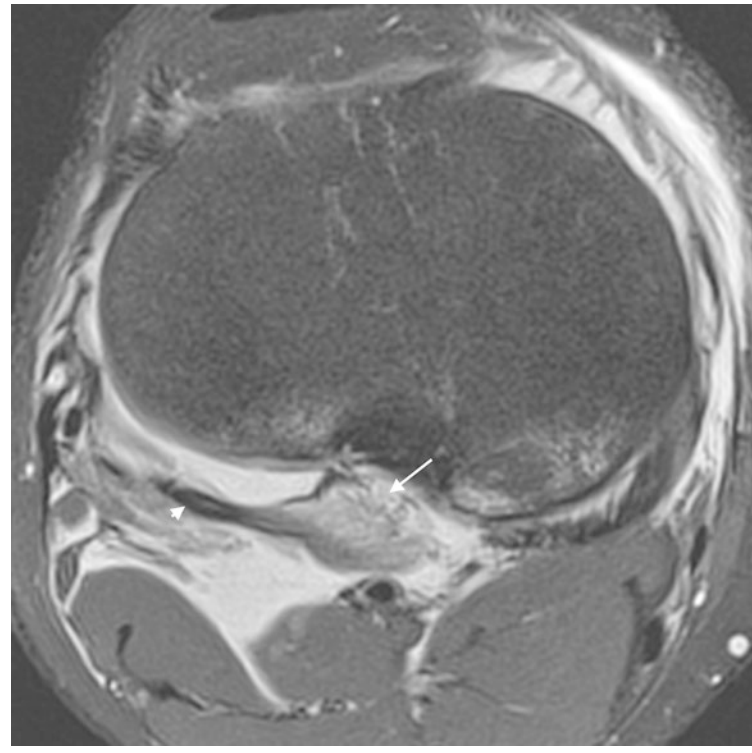

Fig. 38 Popliteus tear. Axial fat-suppressed proton density MR image revealing disruption of the musculotendinous junction (arrow). The tendon (arrowhead) is shown

Fig. 39 Popliteofibular ligament injury. Coronal fat-saturated proton density MR image. The PFL is torn (arrow) with the fibular attachment still intact (arrowhead). The popliteus tendon (asterisk) is the usual proximal attachment of the PFL

these ligaments, in the author's view, is to determine whether there is significant capsular ligament disruption by identifying abnormal pericapsular fluid with loss of the normal fat plane around the geniculate vessels (Fig. 40) or frank capsular disruption (Fig. 41), best visualised in the axial plane (Rosas 2016). The presence of fluid in the posterolateral popliteal fossa is an important finding to transmit to the referring clinician particularly if the patient is to undergo arthroscopy for associated internal derangement. In the presence of an unsealed capsular leak fluid flowing into the knee during arthroscopy can fill the posterior calf and precipitate compartment syndrome. Avulsion fractures of the fibular head also involve the styloid attachment of the PFL and arcuate ligament, but small styloid tip avulsion fractures involving only the PFL/arcuate ligament are harder to appreciate (Fig. 42).

Chronic injuries to these structures are less easy to appreciate on both clinical and imaging. Popliteomeniscal ligament tears in college wrestlers have been described (LaPrade and Konowalchuk 2005). Increased lateral meniscal motion on flexion may be a clue (Staubli and Birrer 1990) though the imaging appearances have not been described. The fascicles may also be congenitally absent (Fig. 43), either with or without a discoid meniscus, leading to instability (Van Steyn et al. 2016). There are normal deficiencies in the superior and inferior popliteomeniscal fascicles as the popliteal tendon passes through the hiatus from lateral to medial which should not be mistaken for injury.

The common peroneal nerve is fixed at its entry to the anterolateral compartment deep to peroneus longus and may be injured. The nerve should be examined for thickening and oedema. In severe injuries, total nerve disruption may occur (Fig. 44).

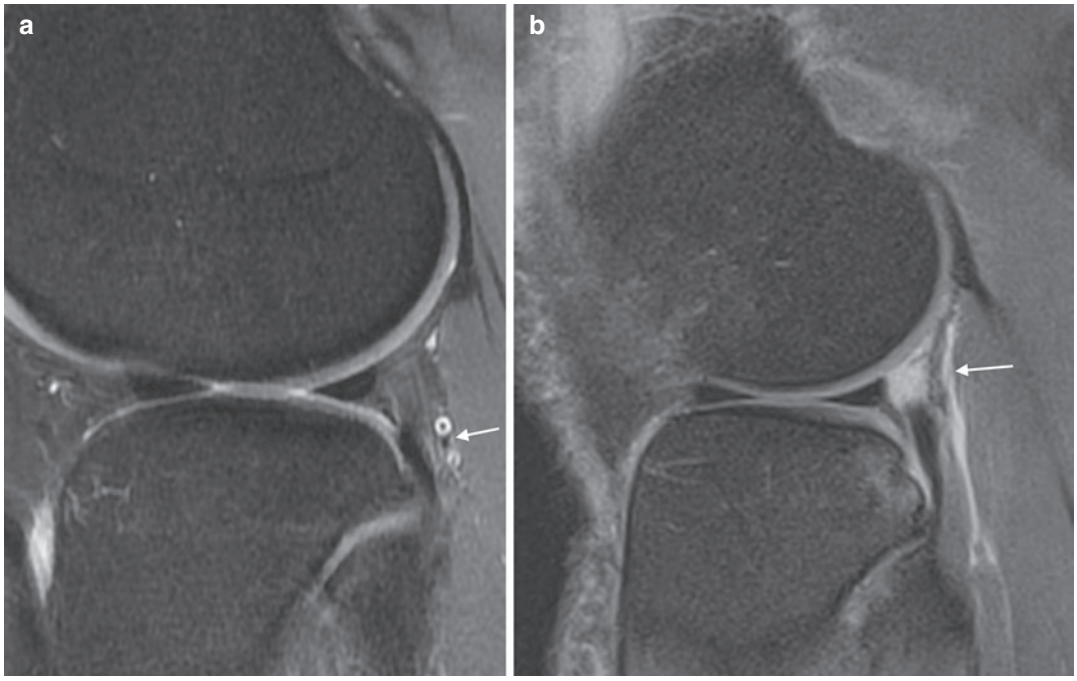

Fig. 40 (**a**, **b**) Posterolateral capsular injury. Sagittal fat-saturated proton density MR images. The geniculate vessels (arrow in **a**) are well visualised in the fat pad immediately posterior to the capsule/arcuate ligament. Fluid signal and loss of definition of the fat (arrow in **b**) are suggestive of a capsular injury and should be mentioned

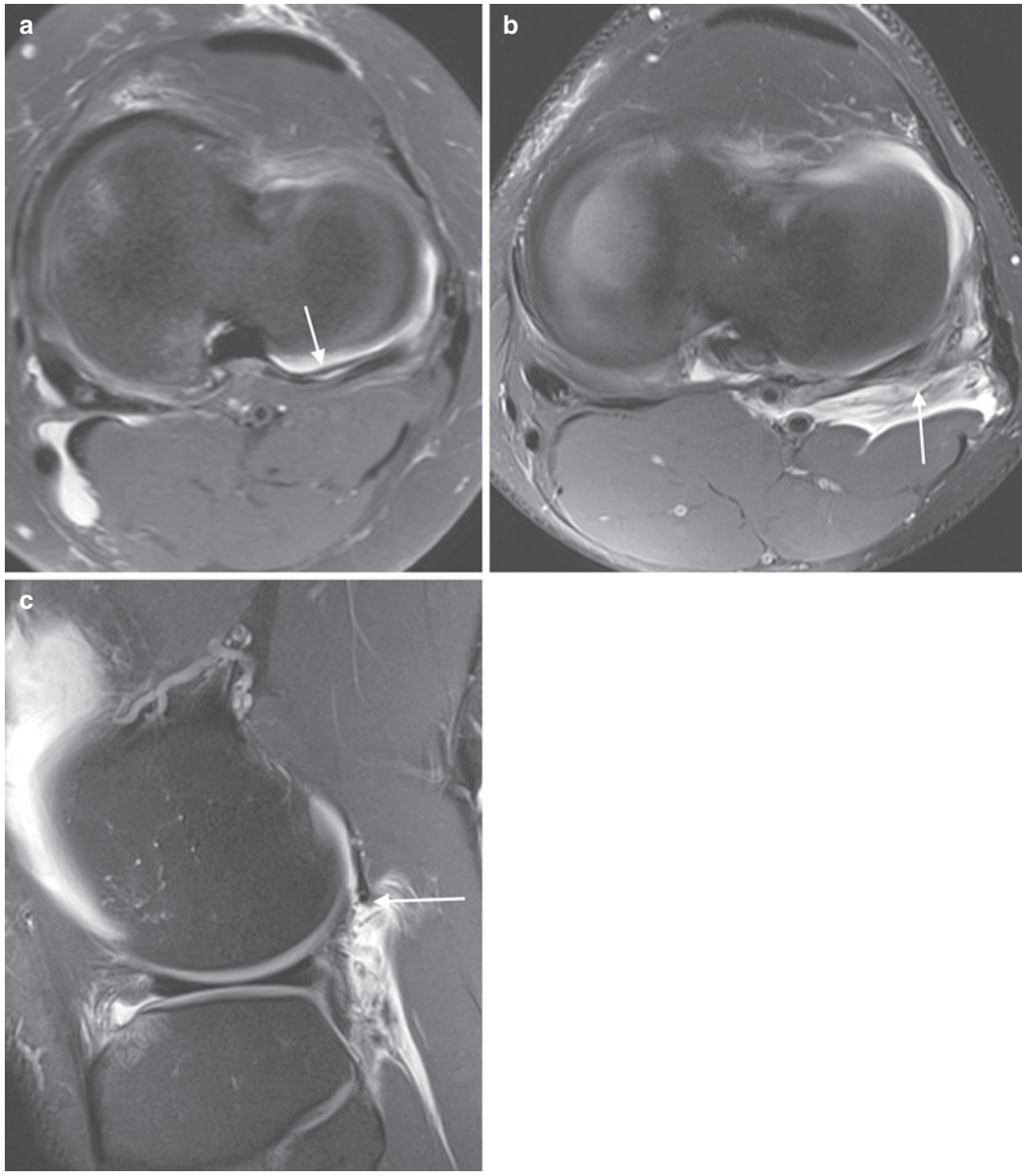

Fig. 41 (**a**–**c**) Posterolateral capsular tear. (**a**, **b**) Axial and (**c**) sagittal fat-suppressed proton density MR images. The capsule can often be seen on normal axial images (arrow in **a**). Loss of definition of the capsule with haemorrhagic fluid in the popliteal fossa in keeping with rupture. The sagittal image shows the edge of the torn capsule (arrow in **c**)

MRI plays an important role in the detection of posterolateral corner injuries as, although surgical indications and technique are still debated, if it is to be performed, then early detection and treatment (<3 weeks) are associated with improved outcomes (Geeslin and LaPrade 2011).

3.1.3 Anterolateral Ligament Injury

The anterolateral ligament, like the deep MCL, is a thickening of the anterolateral capsule which extends from the femur anterior to the LCL, to the tibia between Gerdy's tubercle and the fibular head, about 5 mm below the joint line (Patel and

Fig. 42 Arcuate ligament avulsion. Sagittal fat-saturated proton density MR image. The arcuate ligament (arrows) has avulsed a small cortical fragment from the fibular styloid (arrowhead)

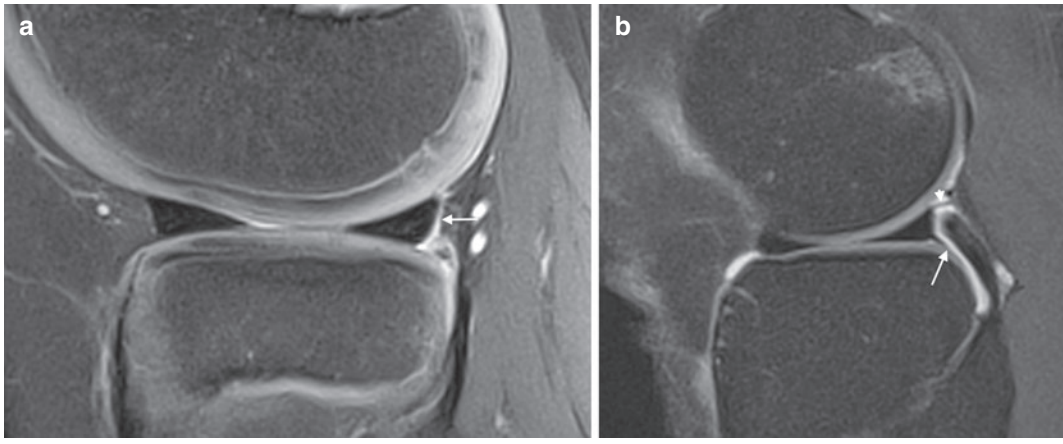

Fig. 43 Congenital absence of the popliteomeniscal fascicles. (**a**, **b**) Sagittal fat-saturated proton density MR images. The lateral meniscus is separated from the capsule (arrow in **a**) leading to instability. This can also occur as an injury. The fascicles are normally deficient where the popliteus tendon passes through (arrow in **b**)

Brophy 2018). In its course to the tibia it attaches to the body of the lateral meniscus at which point the geniculate vessels lie between it and the meniscal periphery (Van Dyck et al. 2016). There is a strong association with ACL injuries and persistent anterolateral rotational instability has been reported in 10–30% of patients after ACL reconstruction (Van Dyck et al. 2016), but the role of the anterolateral ligament is still debated and the structure is not reliably visualised on all studies. It is worth knowing that the Segond fracture is an avulsion of the meniscotibial component of the ALL (Fig. 45) and that primary fixation of the bone fragment has a good out-

Fig. 44 Peroneal nerve injury. Coronal proton density MR image. The common peroneal nerve is disrupted and recoiled (arrows) in this multiligamentous injury. The point at which the nerve is fixed at the fibular neck is shown (arrowhead)

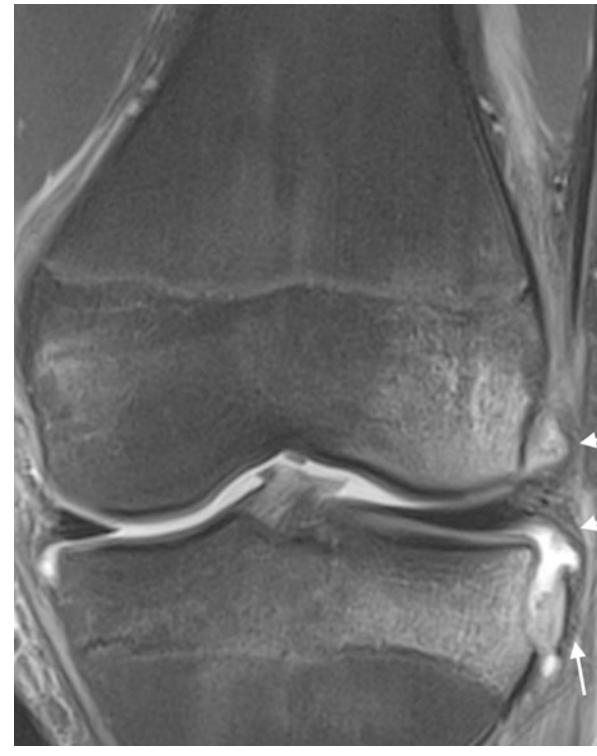

Fig. 45 Segond fracture. Coronal fat-saturated proton density MR image. The Segond avulsion fragment (arrow) is attached to the anterolateral ligament (arrowheads)

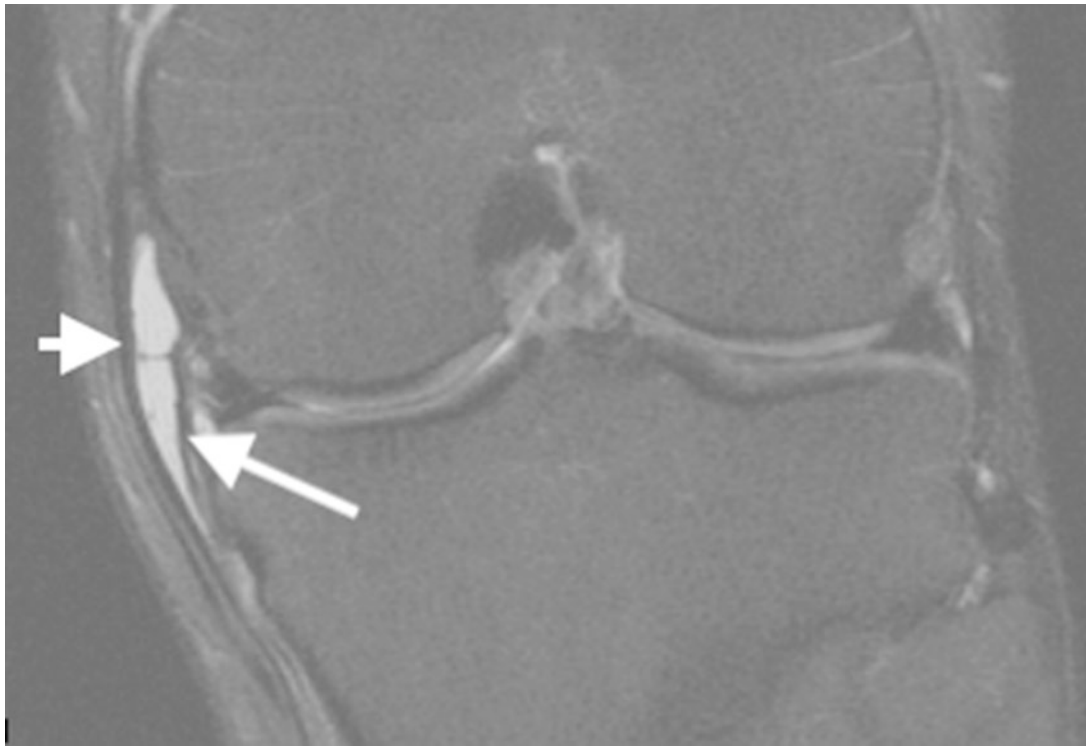

Fig. 46 Tibial collateral bursa. Coronal fat-suppressed proton density MR image. Fluid fills the TCL bursa separating the superficial fibres of the MCL (arrowhead) and the deep fibres (arrow)

come. Reconstruction, which is still not universally accepted, may be via a free graft from the ITB or lateral extra-articular tenodesis. Indications for surgery would include repeat ACL graft failure and those at a high level of sports involving pivot shift (Geeslin et al. 2017).

3.1.4 Lateral Compartment Ganglia

Just as ganglia have been described in relation to the intra-articular ligaments there are also ganglia that have been associated with the lateral ligament complex involving both the iliotibial tract (Simoens et al. 2002) and fibular collateral ligament. A more common cause of an apparent ganglion or synovial cyst posterolaterally is a synovial outpouching from the proximal tibiofibular joint.

3.2 The Medial Stabilisers

The medial knee is stabilised by the deep static components of the medial collateral ligament (MCL) and the dynamic posteromedial corner. Anteriorly the medial retinaculum and fibres of the vastus medialis obliquus provide additional support.

3.2.1 The Medial Collateral Ligament

The medial collateral ligament is made up of a number of layers. The strongest, outermost layer is the dominant structure and comprises two portions. The anterior is a strong low-signal ligament that extends from approximately 5 cm above the knee joint from the medial femoral condyle to insert 6 cm below the knee joint in a broad elongated insertion. The posterior, oblique portion of this ligament arises from the adductor tubercle, posterior to the medial epicondyle. Its insertion has three components: a tibial insertion close to the margin of the articular surface with a strong attachment to the medial meniscus, a capsular insertion and an insertion reinforcing the semimembranosus tendon. Because of the separate origin, it is often referred to as a separate

Fig. 47 Grade 1 MCL injury. Coronal fat-suppressed proton density MR image. Note the oedema medial to an intact ligament. Other evidence of valgus strain is an impaction injury to the lateral femoral condyle (arrowhead). The MCL femoral origin is of partial volume

ligament, the posterior oblique ligament (POL). Beneath the superficial MCL are the deep fibres which comprise two separate components, the meniscal femoral ligament and the meniscal tibial ligament. These are separated from the outer or superficial fibres by potential space generally only filled with connective tissue but which may fill with a bursa termed 'the tibial collateral ligament bursa' (Fig. 46). Other authors define three layers of the medial stabilisers: layer 1 is the most superficial represented by the deep fascia and forms the medial retinaculum by combining with some fibres from layer 2. Layer 2 is the superficial MCL and POL and layer 3 is represented by the capsule proper, but includes the deep layer of the MCL.

Just like the lateral collateral ligament the immediate external relationship of the MCL is subcutaneous fat. Consequently injuries to the collateral ligaments are best appreciated on coronal fat-suppressed images. For simple MCL injury, there is a good correlation between clinical and MRI staging. A grade 1 injury clinically has medial sided pain and some laxity but with a firm end point. The MRI findings under these circumstances are generally limited to oedema around the ligament (Fig. 47). Care should be taken not to misinterpret the capsular and soft-tissue oedema related to meniscal tears and OA as a ligament sprain. The injury context is useful in this regard. A grade 2 injury has a valgus laxity with a soft but definable end point. Under these circumstances the ligament shows internal structural changes; often it is multilayered giving an onion skin appearance (Fig. 48). This is also associated with oedema surrounding the ligament in the acute stages. A stage 3 lesion where there is valgus laxity without a defined end point is correlated with complete rupture on MRI (Fig. 49). Femoral insertion injuries are commonest but midsubstance and distal tears also occur. Osseous femoral avulsions may occur (Fig. 50). Occasionally grade 3 tears of the distal ligament result in retraction of the ligament above and superficial to the pes anserine tendons, preventing ligament healing and requiring surgery (Fig. 51). This has been termed an MCL 'Stener lesion' (Alaia et al. 2019). Tears of the deep MCL or

Fig. 48 Grade 2 MCL injury. Coronal fat-suppressed proton density MR image, showing an 'onion skin' configuration to the ligament (arrow) and oedema. The valgus impaction on the tibia is shown (arrowhead)

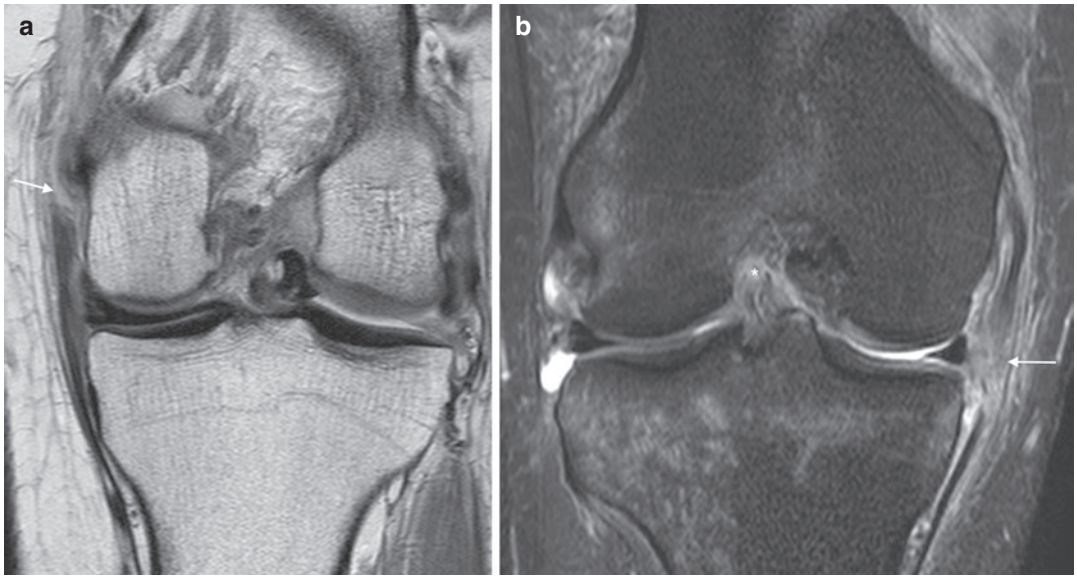

Fig. 49 Complete rupture of the MCL. (**a**, **b**) Coronal proton density MR images. The tears are located proximally (arrow in **a**) and in its midsubstance (arrow in **b**)

meniscofemoral/tibial ligaments may also be seen (Fig. 52), but are more difficult to detect due to their variable appearance. Most medial collateral ligament injuries resolve with conservative treatment, in some cases without the patient being particularly aware that they have been torn.

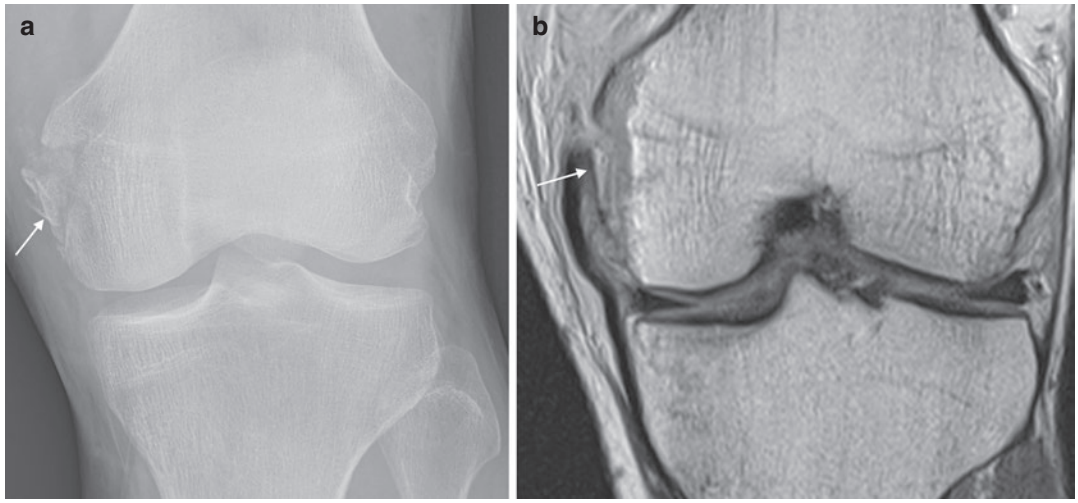

Fig. 50 (**a**, **b**) MCL avulsion. (**a**) X-ray and (**b**) coronal proton density MR image. The MCL has avulsed a fragment of bone from the femoral origin (arrows)

Fig. 51 MCL Stener lesion. Coronal proton density MR image. The MCL (arrow) is retracted above the pes anserine tendons (arrowheads)

Healing leaves only a thickened ligament which may persist for many years. Occasionally ossification can occur adjacent to the ligament termed the 'Pellegrini-Stieda' lesion. One possible cause for this lesion is the full-thickness femoral avulsion which remains continuous with a stripped femoral periosteum. Despite being avulsed, because of the periosteal attachment, the ligament may not be redundant. In paediatric patients the stripped periosteum may become entrapped in a

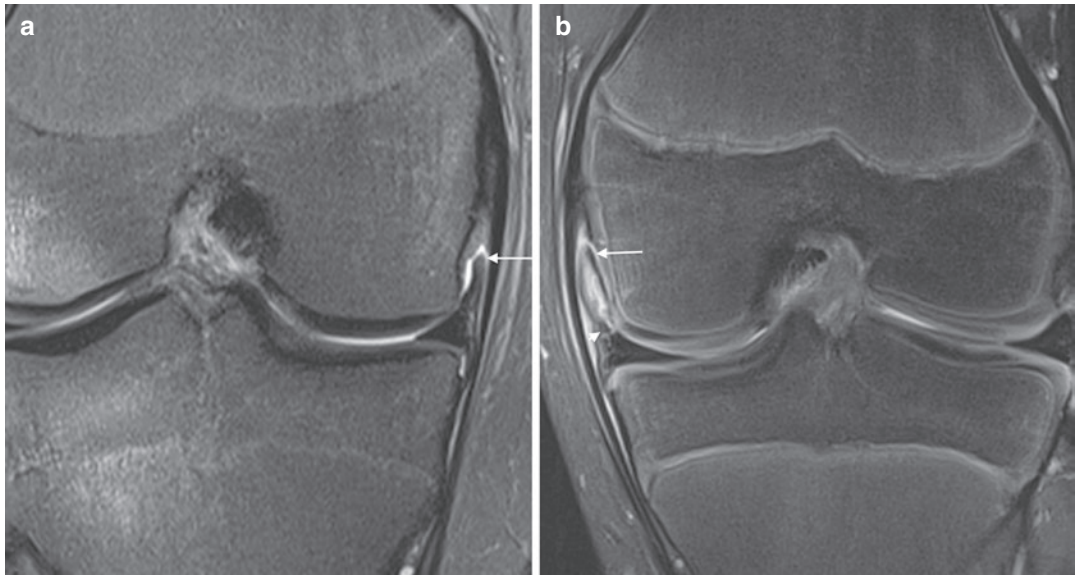

Fig. 52 Deep MCL injury. (**a**, **b**) Coronal fat-saturated proton density MR images. In (**a**) the meniscofemoral component of the deep MCL is torn (arrow). In (**b**) the meniscofemoral component has avulsed the perichondrium at the femoral attachment (arrow). There is also a separated fragment of meniscus at the meniscal attachment (arrowhead)

physeal injury (Fig. 53), preventing healing and leading to premature closure (Pedersen 2016).

3.2.2 The Posteromedial Corner

The posteromedial corner, between the MCL and PCL, has several major components: the semimembranosus tendon, the posterior oblique ligament, the posteromedial capsule which includes the oblique popliteal ligament and the medial meniscus (Lundquist et al. 2015). The semimembranosus tendon is the main dynamic stabiliser of the PMC, with a complex of five arms: The direct tibial arm is augmented by two additional anterior arms and two posterior. The anterior two are the pars reflexa inferiorly, which passes anteriorly in the axial plane to insert on the tibia deep to the MCL, and an expansion to the POL superiorly. The posterior arms are the oblique popliteal ligament superiorly and the popliteus aponeurosis inferiorly (Sims 2004). The direct arm attaches to the meniscotibial ligament of the posterior horn of the medial meniscus and the tendon pulls on the meniscus and prevents it from being compressed between tibia and femur in knee flexion. Sims and Jacobson (2004) have divided medial complex injuries into simple valgus injury with MCL tear, and anteromedial rotatory instability (AMRI), which they describe as an abnormal opening of the medial joint space in abduction at 30° of knee flexion, with a simultaneous anteromedial rotatory subluxation of the medial tibial condyle on the central axis of the intact posterior cruciate ligament.

When MCL injuries are detected, a careful study of the posteromedial structures is warranted, as in a small proportion tears of the semimembranosus tendon and associated insertions may be found (Fig. 54). These may be repaired when contributing to cruciate graft failure or when they are a part of multiligamentous injuries. As with the posterolateral corner, frank posteromedial capsular rupture may be seen. Chronic overuse semimembranosus tendinopathy is more common than acute injury and will be described elsewhere.

3.2.3 Medial Compartment Ganglia

As with ligaments elsewhere, ganglion cysts can occasionally be associated with the medial collateral ligament. These need to be distinguished from the tibial collateral ligament bursa,

Fig. 53 Entrapped periosteum. Coronal fat-saturated proton density MR image. The MCL has stripped the femoral periosteum which has become trapped in the femoral physis (arrow). This may lead to premature physeal closure

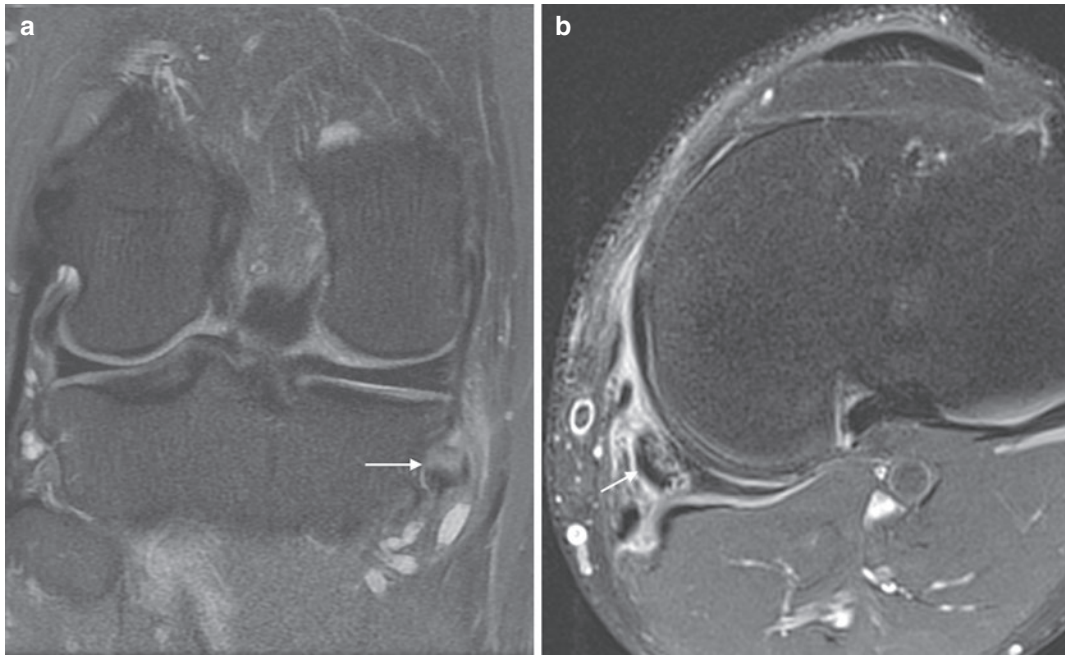

Fig. 54 (**a**, **b**) Posteromedial corner lesion. (**a**) Coronal and (**b**) axial fat-suppressed proton density MR images. Cyclist with a tear of the anterior arm or pars reflex of semimembranosus (arrow in **a**). Axial image in a patient with posteromedial pain and previous injury shows a tear of the direct head of semimembranosus

the semimembranosus bursa and the pes anserine bursa (Vanhoenacker et al. 2003). The semimembranosus bursa and pes anserine bursa are distinguished by the presence of a central tendon. The two bursae themselves are distinguished by their position, with the semimembranosus bursa lying superior to the pes anserine bursa. The tibial collateral ligament bursa lies deep to the superficial MCL and superficial to the meniscofemoral and meniscotibial ligaments.

4 Dislocation

An important subset of ligament and tendon injuries in the knee is dislocation. This involves disruption of three or more ligaments, with the exception being a bicruciate injury, where only the ACL and PCL are torn. The importance for radiologists is that the knee has often reduced by the time the patient presents for X-ray and severe injuries, particularly those to neurovascular structures, may be overlooked. The radiologist may thus be the first to suggest the diagnosis (Walker et al. 2013). The popliteal artery may be acutely torn or occluded (Fig. 55), but occasionally an intimal injury may result in delayed occlusion with resultant limb loss. Most institutions will perform CT angiography on all multiligamentous injuries to avoid this outcome.

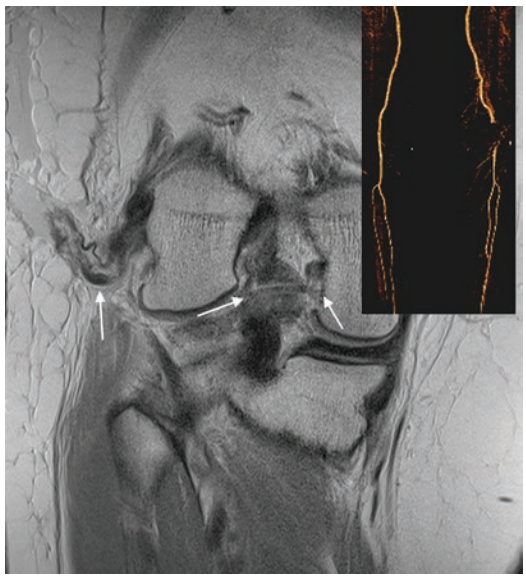

Fig. 55 Dislocation. Coronal proton density MR image and inset of CTA VRT. Note the multiligamentous injury (arrows) consistent with dislocation and the CTA with an occluded popliteal artery (inset)

5 Conclusion

MRI plays a key role in the assessment of suspected ligamentous disruption of the knee. The LCL and MCL are key stabilisers to varus and valgus stress, but injuries to secondary supporting structures in the corners of the knee have been recognised as potential causes of cruciate graft failure. The radiologist should be alert for oedema and fluid in the known position of these structures and alert the surgeon to possible injury.

Things to Remember

- The anterior cruciate ligament should be identified on all MR examinations as a sagittal line of low signal intensity.
- The radiologist may be the first to recognise knee dislocation and the resultant neurovascular injuries.
- In the presence of a tear of the anterior cruciate ligament, it is important to carefully scrutinise the posterolateral corner.
- The immediate external relationship of the collateral ligaments is subcutaneous fat. Coronal orientated fat-saturated images are most efficient in assessing injury to these structures.

References

Alaia EF, Rosenberg ZS, Alaia MJ (2019) Stener-like lesions of the superficial medial collateral ligament of the knee: MRI features. Am J Roentgenol 213:W272–W276

Anderson AF, Awh MH, Anderson CN (2004) The anterior meniscofemoral ligament of the medial meniscus: case series. Am J Sports Med 32:1035–1040

Bach BR Jr, Minihane K (2001) Subluxating biceps femoris tendon: an unusual case of lateral knee pain in a soccer athlete: a case report. Am J Sports Med 29:93–95

Bradley JP, Rytel MJ, Klimkiewicz JJ, Powell JW (2002) Anterior cruciate ligament injuries in the National

Football League: epidemiology and current treatment trends among team physicians. Arthroscopy 18:502
Bui Mansfield LT, Youngberg RA (1997) Intraarticular ganglia of the knee: prevalence, presentation, etiology, and management. AJR Am J Roentgenol 168: 123–127
Chan WP, Peterfy C, Fritz RC et al (1994) MR diagnosis of complete tears of the anterior cruciate ligament of the knee: importance of anterior subluxation of the tibia. Am J Roentgenol 162:355–360
Chan KK, Resnick D, Goodwin D et al (1999) Posteromedial tibial plateau injury including avulsion fracture of the semimembranosus tendon insertion site: ancillary sign of anterior cruciate ligament tear at MR imaging. Radiology 211:754–758
Charlton WPH, St. John TA, Ciccotti MG et al (2002) Differences in femoral notch anatomy between men and women. A magnetic resonance imaging study. Am J Sports Med 30:329
Cobby MJ, Schweitzer ME, Resnick D (1992) The deep lateral femoral notch: an indirect sign of a torn anterior cruciate ligament. Radiology 184:855–858
Cooper DE (1999) Snapping popliteus tendon syndrome: a cause of mechanical knee popping in athletes. Am J Sports Med 27:671–674
Cross MJ, Powell JF (1984) Long-term follow-up of posterior cruciate ligament rupture: a study of 116 cases. Am J Sports Med 12:292–297
De Maeseneer M, Shahabpour M, Vanderdood K et al (2001) Posterolateral supporting structures of the knee: findings on anatomic dissection, anatomic slices and MR images. Eur Radiol 11:2170–2177
De Smet AA, Graf BK (1994) Meniscal tears missed on MR imaging: relationship to meniscal tear patterns and anterior cruciate ligament tears. Am J Roentgenol 162:905–911
Duncan JB, Hunter R, Purnell M, Freeman J (1995) Meniscal injuries associated with acute anterior cruciate ligament tears in alpine skiers. Am J Sports Med 23(2):170–2
Fanelli GC (1993) Posterior cruciate ligament injuries in trauma patients. Arthroscopy 9:291–294
Filli L, Rosskopf AB, Sutter R et al (2018) MRI predictors of posterolateral corner instability: a decision tree analysis of patients with acute anterior cruciate ligament tear. Radiology 289(1):170–180
Flato R, Passanante GJ, Skalski MR et al (2017) The iliotibial tract: imaging, anatomy, injuries, and other pathology. Skelet Radiol 46:605
Gabbe B, Finch C (2001) A profile of Australian football injuries presenting to sports medicine clinics. J Sci Med Sport 4:386
Geeslin AG, LaPrade RF (2011) Outcomes of treatment of acute grade-III isolated and combined posterolateral knee injuries: a prospective case series and surgical technique. J Bone Joint Surg Am 93(18):1672–1683
Geeslin AG, Geeslin MG, LaPrade RF (2017) Ligamentous reconstruction of the knee: what orthopaedic surgeons want radiologists to know. Semin Musculoskelet Radiol 21(2):75–88
Gentili A, Seeger LL, Yao L et al (1994) Anterior cruciate ligament tear: Indirect signs at MR imaging. Radiology 193:835–840
Girgis FG, Marshall JL, Monajem A (1975) The cruciate ligaments of the knee joint. Anatomical, functional and experimental analysis. Clin Orthop Relat Res 106:216–231
Grover JS, Bassett LW, Gross ML et al (1990) Posterior cruciate ligament: MR imaging. Radiology 174:527–530
Guha AR, Gorgees KA, Walker DI (2003) Popliteus tendon rupture: a case report and review of the literature. Br J Sports Med 37:358–360
Gunter P, Schwellnus MP, Fuller PJ (2004) Local corticosteroid injection in iliotibial band friction syndrome in runners: a randomised controlled trial—Commentary. Br J Sports Med 38:269–272
Gupte CM, Smith A, McDermott ID et al (2002) Meniscofemoral ligaments revisited: anatomical study, age correlation and clinical implications. J Bone Joint Surg Br 84-B:846–851
Heller L, Langman J (1964) The menisco-femoral ligaments of the human knee. J Bone Joint Surg Br 46:307–313
Holmes JC, Pruitt AL, Whalen NJ (1993) Iliotibial band syndrome in cyclists. Am J Sports Med 21:419–424
Huang G-S, Lee C-H, Chan WP et al (2002) Acute anterior cruciate ligament stump entrapment in anterior cruciate ligament tears: MR imaging appearance. Radiology 225:537–540
Huang G-S, Yu JS, Munshi M, Chan WP et al (2003) Avulsion fracture of the head of the fibula (the "Arcuate" sign): MR imaging findings predictive of injuries to the posterolateral ligaments and posterior cruciate ligament. Am J Roentgenol 180:381–387
Jadhav SP, More SR, Riascos RF et al (2014) Comprehensive review of the anatomy, function, and imaging of the popliteus and associated pathologic conditions. Radiographics 34(2):496–451
Jarvinen M, Natri A, Laurila S et al (1994) Mechanisms of anterior cruciate ligament ruptures in skiing. Knee Surg Sports Traumatol Arthrosc 2:224–228
Kaplan PA, Walker CW, Kilcoyne RF et al (1992) Occult fracture patterns of the knee associated with anterior cruciate ligament tears: assessment with MR imaging. Radiology 183:835–838
LaPrade RF, Konowalchuk BK (2005) Popliteomeniscal fascicle tears causing symptomatic lateral compartment knee pain: diagnosis by the figure-4 test and treatment by open repair. Am J Sports Med 33: 1231–1236
LaPrade RF, Gilbert TJ, Bollom TS et al (2000) The magnetic resonance imaging appearance of individual structures of the posterolateral knee. A prospective study of normal knees and knees with surgically verified grade III injuries. Am J Sports Med 28:191–199

LaPrade RF, Ly TV, Wentorf FA et al (2003) The posterolateral attachments of the knee: a qualitative and quantitative morphologic analysis of the fibular collateral ligament, popliteus tendon, popliteofibular ligament, and lateral gastrocnemius tendon. Am J Sports Med 31:854–860

Lawrance JA, Ostlere SJ, Dodd CA (1996) MRI diagnosis of partial tears of the anterior cruciate ligament. Injury 27:153–155

Lee JK, Yao L, Phelps CT et al (1988) Anterior cruciate ligament tears: MR imaging compared with arthroscopy and clinical tests. Radiology 166:861–864

Lee K, Siegel MJ, Lau DM et al (1999) Anterior cruciate ligament tears: MR imaging-based diagnosis in a pediatric population. Radiology 213:697–704

Lee BY, Jee WH, Kim JM et al (2000) Incidence and significance of demonstrating the meniscofemoral ligament on MRI. Br J Radiol 73:271–274

Lundquist RB, Matcuk GR, Schein AJ et al (2015) Posteromedial corner of the knee: the neglected corner. Radiographics 35(4):1123–1137

Mair SD, Schlegel TF, Gill TJ et al (2004) Incidence and location of bone bruises after acute posterior cruciate ligament injury. Am J Sports Med 32:1681–1687

Maynard MJ, Deng X, Wickiewicz TL et al (1996) The popliteofibular ligament. Rediscovery of a key element in posterolateral stability. Am J Sports Med 24:311–316

McAllister DR, Parker RD (1999) Bilateral subluxating popliteus tendons: a case report. Am J Sports Med 27:376–379

McCarthy CL, McNally EG (2004) The MRI appearance of cystic lesions around the knee. Skelet Radiol 33:187–209

McCauley TR, Moses M, Kier R et al (1994) MR diagnosis of tears of anterior cruciate ligament of the knee: importance of ancillary findings. Am J Roentgenol 162:115–119

McKean D, Yoong P, Yanny S et al (2015) The popliteal fibular ligament in acute knee trauma: patterns of injury on MR imaging. Skelet Radiol 44:1413

Meister BR, Michael SP, Moyer RA, Kelly JD, Schneck CD (2000) Anatomy and kinematics of the lateral collateral ligament of the knee. Am J Sports Med 28:869–878

Mellado JM, Calmet J, Olona M et al (2004) Magnetic resonance imaging of anterior cruciate ligament tears: re-evaluation of quantitative parameters and imaging findings including a simplified method for measuring the anterior cruciate ligament angle. Knee Surg Sports Traumatol Arthrosc 12:217–224

Murao H, Morishita S, Nakajima M et al (1998) Magnetic resonance imaging of anterior cruciate ligament (ACL) tears: diagnostic value of ACL-tibial plateau angle. J Orthop Sci 3:10–17

Murphy BJ, Smith RL, Uribe JW et al (1992) Bone signal abnormalities in the posterolateral tibia and lateral femoral condyle in complete tears of the anterior cruciate ligament: a specific sign? Radiology 182:221–224

Nelson EW, LaPrade RF (2000) The anterior intermeniscal ligament of the knee: an anatomic study. Am J Sports Med 28:74–76

Nokes SR, Koonce TW, Montanez J (1994) Ganglion cysts of the cruciate ligaments of the knee: recognition on MR images and CT-guided aspiration. AJR Am J Roentgenol 162:1503

Park LS, Jacobson JA, Jamadar DA et al (2007) Posterior horn lateral meniscal tears simulating meniscofemoral ligament attachment in the setting of ACL tear: MRI findings. Skelet Radiol 36:399

Parolie JM, Bergfeld JA (1986) Long-term results of nonoperative treatment of isolated posterior cruciate ligament injuries in the athlete. Am J Sports Med 14:35–38

Patel RM, Brophy RH (2018) Anterolateral ligament of the knee: anatomy, function, imaging, and treatment. Am J Sports Med 46(1):217–223

Pedersen RR (2016) The medial and posteromedial ligamentous and capsular structures of the knee: review of anatomy and relevant imaging findings. Semin Musculoskelet Radiol 20(1):12–25

Pereira MT, Nanni G, Roi GS (2003) Epidemiology of anterior cruciate ligament injuries in professional football players [Epidemiologia de las lesiones del ligamento cruzado anterior en el futbolista profesional]. Archivos de Medicina del Deporte 20:299

Prince JS, Laor T, Bean JA (2005) MRI of anterior cruciate ligament injuries and associated findings in the pediatric knee: changes with skeletal maturation. Am J Roentgenol 185:756–762

Recondo JA, Salvador E, Villanua JA et al (2000) Lateral stabilizing structures of the knee: functional anatomy and injuries assessed with MR imaging. Radiographics 20:91S–102S

Remer EM, Fitzgerald SW, Friedman H et al (1992) Anterior cruciate ligament injury: MR imaging diagnosis and patterns of injury. Radiographics 12: 901–915

Robertson PL, Schweitzer ME, Bartolozzi AR et al (1994) Anterior cruciate ligament tears: evaluation of multiple signs with MR imaging. Radiology 193:829–834

Rosas HG (2016) Unraveling the posterolateral corner of the knee. Radiographics 36(6):1776–1791

Roychowdhury S. Fitzgerald SW, Soniri AH (1997) Using MR imaging to diagnose partial (ears of the anterior cruciate ligament: value of axial images. AJR Am J Roentgenol 168:1487–1491

Sanders TG, Linares RC, Lawhorn KW et al (1999) Oblique meniscomeniscal ligament: another potential pitfall for a meniscal tear-anatomic description and appearance at MR imaging in three cases. Radiology 213:213–216

Schweitzer ME, Cervilla V, Kursunoglu-Brahme S et al (1992) The PCL line: an indirect sign of anterior cruciate ligament injury. Clin Imaging 16:43

Schweitzer ME, Mitchell DG, Ehrlich SM (1993) The patellar tendon: thickening, internal signal buckling, and other MR variants. Skelet Radiol 22:411–416

Segond P (1879) Recherches cliniques et expérimentales sur les épanchements sanguins du genou par entorse. Prog Med 7:297

Shahane SA, Ibbotson C, Strachan R et al (1999) The popliteofibular ligament: an anatomical study of the posterolateral corner of the knee. J Bone Joint Surg Br 81-B:636–642

Shelbourne KD, Nitz PA (1991) The O'Donoghue triad revisited. Combined knee injuries involving anterior cruciate and medial collateral ligament tears. Am J Sports Med 19:474–477

Shelbourne KD, Davis TJ, Patel DV (1999) The natural history of acute, isolated, nonoperatively treated posterior cruciate ligament injuries: a prospective study. Am J Sports Med 27:276–283

Simoens WA, Vanhoenacker FM, Willemen D et al (2002) Iliotibial band friction syndrome. JBR-BTR 85:152–153

Sims WF, Jacobson KE (2004) The posteromedial corner of the knee: medial-sided injury patterns revisited. Am J Sports Med 32:337–345

Siwinski D, Ziemianski A (1998) Value of posterior cruciate ligament index in the diagnosis of anterior cruciate ligament injuries. Arch Orthop Trauma Surg 118:116–118

Sonin AH, Fitzgerald SW, Friedman H et al (1994) Posterior cruciate ligament injury: MR imaging diagnosis and patterns of injury. Radiology 190: 455–458

Sonin AH, Fitzgerald SW, Hoff FL et al (1995) MR imaging of the posterior cruciate ligament: normal, abnormal, and associated injury patterns. Radiographics 15:551–561

Staubli HU, Birrer S (1990) The popliteus tendon and its fascicles at the popliteal hiatus: gross anatomy and functional arthroscopic evaluation with and without anterior cruciate ligament deficiency. Arthroscopy 6:209–220

Sugita T, Amis AA (2001) Anatomic and biomechanical study of the lateral collateral and popliteofibular ligaments. Am J Sports Med 29:466–472

Temponi EF, de Carvalho Júnior LH, Saithna A et al (2017) Incidence and MRI characterization of the spectrum of posterolateral corner injuries occurring in association with ACL rupture. Skelet Radiol 46(8):1063–1070

Terry GC, LaPrade RF (1996a) The biceps femoris muscle complex at the knee. Its anatomy and injury patterns associated with acute anterolateral-anteromedial rotatory instability. Am J Sports Med 24:2–8

Terry GC, LaPrade RF (1996b) The posterolateral aspect of the knee. Anatomy and surgical approach. Am J Sports Med 24:732–739

Tung GA, Davis LM, Wiggins ME et al (1993) Tears of the anterior cruciate ligament: primary and secondary signs at MR imaging [see comments]. Radiology 188:661–667

Tyler P, Datir A, Saifuddin A (2010) Magnetic resonance imaging of anatomical variations in the knee. Part 1: ligamentous and musculotendinous. Skelet Radiol 39:1161

Umans H, Wimpfheimer O, Haramati N et al (1995) Diagnosis of partial tears of the anterior cruciate ligament of the knee: value of MR imaging. Am J Roentgenol 165:893–897

Van Dyck P, De Smet E, Lambrecht V et al (2016) The anterolateral ligament of the knee: what the radiologist needs to know. Semin Musculoskelet Radiol 20(1):26–32

Van Steyn MO, Mariscalco MW, Pedroza AD et al (2016) The hypermobile lateral meniscus: a retrospective review of presentation, imaging, treatment, and results. Knee Surg Sports Traumatol Arthrosc 24: 1555–1559

Vanek J (1994) Posteromedial fracture of the tibial plateau is not an avulsion injury. A case report and experimental study. J Bone Joint Surg Br 76:290–292

Vanhoenacker FM, Vanhoenacker P, Crevits I et al (2001) MR imaging anatomy of the knee. JBR-BTR 84:10–15

Vanhoenacker FM, Van de Perre S, De Vuyst D et al (2003) Cystic lesions around the knee. JBR-BTR 86: 302–304

Vinson EN, Major NM, Helms CA (2008) The posterolateral corner of the knee. Am J Roentgenol 190(2):449–458

Walker RE, McDougall D, Patel S (2013) Radiologic review of knee dislocation: from diagnosis to repair. Am J Roentgenol 201(3):483–495

Wan AC, Felle P (1995) The menisco-femoral ligaments. Clin Anat 8:323–326

Weber WN, Neumann CH, Barakos JA et al (1991) Lateral tibial rim (Segond) fractures: MR imaging characteristics. Radiology 180:731–734

Wind WM Jr, Bergfeld JA, Parker RD (2004) Evaluation and treatment of posterior cruciate ligament injuries: revisited. Am J Sports Med 32:1765–1775

Yao L, Lee JK (1989) Avulsion of the posteromedial tibial plateau by the semimembranosus tendon: diagnosis with MR imaging. Radiology 172:513–514

Imaging of Anterior Knee Pain and Maltracking

Simon Ostlere and Graeme Thompson

Contents

Abstract

Symptoms related to the anterior knee are common in athletes. Most of the conditions are related to overuse injury of the tendons or chronic patellofemoral instability. Acute trauma is less common. Athletes with patellofemoral dysplasia will be at risk of symptoms related to patellofemoral maltracking including acute patellar dislocation. Acute tendon rupture is a rare complication of tendinosis. A direct blow to the kneecap may result in patellar fracture, prepatellar bursal haemorrhage or Morel-Lavallée syndrome. Imaging may reveal signs of pathology of Hoffa's fat pad or knee plica, although often these findings are not clinically significant. In many cases of retropatellar pain, there is no identifiable cause, which has led to the use of the term 'patellofemoral pain syndrome'. In most cases of nonspecific patellofemoral pain, no imaging is required unless there has been a poor response to standard conservative treatment.

1 Introduction

Symptoms related to the anterior knee are common in athletes. There are specific conditions of the patellar tendon, patellofemoral joint and Hoffa's fat pad, but in many cases of retropatellar pain there is no identifiable cause, which has led

S. Ostlere (✉) · G. Thompson
Oxford University Hospitals and Oxford Musculoskeletal Radiology, Oxford, UK
e-mail: sjostlere@me.com

Med Radiol Diagn Imaging (2021)
https://doi.org/10.1007/174_2020_269, © Springer Nature Switzerland AG
Published Online: 23 February 2021

to the use of the term 'patellofemoral pain syndrome'. In most cases of non-specific patellofemoral pain, no imaging is required unless there has been a poor response to standard conservative treatment.

2 Acute Trauma to the Extensor Mechanism

The most common acute injury to the anterior knee is patellar dislocation. More unusual injuries include patellar and quadriceps tendon rupture and direct trauma may result in patellar fractures or haemorrhage into the prepatellar bursa. In children, avulsion fractures of the inferior patella and tibial tubercle may occur.

2.1 Patellar Dislocation

Most acute patellar dislocations occur during sporting activity. Typically the patient experiences acute pain and swelling following a twisting injury. Examination of the knee is difficult in the acute setting and the diagnosis may not be suspected before imaging. Radiographic signs include patellofemoral dysplasia, displaced patella, large haemarthrosis or lipohaemarthrosis and osteochondral fragment (Duthon 2015). MR is indicated in most patients to assess the extent of the soft tissue and bone and to identify and quantify any predisposing patellofemoral dysplasia (see below). At the time of injury, the patella initially subluxes laterally until the medial patellofemoral ligament ruptures, usually at its femoral or patellar attachments (Cao et al. 2019). The patella then dislocates and its medial aspect impacts the anterolateral aspect of the lateral femoral condyle. This often results in an osteochondral fragment originating from the medial patellar facet and/or the lateral femoral condyle. The typical MR signs are therefore ruptured medial patellofemoral ligament, and subcortical oedema/haemorrhage in the anterolateral aspect of the lateral femoral condyle with a corresponding 'kissing' lesion in the medial aspect of the patella, with or without a patellar or femoral osteochondral fracture (Fig. 1) (Sanders et al. 2006). Sometimes the medial retinaculum and medial patellofemoral ligament remain intact (Kirsch et al. 1993).

2.2 Patellar Tendon Rupture

Patellar tendon rupture is a rare injury in athletes. Predisposing factors are patellar tendinosis, previous steroid injections, fluoroquinolone therapy, previous ACL repair with patellar graft and chronic medical disorders. In the immature skeleton, tibial tubercle avulsion fractures are more common than rupture of the tendon. The patient complains of sudden pain and the inability to extend the knee. Early surgical repair is indicated so it is important to make a timely diagnosis. The tear usually involves the proximal or middle parts of the tendon. Distal tendon ruptures are usually associated with high-energy injuries (Capogna et al. 2017). Signs of patellar tendon rupture on the lateral radiograph are patella alta and patellar avulsion fracture. Ultrasound is the easiest and quickest method to make the diagnosis and determine the site and extent of the tear, although MR provides similar information (Fig. 2).

2.3 Quadriceps Tendon Rupture

Rupture of the quadriceps tendon tends to occur in older athletes with multiple medical conditions that may predispose to quadriceps rupture. The quadriceps tendon consists of three layers related to the rectus femoris, vastus medialis/lateralis and vastus intermedius, respectively. Tears usually occur close to the tendon insertion at the patella and are often partial. Radiographs may show avulsion fracture and patella baja. Abnormal contour of the tendon and avulsion fracture may be seen on the radiograph (Fig. 3). MR is thought to be more specific than ultrasound for identifying a tear and more suitable for assessing the severity of partial tears (Perfitt et al. 2013). In acute tears, both ultrasound and MR will show

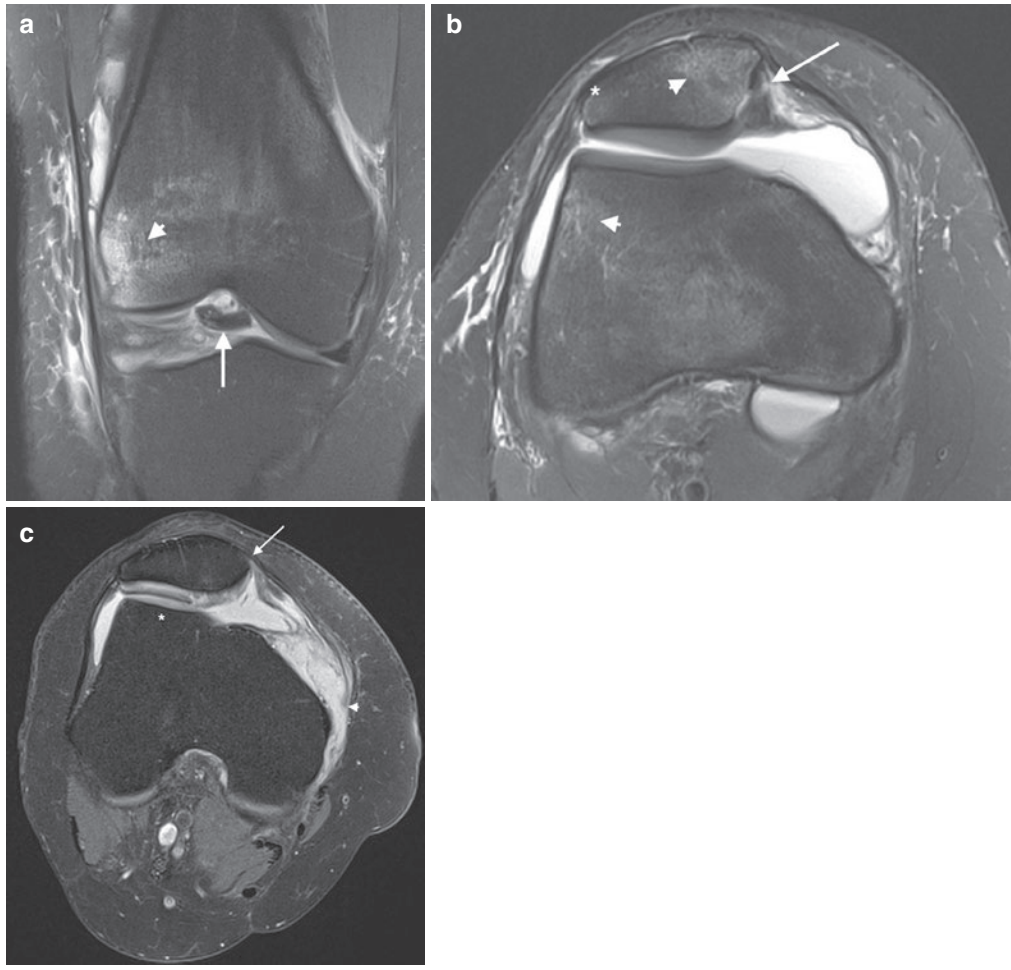

Fig. 1 (**a**–**c**) Acute patellar dislocation. (**a**) Coronal and (**b**) axial proton-density fat-saturated MR images. A large osteochondral fragment (arrow in **a**) has been sheared off the medial patellar facet (arrow in **b**). Marrow oedema is evident in the medial patellar and lateral femoral condyle (arrowheads). The patellar attachment of the MPFL (asterisk) is intact. (**c**) Axial proton-density fat saturation MR image shows avulsion of the femoral end of the medial patellofemoral ligament (arrowhead). The patellar attachment is intact (arrow). Note the dysplastic 'plateau' of the trochlea (asterisk)

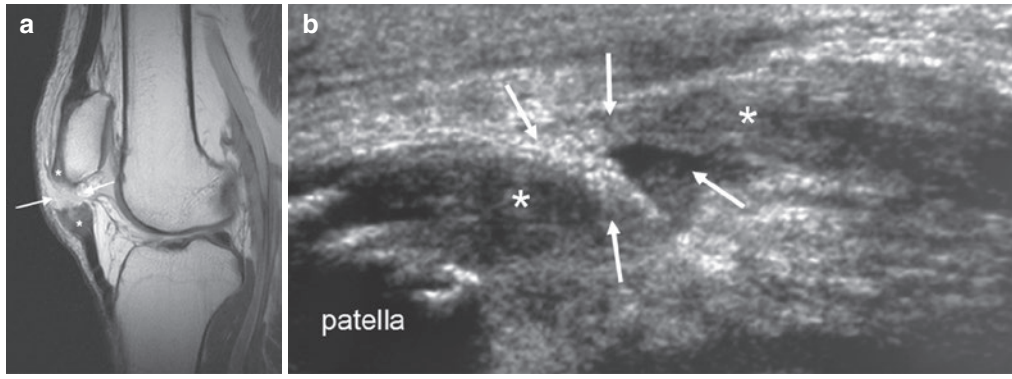

Fig. 2 (**a**, **b**) Patellar tendon rupture. (**a**) Sagittal proton density and (**b**) ultrasound show a defect in the proximal portion of the tendon (arrows). The asterisks mark the free ends of the tendon

disruption of the tendon, either partial or complete, with haematoma (Fig. 4). When tears are complete the torn quadriceps tendon will retract and the patella will migrate inferiorly.

Fig. 3 Quadriceps tendon rupture. Lateral X-ray image showing patella baja (double arrow) and a retracted quadriceps containing a flake of bone (arrowhead) with a resultant soft-tissue gap (arrow)

2.4 Prepatellar Bursa

Prepatellar bursitis is a common condition in the general population, particularly in occupations requiring kneeling. In athletes, the commonest problem is an acute haemorrhagic bursitis resulting from a direct blow. The diagnosis is usually obvious on clinical inspection and can be easily confirmed on ultrasound or MR (Fig. 5). The bursa is a trilaminate structure overlying the patella. The bursa may extend a short distance lateral or medial to the patella (Aguiar et al. 2007). A Morel-Lavallée lesion of the knee is a shearing injury to the soft tissues that can mimic haemorrhagic bursitis on imaging. In this condition, the lesion extends beyond the expected margins of the bursa (Fig. 6) (Tejwani et al. 2007).

2.5 Fractures

In the adult, patellar fractures may occur secondary to a direct blow. In the child, the patellar sleeve avulsion fracture is a rare but important lesion in which the unossified inferior pole plus a small amount of bone is avulsed along with a sleeve of retropatellar articular cartilage and periosteum (Hunt and Somashekar 2005). This can also occur at the quadriceps insertion (Fig. 7) (Gettys et al. 2010). This fracture requires fixa-

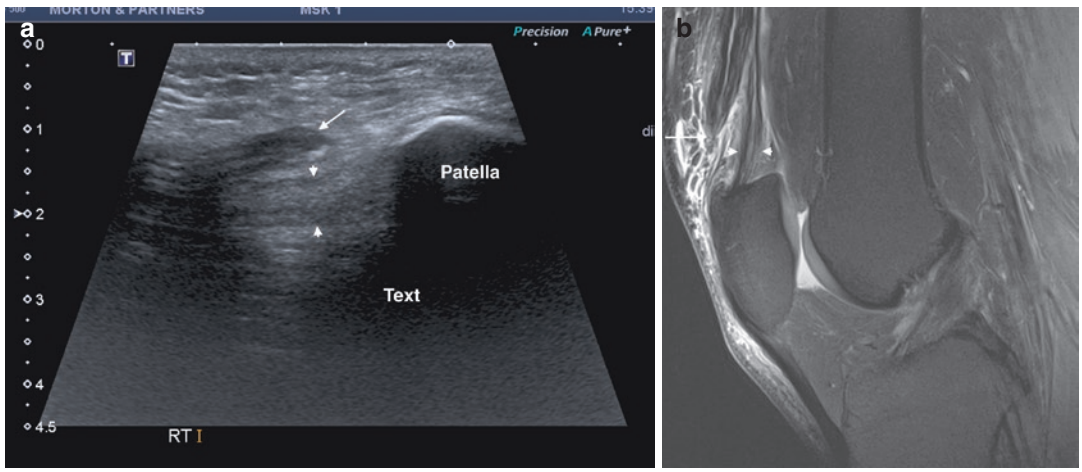

Fig. 4 (**a**, **b**) Partial quadriceps tendon tear. (**a**) Sagittal ultrasound and (**b**) sagittal proton-density fat-saturated images showing the retracted superficial tendon (arrow) with an intact posterior component (arrowheads)

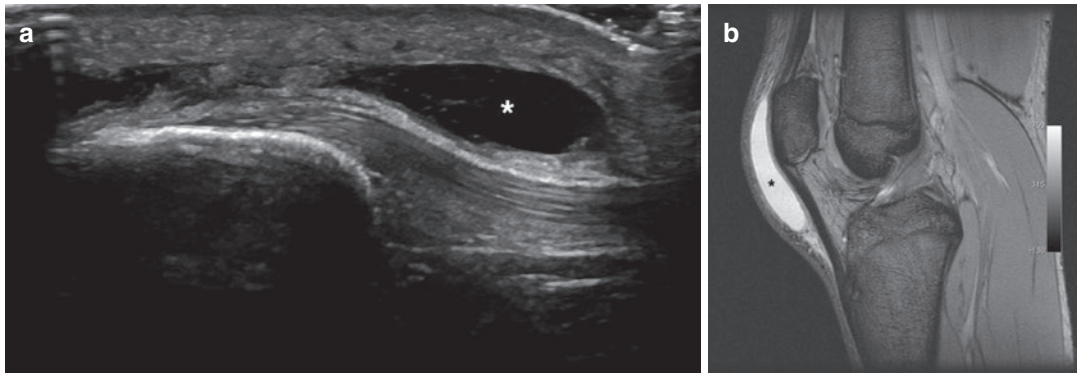

Fig. 5 (**a**, **b**) Prepatellar bursitis. (**a**) Axial ultrasound and (**b**) sagittal gradient-echo images demonstrate fluid distention of the prepatellar bursa (asterisks) which normally covers the upper portion of the infrapatellar tendon

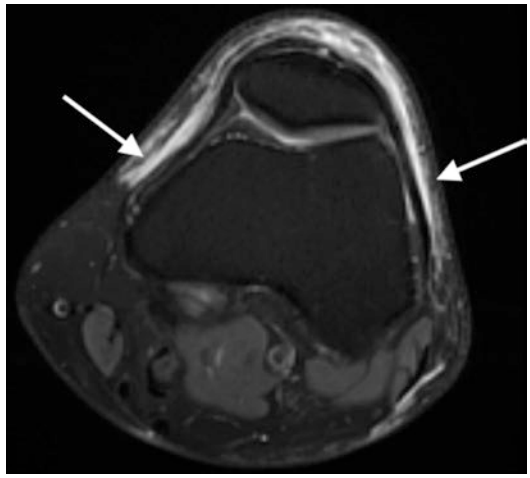

Fig. 6 Morel-Lavallée lesion. Axial T2 fat-saturated image shows a fluid-filled structure beyond the normal confines of the prepatellar bursa (arrows)

tion. Another rare fracture is avulsion of the unfused tibial tubercle, which may occur on a background of Osgood-Schlatter disease.

3 Anterior Knee Pain Without Acute Trauma

Anterior knee pain is a common complaint in athletes and general population. In most cases, symptoms are due to pathology of the patellar tendon, patellofemoral joint or Hoffa's fat pad. Most patients do not require imaging. In certain circumstances, imaging will help to make a diagnosis,

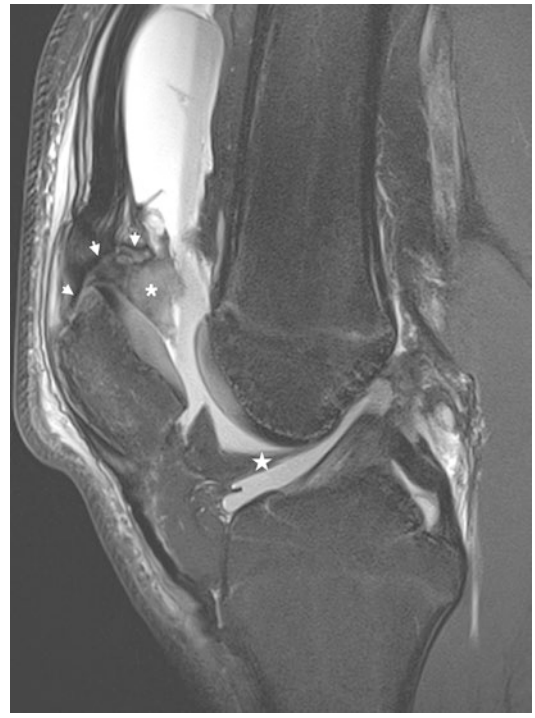

Fig. 7 Periosteal sleeve avulsion of the quadriceps tendon. Sagittal proton-density fat saturation image. The tendon has avulsed periosteum (arrowheads) and cartilage (asterisk) from the patella. Incidental ligamentum mucosum or infrapatellar plica is shown (star)

assess the degree of abnormality or guide therapy. MR and ultrasound are the most useful techniques in investigating anterior knee pain. Radiographs have a limited role and are not required in most cases. Ultrasound is the easiest method of investi-

gating suspected patellar tendon pathology. MR is used for suspected patellofemoral problems and when the symptoms are non-specific.

3.1 Disorders of the Patellar Tendon

The patellar tendon is vulnerable to overuse-type injuries. In the adolescent, the commonest condition is Osgood-Schlatter disease, which is a chronic traction injury at the tibial tubercle apophysis (traction apophysitis). The condition is more common in males and is associated with running sports. A tender bony swelling at the tibial tubercle is found on clinical inspection. Imaging is rarely required and is usually requested to reassure the patient or their parents that there is no sinister pathology. Radiographs will show fragmentation of the tibial tubercle, accompanied by some soft-tissue swelling representing thickened tendon and fluid in the deep infrapatellar bursa. Ultrasound and MR will demonstrate the fragmentation of the tibial tubercle apophysis, tendinosis and infrapatellar bursitis (Fig. 8) (Sailly et al. 2012; Suzue et al. 2015). Early stages of the disease may only show marrow oedema in the apophysis and tibia on MR (Fig. 9). Osgood-Schlatter disease is considered to be a self-limiting condition in most cases with symptoms resolving within 1–2 years, although a substantial proportion of cases requiring hospital assessment suffer from a more chronic course (Guldhammer et al. 2019). Sinding-Larsen-Johansson syndrome is a similar traction apophysitis that occurs at the proximal end of the tendon. The prognosis is better than Osgood-Schlatter disease. Radiographs will show fragmentation of the inferior pole of the patella. Ultrasound and MR will typically demonstrate separation and

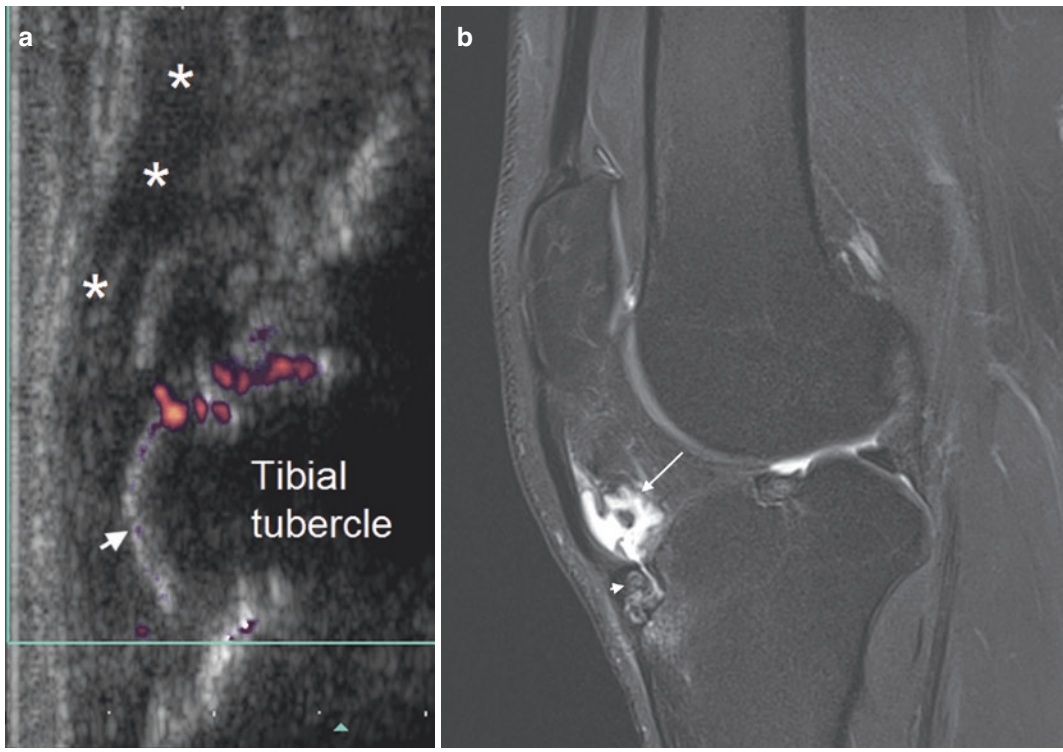

Fig. 8 (**a**, **b**) Osgood-Schlatter disease. (**a**) Sagittal ultrasound and (**b**) proton-density fat-saturated MR images show separation and fragmentation of the tibial tuberosity apophysis (arrowheads) and hypervascularity on Doppler (**a**). There is associated infrapatellar bursitis (arrow in **b**). Patellar tendon (asterisk in **a**)

Fig. 9 Early Osgood-Schlatter disease. Sagittal proton-density fat saturation image shows marrow oedema in the apophysis (arrow) and the subjacent tibia and infrapatellar fat (arrowheads)

fragmentation of the secondary apophysis at the inferior pole of the patella and a swollen hypervascular tendon (Fig. 10) (Draghi et al. 2008; Suzue et al. 2015). Jumper's knee (patellar tendinosis) is a chronic overuse injury of the proximal patellar tendon seen in young adult athletes. The condition may be resistant to treatment. The pathology is degeneration of the proximal tendon directly adjacent to the inferior pole of the patella. The abnormality is typically confined to the deep surface of the central portion of the tendon (Fig. 11). The diagnosis and management are usually based solely on clinical evaluation. When imaging is indicated ultrasound is the technique of choice. A focal swelling of the tendon with hypervascularity is seen adjacent to the inferior pole of the patella (Terslev et al. 2001). Calcification is not uncommon. On MR the abnormal tendon shows increased signal on all sequences (Fig. 12a). Magic-angle effect (Fig. 12b) can cause mild or moderate high signal within the proximal patellar tendon simulating tendinosis on MR, so clinical correlation is important (Levin et al. 2019). Less commonly the

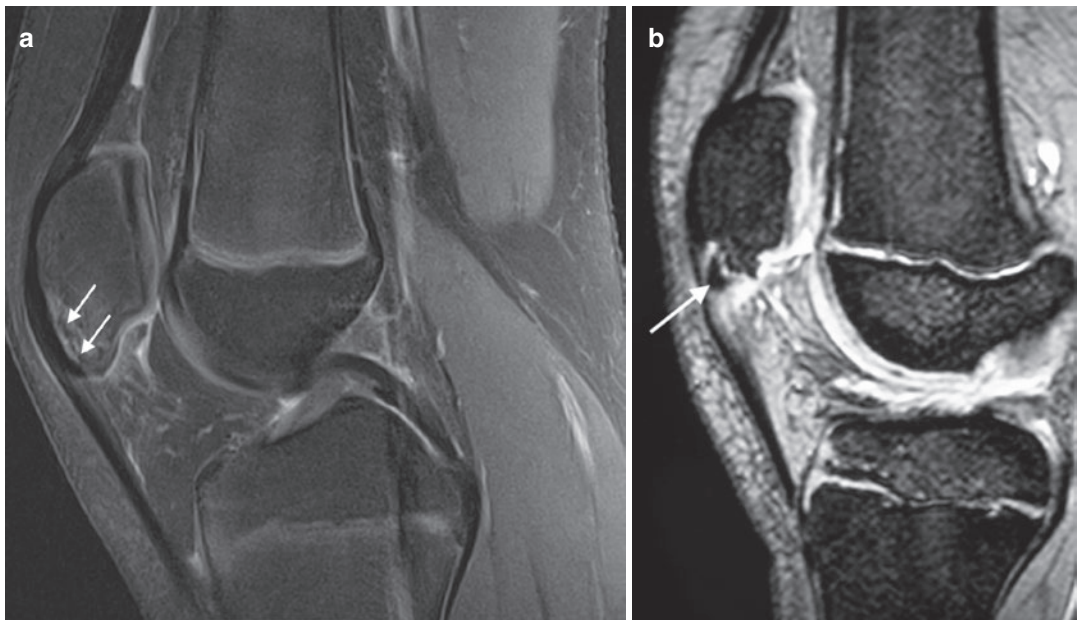

Fig. 10 (**a**, **b**) Sinding-Larsen-Johansson syndrome. (**a**) Sagittal proton-density fat saturation and (**b**) gradient-echo MR images. In an earlier stage (**a**) the apophysis is partially separated (arrows) with associated oedema. Later the apophysis may fragment and ossify (arrow in **b**)

tendinosis may be more diffuse (Fig. 13). Imaging evidence of patellar tendinosis in asymptomatic athletes is a risk factor for developing symptoms in the future (McAuliffe et al. 2016).

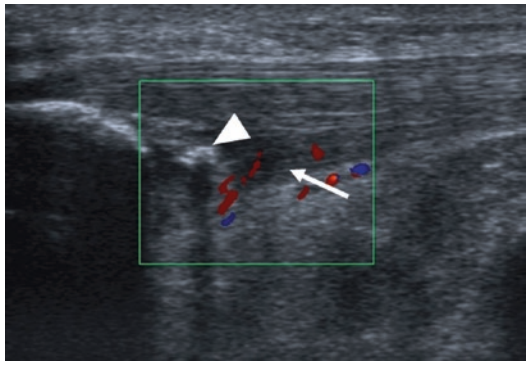

Fig. 11 Jumper's knee. Sagittal ultrasound image showing the thickened, hypoechoic and hypervascular deep portion of the infrapatellar tendon (arrow) with a focus on calcification (arrowhead)

3.2 Medial Patellar Plica

Impingement of the medial patellar plica between the patella and the medial condyle has been implicated as a cause of anterior knee pain. The patient may experience pain, clicking, pseudolocking and tenderness over the medial plica. The normal plica is commonly identified on MR when there is an effusion. In medial patellar plica syndrome, the plica is seen to be thickened and covers the medial side of the medial femoral condyle. There may be an associated chondral defect (Fig. 14) (Nixion et al. 2017).

3.3 Hoffa's Fat Pad

Hoffa's fat pad lies deep to the patellar tendon and has an apex pointing toward the ACL insertion. Cysts, neoplasms and inflammatory conditions can occur in the fat pad (Saddik et al. 2004). The

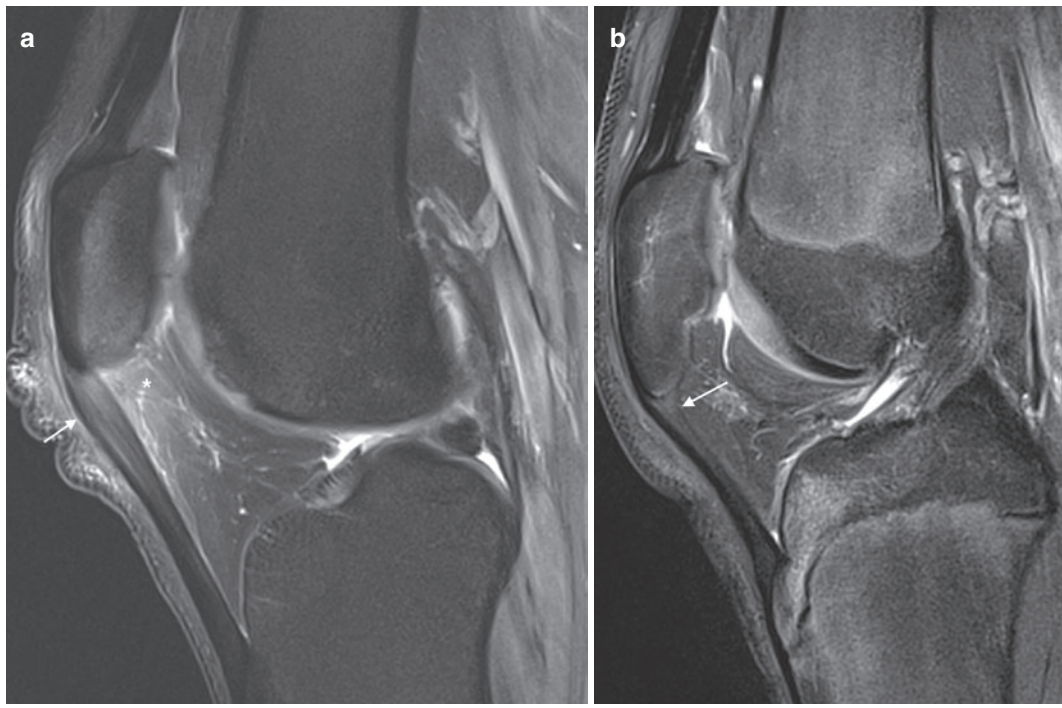

Fig. 12 (**a**, **b**) Jumper's knee and magic angle. (**a**) Sagittal proton-density fat saturation MR image shows a thickened and hyperintense tendon. Note the adjacent fat pad oedema as a supporting sign (asterisk). (**b**) Sagittal proton-density fat-saturated image shows magic-angle artefact (arrow) producing hyperintensity in the deep portion of the tendon. The tendon is not thickened and the fat is normal

Fig. 13 Severe infrapatellar tendinosis. Sagittal proton-density fat saturation image showing extensive tendinosis (arrows). This can lead to tendon shortening and patella baja

concept of Hoffa's fat pad impingement syndrome is controversial but oedema is sometimes seen in the pad without any obvious explanation. In chronic impingement, there may be chondral and osseous metaplasia. The normal infrapatellar plica (ligamentum mucosum) can be frequently identified on MR as it runs through the fat pad and attaches to the inferior pole of the patella (Fig. 7). Occasionally high signal is seen surrounding the plica on MR (Radu et al. 2015). How frequently this abnormality itself is related to symptoms is open to question. The most common lesion found in the fat pad is a ganglion often arising from the ACL (Fig. 15). Ganglia are usually diagnosed on MR but ultrasound is useful to confirm their cystic nature. Ultrasound-guided aspiration and injection may be beneficial. The commonest solid tumours are the nodular form of pigmented villonodular synovitis (PVNS) and synovial osteochondromatosis. Focal PVNS contains haemosiderin and fibrosis which is seen as low signal intensity on T2-weighted images (Fig. 16). Synovial osteochondromatosis is usually calcified to a varying degree (Helpert et al. 2004).

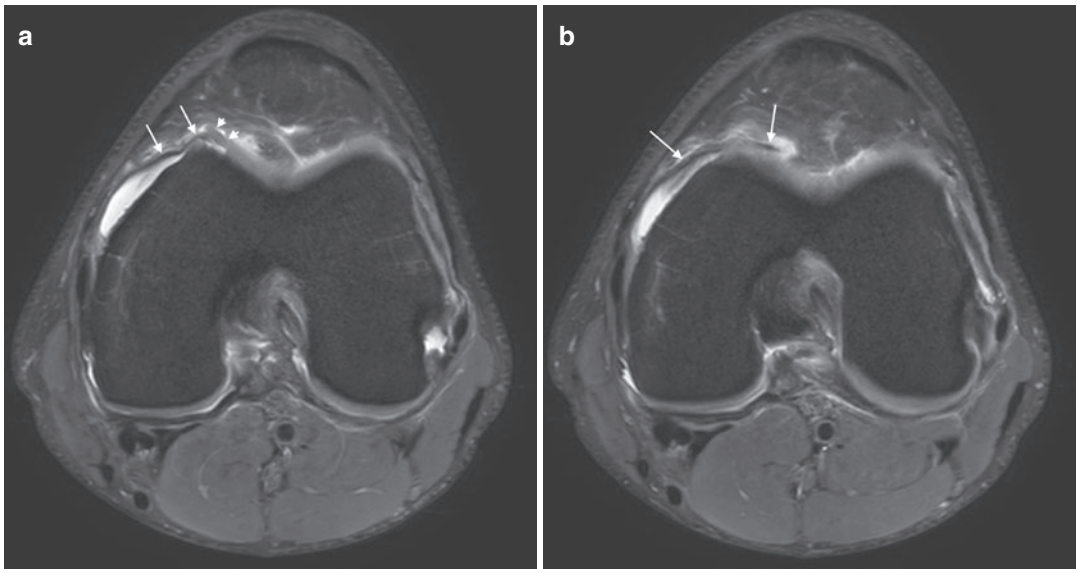

Fig. 14 (**a**, **b**) Medial patellar plica. Professional footballer. Sequential axial proton-density fat-saturated MR images. (**a**) The medial plica (arrows) has lifted and become trapped under a cartilage flap (arrowheads). (**b**) The thickened plica is draped over the medial trochlea (arrows)

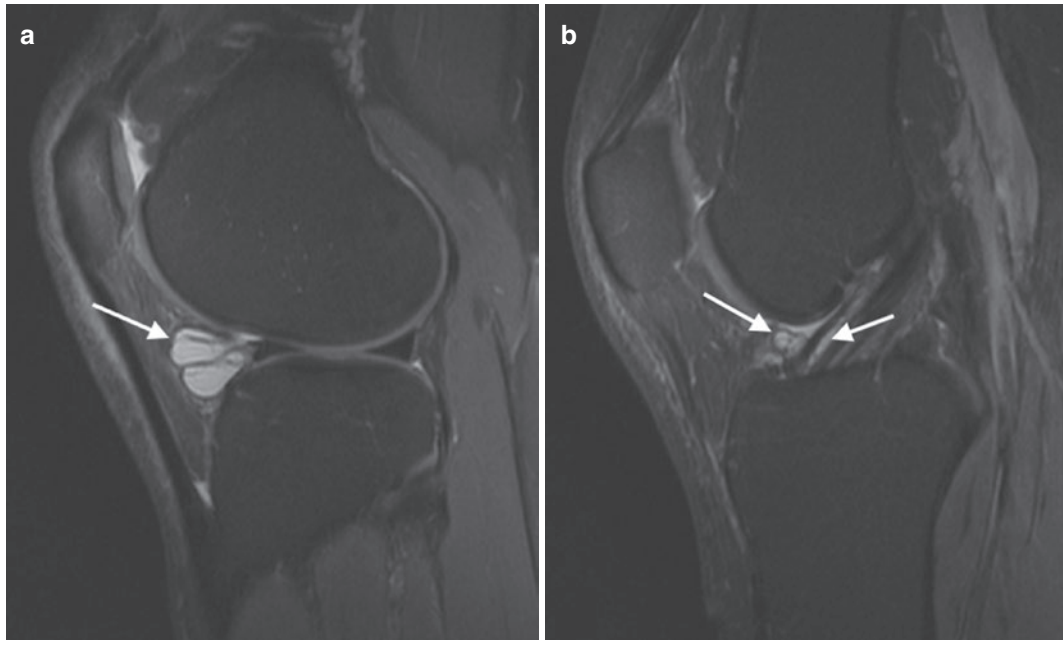

Fig. 15 (**a**, **b**) Hoffa's fat pad ganglion. (**a**, **b**) Proton-density fat-suppression sagittal MR image showing lobulated cystic mass (arrow in **a**). The mass arises from the ACL (arrows in **b**)

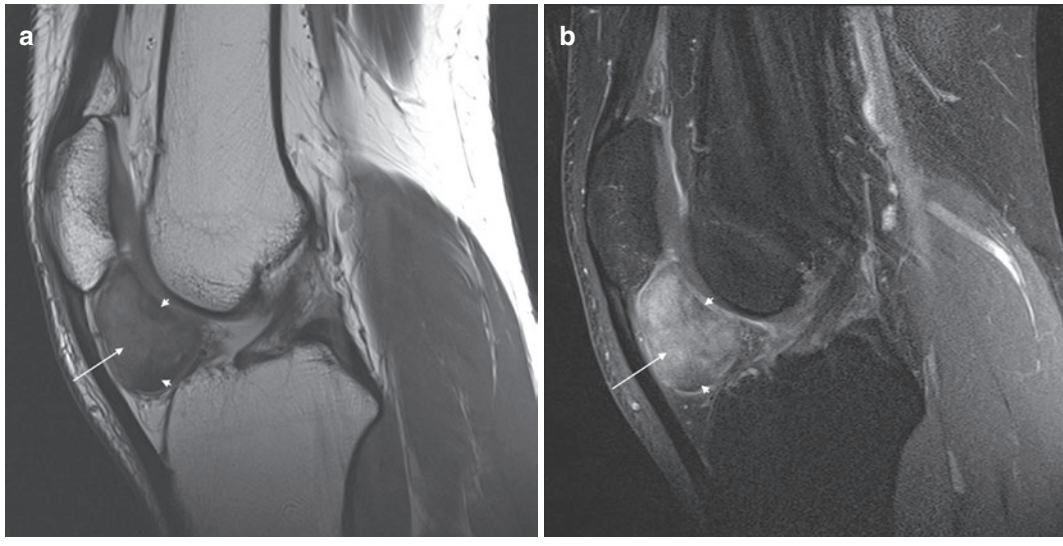

Fig. 16 (**a**, **b**) Focal PVNS. (**a**) Sagittal T1 and (**b**) sagittal proton-density fat-suppression MR image shows a well-defined mass (arrows) in Hoffa's fat pad which contains some low signal intensity on the fat-suppression images representing haemosiderin and fibrosis (arrowheads in **b**), although this may be absent in the localised form

A common finding on MR is oedema involving the superolateral Hoffa's fat pad due to impingement of the lateral aspect of the patellar tendon on the anterolateral articular margin of the lateral femoral condyle. Some minor high signal may be detected in the fat that is interposed between the tendon and the condyle. Although this entity may be seen in patients with anterior or anterolateral pain, it is so common a finding on routine MR that its significance is open to question (Fig. 17). There is evidence of an association with patellofemoral dysplasia, in particular with patella alta, maltracking and patellofemoral osteoarthritis (Li et al. 2019; Kim et al. 2019). Fat pad induration may be identified with ultrasound and addressed with guided steroid injection (Fig. 18).

3.4 Patellofemoral Joint

Definable conditions of the patellofemoral joint that cause anterior knee pain are chondromalacia, osteochondritis dissecans and patellar maltracking. 'Patellofemoral pain syndrome' is a term usually reserved for cases of retropatellar knee pain without an identifiable cause.

3.4.1 Patellofemoral Pain Syndrome

The term is usually reserved for patients with anterior knee pain without a detectable structural abnormality and is common in athletes and non-athletes alike (Thomeé et al. 1999). The condition is much more common in females. Imaging is rarely required as achieving a more specific diagnosis does not usually alter management. Most patients have normal imaging including normal patellofemoral anatomy. A proportion of patients will have demonstrable chondromalacia of the retropatellar cartilage but this is a common finding in individuals without pain (van der Heijden et al. 2016).

Some patients will have anatomical abnormality predisposing to maltracking of the patella (Drew et al. 2016).

Imaging is indicated if symptoms are atypical or persistent, mainly to rule out treatable pathology such as osteochondritis dissecans. If

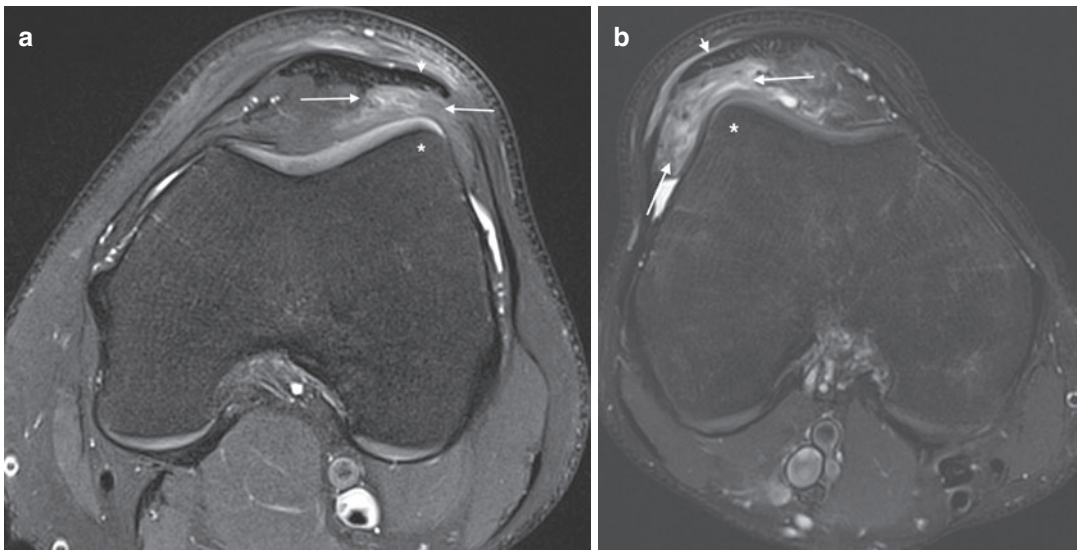

Fig. 17 (**a**, **b**) Superolateral Hoffa's fat pad impingement. Axial proton-density fat-saturated MR images. (**a**) Mild oedema (arrows in **a**) is seen in the fat pad between the lateral margin of the tendon (arrowhead) and the lateral condyle (arrowhead). (**b**) More severe changes

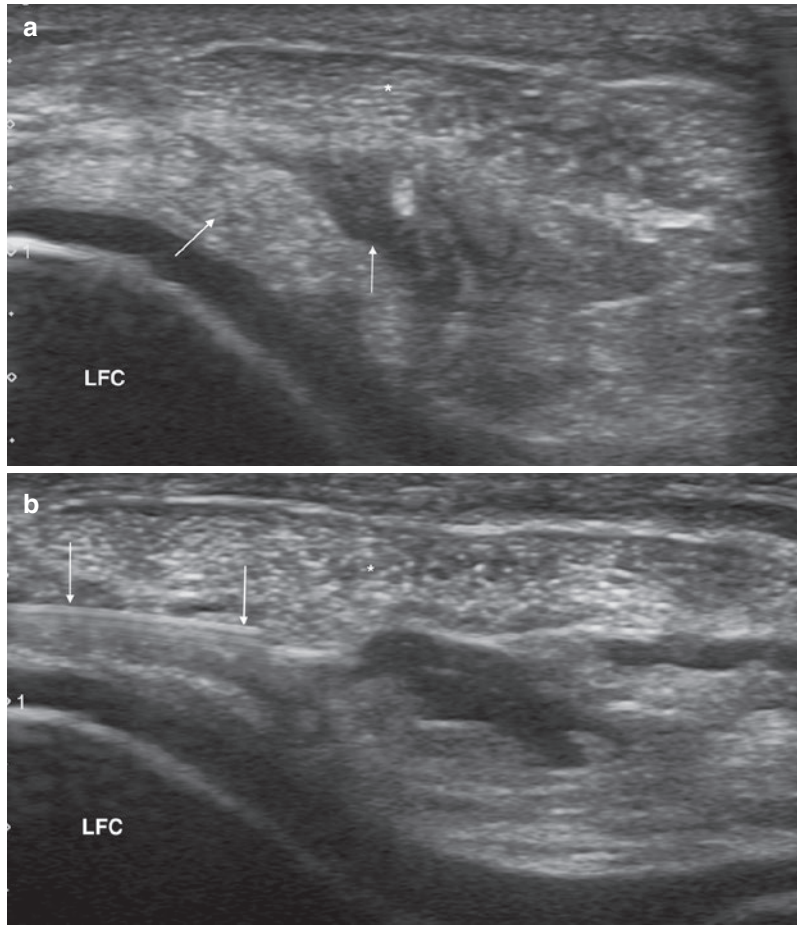

Fig. 18 (**a**, **b**) Fat pad impingement. Axial ultrasound images over the proximal, lateral infrapatellar tendon. (**a**) Echogenic oedematous fat (arrows) under the later margin of the tendon (asterisk). (**b**) Needle (arrows) introduced into the fat pad for steroid injection

maltracking is suspected and surgery is being considered then MR is useful to document any dysplasia. Dynamic imaging may be used to detect and quantify maltracking. Imaging is not always performed for suspected chondromalacia although macroscopic lesions may be reliably seen on good-quality MR (Fig. 19). Patients may rarely present with acute chondral injuries (Fig. 20).

3.4.2 Bipartite Patella

Bipartite patella is a normal variant where there is a small separate ossification usually at the superolateral aspect of the patella. Bipartite patella can be easily identified on radiographs and MR. In asymptomatic cases, a layer of high signal may be seen in a cleft at the articulation but the overlying articular cartilage is intact. Symptomatic cases are rare but persistent localised pain following injury has been reported. On MR, oedema on either side of the divide between the accessory ossification and the main body of the patella may be encountered, as well as disruption of the cartilage (Fig. 21) (Radha et al. 2017).

3.4.3 Osteochondritis Dissecans

Osteochondritis dissecans is a disease of childhood and adolescence thought to be due to

localised failure of endosteal ossification resulting in a cartilage-filled crater of the subchondral bone plate, which is vulnerable to calcification and fragmentation. It is more common in athletic individuals and is due to repetitive loading on the articular surface. In the knee osteochondritis dissecans typically involves the lateral aspect of the medial femoral condyle or the weight-bearing portion of the lateral femoral condyle, but the patella and the lateral facet of the trochlea are also recognised sites (Fig. 22) (Kramer et al. 2015). The patient may present with anterior pain when the lesion involves the patellofemoral joint or the anterior aspects of the femoral condyles. Osteochondritis dissecans can usually be identified on plain films but MR is more sensitive. Radiographically osteochondritis dissecans is seen as a subchondral lucency that may contain a density representing the osteonecrotic fragment. Intra-articular loose bodies may also be seen. On

Fig. 19 Chondromalacia. Axial T2 fat-suppression image showing a full-thickness fissure in the articular cartilage (arrow)

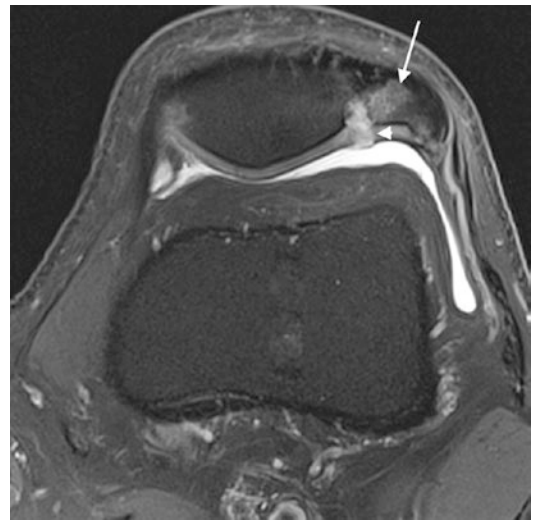

Fig. 21 Bipartite patella. Axial proton-density fat saturation MR image showing bipartite patella with oedema in the ossicle (arrow). The overlying cartilage is disrupted (arrowhead)

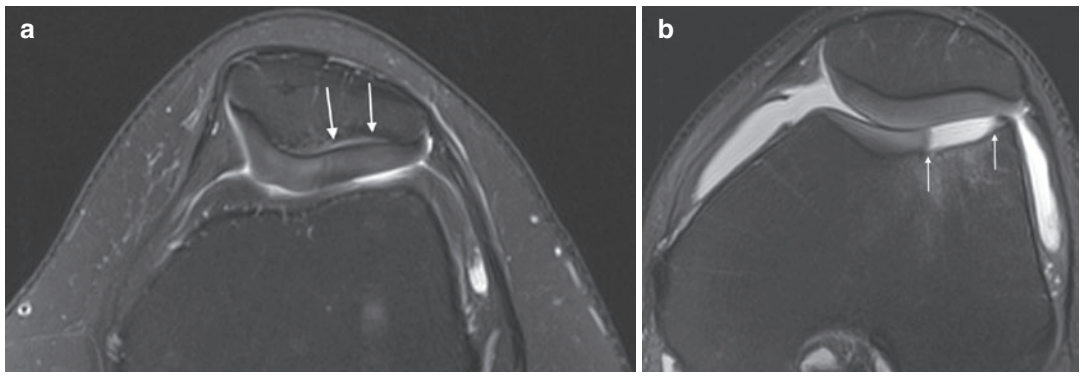

Fig. 20 (**a**, **b**) Chondral injuries. Axial proton-density fat saturation images. (**a**) Delamination of cartilage at the tidemark between calcified and uncalcified cartilage (arrows). (**b**) Acute chondral fracture of the trochlea leaving a well-defined defect (arrows)

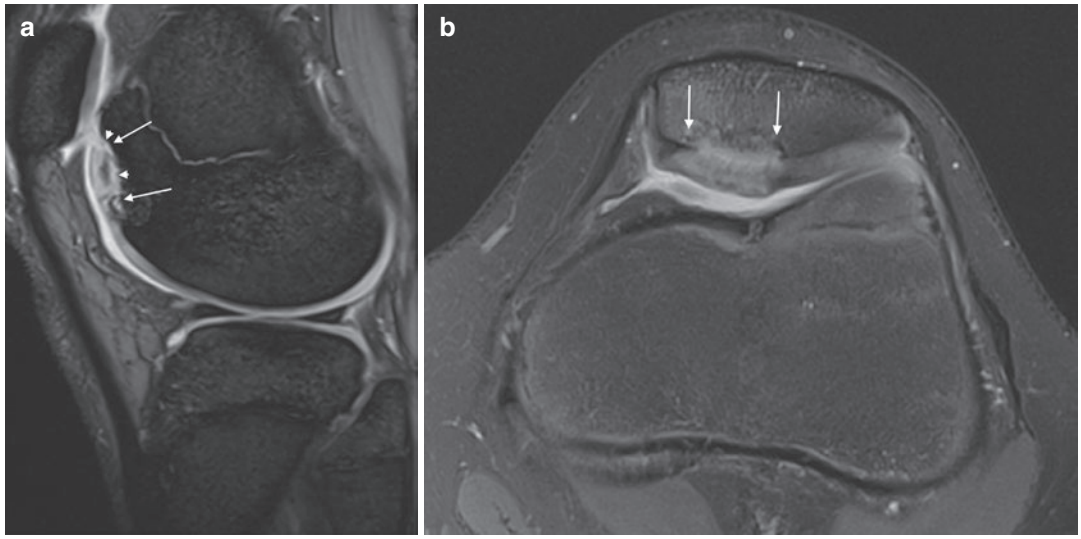

Fig. 22 (**a**, **b**) Osteochondritis dissecans of the patellofemoral joint. (**a**) Sagittal gradient-echo MR image showing an osteochondral lesion in the lateral trochlea (arrows). Fluid subtends this unstable lesion (arrowheads). (**b**) Axial proton-density fat saturation MR image showing a focus of osteochondritis in the medial patellar facet. There is a cystic change below the absent subchondral bone plate, which suggests instability

MR the defect may be seen to be filled with fibrocartilage or to contain the necrotic fragment. The generally accepted criteria for diagnosing an unstable lesion is high-signal fluid lying deep to the fragment and breach of the articular cartilage (De Smet et al. 1997). Multiple cysts at the edge of the lesion may also suggest instability (Grimm et al. 2014). Accurate staging of osteochondritis dissecans usually requires arthroscopy. Normal irregularity of the posterior aspect of the medial femoral condyle in children may simulate osteochondritis dissecans (Gebarski and Hernandez 2005).

3.4.4 Patellar Maltracking

Patients with maltracking may present with nonspecific retropatellar pain or symptoms of patellofemoral joint instability including dislocation. Imaging is useful in suspected acute patellar dislocation (see above) and in patients with chronic patellofemoral instability who are being considered for surgery.

Bony factors that predispose to patellofemoral instability are a high-riding patella (patella alta), a flat or convex trochlear, laterally positioned tibial tubercle and genu valgum. The soft tissue factors include a deficient vastus medialis and medial patellofemoral ligament. The relative contribution of each of these factors may influence clinical management. Most patients are managed conservatively. Popular surgical options are medial or anteromedial transfer of the tibial tubercle and repair of the medial patellofemoral ligament (Erickson et al. 2019). Refashioning of the trochlear groove (trochleoplasty) is usually reserved for severe forms of trochlear dysplasia (Balcarek and Zimmermann 2019). Popularity of lateral retinaculum release has waned and now has a limited role in the treatment of instability (da Fonseca et al. 2017).

MRI is the most useful technique for assessing the relevant anatomy. The commonest measurement used to diagnose patella alta is the Insall-Salvati ratio (patellar tendon-patella ratio) which can be measured on MR or, more reliably, a lateral radiograph (Verhulst et al. 2020). The normal ratio should be less than 1.3–1.5 (Shabshin et al. 2004). The trochlear groove is best assessed on the axial MR. When abnormal, the groove may be shallow, or the surface may be flat or even convex in its most proximal part (Fig. 23). The relative position of the tibial tubercle is clinically estimated by

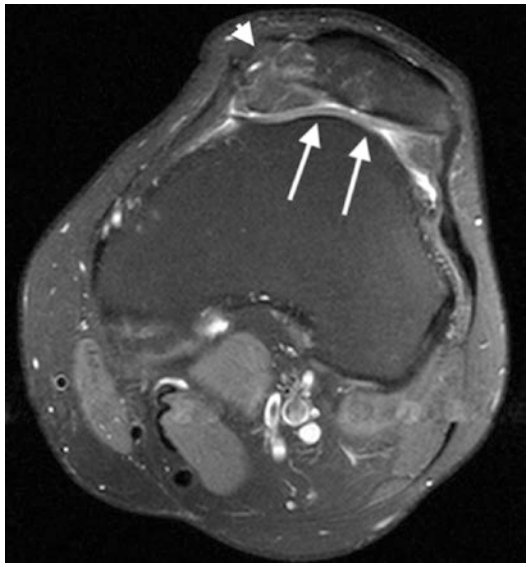

Fig. 23 Patellofemoral dysplasia. Axial proton-density fat suppression MR image through the proximal part of a dysplastic convex trochlear 'groove' (arrows). There is chronic disruption of the medial patellofemoral ligament

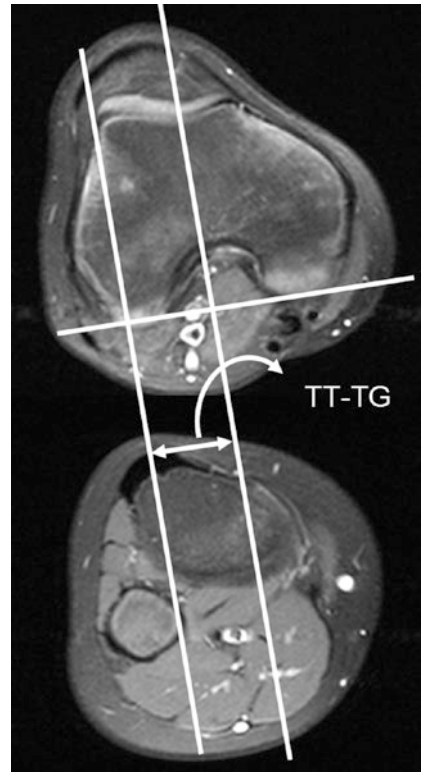

Fig. 24 Laterally positioned tibial tubercle. The TT-TG distance is measured on axial proton-density fat-saturated images at the trochlear notch and tibial tuberosity

measuring the Q angle, which is the angle between a line drawn from the anterosuperior iliac spine to the centre of the patella and a line drawn from the centre of the patella to the tibial tubercle. The MR equivalent is the tibial tubercle-trochlear groove (TT-TG) distance. This is the distance between the deepest point of the trochlear groove and the tibial tubercle in the sagittal plane. Two axial slices are selected, one at the level of the trochlear groove and the other at the level of the attachment of the patellar tendon at the tubercle. The two slices are superimposed. A baseline is drawn along the back of the femoral condyles. Two lines are drawn perpendicular to this baseline, one through the tibial tubercle and the other through the deepest point of the trochlear groove. The TT-TG is the distance between these two lines (Fig. 24). The upper limit of normal is about 1.7–1.8 cm. In almost all cases with a value above 2 cm, maltracking can be demonstrated on dynamic imaging (McNally et al. 2000). Patients with high TT-TG distance are likely to benefit from tibial tubercle medialisation.

In patients with suspected chronic instability, it may also be helpful to document whether or not a patient is indeed maltracking. In some cases, this may be obvious on clinical examination but often imaging is required, particularly in obese patients and those with relatively minor degrees of maltracking. Lateral subluxation may be demonstrated on skyline radiographs but this is an insensitive test as maltracking is maximal from 30° of flexion to full extension (Fig. 25). CT and MR have the advantage of being able to provide axial images of the knee within this range of flexion. Axial images through the centre of the patella are obtained while the knee is extended from 30° of flexion to full extension. Dynamic imaging acquires data while the knee is moving. One MR method is to acquire multiple rapid axial images through the patella during a slow controlled extension. A continually repeated series of around five axial images and one sagittal image are obtained through the patella during extension. For each series, the slice through the centre of the patella is

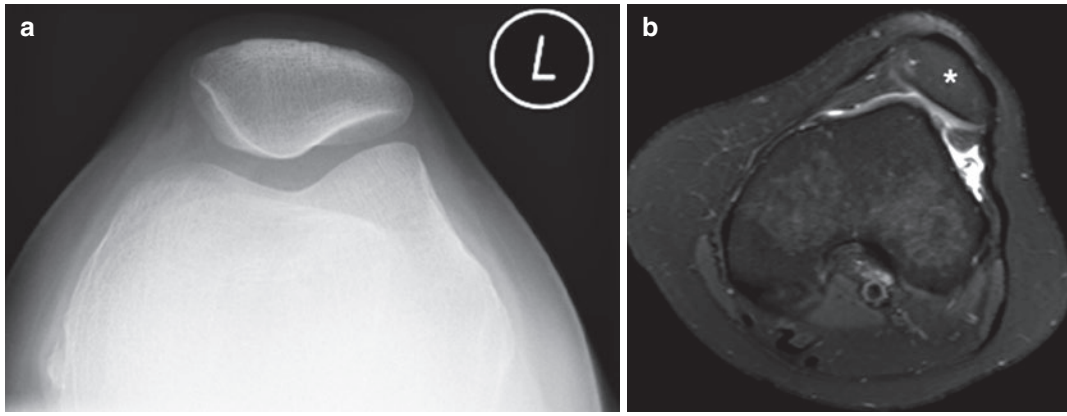

Fig. 25 (**a**, **b**) Patellar subluxation. (**a**) Skyline X-ray image shows a normal position. (**b**) Axial T2 fat saturation MR image in the same patient with the knee in slight flexion shows a sublimed patella (asterisk)

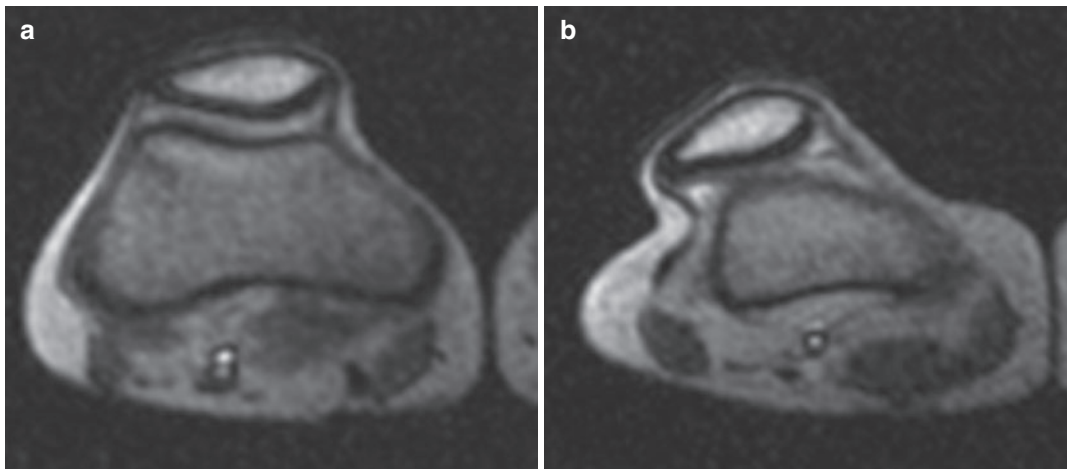

Fig. 26 Patellar maltracking. Axial images with 1-s acquisition time in (**a**) 30° of flexion and (**b**) full extension. There is lateral subluxation and tilt of the patella in extension

selected and a cine loop created (Fig. 26). True real-time dynamic images are now possible with the development of new fast acquisition sequences or real-time CT (Burke et al. 2018). The degree of maltracking correlates with symptoms and TT-TG (O'Donnell et al. 2005; Williams et al. 2016).

4 Conclusion

Most cases of anterior knee pain originate from the patellar tendon, Hoffa's fat pad or patellofemoral joint. Most cases do not require imaging. Acute traumatic pain requires plain films to exclude fracture supplemented by MR if patellar dislocation is considered a possibility. Soft-tissue overuse injuries of the patellar tendon are best assessed by ultrasound. MR is the technique of choice for assessing the patellofemoral joint and abnormalities of Hoffa's fat pad. Plain films are of limited value in the assessment of chronic anterior knee pain.

Things to Remember

- The triad of MR findings found in patellar dislocation is specific for this injury.

- Ultrasound is an excellent method of assessing the patellar tendon and other superficial soft-tissue injuries. No other imaging is required in the vast majority of cases.
- Patellofemoral dysplasia, a complex disorder involving the position of the patella and the tibial tubercle and the shape of the trochlear groove, is best assessed by MR.
- True dynamic imaging is possible with MR to demonstrate maltracking.

Imaging Technique Boxes

CT

High radiation dose.

Poor soft-tissue contrast.

Not indicated in the assessment of anterior knee pain except in exceptional circumstances.

Radiography

Indicated in acute trauma.

Has a lower sensitivity for almost all pathologies when compared to MR.

Not routinely indicated in anterior knee pain in the athlete.

Occasionally useful as second-line investigation to clarify an abnormality seen on MR.

Ultrasound

Excellent tool for assessing the superficial soft tissues.

Quick, easy and cheap.

Patient friendly.

Dynamic and Doppler imaging useful.

Direct interaction with the patient often helpful.

MR

Excellent tool for assessing joints, bones and soft tissues.

Sensitive and specific for most conditions causing anterior knee pain.

Expensive and not very patient friendly.

First-line test for assessment of all pathologies of the patellofemoral joint.

References

Aguiar RO, Viegas FC, Fernandez RY et al (2007) The prepatellar bursa: cadaveric investigation of regional anatomy with MRI after sonographically guided bursography. Am J Roentgenol 188: W355–W358

Balcarek P, Zimmermann F (2019) Deepening trochleoplasty and medial patellofemoral ligament reconstruction normalize patellotrochlear congruence in severe trochlear dysplasia. Bone Joint J 101-B:325–330

Burke CJ, Kaplan D, Block T et al (2018) Clinical utility of continuous radial magnetic resonance imaging acquisition at 3 T in real-time patellofemoral kinematic assessment: a feasibility study. Arthroscopy 34:726–733

Cao H, An Q, Gou B et al (2019) A new classification of injury patterns of the medial patellofemoral ligament after acute lateral patella dislocation detected using magnetic resonance imaging studies. Injury 50:534–540

Capogna B, Strauss E, Konda S et al (2017) Distal patellar tendon avulsion in association with high-energy knee trauma: a case series and review of the literature. Knee 24:468–476

da Fonseca LPRM, Kawatake EH, de Pochini A (2017) Lateral patellar retinacular release: changes over the last ten years. Revista Brasileira de Ortopedia (English Edition) 52(4):442–449

De Smet AA, Ilahi OA, Graf BK (1997) Untreated osteochondritis dissecans of the femoral condyles: prediction of patient outcome using radiographic and MR findings. Skelet Radiol 26:463–467

Draghi F, Danesino GM, Coscia D et al (2008) Overload syndromes of the knee in adolescents: sonographic findings. J Ultrasound 11:151–157

Drew BT, Redmond AC, Smith TO et al (2016) Which patellofemoral joint imaging features are associated with patellofemoral pain? Systematic review and meta-analysis. Osteoarthritis Cartilage 24: 224–236

Duthon VB (2015) Acute traumatic patellar dislocation. Orthop Traumatol Surg Res 101:S59–S67

Erickson BJ, Nguyen J, Gasik K et al (2019) Isolated medial patellofemoral ligament reconstruction for patellar instability regardless of tibial tubercle–trochlear groove distance and patellar height: outcomes at 1 and 2 Years. Am J Sports Med 47: 1331–1337

Gebarski K, Hernandez RJ (2005) Stage-I osteochondritis dissecans versus normal variants of ossification in the knee in children. Pediatr Radiol 35:880–886

Gettys FK, Morgan RJ, Fleischli JE (2010) Superior pole sleeve fracture of the patella: a case report and review of the literature. Am J Sports Med 38:2331–2336

Grimm NL, Weiss JM, Kessler JI et al (2014) Osteochondritis dissecans of the knee: pathoanatomy, epidemiology, and diagnosis. Clin Sports Med 33:181–188

Guldhammer C, Rathleff MS, Jensen HP et al (2019) Long-term prognosis and impact of Osgood-Schlatter disease 4 years after diagnosis: a retrospective study. Orthop J Sports Med 7:2325967119878136

Helpert C, Davies AM, Evans N et al (2004) Differential diagnosis of tumours and tumour-like lesions of the infrapatellar (Hoffa's) fat pad: pictorial review with an emphasis on MR imaging. Eur Radiol 14:2337–2346

Hunt DM, Somashekar N (2005) A review of sleeve fractures of the patella in children. Knee 12:3–7

Kim JH, Lee SK, Jung JY (2019) Superolateral Hoffa's fat pad oedema: relationship with cartilage T2* value and patellofemoral maltracking. Eur J Radiol 118:122–129

Kirsch MD, Fitzgerald SW, Friedman H, Rogers LF (1993) Transient lateral patellar dislocation: diagnosis with MR imaging. Am J Roentgenol 161:109–113

Kramer DE, Yen YM, Simoni MK et al (2015) Surgical management of osteochondritis dissecans lesions of the patella and trochlea in the pediatric and adolescent population. Am J Sports Med 43:654–662

Levin ES, Plotkin B, Levine BD et al (2019) Increased signal in the proximal patellar tendon: normal or pathologic? Skelet Radiol 48:1747–1751

Li J, Sheng B, Yu F et al (2019) Quantitative magnetic resonance imaging in patellar tendon-lateral femoral condyle friction syndrome: relationship with subtle patellofemoral instability. Skelet Radiol 48:1251–1259

McAuliffe S, McCreesh K, Culloty F et al (2016) Can ultrasound imaging predict the development of Achilles and patellar tendinopathy? A systematic review and meta-analysis. Br J Sports Med 50:1516–1523

McNally EG, Ostlere SJ, Pal C et al (2000) Assessment of patellar maltracking using combined static and dynamic MRI. Eur Radiol 10:1051–1055

Nixion A, Chandratreya A, Murray J et al (2017) Synovial plica syndrome of the knee: a commonly overlooked cause of anterior knee pain. Surg J (N Y) 3:e9–e16

O'Donnell P, Johnstone C, Watson M et al (2005) Evaluation of patellar tracking in symptomatic and asymptomatic individuals by magnetic resonance imaging. Skelet Radiol 34:130–135

Perfitt JS, Petrie MJ, Blundell CM et al (2013) Acute quadriceps tendon rupture: a pragmatic approach to diagnostic imaging. Eur J Orthop Surg Traumatol 24:1237–1241

Radha S, Shenouda M, Konan S et al (2017) Successful treatment of painful synchondrosis of bipartite patella after direct trauma by operative fixation: a series of six cases. Open Orthop J 11:390–396

Radu A, Discepola F, Volesky M et al (2015) Posterior Hoffa's fat pad impingement secondary to a thickened infrapatellar plica: a case report and review of the literature. J Radiol Case Rep 9:20–26

Saddik D, McNally EG, Richardson M (2004) MRI of Hoffa's fat pad. Skelet Radiol 33:433–444

Sailly M, Whitele R, Johnson A (2012) Doppler ultrasound and tibial tuberosity maturation status predicts pain in adolescent male athletes with Osgood-Schlatter's disease: a case series with comparison group and clinical interpretation. Br J Sports Med 47:93–97

Sanders TG, Paruchuri NB, Zlatkin MB (2006) MRI of osteochondral defects of the lateral femoral condyle: incidence and pattern of injury after transient lateral dislocation of the patella. Am J Roentgenol 187:1332–1337

Shabshin N, Schweitzer ME, Morrison WB et al (2004) MRI criteria for patella alta and baja. Skelet Radiol 33:445–450

Suzue N, Matsuura T, Iwame T et al (2015) State-of-the-art ultrasonographic findings in lower extremity sports injuries. J Med Investig 62:109–113

Tejwani SG, Cohen SB, Bradley JP (2007) Management of Morel-Lavallee lesion of the knee. Am J Sports Med 35:1162–1167

Terslev L, Qvistgaard E, Torp-Pedersen S et al (2001) Ultrasound and power doppler findings in jumper's knee—preliminary observations. Eur J Ultrasound 13:183–189

Thomeé R, Augustsson J, Karlsson J (1999) Patellofemoral pain syndrome: a review of current issues. Sports Med 8:245–262

van der Heijden RA, de Kanter JLM, Bierma-Zeinstra SMA et al (2016) Structural abnormalities on magnetic resonance imaging in patients with patellofemoral pain. Am J Sports Med 44:2339–2346

Verhulst FV, van Sambeeck JDP, Olthuis GS et al (2020) Patellar height measurements: Insall–Salvati ratio is most reliable method. Knee Surg Sports Traumatol Arthrosc 28(3):869–875. https://doi.org/10.1007/s00167-019-05531-1

Williams AA, Elias JJ, Tanaka MJ et al (2016) The relationship between tibial tuberosity–trochlear groove distance and abnormal patellar tracking in patients with unilateral patellar instability. Arthroscopy 32:55–61

Injuries of the Ligaments and Tendons in Ankle and Foot

Arn Van Royen, Maryam Shahabpour, Dima Al Jahed, Wiem Abid, Filip Vanhoenacker, and Michel De Maeseneer

Contents

A. Van Royen · M. Shahabpour (✉) · D. Al Jahed
W. Abid · M. De Maeseneer
Department of Radiology, University Hospital Brussels – Vrije Universiteit Brussel (VUB), Brussels, Belgium
e-mail: maryam.shahabpour@uzbrussel.be

F. Vanhoenacker
Department of Radiology, AZ Sint-Maarten Hospital, University of Antwerp, Ghent University, Mechelen, Belgium

Abstract

This chapter addresses sports-related injuries of ligaments and tendons of the ankle and foot with emphasis on trauma mechanisms and optimal imaging modalities and findings. The ankle is one of the most common sites of injury in sports with ankle sprain being the most frequent injury. Ligamentous elongations or tears tend to be acute whereas tendinosis is more typically due to overuse and repetitive trauma. Acute tendon tears usually occur in an already diseased tendon. Clinical diagnosis can be challenging due to the complex anatomy and multiple sites of potential injury. Ultrasound is perfectly suited for foot and ankle evaluation as most structures are located superficially. Moreover it allows dynamic assessment of ligaments and tendons towards the static CT or MRI. MRI is also an ideal modality because of the high soft-tissue contrast. It is essential in assessing associated intra-articular lesions and bone marrow oedema. Radiography and CT are a good complement of MRI for detection of bony avulsions and soft-tissue calcifications. Early MRI of the sprained ankle in the athlete can help to assess the severity of ligament injuries (involving lateral ligament complex, syndesmotic complex, deltoid complex, spring or subtalar ligaments as well as Chopart and Lisfranc ligaments in the midfoot). MRI is also capable to depict the first MTP joint ligamentous inju-

Med Radiol Diagn Imaging (2020)
https://doi.org/10.1007/174_2020_257, © Springer Nature Switzerland AG
Published Online: 01 January 2021

ries. Tendon disorders can be analysed on US and MR images based on the clinical findings and the tendon location (peroneal, flexor, extensor, plantar and posterior).

1 Ankle Ligament Tears

Ankle sprains are one of the most frequent sports-related injuries in both recreational and professional athletes. They account for up to 5% of all emergency department admissions and result in a variety of ligamentous injuries (Doherty et al. 2014). The trauma mechanism is often inversion and adduction with plantar flexion of the foot. Depending on the severity of injury, different ligaments can be involved. Most ankle sprains can be treated conservatively and overall outcome is excellent (Box 1).

Box 1 Standard Radiography and Computed Tomography

Standard Radiography

- Useful in acute setting to rule out fractures and small bone avulsions.
- May show aspecific soft-tissue swelling indicative of ligament or tendon injury.
- Ligaments and tendons themselves cannot be assessed, except on dynamic stress radiographs.

Computed Tomography: Same as Radiography

- May aid in the assessment of acute injuries.
- Helps to evaluate bone alignment and to detect tendon/ligament avulsion.
- Useful for preoperative planning of complex fractures.
- Good complement to MRI in chronic post-traumatic ankle or foot pain to detect small bone avulsions.

Imaging is often not necessary in the acute phase apart from radiographs to rule out fracture especially when there is an elective pain at clinical examination. Further imaging studies are indicated in cases that are refractory to conservative treatment. MRI in particular is the modality of choice in patients presenting chronic persistent ankle pain and/or instability to rule out lesions that were initially overlooked and to detect post-traumatic complications. Dynamic radiographs could assess ligament integrity but have a low specificity. Ultrasound (US) is efficient in acute ankle sprains and also allows dynamic evaluation of ligament integrity. Lateral, syndesmotic and medial ligaments are superficial structures, easily visualised on US. This method has the advantage towards MRI to be cheap and fast. MRI is an ideal technique not only for ligament evaluation but also for detection of commonly associated intra-articular lesions such as osteochondral injuries of the talus or injury of the subtalar ligament, which may cause persistent ankle pain or instability (Linklater et al. 2017; Mansour et al. 2011). In general ligamentous injuries can be classified into three categories. Grade I: The ligament is stretched but not torn. Grade 2: The ligament is partially ruptured. Grade III: The ligament is completely torn. Imaging findings of different ligamentous injuries are addressed in the following sections.

1.1 Lateral Ligament Complex

The lateral ligament complex of the ankle consists of the anterior talofibular ligament (ATFL), calcaneofibular ligament (CFL), and posterior talofibular ligament (PTFL) (Fig. 1). It is the most commonly involved in ankle sprains, especially the ATFL and middle CFL. The ATFL is the weakest of the three compounds and is injured in up to 85% of ankle sprains. The CFL is involved in 50–75% of cases. Tears of the PTFL (Fig. 28) are rare, with less than 10% of ankle injuries, and occur in severe trauma with ankle dislocation (Roemer et al. 2014; Mansour et al. 2011).

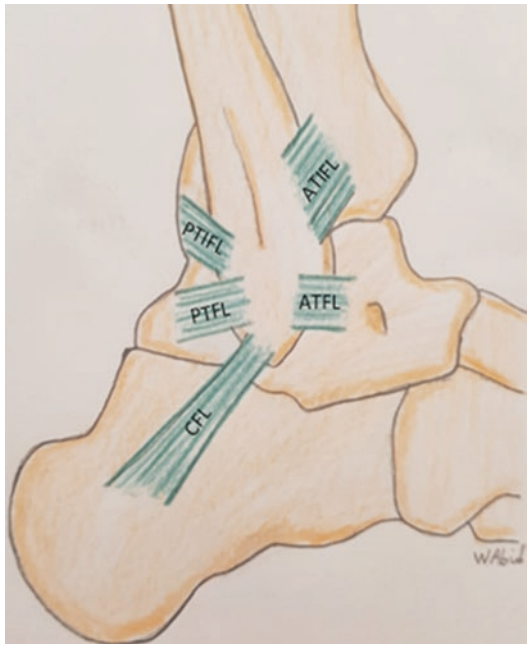

Fig. 1 Lateral ligament complex on a drawing with ATFL, PTFL and CFL as well as inferior tibiofibular ligaments ATIFL and PTIFL

Imaging On US the *ATFL* is a thin hyperechoic linear band running from the anterior rim of the distal fibula to the anterior lateral border of the talus. US has the advantage to show the ligament fibres. A normal ATFL is 2 mm thick. A grade I injury or sprain shows only mild oedema, fluid and a thickened ligament. A grade II or partial tear is characterised by a hypoechoic ligament, markedly thickened with presence of haematoma at one side. In grade III or complete tear, the ligament is discontinuous with a complete hypoechoic gap extending through the entire ligament with haematoma at both sides (Fig. 2). Thanks to the dynamic approach, we can state that the torn ligament end does not move and explain to the clinician that the ligament is incompetent; it cannot keep the ankle stable (the ankle being most probably unstable) and needs to be treated (first conservatively) (Sconfienza et al. 2015; McKiernan et al. 2017).

On MRI the ATFL is a 2 mm thick linear band with homogeneous hypointense signal on all

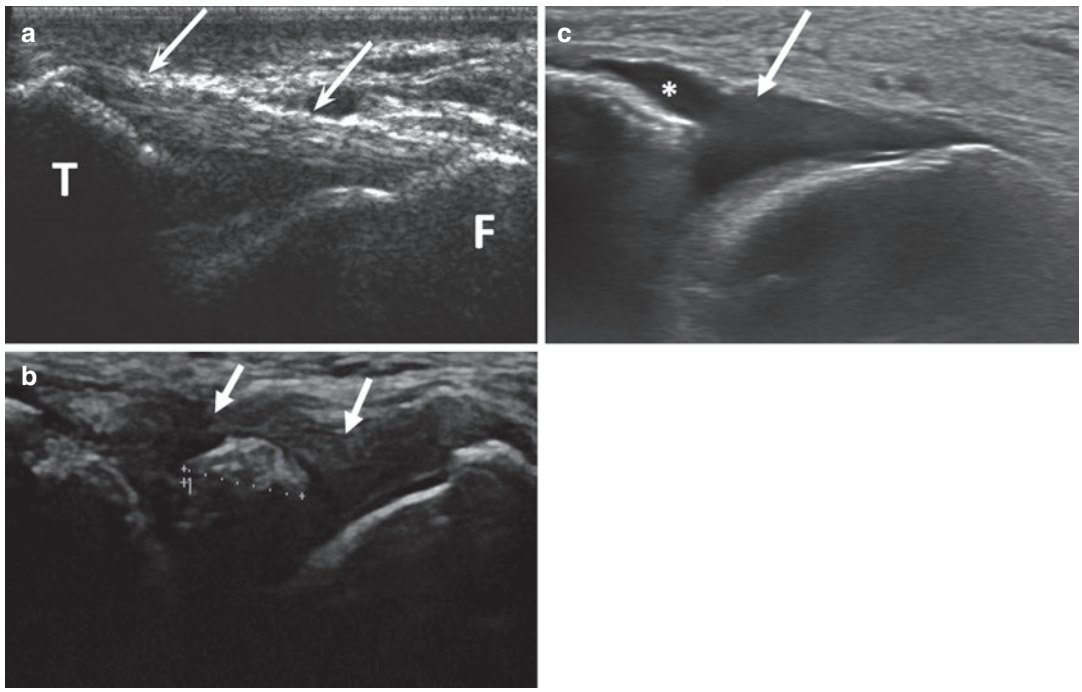

Fig. 2 (**a**–**c**) Normal ATFL and ATFL rupture on transverse US images. (**a**) Normal ligament (arrows) running from the lateral malleolus (F) to the talus (T). (**b**) Sequel of ATFL tear with bony avulsion (callipers) with thickened and hypoechoic ligament (arrows). (**c**) Complete tear of ATFL. Absent ligament (arrow) with fluid effusion protruding out of the joint space (asterisk)

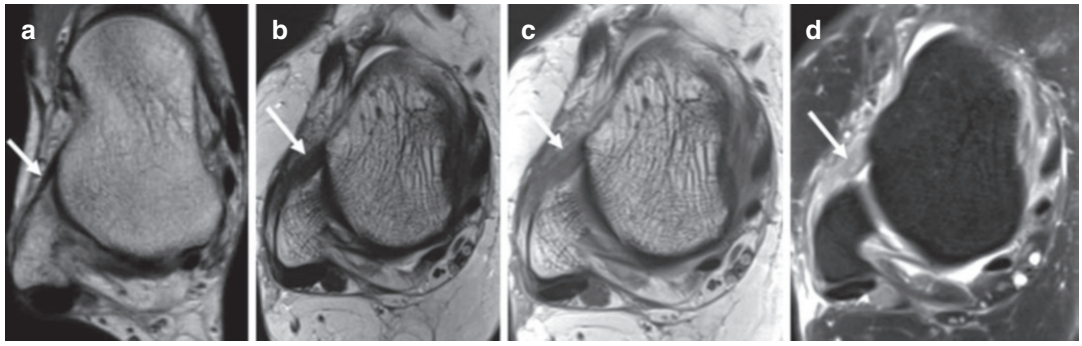

Fig. 3 (a–d) Normal ATFL and chronic tear on axial MR images. (**a**) Normal ATFL demonstrated on PD image through the pear-shaped talar body (arrow). (**b**–**d**) Chronic 3-month-old ATFL tear (arrow) with hypointense scar tissue infiltration on T2 (**b**). The signal intensity is increased and appears intermediate on PD (**c**) and higher on PD fat sat (**d**)

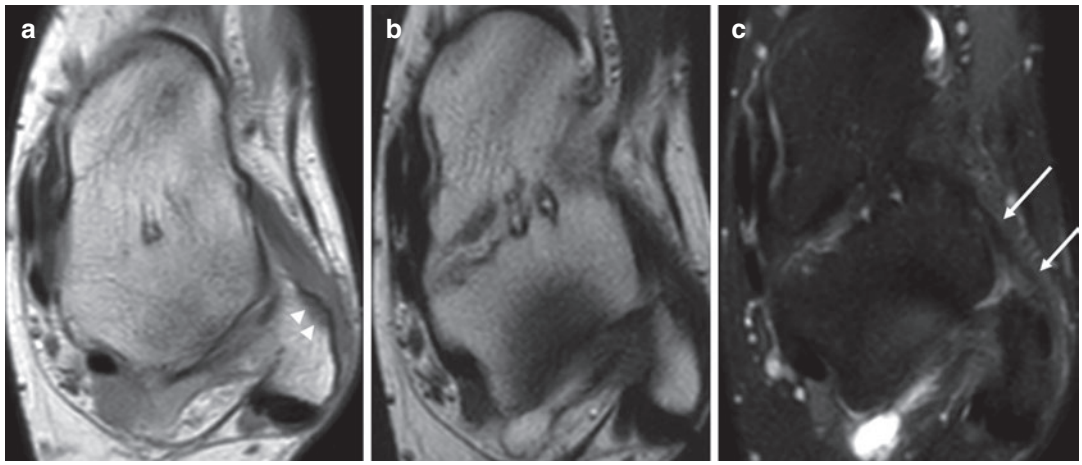

Fig. 4 (**a**–**c**) Chronic ATFL partial tear. Axial MR images of a 26-year-old female athlete obtained 6 m after a severe ankle sprain. PD (**a**), T2 (**b**) and PD fat sat (**c**) depict an attenuated ligament with still some continuous fibres, best visualised on **c** (arrows) and hypointense scar tissue infiltration (displayed on **b**). Slight irregular outline of the fibular cortical bone attachment (arrowheads on **a**)

sequences. It is readily visible in the axial plane and runs at the level of the talus body, which has a pear-like appearance at this level when the foot is in 90° flexion (using the boot-shaped ankle and foot coil) (Fig. 3a). In grade I and II acute injuries, the ligament has an increased signal intensity on fluid-sensitive sequences (such as proton density (PD), T2 or fat-suppressed PD). In case of full-thickness tear the ligament shows a complete discontinuity or is poorly visualised with frayed and wavy margins. Associated signs include fluid or haemorrhage in the anterolateral pouch and oedema in the surrounding capsular and fatty structures (Linklater et al. 2017; Mansour et al. 2011). In most cases the tears will heal, a process that takes up to 6–12 months. After a few days, the attenuated ligament infiltrated by granulation tissue will progressively be replaced by scar remodelling into parallel collagen bundles leading to a thickened ligament (with intermediate signal on T1 or PD images and low signal on T2) (Figs. 3b–d and 4). And approximately 1 year after trauma, MRI depicts a mature reconstructed low signal ligament on all sequences. Similarly on ultrasound, a scarred ligament is thickened and hypoechoic (Linklater et al. 2017; Mansour et al. 2011).

The *CFL* runs from the tip of the lateral malleolus to the lateral aspect of the calcaneus. It has

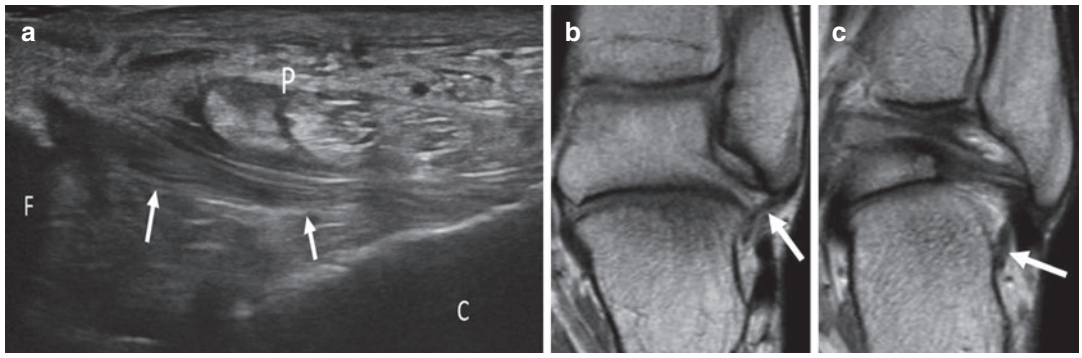

Fig. 5 (**a**–**c**) Normal CFL. (**a**) On a long-axis US image with the foot in dorsiflexion, the normal CFL (arrows) is running from the distal fibula (F) to the calcaneus (C). The ligament is positioned deep to the peroneal tendons (P). (**b**, **c**) Consecutive coronal PD MR images (from anterior to posterior) show the proximal (**b**) and distal (**c**) attachments of the CFL (arrow) running deep to the hypointense (dark) peroneal tendons

an oblique course from anterior to posterior and is located deep to the peroneal tendons; it forms a hammock for the peroneal tendons. It is more difficult to visualise than the ATFL on ultrasound and MRI. Dorsiflexion of the foot stretches the ligament making it more apparent on US (McKiernan et al. 2017). On MRI the ligament is best evaluated on consecutive coronal images when the foot is in 90° flexion (using a boot-shaped coil) (Fig. 5). When the foot is in plantar flexion, the CFL has a horizontal course and can be visualised through the whole length on axial images (Fig. 6). Imaging findings of CFL injuries are similar to ATFL (Figs. 7 and 8). Because of the close relation of the CFL to the peroneal tendons, effusion in the peroneal tendon sheath can be present in cases of CFL tear. The *PTFL* originates from the posterior rim of the lateral malleolus and inserts on the posterior side of the talus. It is composed of different bundles separated by fat resulting in an inhomogeneous appearance on MRI. Due to its deep location it is very difficult to identify on ultrasound (Linklater et al. 2017; Madani et al. 2016).

Fig. 6 Normal CFL. On the axial PD MR image obtained with the foot in plantar flexion (passing through the talocalcaneal joint), the CFL (arrows) has a horizontal course and can be visualised through its whole length (on a single transverse view)

1.2 Distal Syndesmotic Tibiofibular Complex

The distal syndesmotic ligament complex consists of the anterior inferior tibiofibular ligament (ATIFL), the inferior interosseous ligament (IIOL) and the posterior tibiofibular ligament (PTIFL). The ATIFL and PTIFL run, respectively, from the anterior and posterior sides of the distal tibia and of the distal fibula (McKiernan et al. 2017) (Fig. 1). The distal tibiofibular or

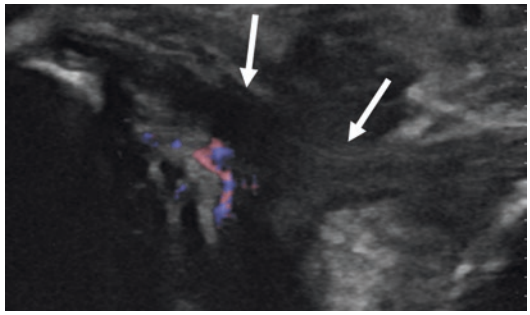

Fig. 7 CFL sprain. Long-axis US image (arrows) demonstrates a thickened and hypoechoic CFL with increased Doppler signal

syndesmotic ligament complex is less frequently injured (in up to 18% of cases in athletes). These injuries also referred to as "high ankle sprains" more typically occur in twisting injuries of the ankle and are common in skiing and football. The trauma mechanism is external rotation of the foot in dorsiflexion combined with internal rotation of the knee. The ATIFL is the first to tear followed by the stronger PTIFL. Bone avulsion is frequent in syndesmotic injury; a PTIFL tear for example will often start at the posterolateral tibial insertion. Posterior malleolar fracture is a type of syndesmotic injury where the PTIFL remains intact. Tibiofibular ligament injury may be a cause of persistent pain prolonging abstinence of activity. Syndesmotic ligament sprains are often overlooked; they are associated with a substantially longer recovery time compared with current lateral ankle sprains. An early and accurate imaging diagnosis is therefore critical to guide patient treatment (Nussbaum et al. 2001; Linklater et al. 2017; Mansour et al. 2011; Roemer et al. 2014).

Imaging Radiographs or CT may depict the bony avulsions and fractures as well as widening of the tibiofibular space. This should not exceed 2 mm at the narrowest interval (Fig. 9). After scar formation there may be bony hypertrophy at the tibial attachment of the PTIFL (De Brucker and Shahabpour 2016; Linklater et al. 2017). On ultrasound the ATIFL is located right above the level of the ATFL on the anterior side of the ankle (Fig. 1). It appears as a thin hyperechoic band with a width of 2 mm, running slightly oblique to the axial plane (Döring et al. 2018) (Fig. 10). When injured it is thickened or interrupted with an anechoic cleft. Dorsiflexion and external rotation of the ankle during ultrasound may help making the diagnosis as it will further widen the tibiofibular interval in case of tear. On MRI, the chronically injured ATIFL can be infiltrated by scar tissue (Fig. 11), sometimes leading to a nodular thickening of the fibrous scarred ligament, that may result in residual ankle stiffness (McKiernan et al. 2017; Linklater et al. 2017; De Brucker and Shahabpour 2016).

The other syndesmotic ligaments are not visible on ultrasound and have to be assessed on MRI. The IIOL is best visualised in the coronal plane while the PTIFL can be visualised in both axial and coronal planes. Bone marrow oedema is often present at the tibial insertion of the injured PTIFL (Linklater et al. 2017).

1.3 Deltoid Ligament Complex

The deltoid ligament is a fan-shaped ligamentous complex on the medial side of the ankle joint which comprises multiple individual ligaments. They can be divided into deep and superficial ligaments. The deep deltoid ligament is further subdivided into an anterior and a posterior tibiotalar component which runs from the medial malleolus to the medial side of the talus. The tibiocalcaneal, tibiospring and tibionavicular ligaments make up the superficial deltoid ligament (Fig. 12). Tears of the deltoid (or medial collateral) ligament complex occur more often in pronation trauma and fractures of the medial malleolus. Injury to the deltoid ligament is less common in inversion trauma, where the proposed mechanism of injury is contusion. Deltoid ligament lesions secondary to ankle inversion are often associated with medial-sided talar dome contusions. Injuries of deltoid ligament have a significant impact on lateral ankle instability but

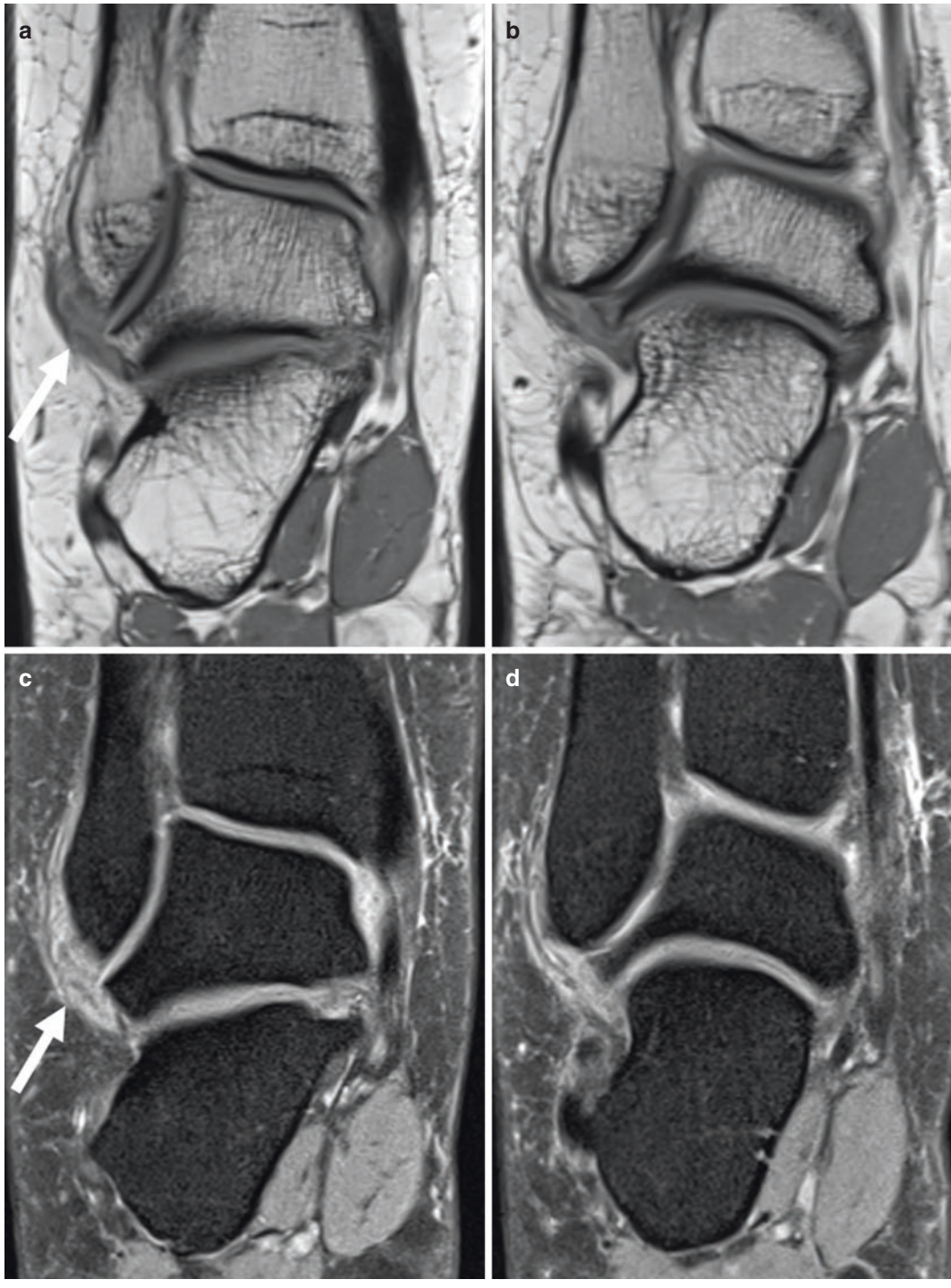

Fig. 8 (**a**, **b**) CFL tear. Consecutive (anterior to posterior) coronal PD (**a**, **b**) and PD fat sat (**c**, **d**) MR images through the posterior and distal part of the fibula show an infiltration of the submalleolar fat tissues along the normal course of the CFL. The CFL and surrounding oedematous infiltration (arrow) present an increased signal intensity (intermediate on PD and higher on PD fat sat)

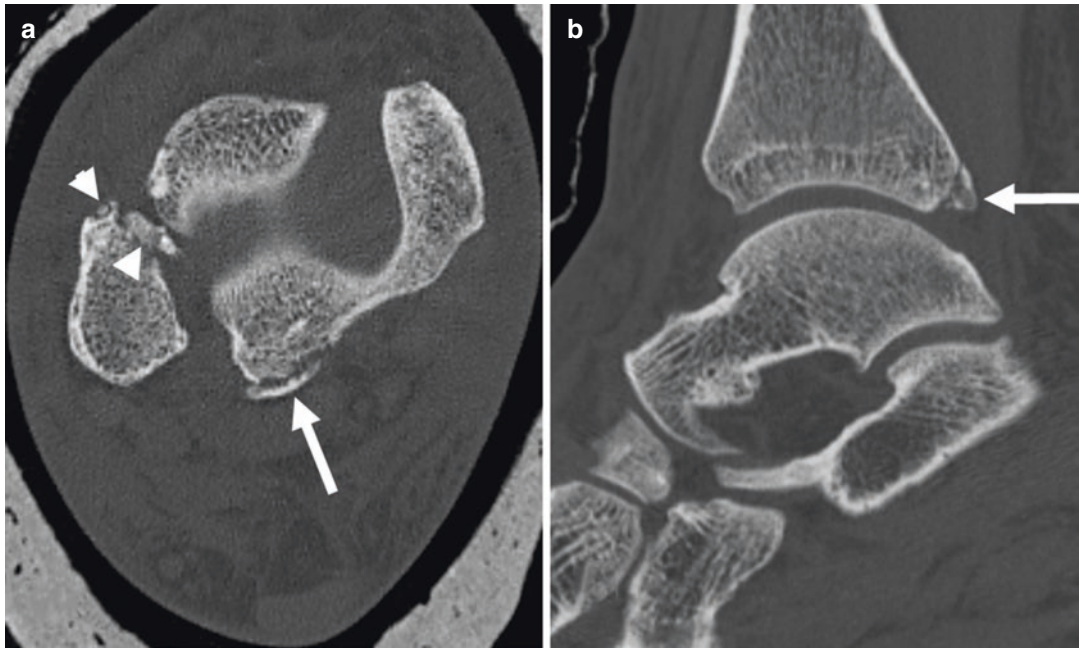

Fig. 9 (**a**, **b**) Tibiofibular syndesmotic injury. Transverse (**a**) and sagittal (**b**) plain CT images depict small bony avulsion at the tibial attachment of PTIFL (arrow). The posterior tibiofibular interval is widened secondary to the syndesmotic injury. Tiny bone avulsions (short arrows on **a**) are also seen at the ATIFL

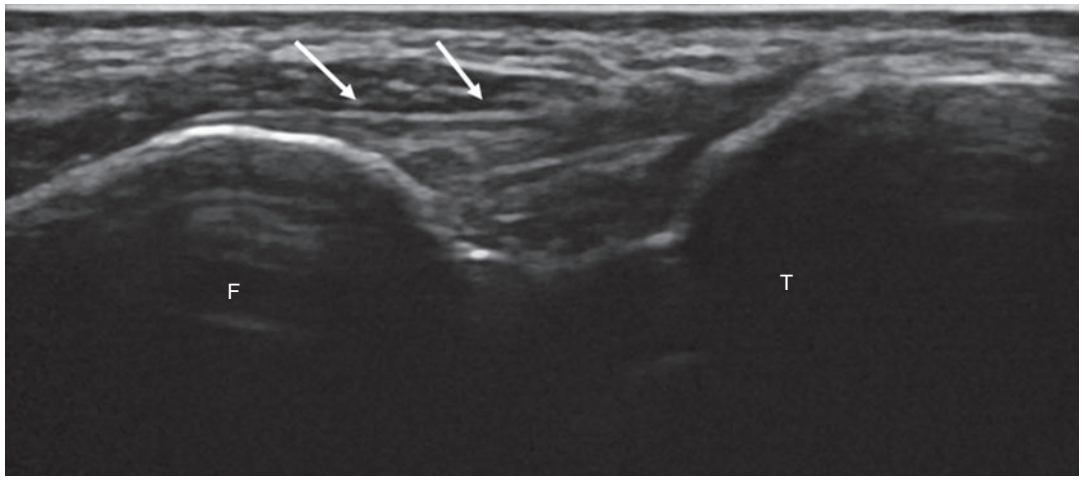

Fig. 10 Normal ATIFL (arrows) on a transverse US image with oblique positioning of the probe with the foot in dorsiflexion (*F* fibula, *T* tibia)

can be overlooked in patients with lateral ligament injuries. The deltoid ligament can be injured in isolation, but in more severe injuries, there is a fibular fracture or an associated tear of the tibiofibular syndesmosis (Roemer et al. 2014; Crim 2016; Mansour et al. 2011).

Imaging The posterior tibiotalar ligament can be visualised on US posterior to the medial malleolus and located deep to the posterior tibial tendon. The superficial ligaments are also easily demonstrated on US (Fig. 13a). On MRI the normal deep posterior tibiotalar ligament has a

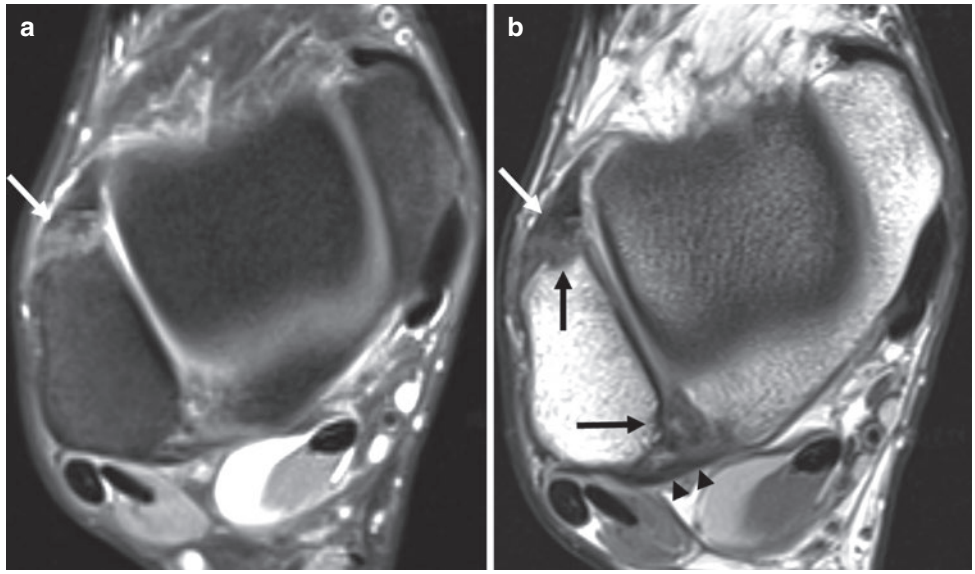

Fig. 11 (**a**, **b**) ATIFL and PTIFL sprain. Transverse PD fat sat (**a**) and PD (**b**) MR images show thickened and infiltrated fibular insertion of both ligaments with slight inhomogeneous signal increase (ATIFL, white arrow; PTIFL, arrowheads on **b**). This is associated to irregular anterior and posteromedial cortical outline of the fibula (dark arrows on **b**)

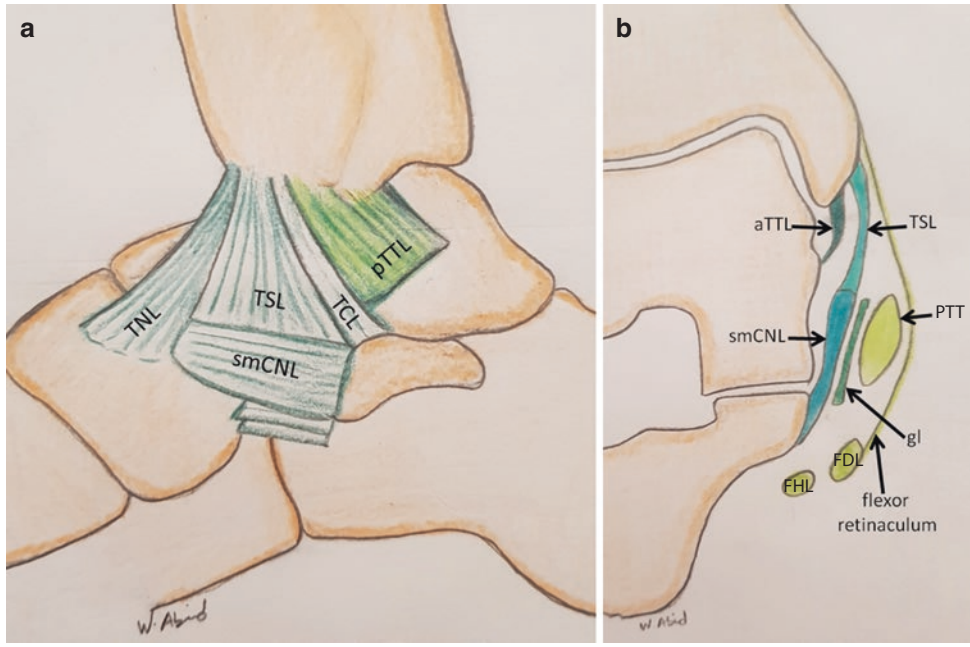

Fig. 12 (**a**, **b**) Deltoid ligament complex on (**a**) sagittal drawing demonstrating the deep posterior tibiotalar ligament (pTTL) and the superficial bundles: tibionavicular ligament (TNL), tibiospring ligament (TSL) and tibiocalcaneal ligament (TCL). The main superomedial calcaneonavicular portion (smCNL) of the spring ligament complex is also displayed. (**b**) is a coronal drawing showing the deep anterior tibiotalar ligament (aTTL) and the more superficial TSL originating from the anterior segment of the medial malleolus and inserting on the smCNL. Between the smCNL and the distal portion of the posterior tibial tendon (PTT), there is a gliding zone (gl) for the PTT which is covered by the FR (flexor retinaculum). *FDL* flexor digitorum longus, *FHL* flexor hallucis longus. (Redrawn from Mengiardi)

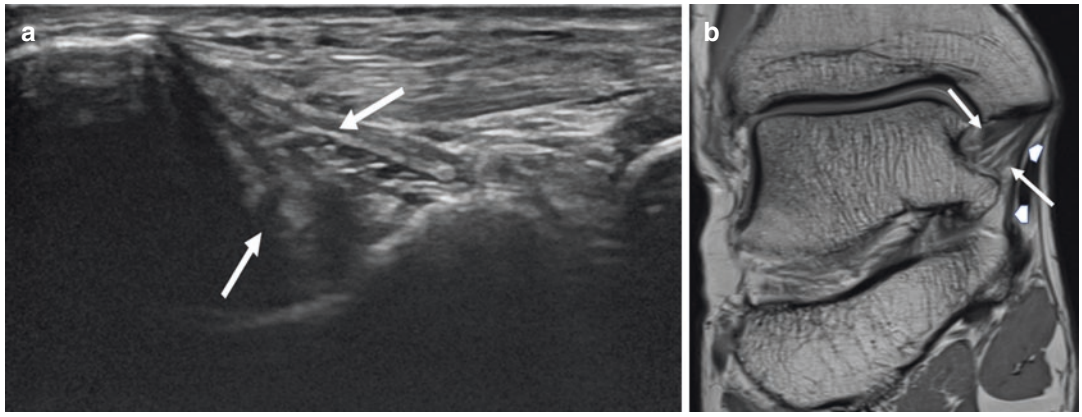

Fig. 13 (**a**, **b**) Normal deltoid ligament on (**a**) coronal US image and (**b**) coronal PD MR image. The deeper tibiotalar bundle (arrows) has a fan-like striated appearance with fatty interdigitations. This should not be mistaken for injury. The tibiocalcaneal bundle is more superficial and thinner with a homogeneous low signal intensity on MRI (arrowheads)

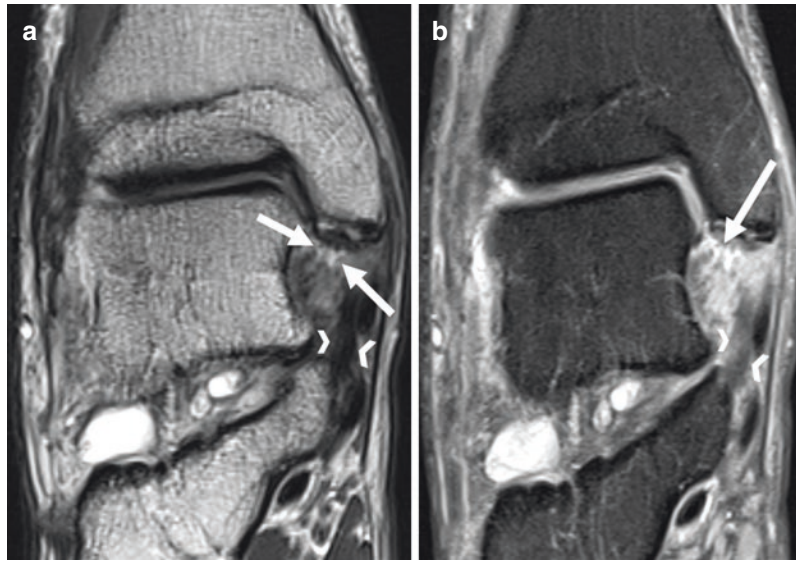

Fig. 14 (**a**, **b**) Partial tear of the deltoid ligament on coronal T2 (**a**) and PD fat-sat (**b**) MR images. The focal markedly hyperintense gap (arrows) corresponds to the interrupted fibres of the deep tibiotalar bundle. The still continuous fibres of this bundle demonstrate a slightly oedematous infiltration with increased signal (especially on PD fat sat) with loss of striated appearance. The superficial tibiocalcaneal bundle (arrowheads on **a**) has a thickened appearance with irregular outline and inhomogeneous signal on PD fat sat (**b**) and low signal on T2 (**a**) corresponding to chronic elongation (sprain)

striated appearance with multiple hyperintense fatty bands running through the ligament. The normal superficial bundles are thinner with a homogeneous low signal intensity (Fig. 13b). Loss of striated appearance of the deep posterior tibiotalar ligament or interruption of the fibres indicates ligament injury (Fig. 14). Chronic lesions of the thinner superficial bands appear as periligamentous infiltration with a thickened appearance due to scar tissue infiltration (Fig. 14). After ligament repair, the deltoid ligament may be hypertrophic causing medial-sided

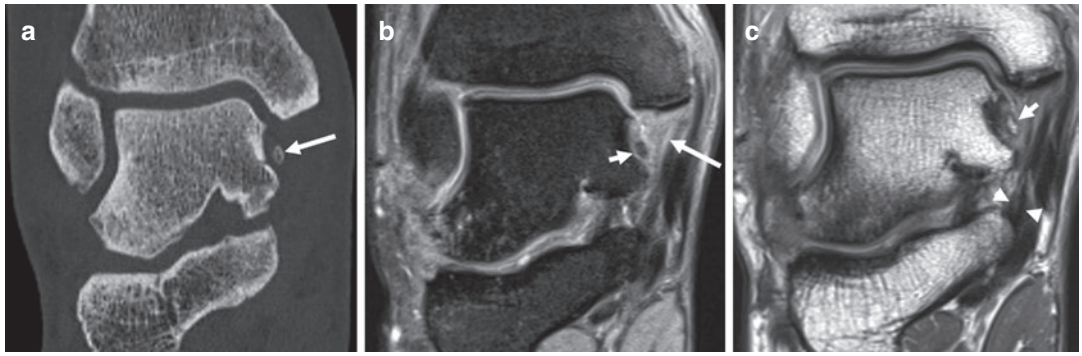

Fig. 15 (**a**–**c**) Sequela of deltoid ligament tear. Coronal CT reconstruction (**a**) detects an osseous fragment at the talar insertion of the deep fibres of the deltoid ligament (arrow). Coronal PD fat sat (**b**) and PD (**c**) demonstrate loss of the striated pattern of the tibiotalar bundle (arrow on **b**) and the bony avulsion on the medial side of the talus which has the same signal intensity as the other bone structures (short arrow). The tibiocalcaneal bundle looks partially fissured on PD (arrowheads on **c**)

impingement. Focal ossification within the scarred ligament is also described after healing (Linklater et al. 2017; Mansour et al. 2011; Crim 2016) (Fig. 15).

1.4 Subtalar Ligaments

The intrinsic ligaments of the sinus tarsi are the interosseous talocalcaneal ligament and the cervical ligament. They prevent inversion and preserve ankle alignment. The medial root of the inferior extensor retinaculum runs above these two ligaments covering the sinus tarsi. The interosseous talocalcaneal ligament runs from the tarsal sulcus to the calcaneal sulcus and is found posteromedially in the sinus tarsi. The cervical ligament is positioned more anterolaterally connecting the superior surface of the calcaneus to the inferolateral aspect of the talar neck (Fig. 16). Damage to these ligaments occurs after forced inversion of the ankle resulting in sinus tarsi syndrome. Patients present an elective pain and tenderness in the subtalar area, usually without signs of tibiotalar instability. They complain of a feeling of walking insecurity with pure subtalar instability aggravated by weight-bearing activity. The symptoms are often responsive to injection of local anaesthetic. Most cases arise following trauma, but the syndrome can be associated with inflammatory arthritis or foot deformities such as pes planus. Associated features include lateral ligament tears, posterior tibial tendon tears and ganglia arising from the posterior subtalar joint. Conservative treatment consists of corticosteroid injections, along with physiotherapy and correction of foot biomechanics. Sinus tarsectomy or subtalar joint synovectomy is reserved for persistent symptoms (Teh et al. 2011).

Imaging US does not allow visualisation of the ligaments themselves but fluid or scar tissue in the sinus tarsi may be indirect signs of ligament injury. MRI is the modality of choice to evaluate sinus tarsi syndrome. T1 and PD images can demonstrate replacement of the normal fatty tissue present in the sinus tarsi with fluid or inflammatory tissue, resulting in decrease of signal intensity on T1 and increase on T2. Tear of the cervical ligament is best seen on sagittal images while tear of the interosseous ligament is better visualised on coronal images. Chronic cystic distension or secondary osteoarthritis may also develop in an unstable joint (Döring et al. 2018; Mansour et al. 2011; Nazarenko et al. 2013) (Fig. 17).

1.5 Spring Ligament

The spring ligament, together with the posterior tibial tendon, is an important stabiliser of the

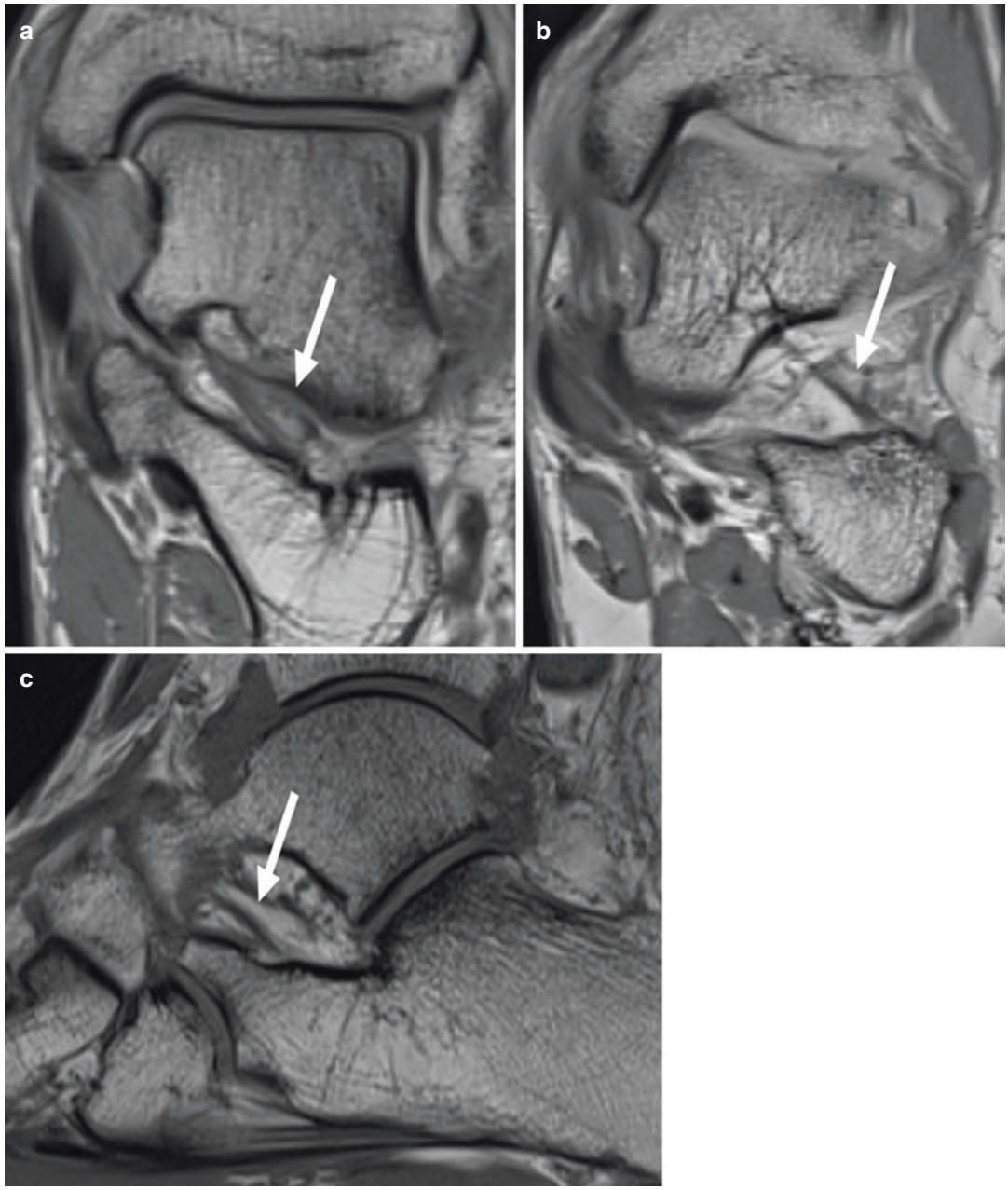

Fig. 16 (**a**–**c**) Subtalar ligaments. (**a**) Coronal PD MR image through the posterior part of the sinus tarsi demonstrates the interosseous talocalcaneal ligament (arrow) running posteromedially. (**b**) Coronal PD MR through the anterior part of the sinus tarsi shows the cervical ligament coursing anterolaterally (arrow). (**c**) Sagittal PD MR through the sinus tarsi also depicts the cervical ligament (arrow)

medial plantar arch of the foot. Three different ligaments make up the spring ligament: the superomedial calcaneonavicular, medioplantar calcaneonavicular and inferoplantar calcaneonavicular ligaments. Acute injury of the spring ligament is uncommon and usually involves the superomedial calcaneonavicular ligament, which is also functionally the most important. The

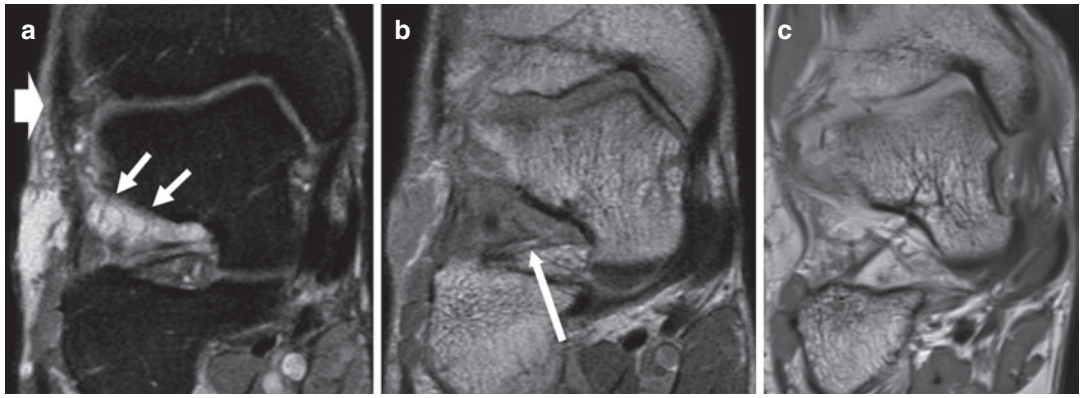

Fig. 17 (**a**–**c**) Sinus tarsi syndrome. Coronal PD fat-sat (**a**) and PD (**b**) MR images of a patient complaining 2 years after an ankle sprain of persisting elective pain at the opening of the sinus tarsi with pure hindfoot instability. MR images (through the anterior part of the medial malleolus) show an abnormal multiloculated high signal collection (small arrows) corresponding to a ganglion cyst pushing down the horizontalised cervical ligament (long arrow). The cyst extends outside the inferior extensor retinaculum which appears thickened with irregular outlines (thick arrow). **c** shows a normal sinus tarsi (with fat signal on PD) and cervical ligament (thin low signal oblique band)

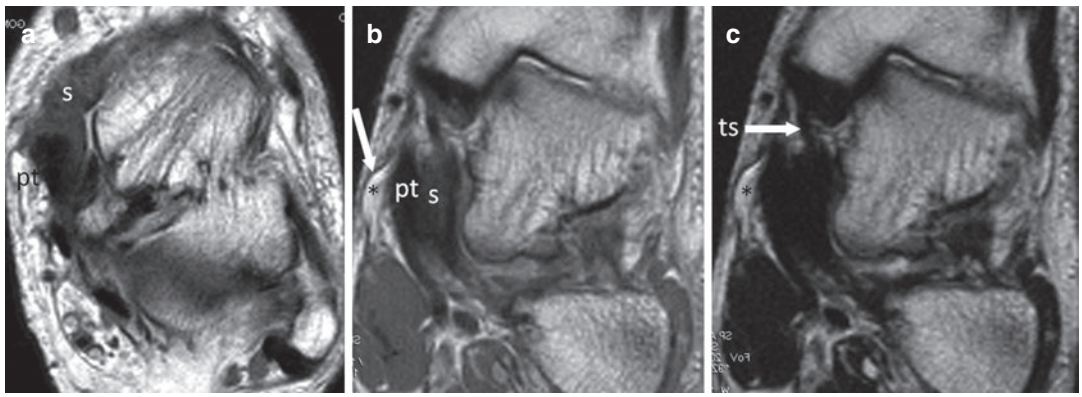

Fig. 18 (**a**–**c**) Chronic spring ligament tear associated with posterior tibial (pt) tendinopathy and tenosynovitis. Axial T1 (**a**) and anterior coronal PD (**b**) and T2 (**c**) MR images show a chronic thickening and infiltration of spring (s) ligament (smCNL). Associated thickening of PT tendon is detected on axial T1 behind the spring ligament. The PT tendon sheath is distended by fluid (arrow*) on coronal PD (**b**) and T2 (**c**). The spring ligament is in continuity with and beneath the tibiospring (ts) bundle of the deltoid ligament

superomedial bundle connects the superomedial edge of the sustentaculum tali and anterior facet of the calcaneus with the navicular bone. Such injuries can result in pes planovalgus deformity; they are often associated with posterior tibial tendinopathy (Mengiardi et al. 2016).

Imaging US allows imaging of the superomedial calcaneonavicular ligament which is a slightly hyperechoic structure deep to the posterior tibial tendon (Fig. 18). Abduction and pronation of the foot may help to visualise it. Os naviculare accessorius may obscure the ligament. On MRI discontinuity of the superomedial bundle is best visualised on coronal and axial images. Periligamentous infiltration of the ligament is nonspecific as it may also indicate a chronic stress response in an intact ligament. The other two bundles are best demonstrated on axial images (Linklater et al. 2017; Mansour et al. 2011; Crim 2016). Abnormality of the spring ligament is often associated with

advanced posterior tibial tendon injury (Balen and Helms 2001) (Box 2).

Box 2 US and MRI for Ligaments

Ultrasound

- Excellent for superficial soft-tissue injuries of ankle and foot.
- Dynamic ultrasound (US) helps differentiate partial from complete tears in acute setting and assess ankle stability.
- Deep ligaments cannot be visualised (e.g. in sinus tarsi).
- In persisting pain after ankle sprain, dynamic US can detect peroneal tendon dislocation (missed on static MRI).
- No radiation, cheap, quick and accessible but user dependant.

MRI

- High sensitivity and specificity for ligament injuries.
- Allows visualisation of associated intra-articular lesions and bone abnormalities (including BME).
- Advantage of MRI is the detection of painful unstable fragments (showing BME).
- Useful in workup of chronic post-traumatic pain caused by synovitis, impingement or OCL.
- May be necessary to assess structures that cannot be imaged with ultrasound (as for subtalar ligaments).
- Allows imaging with a larger field of view than ultrasound with assessment of adjacent structures.
- But is a static imaging modality.

2 Midfoot Ligament Injuries

2.1 Chopart Joint Ligaments

The Chopart ligament complex is located between the hindfoot and midfoot. It consists of the talonavicular and calcaneocuboid joints. The talonavicular joint is stabilised by the bifurcate ligament, the dorsal talonavicular ligament and the spring ligament. The dorsal talonavicular ligament is a capsular thickening on the dorsal side of the joint (Fig. 19). The bifurcate ligament has two bundles: a lateral calcaneocuboid bundle and a medial calcaneonavicular bundle supporting both joints (Fig. 20). Dorsal and plantar calcaneocuboid ligaments further stabilise the calcaneocuboid joint. The dorsal calcaneocuboid ligament is a broad band on the lateral side of the midfoot, inferior to the bifurcate ligament (Döring et al. 2018).

Half of the midfoot sprains are due to sports injuries, and females are generally at higher risk than males. They commonly occur after low-energy inversion injury (such as a missed step) causing distraction of the dorsolateral side of the calcaneocuboid joint. Inversion results in injury of the bifurcate and dorsal calcaneocuboid ligaments. When inversion happens with the ankle in plantar flexion (as in ballet dancing or when wearing high heels) the dorsal talonavicular ligament is often involved. Osseous avulsions are frequent in these kinds of sprain. Typical sites of avulsion are the anterior process of the calcaneum in case of dorsal calcaneocuboid or bifurcate ligament injury and dorsal navicular or talar avulsion in case of dorsal talonavicular ligament tear. Eversion of the foot (less common mechanism) may lead to compressive impaction injury of the calcaneocuboid joint, producing impaction fractures of the anterior process of the calcaneus and posterolateral cuboid, referred to as "nutcracker" injuries (Walter et al. 2018; Linklater et al. 2017).

Imaging On MRI both the bifurcate (Fig. 20) and calcaneocuboid ligaments are well visualised in different planes while the dorsal talonavicular ligament is best seen on sagittal images (Fig. 19). These superficial ligaments can easily be assessed with ultrasound. On MRI bone marrow oedema at the site of avulsion is indicative of ligamentous injury. Subchondral bone oedema along the Chopart joint may be present following bone contusion. Small avulsion fracture fragments detected at typical locations on standard radiographs and CT provide the first clue to the diagnosis (Walter et al. 2018; Linklater et al. 2017).

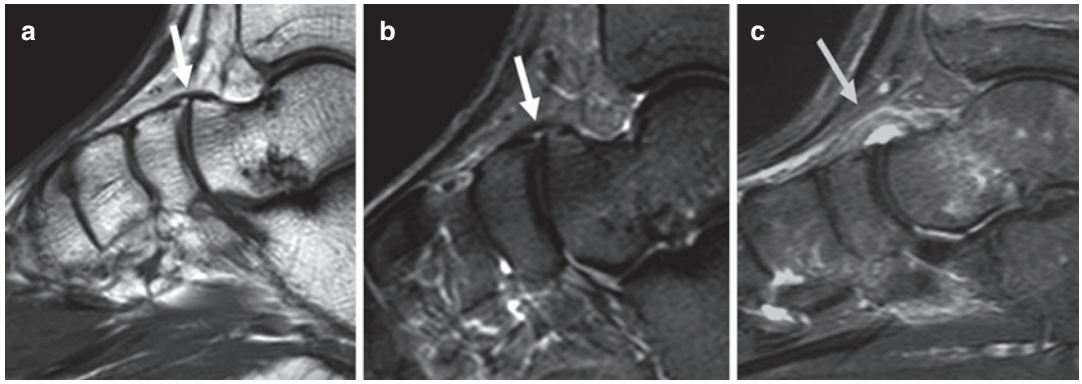

Fig. 19 (**a**–**c**) Dorsal talonavicular ligament. (**a**, **b**) Sagittal T1 and STIR MR images display a normal dorsal talonavicular ligament (arrow). The ligament is thin and hypointense on both sequences. (**c**) Sagittal STIR of another patient demonstrates a dorsal talonavicular ligament sprain. The ligament is markedly thickened and has an increased signal intensity. This is associated with a focal fluid distension of the dorsal talonavicular joint recess (arrow)

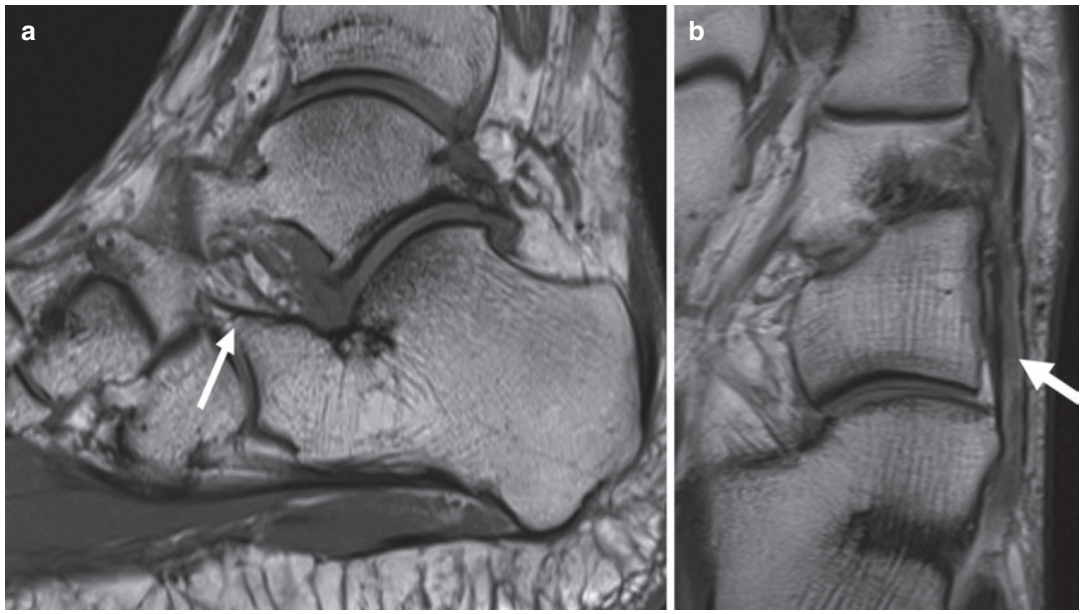

Fig. 20 (**a**, **b**) Bifurcate ligament. (**a**) Sagittal PD MR image depicts the calcaneonavicular component (arrow). (**b**) Axial PD shows the calcaneocuboid component (arrow)

2.2 Lisfranc Ligament Injuries

The Lisfranc ligament complex runs obliquely from the medial cuneiform to the base of the second metatarsal and has three components: an interosseous ligament, as well as a plantar and a dorsal ligament (Döring et al. 2018) (Fig. 21).

Lisfranc sprains are low-energy injuries commonly seen in football, basketball, gymnastics and ballet dancing. Injuries result from axial loading to the foot with the foot in plantar flexion. These kind of sprains can be very subtle injuries, easily overlooked on imaging. Early detection is important as they can result in midfoot instability and early osteoarthritis (Linklater et al. 2017).

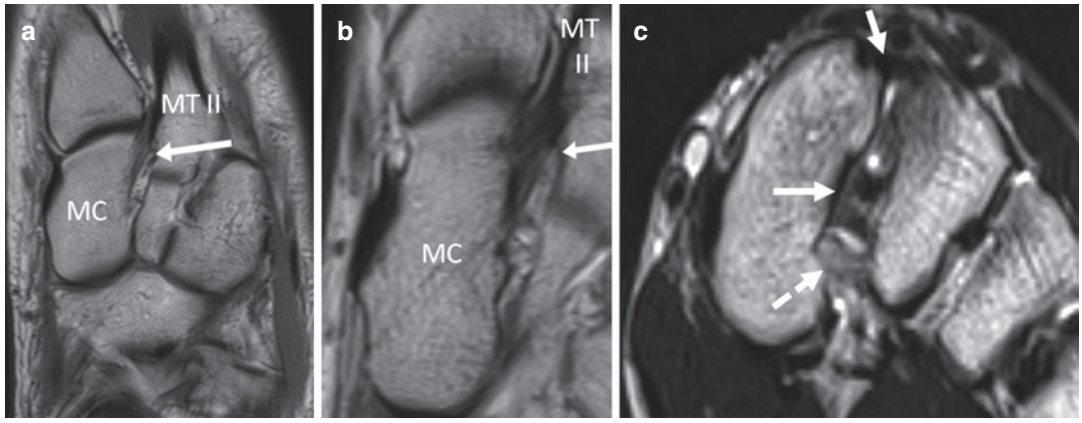

Fig. 21 (**a**–**c**) Normal Lisfranc ligament (arrow) detected on transverse PD MR images along the midfoot (**a**, zoomed on **b**) extending from the medial cuneiform (MC) to the base of the second metatarsal (MT II). Coronal T2 (**c**) proximal to the tarsometatarsal I joint demonstrates the three components of the Lisfranc ligament: dorsal (short arrow), interosseous (arrow) and plantar (dashed arrow) ligaments

Imaging Lisfranc sprains can be suspected on radiographs when there is abnormal midfoot alignment or widening of the interval between the base of the first and second metatarsals or between the medial cuneiform and second metatarsal. Comparative weight-bearing radiographs increase sensitivity. Bony avulsions between the medial cuneiform and second metatarsal are also indicative of a sprain. Preoperative CT is often performed to assess complex fractures or to rule out occult fractures. MRI allows interpretation of the different components of the Lisfranc ligament complex which are best visualised in axial oblique plane along the axis of the foot or in coronal plane (Fig. 21). Bone marrow oedema may be present in cases of bony avulsion, indicating that the avulsed fragment might be unstable (Kitsukawa et al. 2015; Llopis et al. 2016; Linklater et al. 2017) (Fig. 22).

3 Forefoot Ligament Tears

3.1 First Metatarsophalangeal Joint Ligaments

Much stress is exerted on the first metatarsophalangeal (MTP I) joint during running and jumping. Consequently injury of the MTP I joint ligaments is frequent in sports. Ligaments withstanding these forces include the medial and lateral sesamophalangeal ligaments and the medial and lateral collateral ligaments. The collateral ligaments are formed by a proper collateral ligament (metatarsophalangeal) more anteriorly and a metatarsosesamoid ligament more posteriorly. The intersesamoid ligament connects both sesamoid bones. These ligaments together with other fibrocartilaginous structures form the "plantar plate" of the hallux. The plantar plate is a stabiliser on the plantar side of the joint with a strong distal attachment on the base of the proximal phalanx and a looser proximal attachment to the metacarpal head (De Maeseneer et al. 2018a; Linklater et al. 2017; Srinivasan 2016).

Injury to any component of the plantar plate is termed "turf toe". The term turf toe was introduced as a forced hyperextension injury on artificial turf surface. The most common type of injury mechanism is valgus and hyperextension resulting in bony avulsion at the metatarsal insertion or tear of the medial collateral ligament. Isolated injury to the plantar plate is frequent after traumatic hyperextension (De Maeseneer et al. 2018a; Linklater et al. 2017).

Imaging Radiography is often normal in MTP I ligament injury. Comparative radiographs may show subtle differences in sesamoid position or

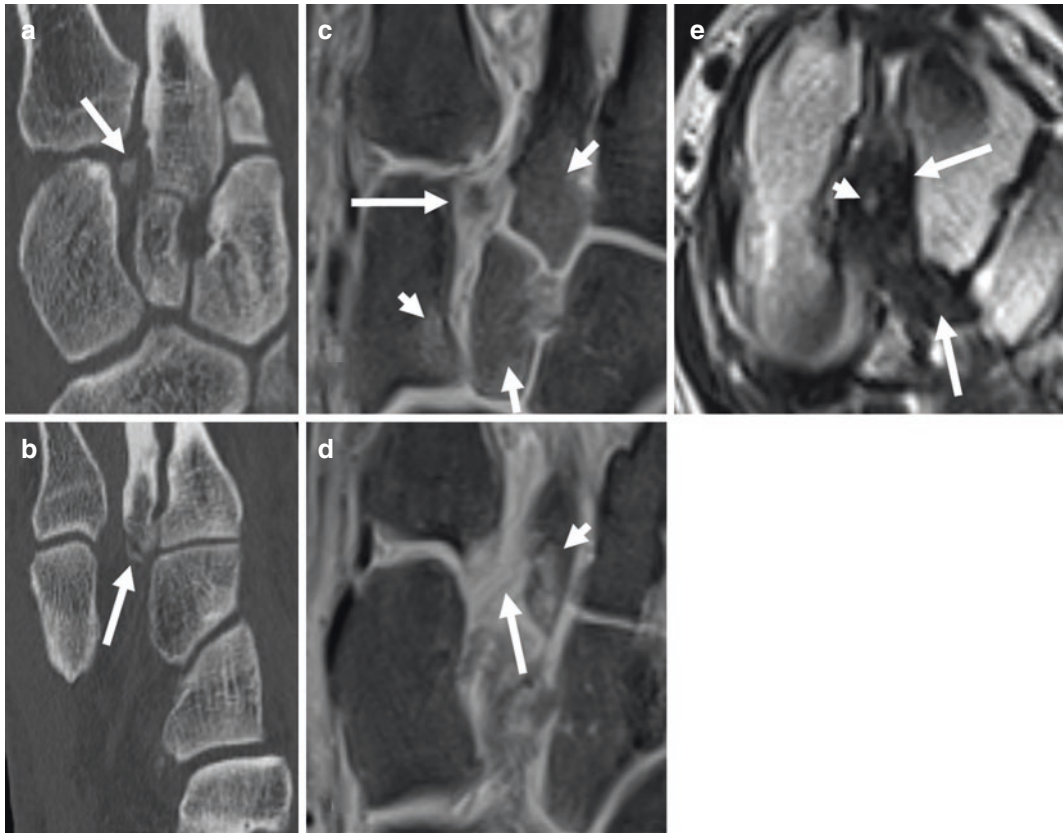

Fig. 22 (**a**–**e**) Lisfranc injury. Axial CT images at the level of the midportion (**a**) and plantar side (**b**) of the second metatarsal base depict bony avulsions (arrow). On the corresponding axial PD fat-sat MR images obtained at the same levels (**c**, **d**), the bone fragment appears as a central hypointense zone (arrow on **c**) and the plantar Lisfranc ligament presents an increased signal (arrow on **d**). Bone marrow oedema is detected in the base of metatarsal II (short arrows on **c** and **d**) as well as in the medial and middle cuneiforms (short arrows on **c**). Coronal T2 through the tarsometatarsal I and II joints shows the Lisfranc ligaments infiltrated by hypointense scar tissue (arrows on **e**). The short arrow displays the bony fragment with fat signal

alignment as well as bony avulsion. Medial collateral ligament tear may also result in acute hallux valgus. On MRI plantar ligaments are readily visualised in the sagittal plane. The metatarsosesamoid ligament is best demonstrated in a coronal plane perpendicular to the hallux whereas the proper collateral ligament is better seen in a longitudinal (axial) plane along the foot axis. Partial ligament tear results in intermediate signal changes while complete tear causes disruption with hyperintense signal on fluid-sensitive images. Full-thickness tears appear as discontinuity of the plantar plate with a fluid signal in the defect (Srinivasan 2016; Linklater et al. 2017; Burge et al. 2012) (Fig. 23).

4 Tendon Disorders

4.1 Lateral Tendons: Peroneal Tendons

The peroneus brevis (PB) and peroneus longus (PL) tendons arise in the lateral compartment. The PB is anterosuperior to the PL tendon and passes beneath the fibula within the bony retromalleolar groove where the peroneal tendons are covered by the superior peroneal retinaculum (SPR). Distally, the PL tendon courses medially in the peroneal groove of the cuboid to insert into the first metatarsal and the medial cuneiform. The PB tendon courses laterally to insert into the

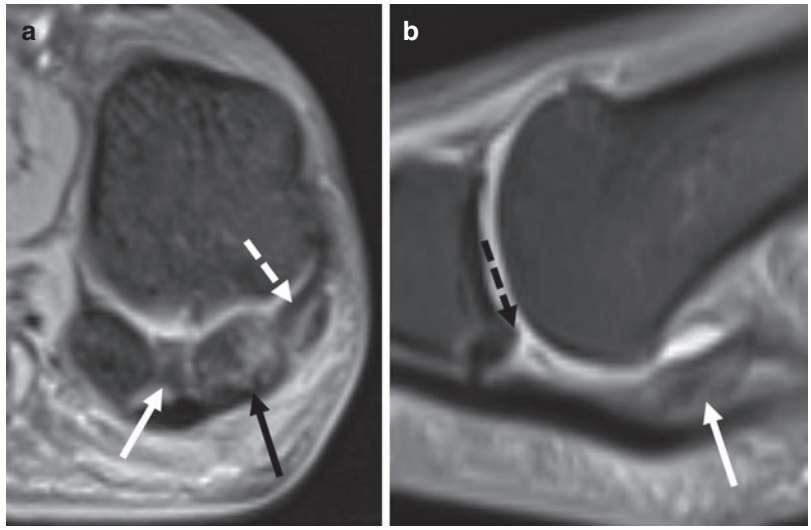

Fig. 23 (**a**, **b**) Turf toe. Coronal (**a**) and sagittal (**b**) PD fat-sat MR images obtained at the level of the MTP I joint detect increased signal in the plantar plate corresponding to a partial tear (white arrow). The medial collateral ligament complex has an intermediate signal, characteristic of a partial tear (white dashed arrow). Bone marrow oedema is depicted in the medial sesamoid (black arrow). The torn plantar plate is absent at the distal insertion (black dashed arrow)

base of the fifth metatarsal. The peroneal tendons are surrounded by a common synovial tendon sheath containing a small amount of synovial fluid. The sheath allows smooth gliding of the two tendons against the bone structures and inside the osteofibrous tunnels during contractions of the muscles and movements of the foot (Bianchi et al. 2010).

Peroneal tendon injuries are common after ankle trauma or sports-related activities with repetitive microtrauma. Acute peroneal dislocations are misdiagnosed in up to 40% of cases, often mistaken for lateral ankle ligament sprains. Therefore, they should be considered in every patient who presents with chronic persistent lateral pain and instability after severe ankle sprain. Chronic lateral ankle pain can also be associated with pathologic conditions such as peroneal tendinosis or tendinopathy, tenosynovitis, partial- and full-thickness tendon tears, peroneal retinaculum injuries and tendon subluxations and dislocations. These disorders are associated with traumatic injuries (typically inversion), and several chronic diseases. Often patients cannot recall a specific traumatic event. They typically present with chronic lateral ankle or hindfoot pain that worsens with activity. Often several peroneal tendon disorders occur simultaneously, such as a combination of tenosynovitis, tendon tear and ankle instability. Spontaneous tendon ruptures are typically associated with pre-existing tendinopathy (Taljanovic et al. 2015; Wang et al. 2005; Lee et al. 2013).

Careful clinical examination and imaging studies are critical to accurate diagnosis. The initial imaging evaluation of patients with lateral ankle and hindfoot pain and/or injury usually consists of radiographs and/or CT, which are helpful in diagnosing osseous abnormalities, such as avulsion injuries and fractures. CT may also show tendinopathy as loss of normal dense appearance of peroneal tendons, tendon entrapment at calcaneal or fibular fracture site or tendon dislocation from the peroneal groove (Demehri et al. 2014). Imaging with high-resolution ultrasound and high-field MRI provide superior soft-tissue contrast evaluation and ability to perform kinematic assessment (Kumar et al. 2017). A normal tendon has a homogeneous low signal intensity on MRI. It appears hyperechoic on ultrasound due to its dense collagen and fibrillar structure (Taljanovic et al. 2015; Wang et al. 2005; Lee et al. 2013; Bianchi et al. 2010).

4.1.1 Peroneal Tendinosis, Tendinopathy and Tenosynovitis

Tendinosis (or tendinopathy) of the peroneal tendons represents a noninflammatory degenerative process that is most commonly caused by repetitive stress on the lateral ankle tendons in athletes. Sporting activities include running, competitive walking, ballet dancing, etc. However, the condition has also been described in older individuals with subfibular impingement (as patients with diabetic foot, inflammatory or metabolic arthritis and individuals with displaced fractures of the lateral malleolus and calcaneus) (Wang et al. 2005; Lee et al. 2013; Taljanovic et al. 2015). Patients typically present with posterolateral ankle pain increasing with activity and improving with rest. Clinical examination can reveal tenderness over the peroneal tendons; a palpable mass that moves with the tendon is suggestive of tendinosis. The condition is characterised by thickening and focal tendon degeneration and swelling, more commonly seen in the inframalleolar portion. There is often associated nodular thickening, splits or tears of the tendon (Davda et al. 2017).

Imaging *Peroneal tendinosis (or tendinopathy)* is well depicted on both MRI and ultrasound (US). It appears on MRI as a tendon thickening with intermediate or slightly increased intratendinous signal intensity on proton density (PD) and fat-saturated PD. US depicts a hypoechoic and thickened tendon without discontinuity (Taljanovic et al. 2015; Lee et al. 2013). Tendinosis can be associated to a *tenosynovitis* characterised on MRI by an increased signal intensity within the distended common peroneal tendon sheath. Although a small amount of fluid within the tendon sheath could be seen in asymptomatic ankles, a circumferential fluid, more than 2 mm thick, is commonly seen in symptomatic subjects with tenosynovitis (Fig. 24). T1-weighted images after administration of intravenous contrast or T2-weighted images without fat saturation could help to differentiate mechanical fluid (with low signal intensity on T1 with intravenous contrast and high and homogeneous signal intensity on T2 without fat saturation) from inflamed synovium within the tendon sheath (showing contrast enhancement on T1). On US, synovial fluid is anechoic, while the thickened and frequently irregular synovium and the inflamed tendon appear hypoechoic. Colour Doppler can help to determine the degree of activity of the tendon sheath inflammation and can detect increased vascularity and hyperaemia inside the inflamed

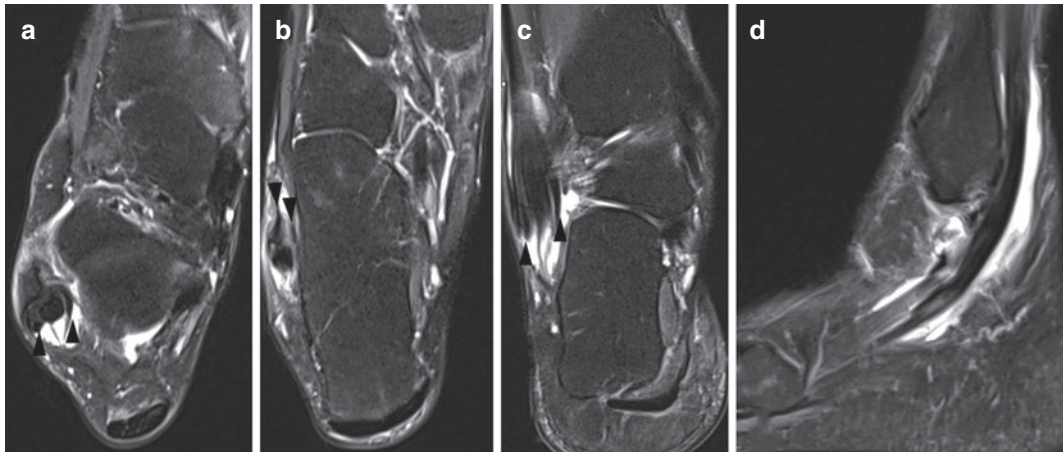

Fig. 24 (**a**–**d**) Partial longitudinal peroneus brevis (PB) tendon tear and tenosynovitis on axial PD fat-sat MR image at retromalleolar (**a**) and at inframalleolar (**b**) level and on coronal (**c**) and sagittal (**d**) PD fat-sat images. The PB tendon is split up into two parts (arrowheads on **a**–**c**) with anterior displacement of the peroneus longus tendon between the PB fragments. Associated tenosynovitis appears as a distension of the peroneal tendon sheath with hyperintense fluid

synovium or pathological tendon. However, in ankle sprain with calcaneofibular ligament tear, fluid may accumulate in the common peroneal tendon sheath (because of the intimate relationship between the calcaneofibular ligament and the common peroneal tendon sheath) and may mimic tenosynovitis (Taljanovic et al. 2015; Lee et al. 2013; Kijowski et al. 2007).

Stenosing tenosynovitis is due to chronic friction of the peroneal tendons inside a narrowed inferior osteofibrous tunnel. It can be associated to a thickening of the peroneal retinaculum, especially in the presence of hypertrophy of the peroneal tubercle or an os peroneum or when the patient has undergone ligament repair (Vuillemin et al. 2012; Bianchi et al. 2010; Saupe et al. 2007; Kijowski et al. 2007; Wang et al. 2005).

4.1.2 Peroneal Tendon Tears

Peroneal tendon tears should be considered in every patient who presents with chronic lateral ankle pain. Tears occur as a result of trauma (including ankle sprains), in tendons with preexisting tendinopathy and in repetitive microtrauma due to instability in recurrent subluxation. Longitudinal split tears of the PB tendon are common in young athletes and in the elderly. PL tears are less common than PB tears (Lee et al. 2013; Taljanovic et al. 2015; Hallinan et al. 2019).

Imaging In *full-thickness tears*, complete discontinuity of the fibres can be depicted with a high signal intensity gap. In *partial-thickness tears*, the tendons can be attenuated with frayed outlines or thickened with irregular intermediate or high signal intensity on MRI (Figs. 24 and 25). On US, the tendons appear hypoechoic or anechoic, with fluid seen at the site of tearing and loss of the normal fibrillar appearance. When it is associated with tendon thickening, a partial-thickness tear is difficult to distinguish from tendinopathy while tendon thinning is always associated with partial-thickness tears. For the diagnosis of acute peroneal tendon tears (caused by direct trauma or sports-related injury), US is proved to be highly effective, and colour Doppler can also show hyperaemia when the synovial membrane is inflamed (Taljanovic et al. 2015).

Peroneus brevis tendon is located between the bony retromalleolar groove and the PL tendon, thereby being susceptible to degenerative tears. When a tear is initiated, the PL tendon can migrate forward into the tendon cleft of the PB (Philbin et al. 2009). Associated conditions of PB tears include a decreased space in the retromalleolar groove due to a low-lying PB muscle belly, presence of a peroneus quartus muscle and insufficiency of the superior peroneal retinaculum (SPR). Tears of the PB can also be associated to an avulsion fracture of the distal attachment on the fifth metatarsal base during ankle inversion injury (Lee et al. 2013; Roster et al. 2015).

Imaging On US, key findings include complete cleft with the formation of two distinct hemi-

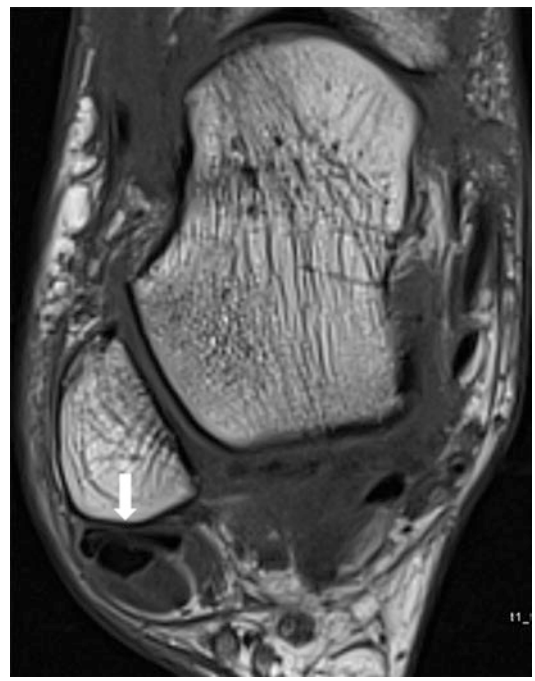

Fig. 25 Partial longitudinal peroneus brevis (PB) tendon tear associated to a slightly convex margin of the posterior aspect of the fibula. On axial T1 MR image obtained at the retromalleolar level the PB tendon has an abnormal boomerang shape with central thinning (arrow) associated to anterior displacement of the peroneus longus tendon between the PB fragments

tendons, irregularities of the tendon, or signs of associated tenosynovitis. An early form of PB longitudinal tear can present a boomerang-shape appearance, corresponding to weakening and thinning of the central part of the tendon. On axial MRI, a longitudinal split of the PB tendon is defined as chevron shaped or boomerang shaped, partially enveloping the PL tendon (Lee et al. 2013) (Fig. 25). Thin 0.5 mm sagittal images obtained with 3D sequences can help to delineate the full longitudinal extent of peroneal tendon tears. Because the peroneal tendons have a curved course around the lateral malleolus, magic angle artifact and partial volume effect can cause falsely increased signal intensity. These could be avoided using coronal oblique images (perpendicular to the peroneal tendon course) with T2-weighted sequences with longer echo times and STIR which are less disturbed than T1 (Wang et al. 2005).

Peroneus longus tendon tears (less common than PB tendon tears) are most commonly caused by acute direct trauma or sports-related injuries. They can be partial- or full-thickness tears. Isolated PL tendon tears are uncommon. Predisposing factors increasing mechanical friction upon the PL tendon include peroneal tubercle hypertrophy, cavovarus foot deformity and peroneus quartus muscle. PL tendon tears most frequently occur at the level of the cuboid tunnel in the midfoot or the os peroneum (or either distal or proximal to the os peroneum) (Wang et al. 2005; Lee et al. 2013; Bianchi et al. 2010; Schubert 2013; Roster et al. 2015) (Fig. 27).

Imaging US or MRI findings of PL tendon partial-thickness tears include irregularity of the tendon contour, longitudinal split and shredded appearance with multiple splits with or without fluid gap. Full-thickness tears may be seen as tendon discontinuity with retraction of the tendon fragments or an empty fluid-filled peroneal tendon sheath. Proximal retraction (migration) of an os peroneum (which is normally located at the level of the calcaneocuboid joint) is a clue for the diagnosis of PL complete tear. Associated signs of PL tears include hypertrophied peroneal tubercle and subtendinous bone marrow oedema on MRI in the tubercle, at the lateral aspect of the calcaneus or cuboid (Wang et al. 2005; Taljanovic et al. 2015; Kumar et al. 2017; Hallinan et al. 2019) (Fig. 27) (Box 3).

Box 3 US and MRI for Tendons

- Dynamic ultrasound (US) aids in diagnosis of tendon tears.
- Colour Doppler US can detect neovascularisation in chronically damaged tendons.
- MRI can demonstrate all tendons and also detect deep tendon injuries.
- Tendon discontinuity is evaluated on axial or coronal MR images perpendicular to the tendon course.
- MRI may show causes of unexplained pain.

4.1.3 Anatomical Muscle and Osseous Variants and Pitfalls

Accurate diagnosis of pathology requires good knowledge of the various anatomical variants present in the muscles, tendons and osseous structures of the ankle and midfoot that may mimic pathologies.

- *Peroneus quartus muscle* (PQ) is the most frequent accessory muscle of the ankle, seen in 7–22% of patients (Saupe et al. 2007; Hallinan et al. 2019). Its origin includes the posterior surface of the fibula or the PL or PB muscle. It courses medial and posterior to the peroneal tendons. The insertion site includes the retrotrochlear eminence of the calcaneus (most common) (Bianchi et al. 2010). Although generally asymptomatic, the PQ muscle may cause crowding and tendon friction in the retromalleolar groove and lead to peroneal tendinopathy or tenosynovitis and to subsequent PB tendon partial-thickness and longitudinal split tears. Patients can present retromalleolar pain and oedema.

Imaging This muscle can be seen on MRI and US posteromedial to the peroneus longus and brevis and can appear as a small muscle or tendon structure, separated from the adjacent peroneus muscles by a fat plane (Hallinan et al. 2019).

- *Low-lying peroneus brevis muscle belly* is an anomalous extension of the PB muscle into and distal to the retromalleolar fibular groove. It may also cause crowding of the groove and the same peroneal tendon pathologies as for the PQ (Lee et al. 2013; Taljanovic et al. 2015; Cheung 2017; Hallinan et al. 2019).
- *Peroneus tertius* is another accessory muscle which lies anterior to the lateral malleolus and belongs to the anterior tendon group (see below) (Choudhary and McNally 2011).
- *Hypertrophy of the peroneal tubercle* (a bony protuberance located at the lateral aspect of the calcaneus) is seen in 40% of individuals and separates the PL from the PB tendon. A bony prominence greater than 5 mm is more likely to be symptomatic; it may irritate the peroneal tendons and tendon sheath and lead to tenosynovitis and rupture or development of an adventitial bursa that may be inflamed and symptomatic (Wang et al. 2005; Lee et al. 2013; Taljanovic et al. 2015) (Fig. 26).
- *Os peroneum* is a sesamoid bone within the PL tendon, located in the region of the cuboid tunnel at the lateral aspect of the cuboid bone. It is present in approximately 20% of individuals (Choudhary and McNally 2011). An ossified os peroneum is seen on up to 30% of foot radiographs and is bilateral in nearly 60% of individuals. The ossicle may be bipartite or multipartite. The term *"painful os peroneum syndrome" (POPS)* includes an acute or chronic os peroneum fracture or diastasis of a bipartite or multipartite os peroneum (with possible callus formation), attrition or partial rupture of the PL tendon (either distal or proximal to the os peroneum) and os peroneum entrapment secondary to peroneal tubercle hypertrophy. Healing of os peroneum fracture or diastasis of multipartite os peroneum with callus formation can result in a stenosing PL tenosynovitis. Patients with POPS present with tenderness along the lateral side of the foot at the level of the calcaneocuboid joint (Sobel et al. 1994; Roster et al. 2015; Hallinan et al. 2019).

Imaging Os peroneum and POPS are well documented on standard radiographs, plain CT, US and MRI. On radiographs and plain CT, os peroneum fragment separation of 6 mm or more suggests an os peroneum fracture and associated

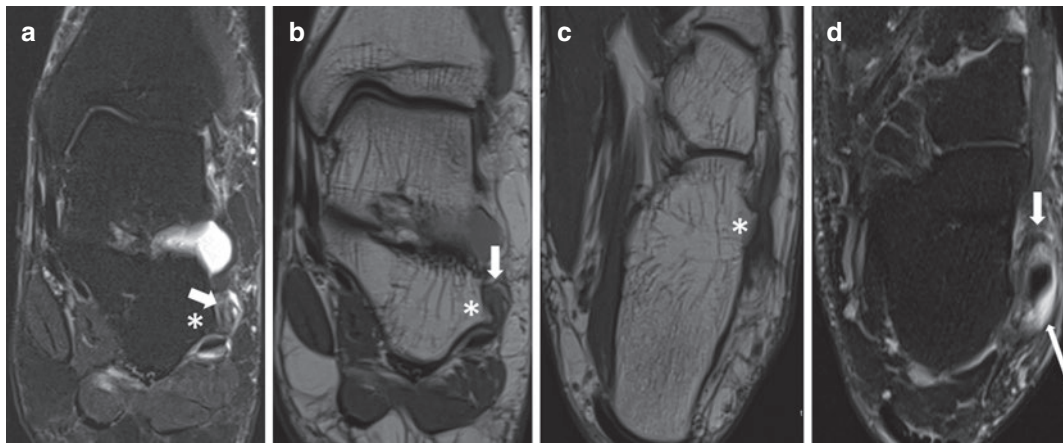

Fig. 26 (**a**–**d**) Prominent peroneal tubercle associated to longitudinal splitting of the peroneus brevis (PB) tendon. Coronal PD fat-sat (**a**) and PD (**b**), axial T1 (**c**) and PD fat-sat (**d**) MR images show a large peroneal tubercle at the lateral aspect of the calcaneum (asterisk on **a**–**c**). The PB tendon is attenuated with longitudinal splitting (short arrow on **a**, **b**, **d**) with increased signal of the peroneal tendon sheath (long arrow on **d**)

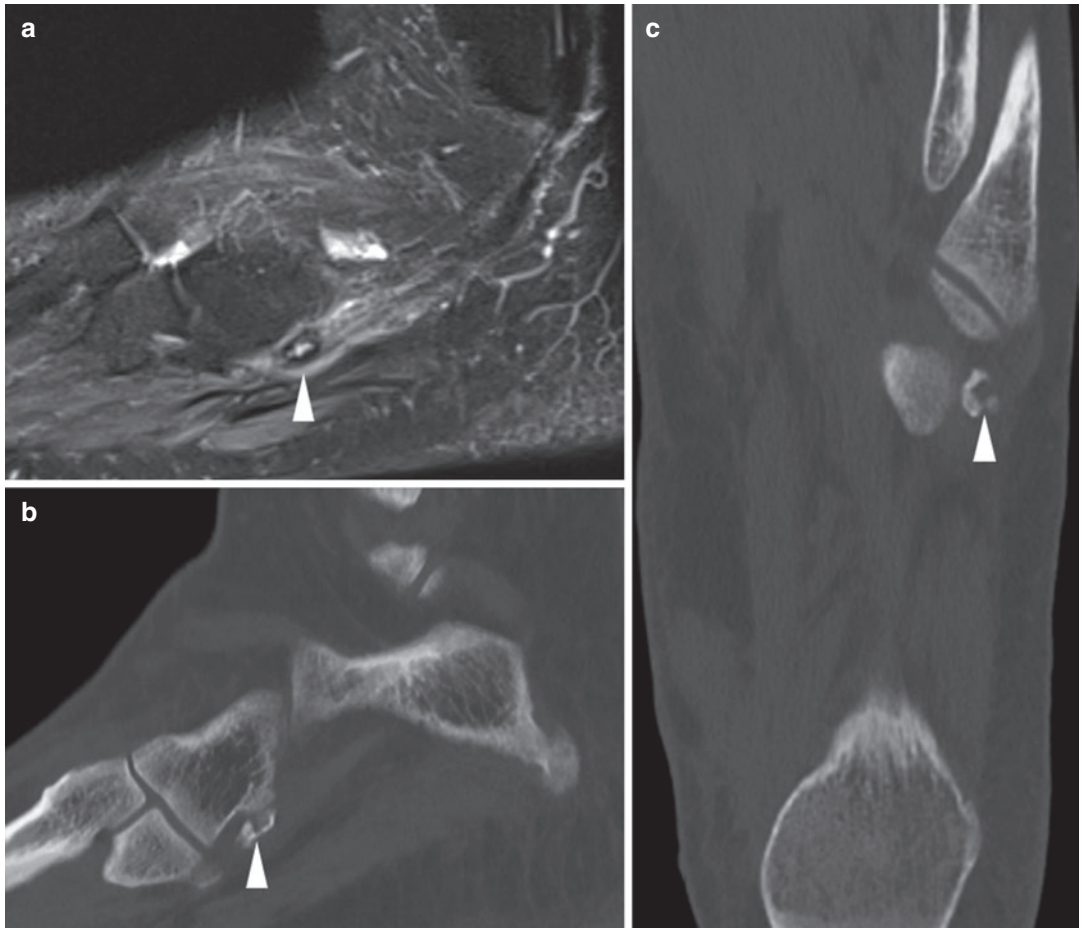

Fig. 27 (**a**–**c**) Painful os peroneum syndrome (POPS) in a female with lateral tenderness at the midfoot level. Sagittal PD fat-sat MR image (**a**) shows hyperintense bone marrow signal within the os peroneum (arrowhead) indicating fractured or unstable ossicle. A very subtle soft-tissue oedema is also displayed along the distal aspect of the peroneus longus tendon. Sagittal (**b**) and axial (**c**) CT images depict inhomogeneous sclerosis and subtle fragmentation of the os peroneum (arrowhead)

full-thickness PL tendon tear. Separation of 2 mm or less may be seen in undisplaced os peroneum fracture and bipartite os peroneum. Bony fragments with non-corticated irregular margins on radiographs or CT are indicative of a fracture (rather than a variant). Os peroneum should also be distinguished from avulsion fractures of the fifth metatarsal or the cuboid (Sobel et al. 1994; Brigido et al. 2005; Choudhary and McNally 2011). On US, an ossified os peroneum appears hyperechoic with posterior acoustic shadowing within the PL tendon. On MRI, an ossified os peroneum appears as a small structure with bone marrow signal intensity on all sequences and should not be confused with PL tendinosis or intrasubstance tear. Presence of oedematous changes within the ossicle and the surrounding soft tissues would be more suggestive of an acute fracture or an unstable ossicle (Wang et al. 2005; Lee et al. 2013; Donovan et al. 2013; Taljanovic et al. 2015) (Fig. 27).

4.1.4 Peroneal Retinaculum Injuries and Tendon Dislocation

Peroneal tendon subluxation and dislocation are usually from post-traumatic origin and may be acute or chronic recurrent. Most dislocations follow sport trauma (typically in skiing, soccer or skating). The mechanism of injury is a forceful

dorsiflexion and eversion of the ankle (with concomitant reflex forceful contraction of the peroneal muscles) causing disruption of the superior peroneal retinaculum (SPR) or an avulsion of the bone insertion. A convex retromalleolar groove and a varus heel are risk factors causing instability and tendon pathology (Davda et al. 2017) (Figs. 28 and 29). Patients present with a swollen ankle and elective pain at the posterolateral aspect of the ankle and sometimes a popping or snapping sensation. The clinical diagnosis can be difficult in the acute patient, while early surgical treatment is warranted, particularly in young athletes, to restore an optimal function of the ankle (Bianchi et al. 2010; Khoury et al. 2007). Peroneus brevis (most commonly), peroneus longus or both tendons may dislocate anteriorly. The tendons may also remain in the fibular groove but sublux and reverse their anatomic location within the peroneal groove (snapping over one another with an audible click and retromalleolar pain), a condition termed "retromalleolar intrasheath subluxation" (Khoury et al. 2007; Bianchi et al. 2010; Taljanovic et al. 2015).

The diagnosis of peroneal retinaculum tear associated with tendon subluxation or dislocation and lateral ankle instability is frequently missed after acute ankle sprains and should be considered in patients presenting chronic persistent lateral ankle pain and instability. Repeated subluxations often lead to PB tendon damage. The sharp posterolateral edge of the fibula can create a small hole in the tendon as it repeatedly subluxes over the ridge that can result into a longitudinal tear. The presence of a peroneus quartus muscle can also increase SPR laxity, which in turn can increase the risk for subluxation (Roster et al. 2015).

Imaging Because of the dynamic approach, US is the imaging method of choice. The foot should be actively dorsiflexed and everted while the

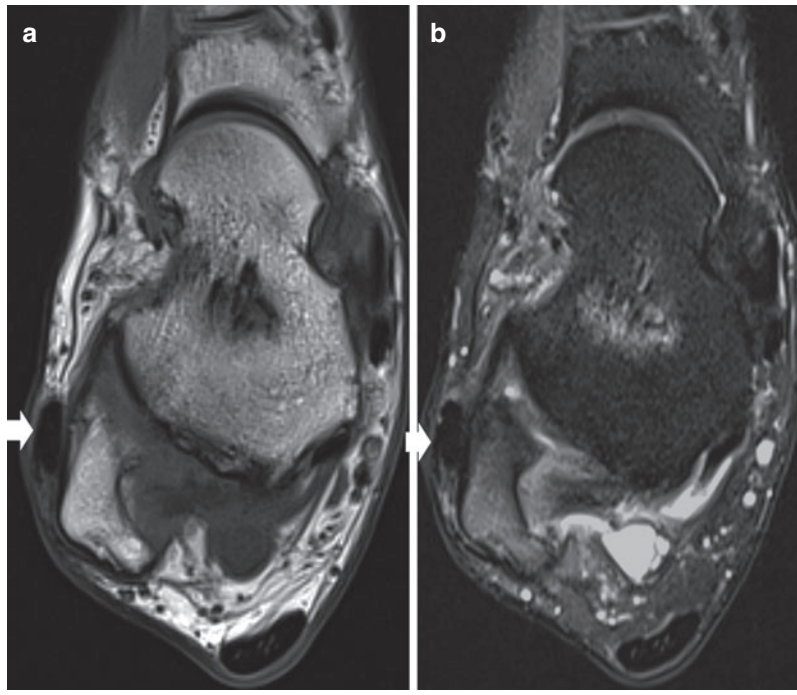

Fig. 28 (**a**, **b**) Peroneal tendon dislocation in a netball player with a previous history of fibula fracture. The patient felt a sudden "pop" at the lateral ankle after a fall during a game. Axial T1 (**a**) and PD fat-sat (**b**) MR images show anterior dislocation of the peroneal tendons (arrow) underneath the peroneal retinaculum. The retinacular tear appears as a hypointense infiltration of the perimalleolar fat on T1-WI with heterogeneous signal increase (on PD fat sat). Chronic post-traumatic deformity of the distal fibula is also demonstrated with subtle bone marrow oedema (intense on **b**). Note also sprain of the fibular attachment of PTF ligament

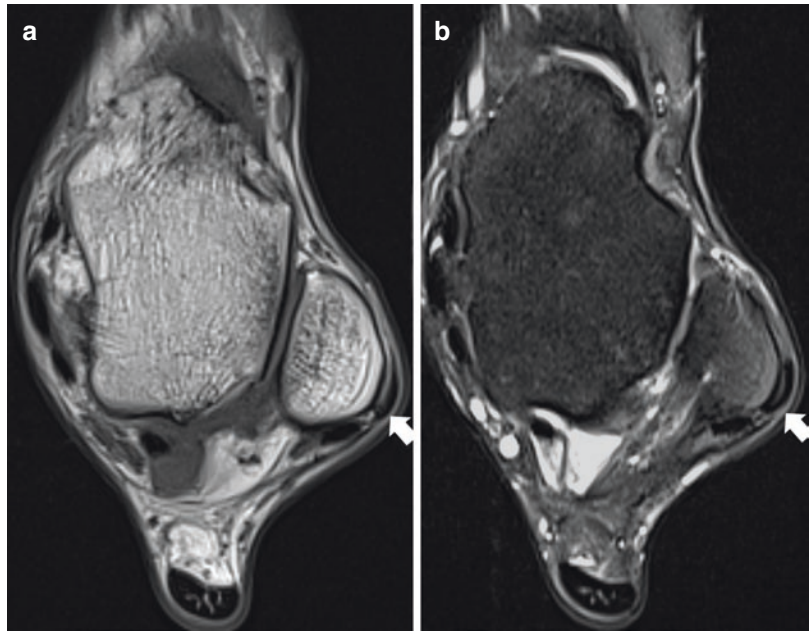

Fig. 29 (**a**, **b**) Chronic peroneus brevis tendon dislocation in an 18-year-old wall climber on axial T1 (**a**) and PD fat-sat (**b**) MR images (arrow). The patient fell down with forceful dorsiflexion and eversion of the ankle

radiologist applies an opposing force on the lateral aspect of the hindfoot. MRI only shows associated signs as peritendinous oedematous infiltration of the peroneal retinaculum (Fig. 29) and most often misses the diagnosis (Taljanovic et al. 2015).

4.2 Medial Flexor Tendons

The medial tendons are flexor tendons located on the medial side of the ankle behind the medial malleolus. They consist of the posterior tibial tendon (PTT), the flexor digitorum longus tendon (FDL) and the flexor hallucis longus tendon (FHL), respectively, from medial to lateral and from anterior to posterior (to remind as "Tom", "Dick" and "Harry"). All tendons are surrounded by individual tendon sheaths and pass through the tarsal tunnel limited by the posteromedial aspect of the distal tibia and the overlying flexor retinaculum (Bianchi et al. 2005; Crim 2016) (Fig. 12).

4.2.1 Posterior Tibial Tendon Dysfunction

The PTT is the largest tendon of the group (twice larger than the FDL). The posterior tibial muscle is the most important dynamic stabiliser of the medial longitudinal arch of the foot (together with the spring ligament complex). Sports-related PTT injury most commonly presents as acute tenosynovitis related to overuse. Tenosynovitis may develop in sports with high stress or repetitive activities as soccer, basketball, running, ice hockey, gymnastics and ballet dancing. PTT rupture is rare in this younger athletic population and is usually acute and typically located near the navicular insertion (Soliman et al. 2019; Khoury et al. 2007). Most PTT pathologies are chronic degenerative abnormalities; they occur most commonly in middle-aged women over weight presenting pre-existing or progressive flatfoot deformity with chronic stress on the tendon. Degenerative PTT tears are located at the level of the medial malleolus and are a common cause of chronic medial ankle pain, almost always associated with abnormalities of the spring or deltoid ligament or flexor retinaculum (Gluck et al. 2010). Tears follow a predictable progression, starting with tenosynovitis, tendinosis with mild-to-severe degeneration progressing to intrasubstance splitting, and partial and complete tear. As the tendon abnormalities progress, the patients also develop elongation and insufficiency of the spring ligament and finally the deltoid ligament (Balen and Helms 2001; Crim 2016). PTT injuries are common but often missed; however early

detection of PTT injuries and appropriate treatment are necessary to prevent disease progression to flatfoot deformity, chronic foot and ankle dysfunction and subsequent severe disability (Khoury et al. 2007).

Using a combination of the clinical stages described by Johnson and Strom and the imaging findings (on radiographs, US and MRI), PTT dysfunction can be subdivided into four stages:

- In *stage I*, patients may present medial foot and ankle pain, swelling and mild weakness but no deformity. Stage I is characterised by tendinosis or tenosynovitis (the last may be acute and symptomatic particularly in the younger athletic population).

Imaging On US, a small amount of compressible, anechoic, physiological fluid can normally be seen in the PTT sheath; however, this should be less than 1–2 mm thick and never circumferential. Tenosynovitis is described when a circumferential amount of fluid with more than 2 mm thickness is detected. The sheath often has an irregular, lobulated outline and there may be synechiae visible within the fluid (Donovan and Rosenberg 2009; Crim 2016). Tenosynovitis may appear as a hypoechoic ring surrounding the tendon within the PTT sheath, corresponding to complex fluid with associated hyperechoic debris or thickened synovium. This may occur with or without hyperaemia on colour Doppler (Soliman et al. 2019). Tendinosis appears hypoechoic and can lose its normal defined fibrillar architecture. On MRI, tendinosis is characterised by slightly increased signal intensity on T2 (less than fluid). In degenerative tears, longitudinal splits (with high signal intensity streaks between the tendon fibres) can develop and the tendon becomes thickened with a fusiform enlargement (Fig. 30). Increased signal on short TE sequences (as T1 and proton density) seen in early degeneration may be difficult to differentiate from magic angle effect. Some authors perform MRI in the prone position with the ankle in plantar flexion to avoid this effect. Coronal oblique planes perpendicular to the oblique PTT course can be obtained to decrease partial volume effect (Crim 2016; Mengiardi et al. 2016).

- In *stage II*, patients have difficulty and pain when standing on their toes, with inability to perform a single heel rise test. It is described as tendon elongation with tendon lengthening and laxity in Johnson and Strom clinical staging.

Imaging A fixed pes planus can be demonstrated on weight-bearing radiographs. US and MRI can detect a significant PTT attenuation (Fig. 30) corresponding to severe PT tendinosis, partial-thickness tear or partial rupture. Partial-thickness tears and longitudinal split tears present on US as linear hypoechoic or anechoic clefts (Soliman et al. 2019; Mengiardi et al. 2016; Cheung et al. 1992; Schweitzer and Karasick 2000).

- In *stage III*, patients develop a clinically rigid and radiographically fixed hindfoot planovalgus deformity and subtalar joint osteoarthrosis and talocalcaneal impingement.

Imaging A PTT rupture is demonstrated on US and MRI as a tendon gap filled with fluid and with associated proximal and distal retraction of the opposing tendon stumps. The differential diagnosis with partial-thickness tear can be validated by the dynamic manoeuvres of US (Soliman et al. 2019) (Figs. 30 and 31).

- *Stage IV* introduced by Myerson occurs when the rigid and fixed hindfoot planovalgus progresses to extra-articular lateral hindfoot impingement with talocalcaneal impingement and progressively subfibular impingement (that can also affect the adjacent peroneal tendons) (Mengiardi et al. 2016; Soliman et al. 2019; Donovan and Rosenberg 2009; Gluck et al. 2010).

4.2.2 Flexor Retinaculum Injuries and Dislocation of PTT

The flexor retinaculum is an important structure for preventing subluxation, dislocation and

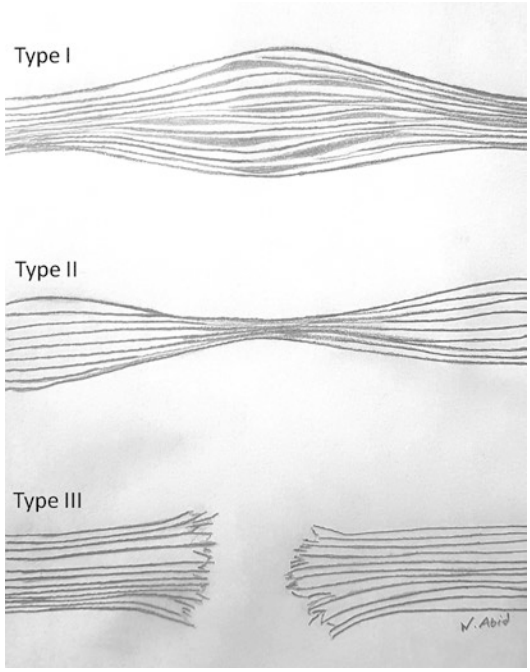

Fig. 30 Classification of PT tendon ruptures: partial (type I hypertrophic; type II atrophic) and complete (type III) rupture. (Redrawn from Rosenberg)

bowstringing of the flexor tendons of the ankle. It maintains the position of the flexor tendons posterior to the medial malleolus. It is located proximal and superficial, forming a roof to the tarsal tunnel. It is immediately superior to the medial malleolus and attaches on the posteromedial corner of the tibia. The PTT continues inferiorly distally to the medial malleolus within the tarsal tunnel (Soliman et al. 2019).

Flexor retinaculum injuries are often associated with a tear of the superficial deltoid ligament or with ankle fractures. Tears of the flexor retinaculum are uncommon but important because they result in PTT subluxation or dislocation. This is the second most common dislocation of ankle tendons after peroneal tendons. An isolated tear of the flexor retinaculum is rare and may occur because of a twisting injury often with dorsiflexion. It is often lately diagnosed. The PTT is often but not always subluxed medially. The retromalleolar groove is usually shallow in patients who dislocate the PTT (Crim 2016; Schweitzer and Karasick 2000). Acute dislocation or recurrent subluxation of the PTT is most commonly seen in athletes and is often the result of a traumatic event or repetitive microtrauma. It may destabilise the PTT resulting in abrasion against the sharp posteromedial border of the tibia and development of interstitial tears, which can progress to complete tear. It is rare for the tendon to dislocate in the absence of ankle fracture (Gluck et al. 2010; Khoury et al. 2007).

Imaging A small avulsion fracture at the insertion of the flexor retinaculum on the medial malleolus can be visualised on radiographs or CT. Dynamic ultrasound is superior to MRI in diagnosing PTT dislocation. On US, the normal flexor retinaculum appears uniformly thin and hyperechoic. In PTT dislocation, the flexor retinaculum may appear thickened, hypoechoic or absent. Occasionally, an associated cortical avulsion can be seen as an adjacent, usually linear, hyperechoic osseous fragment. In chronic injuries of the flexor retinaculum, chronic subluxation or chronic tenosynovitis, the sonographic finding of cortical irregularity may be seen along the distal medial tibia corresponding to the hypertrophic ridge or associated periosteal reaction. MRI of isolated flexor retinaculum injury shows focal discontinuity of the retinaculum, reliably occurring at its insertion on the posteromedial corner of the tibia (Soliman et al. 2019; Crim 2016).

4.2.3 Accessory Navicular Syndrome and PTT Injuries

The accessory navicular bone (also called os tibiale externum) is the second most common accessory bone of the foot with reported prevalence from 4% to 21%. It is bilateral in 50% of cases and best detected on anteroposterior (AP) radiographs of the foot. Three types have been reported based on morphology with their own characteristic imaging appearance and clinical significance. Although most patients with an accessory navicular do not have symptoms, both types II and III increase the risk of PTT dysfunction and resultant pes planus. Symptomatic accessory navicular typically develops in young athletes and like previously mentioned, PTT

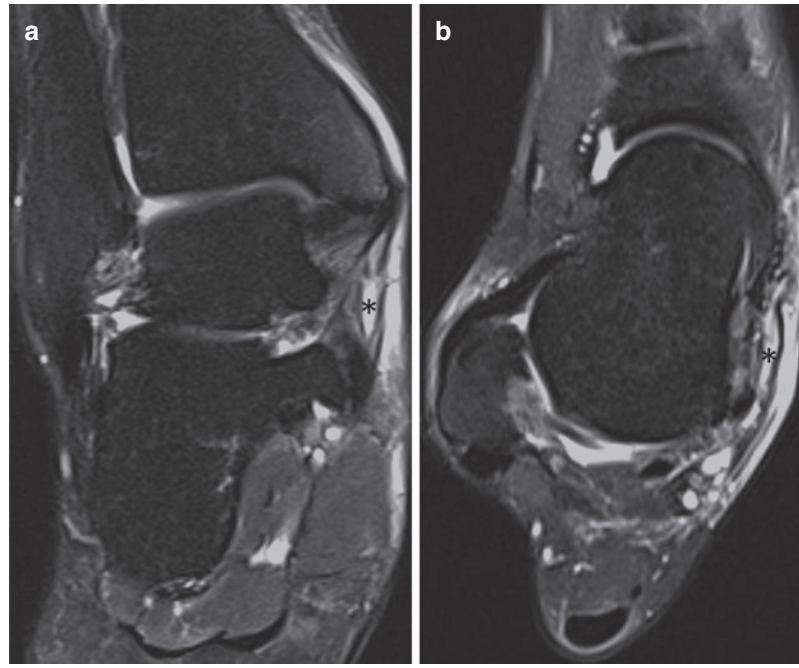

Fig. 31 (**a**, **b**) Complete rupture of posterior tibial tendon (PTT) in a 50-year-old female presenting an acquired flatfoot. Coronal (**a**) and axial (**b**) PD fat-sat MR images show absence of the PTT at inframalleolar level with increased fluid in the tendon sheath (asterisk) and surrounding fat tissues

tears in young athletes are usually located at the navicular insertion (Chan et al. 2019; Aparisi Gómez et al. 2019; Nwawka et al. 2013; Jegal et al. 2016; Khoury et al. 2007).

- *Type I* (30%) is a small ossicle located within the distal portion of PTT. It has no cartilaginous or fibrous connection to the medially located navicular tuberosity and is not associated with tendon abnormalities; it is usually asymptomatic.

Imaging Type I shows normal bone marrow signal with a thin hypointense cortical outline on MRI (Aparisi Gómez et al. 2019; Nwawka et al. 2013).

- *Type II* is the most common variant (50%) and is also called os naviculare with an estimated prevalence of 2–12%. It consists of a triangular or heart-shaped unfused accessory ossification centre separated from the navicular tubercle by a 1–2 mm thick synchondrosis. The ossicle has a broad articulating facet with the navicular tuberosity. The PTT attaches at least partly to the ossicle. Type II accessory navicular is the most commonly symptomatic. Clinical symptoms (medial-sided midfoot pain and shoe irritation) may be attributed to repetitive shearing stress in the synchondrosis transmitted through the powerful PTT, resulting in disruption of the synchondrosis. The biomechanical stress on the PTT fibres will increase the risk of chronic PTT tendinosis and tears followed by flat foot deformity.

Imaging The "accessory navicular syndrome" (also called "painful os naviculare syndrome" or PONS) is characterised by irregularity or widening of the synchondrosis and subjacent sclerosis well demonstrated on radiographs or CT. CT may also show degenerative changes at the synchondrosis and increased bone density and fragmentation of the ossicle. Either MRI or US can assess the condition of PTT and its attachment site relative to the accessory ossicle. A major advantage of MRI over US and radiographs is the ability to detect associated bone marrow oedema within the ossicle (which may indicate instability) and/or the navicular tuberosity (Fig. 32). Be aware

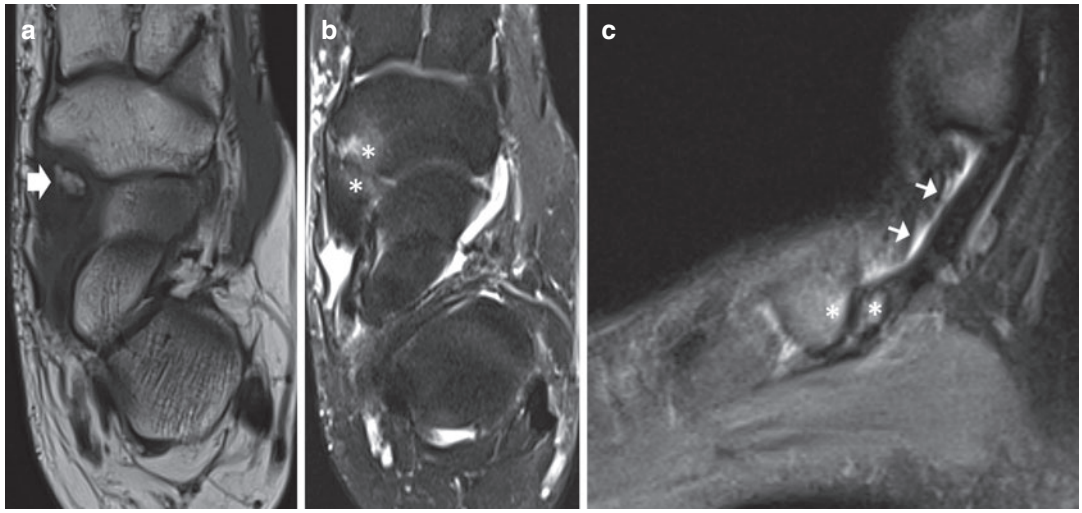

Fig. 32 (**a**–**c**) Painful type II accessory navicular bone with tenosynovitis of posterior tibial tendon (PTT) in a 50-year-old male with medial foot pain during walking. Axial T1 MR image better demonstrates the accessory navicular bone (arrow on **a**) with a slightly decreased signal. Axial (**b**) and sagittal (**c**) PD fat-sat images detect bone marrow oedema in the accessory bone and adjacent navicular bone (asterisk) with slight irregularity of the articular margins. Subtle thickening with adjacent fluid is seen at the distal PTT (small arrows on **c**)

that when bone marrow oedema is present, a small type II ossicle is easily overlooked on fat-saturated sequences (and sometimes on T1). Therefore a gradient echo sequence could be performed in the same plane to detect increased trabeculations due to increased susceptibility artefacts. Besides, MRI should be interpreted together with radiographs or CT. The synchondrosis is often only mildly widened (or is normal in width) but contains fluid signal on MRI. Oedematous infiltration can also be demonstrated within the adjacent soft tissues and in the PTT (Nwawka et al. 2013; Aparisi Gómez et al. 2019; Chan et al. 2019; Gluck et al. 2010) (Fig. 32).

- *Type III* also known as a cornuate navicular (20%) is an often horn-shaped prominent navicular tuberosity, resulting from fusion of the ossification centre with the navicular bone. It may become symptomatic by irritation of the surrounding tissues, with possible adventitial bursa formation and flat foot deformity (Nwawka et al. 2013) (Fig. 33).

4.2.4 Flexor Hallucis Longus Disorders

The FHL tendon arises from the inferior two-thirds of the posterior fibula. It crosses the ankle adjacent to the posterior surface of the sustentaculum tali where it is covered by a retinaculum. More distally, it courses under the sustentaculum tali. At the level of the knot of Henry, it crosses over the FDL tendon. In this area tenosynovitis may occur and when this increases, it may compress the adjacent medial plantar nerve. Fluid in the retromalleolar part of FHL is seen in 54% and in the inframalleolar part in 40% of normal individuals (De Maeseneer et al. 2018b; Willekens et al. 2019).

- *FHL tendinopathy, tenosynovitis and tears* usually occur either at the posterior groove between the lateral and medial tubercles of the talus or just distal to the groove or at the knot of Henry. These are typically seen in athletes, especially runners and classical ballet dancers performing repetitive forceful push-offs with the forefoot (Rosenberg et al. 2000; Tuite

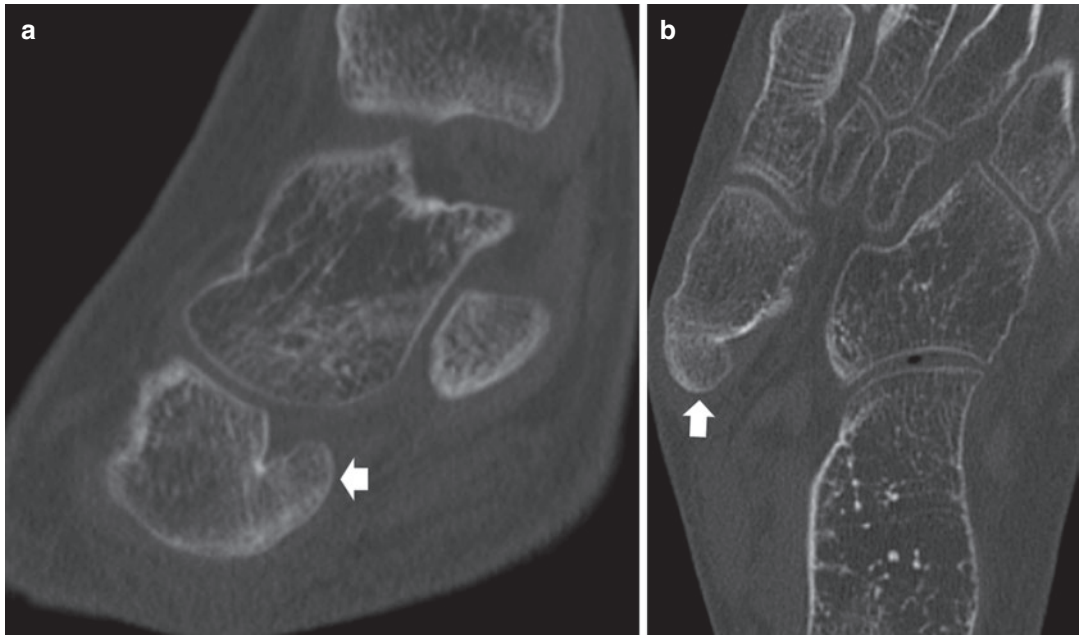

Fig. 33 (**a**, **b**) Accessory type III navicular bone in a 12-year-old sportive female presenting a prominent bone deformity at the medial aspect of the foot. Sagittal (**a**) and axial (**b**) reformatted CT images confirm the osseous excrescence at the proximal aspect of the navicular bone with a horn-like morphology (arrows)

2002; Wong and Tan 2016). The FHL is also vulnerable to *entrapment* at the level of the posterior talus. This condition is usually seen in patients with a large os trigonum (Tuite 2002; Kelikian et al. 2011; Lo et al. 2001). Patients (especially ballet dancers and high jumpers) can present clinical signs of posterior impingement with painful limitation of movements along the course of the FHL, from the posterior ankle down to the base of the distal phalanx of the hallux between the two sesamoids (Vuillemin et al. 2012). Clinical examination may demonstrate swelling, tenderness and crepitus with pain elicited by resisted plantar flexion of the hallux (Tenforde et al. 2016). When conservative treatment fails to improve symptoms, surgical intervention is considered to restore mobility of the hallux and provide improvement of the articular function (Sanhudo 2002).

- *Tenosynovitis* refers to an inflammatory condition involving the synovial sheath of the tendon. It should be taken into consideration in the differential diagnosis of FHL rupture (Sanhudo 2002).

Imaging The diagnosis can be made on T2-weighted MR images if there is a large amount of high signal fluid behind the talus within the tendon sheath in the absence of ankle joint effusion (Rosenberg et al. 2000; Tuite 2002) (Fig. 34).

- *Stenosing tenosynovitis* may complicate an untreated FHL tenosynovitis; it can result from overuse, repetitive movements, and sports-related and professional activities.

Imaging On MRI, the FHL tendon sheath will appear thickened with decreased signal on both T1 and T2 (Tuite 2002; Wong and Tan 2016). A typical sonographic finding is a thickened retinaculum that constricts the osteofibrous tunnel through which the tendon runs and that reduces movements of the tendon during dynamic manoeuvres (Vuillemin et al. 2012).

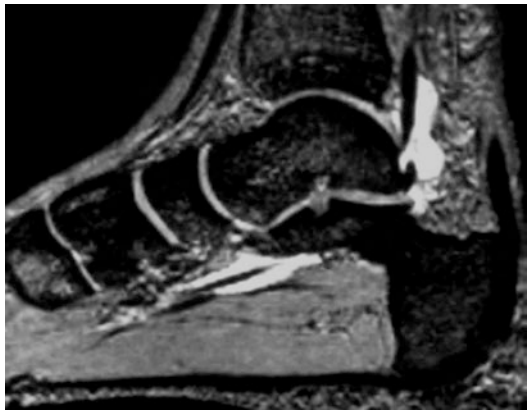

Fig. 34 Tenosynovitis of flexor hallucis longus (FHL) in a high jumper of high level with clinical signs of posterior ankle impingement with swelling, tenderness and painful limitation of movements. The pain is present along the course of the FHL and is elicited by resisted plantar flexion of the hallux. Sagittal image from a 3D gradient echo DESS sequence reveals a large amount of high signal fluid within the tendon sheath behind the talus and in the midfoot

- *FHL rupture or laceration* is uncommon in healthy young athletes; the most common mechanism is direct trauma. FHL rupture occurs at various anatomic locations, including posterior to the talus and at the knot of Henry (as it traverses the medial plantar foot). Physical examination is important in determining complete versus partial rupture and whether there is an associated injury of the flexor hallucis brevis tendon (Hunt et al. 2013).

4.3 Anterior Extensor Tendons

The anterior group consists from medial to lateral of the anterior tibial (AT), extensor hallucis longus (EHL), extensor digitorum longus (EDL) (to remind as "Tom" Hates "Dick") and peroneus tertius tendons. All anterior tendons are covered by the extensor retinaculum, a fibrous band that stabilises the tendons in the anterior aspect of the ankle and foot and prevents tendon bowstringing during dorsal flexion (De Maeseneer et al. 2018b; Sarrafian 1983) (Fig. 35).

Pathology of the anterior tendons is uncommon, since they are usually only exposed to minor mechanical stress owing to their straight course. Overuse and traumatic lesions of the anterior tendons include tendinosis, tenosynovitis, stenosing tenosynovitis, rupture and dislocation, and they have the same sonographic features as elsewhere in the body (Mengiardi et al. 2005; Khoury et al. 2007).

4.3.1 Anterior Tibial Tendon Injuries

The AT is the largest and strongest of the extensor tendons. It begins at the junction of the middle and lower thirds of the tibia and courses at the anteromedial aspect of the ankle. It descends obliquely to insert into the medial aspect of the first cuneiform and the base of the first metatarsal. The tendon passes beneath two retinacula, the superior extensor retinaculum above the ankle joint and the inferior extensor retinaculum below it. The tendon sheath around the AT forms several centimetres above the ankle joint. Unlike the Achilles and PT tendons, the AT tendon is well vascularised throughout its course. It is responsible for 80% of dorsiflexion and inversion of the foot. It prevents the forefoot slapping and scraping of the ground and helps support the longitudinal arch (De Maeseneer et al. 2018b; Tuite 2002).

Closed injuries of the AT tendon are uncommon because of the straight course and the strong vascular supply of the anterior tibia. But the AT tendon can be injured by friction against the inferior extensor retinaculum, talonavicular osteophytes or bony excrescences; the mechanical wear could lead to tenosynovitis or rupture. The most common pathology is *tenosynovitis* seen in downhill runners, football players and skiers who are subject to forced plantar flexion. Tenosynovitis and tendinosis of the AT tendon are more prevalent than tendon tears, and they are an underestimated cause of dorsomedial chronic pain of the foot in older individuals (Teh et al. 2011; Mengiardi et al. 2005).

Tendinopathy may cause anterior leg or ankle pain in a runner. Weakness and pain with dorsiflexion are the primary clinical finding. And pain

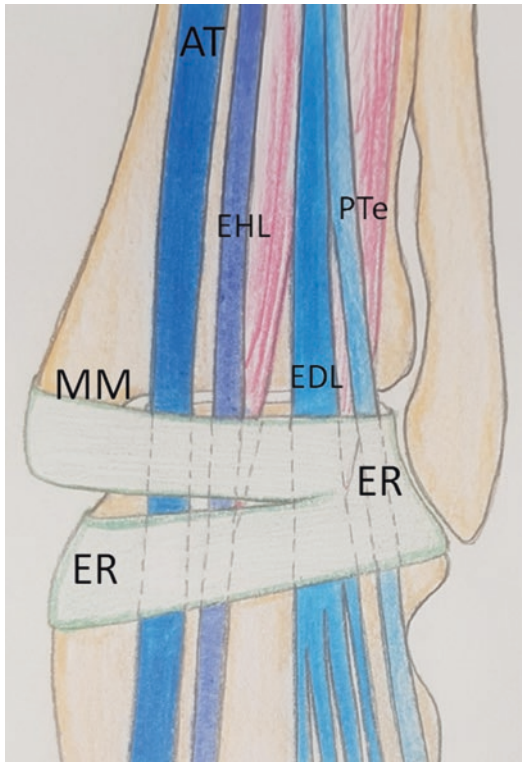

Fig. 35 Coronal drawing of anterior ankle tendons covered by the inferior extensor retinaculum (ER). *AT* anterior tibial, *EHL* extensor hallucis longus, *EDL* extensor digitorum longus, *PTe* peroneus tertius, *MM* medial malleolus

along the AT tendon with resisted dorsiflexion can be helpful to distinguish this condition from pain originating from the tibiotalar joint (Tenforde et al. 2016).

Tendon ruptures are rare and commonly caused by direct trauma. The classic mechanism of AT tendon rupture is sudden eversion and plantar flexion of a dorsiflexed foot with buckling of the tendon against the sharp edge of the retinaculum like when missing a stair step. The disruption usually occurs 0.5–3.0 cm proximal to the tendon insertion site, where the tendon passes deep to the inferior extensor retinaculum (Ng et al. 2013). Patients may have a history of a minor trauma with forceful plantar flexion (Khoury et al. 2007). The injury may be overlooked by the patient which often presents relatively mild symptoms. However the clinical presentation of a tender bulbous mass on the dorsum of the foot (due to the thickened retracted stump of the tendon) without awareness of functional impairment may cause concern for a neoplasm (Lee et al. 2006). Although some patients have localised pain with a foot drop, dorsiflexion is often preserved by the EHL and EDL muscles; therefore the diagnosis of an AT tendon tear may be missed. Delayed diagnosis may hamper primary surgical repair. There is no consensus on the management of AT tendinopathy and tear. Conservative management is reasonable for tendinopathy without significant tear; surgical management seems to provide good outcomes for many patients with AT tendon rupture (Tenforde et al. 2016). *Spontaneous rupture* of the AT is rare; it has been reported in systemic diseases such as gout, rheumatoid arthritis and diabetes mellitus (Tuite 2002; Mengiardi et al. 2005; Teh et al. 2011).

Distal insertional tendinopathy is a less frequent abnormality, rather encountered in middle-aged women who complain of swelling and pain over the AT insertion. It typically occurs as an overuse injury, also secondary to irritation due to tight shoes or ski boots. The medial cuneiform is the most common site of distal pathology including tendinopathy and partial tears of the tendon. The presence of multiple tendon slips at the distal insertion into the base of the first metatarsal and medial cuneiform (variant) should not be mistaken with longitudinal split tears (De Maeseneer et al. 2018b; Mengiardi et al. 2005).

Imaging Characteristic MRI findings of AT injuries include fusiform tendon thickening (more or equal to 5 mm) with intrasubstance increase of signal intensity indicating tendinosis or partial rupture. The intratendinous signal abnormalities are usually located within the deep fibres of the AT distal attachment (or more diffuse) on coronal sections perpendicular to the tendon course (Mengiardi et al. 2005) (Fig. 36). Partial rupture may be seen as longitudinal splitting (Fig. 37). MRI can demonstrate the presence of occasionally associated bone marrow oedema at the distal insertion site; it could be correlated

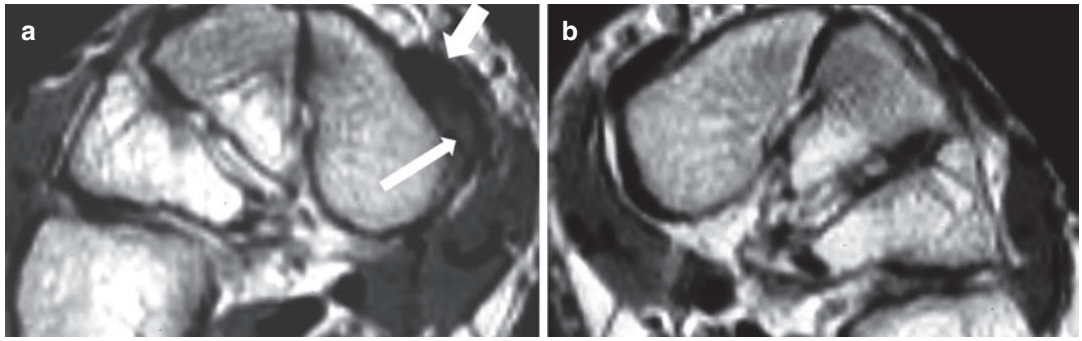

Fig. 36 (**a**, **b**) Tendinopathy of the distal attachment of the anterior tibial tendon in a downhill runner presenting chronic medial cuneometatarsal pain. Coronal PD MR image (**a**) shows an enlarged tendon (arrow) with inhomogeneous signal, increased at the medial attachment (thin arrow) corresponding to intratendinous fissures within the deep fibres. Compare with the normal contralateral side (**b**)

Fig. 37 Partial rupture of the anterior tibial tendon due to tight ski boots. The sagittal PD MR image demonstrates a fusiform tendon thickening with a diffuse intrasubstance increase of signal intensity corresponding to longitudinal splits (arrow)

with pain and used as a marker for adjacent tendon injury (Ng et al. 2013; Tuite 2002). Circumferential fluid distension of the tendon sheath is highly specific of tenosynovitis when greater than 3 mm (Kijowski et al. 2007; Zember et al. 2016). In complete rupture, the torn proximal tendon stump commonly retracts above the level of the ankle joint; a focal segment of empty tendon sheath filled with fluid may be seen. Depending on the age of the rupture, the tendinous gap can be filled with fluid, fat or scar tissue (Lee et al. 2006; Khoury et al. 1996; Cheung et al. 1992). MRI allows evaluation of the extent of injury and tendon retraction (Fig. 38). It can identify predisposing factors and it provides preoperative information in cases that require surgical repair (Khoury et al. 1996; Tuite 2002; Mengiardi et al. 2005; Ng et al. 2013).

On US, the extensor tendons are easily evaluated because of their superficial location. Besides, US is a cost-effective method for dynamic evaluation of the tendons and it also allows the injection of diagnostic or therapeutic steroids and platelet-rich plasma into the site of pain (Ng et al. 2013). Ultrasound allows excellent depiction of AT tendinopathy. Signs of tendinosis include thickening of the tendon, focal or diffuse hypoechoic areas with loss of fibrillar appearance in the longitudinal plane. It may occasionally be difficult to differentiate an area of tendinosis from a small partial-thickness tear. A partial-thickness tendon tear usually manifests as an incomplete discontinuity or focal defect within

Fig. 38 Complete rupture of the anterior tibial tendon with retraction of the torn proximal tendon stump (arrow). The sagittal STIR MR image shows a focal segment of empty tendon sheath filled with fluid

the fibrillar architecture. Tenosynovitis appears as anechoic fluid in the tendon sheath with a "target sign" in the transverse plane and a "rail track" appearance in the longitudinal plane (Khoury et al. 2007). Complete rupture appears as a discrete gap within the tendon, filled with either haematoma in acute injury or scar and granulation tissue in chronic injury, with associated retraction of the proximal and distal tendon stumps. US is useful for marking the extent of tendon retraction before surgery (Mengiardi et al. 2005; Teh et al. 2011; Ng et al. 2013). US is also well suited to demonstrate tendon impingement during tendon motion and underlying osseous abnormality (Khoury et al. 2007).

4.3.2 Extensor Hallucis Longus, Digitorum Longus and Peroneus Tertius Tendon Injuries

The EHL tendon is thinner and runs parallel to the AT lateral to it. The EDL and the peroneus tertius are located more laterally (Fig. 35). The EHL is a thin muscle arising from the anterior surface of the fibula and the interosseous membrane. The EDL arises from the lateral condyle of the tibia, the anterior surface of the fibula and the interosseous membrane. At the level of the ankle, the EDL muscle is held in position along the dorsum of the ankle by both the superior and inferior extensor retinaculum and is subdivided into four tendons coursing over the dorsal aspect of the foot (De Maeseneer et al. 2018b; Ng et al. 2013; Zember et al. 2016). The EDL muscle (situated along the lateral aspect of the leg and ankle) aids in extension of the second through fifth toes.

The peroneus tertius (as mentioned above in the lateral peroneal tendon group—Sect. 4.1.3 on anatomical muscle variants and pitfalls) is an accessory muscle/tendon (present in 10% of individuals) which lies anterior to the lateral malleolus and also belongs to the anterior tendon group. The peroneus tertius muscle originates from the distal anterior fibula and ends proximal to the inferior extensor retinaculum. The peroneus tertius tendon courses beneath the retinaculum and is inserted dorsally onto the base of the fifth metatarsal (De Maeseneer et al. 2018b).

Lesions of EHL and EDL tendons are quite uncommon because these tendons are subject to low mechanical stress (as for the AT). Friction with shoes or impingement with underlying degenerative or post-traumatic osseous remodelling is reported to be a cause of tenosynovitis. One of the more common injuries in ultramarathoners has been reported at the EDL tendon whether related to repetitive friction of the tendon against the retinaculum or a talar head exostosis (Zember et al. 2016).

The *peroneus tertius* rarely could cause anterolateral and hindfoot pain (Iceman et al. 2020; Choudhary and McNally 2011) (Fig. 39).

Imaging Dynamic sonography with plantar flexion may show an impingement between EDL tendon and a dorsal talar ridge (Khoury et al. 2007). Visualisation of peroneus tertius tendon with US is easier than with MRI, as the probe can be placed exactly along the long axis of the

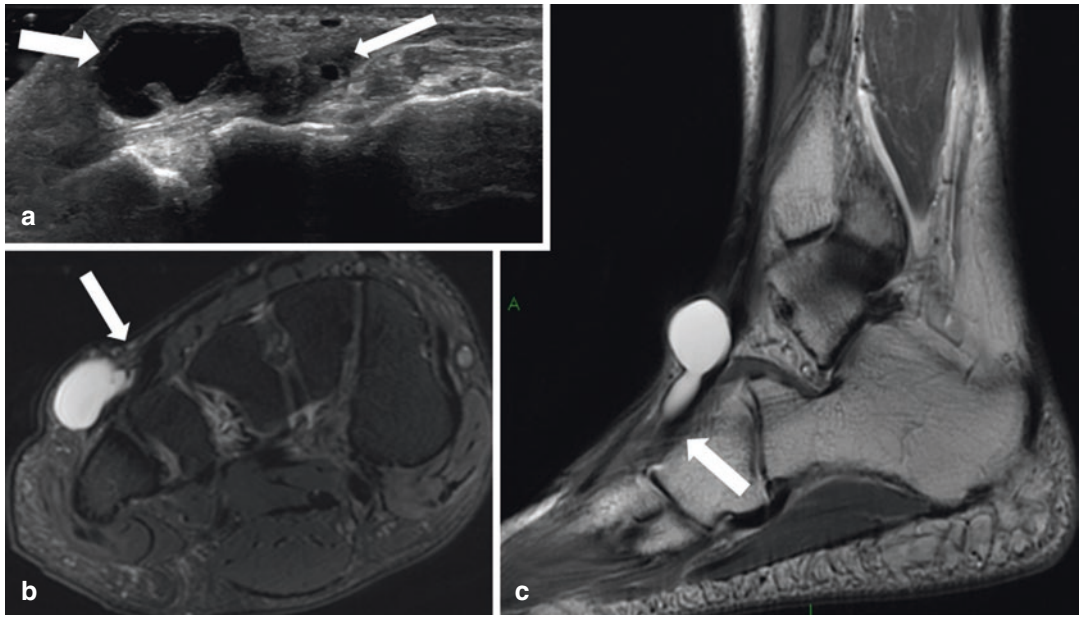

Fig. 39 (**a**–**c**) Subcutaneous cyst of the dorsolateral midfoot associated to a degenerative peroneus tertius tendon in a 37-year-old man with swelling and difficulty to close his right shoe. (**a**) Axial US (thick arrow) image shows a subcutaneous lobulated anechoic mass connected to a degenerative tendon (thin arrow) that courses lateral to the EDL and is inserted distally between the base of metatarsals 4 and 5. The cyst presents on coronal T2 fat sat and sagittal PD MR images a small pedicle to the peroneus tertius (arrow on **b** and **c**). The tendon has an irregular outline on **b** (arrow). (*Courtesy of A. Baetslé and T. Jager*)

tendon (De Maeseneer et al. 2018b). MRI findings of the EHL and EDL tears are similar to AT injuries (Fig. 40).

4.4 Plantar Fascia

The plantar fascia (PF) or plantar aponeurosis is made up of different bands of connective tissue. It helps maintain the longitudinal arch of the foot. The PF is subdivided into a medial, central and lateral bundle. The central bundle is the thickest one and is most frequently involved in PF pathology. This bundle is thick at the proximal insertion on the medial tubercle of the calcaneum and becomes thinner as it progresses distally into a fan-shaped structure with different slips attaching to the base of the proximal phalanx of each toe. The fascia overlies the central band of the flexor digitorum brevis. A normal PF has a thickness of 2–4 mm and is seen as a striated hyperechoic band on ultrasound and a uniform hypointense structure on all MRI sequences (Draghi et al. 2017; Lawrence et al. 2013; Khoury et al. 2007).

4.4.1 Plantar Fasciitis

Plantar fasciitis is an overuse injury typically seen in runners and patients over weight. It is the result of repetitive trauma leading to microtears most commonly at the proximal insertion of the fascia. It is the most frequent common cause of heel pain and can be associated with swelling and local tenderness. It can be associated to bone erosions in seronegative inflammatory spondylarthropathies (as ankylosing spondylitis, Reiter and psoriatic arthritis) (Lawrence et al. 2013).

Imaging Although it is a clinical diagnosis, imaging is sometimes needed in unclear cases to rule out other causes of heel pain. Lateral radio-

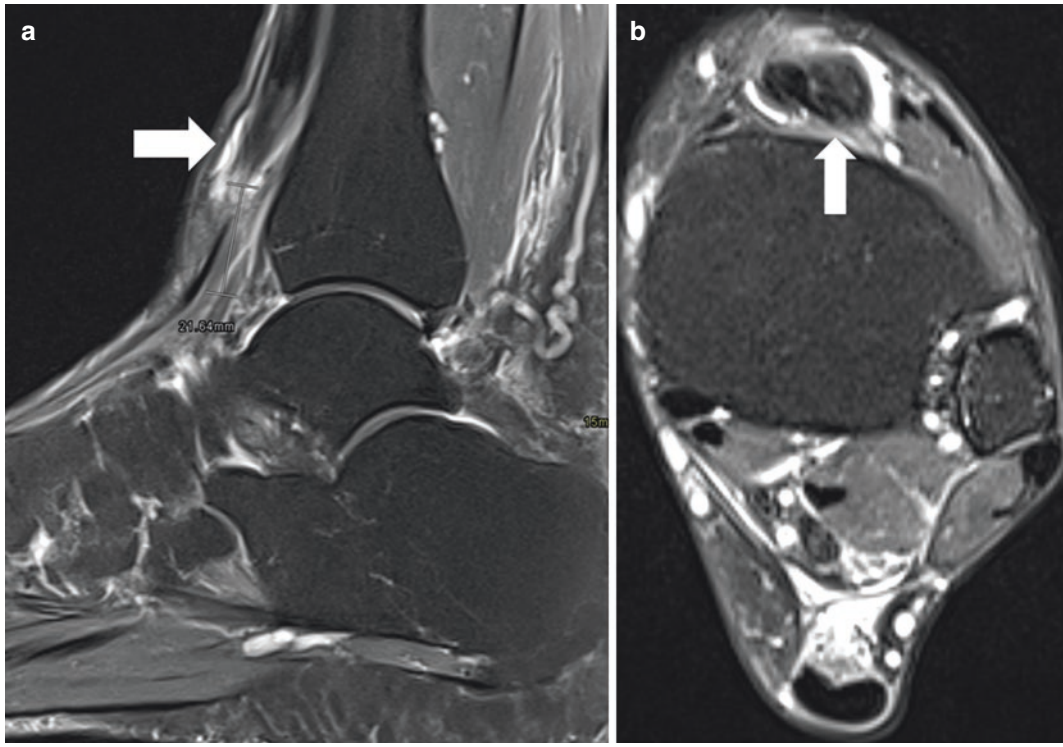

Fig. 40 (**a**, **b**) Complete rupture of the extensor hallucis longus (EHL) tendon in a 55-year-old female presenting a soft-tissue swelling at the anterior aspect of the distal tibia. (**a**) Sagittal PD fat-sat MR image shows discontinuity of the EHL with tendon retraction above the tibiotalar joint (arrow). (**b**) Axial PD fat-sat image depicts a thickening with increased signal of the retracted EHL tendon stump (located lateral to the still low-signal anterior tibial tendon) causing a pseudotumoral mass (arrow). High signal fluid is detected around the EHL tendon stump on **a** and **b**

graph of the ankle can demonstrate proximal subcalcaneal soft-tissue swelling as well as bone erosions or spur (also known as enthesophyte) at the calcaneal insertion. This is indicative of plantar fasciitis, but the definitive diagnosis needs US (or MRI). On ultrasound the injured FP is hypoechoic and markedly thickened, the cut-off being more than 4 mm (Fig. 41). There is a loss of the fibrillar structure and hypervascularisation can be present on colour Doppler. MRI characteristics include thickening over 3 mm and heterogeneous increased signal on fluid-sensitive sequences and oedema in the surrounding soft tissues, sometimes associated to bone marrow oedema in the calcaneal tuberosity (Draghi et al. 2017; Lawrence et al. 2013; Khoury et al. 2007) (Fig. 42).

4.4.2 Plantar Fascia Tear

Tears of the PF can occur at the proximal or middle portion of the aponeurosis. They are uncom-

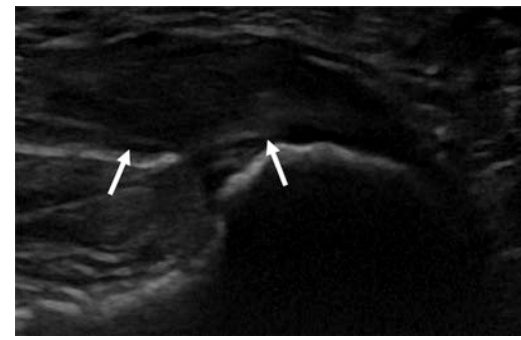

Fig. 41 Plantar fasciitis on longitudinal US image. The fascia is markedly thickened and hypoechoic (arrows) with loss of the fibrillar pattern

mon compared to plantar fasciitis and can be partial or complete. Mechanism of injury is a forced plantar flexion of the foot in competitive athletes, generally runners and jumpers. Patients with chronic plantar fasciitis receiving local corticosteroid injections could develop a spontaneous proximal rupture; they could present acute pain and swelling accompanied by an audible "snap" (Lawrence et al. 2013; Draghi et al. 2017).

Imaging US and MRI are the modality of choice. On US a tear is characterised by disruption of the fibres with a hypoechoic cleft representing fluid and haematoma. Dorsiflexion of the toes can increase conspicuity of PF tears. Similarly to US, MRI shows complete or partial interruption of the PF which is replaced by a hyperintense signal on fluid-sensitive images (Fig. 43). Tear of the flexor digitorum brevis muscle underlying the FP is often associated with FP tears. This should also be ruled out when FP tear is suspected (Draghi et al. 2017; Lawrence et al. 2013; Khoury et al. 2007).

4.5 Achilles Tendon

The Achilles tendon is the thickest, strongest as well as longest tendon in the body. The tendon is the distal insertion of the triceps surae, which consists of the gastrocnemius and soleus mus-

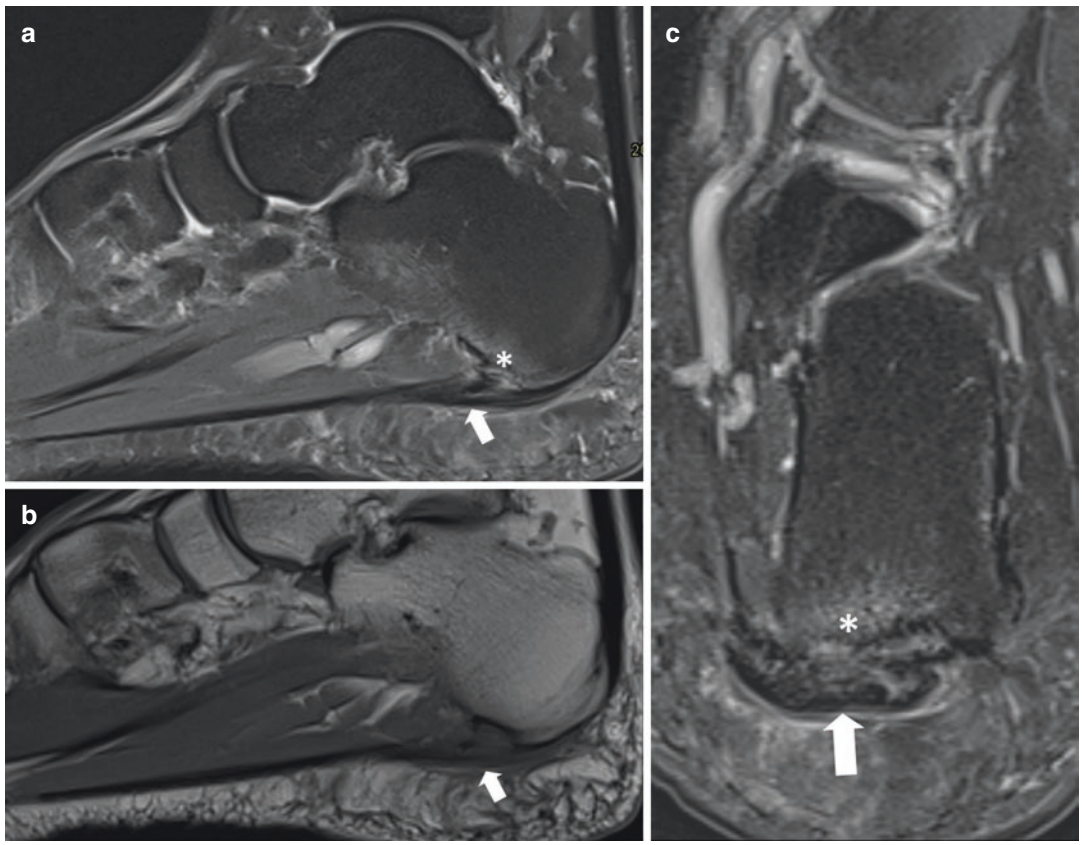

Fig. 42 (**a**–**c**) Plantar fasciitis in a 50-year-old female complaining of plantar pain during walking. Sagittal PD fat-sat (**a**) and T1 (**b**) MR images and coronal PD fat sat show a proximal thickening of the middle and medial bundles of the plantar fascia (arrow) and underlying bone marrow oedema at the plantar aspect of the calcaneum (asterisk on **a** and **c**). There is also subtle soft-tissue oedema in the perifascial fat pad of the heel

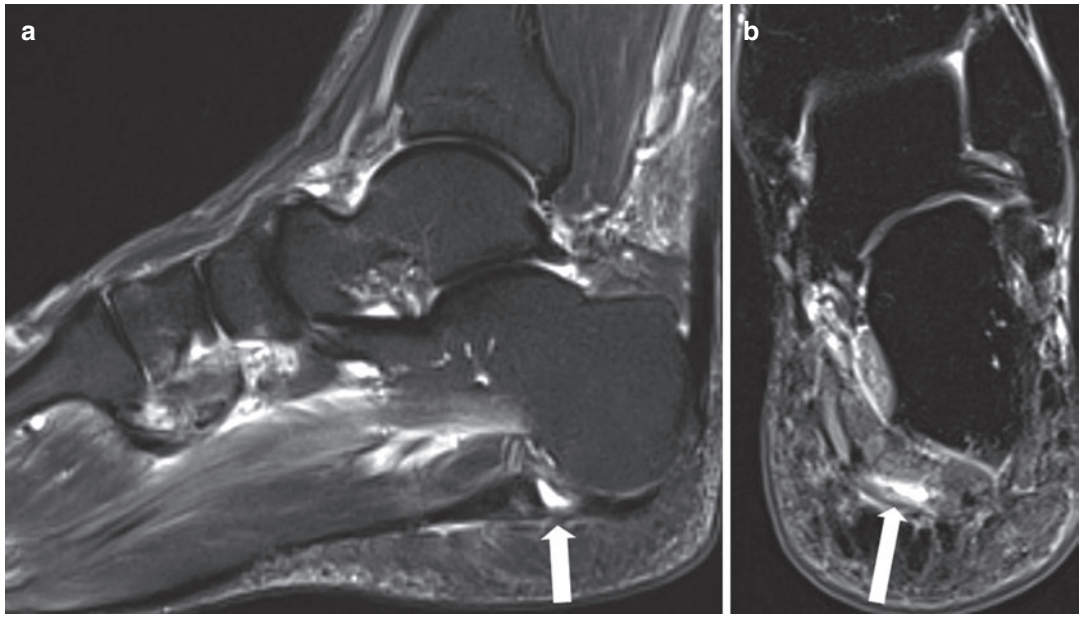

Fig. 43 (**a**, **b**) Complete rupture of the plantar fascia in a 62-year-old female over weight with sudden onset of heel pain during walking. Sagittal STIR (**a**) and coronal PD fat-sat MR images (**b**) disclose discontinuity with a small fluid-filled gap at the proximal attachment (arrow)

cles. Both contribute to form the Achilles tendon. Distally the tendon inserts onto the calcaneum. The insertion is bordered anteriorly and superiorly by the retrocalcaneal bursa and posteriorly by the retro-Achilles bursa. In healthy subjects these should barely be visible on imaging studies. Along its course from proximal to distal, the shape of the tendon changes; it is important to appreciate these changes when evaluating Achilles tendon on imaging. The proximal part of the tendon is flat while the descending part of the tendon has a concave surface anteriorly and a flat surface posteriorly. Just above the distal insertion, the anterior margin of the tendon is convex rather than concave (Chew et al. 2010).

Contrarily to other tendons the Achilles tendon does not have a synovial sheath. It is rather surrounded by a thin membrane called the paratenon, which is richly vascularised and largely responsible for the tendon's blood supply. Kager's fat pad is a triangular shaped area of adipose tissue anterior to the Achilles tendon. Injury of the tendon may result in oedema in Kager's fat pad (Calleja and Connell 2010).

4.5.1 Achilles Tendinopathy

Achilles tendinopathy is very common in athletes participating in running, track and field, soccer and racquet sports. The mechanism responsible for tendon injury is sudden dorsiflexion of a plantar flexed foot. Direct blow to the tendon is less common. The spectrum of injury includes tendinosis, insertional tendinopathy, bursitis and paratendonitis (Khoury et al. 2007; Calleja and Connell 2010).

Both ultrasound and MRI are ideal imaging modalities for evaluating Achilles tendon injury (Weinfeld 2014). Radiography may demonstrate tendon swelling or calcification, but has a low specificity.

Achilles tendinosis is an overuse-type injury secondary to excessive loading. Midsubstance involvement is most common, occurring at around 5—8 cm proximal to the insertion. Patients complain of pain and difficulty doing

steps. Swelling and local tenderness are often present (Weinfeld 2014).

Imaging Tendinosis is usually characterised by a fusiform swelling of the tendon on a longitudinal view. The tendon is thickened in transverse plane with loss of the concave anterior border in the mid portion of the tendon. The affected tendon is hypoechoic on US (Fig. 44) and can demonstrate patchy increased signal intensity on fluid-sensitive MR sequences (Fig. 45). In contrast to the more common fusiform involvement, tendinosis can also be nodular resulting in smaller hypoechoic areas on US. Associated abnormalities include oedema in Kager's fat pad, peritendinous fluid and possible intratendinous tears (Khoury et al. 2007; Calleja and Connell 2010).

Insertional tendinosis is another type of overuse injury secondary to excessive use of the calf muscles. It is most frequently seen in runners, ballet dancers and in jumping sports. Another common cause of posterior heel pain is *retrocalcaneal or retrotendinous bursitis*. These conditions are associated with Haglund deformity (a bony prominence on superior posterior aspect of the calcaneal tuberosity), rheumatoid and seronegative arthritis. The combination of soft-tissue abnormalities and a Haglund deformity is termed "Haglund syndrome" (Lawrence et al. 2013; Calleja and Connell 2010) (Fig. 45).

Imaging For insertional tendinosis, US and MRI findings are those of tendinosis but at the level of the calcaneal insertion. There may be bony erosions present on plain films and oedema in the calcaneal tuberosity on MRI both secondary to local inflammation, as well as calcifications (Fig. 45). In case of bursitis, fluid accumulation may be visible anterior or posterior to the tendon, depending on which bursa is involved. The retrocalcaneal bursa sometimes has a physiological amount of fluid but should not exceed an anteroposterior width of 1 mm on MRI and 1.5 mm on US. In case of bursitis, involvement of the surrounding soft tissues is expected (Lawrence et al. 2013; Calleja and Connell 2010; Khoury et al. 2007). *Paratenonitis* is an inflammation of the paratenon that often occurs in conjunction with tendinosis, but may also be isolated. It is an acute inflammation most prevalent in long-distance runners. Like in tendinosis there is swelling and palpation can be extremely painful. This condition may result in scar formation and adhesions around the Achilles tendon which can cause impingement (Weinfeld 2014; Calleja and Connell 2010).

Imaging Ultrasound reveals hypoechoic thickening of the paratenon, most frequently posteriorly. Fluid accumulation between the tendon and the paratenon as well as increased vascularity on Doppler ultrasound may also be present (Fig. 44). On fluid-sensitive MRI the paratenon is thickened and hyperintense; this is best visualised in the axial and sagittal plane. The paratenon also enhances after gadolinium administration. Oedema in the surrounding soft tissues may be present. In patients with chronic paratendonitis irregular signal intensity changes extending into Kager's fat pad represent adhesions (Weinfeld 2014; Calleja and Connell 2010; Chew et al. 2010).

4.5.2 Achilles Tendon Rupture

Tears almost always occur in an already diseased tendon. Rupture results from a sudden contraction of the gastrocnemius and soleus muscles and most often occurs in sports such as tennis, badminton, football or basketball. Corticosteroid injection is another cause of Achilles tendon tear. Symptoms include acute pain and swelling and the inability to walk. Tears are localised either at the hypovascular mid portion of the tendon, about 6 cm proximal to the insertion, or at the myotendinous junction. They can be either partial or complete. Plantar flexion of the foot may be preserved when the plantaris tendon is still intact (Weinfeld 2014; Calleja and Connell 2010; Chew et al. 2010).

Imaging It helps to determine the severity of a tendon tear and may help planning surgical treatment. On US a complete tear has a hypoechoic defect along the tendon representing haematoma.

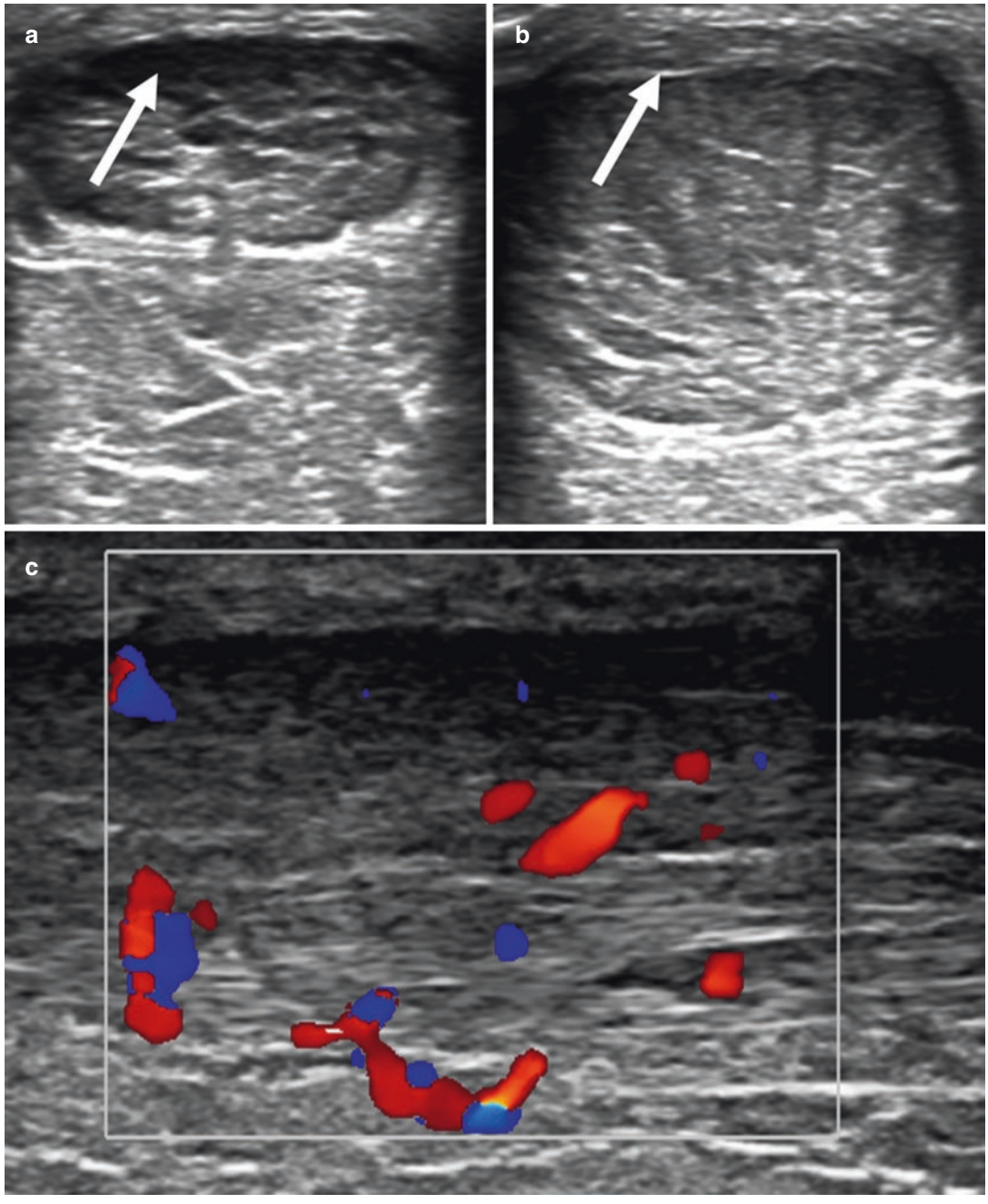

Fig. 44 (**a**–**c**) Achilles tendinosis and paratenonitis on axial US images. The diseased tendon (**b**) is markedly thickened with a rounded shape in the axial plane and diffuse hypoechoic foci. Compare with a normal Achilles tendon (**a**). In addition to tendinosis, the paratenon is also thickened (arrow on **b**) characteristic for paratenonitis. There is loss of fibrillar structure on the longitudinal view (**c**). Doppler US image demonstrates increased vascularisation in and around the tendon (**c**)

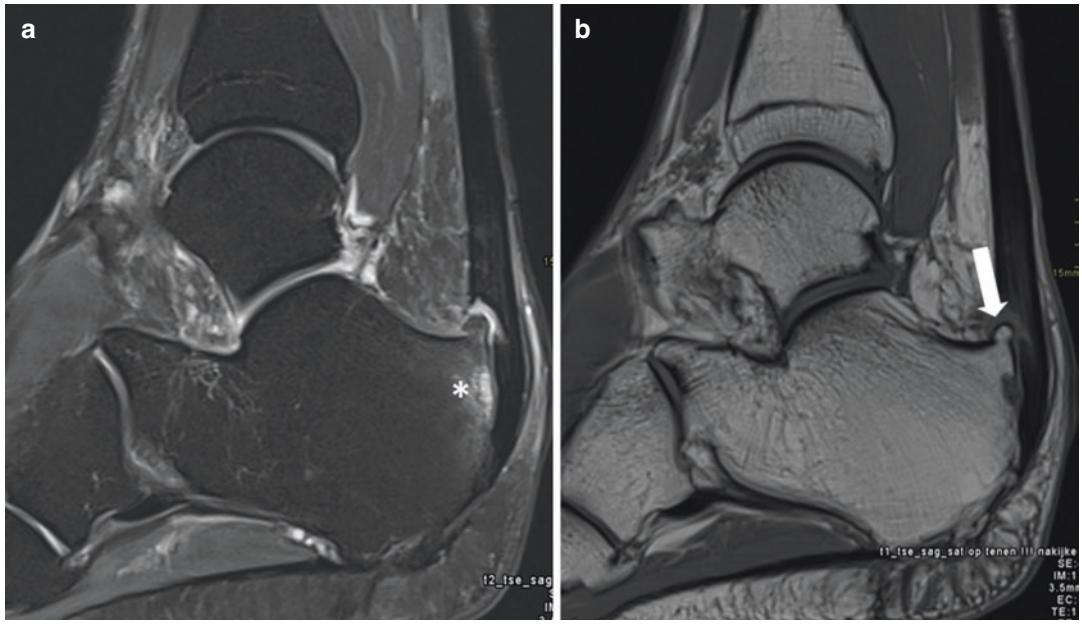

Fig. 45 (**a**, **b**) Insertion Achilles tendinopathy with Haglund deformity of the calcaneal tuberosity (arrow) in a 55-year-old recreative triathlon athlete. Sagittal PD fat-sat (**a**) and T1 (**b**) MR images show thickening of the distal Achilles tendon with intratendinous increased signal, bone marrow oedema in the calcaneal tuberosity (asterisk on **a**) and irregular posterior and inferior calcaneal bone outline on **b**

Torn ends of the tendon are visible on each side of the gap. The distance of the gap should be measured with the foot in plantar flexion (Fig. 46). Herniation of the anterior fat can also be present. Depending on the age of the haematoma it may be more isoechoic obscuring the tear. In these cases dynamic ultrasound with dorsiflexion of the foot is very helpful as this will reveal separation of the tendon. A partial tear demonstrates a focal hypoechoic area with loss of fibrillation parallel to the tendon fibres. MRI is helpful especially in cases where US is equivocal. Complete tears are identified by discontinuity of the tendon with a fluid intensity gap interposed between the torn ends (Fig. 47). A partial tear on MRI demonstrates a more heterogeneous increased signal on fluid-sensitive images and partial disruption of the tendon fibres. After healing, scar formation results in a tendon with intermediate signal intensity (Weinfeld 2014; Chew et al. 2010; Lawrence et al. 2013; Calleja and Connell 2010; Khoury et al. 2007).

4.6 Plantaris Tendon

The plantaris tendon is the longest tendon in the human body, but has a much smaller diameter than the adjacent Achilles tendon. The plantaris muscle originates from the posterior knee capsule and the lateral posterior femur below the linea aspera. The tendon runs between the gastrocnemius and soleus muscles and crosses medially to run anteromedially to the Achilles tendon. In 20% of individuals the tendon merges distally with the Achilles tendon. The site where the tendons merge can mimic a tear on MRI, so it is important to consider and localise the plantaris tendon when this is suspected (Fig. 47).

Plantaris tendon tears are classically seen in tennis players, who complain of pain in the posterior lower leg after an injury. The tendon may retract, and patients will typically have oedema between the soleus and gastrocnemius muscles in the calf on MRI (Tuite 2002).

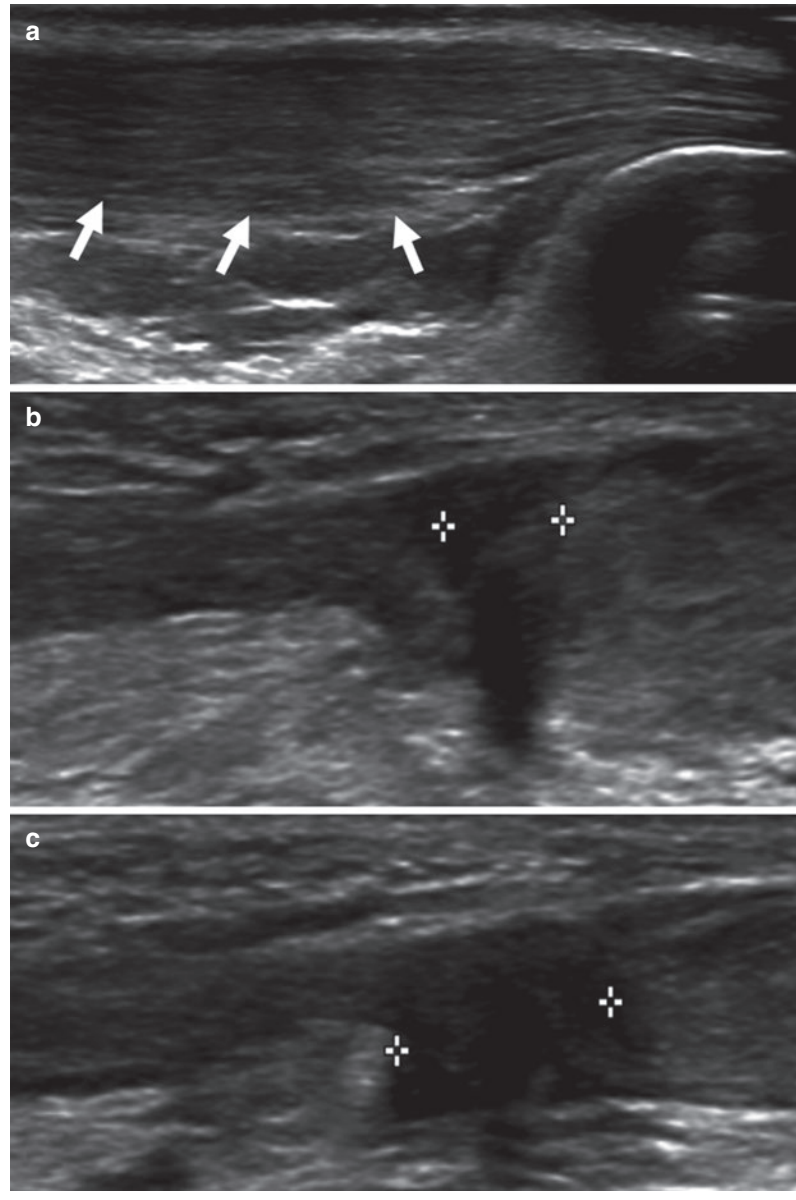

Fig. 46 (**a**–**c**) Complete Achilles tendon tear on dynamic US in a 31-year-old male. (**a**) Longitudinal US image near the calcaneal insertion shows thickening of the tendon characteristic for tendinosis (arrows). (**b**) Longitudinal US image obtained more proximal demonstrates interruption of the fibres with a hypoechoic cleft (callipers) corresponding to an Achilles tendon tear. (**c**) On the same image as **b** but with the foot in dorsiflexion, the gap between the tendon fibres increases confirming a complete tear

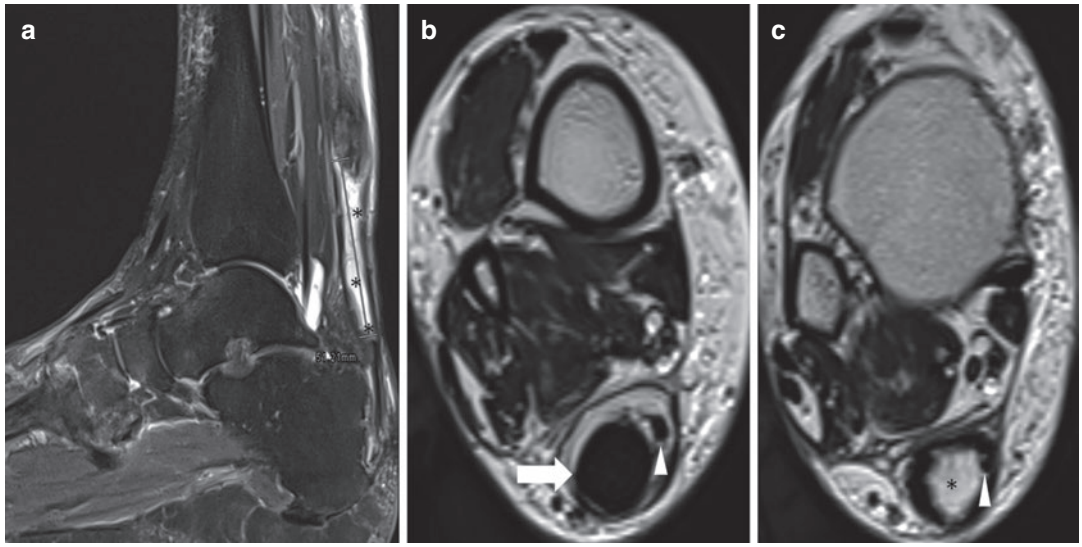

Fig. 47 (**a**–**c**) Complete Achilles tendon tear in a 66-year-old recreative jogger. Sagittal PD fat-sat MR image (**a**) shows discontinuity of the Achilles tendon with proximal retraction and a fluid-filled gap asterisks (2). Axial T2 images at two different levels show thickening of the retracted stump (arrow on **b**) and a fluid-filled gap distal to the stump (asterisk on **c**). The plantaris tendon is intact (arrowhead on **b** and **c**)

Things to Remember

- Ankle and foot are common sites of sports-related injuries; ankle inversion injuries are most prevalent.
- Although ankle sprains usually have a good outcome, unrecognised lesions can delay return to play.
- Ankle inversion can involve most frequently the anterior talofibular ligament followed by the calcaneofibular ligament.
- Medial collateral (deltoid) ligaments and distal tibiofibular syndesmosis are involved in more severe ankle sprains.
- Osteochondral lesions of the talus and peroneal tendon injury can be associated to ankle sprain.
- The most commonly injured tendon in sports is the Achilles tendon.
- Ultrasound (US) is an ideal modality to assess soft-tissue injury of ankle and foot in acute setting.
- MRI may be necessary to rule out intra-articular lesions and bone abnormalities or to assess deep structures that cannot be imaged with US.

References

Aparisi Gómez MP, Aparisi F, Bartoloni A et al (2019) Anatomical variation in the ankle and foot: from incidental finding to inductor of pathology. Part II: Midfoot and forefoot. Insights Imaging 10(1):69

Balen PF, Helms CA (2001) Association of posterior tibial tendon injury with spring ligament injury, sinus tarsi abnormality, and plantar fasciitis on MR imaging. Am J Roentgenol 176:1137–1143

Bianchi S, Martinoli C, Gaignot C, De Gautard R, Meyer JM (2005) Ultrasound of the ankle: anatomy of the tendons, bursae, and ligaments. Semin Musculoskelet Radiol 9(3):243–259

Bianchi S, Delmi M, Molini L (2010) Ultrasound of the ankle: anatomy of the tendons, bursae, and ligaments. Semin Musculoskelet Radiol 14(3):292–306

Brigido MK, Fessell DP, Jacobson JA et al (2005) Radiography and US of os peroneum fractures and associated peroneal tendon injuries: initial experience. Radiology 237(1):235–241

Burge AJ, Gold SL, Potter HG (2012) Imaging of sports-related midfoot and forefoot injuries. Sports Health 4(6):518–534. https://doi.org/10.1177/1941738112459489

Calleja M, Connell DA (2010) The achilles tendon. Semin Musculoskelet Radiol 14(3):307–322. https://doi.org/10.1055/s-0030-1254520

Chan BY, Markhardt BK, Williams KL, Kanarek AA, Ross AB (2019) Os conundrum: identifying symptomatic sesamoids and accessory ossicles of the foot. Am J

Roentgenol 213(2):417–426. https://doi.org/10.2214/AJR.18.20761
Cheung Y (2017) Normal variants: accessory muscles about the ankle. Magn Reson Imaging Clin N Am 25(1):11–26
Cheung Y, Rosenberg ZS, Magee T, Chinitz L (1992) Normal anatomy and pathologic conditions of ankle tendons: current imaging techniques. Radiographics 12(3):429–444
Chew NS, Lee J, Davies M, Healy J (2010) Ankle and foot injuries. In: Philip R (ed) Essential radiology for sports medicine. Springer, New York, pp 69–72. pp 256
Choudhary S, McNally E (2011) Review of common and unusual causes of lateral ankle pain. Skelet Radiol 40(11):1399–1413
Crim J (2016) Medial-sided ankle pain: deltoid ligament and beyond. Magn Reson Imaging Clin N Am 25(1):63–77
Davda K, Malhotra K, O'Donnell P, Singh D, Cullen N (2017) Peroneal tendon disorders. EFORT Open Rev 2(6):281–292. https://doi.org/10.1302/2058-5241.2.160047
De Brucker Y, Shahabpour M (2016) Distal tibiofibular syndesmosis. In Kramer J and Karantanas A. MRI foot and ankle. Breitenseher Publisher, Horn, Austria; 53–62. p 357
De Maeseneer M, Moyson N, Lenchik L, Cattrysse E, Scafoglieri A, Roose R, Shahabpour M (2018a) MR imaging-anatomical correlation of the metatarsophalangeal joint of the hallux: ligaments, tendons, and muscles. Eur J Radiol 106:14–19
De Maeseneer M, Madani H, Lenchik L, De Mey J, Provyn S, Shahabpour M (2018b) Ultrasound of the distal insertions of the ankle and foot tendons with anatomical correlation: a review. Can Assoc Radiol J 69(3):282–292
Doherty C, Delahunt E, Caulfield B, Hertel J, Ryan J, Bleakley C (2014) The incidence and prevalence of ankle sprain injury: a systematic review and meta-analysis of prospective epidemiological studies. Sports Med 44(1):123–140
Demehri S, Chalian M, Farahani SJ, et al (2014) Detection and characterization of tendon abnormalities with multidetector computed tomography. Journal of Computer Assisted Tomography 38:299–307
Donovan A, Rosenberg ZS (2009) Extraarticular lateral hindfoot impingement with posterior tibial tendon tear: MRI correlation. Am J Roentgenol 193(3):672–678. https://doi.org/10.2214/AJR.08.2215
Donovan A, Rosenberg ZS, Bencardino JT et al (2013) Plantar tendons of the foot: MR imaging and US. Radiographics 33(7):2065–2085. https://doi.org/10.1148/rg.337125167
Döring S, Provyn S, Marcelis S et al (2018) Ankle and midfoot ligaments: ultrasound with anatomical correlation: a review. Eur J Radiol 107:216–226
Draghi F, Gitto S, Bortolotto C, Draghi AG, Ori Belometti G (2017) Imaging of plantar fascia disorders: findings on plain radiography, ultrasound and magnetic resonance imaging. Insights Imaging 8(1):69–78
Gluck GS, Heckman DS, Parekh SG (2010) Tendon disorders of the foot and ankle, Part 3: The posterior tibial tendon. Am J Sports Med 38(10):2133–2144
Hallinan JTPD, Wang W, Pathria MN, Smitaman E, Huang BK (2019) The peroneus longus muscle and tendon: a review of its anatomy and pathology. Skelet Radiol 48(9):1329–1344
Hunt KJ, Githens M, Riley GM, Kim M, Gold GE (2013) Foot and ankle injuries in sport: imaging correlation with arthroscopic and surgical findings. Clin Sports Med 32(3):525–557
Iceman K, Magnus MK, Thompson MJ, Abicht BP (2020) Peroneus tertius syndrome: a rare cause of anterolateral ankle and rearfoot pain. J Foot Ankle Surg 59(1):131–135. https://doi.org/10.1053/j.jfas.2019.04.015
Jegal H, Park YU, Kim JS, Choo HS, Seo YU, Lee KT (2016) Accessory navicular syndrome in athlete vs general population. Foot Ankle Int 37(8):862–867. https://doi.org/10.1177/1071100716644791
Kelikian AS, Sarrafian SK, et al. (2011) Sarrafian's Anatomy of the Foot and Ankle: Descriptive, Topographic, Functional. Lippincott Williams & Wilkins (Wolters Kluwer) Philadelphia
Khoury NJ, El-Khoury GY, Saltzman CL, Brandser EA (1996) Rupture of the anterior tibial tendon: diagnosis by MR imaging. AJR Am J Roentgenol 167(2):351–354
Khoury V, Guillin R, Dhanju J, Cardinal E (2007) Ultrasound of ankle and foot: overuse and sports injuries. Semin Musculoskelet Radiol 11(2):149–161. https://doi.org/10.1055/s-2007-1001880
Kijowski R, de Smet A, Mukharjee R (2007) Magnetic resonance imaging findings in patients with peroneal tendinopathy and peroneal tenosynovitis. Skelet Radiol 36(2):105–114. https://doi.org/10.1007/s00256-006-0172-7
Kitsukawa K, Hirano T, Niki H, Tachizawa N, Nakajima Y, Hirata K (2015) MR imaging evaluation of the Lisfranc ligament in cadaveric feet and patients with acute to chronic Lisfranc injury. Foot Ankle Int 36(12):1483–1492. https://doi.org/10.1177/1071100715596746
Kumar Y, Alian A, Ahlawat S, Wukich DK, Chhabra A (2017) Peroneal tendon pathology: pre- and post-operative high resolution US and MR imaging. Eur J Radiol 92:132–144
Lawrence DA, Rolen MF, Morshed KA, Moukaddam H (2013) MRI of heel pain. Am J Roentgenol 200(4):845–855
Lee MH, Chung CB, Cho JH et al (2006) Tibialis anterior tendon and extensor retinaculum: imaging in cadavers and patients with tendon tear. AJR Am J Roentgenol 187(2):W161–W168. https://doi.org/10.2214/AJR.05.0073

Lee SJ, Jacobson JA, Kim SM et al (2013) Ultrasound and MRI of the peroneal tendons and associated pathology. Skelet Radiol 42(9):1191–1200

Linklater JM, Hayter CL, Vu D (2017) Imaging of acute capsuloligamentous sports injuries in the ankle and foot: sports imaging series. Radiology 283(3):644–662. https://doi.org/10.1148/radiol.2017152442

Llopis E, Carrascoso J, Iriarte I, Serrano Mde P, Cerezal L (2016) Lisfranc injury imaging and surgical management. Semin Musculoskelet Radiol 20(2):139–153. https://doi.org/10.1055/s-0036-1581119

Lo LD, Schweitzer ME, Fan JK, Wapner KL, Hecht PJ (2001) MR imaging findings of entrapment of the flexor hallucis longus tendon. Am J Roentgenol 176(5):1145–1148. https://doi.org/10.2214/ajr.176.5.1761145

Madani H, De Brucker Y, De Maeseneer M, Shahabpour M (2016) Lateral collateral ligament complex of the ankle. In: Kramer J, Karantanas A (eds) MRI foot and ankle. Breitenseher Publisher, Horn, Austria, pp 45–52. p 357

Mansour R, Jibri Z, Kamath S, Mukherjee K, Ostlere S (2011) Persistent ankle pain following a sprain: a review of imaging. Emerg Radiol 18(3):211–225

McKiernan S, Fenech M, Fox D, Stewart I (2017) Sonography of the ankle: the lateral ankle and ankle sprains. Sonography 4:146–155. https://doi.org/10.1002/sono.12120

Mengiardi B, Pfirrmann CWA, Vienne P et al (2005) Anterior tibial tendon abnormalities: MR imaging findings. Radiology 235(3):977–984. https://doi.org/10.1148/radiol.2353040617

Mengiardi B, Pinto C, Zanetti M (2016) Spring ligament complex and posterior tibial tendon: MR anatomy and findings in acquired adult flatfoot deformity. Semin Musculoskelet Radiol 20(1):104–115. https://doi.org/10.1055/s-0036-1580616

Nazarenko A, Beltran LS, Bencardino JT (2013) Imaging evaluation of traumatic ligamentous injuries of the ankle and foot. Radiol Clin N Am 51(3):455–478

Ng JM, Rosenberg ZS, Bencardino JT, Restrepo-Velez Z, Ciavarra GA, Adler RS (2013) US and MR imaging of the extensor compartment of the ankle. Radiographics 33(7):2047–2064. https://doi.org/10.1148/rg.337125182

Nussbaum ED, Hosea TM, Sieler SD, Incremona BR, Kessler DE (2001) Prospective evaluation of syndesmotic ankle sprains without diastasis. Am J Sports Med 29(1):31–35. https://doi.org/10.1177/03635465010290011001

Nwawka OK, Hayashi D, Diaz LE et al (2013) Sesamoids and accessory ossicles of the foot: anatomical variability and related pathology. Insights Imaging 4(5):581–593

Philbin TM, Landis GS, Smith B (2009) Peroneal tendon injuries. J Am Acad Orthop Surg 17(5):306–317

Roemer FW, Jomaah N, Niu J et al (2014) Ligamentous injuries and the risk of associated tissue damage in acute ankle sprains in athletes: a cross-sectional MRI study. Am J Sports Med 42(7):1549–1557. https://doi.org/10.1177/0363546514529643

Rosenberg ZS, Beltran J, Bencardino JT (2000) MR imaging of the ankle and foot. Radiographics 20:S153–S179

Roster B, Michelier P, Giza E (2015) Peroneal tendon disorders. Clin Sports Med 34(4):625–641. https://doi.org/10.1016/j.csm.2015.06.003

Sanhudo J (2002) Stenosing tenosynovitis of the flexor hallucis longus tendon at the sesamoid area. Foot Ankle Int 23(9):801–803. https://doi.org/10.1177/107110070202300905

Sarrafian SK (1983) Anatomy of the foot and ankle: descriptive, topographic, functional. Lippincott, Philadelphia. p 433

Saupe N, Mengiardi B, Pfirrmann CWA, Vienne P, Seifert B, Zanetti M (2007) Anatomic variants associated with peroneal tendon disorders: MR imaging findings in volunteers with asymptomatic ankles. Radiology 242(2):509–517. https://doi.org/10.1148/radiol.2422051993

Schubert R (2013) MRI of peroneal tendinopathies resulting from trauma or overuse. Br J Radiol 86(1021):20110750. https://doi.org/10.1259/bjr.20110750

Schweitzer ME, Karasick D (2000) MR imaging of disorders of the posterior tibialis tendon. Am J Roentgenol 175(3):627–635

Sconfienza LM, Orlandi D, Lacelli F, Serafini G, Silvestri E (2015) Dynamic high-resolution US of ankle and midfoot ligaments: normal anatomic structure and imaging technique. Radiographics 35(1):164–178. https://doi.org/10.1148/rg.351130139

Sobel M, Pavlov H, Geppert MJ, Thompson FM, DiCarlo EF, Davis WH (1994) Painful os peroneum syndrome: a spectrum of conditions responsible for plantar lateral foot pain. Foot Ankle Int 15(3):112–124. https://doi.org/10.1177/107110079401500306

Soliman SB, Spicer PJ, van Holsbeeck MT (2019) Sonographic and radiographic findings of posterior tibial tendon dysfunction: a practical step forward. Skelet Radiol 48(1):11–27

Srinivasan R (2016) The hallucal-sesamoid complex: normal anatomy, imaging, and pathology. Semin Musculoskelet Radiol 20:224–232

Taljanovic MS, Alcala JN, Gimber LH, Rieke JD, Chilvers MM, Latt LD (2015) High-resolution US and MR imaging of peroneal tendon injuries. Radiographics 35(1):179–199. https://doi.org/10.1148/rg.351130062

Teh J, Suppiah R, Sharp R, Newton J (2011) Imaging in the assessment and management of overuse injuries in the foot and ankle. Semin Musculoskelet Radiol 15(1):101–114

Tenforde AS, Yin A, Hunt KJ (2016) Foot and ankle injuries in runners. Phys Med Rehabil Clin N Am 27(1):121–137. https://doi.org/10.1016/j.pmr.2015.08.007

Tuite MJ (2002) MR imaging of the tendons of the foot and ankle. Semin Musculoskelet Radiol 6(2):119–131

Vuillemin V, Guerini H, Bard H, Morvan G (2012) Stenosing tenosynovitis. J Ultrasound 15(1):20–28. https://doi.org/10.1016/j.jus.2012.02.002

Walter WR, Hirschmann A, Tafur M, Rosenberg ZS (2018) Imaging of Chopart (midtarsal) joint complex: normal anatomy and posttraumatic findings. Am J Roentgenol 211:416–425

Wang XT, Rosenberg ZS, Mechlin MB, Schweitzer ME (2005) Normal variants and diseases of the peroneal tendons and superior peroneal retinaculum: MR imaging features. Radiographics 25(3):587–602

Weinfeld SB (2014) Achilles tendon disorders. Med Clin N Am 98(2):331–338

Willekens I, Shahabpour M, Lenchik L et al (2019) Fluid distribution in ankle tendon sheaths in healthy volunteers: MRI findings. Surg Radiol Anat 41(12):1445–1449. https://doi.org/10.1007/s00276-019-02355-z

Wong GNL, Tan TJ (2016) MR imaging as a problem solving tool in posterior ankle pain: a review. Eur J Radiol 85(12):2238–2256

Zember J, Rosenberg Z, Rossi I, Mba-Jones C, Bencardino J (2016) The frondiform ligament and pseudotenosynovitis of the extensor digitorum longus tendon: MRI evaluation with cadaveric correlation. Skelet Radiol 45(8):1089–1095. https://doi.org/10.1007/s00256-016-2395-6

Ankle and Foot: Osteochondral Injuries

Onno L. G. Baur, Jari Dahmen,
Gino M. M. J. Kerkhoffs, and Mario Maas

Contents

O. L. G. Baur · M. Maas (✉)
Department of Radiology and Nuclear Medicine, Amsterdam University Medical Centers, Amsterdam Movement Sciences, Amsterdam, Academic Center for Evidence Based sports Medicine, University of Amsterdam, Amsterdam, The Netherlands
e-mail: O.l.baur@amsterdamumc.nl; m.maas@amsterdamumc.nl

J. Dahmen · G. M. M. J. Kerkhoffs
Department of Orthopaedic Surgery, Amsterdam University Medical Centers, Academic Center for Evidence Based Sports Medicine, University of Amsterdam, Amsterdam, The Netherlands
e-mail: j.dahmen@amsterdamumc.nl; g.m.kerkhoffs@amsterdamumc.nl

Abstract

This chapter focuses on subchondral bone injuries related to sports. Ankle sprains are the most common ankle injury which can result in an osteochondral defect. The diagnosis of osteochondral pathology is often confirmed by imaging. The different modalities all have advantages and disadvantages. This chapter examines in detail the pathophysiology of osteochondral defects and foot injuries and the added value of different imaging modalities.

Med Radiol Diagn Imaging (2021)
https://doi.org/10.1007/174_2020_258, © Springer Nature Switzerland AG
Published Online: 19 March 2021

1 Introduction: Specific Anatomy and Incidence

This chapter describes the sport-related osteochondral injuries of the ankle. Since the sports-related biomechanics of osteochondral injuries of the ankle is closely related to osteochondral defects (OCDs) we will discuss the pathology extensively. Osteochondral defects are defined as injuries involving both articular cartilage and subchondral bone. The term covers a wide spectrum of pathologies including (sub)chondral contusion, osteochondritis dissecans, osteochondral fracture, and osteoarthritis. Osteochondral injuries of the ankle often coincide with ligamentous ankle injuries and ankle sprains, which are discussed in (Van Royen et al. 2020). The entire anatomy of the ankle will not be described, but to have a better understanding about osteochondral injury we will describe the cartilaginous anatomy briefly.

1.1 Cartilage Anatomy

Osteochondral injuries in the ankle often occur in the tibiotalar joint. Cartilage is found on top of the talar dome and on the medial and lateral facets facing the medial malleolus and the fibula. Sugimato et al. examined the thickness of the cartilage at the talar surface. Specific interest was paid to those regions where osteochondral injuries predominantly occur (Sugimoto et al. 2005). The average cartilage thickness of the total area was 1.35 mm (±0.22) in males and 1.11 mm (±0.28) in females. The difference was considered statistically significant between the sexes (p = 0.025). The mean thickest area was found in the medial talar corner (1.56 mm in males, 1.42 mm in females). The thinnest cartilage was found in the lateral fibular surface (1.00 mm in males, 0.86 mm in females). Compared to the knee, the cartilage in the ankle is thin. This is thought to be due to the fact that the ankle joint is a congruent joint, compared to the knee.

2 Historical Background and Terminology

An osteochondral defect (OCD) is an idiopathic lesion of the cartilage and adjacent subchondral bone. The first documentation of an OCD dates back to 1560 when Ambroise Paré wrote about a surgical intervention were he removed loose bodies from the inside of a joint cavity (Paré and Malgaigne 1560). In 1738, surgeon and anatomist Alexander Monro was probably the first to describe the disease called "cartilaginous bodies of the joint" (Monro 1752). A couple of years later, Hunter (1743) described it as cartilaginous ulcerations and stated the following regarding treatment: "From Hippocrates down to the present age, ulcerated cartilage is a troublesome disease; when destroyed, it is not recovered" (Hunter 1743). It was König (1888) who first introduced the term osteochondritis dissecans and since Kappis (1922) the disease became known as the osteochondral lesion of the talus (König 1888; Kappis 1922).

In 1932 a paper was reported by Rendu, describing an intra-articular fracture of the talus which appeared similar to an osteochondral lesion (Rendu 1932). Then Rödén et al. (1953) were the first to describe a series of 55 cases which looked like osteochondritis dissecans lesions of the talus (Rödén et al. 1953).

Different aliases are known in the literature such as osteochondritis dissecans, osteochondral lesions of the talus (OLT), flake fracture, osteochondral fracture, and osteochondral defect. Currently the most accepted term is osteochondral defects or osteochondral lesions (van Bergen et al. 2015; Murphy et al. 2019).

3 Incidence

OCDs are often described as sequelae of inversion sprains. Ankle sprains are a common phenomenon among athletes with >300,000 injuries per year reported in the USA, and an estimated 52.3 ankle injuries per 1000 athletic exposures in high school-aged athletes (Delco et al. 2017).

Indoor sport athletes are particularly prone to ankle sprains (Doherty et al. 2014). Especially basketball, handball, and volleyball players have a high incidence of ankle sprains. In outdoor sports, soccer players are most prone to an ankle sprain. Although most patients with an ankle sprain have an uncomplicated recovery a small percentage will develop an OCD. It is not entirely clear what the overall incidence of OCD in the ankle is. Based on the literature, the incidence is approximately 0.09% with a prevalence of 0.002/100.000 person/year. OCD is usually diagnosed between the age of 10 and 30 years (Loomer et al. 1993; Bauer et al. 1987; Orr et al. 2011; Weiss et al. 2016). Second to inversion sprains, ankle fractures seem to be related to the formation of an ankle OCD in 10–40% of the cases (Nosewicz et al. 2016). Although no clear association has been established, displaced fractures Lauge-Hansen stage III/IV seem to be most prone to forming an OCD of the talar joint (Nosewicz et al. 2016; Regier et al. 2016; Lambers et al. 2019).

4 Etiology

4.1 Biomechanical Etiology

Traumatic events are regarded as the predominant cause of an OCD, as research indicated that in up to 70% of acute ankle fractures and sprains osteochondral defects can occur (Hintermann et al. 2000; Saxena and Eakin 2007; Blom et al. 2019). Repetitive trauma may also play a role, especially in athletes. Research indicates that these repetitive traumas occur, in 55–60% of patients with an OCD, during sport activities (Tol et al. 2000; Aichroth 1971). Nevertheless, trauma does not explain all cases of OCD.

4.2 Biological Etiology

Other etiologies mentioned in the literature are ischemic, inflammatory, and hereditary factors; osteonecrosis and gradual development following an injury to the endochondral epiphyseal growth plate; and idiopathic, potentially making it a multifactorial disease (Bruns et al. 2018; Robertson et al. 2003; Tóth et al. 2015; Krishnan and Grodzinsky 2018). OCDs occur in both children and adults. The distinction between children and adults is based on whether the growth plates are open or closed (Uppstrom et al. 2016; Schenck and Goodnight 1996).

Next to the traumatic and ischemic hypotheses, several authors have indicated that a genetic component might play a factor as well (Gorter and van Raay 2015; Stattin et al. 2010; Gornitzky et al. 2017). Mutations of the aggrecan (ACAN) and COL9A2 gene have been associated with familial OCD (Stattin et al. 2010; Jackson et al. 2010). The ACAN genes are proteins involved in the development of the aggrecan network. Mutation of the ACAN gene causes an inadequate formation of the aggrecan network leading to a disruption of the extracellular matrix interactions within the cartilage (Stattin et al. 2010).

5 Pathophysiology

The pathophysiological mechanism behind OCDs remains unknown. There are several hypotheses proposed (van Dijk et al. 2010).

Biomechanical trauma mechanisms have gained the most attention. The trauma hypothesis assumes that an inversion trauma or fracture of the ankle causes a flake or fissure of the cartilage and microfractures of the subchondral bone. Continuous loading will eventually lead to pressurized synovial and/or cartilage fluid between the cartilage and into the subchondral bone. The continuous high fluid pressure induces osteolysis of the subchondral bone, resulting in cysts (Reilingh et al. 2013; Cox et al. 2011; Posadzy et al. 2017).

A second hypothesis is based on current animal literature in which ischemia might play an important role in the development of OCD (Ytrehus et al. 2004; Olstad et al. 2008). During the endochondral ossification process cartilage channels are formed. These channels arise from

the perichondrium into the epiphyseal cartilage. As the patient becomes of age the channels regress and cartilage is formed by the process called chondrification. Premature cessation of these channels results in disintegration of the endothelial cells and transformation of perivascular cells. As a consequence the subchondral bone progresses to avascular necrosis (Ytrehus et al. 2004; Olstad et al. 2008). If the overlying articular cartilage is intact, spontaneous healing may occur. On the other hand, detachment of the subchondral bone could result in an osteochondral fragment (Zanon et al. 2014).

6 Location of Osteochondral Defects

Several studies described the location of OCDs in the ankle (Dahmen et al. 2018). Based on a nine-piece grid, between 63 and 77% of the lesions were found on the medial talar dome (zones 1, 4, and 7); 21 and 33% originated in the lateral talar dome (zones 3, 6, and 9); and 2 and 3.7% of the OCDs were localized to the center third of the dome (zones 2, 5, and 8) (Raikin et al. 2007; Dahmen et al. 2018). In addition to OCD of the talus in 5% of the cases an OCD is observed in the tibial plafond. A kissing lesion is found on both sides. Osteochondral defects of the tibial plafond account for approximately 2.6% of all lesions of the ankle with less than 20–35% being a kissing lesion (Mologne and Ferkel 2007; Cuttica et al. 2012; Irwin et al. 2018). Zone six (20%), zone two (16%), zone five (13%), and zone eight (13%) are the most frequent tibial plafond locations(Elias et al. 2009; Irwin et al. 2018). Common lesion locations are illustrated in Fig. 1 (Elias et al. 2009; Raikin et al. 2007). Furthermore, one case report has described an OCD of the distal fibula (Riaz et al. 2012). Clinical implications of an OCD in this location remain unknown.

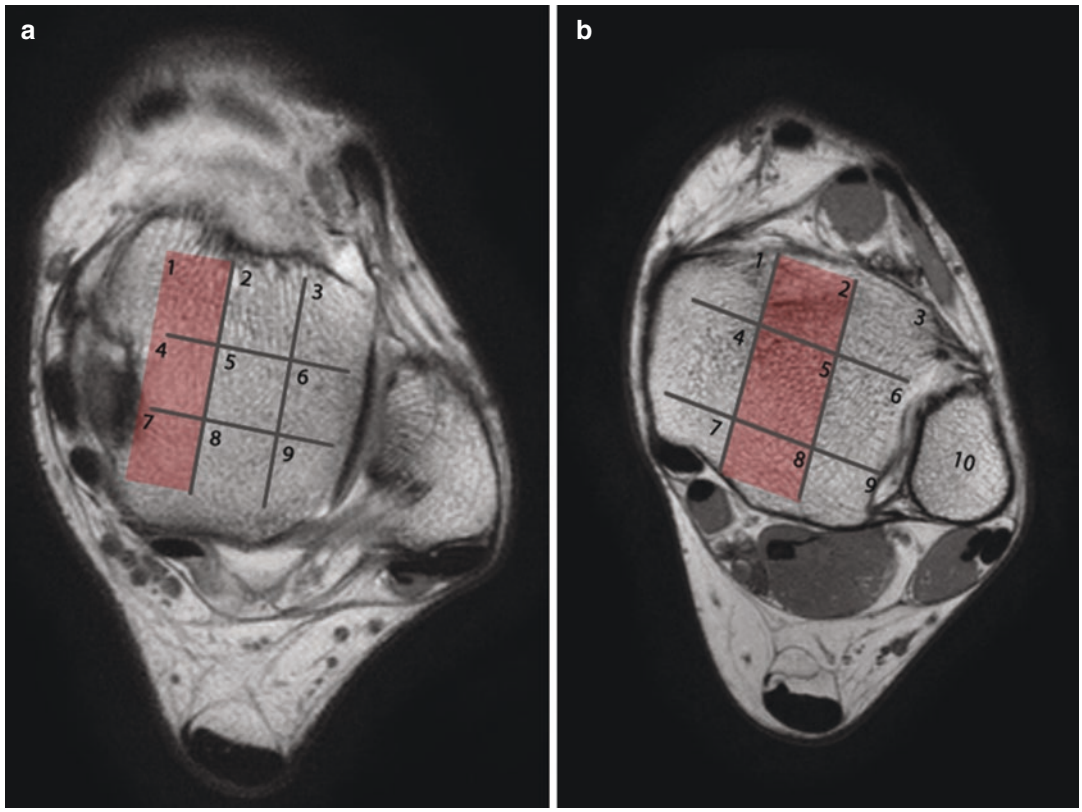

Fig. 1 (**a**) Nine-grid scheme grid of the talar cartilage. (**b**) The ten-piece grid of the tibial bone on the right

7 Diagnostic Imaging

7.1 Conventional Radiography

7.1.1 Hardware and Positioning

A conventional radiograph of the ankle should consist of an AP view, a mortise view, and a lateral view (Reilingh et al. 2010).

7.1.2 Scan Protocol and Post-processing

7.1.2.1 AP View

In AP view the patient should be sitting upright in supine position with a straight leg. The foot is in dorsal flexion with the toes facing the ceiling. In the right position this should result in an image where the tibia, distal fibula, and lateral and medial malleolus are in profile (Fig. 2).

7.1.2.2 Mortise View

The mortise view is an AP view in a 15–25° of endorotation. This view enables visualization of the lateral and medial joint spaces and is necessary because a part of the talus overlaps a part of the lateral malleolus in AP view, concealing the lateral aspect of the ankle (Fig. 2).

7.1.2.3 Lateral View

The lateral view is obtained with the patient in lateral recumbent position. The lateral part of the knee and ankle should make contact with the table with the foot still in dorsal flexion. The talar dome should be open, uniform, and without overprojection for adequate assessment (Fig. 3).

Fig. 2 (**a**) Anteroposterior view (AP view) of the ankle. Note that the midpoint of the AP view is in the center of the lateral and medial malleoli. The tibiotalar joint should be open, without revealing the mortise, and the distal fibula should be slightly overlaying the distal fibula. (**b**) Mortise view of the ankle with a 15° angle visualizing the lateral and medial joint space illustrating a hypointense lesion can be seen at the medial side of the talus

Fig. 3 Lateral view of the talar joint. Note that the talar dome is open and uniform for adequate assessment. As can be seen, the hypointense lesion that can be seen in Fig. 2b is not visible in a lateral view

7.1.3 Conventional Radiography of an OCD

Conventional radiography is the first step in the diagnostic process of ankle pain. It has a sensitivity of 59% and a specificity of 91%. It is important to remember that conventional radiography underestimates the incidence and size of osteochondral defects and fails to detect an OCD in 30–60% of the cases (Magee and Hinson 1998; van Bergen et al. 2015; Nosewicz et al. 2016). The AP and mortise view provides subtle clues such as flattening of the joint space or indistinct radiolucency of the subchondral bone. The lateral view provides no additional information with regard to OCD but could be helpful in the detection of other pathologies. In case of a more advanced OCD, additional anomalies could be seen such as fragmentation of the subchondral bone, more pronounced flattening/abnormalities of the joint space, or larger radiolucent and sclerotic areas (Resnick and Kransdorf 2005).

7.2 Computed Tomography

7.2.1 Hardware and Positioning Multi-Helical Systems

Modern computed tomography (CT) scanners are multi-slice helical systems. These systems are equipped with multiple detector arrays to simultaneously collect data at different slice locations. Patients need to be scanned in a supine position, with extended legs flat on the table, and the foot should be in dorsal flexion with the toes facing the ceiling (Johnson and Timins 1998).

7.2.2 Hardware Dual-Energy Systems

The latest edition of CT scanners is dual-energy system. There are currently three dual-energy CT imaging methods: (1) two separate sequential scans with single energy sources with different energy levels: the hardware is the same as the multi-slice helical systems; (2) dual-source imaging which uses two X-ray tubes and two detector plates: each of the tubes uses a different energy level to obtain an image simultaneously; and (3) rapid kilovoltage (kV) switching which uses a single tube with rapidly changing energy levels (Mallinson et al. 2016).

7.2.3 Scan Protocol and Post-processing Software Multi-Helical Systems

For adequate assessment of an OCD, a suitable scan protocol is recommended. X-ray beam settings for an ankle CT are 120 kV with 80 mAs with an exposure time of approximately 1 s. The field of view (FOV) should cover both ankles. A slice thickness of 0.3 is recommended with a maximum of 1 mm.

Post-processing reconstruction software makes it possible to create both 2D and 3D reconstructions with matching filters such as soft-tissue setting and bone setting in axial plane.

7.2.4 Scan Protocol and Post-processing Software Dual-Energy Systems

The X-beam settings for a dual-energy CT are 150 Kv and 80 Kv with 85 mAs and 125 mAs, respectively. The exposure time should be the

same (1 s) as for a multi-helical system with the same FOV and slice thickness. Dual-energy CT scanning can make a substantial difference concerning the post-processing capabilities (Mallinson et al. 2016). Material-specific and energy-specific post-processing techniques are the most valuable for OCD pathology. Material-specific post-processing compares the attenuation values between low- and high-kV datasets allowing specific materials to be color coded. Especially virtual non-calcium images could be useful for the assessment of bone marrow edema (Kaup et al. 2016). Energy-specific post-processing enables reconstruction algorithms to generate virtual monochromatic images forming the basis for metal artifact reduction (Wellenberg et al. 2018).

7.2.5 CT Imaging of an OCD

CT imaging has a sensitivity of 81% and a specificity of 99% in detecting OCDs. OCDs can have numerous dimensions. Assessment concerning the size should be performed in all three dimensions, namely anteroposterior, mediolateral, as well as depth. The smallest OCD size which can be imagined is 0.3–1.0 mm, depending on the scan resolution. An OCD can contain cortical irregularities, osteophytes, and/or cystic changes of the subchondral bone (Fig. 4). These changes are depicted on a CT scan as irregular borders, with white cortical lines or dentate appearances of the talus or tibia. The cortical irregularities are suggestive of adjacent cartilaginous lesions. Lucent and dark gray areas of the irregular cortex are indicative of a cyst. In more advanced and larger OCDs the cartilage will disappear and the cortex will become more profound on CT. Larger defects are sometimes accompanied by loose bodies of the joint. In case of large defects, the joint should be scrutinized for loose body at a remote location from the defect (Korteweg et al. 2014).

New imaging techniques such as cone beam CT are currently being researched. Several studies have shown that cone beam has added value in terms of fissures, fractures, and osteomyelitis in the upper and lower extremities compared to conventional radiography (De Smet et al. 2015). Cone beam CT might also offer added value in the field of staging for OCD pathology (Posadzy

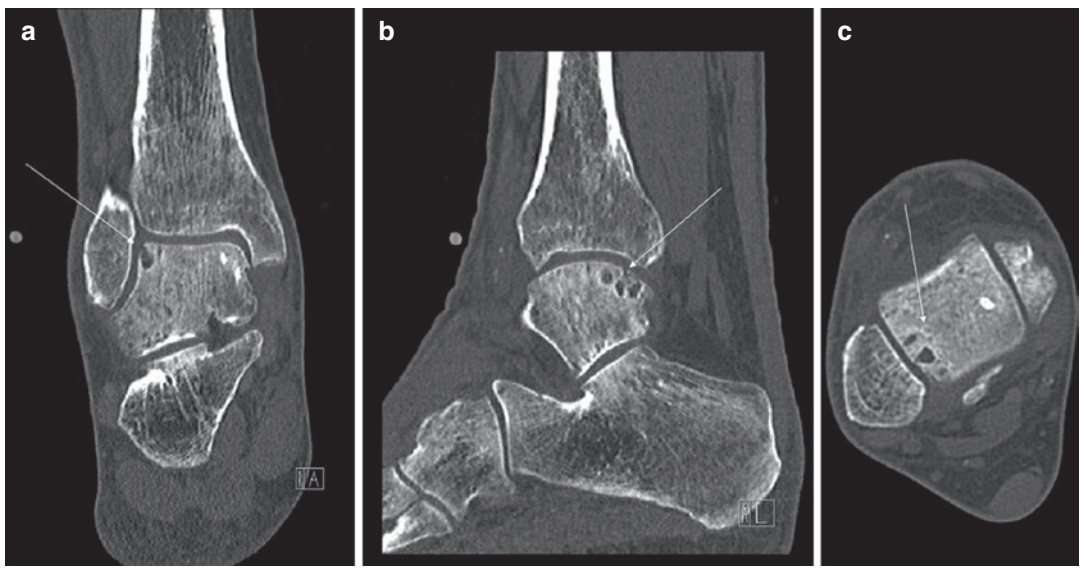

Fig. 4 Appearance of an OCD on CT. (**a**) Coronal, (**b**) sagittal, (**c**) axial. A huge defect at the posteromedial part of the talus is seen (white arrows), while standard radiography was negative. A large osteochondral lesion is seen with multiple cysts in the subchondral bone (arrows) (**a**, **b**). The axial images show that the lesion is located at the lateral talar dome (arrow) (**c**)

et al. 2017). In particular, weight-bearing cone beam CT may be a better illustration of the actual stage of the disease. However, further comparative research is needed.

7.3 Single-Photon Emission Computed Tomography

7.3.1 Hardware and Positioning

Single-photon emission computed tomography (SPECT-CT) is a combination of a 3-dimensional scintigraphy bone scan and a CT scan. SPECT has a sensitivity of 94% and a specificity of 57% (Claassen et al. 2014). SPECT-CT is a combination of CT and gamma radiation distribution radioactive isotopes. The CT provides anatomical information regarding the injury and the radioactive isotope provides information in terms of biological activity. The patient should be positioned the same as on a CT scanner.

7.3.2 Scan Protocol and Post-processing Software

A triple-phase bone scan is accomplished with a dose of 500 MBq Technetium-99 (99Tc), an isotope derived from Rubidium-99 (99Ru). The radioactive tracer should be administered directly and followed by a blood pool-phase scan and a diffusion-phase scan. Afterwards, an intermission of two and a half–three hours should be accounted for before preforming a late-phase scan. A high-resolution image protocol should be acquired in order to compete with MRI. Therefore, an adequate scan protocol for SPECT-CT has the same X-ray beam settings as a regular CT of 120 kv and 80 mA.

To analyze the images a post-processing software program with fusion capabilities enables assessment by a nuclear medicine specialist.

7.3.3 SPECT-CT of an OCD

SPECT-CT provides additional information with regard to biological activity of an osteochondral defect. It enhances regions of increased bone turnover due to a more profound vascularity and osteoblastic activity. In addition to the CT scan SPECT provides additional information on the activity of the subchondral bone (Leumann et al. 2011). The CT scan can be assessed as described in the previous section. The advantage of SPECT in comparison to MRI can be found in a more accurate lesion size estimation. However, SPECT has a lower specificity and high radiation burden and is therefore only of additional value in complex cases with coexisting pathology where MRI or CT does not provide enough information on the status of the subchondral bone (van Bergen et al. 2015; Leumann et al. 2011).

7.4 Magnetic Resonance Imaging

7.4.1 Hardware and Positioning

Magnetic resonance imaging (MRI) of the ankle is considered challenging. For adequate assessment of an OCD high-field scanners at 1.5 or 3.0 T are required. 3.0 T systems are preferred considering their superior image contrast and cartilage visualization (Barr et al. 2007; Bauer et al. 1987). Second, adequate multichannel surface coils are recommended with parallel imaging and/or compressed sensing capability. In the literature knee coils have been used as well; however positioning of the ankle can be challenging and reproducibility is questionable (Muhle et al. 1999). The patient should be positioned in supine position with extended legs on the table and the foot should be in dorsal flexion with the toes facing the ceiling in case of a regular foot and ankle coil.

7.4.2 Scan Protocol and Post-processing Software

In addition to the hardware, adequate imaging sequences are mandatory to detect OCDs of the ankle. Most imaging protocols consist of multiple spin-echo sequences, including fluid-sensitive intermediate-weighted fast spin-echo sequences as well as nonfat-saturated T1-weighted and proton density-weighted sequences. Fat-saturated intermediate-weighted fast spin-echo sequences are used for tendon, ligament, cartilage, and bone marrow assessment (Link et al. 2014). This sequence reduces chemical shift artifacts between the subchondral bone and the cartilage for better assessment of the OCD and the bone marrow

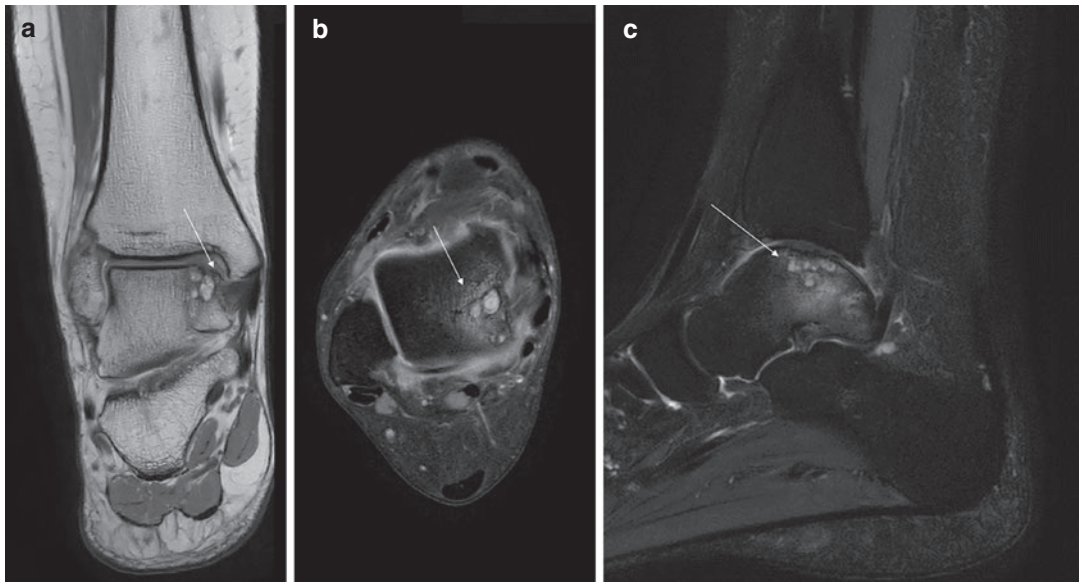

Fig. 5 OCD appearance on various MR sequences. (**a**) Pd-TSE-Dixon, coronal in phase image, (**b**) Pd-TSE-Dixon, axial, water-only image, (**c**) T2W-TSE-Dixon, sagittal, water-only image. On the Pd-Dixon in phase images the cystic changes within the lesion are hyperintense, whereas the sclerosis is hypointense (arrow).On the Pd- and T2w-Dixon water-only images the edema surrounding the cystic lesions is seen (arrow). The true extent of the lesion is not clearly delineated

edema surrounding the defect. It remains hard to accurately assess subtle articular cartilage defects of the ankle due to the lack of spatial resolution, and partial volume effects of 2D sequences. Studies with 3D fast spin-echo sequences may be superior in the visualization of these subtle cartilage defects and subchondral bone changes (Chen et al. 2010). To better depict the subchondral bone, bone marrow abnormalities, and tendons a short-tau inversion recovery (STIR) sequence might be considered, as this sequence reduces the amount of magic angle effects (Srikhum et al. 2013).

7.4.3 MR Imaging of an OCD

MRI is considered the best available option for the detection of OCDs. It has a sensitivity of 96% and a high specificity of 96% in detecting OCDs of the ankle (van Bergen et al. 2015; Verhagen et al. 2005). Adequate assessment includes lesion location, size in three planes, subchondral bone marrow edema, subchondral sclerosis and/or cyst formation, general state of talar and tibial cartilage, and amount of delineation of the articular bone plate (Fig. 5). However, due to the presence of bone marrow edema the lesion size is known to be overestimated. The usefulness of MRI in determining the lesion size for preoperative planning is therefore controversial. Nevertheless, the degree of bone marrow edema (BME) has been associated with a worse clinical outcome, following a microfracture procedure, than patients that did not have BME (Shimozono et al. 2018). The added value of MRI for postoperative evaluation is less controversial and is gaining popularity, especially in the assessment of OCD repair tissue. For postoperative evaluation quantitative imaging sequences such as T1rho, T2 mapping, and delayed gadolinium-enhanced MR imaging of cartilage (dGEMRIC) are being used to evaluate the success of the procedure.

7.5 Imaging ACR Appropriateness Criteria

An Expert Panel of Musculoskeletal Imaging published the ACR Appropriateness Criteria for

Table 1 Table of the ACR appropriateness criteria for chronic ankle pain specified to osteochondral lesions

ACR Appropriateness Criteria osteochondral defects		
Procedure	Appropriateness category	Relative radiation level
MRI ankle without IV contrast	Usually appropriate	O
CT arthrography ankle	May be appropriate	⊛
MR arthrography ankle	May be appropriate	O
Bone scan with SPECT or SPECT/CT ankle	May be appropriate (disagreement)	⊛⊛⊛
CT ankle without IV contrast	May be appropriate	⊛
MRI ankle without and with IV contrast	Usually not appropriate	O
CT ankle with IV contrast	Usually not appropriate	⊛
CT ankle without and with IV contrast	Usually not appropriate	⊛
X-ray ankle stress views	Usually not appropriate	⊛
Ultrasound ankle	Usually not appropriate	O
X-ray arthrography ankle	Usually not appropriate	⊛
Image-guided anesthetic injection ankle	Usually not appropriate	Varies

chronic ankle pain to select the appropriate imaging technique (Chang et al. 2018). It is recommended to follow these guidelines concerning ankle OCD pathology (Table 1).

8 Imaging Assessment

8.1 Alignment

Alignment of the ankle should be described as it influences joint biomechanics, and may play a role in decision-making. An orthopedic surgeon may choose to perform a concomitant osteotomy of the calcaneus or the distal tibia (supramalleolar) in order to correct a varus or valgus malalignment. It is therefore advised that radiologist assess hindfoot alignment through a bilateral long axial view or a "conventional" hindfoot alignment view (Reilingh et al. 2010).

8.2 Morphology

Concerning the morphology of the defect, a systematic approach is recommended. It should be emphasized that a good description of the subchondral bone plate, size of the fragments, and overall size is most essential for the choice of treatment (Fig. 6). The following characteristics that should be assessed are summarized in Table 2.

8.3 Location

The location of the defect is important, as this influences whether the treatment of choice can be performed arthroscopically or should be done in an open manner. One could consider using a CT or MRI in (full) plantar flexion in order to assess accessibility of an anterior ankle arthroscopy (van Bergen et al. 2012). Reporting of the location guided by the nine-grid scheme as presented by Raikin and Elias et al. can standardize the location reporting as illustrated in Fig. 1 (Elias et al. 2009; Raikin et al. 2007).

8.4 Size

Assessment concerning lesion size should be performed in all three dimensions, namely anteroposterior, mediolateral, as well as depth (Fig. 7). In case of multiple assessments in time, any change in morphology as well as sizes (in all dimensions) should be described. Previous research has shown that bone marrow stimulation may be best suitable for defects with sizes less than 107.4 mm^2 in area and/or 10.2 mm in diam-

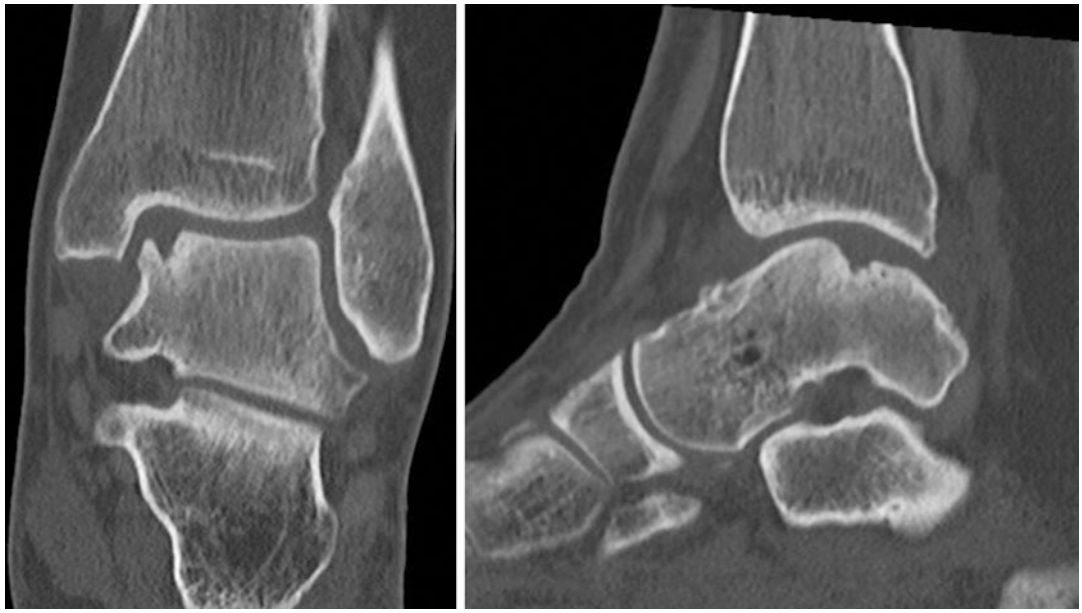

Fig. 6 Description of the subchondral bone plate: presence of a bare area, sometimes referred to as a crater

Table 2 A description the radiological report must comply with for a targeted osteochondral defect treatment plan

Radiologic description of an osteochondral defect

- Number of osteochondral defects
- Fragmentation of cartilage*
- Sclerosis around the lesion
- Subchondral bone plate quality
- Description of cysts**

* Fragmentation
- Size of fragment
- Attachment: loose or stable

** Cysts
- Number of cysts
- Size of cysts (three dimensions
- Open or enclosed cyst

eter (Ramponi et al. 2017). In case fixation of a defect is considered, a clear description of the defect is recommended. Fixation procedures are considered to be technically "more" amenable (Lambers et al. 2020).

8.5 Bone Marrow Edema (BME)

Subchondral bone marrow edema and its extent should be assessed on fat-suppressed T2-weighted (coronal or sagittal) sequences of the MRI. The extent of the BME can be determined by relating the volume of the BME to the total volume of the talar bone, in order to make an estimate of the involved area of interest. This can be done in the following manner: 0 accounts for absence of BME, 1 accounts for involved BME area less than 25% of talar volume, 2 accounts for an area between 25 and 50% of the talar volume, and 3 should be referred to when more than 50% of the talar volume contains BME (Shimozono et al. 2018).

It should be mentioned that subchondral bone marrow edema should be interpreted in conjunction with the clinical complaints of the patient. The presence of BME should always be related to time-nature of an injury, i.e., whether the injury is acute or chronic (mostly referred to as <6 weeks or >6 weeks, respectively), as the timing of the

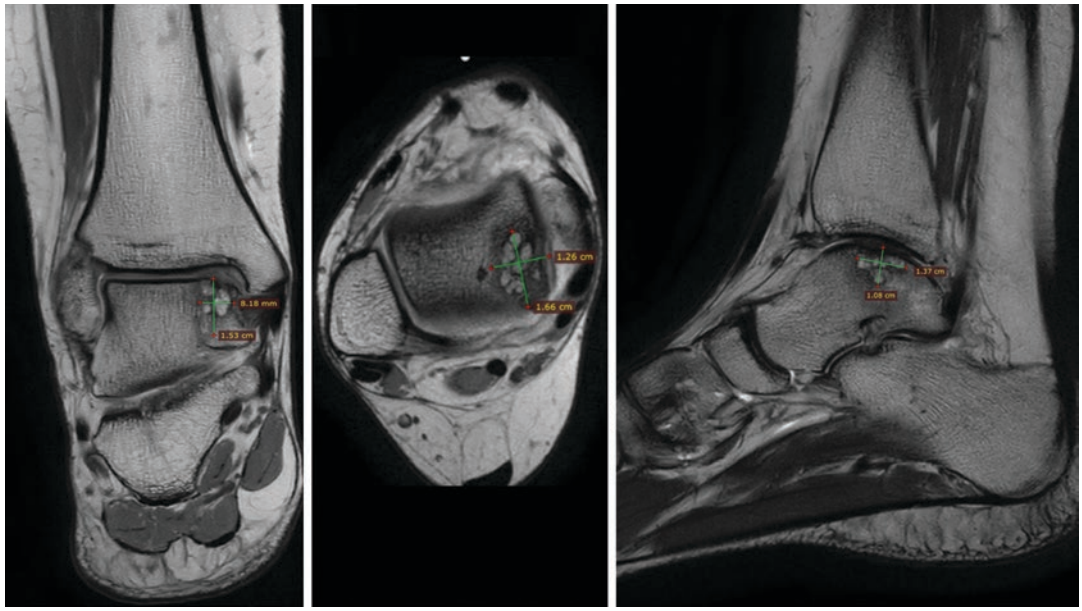

Fig. 7 OCD measurements should be described in all three planes. Adequate measurements should be assessed perpendicular to the other direction as illustrated. Note subchondral cyst formation and surrounding sclerosis

Table 3 Berndt and Harty classification based on CT and MRI imaging

Berndt and Harty classification for osteochondral defects
Stage 1: Small area of compression of the subchondral bone.
Stage 2: Subchondral bone becomes partially avulsed
Stage 3: Complete avulsion of the subchondral bone without displacement
Stage 4: Subchondral bone is completely avulsed and displaced

injury correlates largely with BME presence. However, it can certainly occur in later stages of the injury corresponding to damage of the subchondral bone, subchondral collapse, (ongoing) cyst formation, cartilage loss, and, in later stages, osteoarthritis (Rios et al. 2011; Weishaupt and Schweitzer 2002).

8.6 Staging

Staging of an OCD in the ankle is important and can contribute to the choice of treatment.

The purpose of a classification system should be to include the currently available diagnostic tools, address the etiology of the OCD, and direct treatment. However, it should be noted that the majority of the classification systems currently being used are of importance in creating (sub) groups for scientific research rather than having a decisive role in treatment choice. The first classification system that was introduced for osteochondral defects of the ankle was the one by Berndt and Harty (1959). The staging system is based on the radiological appearance of an OCD and assesses an OCD as a fracture, where the fracture model focuses on bone rather than cartilage. Although the classification system is frequently used in practice, it does not direct treatment and is not based on current imaging (CT, MRI). The four stages as mentioned by Berndt and Harty are listed in Table 3.

In 1993, Loomer et al. adjusted the classification system by Berndt and Harty through the addition of a fifth stage indicating a cystic component of the lesion (Loomer et al. 1993).

Table 4 Osteochondral defect classification system by Mintz et al. based on MRI imaging

Magnetic resonance imaging osteochondral defect classification system
Stage 0: normal cartilage;
Stage 1: intact cartilage but abnormal MRI signal;
Stage 2: fibrous cartilaginous fissures or lesions but bone intact;
Stage 3: cartilaginous flap or subchondral bone exposed;
Stage 4: free but nondisplaced cartilaginous fragment;
Stage 5: free displaced fragment.

Table 5 Osteochondral defect classification system by Ferkel et al. based on CT imaging

Computed tomography osteochondral defect classification system
Stage 1: Cystic lesion within dome of talus, intact roof on all views
Stage 2A: Cystic lesion with communication to talardome surface
Stage 2B: Open articular surface lesion with overlying nondisplaced fragment
Stage 3: Non-displaced lesion with lucent area
Stage 4: Displaced fragment

Due to the fact that the aforementioned classification does not incorporate any currently applied radiological assessment (through MRI or CT), different MRI classification systems were introduced in the late 1990s, by Dipaola et al. (1991), Taranow et al. (1999), and Hepple et al. (1999).

In 2003, Mintz et al. proposed a novel classification system based on MRI with arthroscopic correlation with the aim to introduce a classification system applicable to both MRI and ankle arthroscopy. The classification system is similar to the one by Hepple et al. with both having involvement of the osseous part of the osteochondral defect from stage 3 onwards (Mintz et al. 2003).

The majority of the classification systems are based on MRI (Table 4); solely one classification system has been proposed based on CT (Table 5) (Ferkel et al. 2008).

9 Pitfalls in Imaging

The presence of kissing lesions, both in the talus and tibia, is a well-known entity. The literature states that kissing lesions are found in about 5% of the cases (Verhagen et al. 2005; Labovitz and Schweitzer 1998). Kissing lesions may be missed due to a phenomenon known as "satisfaction of search" (Samuel et al. 1995) (Verhagen et al. 2005). Kissing lesions should not be confused with osteoarthritis, especially when other signs such as sclerosis, joint space narrowing, and osteophytes are lacking (Fig. 8).

With MR imaging bone marrow edema might be present and obscure the accuracy of size measurements (Yasui et al. 2019). One should be aware of this inaccuracy and consider making a CT preoperatively if there is any doubt about the treatment decision based on the OCD size.

10 Osseous Injury

In any sports an unexpected movement may cause acute osseous injury. The trauma mechanism will easily explain the fracture extension. The more frequent encountered fractures in the ankle are beyond the scope of this chapter. However a specific sports-related fracture is discussed below.

10.1 Snowboarder's Fracture

A well-documented sports-related fracture is the fracture of the lateral process of the talus. In a prospective study of foot and ankle injuries in snowboarders a very high incidence of these fractures was found (Kirkpatrick 1998). It should be noted that many of these fractures are not visible on

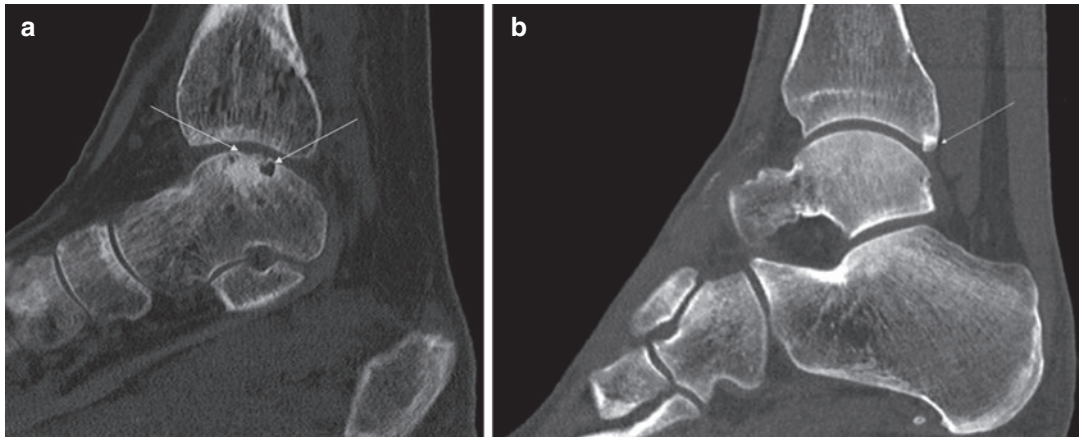

Fig. 8 Osteochondral defect with multiple cysts, irregular cortical subchondral bone plate, and osteophyte on the posterior side of the talar joint (arrow, right image)

standard radiography. When MRI is performed, usually in a later stage, when the patient is complaining of chronic lateral ankle pain, bone marrow edema is seen. However it may still be hard to diagnose the fracture. MDCT will aid in diagnosing this lesion and can help the surgeon to tailor therapy.

11 The Foot

11.1 Osteochondral Injuries

Osteochondral defects of the foot can occur in the toes, especially in the first toe. It has been described in adolescent population, beach soccer players, soccer players, and elite ballet dancers and is characterized by pain, swelling, and tenderness at the interphalangeal joint (Kinoshita et al. 1998; Altman et al. 2008). Radiographic appearance is similar to an OCD of the ankle. Therapy often consists of microfracturing.

11.2 Skimboarder's Toe

An injury of the dorsal aspect of the first metatarsophalangeal joint is described as a skimboarder's toe (Donnelly et al. 2005). In this beachside sport a hyperdorsal flexion of the MTP joint causes injury to the extensor muscle, and the extensor expansion. On MRI a soft-tissue swelling with edema is seen. The dorsal aspect of the extensor expansion is disrupted, while the plantar plate is intact. Bone marrow edema or joint effusion can accompany the lesion.

12 Overuse Injury of the Foot

12.1 Navicular Stress Fracture

Stress fractures of the navicular bone are familiar lesions in athletes (Pećina 2004). They most often occur in explosive athletic activities, involving jumping, sprinting, and hurdling. Chronic stress usually produces sagittal fractures of the navicular bone. Patients typically present with complaints of poorly localized, midfoot tenderness or ill-defined soreness/cramping sensation in the foot that is aggravated by weight bearing and initiation of activity (Shakked et al. 2017). On physical examination a localized painful point may be found on the proximal dorsal border. The navicular stress fracture will generally not be detected by plain radiology. As a rule of thumb, conventional radiography is not sensitive enough to detect these stress fractures (Gross and Nunley 2015). When there is a high clinical suspicion, further modalities can be used. Bone marrow edema is the key finding in diagnosing stress fractures with MRI. A linear hypointense configuration on T1-weighted MR sequences should

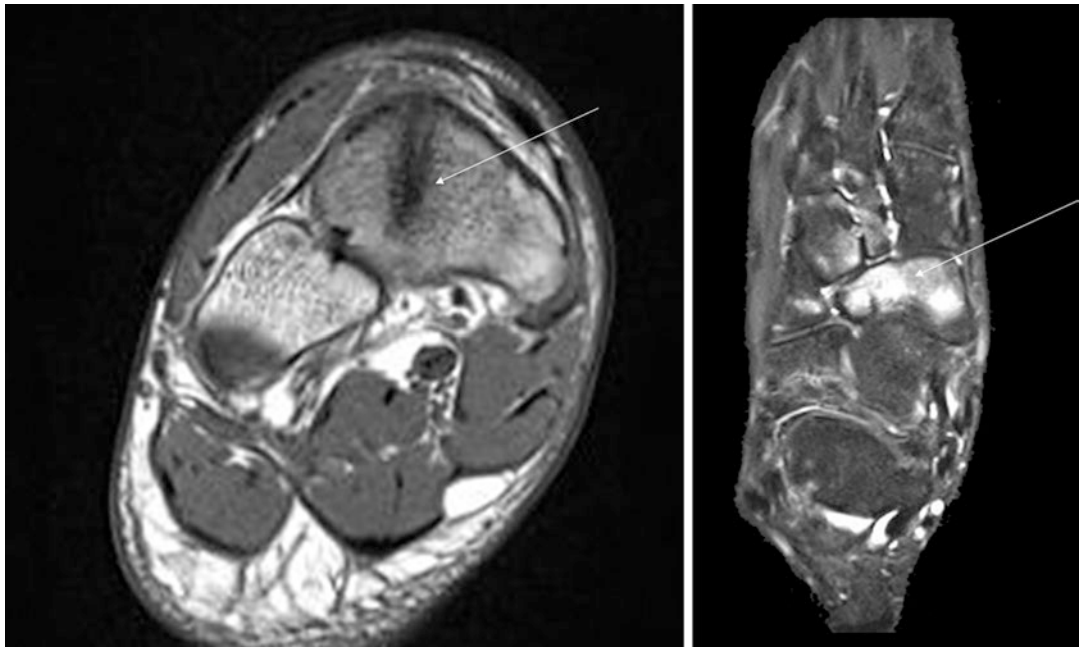

Fig. 9 Stress fracture of the navicular bone. The fracture line (arrow) can be seen on a coronal Pd-TSE-Dixon, fat-only image. Diffuse edema surrounding the fracture line is seen (arrow) on the axial Pd-TSE-Dixon, water-only image. To visualize the extent of the fracture an additional CT scan is recommended as illustrated in Fig. 10

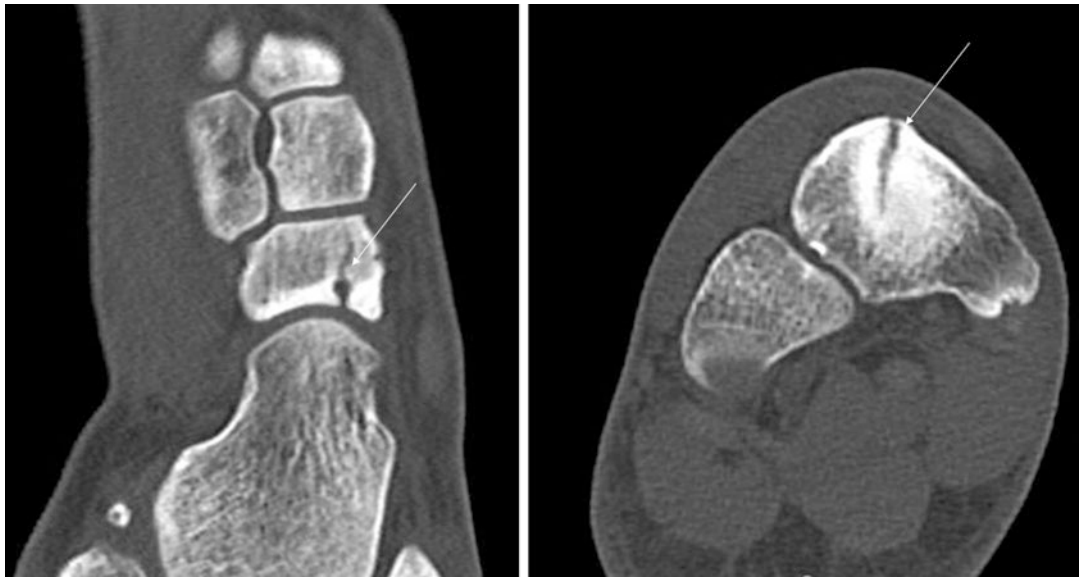

Fig. 10 Stress fracture of the navicular bone. CT scan shows the precise extent of stress fracture of the navicular bone

be present when diagnosing a true fracture (Fig. 9). The use of high-resolution CT with 0.6 mm axial source images and MPR in any given plane aids in making a final diagnosis and is useful for preoperative planning purposes and follow-up (Fig. 10). Dorsal cortical proliferation can be expected as early as 6 weeks following the injury using CT (Hossain et al. 2015).

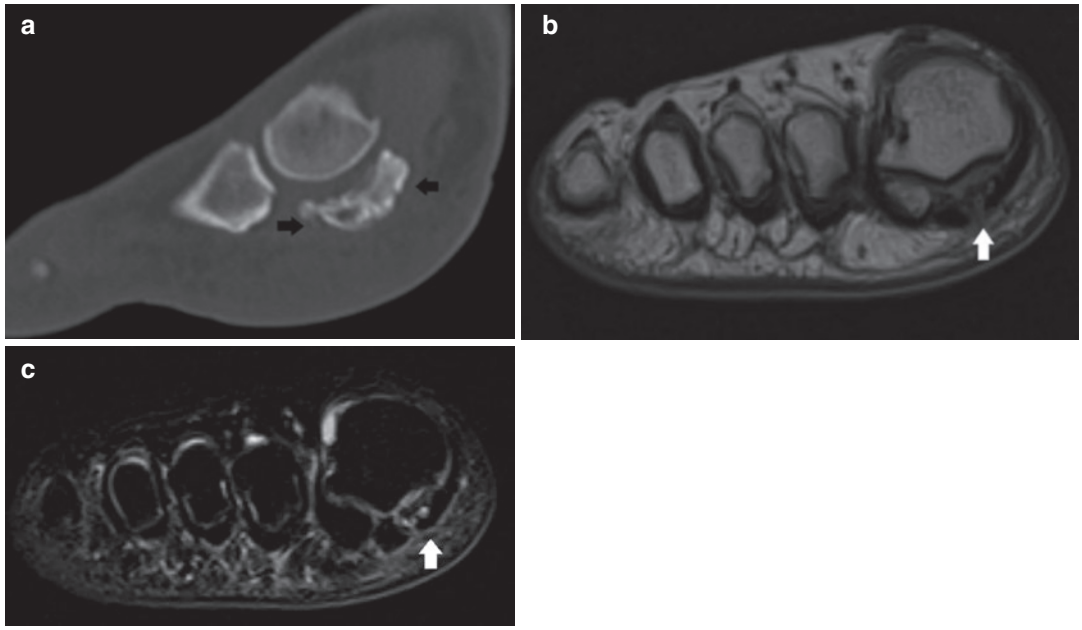

Fig. 11 Sesamoid stress fracture. (**a**) Sagittal reformatted CT images show sclerosis, collapse, and fragmentation of the medial sesamoid bone (black arrows) of the right foot. (**b**) Short-axis T1- and (**c**) FS T2-WI shows fragmentation, collapse, and abnormal signal of the medial sesamoid (white arrow) compared to the normal lateral sesamoid (case courtesy F.M. Vanhoenacker)

12.2 Sesamoid Overuse Injury

Stress-related injury to the sesamoid bones, also known as sesamoiditis, is a common problem in athletes, who require maximum dorsiflexion of the great toe. Athletes at risk are joggers, sprinters, figure skaters, ballet dancers, basketball players, football players, and tennis players. It is a painful condition increased with weight bearing under the first metatarsal head, usually in the region of the medial rather than the lateral sesamoid.

Sesamoiditis may have a variable appearance on imaging (Fig. 11). Sesamoiditis can be represented as a stress fracture of the sesamoid bone. However this has to be differentiated from bipartite sesamoids, which can occur in up to 75% of patients (Biedert and Hintermann 2003; Robertson et al. 2017). Other findings include bone marrow edema without a fracture line, reactive soft-tissue edema, and tendinosis of the flexor hallucis tendon. Synovitis and bursitis are frequently associated. Some authors state that when edema is seen on TSTIR or fat-suppressed T2-weighted MR images with absence of abnormalities on T1-weighted MR images, this is favorable for sesamoiditis (Schein et al. 2015).

Things to Remember

1. Think about an osteochondral defect of the ankle in a patient with chronic ankle pain.
2. Standard radiography may detect but cannot exclude osteochondral defects.
3. The most important features of the osteochondral defect of the talus are the exact location, size, and extent. This is the surgical question that imaging needs to address.
4. Both MRI and CT imaging with MPR may document an osteochondral defect.

Imaging Boxes

Standard Radiography

Used for initial survey and to define additional pathology.
AP view most helpful, lateral not in detecting OCD.
When negative, OCD is not ruled out.
Additional AP view with 4 cm heel rise may be beneficial.

MRI

Golden standard in detecting OCD.
Bone marrow edema detection is important, yet hampering adequate true lesion demarcation.
All three imaging planes must be used to rule out or to detect concomitant lesions.
Quantitative sequences can be used to monitor treatment effectiveness.

Computed Tomography

Axial high-resolution (0.5/0.6 mm) acquisition with coronal and sagittal MPR.
Is as powerful as MRI in the diagnostic workup of a patient with chronic ankle pain. Enables exact delineation of the OCD.
Provides surgeon with adequate information on location and especially the extent of the OCD.

References

Aichroth P (1971) Osteochondritis dissecans of the knee. A clinical survey. J Bone Joint Surg Br 53:440–447

Altman A, Nery C, Sanhudo A, Pinzur MS (2008) Osteochondral injury of the hallux in beach soccer players. Foot Ankle Int 29:919–921

Barr C, Bauer JS, Malfair D, Ma B, Henning TD, Steinbach L, Link TM (2007) MR Imaging of the ankle at 3 tesla and 1.5 tesla: protocol optimization and application to cartilage, ligament and tendon pathology in cadaver specimens. Eur Radiol 17:1518–1528

Bauer M, Jonsson K, Linden B (1987) Osteochondritis dissecans of the ankle. A 20-year follow-up study. J Bone Joint Surg Br 69:93–96

Berndt AL, Harty M (1959) Transchondral fractures (osteochondritis dissecans) of the talus. J Bone Joint Surg Am 41-A:988–1020

Biedert R, Hintermann B (2003) Stress fractures of the medial great toe sesamoids in athletes. Foot Ankle Int 24:137–141

Blom RP, Mol D, Van Ruijven LJ, Kerkhoffs G, Smit TH (2019) A single axial impact load causes articular damage that is not visible with micro-computed tomography: an ex vivo study on caprine tibiotalar joints. Cartilage:1947603519876353

Bruns J, Werner M, Habermann C (2018) Osteochondritis dissecans: etiology, pathology, and imaging with a special focus on the knee joint. Cartilage 9:346–362

Chang EY, Tadros AS, Amini B, Bell AM, Bernard SA, Fox MG, Gorbachova T, Ha AS, Lee KS, Metter DF, Mooar PA, Shah NA, Singer AD, Smith SE, Taljanovic MS, Thiele R, Kransdorf MJ (2018) ACR appropriateness criteria((R)) chronic ankle pain. J Am Coll Radiol 15:S26–S38

Chen CA, Kijowski R, Shapiro LM, Tuite MJ, Davis KW, Klaers JL, Block WF, Reeder SB, Gold GE (2010) Cartilage morphology at 3.0t: assessment of three-dimensional magnetic resonance imaging techniques. J Magn Reson Imaging 32:173–183

Claassen L, Uden T, Ettinger M, Daniilidis K, Stukenborg-Colsman C, Plaass C (2014) Influence on therapeutic decision making of SPECT-CT for different regions of the foot and ankle. Biomed Res Int 2014:927576–927576

Cox LGE, Lagemaat MW, Van Donkelaar CC, Van Rietbergen B, Reilingh ML, Blankevoort L, Van Dijk CN, Ito K (2011) The role of pressurized fluid in subchondral bone cyst growth. Bone 49:762–768

Cuttica DJ, Smith WB, Hyer CF, Philbin TM, Berlet GC (2012) Arthroscopic treatment of osteochondral lesions of the tibial plafond. Foot Ankle Int 33:662–668

Dahmen J, Lambers KTA, Reilingh ML, Van Bergen CJA, Stufkens SAS, Kerkhoffs GMMJ (2018) No superior treatment for primary osteochondral defects of the talus. Knee Surg Sports Traumatol Arthrosc 26:2142–2157

De Smet E, De Praeter G, Verstraete KL, Wouters K, De Beuckeleer L, Vanhoenacker FM (2015) Direct comparison of conventional radiography and cone-beam CT in small bone and joint trauma. Skelet Radiol 44:1111–1117

Delco ML, Kennedy JG, Bonassar LJ, Fortier LA (2017) Post-traumatic osteoarthritis of the ankle: a distinct clinical entity requiring new research approaches. J Orthop Res 35:440–453

Dipaola JD, Nelson DW, Colville MR (1991) Characterizing osteochondral lesions by magnetic resonance imaging. Arthroscopy 7:101–104

Doherty C, Delahunt E, Caulfield B, Hertel J, Ryan J, Bleakley C (2014) The incidence and prevalence of ankle sprain injury: a systematic review and meta-analysis of prospective epidemiological studies. Sports Med 44:123–140

Donnelly LF, Betts JB, Fricke BL (2005) Skimboarder's toe: findings on high-field MRI. Am J Roentgenol 184:1481–1485

Elias I, Raikin SM, Schweitzer ME, Besser MP, Morrison WB, Zoga AC (2009) Osteochondral lesions of the distal tibial plafond: localization and morphologic characteristics with an anatomical grid. Foot Ankle Int 30:524–529

Ferkel RD, Zanotti RM, Komenda GA, Sgaglione NA, Cheng MS, Applegate GR, Dopirak RM (2008) Arthroscopic treatment of chronic osteochondral lesions of the talus: long-term results. Am J Sports Med 36:1750–1762

Gornitzky AL, Mistovich RJ, Atuahuene B, Storey EP, Ganley TJ (2017) Osteochondritis dissecans lesions in family members: does a positive family history impact phenotypic potency? Clin Orthop Relat Res 475:1573–1580

Gorter J, Van Raay JJ (2015) A suspected genetic form of bilateral osteochondritis dissecans of the knee in a Dutch family. Knee 22:677–682

Gross CE, Nunley JA 2nd (2015) Navicular stress fractures. Foot Ankle Int 36:1117–1122

Hepple S, Winson IG, Glew D (1999) Osteochondral lesions of the talus: a revised classification. Foot Ankle Int 20:789–793

Hintermann B, Regazzoni P, Lampert C, Stutz G, Gachter A (2000) Arthroscopic findings in acute fractures of the ankle. J Bone Joint Surg Br 82:345–351

Hossain M, Clutton J, Ridgewell M, Lyons K, Perera A (2015) Stress fractures of the foot. Clin Sports Med 34:769–790

Hunter W (1743) Vi. Of the structure and diseases of articulating cartilages. Phil Trans 9:267

Irwin RM, Shimozono Y, Yasui Y, Megill R, Deyer TW, Kennedy JG (2018) Incidence of coexisting talar and tibial osteochondral lesions correlates with patient age and lesion location. Orthop J Sports Med 6:2325967118790965

Jackson GC, Marcus-Soekarman D, Stolte-Dijkstra I, Verrips A, Taylor JA, Briggs MD (2010) Type IX collagen gene mutations can result in multiple epiphyseal dysplasia that is associated with osteochondritis dissecans and a mild myopathy. Am J Med Genet A 152:863–869

Johnson JE, Timins ME (1998) Optimal computed tomography imaging of the midfoot: an improved technique. Foot Ankle Int 19:825–829

Kappis M (1922) Weitere Beiträge zur traumatisch-mechanischen Entstehung der "spontanen" Knorpelablösungen (sogen. Osteochondritis dissecans). Deutsche Zeitschrift für Chirurgie 171:13–29

Kaup M, Wichmann JL, Scholtz J-E, Beeres M, Kromen W, Albrecht MH, Lehnert T, Boettcher M, Vogl TJ, Bauer RW (2016) Dual-energy CT-based display of bone marrow edema in osteoporotic vertebral compression fractures: impact on diagnostic accuracy of radiologists with varying levels of experience in correlation to Mr Imaging. Radiology 280: 510–519

Kinoshita M, Okuda R, Morikawa J, Yasuda T, Jotoku T, Abe M (1998) Osteochondral lesions of the proximal phalanx of the great toe: a report of two cases. Foot Ankle Int 19:252–254

Kirkpatrick DP, Hunter RE, Janes PC et al (1998) The snowboarder's foot and ankle. Am J Sports Med 26:271–277

König F (1888) Über freie Körper in den Gelenken. Dtsch Z Chir 27:90–109

Korteweg M, Wiewiorski M, Streekstra G, Strobel K, Valderrabano V, Maas M (2014) Diagnosis of osteochondral defects of the talus by computerized tomography (CT) and single-photon emission computed tomography (SPECT-CT)

Krishnan Y, Grodzinsky AJ (2018) Cartilage diseases. Matrix Biol 71-72:51–69

Labovitz JM, Schweitzer ME (1998) Occult osseous injuries after ankle sprains: incidence, location, pattern, and age. Foot Ankle Int 19:661–667

Lambers KTA, Saarig A, Turner H, Stufkens SAS, Doornberg JN, Kerkhoffs G, Jaarsma R (2019) Prevalence of osteochondral lesions in rotational type ankle fractures with syndesmotic injury. Foot Ankle Int 40:159–166

Lambers KTA, Dahmen J, Reilingh ML, Van Bergen CJA, Stufkens SAS, Kerkhoffs GMMJ (2020) Arthroscopic lift, drill, fill and fix (LDFF) is an effective treatment option for primary talar osteochondral defects. Knee Surg Sports Traumatol Arthrosc 28:141–147

Leumann A, Valderrabano V, Plaass C, Rasch H, Studler U, Hintermann B, Pagenstert G (2011) A novel imaging method for osteochondral lesions of the talus-comparison of SPECT-CT with MRI. Am J Sports Med 39:1095–1101

Link TM, Vavken P, Valderrabano V (2014) Diagnosis of osteochondral lesions by MRI. In: Van Dijk CN, Kennedy JG (eds) Talar osteochondral defects: diagnosis, planning, treatment, and rehabilitation. Springer, Berlin, Heidelberg

Loomer R, Fisher C, Lloyd-Smith R, Sisler J, Cooney T (1993) Osteochondral lesions of the talus. Am J Sports Med 21:13–19

Magee TH, Hinson GW (1998) Usefulness of MR imaging in the detection of talar dome injuries. Am J Roentgenol 170:1227–1230

Mallinson PI, Coupal TM, Mclaughlin PD, Nicolaou S, Munk PL, Ouellette HA (2016) Dual-energy CT for the musculoskeletal system. Radiology 281:690–707

Mintz DN, Tashjian GS, Connell DA, Deland JT, O'malley M, Potter HG (2003) Osteochondral lesions of the talus: a new magnetic resonance grading system with arthroscopic correlation. Arthroscopy 19:353–359

Mologne TS, Ferkel RD (2007) Arthroscopic treatment of osteochondral lesions of the distal tibia. Foot Ankle Int 28:865–872

Monro A (1752) Medical essays and observations. Pub By A Society In Edinburgh 4:276

Muhle C, Frank LR, Rand T, Yeh L, Wong EC, Skaf A, Dantas RWM, Haghighi P, Trudell D, Resnick D (1999) Collateral ligaments of the ankle: high-

resolution MR imaging with a local gradient coil and anatomic correlation in cadavers. Radiographics 19:673–683

Murphy EP, Mcgoldrick NP, Curtin M, Kearns SR (2019) A prospective evaluation of bone marrow aspirate concentrate and microfracture in the treatment of osteochondral lesions of the talus. Foot Ankle Surg 25:441–448

Nosewicz TL, Beerekamp MS, De Muinck Keizer RJ, Schepers T, Maas M, Niek Van Dijk C, Goslings JC (2016) Prospective computed tomographic analysis of osteochondral lesions of the ankle joint associated with ankle fractures. Foot Ankle Int 37: 829–834

Olstad K, Ytrehus B, Ekman S, Carlson CS, Dolvik N (2008) Epiphyseal cartilage canal blood supply to the tarsus of foals and relationship to osteochondrosis. Equine Vet J 40:30–39

Orr JD, Dawson LK, Garcia EJ, Kirk KL (2011) Incidence of osteochondral lesions of the talus in the United States military. Foot Ankle Int 32:948–954

Paré A, Malgaigne J-F (1560) The case reports and autopsy records of Ambroise Paré. In: Hamby WB (ed) Translated from J. P.Malgaigne's Oeuvres completes D'amboise Paré. Charles C Thomas, Spring, Paris

Pećina MM, Bojanić I (2004) Stress fractures. Overuse injuries of the musculoskeletal system, 2nd edn, Chap. 12. CRC Press, Boca Raton 315–349

Posadzy M, Desimpel J, Vanhoenacker F (2017) Staging of osteochondral lesions of the talus: MRI and cone beam CT. J Belgian Soc Radiol 101:1–1

Raikin SM, Elias I, Zoga AC, Morrison WB, Besser MP, Schweitzer ME (2007) Osteochondral lesions of the talus: localization and morphologic data from 424 patients using a novel anatomical grid scheme. Foot Ankle Int 28:154–161

Ramponi L, Yasui Y, Murawski CD, Ferkel RD, Digiovanni CW, Kerkhoffs GMMJ, Calder JDF, Takao M, Vannini F, Choi WJ, Lee JW, Stone J, Kennedy JG (2017) Lesion size is a predictor of clinical outcomes after bone marrow stimulation for osteochondral lesions of the talus: a systematic review. Am J Sports Med 45:1698–1705

Regier M, Petersen JP, Hamurcu A, Vettorazzi E, Behzadi C, Hoffmann M, Grossterlinden LG, Fensky F, Klatte TO, Weiser L, Rueger JM, Spiro AS (2016) High incidence of osteochondral lesions after open reduction and internal fixation of displaced ankle fractures: medium-term follow-up of 100 cases. Injury 47:757–761

Reilingh ML, Beimers L, Tuijthof GJM, Stufkens SAS, Maas M, Van Dijk CN (2010) Measuring hindfoot alignment radiographically: the long axial view is more reliable than the hindfoot alignment view. Skelet Radiol 39:1103–1108

Reilingh ML, Blankevoort L, Van Eekeren ICM, Van Dijk CN (2013) Morphological analysis of subchondral talar cysts on micro-CT. Knee Surg Sports Traumatol Arthrosc 21:1409–1417

Rendu A (1932) Fracture intra-articulaire Parcellaire De La Poulie Astragalienne. [Fragmented Intra-articular fractures of the Talar Dome]. Lyon Med 150: 220–222

Resnick D, Kransdorf MJ (2005) Bone and joint imaging. Elsevier, Saunders, Philadelphia

Riaz O, Boyce Cam N, Shenolikar A (2012) An osteochondral lesion in the distal fibula: a case report. Foot Ankle Spec 5:394–396

Rios AM, Rosenberg ZS, Bencardino JT, Rodrigo SP, Theran SG (2011) Bone marrow edema patterns in the ankle and hindfoot: distinguishing MRI features. Am J Roentgenol 197:W720–W729

Robertson W, Kelly BT, Green DW (2003) Osteochondritis dissecans of the knee in children. Curr Opin Pediatr 15:38–44

Robertson GAJ, Goffin JS, Wood AM (2017) Return to sport following stress fractures of the great toe sesamoids: a systematic review. Br Med Bull 122:135–149

Rödén S, Tillegard P, Unander-Scharin L (1953) Osteochondritis dissecans and similar lesions of the talus. report of fifty-five cases with special reference to etiology and treatment. Acta Orthop Scand 23:51–66

Samuel S, Kundel HL, Nodine CF, Toto LC (1995) Mechanism of satisfaction of search: eye position recordings in the reading of chest radiographs. Radiology 194:895–902

Saxena A, Eakin C (2007) Articular talar injuries in athletes: results of microfracture and autogenous bone graft. Am J Sports Med 35:1680–1687

Schein AJ, Skalski MR, Patel DB, White EA, Lundquist R, Gottsegen CJ, Forrester DM, Matcuk GR Jr (2015) Turf toe and sesamoiditis: what the radiologist needs to know. Clin Imaging 39:380–389

Schenck RC Jr, Goodnight JM (1996) Osteochondritis dissecans. J Bone Joint Surg Am 78:439–456

Shakked RJ, Walters EE, O'malley MJ (2017) Tarsal navicular stress fractures. Curr Rev Musculoskelet Med 10:122–130

Shimozono Y, Hurley ET, Yasui Y, Deyer TW, Kennedy JG (2018) The presence and degree of bone marrow edema influence midterm clinical outcomes after microfracture for osteochondral lesions of the talus. Am J Sports Med 46:2503–2508

Srikhum W, Nardo L, Karampinos DC, Melkus G, Poulos T, Steinbach LS, Link TM (2013) Magnetic resonance imaging of ankle tendon pathology: benefits of additional axial short-tau inversion recovery imaging to reduce magic angle effects. Skelet Radiol 42:499–510

Stattin EL, Wiklund F, Lindblom K, Onnerfjord P, Jonsson BA, Tegner Y, Sasaki T, Struglics A, Lohmander S, Dahl N, Heinegard D, Aspberg A (2010) A missense mutation in the aggrecan C-type lectin domain disrupts extracellular matrix interactions and causes dominant familial osteochondritis dissecans. Am J Hum Genet 86:126–137

Sugimoto K, Takakura Y, Tohno Y, Kumai T, Kawate K, Kadono K (2005) Cartilage thickness of the talar dome. Arthroscopy 21:401–404

Taranow WS, Bisignani GA, Towers JD, Conti SF (1999) Retrograde drilling of osteochondral lesions of the medial talar dome. Foot Ankle Int 20:474–480

Tol JL, Struijs PA, Bossuyt PM, Verhagen RA, Van Dijk CN (2000) Treatment strategies in osteochondral defects of the talar dome: a systematic review. Foot Ankle Int 21:119–126

Tóth F, Nissi MJ, Ellermann JM, Wang L, Shea KG, Polousky J, Carlson CS (2015) Novel application of magnetic resonance imaging demonstrates characteristic differences in vasculature at predilection sites of osteochondritis dissecans. Am J Sports Med 43:2522–2527

Uppstrom TJ, Gausden EB, Green DW (2016) Classification and assessment of juvenile osteochondritis dissecans knee lesions. Curr Opin Pediatr 28:60–67

Van Bergen CJA, Tuijthof GJM, Blankevoort L, Maas M, Kerkhoffs GMMJ, Van Dijk CN (2012) Computed tomography of the ankle in full plantar flexion: a reliable method for preoperative planning of arthroscopic access to osteochondral defects of the talus. Arthroscopy 28:985–992

Van Bergen CJ, Gerards RM, Opdam KT, Terra MP, Kerkhoffs GM (2015) Diagnosing, planning and evaluating osteochondral ankle defects with imaging modalities. World J Orthop 6:944–953

Van Dijk CN, Reilingh ML, Zengerink M, Van Bergen CJA (2010) Osteochondral defects in the ankle: why painful? Knee Surg Sports Traumatol Arthrosc 18:570–580

Van Royen A, Shahabpour M, Al Jahed D, Abid W, Vanhoenacker F, De Maeseneer M (2020) Injuries of the ligaments and tendons in ankle and foot. MedRadiol. https://doi.org/10.1007/174_2020_257

Verhagen RA, Maas M, Dijkgraaf MG, Tol JL, Krips R, Van Dijk CN (2005) Prospective study on diagnostic strategies in osteochondral lesions of the talus. Is MRI superior to helical CT? J Bone Joint Surg Br 87:41–46

Weishaupt D, Schweitzer ME (2002) MR Imaging of the foot and ankle: patterns of bone marrow signal abnormalities. Eur Radiol 12:416–426

Weiss JM, Nikizad H, Shea KG, Gyurdzhyan S, Jacobs JC, Cannamela PC, Kessler JI (2016) The incidence of surgery in osteochondritis dissecans in children and adolescents. Orthop J Sports Med 4:2325967116635515

Wellenberg RHH, Hakvoort ET, Slump CH, Boomsma MF, Maas M, Streekstra GJ (2018) Metal artifact reduction techniques in musculoskeletal CT-imaging. Eur J Radiol 107:60–69

Yasui Y, Hannon CP, Fraser EJ, Ackermann J, Boakye L, Ross KA, Duke GL, Shimozono Y, Kennedy JG (2019) Lesion size measured on MRI does not accurately reflect arthroscopic measurement in talar osteochondral lesions. Orthop J Sports Med 7:2325967118825261–2325967118825261

Ytrehus B, Ekman S, Carlson CS, Teige J, Reinholt FP (2004) Focal changes in blood supply during normal epiphyseal growth are central in the pathogenesis of osteochondrosis in pigs. Bone 35:1294–1306

Zanon G, Di Vico G, Marullo M (2014) Osteochondritis dissecans of the talus. Joints 2:115–123

Acute and Overuse Lesions of the Leg and Calf

Veronica Attard, Emma Rowbotham, and Philip Robinson

Contents

Abstract

Lower limb injuries are extremely common in sports, particularly contact sports. The injuries can be divided into acute and chronic causes. It is important for the radiologist to be aware of all the possible causes of both acute and chronic symptoms within the lower leg and also any subsequent complications so that the correct imaging modalities can be selected and the possible range of pathologies considered. This chapter discusses the biomechanics of lower limb injury as well as the most common acute and chronic causes seen in sports and also any potential complications and their characteristic imaging findings. The most appropriate imaging modalities for each of the conditions are also described.

V. Attard
Musculoskeletal Centre X-Ray Department, Leeds Teaching Hospitals Trust, Chapel Allerton Hospital, Leeds, UK

E. Rowbotham · P. Robinson (✉)
Musculoskeletal Centre X-Ray Department, Leeds Teaching Hospitals Trust, Chapel Allerton Hospital, Leeds, UK

Leeds Musculoskeletal Biomedical Research Centre, University of Leeds, Leeds, UK
e-mail: philip.robinson10@nhs.net

Med Radiol Diagn Imaging (2021)
https://doi.org/10.1007/174_2020_268, © Springer Nature Switzerland AG
Published Online: 12 March 2021

1 Introduction

The lower limb is subject to marked biomechanical stresses during the majority of athletic activity (Dvorak and Junge 2000). This region is the most frequently injured area in a number of sports with audits in professional football demonstrating 87% of all injuries occurring here, in particular the thigh (23%), ankle (14%), knee (18%), leg (11%) and groin (14%). Among acute lower extremity injuries, ankle sprain occurred in 7% and thigh strain in 17% (Ekstrand et al. 2011).

This chapter discusses the biomechanics of lower limb injuries and also the role of imaging in their management, highlighting specific acute and chronic osseous, muscle and tendon injuries commonly encountered in athletes. Injuries relating to the pelvis, knee, ankle and foot will not be discussed in detail as these areas are covered in their specific chapters.

2 Acute Osseous Injury

Biomechanically the cortex provides the majority of a bone's strength for force absorption (Nordin and Frankel 2001a). The trabecular bone and marrow contribute relatively little to the overall strength but do determine the bone's cross-sectional area influencing the distribution of applied forces, important for resisting chronic stress and explaining the subsequent distribution of injuries particularly seen in the tibia.

Acute trauma in the context of sporting injuries frequently results in soft-tissue injury; however, in contact sports acute fractures may also occur on tackling or player collision (Hawkins et al. 2001; Fuller et al. 2004; Chomiak et al. 2000). In the context of sports injuries, acute fractures of the femur and hip are rare but injuries of the tibia, fibula, ankle and foot are more frequent.

In contrast to chronic osseous injuries where concomitant injuries and local muscle imbalance are important for injury development, in acute injury the forces applied are usually sudden and excessive leading to acute structural failure (fracture) not dependent on concomitant injuries (Nordin and Frankel 2001a). The rate of force application is also important, as forces applied at a high rate induce increased bone stiffness resulting in shattering if the bone strength limit is exceeded. As bone fails, the energy producing the fracture is dissipated into the soft tissues resulting in significant associated injury due to the high energies involved (Nordin and Frankel 2001a).

The forces applied to the tibia and fibula can be direct, torsional or bending which influence the subsequent fracture configuration. The majority of fractures of the tibia and fibula usually have an oblique orientation in the mid to distal shaft resulting from the lateral or medial oblique forces produced from a direct blow during a fall, from tackling or from falling players (Figs. 1, 2, 3, and 4) (Giza et al. 2003; Fuller et al. 2004). This particular fracture pattern involving a direct blow and low velocity is sometimes termed 'footballer's fracture' (Boden et al. 1999; Chang et al. 2007).

2.1 Imaging Strategy and Management

For fractures of the tibia and fibula radiographs are usually sufficient to confirm the diagnosis and fracture configuration (Figs. 1 and 2). CT and MR imaging can be used to confirm fractures when radiographs are negative and an undisplaced fracture rather than just soft-tissue contusion is suspected (Figs. 3 and 4) (Jarraya et al. 2013).

CT is the method of choice in detecting osteopenia, one of the earliest imaging findings in fatigue cortical bone injury (Gaeta et al. 2005). Moreover, CT utilising dual energy via the virtual non-calcium-subtraction technique can be used for the detection of bone marrow oedema after trauma, especially in cases when MR imaging is contraindicated (Nicolaou et al. 2012).

MR imaging demonstrates soft-tissue oedema in the area of impact but also allows evaluation of the cortical and trabecular bone for oedema and

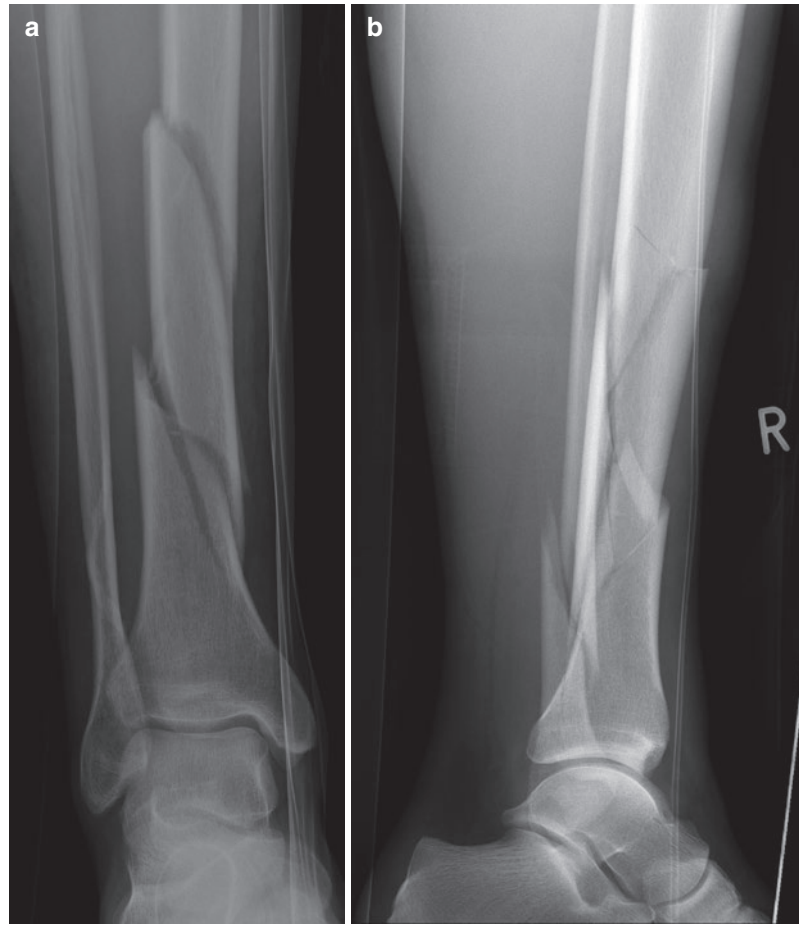

Fig. 1 (**a**, **b**) Footballer with acute severe leg pain after a tackle. (**a**) Anteroposterior (AP) and (**b**) lateral radiographs, both showing a comminuted oblique displaced fracture through the diaphysis of the tibia and an oblique fracture of the distal fibula. The player went on to have plate fixation of the fractures

low-signal fracture lines. Cortical abnormalities include buckling or increased thickness with high T2-weighted signal due to periosteal haematoma (Fig. 3).

Treatment for tibia and fibula fractures is often conservative with casting, but if the injury is of high velocity resulting in bone comminution and soft-tissue disruption, internal fixation and soft-tissue reconstruction will be required. In these cases, CT examination can be useful to define the exact fracture configuration and extent for surgical treatment. Despite the soft-tissue damage subsequent reconstruction (primary or grafting) does not require MR or ultrasound imaging unless there are specific vascular complications.

The recovery time for these injuries will depend on the fracture position and severity of associated injuries. While the majority of patients sustaining a lower limb fracture will return to their sport, fracture of the tibia and fibula can be career ending for athletes involved in contact sports (Chomiak et al. 2000). One series on 357 soccer players presenting with fractures reported that 83% of players made a full return to sport taking a mean of 15 ± 17 weeks with fractures of the distal tibial diaphysis having the highest rate of morbidity and non-return to soccer (Robertson and Wood 2017). Non-union is the most significant complication and if appearances are indeterminate on radiographs ultrasound or CT can be used to give a more accurate assessment of callus formation. If non-union is confirmed internal fixation and bone grafting may be required, which is not without complication (Fig. 2).

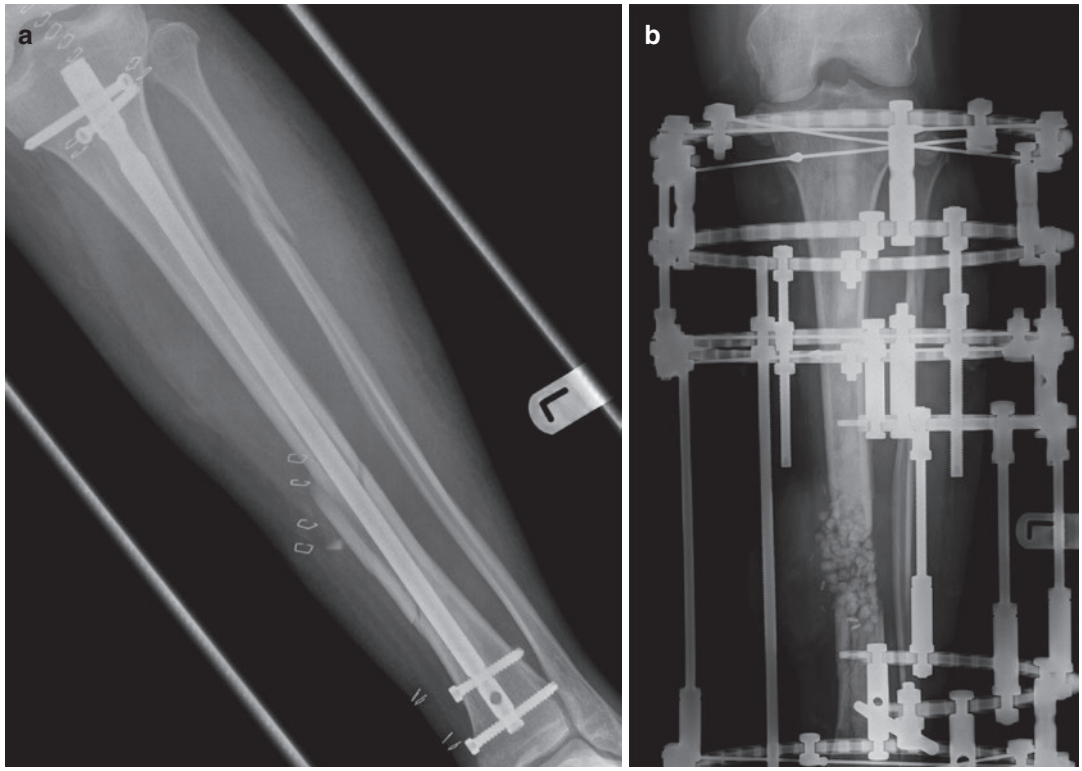

Fig. 2 (**a**) AP radiograph of a tibial fracture and a proximal fibular fracture in a professional footballer treated with intramedullary nail. There is persistent non-union across the fracture site. (**b**) The intramedullary nail had to be removed and a circular frame was applied due to non-union secondary to infection. Antibiotic beads were implanted providing a method for antibiotic delivery

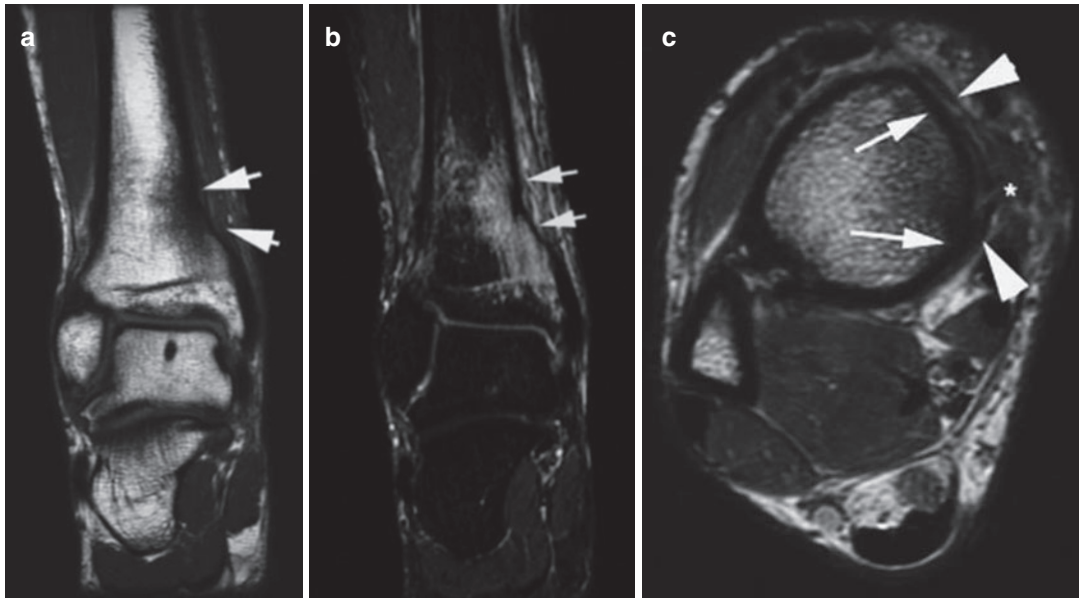

Fig. 3 (**a**–**c**) Professional footballer with severe lower leg pain after stamping; radiographs showed some cortical irregularity. (**a**) Coronal T1-weighted and (**b**) T2-weighted fat-suppressed MR images show depression of the distal medial tibial cortex (arrows) with associated bone marrow oedema. (**c**) Corresponding axial T1-weighted MR image shows the main cortex (arrows) with periosteal haematoma and elevation (arrowheads). Note the defect in the elevated periosteum with haematoma (*)

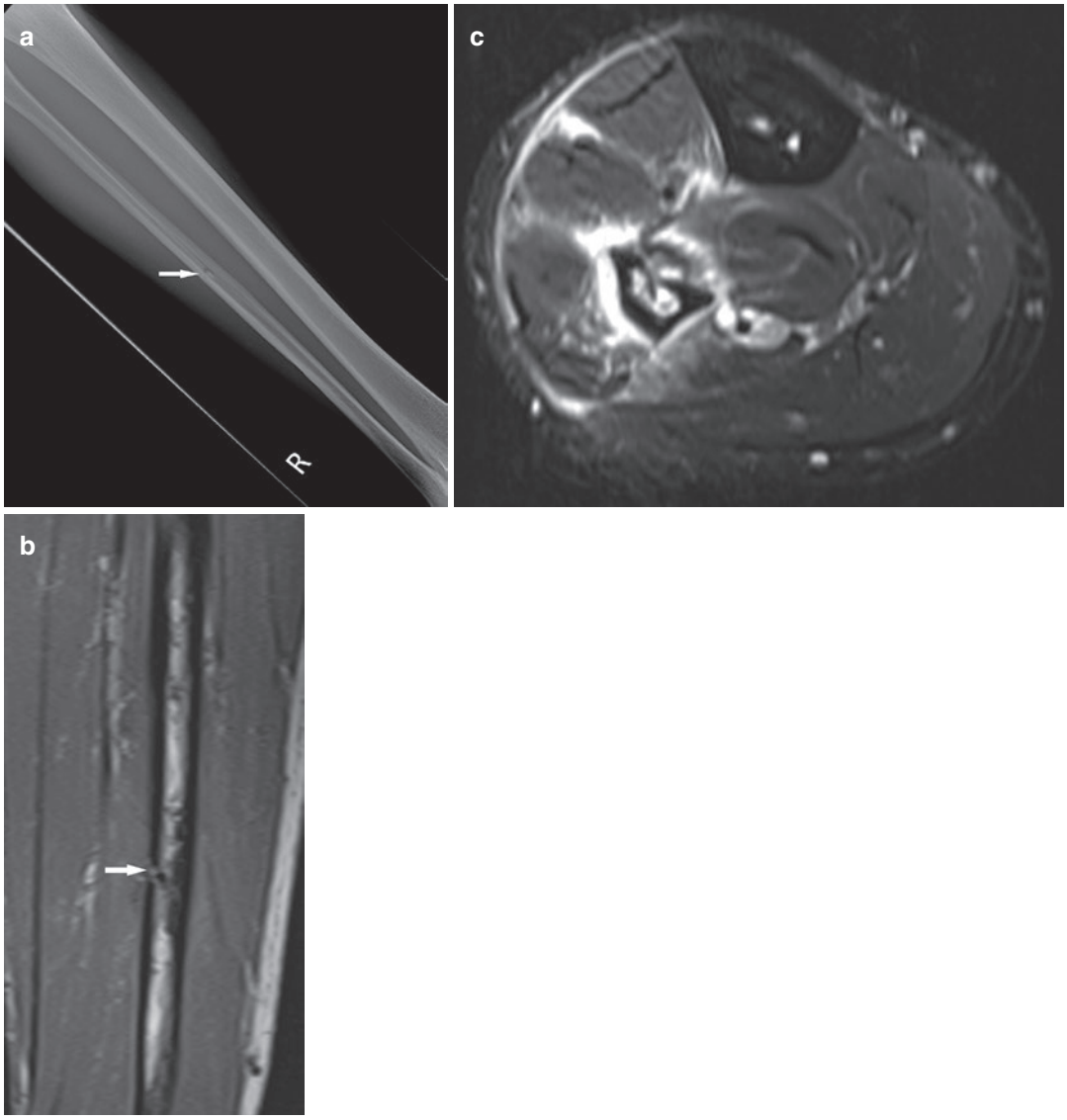

Fig. 4 (**a**–**c**) Footballer with lateral leg pain following a tackle. (**a**) Plain-film radiograph—lateral view of the right fibula fracture. (**b**) Coronal T1-weighted MR image showing a cortical defect in the mid-shaft of the fibula (arrow). (**c**) Axial T2-weighted fat-suppressed MR image showing muscle contusion and a fibular fracture with associated bone marrow oedema

3 Chronic Exertional Leg Pain

The commonest causes of chronic exertional athletic lower extremity pain include medial tibial stress syndrome, stress fractures, chronic exertional compartment syndrome and popliteal artery and nerve entrapment (Gaeta et al. 2008). Several series have found slightly different incidences for each type of injury but together these processes most frequently occurr in athletes (Kaufman et al. 2000; Edwards Jr. et al. 2005; Bonasia et al. 2015).

3.1 Chronic Osseous Stress Response and Injury

Overuse injuries occur when the ability of cortical bone to remodel and compensate is exceeded by chronic excessive forces not individually

reaching acute overload (Nordin and Frankel 2001a; Anderson et al. 1997). Causes of increased stress normally relate to a sustained increase in training and more commonly present in athletes who are female, have suffered prior osseous injury and have concomitant lower limb injuries (e.g., muscle strain) and especially in the lower leg, if there is ankle pronation (Anderson et al. 1997; Batt et al. 1998; Fredericson et al. 1995; Gaeta et al. 2008). Causes of increased stress include low bone mineral density, hormone imbalance, low-fat diet, high-mileage running, leg length discrepancy, high longitudinal arch of the foot and excessive forefoot varus (Bonasia et al. 2015).

Studies of military recruits have shown that stress injuries and fractures most commonly affect the calcaneus and metatarsals (Jarraya et al. 2013). In the femur stress reactions most frequently occur in the femoral neck and are important to detect early as the consequences for osteonecrosis or complete fracture are serious (Robertson and Wood 2017).

3.1.1 Tibia and Fibula

In the tibia the fracture position can vary according to sporting activity, with runners experiencing middle to distal third, dancers middle third and jumping athletes (e.g., tennis, basketball and volleyball) proximal third injuries (Batt et al. 1998). The mid and distal diaphysis of the tibia is thought to be the most vulnerable region as this is the narrowest cross-sectional area of the bone and has relatively little surrounding musculature to dissipate applied forces. In the tibia, compressive forces concentrate medially and fractures can present here or be part of medial tibial stress syndrome (MTSS, see below) (Gaeta et al. 2008). Fractures that develop on the anterolateral tibia occur as a result of tensile forces and subsequently have a higher risk of non-union, especially if the orientation is longitudinal and not perpendicular to the cortex (Fredericson et al. 1995; Edwards Jr. et al. 2005; Green et al. 1985). Fibular stress fractures are much less frequent and usually occur at the distal shaft, 5–6 cm proximal to the lateral malleolus (Bonasia et al. 2015).

Symptoms are usually of insidious onset, occurring on exertion, and are a differential diagnosis for chronic exercise-induced pain. However, if allowed to progress pain can be present at rest or on weight bearing (Fredericson et al. 1995; Edwards Jr. et al. 2005). In contrast, in chronic exertional compartment syndrome pain subsides after cessation of exercise (Ringler et al. 2013).

Clinical findings include localised tenderness and indirect pain produced by tibial percussion at a distant site (Batt et al. 1998; Yates and White 2004; Bonasia et al. 2015). This latter finding is thought to correlate well with more severe clinical and imaging extent (Fredericson et al. 1995).

3.2 Medial Tibial Stress Syndrome (MTSS)

This is an overuse syndrome in running and jumping athletes which is defined as involving the posteromedial tibial periosteum (Batt et al. 1998; Yates and White 2004). There has been previous controversy concerning the aetiology of this condition with initial theories suggesting a chronic periosteal traction injury from adjacent muscles (Anderson et al. 1997; Batt et al. 1998; Fredericson et al. 1995; Yates and White 2004). However, the osseous changes are usually distal to the main muscle origins and it is now thought to be the beginning of the spectrum of osseous stress reaction of the tibia (Figs. 5 and 6). This condition is interchangeable with posterior ‘shin splints’ and some clinicians define both terms as lower leg exertional pain not due to a compartment syndrome, fracture or muscle hernia (Batt et al. 1998; Edwards Jr. et al. 2005).

Compressive stresses are concentrated on the concave aspect of the posteromedial tibial cortex stimulating osteoblastic and osteoclastic activity as the bone remodels (Anderson et al. 1997, Batt et al. 1998, Fredericson et al. 1995, Yates and White 2004). As with other osseous stress reactions, as the repetitive loading continues, trabecular failure may occur, ultimately resulting in cortical fracture (Fig. 7).

MTSS is a very common cause of overuse leg injury, with an incidence ranging from 4% to 35% in athletic and military recruits (Bonasia et al. 2015). As in other osseous stress injuries the development of this condition is increased in athletes that are female, have a pronated foot or have injury elsewhere within the lower limb kinetic

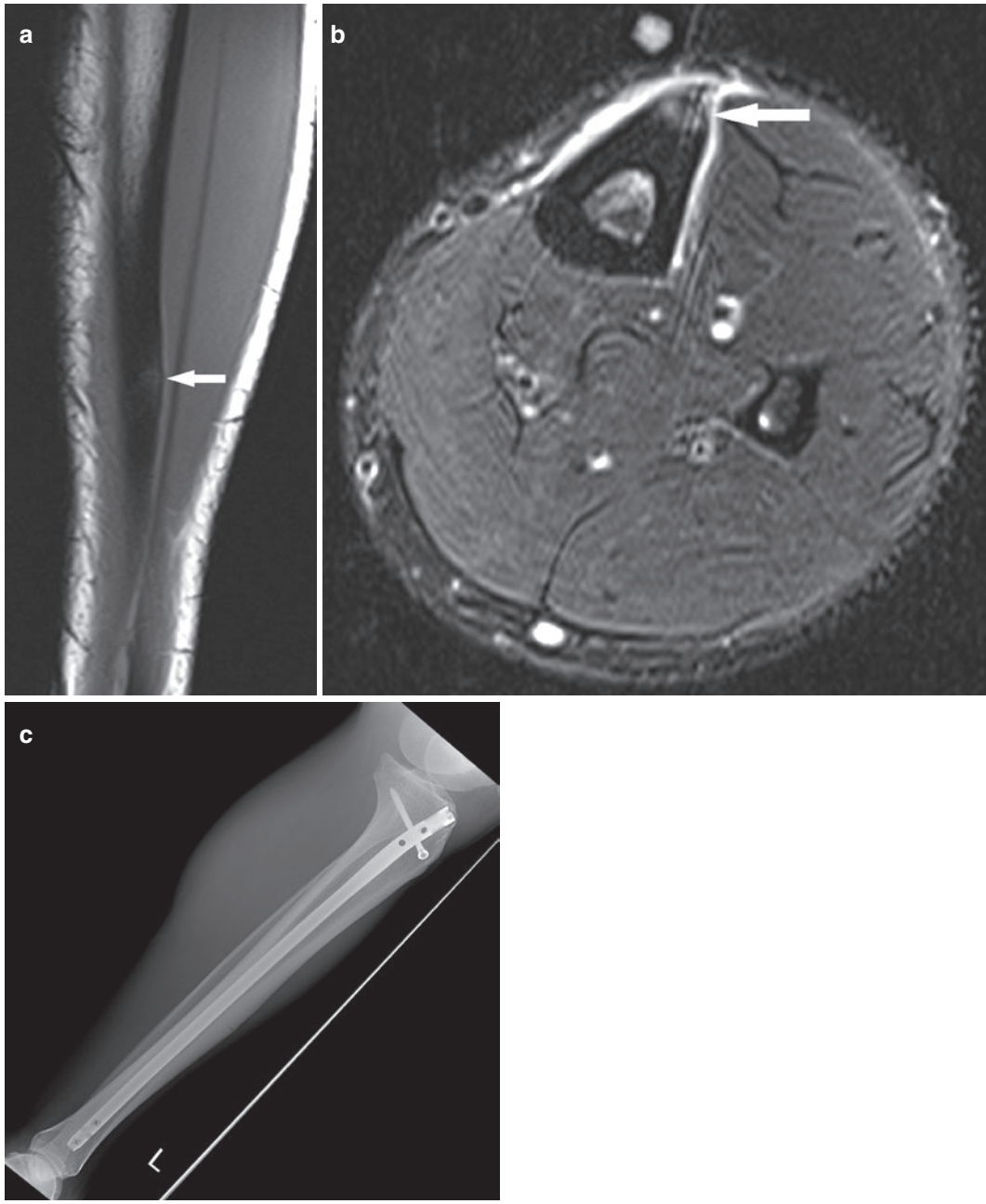

Fig. 5 (**a**–**c**) Long-distance runner with recurrent anterior lower leg pain. (**a**) Coronal proton-density MR image of the tibia showing a fracture line (arrow) in the anterior tibial cortex and associated marrow oedema-like signal intensity in keeping with a stress fracture. (**b**) Axial proton-density-weighted MR image of the tibia showing marrow oedema-like signal intensity (arrow) in the anterior cortex of the tibia. (**c**) Lateral radiograph shows cortical hypertrophy and a 'black line' defect on the anterior cortex of the middle third of the tibia. Persistent fracture in this case resulted in the need for IM nail insertion in order to aid healing

chain (Batt et al. 1998; Yates and White 2004). It is bilateral in over 70% of cases which is thought to relate to running and jumping (e.g., basketball and tennis) being the most common underlying mechanisms of injury. The area of diaphysis affected can vary depending on sporting activity but the majority of injuries involve the mid and distal diaphyseal region where the cross-sectional

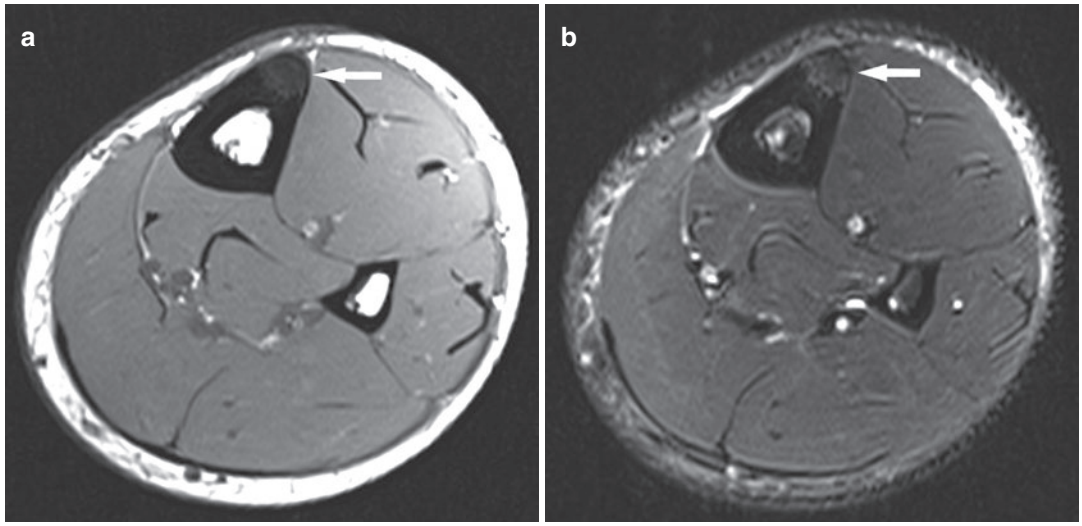

Fig. 6 (**a**, **b**) Professional athlete with persistent anterior lower leg pain. (**a**) Axial T1-weighted MR image and (**b**) axial proton-density-weighted fat-suppressed MR image reveal bone marrow and endosteal oedema (arrow) involving the anterior aspect of the mid diaphysis of the tibia, in keeping with a stress reaction, but no fracture is seen here

Fig. 7 Female marathon runner presenting at major games with continuous anterior tibial pain. Lateral radiograph of the tibia shows anterior cortical thickening and multiple stress fractures. The athlete had to withdraw from competition

area is smallest (Batt et al. 1998; Anderson et al. 1997; Fredericson et al. 1995; Yates and White 2004). Clinical findings include diffuse posteromedial tibial tenderness which is unaffected by ankle or knee movement (Batt et al. 1998; Edwards Jr. et al. 2005; Bonasia et al. 2015).

3.2.1 Imaging and Management of Osseous Stress Reaction

In athletes it is especially important to make an early diagnosis and determine the extent of osseous damage to give prognostic information (Ohta-Fukushima et al. 2002). Radiographs are insensitive and can be negative in up to 85% of cases but are usually performed initially to exclude a complete fracture (Fig. 6) (Anderson et al. 1997; Ohta-Fukushima et al. 2002; Batt et al. 1998; Fredericson et al. 1995; Gaeta et al. 2005; Bonasia et al. 2015). MR imaging has been repeatedly shown to be an accurate, sensitive and specific technique compared to CT and isotope scanning (Anderson et al. 1997; Milgrom et al. 1984; Batt et al. 1998; Fredericson et al. 1995; Gaeta et al. 2005).

T2-weighted (fat-suppressed) MR sequences are most sensitive for detecting periosteal, cortical and bone marrow oedema (Fig. 8) (Anderson et al. 1997; Batt et al. 1998; Gaeta et al. 2005). Isotope bone scans show increased activity but

lack spatial resolution (Fig. 9) and can be negative if osteoblastic activity is markedly reduced (Milgrom et al. 1984).

The MR classification and the management of osseous stress reaction are summarised in Table 1. Further discussion is beyond the scope of this chapter (see Lefere et al. 2021 and Karantanas 2021, respectively).

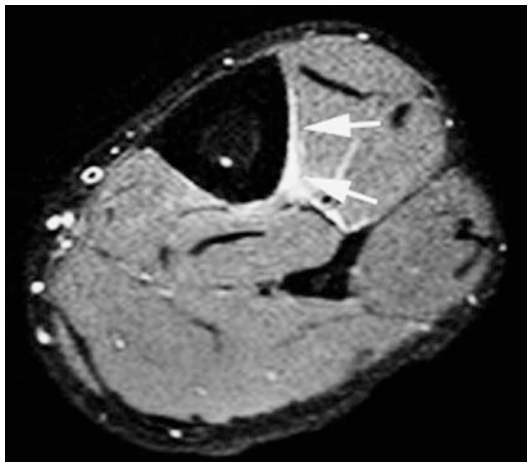

Fig. 8 Running athlete with clinical diagnosis of anterior shin splints. Axial T2-weighted fat-suppressed MR image shows marked anterolateral periosteal oedema of the tibia with no associated intracortical or bone marrow change

3.3 Chronic Exertional Compartment Syndrome (CECS)

Compartment syndrome is defined as increased interstitial pressure within an anatomically confined compartment that interferes with neurovascular function. Normal pressures within a muscle compartment are between 0 and 4 mmHg and can peak above 60 mmHg on exercise but quickly dissipate on cessation. However, if this pressure is sustained above 15 mmHg blood flow is compromised and muscle ischaemia can occur (Zabetakis 1986). The pathophysiology of increased tissue pressures is not yet fully understood (Guermazi et al. 2017).

Chronic exertional compartment syndrome commonly affects the anterior and lateral calf lower leg muscular compartments (Peterson and Renstrom 1986; Zabetakis 1986; Martens et al. 1984; Gaeta et al. 2008). It is thought to occur because of abnormally increased pressure within muscle compartments enclosed by relatively noncompliant fasciae. Potentially any athlete can be affected but it is particularly common in distance runners, cyclists and cross-country skiers. The athlete usually presents with crescendo pain

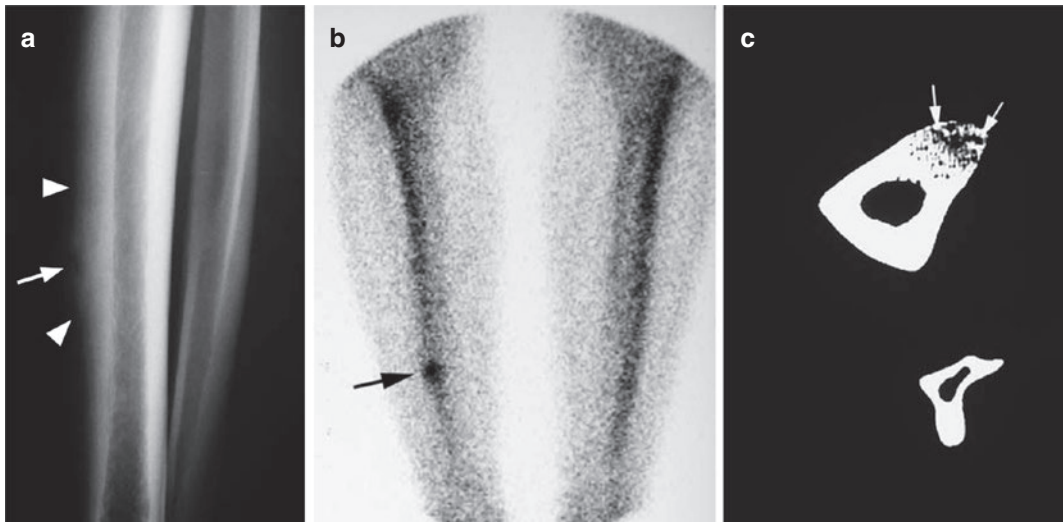

Fig. 9 (**a**–**c**) Running athlete with tibial pain. (**a**) Lateral radiograph shows diffuse anterior cortical thickening (arrowheads) with an ill-defined lucency in the superficial cortex (arrow). (**b**) Isotope bone scan image shows increased uptake (arrow) in the region. (**c**) Corresponding axial CT shows diffuse resorption through the anterior cortex but also a linear fracture (arrows)

and paraesthesia after exercise which eases on ceasing activity and unlike popliteal artery syndrome is not posture dependant (Martens et al. 1984; Nicholas and Hershman 1986). There may also be muscle swelling and it is important to rule out an underlying muscle hernia which usually exists in 40–60% of patients (Bonasia et al. 2015). The diagnosis can sometimes be made with history alone but intracompartmental pressure monitoring, MRI and near-infrared spectroscopy are useful to establish a diagnosis (Bonasia et al. 2015). Recent work has demonstrated that the sensitivity of MRI in the diagnosis of chronic exertional compartment syndrome was comparable to measuring compartment pressure with a slit or weak catheter (Gaeta et al. 2008).

Table 1 Summary of MR imaging classification and potential relationship with return to weight bearing for osseous stress injuries (Fredericson et al. 1995)

MR grade	Grade 1	Grade 2	Grade 3	Grade 4
Periosteal and adjacent soft-tissue oedema	–	+	+	+
Bone marrow oedema	–	–	+	+
Cortical fracture	–	–	–	+
Typical time to weight bearing (weeks)	2–3	3–6	6–9	12+ (including 6 weeks in cast)

3.3.1 Imaging

The role of near-infrared spectroscopy and MRI is yet to be established in the diagnosis of chronic exertional compartment syndrome (Bonasia et al. 2015) and it is not routinely used in clinical practice at present.

On ultrasound the muscle can appear echogenic with relative sparing of periseptal areas which are still receiving sufficient blood flow from the adjacent fascia (Van Holsbeeck and Introcasco 2001). Studies evaluating muscle cross-sectional area on ultrasound both before and after exercise describe two different patterns in symptomatic patients. In one group the muscle compartment cannot expand with a relatively rigid fascia compared to normal subjects (where muscle volume can increase by 10–15%). In the other symptomatic group, although the muscle compartment does expand during exercise, there is a slow reduction in volume post-exercise compared to normal subjects (Van Holsbeeck and Introcasco 2001).

Post-exercise MR imaging can show oedema in the clinically affected muscles confirming the diagnosis (Fig. 10). However, this technique

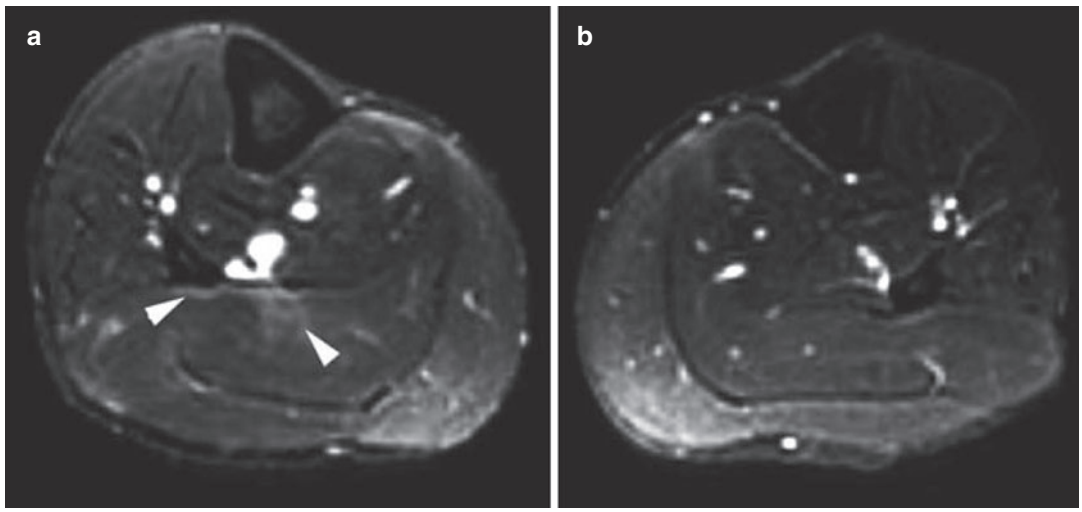

Fig. 10 (**a**, **b**) Running athlete with chronic exertional right-leg pain. Axial T2-weighted fat-suppressed MR image post-exercise shows persisting soleus oedema (arrowheads) (**a**), on right right side, and (**b**) normal appearances on the left asymptomatic side. The athlete underwent fasciotomy

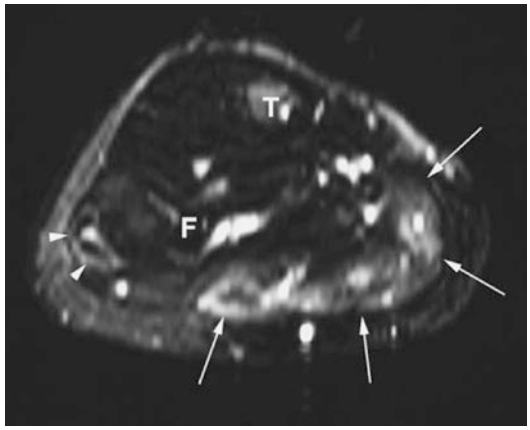

Fig. 11 Running athlete with chronic exertional right-leg pain, clinically related to soleus. Axial T2-weighted fat-suppressed MR image post-exercise shows soleus oedema (arrows). Note asymptomatic peroneus muscle oedema (arrowheads)

despite being sensitive post-exercise is not completely specific with oedema being found in asymptomatic athletes and normal muscle appearances occurring in athletes with objective clinical features (Fig. 11) (Tucker 2010).

The initial treatment of chronic exertional compartment syndrome includes training modifications and assessment for orthotics; however, if symptoms persist fasciotomy of the muscle compartment is performed. Morbidity can potentially result if there is subsequent muscle herniation or scarring (Van Holsbeeck and Introcasco 2001).

3.4 Vascular and Nerve Compression

3.4.1 Vascular

Popliteal artery entrapment is an uncommon cause of chronic exertional calf pain which can occur during exercise or on particular postural changes (Atilla et al. 1998; Elias et al. 2003). The condition is usually precipitated in young male athletes by a change in muscle bulk due to adolescent growth or increased training (Atilla et al. 1998; Collins et al. 1989; Edwards Jr. et al. 2005). This most commonly occurs in sports which involve high-intensity repetitive plantar and dorsiflexion such as soccer, basketball and running. Repeated knee flexion resulting in microtrauma and intimal fibrosis of the artery resulting in this condition have been described in a skier (Toorop et al. 2004).

Symptoms occur due to muscle ischaemia from compression of the popliteal artery (and occasionally vein) at the level of the medial head of gastrocnemius (MHG). The MHG can be normal with compression resulting from muscle hypertrophy; however, more frequently there is also a congenital anomalous origin or fibrous slip. Causes of the condition can be classified into six types (Fig. 12): medial deviation of popliteal artery and normal MHG (type 1), aberrant origin of MHG from intercondylar notch compressing the artery (type 2), slip of MHG compressing the popliteal artery (type 3), popliteal artery passing deep to popliteus muscle or fibrous band in the popliteal fossa (type 4), any entrapment also resulting in the involvement of the popliteal vein (type 5) and compression of a normal artery by a normal but hypertrophied MHG (type 6) (Collins et al. 1989; Rich et al. 1979; Labmayr et al. 2019).

The diagnosis is clinical with complete loss or a decrease in ankle pulses between dorsiflexion and plantarflexion associated with calf and foot pain. The underlying abnormality can be bilateral in up to 67% but does not always result in bilateral symptoms (Collins et al. 1989; Chernoff et al. 1995; Hai et al. 2008).

3.4.2 Imaging and Management

The diagnosis, extent and severity of compression can be confirmed by imaging using a combination of ultrasound, MR imaging (angiography) or conventional arteriography. Ultrasound is typically the first technique used and can depict change in vessel calibre and distal flow showing systolic peaks and dampening during dynamic manoeuvres (Fig. 13a, b). The artery may be medially deviated by muscle, but this is present in less than 25% of cases. MR imaging is nearly always then performed as it allows complete non-invasive investigation of muscular anatomy while time-of-flight angiography can depict vessel compression in different foot positions (Fig. 13c) (Atilla et al. 1998). Subsequent complications

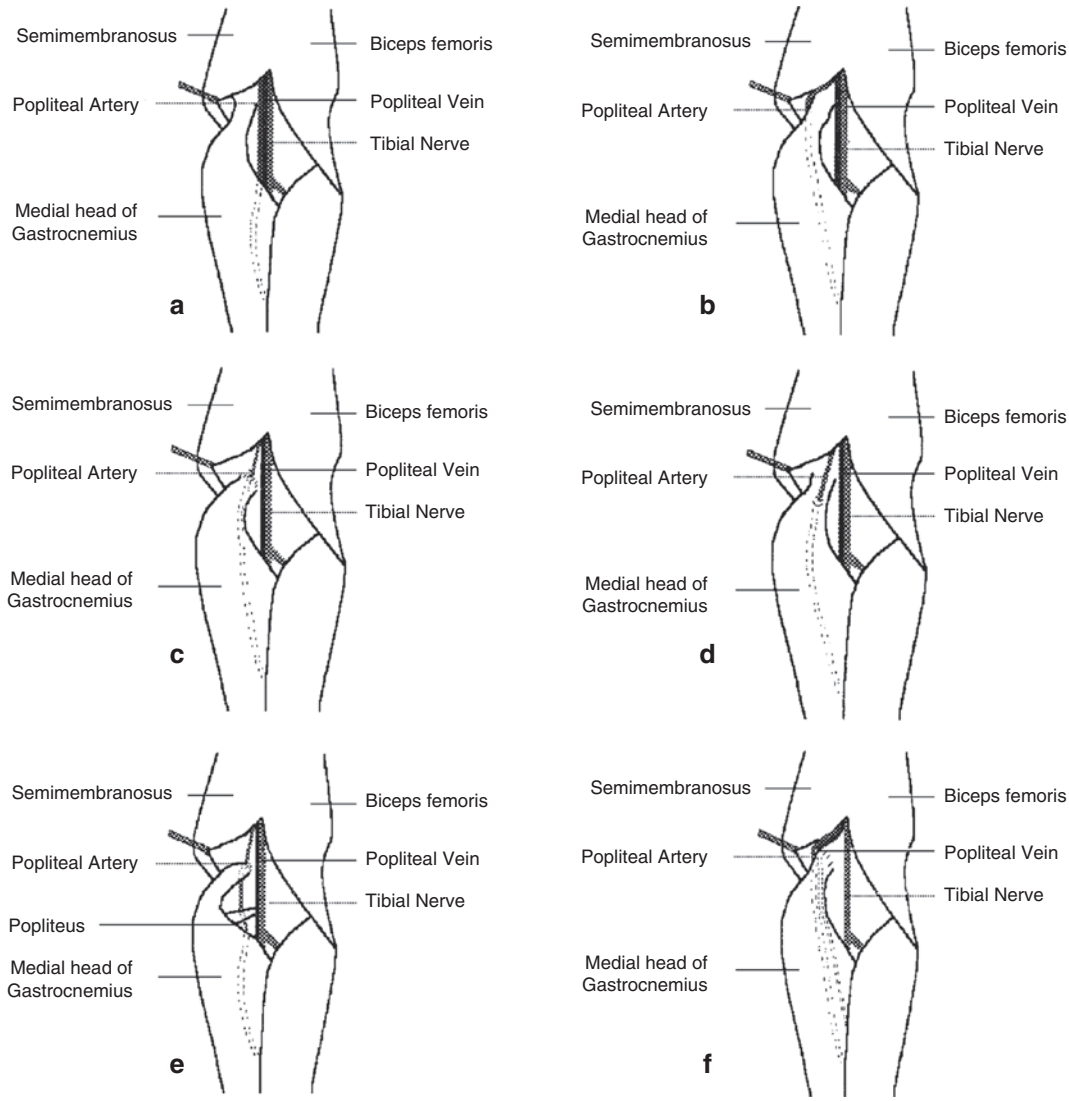

Fig. 12 Line drawing of PAES

such as adventitial disease or post-stenotic aneurysms can also be demonstrated by MR imaging although this is rare in true athletic-induced pain. If MR imaging features are equivocal angiography may be required to more accurately define the degree of compression (Fig. 13d, e) (Atilla et al. 1998; Edwards Jr. et al. 2005).

3.4.3 Nerve Compression

Treatment in athletes usually requires surgical release of the MHG and anomalous slips:

In the lower limb this most commonly involves the common or superficial peroneal nerves. This is usually thought to be due to fascial thickening or scarring (see later) or less commonly because of an adjacent bony abnormality, ganglion cyst or an intraneural ganglion (Nicholas and Hershman 1986; Yablon et al. 2016). Superficial peroneal injury can occur secondary to trauma and is seen in dancers, football players and runners. The peroneal nerve has a superficial course and lacks epineural supporting tissue with traction injuries, contusion and penetrating trauma being the three mechanisms involved in the spectrum of pathological conditions. Traction injuries of the peroneal nerve can occur following ankle inversion,

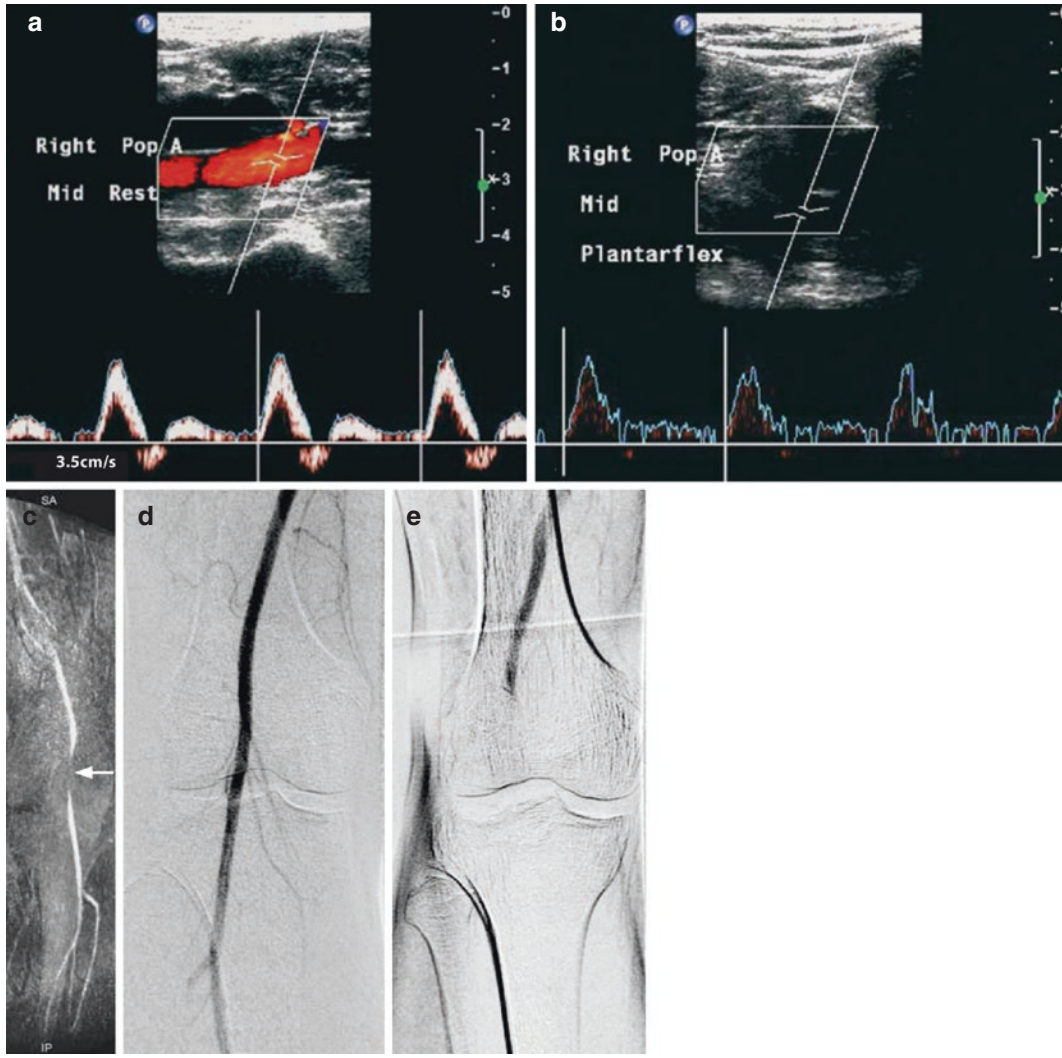

Fig. 13 (**a**–**e**) Male track hurdler with recent onset of intermittent calf pain. (**a**) Doppler ultrasound evaluation of the right popliteal artery shows normal systolic and diastolic waveform. (**b**) Corresponding evaluation with plantarflexion shows dampening of the systolic and diastolic variation consistent with arterial compression. (**c**) Time-of-flight MR angiography image shows complete vessel occlusion on plantarflexion (arrow). (**d**) Subtraction angiography image shows normal vessel calibre in neutral position and (**e**) subsequent complete occlusion on plantarflexion. At surgery an anomalous slip of the medial head of the gastrocnemius was identified (grade 3 abnormality)

high-grade varus sprains of the knee, proximal fibular fractures, dislocation of the knee and posterolateral corner injury. Oblique locking screws in intramedullary tibial nailing may also result in peroneal nerve palsy.

Direct impact in contact sports and football may result in peroneal nerve contusion. The nerve will appear hyperintense on T2-weighted imaging, hypointense on T1-weighted imaging and thickened. Oedema in the adjacent lateral compartment muscles and in the proximal fibula should alert the reporting radiologist to a potential peroneal nerve lesion. Other miscellaneous lesions resulting in peroneal nerve injuries include anterior or lateral compartment syndrome after minor trauma and a Morel-Lavallée lesion (Van Den Bergh et al. 2013).

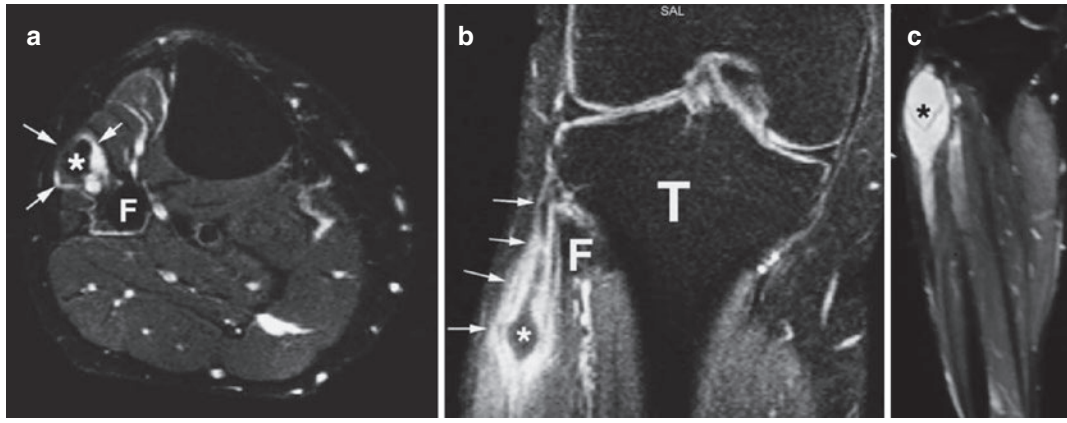

Fig. 14 (**a**–**c**) Two runners with lateral calf pain on exertion. (**a**) Axial T2-weighted fat-suppressed MR image shows a ganglion (arrows) extending into the peroneus muscles adjacent to the fibula (F). Note low-signal fibrous tissue (*) within the ganglion. (**b**) Coronal T1-weighted fat-suppressed post-IV gadolinium MR image shows low-signal fluid (*) and the enhancing ganglion wall (arrows) tracking to the tibiofibular joint (T = tibia, F = fibula). (**c**) Coronal T2-weighted fat-suppressed MR image in a different runner shows a high signal and enlarged common peroneal nerve (*). At surgery this was found to be a neural cyst originating from the tibiofibular joint

A ganglion of the proximal tibiofibular joint can result in direct compression of the common peroneal nerve (Fig. 14a, b) or actually extend into and along the nerve sheath (Fig. 14c) (Ilahi et al. 2003; Miskovsky et al. 2004; Spinner et al. 2000).

Traditionally the diagnosis of peripheral neuropathy has been based on history, clinical findings and electromyography. Imaging also plays an important role and magnetic resonance neurography is gaining an increasing role in the diagnosis of peripheral nerve disorders (Chhabra et al. 2012).

4 Acute Lower Limb Muscle Injury

Muscle and tendon injury most commonly occurs at zones of anatomical or functional transition as these sites generate the greatest concentrations of intrinsic forces (Garrett Jr. et al. 1987; Nordin and Frankel 2001b). These are the commonest injuries in all sporting activities because the lower limb is essential for athletic movement.

4.1 Biomechanical Basis of Acute Lower Limb Muscle Injury

Lower limb muscles experience a wide range of physiological movement and must be able to maintain significant stamina while undergoing repetitive explosive activity. Studies have shown that acute muscle injury, especially of the lower limb, accounts for more than 37% of all athletic injuries. The hamstring muscle complex is the most commonly affected (Guermazi et al. 2017). The rectus femoris and gastrocnemius muscles are also frequently affected. These muscles are more susceptible because they contain a high proportion of fast-twitch type 2 fibres and span multiple joints (Guermazi et al. 2017).

4.2 Imaging of Acute Lower Limb Muscle Injury

In experienced hands and with modern equipment MR imaging and ultrasound are both accurate techniques for the evaluation of lower limb muscle injury (Robinson 2004; Van Holsbeeck and Introcasco 2001; Connell et al. 2004; Cross

et al. 2004; Steinbach et al. 1998; Flores et al. 2018). However, the large muscle bulk often present in athletes means that the depth of resolution and field of view offered by ultrasound can be limiting especially in the pelvis and proximal thigh. Acute muscle injuries can be classified as direct or indirect, with direct injuries resulting in lacerations and contusions and indirect injuries in muscle tears. The latter account for the majority of significant muscle injuries in high-level athletes (Purohit and King 2015). In mild contusion, US shows focal isoechoic muscle swelling and the lesion usually resolves quickly. With more severe contusions, the haematoma may vary in appearance depending on the time between injury and examination. Initially within the first 20 h haematomas may appear both hyperechoic and hypoechoic. Within the following days, haematomas tend to appear hypoechoic or anechoic and will subsequently resolve, possibly resulting in scar tissue (Draghi et al. 2013).

4.2.1 Hamstring Injuries

This muscle group is particularly susceptible to strain with injury occurring during running and sprinting as the muscles eccentrically contract decelerating knee extension (Mink 1992; Shellock et al. 1991; Nicholas and Hershman 1986; Garrett Jr. 1988; Slavotinek et al. 2000; De Smet and Best 2000; Garrett Jr. et al. 1984; Speer et al. 1993; Taylor et al. 1993; Rubin 2012). Contusions to the hamstrings are rare (Rubin 2012). The three muscles (semimembranosus, semitendinosus and biceps femoris) cross two joints (hip and knee) and have the largest proportion of type 2 fast-twitch fibres in the body. A number of clinical and imaging studies have confirmed that the long head of biceps femoris is the most commonly injured muscle accounting for over 80% of all injuries (alone or in combination) with partial tears more common than complete tears (De Smet and Best 2000; Slavotinek et al. 2000; Speer et al. 1993; Rubin 2012). In comparison to the other muscles within the group it has two heads proximally (long and short), which mechanically reduces the elasticity of the muscle making it more susceptible to acute injury (Fig. 15). The proximal or distal myotendinous area can be injured with almost equal incidence and strains can appear intramuscular as histologically the tendons extend throughout a large proportion of the main muscle (Fig. 16) (Garrett Jr. et al. 1984). Acute injuries are more frequent in older players and those with previous identical

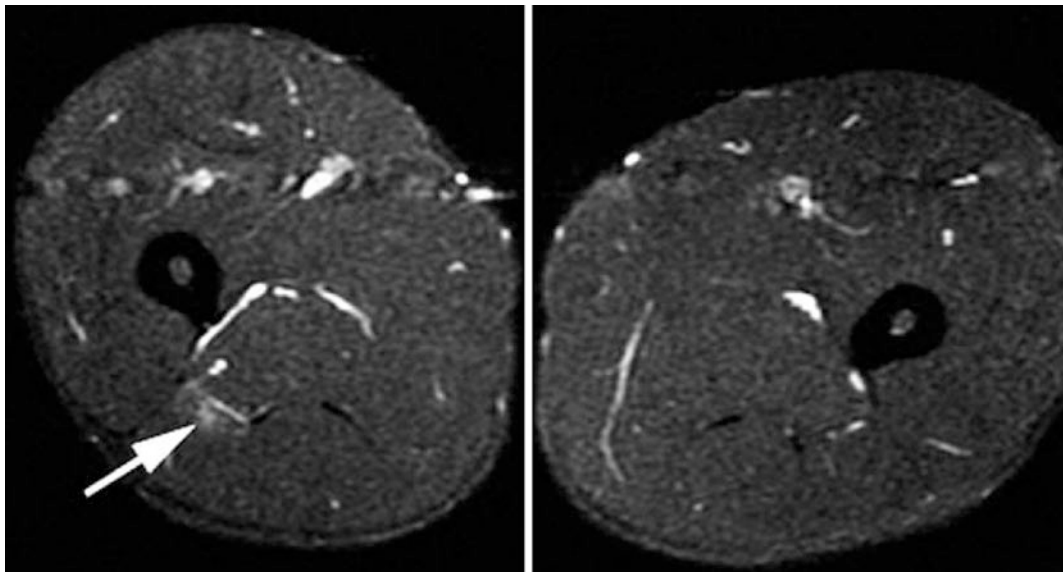

Fig. 15 Professional footballer with acute-onset thigh pain. Axial T2-weighted fat-suppressed MR image shows minor area of oedema (arrow) within the long head of biceps femoris (grade 1 injury)

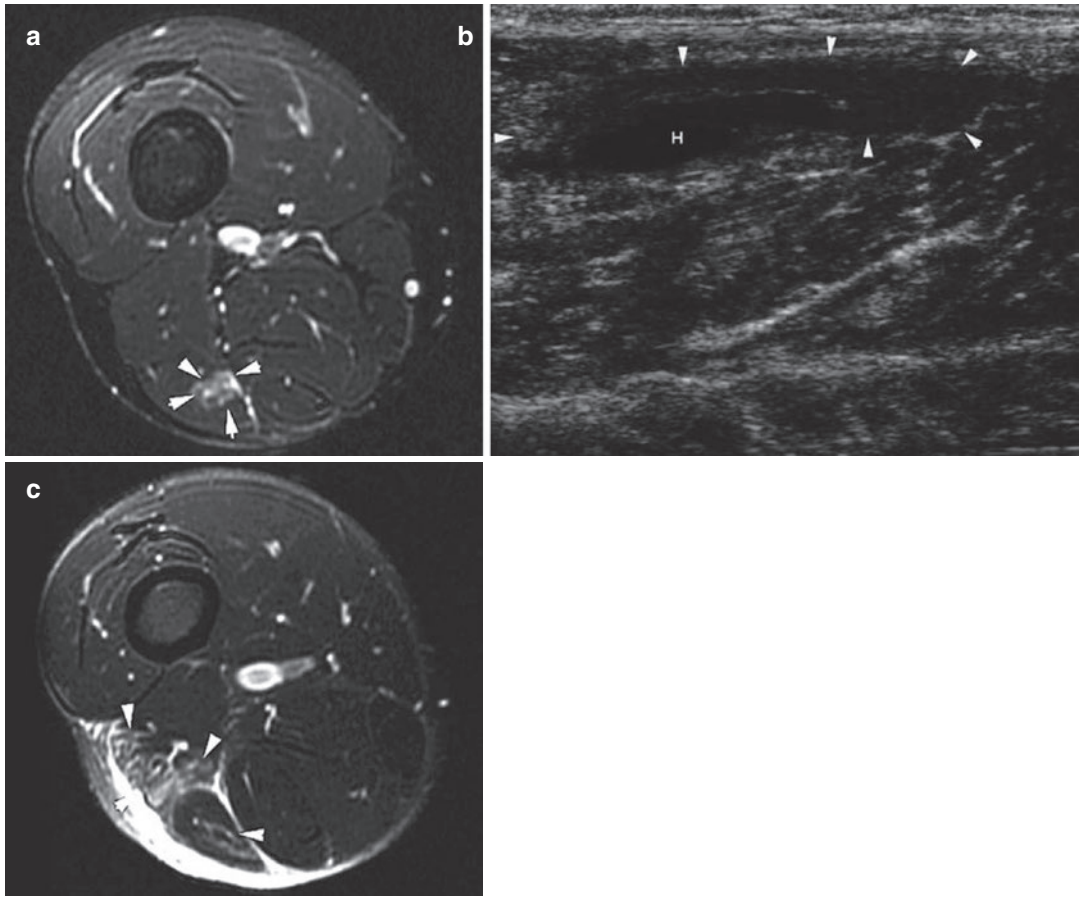

Fig. 16 (**a**–**c**) Professional footballer with recurrent hamstring injuries. (**a**) Axial T2-weighted fat-suppressed MR image from 2002 shows an acute grade 2 injury involving the long head of biceps femoris (small arrowheads). (**b**) Corresponding longitudinal ultrasound image 1 week later shows a hypoechoic haematoma (H) with an area (arrowheads) occupying 10–20% of the muscle diameter (grade 2 injury). (**c**) Axial T2-weighted fat-suppressed MR image from new injury in 2005 shows marked oedema involving the myotendinous junction of the short and long heads (arrowheads) of biceps femoris

hamstring injuries. Hamstring injuries increase during the competitive season (Hagglund et al. 2013).

Semimembranosus and semitendinosus are rarely affected on their own although isolated semitendinosus tears can occur particularly in running and jumping athletes (De Smet and Best 2000). This is thought to be secondary to sudden forced hip flexion with knee extension which is required to hurdle or perform the long jump.

Several studies have evaluated specific imaging factors for hamstring injury and subsequent time to recovery. There are numerous imaging systems for grading of acute muscle injury with the most widely used being the 'modified Peetrons' and BAMIC (British Athletics Muscle Injury Classification) methods (Pollock et al. 2014). Studies have shown that these techniques are reasonably reproducible; however their isolated use for predicting return to play is less so. Higher grade (severe) injuries do correlate with a significantly longer return to sport but the lower grades in these classifications are less discriminatory.

The British Athletics Muscle Injury Classification grades hamstring injuries from 0 to 4 based on MRI indicators of injury extent (cross-sectional area and length of injury) and classifies

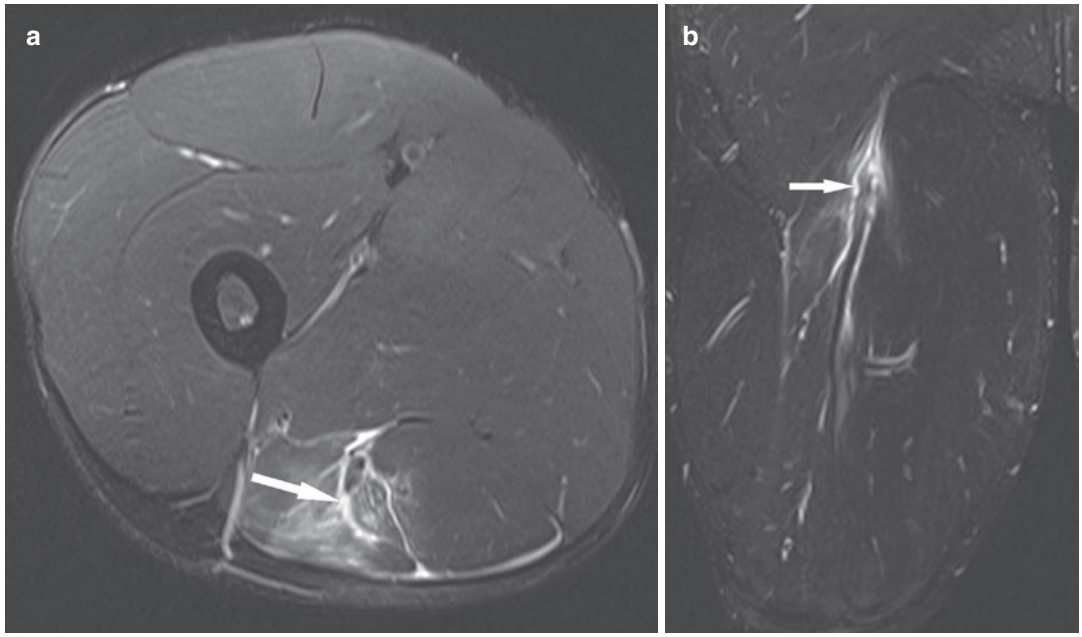

Fig. 17 (**a**, **b**) Professional footballer with acute-onset thigh pain. (**a**) Axial proton-density-weighted fat-suppressed MR image and (**b**) corresponding coronal proton-density-weighted fat-suppressed MR image demonstrate a hamstring tear (arrow) represented by a region of high signal intensity adjacent to the myotendinous junction of the long head of biceps femoris with interstitial feathery high signal. The tendon demonstrates features of laxity indicative of tendon involvement (BAMIC grade 2c injury). Moderate perifascial fluid is also present

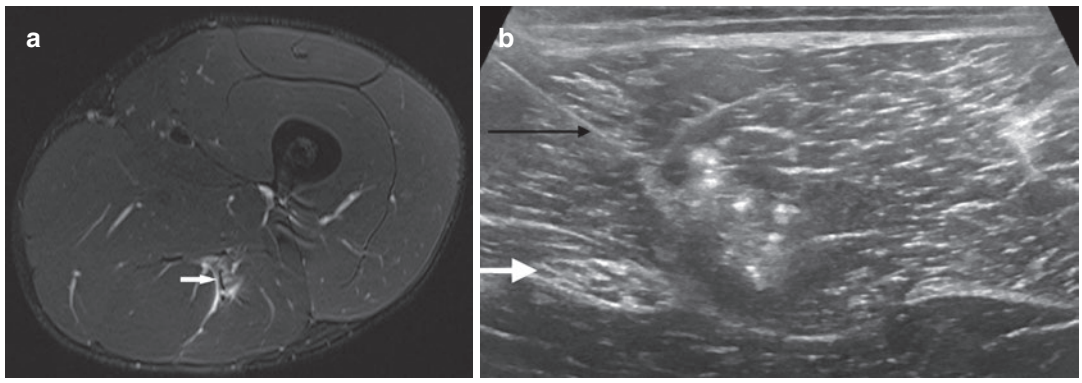

Fig. 18 (**a**) Axial proton-density-weighted fat-suppressed MR image showing a grade 2 biceps femoris tear (arrow) with oedematous change around the sciatic nerve. (**b**) Transverse ultrasound image of the conjoint tendon demonstrating a heterogeneous mass with mixed hypo- and hyperechogenicity compatible with a haematoma around the conjoint tendon. The site of tear was treated with platelet-rich plasma (PRP) injection (black arrow shows needle) as the patient was symptomatic, avoiding the sciatic nerve (arrow)

location according to their anatomical site: myofascial (a), musculotendinous (b) or intratendinous (c).

Grade 0 injuries encompass injuries that are MRI negative reflecting a focal neuromuscular injury or muscle injury consistent with DOMS. Grade 1–3 injuries are small, moderate or extensive tears of muscle tissue, respectively (Figs. 16, 17, and 18). Grade 4 injuries are complete tears to either muscle or tendon.

Hamstring injuries that are intratendinous are more prone to re-injury and result in a delay in

time to return to full training. This study also demonstrated an increased time to return to full training in the more extensive grade of tendon injury, i.e., grade 3 injury (Pollock et al. 2016).

4.2.2 Quadriceps

Rectus femoris is the most commonly injured muscle within the quadriceps group and the second or third most injured after hamstring strains (Speer et al. 1993; Peterson and Renstrom 1986; Garrett Jr. 1988; Garrett Jr. 1990; Noonan and Garrett Jr. 1999; Taylor et al. 1993; Kassarjian et al. 2014). The rectus femoris differs from the other group muscles in that it spans two joints, the hip and the knee joint, and originates from two heads (indirect and direct).

The rectus femoris outer unipennate muscle originates from the anterior aponeurosis which forms the direct tendon and attaches to the anterior inferior iliac spine. The inner bipennate muscle originates from the central aponeurosis which forms the indirect tendon and is inserted into the superior acetabular ridge and posterolateral aspect of hip joint capsule. This envelopment results in a muscle-within-a-muscle configuration.

Due to its complex anatomy and muscle-within-a-muscle structure, injuries to the rectus femoris muscle may not always be classified according to the traditional three-point muscle injury grading system.

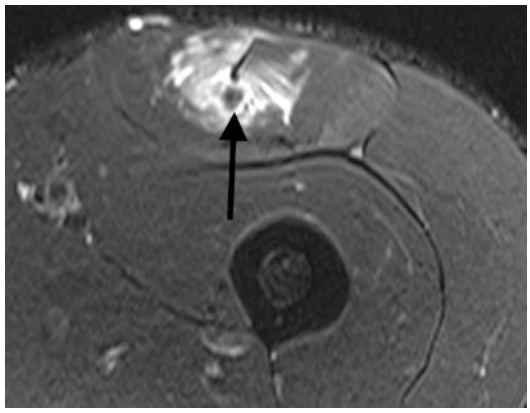

Fig. 19 Professional footballer with distal thigh pain 1 week after acute injury. Axial T2 weighted fat suppressed MR image of the mid thigh shows a region of injury centred around the myotendinous junction with feathery oedema surrounding the central tendon. There is a region of haematoma formation (arrow) also seen which is low in signal in this subacute injury

The most common site of rectus femoris injury in football involves injury of the distal myotendinous junction when the muscle belly strips from the undersurface of the distal tendon (Fig. 19).

The indirect component of rectus femoris has a long intramuscular myotendinous junction and is susceptible to a more unique longitudinally oriented injury. This results in not only myotendinous injury, but also in separation and dissociation of the inner bipennate component from the outer unipennate muscle (a type of intramuscular degloving injury), and may lead to retraction of the inner muscle belly. This degloving injury differs from the typical myotendinous injury of the indirect portion of the rectus femoris and occurs in the periphery of the fibres of inner bipennate muscle (Figs. 20 and 21) (Kassarjian et al. 2014).

4.2.3 Calf

The gastrocnemius-soleus muscles eccentrically contract to modulate dorsiflexion at the ankle during normal gait and heel strike. However, in sprinting the foot initially strikes the ground with the distal first and second rays and not the heel resulting in more forceful ankle dorsiflexion (Lees and Nolan 1998; Novacheck 1998; Sammarco and Hockenbury 2001). This muscle complex also concentrically contracts on push-off for sprinting, jumping and cutting-in.

Aponeurosis distraction is a specific type of injury which occurs at the margin of two synergistic muscles. The muscles most frequently involved are the medial head of gastrocnemius and soleus or, less commonly, semimembranosus and semitendinosus (Bianchi et al. 1998). When this involves the medial head of gastrocnemius it is known as ‘tennis leg’ (Bianchi et al. 1998; Mink 1992; Harwin and Richardson 2017). This injury typically occurs during forced dorsiflexion with the knee in extension causing powerful eccentric loading of the gastrocnemius and soleus muscles. Although in the past there has been debate over whether plantaris is primarily involved (Helms et al. 1995), larger reviews of this condition have subsequently shown little or no involvement of plantaris with the medial head

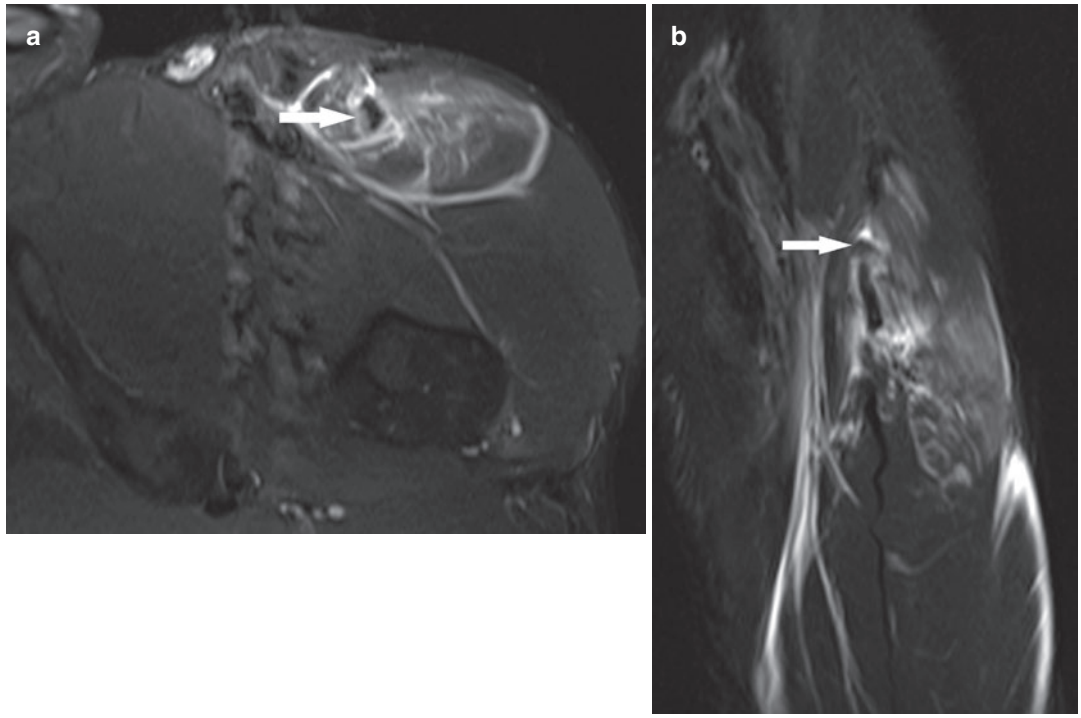

Fig. 20 (**a**, **b**) Professional footballer with severe proximal thigh pain. (**a**) Axial T2-weighted fat-suppressed MR image showing an acute tear of the myotendinous junction of the indirect head of the rectus femoris (arrow) and a heterogeneous area of intramuscular oedema. (**b**) Coronal proton-density-weighted fat-suppressed MR image shows a full-thickness tear of the indirect head of rectus femoris tendon with complete disruption of the musculotendinous junction (arrow)

of gastrocnemius being the primary site of injury with fluid between the soleus and gastrocnemius muscles (Fig. 23) (Bianchi et al. 1998; Delgado et al. 2002; Speer et al. 1993; Harwin and Richardson 2017). The aponeurosis between the two muscles is a potentially weak area as soleus consists mainly of T1 fibres and is relatively inelastic compared to the gastrocnemius which also spans two joints and consists of T2 fibres (Bianchi et al. 1998; Mink 1992). The Achilles tendon is usually not injured.

Ultrasound or MR imaging can demonstrate muscle fibre disruption adjacent to the aponeurosis and the presence of perifascial fluid and haematoma (most commonly a grade 2 injury) (Fig. 22) (Bianchi et al. 1998; Delgado et al. 2002). These injuries respond well to conservative treatment although scarring can occur in the region of the aponeurosis (Fig. 23) (Bianchi et al. 1998).

Soleus muscle injuries have been previously considered rare, potentially due to the widespread use of sonographic assessment; however, they are now felt to be more frequent than previously thought as a result of increased use of MR imaging.

Ultrasound is not sensitive enough in assessing soleus traumatic tears compared with MR imaging (Fig. 24). Injuries at the myofascial junction are more readily identified than those at the musculotendinous units. Factors which contribute to difficult visualisation and underappreciation of soleus injuries include the deep location of the soleus muscle and the fact that soleus is often extensively vascularised. Moreover, soleus injuries may be underappreciated in the context of a more superficial (and therefore easily detectable) gastrocnemius strain (Balius et al. 2014). Therefore, subtle soleus injuries may be missed sonographically. MR imaging has become the modality of choice for detection of soleus strains. Soleus injuries on MRI may be classified as musculotendinous or myofascial.

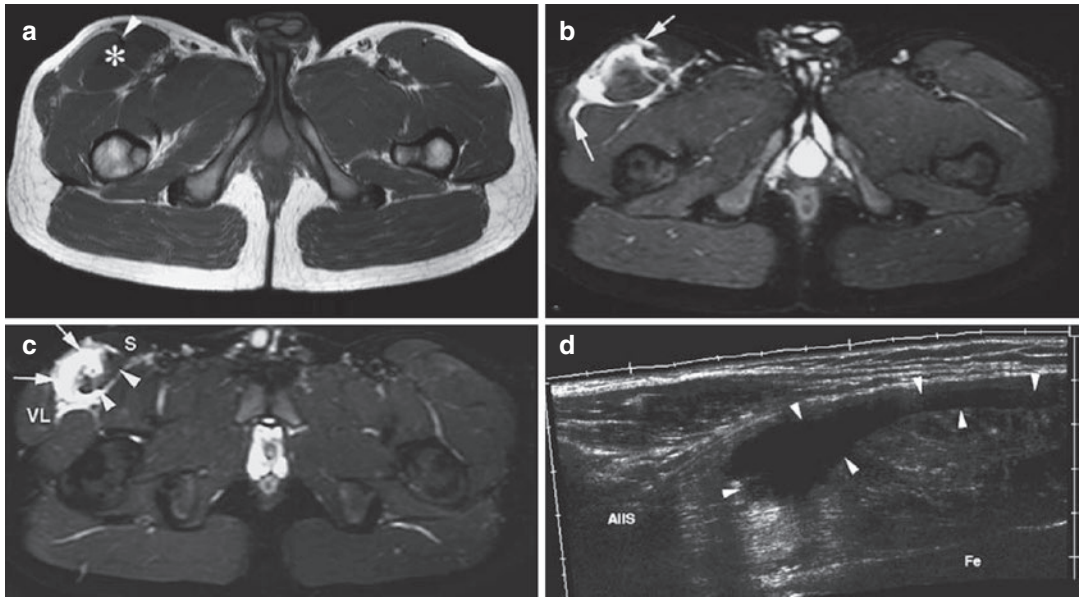

Fig. 21 (**a**–**d**) Professional footballer with severe acute proximal thigh pain. (**a**) Axial T1- and (**b**) T2-weighted fat-suppressed MR images show a swollen and oedematous proximal right rectus femoris (*), extensive perifascial fluid (arrows) and intact low-signal tendon (arrowhead). (**c**) Axial T2-weighted fat-suppressed MR image above the level of the previous images shows more extensive muscle oedema and fluid (arrows) extending towards vastus lateralis (VL) and overlying sartorius (S). A small remnant of muscle is seen intact (arrowheads). (**d**) Longitudinal extended field-of-view ultrasound image confirms grade 2 injury (arrowheads) just distal to the origin from the anterior inferior iliac spine (AIIS). The muscle deep to the area and adjacent to the femur (Fe) appears intact (arrows)

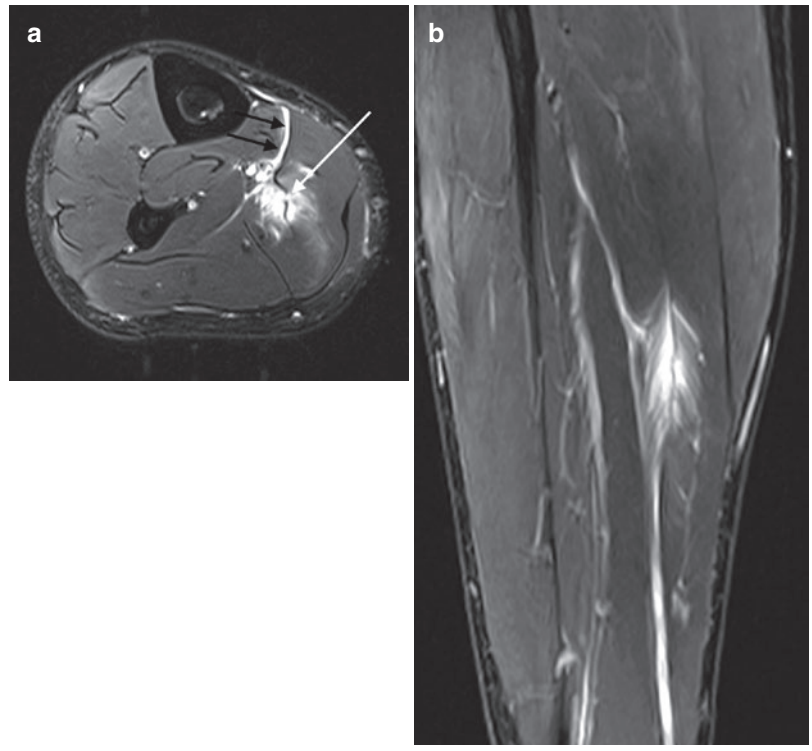

Fig. 22 (**a**, **b**) Rugby league player with acute onset calf pain. (**a**) Axial T2-weighted fat-suppressed and (**b**) sagittal T2 weighted fat suppressed MR imaging of the calf showing acute injury to the soleus myotendinous junction with muscle fibre disruption seen around the central tendon. A small tendon defect (white arrow) is seen in this grade 2c soleus injury. Haematoma formation is seen deep to the medial soleus muscle belly (black arrow)

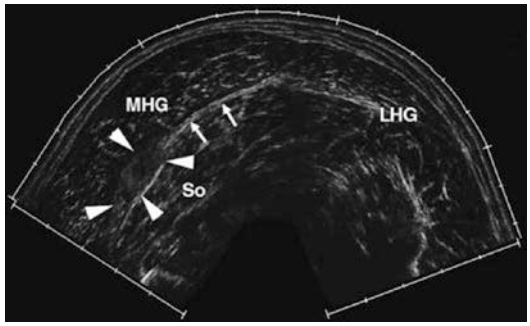

Fig. 23 Professional ballet dancer with previous calf pain and persisting swelling but relatively little symptoms. Transverse extended field-of-view ultrasound image shows a normal-appearing lateral head of gastrocnemius (LHG) but hyperechoic nodular thickening (arrowheads) between the medial head of gastrocnemius (MHG) and soleus (So). This is consistent with scar tissue and adjacent fascia appears of more normal thickness (arrows)

4.3 Delayed-Onset Muscle Soreness

Delayed-onset muscle soreness (DOMS) develops when specific muscle groups undergo unaccustomed vigorous exercise (Flores et al. 2018). This usually occurs in recreational athletes who sporadically participate in sport; however, this can also occur in professional athletes when training is intensified after injury. The aetiology of DOMS is thought to be due to increased compartment pressure and water content affecting type 2 fast-twitch fibres with resultant disruption of the Z bands of sarcomeres within the muscle (Flores et al. 2018).

Clinically diffuse lower limb muscle pain develops 12–24 h after activity and is exacerbated by eccentric contraction (Noonan and Garrett Jr. 1999; Newham et al. 1983; Zabetakis 1986). This helps to clinically differentiate DOMS from a muscle tear or strain, which usually causes immediate focal pain and is exacerbated by concentric contraction. Additionally DOMS usually resolves within 7 days without any specific treatment (Peterson and Renstrom 1986; Mink 1992).

Imaging is rarely necessary in the majority of cases (Fornage 2000) but can be useful in excluding other causes of severe pain if the clinical history is not clear. MR imaging can show oedema in multiple muscles, but this is not a specific or sensitive finding with the abnormality persisting up to 82 days after clinical resolution (Marcantonio and Cho 2000; Steinbach et al. 1998). At the early phase of injury perifascial fluid may be demonstrated. The involved muscle belly may also demonstrate diffuse muscle oedema without the feathery pattern typical of strain or perifascial fluid (Guermazi et al. 2017). Ultrasound is usually normal, but its main role is for excluding a significant muscle strain or tear, which allows appropriate rehabilitation to continue.

4.4 Muscle Contusion

Muscle contusion occurs secondary to direct nonpenetrating trauma causing muscle fibre disruption and haematoma. This usually results from muscle being compressed against bone but can also occur when superficial muscle is compressed against a contracted underlying muscle (Jarvinen et al. 2005). Muscle contusion is commonly seen in contact sports (‘dead leg’) with rectus femoris and vastus intermedius being the most affected muscles (Flores et al. 2018). It is a clinical diagnosis obtained from patient history, but on examination, compared to a severe muscle tear, muscle function is relatively normal given the degree of pain (Zarins and Ciullo 1983; Jarvinen et al. 2005; Armstrong 1984; Stauber 1988; Jackson and Feagin 1973).

4.4.1 Imaging

In a similar manner to muscle strain MR imaging or ultrasound can be used to evaluate the muscle and underlying periosteum although MR imaging is preferable if an associated bone injury is suspected. The difficulty for either imaging modality is defining if there is muscle distraction especially if the clinical history is unclear.

On ultrasound an acute contusion (0–48 h) appears ill defined with irregular margins and marked echogenic swelling of the fascicles and entire muscle (Fig. 25) (Aspelin et al. 1992). MR imaging also demonstrates oedema and mixed intrinsic signal as the blood products develop. In

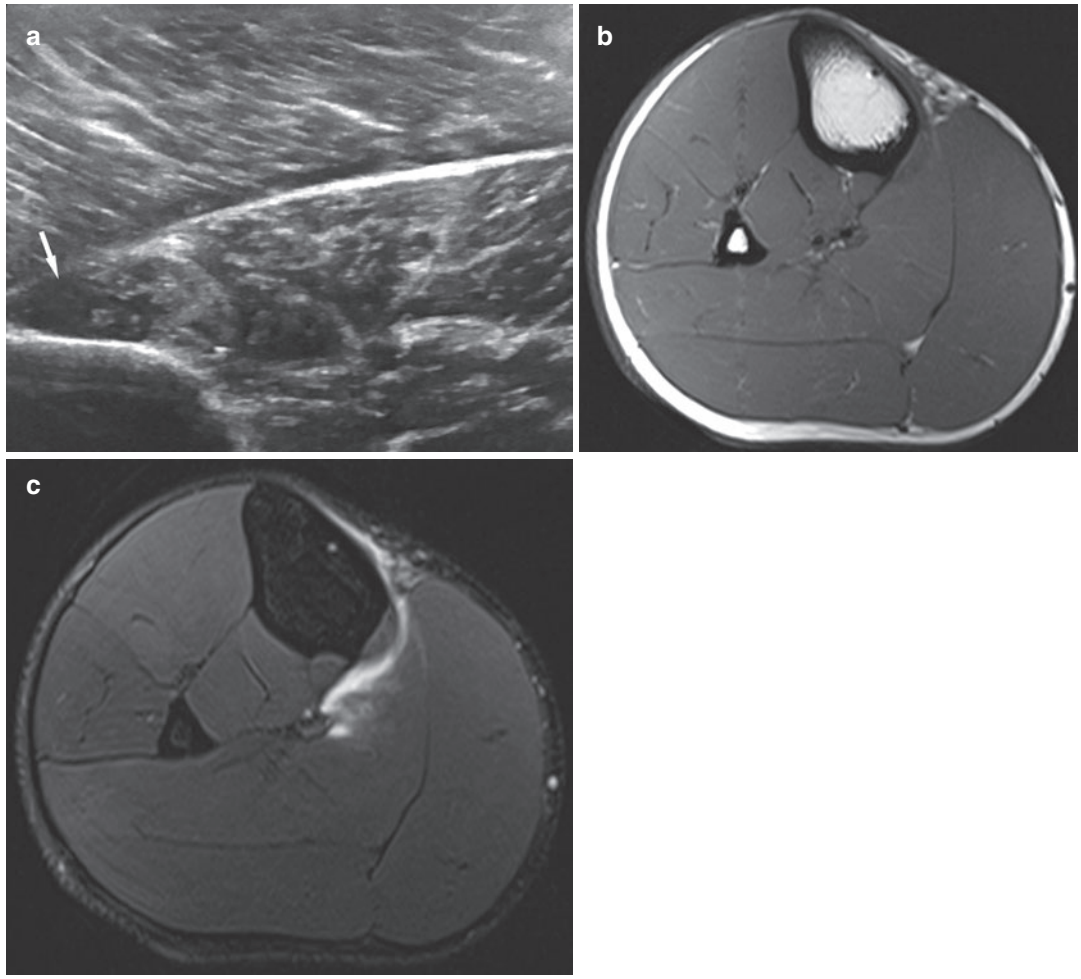

Fig. 24 (**a**–**c**) Professional rugby league player with acute calf pain. (**a**) Longitudinal ultrasound image shows subtle soleus injury with hypoechoic change abutting the posterior cortex of the tibia (arrow). (**b**) Axial T1-weighted MR image and **c** axial T2-weighted fat-suppressed MR image showing grade 2 injury of the soleus muscle with low-grade muscle fibre disruption

comparison to muscle strain, contusion is characterised by the haematoma crossing aponeurotic boundaries representing the demarcation of the impact (Robinson 2004; Van Holsbeeck and Introcasco 2001).

In severe clinical cases, dynamic ultrasound imaging may be helpful to confirm that a complete tear is not present and to document the extent of muscle damage and any retraction. At 48–72 h ultrasound appearances become better defined with the haematoma appearing hypoechoic and a clearer echogenic margin which expands centrally as the muscle repairs (Van Holsbeeck and Introcasco 2001; Robinson 2004). MR imaging also demonstrates these changes although the degree of adjacent muscle and soft-tissue oedema can persist for some time.

In the following weeks the contusion can be monitored for regeneration of muscle, scar tissue or more rarely myositis ossificans (Zarins and Ciullo 1983; Garrett Jr. 1988). However, in sporting injuries, the majority of contusions heal with normal muscle regeneration and chronic

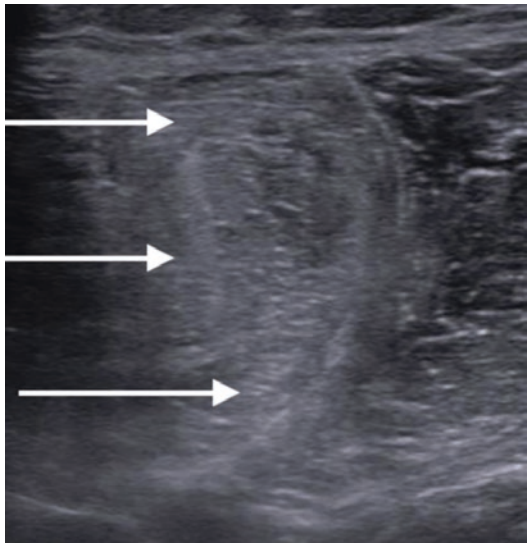

Fig. 25 Rugby player with lower leg pain following a direct impact injury. Transverse ultrasound image of the lateral aspect of the lower leg with diffuse hyperechoic change present within the peroneal muscle compartment and also in the overlying subcutaneous tissues in keeping with a muscle contusion

complications are relatively rare (Peterson and Renstrom 1986; Jarvinen et al. 2005).

5 Complications of Lower Limb Muscle Injury

5.1 Fibrous Scarring

Scar tissue can restrict muscle function resulting in reduced contractile strength increasing the risk of re-injury at the junction of the muscle and scar (Fig. 26) (Speer et al. 1993; Jarvinen et al. 2005; Taylor et al. 1993). Scar tissue, especially after hamstring tears, can also involve adjacent nervous tissue and cause referred symptoms which produce significant pain on sprinting or sudden movement (Fig. 27).

MR imaging usually defines scar tissue as a low-signal soft-tissue thickening either paralleling the tendon (Fig. 26) or with a more amorphous appearance at the muscle periphery (Fig. 27). Ultrasound detects fibrotic scarring as an echogenic focus, but dynamic stressing can assess the relative inelasticity of this tissue and any adherence to adjacent structures which is why this technique is most useful for initial evaluation in athletes (Fig. 28).

5.2 Myositis Ossificans

Myositis ossificans is a rare complication of muscle injury and usually develops after injuries associated with a large haematoma or contusion.

Clinically the development of myositis ossificans should be suspected when the degree of pain and soft-tissue swelling persists and is out of proportion to the original injury (Peterson and Renstrom 1986; Lacout et al. 2012). The commonest muscle group involved by this condition is the quadriceps, as this area is most commonly affected by muscle contusion.

Prior to the development of calcification or ossification ultrasound appearances are similar to an organising haematoma (see contusion before). However, an advantage of ultrasound is that it can depict the zone phenomenon with calcification being peripheral and centripetal (Lacout et al. 2012) and demonstrate the relatively well-defined peripheral margins and borders with adjacent soft tissues (Bodley et al. 1993; Peck and Metreweli 1988). MR imaging performed at this stage can show an extremely heterogeneous appearance with surrounding oedema that can sometimes be misinterpreted as an aggressive or even malignant process (Fig. 29) (De Smet et al. 1992; Shirkhoda et al. 1995). Ultrasound can also demonstrate peripheral calcification and ossification, as early as 2–3 weeks, before it is clearly evident on plain-film or MR imaging (Bodley et al. 1993; Peck and Metreweli 1988; Lacout et al. 2012).

5.3 Muscle Atrophy/Hypertrophy/Hernia

On MR imaging muscle atrophy shows decreased muscle bulk and increased T1-weighted signal due to fat deposition between the muscle fibres.

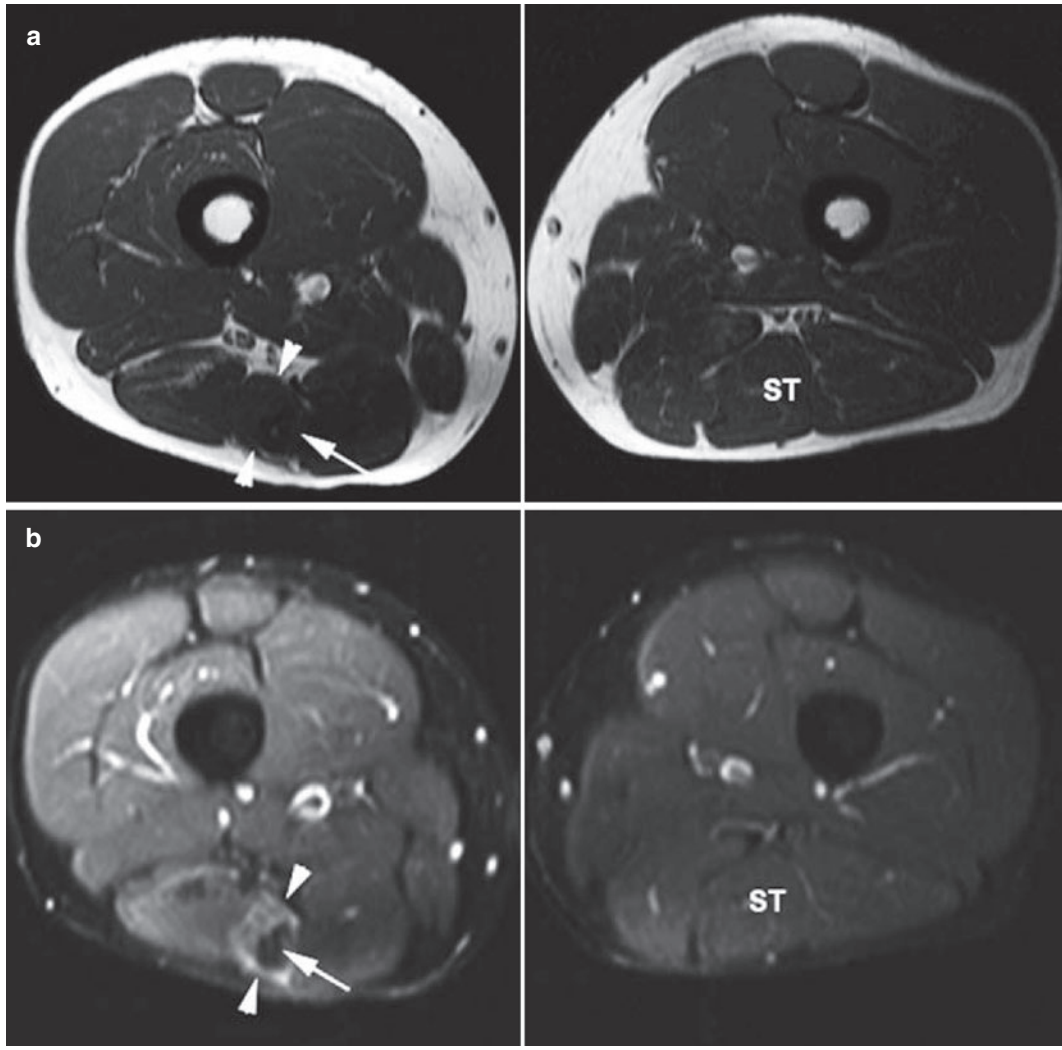

Fig. 26 (**a**, **b**) Professional footballer with previous hamstring injury complaining of recurrent pain. (**a**) Axial T1- and (**b**) T2-weighted fat-suppressed MR images show normal left semitendinosus (ST). There is reduced muscle bulk on the right, thickened (scarred) low-signal tendon (arrow) and oedema (arrowheads) within the remaining muscle indicating a retear

These features are not uncommonly seen in muscles which retear (Fig. 30). On ultrasound the muscle echotexture is increased due to fat deposition with additional loss of fascial plane definition.

A muscle hernia, also known as myofascial herniation, is defined as an abnormal protrusion of muscular tissue through a fascial defect, initially described by Richet in 1853 (Naffaa et al. 2017). This commonly occurs in the anterior and lateral muscle groups of the lower leg (especially tibialis anterior) (Fig. 31) but is also recognised within peroneus longus, peroneus brevis, extensor digitorum longus, gastrocnemius and flexor digitorum longus (Bianchi et al. 1995). It is thought that the fascia overlying tibialis anterior has an area of potential weakness due to penetrating branches of the peroneal nerve and vessels (Khaladkar et al. 2016).

The hernia usually presents as a mass which may only appear after exercise or on standing (Bianchi et al. 1995). The hernia may be painful

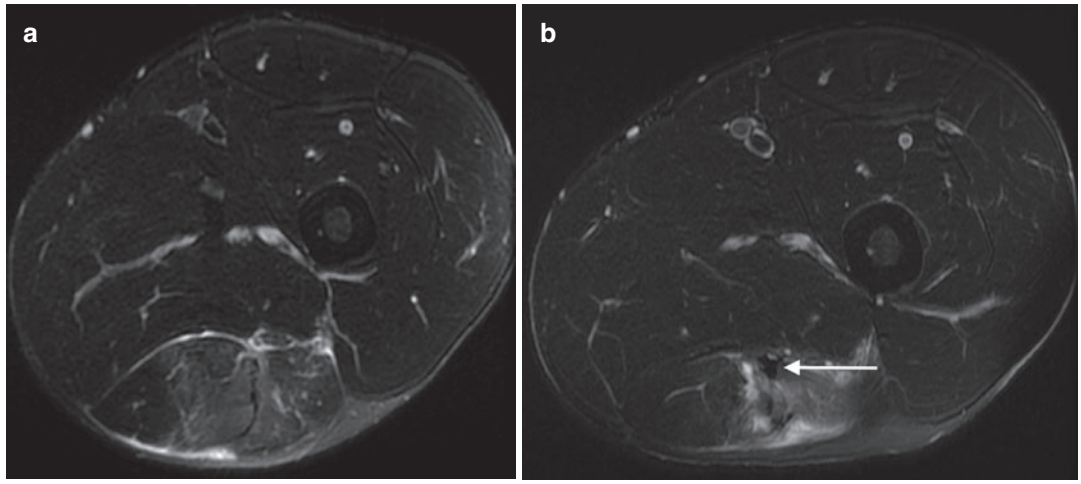

Fig. 27 (**a**, **b**) Professional footballer with previous hamstring injury. (**a**) Axial proton-density-weighted fat-suppressed MR image showing conjoint tendon injury with oedema and (**b**) axial proton-density-weighted fat-suppressed MR image obtained 6 weeks after the initial injury showing a further acute injury at the same site where there is thickening of the tendon (white arrow) at the site of previous healing

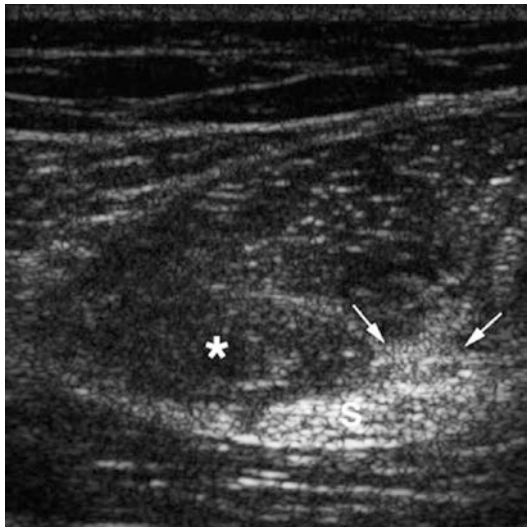

Fig. 28 Professional football player with previous hamstring tear and leg pain on sprinting. Transverse ultrasound image shows peripheral echogenic scar tissue (arrows) of semitendinosus adherent to the sciatic nerve (S) with some loss of the normal muscle echotexture (*) due to previous injury

on exertion and the clinical differential diagnosis includes an incompetent perforating vein or chronic exertional compartment syndrome.

Ultrasound can accurately identify the normal thick echogenic muscle fascia with any defect seen as a hypoechoic gap (Fig. 31) (Bianchi et al. 1995). Dynamic manoeuvres (using a gel stand-off) can be performed to reproduce the muscle hernia if it is currently reduced. On acute herniation the muscle may appear hyperechoic due to compression of the fascial planes within it. However, if chronic it may appear hypoechoic and ill defined due to a degree of oedema (Bianchi et al. 1995). MR imaging can demonstrate a hernia if present at rest but may be relatively ineffective in demonstrating small or exertional lesions (Bianchi et al. 1995; Steinbach et al. 1998).

5.4 Morel-Lavallée Lesion and Periosteal Haematoma

5.4.1 Morel-Lavallée Lesion

Athletes can develop Morel-Lavallée lesion through contact injuries most commonly in football and rugby when tackling involves the lower limb. The injury is usually a direct force which causes a shearing injury between the subcutaneous fat and underlying deep fascia and muscles. The areas most commonly affected are the lateral hip where the overlying subcutaneous fat may shear from the tensor fascia lata and the anteromedial or anterolateral knee where the fat shears

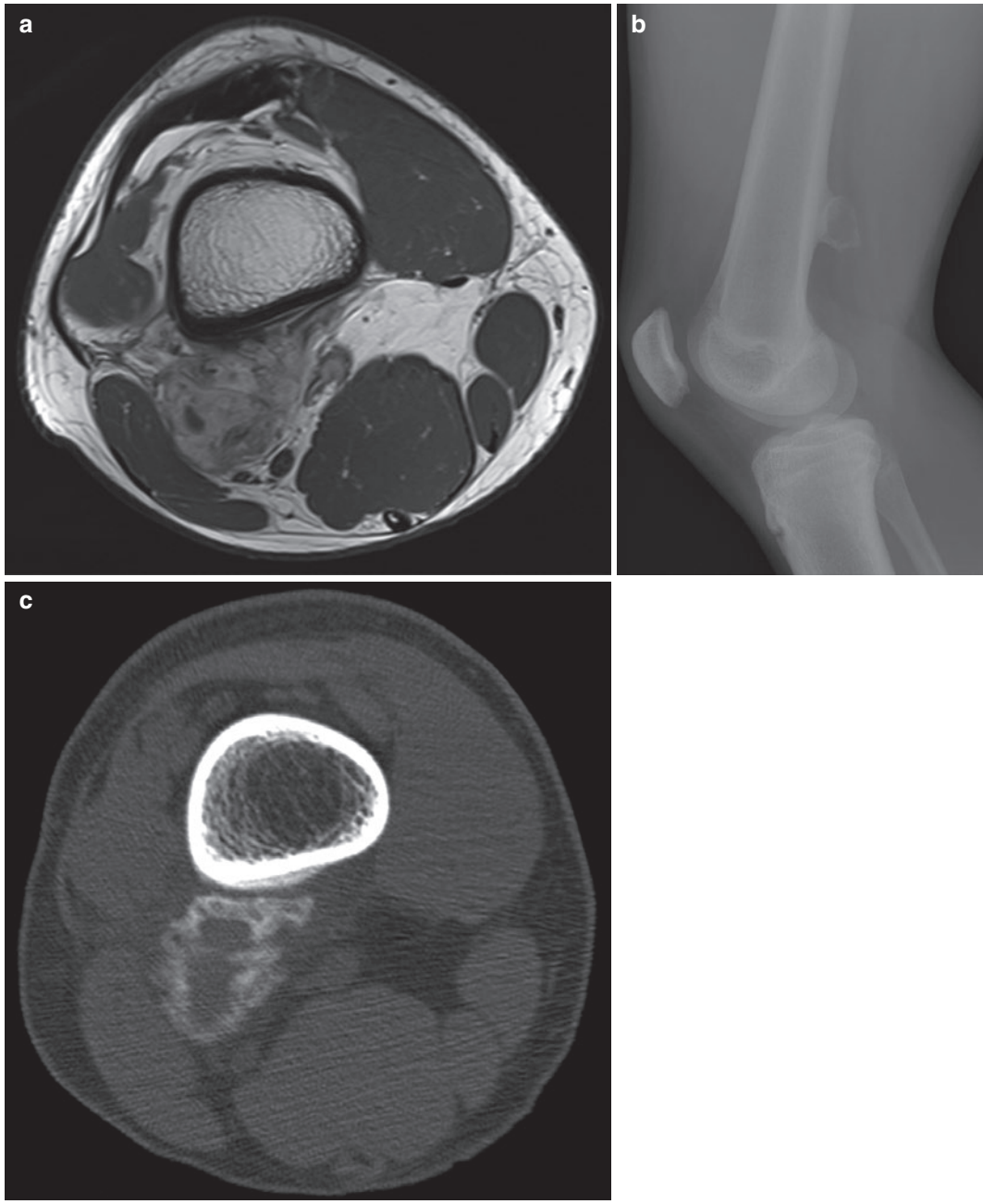

Fig. 29 (**a**–**c**) Painful rapidly growing mass in a professional footballer following previous direct blow to the distal hamstring region. (**a**) Axial T1-weighted MR image showing a hyperintense mass abutting the posterior femoral cortex. (**b**) Lateral radiograph of the thigh shows an ossified lesion with a noncalcified central area arising from the posterior cortex of the femur. (**c**) Axial CT image showing a mass typical of myositis ossificans in the posterior thigh muscles, with peripheral ossification

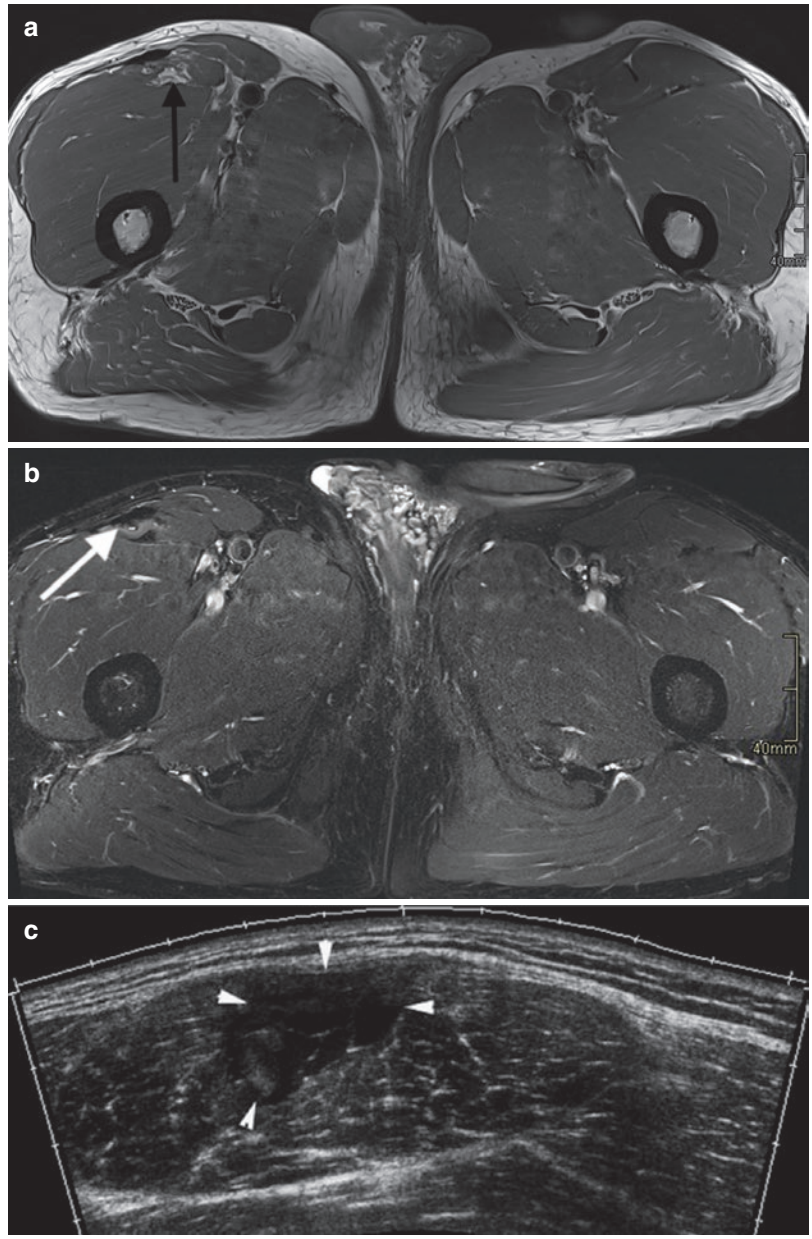

Fig. 30 (**a**, **b**) Triathlete with previous high grade right sided proximal rectus femoris injury. (**a**) T2 weighted fat suppressed axial MR imaging shows here is thickening of the rectus femoris tendon at the site of previous injury (arrow). (**b**) T2 weighted axial imaging - there is adjacent fat atrophy change within the muscle around the myotendinous junction and relative loss of muscle bulk

from the underlying vastus retinaculum and extensor mechanism (Robinson et al. 2008). During the acute phase, ultrasound shows haematoma and oedema between fascia and fat. The underlying muscles often appear normal. Individual fat lobules can be visualised as separated by blood products and fluid and over time a pseudocapsule may form (Mclean and Popovic 2017). The resulting mass has been named a Morel-Lavallée lesion. Appearances are variable but are generally hypoechoic with hyper- and hypoechoic fat lobules separated by septa and hypoechoic fluid, surrounded by the hyperechoic pseudocapsule. MRI shows fluid and fat oedema at the fascial interface with subcutaneous haemorrhage in the acute phase (Fig. 32). Sedimentation of blood components can also result in a fluid-fluid levels. Slow growth can occur over time due to reaccumulation of fluid and the appearance, along with the associated pain, can be

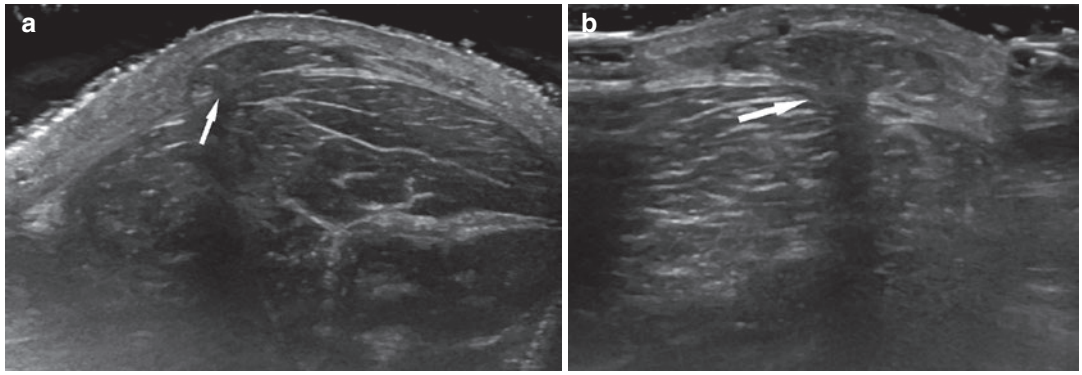

Fig. 31 (**a**) Transverse and (**b**) longitudinal ultrasound images of the anterolateral aspect of the leg showing an acute muscle hernia in a professional footballer after blunt trauma of the anterolateral aspect of the leg. Protrusion of the extensor digitorum longus muscle through a defect in the overlying fascia is shown (arrow)

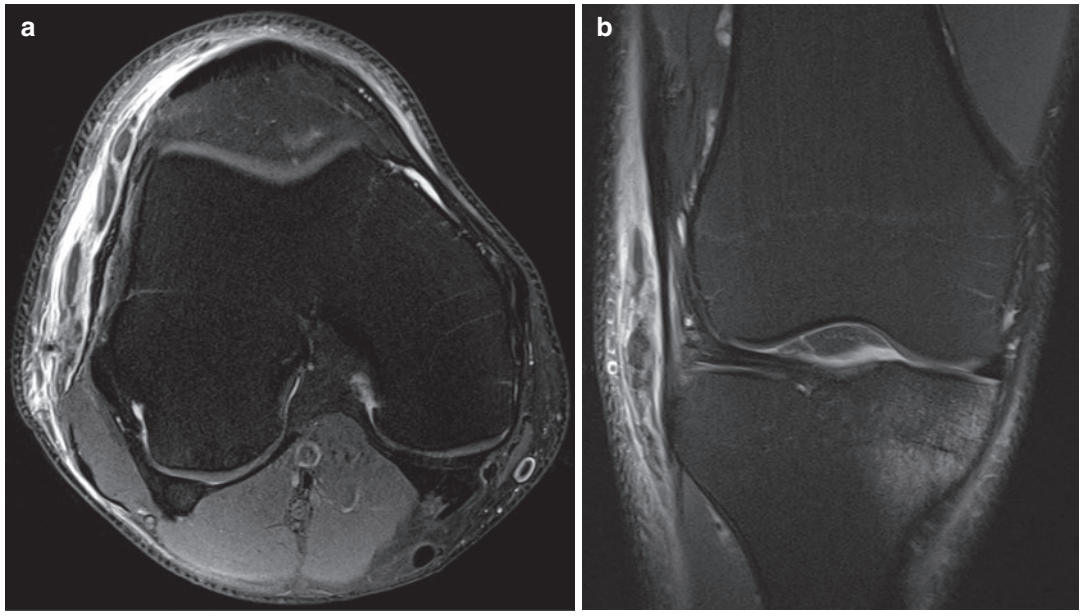

Fig. 32 (**a**, **b**) Pain and swelling of the lateral knee in a professional footballer caused by a chronic haematoma after a sheering injury. (**a**) Axial proton-density-weighted fat-suppressed MR image and (**b**) coronal proton-density fat-suppressed MR image showing a Morel-Lavallée lesion located over the lateral aspect of the knee with areas of heterogeneous hyperintensity and septa formation secondary to shearing of the subcutaneous tissues away from underlying fascia

misdiagnosed as soft-tissue tumour, particularly if the trauma has been omitted from the history. Chronic lesions may develop a fibrous pseudocapsule and calcify with reaccumulation of fluid causing growth. MRI may be useful to further evaluate uncertain cases, as is follow-up interval scanning.

5.5 Periosteal Haematoma

Periosteal haematoma may be seen after a direct-impact injury and represents a collection of blood underneath the periosteum. The imaging findings are initially of smooth periosteal reaction which matures over time, often with associated new

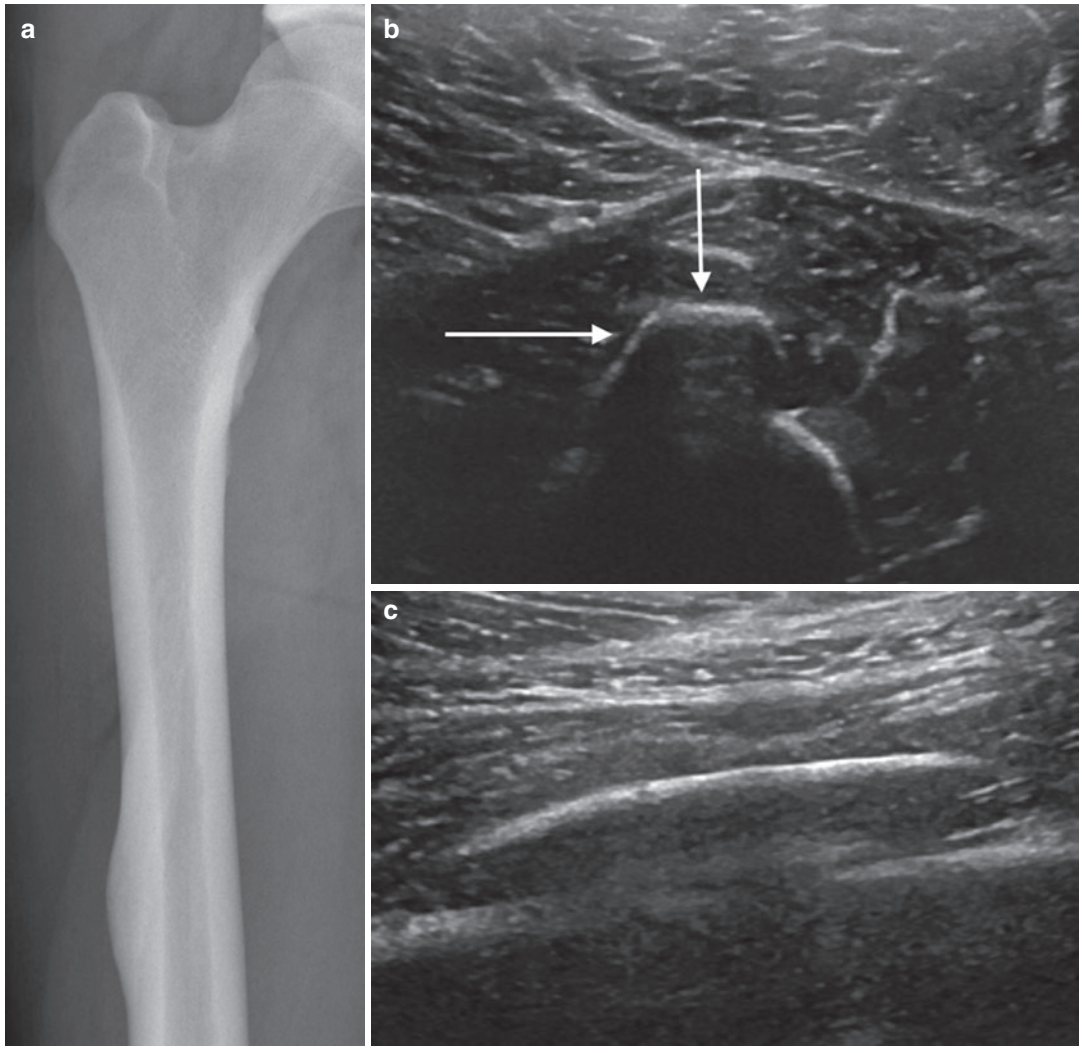

Fig. 33 (**a**–**c**) Pain in the quadriceps compartment 2 months following direct-impact injury. (**a**) Plain-film and (**b**, **c**) **u**ltrasound images showing periosteal haematoma within the mid-shaft of the femur. There is smooth, well-established periosteal reaction. The adjacent musculature images normally

bone formation. Imaging may be helpful in order to differentiate between myositis ossificans and periosteal haematoma (Fig. 33).

6 Conclusion

Imaging injuries in high-level athletes is a complex but rewarding process as the diagnosis can markedly influence treatment and performance. There are a number of imaging techniques available for evaluating lower limb osseous and soft-tissue injuries, and choice can be limited by local availability and radiologist preference. The radiologists' role in assessing injury is to grade the severity and extent of injury so appropriate treatment can be implemented.

In acute osseous injuries, radiographs are usually sufficient to confirm or exclude immediate severe injury. In acute and overuse injuries of the leg and calf, several imaging modalities play a role in depicting findings, with US and MR imaging being the most frequently utilised.

Each of the modalities has both strengths and weaknesses and the utility of each will depend

upon the particular clinical scenario and the question which needs to be answered. Ultimately more than one imaging modality may be needed in conjunction with clinical examination in order to best assess overuse injuries of the leg and calf.

Things to Remember

1. The lower limb is essential for all athletic movements and is the most commonly injured area for all sporting activities.
2. Radiographs are the first-line imaging investigation for evaluating acute osseous injury but MR imaging is a sensitive technique for acute complications and overuse injuries.
3. MR imaging and ultrasound are both accurate techniques for assessing acute and chronic soft-tissue injuries as well as subsequent complications.
   (a) Ultrasound provides a rapid and dynamic assessment.
   (b) MR imaging is sensitive for very-low-grade injuries and also maintains its field of view in athletes with large muscle bulk or diffuse symptoms.

7 Boxes

Box 1: Acute Osseous Injury

Radiographs—sufficient in majority of cases.

CT—to define complex fracture patterns prior to treatment.

MRI—for suspected radiographically occult injuries.

Box 2: Chronic Osseous Stress

MRI most useful for defining the severity of cortical and bone marrow changes.

Radiographs—usually negative but performed initially.

CT—can be helpful in ruling out a cortical fracture.

Isotope bone scanning—sensitive but lacks spatial resolution compared to MRI.

Box 3: Acute Lower Limb Muscle Injury

Ultrasound—accurate, fast and dynamic. Particularly useful in differentiating large grade 2 from grade 3 injuries. Can be negative in very-low-grade injury.

MRI—accurate and useful in athletes with large muscle bulk or diffuse symptoms.

Box 4: Complications of Muscle Injury

Ultrasound—particularly useful in diagnosing early myositis ossificans, muscle hernias and adherence of scar tissue.

MRI—particularly useful in defining subtle atrophic changes.

Acknowledgments The author would like to thank Drs. P. Bearcroft, A.J. Grainger and P.J. O'Connor for contributing images to this chapter.

References

Anderson MW, Ugalde V, Batt M, Gacayan J (1997) Shin splints: MR appearance in a preliminary study. Radiology 204:177–180

Armstrong RB (1984) Mechanisms of exercise-induced delayed onset muscular soreness: a brief review. Med Sci Sports Exerc 16:529–538

Aspelin P, Ekberg O, Thorsson O, Wilhelmsson M, Westlin N (1992) Ultrasound examination of soft tissue injury of the lower limb in athletes. Am J Sports Med 20:601–603

Atilla S, Ilgit ET, Akpek S, Yucel C, Tali ET, Isik S (1998) MR imaging and MR angiography in popliteal artery entrapment syndrome. Eur Radiol 8:1025–1029

Balius R, Rodas G, Pedret C, Capdevila L, Alomar X, Bong DA (2014) Soleus muscle injury: sensitivity of ultrasound patterns. Skelet Radiol 43:805–812

Batt ME, Ugalde V, Anderson MW, Shelton DK (1998) A prospective controlled study of diagnostic imaging for acute shin splints. Med Sci Sports Exerc 30:1564–1571

Bianchi S, Abdelwahab IF, Mazzola CG, Ricci G, Damiani S (1995) Sonographic examination of muscle herniation. J Ultrasound Med 14:357–360

Bianchi S, Martinoli C, Abdelwahab IF, Derchi LE, Damiani S (1998) Sonographic evaluation of tears of the gastrocnemius medial head ("tennis leg"). J Ultrasound Med 17:157–162

Boden BP, Lohnes JH, Nunley JA, Garrett WE Jr (1999) Tibia and fibula fractures in soccer players. Knee Surg Sports Traumatol Arthrosc 7:262–266

Bodley R, Jamous A, Short D (1993) Ultrasound in the early diagnosis of heterotopic ossification in patients with spinal injuries. Paraplegia 31:500–506

Bonasia DE, Rosso F, Cottino U, Rossi R (2015) Exercise-induced leg pain. Asia Pac J Sports Med Arthrosc Rehabil Technol 2:73–84

Chang WR, Kapasi Z, Daisley S, Leach WJ (2007) Tibial shaft fractures in football players. J Orthop Surg Res 2:11

Chernoff DM, Walker AT, Khorasani R, Polak JF, Jolesz FA (1995) Asymptomatic functional popliteal artery entrapment: demonstration at MR imaging. Radiology 195:176–180

Chhabra A, Faridian-Aragh N, Chalian M, Soldatos T, Thawait SK, Williams EH, Andreisek G (2012) High-resolution 3-T MR neurography of peroneal neuropathy. Skelet Radiol 41:257–271

Chomiak J, Junge A, Peterson L, Dvorak J (2000) Severe injuries in football players. Influencing factors. Am J Sports Med 28:S58–S68

Collins PS, Mcdonald PT, Lim RC (1989) Popliteal artery entrapment: an evolving syndrome. J Vasc Surg 10:484–489; discussion 489–90.

Connell DA, Schneider-Kolsky ME, Hoving JL, Malara F, Buchbinder R, Koulouris G, Burke F, Bass C (2004) Longitudinal study comparing sonographic and MRI assessments of acute and healing hamstring injuries. AJR Am J Roentgenol 183:975–984

Cross TM, Gibbs N, Houang MT, Cameron M (2004) Acute quadriceps muscle strains: magnetic resonance imaging features and prognosis. Am J Sports Med 32:710–719

De Smet AA, Best TM (2000) MR imaging of the distribution and location of acute hamstring injuries in athletes. AJR Am J Roentgenol 174:393–399

De Smet AA, Norris MA, Fisher DR (1992) Magnetic resonance imaging of myositis ossificans: analysis of seven cases. Skelet Radiol 21:503–507

Delgado GJ, Chung CB, Lektrakul N, Azocar P, Botte MJ, Coria D, Bosch E, Resnick D (2002) Tennis leg: clinical US study of 141 patients and anatomic investigation of four cadavers with MR imaging and US. Radiology 224:112–119

Draghi F, Zacchino M, Canepari M, Nucci P, Alessandrino F (2013) Muscle injuries: ultrasound evaluation in the acute phase. J Ultrasound 16:209–214

Dvorak J, Junge A (2000) Football injuries and physical symptoms. A review of the literature. Am J Sports Med 28:S3–S9

Edwards PH Jr, Wright ML, Hartman JF (2005) A practical approach for the differential diagnosis of chronic leg pain in the athlete. Am J Sports Med 33:1241–1249

Ekstrand J, Hagglund M, Walden M (2011) Injury incidence and injury patterns in professional football: the Uefa injury study. Br J Sports Med 45:553–558

Elias DA, White LM, Rubenstein JD, Christakis M, Merchant N (2003) Clinical evaluation and MR imaging features of popliteal artery entrapment and cystic adventitial disease. AJR Am J Roentgenol 180:627–632

Flores DV, Mejia Gomez C, Estrada-Castrillon M, Smitaman E, Pathria MN (2018) MR imaging of muscle trauma: anatomy, biomechanics, pathophysiology, and imaging appearance. Radiographics 38:124–148

Fornage BD (2000) The case for ultrasound of muscles and tendons. Semin Musculoskelet Radiol 4:375–391

Fredericson M, Bergman AG, Hoffman KL, Dillingham MS (1995) Tibial stress reaction in runners. Correlation of clinical symptoms and scintigraphy with a new magnetic resonance imaging grading system. Am J Sports Med 23:472–481

Fuller CW, Smith GL, Junge A, Dvorak J (2004) The influence of tackle parameters on the propensity for injury in international football. Am J Sports Med 32:43S–53S

Gaeta M, Minutoli F, Scribano E, Ascenti G, Vinci S, Bruschetta D, Magaudda L, Blandino A (2005) CT and MR imaging findings in athletes with early tibial stress injuries: comparison with bone scintigraphy findings and emphasis on cortical abnormalities. Radiology 235:553–561

Gaeta M, Minutoli F, Mazziotti S, Visalli C, Vinci S, Gaeta F, Blandino A (2008) Diagnostic imaging in athletes with chronic lower leg pain. AJR Am J Roentgenol 191:1412–1419

Garrett WE Jr (1988) Injuries to the muscle-tendon unit. Instr Course Lect 37:275–282

Garrett WE Jr (1990) Muscle strain injuries: clinical and basic aspects. Med Sci Sports Exerc 22:436–443

Garrett WE Jr, Califf JC, Bassett FH 3rd (1984) Histochemical correlates of hamstring injuries. Am J Sports Med 12:98–103

Garrett WE Jr, Safran MR, Seaber AV, Glisson RR, Ribbeck BM (1987) Biomechanical comparison of stimulated and nonstimulated skeletal muscle pulled to failure. Am J Sports Med 15:448–454

Giza E, Fuller C, Junge A, Dvorak J (2003) Mechanisms of foot and ankle injuries in soccer. Am J Sports Med 31:550–554

Green NE, Rogers RA, Lipscomb AB (1985) Nonunions of stress fractures of the tibia. Am J Sports Med 13:171–176

Guermazi A, Roemer FW, Robinson P, Tol JL, Regatte RR, Crema MD (2017) Imaging of muscle injuries in sports medicine: sports imaging series. Radiology 285:1063

Hagglund M, Walden M, Ekstrand J (2013) Risk factors for lower extremity muscle injury in professional soccer: the UEFA injury study. Am J Sports Med 41:327–335

Hai Z, Guangrui S, Yuan Z, Zhuodong X, Cheng L, Jingmin L, Yun S (2008) CT angiography and MRI in patients with popliteal artery entrapment syndrome. AJR Am J Roentgenol 191:1760–1766

Harwin JR, Richardson ML (2017) "Tennis leg": gastrocnemius injury is a far more common cause than plantaris rupture. Radiol Case Rep 12:120–123

Hawkins RD, Hulse MA, Wilkinson C, Hodson A, Gibson M (2001) The association football medical research programme: an audit of injuries in professional football. Br J Sports Med 35:43–47

Helms CA, Fritz RC, Garvin GJ (1995) Plantaris muscle injury: evaluation with MR imaging. Radiology 195:201–203

Ilahi OA, Younas SA, Labbe MR, Edson SB (2003) Prevalence of ganglion cysts originating from the proximal tibiofibular joint: a magnetic resonance imaging study. Arthroscopy 19:150–153

Jackson DW, Feagin JA (1973) Quadriceps contusions in young athletes. Relation of severity of injury to treatment and prognosis. J Bone Joint Surg Am 55:95–105

Jarraya M, Hayashi D, Roemer FW, Crema MD, Diaz L, Conlin J, Marra MD, Jomaah N, Guermazi A (2013) Radiographically occult and subtle fractures: a pictorial review. Radiol Res Pract 2013:370169

Jarvinen TA, Jarvinen TL, Kaariainen M, Kalimo H, Jarvinen M (2005) Muscle injuries: biology and treatment. Am J Sports Med 33:745–764

Karantanas AH (2021) Natural history and monitoring of fractures and microfractures. Med Radiol https://doi.org/10.1007/174_2020_271

Kassarjian A, Rodrigo RM, Santisteban JM (2014) Intramuscular degloving injuries to the rectus femoris: findings at MRI. AJR Am J Roentgenol 202:W475–W480

Kaufman KR, Brodine S, Shaffer R (2000) Military training-related injuries: surveillance, research, and prevention. Am J Prev Med 18:54–63

Khaladkar SM, Kondapavuluri SK, Kamal A, Kalra R, Kamal V (2016) Detection of myofascial herniation on dynamic sonography and magnetic resonance imaging. Case Rep Radiol 2016:4245189

Labmayr V, Aliabadi A, Tiesenhausen K, Brodmann M, Schmid F, Moore D (2019) Popliteal artery entrapment syndrome (PAES) in a 17-year-old adolescent. Case Rep Vasc Med 2019:8540631

Lacout A, Jarraya M, Marcy PY, Thariat J, Carlier RY (2012) Myositis ossificans imaging: keys to successful diagnosis. Indian J Radiol Imaging 22:35–39

Lees A, Nolan L (1998) The biomechanics of soccer: a review. J Sports Sci 16:211–234

Lefere M, Demeyere A, Vanhoenacker F (2021) Overuse bone trauma and stress fractures. Med Radiol https://doi.org/10.1007/174_2020_240

Marcantonio DR, Cho GJ (2000) Focus on muscle in orthopedic MRI. Semin Musculoskelet Radiol 4:421–434

Martens MA, Backaert M, Vermaut G, Mulier JC (1984) Chronic leg pain in athletes due to a recurrent compartment syndrome. Am J Sports Med 12:148–151

Mclean K, Popovic S (2017) Morel-Lavallee lesion: AIRP best cases in radiologic-pathologic correlation. Radiographics 37:190–196

Milgrom C, Chisin R, Giladi M, Stein M, Kashtan H, Margulies J, Atlan H (1984) Negative bone scans in impending tibial stress fractures. A report of three cases. Am J Sports Med 12:488–491

Mink JH (1992) Muscle injuries. In: Deutsch A, Mink JH, Kerr R (eds) MRI of the foot and ankle, 1st edn. Raven Press, New York

Miskovsky S, Kaeding C, Weis L (2004) Proximal tibiofibular joint ganglion cysts: excision, recurrence, and joint arthrodesis. Am J Sports Med 32:1022–1028

Naffaa L, Moukaddam H, Samim M, Lemieux A, Smitaman E (2017) Semimembranosus muscle herniation: a rare case with emphasis on muscle biomechanics. Skelet Radiol 46:373–378

Newham DJ, Mills KR, Quigley BM, Edwards RH (1983) Pain and fatigue after concentric and eccentric muscle contractions. Clin Sci (Lond) 64:55–62

Nicholas J, Hershman E (1986) The lower extremity and spine in sports medicine. Mosby, St Louis

Nicolaou S, Liang T, Murphy DT, Korzan JR, Ouellette H, Munk P (2012) Dual-energy CT: a promising new technique for assessment of the musculoskeletal system. AJR Am J Roentgenol 199:S78–S86

Noonan TJ, Garrett WE Jr (1999) Muscle strain injury: diagnosis and treatment. J Am Acad Orthop Surg 7:262–269

Nordin M, Frankel VH (2001a) Biomechanics of bone. In: Nordin M, Frankel VH (eds) Basic biomechanics of the musculoskeletal system, 3rd edn. Lippincott Williams and Wilkins, Philadelphia

Nordin M, Frankel VH (2001b) Biomechanics of skeletal muscle. In: Nordin M, Frankel VH (eds) Basic biomechanics of the musculoskeletal system, 3rd edn. Lippincott Williams and Wilkins, Philadelphia

Novacheck TF (1998) The biomechanics of running. Gait Posture 7:77–95

Ohta-Fukushima M, Mutoh Y, Takasugi S, Iwata H, Ishii S (2002) Characteristics of stress fractures in young athletes under 20 years. J Sports Med Phys Fitness 42:198–206

Peck RJ, Metreweli C (1988) Early myositis ossificans: a new echographic sign. Clin Radiol 39:586–588

Peterson L, Renstrom P (1986) Sports injuries. Year Book Medical, Chicago

Pollock N, James SL, Lee JC, Chakraverty R (2014) British athletics muscle injury classification: a new grading system. Br J Sports Med 48:1347–1351

Pollock N, Patel A, Chakraverty J, Suokas A, James SL, Chakraverty R (2016) Time to return to full training is delayed and recurrence rate is higher in intratendinous ('c') acute hamstring injury in elite track and field athletes: clinical application of the British Athletics Muscle Injury Classification. Br J Sports Med 50:305–310

Purohit NB, King LJ (2015) Ultrasound of lower limb sports injuries. Ultrasound 23:149–157

Rich NM, Collins GJ Jr, Mcdonald PT, Kozloff L, Clagett GP, Collins JT (1979) Popliteal vascular entrapment. Its increasing interest. Arch Surg 114:1377–1384

Ringler MD, Litwiller DV, Felmlee JP, Shahid KR, Finnoff JT, Carter RE, Amrami KK (2013) Mri accurately detects chronic exertional compartment syndrome: a validation study. Skelet Radiol 42:385–392

Robertson GA, Wood AM (2017) Femoral neck stress fractures in sport: a current concepts review. Sports Med Int Open 1:E58–E68

Robinson P (2004) Ultrasound of muscle injury. In: Mcnally E (ed) Practical musculoskeletal ultrasound. Churchill Livingston, London

Robinson P, Farrant JM, Bourke G, Merchant W, Mckie S, Horgan KJ (2008) Ultrasound and MRI findings in appendicular and truncal fat necrosis. Skelet Radiol 37:217–224

Rubin DA (2012) Imaging diagnosis and prognostication of hamstring injuries. AJR Am J Roentgenol 199:525–533

Sammarco GJ, Hockenbury RT (2001) Biomechanics of the foot and ankle. In: Nordin M, Frankel VH (eds) Basic biomechanics of the musculoskeletal system, 3rd edn. Lipponcott Williams and Wilkins, Philadelphia

Shellock FG, Fukunaga T, Mink JH, Edgerton VR (1991) Exertional muscle injury: evaluation of concentric versus eccentric actions with serial MR imaging. Radiology 179:659–664

Shirkhoda A, Armin AR, Bis KG, Makris J, Irwin RB, Shetty AN (1995) MR imaging of myositis ossificans: variable patterns at different stages. J Magn Reson Imaging 5:287–292

Slavotinek JP, Stilger VG, Fon GT (2000) Hamstring injuries in footballers: the prevalence and prognostic value of MRI findings. Radiology 217:191

Speer KP, Lohnes J, Garrett WE Jr (1993) Radiographic imaging of muscle strain injury. Am J Sports Med 21:89–95; discussion 96.

Spinner RJ, Atkinson JL, Harper CM Jr, Wenger DE (2000) Recurrent intraneural ganglion cyst of the tibial nerve. Case report. J Neurosurg 92: 334–337

Stauber W (1988) Eccentric action of muscles: physiology, injury, and adaption. In: Stauber W (ed) Exercise and sports sciences reviews. Franklin Institute, Philadelphia

Steinbach L, Fleckenstein J, Mink J (1998) MR imaging of muscle injuries. Semin Musculoskelet Radiol 1:128–141

Taylor DC, Dalton JD Jr, Seaber AV, Garrett WE Jr (1993) Experimental muscle strain injury. Early functional and structural deficits and the increased risk for reinjury. Am J Sports Med 21:190–194

Toorop R, Poniewierski J, Gielen J, Maes M, Van Schil P, D'archambeau O (2004) Popliteal artery entrapment syndrome. Jbr-Btr 87:154–155

Tucker AK (2010) Chronic exertional compartment syndrome of the leg. Curr Rev Musculoskelet Med 3:32–37

Van Den Bergh FR, Vanhoenacker FM, De Smet E, Huysse W, Verstraete KL (2013) Peroneal nerve: normal anatomy and pathologic findings on routine MRI of the knee. Insights Imaging 4:287–299

Van Holsbeeck M, Introcasco J (2001) Musculoskeletal ultrasound. St Louis, Miss, Mosby

Yablon CM, Hammer MR, Morag Y, Brandon CJ, Fessell DP, Jacobson JA (2016) US of the peripheral nerves of the lower extremity: a landmark approach. Radiographics 36:464–478

Yates B, White S (2004) The incidence and risk factors in the development of medial tibial stress syndrome among naval recruits. Am J Sports Med 32:772–780

Zabetakis P (1986) Muscle soreness and rhabdomyolysis. In: Nicholas J, Hershman E (eds) The lower extremity and spine in sports medicine. Mosby, St Louis

Zarins B, Ciullo JV (1983) Acute muscle and tendon injuries in athletes. Clin Sports Med 2:167–182

The Spine in Sports Injuries: The Cervical Spine

Sven Dekeyzer, Filip M. Vanhoenacker, Stephanie Van den Bossche, Luc van den Hauwe, and Paul M. Parizel

Contents

S. Dekeyzer (✉) · S. Van den Bossche
L. van den Hauwe
Department of Radiology, University Hospital Antwerp, Edegem, Belgium
e-mail: sven.dekeyzer@gmail.com

F. M. Vanhoenacker
Department of Radiology, University Hospital Antwerp, Edegem, Belgium

Department of Radiology, AZ Sint Maarten, Mechelen, Belgium

Faculty of Medicine and Health Sciences, University of Antwerp and Ghent University, Ghent, Belgium

P. M. Parizel
Department of Radiology, Royal Perth Hospital (RPH), University of Western Australia (UWA) Medical School, Perth, WA, Australia

Abstract

Cervical spine injuries are extremely common in athletes and range from minor strains and sprains to severe, life-threatening cervical fractures with spinal cord injuries. A basic understanding of cervical spine anatomy and biomechanics, imaging indications, and most appropriate imaging techniques, as well as of the most common types of injury, is necessary for any physician ordering and/or interpreting imaging studies of athletes who suffer from acute or chronic cervical spine injury. Furthermore, radiologists should be able to recognize predisposing conditions, more specifically congenital spinal stenosis, which increase the risk for serious cervical spine injury in athletes even after a minor trauma. This chapter provides multiple examples of cervical spine injuries in athletes, highlighting the imaging findings in these injuries and the imaging modalities that can be used to assess such injuries.

1 Introduction

Injuries to the spine are commonly associated with all kinds of sports activities, both contact and noncontact sports, and at all levels of compe-

Med Radiol Diagn Imaging (2020)
https://doi.org/10.1007/174_2020_259, © Springer Nature Switzerland AG
Published Online: 10 December 2020

tition ranging from the high school level to the professional level (Boden and Jarvis 2008). They are most common in athletes younger than 30 years of age, and the associated activity varies by region. Ice hockey injuries are common in Canada, while rugby injuries are common in Europe, South Africa, and Australia. In the United States, (American) football is the leading cause of sports-related cervical injury, although the majority of injuries are sprains. Within Europe, the epidemiology is variable (Schroeder and Vaccaro 2016).

The spectrum of potential spinal injuries is wide; the vast majority of injuries are self-limiting, others require conservative therapy, and a minority require surgical intervention. Sports injuries involving the cervical spine include acute cervical sprain/strain, intervertebral disc lesions, burners/stingers, nerve root and brachial plexus injuries, transient (or in rare cases permanent) quadriplegia, and unstable injuries with and without fracture-dislocation.

In the popular media covering sports events, tragic cervical spine injuries of well-known professional athletes are often brought to national attention. These catastrophic cervical spine injuries most commonly occur in collision sports or motorized sports and can lead to devastating consequences for the athlete (Banerjee et al. 2004). Fortunately, these severe injuries are rare in sports. An elaborate review of epidemiologic studies, involving all types of sports activities at all levels of competition, reveals that the overwhelming majority of sports injuries related to the spine are soft-tissue injuries (sprains and strains) and are self-limiting (Tall and DeVault 1993). It is relatively rare for athletic injuries to the spine to result in significant neurologic compromise. However, in cases with neurologic symptoms, the cervical spine is most commonly involved.

Accurate and timely radiological examination of the cervical spine in athletes is therefore essential to establish a correct diagnosis and to prevent further injury.

2 Anatomical Considerations

Before proceeding to the radiological examination of the spine, we shall present a brief overview of cervical spine anatomy. The cervical spine consists of seven vertebrae, numbered from C1 to C7. The occipital condyles, atlas (C1) and axis (C2), comprise the upper cervical spine. The lower cervical spine consists of the cervical vertebra C3 through C7. Cervical vertebrae are the smallest of the true vertebrae and can be readily distinguished from those of the thoracic or lumbar regions by the presence of a foramen in each transverse process. They are ring shaped with the vertebral body anteriorly, the pedicles laterally, and the laminae and spinous process posteriorly. The first cervical vertebra (C1), also known as the atlas because it supports the globe of the head, does not possess a vertebral body but has two lateral masses, which articulate with the occipital condyles. The atlanto-occipital articulation accounts for 50% of cervical flexion-extension motion. The second cervical vertebra (C2), also known as the axis because it forms the pivot on which the first vertebra rotates, has a vertical toothlike projection called the dens or odontoid process, on which the atlas (C1) pivots. Embryologically, the odontoid process can be thought of as representing the vertebral body of the C1 and articulates with the anterior arch of C1. With the notable exception of C1–C2, the cervical vertebrae articulate with one another anteriorly via the intervertebral disc and two uncovertebral joints. Laterally, they articulate via the facet joints (also known as zygapophyseal joints).

The successive openings in the articulated ring-shaped vertebrae, which are stacked upon one another, enclose the spinal canal (also known as vertebral or neural canal). On cross section, the spinal canal presents an isosceles triangular shape, with the base of the triangle anteriorly (formed by the posterior wall of the vertebral bodies and intervertebral discs), and the sides posterior and lateral (formed by the lamina on either side). The angle between the laminae

(interlaminar angle) determines to a large extent the anteroposterior diameter of the spinal canal. Progressing down the spinal column, the diameter of the bony canal gradually narrows as the diameter of the spinal cord widens, thus reducing the space available for the cord in the inferior cervical spine.

The spinal canal contains the spinal cord, nerve roots, blood vessels, and meninges. At each intervertebral disc level, cervical spinal nerves originate from the spinal cord as the anterior (motor) and posterior (sensory) rootlets. Posterior and anterior rootlets join to form a spinal nerve, which lies within the intervertebral foramen. The posterior rootlet has a nerve root ganglion at the inner portion of the intervertebral foramen. The spinal nerve divides into a posterior and anterior ramus at the outlet of the intervertebral foramen. In the cervical spine, the spinal nerves exit the intervertebral foramen above the same-numbered cervical vertebra (e.g., the seventh spinal nerve exits at the C6–C7 level). Though there are only seven cervical vertebrae, there are eight spinal nerves on either side. The eighth cervical nerve exits between the C7 and T1 segment.

The cervical intervertebral disc constitutes a separate anatomic and functional entity, and is distinctly different from the lumbar intervertebral disc (Mercer and Bogduk 1999). The annulus fibrosus of the cervical intervertebral disc does not consist of concentric laminae of collagen fibers, as in the lumbar discs. Instead, the annulus forms a crescent-shaped mass of collagen, which is thickest anteriorly and tapers laterally toward the uncinate processes. Posteriorly, the annulus is merely a thin layer of paramedian vertically oriented fibers. The anterior longitudinal ligament (ALL) covers the front of the disc, and the posterior longitudinal ligament (PLL) reinforces the deficient posterior annulus fibrosus with longitudinal and alar fibers. In this way, the cervical annulus fibrosus is likened to a crescentic anterior interosseous ligament, rather than a ring of fibers surrounding the nucleus pulposus (Mercer and Bogduk 1999).

3 Biomechanics of the Cervical Spine

The cervical spine is the most mobile of all the segments of the vertebral column. It allows an extensive range of motion in flexion and extension, which is mainly due to the upwardly oriented inclination of the superior articular surfaces. In *flexion* (forward movement), the anterior longitudinal ligament (ALL) is relaxed, while the posterior longitudinal ligament (PLL), the ligamenta flava, and the inter- and supraspinous ligaments are stretched. During flexion, the intervertebral discs are compressed anteriorly, the interspaces between the laminae are widened, and the inferior articular processes glide upward, upon the superior articular processes of the subjacent vertebrae. Flexion of the cervical spine is arrested just beyond the point where the cervical convexity is straightened. In *extension* (backward movement), the opposite motions occur. Extension can be carried farther than flexion and is limited by stretching of the anterior longitudinal ligament (ALL), and by the approximation of the spinous processes. In the cervical spine *lateral flexion and rotation* always occur as combined movements. The upward and medial inclinations of the superior articular facet joint surfaces convey a rotary movement during lateral flexion, while pure rotation is prevented by their slight medial slope. During lateral flexion, the sides of the intervertebral discs are compressed, and the extent of motion is limited by the resistance offered by the surrounding ligaments.

In sports-related injuries, the most common mechanism of cervical spine trauma is neck flexion with axial loading (Torg et al. 2002a). In a neutral position, the overall alignment of the cervical spine is lordotic. When engaging in collision sports, the majority of the force is dissipated by the paravertebral musculature. Neck flexion causes the physiological cervical lordosis to disappear, however. When for instance a tackle is made in this position, the axial load is dissipated through and absorbed by a straight spine, causing

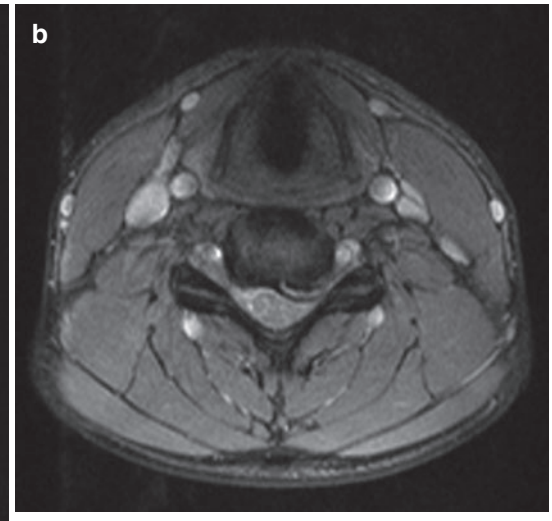

Fig. 1 Cervical disc herniation in a 32-year-old professional soccer player and fitness enthusiast with cervicalgia and paresthesia in the left arm since 2 years. **a** MRI of the cervical spine with sagittal T2-weighted images shows a disc herniation at the C5–C6 level. **b** Axial gradient-echo T2*-weighted images confirm the presence of a left paracentral disc herniation with asymmetric deformation of the dural sac and impingement on the left C6 nerve root

cervical spine compression and possibly resulting in catastrophic spine injury (Torg et al. 2002b).

Examples of axial loading injuries to the cervical spine are found in a variety of sports, such as:

- American football (Fig. 1) (player striking opponent with the crown of his/her helmet) or rugby (Fig. 2) (during the scrum phase of the game)
- Ice hockey (player striking his/her head on the board while doing a push or check)
- Diving in shallow water (Figs. 3 and 4) (head striking the ground)
- Gymnastics (Fig. 5) (athlete accidentally landing head down while performing a somersault on a trampoline)

The spectrum of cervical spine injury is related to the mechanism, the force involved, and the point of application of the force (Tall and De vault 1993). Axial loading injuries of the cervical spine include vertebral fractures (Figs. 2 and 3), cervical disc herniations (Fig. 1), ligament rupture, facet fracture, and dislocations (Figs. 5 and 6). Neurologic deficits tend to be more severe in athletes with spinal stenosis (Fig. 7), either developmental or acquired through degenerative disease (Torg et al. 1997).

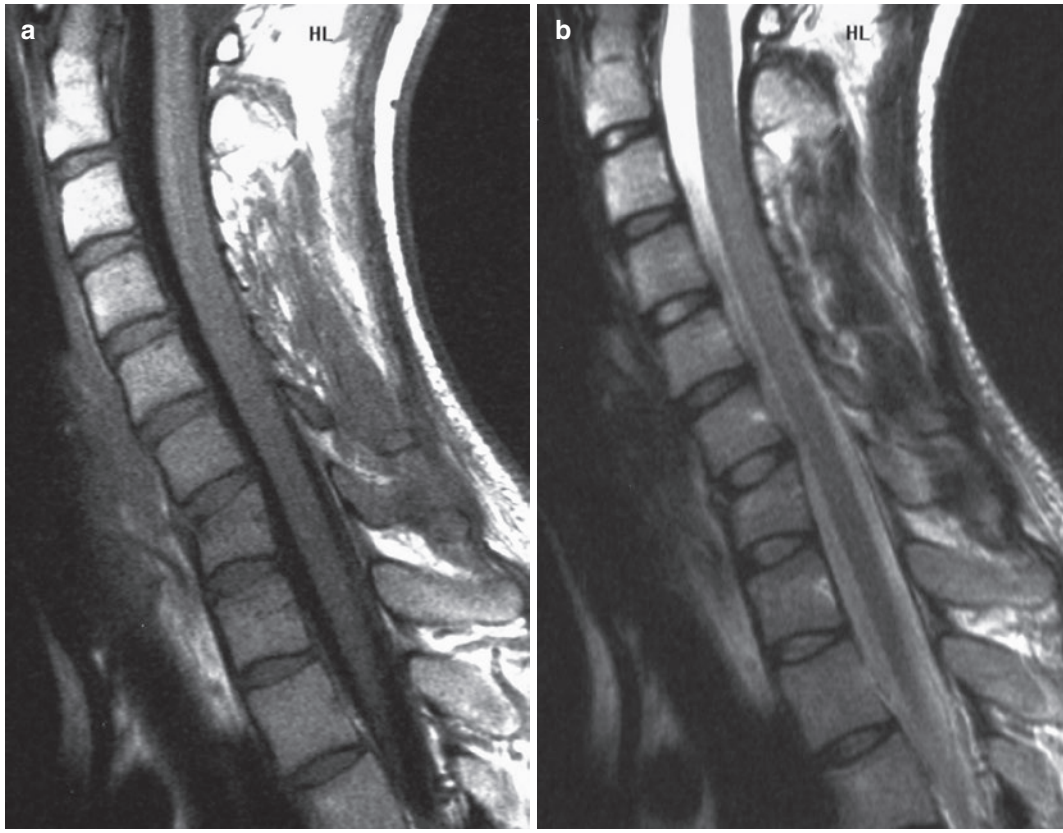

Fig. 2 Hyperflexion injury with simple anterior wedge fracture of C7 in a 23-year-old rugby player. **a** MRI scan with sagittal T1-weighted images shows that the anterosuperior corner of the vertebral body C7 is depressed. **b** Sagittal T2-weighted images show a band of bone marrow edema subjacent to the upper endplate. The posterior wall is not displaced, the diameter of the spinal canal remains normal, and there is no medullary contusion

Moreover, the biochemistry and biomechanics of the intervertebral disc and spine are age related. Thus, the adolescent and older athlete may have different concerns with regard to diagnosis, treatment, and prognosis after an injury to the spine.

Some studies have indicated that there is also a gender differential regarding injuries of the cervical spine. Compared with females, the incidence of injuries in males was 1.7 times higher for neck sprains and 3.6 times higher for fractures (Depasse et al. 2019). Football was the most common cause of cervical sprains in males, followed by cycling and weight lifting/aerobics. Females sustained most neck sprains in weight lifting/aerobics, trampoline, and cheerleading. In males cycling is the most common cause of fracture, followed by diving/swimming and football. For females, horseback riding is the most common, followed by cycling and diving/swimming (Depasse et al. 2019).

The radiologist examining an athlete with cervical spine trauma should recognize and understand the mechanism of injury (Pavlov and Torg 1987). Accurate radiological evaluation of the cervical spine must be performed immediately following the possibility of injury and in such a manner so as not to compromise the neurologic status of the patient. Subtle radiographic findings indicating ligamentous injuries must be recognized in order to prevent cervical spine instability. Occult fractures are often difficult to diagnose on plain films and CT has replaced traditional X-rays as the first imaging examination to be performed in patients with suspected cervical spinal trauma.

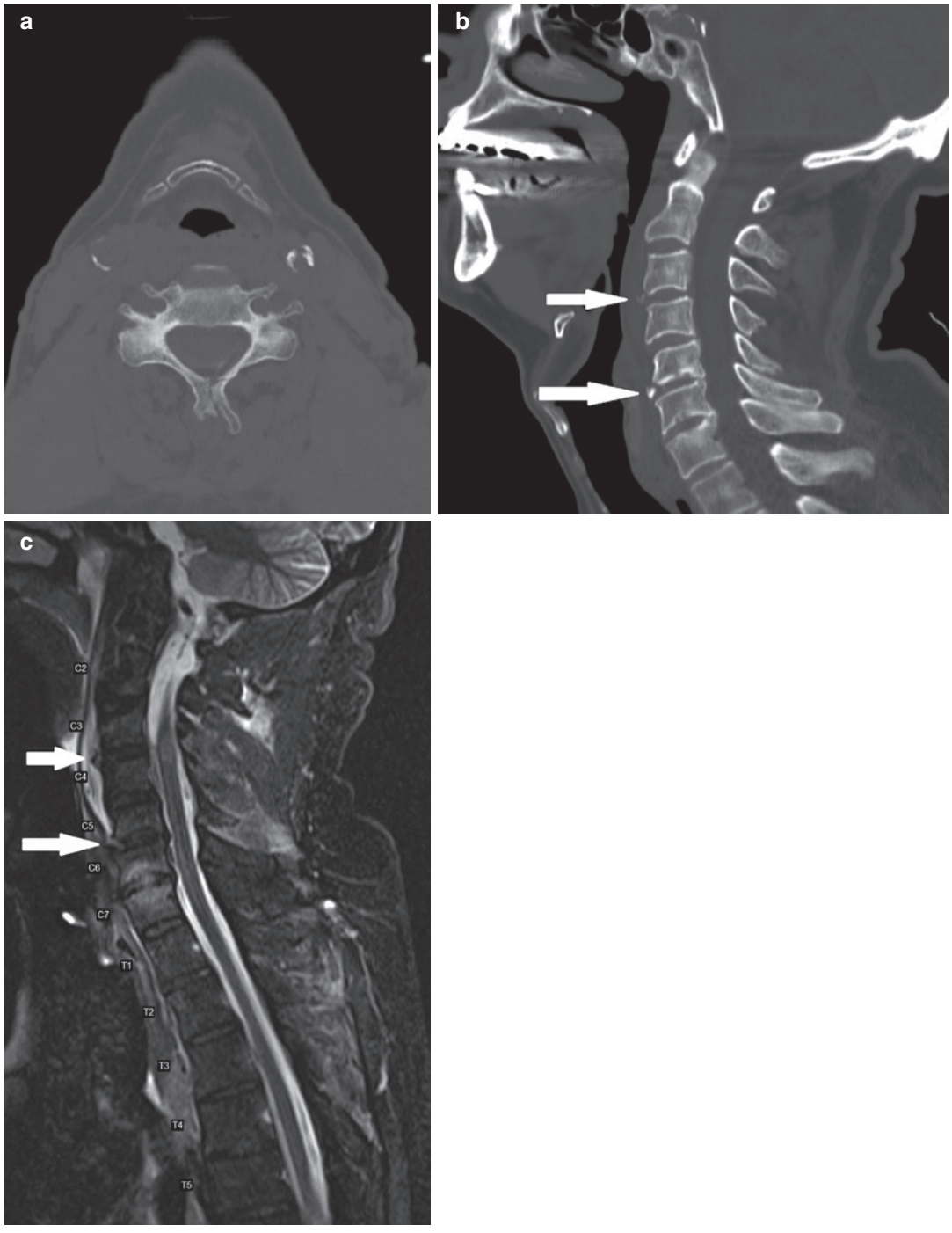

Fig. 3 Catastrophic cervical spine injury in a 26-year-old man who was injured in a mountain bike accident. **a** Non-contrast axial CT scan with **b** sagittal reformatted images. There is a flexion teardrop fracture of the inferior corner of the C3 and C5 endplates (white arrows in **b**) as well as a linear fracture of the posterior arch of C5 (**a**). **c** MRI with sagittal T2-STIR images shows associated tearing of the anterior longitudinal ligament at the C3 and C5 levels (white arrows), a medullary contusion at the C3–C4 level, and extensive edema in the cervical and thoracic interspinous ligaments

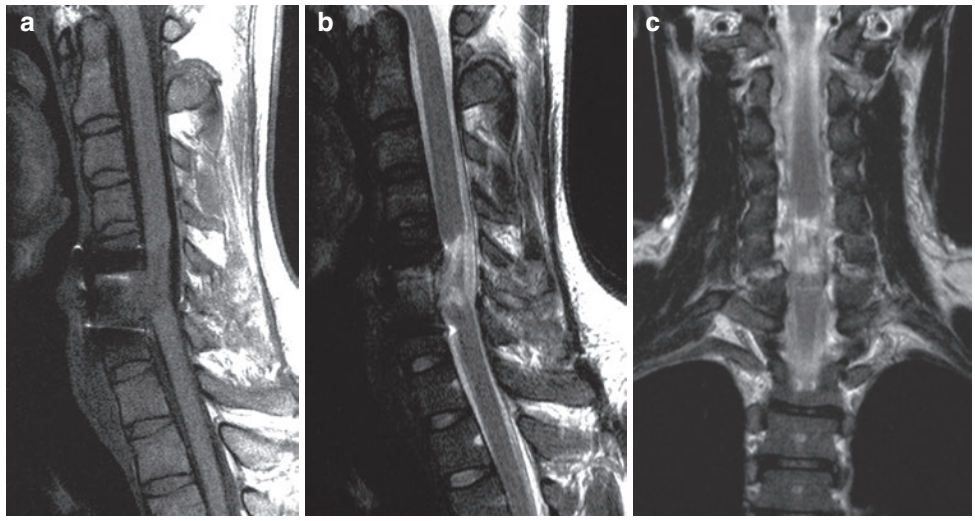

Fig. 4 Catastrophic neck injury (diving accident) with contusion and partial transection of the spinal cord in a 23-year-old man. **a** MRI examination with sagittal T1-weighted, **b** sagittal T2-weighted, and **c** coronal T2-weighted images. The study was obtained after anterior fixation at C5–C6–C7 with titanium plate. Despite the magnetic susceptibility artifacts caused by the instrumentation, the spinal cord contusion is clearly identified as a focal intramedullary high signal intensity on the T2-weighted scans

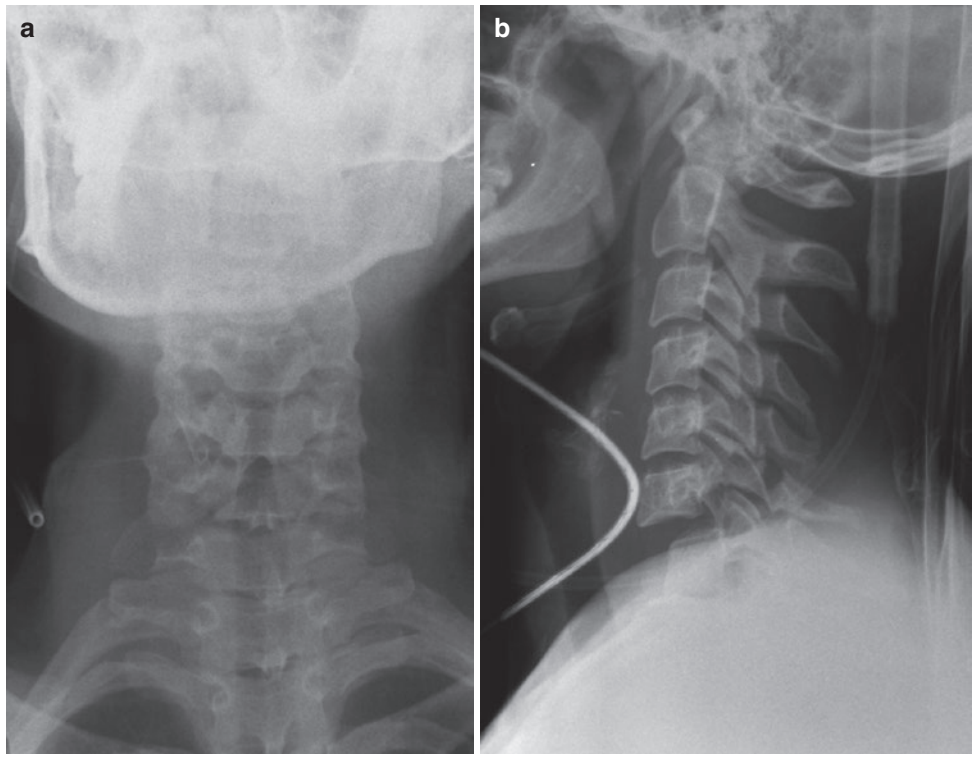

Fig. 5 Distracted hyperflexion injury in a young gymnast with anterior subluxation at C6–C7. **a** Plain radiographs of the cervical spine in AP and **b** cross-table lateral projection. The marked anterior displacement of C6 indicates disruption of all ligamentous structures and interfacetal dislocation. The cervicothoracic prevertebral soft-tissue shadow is widened, indicating the presence of a hematoma secondary to the injury

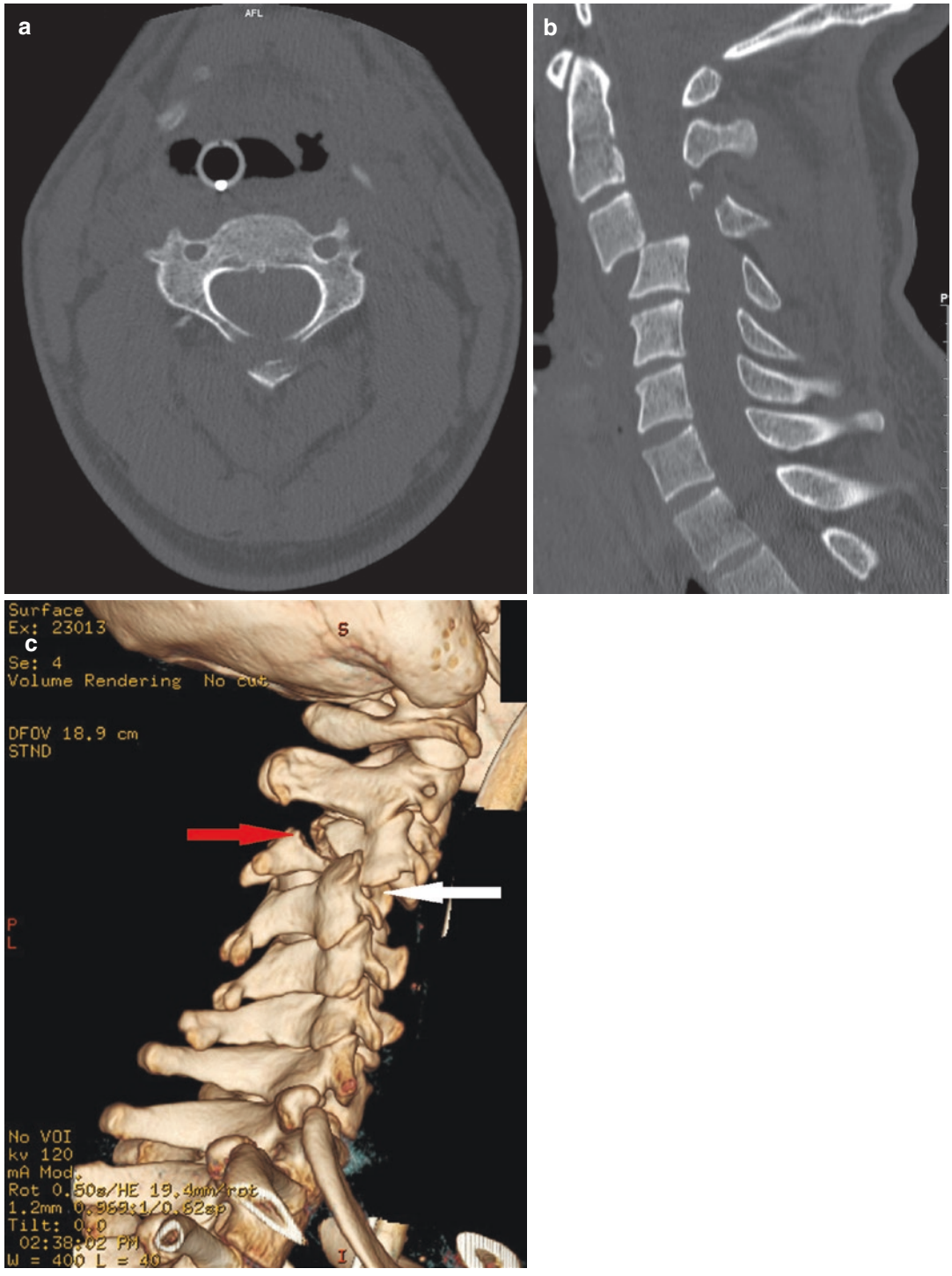

Fig. 6 Bilateral interfacetal dislocation with anterior translation of C3 with regard to C4 in a 34-year-old man following a severe fall during a soccer game. **a** Non-contrast CT scan with axial and **b** midsagittal reformatted images showing a fracture of the lamina of C3 and anterior displacement of C3 on C4 with marked steplike deformation of the spinal canal. **c** The 3D volume-rendered image confirms the fracture of the posterior elements of C3 (red arrow) and the facetal dislocation (white arrow)

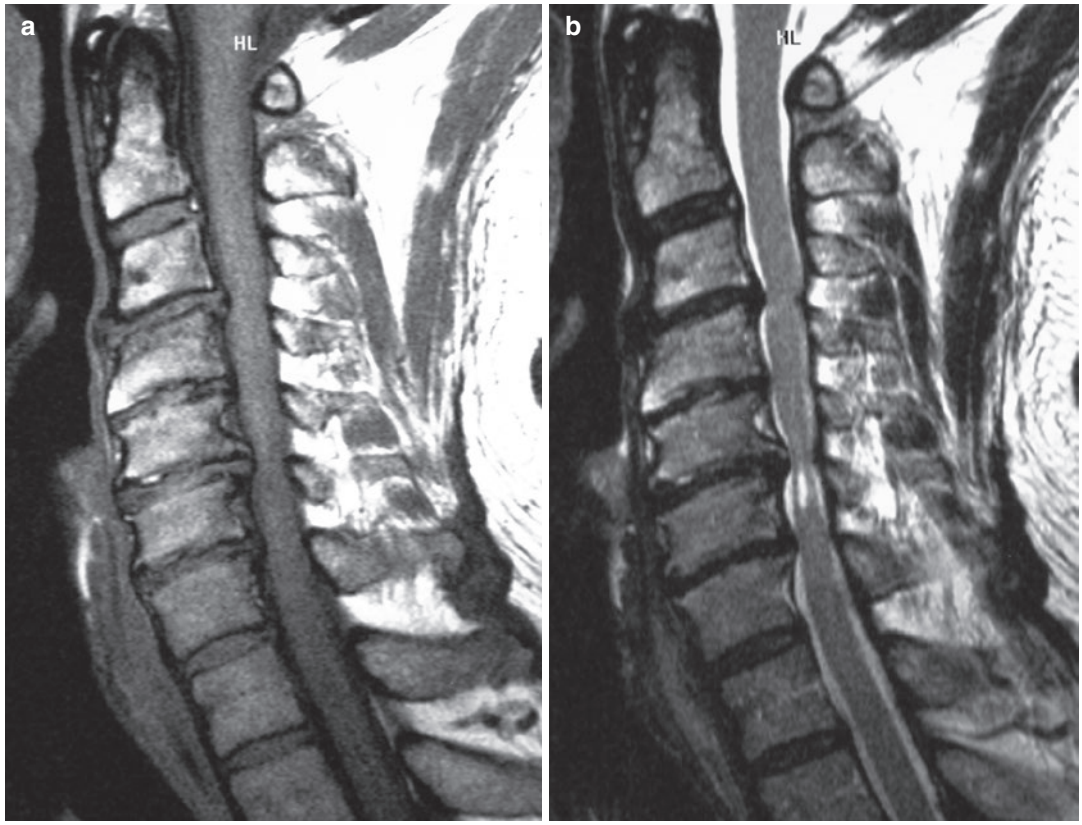

Fig. 7 Cord contusion secondary to spinal stenosis in a 49-year-old recreational tennis player, who complained of neck pain and paresthesia in both arms after a collision with another player. **a** MRI examination with sagittal T1-weighted and **b** sagittal T2-weighted images. Sagittal images show severe narrowing of the spinal canal due to chronic disc herniations and posterior osteophytes. There is a focal intramedullary area of increased T2 signal intensity indicating cord contusion

4 Radiological Examination

The purpose of the radiological investigation in the injured athlete is to document lesions that must be treated, such as disc disease or instability. Pain in itself is not an indication for imaging (for example, most acute burner or stinger injuries do not require imaging) (Mintz 2004). On the other hand, when the athlete shows signs or symptoms of instability or neurological deficit, imaging studies are required to document potentially serious lesions.

One of the most important questions to be answered concerning patients with possible cervical spine trauma is the following: *Who should be imaged*? Two large studies developed a set of criteria to determine which trauma patients do not require cervical spine imaging: The National Emergency X-ray Utilization Study (NEXUS) (Hoffman et al. 2001) and the Canadian Cervical Spine Rule Group (CCR) (Stiell et al. 2001). According to the NEXUS study, imaging is not necessary if all the following criteria are met: no midline cervical tenderness, no focal neurological deficits, normal level of alertness, no intoxication, and no painful distracting injury. The CCR criteria are more elaborate and include an absence of high-risk criteria, the presence of any low-risk factor, and the ability to actively rotate the neck 45°. A detailed overview of the CCR criteria is presented in Table 1.

Table 1 The Canadian C-spine rules for cervical spine imaging in trauma patients

High-risk factors	Low-risk factors
≥65 years	Simple rear-end motor vehicle collision
A dangerous mechanism:	Sitting position in emergency department
Fall from elevation >3 ft (or five stairs)	Ambulatory at any time since the injury
Axial load to head	Delayed onset of neck pain
High-speed motor vehicle collision	Absence of midline C-spine tenderness
Motorized recreational vehicles	
Bicycle collision	
Paresthesias in extremities	

If any high-risk factor is present → cervical spine imaging is warranted.
If the patient does not meet the criteria of a low-risk injury → cervical spine imaging is warranted.
If the patient meets the criteria of a low-risk injury → assess whether the patient can rotate the neck 45°.
If low-risk injury and the patient can rotate the neck 45° → no cervical imaging is required.
If low-risk injury and the patient cannot rotate the neck 45° → cervical spine imaging is warranted.

The next question to be answered is this: *What imaging modality should be used* in a patient with suspected cervical spine trauma? In many centers radiographs of the cervical spine, including frontal, lateral, and odontoid projections, are the first imaging study to be performed, with additional CT and/or MRI examinations in the function of clinical and/or radiological findings. Due to the increased sensitivity of CT, and especially multidetector CT (MDCT), compared to conventional radiographs, this stepwise approach of ordering imaging examinations is no longer recommended (Fisher and Young 2008). In 2007, the American College of Radiology formulated appropriateness criteria in the setting of cervical spine trauma after an investigation of over 5700 patients and a literature review involving more than 55,000 patients (Daffner and Hackney 2007). The ACR stated that (1) if NEXUS or CCR criteria indicate low risk, then no imaging should be performed, and (2) if NEXUS or CCR criteria indicate imaging, then a CT of the cervical spine with sagittal and coronal reformations is highly recommended.

The role of MRI in acute cervical trauma is still being defined. Even though MDCT remains superior in assessing bone injuries, MRI is more sensitive for the detection of soft-tissue injury and spinal cord damage. The American College of Radiology has identified the following indications for MRI in cervical spine trauma (Beckmann et al. 2019):

1. *Possible spinal cord or nerve injury*. Regardless of whether a fracture has been identified on CT, MRI should be performed in patients who have possible spinal cord or nerve injury, and in whom there is clinical concern for cord compression due to disc herniation, hematoma, or fracture.
2. *Treatment planning for the unstable spine*. MRI is complementary to CT in preoperative assessment of the unstable cervical spine and should be performed for adequate treatment planning. Assessment of the integrity of the discoligamentous complex is crucial in preoperative cervical spine assessment.
3. *Obtunded patient with no traumatic injury identified on CT*. This is a controversial indication. MRI is superior to CT in identifying cervical spine ligamentous injuries. Studies looking at the presence of soft-tissue injury on MRI of the cervical spine in patients with negative CT and unreliable physical or neurological examination found MRI to be positive in 6–49% of patients. Most of these injuries were minor, requiring no significant changes in management. However, approximately 1%

of patients with an unreliable clinical examination and negative cervical spine CT will have an unstable cervical spine injury identified on MRI that requires surgical stabilization.

4. *Clinical or imaging findings suggesting ligamentous injury*. MRI is the most sensitive imaging study for the detection of ligamentous injury. MRI of the cervical spine should be performed after CT when ligamentous injury is suspected.

5 Cervical Strain and Sprain

Paraspinal muscle strain and cervical ligament sprain are the most common cervical spine injuries in athletes. Muscle strains are caused by direct blows or rapid eccentric muscle contraction. Ligamentous sprains or capsular injuries of the facets are caused by forced neck flexion. Clinically, patients present with localized pain without neurological deficits or irradiation. There can be an antalgic limitation of the range of motion. Treatment is conservative and consists of immobilization and anti-inflammatory medication until the pain resolves. Imaging is generally negative, and the role of imaging is mainly to rule out more serious spinal injury.

6 Burners and Stingers

The most common cervical injury in players of contact sports is a transient loss of function (weakness) of the upper extremity with burning pain, numbness, or tingling along the affected upper extremity following a collision (Tosti et al. 2016). This phenomenon is known as a "stinger" or "burner" injury. A stinger or burner injury is a transient neuropraxia of the brachial plexus caused by stretching or compression of the brachial plexus fibers between the neck and shoulder. Symptoms are usually transient and full recovery usually occurs within 10 min. The most commonly affected muscle groups in terms of motor weakness are shoulder abductors, elbow flexors, external humeral rotators, and wrist and finger extensors. Function gradually returns from the proximal muscle groups to the distal muscle groups. Though the burner or stinger syndrome is one of the most common injuries in football, it can occur in other sports such as wrestling, hockey, basketball, boxing, and weight lifting (Feinberg 2000).

The stinger or burner syndrome most likely represents an upper cervical root injury and occurs most commonly at the C5 or C6 distribution. Three possible mechanisms have been identified that may lead to burner/stinger injuries: traction, compression, and direct blows.

- *Traction* occurs with increases in the neck-shoulder angle (through forced depression of the ipsilateral shoulder in combination with forcible lateral bending away of the head to the opposite side) resulting in stretching or distraction injury to the upper cords of the brachial plexus.
- *Compression* occurs through rotation of the cervical spine toward the painful arm. The cervical foramina are narrowed transiently when the cervical spine is forced into hyperextension, either alone or in combination with lateral flexion or shoulder elevation to the affected side, causing transient nerve root compression.
- *Direct blows* occur from a percussive mechanism to the brachial plexus cords and trunks.

The severity of the injury correlates with the underlying pathophysiology. *Neuropraxia* refers to selective demyelination of the nerve sheath, and it is the most benign form of injury. *Axonotmesis* is a disruption of the axon and the myelin sheath, but the epineurium remains intact. The most severe injury is *neurotmesis* or a complete disruption of the endoneurium. This injury is associated with the most unfavorable prognosis.

A stinger or burner injury is a neuropraxia or low-grade axonotmesis by definition. Hence, symptoms often resolve within a few minutes but may last up to 24 h. In symptoms persisting longer than 24 h, suspicion should be raised for a more severe injury or another diagnosis. Imaging is indicated in symptoms persisting over 24 h, or if there are other symptoms, such as decreased or painful neck motion, to rule out possible fractures or dislocations or disc herniations. If the symptoms persist for 3–4 weeks following injury, an electromyogram should be obtained to evaluate upper trunk function and MRI should be considered.

7 Nerve Root and Plexus Avulsion

A severe type of brachial plexus lesion is the brachial plexus avulsion, which is an uncommon but serious injury associated with contact sports (Williams and Hoeper 2004), and motorized sports, especially motorcycle racing. The term refers to complete or incomplete avulsion of one or more cervical nerve roots from the spinal cord. Brachial plexus injuries can be classified as preganglionic or postganglionic, although in clinical practice injuries can be mixed. The distinction is important however, as management and prognosis differ between these two types of injuries.

- *Preganglionic nerve root injury*: avulsion injury or nerve rupture proximal to the dorsal root ganglion, causing a disconnection between the central and peripheral nervous system. Preganglionic avulsion injuries are associated with a marked and progressive death of motor neurons and are associated with a poor functional outcome. Preganglionic injuries are not considered amenable to repair.
- *Postganglionic nerve root avulsion*: injuries distal to the dorsal root ganglion. They can be further classified into *nerve ruptures* and *lesions in continuity*. Depending on the severity of the injury, function may either spontaneously return with time or, when loss of nerve continuity occurs, can be repaired with nerve grafting—that is, excision of the damaged nerve segment and interposition of a nerve autograft between the nerve ends.

Traumatic brachial plexus avulsion is usually associated with a dural tear, through which CSF leakage occurs to form a pseudomeningocele. Traditionally cervical myelography, followed by CT myelography, used to be the gold standard for demonstration of these lesions, showing both complete and incomplete traction injuries (Yoshikawa 2006). The combination of CT and CT myelography can differentiate pre- from postganglionic lesions, and this information is essential for deciding whether exploration of the plexus or a motor substitution operation is indicated (Yoshikawa 2006). Moreover, CT has the added advantage of being able to rule out an associated fracture of the spinal column. Conventional MRI scanning of the cervical spine provides additional anatomic and physiologic information on injuries, such as signal intensity changes in the spinal cord (seen in about 20% of patients with preganglionic nerve root injuries) or additional lesions, such as intramedullary or extradural hematomas. Visualization of the intradural nerve roots is inadequate at MR imaging (Yoshikawa 2006). With the use of high-resolution, thin-section slices (Fig. 8), the sensitivity for detection of cervical nerve root avulsion was the same (92.9%) with MRI as myelography/CT myelography (DOI et al. 2002). Alternatively, MR myelography provides high-quality images with excellent visualization of nerve roots in healthy volunteers and in 60% of patients with brachial plexus injury (Yoshikawa 2006). However, visualization was only fair in the remaining 40% of patients with brachial plexus injury, implying that even if MR myelography can partially replace CT myelography, CT myelography is still needed in some patients.

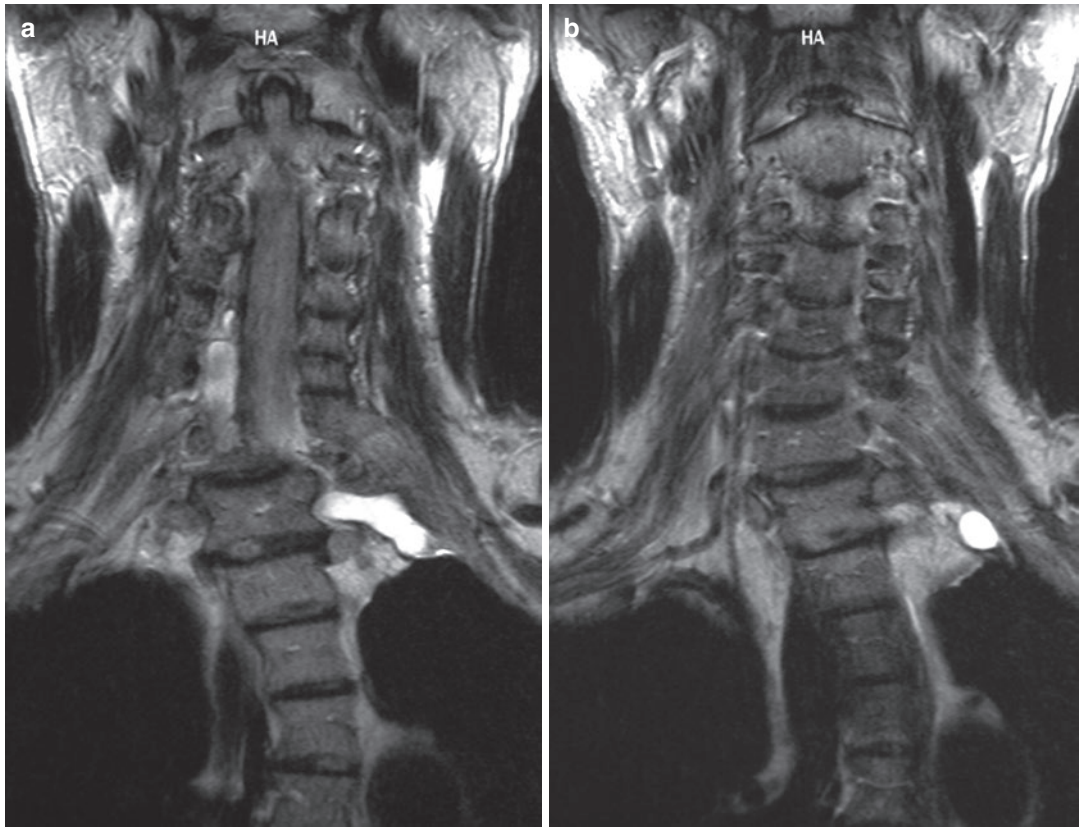

Fig. 8 Left brachial plexus nerve root avulsion with formation of a pseudomeningocele filled with cerebrospinal fluid. The patient is a 29-year-old man who was injured in a cross-country motorcycle racing accident. **a, b** Coronal thin-section turbo spin-echo T2-weighted MRI scans reveal a CSF-filled pseudomeningocele extending to the apex of the left lung

8 Cervical Disc Herniation

Traumatic sports injuries of the cervical spine can occur at the level of the disc, resulting in *acute disc herniation* or *chronic disc degeneration*.

Acute disc pathology results from an axial load that rapidly increases intradiscal pressure. The nucleus pulposus is then extruded through the annulus fibrosus into the spinal canal or neuroforamen. It can cause a variety of neurological complications, which may be transient or permanent, including tetraparesis, paraparesis, and neuralgia due to compression of the spinal nerve roots and/or the spinal cord. Although acute disc herniations are uncommon, making up only 5.8% of cervical spine injuries in a large study of 987 national football league (NFL) players who suffered cervical spine trauma, they can result in a considerable functional impairment and days lost to play for elite athletes (Mall et al. 2012).

Whether or not long-standing sports participation results in an increased incidence of *chronic cervical disc degeneration* remains unclear. There is some evidence to suggest that participation in collision sports is implicated in the premature degeneration of the cervical spine, and that

the same is true for non-collision sports and activities that result in direct and indirect repetitive loads to the cervical spine over time. The risk factors, natural history, and clinical relevance of this premature cervical degeneration remain unclear, however (Triantafillou et al. 2012).

Structurally, cervical disc disease can be classified as either soft- or hard-disc disease, which generally corresponds to acute and chronic disc disease, respectively. Soft-disc herniation generally refers to an acute process in which the nucleus pulposus herniates through the annulus fibrosus, which might result in spinal cord or nerve root compression. Hard-disc disease represents a chronic, degenerative process with loss of disc height and formation of marginal osteophytes. On MRI, it can be difficult to distinguish between a disc herniation ("soft" disc) and an osteophyte ("hard" disc). Recent disc herniations tend to have a higher signal intensity on T2- or T2*-weighted images, whereas osteophytes present a low signal intensity. T2-weighted MR images are the method of choice to demonstrate abnormal intramedullary signal intensity due to extrinsic compression by an intervertebral disc.

9 Transient Quadriparesis and Spinal Stenosis

Transient quadriparesis is a temporary loss of motor and often sensory function in the arms and legs, and is typically seen in athletes following a blow to the head or whiplash injury. Motor symptoms can range from weakness in the arms and legs to complete quadriplegia. Sensory symptoms may include numbness, paresthesia, and burning pain. Transient quadriparesis has been described in the medical literature under many other names, including cervical cord neuropraxia, burning hands syndrome, commotio spinalis, and spinal cord concussion. Symptom duration varies from less than 15 min (grade 1) to over 24 h (grade 3).

Transient quadriparesis is assumed to be a transient postconcussive neuropraxia of the spinal cord and can be caused by hyperextension or hyperflexion. Hyperextension can cause infolding or bunching of the ligamentum flavum, resulting in a dynamic narrowing of the canal of up to 30% in the sagittal plane, and compression of the spinal cord by the inferior portion of the superior vertebral body anteriorly, and by the lamina of the inferior vertebra posteriorly. In hyperflexion the opposite phenomenon may occur, with compression of the spinal cord against the lamina of the superior vertebra and the endplate of the inferior vertebra. Brief compression of the cord by either hyperflexion or hyperextension creates a "postconcussive" effect on the cord.

In line with this proposed mechanism, athletes with cervical spinal stenosis may be predisposed to transient quadriparesis. One of the difficulties when it comes to the relationship between transient quadriparesis and spinal stenosis is the variable definition of spinal stenosis in the medical literature. Prior to the advent of more advanced imaging, radiographs were used to evaluate spinal stenosis. This was done by simply measuring the anteroposterior diameter of the spinal canal at the C3–C6 level from the posterior aspect of the vertebral body to the most anterior point on the spinolaminar line. Values greater than 15 mm were considered normal, while 13 mm or less was considered consistent with stenosis (Cantu 1997).

In a further attempt to radiographically define spinal stenosis, Pavlov and Torg (1987) described a ratio (the *Pavlov–Torg ratio*) between the sagittal diameter of the spinal canal measured from the mid-height of the posterior aspect of the vertebral body to the spinolaminar line, divided by the anterior-posterior diameter of the corresponding vertebral body. A normal ratio is 1.0, and values lower than 0.8 are consistent with stenosis. A Pavlov–Torg ratio of less than 0.8 was found in 93% of football players with transient quadriparesis. However, it was also demonstrated by the same authors that the positive predictive value of having a Pavlov–Torg ratio less than 0.80 and subsequently experiencing an episode of transient neurapraxia is only 0.2%. Specificity of the Pavlov–Torg ratio is further hampered by the fact that professional athletes may have larger vertebral bodies than the general population, leading

to a low Pavlov–Torg ratio despite normal spinal canal diameter (Herzog et al. 1991).

A more recent attempt to define cervical spinal stenosis is coined "functional cervical spinal stenosis." This definition is based on MRI in which a functional reserve of cerebral spinal fluid (CSF) remains around the spinal cord at all levels. Functional cervical spinal stenosis is defined as a cervical spinal canal so small as to obliterate the protective cushion of CSF, or in more extreme cases it causes deformation of the spinal cord itself (Dailey et al. 2010). This criterion has not yet been thoroughly evaluated in the literature, however.

Professional athletes, especially those involved in contact sports, who experience an episode of transient quadriparesis with rapid and complete symptom resolution should have plain radiographs and MRI to rule out spinal canal stenosis, spinal cord abnormality, and neural compression. In athletes without evidence of spinal stenosis or spinal cord injury, the player may resume sport activities when an asymptomatic and full range of neck motion is regained. Players with mild or moderate cervical spinal canal stenosis and no evidence of spinal cord injury with quick symptom resolution and complete regain of neck mobility are considered to have a relative contraindication to returning to contact sports. The decision whether or not someone should be allowed to return to play should be made based on the degree of stenosis, propensity for injury based on the involved sport, and symptom severity during the episode of transient quadriparesis. Players who have sustained a single episode of transient quadriparesis and severe spinal stenosis, or who experienced more than one episode of transient quadriparesis, should not be allowed to return to play (Kepler and Vaccaro 2012).

10 Catastrophic Cervical Spine Injuries

A catastrophic cervical spine injury can be defined *as a structural distortion of the cervical spinal column associated with actual or potential damage to the spinal cord*, and can lead to devastating and irreversible neurologic consequences for the athlete (Banerjee et al. 2004). Contact and collision sports, such as rugby, American football, or ice hockey, expose the athlete to a wide array of potential injuries to the spinal cord (Wilson et al. 2006). This is equally true for motorized sports involving high speeds. The outcome of athletic neck injuries ranges from complete recovery to death, depending on the degree of spinal cord damage sustained (Quarrie et al. 2002).

Despite the potentially devastating consequences of catastrophic cervical spine injuries and the high profile and attention given to these injuries when occurring in elite athletes, the frequency of these injuries remains poorly studied. Current evidence, consisting mainly of low-quality studies, indicates that catastrophic cervical spine injuries are infrequent among elite athletes (Hutton et al. 2016). *Potentially* catastrophic cervical spine injuries were reported to occur in as many as 10–15% of all American football players (Torg et al. 1979). However, the introduction of the antispearing rule implemented in 1976, which outlawed making a tackle or block by leading with the head or face, essentially using the helmet as a weapon, reduced the incidence of spine injuries from 20 per year during 1971 through 1975 to 7.2 per year after 1976 (Cantu and Mueller 2003).

Unstable fractures and/or dislocations are the most common causes of catastrophic cervical spinal injuries in collision sport athletes. A cervical spine injury is considered unstable when it results in loss of the ability of the spine under physiological loads to maintain its premorbid patterns of motion so that no additional damage to the spinal cord or nerve roots or major deformity may occur. The majority of catastrophic cervical spine injuries, associated with spinal cord injury, occur in the lower cervical region. Spinal cord damage due to fractures or dislocation involving the upper cervical spine is unusual, because there is proportionately more space available within the spinal canal compared with the lower cervical segments. The spinal cord occupies less than half of the spinal canal's cross-sectional area at the level of the atlas. At the lower cervical levels on the other hand, due to a

combination of progressive narrowing of the bony spinal canal and gradual widening of the spinal cord diameter, the spinal cord fills approximately 75% of the canal's cross-sectional area.

With respect to the trauma mechanism, two major patterns of spinal column damage can be identified. Pure compressive forces will result in *burst fractures*. The vertebral body looks "exploded," posterior vertebral body cortex is always involved, and retropulsion of bony fragments in the spinal canal may occur. *Compression-flexion injuries* are more frequent than burst fractures and result from a combination of neck flexion and an axial force. These lead to a characteristic pattern of injuries, consisting of the following:

- *Compression fracture along the anterior vertebral body*, often isolating a triangular anterior bony fragment (the so-called teardrop in "flexion teardrop injuries") and associated with rupture of the anterior longitudinal ligament: The fracture may continue through the vertebral subchondral endplate, with shearing/rotational injury of the posterior discoligamentous complex and rupture of the posterior longitudinal ligament.
- *Distraction injury of the posterior elements* and tensile rupture of the posterior ligaments (such as the ligamentum flavum and interspinous ligaments).

11 Differential Diagnosis

Finally, as a word of caution, it should be remembered that injuries are not the only cause of neck or back pain in the athlete. Disorders simulating athletic injury include, among others, tumors and inflammatory connective tissue disease. As the number of middle-aged or elderly recreational athletes increases steadily, we should keep in mind that these athletes can also have tumors, infection, rheumatologic disorders, and other nontraumatic etiologies of pain. For these conditions, radiological examination should be guided by an adequate and precise clinical workup.

Things to Remember

- Cervical spine injuries occur in many sports. Most lesions are benign and resolve spontaneously; serious injuries are mostly associated with contact sports and motorized sports.
- In sports-related injuries, the most common mechanism of cervical spine trauma is neck flexion with axial loading.
- Pain in itself is not an indication for imaging. Validated criteria (NEXUS, C-Spine Rules) have been developed to determine which patients need further imaging studies.
- Multidetector CT (MDCT) is the imaging modality of choice in patients with suspected cervical spine trauma.
- MRI is the preferred imaging technique to demonstrate soft-tissue injuries, e.g., possible spinal cord or nerve injury, as well as ligamentous injury.
- Sports-related injuries of the cervical spine can occur in athletes with spinal canal stenosis (developmental and/or acquired degenerative changes). Imaging studies must take into account the relative diameter of the spinal canal.
- Nerve root and brachial plexus avulsion is an unusual but severe type of sports injury. It can be investigated with myelography and CT myelography, or with MRI.

Imaging Technique Boxes

Plain Radiographs

- No longer indicated as the first imaging study in suspected cervical spine trauma.
- Underestimate fractures, especially near the cervicothoracic junction

CT

- First-choice imaging modality in suspected cervical spine trauma
- Very fast (MDCT requires only seconds to scan the cervical spine)
- Provides limited soft-tissue contrast

Myelography and CT Myelography

- Supplanted by noninvasive cross-sectional imaging techniques
- Remain useful in the diagnosis of nerve root and brachial plexus avulsion

MR

- Method of choice for assessing spinal cord, ligaments, muscles, and soft tissues
- Fat-suppressed sequences are sensitive to bone marrow edema
- Not always readily available in the emergency setting

References

Banerjee R, Palumbo MA, Fadale PD (2004) Catastrophic cervical spine injuries in the collision sport athlete, part 1: epidemiology, functional anatomy, and diagnosis. Am J Sports Med 32:1077–1087

Beckmann NM, West OC, Nunez D Jr, Kirsch CFE, Aulino JM, Broder JS, Cassidy RC, Czuczman GJ, Demertzis JL, Johnson MM, Motamedi K, Reitman C, Shah LM, Than K, Ying-Kou Yung E, Beaman FD, Kransdorf MJ, Bykowski J (2019) ACR Appropriateness Criteria(®) suspected spine trauma. J Am Coll Radiol 16(5S):S264–S285. https://doi.org/10.1016/j.jacr.2019.02.002

Boden BP, Jarvis CG (2008) Spinal injuries in sports. Neurol Clin 26:63–78. https://doi.org/10.1016/j.ncl.2007.12.005

Cantu RC (1997) Stingers, transient quadriplegia, and cervical spinal stenosis: return to play criteria. Med Sci Sports Exerc 29(Suppl. 7):S233Y5

Cantu RC, Mueller FO (2003) Catastrophic spine injuries in American football, 1977–2001. Neurosurgery 53:358–363

Daffner RH, Hackney DB (2007) ACR Appropriateness Criteria on suspected spine trauma. J Am Coll Radiol 4:762–775

Dailey A, Harrop JS, France JC (2010) High-energy contact sports and cervical spine neuropraxia injuries: what are the criteria for return to participation? Spine (Phila Pa 1976) 35(21 Suppl):S193–S201

DePasse JM, Durand W, Palumbo MA, Daniels AH (2019) Sex- and sport-specific epidemiology of cervical spine injuries sustained during sporting activities. World Neurosurg 122:e540–e545. https://doi.org/10.1016/j.wneu.2018.10.097

Doi K, Otsuka K, Okamoto Y et al (2002) Cervical nerve root avulsion in brachial plexus injuries: magnetic resonance imaging classification and comparison with myelography and computerized tomography myelography. J Neurosurg 96:277–284

Feinberg JH (2000) Burners and stingers. Phys Med Rehabil Clin N Am 11:771–784

Fisher A, Young WF (2008) Is the lateral cervical spine X-ray obsolete during the initial evaluation of patients with acute trauma? Surg Neurol 70:53–57

Herzog RJ, Weins MF, Dillingham MF, Sontag MJ (1991) Normal cervical spine morphometry and cervical spinal stenosis in asymptomatic professional football players. Spine 16:178Y86

Hoffman JR, Mower WR, Wolfson AB, Todd KH, Zucker MI (2001) Validity of a set of clinical criteria to rule out injury to the cervical spine in patients with blunt trauma. National Emergency X-radiography utilization study group. N Engl J Med 343:94–99

Hutton MJ, McGuire RA, Dunn R et al (2016) Catastrophic cervical spine injuries in contact sports. Global Spine J 6:721–734. https://doi.org/10.1055/s-0036-1586744

Kepler CK, Vaccaro AR (2012) Injuries and abnormalities of the cervical spine and return to play criteria. Clin Sports Med 31:499–508. https://doi.org/10.1016/j.csm.2012.03.005

Mall NA, Buchowski J, Zebala L et al (2012) Spine and axial skeleton injuries in the National Football League. Am J Sports Med 40:1755–1761. https://doi.org/10.1177/0363546512448355

Mercer S, Bogduk N (1999) The ligaments and annulus fibrosus of human adult cervical intervertebral discs. Spine 24:619–626

Mintz DN (2004) Magnetic resonance imaging of sports injuries to the cervical spine. Semin Musculoskelet Radiol 8:99–110

Pavlov H, Torg JS (1987) Roentgen examination of cervical spine injuries in the athlete. Clin Sports Med 6:751–766

Quarrie KL, Cantu RC, Chalmers DJ (2002) Rugby union injuries to the cervical spine and spinal cord. Sports Med 32:633–653

Schroeder GD, Vaccaro AR (2016) Cervical spine injuries in the athlete. J Am Acad Orthop Surg 24(9):e122–e133. https://doi.org/10.5435/JAAOS-D-15-00716

Stiell IG, Wells GA, Vandemheen KL et al (2001) The Canadian C-spine rule for radiography in alert and stable trauma patients. JAMA 286:1841–1848

Tall RL, DeVault W (1993) Spinal injury in sport: epidemiologic considerations. Clin Sports Med 12:441–448

Torg JS, Corcoran TA, Thibault LE et al (1997) Cervical cord neurapraxia: classification, pathomechanics, morbidity, and management guidelines. J Neurosurg 87:843–850

Torg JS, Guille JT, Jaffe S (2002a) Injuries to the cervical spine in American football players. J Bone Joint Surg 84-A:112–122

Torg JS, Guille JT, Jaffe S (2002b) Current concepts review: injuries to the cervical spine in American football players. J Bone Joint Surg Am 84:112–122

Torg JS, Truex R Jr, Quedenfeld TC et al (1979) The National Football Head and Neck Injury Registry. Report and conclusions 1978. JAMA 241:1477–1479

Tosti R, Rossy W, Sanchez A, Lee SG (2016) Burners, stingers and other brachial plexus injuries in the contact athlete. Oper Tech Sports Med. https://doi.org/10.1053/j.otsm.2016.09.006

Triantafillou KM, Lauerman W, Kalantar SB (2012) Degenerative disease of the cervical spine and its relationship to athletes. Clin Sports Med 31:509–520. https://doi.org/10.1016/j.csm.2012.03.009

Williams J, Hoeper E (2004) Brachial plexus injury in a male football player. Curr Sports Med Rep 3: 125–127

Wilson JB, Zarzour R, Moorman CT 3rd (2006) Spinal injuries in contact sports. Curr Sports Med Rep 5:50–55

Yoshikawa et al (2006) Brachial plexus injury: clinical manifestations, conventional imaging findings, and the latest imaging techniques. Radiographics 26:S133–S143

The Spine in Sports Injuries: Thoracic and Lumbar Spine

Klaus Friedrich and Franz Kainberger

Contents

Abstract

This book chapter provides an overview of imaging in sports injuries of the thoracic and lumbar spine. Indications for imaging in trauma, overuse, as well as osteoporosis are discussed. Imaging findings in the most important diagnoses and differential diagnoses are explained in detail. Within those, overuse plays a significant role. It is important to keep in mind that congenital and developmental disorders are risk factors for overuse syndromes and degenerative diseases of the spine. Overuse trauma is most mainly seen at the lumbar spine in children or adolescents performing sports activities associated with repetitive lumbar hyperextension. Spondylosis, apophyseal damage, and scoliosis form a typical triad of overuse of the thoracic and lumbar spine. Especially, in young patients correct diagnosis not only is the basis for a successful treatment, but might also help to prevent sequelae in later days.

1 Introduction

Spinal manifestations of sports injuries or of overuse at the spine mainly result from activities in certain trend sports with high deceleration or from monotonous repetitive movement patterns. An involvement of the spine has been reported in 10–15% of sports injuries (Tall and DeVault

K. Friedrich · F. Kainberger (✉)
Department of Biomedical Imaging and Image-Guided Therapie, Medical University of Vienna, Vienna, Austria
e-mail: klaus.friedrich@meduniwien.ac.at; franz.kainberger@meduniwien.ac.at

Med Radiol Diagn Imaging (2020)
https://doi.org/10.1007/174_2020_260, © Springer Nature Switzerland AG
Published Online: 01 January 2021

1993). For many forms of sports-associated overuse, especially those located at the vertebral arches, childhood and adolescence form more than 60% of the "vulnerable phases" of life, whereas degenerative disc disease is more commonly observed in adults and has been reported to occur in only 10% in earlier decades (Micheli and Wood 1995). Among the various forms of sports injury and overuse certain relationships exist as "structures of weakness" within a kinetic chain may be prone to earlier or more severe degeneration than others.

The imaging modalities used for documenting sports injuries include conventional radiography (Box 1), computed tomography (CT, Box 2) with multiplanar reformations, and magnetic resonance imaging (MRI, Box 3). Bone scintigraphy with 99m-Tc-diphosphonates has been advocated especially for detecting stress reactions but is of limited value with respect to the continuous improvements of the spatial resolution gained with CT and MRI. Ultrasound has been described for measuring the width of spondylolytic clefts and the thickness of spinal muscles but has not been established in clinical routine (Hides et al. 1995). In the context of biomechanical concepts of trend sports the indications for imaging, the techniques of investigation, and the interpretation of normal and abnormal findings will be reviewed.

Box 1: Plain Radiography
- In many cases the primary investigation
- Enables documentation of segmental abnormalities of flexion and extension
- Evaluation of the spinal alignment
- Evaluation of fractures

Box 2: Computed Tomography
- Should be performed after severe acute traumatic events
- Enables multiplanar reformations in three planes and 3D volume reconstructions
- Shows fractures, especially tiny avulsions

Box 3: MR Imaging
- Should be performed in case of neurological deficit and can also be helpful as second-line investigation in the chronic setting
- Detection of bone marrow edemas, especially in stress reactions
- Evaluation of disc disease, spinal cord, and soft-tissue edema
- Evaluation of rupture of joint capsules/ligaments and of fractures

2 Indications

As a general recommendation based on European referral criteria and the American College of Radiology Appropriateness Criteria, CT without intravenous contrast should be used as a primary investigation in adult patients after blunt trauma of the thoracic or lumbar spine. In cases with neurological abnormalities MR imaging is thought to be the most appropriate next imaging study. Performing a CT study should usually be sufficient in patients without neurologic signs. However, due to the increasing use of the thoracolumbar injury classification and severity score (TLICS), MR imaging is requested more and more often to rule out nonstable fractures, since those normally require surgical stabilization. Patients with chronic complaints should only be evaluated radiologically if clinically indicated in most cases starting with conventional radiographs, eventually followed by MR imaging (De Jonge and Kramer 2014). An important advantage of projection radiography is its potential to document segmental abnormalities of flexion and extension. Such direct information about malalignment may also be appreciated with dedicated low-field MR units, which, however, are still infrequently available.

Specific aspects in sports medicine that should be mentioned in the referral with respect to a dedicated treatment plan include the following:

- The symptoms and signs of the biomechanical "kinetic chain" associated with the type of

trauma or overuse (Kainberger et al. 2006; Lennard and Crabtree 2005).
- Red flags, i.e., signs of severe trauma that may be associated with a neurologic deficit: They should be differentiated from less severe and more commonly observed signs of pain and movement disorders due to self-limiting muscle strains.
- The urgency of "return to play," whether the patient is a professional athlete or is involved in recreational sporting activities (Eck and Riley III 2004).

These general, as well as specific, recommendations are also true for back pain in children which is most commonly observed at the lumbar segment in conjunction with sports.

2.1 Trauma

Fractures mainly result from compression or from a hyperflexion-hyperextension movement pattern with high deceleration, acceleration, or an abrupt change of the direction of movement. With increasing frequency they are associated with trend sports with high speed or jumping movements like motor sports or kite surfing. A typical location is at the thoracolumbar junction.

After acute traumatic events, CT should be performed with multiplanar reformations in three planes. Three-dimensional volume reconstructions are helpful for documenting complex rotational malalignment but its interpretation is associated with a flat learning curve, so that specific experience is needed in using this technique (Schroder et al. 2003). MRI is especially indicated if neural structures seem to be involved which may be caused by a hematoma or by direct violation. MRI is further helpful for documenting a rupture of joints or ligaments, or a disc herniation that in the adolescent athlete may result from abrupt rotational or hyperflexion movements (Fig. 1).

Late sequelae of macro- or microtrauma are degeneration of discs or facet joints and may be documented with conventional radiographs, CT, or MRI (Fig. 2).

Fig. 1 A 17-year-old professional basketball player with lumbar disc dehydration and extrusion at L5/S1 on a sagittal TSE T2-weighted MR image. Additionally, multilevel Schmorl's nodes

2.2 Overuse

Stress reactions of the bone most commonly manifest at the caudal lumbar spine and are associated with track-and-field athletics, dancing, and various activities associated with lumbar hyperextension. Conventional radiographs which include views in two plains and a lateral view of the lumbosacral junction should be exposed. They are generally more reliable than oblique views which, especially in case of an associated scoliosis, may be difficult to be interpreted

Fig. 2 A 21-year-old male high jumper. Sagittal T2-weighted MR image reveals a single Schmorl's node with surrounding bone marrow edema (in keeping with an "acute" Schmorl's node) at the upper endplate L5. The presence of bone marrow edema may correlate with the patient's symptoms

(Amato et al. 1984). A CT with multiplanar reconstructions may be added in equivocal cases. MRI should be performed for assessing the width of the spinal canal and for an associated degenerative disc disease. Sacral stress fractures are less commonly observed and result from excessive transmission of load from the spine to the lower extremities due to jogging, basketball, volley ball, or aerobics (White et al. 2003). MRI is the modality of choice in these cases whilst the diagnosis may be missed with conventional radiographs (Fig. 3).

Imminent spondylolysis should be suspected and radiologically detected in adolescents with unspecific activity-related lower back pain for more than 3–4 weeks (Leone and Cassar-Pullicino 2019); thereby healing can be enabled, progression can be prevented, and a return to sport is possible. This requires activity restriction, rest, and physical therapy with or without a spinal brace for 3–6 months, from the point that a stress reaction was diagnosed; otherwise non-union/olisthesis occur and surgical interventions might be necessary (Overley et al. 2018).

Overuse of the sacroiliac joints in the athlete is often associated with asymmetric load on the pelvic ring and imaging, especially MRI, should be performed to document bone marrow or soft-tissue edema as being important footprints of stress or trauma (Brolinson et al. 2003). Hypertrophy of the piriformis muscle with or without additional muscle fibers originating from the anterior sacral surface may be associated with sciatic nerve entrapment and cross-sectional imaging may have the potential to clarify its clinical appearance (McCrory and Bell 1999).

2.3 Osteoporosis

A decreased bone mineral density has been described in young gymnasts or in ballet dancers with or without secondary amenorrhea (Kaufman et al. 2002). A bone densitometry should be performed in any case of an unclear stress fracture, especially in young active women, as high-intensity training may be regarded as a significant risk factor for developing osteoporosis (Braam et al. 2003). Positive effects of sporting activities on bone density, on the other hand, have been reported for short-term high-performance activities such as sprint, tennis, fencing, as well as weight lifting or heavy athletics (Felsenberg and Gowin 1998; Sabo et al. 1996; Seidl et al. 1993).

3 Image Interpretation

The image analysis has to be focused on the distribution, characteristics, and differential diagnosis of so-called footprints of kinetic chains. The

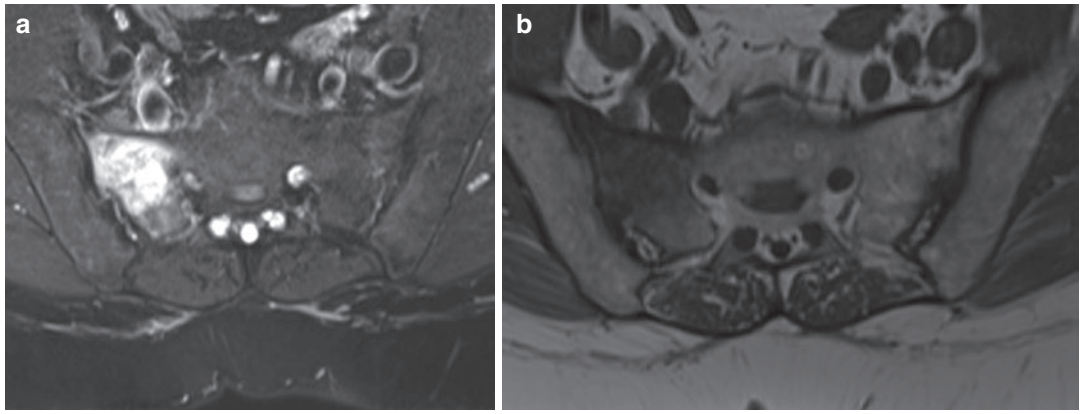

Fig. 3 27-Year-old judoka athlete with right-sided pain since 5 weeks. Unilateral, right-sided stress fracture of the massa lateralis S1. MRI with **a** para-axial STIR and **b** para-axial T1-weighted MR image shows bone marrow edema at the right hemisacrum (case courtesy of F.M. Vanhoenacker)

spinal kinetic chains associated with sports are caused by the effects of high kinetic energies in cases with acute trauma and by effects from monotonous repetitive forces (rowing), asymmetric forces (golf, cricket), or various and less standardized movement patterns (gymnastics).

3.1 Imaging Findings

3.1.1 Trauma

Osseous lesions occur, in contrast to injuries of the cervical spine, less commonly and with less severity observed at the thoracolumbar spine as it has been described in detail for pole-vaulters (Boden et al. 2001). Reports include compression fractures, mainly in contact sports, cycling, or skiing, and flexion-distraction injuries in gymnasts (Katz and Scerpella 2003). The facet lamina fractures (posterior column fractures) of the thoracic spine and the facet posterior fractures of the lumbar spine are typical fracture types that are associated with sports. The concept of the functional reserve of spinal capacity, originally developed by Burrows, may be applied on the thoracolumbar spine (Prasad et al. 2003). Rarely fractures of the superior articular process of S1 can be a source of pain in elite athletes; thus this diagnosis should be kept in mind and it should be noted that in some cases such fractures might be easier to detect on CT than on MRI (Skaggs et al. 2012; Kojima and Asamoto 2017).

Physeal injuries are referred to as the vertebral growth plate. Slipped vertebral ring apophysis may occur in childhood if the apophysis together with the adjacent disc that is tightly fixed by the annulus fibers is displaced posteriorly into the spinal canal. It is a rare entity which usually results from lifting heavy weights.

Spinal cord injury without radiographic abnormality (SCIWORA) is an entity described for children whose spinal structures are of less stiffness than in adulthood. In a meta-analysis it was shown that, in 13%, SCIWORA was associated with sports injuries and 26% occurred at the thoracic spine whereas it was virtually never observed at the lumbar spine (Launay et al. 2005). The prognosis can be improved if the syndrome is diagnosed early and adding MRI to the diagnostic workup may show neural and extraneural injuries.

Muscle strains may be detected rarely with MRI (Bennett et al. 2006).

3.1.2 Congenital and Developmental Disorders

Variants and congenital diseases occur especially at the lumbosacral junction and have, as intrinsic risk factors for overuse syndromes and degenerative diseases, to be assessed radiologically. An incomplete fusion of the vertebral arch at the level of S1 may be associated with a spondylolysis of L5. From the three patterns of incomplete fusion (type I with a wide cleft, type II with small contact between the divided branches, and type

III with overlapping borders), types II and III are regarded as parts of retarded spinal development and are typically observed together with a spondylolysis of L5 (Fig. 4) (Niethard et al. 1997).

In the radiological assessment of scoliosis with respect to sports the Cobb angle should be measured to differentiate more severe forms (higher than 20°) in which axial load should be prohibited from less severe forms (Hochmuth et al. 2002).

3.1.3 Stress Reactions of the Bone and the Discovertebral Junction

Spondylolysis and apophyseal damage form, together with scoliosis, a characteristic triad of overuse of the thoracic and the lumbar spine. Accelerated growth (growth spurt) during adolescence is regarded as an important trigger mechanism in its development (Seitsalo et al. 1991).

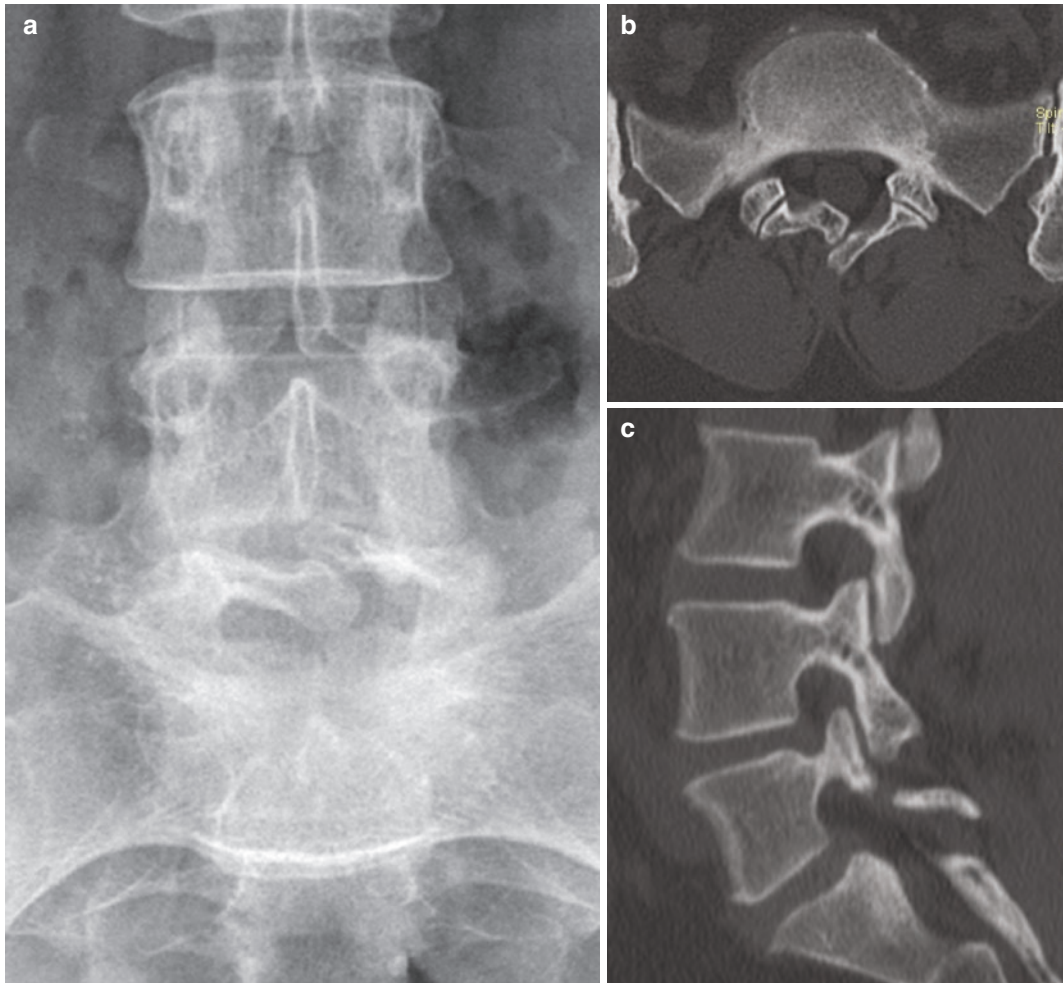

Fig. 4 Former gymnast with incomplete fusion of the vertebral arch of S1 on **a** plain radiograph (type III) and **b** axial CT image and **c** interruption of pars interarticularis of L5 on CT (case courtesy of F.M. Vanhoenacker). **d** Sagittal T2-weighted MR image in another 29-year-old athlete with spondylolysis and anterolisthesis L5 as well as disc bulging L5/S1 and consecutive stenosis of the neuroforamen. **e** Axial CT scan in another gymnast with unilateral left spondylolysis shows an "incomplete ring sign" at the left side and contralateral sclerosis of the right pedicle (case courtesy of F.M. Vanhoenacker)

Fig. 4 (continued)

3.1.4 Osseous Stress Reactions

Spondylolysis manifests typically at the age of 6 years and is in more than 90% located at the fifth lumbar vertebra (Fig. 4), and less commonly at the fourth or at other segments. Sometimes, two or more segments of the lumbar spine may be involved. A reduced resistance of the interarticular portion of the vertebral arch and increased stress due to hyperlordosis are regarded as main causative factors. Therefore, spondylolysis is defined as a stress fracture and many concepts about its etiology and its treatment are based on this definition (Standaert and Herring 2000). According to Vialle et al. (2005), radiologic signs support the concept that a global dystrophic pattern of the lumbosacral junction is an underlying cause of severe spondylolisthesis with increased shear stresses. Spondylolysis seems to be, although asymptomatic forms have been observed in rare cases, the most common cause of back pain in athletes and occurs with higher frequency than in the general population in which it occurs in about 10% (Rossi and Dragoni 1990; Soler and Calderon 2000). There is a racial preponderance with a prevalence of 5–7% in Europeans, 9% in Bantus, 7–10% in Japanese, and up to 50% in Eskimos (Engelhardt et al. 1997). Typical movement patterns for the development of spondylolysis have been described (Table 1) (Bono 2004).

In tennis players, the pars interarticularis is a common site of stress injury with sudden hyperextension of the spine secondary to the serving

Table 1 Common forms of applied forces leading to spondylolysis (modified from Junghanns 1986)

Applied force	Type of activity
Repetitive hyperextension maneuvers	Gymnastics, wrestling, diving, throwing sports, basketball, volleyball, pole vaulting, certain swimming styles (butterfly), high diving
Strong muscle forces	Body building, wrestling, hockey
Repeated monotonous exercises	Rowing
Rotational motion creating unilateral defects	Throwing sports, golf
High and various degrees of movement	Football, track-and-field athletics, dancing, figure skating

and ground stroke motions, increased repetitive motion due to double-handed ground strokes, and increased use of the top spin on hard courts being some of the many potential etiological factors (Rajeswaran et al. 2014).

Spondylolysis results from a low stress resistance of the pars interarticularis of the vertebral arch on one side, and from high stress applied to this structure on the other side. Low stress resistance is mainly due to an elongation and thinning of the pars and is exaggerated by a prominent lordosis of the lumbar spine. Such lordosis especially develops at between 6 and 8 years and is associated with a physiological flexion of the hip joints. Radiological evidence of a lumbosacral transitional vertebra, a congenital cleft of the posterior arch of the S1 segment (spina bifida occulta), or a facet joint anomaly is strongly associated with spondylolysis of L5 (Standaert and Herring 2000). A spina bifida occulta has been described to occur between 13% and 58% concomitant with spondylolysis (Niethard et al. 1997). Spondylolysis also occurs in patients with Marfan syndrome and Ehlers-Danlos syndrome; in the latter disorder it may be severe. Osteogenesis imperfecta and osteopetrosis are other forms of systemic diseases related to spondylolysis. Repeated microfractures are mainly related to hyperextension movements, thus amplifying the lordotic state. Muscle strength and tension may influence the development of spondylolysis by shortening or tightness of the hamstring muscles of the thigh with increased tension on the posterior vertebral arches of the lower lumbar spine. Weakening of the spinal and the anterior abdominal wall muscles is a precursor in the development of spondylolysis, too, whereas strengthening parts of these muscles should have a preventive effect.

In the later course of spondylolysis, fibrous or bony callus formation at the pars defect site may develop. Bony outgrowths, facet joint arthrosis, or instability may lead to nerve root impingement with leg pain, numbness, or weakness.

A cleft of the vertebral arch detected on oblique views ("Scotty dog" or "LaChapel's dog") is a direct sign of spondylolysis. More sensitive imaging techniques for the diagnosis may be a lateral view of the lumbosacral junction, multiplanar CT, and MRI. Flexion and extension views are helpful to document signs of hypermobility. These findings and a cleft of more than 3 mm width are indicators of a late phase of spondylolysis with a poorer prognosis than during the early phase (Engelhardt et al. 1997). During anteflexion, a complex gliding mechanism may be observed fluoroscopically: the vertebra, partially fixed at the facet joints, moves with a sudden jump in a retrolisthetic position. With such abnormal movements the increased stress on the facet joints and the spinal nerves in the adjacent intervertebral foramina may be explained. On axial CT or MR images, the spondylolytic clefts adjacent to the facet joint spaces may appear as the "double facet joint" or "incomplete ring" sign (Fig. 4). In the case of unilateral spondylolysis, reactive sclerosis may develop at the contralateral pedicle (Fig. 4). On MR images, bone marrow edema within the vertebral arch or a bony sclerosis may be observed in 40% and MR imaging may be used as a reliable modality for the diagnosis of juvenile spondylolysis (Campbell et al. 2005; Ulmer et al. 1997). Stäbler et al. (2000) have described the importance of detecting stress reactions (T1-weighted hypointense and T2-weighted hyperintense; bone marrow edema) without visible fracture lines for early diagnosis.

The degree of destruction of the interarticular portion may be graded as follows: 0, normal; I, intact with bone marrow edema (stress reaction); II, sclerosis or low signal with intact cortex; III, indeterminate; IVa, cortical discontinuity on one side of pars; iVb, complete discontinuity of pars (Campbell et al. 2005). Sherif and Mahfouz (2004) mentioned the interposition of fatty tissue between the dural sac and the spinous process of L5 as a helpful indirect sign of spondylolysis.

An isthmic spondylolisthesis may develop in 4% of spondylolysis (Fig. 4) (Danielson et al. 1991). It is a forward movement of the body of one of the lumbar vertebrae on the vertebra below it, whereas the posterior joints and the neural arches are aligned with the posterior elements of the inferior vertebral body. Spondyloptosis is a fully dislocated vertebral body. Spondylolisthesis occurs in preadolescents and is found in up to 50% of athletes with persistent back pain. Symptoms may not occur until later in life. In a longitudinal study by Fredrickson et al. (1984), three-quarters of all individuals with spondylolysis had an identifiable pars defect on plain films by age 6, and approximately 75% of these patients had evidence of a slip at that time. Further progression of the slip in adulthood is rare (Floman 2000).

An early gliding of more than 20% is the only predictor for spondylolisthesis that has been described (Seitsalo et al. 1991). Muschik et al. (1996) observed a progression of this entity especially during growth spurt. Meyerding grading into four stages oriented on the sagittal diameter of the subjacent vertebra has been generally accepted (Meyerding 1932). On axial CT or MR images, an oval elongation of the spinal canal and a stenosis of the intervertebral foramina with atrophied perineural fat are associated findings.

Other forms of spinal stress fractures are rare and may be observed at the cervical spine. At the chest, such fractures generally occur at the ribs rather than at the thoracic spine (Karlson 2004). The ribs of the lower chest may be injured in golfers or rowers, whereas fractures of the first rib may occur in weight lifters, throwers, or rucksack-carrying hikers.

3.1.5 Discovertebral Overuse

Apophyseal damage or microfractures of the vertebral endplates are typical findings in weight lifters, wrestlers, and track-and-field athletes and are part of Scheuermann's disease. It is also observed in professional downhill skiers (Ogon et al. 2001). There is a clear genetic predisposition for developing Scheuermann's disease, but observations in adolescents with high athletic activity underline the aspect of overuse in its etiology especially in the "atypical" or "traumatic" subtype which is located at the thoracolumbar junction (Alexander 1977).

With respect to the different types of endplate reactions that may or may not be associated with Scheuermann's disease, there is general agreement that Schmorl's nodes, especially their chronic forms, are not indicators of athletic injury, whereas anterior lesions are related to sports and may be associated with back pain (Ogon et al. 2001).

These anterior lesions (Fig. 5), the limbus vertebrae (LV) or slipped vertebral apophysis, are a disorder with cartilaginous node formation due to intraosseous disc penetration at the border of the rim apophysis. During flexion, the anterior part of the disc is pressed under the superior nonfused endplate. It typically occurs during the second decade of life after the rim apophysis has formed (7–9 years) and before its fusion with the vertebral body. The abnormality is typically observed in athletic adolescents (Ross et al. 2004).

The degree of thoracic kyphosis is increased in adolescent gymnasts but, in contrast to heavy workers, does not reach the pathologic ranges that are associated with Scheuermann's disease (Hochmuth et al. 2002).

3.1.6 Degenerative Joint and Disc Disease

Degeneration, despite its higher frequency in the later decades of life, may be observed in young athletes—especially gymnasts and wrestlers—and occurs rather in the nucleus than in the annulus (Sward 1992). It has also been described that disc herniations occur slightly more often in elite tennis players than in asymptomatic nonathletes

Fig. 5 Limbus vertebrae in two different patients. **a** Sagittal TSE T2-weighted MR image shows a sequela of an intravertebral herniation separating the anterosuperior ring apophysis L4 in a 33-year-old swimmer and biker. Note also disc degeneration at L3/L4. **b** Conventional radiograph and **c** CT scan in another gymnast showing separation of the rim apophyses at multiple levels (cases courtesy of F.M. Vanhoenacker)

(Rajeswaran et al. 2014), which can be explained by the repeatedly high degree of axial loading and axial rotation during the serving and ground stroke motions; the majority of these disc herniations were at the levels L5/S1 and L4/L5. In the same way as with Scheuermann's disease, a

genetic influence has been proposed for the development of disc degeneration in children. Abnormal segmental movement patterns in the forms of hyper- or hypomobility or of instability may be best documented on flexion and extension views.

Facet joint arthropathy has been described as the most common abnormality in almost 90% of asymptomatic elite junior tennis players; it is thought to be the result of repeatedly axial rotation and impaction of the facet joints, which occurs during the tennis serve, and ground top spin strokes. Synovial cyst formation arising from the facet joints has also been described to be relatively prevalent in young elite tennis players; however, most of those synovial cyst formations occurred posteriorly (Rajeswaran et al. 2014).

3.2 Differential Diagnosis

Back pain in athletes not resulting from sporting activities may be due to diseases commonly occurring in adolescents and young adults, especially rheumatic diseases, tumors, or unexpected trauma. Their first clinical manifestation may, however, be in conjunction with sporting activities and characteristic imaging findings can be a hallmark of the correct diagnosis.

Inflammatory back pain is a typical symptom of seronegative spondylarthropathies (ankylosing spondylitis, psoriatic arthropathy, and reactive arthritis). Bone marrow edema, sclerosis, or erosions may be observed at the sacroiliac joints or in the form of anterior spondylitis at the thoracolumbar junction; endplate changes, like the Andersson lesions, are well-known manifestations of ankylosing spondylitis. However, also bone marrow as well as soft-tissue edema of the facet and the costovertebral joints are typically seen in patients with seronegative spondylarthropathies.

Osteoid osteoma is typically located at the pedicle roots of the lumbar spine with a characteristic calcified nidus within an osteolysis. CT is the modality of choice for its detection, whereas MRI may be difficult to be interpreted because of the various tissue contrast of the nidus. However, osteoid osteoma should always be considered in case of marked bone marrow and adjacent soft-tissue edema in the typical location in a patient without trauma between 10 and 35 years; to identify a nidus, CT is recommended. Bone scintigraphy is helpful especially if performed with single-photon emission computed tomography (SPECT). Primary malignant bone tumors (osteosarcoma, chondrosarcoma, chondroma) or malignant bone marrow diseases are generally rare and present with osteolysis and typical calcification patterns.

Non-accidental trauma (battered child syndrome) has to be considered in any case of unclear trauma, especially if manifestations do not match with patterns of kinetic chains of if they are observed asynchronically. Apophyseal injuries at the thoracic or lumbar spine have been described to be associated with this entity (Levin et al. 2003).

Congenital vertebral clefts at the lumbar spine are in most cases observed as median interruptions of the vertebral arch, and less commonly as paraspinal, retroisthmic, or retrosomatic forms. They have to be differentiated from spondylolysis vera.

4 Conclusion

The biomechanics of all major types of sports with spinal involvement along with the typical movement patterns is the basis for the diagnosis and treatment of pain, restricted motion, or other associated findings (Lennard and Crabtree 2005). Cross-sectional imaging modalities and attempts to document the spinal kinematics are promising techniques to document normal as well as abnormal states and movement patterns. Imaging interpretation should therefore be based on "footprint" patterns of kinetic chains associated with certain athletic activities.

Things to Remember

- The spine is involved in 10–15% of sports injuries.
- Overuse trauma of the vertebral arches is mainly seen in childhood and adolescence,

whereas degenerative disc disease is most commonly seen in older athletes.

- Overuse trauma is most commonly seen at the lumbar spine in sports activities associated with lumbar hyperextension. Spondylosis, apophyseal damage, and scoliosis form a typical triad of overuse of the thoracic and lumbar spine.
- Congenital and developmental disorders are risk factors for overuse syndromes and degenerative diseases of the spine.
- A limbus vertebra occurs typically in athletic adolescents.

References

Alexander C (1977) Scheuermann's disease: a traumatic spondylodystrophy? Skelet Radiol 1:209–221

Amato M, Totty WG, Gilula LA (1984) Spondylolysis of the lumbar spine: demonstration of defects and laminal fragmentation. Radiology 153:627–629

Bennett DL, Nassar L, Delano MC (2006) Lumbar spine MRI in the elite-level female gymnast with low back pain. Skelet Radiol 35:503–509

Boden BP, Pasquina P, Johnson J et al (2001) Catastrophic injuries in pole-vaulters. Am J Sports Med 29: 50–54

Bono CM (2004) Low-back pain in athletes. J Bone Joint Surg Am 86A:382–396

Braam LA, Knapen MH, Geusens P et al (2003) Factors affecting bone loss in female endurance athletes: a two-year follow-up study. Am J Sports Med 31:889–895

Brolinson PG, Kozar AJ, Cibor G (2003) Sacroiliac joint dysfunction in athletes. Curr Sports Med Rep 2:47–56

Campbell RS, Grainger AJ, Hide IG, Papastefanou S, Greenough CG (2005) Juvenile spondylolysis: a comparative analysis of CT, SPECT and MRI. Skelet Radiol 34:63–73

Danielson BI, Frennered AK, Irstam LK (1991) Radiologic progression of isthmic lumbar spondylolisthesis in young patients. Spine 16:422–425

De Jonge M, Kramer J (2014) Spine and sport. Semin Musculoskelet Radiol 18:246–264

Eck JC, Riley LH III (2004) Return to play after lumbar spine conditions and surgeries. Clin Sports Med 23:367–379

Engelhardt M, Reuter I, Freiwald J et al (1997) Spondylolysis and spondylolisthesis and sports. Orthopade 26:755–759

Felsenberg D, Gowin W (1998) Bone densitometry: applications in sports-medicine. Eur J Radiol 28:150–154

Floman Y (2000) Progression of lumbosacral isthmic spondylolisthesis in adults. Spine 25:342–347

Fredrickson BE, Baker D, McHolick WJ et al (1984) The natural history of spondylolysis and spondylolisthesis. J Bone Joint Surg Am 66:699–707

Hides JA, Richardson CA, Jull GA (1995) Magnetic resonance imaging and ultrasonography of the lumbar multifidus muscle. Comparison of two different modalities. Spine 20:54–58

Hochmuth K, Mack MG, Kurth AA et al (2002) Sports-related injuries of the spine. Radiologe 42: 823–832

Junghanns H (1986) Die Wirbelsäule unter den Einflüssen des täglichen Lebens, der Freizeit, des sports, vol 35. Thieme, Stuttgart

Kainberger F, Weidekamm CM, Trieb K (2006) Sports injury of the spine: imaging diagnosis. Rontgenpraxis 56:47–57

Karlson KA (2004) Thoracic region pain in athletes. Curr Sports Med Rep 3:53–57

Katz DA, Scerpella TA (2003) Anterior and middle column thoracolumbar spine injuries in young female gymnasts. Report of seven cases and review of the literature. Am J Sports Med 31:611–616

Kaufman BA, Warren MP, Dominguez JE et al (2002) Bone density and amenorrhea in ballet dancers are related to a decreased resting metabolic rate and lower leptin levels. J Clin Endocrinol Metab 87: 2777–2783

Kojima K, Asamoto S (2017) Bilateral fracture of the superior articular process of S1 – an unusual fracture seen in a speed skater. Br J Neurosurg 31:273–274

Launay F, Leet AI, Sponseller PD (2005) Pediatric spinal cord injury without radiographic abnormality: a meta-analysis. Clin Orthop Relat Res 2005:166–170

Lennard T, Crabtree H (2005) Spine in sports. Elsevier Mosby, Philadelphia, pp 57–220

Leone A, Cassar-Pullicino VN (2019) Sports overuse and injury: the spine. Imaging of motion and performance – stress and strain. The European Society of Radiology, Vienna, pp 79–81

Levin TL, Berdon WE, Cassell I et al (2003) Thoracolumbar fracture with listhesis – an uncommon manifestation of child abuse. Pediatr Radiol 33:305–310

McCrory P, Bell S (1999) Nerve entrapment syndromes as a cause of pain in the hip, groin and buttock. Sports Med 27:261–274

Meyerding H (1932) Spondylolisthesis. Surg Gynec Obstet 54:371–377

Micheli LJ, Wood R (1995) Back pain in young athletes. Significant differences from adults in causes and patterns. Arch Pediatr Adolesc Med 149:15–18

Muschik M, Hahnel H, Robinson PN et al (1996) Competitive sports and the progression of spondylolisthesis. J Pediatr Orthop 16:364–369

Niethard FU, Pfeil J, Weber M (1997) Etiology and pathogenesis of spondylolytic spondylolisthesis. Orthopade 26:750–754

Ogon M, Riedl-Huter C, Sterzinger W et al (2001) Radiologic abnormalities and low back pain in elite skiers. Clin Orthop Relat Res 390:151–162

Overley SC, McAnany SJ, Andelman S et al (2018) Return to play in adolescent athletes with symptomatic spondylolysis without listhesis: a meta-analysis. Global Spine J 8:190–197

Prasad SS, O'Malley M, Caplan M et al (2003) MRI measurements of the cervical spine and their correlation to Pavlov's ratio. Spine 28:1263–1268

Rajeswaran G, Turner M, Gissane C, Healy JC (2014) MRI findings in the lumbar spines of asymptomatic elite junior tennis players. Skelet Radiol 43:925–932

Ross J, Brant-Zawadzki M, Moore K et al (2004) Diagnostic imaging: spine. Amirsys, Salt Lake City 1:82–85

Rossi F, Dragoni S (1990) Lumbar spondylolysis: occurrence in competitive athletes. Updated achievements in a series of 390 cases. J Sports Med Phys Fitness 30:450–452

Sabo D, Bernd L, Pfeil J et al (1996) Bone quality in the lumbar spine in high-performance athletes. Eur Spine J 5:258–263

Schroder RJ, Albus M, Kandziora F et al (2003) Diagnostic value of three-dimensional reconstruction in CT of traumatic spinal fractures. Rofo 175:1500–1507

Seidl G, Kainberger F, Haber P et al (1993) Systematisches Krafttraining in der Postmenopause: begleitende densitometrische Kontrolle mittels DXA. Radiologe 33:452–456

Seitsalo S, Osterman K, Hyvarinen H et al (1991) Progression of spondylolisthesis in children and adolescents. A long-term follow-up of 272 patients. Spine 16:417–421

Sherif H, Mahfouz AE (2004) Epidural fat interposition between dura mater and spinous process: a new sign for the diagnosis of spondylolysis on MR imaging of the lumbar spine. Eur Radiol 14:970–973

Skaggs DL, Avramis I, Myung K, Weiss J (2012) Sacral facer fractures in elite athletes. Spine 37:E514–E517

Soler T, Calderon C (2000) The prevalence of spondylolysis in the Spanish elite athlete. Am J Sports Med 28:57–62

Stäbler A, Paulus R, Steinborn M et al (2000) Spondylolysis in the developmental stage: diagnostic contribution of MRI. Rofo 172:33–37

Standaert CJ, Herring SA (2000) Spondylolysis: a critical review. Br J Sports Med 34:415–422

Sward L (1992) The thoracolumbar spine in young elite athletes. Current concepts on the effects of physical training. Sports Med 13:357–364

Tall RL, DeVault W (1993) Spinal injury in sport: epidemiologic considerations. Clin Sports Med 12:441–448

Ulmer JL, Mathews VP, Elster AD et al (1997) MR imaging of lumbar spondylolysis: the importance of ancillary observations. AJR Am J Roentgenol 169:233–239

Vialle R, Schmit P, Dauzac C et al (2005) Radiological assessment of lumbosacral dystrophic changes in high-grade spondylolisthesis. Skelet Radiol 34:528–535

White JH, Hague C, Nicolaou S et al (2003) Imaging of sacral fractures. Clin Radiol 58:914–921

Sports-Related Maxillofacial Injuries

Anja Bernaerts, Barbara Veys, Johan Abeloos, Kathleen Dhont, Jan Casselman, and Bert De Foer

Contents

A. Bernaerts (✉) · K. Dhont · B. De Foer
Department of Radiology, GZA Hospitals, Wilrijk, Belgium
e-mail: Anja.Bernaerts@gza.be

B. Veys · J. Abeloos
Department of Maxillo-Facial Surgery, AZ Sint-Jan Brugge-Oostende AV, Bruges, Belgium

J. Casselman
Department of Radiology, GZA Hospitals, Wilrijk, Belgium

Faculty of Medicine and Health Sciences, Ghent University, Ghent, Belgium

Department of Radiology, AZ Sint-Jan Brugge-Oostende AV, Bruges, Belgium

Abstract

Sports-related trauma may have a significant impact on both function and aesthetics of the maxillofacial region. Although the majority of sports-related maxilla-facial injuries are of minor nature, such as soft tissue lacerations, dentoalveolar fractures and minor facial bone fractures, sports-related facial fractures are reported to account up to 42% of all facial bone fractures. This article highlights the injury mechanism in different sports-related facial trauma. In addition, it provides an overview of the imaging strategy and classification systems of dental, mandibular and maxillofacial injuries and fractures as a framework for an effective radiological approach and clinically beneficial reports. The key imaging features that are critical for clinical management are emphasized.

1 Introduction

Sports-related trauma may have a significant impact on both function and aesthetics of the maxillofacial region. The most common maxil-

Med Radiol Diagn Imaging (2020)
https://doi.org/10.1007/174_2020_261, © Springer Nature Switzerland AG
Published Online: 10 December 2020

lofacial injuries due to sports are soft tissue lacerations followed by dentoalveolar fractures and minor facial bone fractures, respectively (Hill et al. 1998; Tuli et al. 2002). The most frequently recorded facial bone fractures involve in descending order, the nose, zygoma and mandible (Maladiere et al. 2001; Ruslin et al. 2016; Viozzi 2017).

According to different reports, sports-related facial fractures account for 10–42% of all facial bone fractures (Viozzi 2017). This variation in occurrence may reflect the geographic differences in the level of participation in sports activities and the type of popular sports. Fractures of the maxillofacial region are more frequent in males and between the ages of 20 and 30 years, most likely reflecting the high levels of physical activity, the riskier behaviour as well as higher impact forces during sporting activities in this sex and age group (Ruslin et al. 2016). Children are less prone to facial fractures than adults due to certain anatomical attributes (less calcified facial bones and a higher cranial-to-facial ratio than adults); however when they do occur, they tend to have more severe concomitant injuries due to the higher threshold of force required for injury (Gassner et al. 2004). These injuries include intracranial haemorrhage and traumatic brain injury (Dobitsch et al. 2019).

The sport responsible for the majority of injuries varies above all according to the popularity of each sport activity in a particular country. The majority of facial fractures in western countries today occur during team sports, such as soccer, basketball, rugby and hockey and are most often due to direct hits with a ball or player-to-player contact (Ruslin et al. 2016).

Various sports committees have adopted specific guidelines for the prevention of dental and craniomaxillofacial injuries (helmets, safety glasses, etc.). Sports such as hockey and American football have even adopted full facial and cranial protective headgear. Evolution of these protective devices had significantly reduced many types of head and neck injuries in these sports (Greenberg and Haug 2005). However, this decreasing trend is attenuated to a certain degree by the emergence of relatively new, more dangerous sports activities such as high-velocity vehicular and high altitude-dependent activities. Moreover, amateur athletes often do not use any protection in sports in which the use of protective gear is recommended.

This article highlights the injury mechanism in different sports-related facial trauma in support of clinical history taking and physical examination. In addition, it provides an overview of the imaging strategy and classification systems of facial fractures as a framework for effective radiological approach and clinically beneficial reports. The key imaging features that are critical for clinical management are emphasized.

2 Correlation Between Injury Type and Injury Mechanism Among Sports

There have been few studies that have been directed towards the biomechanics of maxillofacial injuries associated with sports. Perhaps the difficulty of engaging in such a study is the large variety of sports activities that are available today ranging from those with minimal interpersonal contact to those with high-energy contact. In addition, comparative analysis of these studies is hampered by varied selection criteria and the use of retrospective non-consecutive data.

2.1 Dentoalveolar Fractures

In dentoalveolar fractures, a high-velocity trauma, such as a baseball that takes a bad hop and strikes the maxillary incisors, is more likely to cause a tooth fracture, whereas a low-velocity trauma is more expected to cause a luxation or avulsion. Fractures due to traumatic incidents are mainly horizontal unlike fractures due to iatrogenic conditions (e.g. endodontic treatment) which cause primarily vertical fractures (Alimohammadi 2018). Children with a type 2 malocclusion (so-called retrognathism or overbite) in particular will be prone to sports-related dentoalveolar injuries of the upper incisors.

Another mechanism, indirect trauma, occurs when the mandible whiplashes into collision with the maxilla. This trauma can occur from a blow to the chin, such as an uppercut in boxing, a football tackle, or a hockey stick. The concussion is capable of shattering posterior teeth.

Enamel infraction can be caused by acute or chronic trauma such as grinding or clenching (e.g. weightlifting) (Kurtz et al. 2005).

2.2 Facial Bone Fractures

Sporting activities can be grouped into different categories in order to better understand the injury mechanism in sports-related facial bone fractures:

- *Team sports*: soccer, rugby, basketball, football, handball, hockey
- *Vehicular sports*: bicycling, mountain biking, horse riding, skiing, snowboarding, ice hockey, in-line skating
- *Sports with small balls*: tennis, baseball, cricket, golf, squash
- *Combat sports*: boxing, wrestling, martial arts
- *Individual sports*: swimming, diving, gymnastics, bodybuilding, etc.

In team sports the main type of impact in facial bone fractures appears to be a collision with another player that takes place for instance when the ball is played with the forehead. At this moment there can be an elbow-head impact or a head-head impact. An analysis of the anatomic distribution of facial fractures sustained during team sports showed that the nose followed by the zygomatic complex and the mandible are most commonly involved (Ruslin et al. 2016; Bobian et al. 2016). Coronoid process fractures are almost exclusively observed in soccer players whereas mandible angle fractures are relatively more frequent in rugby players (Ruslin et al. 2016). Football players do not encounter orofacial injuries as often as other athletes because faceguards and mouth protectors are now mandatory (Flanders and Bhat 1995; Sane 1988).

In vehicular, non-car, sports, a fall to the ground is the most commonly reported type of impact. Fractures of the mandible and zygoma are most prominent in vehicular sports as well, but unlike team sports, the frontal sinus and central midface are commonly affected too (Gassner et al. 1999; Maladiere et al. 2001). Generally, mountain bikers sustain more severe maxillofacial injuries in comparison with bicyclists. The dominant fracture site in bicyclists is the zygoma, whereas mountain bikers and motorcyclists encounter more serious midface fractures such as Le Fort I, II, and III fractures (Gassner et al. 1999). In horse riding, being kicked by the horse is also correlated with more severe injuries (Ueeck et al. 2004).

A missile type of injury to the head caused by a ball or other implement is mostly mentioned in sports with small balls such as baseball (Bak and Doerr 2004; Delilbasi et al. 2004; Maladiere et al. 2001). Contact with a racquet, a bat or club also is a common cause of injury in this category (Lim et al. 1993). Although small ball-related ocular injuries are uncommon in sports-related traumas, when they do occur, they are often devastating and can even require enucleation in case of rupture (Park et al. 2014).

Combat sports-related facial injuries occur most frequently in wrestling, followed by martial arts and only then in boxing. This might be due to the protective headgear, which is used during boxing. Nasal bone fractures account for the majority of facial fractures, followed by orbital, mandibular and zygomaticomaxillary complex (ZMC) fractures (Hojjat et al. 2016).

Scuba diving entails risks to the maxillofacial region in a specific way. The mechanical effects from changes in ambient pressure may cause paranasal sinus barotraumas. More than 10% of experienced divers have a history of paranasal sinus barotrauma in their career. During descent, air in the paranasal sinuses is compressed according to Boyle's law. In the event of any blockage of the drainage pathways secondary to an acute upper respiratory tract infection or chronic rhinosinusitis, pressures cannot be equalized with air passing into the sinuses. The diver complains of pain over the affected sinus during descent. The

relatively low pressures cause mucosal oedema and effusion with rupture of small blood vessels, causing bleeding into the sinuses, thereby reducing the pressure and the degree of pain and discomfort. During ascent, this air then expands in the paranasal sinuses with drainage of mucus and blood from the sinuses (often visible in the diver's mask). Rarely, the drainage pathways are blocked to an extent that the pressure inside the sinuses cannot overcome the blockage and the expanding air may fracture the walls of the sinuses, tracking along the soft tissues. This may cause emphysema, bruising, and haemorrhage in adjoining skin and damage to the orbital content and vision. If air tracks intracranially, this leads to pneumocephalus. Furthermore, temporomandibular joint dysfunction may result from repeated use of the mouthpiece of the regulator (Lechner et al. 2018).

3 Imaging Strategy

The diagnosis of facial fractures usually is accomplished by a combination of clinical and imaging examinations. Often, deformity of the facial skeleton is initially concealed by overlying oedema, haemorrhage and soft tissue injury. Therefore, the clinician is primarily concerned with the detection of malocclusion, abnormal mobility and crepitation as a sign of fracture. Any evidence of a palpable step-off at the orbital rim, diplopia, hypertelorism, midfacial elongation, cerebrospinal fluid rhinorrhoea, or flattening of the cheek further helps the clinician to identify the type of fracture present. Radiological evaluation is however of utmost importance in the diagnosis and classification of fractures and traumatic injuries of the facial skeleton. It helps in making a correct diagnosis, in describing the exact extent of these fractures and in optimal treatment planning (Greenberg and Haug 2005).

3.1 Plain Radiography

The orthopantomogram (OPG) is still a highly cost-effective and accurate method for the diagnosis of dental, dentoalveolar and mandibular fractures. It can be used as an initial survey in all mandibular and maxillofacial fractures (Fig. 1) (Box 1). In case of a dental trauma, supplementary intraoral periapical radiographs—usually in multiple projections—are always required to

Fig. 1 26-year-old medical doctor complaining of pain after a kick on his cheek during mixed martial arts. He also reported hearing a "crackling" sound. Orthopantomogram shows a fracture line running through the mandibular angle on the right side, just posterior to the third molar tooth. There is a minimal displacement. *Courtesy: Frank Pameijer, MD, PhD, Utrecht, The Netherlands*

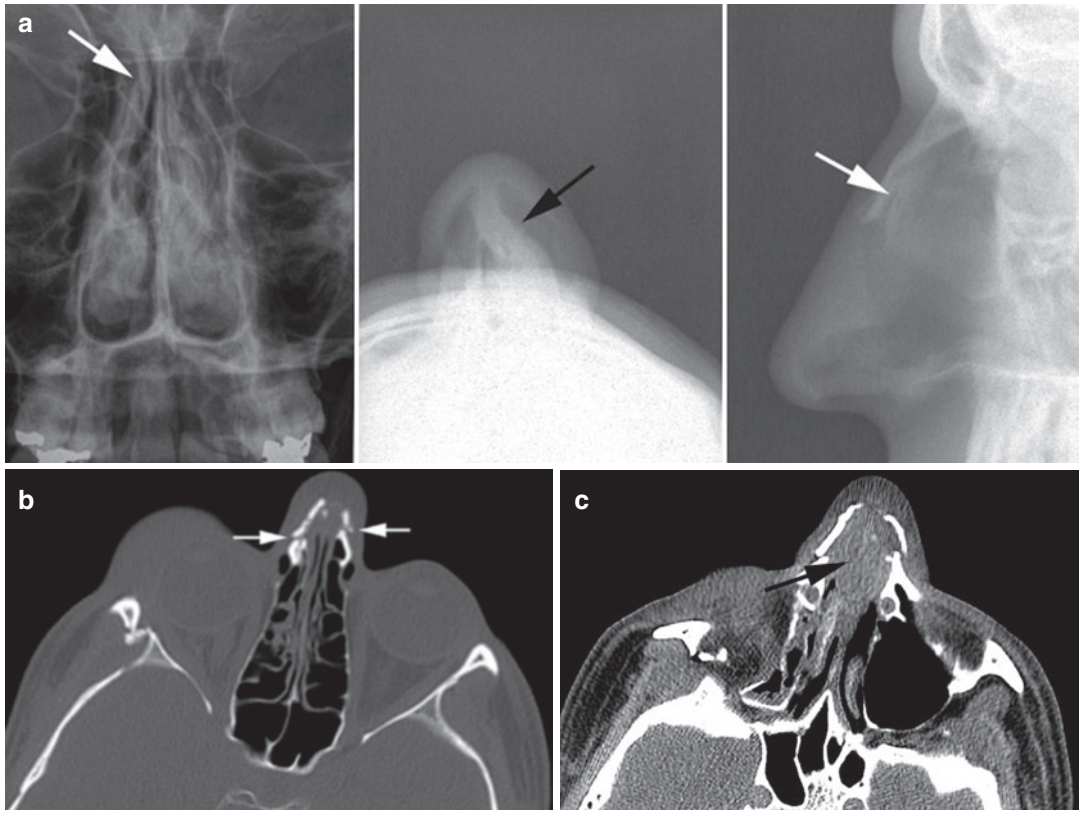

Fig. 2 25-year-old male soccer player who encountered a complex nasal fracture after being kicked in the face by an opponent's foot. **a** Radiographic evaluation of the nasal bone including a frontal, superior-inferior and lateral view confirms a fracture of the nasal bone (*white arrows*). A deviation of the cartilaginous portion of the nasal septum is noted (*black arrow*). **b** Axial CT scans viewed at "bone" and **c** "soft-tissue" window settings show comminuted fractures of both nasal bones and right frontal process of the maxilla (*white arrows*). Also note the presence of a septal haematoma (*black arrow*) and an associated displaced fracture at the right zygomaticosphenoid suture

obtain adequate image detail and to visualize the fracture (White and Pharoah 2000).

In the evaluation of a (complex) facial trauma, the use of plain radiographs is nowadays limited to the evaluation of the (isolated) nasal bone fracture. Nasal bone radiographs generally give no additional information that is helpful either in reaching a diagnosis or in deciding on the therapeutic management, but it can be performed to confirm a clinical diagnosis, to verify the displacement of the various and/or for medical–legal purposes (Fig. 2) (Marston et al. 2017).

With the advent of 3-dimensional (3D) imaging, the use of various standard skull radiographs such as PA view, AP view and lateral view as well as more specific incidences such as Towne view, Caldwell view and (reverse) Waters view are no longer advocated (Alimohammadi 2018).

3.2 Multidetector Versus Cone Beam Computed Tomography (CT)

Radiological evaluation of maxillofacial trauma using plain radiographs delivers information based upon bidimensional geometric projections. These techniques hence suffer

Box 1: Orthopantomogram (OPG)
- Easy interpretation
- Cost-effective
- Initial survey in case of isolated trauma of the mandible
  - Dentoalveolar injuries
  - Mandibular fractures

from superposition due to the curved configuration and complex anatomy of the mandible and maxilla, allowing them to conceal a lesion or anatomical structures of interest. As a consequence, the traditional strong role of conventional X-ray imaging of patients with facial bone fractures nearly completely has disappeared.

3D cross-sectional imaging is able to overcome these obstacles and results in superior diagnostic capabilities. It allows accurate information about bone morphology and structure, as well as information about the location of critical anatomical structures such as neurovascular canals, paranasal sinuses and the nasal cavity. 3D cross-sectional imaging has become the imaging tool of choice in the evaluation of the patient with a maxillofacial trauma. It is able to evaluate the bony as well as the soft tissue structures and to describe the exact extent and displacement of the various fractures enabling adequate classification of these fractures as well as appropriate treatment. Based upon the acquired 3D data set, contiguous multiplanar reconstructions (MPR) in the three different planes (axial, coronal and sagittal) are acquired on a routine basis, with a slice thickness of 1–2 mm. 3D volume rendering and surface shaded display CT reconstructions deliver a real 3-dimensional image at one glance and are particularly helpful for treatment in case of multiple fragments and/or severe fragment dislocation. Using various software programs, the surgeon can also even plan and optimize the surgery in advance using these 3D images. Mirroring techniques for zygomatic complex fractures, navigational surgery for orbital floor and even patient specific implants (3D printing) can be provided.

Two types of 3D cross-sectional imaging currently are available for the radiological evaluation of a patient with a mandibular or midface trauma: Multidetector Computed Tomography (MDCT) as well as Cone Beam Computed Tomography (CBCT).

Multidetector Computed Tomography Scan (MDCT) uses a "fan beam" X-ray in combination with multiple rows of detectors while the patient is moving through this X-ray detector combination in the *z*-axis during data acquisition. Essentially, MDCT is acquiring multiple slices put together to form a volumetric data set. Slice thickness of 0.4–0.6 mm can be acquired. The smallest picture element of an acquired 3D imaging volume is called a voxel. A voxel is represented as a cube, with a certain height, width and depth. MDCT voxels are non-isotropic, meaning that 2 sides of the voxels are equal, but that the 3rd side has a selectable width, determined by the distance the patient moves through the gantry in the z-plane. As a result, axial reconstructions in MDCT are of a higher quality than the reconstructions into the coronal and sagittal plane. Metal artefacts from tooth filling or osteosynthesis material can also degrade imaging quality. On the other hand, evaluation can be done in bone window setting as well in soft tissue setting.

CBCT uses a "cone beam" X-ray in combination with a flat panel detector resulting in the acquisition of a volume scan during a single rotation around the patient. It provides a high isotropic spatial resolution with a relatively low patient dose, compared to MDCT, and at a lower cost. CBCT voxels are isotropic, resulting in images reconstructed in any plane with high fidelity (Miracle and Mukherji 2009; Shintaku et al. 2009; Doğan et al. 2018). To be able to differentiate between small structures, the voxel size needs to be smaller than the desired structure that has to be visualized. The small field-of-view units of a CBCT can use a voxel size down to 0.075 mm, which enables visualization of small structures with high fidelity. Therefore, CBCT is—due to

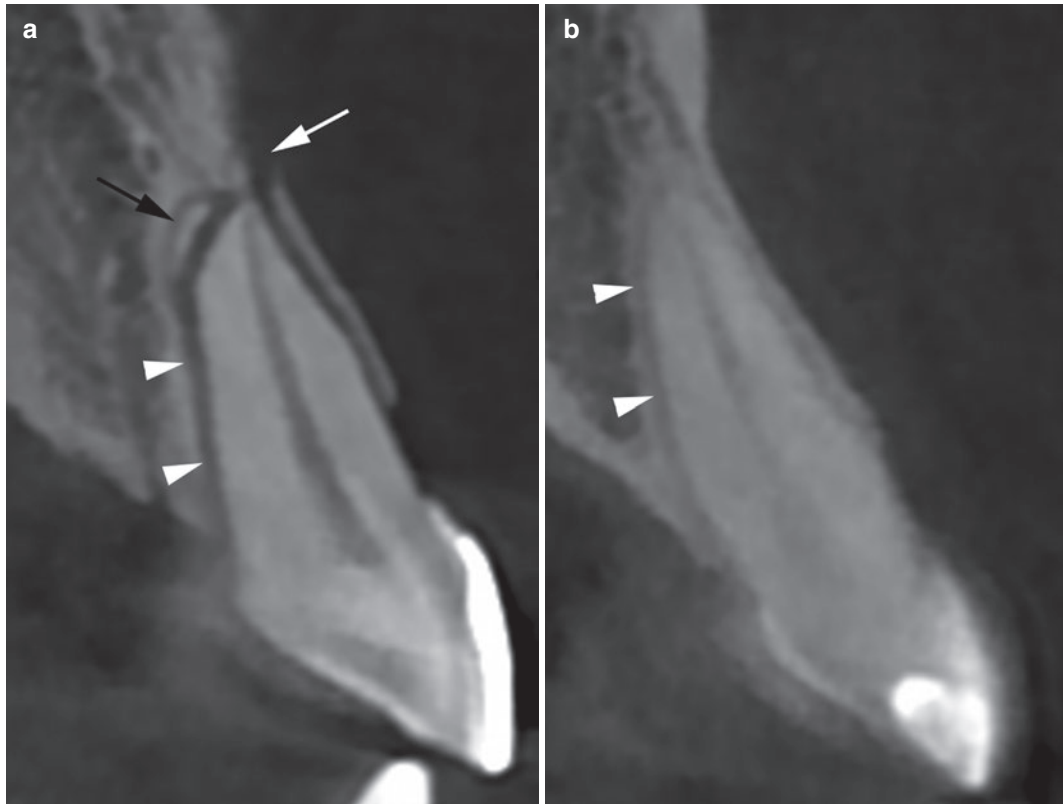

Fig. 3 25-year-old male presenting with tooth pain after a fall with his bicycle. **a** Sagittal CBCT reformation through the left central maxillary incisor not only demonstrates a fracture line (white arrow) at the labial plate but also a small fracture of the apex of the tooth (black arrow). The extrusive luxation is also visible as a widening of the periodontal ligament space (arrowheads). Compare to figure **b**. **b** Sagittal CBCT reformation at the level of the left lateral maxillary incisor illustrating the normal periodontal ligament space, visible as a very thin radiolucent line between the tooth and the tooth socket (arrowheads). Compare to figure **a**. Conclusion: extrusive luxation of the left central maxillary incisor with an associated fracture of the labial plate

its very high spatial resolution—considered the imaging technique of choice for the evaluation of mandibular and/or maxillary trauma, dental trauma and temporal bone trauma (Fig. 3). CBCT also has the advantage of being less vulnerable to metal artefacts, when compared to MDCT (Box 2). The disadvantage of CBCT is its poor contrast resolution making it difficult to evaluate soft tissues. In the evaluation of orbital trauma, where the detection of orbital and periorbital soft tissues is mandatory, a MDCT scan will therefore be the imaging tool of choice (Fig. 4) (Box 3).

Box 2: Cone Beam Computed Tomography (CBCT)

- Very high spatial resolution
- Less vulnerable to metal artefacts
- Cost-effective
- Lower radiation dose
- Low contrast resolution
- Diagnostic workup
  - Dentoalveolar fractures
  - Mandibular and midface trauma
  - Temporal bone trauma

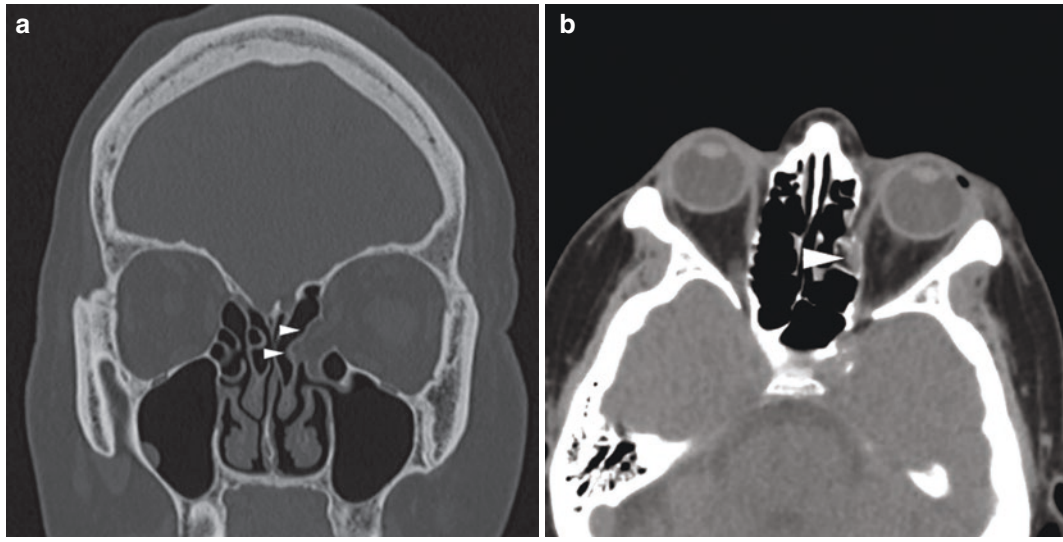

Fig. 4 59-year-old female who was watching the soccer game of her grandson at the sideline of the field and was forcefully hit by a football in the midface. **a** Coronal CT reformation in bone windows at retrobulbar level. Note the medial deviation of the medial orbital wall (lamina papyracea) into the anterior ethmoidal cells (arrowheads). **b** Axial CT image in soft tissue window setting at the mid-orbital level. There is displacement of orbital fat into the defect. Note also the displacement of the medial rectus muscle into the defect (arrowhead). Conclusion: Medial blow-out fracture with entrapment of the medial rectus muscle into the defect, causing visual disturbances in this patient. Reconstruction of the medial orbital wall was performed. *Courtesy: Steven Schepers, MD, Hasselt, Belgium*

Box 3: Multidetector Computed Tomography (MDCT)

- Bone and soft tissue evaluation
- Investigation of complex, high-velocity or high-energy mandibular and midface trauma
- Description and classification of complex fractures
- Multiplicity of fragments
- Degree of displacement
- Orbital soft tissue—muscles and nerves—involvement
- Cribriform plate, lacrimal duct, optic canal, superior orbital fissure or infraorbital canal involvement
- Skull base involvement

3.3 Magnetic Resonance (MR) Imaging

MR imaging does not visualize the bone directly and therefore small, yet unstable nondisplaced facial fractures may not be seen. Nevertheless, supplementary MR examinations are required when cranial nerve palsy occurs in order to recognize neural compression (Fig. 5). It is required in case of an immediate post-traumatic cranial nerve palsy as well as a delayed cranial nerve palsy. MR imaging is more sensitive to detect nerve compression due to hematoma, nerve transection or axonal injury. It is also the most sensitive technique to evaluate traumatic damage to the temporomandibular joint disc (Fig. 6) (Box 4).

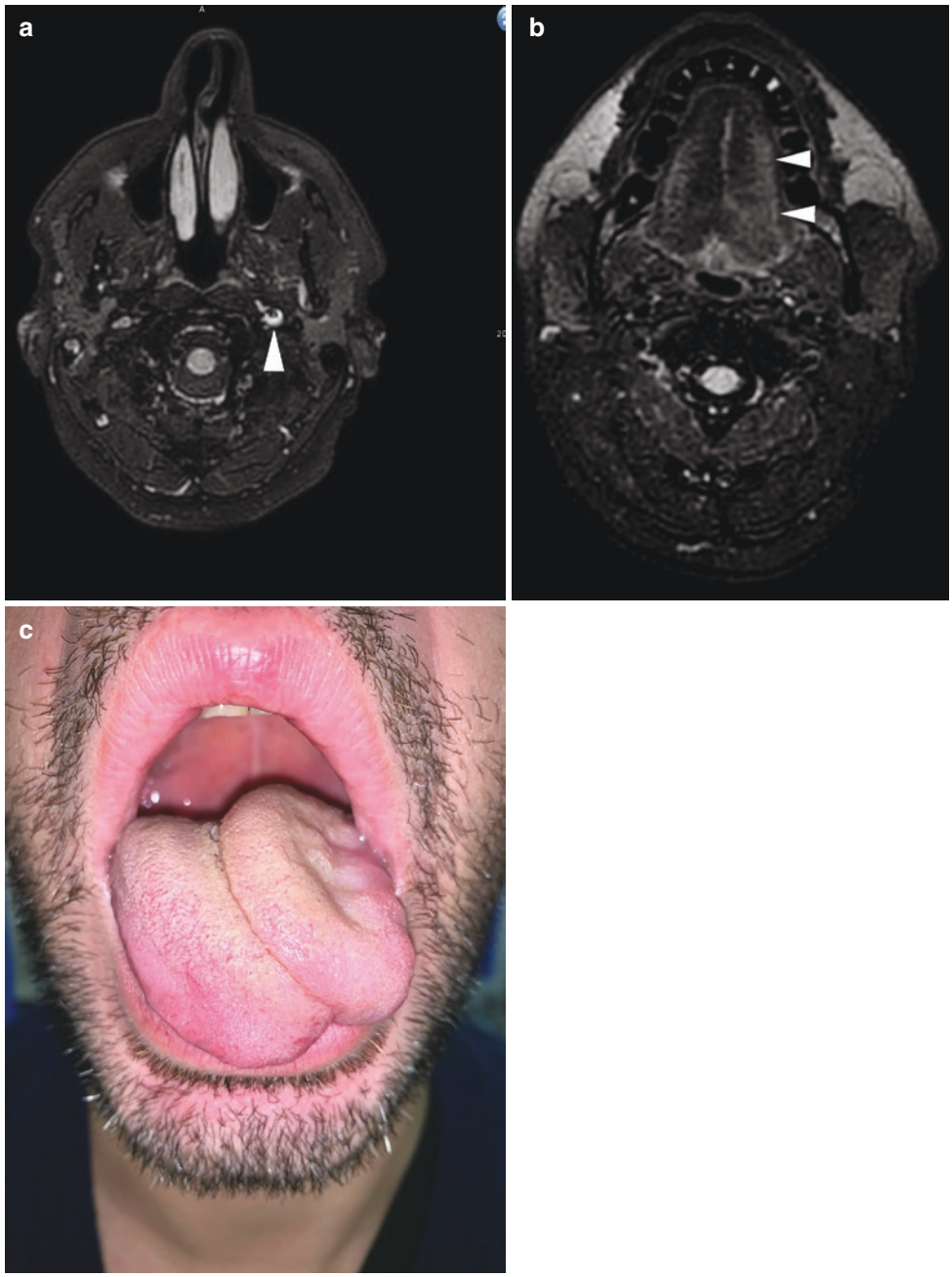

Fig. 5 26-year-male accidently hit by a football on the left side of his neck by force. **a** Axial T2-weighted MR image with fat saturation technique at the level of the entrance of the internal carotid artery in the skull base, nicely demonstrates a semilunar hyperintensity in the posterior and medial wall of the internal carotid artery (large arrowhead) compatible with a hematoma in the wall and internal carotid artery dissection. **b** Axial T2-weighted MR image with fat saturation technique at the level of the oral tongue showing the larger volume and the hyperintense aspect of the left side of the tongue (small arrowheads), compatible with oedema indicating an acute left-sided hypoglossal nerve palsy secondary to the post-traumatic internal carotid artery dissection. **c** Clinical image demonstrating the swollen aspect of the left side of the tongue and the left-sided deviation of the tongue. *Courtesy: Sofie Van Cauter, MD, PhD, Genk, Belgium*

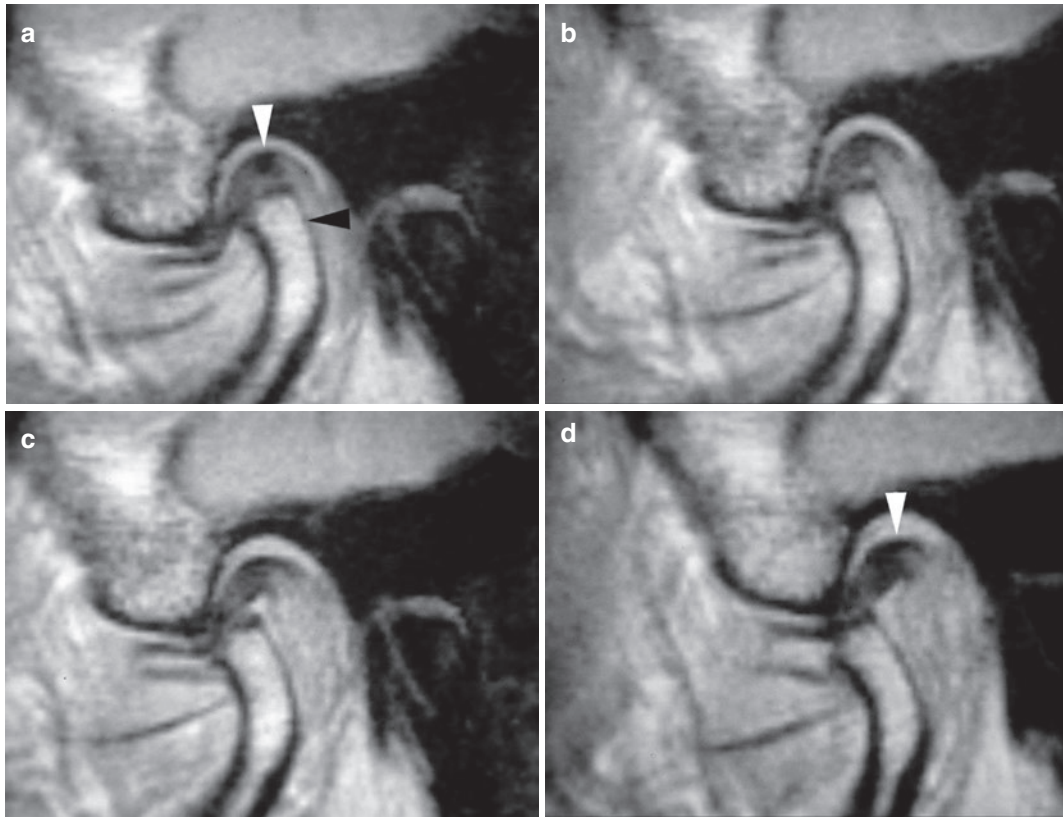

Fig. 6 Post-traumatic disc adhesion demonstrated by T1-weighted MR images. **a** Closed-mouth image shows a normal position of the disc (*white arrowhead*) and the condyle (*black arrowhead*) relative to the glenoid fossa. **b–d** Upon opening of the mouth, the condyle moves inferior to the articular eminence, however the disc (*white arrowhead*) remains stuck in the glenoid fossa

Box 4: Magnetic Resonance (MR) Imaging

- Cranial nerve palsy
  - Nerve compression due to haematoma
  - Nerve transection
  - Axonal injury
  - Carotid artery dissection
- Traumatic damage to the temporomandibular joint disc
- Brain concussion
- Post-traumatic meningocele
- Post-traumatic meningitis
  - Inflammatory collections
  - Abscess formation

4 Specific Sports-Related Maxillofacial Injuries

4.1 Soft Tissue Injuries

Soft tissue injuries are by far the most common maxillofacial injuries associated with sports. Soft tissue injuries may be classified as abrasions, lacerations, cuts, haematomas and burns (Lanzi 2017).

Furthermore, ocular soft tissue injuries are frequently seen in sports-related trauma, mainly in racquet sports (squash, tennis, and badminton) and soccer (Barr et al. 2000). Problems such as

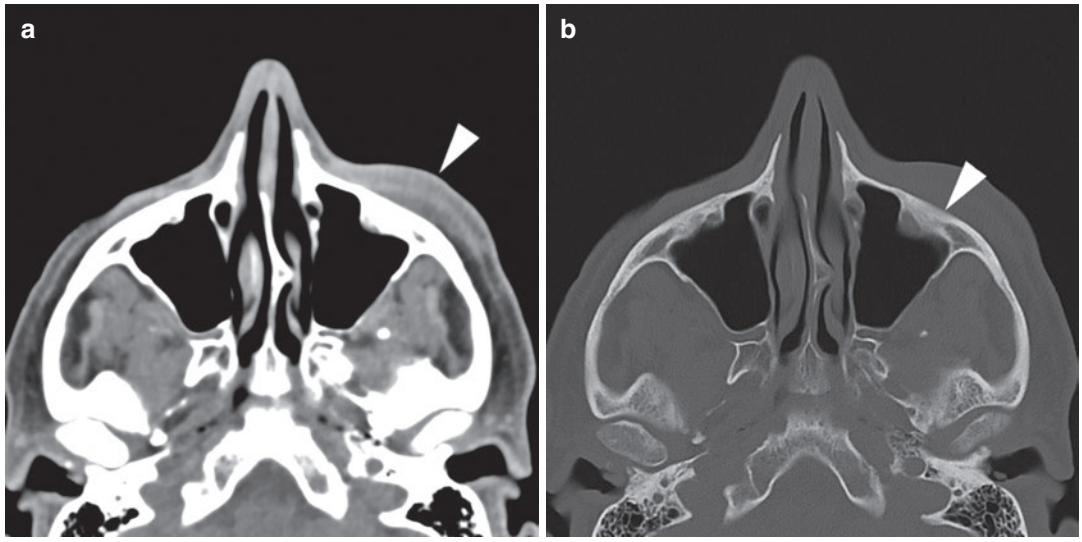

Fig. 7 60-year-old male complaining of left-sided premaxillary numbness after being hit by a golf ball on the left side of the maxilla. **a** Axial CT image in soft tissue windows at the level of the zygoma. Note the asymmetrical hyperdense swelling of the left premaxillary soft tissues (arrowhead), compared to the normal right side, compatible with a premaxillary hematoma. **b** Axial CT image in bone windows at the same level. There is no associated fracture of the wall of the maxillary sinus or the zygoma neither of the infraorbital nerve canal. *Courtesy: Christoph Kenis, MD, Heusden Zolder, Belgium*

hyphaemia (bleeding in the anterior chamber), retinal tears, lens dislocation, penetrating globe injury, optic nerve compression, superior orbital fissure syndrome (cranial nerve III to VI paralysis) and retrobulbar hematoma should be cautiously looked after (Greenberg and Haug 2005).

Radiologic examination should be carefully considered in each patient to spot underlying fractures (Fig. 7).

4.2 Dentoalveolar Injuries

Dental trauma is the second most common injury in sports after soft tissue injuries and range from minor enamel fragments to complete tooth avulsion. About 80% of all dental sports injuries occur in the 4 maxillary incisor teeth (Piccininni et al. 2017). These types of injuries are highly preventable with the use of mouthguards (Greenberg and Haug 2005). Especially children are adversely affected by dental injuries. Tooth germs in the fracture line are at risk for delayed development, deformity or premature loss (Som and Brandwein 2003).

Dental trauma can be classified into fracture, luxation and avulsion. A *fracture* is a discontinuity of any dental component and can result in loss of a part of the tooth. It can be classified according to the affected segment of the tooth: crown, crown-root and root fractures (Fig. 8). It is fundamental to assess the extent of the fracture through the tooth layers (the enamel, the dentin and pulp) since fractures affecting the pulp (pulp chamber or root canal) are detrimental for the tooth vitality. When the fracture involves the alveolar process, it is called a dentoalveolar fracture.

Dental luxation is a general term that covers multiple types of injuries to the tooth support structures, particularly the periodontal ligament. Dental luxation injuries are divided into concussion, subluxation, extrusive luxation, intrusive luxation and lateral luxation. They can be associated with dental fracture but can also manifest without dental fracture. While radiologic abnormalities are not expected in concussion and subluxation, tooth displacement and widening of the periodontal ligament space (PLS) (radiolucency between the cementum of the root and the lamina dura of the bony socket) are

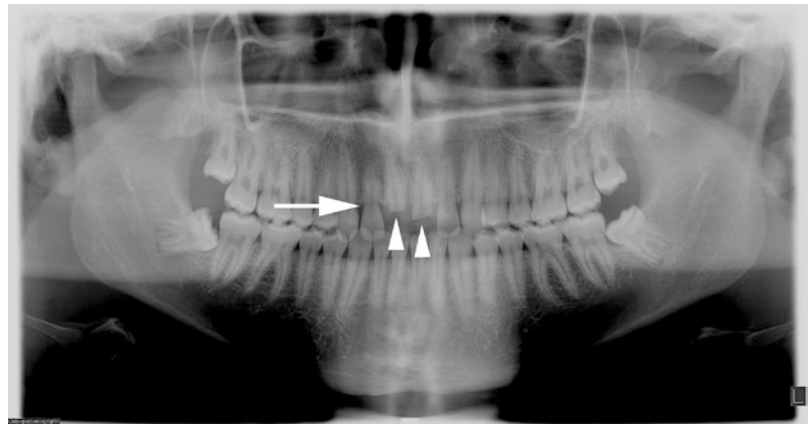

Fig. 8 18-year-old male who was hit by an ice hockey puck. Orthopantomogram, displaying a horizontal crown-root fracture of tooth 12 (arrow) and a crown avulsion fracture of teeth 11 and 21 (arrowheads). *Courtesy: Marianne Suuronen, MSD, Helsinki, Finland*

observed in extrusive luxation and lateral luxation, the latter accompanied by fracture of the alveolar process (Fig. 3). Despite its name, *lateral luxation* consists of eccentric displacement of the tooth, usually in the palatal, lingual or labial direction. On the other hand, *intrusive luxation* appears on images as a narrowed or absent PLS, with a tooth displaced into the alveolar bone. A potential pitfall to be aware of is that a widened PLS can develop in patients receiving orthodontic treatment, usually in multiple teeth, mimicking extrusive luxations. In these cases, the brackets and wires are easily seen on CT images and radiographs.

Finally, *avulsion* is the term used when the tooth is completely displaced out of the alveolar socket (Loureiro et al. 2019).

Accurate description of all injuries of the teeth can be important in case of insurance problems, as dental reconstruction can be very expensive.

4.3 Mandibular Fractures

There is a variety of causes for mandibular fractures predominated by assaults and motor vehicle collisions, with sports as a smaller aetiology (2–6%) (Greenberg and Haug 2005). However, according to the investigations of Emshoff et al., sports are increasingly involved in the causes of mandibular fractures. His study showed sporting activities to be the main causative factor of mandibular fractures, accounting for 31.5% (Emshoff et al. 1997). The difference may be attributable to the extensive sports facilities and tourism industry in the studied region (Innsbruck).

Mandibular fractures are generally described by the part of the mandible that is involved. The mandible can be divided into the following components: symphyseal, para-symphyseal body, angle, ramus, coronoid process and condyle (Fig. 9a). The body is defined as the region between the posterior aspect of the mandibular canine and the posterior aspect of the second molar. The angle is delimited by the anterior and posterior margins of the 3rd molar tooth socket superiorly and the margins of the masseter muscle inferiorly. Fractures of the mandibular condyle can be further divided into condylar head (also referred as intra-capsular fractures), condylar neck and subcondylar fractures (extra-capsular fractures) (Fig. 9b). The condylar neck is the thin constricted portion just below the condylar head. The subcondylar area is superiorly confined to the line passing through the sigmoid notch and inferiorly to the line obliquely connecting the sigmoid notch to the masseter tuberosity (Dreizin et al. 2016; Alimohammadi 2018).

The location and type of the fracture are used to determine the treatment strategy and surgical access route. Condylar head fractures, for example, are generally managed with closed reduction and intermaxillary fixation regardless of comminution, as opposed to extra-capsular fractures in which open repair might be indicated. Displaced condylar head fractures are occasionally reduced and internally fixed to prevent malocclusion (Fig. 10) (Patel et al. 2012). Body fractures are

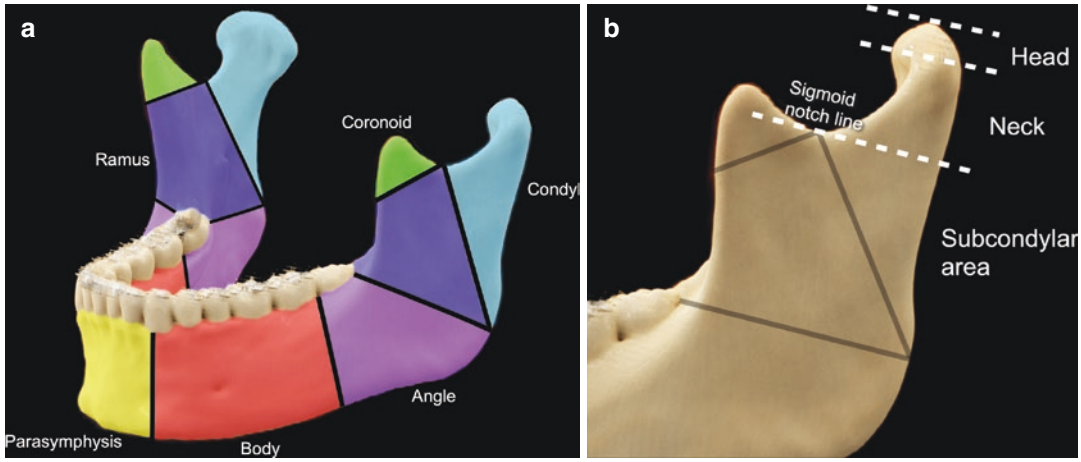

Fig. 9 **a** Volume rendered image with colour overlay showing the regions of the mandible and their approximate demarcations. An imaginary line drawn down from the canine teeth separates the para-symphyseal region from the body of the mandible. The angle is delimited by the anterior and posterior margins of the third molar tooth socket superiorly and the anterior and posterior margins of the masseter muscle insertion inferiorly. The condyles and coronoid processes form the superior projections of the mandible. **b** Volume rendered image of the mandibular condyle with its different anatomical parts. The condyle can be divided into three parts: the condylar head, which articulates with the glenoid fossa; the neck, which is below the lateral pterygoid muscle insertion and above the sigmoid notch, and the subcondylar area, which is below the sigmoid notch

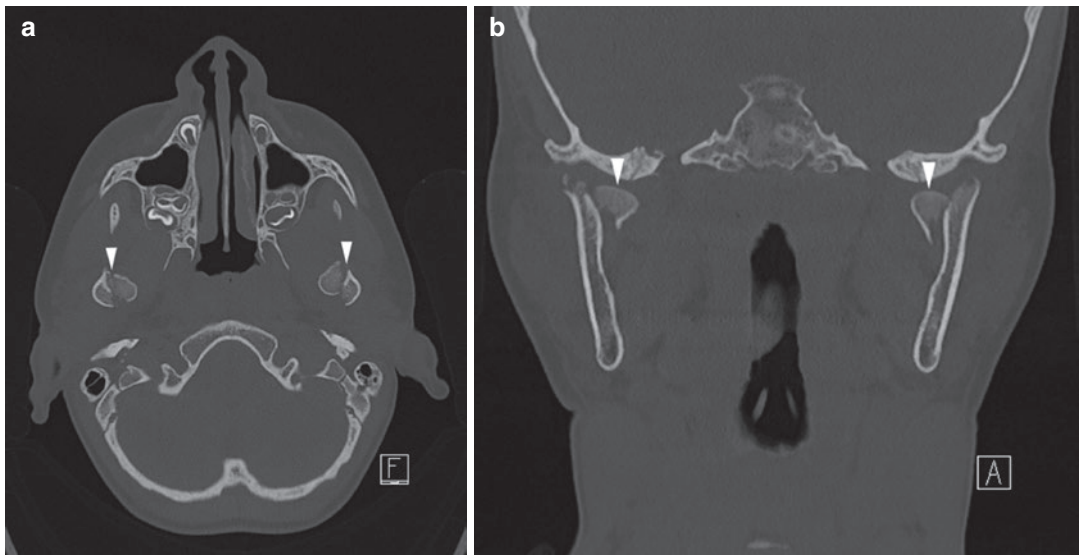

Fig. 10 10-year-old boy who fell from his horse. **a** Axial CT image at the level of the condylar heads, demonstrating the fracture line (arrowheads) running in an anteroposterior direction through the condylar head on both sides. **b** Coronal CT reconstruction at the level of the condylar heads, showing the bilateral intra-capsular fracture of the condylar head (arrowheads) with downwards displacement of the medial fragments. *Courtesy: Christoph Kenis, MD, Heusden, Belgium*

often unfavourable and need open reduction because of the actions of the masseter, temporalis and medial pterygoid muscles, which distract the proximal segment superior and medially. Additionally, the mylohyoid muscle and anterior belly of the digastric muscle may contribute to

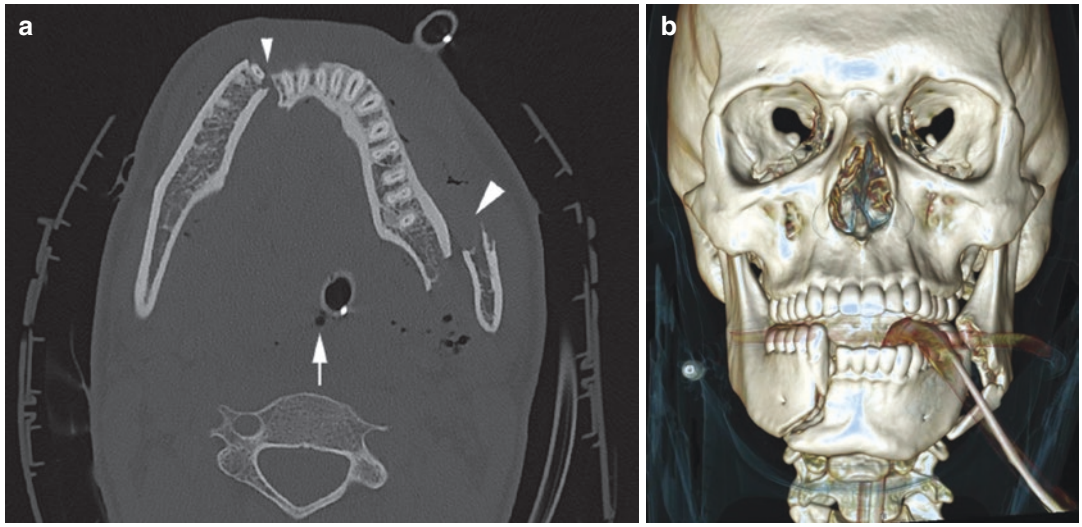

Fig. 11 19-year-old male involved in a motorcycle accident. He died a few hours after admission to the hospital. **a** Axial CT image through the mandibular body, demonstrating a fracture through the right para-symphyseal mandibular area (small arrowhead) as well as a fracture at the level of the left mandibular angle (large arrowhead). Note the severe posterior displacement of the mandibular fragment in between both fracture lines. Patient is intubated as there is a nearly complete obliteration of the oropharyngeal air space (arrow). **b** Anterior view of a 3D volume rendered and surface shaded CT volume showing a double mandibular fracture with the typical pattern of the para-symphyseal involvement on one side and involvement of the angle on the other side resulting in a flail mandible. There is a severe displacement of the free mandibular segment posteriorly and inferiorly by the force of the supra-hyoid mandibular depressors causing a nearly complete obstruction of the oropharyngeal air space. *Courtesy: Christoph Kenis MD, PhD, Heusden-Zolder, Belgium*

the unfavourable nature of this fracture by displacing the anterior fractured segment posteriorly and inferiorly (Alimohammadi 2018). In case of body fractures, the fracture line may cross the inferior alveolar canal which may lead to neurosensory disturbances. The risk is much greater when the displacement exceeds 5 mm (Dreizin et al. 2016).

The mandible is a U-shaped structure that frequently fractures in 2 locations rather than in 1. A common pattern is a mandibular angle or symphyseal fracture on 1 side, with a contralateral body or condyle fracture (Viozzi 2017). Trifocal (para-symphyseal and bicondylar) fractures, bilateral angle fractures and bilateral body fractures—so-called flail mandible—can result in unrestricted posterior and inferior pull of the free anterior mandibular segment, with loss of anterior support of the tongue from the genioglossus (Fig. 11). The ptosis of the tongue, the sublingual and submandibular hematomas and intraoral bleeding commonly associated with these fractures may contribute to airway compromise. Therefore, identifying flail mandible and associated soft tissue injuries as airway compromise risks is critical (Dreizin et al. 2016).

4.4 Central Midface Fractures

Central midface fractures are classified into fractures of the nose, naso-orbito-ethmoid complex fractures and Le Fort I, II and III types of fractures (Som and Brandwein 2003).

Nasal fractures are the most common sports-related facial fractures with sports accounting for up to 27% of all nasal fractures (Greenberg and Haug 2005). With the nasal pyramid projecting from the midface, it is the most vulnerable to injury of all facial bones. The major features that should be mentioned in the radiological report include: (1) unilateral versus bilateral, (2) simple versus comminuted, (3) displacement with or without depression and (4) associated septal

fractures. If the fracture is comminuted, one has to look for depression or telescoping of the fracture as they are almost universally treated with open reduction (Patel et al. 2012).

Identification and drainage of a septal hematoma following injury to the nose is important to minimize postoperative morbidity (Fig. 2). The perichondrium adheres tightly to the septal cartilage and provides its blood supply. A septal hematoma occurs between the septal cartilage and perichondrium, effectively separating the cartilage from its nutrient source. If a septal hematoma is not properly drained, pressure-induced avascular necrosis can occur within 3 days, and if not treated, lead to nasal deviation and (saddle) nose deformity (Marston et al. 2017).

Naso-orbital-ethmoid (NOE) fractures commonly occur following blunt trauma to the upper part of the central midface or an isolated impact to the bridge of the nose resulting in posterior displacement of the nasal bones and frontal process of the maxilla with telescope-like deformation and collapse of the anterior ethmoid. The most common classification of these fractures is the Markowitz classification. This classification system is based around a central fragment from the medial orbital rim, which contains the attachment for the medial canthal tendon. In the first 2 types of NOE fractures (Markowitz types I and II), the fracture lines are around the central fragment and thus the medial canthal tendon is intact. Type I fractures are those with a single-fracture fragment, whereas type II fractures are comminuted. The type III NOE fractures are also comminuted, but the medial canthal tendon is disrupted from the bone. The medial canthal tendon is important because it contributes to the normal definition and spacing of the eyes. If not repaired, then the eyes may appear too far apart (telecanthus). Therefore, it is important to mention in the radiological report whether the fracture fragment is single or comminute, in which case medial canthal tendon injury is possible (Fig. 12) (Patel et al. 2012). Commonly associated injuries include lacrimal duct injury and fractures of the cribriform plate (Schuknecht and Graetz 2005; Som and Brandwein 2003).

Complex midface fractures are typically referred to in the context of Le Fort's early anatomic studies. Although visualization of injury to the struts and buttresses of the face is required for repair of these fractures with restoration of the 3D stability and symmetry of the face, the Le Fort classification still appears to be a succinct way of summarizing and communicating the major planes of certain fractures. The greatest frequency of *Le Fort types of fractures* results from assaults and motor-vehicle collisions, with sports accounting for only 5–8% of such fractures (Greenberg and Haug 2005).

Common to all Le Fort fractures is the fracture of the pterygoid processes. In addition, each Le Fort fracture has a unique component (Fig. 13) (Rhea and Novelline 2005). The Le Fort I fracture runs horizontally above the maxillary alveolar process and is the only one that involves the anterolateral margin of the nasal fossa just above the maxillary alveolar process. The Le Fort II

Fig. 12 25-year-old male scanned after head-knee collision during a football game. Right anterior oblique view of a 3D volume rendered and surface shaded CT volume showing a depression of the naso-fronto-ethmoidal complex into the ethmoidal sinuses. The right medial orbital wall consists of a large single bony fracture fragment (asterisk) compatible with a Markowitz type I naso-orbital-ethmoidal (NOE) fracture. There is an associated right-sided inferior orbital rim fracture. *Courtesy: Riste Saat, MD, Tallinn, Lithuania*

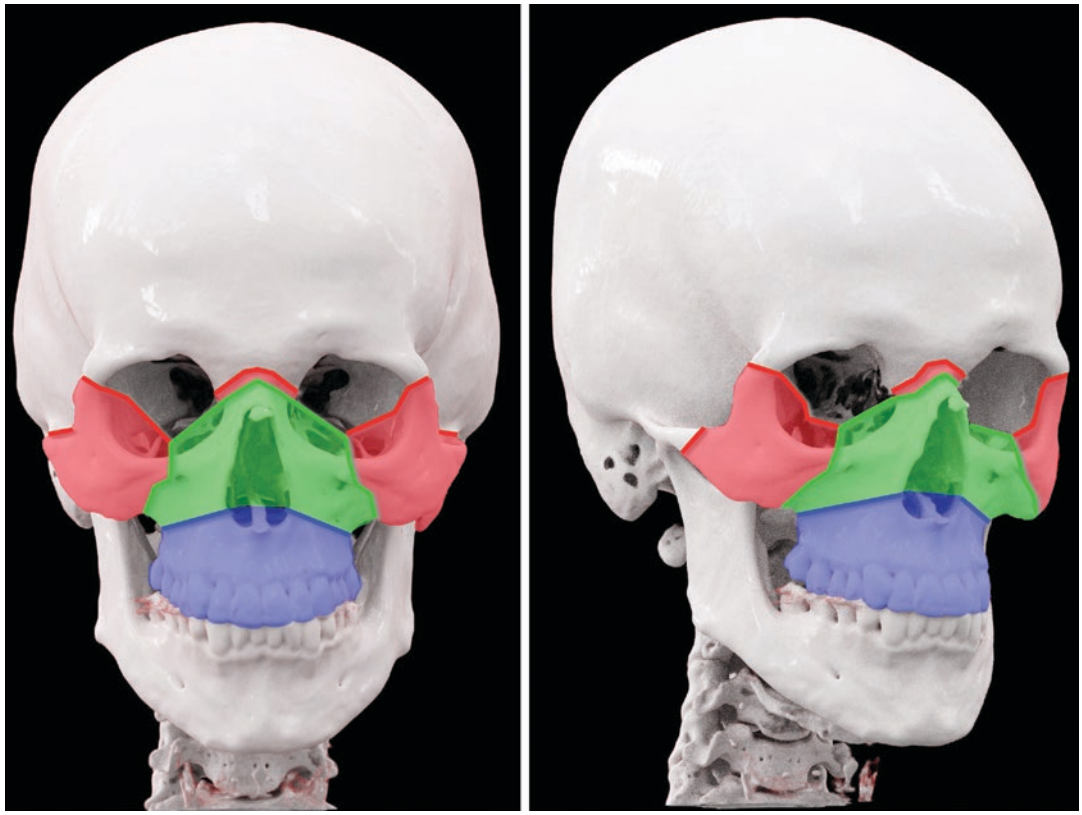

Fig. 13 Schematic drawing of the Le Fort fractures on an anterior and right anterior oblique view of a 3D volume rendered and surface shaded CT. The blue volume represents the Le Fort 1 fracture also known as the "floating teeth" fracture with complete detachment of the lower maxilla from the face. The green volume represents the Le Fort 2 fracture also known as the "pyramidal fracture" (due to pyramidal shape of the detached maxilla) or "floating maxilla" fracture with a complete detachment of the maxilla from the skull base. The red volume represents the Le Fort 3 fracture also known as the "floating face" fracture with a complete detachment of the maxillofacial complex of the skull base and the rest of the skull

fracture is pyramidal in shape with the teeth at the base of the pyramid and the nasofrontal suture at the apex of the pyramid. This type of fracture is the only one that involves the inferior orbital rim. Posterior and lateral walls of maxillary sinuses are also broken. The Le Fort III fracture separates the facial bones from the rest of the skull. This fracture crosses the frontonasal suture, runs through the ethmoid bone or the lamina papyracea into the orbit to the inferior orbital fissure and courses laterally to involve the sphenozygomatic and fronto-zygomatic suture. The Le Fort III fracture is the only one that involves the zygomatic arch. Keep in mind that multiple types of Le fort fractures may be present and that each side of the face may be fractured differently (Fig. 14). Patients with Le Fort II and III fractures are also at a higher risk for associated vascular or cranial injuries (Patel et al. 2012).

4.5 Lateral Midface Fractures

Lateral midface fractures consist of zygomatic arch fractures, zygomaticomaxillary complex (ZMC) fractures and fractures of the orbit (Som and Brandwein 2003). Sports injuries account for 4–11% of all zygomatic (Greenberg and Haug 2005) and 13% of all orbital fractures (Lock et al. 2017).

When there is an *isolated fracture of the zygomatic arch*, there usually are at least three

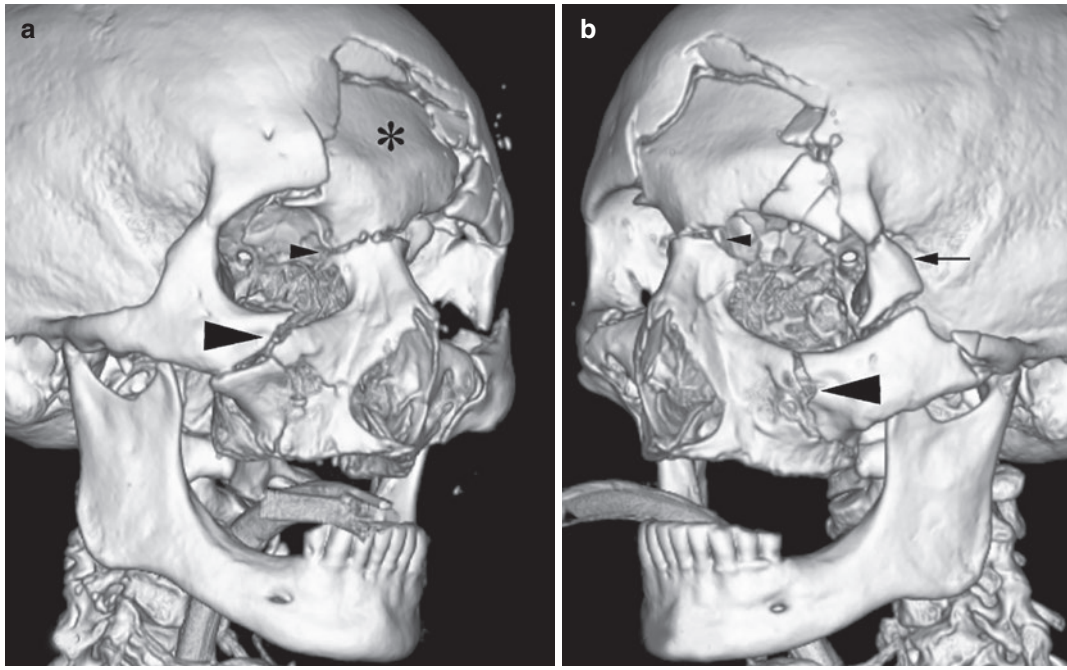

Fig. 14 54-year-old male bicycle racer, ran in a ditch, hitting a wall with the forehead. **a** Right and **b** left anterior oblique view of a 3D volume rendered and surface shaded CT volume. There is a bilateral fracture of the anterior wall of the maxillary sinus and the inferior orbital rim (large arrowheads) extending into the medial orbital wall cranially and ending in a transverse fracture of the nasal bone (small arrowheads), compatible with a bilateral Le Fort 2 fracture. Note the associated fracture of the lateral orbital wall on the left side (arrow), compatible with a Le Fort 3 fracture on the left side. There is also an associated comminuted depression fracture of the frontal sinus anterior wall (asterisk)

discrete fracture lines, creating two fracture segments. As with other facial fractures, zygomatic fractures should be described in terms of displacement and comminution, as these are important indicators for surgical planning (Fig. 15). Usually, these pieces are displaced medially and downwards, reflecting the direction of the impact force.

In *zygomaticomaxillary complex (ZMC) fractures* also-called *tetrapod fracture*, the fracture line extends from the lateral orbital wall (zygomaticofrontal suture and the zygomaticosphenoid suture) to the inferior orbital floor and the anterior maxilla near the zygomaticomaxillary suture, and along the weakest part of the zygomatic arch, which is about 1.5 cm dorsal to the zygomaticotemporal suture. Associated enophthalmos, ocular injury or involvement of the infraorbital nerve should be described (Fig. 16) (Patel et al. 2012).

One-third of *orbital blow-out fractures* are sustained during sports. Soccer is most commonly involved. A blow to the orbit by an object that is too large to enter the orbit (baseball, fist, etc.) may cause a fracture of the orbital floor and leaving the inferior orbital rim intact. Herniation of orbital fat, inferior rectus muscle and inferior oblique muscle can occur. Additionally, or rarely alternatively, the medial orbital wall—lamina papyracea—may be displaced into the ethmoid resulting in the so-called "*medial blow-out*" *fracture* with potential herniation of the medial rectus muscle (Fig. 4). Supraorbital roof fractures (also called "*blow-up*" *fractures*) are uncommon (Schuknecht and Graetz 2005; Som and Brandwein 2003). Indications for surgery include a large fracture involving >1 cm^2 of the orbital floor (whether there is associated enophthalmos) and rounding or kinking of the medial or inferior rectus muscle as a sign of entrapment. If left

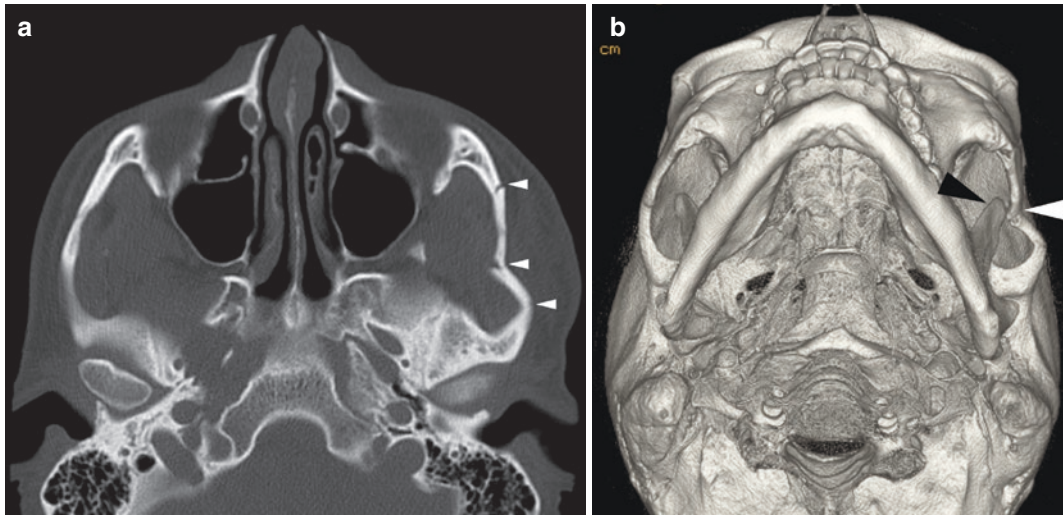

Fig. 15 59-year-old male who was kicked by his horse onto the left lateral side of his face. **a** Axial CT image in bone windows at the level of the zygoma. The left zygoma is fractured at 3 places (small arrowheads). Note the depression of the left zygoma towards the depth of the left infratemporal fossa. **b** Inferior view of a 3D volume rendered and surface shaded CT volume showing the left-sided zygoma fracture. Note the depressed left zygomatic arch (white arrowhead), nearly touching the left coronoid process (black arrowhead). The fracture was repaired surgically and the form and position of the left zygoma was restored in order to avoid restriction of the mouth opening and development of ankylosis

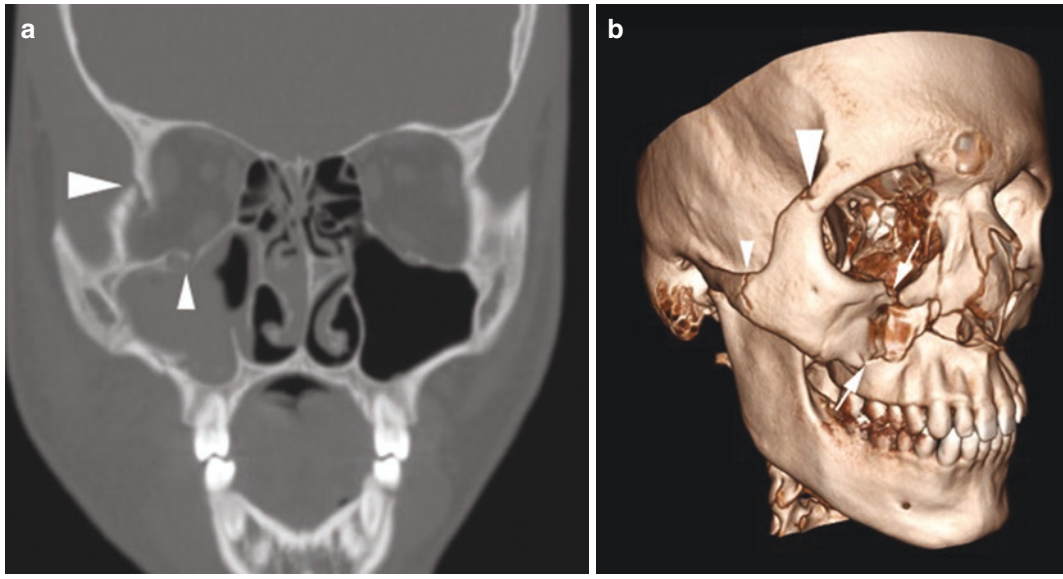

Fig. 16 16-year-old male hit by a baseball to the right side of his face. **a** Coronal CT reconstruction at the retrobulbar level demonstrating the fracture through the lateral orbital wall (large arrowhead) and the orbital floor (small arrowhead), running through the inferior orbital canal, which gives hypaesthesia/anaesthesia in the area of the infraorbital nerve. **b** Right anterior oblique view of a 3D volume rendered and surface shaded CT volume showing the fractures of the right zygomatic arch (small arrowhead), the fronto-zygomatic suture (large arrowhead), as well as the right anterior maxillary sinus wall (arrows). Conclusion: right-sided zygomaticomaxillary complex (ZMC) fracture. *Courtesy: Frank Pameijer MD, PhD, Utrecht, the Netherlands*

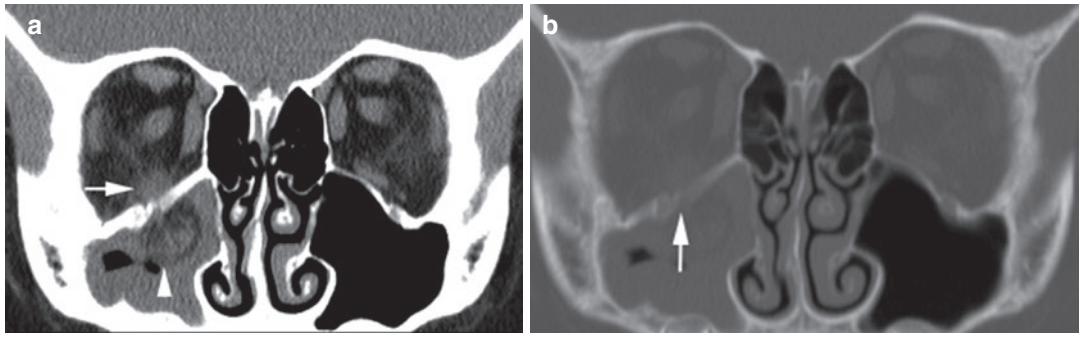

Fig. 17 26-year-old male complaining of double vision after being hit by a squash ball to the orbit. **a** Coronal CT reformation in soft tissue window at the retrobulbar level. Note the descent of orbital fat into a small defect of the right orbital floor (arrowhead). The inferior rectus muscle has a rounded shape and is attracted to the defect (arrow). **b** Coronal CT reformation in bone windows at the same level. Note the opacification of the right maxillary sinus and the almost intact aspect of the orbital floor, apart from a small fracture line (arrow). Conclusion: Orbital floor "trapdoor" fracture. In this type of fracture, the inferiorly displaced fracture segment has jumped back into its normal position—like a trapdoor—with entrapment of orbital fat and/or the inferior rectus muscle. This entrapment makes it a surgical emergency as the muscle can become ischaemic. *Courtesy: Steve Connor, MD, London, UK*

untreated, entrapped muscles can undergo progressive fibrosis. A specific type of blow-out fracture that occurs in the paediatric population is the *"trapdoor" fracture*. The "trapdoor" fracture is similar to other blow-out fractures in injury mechanism and bones involved. However, in children, the fracture fragment can jump back into place and trap the muscle outside of the orbital wall (Fig. 17). This type of fracture is considered a surgical emergency, as the muscle can become ischemic (Patel et al. 2012).

Attention should be paid to potential associated ocular injuries in orbital fractures including globe rupture, retrobulbar hematoma, optic nerve injury or lens dislocation.

4.6 Frontal Sinus Fractures

Frontal sinus fractures are less common than other fractures of the craniomaxillofacial skeleton because of their greater thickness and biomechanical advantages. Sports injuries account for 3–5% of all frontal sinus fractures (Greenberg and Haug 2005). Frontal bone fractures are classified according to the involvement of the anterior or posterior walls (or tables) (Som and Brandwein 2003). The nasofrontal duct normally drains the frontal sinus, and occlusion potentially leads to the development of mucoceles, mucopyoceles, osteomyelitis or abscess. The nasofrontal duct may be difficult to evaluate by imaging alone. However, nasofrontal duct injury should be strongly suspected if one of the three findings are present: fracture fragments in the nasofrontal outflow tract, fracture of the frontal sinus floor, or fracture of the medial wall of the anterior table (Fig. 14) (Patel et al. 2012). Associated intracranial haemorrhage and pneumocephalus should also be excluded when a frontal sinus fracture is present. Such findings are suspicious for dural violation, and when present, should prompt prophylactic antibiotics administration to prevent intracranial infection (Patel et al. 2012).

5 Conclusions

In conclusion, the vast majority of sports-related maxillofacial injuries are of minor nature. These typically include soft tissue lacerations followed by dentoalveolar fractures and minor facial bone fractures. The most frequently occurring facial fractures in sports are (in descending order): nasal, mandibular and zygomatic fractures. The vast majority of facial fractures are encountered during team sports such as soccer and rugby. This is usually the result of an impact with another

player. Dentoalveolar and mandibular fractures always require initial investigation by intraoral periapical films and OPG. CBCT is used for further diagnostic workup. MDCT is the modality of choice for a complete evaluation of the facial skeleton and facial soft tissues in case of a complex, high-velocity or high-energy mandibular and maxillofacial trauma.

Things to Remember

- The majority of sports-related maxillofacial injuries are of minor nature. These typically include soft tissue lacerations, dentoalveolar injuries and minor facial bone fractures.
- The most frequently occurring facial fractures in sports comprise in descending order: nasal, mandibular and zygomatic fractures.
- The vast majority of facial fractures are encountered during team sports, such as soccer and rugby. This is usually the result of an impact with another player.
- Ball sports can cause severe orbital injuries and fractures.
- In vehicular sports, a fall to the ground is the most commonly reported type of impact which usually involves the frontal sinus and central midface.

References

Alimohammadi R (2018) Imaging of dentoalveolar and jaw trauma. Radiol Clin N Am 56(1): 105–124

Bak MJ, Doerr TD (2004) Craniomaxillofacial fractures during recreational baseball and softball. J Oral Maxillofac Surg 62(10):1209–1212

Barr A, Baines PS, Desai P et al (2000) Ocular sports injuries: the current picture. Br J Sports Med 34(6):456–458

Bobian MR, Hanba CJ, Svider PF, Hojjat H, Folbe AJ, Eloy JA, Shkoukani MA (2016) Soccer-related facial trauma: a nationwide perspective. Ann Otol Rhinol Laryngol 125(12):992–996

Delilbasi C, Yamazawa M, Nomura K et al (2004) Maxillofacial fractures sustained during sports played with a ball. Oral Surg Oral Med Oral Pathol Oral Radiol Endod 97(1):23–27

Dobitsch AA, Oleck NC, Liu FC, Halsey JN, Hoppe IC, Lee ES, Granick MS (2019) Sports-related pediatric facial trauma: analysis of facial fracture pattern and concomitant injuries. Surg J (N Y) 5(4): e146–e149

Doğan MS, Callea M, Kusdhany LS, Aras A, Maharani DA, Mandasari M, Adiatman M, Yavuz I (2018) The evaluation of root fracture with Cone Beam Computed Tomography (CBCT): an epidemiological study. J Clin Exp Dent 10(1):e41–e48

Dreizin D, Nam AJ, Tirada N, Levin MD, Stein DM, Bodanapally UK, Mirvis SE, Munera F (2016) Multidetector CT of mandibular fractures, reductions, and complications: a clinically relevant primer for the radiologist. Radiographics 36(5):1539–1564

Emshoff R, Schoning H, Rothler G et al (1997) Trends in the incidence and cause of sport-related mandibular fractures: a retrospective analysis. J Oral Maxillofac Surg 55(6):585–592

Flanders RA, Bhat M (1995) The incidence of orofacial injuries in sports: a pilot study in Illinois. J Am Dent Assoc 126(4):491–496

Gassner R, Hackl W, Tuli T et al (1999) Facial injuries in skiing. A retrospective study of 549 cases. Sports Med 27(2):127–134

Gassner R, Tuli T, Emshoff R et al (1999) Mountainbiking–a dangerous sport: comparison with bicycling on oral and maxillofacial trauma. Int J Oral Maxillofac Surg 28(3):188–191

Gassner R, Tuli T, Hachl O et al (2004) Craniomaxillofacial trauma in children: a review of 3,385 cases with 6,060 injuries in 10 years. J Oral Maxillofac Surg 62(4):399–407

Greenberg AM, Haug RH (2005) Craniofacial injuries. In: Scuderi GR, McCann PD (eds) Sports medicine: a comprehensive approach, 2nd edn. Mosby, Philadelphia, pp 132–151

Hill CM, Burford K, Martin A et al (1998) A one-year review of maxillofacial sports injuries treated at an accident and emergency department. Br J Oral Maxillofac Surg 36(1):44–47

Hojjat H, Svider PF, Lin HS, Folbe AJ, Shkoukani MA, Eloy JA, Zuliani G (2016) Adding injury to insult: a national analysis of combat sport-related facial injury. Ann Otol Rhinol Laryngol 125(8): 652–659

Kurtz MD, Camp JH, Andreasen JO (2005) Dental injuries. In: Scuderi GR, McCann PD (eds) Sports medicine: a comprehensive approach, 2nd edn. Mosby, Philadelphia, pp 152–178

Lanzi GL (2017) Facial injuries in sports, soft tissue injuries (Abrasions, Contusions, Lacerations). Clin Sports Med 36(2):287–298

Lechner M, Sutton L, Fishman JM, Kaylie DM, Moon RE, Masterson L, Klingmann C, Birchall MA, Lund VJ, Rubin JS (2018) Otorhinolaryngology and diving-part 1: otorhinolaryngological hazards related to compressed gas scuba diving: a

review. JAMA Otolaryngol Head Neck Surg 144(3): 252–258

Lim LH, Moore MH, Trott JA et al (1993) Sports-related facial fractures: a review of 137 patients. Aust N Z J Surg 63(10):784–789

Lock JZ, Hegde R, Young S, Lim TC, Amrith S, Sundar G (2017) A study of sports-related orbital fractures in Singapore. Orbit 36(5):301–306

Loureiro RM, Naves EA, Zanello RF, Sumi DV, Gomes RLE, Daniel MM (2019) Dental emergencies: a practical guide. Radiographics 39(6):1782–1795

Maladiere E, Bado F, Meningaud JP et al (2001) Aetiology and incidence of facial fractures sustained during sports: a prospective study of 140 patients. Int J Oral Maxillofac Surg 30(4):291–295

Marston AP, O'Brien EK, Hamilton GS 3rd (2017) Nasal injuries in sports. Clin Sports Med 36(2): 337–353

Miracle AC, Mukherji SK (2009) Cone beam CT of the head and neck, part 1: physical principles. Am J Neuroradiol 30:1285–1292

Park SJ, Park KH, Heo JW, Woo SJ (2014) Visual and anatomic outcomes of golf ball-related ocular injuries. Eye (Lond) 28(3):312–317

Patel R, Reid RR, Poon CS (2012) Multidetector computed tomography of maxillofacial fractures: the key to high-impact radiological reporting. Semin Ultrasound CT MR 33(5):410–417

Piccininni P, Clough A, Padilla R, Piccininni G (2017) Dental and orofacial injuries. Clin Sports Med 36(2):369–405

Rhea JT, Novelline RA (2005) How to simplify the CT diagnosis of Le fort fractures. AJR Am J Roentgenol 184(5):1700–1705

Ruslin M, Boffano P, ten Brincke YJ, Forouzanfar T, Brand HS (2016) Sport-related maxillo-facial fractures. J Craniofac Surg 27(1):e91–e94

Sane J (1988) Comparison of maxillofacial and dental injuries in four contact team sports: American football, bandy, basketball, and handball. Am J Sports Med 16(6):647–651

Schuknecht B, Graetz K (2005) Radiologic assessment of maxillofacial, mandibular, and skull base trauma. Eur Radiol 15(3):560–568

Shintaku WH, Venturin JS, Azevedo B, Noujeim M (2009) Applications of cone-beam computed tomography in fractures of the maxillofacial complex. Dent Traumatol 25(4):358–366

Som PM, Brandwein MS (2003) Facial fractures and postoperative findings. In: Som PM, Curtin HD (eds) Head and neck imaging, 4th edn. Mosby, St. Louis, pp 374–438

Tuli T, Hachl O, Hohlrieder M et al (2002) Dentofacial trauma in sport accidents. Gen Dent 50(3):274–279

Ueeck BA, Dierks EJ, Homer LD et al (2004) Patterns of maxillofacial injuries related to interaction with horses. J Oral Maxillofac Surg 62(6):693–696

Viozzi CF (2017) Maxillofacial and mandibular fractures in sports. Clin Sports Med 36(2):355–368

White S, Pharoah M (2000) Trauma to teeth and facial structures. In: White S, Pharoah M (eds) Oral radiology: principles and interpretation, 4th edn. Mosby, St. Louis, pp 566–587

Thoracic and Abdominal Wall Injuries in Sports

Jan L. M. A. Gielen, Filip M. Vanhoenacker, and Pieter Van Dyck

Contents

Abstract

Specific imaging literature on abdominal and thoracic wall injuries is relatively uncommon compared to the overall incidence in sports medicine. However radiological grading and follow-up of musculotendinous unit (MTU) elongation may be significant in athletes. Moreover radiological diagnosis is relevant in specific circumstances. During the past two decades, the frequency of pectoralis major muscle injuries has increased. Ultrasound and magnetic resonance imaging are helpful for treatment planning. A thorough understanding of the complex anatomy of the pectoralis major is crucial. Rectus abdominis sheath haematoma has to be excluded in cases of muscular tear as it might not self-tamponade. Clinical diagnosis of groin lesions is difficult and therefore radiological procedures may be of additional help in the diagnosis of groin lesions. An in-depth knowledge of the anatomy and biomechanics of the thoracic and abdominal wall is a prerequisite for understanding the pathological conditions of this area. Handlebar injuries are a significant cause of both blunt abdominal

J. L. M. A. Gielen (✉)
University of Antwerp, University Hospital, Antwerp, Belgium
e-mail: Jan.gielen@uza.be

F. M. Vanhoenacker
Department of Radiology, AZ Sint-Maarten Mechelen, Mechelen, Belgium

Department of Radiology, Antwerp University Hospital, University of Antwerp, Antwerp, Belgium

Faculty of Medicine and Health Sciences, Ghent University, Ghent, Belgium

P. Van Dyck
Department of Radiology, University of Antwerp, Antwerp, Belgium

Med Radiol Diagn Imaging (2021)
https://doi.org/10.1007/174_2020_267, © Springer Nature Switzerland AG
Published Online: 16 March 2021

trauma and lacerations to the contact area in children. The high proportion of lacerations observed in this type of trauma result from the sharp metallic end of the handlebar cutting through the soft rubber handle. Arterial endofibrosis at the external iliac artery is found in cyclists. It is characterized by thickening of the intima and/or adventitia. Angiographic examination demonstrates tapering of the arterial lumen with elongation of the artery.

1 Introduction

Specific imaging literature on abdominal and thoracic wall injuries is relatively uncommon compared to the overall incidence in sports medicine. This is because the clinical diagnosis is usually straightforward and imaging is only needed to exclude anatomical variants (scapulothoracic crepitus) and concomitant lesions (rib fractures, handlebar trauma of the abdomen). However radiological grading and follow-up of musculotendinous unit (MTU) elongation may be significant in athletes. Moreover radiological diagnosis is relevant in specific circumstances. Rectus abdominis sheath haematoma has to be excluded in cases of muscular tear as it does not self-tamponade. Clinical diagnosis of groin lesions is difficult and therefore radiological procedures may be of additional help in the diagnosis of sports hernia and groin disruption.

A thorough knowledge of the anatomy, variant anatomy and biomechanics of the thoracic and abdominal wall is a prerequisite for understanding the pathological conditions of this area (Figs. 1 and 2). The anatomy and biomechanics of the thoracic and abdominal wall are summarized in Fig. 3 and Tables 1 and 2, respectively.

2 Rib Cage and Thoracic Wall

Rib and sternum injuries are relatively rare in athletes. Rib fractures can be divided into two main categories: traumatic fractures and stress fractures.

2.1 Rib Fractures and Chondral Lesions

Rib fractures are the most common injury of the chest wall. Mostly, they occur at the middle and lower ribs with blunt trauma. Lateral rib fracture or injury to the costochondral junction is caused by a direct force to a small area most often coming from an anterior direction. Compression of the entire thorax results in fractures of multiple ribs.

Fractures of the first four ribs or the last two ribs, multiple fractures and flail segments have a less benign cause than other rib fractures, as they may result in injury to surrounding structures. In lower left or right rib fractures associated splenic or hepatic trauma is reported in up to 20% and 10%, respectively. Ultrasound is an excellent tool to detect occult fracture. The term *flail chest* is used if three or more ribs are fractured in two or

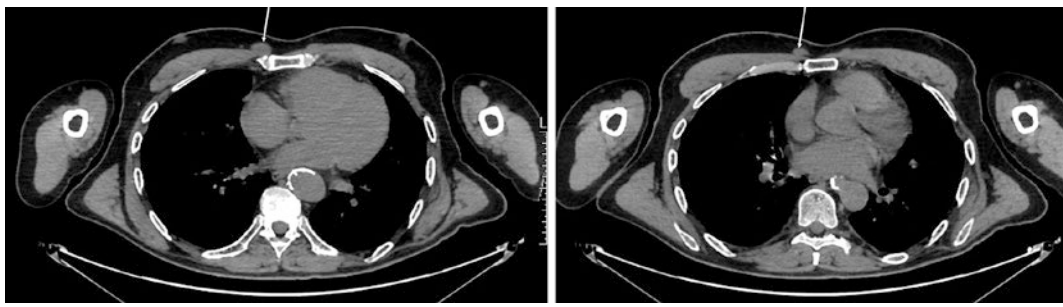

Fig. 1 Sternalis muscle. Male 66 years old. Axial CT images reveal a unilateral sternalis muscle at the right hemithorax, which is a normal variant (arrow)

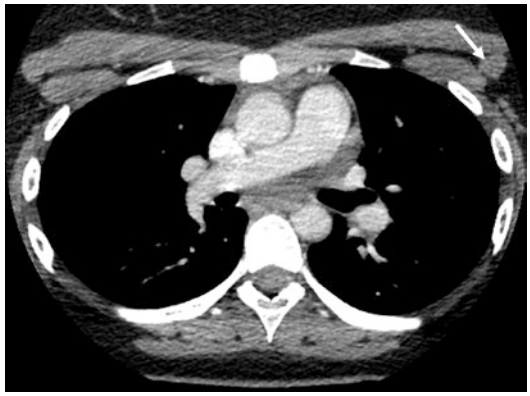

Fig. 2 Accessory pectoralis muscle. Nineteen-year-old female with left-sided accessory pectoralis muscle (arrow). This finding should not be confused with an adenopathy

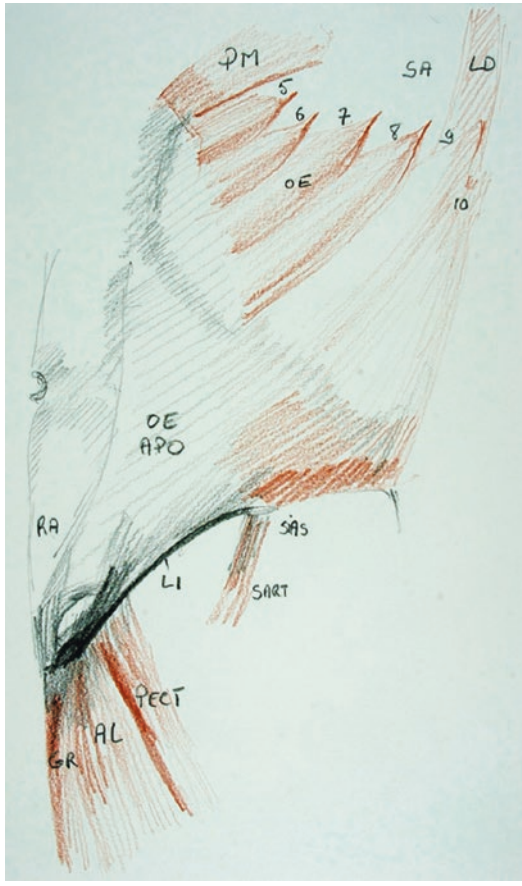

Fig. 3 Superficial muscles of the groin and abdominal wall. *AL* adductor longus muscle, *GR* gracilis muscle, *LI* ligamentum inguinale, *LD* latissimus dorsi, *OE* obliquus externus abdominis muscle, *OE APO* aponeurosis, external inguinal ring, *PECT* pectineus muscle, *PM* pectoralis major, *RA* rectus abdominis muscle, *SART* sartorius muscle, *SIAS* spina iliaca anterior superior

more locations provoking paradoxical motion during respiration.

Rib fractures may also be caused by violent muscle contractions. First rib and floating rib fractures are uniquely athletic fractures, caused by a sudden vigorous contraction in different directions of pull (Miles and Barrett 1991; Coris and Higgins 2nd. 2005). Fractures of the first rib have been reported in basketball players.

Fracture diagnosis is generally straightforward on standard radiographs (chest series and rib series). The differential diagnosis includes severe rib contusion, costochondral separations, muscle elongation and pneumothorax.

Furthermore, chondral lesions, costochondral separations and rib fractures may be dynamically examined with ultrasound. By using ultrasonographic palpation to detect the pain at the region of interest (ROI) the accuracy of the technique is improved (Fig. 4). Examination of the painful ROI is performed during inspiration, expiration and pain-provoking manipulations. A short video sequence can be used to capture the intermittent step off at a costochondral separation or the snapping movement at the region of interchondral friction.

2.2 Stress Fractures of the Ribs

Stress fractures of the rib have been reported in throwing, golf, rowing, canoeing and swimming (Iwamoto and Takeda 2003) and occasionally in soccer (Matsumoto et al. 2003), kickboxing (Sakellaridis et al. 2004) and baseball players (Curran and Kelly 1966; Gurtler et al. 1985). In soccer, fractures are located at the first rib, whereas the lower ribs are involved in golfers and rowers. Fractures at the antero- to posterolateral aspects of ribs five through nine were most often associated with long-distance training and heavy load per stroke. Clinically, patients present with difficulty in abducting the arm (Gaffney 1997). A mechanism involving pull of the serratus anterior and external oblique muscles on the rib has been proposed as the cause of repetitive bending of the rib, leading to stress fracture. A modified technique using less reach, pull-through and layback

Table 1 Anatomy of the thoraco-abdominal wall muscles

Muscle	Origin	Insertion	Comment
M. Obliquus externus abdominis	8 Lower rib (cartilages)	Outer lip of iliac crest Anterior superior iliac crest Aponeurosis – Symphysis pubis – Inguinal ligament	Interdigitate with serratus anterior Outer layer of abdominal wall
M. Obliquus internus abdominis	Lateral two-thirds of inguinal ligament Anterior two-thirds of the iliac crest Thoracolumbar fascia	Lower three or four ribs Rectus abdominis Linea alba	Middle layer of abdominal wall
M. Transversus abdominis	Lateral third of inguinal ligament Anterior two-thirds of the iliac crest Twelfth rib Lower six costal cartilages	Aponeurosis toward obliquus internus abdominis Crista and pecten ossis pubis (conjoined tendon)	Innermost layer of abdominal wall
M. Rectus abdominis	Pubic crest, pecten ossis pubis Front of pubis	Fifth through seventh costal cartilages	Interconnection: linea alba Intersected with tendinous intersections
M. Latissimus dorsi	Spina vertebra Th 6–12 Thoracolumbar fascia – Spinous process vertebra L1–L6 – Spine vertebra sacrum Posterior lip of iliac crest Three or four lower ribs	Sulcus intertubercularis of humerus (common insertion with teres major tendon)	
M. Serratus anterior	Upper eight or nine (ten) ribs	Medial border of the scapula	Frequent variations at the origin

Table 2 Biomechanics of the thoraco-abdominal wall

Muscle	Bilateral actions	Unilateral actions	Strains
Iliopsoas muscle	Forward bending of trunk	Hip flexion	Resisted hip flexion, soccer
Obliquus externus abdominis	Aids in expiration Forward bending of trunk	Contralateral bending	Twisting motions Tennis, football, hockey, groin disruption
Obliquus internus abdominis	Retains abdominal viscera in position Bending of trunk forward	Ipsilateral bending	Twisting motions, tennis, groin disruption
Transversus abdominis	Retains abdominal viscera in position		
Rectus abdominis	Retains abdominal viscera in position Forward bending of trunk		Groin disruption
Serratus anterior		Pulls scapula anterior, reaching and pushing movements	Swimming, baseball pitcher (rare)
Latissimus dorsi	Violent expiratory movements (coughing, sneezing)	Adduction, extension, medial rotation of the ipsilateral humerus	Throwing sports (rare)

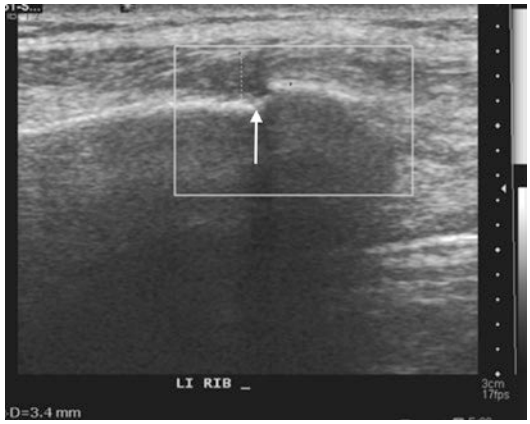

Fig. 4 Rib fracture. Rib fracture in an 82-year-old male with local pain at the anterior part of the left second rib. Chest and rib radiographs show no rib abnormality. Ultrasound examination and palpation along the long axis of the rib. Cortical interruption at the point of tenderness with subtle step off (arrow) and small haematoma (arrowhead)

should decrease the forces transmitted to the rib by these muscles, and decrease the risk for stress fractures (Karlson 1998).

Avulsion fractures of the floating ribs may also result from the opposing pulls of the latissimus dorsi, the internal obliques and the serratus posterior inferior muscles (Tullos et al. 1972). Diagnosis is confidently made by bone scintigraphy.

2.3 Injuries to the Sternum

Injuries of the sternum in athletes are rare. Most sternal injuries occur in automobile racing. Fowler (1957) reported three mechanisms of trauma: direct, indirect and muscular. Direct injuries occur when either a helmet, steering wheel or elbow (basketball players) strikes the sternum directly producing an inward displacement of the lower portion of the sternum. Indirect injury results from flexion compression injury of the cervicothoracic spine leading to posterior displacement of the cranial part of the sternum with manubriosternal dislocation due to direct strike of the chin to the manubrium. This has been reported in a football player.

Barbaix (2000) and Keating (1987), respectively, reported stress fractures of the sternum in a golfer and a wrestler.

2.4 Injuries to the Pectoralis Major, Latissimus Dorsi and Teres Major

Pectoralis major injuries were rare, typically occurring in active individuals participating in manual labour or sports. During the past two decades, the frequency of pectoralis major muscle injuries has increased in association with the increased popularity of bench press exercises (Lee et al. 2017). Diagnosis can usually be made based on a patient's history and physical examination. Injury of the pectoralis major can occur at the sternal muscle origin, muscle belly, musculotendinous junction, intratendinous region and/or humeral insertion—with or without bone avulsion. The extent of the tendon injury ranges from partial to complete tears. Specific treatment options, conservative or surgical, should be based on the severity of the injury and the patient's individual needs. In recent studies, operative repair of pectoralis major rupture has been shown to restore normal chest-wall muscle contours and preoperative strength (even in competitive athletes) (Dodds and Wolfe 2002; Neitzschman and Wilson 1999). Ultrasound and magnetic resonance imaging grading and characterization are helpful for treatment planning, conservative or surgical (Figs. 5 and 6). US may be useful for the initial screening of injuries, but MR imaging should be used invariably for patients in whom surgery is being considered and a more thorough evaluation is required (Lee et al. 2017). A thorough understanding of the complex anatomy of the pectoralis major is crucial. The pectoralis major has a parallel muscle fibre architecture with a broad clavicular, sternal and variable abdominal origin (Fig. 7a). The abdominal origin originates from the rectus abdominis fascia. The sternal head with origin at the anterior manubrium, sternum and second to sixth rib cartilages constitutes 80% of the muscle. This sternal part is divided by fascial planes in five segments for

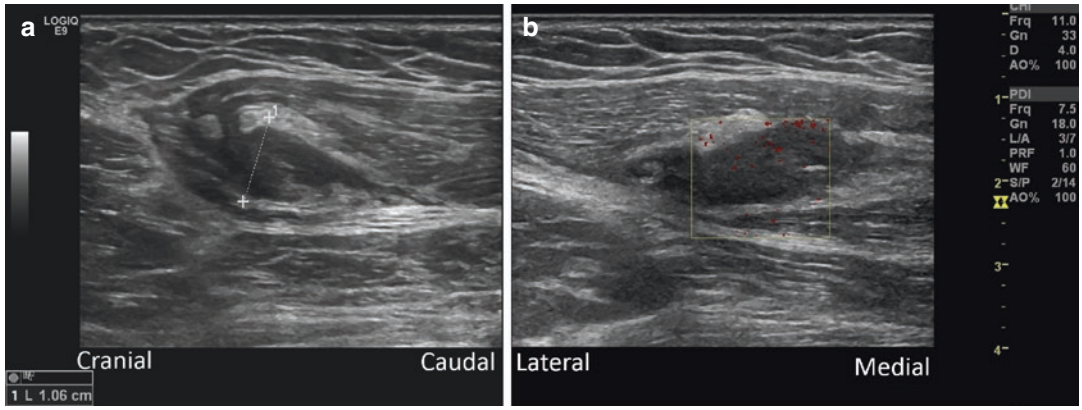

Fig. 5 (**a**, **b**) Haematoma at the muscle belly of the clavicular part of the pectoralis major muscle in a 46-year-old male patient. (**a**) Transverse US view. (**b**) Longitudinal US view. Notice a structural anomaly with fluid infiltration at the muscle

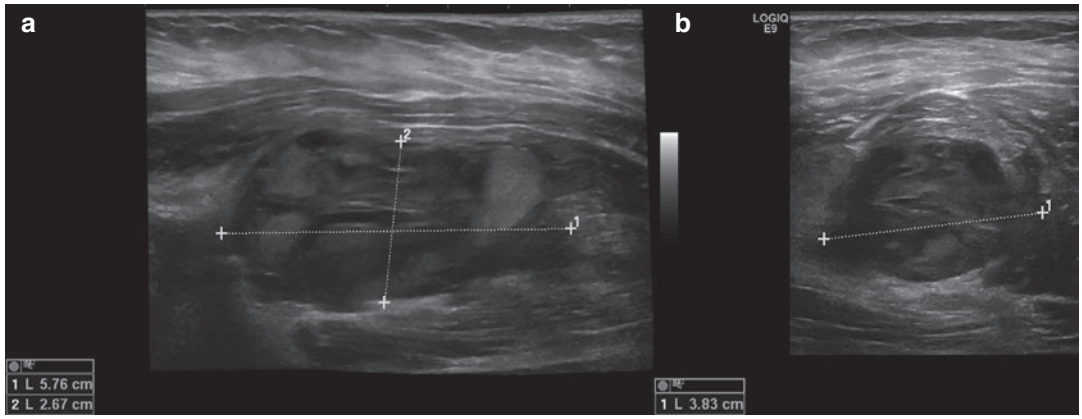

Fig. 6 (**a**, **b**) Ultrasound demonstration of a 1-day-old pectoralis major haematoma in a 33-year-old male. (**a**) Longitudinal US view. (**b**) Transverse US view. Note the heterogeneous mass of mixed reflectivity at the medial-cranial half of the pectoralis muscle belly

each rib 2–6. A specific partial overlap of the cranial over the caudal neighbouring muscle division creates the aspect of a Chinese fan (Fig. 7a). The caudal parts are most commonly involved in elongation injury. Distally a short MTJ is inserted into a common tendon with a length of about 5 cm and a width of about 4 cm craniocaudally. The tendon is an inferiorly connected double-layered U-shaped sulcus: the cranial half of the muscle (sternal and manubrial) and caudal half of the muscle (manubrial and abdominal) form the anterior and posterior tendon components, respectively (Fig. 7b). Distally these two layers fuse and run anterior to the coracobrachialis, short and long head of the biceps, respectively, to get inserted at the lateral margin of the intertubercular sulcus of the humerus (crista tuberculi majoris) at the same level of the teres major and latissimus dorsi (Figs. 7c, 8a–c, and 9a, b). The latter run deep to the coracobrachialis and the short head of the biceps and get inserted on the medial margin of the intertubercular sulcus (crista tuberculi minoris). Eighty-three percent of injuries to the pectoralis major are elongation related during eccentric contraction with extended humerus; 48% of them are bench pressing related (Elmaraghy and Devereaux 2012) and others are related to rugby, wrestling, ju-jitsu

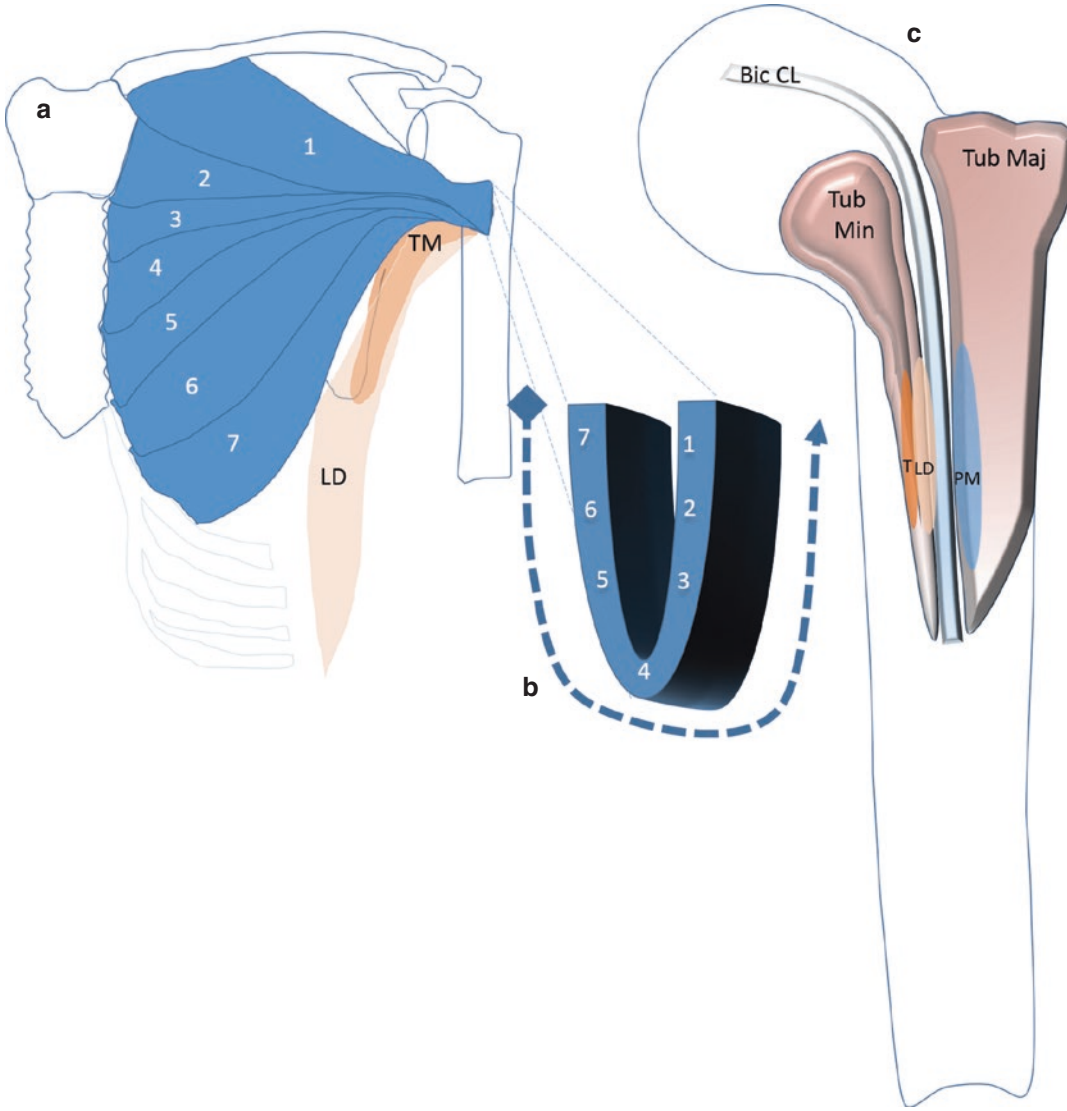

Fig. 7 (**a**–**c**) Normal anatomy of the pectoralis major, latissimus dorsi and teres major. (**a**) Clavicular (1), sternal (2–5) and abdominal (6, 7) pectoralis major segments. Fanlike partial overlap of the segments. (**b**) Distal tendon is U-shaped with segments 1–3 anterior and 5–7 posterior and inferior connecting segment 4. Tear of the pectoralis major tendon starts inferior/anterior (curved arrow). Four consecutive tear types are recognized: (*1*) Partial width partial thickness: tear of segments 7–6 (abdominal portion). (*2*) Full width partial thickness: tear of segments 7–3 (abdominal and sternal portion). (*3*) Full-width tear of the posterior portion and partial width tear of the anterior portion: tear of segments 7–2 (two-layer component). (*4*) Full-thickness/full-width tear: complete tear of all segments. (**c**) Fusion of the anterior and posterior tendon at the insertion on the crista tuberculi majoris (tub maj). Caput longum tendon of the biceps (*Bic CL*) at the intertubercular sulcus. Insertion of the teres major (*TM, T*) and latissimus dorsi (*LD*) tendon, respectively, into medial and lateral on the crista tuberculi minoris (*tub min*)

gymnastics and boxing. Contusion injury is most often located at the muscle origin and muscle belly. Pectoralis major elongation injury is classified according to Tietjen and later on according to ElMaraghy and Deveraux (Tietjen 1980; Elmaraghy and Devereaux 2012); actually this classification is adapted to the BAC muscle injury classification system (Gielen et al. 2021, Table 3) taking into account the location and extent. Muscular origin, intramuscular and subfascial

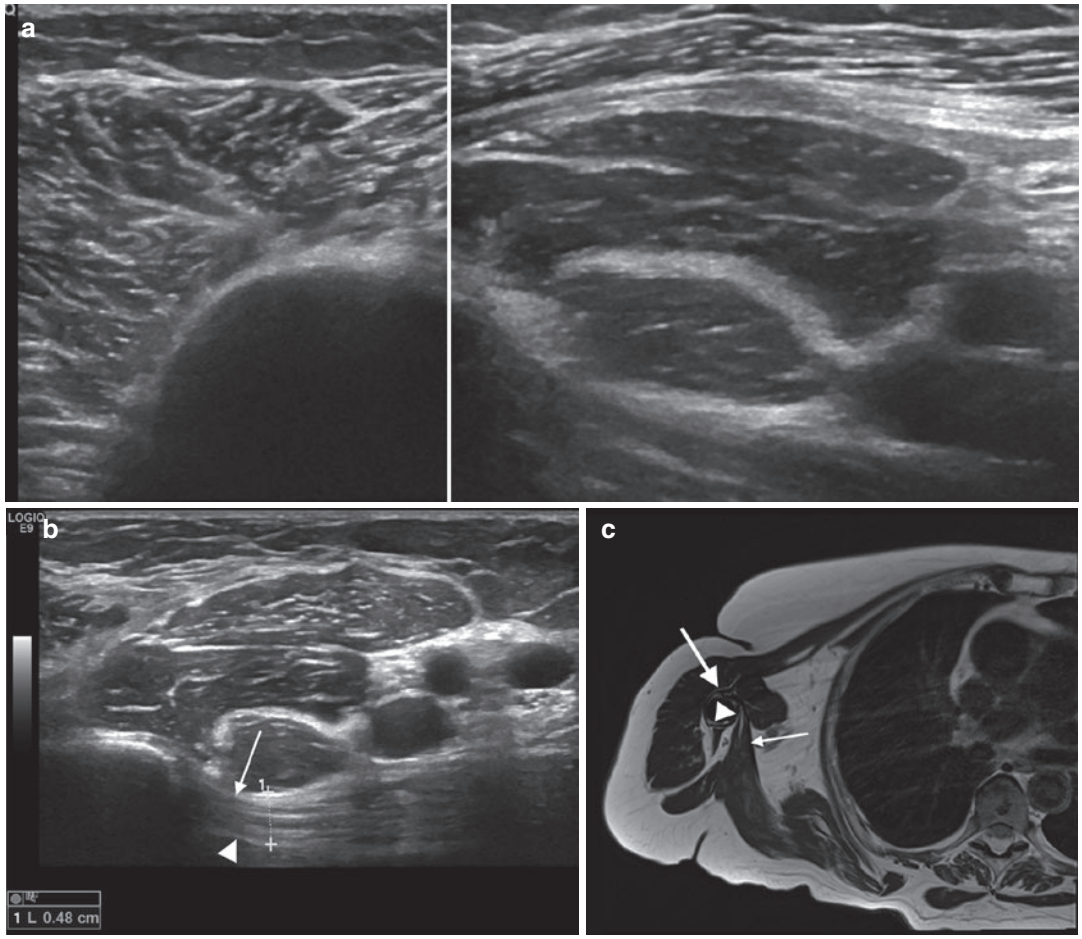

Fig. 8 (**a**–**c**) US and MRI demonstration of distal insertion pectoralis major, teres major and latissimus dorsi. (**a**) Longitudinal pectoralis major view with demonstration of the double-layered pectoralis major tendon. (**b**) Longitudinal pectoralis major view with demonstration of the teres major and latissimus dorsi tendons. (**c**) Axial TSE T1-WI. Pectoralis major tendon (arrows) anterior to the coracobrachialis and short head of the biceps muscle bellies. Posterior to these muscle bellies location of the teres major (arrowhead) and latissimus dorsi tendons (small arrow) with insertion on the crista tuberculum minoris

lesions (BAC suffix a) have the best prognosis and generally are treated conservatively; lesions located at the MTJ (BAC suffix b, prevalence 24%) (Fig. 10a–c) tend to have a longer rehabilitation period; and lesions with involvement of the tendon (BAC suffix c, prevalence 59%) have the longest rehabilitation period, might show tendon retraction and often need surgical repair (Haley and Zacchilli 2014). The tendon tears in a characteristic sequence starting from the inferior segments (7 and 6) which is the location of the greatest strain resulting in BAC suffix c partial lesions that often involve only part of or the whole posterior abdomino-sternal segments (Fig. 7b). These partial lesions are quantified by measuring the length (retraction), width (full or partial thickness) and craniocaudal extent (partial or complete) (Fig. 7b). In complete tendon lesions both anterior clavicular and posterior abdomino-sternal segments are involved with retraction of the tendon and anterior displacement of the tendon of the long head of the biceps (Fig. 7b). Distal lesions with bony avulsion also exist and might need primary fracture fixation. A distinction is made between acute and chronic tears because with chronic injuries, a delay in

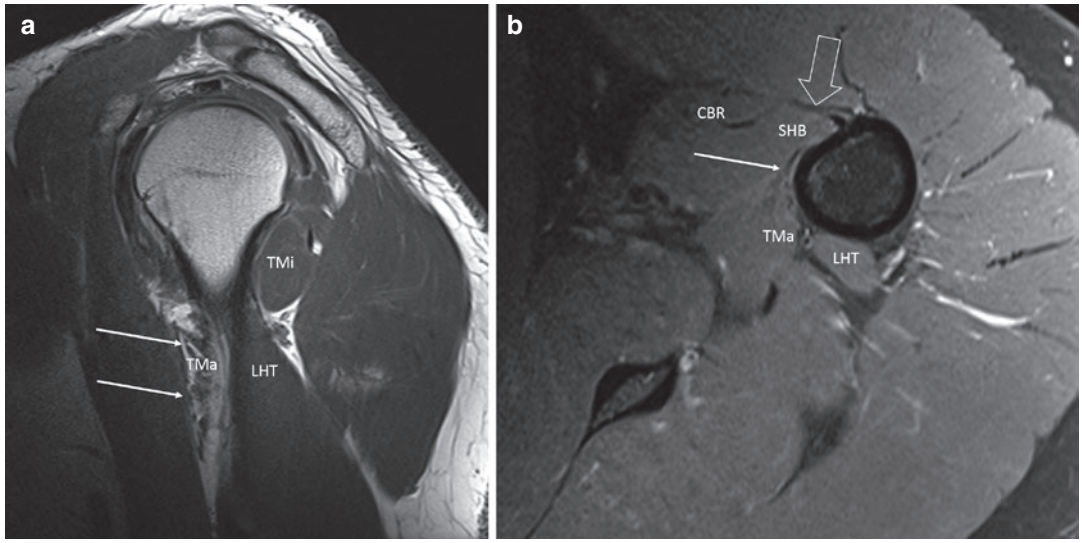

Fig. 9 (**a**, **b**) Normal anatomy tendon and distal insertion of the pectoralis major, latissimus dorsi and teres major muscle. (**a**) Sagittal T1-WI. (**b**) Axial fat-suppressed T2-WI. Latissimus dorsi tendon (**a**, **b** arrows). Pectoralis major tendon (thick arrow). Biceps muscle, short head (*SHB*). Coracobrachialis muscle (*CBR*). Long head of triceps (*LHT*). Teres major (*TMa*). Teres minor (*TMi*)

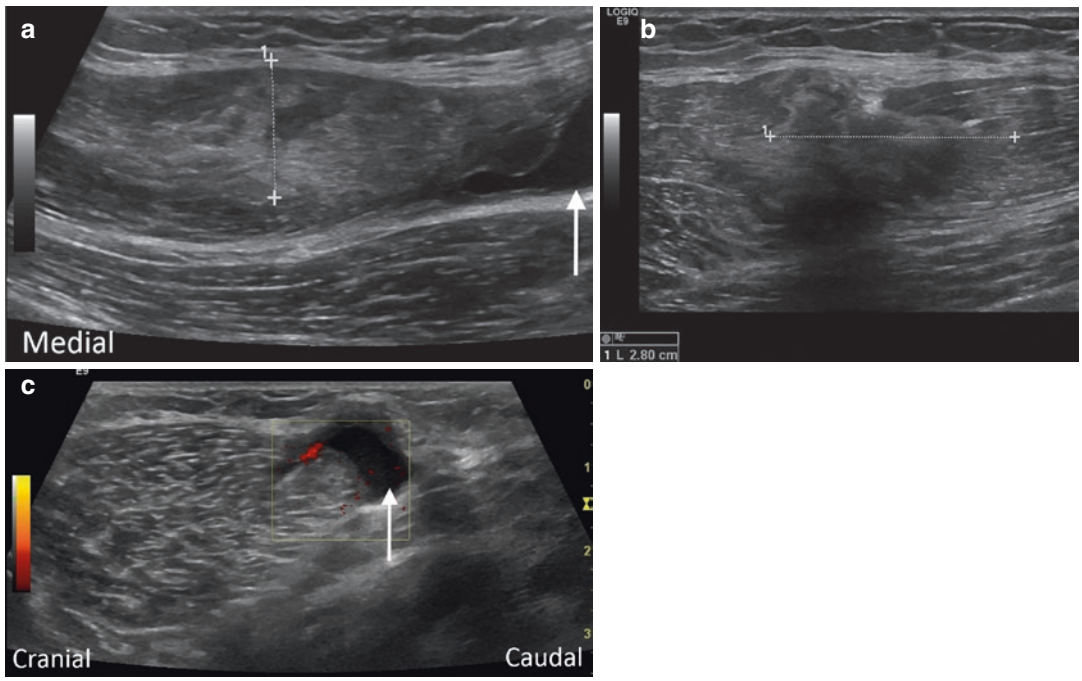

Fig. 10 (**a**–**c**) Partial tear at the MTJ of the abdominosternal segments of the pectoralis major in a 47-year-old male patient. (**a**) Longitudinal view of the inferior part of the pectoralis major with fluid collection (arrow) and distracted tendon (arrowhead) of the abdominal and lower sternal head (see also Fig. 7b (*2*)). (**b**) Longitudinal view of the central part of the pectoralis major with structural anomaly at the central sternal head of the pectoralis major. (**c**) Transverse view of the pectoralis major with fluid-filled collection (arrow) at the lower lining of the muscle belly: abdominal and lower sternal head

surgery of a few weeks to a few months is associated with the development of adhesions, muscular contraction, atrophy and worsened functional outcome (Lee et al. 2017). Distal pectoralis major lesions have to be discriminated from distal acute and chronic overuse and elongation lesions to the latissimus dorsi and teres major; these lesions are also the result of forceful resisted arm adduction. The distal insertion is located at the crista tuberculum minoris at the same level as the distal pectoralis major insertion (Figs. 7a–c, 8a–c, and 9a, b). Both tendons may be involved in the same elongation injury. They are rare and reported in baseball pitching, golf, gymnastics, rock climbing, volleyball and water ski (Anderson et al. 2005; Schickendantz et al. 2009).

2.5 Scapulothoracic Crepitus and Bursitis

Symptomatic scapulothoracic crepitus is also known as the snapping scapula, the washboard syndrome or the scapulothoracic syndrome. This is due to repetitive friction of the scapula against the thoracic wall. A gentle friction (*froissement*) is described as physiologic but grating (*frottement*) and loud snapping (*craquement*) are definitively pathologic. Symptomatic scapulothoracic bursitis affects the superomedial and the inferior angle of the scapula. Predisposing anatomic conditions include osteochondroma or malunion of rib of scapula, and hooked superomedial angle of the scapula. A common cause of scapulothoracic crepitus in athletes involves abnormalities in congruence of the scapulothoracic articulation (i.e., scoliosis and thoracic kyphosis) (Hellstrom et al. 1990; Wojtys et al. 2000). In scapula infracoracoid dyskinesis syndrome—frequently seen in throwing athletes—the scapula assumes a protracted and depressed position, with the inferior angle deviating laterally and leading to scapulothoracic crepitus (Kuhn 2003). Athletes who participate in sports that require repetitive overhead activity are also commonly affected. Repetitive motion may irritate soft tissues until chronic inflamed adventitious bursitis and inflammation develop. The bursa then undergoes scarring and fibrosis, with crepitus and pain to follow. MRI will occasionally demonstrate increased signal and even fluid collections in an inflamed bursa on T2-WI. This finding is highly specific for bursitis, but in case of fibrosis, there may be absence of high signal changes. Ultrasound may detect these fibrotic adventitious bursae by revealing a volume increase in comparison with the normal side (Fig. 11a–c) (Huang et al. 2005). Radiographs with tangential views of the lateral scapula, computed tomography (CT) or magnetic resonance imaging (MRI) may be helpful in identifying predisposing anatomic disease.

3 Abdominal Wall

3.1 Introduction

Sports injuries to the hip and groin region have been noted in 5–9% of high school athletes (Morelli and Weaver 2005). Abdominal wall injuries occur in nearly one of ten patients coming to the emergency department after nonpenetrating trauma (Matalon et al. 2017). Injuries range from minor, such as abdominal wall contusion, to severe, such as abdominal wall rupture with evisceration of abdominal contents (Matalon et al. 2017). These injuries occur most commonly in athletes participating in sports involving side-to-side cutting, quick accelerations and decelerations, and sudden directional changes.

Injuries related to the abdominal wall fall into three basic categories: abdominal wall muscle and tendon injuries, acute and chronic groin lesions and nerve compression injuries. The muscle groups that are susceptible to elongation injury are the internal and external obliques, rectus abdominis and pyramidalis, adductor and obturator muscle groups, gracilis, pectineus, rectus femoris and iliopsoas. This chapter focuses on trauma of the abdominal wall, iliopsoas and acute groin lesions. The other groin lesions are studied in Prasad et al. (2021).

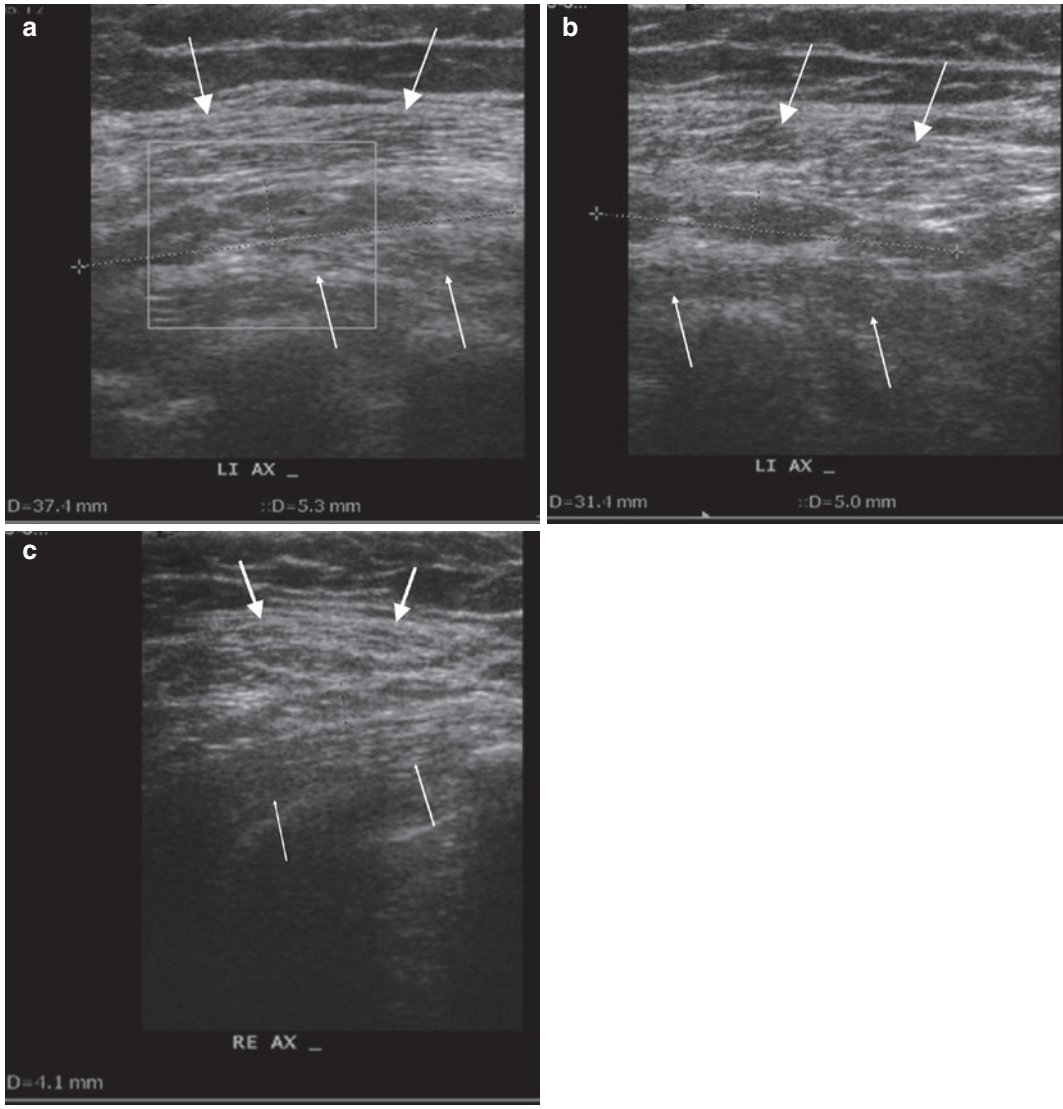

Fig. 11 (**a**–**c**) Scapulothoracic crepitus. Scapulothoracic crepitus in a 25-year-old female with pain and snapping during left shoulder abduction-elevation at the level of the angulus inferior of the scapula. Patient with hyperkyphosis of the thoracic spine. Ultrasound (**a**) axial and (**b**) sagittal (**b**, cranial = left) imaging plane at the painful region of the latero-inferior margin of the left and right scapula, respectively. Thickening of the tissue in between m. serratus anterior (arrows), m. latissimus dorsi (small arrows) and adjacent to the angulus inferior of the scapula at the left side. Aspect of adventitious bursa with nonhomogeneous low-reflective tissue that is slightly compressible and demonstrates no vascularization on power Doppler technique. (**c**) Comparison with right side, asymmetry with smaller volume of the interposed tissue. Within 4 weeks after ultrasound-guided locoregional corticosteroid infiltration, there is gradual reduction of pain and snapping

3.2 Abdominal Wall Muscle Lesions

Most commonly, there is a typical history of a sudden violent contraction of the muscle against resistance with the muscle maximally stretched. Nearly all muscle elongations occur just adjacent to the musculotendinous junction (Garret et al. 1993). In the abdominal region most muscles have short tendons or muscular origins and insertions, and therefore muscle elongation is often found near its origin or insertion (except for the rectus abdominis).

Injury to the oblique muscles of the abdomen will occur during twisting motions of the trunk. Lacroix et al. (1998) reported on operative findings of varying degrees of tearing of the external oblique aponeurosis and external oblique muscle associated with ilioinguinal nerve entrapment in 11 elite ice hockey players. In this study, preoperative physical examination and imaging findings (scintigraphy, US, CT, MRI) were consistently negative. Despite the lack of specific literature on the subject, it is our personal experience however that state-of-the-art ultrasound and MR imaging techniques are valuable methods for diagnosis, grading and follow-up of abdominal muscle elongations.

3.2.1 Side Strain and Hip Pointer

Side strain tears are rarely a diagnostic dilemma for clinicians. The study of Connell et al. (2003) showed that side strain is caused by an acute tear of the internal oblique musculature where it originates on the undersurface of the 9th, 10th, or, most commonly, the 11th rib or costal cartilages. Movements associated with bowling (cricket), rowing, swimming and golf cause lengthening of the muscle and superimposed eccentric contraction, making it vulnerable to rupture. MRI can depict the site of a muscle tear, characterize the severity of injury and monitor healing. Sagittal oblique muscle images are most useful for assessing the degree of muscle injury (Fig. 12). Stripping of the periosteum occurs as the muscular attachment is avulsed from the osseous or cartilaginous origin. This may result in excessive haemorrhage even though the muscle tear may be of low grade. The presence of a haematoma often aids in the identification of the site of muscle injury. The MR signal characteristics of haemorrhage vary with different sequences and are time dependent. Follow-up MRI may be useful for monitoring healing and scar formation in patients who fail to respond to treatment.

Rarely fibres inserted on the anterior portion of the iliac crest may be disrupted, resulting in the so-called hip pointer. The equivalent in adolescent patients is acute iliac crest apophyseal avulsion fracture (Fig. 13). Patients present with local tenderness along the injured muscle and iliac crest. Pain is aggravated by passive stretching of the muscles due to contralateral bending and activation of the muscle by twisting and flexing the abdomen. Ultrasound and MRI documented the tear with fluid collection at the iliac

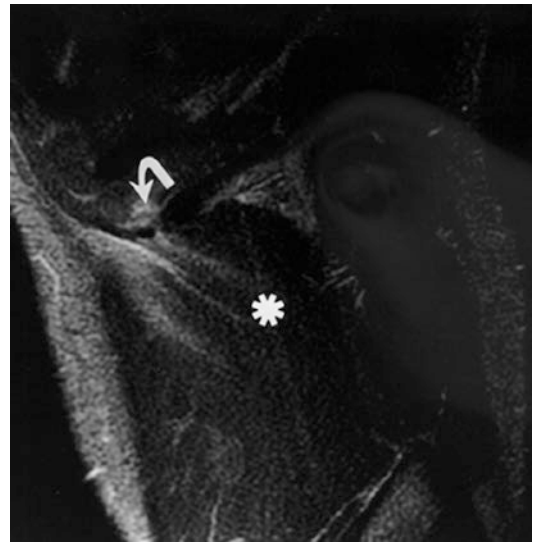

Fig. 12 Side strain. Side strain in a 23-year-old male javelin thrower with point tenderness and pain during competition. Sagittal oblique STIR MR image (5300/38; inversion time, 120 ms) shows high signal at the origin of the m. obliquus internus at the undersurface of tenth rib (curved *arrow*). Haematoma tracks along muscle fibres of m. obliquus internus abdominis (*asterisk*) (reprinted with permission from Connell et al. 2003)

Fig. 13 Radiograph of the pelvis in a 16-year-old male soccer player with acute crista iliaca (CI) apophyseal avulsion fracture 2 weeks ago. Widening of the physis at the left CI (arrow)

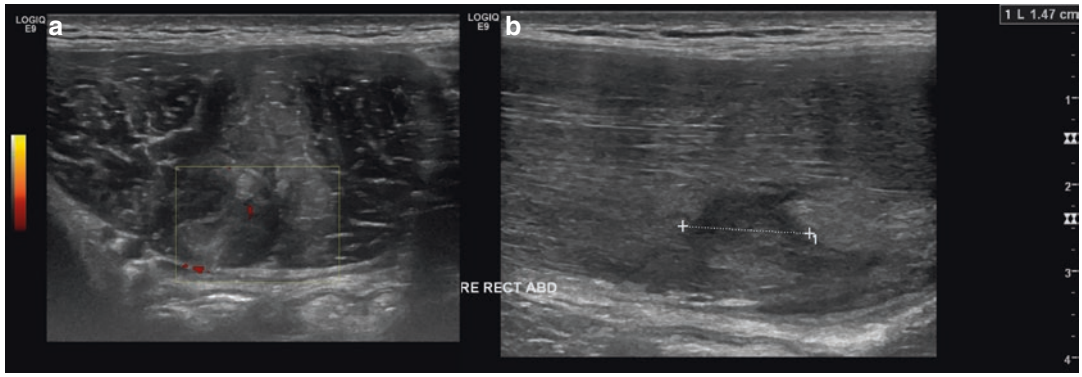

Fig. 14 (**a**, **b**) Two-week-old tear at the right rectus abdominis in a 19-year-old soccer player. (**a**) Axial US image. (**b**) Longitudinal US image. Hyporeflective collection (1.5 cm) surrounded with hyperreflective infiltration located at the posterior subfascial area of the muscle belly. Grading BAC 2a (see Table 3 in Gielen et al. 2021)

crest in an Australian football player (Murphey et al. 2016).

3.2.2 Rectus Abdominis Lesions

Similar problems result from elongation of the rectus abdominis muscle. This paragraph discusses the elongations and lesions after blunt trauma of the rectus abdominis. Elongation lesions are typically located at different levels near its tendinous intersections (Figs. 14 and 15). After blunt trauma to the abdomen, patients present with lower grade injuries ranging from subcutaneous contusion to abdominal wall haematoma (Dennis et al. 2009; Matalon et al. 2017). It is however not uncommon to have injury to several muscle groups of the abdomen at the same time.

Johnson (2006) acknowledges the importance of rectus sheath haematoma (RSH) in cases of muscular tear or contusion from damage of the superior or inferior epigastric arteries or their branches. Above the arcuate line, the superior epigastric arteries are usually involved; below the arcuate line, the inferior epigastric arteries are most commonly implicated (Matalon et al. 2017). Rectus sheath haematoma is not always self-limiting and can cause hypovolemic shock with associated mortality. RSH caused by bleeding from the superior epigastric arteries is more likely to result in self-tamponade because of compression by the circumferential rectus sheath, and RSH caused by bleeding from the inferior epigastric arteries is less constrained by the absent posterior sheath (Matalon et al. 2017). Ultrasonography (Fig. 16), CT and MR imaging are valuable tools for evaluation of the possible haematoma.

3.2.3 Iliopsoas Injury

Iliopsoas injuries occur during forceful resisted hip flexion. Clinically, the athlete will feel a sharp pain in the groin region that may radiate into the lower abdomen. Passive external rotation and hip extension and resisted hip flexion will be painful. In adolescents, an avulsion fracture of the lesser tuberosity may occur, ***whereas*** adults will present with an injury to the musculotendinous junction. Therefore radiographs are sufficient for diagnosis in adolescents, whereas in adults, MRI is needed for a reliable diagnosis (Shin et al. 1996) (Fig. 21, see Gielen et al. 2021).

3.2.4 Acute Groin Disruption

Profound knowledge of the anatomical relationships is a condition sine qua non to understand the pathology at this area.

Literature on acute groin disruption is rare. Our personal experience includes two cases of acute groin disruption that occurred in skiing (alpine ski and water ski with right and left lesions, respectively). The patients experienced hyperextension of the spine-abdomen and abduction-extension of the hip while making a slip and fall. Both patients were diagnosed on ultrasound and MRI (Fig. 17a–f). In both patients ipsilateral elongation with

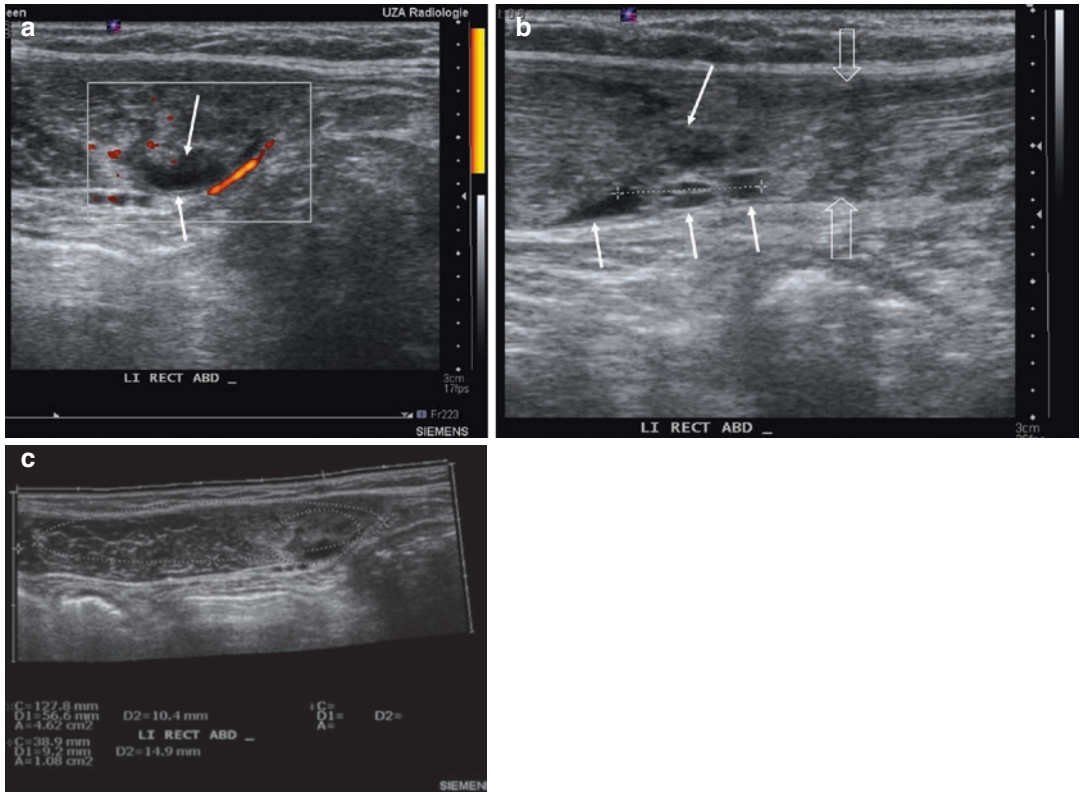

Fig. 15 (**a**–**c**) Left rectus abdominis elongation injury in a 21-year-old right-handed female tennis player. (**a**) Axial US image. (**b**) Longitudinal US image. (**c**) Transverse extended field of view. US examination 1 week after the injury demonstrating an area of fibre disruption with small fluid collection (**a** and **b**, arrows) at the MTJ of infraumbilical fibrous intersection (**b**, transparent arrows). Length 10 mm and a SCA of 20% (**c**). Grading BAC 2b (see Table 3 in Gielen et al. 2021)

oedema was found at the external oblique aponeurosis, rectus abdominis/pyramidalis tendon and anterior pubic ligament with avulsed fragment of the adductor longus with haematoma, elongation grade 2 at the origin at the gracilis, and pectineus and dehiscence of these structures from the anterior pubis. This finding favours the PLAC concept (see Prasad et al. 2021) for more in-depth discussion) and confirms the hypothetic mechanism of injury with the pubic bone as pivot point. In this concept lower abdominal structures (pyramidalis muscle and medial slender tendon/aponeurosis of the rectus abdominis) are inserted to adductor longus/anterior pubic ligament and gracilis, respectively (Schilders et al. 2017) (Fig. 18a, b). A similar pivot shift mechanism may contribute to the development of chronic overuse-related groin pain.

3.2.5 Groin Pain in Athletes

The Doha agreement in 2015 on terminology and definitions in groin pain in athletes tries to unravel the confusion in this complicated area (Weir et al. 2015). In this meeting clinical entities for groin pain were defined. These major four clinical entities are adductor-related (adductor tenderness and pain on resisted adduction testing), iliopsoas-related (pain on resisted hip flexion AND/OR stretching of the hip flexors), inguinal-related (inguinal canal region pain without palpable inguinal hernia, aggravated with resistance testing of the abdominal muscles OR Valsalva) and pubic-related groin pain (symphysis and adjacent bone pain WITHOUT pain with resistance testing). The fifth entity is hip-related groin pain. Other musculoskeletal causes of groin pain have to be evaluated: inguinal or femoral hernia and

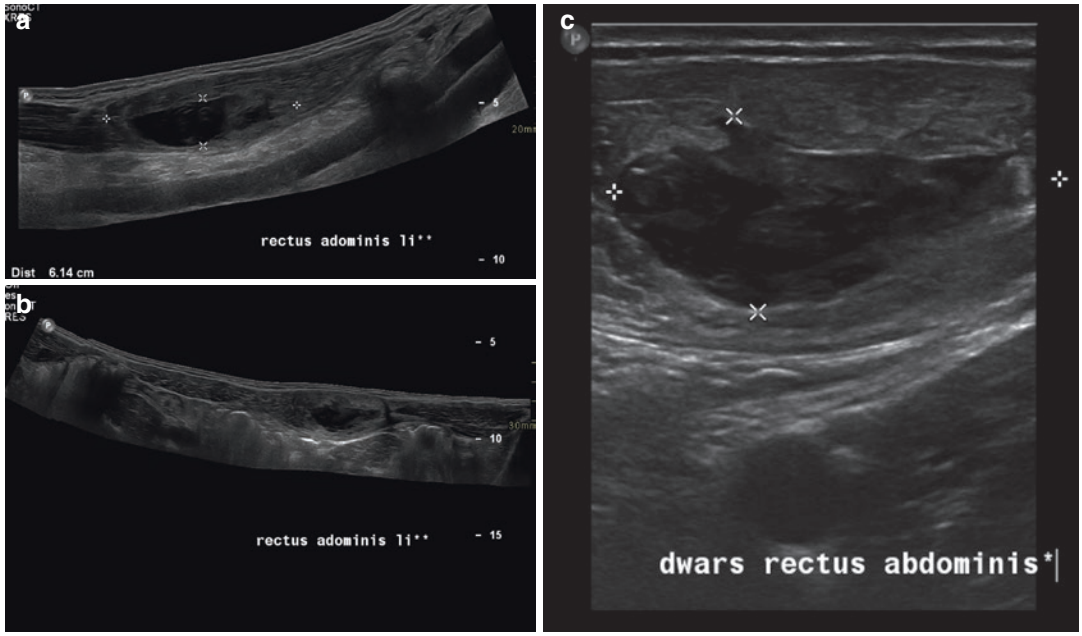

Fig. 16 (**a**–**c**) Self-limiting left rectus abdominis haematoma above the arcuate line. (**a**) Longitudinal extended field of view. (**b**) Transverse extended field of view. (**c**) Transverse view. Hyporeflective area at the deep half of the muscle belly with maximal dimension 6 cm

posthernioplasty pain, nerve entrapment, referred pain and apophyseal abnormalities of the SIAS (Fig. 19) and SIAI and pubis apophysis. Miscellaneous conditions are not to be missed (stress fracture, adenopathy, intra-abdominal and gynaecological pathology, tumours).

The Doha agreement also avoided several terms related to the lack of specificity, inappropriate or incorrect term and large degree of variation of use. These terms are adductor and iliopsoas tendinitis or tendinopathy, athletic pubalgia, osteitis pubis, sports groin, sports(man's) groin or hernia.

The Doha agreement agreed on the lack of high-quality reviews related to varying definitions and categories and the lack of prospective controlled studies resulting in low level of evidence on epidemiology, risk factors, accuracy of clinical tests, imaging and treatments in groin pain in athletes.

3.2.6 Imaging of Groin Pain

Major imaging findings are discussed in Prasad et al. (2021). Dynamic examination at the inguinal region for evaluation of the inguinal and femoral canal is done with ultrasound.

In athletes with continued groin pain, despite adequate rest and no obvious hernia, herniography was of great value. Smedberg et al. (1990) have shown that herniography is accurate in disclosing nonpalpable hernias (Figs. 20 and 21). Herniography is performed by injecting contrast medium under fluoroscopic control into the peritoneal cavity under local anaesthesia (Smedberg et al. 1985). Few complications have been reported with herniography (Ekberg 1983). Incarcerated or irreducible hernias may give false-negative results because the contrast will be unable to leak through the defect.

Ultrasound is currently the most valuable noninvasive technique to study the inguinal and femoral canal and its contents. It is performed dynamically during rest and Valsalva testing as well as in decubitus dorsalis and prone position. If the ultrasonographer is familiar with the specific anatomy of this region, a good discrimination between femoral and inguinal hernia is possible. Also, direct and nondirect inguinal hernias are discriminated.

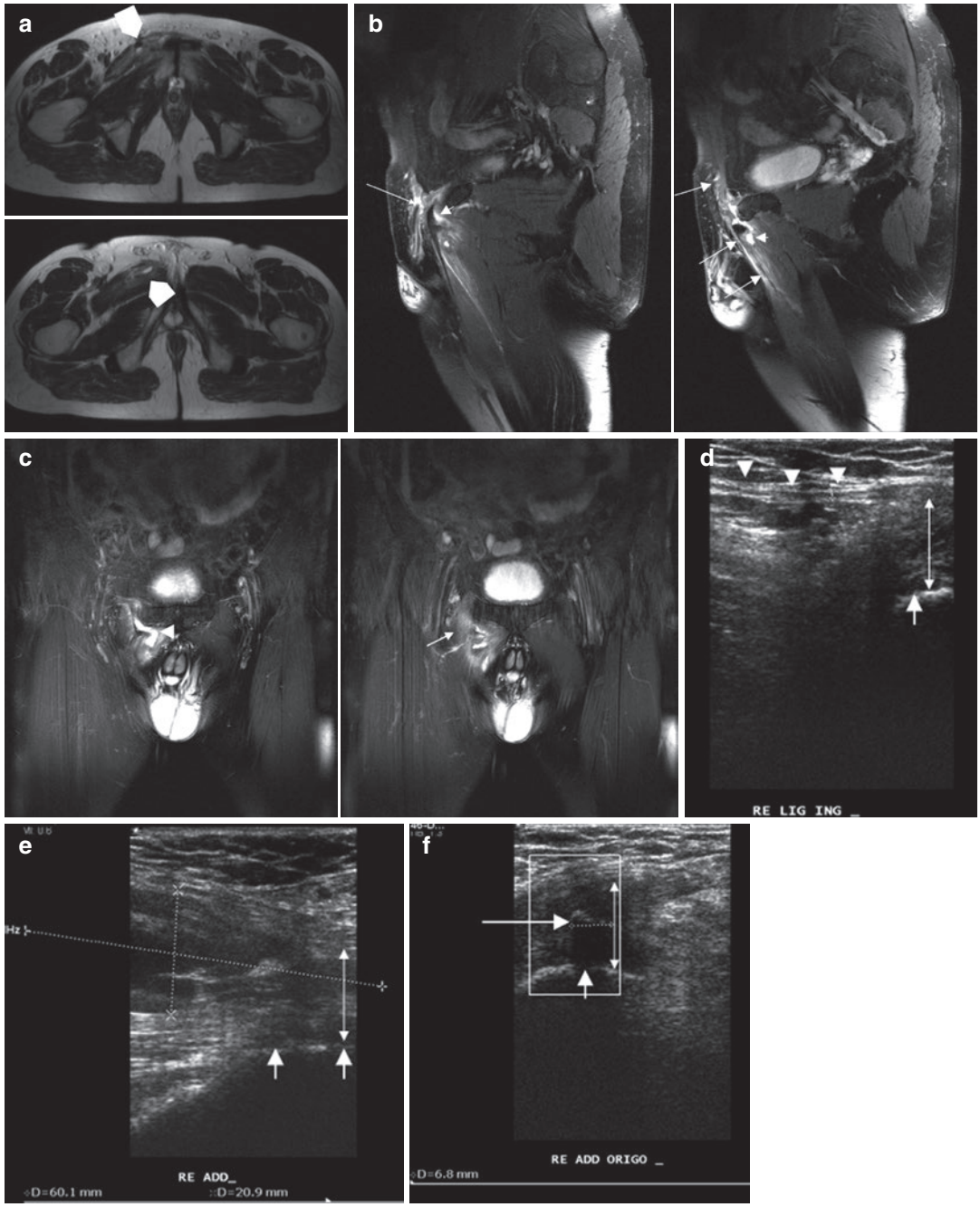

Fig. 17 (**a**–**f**) Acute groin disruption. Acute groin disruption in a 49-year-old male alpine skier after resisted hyper-abduction extension of the right hip and extension of the abdomen. Acute pain and swelling at the right groin. (**a**) Axial TSE T2-weighted MR image, cranial and caudal parts of pubis, respectively. (**b**) Sagittal TSE T2-weighted fat-suppressed MR image (intermediary TE), parasagittal lateral and medial through the right pubic bone, respectively. (**c**) Coronal TSE T2-weighted fat-suppressed MR image (intermediary TE), anterior and midsection through the pubic bone, respectively. High SI haematoma (**a**–**c**, arrowheads) at the right adductor longus, gracilis and rectus abdominis muscle separating the pubic bone and the muscles, surrounded by oedema. Avulsed bone fragment continuously with the adductor longus tendon (hypointense area in **b**, right). Note oedema at the pectineus origin (**b**, left small arrow), the inguinal canal (**b**, left arrow) and the pyramidalis muscle (**b**, right

(continued)

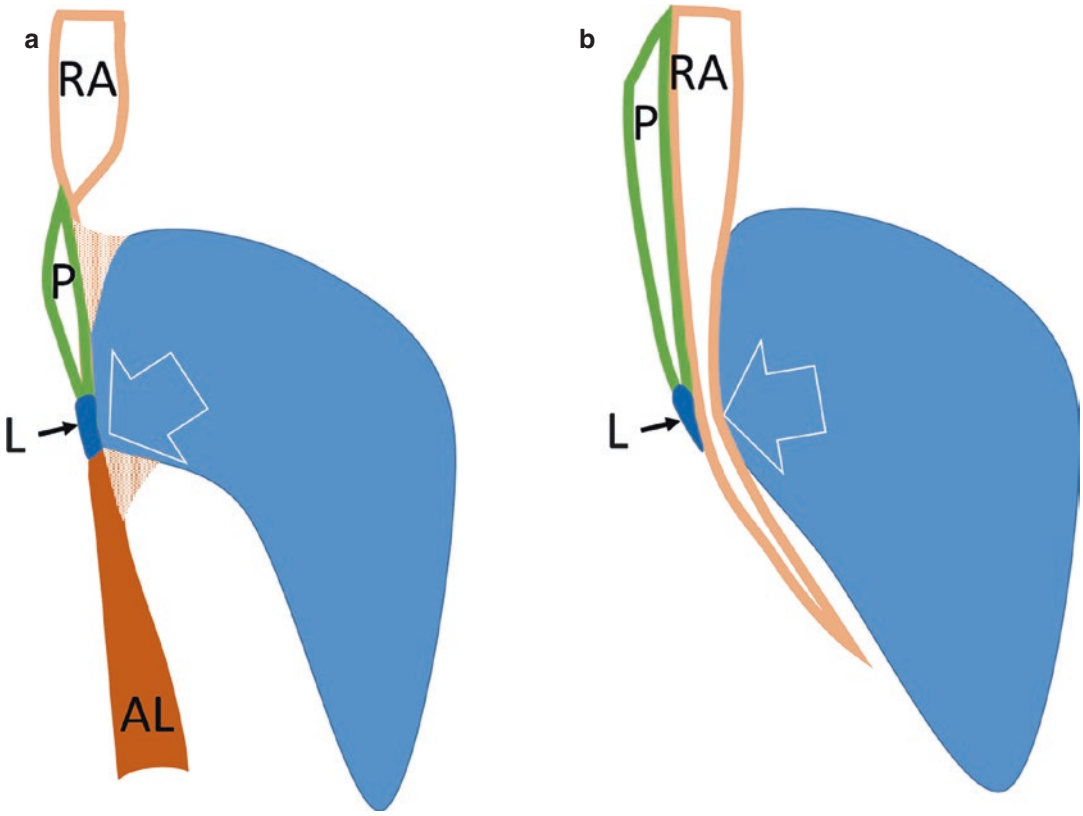

Fig. 18 (**a**, **b**) Diagram of the PLAC concept (Schilders et al. 2017). (**a**) Parasagittal lateral plane. (**b**) Parasagittal medial plane. Blue arrow (**a**, **b**): pubic crest. Blue: pubis. Rectus abdominis (RA), insertion of the lateral tendon (**a**) on the pubic crest. Rectus abdominis (RA) medial slender tendon/aponeurosis (**b**) running in front of the pubis distal to the pubic crest and connecting to the gracilis muscle (not drawn). Pyramidalis muscle (P) anterior to the rectus abdominis, inserted on the anterior pubic ligament (L). Anterior pubic ligament fused with adductor longus tendon (AL)

In concordance with the findings of Orchard et al. (1998), obliquus internus aponeurosis insufficiency (sports hernia) refers on ultrasound to a condition of bulging at the site of the external inguinal ring through sprain of the posterior inguinal wall at this level. Most often this bulging is only present during Valsalva test and is spontaneously reduced at rest. A flank hernia with recognition of a hernial sac is usually not found in sports hernia (Figs. 21 and 22a–d).

arrow superficial) that is continuous in front of the pubis with the adductor longus. Dehiscence of the pyramidalis/rectus abdominis, adductor tendon complex and anterior pubic ligament from the pubic bone is obvious through widening of the distance between the tendon and the bone with interposition of high SI haematoma and oedema (**b**, right double-sided arrow). Continuity of the pyramidalis and adductor longus in front of the pubic bone at the level of the dehiscence (**b**, right large arrows). (**d**) Oblique axial ultrasound view along the axis of the ligamentum inguinale up to the anterior pubic ligament and pubic bone. (**e**) Sagittal ultrasound view at the level of the m. rectus abdominis/pyramidalis up to the pubic bone. (**f**) Axial ultrasound view at the level of the pubic bone at the adductor origin. Dehiscence of the ligamentum inguinale (**d**, arrowheads), adductor complex from the pubic bone (**d**–**f**, small arrows) with small avulsion fracture fragment (**f**, large arrow). Dehiscence distance (**d**–**f**, double-sided arrow). Thickening of the m. rectus abdominis with non-homogeneous reflectivity and disruption of its layered architecture at the distal musculotendinous junction (region within dotted crossing lines)

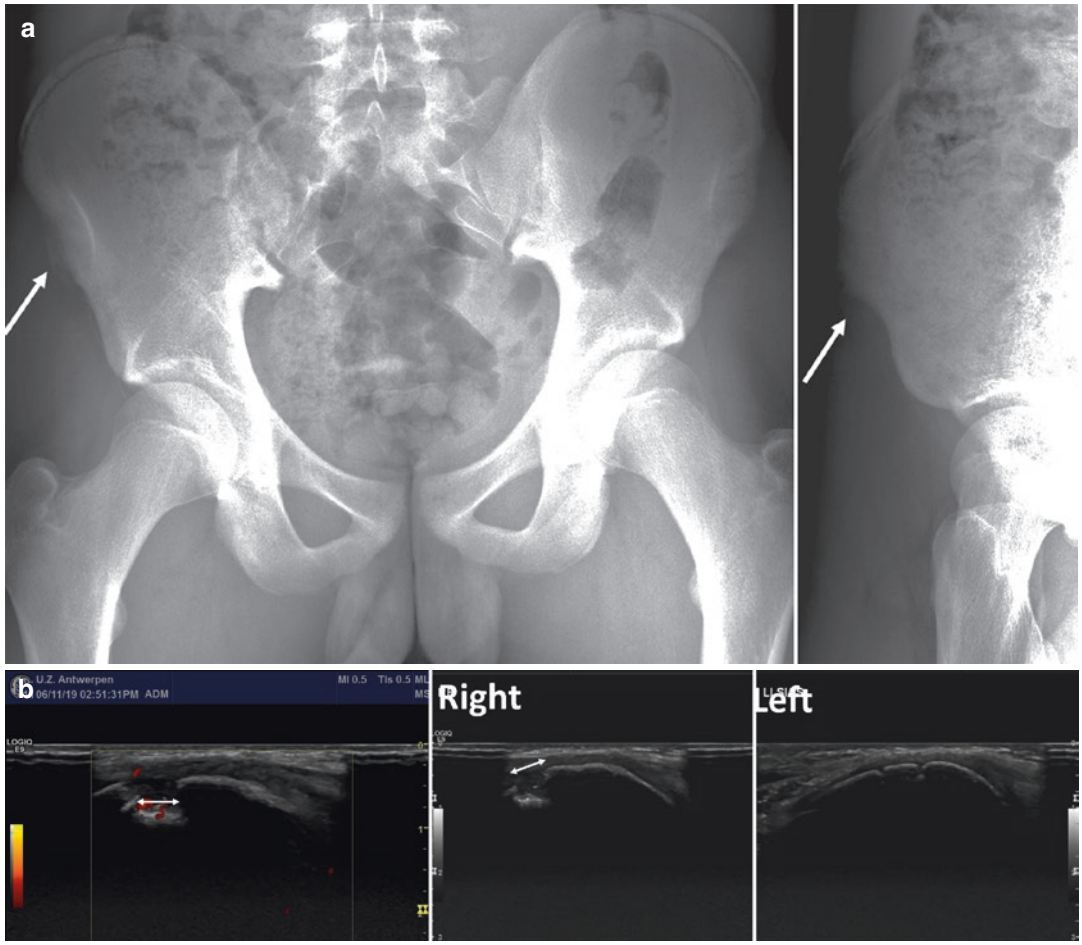

Fig. 19 (**a**, **b**) Sixteen-year-old male with acute apophyseal avulsion fracture of the right spina iliaca anterior superior (SIAS). (**a**) Radiograph (AP (right) and rotated (left)). (**b**) Ultrasound right and left side compared. Note displaced SIAS apophysis (**a**, **b** arrows)

3.3 Traumatic Abdominal Wall Injury and Hernia in Children

Handlebar injuries are a significant cause of both blunt abdominal trauma and lacerations to the contact area. The infrequent finding of external bruising in the presence of major organ damage suggests that, although the velocity at impact may be relatively low, the small cross-sectional area of the end of the handlebar is a major factor contributing to organ damage. The high proportion of lacerations observed in this type of trauma result from the sharp metallic end of the handlebar cutting through the soft rubber handle (Clarnette and Beasley 1997). Erez et al. (2001) reported on children who presented with abdominal injuries caused by bicycle handlebars. In 12 of the 76 children, there was an imprint of the handlebar edge on the hypochondria. The most common injuries were isolated ruptures of spleen or liver, traumatic pancreatitis or transection of the pancreas, renal contusions, duodenal haematoma and bowel perforation. Mesenteric haematoma is relatively uncommon (Chao and Kong 1999). In addition, there may be urethral injuries and lacerations involving the abdominal wall and inguino-scrotal region. CT is most helpful in evaluating children who have sustained blunt abdominal trauma and is usually regarded as the method of choice for diagnosing mesenteric and

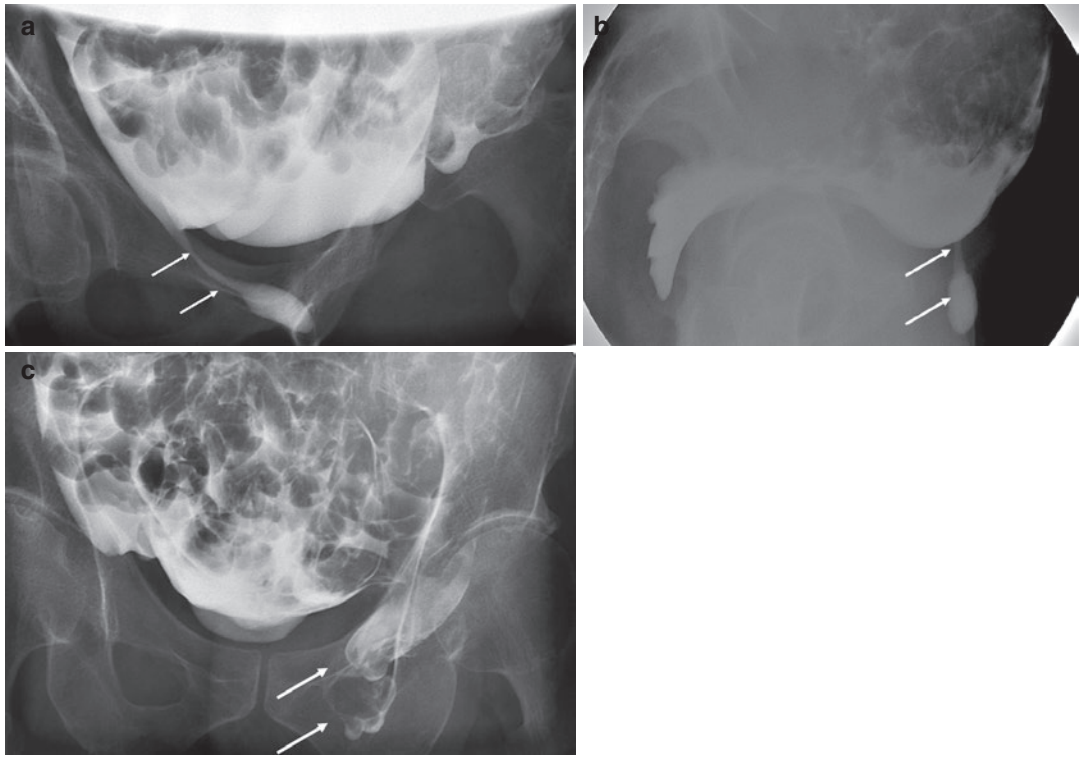

Fig. 20 (**a**–**c**) Inguinal hernia, herniography. Inguinal hernia in a 45-year-old male. Radiograph of the abdomen after herniography, (**a**) AP and (**b**) lateral view in prone position. Peritoneal contrast is visualized below the lining of the inguinal ligament at the right side without small intestine at the hernial sac: non-occupied inguinal hernia. Narrowing of the herniation sac at the level of the gate that is located at the inguinal canal (arrows). (**c**) Fifty-three-year-old male. Radiograph of the abdomen after herniography, AP view in prone position. Peritoneal contrast is visualized below the lining of the inguinal ligament at the left side with small intestine at the hernial sac: occupied inguinal hernia (Courtesy of Salgado R MD. Department of Radiology. University of Antwerp, Belgium)

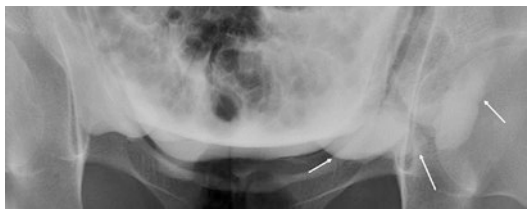

Fig. 21 Obliquus internus aponeurosis insufficiency, herniography. Broad-based bulging in prone position at the left external inguinal ring (Courtesy of Salgado R MD. Department of Radiology. University of Antwerp, Belgium)

abdominal wall lesions (Strouse et al. 1999; Mitchiner 1990).

Handlebar hernia is a rare, traumatic, abdominal wall hernia caused by high-velocity direct trauma. There are only 21 reported cases of handlebar hernias (Goliath et al. 2004). It involves disruption of the abdominal wall muscles, with bowel loop herniated through the defect in the abdominal wall, and may have major or even lethal complications. All layers of the abdominal wall may be disrupted by a fall when bicycling, although skin and intra-abdominal organs may be completely intact. Computed tomography demonstrates subcutaneous intestinal loops protruding through the rent (Chen et al. 2005; Holmes et al. 2002; Perez et al. 1998; Linuma et al. 2005).

3.4 Addendum: Endofibrosis of the Iliac Arteries

Arterial endofibrosis is an arterial disease discovered in the 1980s that is specific to endurance athletes. The location at the external iliac artery is most frequent and found in cyclists. The location at the popliteal artery is rarely documented in

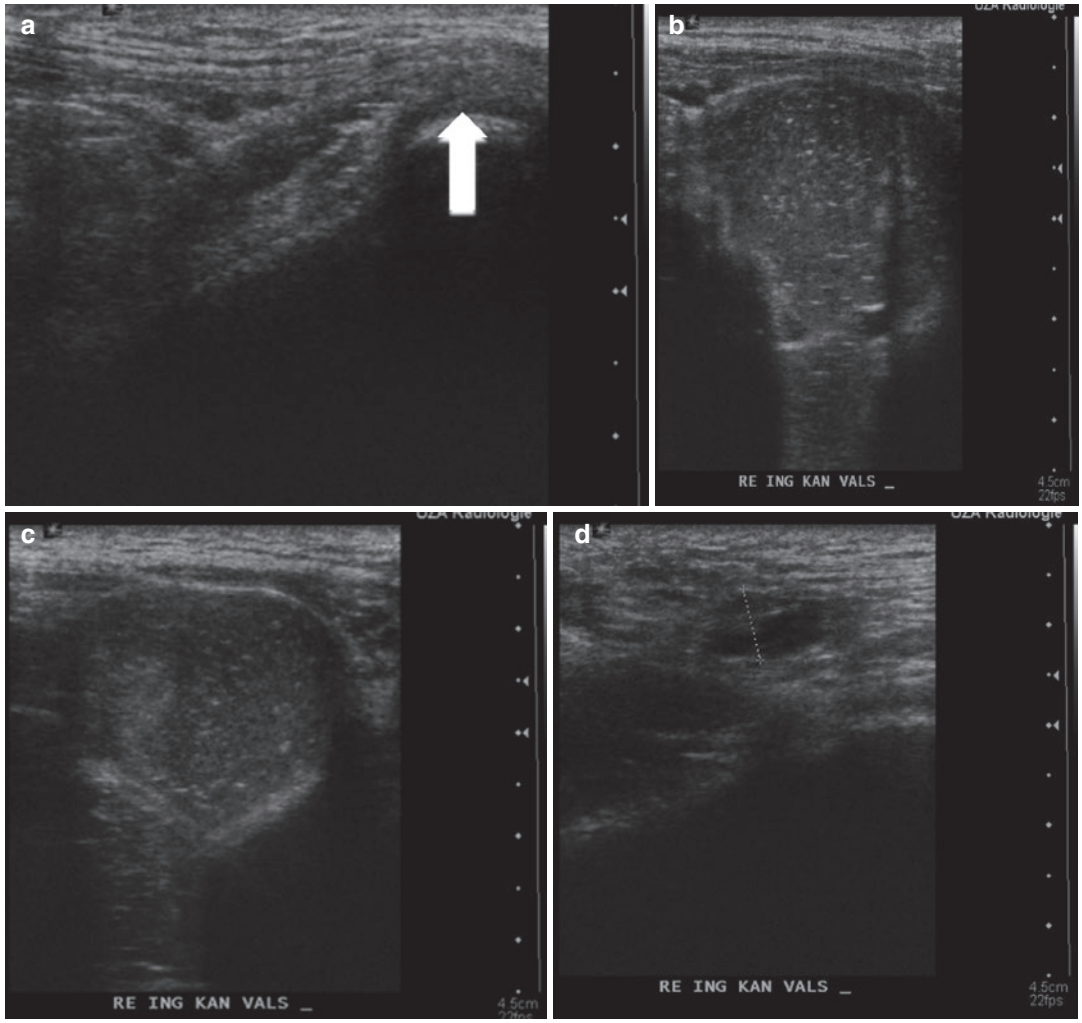

Fig. 22 (**a**–**d**) Obliquus internus aponeurosis insufficiency, ultrasound. Obliquus internus insufficiency in a 20-year-old male soccer player with long-standing pain at the right adductor and inguinal region. (**a**) Oblique axial imaging plane at and parallel to the right ligamentum inguinale at rest. Pubic bone (arrow). (**b**) Identical imaging plane as a (**c**) sagittal imaging plane (left = cranial) at the level of the inguinal ligament both during Valsalva test. Marked external bulging of the inguinal ligament and external oblique aponeurosis with descending bowel during Valsalva test. (**d**) Axial oblique imaging plane at the spermatic cord (between crosses) distal to the inguinal ligament. Neither direct nor indirect inguinal hernia

skiing (Toorop et al. 2004). It is characterized by thickening of the intima and/or adventitia, a result of smooth muscle hyperplasia with only mild collagen or elastin deposition, and/or hypertrophy of the media. There is no inflammation and only rarely calcification of the media. Mural thrombus is found in less than half of the cases (Kral et al. 2002). There is intermittent exercise-induced claudication with lower limb and thigh pain during near-maximal exercise (Feugier and Chevalier 2004; Chevalier et al. 1986). A post-exercise asymmetric measurement of ankle systolic pressure is lower at the symptomatic side, and positive ankle-to-arm systolic pressure index is highly suggestive. Systolic pressure is mostly symmetric with normal ankle-to-arm index at rest. Angiographic examination (conventional arteriography, CT-arteriography or MR-arteriography) demonstrates tapering of the arterial lumen with elongation of the artery (Fig. 23) (Hindryckx et al. 1996). An acute claudication with complete obstruction due to thrombus is rare. Greyscale

Fig. 23 (**a**–**d**) Endofibrosis of the external iliac artery. Endofibrosis in a 33-year-old professional cyclist with claudication-like pain at the right thigh and calf especially during maximum exertion since years. Post-exertion hydrostatic pressure is 105 mmHg at the right calf, 165 mmHg at the left calf and 150 mmHg at the right arm. No difference in hydrostatic pressure between both calves is present at rest. (**a**) Subtraction angiography of the iliac arteries, two right oblique views. Mild regular narrowing of the lumen, *tapering*, of the right arteria iliaca externa at the area between arrows. Twenty percent area reduction of the artery is obvious. The low-grade stenosis only produces symptoms at maximum exertion. (**a** Courtesy of Vanderstraeten G, Department of Physiotherapy, University of Ghent, Belgium). (**b** and **c** Reprinted with permission from Hindryckx, Von Lanz T and Wachsmuth W). (**d**) Kinking of the artery during extreme flexion of the hip. Reduced wall elasticity at the endofibrosis area produces kinking with high-grade stenosis during extreme flexion of the hip (reprinted with permission from Von Lanz T and Wachsmuth W, 1972, Praktische Anatomie, Springer Berlin)

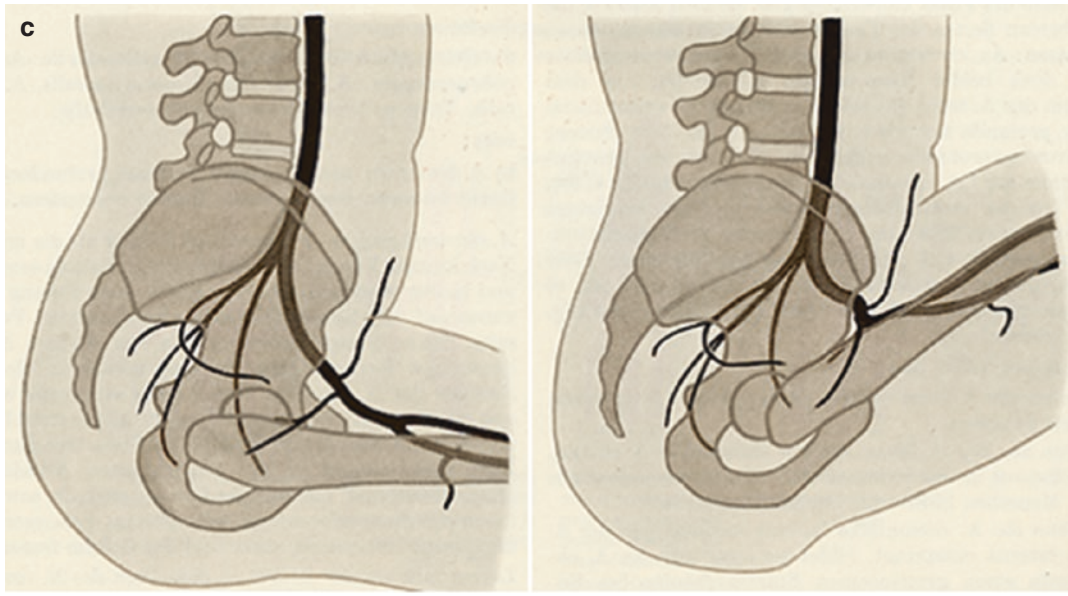

Fig. 23 (continued)

ultrasound findings include parietal thickening and increased echogenicity of the arterial wall with straightness of the abnormal segment. There is a mild narrowing of the involved arterial diameter (Abraham et al. 1993). Abraham et al. (1997) demonstrated normal velocity profiles at rest in 80% of the Doppler ultrasound examinations. Power Doppler appears to be an effective technique to visualize and scale kinks and intravascular lesions (Schep et al. 2001). Conservative treatment mainly consists of advice to change sports activity. Surgical mobilization of the iliac arteries for functional lesions and vascular reconstructions in case of intravascular lesions are possible. Percutaneous transluminal angioplasty and intravascular stent are contraindicated because of high risks for dissection and reactive intimal hyperplasia, respectively (Schep et al. 1999).

4 Conclusions

Abdominal and thoracic wall lesions often are self-evident. Imaging interest is merely confirmation of diagnosis or grading.

Several diagnoses must be considered in patients with groin pain, including musculoskeletal and more severe visceral problems (Renstrom 1992). These other possible diagnoses emphasize the importance of a detailed careful history, physical examination and obtaining the appropriate imaging tests.

Things to Remember

1. Prompt radiological investigation is needed in cases of suspicion of abdominal visceral trauma, pneumothorax and rectus sheath haematoma.
2. The PLAC-related pivot mechanism at the pelvis and pubic bone explains superior and inferior located lesions in groin disruption.
3. Obliquus internus insufficiency is probably a minor form of (chronic) groin disruption. It should be preferentially investigated with dynamic ultrasound.
4. The presence of external bruising in handlebar injury is a poor indicator of underlying damage.

5 Referral Criteria

5.1 Boxes

Box 1: Radiographs

Chest series and rib series—sufficient in majority of cases of rib injury, exclude pneumothorax and visceral laceration.

Box 2: Scintigraphy

Sensitive but non-specific in chronic osseous stress of the ribs and apophysiolysis.

Box 3: Ultrasound

Detection of occult rib fracture and chondral injury.

Acute muscle elongation—accurate, fast and dynamic. Particularly useful in grading.

Can be negative in grade 1 injury.

Probably useful in the detection of obliquus internus insufficiency.

Evaluation of abdominal wall injury and (rectus sheath) haematoma.

Endofibrosis of the iliac arteries: greyscale and power Doppler demonstrate tapering—Doppler only useful after exercise.

Box 4: MRI

Acute groin disruption.

Accurate and useful in athletes for muscle trauma with large muscle bulk.

Box 5: CT

Handlebar injury—evaluation of visceral injury.

Box 6: Angiography, MR angiography, CT angiography

Endofibrosis—specific diagnosis.

References

Abraham P, Leftheriotis G, Bourre Y et al (1993) Echography of external iliac artery endofibrosis in cyclists. Am J Sports Med 21:861–863

Abraham P, Chevalier JM, Leftheriotis G et al (1997) Lower extremity arterial disease in sports. Am J Sports Med 25:581–584

Anderson SE, Hertel R, Johnston JO et al (2005) Latissimus dorsi tendinosis and tear: imaging features of a pseudotumor of the upper limb in five patients. AJR 185:1145–1151

Barbaix E (2000) Stress fracture of the sternum in a golf player. Int J Sports Med 17:304–305

Chao HC, Kong MS (1999) Sonographic diagnosis of mesenteric hematoma. J Clin Ultrasound 27:284–286

Chen HY, Sheu MH, Tseng LM (2005) Bicycle-handlebar hernia: a rare traumatic abdominal wall hernia. J Chin Med Assoc 68:283–285

Chevalier JM, Enon B, Walder J et al (1986) Endofibrosis of the external iliac artery in bicycle racers: an unrecognized pathological state. Ann Vasc Surg 1:297–303

Clarnette TD, Beasley SW (1997) Handlebar injuries in children: patterns and prevention. Aust N Z J Surg 67:338–339

Connell DA, Jhamb A, James T (2003) Side strain: a tear of internal oblique musculature. Am J Roentgenol 181:1511–1517

Coris EE, Higgins HW 2nd. (2005) First rib stress fractures in throwing athletes. Am J Sports Med 33:1400–1404

Curran J, Kelly D (1966) Stress fracture of the first rib. Am J Orthop 8:16–18

Dennis RW, Marshall A, Deshmukh H et al (2009) Abdominal wall injuries occurring after blunt trauma: incidence and grading system. Am J Surg 197:413–417

Dodds SD, Wolfe SW (2002) Injuries to the pectoralis major. Sports Med 32:945–952

Ekberg O (1983) Complication after herniography in adults. Am J Roentgenol 140:491–495

ElMaraghy AW, Devereaux MW (2012) A systematic review and comprehensive classification of pectoralis major tears. J Shoulder Elb Surg 21:412–422

Erez I, Lazar L, Gutermacher M et al (2001) Abdominal injuries caused by bicycle handlebars. Eur J Surg 167:331–333

Feugier P, Chevalier JM (2004) Endofibrosis of the iliac arteries: an underestimated problem. Acta Chir Belg 104:635–640

Fowler AW (1957) Flexion-compression injury of the sternum. J Bone Joint Surg (Br) 39:487–497
Gaffney KM (1997) Avulsion injury of the serratus anterior: a case history. Clin J Sport Med 7:134–136
Garret W, Safran M, Seaber A et al (1993) Biomechanical comparison of stimulated and nonstimulated skeletal muscle pulled to failure. Am J Sports Med 21:89–96
Gielen JLMA, Robinson P, Van Dyck P, Van der Stappen A, Vanhoenacker FM (2021) Muscle injuries. Med Radiol https://doi.org/10.1007/174_2020_247
Goliath J, Mittal V, McDonough J (2004) Traumatic handlebar hernia: a rare abdominal wall hernia. J Pediatr Surg 39:e20–e22
Gurtler R, Pavlov H, Torg J (1985) Stress fractures of the ipsilateral first rib in a pitcher. Am J Sports Med 13:277–279
Haley CA, Zacchilli MA (2014) Pectoralis major injuries: evaluation and treatment. Clin Sports Med 33: 739–756
Hellstrom M, Jacobsson B, Sward L et al (1990) Radiologic abnormalities of the thoracolumbar spine in athletes. Acta Radiol 31:127–132
Hindryckx C, Rousseaux M, Vanderstraeten G et al (1996) Endofibrosis of the external iliac artery: a cyclist's syndrome? A case report. Eur J Phys Med Rehab 6:126–127
Holmes J, Hall R, Schaller R (2002) Thoracic handlebar hernia: presentation and management. J Trauma 52:165–166
Huang CC, Ko SF, Ng SH et al (2005) Scapulothoracic bursitis of the chest wall: sonographic features with pathologic correlation. J Ultrasound Med 24(10):1437–1440
Iwamoto J, Takeda T (2003) Stress fractures in athletes: review of 196 cases. J Orthop Sci 8(3):273–278
Johnson R (2006) Abdominal wall injuries: rectus abdominis strains, oblique strains, rectus sheath hematoma. Curr Sports Med Rep 5:99–103
Karlson D (1998) Rib stress fractures in elite rowers. A case series and proposed mechanism. Am J Sports Med 26:516–519
Keating T (1987) Stress fracture of the sternum in the wrestler. Am J Sports Med 15:92–93
Kral CA, Han DC, Edwards WD et al (2002) Obstructive external iliac arteriopathy in avid bicyclists: new and variable histopathologic features in women. J Vasc Surg 36:565–570
Kuhn JE (2003) Scapulothoracic crepitus and bursitis in athletes. In: Delee JC, Drez D, Miller MD (eds) Orthopedic sports medicine. Principles and practice. 2nd ed. Saunders, Philadelphia, pp 1006–1014
Lacroix VJ, Kinnear DG, Mulder DS et al (1998) Lower abdominal pain syndrome in national hockey league players: a report of 11 cases. Clin J Sport Med 8:5–9
Lee YK, Skalski MR, White EA et al (2017) US and MR imaging of pectoralis major injuries. Radiographics 37:176–189
Linuma Y, Yamazaki Y, Hirose Y et al (2005) A case of a traumatic abdominal wall hernia that could not be identified until exploratory laparoscopy was performed. Pediatr Surg Int 21:54–57
Matalon SA, Askari R, Gates JD et al (2017) Imaging spectrum of abdominal wall injuries after nonpenetrating trauma. Radiographics 37:1218–1235
Matsumoto T, Fujita K, Fujioka H et al (2003) Stress fracture of the first rib in a soccer player: a rare etiology of shoulder pain. J Shoulder Elb Surg 12: 197–199
Miles JW, Barrett GR (1991) Rib fractures in athletes. Sports Med 12:66–69
Mitchiner JC (1990) Handlebar hernia: diagnosis by abdominal computed tomography. Ann Emerg Med 19:812–813
Morelli V, Weaver V (2005) Groin injuries and groin pain in athletes: part 1. Prim Care 32:163–183
Murphey M, Stockden M, Breidahl B (2016) Acute tearing of the oblique abdominal wall insertion onto the iliac crest in an Australian football player: a case report. Int J Sports Phys Ther 11:1125–1134
Neitzschman HR, Wilson S (1999) Radiology case of the month. Tearing pain and swelling in the left chest wall. Grade III muscle strain of the pectoralis major and minor. J La State Med Soc 51:19–20
Orchard JW, Read JW, Neophyton J et al (1998) Groin pain associated with ultrasound finding of inguinal canal posterior wall deficiency in Australian Rules footballers. Br J Sports Med 32:134–139
Perez V, McDonald A, Ghani A et al (1998) Handlebar hernia: a rare traumatic abdominal wall hernia. J Trauma 44:568–570
Prasad R, Abdullah O, Robinson P (2021) Athletic groin pain. Med Radiol https://doi.org/10.1007/174_2020_254
Renstrom AF (1992) Tendon and muscle injuries in the groin area. Clin Sports Med 11:815
Sakellaridis T, Stamatelopoulos A, Andrianopoulos E et al (2004) Isolated first rib fracture in athletes. Br J Sports Med 38:e5
Schep G, Bender MH, Kaandorp D et al (1999) Flow limitations in the iliac arteries in endurance athletes. Current knowledge and directions for the future. Int J Sports Med 20:421–428
Schep G, Bender MH, Schmikli SL et al (2001) Color Doppler used to detect kinking and intravascular lesions in the iliac arteries in endurance athletes with claudication. Eur J Ultrasound 14:129–140
Schickendantz MS, Scott GK, Meister K et al (2009) Latissimus doris and teres major tears in professional baseball pitchers: a case series. Am J Sports Med 37:2016–2020
Schilders E, Bharam S, Golan E et al (2017) The pyramidalis-anterior pubic ligament-adductor longus complex (PLAC) and its role with adductor injuries: a new anatomical concept Knee. Surg Sports Traumatol Arhtrosc 25:3969–3977
Shin AY, Morin WD, Gorman JD et al (1996) The superiority of magnetic resonance imaging in differentiating the cause of hip pain in endurance athletes. Am J Sports Med 24:168–176
Smedberg S, Broome A, Elmer O et al (1985) Herniography in the diagnosis of obscure groin pain. Acta Chir Scand 151:663–667

Smedberg S, Broome A, Elmer O et al (1990) Herniography in primary inguinal and femoral hernia: an analysis of 283 operated cases. Contemp Surg 36: 48–52

Strouse PJ, Close BJ, Marshall KW et al (1999) CT of bowel and mesenteric trauma in children. Radiographics 19:1237–1250

Tietjen R (1980) Closed injuries of the pectoralis major muscle. J Trauma 20:262–264

Toorop R, Poniewierski J, Gielen J et al (2004) Popliteal artery entrapment syndrome. JBR-BTR 87: 154–155

Tullos HS, Erwin WD, Woods GW et al (1972) Unusual lesions of the pitching arm. Clin Orthop 88: 169–182

Weir A, Bruckner P, Delahunt E et al (2015) Doha agreement meeting on terminology and definitions in groin pain in athletes. Br J Sports Med 49:768–774

Wojtys EM, Ashton-Miller JA, Huston LJ et al (2000) The association between athletic training time and the sagittal curvature of the immature spine. Am J Sports Med 28:490–498

Special Considerations in the Immature Skeleton

Anish Patel, Suzanne E. Anderson, and A. Mark Davies

Contents

Abstract

It is well accepted that physical activity is required for the healthy development of the growing child. As the number of children involved in regular sporting activity increases so does the potential risk for injury. This risk of injury is also dependent on the age of the child. The growing skeleton is particularly vulnerable at the time of puberty as rapid growth and the increasingly competitive nature of childhood sports, year-round activity and inadequate rest result in an increasing prevalence of overuse injuries in this population.

This chapter focuses on the multimodality imaging findings of some of the most common overuse injuries in children seen at a variety of anatomical sites. The chapter also covers the variation of skeletal development that may mimic the effects of trauma and also the common acute bony injures specific to the growing skeleton.

A. Patel · A. M. Davies (✉)
The Royal Orthopedic Hospital NHS Trust, MRI Centre, Birmingham, UK
e-mail: anish.patel4@nhs.net; mark.davies8@nhs.net

S. E. Anderson
Kantonsspital Baden, Baden, Switzerland

Sydney School of Medicine, University of Notre Dame Australia, Fremantle, WA, Australia
e-mail: suzanne.anderson1@bluewin.ch

1 Introduction

It is well recognised that physical activity, sporting or otherwise, is required for the healthy development of the growing child into adulthood. While important, the pervasive influence of sport can affect all aspects of our culture including fashion, lifestyles, and institutional and even

Med Radiol Diagn Imaging (2021)
https://doi.org/10.1007/174_2020_266, © Springer Nature Switzerland AG
Published Online: 16 March 2021

national identity (Hyndman 1996). The result can be that the growing skeleton, more susceptible to trauma than the healthy mature skeleton, is exposed to forces well above that which evolution intended or allowed for. Injury is defined as the response in bone and soft tissues to applied kinetic energy. The mode of injury can be classified into three groups. The first occurs as a result of a direct blow. This form of injury in the context of sport can be minimised by the use of protective clothing/equipment. The second occurs as a result of an indirect blow or force such as a fall onto the wrist leading to an injury to the elbow or shoulder. The third group is the chronic repetitive injuries otherwise known as overuse injuries. The mode of injury may be identical be it applied to a child or an adult. How the kinetic energy is dissipated in the tissues and the trauma manifested can be very different depending on age. A fall onto an outstretched hand (FOOSH) in an adolescent typically causes a Salter-Harris (Fig. 1) type 2 fracture/separation of the distal radial growth plate. In the young adult an identical injury may cause a fracture of the scaphoid. However, in the older individual, particularly the postmenopausal woman, a Colles' fracture would be the anticipated result. This is because the physis (growth plate), at the time of the adolescent growth spurt, is up to four times weaker than the adjacent bones, ligaments and tendons (Harsha 1957). It is, therefore, important to stress that the child should not be viewed as a mini-adult. Injuries sustained in the pursuit of sporting excellence depend on the type of sport. There can, therefore, be major geographical differences in the incidence of specific injuries. For example, cases of Little Leaguer's shoulder and elbow are well recognised in adolescent baseball pitchers in North America and are uncommon in the rest of the world. However, adolescent cricketers, with a different bowling action, are susceptible to spondylolysis defects. Cricket is played in the United

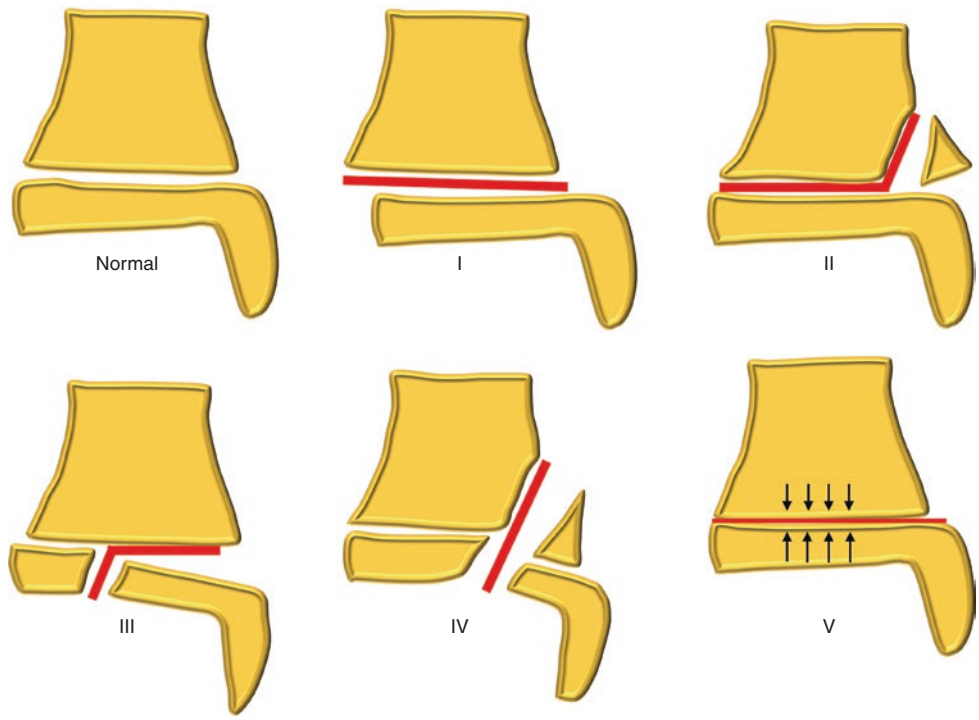

Fig. 1 Diagram showing Salter-Harris classification for physeal injuries. *I*. Fracture plane is through the physis. *II*. Fracture plan is through most of the physis and extends to involve the metaphysis. *III*. Fracture plane is through most of the physis and extends through the epiphysis. *IV*. Fracture plane is through the metaphysis, physis and epiphysis. *V*. Compression fracture of the physis

Kingdom and its former colonies but rarely elsewhere. It has also been shown that individuals who specialise in a single sport at a young age are more likely to sustain an injury in comparison to those who do not specialise (Field et al. 2019). In addition, the risk of injury depends on the sport and the sex of the participant; in males the risk of injury doubles if they specialise in baseball or gymnastics. In females specialisation in running, swimming, soccer or gymnastics is predictive of a higher risk of injury (Field et al. 2019).

A number of overuse injuries, if unrecognised, may simulate a tumour. These conditions are the subject matter of Lunkiewicz et al. (2021). This chapter concentrates predominantly on overuse injuries as seen at different anatomical sites in the paediatric skeleton. We also give a brief mention of important acute bony injuries specific to the paediatric skeleton and variations of skeletal development that may mimic the effects of trauma.

2 Normal Variants Simulating Traumatic Lesions

Normal skeletal development tends to follow a well-ordered pattern. Within this pattern there are numerous minor variations that fall within the spectrum of normal. The extent of these variations is no better illustrated than in Keats' authoritative atlas (Keats and Anderson 2012). All-too-often growth plates and accessory ossification centres may be misinterpreted as fractures. The prudent radiologist will have not only an appropriate atlas to hand when reporting radiographs but also knowledge of the approximate age and normal sequence of appearance of the epiphyses. This is particularly important in the elbow with no less than six separate ossification centres appearing between a few months and 10–13 years of age (Fig. 2). A problematic example is the acute avulsion of the medial epicondyle

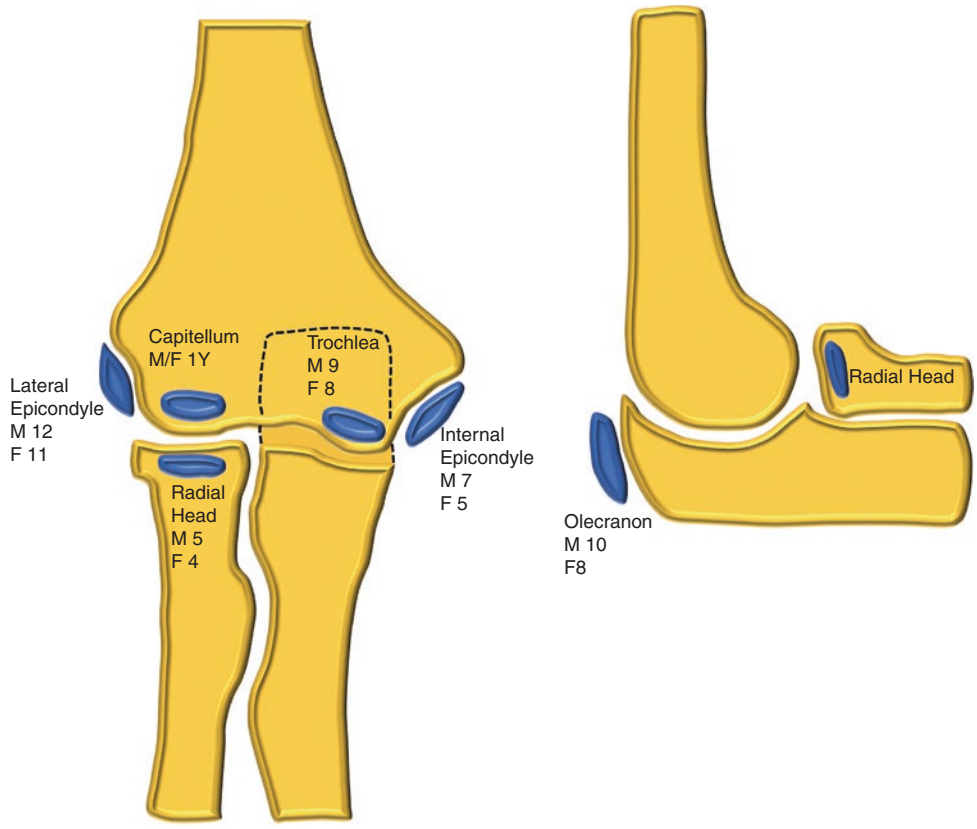

Fig. 2 Diagram showing the elbow ossification centres and when they should be visible in males (*M*) and females (*F*)

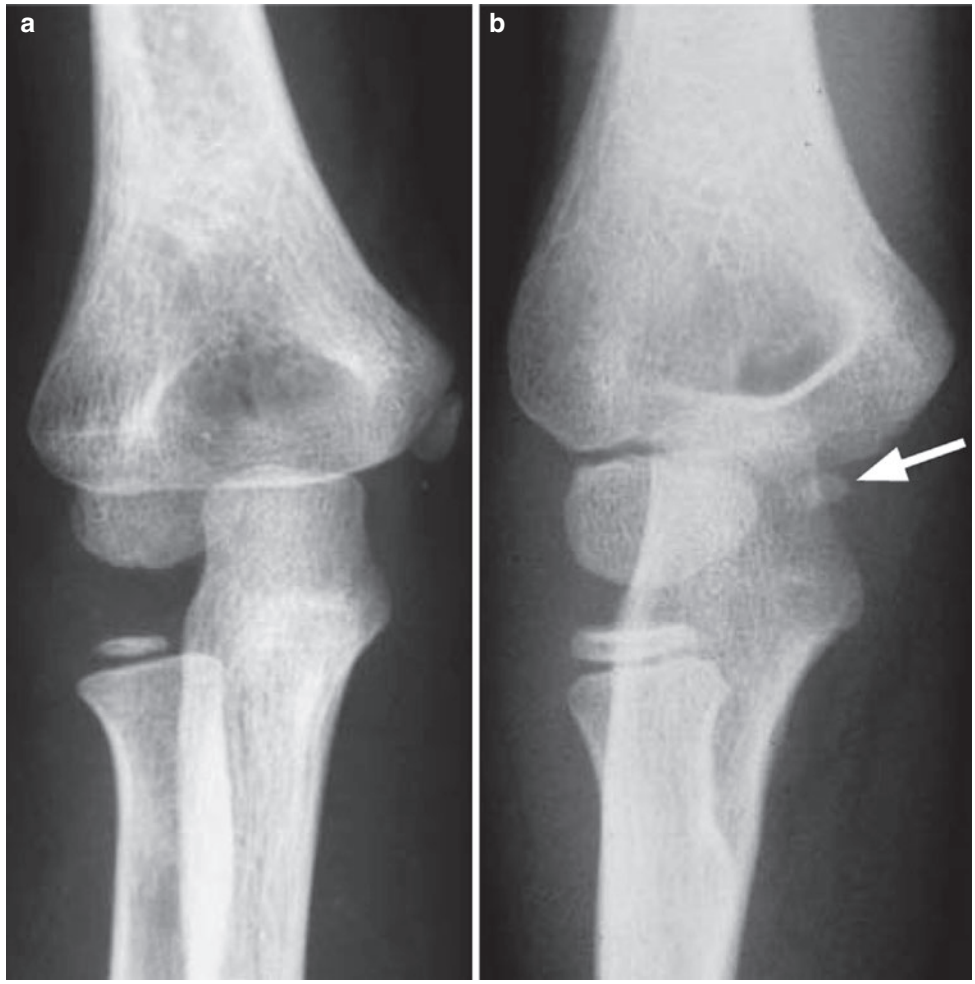

Fig. 3 (**a**, **b**) AP radiographs of the elbow in two 5-year-old children. (**a**) Normal appearances with visible medial epicondyle and absent trochlea. (**b**) Acute avulsion and displacement of the medial epicondyle simulating the trochlea ossification centre

that can become trapped between the trochlea and the ulna. The trochlea ossification centre tends to appear after the medial epicondyle. Therefore, if the "trochlea" is visible in the absence of a medial epicondyle this type of injury has to be seriously considered (Fig. 3). In the past some have advocated obtaining comparison views of the contralateral joint to help confirm/exclude injury. While this has some merit the practice should not be encouraged as it necessitates irradiating an entirely normal structure.

The distinction between a normal variant and a developmental abnormality, be it trauma related or not, may in some instances be blurred. The avulsive cortical irregularity of the posteromedial distal femur, otherwise known as a periosteal desmoid or Bufkin lesion, is frequently attributed to mechanical stresses applied to the insertion of the adductor magnus or the origin of the medial head of the gastrocnemius muscle (Bufkin 1971; Barnes and Gwinn 1974; Resnick and Greenway 1982). Bone scintigraphy tends to show normal skeletal activity that is somewhat atypical for a trauma-related abnormality of bone (Dunham et al. 1980; Burrows et al. 1982; Craigen et al. 1994); however the typical

site of a cortical desmoid is often masked by the physeal activity. MRI and CT are the most sensitive imaging modalities in detecting cortical desmoids due to their excellent cross-sectional detail (Fig. 4). On MRI the lesion is of low signal intensity on the T1 sequence and on the T2 sequences it is of intermediate to high signal with surrounding low signal due to the sclerosis (Yamazaki et al. 1995). These lesions can often be bilateral (Kontogeorgakos et al. 2009). Parosteal osteosarcoma, infection and stress fractures are in the differential diagnosis but

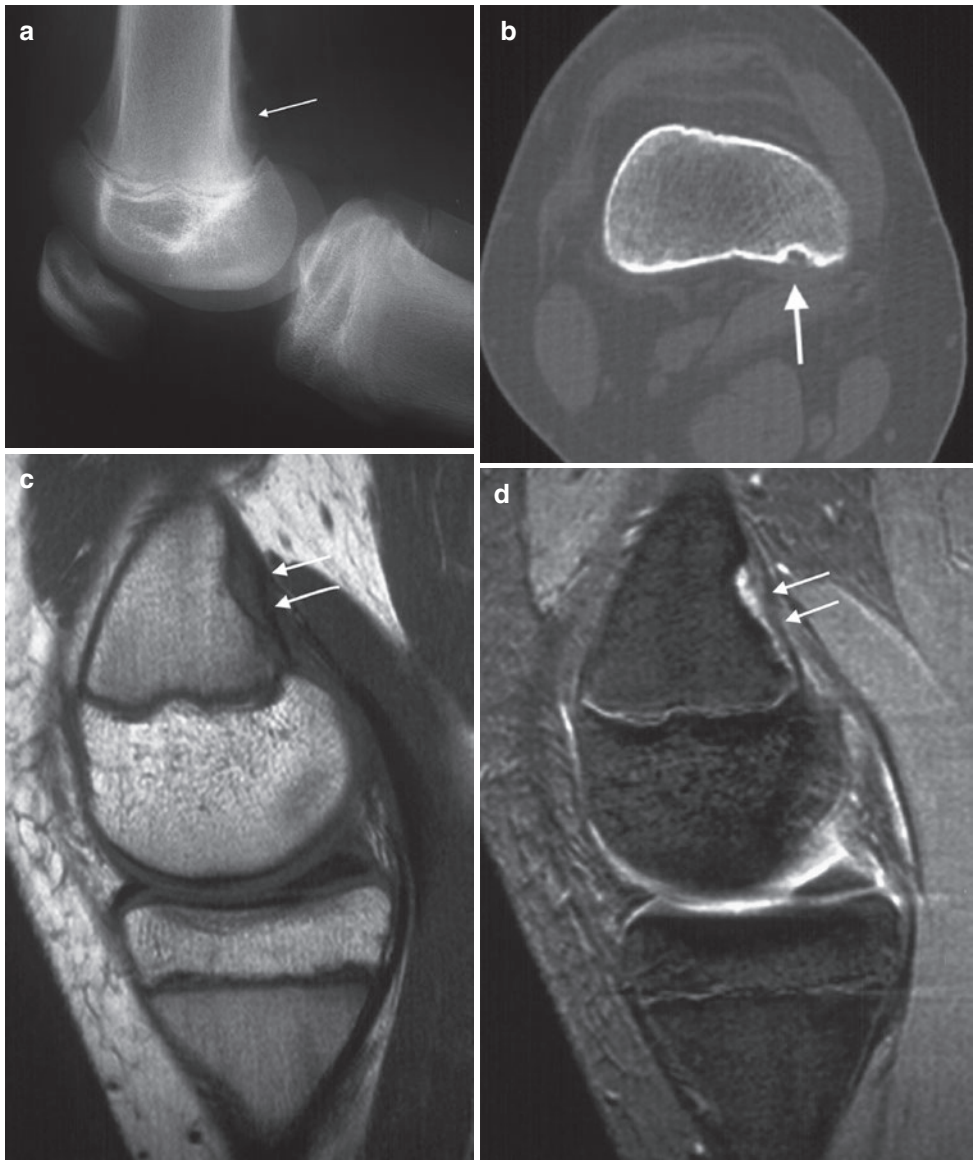

Fig. 4 (**a–d**) Periosteal desmoid. (**a**) Lateral radiograph of an adolescent male showing irregularity of the cortex of the posteromedial aspect of the distal femoral metaphysis (white arrow). (**b**) Axial CT showing posteromedial cortical irregularity (white arrows). (**c**) Sagittal T1-weighted and (**d**) and T2* images show this lesion to be of high signal on T2 weighting and low signal on T1 weighting but no tumour mass is seen (white arrows)

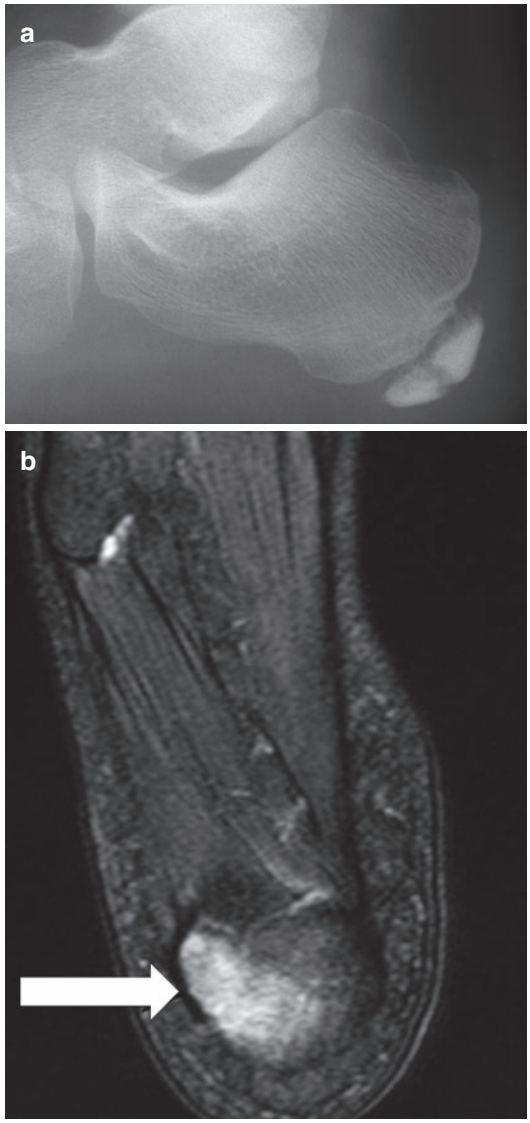

Fig. 5 Sever's disease. (**a**) Lateral radiograph in an 8-year-old male footballer showing sclerosis and fragmentation of the calcaneal apophysis; however this is an unreliable sign. (**b**) Axial STIR MRI showing oedema of the calcaneal apophysis (large white arrow)

these can be effectively excluded with cross-sectional imaging due to a lack of tumour mass. Whatever the precise aetiology the important thing to note is that the process is self-limiting and of no immediate clinical consequence. A heterogeneous group of conditions known as the osteochondroses also fall into this category of self limiting. These include osteochondritis of the calcaneal apophysis (Sever's disease) (Lokiec and Weintroub 1998) (Fig. 5), the tarsal navicular (Kohler's disease) (Borges et al. 1995; Posadzy et al. 2018) (Fig. 6) and the ischiopubic synchondrosis (van Neck disease) (Brower 1983) (Fig. 7). These conditions need to be distinguished from the other articular osteochondroses (e.g., Freiberg's infraction and Kienbock's disease) and the nonarticular osteochondroses (e.g., Osgood-Schlatter disease and Sinding-Larsen-Johansson disease) (Fig. 8) in which trauma is considered a significant contributory factor. Occasionally osteomyelitis, particularly subacute, may present in the child with little or no abnormality detected on routine blood tests such that it may be mistaken for an overuse injury.

3 Upper Limb

3.1 Shoulder

The classic overuse injury seen in the paediatric age group is the Little Leaguer's shoulder first described over 50 years ago (Dotter 1953). It has been variously referred to in the literature as proximal humeral epiphysiolysis (Barnett 1985), osteochondrosis of the proximal humeral epiphysis (Adams 1966; Tullos and King 1972), stress fracture of the proximal humeral epiphyseal plate (Ireland and Andrews 1988) and rotational stress fracture of the proximal humeral epiphyseal plate (Cahill et al. 1974; Tullos and Fain 1974). It is thought to be an overuse injury due to repetitive rotational stress applied to the proximal humeral growth plate (physis) (Carson Jr. and Gasser 1998) and is best considered as a form of Salter-Harris type 1 stress fracture through the growth plate (Fleming et al. 2004). Baseball pitchers are the most commonly affected athletes with an average age of 14 years with a range from 13 to 16 years old (Carson Jr. and Gasser 1998). Cases have also been reported in an adolescent badmin-

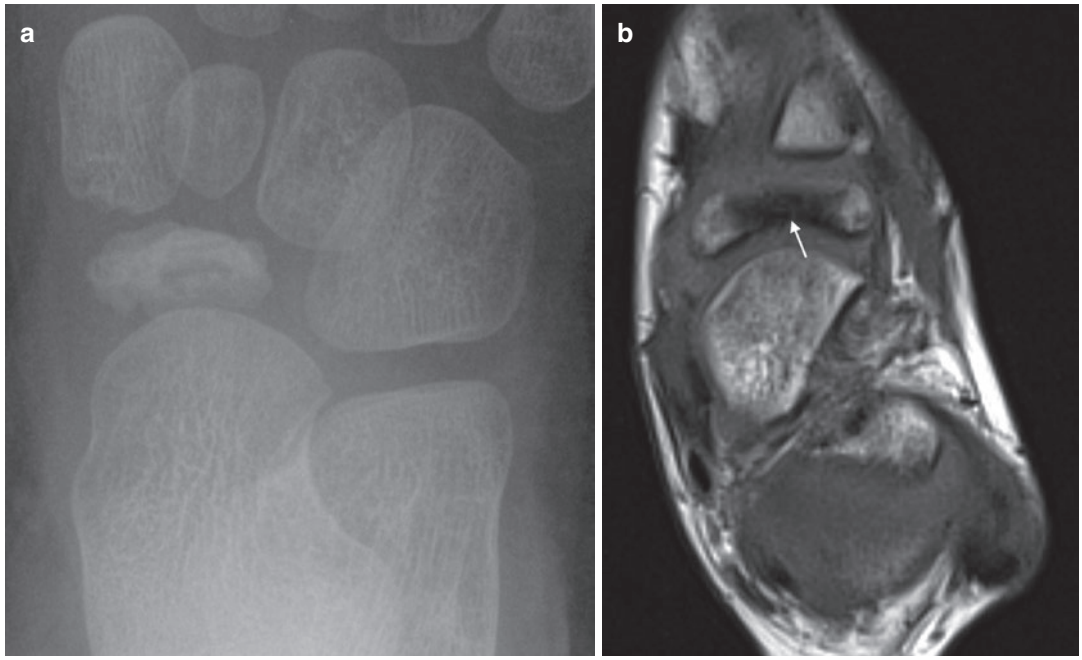

Fig. 6 (**a**, **b**) Kohler's disease. (**a**) AP radiograph of the foot in a 7-year-old male showing an irregular, small and sclerotic navicular. (**b**) Axial T1-weighted MRI shows sclerosis and loss of the normal fatty bone marrow (white arrow) (courtesy F. Vanhoenacker, used with permission from Posadzy et al. 2018)

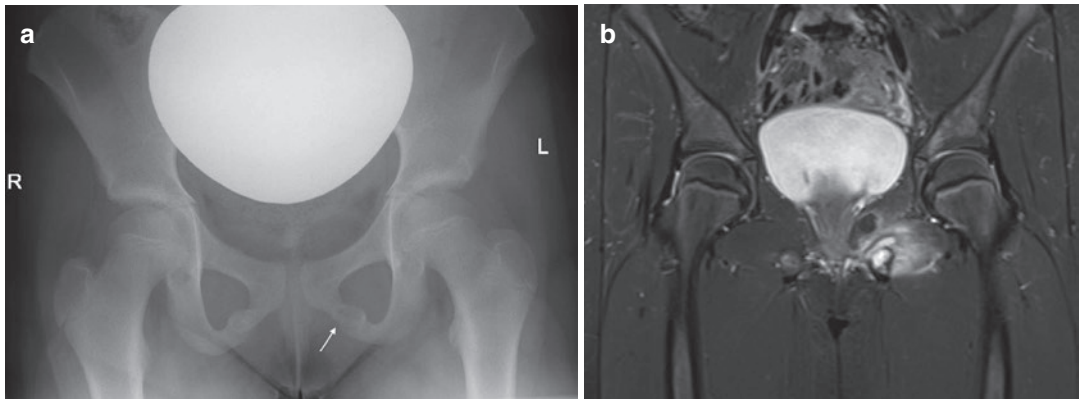

Fig. 7 (**a**, **b**) Van Neck disease. (**a**) AP radiograph of the pelvis in a 6-year-old female with left groin pain showing prominence of the left ischiopubic synchondrosis (white arrow) (there are mild changes on the contralateral side). (**b**) Coronal STIR MRI shows marked osseous and periosteal oedema around the ischiopubic synchondrosis

ton player (Boyd and Batt 1997) and a gymnast (Daldorg and Bryan 1994). Typically, patients present with shoulder pain aggravated by throwing and tenderness over the lateral aspect of the shoulder. Radiographic changes include widening of the proximal humeral growth plate with irregularity and sclerosis of the metaphyseal margin and fragmentation/cystic change laterally (Adams 1966; Barnett 1985; Fleming et al. 2004). The MR imaging findings in Little

Leaguer's shoulder demonstrate asymmetric physeal widening and periphyseal oedema (Fig. 9). Partial-thickness rotator cuff tears and labral tears have also been described (Pennock et al. 2018). Asymptomatic little league baseball players showed similar MRI changes in the dominant throwing arm and these changes were associated with single-sport year-round activity and early single-sport specialisation (Pennock et al. 2018).

Acute avulsion injuries that may occur around the shoulder girdle include the following: avulsion of the coracoid apophysis due to pull of the coracoclavicular ligament usually in association with acromioclavicular separation (Benton and Nelson 1971); avulsion of the acromial apophysis due to pull of the deltoid muscle (Rask and Steinberg 1978); and avulsion of the infraglenoid tubercle at the site of origin of the long head of triceps muscle (Heyes-Moore and Stoker 1982). Avulsions of the greater and lesser tuberosities are uncommon in children. Isolated avulsion of the lesser tuberosity has been reported in children participating in American football, hockey, volleyball, wrestling, skateboarding and baseball (Klasson et al. 1993; Paschal et al. 1995; Ogawa and Takahashi 1997; Sugalski et al. 2004). Rotator cuff tears, in the absence of avulsions, are rare in children (Battaglia et al. 2003) and may involve the subscapularis tendon more commonly than seen in the over-40-years age group (Tarkin et al. 2005).

Fig. 8 Traumatic osteochondritis (Sinding-Larsen-Johansson disease). Lateral radiograph of the knee in an adolescent male showing fragmentation of the lower pole of the patella

In adults, lateral impact of the shoulder commonly leads to an acromioclavicular separation. In the skeletally immature child this can lead to a type 1 Salter-Harris fracture of the lateral clavicle which is called a clavicular periosteal sleeve fracture. On radiographs it may appear as if there is an AC joint dislocation but the unfused lateral epiphysis still maintains its normal position relative to the AC joint with the metaphysis of the clavicle displaced superiorly through a tear in the periosteal sleeve. This can give the pseudo subluxation sign of plain radiographs. MRI will

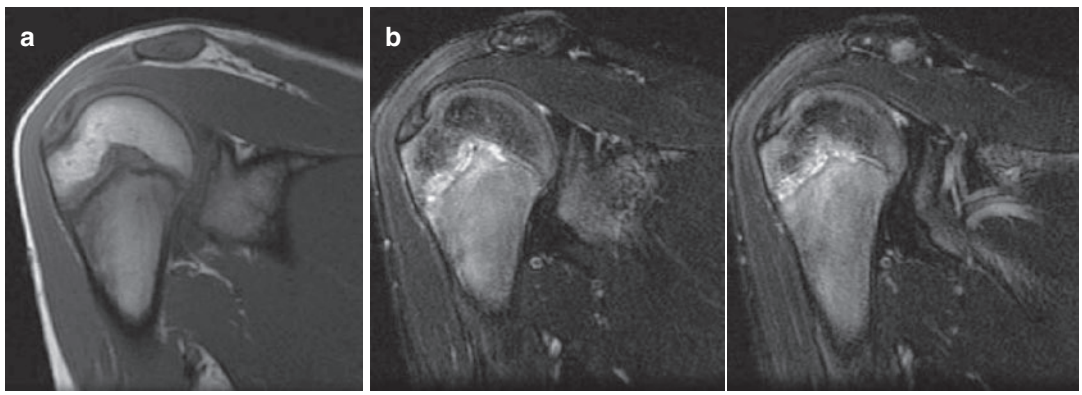

Fig. 9 (**a**, **b**) Little Leaguer's shoulder. (**a**) Coronal oblique T1-weighted and (**b**) fat-suppressed T2-weighted MR images showing widening of the growth plate with surrounding oedema indicating a stress injury (reproduced from Song et al. 2006 with permission)

show non-displacement of the lateral clavicle epiphysis and displacement of the medial fragment through a tear in the periosteal sleeve and allows evaluation of the acromioclavicular and coracoclavicular ligaments (Delgado et al. 2016).

Fatigue-type stress fractures of the humeral diaphysis usually occur secondary to athletic throwing injuries due to repeated muscular torque (Allen 1984) and have been termed "ball-thrower's fractures" (Callaghan et al. 2004). They have even been described with the throwing of hand grenades but mercifully this is not a childhood activity (Chao et al. 1971; Kaplan et al. 1998). One of the authors (AMD) has seen a similar injury in an elite adolescent tennis player due to excessive serving practice (Fig. 10). Keats coined the term tug lesion to describe new bone formation at muscle insertions suggesting that they are due to muscular forces. These may be seen in the humerus at the insertion of the deltoid and latissimus dorsi muscles but are of no clinical significance (Keats 1990).

Fig. 10 Stress fracture in a 12-year-old elite male tennis player with 3-month aching in the dominant upper arm. He sustained a fracture of the humerus while practising serving. The presence of minor periosteal reaction preceding the injury indicates the presence of a stress fracture

3.2 Elbow

The elbow is the focus of loading in many sports and is particularly susceptible to both acute and chronic injuries prior to skeletal fusion. Arguably, it is also the site of the greatest spectrum of skeletal development which can make distinction of normal variants from problematic pathology (Fig. 3) (Silberstein et al. 1979, 1981, 1982a, b; McCarthy and Ogden 1982). Imaging should always start with the conventional radiograph (Sofka and Potter 2002). However, because of the incidence of transphyseal fractures and avulsion injuries both ultrasound and MR imaging can be useful in assessing elbow injuries in the child (Beltran and Rosenberg 1997; Fritz 1999; Markowitz et al. 1992; May et al. 2000). Several sports cause a high incidence of elbow injuries including baseball, javelin, handball and gymnastics (Gregory and Nyland 2013). The baseball pitch is one of the most common causes of overuse elbow injuries. The baseball throwing action produces extreme valgus and extension forces in the elbow especially in the late cocking and the acceleration phases of the throwing action. This results in distraction injuries to the medial compartment and compression injuries to the lateral compartment of the elbow. This characteristic spectrum of injuries that occur are known as "Little Leaguer's elbow" (Adams 1965; Pappas 1982) (Fig. 11). Similar overuse injuries may be seen in those practising racquet sports (Gore et al. 1980; Priest et al. 1974) as well as gymnasts (Goldberg 1980). The type of injury also depends on the skeletal maturity of the individual (Oshlag and Ray 2016). In the younger skeletally immature child, the physis is the weakest link in the medial compartment. In the older adolescent throwing athlete, the weakest part is the ulnar collateral ligament complex and the common flexor origin. Therefore, medial compartment injuries in the skeletally immature ath-

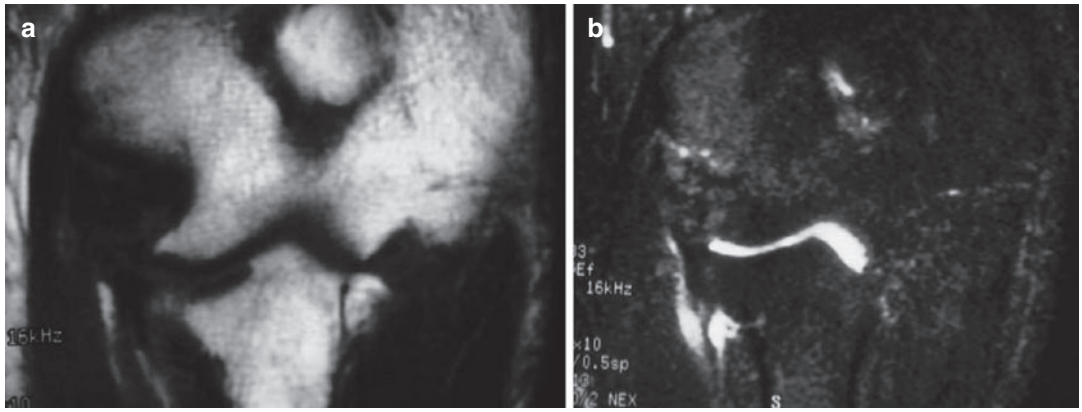

Fig. 11 (**a**, **b**) Little Leaguer's elbow in a 16-year-old baseball player. (**a**) Coronal T1-weighted and (**b**) coronal T2-weighted fat-suppressed MR images showing a partial tear in a chronically thickened medial collateral ligament with early degenerative joint disease

lete usually involves the medial epicondylar physis. Chronic repetitive medial injury results in traction apophysitis of the medial epicondyle. Radiographic changes comprise fragmentation of the medial epicondyle which often has a ragged appearance and can demonstrate sclerosis, coarsened trabeculation and widening of the physis (Hang et al. 2004). MRI demonstrates widening of the physis with associated periphyseal oedema. On T1-weighted sequences there may be loss of the normal fatty marrow of the medial epicondylar apophysis. With repeated sporting activity this can progress to complete dislocation of the apophysis. Chronic overuse delays epiphyseal closure and the medial epicondyle may remain unfused throughout life (Pappas 1982). In the older adolescent athlete, the injury pattern shifts to involve the ulnar collateral ligament (UCL) and the common flexor origin; however, it is not uncommon to see a mixed pattern of injury. UCL injuries range from mild sprains to partial tears and eventually to complete tears. On MRI mild sprains show periligamentous oedema with a grossly intact UCL. Higher grade partial tears show oedema in the ligament with partial disruption of the fibres. There may be bony oedema in the sublime tubercle. Distal partial-thickness tears when present can be identified if there is fluid in the joint or at MRI arthrography by demonstrating fluid between the distal UCL attachment and the sublime tubercle—the "T" sign. Full-thickness tears show ligament discontinuity. They usually involve the mid portion of the ligament but it is not uncommon to see proximal or distal UCL avulsions (Conway et al. 1992; Carrino et al. 2001). MRI can show fluid or contrast extravasation through the torn ligament.

Lateral compression causes forced impaction of the radial head into the capitellum. In full elbow extension, the forces act on the anterior aspect of the radial head causing anterior depression (Ellman 1975). If the excess shear forces continue a chronic Salter-Harris type 4 stress fracture may extend to involve the proximal radial metaphysis (Fig. 12) (Chan et al. 1991). In the immature athlete (6–12 years) osteochondrosis of the capitellum (Panner's disease) may occur. Panner's disease is a self-limiting condition presumed to be due to chronic disruption of the blood supply to the capitellum ossification centre. X-ray shows fragmentation of the capitellar ossification centre with thickening of the trabeculae. A subchondral radiolucent crescent may be seen as well (Anisau et al. 2018). On MRI, the capitellar ossification centre is low on T1 weighting and there is increased signal on fluid-sensitive sequences (Fig. 13), the degree of which is dependent on the stage of the disease (Dwek 2013).

In the slightly older athlete, medial compressive forces can result in subchondral fractures which may progress to capitellar osteochondral lesions with or without loose body formation (Fig. 14). This is recognised in gymnasts (Priest and Weise 1981; Singer and Roy 1984; Jackson et al. 1989; Chan et al. 1991) as well as in sports involving repetitive throwing (Pappas 1982) and use of a racquet (Gore et al. 1980) and in BMX bicycle riding where up to 40% of the weight of the rider is borne by the arms (Fixsen and Maffulli 1989). MR imaging can be helpful in distinguishing stable from unstable lesions and the state of the overlying cartilage. Unstable lesions are surrounded by a rim of high signal intensity on T2-weighted images (Kijowski and De Smet 2005). Other MRI features of instability include a second low-signal rim around the rim of fluid, multiple breaks in the subchondral bone plate and large cysts (Chauvin and Gustas-French 2019).

Explosive extension of the elbow by the triceps muscle exerts both traction and shearing forces on the olecranon. Acute avulsions of the olecranon apophysis are well recognised. In skeletally immature athletes, chronic traction

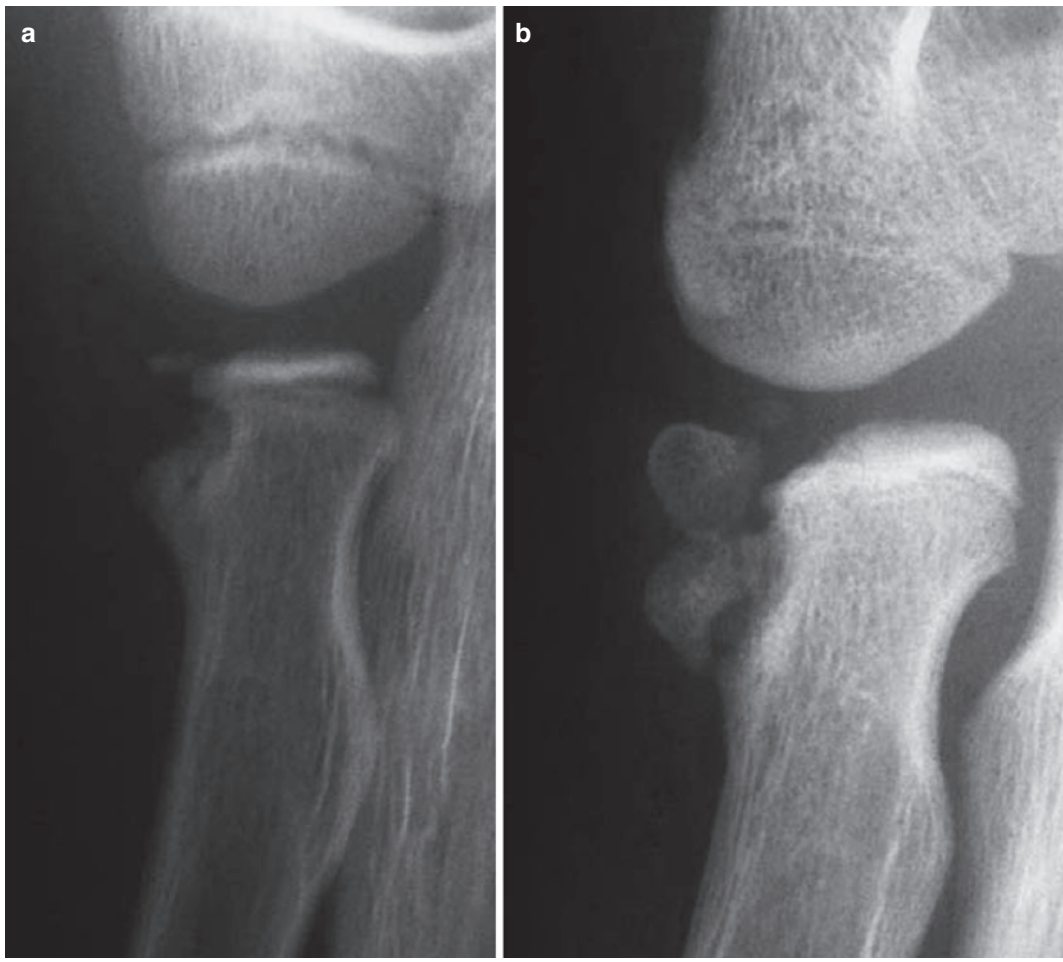

Fig. 12 (**a**, **b**) Salter-Harris type 4 stress fracture of the radial metaphysis. Over-rotated AP radiographs of the elbow in a child gymnast showing (**a**) a lateral epiphyseal cleft with a prominent underlying metaphyseal defect; (**b**) 2 years later the radial head is dysplastic with disordered ossification laterally

Fig. 13 (**a**–**c**) Panner's disease. (**a**) Radiograph in an 8-year-old male patient showing sclerosis and fragmentation of the humeral capitellum. Note the presence of a subchondral radiolucent crescent. (**b**) Coronal T1-weighted and **c** coronal FS T2-MRI show diffuse low signal on the T1 and high signal on the STIR sequence with intact overlying articular cartilage (courtesy F. Vanhoenacker)

can cause olecranon apophysitis (a Salter-Harris type 1 stress fracture) resulting in widening and irregularity of the physis (Fig. 15) and increased signal on either side of the physis on the MRI. This has been reported in gymnasts, baseball pitchers, divers and hockey players (Torg and Moyer 1977; Hunter and O'Connor 1980; Danielsson et al. 1983; Wilkerson and Johns 1990; Chan et al. 1991). This can lead to an unfused olecranon apophysis. In the older skeletally mature adolescent overuse can lead to stress fractures of the olecranon and triceps muscle pathology including tendinopathy or triceps tears.

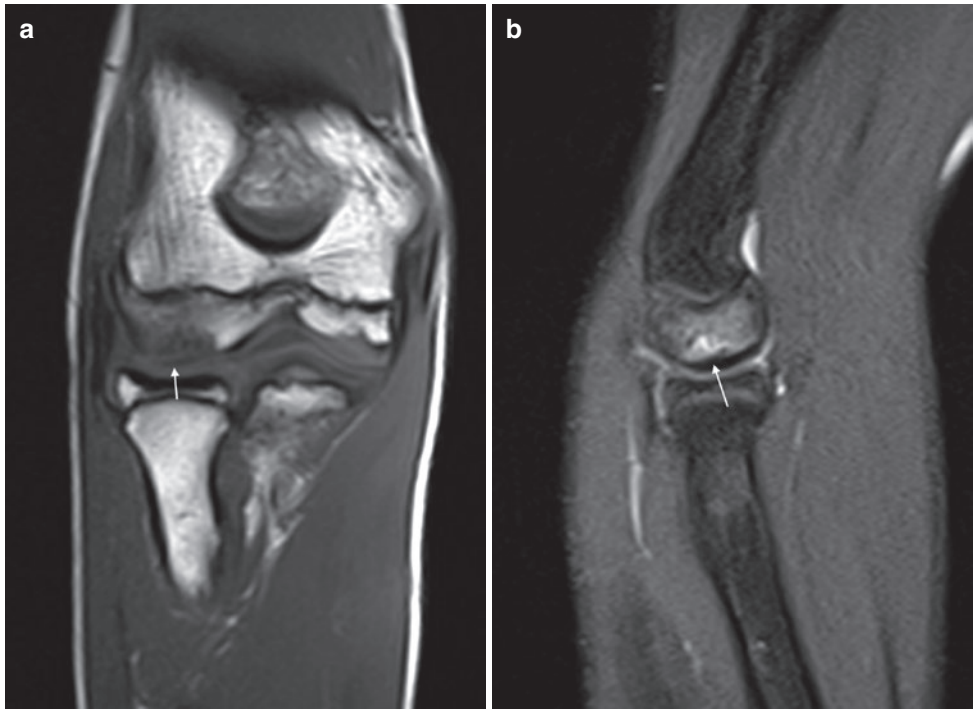

Fig. 14 (**a**, **b**) Capitellar osteochondral lesion in a 14-year-old male. (**a**) Coronal T1 and (**b**) sagittal STIR sequence showing a curvilinear lesion (white arrows) with surrounding oedema and irregularity of the overlying cartilage in keeping with an osteochondral lesion. There is a thin rim of fluid undermining the base of the lesion suggesting that it may be unstable

Fig. 15 Chronic Salter-Harris type 1 stress fracture in a female adolescent gymnast. Lateral radiograph of the elbow showing widening and irregularity of the olecranon growth plate

3.3 Wrist and Hand

Acute injuries of the distal forearm bones in the young child are typically of the torus or greenstick varieties. They occur at the junction between the dense diaphyseal lamellar bone and the softer metaphyseal bone. This type of injury is seen commonest in soccer players (Pannu and Herman 2015). In adolescence the Salter-Harris type 2 fracture-separation of the distal radial growth plate predominates. In the adolescent gymnast chronic wrist pain is a frequent complaint and can be associated with repetitive trauma to the wrist in extension, and is a Salter-Harris type 1 stress fracture of the distal radial growth plate. The radiographic findings are widening and irregularity of the growth plate with normal appearances of the distal ulnar growth plate (Fig. 16) (Read 1981; Roy et al. 1985; Fliegel 1986; Carter et al. 1988). MR imaging will show similar appearances and can also

Fig. 16 Chronic Salter-Harris type 1 stress fracture in an adolescent male gymnast. PA radiograph of the wrist showing widening and irregularity of the distal radial growth plate

demonstrate increased T2 signal in the physis which if untreated can lead to premature closure (Delgado et al. 2016; Liebling et al. 1995). The condition may be subclinical (Auberge et al. 1984) and is often self-limiting (Carter et al. 1988). The use of semi-quantitative Dixon MRI to measure the water signal fraction around the physis has been studied in both symptomatic and asymptomatic gymnasts and has showed significantly higher water content in the symptomatic group and this could be used as an indicator of early physeal injury (Kox et al. 2020). There is some controversy as to whether this form of injury if long-standing results in relatively positive ulnar variance in adulthood (De Smet et al. 1994; DiFiori et al. 2002). Carpal injuries are fairly uncommon preskeletal fusion. Stress fractures may rarely affect the scaphoid (Matzkin and Singer 2000). Acute fractures and dislocations are relatively common in the hand at all ages.

Finger injures can be commonly seen in rock climbing. This activity puts significant strain of the epiphyses and especially the flexor pulleys. This can lead to a Salter-Harris type 2 and 3 fractures of the middle phalanx of the third/fourth digit and pulley injures (Delgado et al. 2016).

4 Spine

Adolescent idiopathic scoliosis is one of the commonest childhood deformities more frequent in girls than boys. The overall prevalence is less than 3% but a much higher incidence of up to 25% has been reported in athletes, particularly ballet dancers (Warren et al. 1986). Increased frequency of scoliosis has also been reported in many other athletes including swimmers (Becker 1986), javelin throwers (Gussbacher and Rompe 1983), and tennis and volleyball players (Hellstrom et al. 1990; Omey et al. 2000). It is thought that the scoliosis is due to excessive lateral torque forces developed in certain activities such as serving and throwing (Omey et al. 2000).

The ring apophysis of the vertebral body is susceptible to axial compressive loading in the adolescent in sports such as gymnastics and water ski jumping (Horne et al. 1987; Sward et al. 1990). Injuries to the apophysis most often occur anteriorly but can arise posteriorly (Gundry and Fritts 1999). If multiple levels are involved then Scheuermann-like changes are seen with Schmorl's nodes, vertebral endplate irregularities, disc space narrowing, minor anterior body wedging and disc dehydration on T2-weighted MR images (Sward et al. 1991) (Fig. 17).

Spondylolysis, considered to be a stress fracture through the pars interarticularis, is a relatively common cause of low back pain in adolescent athletes and dancers (Micheli 1979, 1983, 1985; Soler and Calderon 2000; Rassi et al. 2005). There is a progression from a pre-fracture stress reaction through the pars interarticularis, to a fracture that may be unilateral or more frequently bilateral (spondylolysis), to vertebral displacement (spondylolisthesis) (Jackson et al. 1981). Repetitive load-bearing flexion and extension are considered the major risk factors predisposing to the development of spondylolysis (Letts et al. 1986). It may be seen in almost any

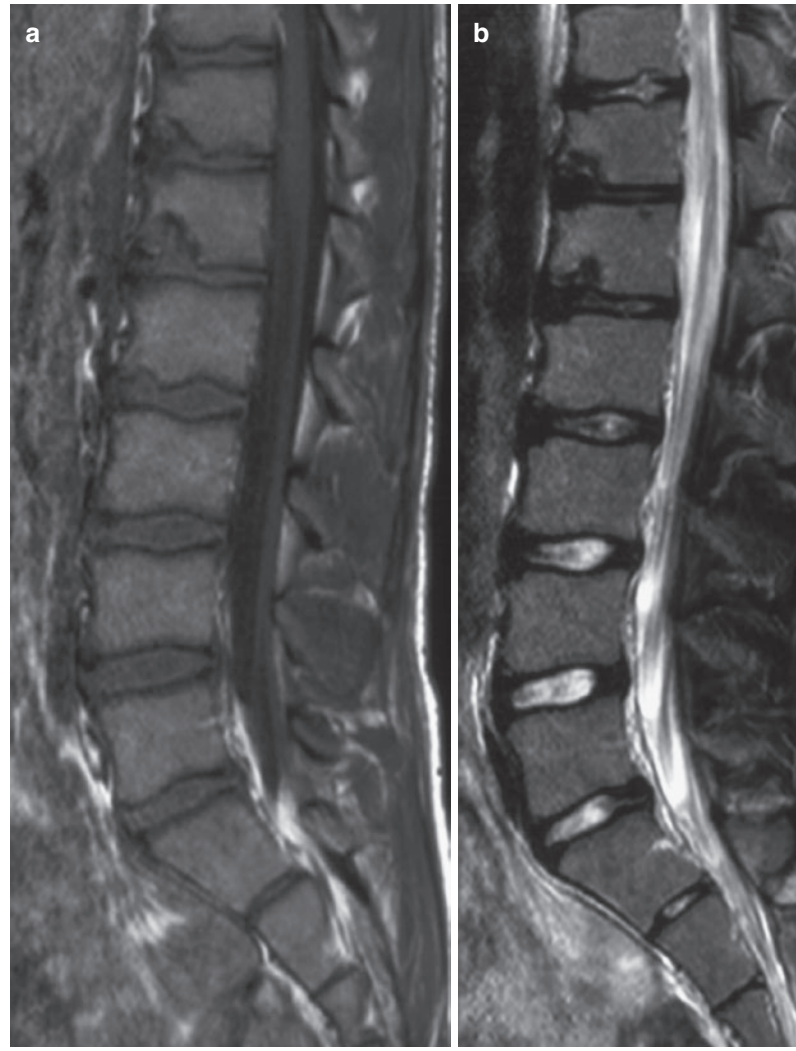

Fig. 17 (**a**, **b**) Adolescent gymnast with multiple-level juvenile vertebral osteochondrosis due to chronic axial compressive loading. (**a**) Sagittal T1- and (**b**) sagittal T2-weighted MRI showing Schmorl's node formation, vertebral endplate irregularities, disc space narrowing, anterior body wedging and disc dehydration

sport associated with high levels of mobility and loading. The incidence in gymnasts can be as high as 32% and divers 63% (Omey et al. 2000). A lateral radiograph of the lumbar spine will demonstrate the fracture if it is relatively well established and show any slip (Fig. 18). In the past oblique radiographs were used to reveal more subtle fractures. A standard bone scan will identify most cases but single-photon emission computed tomography/computed tomography (SPECT/CT) is more sensitive to subtle fractures and pre-fracture stress reactions (Zukotynski et al. 2010) and can assess healing (Fig. 19). Multislice CT with parasagittal reconstructions will allow direct visualisation of the fracture and can be helpful in assessing healing. MR imaging can be useful in the detection of acute and pre-fracture stress reactions owing to its ability to detect focal reactive bone marrow oedema on fluid-sensitive sequences (Ulmer et al. 1995; Gundry and Fritts 1999) (Fig. 20). Rarely, apophysitis of the spinous processes in gymnasts may clinically mimic spondylolysis (Mannor and Lindenfield 2000). Localisation of this particular

Fig. 18 Spondylolisthesis in a 13-year-old girl. Lateral radiograph of the lumbar spine showing bilateral L5 pars defects (white arrow) and a grade 2 spondylolisthesis

condition of abnormality can be readily made with sagittal SPECT/CT images.

Fatigue-type stress fractures of the sacrum are uncommon and tend to affect running athletes such as cross-country and marathon runners (Johnson et al. 2001). The fractures are more common in female athletes but have also been reported in males (Featherstone 1999; Shah and Stewart 2002). These fractures are notoriously difficult to detect on radiographs and some other form of imaging be it CT, MR imaging or bone scintigraphy is usually required (Fig. 21). In female athletes the identification of a sacral stress fracture should prompt inquiry into the dietary habits of the individual as a concurrent eating disorder might indicate that this was in fact an insufficiency-type stress fracture (Bono 2004).

Acute intervertebral disc herniations, while uncommon, are occasionally seen in young athletes with an incidence of 0.8–3.2% (Dang et al. 2015; Lagerbäck et al. 2015; Strömqvist et al. 2016; Wang et al. 2016). The L4/5 and L5/S1 levels are the commonest affected. Sports such as weightlifting, gymnastics, wrestling and collision sports have a higher incidence of disc herniations (Lagerbäck et al. 2015).

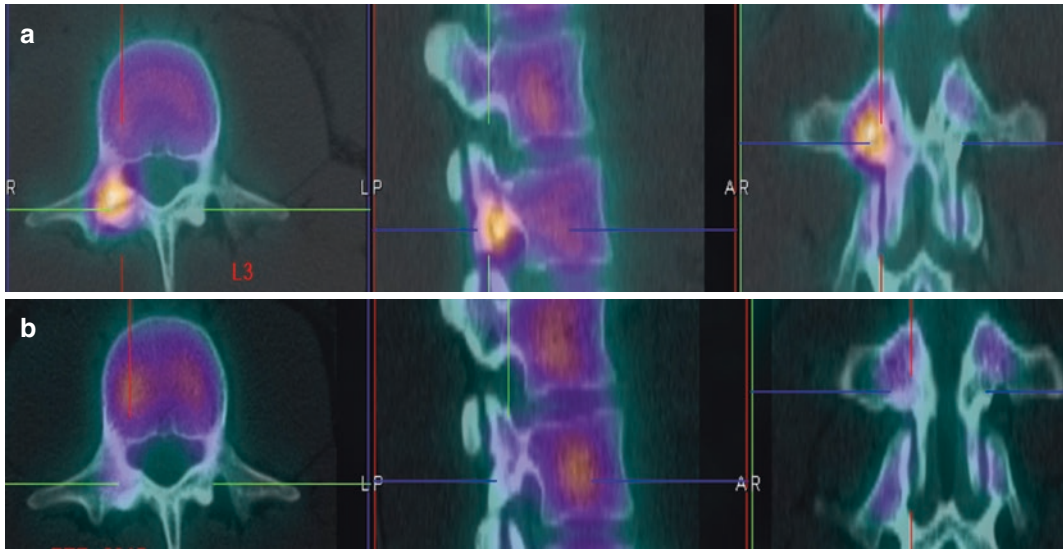

Fig. 19 (**a**, **b**) Spondylolysis in a 16-year-old male cricket player. (**a**) Presentation of SPECT CT showing right L3 pars defect with increased activity in keeping with an acute fracture. (**b**) SPECT CT after 18 months shows healed pars with no osteoblastic activity

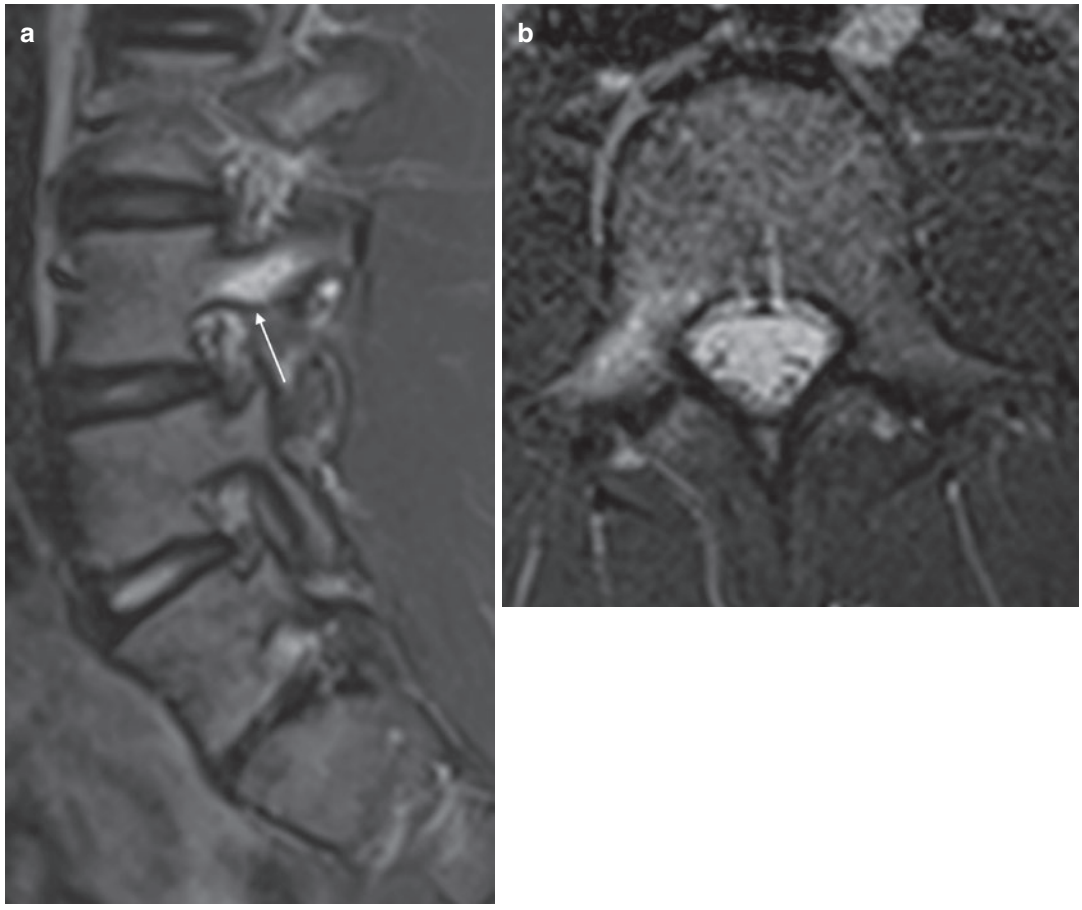

Fig. 20 (**a**, **b**) Stress reaction in the right L3 pars of a 16-year-old male cricket player. (**a**) STIR sagittal and (**b**) STIR axial demonstrating stress reaction in the right pars of L3 (white arrow)

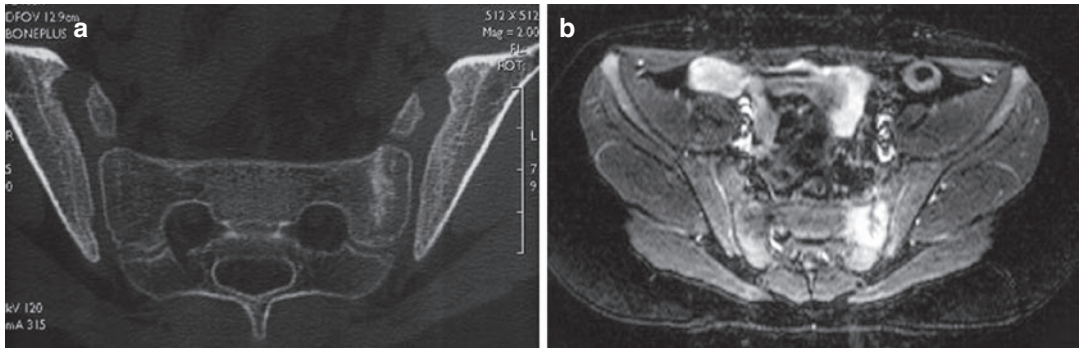

Fig. 21 (**a**, **b**) Stress fracture of the sacrum in an adolescent female cross-country runner. Radiographs of the sacrum were normal. (**a**) CT showing a linear band of sclerosis in the left sacral ala. (**b**) Axial T2-weighted fat-suppressed MR image showing the fracture as a dark line with surrounding marrow oedema

5 Pelvis

The pelvic ring is a strong structure such that most acute bony fractures in a sporting context are a result of major falls, e.g., horse riding. The growth of the bony pelvis is contributed by multiple apophyses that serve as the origin/insertion of a number of major muscle groups (see Table 1). Preskeletal fusion, acute or chronic, loading applied by these muscles can cause an avulsion injury. In the acute injury a small linear fragment of the avulsed apophysis can be identified in the adjacent soft tissues. If there is avulsion of the whole apophysis, with preservation of the blood supply, then it can continue to grow to form a large piece of mature bone within the soft tissues. This is well recognised with ischial injuries (Fig. 22). In a large series of acute pelvic avulsion injuries the mean age was 13.8 years and the sites involved were ischial apophysis (54%), anterior-inferior iliac spine (22%) (Fig. 23) and anterior-superior iliac spine (19%) (Fig. 24) (Rossi and Dragoni 2001). These injuries can be multiple (Sundar and Carty 1994). In the chronic injury there can be a spectrum of radiographic appearances that depend on the severity of the trauma and the degree of repair. The changes can vary from subtle irregularity of the bone surface through to marked irregular new bone formation (Vanhoenacker et al. 2005). It is the latter entity that can readily be mistaken for a malignant tumour of bone (see Lunkiewicz et al. 2021).

Table 1 Avulsion of pelvic apophyses—muscles and sporting activities involved

Apophysis	Muscle(s)	Sport
Iliac crest	Abdominal	Running Jumping Figure skating
Anterior-superior iliac spine	Sartorius/ tensor fascia lata	American football Baseball Running Cycling
Anterior-inferior iliac spine	Rectus femoris	Soccer Field hockey Running
Ischium	Hamstrings	Gymnastics Baseball Figure skating Ice hockey Hurdling American football
Pubis	Adductors	Running American football Soccer

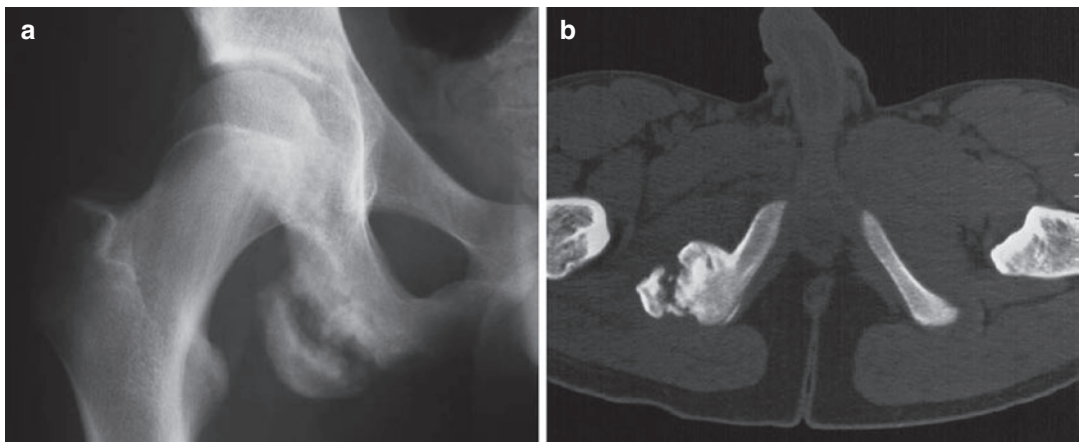

Fig. 22 (**a**, **b**) Chronic ischial avulsion in an adolescent male athlete. (**a**) AP radiograph showing irregularity of the ischial cortex with overgrowth of the avulsed apophysis in the adjacent soft tissues. (**b**) CT showing the deformity of the ischium and new bone formation

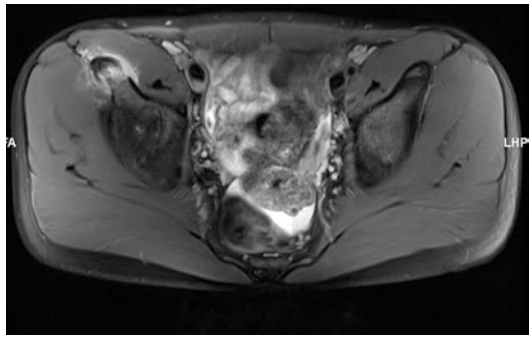

Fig. 23 Avulsion fracture of the anterior inferior iliac spine (AIIS) in a 15-year-old male football player. T2 fat saturation axial image showing avulsion of the AIIS and rectus femoris origin with surrounding oedema

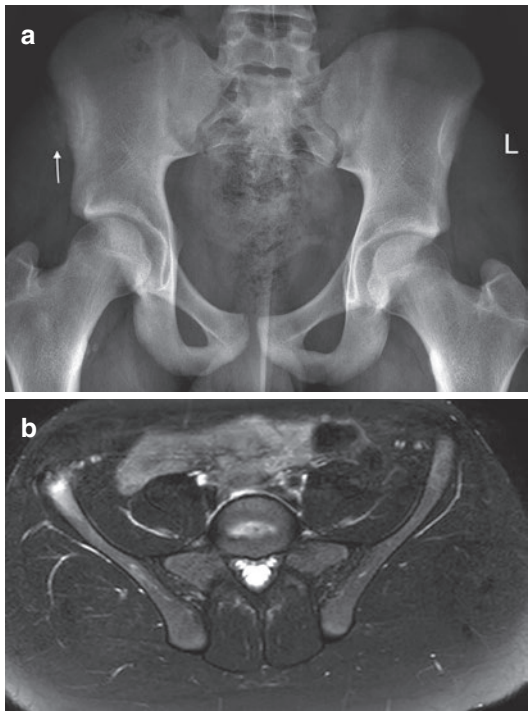

Fig. 24 (**a**, **b**) Avulsion fracture of the anterior superior iliac spine (ASIS) in a 16-year-old male football player. (**a**) AP radiograph showing avulsion of the ASIS with hypertrophic new bone formation. (**b**) T2 fat saturation axial image showing avulsion of the anterior superior iliac spine at the site of the attachment of the sartorius

6 Lower Limb

Fatigue-type stress fractures of the lower limb including the femoral neck, distal femoral diaphysis, proximal tibial diaphysis, distal fibular diaphysis and metatarsals (March fracture) are well recognised in adolescent athletes, particularly runners. The imaging features and differential diagnosis are covered in Lefere et al. (2021) and Lunkiewicz et al. (2021).

6.1 Hip

Developments in MRI imaging and hip arthroscopy techniques in recent years have improved the diagnosis of labral tears in the paediatric athletic patient. Labral tears can occur as an acute traumatic event or a chronic repetitive injury. In femoroacetabular impingement (FAI), the abnormal contact of the femoral head-neck junction and the acetabulum, this can be due to bony overgrowth at the femoral head-neck junction—cam lesion—or the overcoverage of the femoral head—pincer lesion—or a combination of both—mixed lesion. Other bony disorders including acetabular dysplasia, acetabular retroversion, Perthes, slipped upper femoral capital epiphysis (SUFE) and coxa valga increase the risk of labral injury.

Plain radiography can demonstrate any underlying bony disorders (e.g., cam or pincer lesions, acetabular retroversion, acetabular dysplasia, SUFE, Perthes). MRI/MRA can detect any labral pathology and assess the state of the articular cartilage. MRA was preferred as it has a higher sensitivity for labral pathology than plain MRI (Toomayan et al. 2006); however 3 T MRI is at least as good as demonstrating labral pathology and better at detecting chondral loss than 1.5 T MRA (Chopra et al. 2018) (Fig. 25). Most labral tears are located in the antero-superior location; however labral tears can be seen in all quadrants

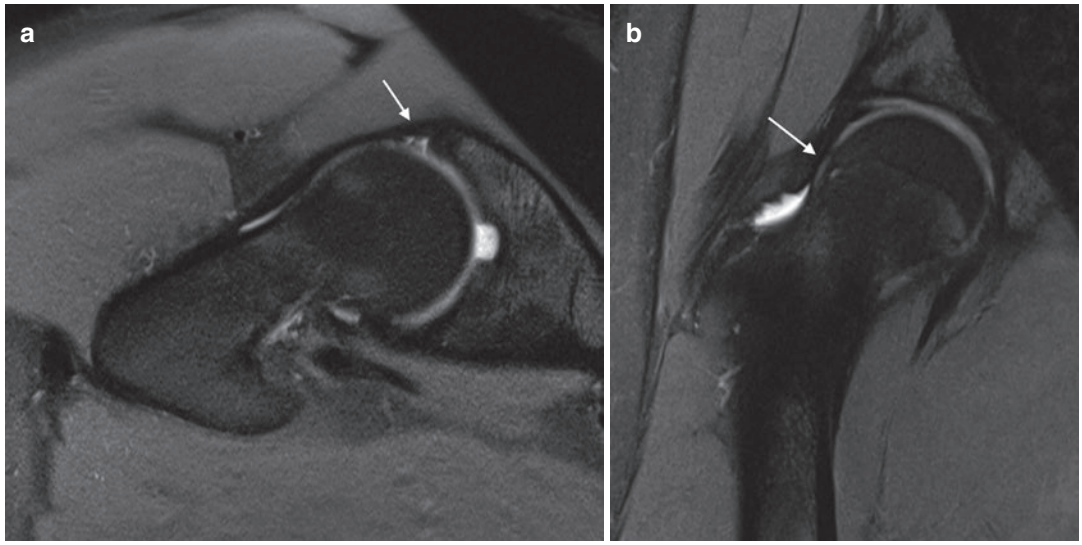

Fig. 25 (**a**, **b**) Labral tear and small cam impingement lesion in a 16-year-old female dancer. (**a**) 3T axial oblique proton-density fat-saturated images (PDFS) show complex labral tear in the anterior superior acetabular labrum (white arrow). (**b**) 3T coronal PDFS image showing mild prominence of the femoral head-neck junction with mild fibrocystic change in keeping with a small cam impingement lesion (white arrow)

(Blankenbaker et al. 2007). CT with 3D reconstructions allows the assessment of the size and location of any bony impingement lesion. CT-based 3D motion analysis can demonstrate the precise motion of a hip joint and can better identify any site of osseous impingement and where in the range of motion they occur.

6.2 Proximal Femur

Fatigue-type stress fractures of the femoral neck are four times more common than elsewhere in the femur (Fig. 26) (see Lefere et al. 2021).

Adductor insertion avulsion syndrome, "thigh splints", has been reported occasionally in skeletally immature individuals (Anderson et al. 2001; Van De Perre et al. 2003). In children the MRI appearances can mimic a sarcoma or osteomyelitis and therefore clinical and MRI follow-up is advised particularly in those who have increased symptoms or altered pain (Tshering-Vogel et al. 2005) (Fig. 27).

Acute avulsion of the lesser trochanteric apophysis, due to pull-off of the iliopsoas tendon,

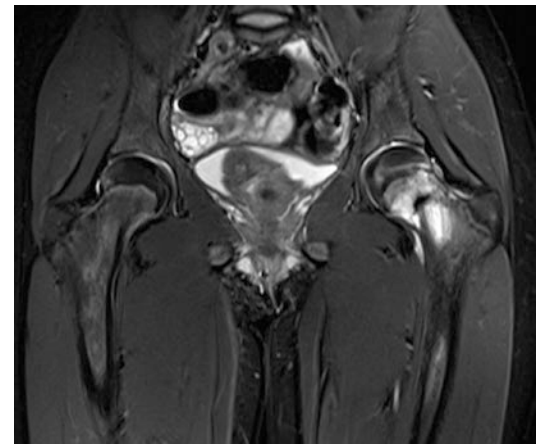

Fig. 26 Femoral neck stress fracture in a 16-year-old female gymnast. Coronal STIR MRI shows florid intramedullary osseous oedema and a low-signal incomplete fracture line

is most commonly seen in adolescents (Fig. 28) (Theologis et al. 1997). It should be distinguished from cases in the middle-aged persons and elderly where avulsion of the lesser trochanter is typically associated with malignant marrow infiltration.

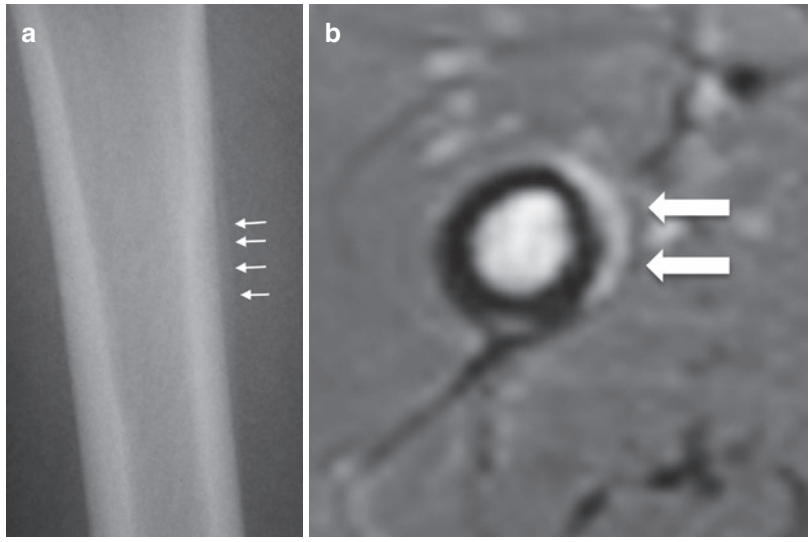

Fig. 27 (**a**, **b**) Adductor insertion avulsion "thigh splints". (**a**) AP radiograph of the proximal/mid femur magnified up shows smooth periosteal reaction of the medial femur. (**b**) Axial fluid-sensitive sequence shows periosteal and intramedullary oedema at the insertion of the adductor longus and brevis. This is on the spectrum of a stress-related injury (courtesy of F. Vanhoenacker, used with permission from Van de Perre S, Vanhoenacker F, De Schepper AM (2003) Thigh splints in a skeletally immature boy. Rofo Forschr Geb Rontgenstr Neuen Bildgeb Verfahr 175(11):1582–1584)

Fig. 28 Young male with avulsion of the right lesser trochanter imaged 2 weeks after acute injury. AP radiograph showing new bone formation around the avulsion simulating a bone forming tumour

6.3 Knee

The commonest acute avulsion around the knee in children and adolescents is at the site of the origin of the anterior cruciate ligament from the anterior tibial spine (Fig. 29). Avulsion of the insertion of the posterior cruciate ligament and origin of the medial collateral ligament are much less frequent. As stated above (see Sect. 2), the avulsive cortical irregularity of the posteromedial distal femur, otherwise known as a periosteal desmoid or cortical irregularity syndrome, may be a normal variant or a self-limiting traumatic lesion (Fig. 4). The presence of marrow oedema in the adjacent bone on MR imaging should not be considered indicative of infection or malignancy (Posch and Puckett 1998).

Stress fractures through the growth plates of the distal femur and proximal tibia, analogous to the Little Leaguer's shoulder and gymnast's wrist, are documented but rare (Godshall and Hansen 1981; Liebling et al. 1995).

Trauma is considered to be an important factor in the development of osteochondral lesions of the distal femur as it is more common in athletes than in those who do not participate in sports (Schenk and Goodnight 1996). It is also much more common in males than females and typically affects the lateral (intercondylar) aspect of the medial femoral condyle (Hefti et al. 1999). The abnormality may be unilateral or bilateral and on radiographs the osteochondral fragment may remain attached to the host bone or form a loose body in the joint (Fig. 30). MR imaging has superseded other imaging techniques in assessing the extent and stability of the lesion (De Smet

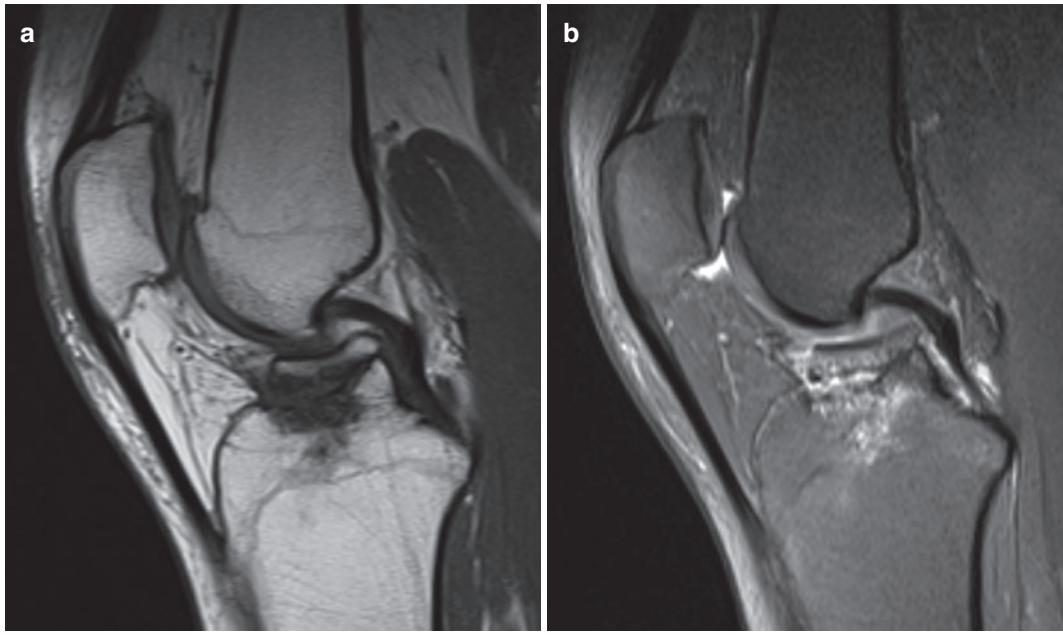

Fig. 29 (**a**, **b**) Adolescent male football player showing avulsion fracture of the ACL footprint. (**a**) T1 sagittal and (**b**) PDFS sagittal images showing avulsion fracture of the tibial spine including the ACL footprint (courtesy F. Vanhoenacker)

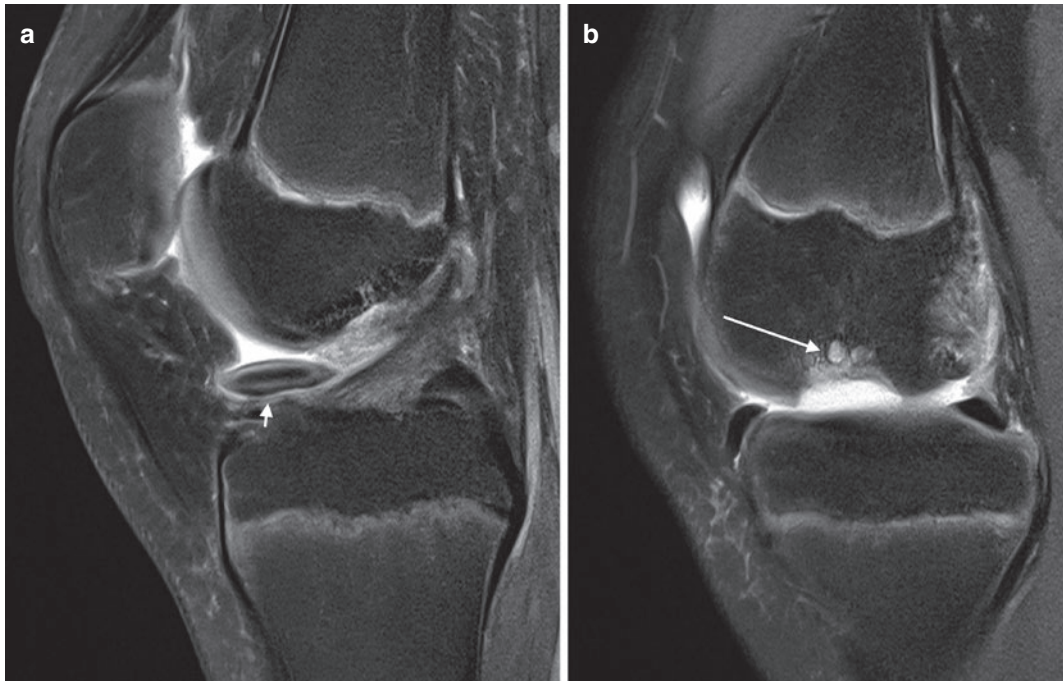

Fig. 30 (**a**, **b**) Unstable osteochondral lesion of the medial femoral condyle in a 16-year-old football player. (**a**, **b**) Consecutive parasagittal PD FS images showing a displaced osteochondral fragment (short white arrow). The cystic change and oedema at the donor site are secondary signs of instability (long white arrow)

et al. 1996). A lesion is considered unstable if one or more of the following MR criteria are present: (1) high-signal-intensity fluid/granulation line deep to the lesion, (2) cysts more than 5 mm in width beneath the lesion, (3) focal cartilage defect and (4) fluid passing through an articular cartilage defect (De Smet et al. 1996).

Congenital intra-articular abnormalities which may predispose to problems in the immature knee include congenital absence of the anterior cruciate ligament (Gabos et al. 2005) and discoid menisci. Discoid menisci are more common laterally, may be bilateral and can be associated with tears, meniscal cysts and premature degenerative joint disease (Rohren et al. 2001) (Fig. 31).

Chronic repetitive trauma can cause pain, tenderness, soft-tissue swelling and bony fragmentation at the origin of the patellar tendon from the inferior pole of the patella (Sinding-Larsen-Johansson disease, aka "jumper's knee") (Fig. 8) and at its insertion into the tibial tubercle (Osgood-Schlatter disease) commonest in adolescent athletes. If required, the clinical diagnosis of both conditions can be confirmed with ultrasound or MR imaging (Hirano et al. 2002). Arguably, the role of imaging in this situation is to exclude other occult pathology. Care should be taken not to overdiagnose minor signal change within the patellar tendon as indicative of chronic trauma without evidence of swelling and oedema as it may be artefactual due to the magic angle phenomenon.

Patella dislocations are a common acute injury in children during athletic activity. It is most frequently seen in basketball, soccer and American football (Waterman et al. 2012). The patella dislocates laterally out of the trochlea groove and may or may not relocate spontaneously. Genu valgum, trochlear dysplasia, increased tibial tuberosity-trochlea groove (TT-TG) distance, patella alta and joint hypermobility are risk factors. Radiographs can be normal if spontaneous relocation occurs but can show a haemarthrosis. MRI can demonstrate typical oedema pattern of the inferomedial patella and lateral femoral condyle and disruption of the medial patellofemoral retinaculum. A haemarthrosis may also be present. MRI can also define morphological abnormalities of the trochlea and patella and help in surgical planning (Diederichs et al. 2010).

Fractures of the patella are relatively rare in children and adolescents accounting for

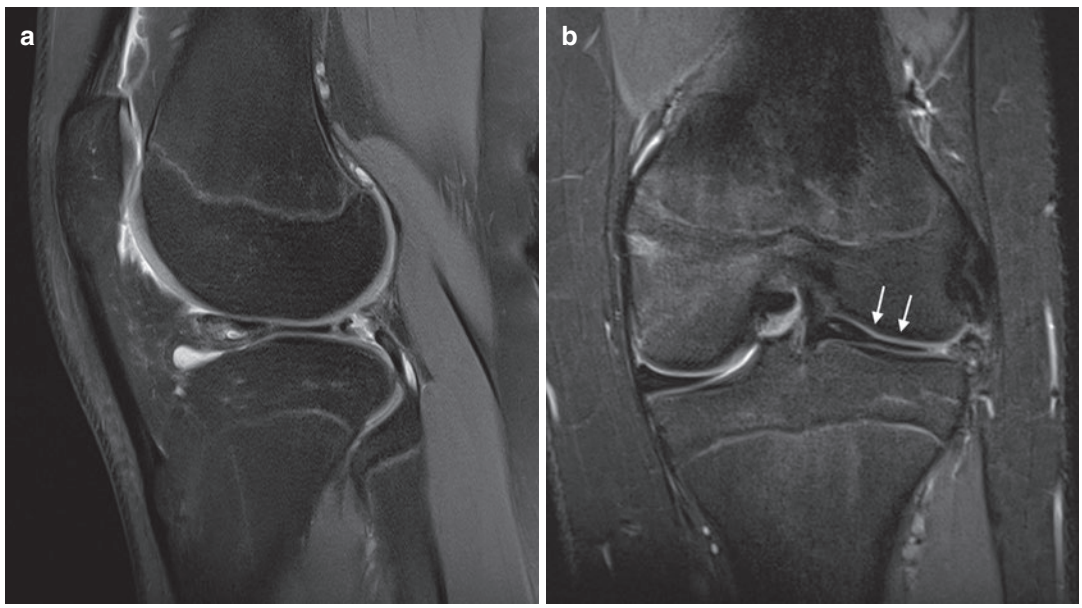

Fig. 31 (**a**, **b**) Discoid lateral meniscus in a 17-year-old male football player. (**a**) Sagittal PD FS and (**b**) coronal PD FS sequences show a discoid lateral meniscus with an associated complex tear (white arrows)

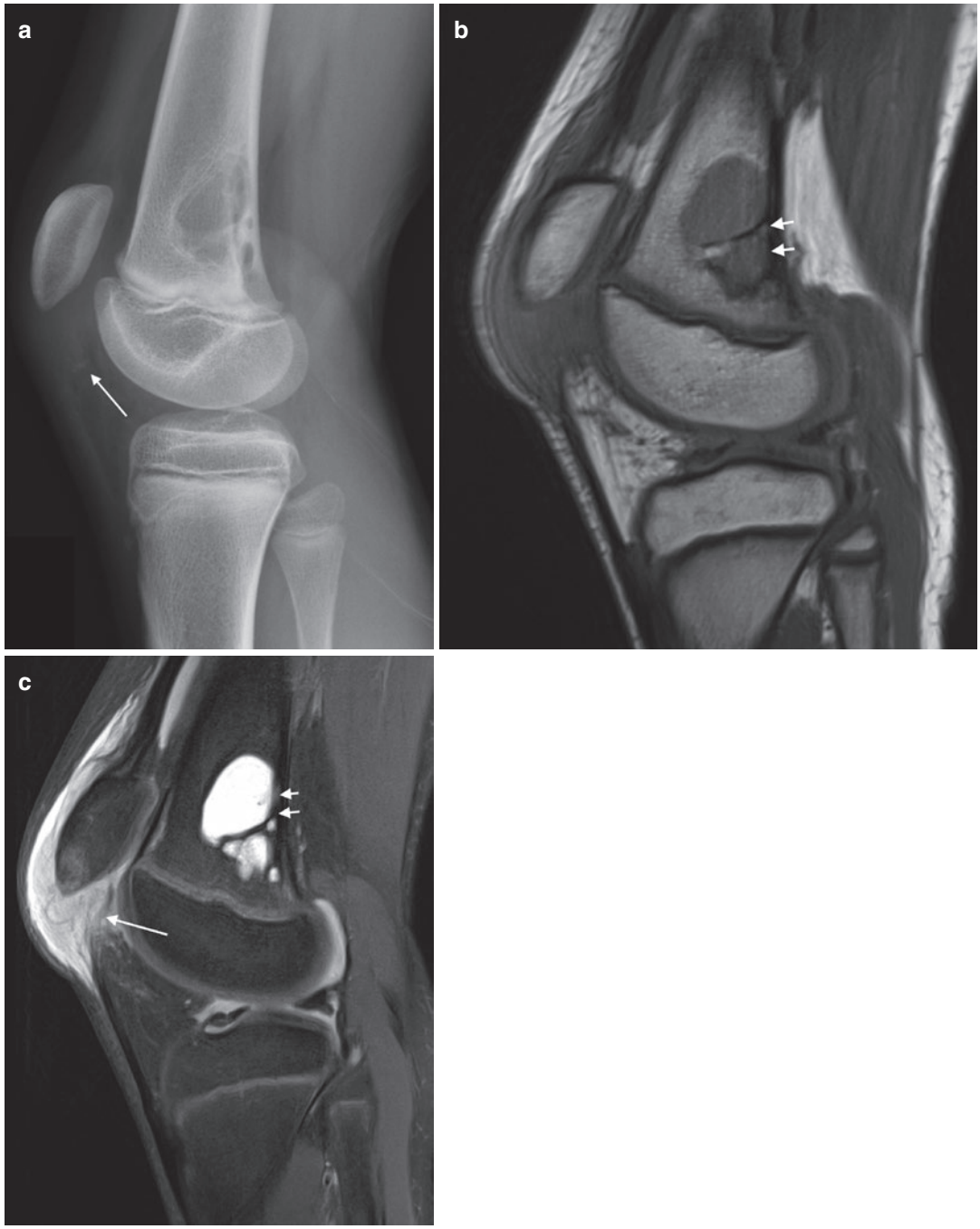

Fig. 32 (**a–c**) Patella sleeve fracture in an 11-year-old female. (**a**) Lateral radiograph showing patella alta; there is a small avulsed bony fragment from the inferior pole of the patella which is just visible (white arrow). (**b**) Sagittal T1 and **c** sagittal STIR sequence shows loss of continuity of the proximal patella tendon and accompanying patella sleeve from the inferior pole of the patella (long white arrows). A benign asymptomatic fibrocystic lesion is also noted in the distal femoral metaphysis (short arrows) (courtesy of Dr. H. Majeed UK)

approximately 1% of all fractures in this age group (Green and Swiontkowski 2002). Sleeve fractures of the patella constitute about 57% of all patella fractures in this age group (Hunt and Somashekar 2005). They are usually caused by forceful extension of the knee with vigorous

contraction of the quadriceps. This results in a "sleeve" of periosteum which is pulled off the patella with or without a bony fragment. The most common pattern of injury involves avulsion of the inferior sleeve but superior, medial and lateral sleeve avulsions can occur. X-rays may or may not show a small avulsed bony fragment, varying degrees of patella alta and a joint effusion; however the extent of the soft-tissue injury is severely underestimated. MRI will assess the full extent of the injury to the extensor mechanism and can identify the presence of a displaced patella fragment if present and the need for surgical management (Dupuis et al. 2009; Bates et al. 1994) (Fig. 32).

"Shin splint" refers to activity-related lower leg pain thought to be related to traction periostitis of the calf muscles along the posteromedial tibia. MR imaging may show juxtacortical and marrow oedema as well as subtle cortical changes (Anderson et al. 1997). It forms part of the spectrum of stress-related pathology affecting the tibial diaphysis, with the fatigue-type stress fracture as the most severe manifestation. MRI is the imaging modality of choice. It is more sensitive than radiography, CT and nuclear medicine studies (Gaeta et al. 2005; Kiuru et al. 2002; Kijowski et al. 2007; Kiuru et al. 2007) (Fig. 33). A classification based on MRI findings was first proposed in 1995 to allow a standardised method of assessing the severity of injury (Fredericson et al. 1995) (Table 2).

Table 2 Fredericson MRI classification for tibial stress injuries

Grade of stress injury	MRI findings
0	No abnormality
1	Periosteal oedema only
2	Periosteal oedema and marrow oedema only visible on T2-weighted sequences
3	Periosteal oedema and marrow oedema visible on T1- and T2-weighted sequences
4a	Multiple focal intracortical signal abnormalities on T1- and T2-weighted sequences
4b	Linear intracortical signal abnormalities on T1- and T2-weighted sequences

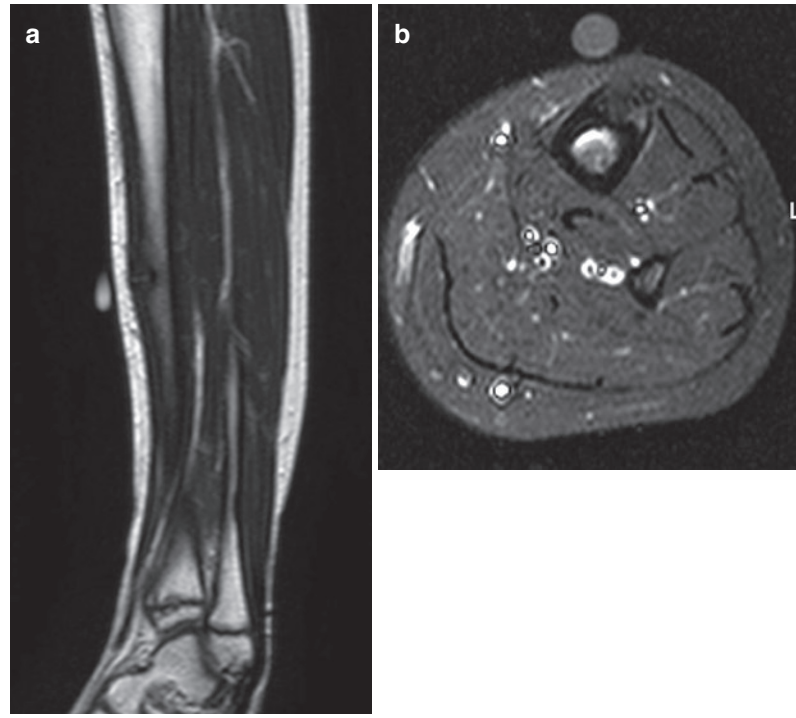

Fig. 33 (**a**, **b**) Medial tibial stress fracture in a 14-year-old female. (**a**) Sagittal T2 and (**b**) axial PD FS sequences showing focal cortical thickening with periosteal and intramedullary oedema with a visible fracture line in keeping with a grade 4b stress fracture

6.4 Ankle and Foot

The foot and ankle are the most commonly injured and imaged parts of the musculoskeletal system affecting athletes of all ages (Dunfee et al. 2002). Ankle injuries account for over one-quarter of all sports-related injuries in school-aged children (Backx et al. 1989). Acute Salter-Harris fractures of the distal tibia are associated with premature fusion of the growth plate in approximately one-third of cases (Barmada et al. 2003). Fatigue-type stress fractures around the ankle and foot preskeletal fusion tend to involve the navicular (Corris et al. 2003), distal fibula and uncommonly medial malleolus (Shabat et al. 2002). Torsional or inversion stress injuries in adolescent athletes may lead to osteochondral lesion of the talar dome (Fig. 34). The average age at presentation is approximately 13 years and the medial dome of the talus is the most commonly affected (Letts et al. 2003a; Vanhoenacker et al. 2002). Both CT and MR imaging can be used to confirm the diagnosis, assess for instability and enable surgical planning.

Fig. 34 Osteochondral lesion of the talar dome in a 13-year-old male. Radiographs showing a displaced osteochondral fragment of the talar dome (white arrow) (courtesy F. Vanhoenacker)

Heel pain is a common presenting symptom in the skeletally immature athlete. Sever's disease is an overuse injury due to traction apophysitis of the calcaneal apophysis. This often occurs at a time of a growth spurt or a rapid increase in training volume which increases the pull of the strong Achilles tendon against the relatively soft calcaneal apophysis. It is often bilateral in up to 60% of patients. It is more common in sports that require running and jumping (James et al. 2016). Year-round activity, improper footwear and biomechanical factors such as a short Achilles tendon, pes cavus, pes planus and genu varum are contributing factors (James et al. 2016; Launay 2015). The diagnosis is usually made clinically but if the diagnosis is in doubt imaging can be performed. Radiographs can often be normal or can show increased sclerosis and fragmentation of the calcaneal apophysis. MRI can show bone marrow oedema and enhancement following contrast in the calcaneal apophysis (Hussain et al. 2013) (Fig. 5).

Ankle sprains are one of the commonest sports-related injuries in adolescence. They can be divided into lateral, high and medial based on their location. Lateral sprains are the commonest type. Inversion and plantar flexion are the commonest mechanisms of injury. Medial and high ankle sprains are usually caused by eversion and external rotation. Most will improve with non-operative management. Imaging of the ligaments and tendons, be it with MR imaging or ultrasound, is best reserved for those cases where surgical intervention is being considered. The severity of injury on MRI can be classified into one of three grades ranging among oedema around the ligament, grade 1; partial tear, grade 2; and full-thickness tear, grade 3. Surgical indications include persistent chronic lateral ankle instability (Letts et al. 2003b) and posterior tibial tendon dysfunction (McCormack et al. 2003).

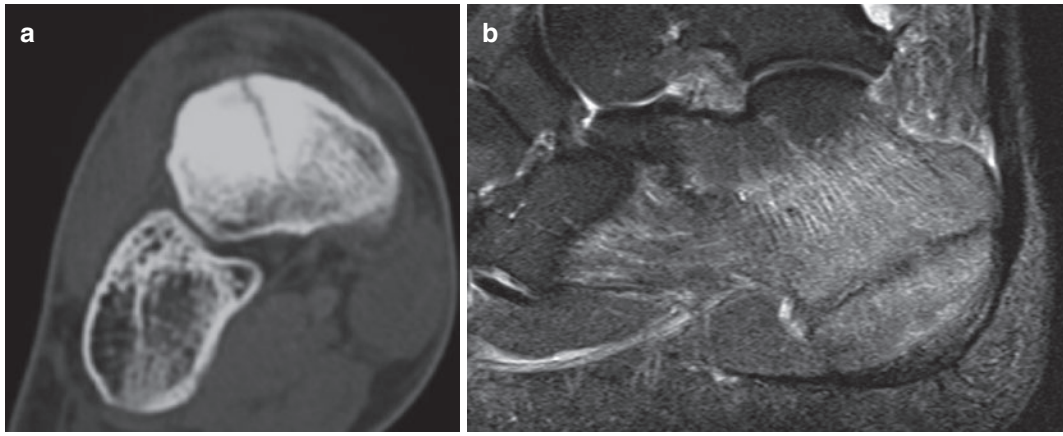

Fig. 35 (**a**, **b**) Stress fractures of the foot. (**a**) Reformatted CT in a 16-year-old female dancer shows incomplete stress fracture of the navicular which does not quite reach the inferior surface. (**b**) Sagittal STIR MRI in a 16-year-old female dancer showing incomplete fracture of the calcaneus with visible low-signal fracture line and marked osseous oedema

Ballet dancers are particularly prone to foot and ankle pain. The causes can be classified into four groups: impingement syndromes, tendon, ligament and osseous pathologies (Hillier et al. 2004). Posterior impingement is a particular problem because of forced plantar flexion in the en pointe and demi-pointe positions where the posterior tibia and the postero-superior aspect of the calcaneus come into close contact; this is aggravated by the presence of an os trigonum or prominent posterolateral talar tubercle (Stieda process). Compression of the osseous and interposed soft tissues can result. MRI can demonstrate the presence of an os trigonum or a Stieda process and associated cystic change, marrow oedema, synovitis, posterior capsule thickening and tenosynovitis of the flexor hallucis longus (Peace et al. 2004). Stress fractures can be seen in any bone of the foot (Fig. 35). The forefoot especially is vulnerable to injury when dancing the en pointe and demi-pointe positions which can place high loads on the metatarsals and the plantar aspect of the MTPJs. Plantar plate injuries, MTPJ chondral injuries and sesamoiditis and sesamoid stress injuries are commonly seen. Midfoot injuries are less commonly seen than injuries to the hind and forefoot but include fractures of the metatarsals and abnormalities of the Lisfranc ligament (Fritz and Kassarjian 2014).

Things to Remember

1. How trauma is manifested in the skeleton depends on the age of the individual.
2. The nature of the sport will determine the pattern of injuries sustained.
3. Overuse injuries are associated with year-round sporting participation and early specialisation in a single sport.
4. In the adolescent the growth plate (physis) is particularly susceptible to trauma.
5. The differential diagnosis of chronic overuse injuries in the immature skeleton includes normal variants, osteomyelitis and primary bone tumours.

Box 1: Standard Radiography

Initial imaging modality for diagnosis of fractures, Salter-Harris fractures or apophyseal avulsion fracture.

Knowledge of age-related anatomy of the patients and normal variants is mandatory for correct image interpretation.

Contralateral/comparison views should be discouraged.

Some type of stress fractures, particularly in complex anatomical areas (e.g., sacrum), may be very difficult to detect on standard radiographs.

Box 2: Other (Cross-Sectional) Imaging Techniques

MRI is useful for early detection of stress fractures or stress reactions, assessment of internal derangement of joints and staging of osteochondral lesions.

US is mainly used for overuse trauma of tendons (e.g., patellar tendon) and can allow guided therapeutic intervention.

Multi-detector CT is the technique of choice to detect fracture lines in spondylolysis.

SPECT/CT is very sensitive to detect subtle spondylolysis; it can also be used for assessment of healing in spondylolysis.

References

Adams JE (1965) Injury to the throwing arm. A study of traumatic changes in the elbow joints of boy baseball players. Calif Med 102:127–132

Adams JE (1966) Little league shoulder: osteochondrosis of the proximal humeral epiphysis in boy baseball pitchers. Calif Med 105:22–25

Allen ME (1984) Stress fracture of the humerus: a case report. Am J Sports Med 12:244–245

Anderson MW, Ugalde V, Batt M, Gacayan J (1997) Shin splints: MR appearance in a preliminary study. Radiology 204:177–180

Anderson SE, Johnston JO, O'Donnell R, Steinbach LS (2001) MR imaging of sports related pseudotumor in children: midfemoral diaphyseal periostitis at insertion site of adductor musculature. AJR Am J Roentgenol 176:1227–1231

Anisau A, Posadzy MS, Mulier E, Vanhoenacker FM (2018) Case 16265: Panne's disease. Eurorad. https://doi.org/10.1594/EURORAD/CASE.16265

Auberge T, Zenny JC, Duvallet A et al (1984) Etude de la maturation osseuse et des lesions ostéo-articulaires des sportifs de haut niveau. J Radiol 65: 555–561

Backx FJ, Erich WB, Kemper AB et al (1989) Sports injuries in school-aged children: an epidemiological study. Am J Sports Med 17:234–240

Barmada A, Gaynor T, Mubarak SJ (2003) Premature physeal closure following distal tibial physeal fractures: a new radiographic predictor. J Pediatr Orthop 23:733–739

Barnes GR, Gwinn JL (1974) Distal irregularities of the femur simulating malignancy. AJR 122:180–185

Barnett LS (1985) Little league shoulder syndrome: proximal humeral epiphysiolysis in adolescent baseball pitchers: case report. J Bone Joint Surg Am 67A:495–496

Bates DG, Hresko MT, Jaramillo D (1994) Patellar sleeve fracture: demonstration with MR imaging. Radiology 193:825–827

Battaglia TC, Barr MA, Diduch DR (2003) Rotator cuff tear in a 13-year-old baseball player. Am J Sports Med 31:779–782

Becker TJ (1986) Scoliosis in swimmers. Clin Sports Med 5:149–158

Beltran J, Rosenberg ZS (1997) MR imaging of pediatric elbow fractures. MRI Clin North Am 5:567–578

Benton J, Nelson C (1971) Avulsion of the coracoid process in an athlete. J Bone Joint Surg Am 53A:356–358

Blankenbaker DG, De Smet AA, Keene JS et al (2007) Classification and localization of acetabular labral tears. Skelet Radiol 36:391–397

Bono CM (2004) Current concepts review: low-back pain in athletes. J Bone Joint Surg Am 86A:382–396

Borges JLP, Guille JT, Bowen JR (1995) Kohler's disease of the tarsal navicular. J Pediatr Orthop 15:956–968

Boyd KT, Batt ME (1997) Stress fracture of the proximal humeral epiphysis in an elite junior badminton player. Br J Sports Med 31:252–253

Brower AC (1983) The osteochondroses. Orthop Clin North Am 14:99–117

Bufkin WJ (1971) The avulsive cortical irregularity. AJR 112:487–492

Burrows PE, Greenberg ID, Reed MH (1982) The distal femoral defect: technetium-99m pyrophosphate bone scan results. J Can Assoc Radiol 33:91–93

Cahill BR, Tullos HS, Fain RH (1974) Little league shoulder: lesions of the proximal humeral epiphyseal plate. J Sports Med 2:150–151

Callaghan EB, Bennett DL, El-Khoury GY et al (2004) Ball-thrower's fracture of the humerus. Skelet Radiol 33:355–358

Carrino JA, Morrison WB, Zou KH et al (2001) Noncontrast MR imaging and MR arthrography of the ulnar collateral ligament of the elbow: prospective evaluation of two-dimensional pulse sequences for detection of complete tears. Skelet Radiol 30: 625–632

Carson WG Jr, Gasser SI (1998) Little Leaguer's shoulder: a report of 23 cases. Am J Sports Med 26:575–580

Carter SR, Aldridge MJ, Fitzgerald R et al (1988) Stress changes of the wrist in adolescent gymnasts. Br J Radiol 61:109–112

Chan D, Aldridge MJ, Maffulli N et al (1991) Chronic stress injuries of the elbow in young gymnasts. Br J Radiol 64:1113–1118

Chao SL, Miller M, Teng SW (1971) A mechanism of spiral fracture of the humerus: a report of 259 cases following the throwing of hand grenades. J Trauma 11:602–605

Chauvin N, Gustas-French CN (2019) Magnetic resonance imaging of elbow injuries in children. Pead Radiol 49:1629–1642

Chopra A, Grainger AJ, Dube B, Evans R, Hodgson R, Conroy J, Macdonald D, Robinson P (2018)

Comparative reliability and diagnostic performance of conventional 3T magnetic resonance imaging and 1.5T magnetic resonance arthrography for the evaluation of internal derangement of the hip. Eur Radiol 28(3):963–971

Conway JE, Jobe FW, Glousman RE (1992) Pink M. medial instability of the elbow in throwing athletes—treatment by repair or reconstruction of the ulnar collateral ligament. Am J Bone Joint Surg 74:67–83

Corris EE, Kaeding CC, Marymont JV (2003) Tarsal navicular stress fractures in athletes. Orthopedics 26:733–737

Craigen MAC, Bennet GC, MacKenzie JR et al (1994) Symptomatic cortical irregularities of the distal femur simulating malignancy. J Bone Joint Surg (Br) 76B:814–817

Daldorg PG, Bryan WJ (1994) Salter-Harris type 1 injury in a gymnast. A slipped capital humeral epiphysis? Orthop Rev 23:538–541

Dang L, Chen Z, Liu X et al (2015) Lumbar disk herniation in children and adolescents: the significance of configurations of the lumbar spine. Neurosurgery 77:954–959; discussion 959.

Danielsson LG, Hedlund ST, Henricson AS (1983) Apophysitis of the olecranon: a report of four cases. Acta Orthop Scand 54:777–778

De Smet L, Claessens A, Lefevre J et al (1994) Gymnast wrist: an epidemiological survey of ulnar variance and stress changes of the radial physis in elite female gymnasts. Am J Sports Med 22:846–850

De Smet AA, Ilahi OA, Graf BK (1996) Reassessment of the MR criteria for stability of osteochondritis dissecans in the knee and ankle. Skelet Radiol 25: 159–163

Delgado J, Jaramillo D, Chauvin NA (2016) Imaging the injured pediatric athlete: upper extremity. Radiographics 36(6):1672–1687. Review.

Diederichs G, Issever AS, Scheffler S (2010) MR imaging of patellar instability: injury patterns and assessment of risk factors. Radiographics 30(4):961–981. https://doi.org/10.1148/rg.304095755

DiFiori JP, Puffer JC, Aish B et al (2002) Wrist pain, distal radial physeal injury, and ulnar variance in young gymnasts: does a relationship exist? Am J Sports Med 30:879–885

Dotter WE (1953) Little Leaguer's shoulder. Guthrie Clin Bull 23:–68

Dunfee WR, Dalinka MK, Kneeland JB (2002) Imaging athletic injuries to the ankle and foot. Radiol Clin N Am 40:289–312

Dunham WK, Marcus NW, Enneking WF et al (1980) Developmental defects of the distal femoral metaphysis. J Bone Joint Surg Am 62A:801–806

Dupuis CS, Westra SJ, Makris J, Wallace EC (2009) Injuries and conditions of the extensor mechanism of the pediatric knee. Radiographics 29: 877–886

Dwek JR (2013) Chung CB. A systematic method for evaluation of pediatric sports injuries of the elbow. Pediatr Radiol 43:S120–S128

Ellman H (1975) Anterior angulation deformity of the radial head: an unusual lesion occurring in juvenile baseball players. J Bone Joint Surg Am 57A:776–778

Featherstone T (1999) Magnetic resonance imaging in the diagnosis of sacral stress fracture. Br J Sports Med 33:276–277

Field AE, Tepolt FA, Yang DS, Kocher MS (2019) Injury risk associated with sports specialization and activity volume in youth. Orthop J Sports Med 7(9):2325967119870124

Fixsen JA, Maffulli N (1989) Bilateral intra-articular loose bodies of the elbow in an adolescent BMX player. Injury 20:363–364

Fleming JL, Hollingsworth CL, Squire DL et al (2004) Little Leaguer's shoulder. Skelet Radiol 33: 352–354

Fliegel CP (1986) Stress related widening of the radial growth plate in adolescents. Ann Radiol 29:374–376

Fredericson M, Bergman AG, Hoffman KL, Dillingham MS (1995) Tibial stress reaction in runners: correlation of clinical symptoms and scintigraphy with a new magnetic resonance imaging grading system. Am J Sports Med 23:472–481

Fritz RC (1999) MR imaging of sports injuries of the elbow. Magn Reson Imaging Clin N Am 7:51–72

Fritz BL, Kassarjian A (2014) MRI of foot and ankle injuries in ballet dancers. Spetar Sports Med J 3:630–637

Gabos PG, El Rassi G, Pahys J (2005) Knee reconstruction in syndromes with congenital absence of the anterior cruciate ligament. J Pediatr Orthop 25:210–214

Gaeta M, Minutoli F, Scribano E et al (2005) CT and MR imaging findings in athletes with early tibial stress injuries: comparison with bone scintigraphy findings and emphasis on cortical abnormalities. Radiology 235:553–561

Godshall RW, Hansen CA (1981) Stress fractures through the distal femoral epiphysis in athletes. Am J Sports Med 9:114–116

Goldberg MJ (1980) Gymnastic injuries. Orthop Clin N Am 11:717–726

Gore RM, Rogers LF, Bowerman J, Suker J, Compere CL (1980) Osseous manifestations of elbow stress associated with sports activity. AJR Am J Roentgenol 134:971–977

Green NE, Swiontkowski MF (eds) (2002) Skeletal trauma in children, 3rd edn. Saunders, Philadelphia, PA

Gregory B, Nyland J (2013) Medial elbow injury in young throwing athletes. Muscles Ligaments Tendons J 3:91–100

Gundry CR, Fritts HM (1999) MR imaging of the spine in sports injuries. Magn Reson Imaging Clin N Am 7:85–103

Gussbacher A, Rompe G (1983) Die dynamische und statische beanspruchung der Wirbelsaule und ihre moglichen auswirkungen bei verschiedenen sportaten. Schweiz Z Sportmed 31:119–124

Hang DW, Chao CM, Hang YS (2004) A clinical and roentgenographic study of Little League elbow. Am J Sports Med 32:79–84

Harsha WN (1957) Effects of trauma upon epiphyses. Clin Orthop 10:140–147
Hefti F, Beguiristain J, Krauspe R et al (1999) Osteochondritis dissecans: a multicenter study of the European Pediatric Orthopedic Society. J Pediatr Orthop B 8(4):231–245
Hellstrom M, Jacobsson B, Sward L et al (1990) Radiological abnormalities of the thoraco-lumbar spine in athletes. Acta Radiol 31:127–132
Heyes-Moore GH, Stoker DJ (1982) Avulsion fractures of the scapula. Skelet Radiol 9:27–32
Hillier JC, Peace K, Hulme A et al (2004) MRI features of foot and ankle injuries in ballet dancers: pictorial review. Br J Radiol 77:532–537
Hirano A, Fukubayashi T, Ishii T et al (2002) MR imaging of Osgood-Schlatter disease: the course of the disease. Skelet Radiol 31:334–342
Horne J, Cockshott WP, Shannon HS (1987) Spinal column damage from water ski jumping. Skelet Radiol 16:612–616
Hunt DM, Somashekar N (2005) A review of sleeve fractures of the patella in children. Knee 12:3–7
Hunter LY, O'Connor GA (1980) Traction apophysitis of the olecranon: a case report. Am J Sports Med 8:51–52
Hussain S, Hussain K, Hussain S et al (2013) Sever's disease: a common cause of paediatric heel pain. BMJ Case Rep 2013:bcr2013009758
Hyndman JC (1996) The growing athlete. In: Harries M, Williams C, Stanish WD, Micheli LJ (eds) Oxford textbook of sports medicine. Oxford University Press, Oxford, pp 620–633
Ireland ML, Andrews JR (1988) Shoulder and elbow injuries in the young athlete. Clin Sports Med 7:473–494
Jackson DW, Wiltse LL, Dingeman RD (1981) Stress reactions involving the pars interarticularis in young athletes. Am J Sports Med 9:304–312
Jackson SW, Silvino N, Reiman P (1989) Osteochondrosis in the female gymnasts elbow. Arthroscopy 5:129–136
James AM, Williams CM, Haines TP (2016) Health related quality of life of children with calcaneal apophysitis: child & parent perceptions. Health Qual Life Outcomes 14:95
Johnson AW, Weiss CB Jr, Stento K et al (2001) Stress fractures of the sacrum. An atypical cause of low back pain in the female athlete. Am J Sports Med 29:498–508
Kaplan H, Kiral A, Kuskucu M et al (1998) Report of eight cases of humeral fractures following the throwing of hand grenades. Arch Orthop Trauma Surg 117:50–52
Keats TE (1990) Radiology of musculoskeletal stress injury. Year Book Medical Publishers, Chicago, p p13
Keats TE, Anderson MW (2012) Atlas of normal roentgen variants that may simulate disease, 9th edn. Mosby Inc, St Louis
Kijowski R, De Smet A (2005) MRI findings in osteochondritis dissecans of the capitellum with surgical correlation. AJR Am J Roentgenol 185:1453–1459
Kijowski R, Choi J, Mukharjee R, De Smet A (2007) Significance of radiographic abnormalities in patients with tibial stress injuries: correlation with magnetic resonance imaging. Skelet Radiol 36: 633–640
Kiuru MJ, Pihlajamaki HK, Hietanen HJ, Ahovuo JA (2002) MR imaging, bone scintigraphy, and radiography in bone stress injuries of the pelvis and the lower extremity. Acta Radiol 43:207–212
Kiuru MJ, Pihlajamaki H, Kijowski R, Choi J, Mukharjee R, De Smet A (2007) Significance of radiographic abnormalities in patients with tibial stress injuries: correlation with magnetic resonance imaging. Skelet Radiol 36:633–640
Klasson SC, Vande Schilden JL, Park JP (1993) Late effect of isolated avulsion fractures of the lesser tubercle of the humerus in children: report of two cases. J Bone Joint Surg Am 75A:1691–1694
Kontogeorgakos VA, Xenakis T, Papachristou D et al (2009) Cortical desmoid and the four clinical scenarios. Arch Orthop Trauma Surg 129:779–785
Kox LS, Kraan RBJ, Mazzoli V, Mens MA, Kerkhoffs GMJJ, Nederveen AJ, Maas M (2020) It's a thin line: development and validation of Dixon MRI-based semi-quantitative assessment of stress-related bone marrow edema in the wrists of young gymnasts and non-gymnasts. Eur Radiol 30(3):1534–1543
Lagerbäck T, Elkan P, Möller H et al (2015) An observational study on the outcome after surgery for lumbar disc herniation in adolescents compared with adults based on the Swedish Spine Register. Spine J 15:1241–1247
Launay F (2015) Sports-related overuse injuries in children. Orthop Traumatol Surg Res 101(1 Suppl):S139–S147
Lefere M, Demeyere A, Vanhoenacker F (2021) Overuse bone trauma and stress fractures. Med Radiol https://doi.org/10.1007/174_2020_240
Letts M, Smallman T, Afanasiev R et al (1986) Fracture of the pars interarticularis in adolescent athletes: a clinical-biomechanical analysis. J Pediatr Orthop 6:40–46
Letts M, Davidson D, Ahmer A (2003a) Osteochondritis dissecans of the talus in children. J Pediatr Orthop 23:617–625
Letts M, Davidson D, Mukhtar I (2003b) Surgical management of chronic lateral ankle instability in adolescents. J Pediatr Orthop 23:392–397
Liebling MS, Berdon WE, Ruzal-Shapiro C et al (1995) Gymnast's wrist (pseudorickets growth plate abnormality) in adolescent athletes: findings on plain films and MR imaging. AJR Am J Roentgenol 164: 157–159
Lokiec F, Weintroub S (1998) Calcaneal osteochondritis: a new overuse injury. J Pediatr Orthop 17:243–245
Lunkiewicz M, Davies AM, Anderson SE (2021) Pseudotumors in sports. Med Radiol https://doi.org/10.1007/174_2020_270
Mannor DA, Lindenfield TN (2000) Spinal process apophysitis mimics spondylolysis. Am J Sports Med 28:257–260

Markowitz RI, Davidson RS, Harty MP et al (1992) Sonography of the elbow in infants and children. AJR Am J Roentgenol 159:829–833
Matzkin E, Singer DI (2000) Scaphoid stress fracture in a 13-year-old gymnast: a case report. J Hand Surg [Am] 25A:710–713
May DA, Disler DG, Jones EA et al (2000) Using sonography to diagnose an unossified medial epicondyle avulsion in a child. AJR Am J Roentgenol 174: 1115–1117
McCarthy SM, Ogden JA (1982) Radiology of postnatal skeletal development: VI. Elbow joint, proximal radius and ulna. Skelet Radiol 9:17–26
McCormack AP, Varner KE, Marymont JV (2003) Surgical treatment for posterior tibial tendonitis in young competitive athletes. Foot Ankle Int 24: 535–538
Micheli LJ (1979) Low back pain in the adolescent: differential diagnosis. Am J Sports Med 7:362–364
Micheli LJ (1983) Back injuries in dancers. Clin Sports Med 2:473–484
Micheli LJ (1985) Back injuries in gymnastics. Clin Sports Med 4:85–93
Ogawa K, Takahashi M (1997) Long-term outcome of isolated lesser tuberosity fractures of the humerus. J Trauma 42:955–959
Omey ML, Micheli LJ, Gerbino PG (2000) Idiopathic scoliosis and spondylolysis in the female athlete. Clin Orthop 372:74–84
Oshlag BL, Ray TR (2016) Elbow injuries in the young throwing athlete. Curr Sports Med Rep 15:325–329
Pannu GS, Herman M (2015) Distal radius-ulna fractures in children. Orthop Clin North Am 46(2):235–248
Pappas AM (1982) Elbow problems associated with baseball during childhood and adolescence. Clin Orthop 164:30–41
Paschal SO, Hutton KS, Weatherall PT (1995) Isolated avulsion fracture of the lesser tuberosity of the humerus in adolescents: a report of two cases. J Bone Joint Surg Am 77A:1427–1430
Peace KA, Hillier JC, Hulme A, Healy JC (2004) MRI features of posterior ankle impingement syndrome in ballet dancers: a review of 25 cases. Clin Radiol 59(11):1025–1033
Pennock AT, Dwek J, Levy E, Stearns P, Manning J, Morgan Dennis M, Davis-Juarez A, Bastrom T, Taylor KS (2018) Shoulder MRI abnormalities in asymptomatic little league baseball players. Orthop J Sports Med 6(2):2325967118756825
Posadzy M, Vanhoenacker C, Vanhoenacker F (2018) Köhler de l'os naviculaire: pathologie ou variante d'ossification? Ortho-Rhumato 16(5):62–64
Posch TJ, Puckett ML (1998) Marrow MR signal abnormality associated with bilateral avulsive cortical irregularities in a gymnast. Skelet Radiol 27:511–514
Priest JD, Weise DJ (1981) Elbow injury in women's gymnastics. Am J Sports Med 9:288–295
Priest JD, Jones HH, Nagel DA (1974) Elbow injuries in highly skilled tennis players. J Sports Med 2:137–149
Rask MR, Steinberg LH (1978) Fracture of the acromion caused by muscle forces: a case report. J Bone Joint Surg Am 60A:1146–1147
Rassi GE, Takemitsu M, Woratanarat P et al (2005) Lumbar spondylolysis in pediatric and adolescent soccer players. Am J Sports Med 33:1688–1693
Read MTF (1981) Stress fractures of the distal radius in adolescent gymnasts. Br J Sports Med 15: 272–276
Resnick D, Greenway G (1982) Distal femoral cortical defects, irregularities and excavations. Radiology 143:345–354
Rohren EM, Kosarek FJ, Helms CA (2001) Discoid lateral meniscus and the frequency of meniscal tears. Skelet Radiol 30:316–320
Rossi F, Dragoni S (2001) Acute avulsion fractures of the pelvis in adolescent competitive athletes: prevalence, location and sports distribution of 203 cases collected. Skelet Radiol 30:127–131
Roy S, Caine D, Singer KM (1985) Stress changes of the distal radial epiphysis in young gymnasts. Am J Sports Med 13:301–308
Schenk RC, Goodnight JM (1996) Current concepts review: osteochondritis dissecans. J Bone Joint Surg Am 78A:439–456
Shabat S, Sampson KB, Mann G et al (2002) Stress fractures of the medial malleolus: review of the literature and report of a 15-year-old elite gymnast. Foot Ankle Int 23:647–650
Shah MK, Stewart GW (2002) Sacral stress fractures: an unusual cause of low back pain in an athlete. Spine 27:E104–E108
Silberstein MJ, Brodeur AE, Graviss ER (1979) Some vagaries of the capitellum. J Bone Joint Surg Am 61A:244–247
Silberstein MJ, Brodeur AE, Graviss ER et al (1981) Some vagaries of the olecranon. J Bone Joint Surg Am 63A:722–725
Silberstein MJ, Brodeur AE, Graviss ER (1982a) Some vagaries of the lateral epicondyle. J Bone Joint Surg Am 64A:444–448
Silberstein MJ, Brodeur AE, Graviss ER (1982b) Some vagaries of the radial head and neck. J Bone Joint Surg Am 64A:1153–1157
Singer KM, Roy SP (1984) Osteochondrosis of the humeral capitellum. Am J Sports Med 12:351–360
Sofka CM, Potter HG (2002) Imaging of elbow injuries in the child and adult athlete. Radiol Clin N Am 40:251–265
Soler T, Calderon C (2000) The prevalence of spondylolysis in the Spanish elite athlete. Am J Sports Med 28:57–62
Strömqvist F, Strömqvist B, Jönsson B et al (2016) Lumbar disc herniation surgery in children: outcome and gender differences. Eur Spine J 25:657–663
Sugalski MT, Hyman JE, Ahmad CS (2004) Avulsion fracture of the lesser tuberosity in an adolescent baseball pitcher: a case report. Am J Sports Med 32: 793–796

Sundar M, Carty H (1994) Avulsion fractures of the pelvis in children: a report of 32 fractures and their outcome. Skelet Radiol 23:85–90

Sward L, Hellstrom M, Jacobsson B et al (1990) Acute injury of the vertebral ring apophysis and intervertebral disc in adolescent gymnasts. Spine 15:144–146

Sward L, Hellstrom M, Jaconsson B et al (1991) Disc degeneration and associated abnormalities of the spine in elite gymnasts: a MR imaging study. Spine 16:437–443

Tarkin IS, Morganti CM, Zillmer DA et al (2005) Rotator cuff tears in adolescent athletes. Am J Sports Med 33:596–601

Theologis TN, Epps H, Latz K et al (1997) Isolated fractures of the lesser trochanter in children. Injury 28:363–364

Toomayan GA, Holman WR, Major NM et al (2006) Sensitivity of MR arthrography in the evaluation of acetabular labral tears. AJR Am J Roentgenol 449-53(28):186

Torg JS, Moyer RA (1977) Non-union of a stress fracture through the olecranon epiphyseal plate observed in an adolescent baseball pitcher: a case report. J Bone Joint Surg Am 59A:264–265

Tshering-Vogel D, Waldherr C, Schindera ST, Steinbach LS, Stauffer E, Anderson SE (2005) Adductor insertion avulsion syndrome, “thigh splints”: relevance of radiological follow-up. Skelet Radiol 34:355–358

Tullos HS, Fain RH (1974) Little League shoulder: rotational stress fracture of the proximal epiphysis. J Sports Med 2:152

Tullos HS, King JW (1972) Lesions of the pitching arm in adolescents. JAMA 220:264–271

Ulmer JL, Elster AD, Mathews VP et al (1995) Lumbar spondylolysis: reactive changes seen in adjacent pedicles on MR images. AJR Am J Roentgenol 164:429–433

Van de Perre S, Vanhoenacker F, De Schepper AM (2003) Thigh splints in a skeletally immature boy. Rofo Forschr Geb Rontgenstr Neuen Bildgeb Verfahr 175(11):1582–1584

Vanhoenacker FM, Bernaerts A, Gielen J et al (2002) Trauma of the pediatric ankle and foot. JBR-BTR 85:212–218

Vanhoenacker FM, Snoeckx A, Gielen JL et al (2005) Imaging of muscle injuries in children and adolescents. Vlaams Tijdschrift Sportgeneeskunde en Wetenschappen 101:39–41

Wang H, Zhang Z, Zhou Y (2016) Irregular alteration of facet orientation in lumbar segments: possible role in pathology of lumbar disc herniation in adolescents. World Neurosurg 86:321–327

Warren MP, Brooks-Gunn J, Hamilton LH, Warren LF, Hamilton WG (1986) Scoliosis and fractures in young ballet dancers. Relation to delayed menarche and secondary amenorrhea. N Engl J Med 314:1348–1353

Waterman BR, Belmont PJ, Owens BD (2012) Patellar dislocation in the United States: role of sex, age, race, and athletic participation. J Knee Surg 25(01):051–058

Wilkerson RD, Johns JC (1990) Nonunion of an olecranon stress fracture in an adolescent gymnast. Am J Sports Med 18:432–434

Yamazaki T, Maruoka S, Takahashi S, Saito H, Takase K, Nakamura M (1995) Sakamoto KMR findings of avulsive cortical irregularity of the distal femur. Skelet Radiol 24(1):43–46

Zukotynski K, Curtis C, Grant FD, Micheli L, Treves ST (2010) The value of SPECT in the detection of stress injury to the pars interarticularis in patients with low back pain. J Orthop Surg Res 5:13

The Aging Athlete

Eva Llopis, Maria Pilar Aparisi Gómez,
Fernando Idoate, and Mario Padrón

Contents

E. Llopis (✉)
Department of Radiology,
Hospital de la Ribera, Valencia, Spain
e-mail: evallopis@gmail.com

M. P. Aparisi Gómez
Department of Radiology/Department of Ultrasound,
National Women's Hospital, Auckland City Hospital,
Greenlane Clinical Center, Auckland District Health
Board, Auckland, New Zealand

Department of Radiology, Hospital Vithas
Nueve de Octubre, Valencia, Spain
e-mail: pilucaparisi@yahoo.es

F. Idoate
Departamento de Radiologia,
Mutua Navarra, Pamplona, Spain
e-mail: fidoate@gmail.com

M. Padrón
Clínica Cemtro, Madrid, Spain
e-mail: mario.padron@clinicacemtro.com

Abstract

Aging is an unavoidable process but the benefits of regular exercise have been proven to have a major impact on maintaining quality of life. A combination of factors at cellular and molecular level, the presence of conditions such as obesity or malalignment problems, together with a history of past injuries (cartilaginous, ligamentous, meniscal as examples) and the distribution of load depending on the type of sporting activity will result in different risks of developing lesions with aging. There is a significant overlap between findings secondary to normal degenerative processes and those that may be symptomatic.

The role of imaging consists of the detection and characterization of injuries that may benefit from treatment or correction through clinical intervention.

In this chapter, we provide an overview of the sport injuries that affect the aging

Med Radiol Diagn Imaging (2021)
https://doi.org/10.1007/174_2020_265, © Springer Nature Switzerland AG
Published Online: 12 March 2021

population. With this purpose, we describe the long-term effects of joint derangement and injury to the muscle and tendon, including some tips on how to discern possible normal findings related to aging processes from those amenable to clinical intervention. As part of the analysis of the particularities of the aging athlete we also review the impact that sporting activity has on bone health and sarcopenia.

1 Introduction

Our society has become fitness oriented; participation in sports has increased over recent decades. The benefits of exercises are extensive and many of the physiological consequences of aging may be mitigated or reversed by regular exercise.

Physical exercise is the most recommended non-pharmacological intervention for osteoarthritis patients, based on the existing evidence supporting that it reduces pain and enhances function of osteoarthritic joints (Soto-Quijano 2017; Rausch Osthoff et al. 2018). Recent evidence also establishes a strong link between obesity, metabolic syndrome, and nutrition and the incidence of OA (Bortoluzzi et al. 2018).

The greatest threat to the health of the aging athlete is not the aging process itself but rather inactivity (Menard and Stanish 1989).

Aging athletes can be divided into those that wish to remain active as they age, weekend warriors, and some of those who have never before exercised and practiced sports.

The American College of Sports Medicine/American Heart Association consider that their "old age" guidelines should apply to individuals aged 65 years or older, but also extend them to adults aged 50–64 with significant chronic conditions or functional limitations (Chodzko-Zajko et al. 2009). However, what represents a "senior athlete" will depend on the sport and events. The World Masters Athletics includes athletes over 35, whereas the Senior Professional Golf Association includes players older than 50. The International Tennis Federation has a cutoff for young senior divisions at 35 years (Brun 2016).

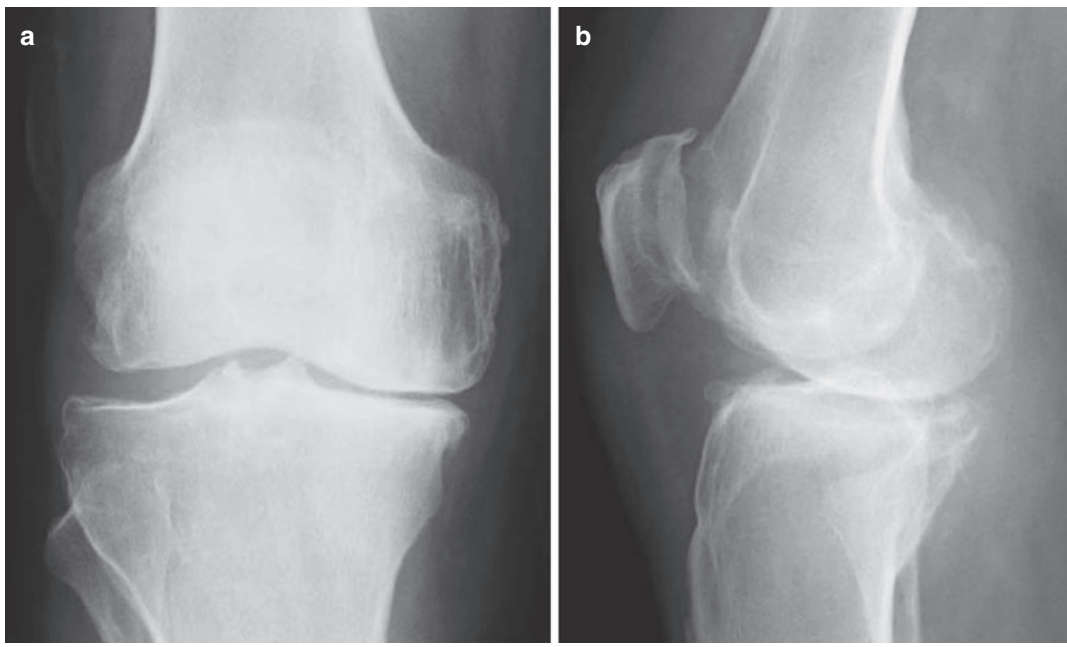

Fig. 1 (**a**, **b**) Knee osteoarthritis in 50-year-old soccer player. (**a**) AP and (**b**) lateral standard radiograph. Joint space narrowing especially at the medial femorotibial and patellofemoral compartments, subchondral sclerosis, and osteophyte formation

Table 1 Radiological musculoskeletal manifestation of normal aging vs. pathologic aging

	Normal aging	Pathologic aging
Bone	Decreased bone density	Stress insufficiency fractures Bone marrow edema
Articular cartilage	Chondromalacia	Osteochondral lesions
Meniscus and fibrocartilage	*Knee* Intrasubstance degeneration Meniscus horizontal tears *Wrist* Triangular fibrocartilage tear type II	*Knee* Radial, vertical, complex, or displaced meniscal tears *Wrist* Ulnar site attachment tears Bone marrow edema and osteochondral associated injuries
Ligament and tendons	Mucoid degeneration of major ligaments, ACL, PCL Mild increased intratendon signal, peritendinitis	Total disruption of fibers Thicker tendon Tears
Muscle	Muscle weakness Musculotendinous unit loss of flexibility	Acute muscular strains or tears Musculotendinous unit rupture

Injuries may result from acute trauma ("macrotrauma"), insidious overuse injuries ("microtrauma"), or a combination of these two mechanisms, although older athletes experience a lower incidence of acute traumatic injuries (Armsey and Hosey 2004; Chen et al. 2005). The risk of lesions is from their current program and past indiscretions (Menard and Stanish 1989). Injuries of master-level practitioners reflect the impact of tissue aging (degenerative disease), repetitive joint stresses (chronic overuse injuries), or long-term effects of athletic injuries (Bert and Gasser 2002; Wolf and Amendola 2005).

The aim of this chapter is to provide an overview of the different specific injuries that aging athletes can sustain, to help to differentiate "normal" from pathological aging, to identify radiological findings that are clearly associated with symptoms or disability, and to provide some guidelines to help the practitioner respond more effectively to each individual patient (Table 1).

2 Impact of Osteoarthritis in Sport Activities: Risk and Consequences

Osteoarthritis (OA) is the progressive loss of normal cartilage structure and function, and involves all the joint tissues, bone, capsule, synovium, and cartilage (Wolf and Amendola 2005). With age, chondrocyte numbers decline. Lower turnover in the cartilage results in a decrease in maintenance capacity, with structural changes in the collagen that increase tissue stiffness. The content of proteoglycans in cartilage changes in response to mechanical loading. Moderate loading results in hypertrophy, and reduced loading in atrophy. In cases of mechanical overload there is proteoglycan loss, and irreversible cartilage damage. Thus, age is a predisposing factor for OA, but mechanical overload acts as a triggering event (Jørgensen et al. 2017).

There are multiple risk factors for osteoarthritis (OA) (Gessel and Harrast 2019) (Table 2), so determining whether an athlete's OA is due to participation in sports or other factors is difficult, and possible cause and effect between sport and osteoarthritis in the aging athlete is still controversial (Tran et al. 2016). A recent systematic review (Runhaar et al. 2015) concluded that the risk of developing osteoarthritis seems to be moderately increased with sporting participation, but mainly linked to the risk of joint injury.

A strong link has been established between obesity, metabolic syndrome, and nutrition and the incidence of OA (Bortoluzzi et al. 2018).

The joints that are particularly susceptible to OA in the general population are those involved in load bearing and a history of high sports participation increases the risk of osteoarthritis. The

Table 2 Risks for osteoarthritis

Non-modifiable	Modifiable
Age >50	Obesity
Strong family history of OA	Propensity to injury
Female	Poor biomechanics
Postmenopausal	Occupational load
Previous joint injury	Sport participation

type of sport is an important factor in the subsequent risk of OA, with high-impact sports being more detrimental. A group of sports with minimal joint impact and torsional loading (walking, swimming, water aerobics, stationary cycling, golf, Tai Chi) have been seen to increase osteophyte formation, but do not increase the risk of osteoarthritis in the context of normal joints and neuromuscular function (Soto-Quijano 2017).

Top athletes that competed in endurance (competitive running, cross-country, skiing), team (soccer, basketball, hockey), or power sports (boxing, wrestling, weight lifting) demonstrate an increase in hip and knee OA, with higher rates in team and power athletes. The risk increases in cases of abnormal joint anatomy or alignment (dysplasias, instability), previous injuries, or background of surgery, when there is neuromuscular impairment or inadequate muscle strength (Bennell et al. 2011).

For some sports, such as running, there has long been controversy as to the role of exercise and the risk of OA; a recent systematic review and meta-analysis of 16 studies concludes that recreational runners have a lower occurrence of hip and knee osteoarthritis compared with competitive runners and controls, but it is not possible to determine whether this association is causative or could be confounded by risk factors such as the incidence of injuries (Alentorn-Geli et al. 2017).

Among the throwing sports MRI revealed increased numbers of rotator cuff tears and acromioclavicular OA in the dominant arm compared with the nondominant limb. In addition, those athletes also displayed radiographic evidence of elbow OA. Increased hand OA has been found in rock climbers.

Chronic tendinosis is related to microtrauma to the tendons, and is therefore more frequent in the adult athlete population. Rotator cuff tendinosis, medial epicondylitis, or wrist tendon tendinosis is common in golfers. Achilles tendinosis is the most common injury in joggers. Lateral epicondylitis is more common in middle-age racquetball players (Chung and Kim 2003; Potter et al. 2004).

Furthermore, the effects of changes due to OA on different joints in the body have different implications for participants in different sports. Degenerative changes to any of the lower extremity joints will be poorly tolerated by those participating in running, cutting, or pivoting sports, such as basketball, football, soccer, and tennis. OA in the shoulder, elbow, wrist, or hands is likely to be well tolerated unless the sport involves some overhead activity. Overhead athletes such as tennis and baseball players or swimmers would be far less tolerant to OA changes involving the upper extremity especially in the dominant arm.

The number of master female athletes has also increased. The majority of injuries sustained by female athletes are due to participation in the sport rather than their sex, but there are anatomic, hormonal, and functional differences between the sexes which must be considered (Ireland and Ott 2004).

Imaging evaluation of early cartilage damage is important for treatment options; focal disease has a different therapeutic approach than diffuse cartilage disease. MRI is a useful tool for the evaluation of subtle OA on cartilage-specific sequences due to its high soft-tissue contrast, and it is currently the most important tool for osteoarthritis research. It allows the assessment of structural and symptomatic changes, relevant for longitudinal studies. Radiographs are a late-stage imaging method and only provide an indirect evaluation, but despite this, plain films remain the most widely available and least expensive imaging method. Joint space narrowing, subchondral sclerosis, subchondral cysts, and osteophytes are classical OA imaging features. The absence of statistical correlation between the severity of the joint degeneration and the high prevalence of asymptomatic imaging findings makes a diagnostic dilemma in determining the cause of the pain.

Subchondral bone marrow lesions (BMLs) on MRI or "edema-like MRI abnormalities" have been seen to be associated with the presence of pain as a symptom.

Bone marrow edema is defined on MRI as ill-defined hyperintensities on STIR images and on fat-suppressed T2-weighted MR images (see Vanhoenacker 2021). These hyperintensities on histopathological examination show fibrosis, areas of osteonecrosis, bony remodeling, and only little real edema. Therefore, some authors have suggested using the term "ill-defined signal intensity abnormality" or "edema-like MRI abnormality" to describe bone marrow lesions. More specific concomitant abnormalities must be ruled out, such as trabecular fracture demonstrated as a well-defined hypointense line within a high signal area (Fig. 2).

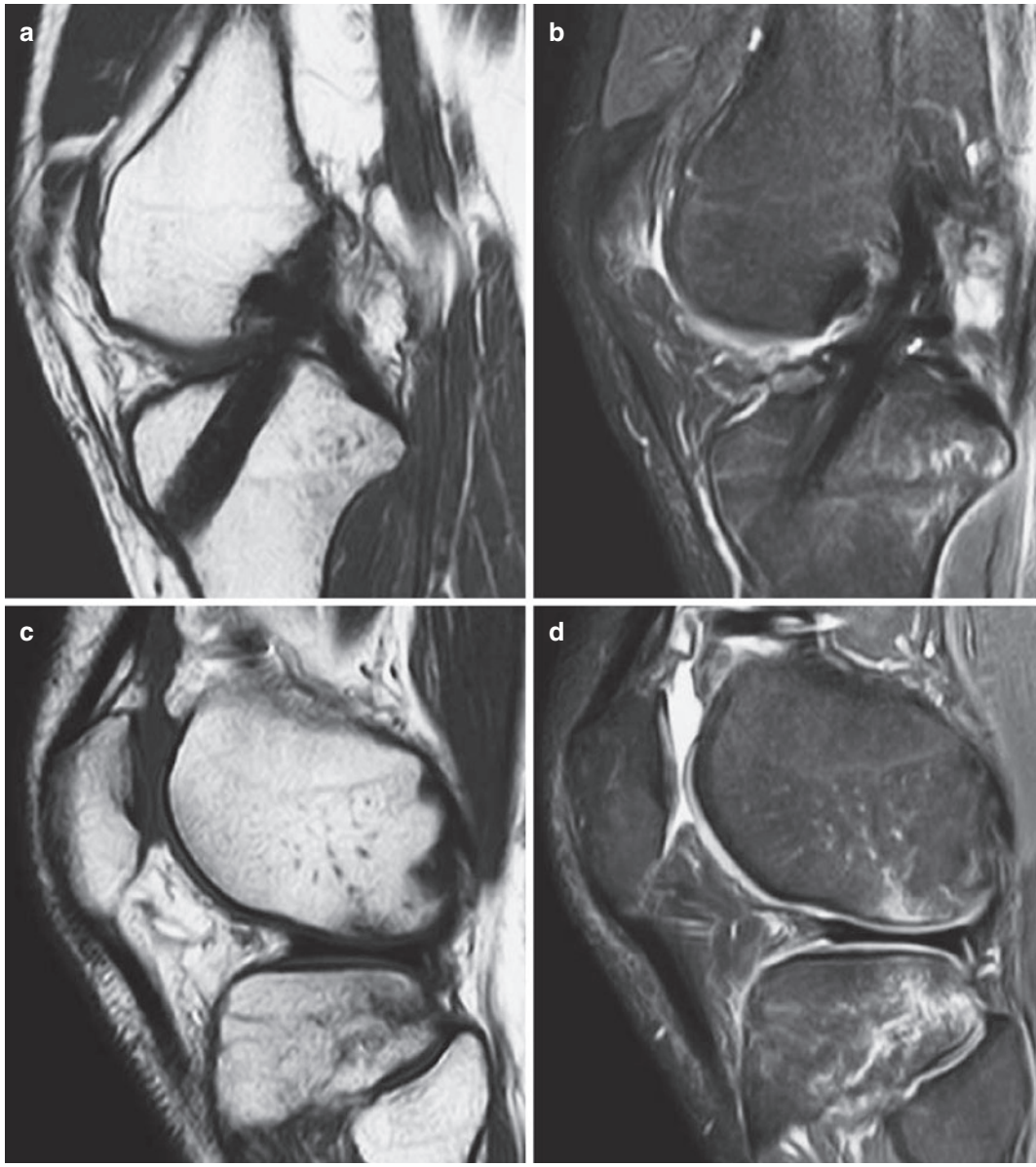

Fig. 2 (**a**–**d**) Trabecular fracture in a 39-year-old man soccer player after a twisting knee motion. Previous history included ACL graft reconstruction. (**a**, **c**) Sagittal FSE T1-weighted MR images and (**b**, **d**) sagittal SE proton-density MR images. The course, signal intensity, and morphology of the ACL graft are normal. More lateral images—however—show bone marrow edema at the posterolateral tibial plateau and in the subchondral area of the lateral femoral condyle surrounding two hypointense linear foci, indicative of trabecular fractures (black arrow)

Recently, derived from the use of MRI, artificial intelligence (AI), with its potential to extract new analytic algorithms, has been applied to the study of OA, but is still at a stage in which it requires further research and validation (Hayashi et al. 2019).

3 Long-Term Joint Injuries

Joint injury during sports activities is frequent, and can be secondary to a single acute trauma or secondary to repetitive loads and microtrauma during sport participation. A history of joint injury increases the incidence rate of joint OA but does not affect the rate of progression of OA. Recently, the tissue homeostasis theory as a model that maintains knee function was introduced. The range of loads that a joint can accept, transfer, and dissipate without failure is represented by an area that can be termed the envelope of function. The envelope of function for a given injured joint can vary significantly and reduces with aging. Loading outside of this threshold induces a loss of tissue homeostasis, resulting in injury (Bartz and Laudicina 2005).

Long-term consequences of the most frequent associated sport injuries are reviewed in this chapter.

3.1 Lower Extremity: Knee

Knee injuries are frequent and associated with contact and noncontact sports, often related to a twisting or pivoting episode and repetitive athletic activity loading.

A recent meta-analysis of 15 studies suggests that the prevalence of knee osteoarthritis in former athletes is as high as 30%, but points out that heterogeneity in the diagnostic criteria and type of sports may have an impact on this estimation and high-quality studies are still needed (Madaleno et al. 2018).

3.1.1 Knee: ACL

ACL injury has a drastic effect on an athlete's ability to perform sports; however there is little consensus on the long-term consequences of isolated ACL tears and the effectiveness of ACL reconstruction on preventing long-term sequelae after an isolated injury. Both surgical and conservative treatment may result in cartilage degeneration and osteoarthritis.

A great number of studies have analyzed the prevalence of OA post-ACL tear. A systematic review found the prevalence of OA in individuals with an isolated ACL injury to be between 0% and 13%, and in individuals with combined injuries, between 21% and 48% (Øiestad et al. 2009). Rates of radiological OA after ACL tears have been shown to be between 16% and 78% (Potter et al. 2012).

The cases in which nonsurgical management is favored or reconstruction is delayed have a higher probability of developing a secondary meniscal tear and being diagnosed with OA compared with patients that choose surgical reconstruction (Sanders et al. 2016).

The current recommendations, especially for athletes returning to pivoting sports, are for early surgery (between 1 and 6 months). The presence of meniscal tears, background of surgery, or performance of meniscectomy at the time of surgical reconstruction of the ACL are the most frequent factors to develop OA (Borchers et al. 2011; Risberg et al. 2016; van Meer et al. 2016). Revision surgery has been found to increase articular cartilage injury compared with primary repair, with higher rates of subsequent OA (Borchers et al. 2011; Kaeding et al. 2015). Overall, approximately 20–50% of patients will have evidence of OA within 10–20 years (Sepúlveda et al. 2017).

Even in older patients, over the age of 50, the ACL can be satisfactorily reconstructed allowing patients to return to sport activity, with outcomes comparable to younger patients (Fig. 2) (O'Neill et al. 2002; Iorio et al. 2018).

Areas of occult bone lesions in the lateral femoral condyle and in the posterolateral corner of the medial plateau are frequently seen on MRI in acute ACL injuries secondary to compressive forces (see Vanhoenacker 2021). However, the most common cartilage lesion in ACL chronic deficient knee is located in the articular surface of

the medial femoral condyle, especially associated with bucket-handle meniscal rupture, while it is infrequent to find lateral femoral condyle cartilage lesion. It is probably due to bone bruise healing in the lateral compartment and persistent rotational instability loading the medial compartment. The presence of a medial femoral condyle osteophyte adjacent to the anterior tibial spine is a radiographic indirect sign of chronic ACL deficiency (Maffulli et al. 2003).

Degenerative changes can occur to the cruciate ligaments with aging. Intrasubstance ganglia, mucoid degeneration, and intraosseous ganglia at the femoral or tibial ACL attachment may be part of a degenerative aging process. MRI findings are fairly specific and should not be mistaken for a tear. MRI of mucoid degeneration shows a mass-like ligament with homogeneous marked increase signal intensity on T2-WI without fiber disruption. McIntyre et al. (2001) concluded, "mucoid degeneration of the ACL must be suspected when an apparently thickened, ill-defined ligament with increased signal intensity, 'celery stick appearance', with absence of discontinuity is identified in a patient with a clinically intact ligament." Clinical significance has to be determined; however pain and restriction to flexion have been reported; those patients respond well to arthroscopic release and notchplasty (McIntyre et al. 2001; Narvekar and Gajjar 2004; Bergin et al. 2004).

3.1.2 Knee: PCL

The natural history and treatment options for PCL rupture are still a matter of debate. PCL injuries may not be benign in the long term. Chronic PCL tears demonstrate a variable progression of articular degeneration and late arthrosis. PCL has a unique feature: it may heal after injury. MRI studies have shown that chronic PCL injuries that develop a continuous low signal intensity pattern on MRI were less unstable. Prognostic factors such as combined injuries predict long-term outcome as well as appropriate treatment. PCL tears without associated intra-articular injury, significant posterior tibial displacement, or multidirectional instability were more likely to remain symptom free, while combined instabilities were more likely to result in a decreasingly functional knee (Bartz and Laudicina 2005; Shelbourne and Muthukaruppan 2005).

The overall incidence of degenerative articular cartilage lesions has been 67.4%, the majority being within the medial femoral condyle. Posterior tibial translation secondary to PCL deficiency alters the kinematics of the knee and results in anterior shifted tibiofemoral contact and increased posterolateral corner stress during knee loading. This unloads the posterior horn of the medial meniscus and leads to increased joint pressure in the anterior medial compartment. The more posterolateral structures involved, the more rotational shift increasing the loads acting on the medial compartment increasing the loads acting on the medial compartment (Strobel et al. 2003; Logan et al. 2004; Bartz and Laudicina 2005).

3.1.3 Knee: Meniscus Tears

Meniscal degeneration contributes to the development of OA. This is caused by various factors, some of them external, like repetitive trauma and malalignment, and some of them internal. Aging is an internal factor, due to cellular and molecular changes. Senescence of the meniscal cells leads to disruption of tissue homeostasis. There is a decreased turnover of collagen, accumulation of glycation end products, and loss of proteoglycans, similar to what happens in cartilage, with an increase in tissue stiffness that raises the risk for tears. Lately, it has been demonstrated that pro-inflammatory factors in joint fluid are also contributory to degeneration (Tsujii et al. 2017).

Athletic activity loads the lateral compartment, especially the anterior horn of the lateral meniscus. Among asymptomatic aging athletes over the age of 50, MR imaging shows a significant number of lateral meniscal anterior horn lesions. Therefore, meniscal tears must be only treated if they are considered to be responsible for the patient's discomfort and it is important to identify those MRI features associated with patient's symptoms.

Horizontal or oblique meniscal tears on MRI are frequently encountered in both asymptomatic and symptomatic knees and do not always

correlate with the patient's symptoms. Radial, vertical, complex, or displaced meniscal tears are found to be more prevalent in symptomatic knees, especially when they have associated collateral ligament, pericapsular soft-tissue strains, or bone marrow abnormalities (Jerosch et al. 1996; Zanetti et al. 2003).

The most common type of tear in the aging population (over 40 years) is degenerative tears. They result from repetitive stress over an aged meniscus, and normally have an insidious onset, with no direct trauma (Feeley and Lau 2018). Degenerative tears are associated with chondral degeneration in 85% of cases (Mesiha et al. 2007).

The development of osteoarthritis is a well-known, relatively frequent adverse outcome of meniscectomy.

After meniscectomy there is an alteration in the load distribution. Medial meniscectomy reduces 50–70% femoral condyle area and leads to a 100% increase in contact stress in the medial compartment. Lateral meniscus meniscectomy has been shown to result in a 40–50% decrease in contact area and a 200–300% increase in contact stress in the lateral compartment (Figs. 3 and 4). Lateral meniscectomy is therefore worse for the biomechanics of the compartment than medial (Klimkiewicz and Shaffer 2002; Bartz and Laudicina 2005). Another of the consequences of arthroscopic partial meniscectomy is an increase in the knee adduction moment (KAM) in the operated leg for up to 1 year after surgery. The adduction moment determines the mediolateral distribution of load across the tibial plateau. Large adduction moments concentrate load on the medial tibiofemoral compartment. Several studies have demonstrated an association between increased KAM and incidence of progression of tibiofemoral OA (Sturnieks et al. 2008; Thorlund et al. 2016). Besides, knee extension and flexion moments also change, with subsequent changes in the load of the patellofemoral joint, also favoring the development of OA (Hall et al. 2015; Thorlund et al. 2016).

A recent systematic review of predictors for the clinical outcome following arthroscopic partial meniscectomy concluded that duration of symptoms for longer than 1 year, presence of OA, resecting more than 50% of the meniscus, and leaving a non-intact meniscal rim (radial resection leading to destruction of the hoop stress function) were associated with worse clinical outcomes following arthroscopic partial meniscectomy. There is moderate evidence that sex, onset of symptoms, type of tear, and sport level before injury do not predict clinical outcome. Evidence was found to be conflicting with regard to age, perioperative chondral damage, and joint alignment (Eijgenraam et al. 2018). They did not consider other associated injuries such as ACL tears or other types of surgical technique, such as meniscal repair or open approaches.

A recent study focused on patients over 60 undergoing medial meniscus partial meniscectomy demonstrated that high BMI ($\geq$26 kg/m^2), an advanced chondral lesion in the medial compartment (Outerbridge grade III or IV), degenerative changes in the patellofemoral joint, and ACL tear or laxity were major predictors for surgical outcome in the elderly age group (Sofu et al. 2016).

An unusual complication of postmeniscectomy is osteonecrosis of the femoral condyle. Its physiopathology is not yet fully understood. The reduction of weight bearing by approximately 50% leads to an increase in tibiofemoral pressure. Altered mechanical force has been suggested to be an etiological factor (Johnson et al. 2000). In the initial phase MRI appearance of postmeniscectomy, osteonecrosis displays a large area of nonspecific intramedullary edema. After 3 months, the edema decreases and the clearly defined central area of necrosis shows high signal intensity on T2-weighted MR images. A subchondral band of low intensity is seen on both pulse sequences, related to a variable portion of impacted and necrotic medullary bone. After this, bone sequestration may occur, loose bodies may develop, or it may resolve with residual flattening of the articular surfaces (Faletti et al. 2002).

The much better understanding of the biomechanical impact of meniscectomy obtained from recent studies has led to the development of

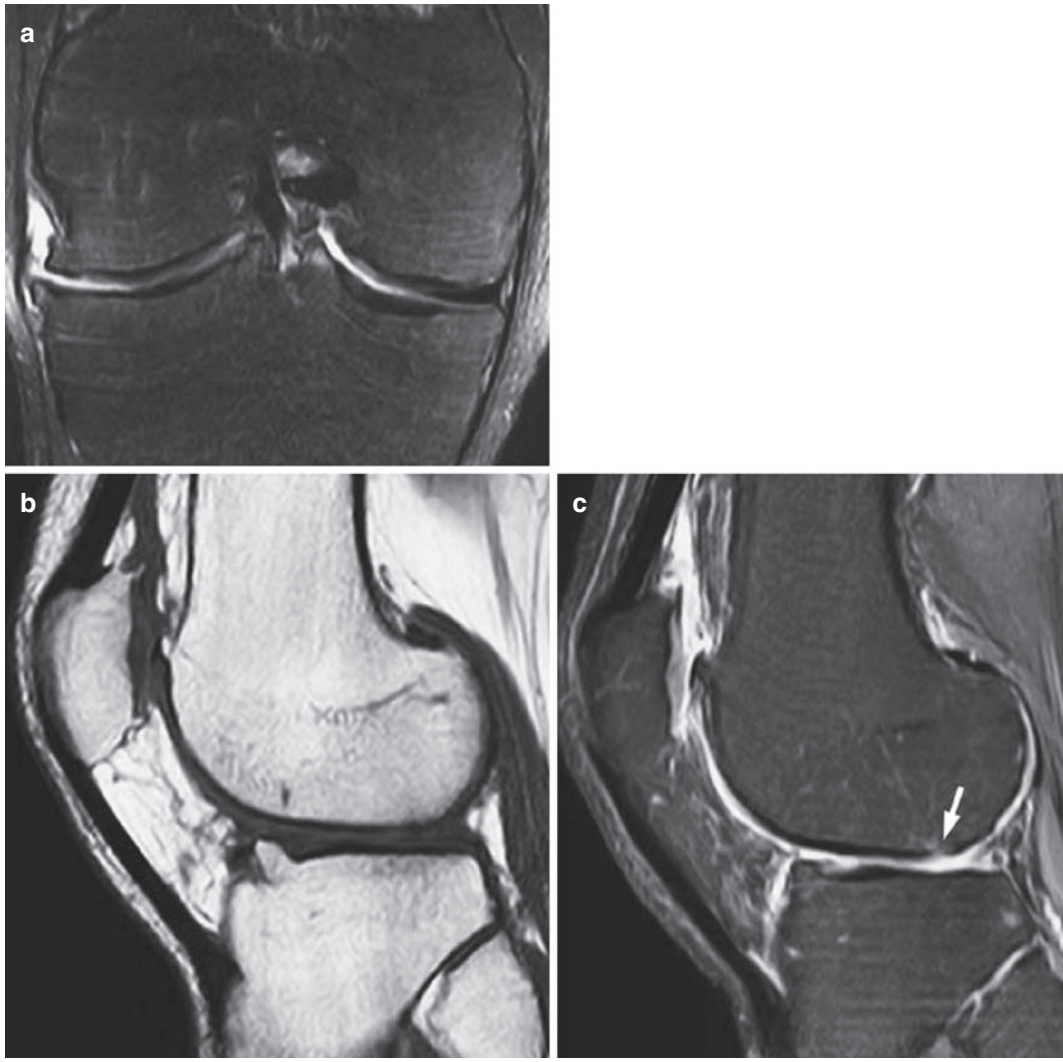

Fig. 3 (**a**–**c**) Post-total meniscectomy osteoarthritis in a 46-year-old male marathon runner. (**a**) Coronal FSE fat-suppressed T2-weighted MR image. Marked decrease of the joint space, waving of the surface of the articular cartilage, and marginal osteophyte formation. (**b**) Sagittal FSE T1-weighted MR image. (**c**) Fat-suppressed proton-density MR images. Note osteophyte formation at the lateral facet of the patella and the anterolateral tibial plateau, and cartilage defect with associated bone marrow edema (grade 5 lesion) at the posterior femoral condyle (white arrow)

surgical techniques aiming at preserving as much meniscal tissue as possible (meniscal repairs). Some studies report an increase in failure rates if the repairs are performed in patients over 40 (Barrett et al. 1998) but others suggest that age does not affect the outcome (Steadman et al. 2015).

Arthroscopic partial meniscectomy remains the preferred technique for the treatment of unstable tears. Current studies suggest that meniscectomy offers a shorter recovery time, earlier return to sport, and less revision surgery than meniscal repair (Feeley and Lau 2018).

Meniscal allograft transplants have also been reported to stop the progression of OA (Drobnič et al. 2019).

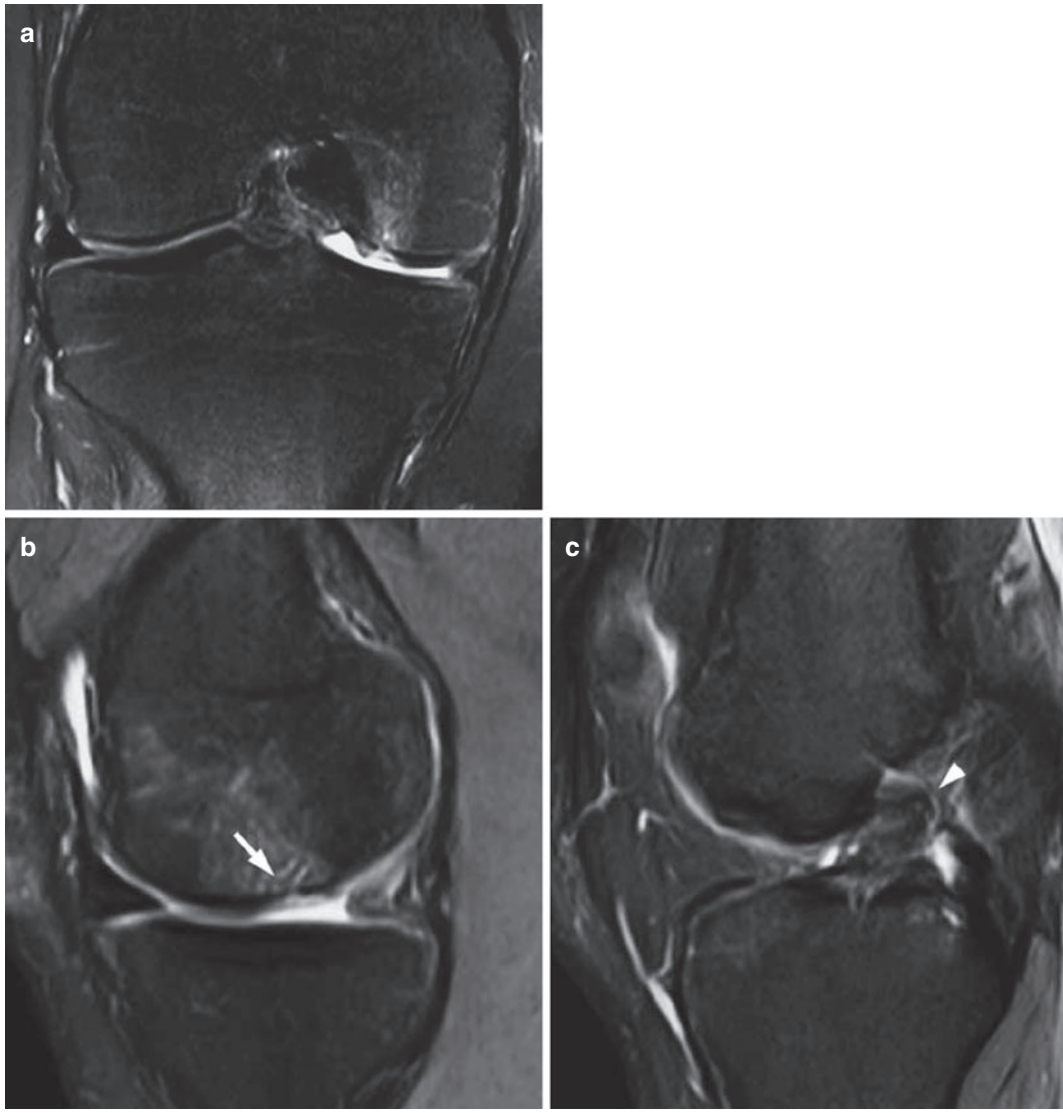

Fig. 4 (**a**–**c**) Post-partial meniscectomy changes, meniscal retear, ACL rupture, and grade 4 cartilage lesion in a 35-year-old basket player. (**a**) Coronal FSE fat-suppressed T2-weighted MR image. (**b**, **c**) Sagittal SE fat-suppressed proton-density MR images. Morphologic changes (blunting and truncation) and increased intrameniscal signal intensity of the posterior horn of the medial meniscus. The retear was confirmed at arthroscopy. A focal cartilage defect with subchondral bone marrow edema is seen at the medial femoral condyle (black arrow). Complete proximal ACL rupture is seen at the level of the intercondylar notch (white arrow)

3.1.4 Articular Cartilage/ Subchondral Bone Injury

The natural history of acute osteochondral or chondral injury to the knee continues to be an object of study.

The subchondral bone is a critical element of the osteochondral unit, and plays an important role in the outcomes from injuries and surgical interventions, as well as in general joint health.

Subchondral bone marrow lesions (BMLs) or "edema-like MRI abnormalities" have been seen to be associated with knee pain in the context of OA.

Sowers et al. (Sowers et al. 2003) demonstrated that in women with full-thickness

articular cartilage defects, if there was bone marrow edema and subchondral bone defect, the likelihood of painful OA was significantly greater than painless OA.

A few years ago, a systematic review of 22 studies suggested moderate evidence associating knee pain with BMLs and effusion/synovitis (Yusuf et al. 2011).

BMLs have been seen to be associated with radiologic progression of joint destruction in the knee (Wluka et al. 2008; Roemer et al. 2010) and with chondral loss (Hunter et al. 2006). This supports the involvement of subchondral bone lesions in OA.

In patients with no trauma, BMLs have been associated with changes in the cartilage in the following 2 years, with the progression of chondral defects seen to be proportional to the size of the lesion (Wluka et al. 2008). In a study with arthroscopic correlation, higher grades of visualized cartilage defects correlated with a higher prevalence and greater depth or cross-sectional area or both of BMLs on MRI (Kijowski et al. 2006).

A relatively recent study showed that MRI signs of cartilage degradation (using quantitative sequences) are directly associated with BML signal intensity (Zhao et al. 2010). Also, subchondral bone uptake on MRI and SPECT/CT (single-photon computed tomography/CT) has been seen to correlate with the grade of overlying cartilage lesions (Maas et al. 2015).

In the setting of early OA changes and varus malalignment, an association between pain in knee OA and presence of BMLs has been proven (Kröner et al. 2007).

However BMLs do not fully explain the presence or absence of knee pain in OA. OA progression is unlikely if bone marrow lesions are absent on MRI (Pessis et al. 2003), but the location of the lesions does not predict reliably the location of pain, suggesting that other factors contribute to pain in OA.

3.2 Lower Extremity: Hip

Osteoarthritis of the hip in athletes is typically the result of cumulative overuse, without specific injury in the majority of cases. It is relatively common, second only to osteoarthritis of the knee. Hip and knee OA has been found to be higher in soccer, football, handball, jumping, and track-and-field sports even without a history of injury, with higher prevalence than age-matched controls. Running, as a recreational activity, has a lower occurrence of OA than competitive running or sedentarism (Alentorn-Geli et al. 2017). Specific risk factors include high loads, sudden or irregular impact, repetitive flexion and internal rotation movements, or preexisting abnormalities such as hip dysplasia, labral tears, or avascular necrosis sequelae. Acute or chronic hip pain presents a diagnostic and therapeutic challenge because of the vague, nonspecific symptoms and signs. Symptoms include pain and lack of range of motion, particularly in internal rotation. The athlete may not specifically complain of pain per se, but rather discomfort or stiffness, usually when starting or after being sedentary (Koh and Dietz 2005; L'Hermette et al. 2006).

Despite the fact that excessive loading to the hip promotes osteoarthritis, it was not until recently that femoroacetabular impingement was associated with the early development of degenerative disease. Femoroacetabular impingement is a condition of abnormal contact between the proximal femur and the acetabulum that may result in lesions of the labrum and cartilage which may progress to osteoarthritis.

Hip arthroscopy is becoming popular and early treatment can alleviate pain and improve function in athletes with OA.

Radiographic features of adult hip dysplasia range from subtle acetabular dysplasia to complex sequelae of development dysplasia. MRI is an accurate method for the diagnosis of hip diseases. MR arthrography is usually performed to assess the acetabular labrum, although its greater accuracy is questioned by some authors. MRI findings include abnormal head-neck or acetabular morphology, juxta-articular cyst formation at the anterosuperior femoral neck, cysts of the acetabular rim, paralabral cyst with or without bone marrow edema, and labral tears (Fig. 5) (Delaunay et al. 1997; Kassarjian et al. 2005; Leunig et al. 2006).

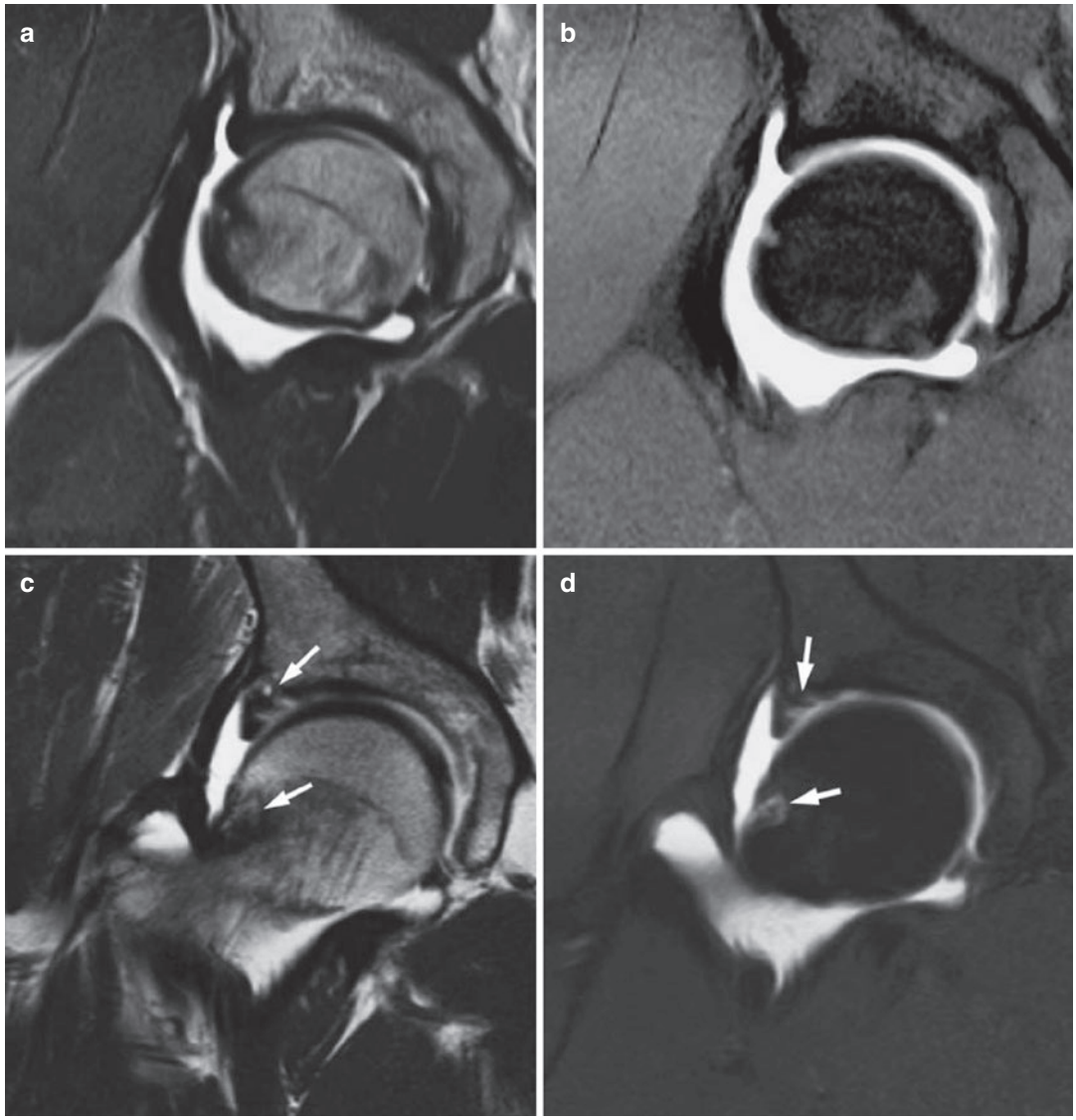

Fig. 5 (**a**–**d**) Femoroacetabular hip impingement. (**a**, **c**) Coronal proton-density direct MR arthrogram. (**b**, **d**) Fat-suppressed T1-weighted direct MR arthrogram. Note a superior labral tear, thickened iliofemoral ligament, and bone marrow edema surrounding a cystic lesion in the femoral head-neck junction (white arrow)

Several recent prospective studies have demonstrated an association between cam morphology and progression to hip OA (Agricola et al. 2013; Thomas et al. 2014; Nelson et al. 2016; Saberi Hosnijeh et al. 2017). The strength of the association depended on the alpha angle. The positive predictive value (PPV) for end-stage OA when having cam morphology within 5 years was 10.9% for an alpha angle >60° and 25.0% for an alpha angle >83° (Agricola et al. 2013).

Also, males participating in high-level-impact sports (basketball, hockey, soccer) are at increased risk of physeal abnormalities of the anterosuperior head-neck junction, resulting in cam deformity at skeletal maturity (Nepple et al. 2015).

A link between pincer morphology (anterior or lateral) and OA has never been identified in epidemiological studies. Moreover, the concurrence of these two morphologies appears to have a protective

effect for the development of end-stage OA (OR 0.34, 95% CI 0.13, 0.87) (Thomas et al. 2014).

However, it is important to mention that there is no role for prophylactic surgery in the asymptomatic hip with anatomy predisposing to impingement; morphology does not mean femoroacetabular impingement, which comprises a range of symptoms and clinical findings.

The labrum is subject to continuous weight-bearing stresses and with age there is an increase in the incidence of asymptomatic tears diagnosed by MR imaging, so imaging findings must be correlated with patient symptoms. The labrum undergoes changes in signal intensity and shape with aging. The shape tends to change from triangular to round and irregular. High signal intensity reflects normal tissue degeneration and may even communicate with the articular surface (Lecouvet et al. 1996; Abe et al. 2000; Mintz et al. 2005). The response to an intra-articular injection of anesthetic is a reliable indicator of intra-articular abnormality (Byrd and Jones 2004).

3.3 Lower Extremity: Ankle

Osteoarthritis of the ankle is more common in professional football, baseball, and soccer players and ballet dancers but not significantly so in high jumpers. Ankle OA can often be asymptomatic (Koh and Dietz 2005).

Osteoarthritis of the ankle is characterized by the formation of impinging bone spurs, loose bodies, and joint space narrowing. Impingement syndromes are painful conditions caused by the friction of joint tissues; they can be classified as anterolateral, anterior, anteromedial, posteromedial, and posterior. Anterior impingement resulting from repetitive dorsiflexion appears typically in soccer players, whereas posterior impingement is more typical in ballet dancers. MR imaging is useful in assessing the distribution of the spurs and osteophytes and detecting bone marrow edema, synovitis, and cartilage lesions (Fig. 6) (Bureau et al. 2000; Cerezal et al. 2003).

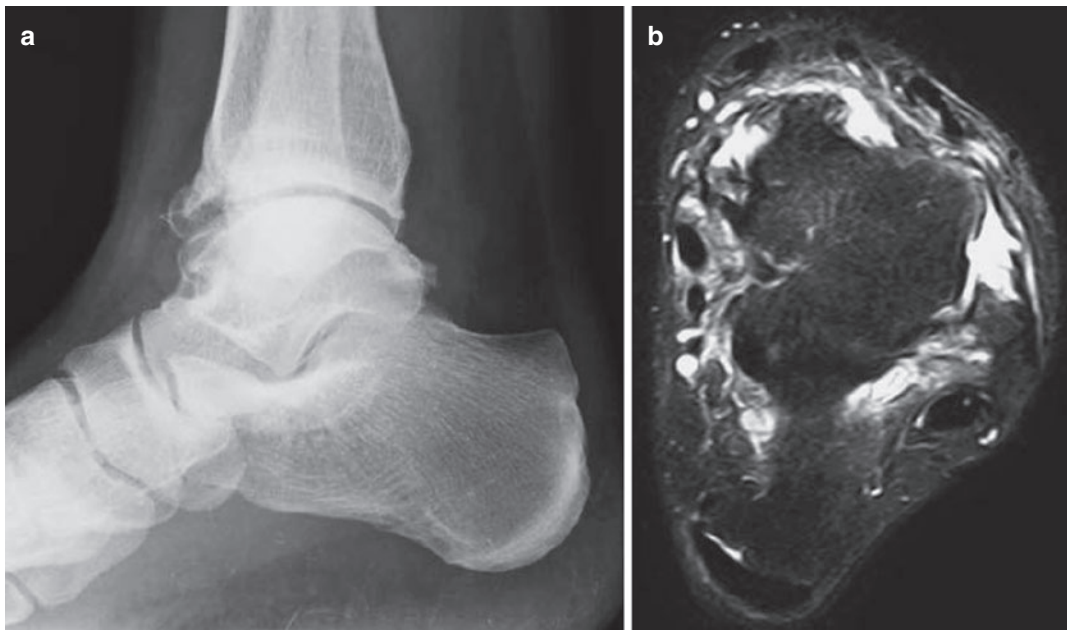

Fig. 6 (**a**–**e**) Ankle osteoarthritis. (**a**) Standard radiograph. (**b**) Axial FSE T1-weighted MR image. (**c**) Axial STIR image. (**d**) Sagittal FSE T1-weighted MR image. (**e**) Sagittal STIR image. Note the anterior tibiotalar spur formation with thickening of the anterior capsule (white arrow), a prominent posterior lateral talar process (double white arrow) with adjacent bone marrow edema and cyst formation, and joint effusion

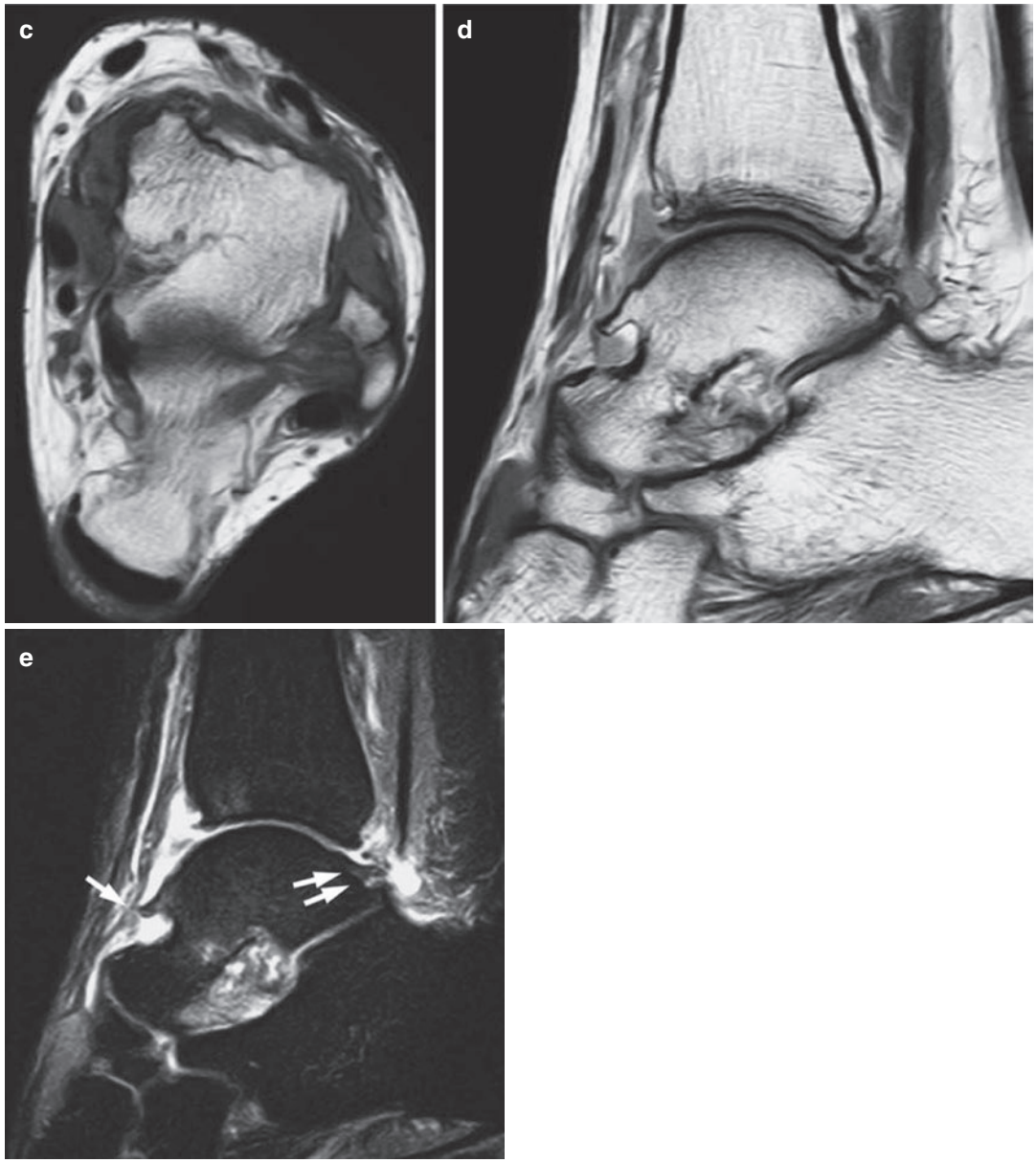

Fig. 6 (continued)

3.4 Upper Extremity: Shoulder

Shoulder pain is a prevalent musculoskeletal symptom, accounting for 16% of all musculoskeletal complaints; the peak age is 45–64 years (Andrews 2005). Shoulder range of motion decreases with aging for all motions except internal rotation. The athletic population such as professional baseball players and tennis players have increased shoulder external rotation and decreased internal rotation in the dominant arm (Barnes et al. 2001). Athletes who train with heavy weights have a higher risk of degenerative changes in the dominant arm (Schmitt et al. 2001). Chronic shoulder pain may result from one of several categories of intra-articular and

extra-articular entities; imaging-guided selective injection of local anesthetic into the subacromial space or acromioclavicular joint helps to localize the origin of the symptoms (Strobel et al. 2003).

Glenohumeral osteoarthritis includes labrum degeneration, cartilage defects, loose bodies, adhesive capsulitis, and osteophytes. A prior shoulder dislocation increases the risk of subsequent shoulder osteoarthritis by 10–20 times compared with an uninjured shoulder. However, how quickly and which patients with instability will worsen in time is unclear and it has not yet been determined whether surgical treatment has an impact on the progression of the degenerative disease (Brophy and Marx 2005).

During repetitive shoulder motion, the rotator cuff can impinge on the coracoacromial arch. Rotator cuff tendinosis represents a combination of mechanical attrition, progression of incompletely healed microtears, and age-related hypovascularity of the supraspinatus tendon and is vulnerable to tearing while playing throwing sports. The cuff tears tend to occur in the anterior supraspinatus tendon (Fig. 7). Another typical injury is the rim rent-type tear just at the insertion onto the greater tuberosity (Tuite 2003; Chen et al. 2005).

Acromioclavicular arthritis manifests as capsular hypertrophy and osteophyte formation. The narrowing of the subacromial space by inferior projecting osteophytes has been associated with subacromial impingement and development of rotator cuff pathology. Radiological acromioclavicular osteoarthrosis is a constant finding in patients over 50 years old. MR imaging shows subchondral cyst formation, osteophytes, and joint effusion, but bone marrow edema in the distal clavicle and acromion and capsular hypertrophy are the only MRI characteristics associated with clinical findings (Fig. 7) (Strobel et al. 2003; Ernberg and Potter 2003).

3.5 Upper Extremity: Elbow

Long-term osteoarthritis changes secondary to repetitive overuse are seen in many throwing athletes. Posterior olecranon osteophytes, osteophytes in the olecranon fossa, coronoid osteophytes, loose bodies, and chondromalacia may be found.

Chronic stress applied to the elbow is the most frequent injury in athletes. Although these entities have been termed "epicondylitis," tendon changes present fibroblastic proliferation with focal hyaline degeneration rather than inflammation; therefore the term tendinosis is recommended (see Bakewell et al. 2020).

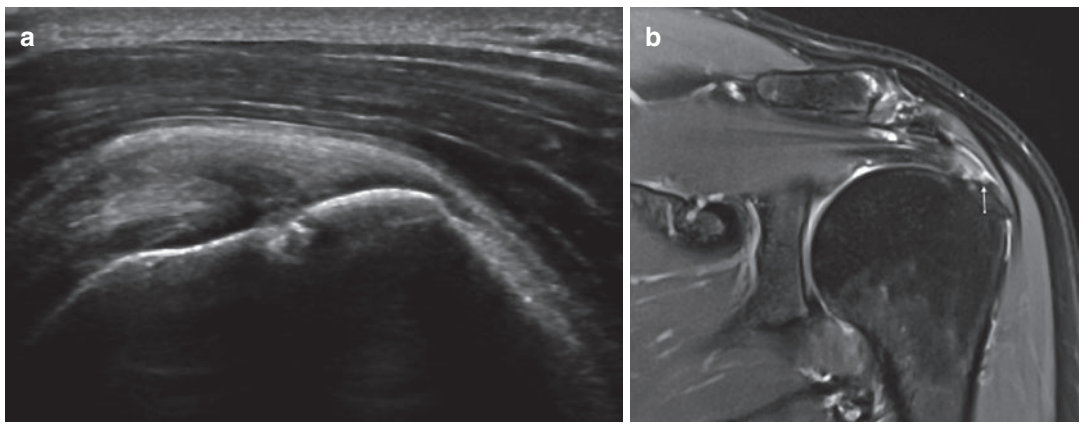

Fig. 7 (**a**, **b**) Small full-thickness supraspinatus tear. (**a**) Ultrasound showing a fluid-filled gap within the supraspinatus; the extension into the subacromial bursa is difficult to show in only one image due to the oblique course of the tear. (**b**) Coronal FSE fat-suppressed T2-weighted MR image shows the small full-thickness supraspinatus tear with fluid extending into the subacromial bursa (arrows). Note the extensive acromioclavicular degenerative changes

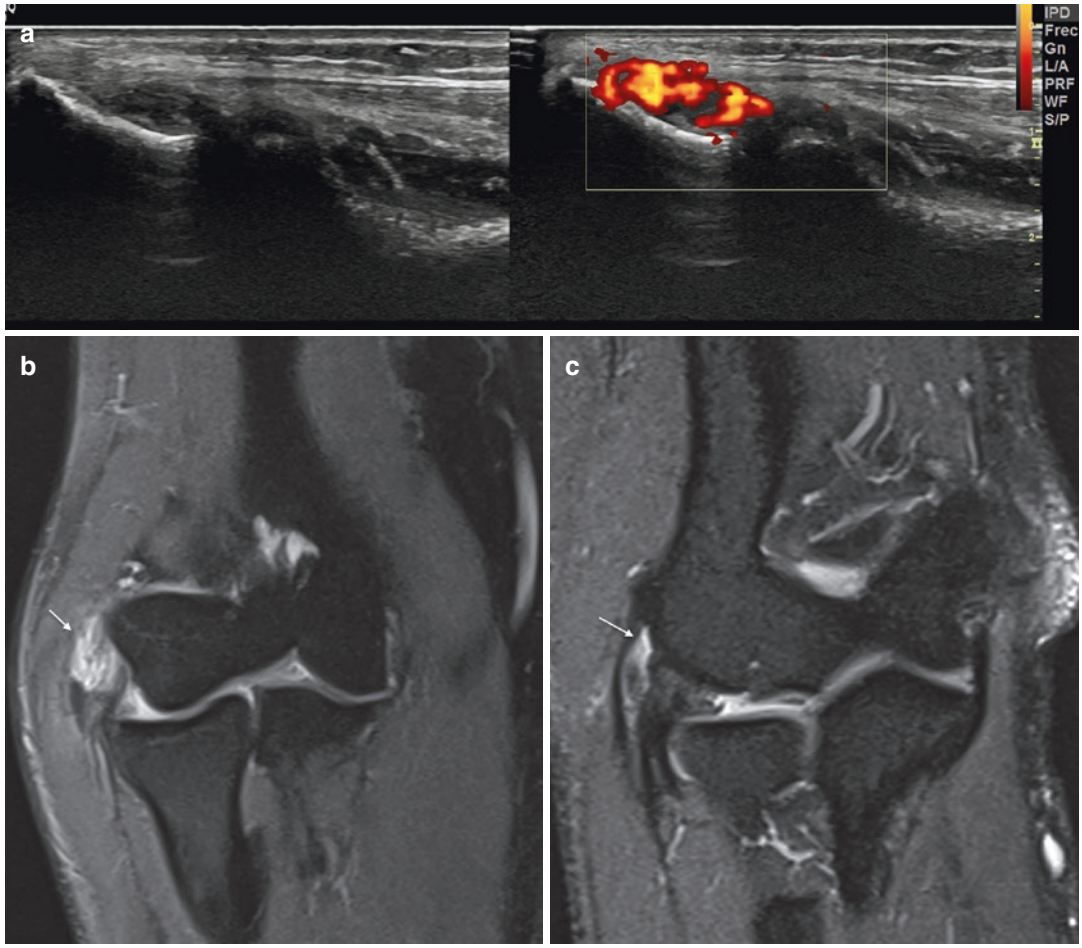

Fig. 8 (**a**–**c**) Chronic elbow common extensor tendinosis and extensive tear in a 48-year-old female golf player. (**a**) US of the elbow showing tear on the extensor common tendon and the color Doppler demonstrating important localized Doppler signal. (**b**, **c**) Corresponding consecutive coronal FSE T2 fat saturation-weighted image showing the extensive tear (white arrow). Note that the radial collateral ligament is normal

In throwing sports high valgus stresses are placed on the medial aspect of the elbow, and involve the pronator teres, flexor carpi radialis, and palmaris longus. Lateral "epicondylitis" is the most common problem in the athlete's elbow; many of the cases occur in non-tennis players, but any sport with overhead arm motion will overuse the extensor muscle. The excessive use of the wrist extensor musculature is associated with lateral "epicondylitis" (tennis, golf, rugby, handball) (Fig. 8) (Chung et al. 2004; Campbell et al. 2013).

3.6 Upper Extremity: Wrist and Hands

Primary osteoarthritis of the wrist is rare. Radiocarpal osteoarthritis is usually secondary to structural changes that are often precipitated by trauma. Traumatic injuries to the wrist are common in the athletic population. Alterations of biomechanics of the carpal bones of the proximal row can lead to the development of radiocarpal osteoarthritis (Koh and Dietz 2005). Racquet sports aggravate pisotriquetral inflammation

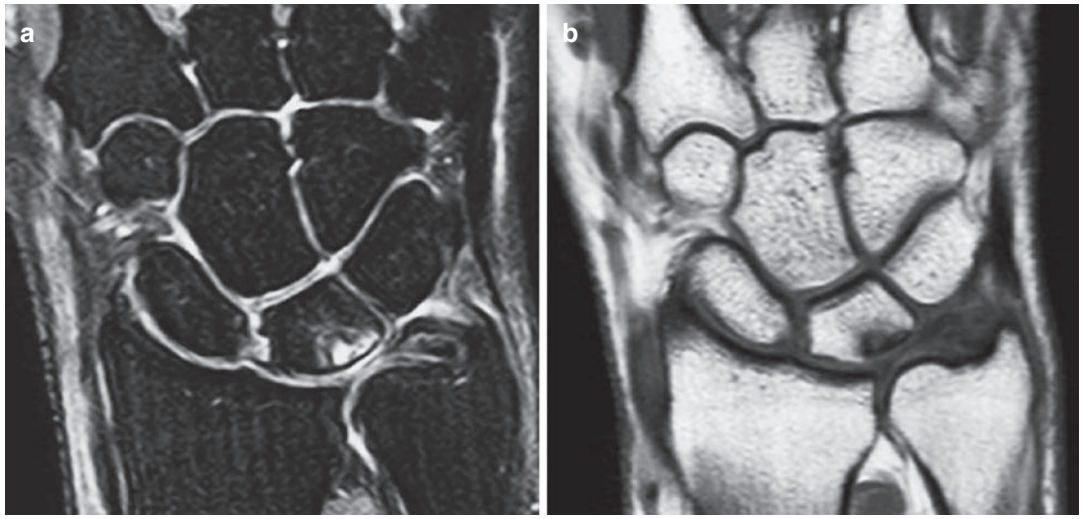

Fig. 9 (**a**, **b**) Ulnar impaction syndrome in a 41-year-old paddle player with 1-year complaints of ulnar-sided pain. (**a**) Coronal fat-suppressed FSE proton-density MR image. (**b**) Coronal FSE T1-weighted MR image. There is a central defect within the triangular fibrocartilage, thinning of the lunate cartilage, and secondary subchondral cystic lesions

secondary to repetitive wrist flexion and direct compression on the joint.

Ulnar-sided pain may be caused by a broad spectrum of disorders, mainly secondary to post-traumatic and overuse syndromes. MRI allows detection of abnormal bones, triangular fibrocartilage tears, bone marrow edema, cartilage lesions, and extensor carpi ulnaris tendinosis (Fig. 9). However determining the clinical relevance is difficult due to high rates of findings in asymptomatic patients (Zanetti et al. 2000; Cerezal et al. 2004; Zlatkin and Rosner 2004).

4 Muscle, Ligament, Tendon

Skeletal muscle becomes weaker and smaller and flexibility decreases as we age, losing the ability to withstand stresses. The slowing of speed and decrease in strength in master athletes are consistent with a loss of type II (fast-twitch) muscle fibers. Chronic endurance training can delay the age of significant decline in peak torque and change in muscle morphology characteristics of the leg. Several cross-sectional studies demonstrated significantly greater muscle mass, architecture preservation, and function in strength-trained master athletes compared with sedentary control participants of similar age. However, the increased incidence of muscle injuries in older athletes compared to other adults, and slower repair rates, makes training and early diagnosis essential (Morley 2000; Hawkins et al. 2003; Tarpenning et al. 2004).

Among aging athletes muscular strains are frequent, especially in the myotendinous junction. Participation in endurance sports (long-distance running) results in muscle fatigue and predisposes to injury (Close et al. 2005; Chen et al. 2005).

Repetitive loading and cumulative microtrauma to tendons lead to tendinosis. Overuse tendon injuries are more common in veteran athletes than in younger athletes. Chronic tendon abnormalities can be found in the midsubstance of the tendon, the insertion site on the bone, and the tenosynovium surrounding the tendon. Different types can also coexist within one tendon (Puddu et al. 1976; Maffulli et al. 1998; Alfredson 2005). Tendinosis affecting the insertion site into the bone or enthesis is a common type, in particular, supraspinatus, common wrist extensor, quadriceps, or patellar tendon (Almekinders et al. 2003).

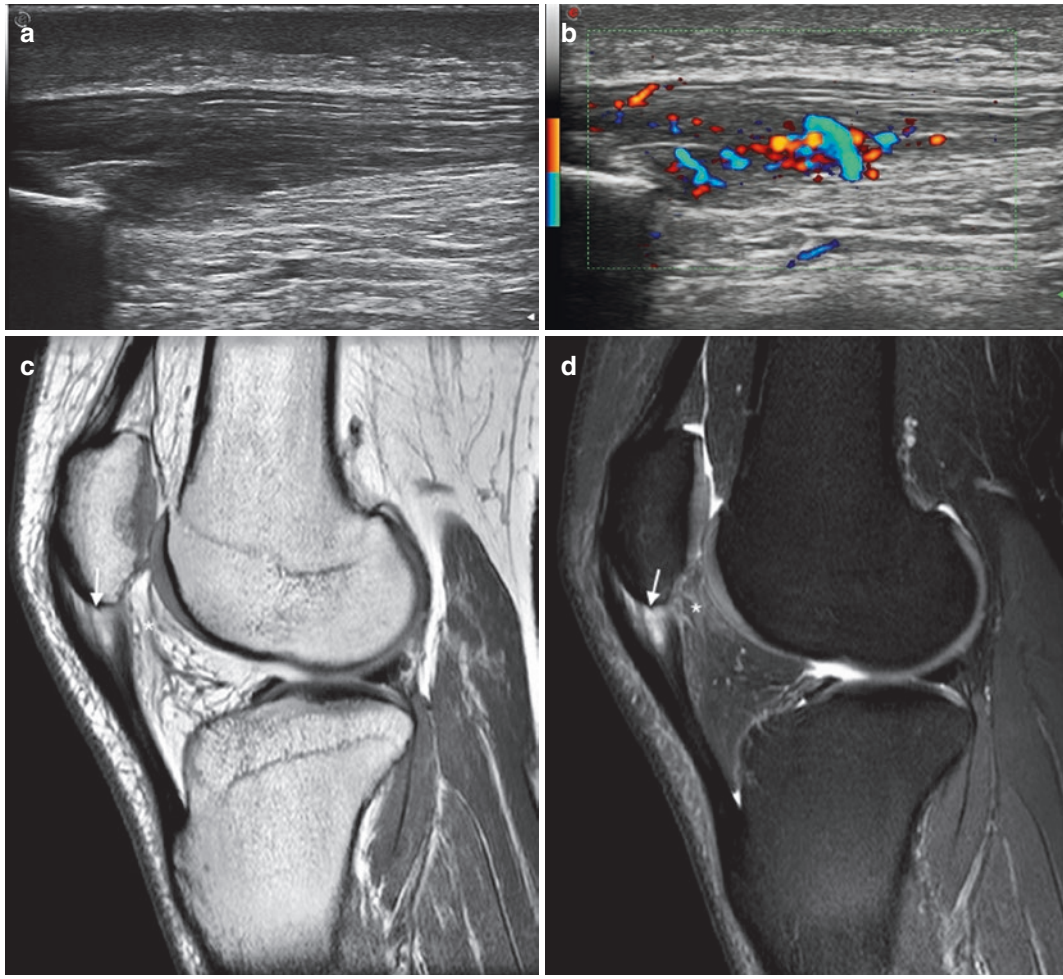

Fig. 10 (**a**–**d**) Patellar tendinosis in a 37-year-old cyclist. (**a**) Longitudinal US view and (**b**) corresponding US with color Doppler in a different patient with patellar tendon partial rupture, demonstrating thickening of the proximal patellar tendon with increased Doppler signal related to neovascularity. Patellar tendinosis with focal tear in a different patient, 42-year-old football player. (**c**) Sagittal FSE proton-density MR image. (**d**) Sagittal FSE with fat suppression T2-weighted image. Patellar tendon shows thickening of the proximal tendon and increase in signal intensity with focal area of fluid signal intensity area indicating partial rupture in the posterior insertion (white arrow). Note the adjacent edema of the Hoffa's fat pad (star).

Midsubstance locations of most common types are Achilles or patellar tendinosis (Fig. 10). Although the etiology is not entirely clear, degenerative changes are found in most ruptured tendons, suggesting that there is a pre-rupture phase and even a predisposition to rupture (Maffulli and Wong 2003). The onset of symptoms is related to a partial rupture or series of microruptures in the area of degeneration. Middle-aged men who suddenly increase their activity after a long period of inactivity seem to be most susceptible to developing micro- or partial ruptures within an area of preexisting tendinosis. In runners, the most common cause of Achilles tendon injuries is training errors, increase in training mileage, change of terrain, or increase in interval training.

Ultrasound is less expensive but examiner dependent. Undetectable tendon at the site of injury, tendon retraction, and posterior acoustic

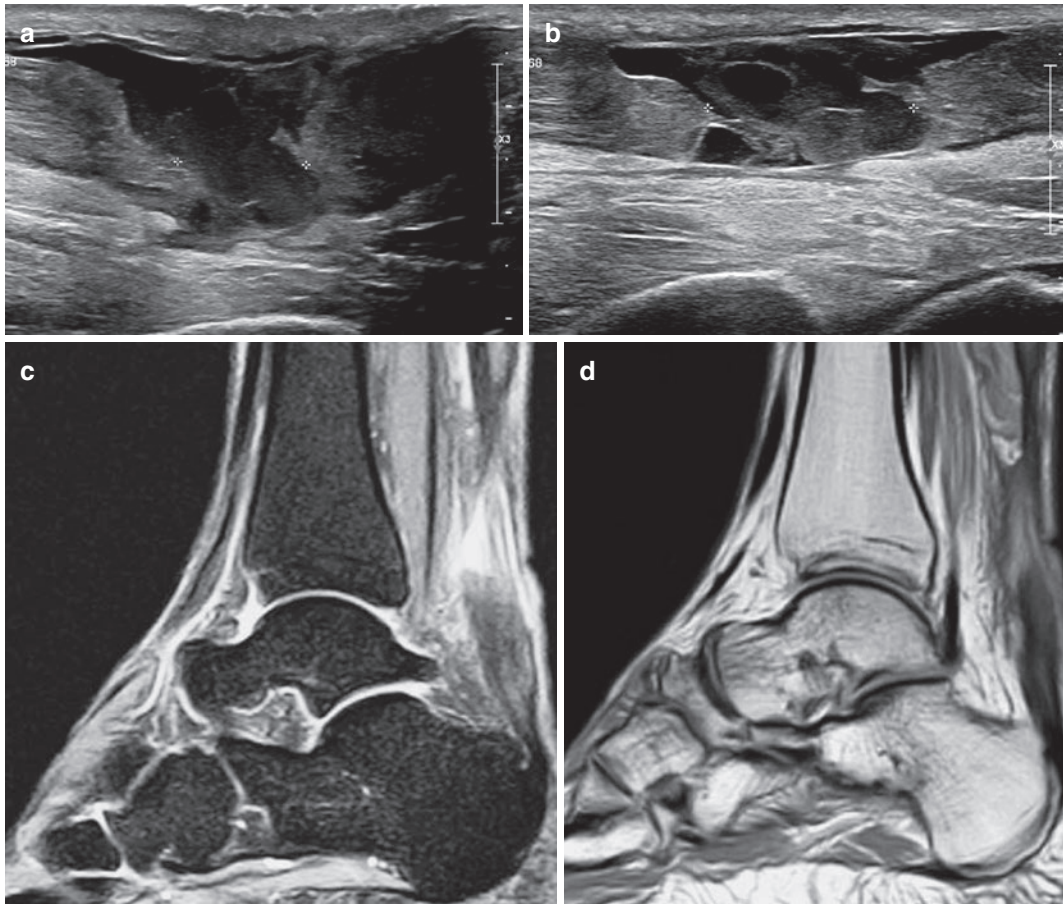

Fig. 11 (**a**–**d**) Full-thickness tear of the Achilles tendon in a 40-year-old tennis teacher. (**a**) Longitudinal US of the Achilles tendon in dorsiflexion; (**b**) longitudinal US of the Achilles tendon in plantar flexion; both show full-thickness tear with fluid between the two ends. Note the increase of size of the rupture that is demonstrated in plantar flexion. (**c**, **d**) Corresponding sagittal FSE T2-weighted MR image and STIR image show a complete Achilles tendon rupture 3–4 cm from its insertion at the calcaneus (black arrow)

shadowing at the ends of a torn tendon are characteristics that can be used to aid the diagnosis of a full-thickness tear (Fig. 11). Tendon thickening and areas of high signal intensity on MRI can be seen in asymptomatic and symptomatic patients, so clinical relevance has to be confirmed (Haims et al. 2000; Schepsis et al. 2002).

The role of US or MRI during the tendon-healing process is limited. Tendon imaging abnormalities may persist even when patients have functionally recovered; thus they should not be used as a guide to whether or not a patient is fit to return to sport (Möller et al. 2002; Khan 2003).

5 Bone Health

There is age-related loss of bone density, increasing bone fragility in men and women (Chen et al. 2005). Weight-bearing physical activity has beneficial effects on bone health across the age spectrum. Exercise and weight-bearing activity have been known to prevent the decline in bone density seen in aging and thus reduce the risk of osteoporotic fractures.

The types of load beneficial to bone (resulting in osteogenesis) are the dynamic, variable, and progressive (assimilated to impact sports). Static

exercise loading does not have the same osteogenic effect (Burr et al. 2002).

Aerobic non-impact activities, like swimming and cycling, would usually lead to a lower BMD than impact sports (Guadalupe-Grau et al. 2009). However, recent evidence suggests that swimming increases bone turnover which results in stronger bone structure and better bone quality (Gómez-Bruton et al. 2013).

In competitive male cyclists, low BMD and a higher risk of fractures have been demonstrated (Nichols and Rauh 2011), and therefore, it is recommended to combine this activity with plyometric, weight lifting, or high-impact exercises.

Other low-impact exercises, like walking, have been seen to improve femoral BMD in postmenopausal women, but have no generalized positive effects on BMD in the spine or other locations (Martyn-St James and Carroll 2008; Ma et al. 2013).

A recent meta-analysis has shown that high-impact exercise training, such as jumping and progressive resistance training, enhances bone health in postmenopausal women (Zhao et al. 2015). Similarly, a relatively recent systematic review reports that a program of moderate- to high-intensity resistance training, with 3–4 bouts of 8–12 repetitions, performed 2–3 times a week has been proven to maintain or improve BMD of the femur in postmenopausal women (Zehnacker and Bemis-Dougherty 2007).

Early postmenopause is a critical time for loss of muscular strength and bone mass in woman. Moreover, female athletes involved in intensive training since childhood are at especially high risk for developing osteoporosis because many experienced delayed menarche, oligomenorrhea, or secondary amenorrhea related to their training and diet. Thus, osteoporosis treatment may be indicated even in female master athletes (Ireland and Ott 2004; Kohrt et al. 2004). Recently, a shift from treating osteoporosis with drugs to preventing falls with PA has been proposed. Osteoporotic fractures tend to be the result of falls, and PA decreases the risk of falls. In this sense, it is more effective than the use of drugs, which have no effect on falls (with the exception of high doses of vitamin D (Bischoff-Ferrari et al. 2004). It has been estimated that using a dual-energy X-ray absorptiometry (DXA) T score of −2.5 to start treatment, the cost of preventing one vertebral fracture is approximately 30,000 USD, and even in most cases, this will still occur (Järvinen et al. 2008).

Preserving muscle quality and quantity and improving balance reduce the risk of falls and fractures, but insufficiency stress fracture incidence increases with aging; therefore moderation is critical for injury avoidance (Hill 2001).

Stress fractures represent the response of normal or abnormal bone to repetitive cyclic loading. The cause of stress fractures changes with aging; fatigue stress fractures are more frequently encountered in young athletes, while older athletes develop insufficiency stress fractures. In younger athletes coordination of muscle action is impaired due to fatigue, but muscle strength and rapid forceful muscle contraction remain; therefore postfatigue impact loading is increased. On the other hand, the loss of muscle strength and endurance with age prevent forceful muscle contraction following fatigue. This may be the cause of the difference in fatigue stress fractures rates between younger and older individuals (Fyhrie et al. 1998). However the normal decrease of bone mineral density increases the risk of fracture.

Clinical symptoms are nonspecific and therefore diagnosis is not suspected in many cases. Radiologists must be aware of stress insufficiency fractures, particularly when a patient over 50 starts a new training regimen. The location, distribution, and associated findings are the clues for the diagnosis. MRI is an excellent tool for diagnosis (see Lefere et al. 2021). Characteristic imaging findings may allow accurate diagnosis, avoid inappropriate studies, and allow start of early treatment (Daffner and Pavlov 1992; Peh et al. 1996; Hosono et al. 1997; Chowchuen and Resnick 1998; Chen et al. 2005).

6 Sports After Total Joint Replacement

The implant designs and surgical advances in joint replacement have allowed patients to return to functional activities. Today it is not uncommon for patients to remain athletically active after total joint replacement. Most patients pursue lower intensity and lower impact activities (golf, walking, swimming, etc.). However, an increasing number of master athletes performing intermediate-intensity and -impact sports (skiing, tennis, running) are seen and have higher injury rates. High-impact loading sports, such as football, soccer, or basketball, are not recommended due to the probability of injury. Sports participation increases the risk of traumatic complications, such as dislocation, implant failure, or periprosthetic fracture (Clifford and Mallon 2005; Chen et al. 2005).

7 Sarcopenia

Skeletal muscle accounts for approximately 40–45% of body mass and plays a vital role in health and disease through its effects on energy metabolism, glucose utilization, and physical function. Skeletal muscle is a remarkably plastic tissue, which continuously adapts to physiological and pathological conditions. The most powerful modulators of the skeletal muscle phenotype are contraction and load, experienced during endurance and resistance exercise, whereas skeletal muscle loss is exacerbated by injury, illness, disuse, insufficient nutrient intake, and aging. This dramatic ability of skeletal muscle to adapt to various stimuli and its connection to morbidity and mortality make it the focus of investigation in frailty, cachexia, sarcopenia, and metabolism-related research (Baracos and Kazemi-Bajestani 2013; Keevil and Romero-Ortuno 2015).

The retention and maintenance of muscle and muscle function are coming under increasing scrutiny in our aging society because of the looming epidemic of sarcopenia and the financial and social impact that this will have. However, the discussion around the diagnosis and prevalence on sarcopenia is centered on the elderly (Bruyère et al. 2016). Sarcopenia is a well-known concept in geriatric medicine (Dawson and Dennison 2016). It is defined by the European Working Group on Sarcopenia in Older People (EWGSOP) as a progressive and generalized muscle loss with decline in muscle mass and muscle function (either low strength or performance) (Cruz-Jentoft et al. 2010), and is accompanied by histologic changes, including intermuscular fat accumulation, fibrosis, selective atrophy of type II fibers, and perfusion changes that lead to deterioration in muscle force generation (Lexell et al. 1983; Korhonen et al. 2006; Alnaqeeb et al. 1984).

7.1 Epidemiology

The European Working Group on Sarcopenia in Older People (EWGSOP) has suggested a conceptual staging system that progresses from "presarcopenia" (low muscle mass only) and "sarcopenia" (low muscle mass with low muscle strength or low physical performance) to "severe sarcopenia" (low muscle mass with low muscle strength and low physical performance) (Cruz-Jentoft et al. 2010). Currently, it affects more than 50 million people and the condition will affect more than 250 million people in the next 40 years. Thus, the EWGSOP suggests that elderly people should be screened routinely in communities.

The negative effects of sarcopenia have been amply demonstrated and include physical impairment, a greater risk of falls and fractures, disability, limited self-sufficiency in activities of daily living, a higher incidence of hospitalizations, and higher mortality (Roubenoff 2000). As a result of these effects and of the increasing prevalence of sarcopenia in the elderly, 1.5% of the total healthcare expenditure in the United States has been attributed to sarcopenia (Janssen et al. 2002).

7.2 Histology

Imaging muscle mass has become more important in recent years for the diagnosis and staging. The loss of muscle mass is accompanied by qualitative changes in muscle fibers, particularly involving a reduction in the size of type II (fast-twitch) fibers and, to a lesser degree, of type I (slow-twitch) fibers.

Another qualitative change occurring in muscle mass with aging involves development of myosteatosis, the process of increased uptake of lipids by muscle adipocytes, which are located in the deep fascia of the muscle (Goodpaster et al. 2001), which seems to increase the risk of mobility impairment in older people (Visser et al. 2005). This phenomenon mainly affects older women with an increasing proportion of fat mass in their body composition (Coin et al. 2008), and individuals who are obese—hence the term "sarcopenic obesity" is used to define the combination of sarcopenia and obesity in the elderly (Stenholm et al. 2008). There are three types of myosteatosis: lipid depositions between muscle groups (intermuscular lipids), lipid depositions between the myocytes (intramuscular lipids), and lipid depositions within the myocytes (intramyocellular lipids) (Fig. 12).

7.3 Imaging Techniques

Thus, accurate measurements of muscle mass, size, and composition are critically important. There are several methods to measure muscle mass, such as ultrasound (US), computed tomography (CT), magnetic resonance imaging (MRI), and DXA.

7.3.1 Muscle Mass

MRI and CT are known as the gold standards for measuring skeletal muscle mass and have been used primarily for basic or clinical research studies. However, these methods are limited because they are expensive and not portable, and CT involves exposure to radiation.

DXA has been widely and commonly used in the diagnosis of sarcopenia. Despite the minimal radiation exposure from DXA, it is difficult to use in community-wide screenings of sarcopenia. DXA-specific measurements of lean mass (LM) include several parameters. Among them, the appendicular lean mass index (ALMI) is of clinical significance, because the maintenance of appendicular skeletal muscle is critical in the preservation of mobility and functional independence (with an impact on mobility) (Janssen et al. 2004). The International Society for Clinical Densitometry (ISCD) suggests that lean mass status could be defined using ALMI Z-scores, but the threshold for the definition of low LM is yet to be set and validated—therefore, the definition of "healthy status" is still unclear (Shepherd et al. 2013). In addition, DXA is not portable.

Sonographic measurements of muscle size have been significantly associated with strength (Strasser et al. 2013). US images have been used to measure both CSA and volume, with inter- and intrareader reliability similar to that for MRI (Gould et al. 2019). Total skeletal muscle mass may be estimated using sonographically measured muscle thickness, with a strong correlation with both MRI (R^2 = 0.94) and DXA (R^2 = 0.95).

7.3.2 Muscle Quality

Previous studies have assessed the quality of skeletal muscle using CT, MRI, and/or US (Kent-Braun et al. 2000; Goodpaster et al. 2001). Goodpaster et al. 2001, in an assessment of muscle quality using CT, showed a reduced attenuation coefficient caused by augmented fat infiltration (Goodpaster et al. 2001). They reported that low CT attenuation values for muscle were associated with lower muscle strength in elderly adults (>65 years old) and that the association between CT attenuation value and muscle strength was independent of muscle size.

Recently, advanced quantitative magnetic resonance (MR) imaging techniques targeting different muscle components have shown promising results for evaluating skeletal muscles by overcoming limitations in visual assessment based on gross morphologic and signal intensity changes. With quantitative MR imaging-derived parameters, noninvasive characterization of changes

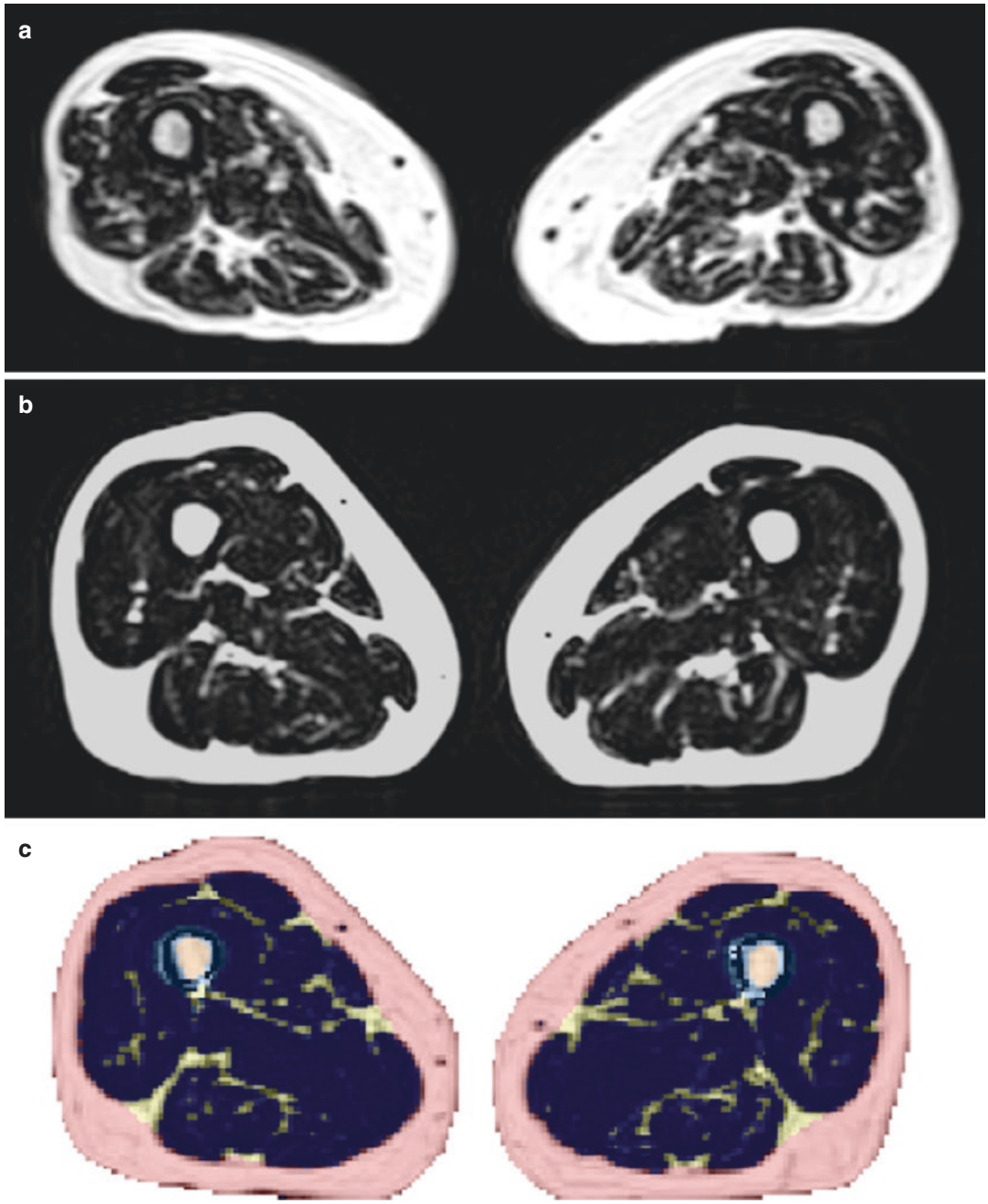

Fig. 12 (**a**–**c**) Dixon 2.0 cross-sectional images (water suppression) obtained in mid-muscle in (**a**) a frail 78-year-old woman and (**b**) non-frail 76-year-old woman. The images show diminished muscle mass relative to subcutaneous fat and mild fatty infiltration of muscles in the patient (**b**). (**c**) Segmented parametric MRI image (pink: subcutaneous adipose tissue; yellow: intermuscular adipose tissue; dark gray: muscle tissue). MRI fat fraction provides quantitative marker of muscle quality and fat content

occurring at cellular or fascicular levels of the muscle is possible, providing information about cellularity and changes in microstructure (Agten et al. 2016; Yoon et al. 2018). These quantitative MR imaging techniques include diffusion-weighted imaging (DWI), diffusion tensor

imaging (DTI), and 2.0 or multiecho Dixon water-fat imaging. Measurement of the muscle's anisotropic microstructure can be derived from DTI (Zaraiskaya et al. 2006). 2.0 and multiecho Dixon imaging allows quantification of fat infiltration, with larger volume coverage than with single-voxel MR spectroscopy.

The quality of skeletal muscle, however, can also be evaluated using noninvasive, easily accessible, and safe ultrasonography (US) imaging.

Muscle thickness, cross-sectional area (CSA), echo intensity, fascicle length, and pennation angle of the lower limbs are the parameters most commonly evaluated by ultrasound examination; in pennate muscles, the pennation angle (angle formed at the attachment site of the fibers into deep and superficial aponeurosis) can be evaluated in static and dynamic conditions and provides information about mechanical and contractile proprieties. All of these parameters are affected by aging to a different extent but need to be further validated. The large majority of the available studies have been conducted with small samples, in healthy patients. As a result, no validated site-specific cutoff points for the ultrasound-based assessment of low muscle mass in aging patients exist (Narici et al. 2016, Ticinesi et al. 2017).

8 Conclusions

Gaining the benefits of participation in athletics while minimizing the risk of injuries requires understanding of the relationship between sports participation and injury, and the relationship between injury and joint degeneration. It is essential for radiologists to differentiate radiological age-related changes from pathological injuries. Knowledge of the spectrum of injuries in the aging athlete will allow correct diagnosis and early return to athletic activity.

Things to Remember

1. The risk of development of osteoarthritis depends on the load bearing and impact distribution, therefore higher loading sports increase hip and knee osteoarthritis WHEREAS throwing and overhead sports predispose to degenerative changes at the upper limb.
2. Due to the high prevalence of degenerative changes in asymptomatic patients, radiological findings must be carefully correlated with clinical presentation, trying to differentiate "normal changes" from pathological aging.
3. Older athletes experience a lower incidence of acute traumatic injuries, and commonly their injuries are related to overuse and repetitive microtrauma. Tendinosis of the rotator cuff, elbow, wrist tendons, Achilles, or patellar tendons is more frequent among aging athletes.
4. High-impact loading results in cartilage microtrauma and degeneration of the weight-bearing joints. Previous injury or injury may exacerbate this effect.

Imaging Technique Boxes

Radiography

1. Late-stage imaging method for osteoarthrosis and not always correlation with pain
2. Limited value in internal joint disease
3. Not indicated for muscle or tendon disease
4. Late imaging method for stress fractures; radiological pattern (linear sclerosis perpendicular to the major trabecular lines) and specific location (pubic rami, femoral neck, metatarsal bones) are the clues to the diagnosis; may be normal, inability to show sacral fractures

Ultrasound

1. Imaging-guided percutaneous technique
2. Excellent tool for assessing the superficial soft tissues, muscles, and tendons
3. Quick, cheap, and available, but operator dependent

CT

1. High radiation
2. Indicated for stress fractures specially in sacrum
3. Indicated in acute trauma

MRI

1. Excellent tool for assessing cartilage and joint, beware of asymptomatic findings with aging
2. Early diagnosis for stress fractures
3. Excellent tool for tendon and muscle evaluation

References

Abe I, Harada Y, Oinuma K et al (2000) Acetabular labrum: abnormal findings at MR imaging in asymptomatic hips. Radiology 216:576–581. https://doi.org/10.1148/radiology.216.2.r00au13576

Agricola R, Heijboer MP, Bierma-Zeinstra SMA et al (2013) Cam impingement causes osteoarthritis of the hip: a nationwide prospective cohort study (CHECK). Ann Rheum Dis 72:918–923. https://doi.org/10.1136/annrheumdis-2012-201643

Alentorn-Geli E, Samuelsson K, Musahl V et al (2017) The association of recreational and competitive running with hip and knee osteoarthritis: a systematic review and meta-analysis. J Orthop Sports Phys Ther 47:373–390. https://doi.org/10.2519/jospt.2017.7137

Alfredson H (2005) Conservative management of Achilles tendinopathy: new ideas. Foot Ankle Clin 10:321–329. https://doi.org/10.1016/j.fcl.2005.01.002

Almekinders LC, Weinhold PS, Maffulli N (2003) Compression etiology in tendinopathy. Clin Sports Med 22:703–710. https://doi.org/10.1016/s0278-5919(03)00067-x

Alnaqeeb MA, Al Zaid NS, Goldspink G (1984) Connective tissue changes and physical properties of developing and ageing skeletal muscle. J Anat 139(Pt 4):677–689

Andrews JR (2005) Diagnosis and treatment of chronic painful shoulder: review of nonsurgical interventions. Arthroscopy 21:333–347. https://doi.org/10.1016/j.arthro.2004.11.003

Agten CA, Rosskopf AB, Gerber C, Pfirrmann CW (2016) Quantification of early fatty infiltration of the rotator cuff muscles: comparison of multi echo Dixon with single-voxel MR spectroscopy. Eur Radiol 26(10):3719–3727

Armsey TD, Hosey RG (2004) Medical aspects of sports: epidemiology of injuries, preparticipation physical examination, and drugs in sports. Clin Sports Med 23:255–279., vii. https://doi.org/10.1016/j.csm.2004.04.007

Bakewell R, Gerety EL, Grainger AJ (2020) Basic imaging principles of tendons and ligaments. Med Radiol https://doi.org/10.1007/174_2020_249

Baracos V, Kazemi-Bajestani SMR (2013) Clinical outcomes related to muscle mass in humans with cancer and catabolic illnesses. Int J Biochem Cell Biol 45:2302–2308

Barnes CJ, Van Steyn SJ, Fischer RA (2001) The effects of age, sex, and shoulder dominance on range of motion of the shoulder. J Shoulder Elb Surg 10:242–246. https://doi.org/10.1067/mse.2001.115270

Barrett GR, Field MH, Treacy SH, Ruff CG (1998) Clinical results of meniscus repair in patients 40 years and older. Arthroscopy 14:824–829. https://doi.org/10.1016/s0749-8063(98)70018-0

Bartz RL, Laudicina L (2005) Osteoarthritis after sports knee injuries. Clin Sports Med 24:39–45. https://doi.org/10.1016/j.csm.2004.08.006

Bennell K, Hinman RS, Wrigley TV et al (2011) Exercise and osteoarthritis: cause and effects. Compr Physiol 1:1943–2008. https://doi.org/10.1002/cphy.c100057

Bergin D, Morrison WB, Carrino JA et al (2004) Anterior cruciate ligament ganglia and mucoid degeneration: coexistence and clinical correlation. AJR Am J Roentgenol 182:1283–1287. https://doi.org/10.2214/ajr.182.5.1821283

Bert JM, Gasser SI (2002) Approach to the osteoarthritic knee in the aging athlete: debridement to osteotomy. Arthroscopy 18:107–110. https://doi.org/10.1053/jars.2002.36513

Bischoff-Ferrari HA, Dawson-Hughes B, Willett WC et al (2004) Effect of Vitamin D on falls: a meta-analysis. JAMA 291:1999–2006. https://doi.org/10.1001/jama.291.16.1999

Borchers JR, Kaeding CC, Pedroza AD et al (2011) Intra-articular findings in primary and revision anterior cruciate ligament reconstruction surgery: a comparison of the MOON and MARS study groups. Am J Sports Med 39:1889–1893. https://doi.org/10.1177/0363546511406871

Bortoluzzi A, Furini F, Scirè CA (2018) Osteoarthritis and its management—epidemiology, nutritional aspects and environmental factors. Autoimmun Rev 17:1097–1104. https://doi.org/10.1016/j.autrev.2018.06.002

Brophy RH, Marx RG (2005) Osteoarthritis following shoulder instability. Clin Sports Med 24:47–56. https://doi.org/10.1016/j.csm.2004.08.010

Brun SP (2016) Clinical considerations for the ageing athlete. Aust Fam Physician 45:478–483

Bruyère O, Beudart C, Locquet M et al (2016) Sarcopenia as a public health problem. Eur Geriatr Med 7:272–275

Bureau NJ, Cardinal E, Hobden R, Aubin B (2000) Posterior ankle impingement syndrome: MR imaging findings in seven patients. Radiology 215:497–503. https://doi.org/10.1148/radiology.215.2.r00ma01497

Burr DB, Robling AG, Turner CH (2002) Effects of biomechanical stress on bones in animals. Bone 30:781–786. https://doi.org/10.1016/s8756-3282(02)00707-x

Byrd JWT, Jones KS (2004) Diagnostic accuracy of clinical assessment, magnetic resonance imaging, magnetic resonance arthrography, and intra-articular injection in hip arthroscopy patients. Am J Sports Med 32:1668–1674. https://doi.org/10.1177/0363546504266480

Campbell D, Campbell R, O'Connor P, Hawkes R (2013) Sports-related extensor carpi ulnaris pathology: a review of functional anatomy, sports injury and management. Br J Sports Med 47:1105–1111. https://doi.org/10.1136/bjsports-2013-092835

Cerezal L, Abascal F, Canga A et al (2003) MR imaging of ankle impingement syndromes. AJR Am J Roentgenol 181:551–559. https://doi.org/10.2214/ajr.181.2.1810551

Cerezal L, del Piñal F, Abascal F (2004) MR imaging findings in ulnar-sided wrist impaction syndromes. Magn Reson Imaging Clin N Am 12:281–299., vi. https://doi.org/10.1016/j.mric.2004.02.005

Chen AL, Mears SC, Hawkins RJ (2005) Orthopaedic care of the aging athlete. J Am Acad Orthop Surg 13:407–416. https://doi.org/10.5435/00124635-200510000-00005

Chodzko-Zajko WJ, Proctor DN et al (2009) American College of Sports Medicine position stand. Exercise and physical activity for older adults. Med Sci Sports Exerc 41:1510–1530. https://doi.org/10.1249/MSS.0b013e3181a0c95c

Chowchuen P, Resnick D (1998) Stress fractures of the metatarsal heads. Skelet Radiol 27:22–25. https://doi.org/10.1007/s002560050329

Chung CB, Chew FS, Steinbach L (2004) MR imaging of tendon abnormalities of the elbow. Magn Reson Imaging Clin N Am 12(233–245):vi. https://doi.org/10.1016/j.mric.2004.02.007

Chung CB, Kim H-J (2003) Sports injuries of the elbow. Magn Reson Imaging Clin N Am 11:239–253. https://doi.org/10.1016/s1064-9689(03)00024-2

Clifford PE, Mallon WJ (2005) Sports after total joint replacement. Clin Sports Med 24:175–186. https://doi.org/10.1016/j.csm.2004.08.009

Close GL, Kayani A, Vasilaki A, McArdle A (2005) Skeletal muscle damage with exercise and aging. Sports Med 35:413–427. https://doi.org/10.2165/00007256-200535050-00004

Coin A, Sergi G, Minicuci N et al (2008) Fat-free mass and fat mass reference values by dual-energy X-ray absorptiometry (DEXA) in a 20–80-year-old Italian population. Clin Nutr 27(1):87–94

Cruz-Jentoft AJ et al (2010) Sarcopenia: European consensus on definition and diagnosis: report of the European Working Group on Sarcopenia in Older People. Age Ageing 39(4):412–423

Daffner RH, Pavlov H (1992) Stress fractures: current concepts. AJR Am J Roentgenol 159:245–252. https://doi.org/10.2214/ajr.159.2.1632335

Dawson A, Dennison E (2016) Measuring the musculoskeletal aging phenotype. Maturitas 93:13–17

Delaunay S, Dussault RG, Kaplan PA, Alford BA (1997) Radiographic measurements of dysplastic adult hips. Skeletal Radiol 26(2):75–81. https://doi.org/10.1007/s002560050197. PMID: 9060097

Drobnič M, Ercin E, Gamelas J et al (2019) Treatment options for the symptomatic post-meniscectomy knee. Knee Surg Sports Traumatol Arthrosc 27:1817–1824. https://doi.org/10.1007/s00167-019-05424-3

Eijgenraam SM, Reijman M, Bierma-Zeinstra SMA et al (2018) Can we predict the clinical outcome of arthroscopic partial meniscectomy? A systematic review. Br J Sports Med 52:514–521. https://doi.org/10.1136/bjsports-2017-097836

Ernberg LA, Potter HG (2003) Radiographic evaluation of the acromioclavicular and sternoclavicular joints. Clin Sports Med 22:255–275. https://doi.org/10.1016/s0278-5919(03)00006-1

Faletti C, Robba T, de Petro P (2002) Postmeniscectomy osteonecrosis. Arthroscopy 18:91–94. https://doi.org/10.1053/jars.2002.25259

Feeley BT, Lau BC (2018) Biomechanics and clinical outcomes of partial meniscectomy. J Am Acad Orthop Surg 26:853–863. https://doi.org/10.5435/JAAOS-D-17-00256

Fyhrie DP, Milgrom C, Hoshaw SJ et al (1998) Effect of fatiguing exercise on longitudinal bone strain as related to stress fracture in humans. Ann Biomed Eng 26:660–665. https://doi.org/10.1114/1.103

Gessel T, Harrast MA (2019) Running dose and risk of developing lower-extremity osteoarthritis. Curr Sports Med Rep 18:201–209. https://doi.org/10.1249/JSR.0000000000000602

Gómez-Bruton A, Gónzalez-Agüero A, Gómez-Cabello A et al (2013) Is bone tissue really affected by swimming? A systematic review. PLoS One 8:e70119. https://doi.org/10.1371/journal.pone.0070119

Goodpaster BH, Carlson CL, Visser M, Kelley DE, Scherzinger A, Harris TB, Stamm E, Newman AB (2001) Attenuation of skeletal muscle and strength in the elderly: The Health ABC Study. J Appl Physiol (1985) 90(6):2157–2165. https://doi.org/10.1152/jappl.2001.90.6.2157. PMID: 11356778

Gould DW, Watson EL, Wilkinson TJ et al (2019) Ultrasound assessment of muscle mass in response to exercise training in chronic kidney disease: a comparison with MRI. J Cachexia Sarcopenia Muscle 10(4):748–755

Guadalupe-Grau A, Fuentes T, Guerra B, Calbet JAL (2009) Exercise and bone mass in adults. Sports Med 39:439–468. https://doi.org/10.2165/00007256-200939060-00002

Haims AH, Schweitzer ME, Patel RS et al (2000) MR imaging of the Achilles tendon: overlap of findings in symptomatic and asymptomatic individuals. Skelet Radiol 29:640–645. https://doi.org/10.1007/s002560000273

Hall M, Wrigley TV, Metcalf BR et al (2015) Mechanisms underpinning the peak knee flexion moment increase over 2-years following arthroscopic partial meniscectomy. Clin Biomech 30:1060–1065. https://doi.org/10.1016/j.clinbiomech.2015.09.006

Hawkins SA, Wiswell RA, Marcell TJ (2003) Exercise and the master athlete—a model of successful aging? J Gerontol A Biol Sci Med Sci 58:1009–1011. https://doi.org/10.1093/gerona/58.11.m1009

Hayashi D, Roemer FW, Guermazi A (2019) Magnetic resonance imaging assessment of knee osteoarthritis: current and developing new concepts and techniques. Clin Exp Rheumatol 37(Suppl 120):88–95

Hill C (2001) Caring for the aging athlete. Geriatr Nurs 22:43–45. https://doi.org/10.1067/mgn.2001.114423

Hosono M, Kobayashi H, Fujimoto R et al (1997) MR appearance of parasymphyseal insufficiency fractures of the os pubis. Skelet Radiol 26:525–528. https://doi.org/10.1007/s002560050279

Hunter DJ, Zhang Y, Niu J et al (2006) Increase in bone marrow lesions associated with cartilage loss: a longitudinal magnetic resonance imaging study of knee osteoarthritis. Arthritis Rheum 54:1529–1535. https://doi.org/10.1002/art.21789

Iorio R, Iannotti F, Ponzo A et al (2018) Anterior cruciate ligament reconstruction in patients older than fifty years: a comparison with a younger age group. Int Orthopaed 42:1043–1049. https://doi.org/10.1007/s00264-018-3860-8

Ireland ML, Ott SM (2004) Special concerns of the female athlete. Clin Sports Med 23(281–298):vii. https://doi.org/10.1016/j.csm.2004.04.003

Janssen I, Heymsfield SB, Ross R (2002) Low relative skeletal muscle mass (sarcopenia) in older persons is associated with functional impairment and physical disability. J Am Geriatr Soc 50:889–896. https://doi.org/10.1046/j.1532-5415.2002.50216.x

Janssen I, Baumgartner RN, Ross R, Rosenberg IH, Roubenoff R (2004) Skeletal muscle cutpoints associated with elevated physical disability risk in older men and women. Am J Epidemiol 159(4):413–421

Järvinen TLN, Sievänen H, Khan KM et al (2008) Shifting the focus in fracture prevention from osteoporosis to falls. BMJ 336:124–126. https://doi.org/10.1136/bmj.39428.470752.AD

Jerosch J, Castro WH, Assheuer J (1996) Age-related magnetic resonance imaging morphology of the menisci in asymptomatic individuals. Arch Orthop Trauma Surg 115:199–202. https://doi.org/10.1007/bf00434553

Johnson TC, Evans JA, Gilley JA, DeLee JC (2000) Osteonecrosis of the knee after arthroscopic surgery for meniscal tears and chondral lesions. Arthroscopy 16:254–261. https://doi.org/10.1016/s0749-8063(00)90049-5

Jørgensen AEM, Kjær M, Heinemeier KM (2017) The effect of aging and mechanical loading on the metabolism of articular cartilage. J Rheumatol 44:410–417. https://doi.org/10.3899/jrheum.160226

Kassarjian A, Yoon LS, Belzile E, Connolly SA, Millis MB, Palmer WE (2005) Triad of MR arthrographic findings in patients with cam-type femoroacetabular impingement. Radiology 236(2):588–92. https://doi.org/10.1148/radiol.2362041987. Epub 2005 Jun 21. PMID: 15972331

Kaeding CC, Pedroza AD, Reinke EK et al (2015) Risk factors and predictors of subsequent ACL injury in either knee after ACL reconstruction: prospective analysis of 2488 primary ACL reconstructions from the MOON cohort. Am J Sports Med 43:1583–1590. https://doi.org/10.1177/0363546515578836

Keevil VL, Romero-Ortuno R (2015) Ageing well: a review of sarcopenia and frailty. Proc Nutr Soc 74:337–347

Kent-Braun JA, Ng AV, Young K (2000) Skeletal muscle contractile and noncontractile components in young and older women and men. J Appl Physiol 88(2):662–668

Khan KM, Forster BB, Robinson J, Cheong Y, Louis L, Maclean L, Taunton JE (2003) Are ultrasound and magnetic resonance imaging of value in assessment of Achilles tendon disorders? A two year prospective study. Br J Sports Med 37(2):149–53. https://doi.org/10.1136/bjsm.37.2.149. PMID: 12663358; PMCID: PMC1724608

Kijowski R, Stanton P, Fine J, De Smet A (2006) Subchondral bone marrow edema in patients with degeneration of the articular cartilage of the knee joint. Radiology 238:943–949. https://doi.org/10.1148/radiol.2382050122

Klimkiewicz JJ, Shaffer B (2002) Meniscal surgery 2002 update: indications and techniques for resection, repair, regeneration, and replacement. Arthroscopy 18:14–25. https://doi.org/10.1053/jars.2002.36505

Koh J, Dietz J (2005) Osteoarthritis in other joints (hip, elbow, foot, ankle, toes, wrist) after sports injuries. Clin Sports Med 24:57–70. https://doi.org/10.1016/j.csm.2004.08.011

Kohrt WM, Bloomfield SA, Little KD et al (2004) American College of Sports Medicine Position Stand: physical activity and bone health. Med Sci Sports Exerc 36:1985–1996. https://doi.org/10.1249/01.mss.0000142662.21767.58

Korhonen MT, Cristea A, Alén M et al (2006) Aging, muscle fiber type, and contractile function in sprint-trained athletes. J Appl Physiol 101(3):906–917

Kröner AH, Berger CE, Kluger R et al (2007) Influence of high tibial osteotomy on bone marrow edema in the knee. Clin Orthop Relat Res 454:155–162. https://doi.org/10.1097/01.blo.0000238806.87411.33

Lecouvet FE, Vande Berg BC, Malghem J et al (1996) MR imaging of the acetabular labrum: variations in 200 asymptomatic hips. AJR Am J Roentgenol 167:1025–1028. https://doi.org/10.2214/ajr.167.4.8819406

Lefere M, Demeyere A, Vanhoenacker F (2021) Overuse bone trauma and stress fractures. Med Radiol https://doi.org/10.1007/174_2020_240

Leunig M, Beck M, Dora C, Ganz R (2006) Femoroazetabuläres Impingement als Auslöser der Koxarthrose [Femoroacetabular impingement: trigger for the development of coxarthrosis]. Orthopade 35(1):77–84. German. https://doi.org/10.1007/s00132-005-0896-4. PMID: 16322969

Lexell J, Henriksson-Larsén K, Winblad B, Sjöström M (1983) Distribution of different fiber types in

human skeletal muscles: effects of aging studied in whole muscle cross sections. Muscle Nerve 6(8): 588–595

L'Hermette M, Polle G, Tourny-Chollet C, Dujardin F (2006) Hip passive range of motion and frequency of radiographic hip osteoarthritis in former elite handball players. Br J Sports Med 40:45–49.; discussion 45–49. https://doi.org/10.1136/bjsm.2005.019026

Logan M, Williams A, Lavelle J et al (2004) The effect of posterior cruciate ligament deficiency on knee kinematics. Am J Sports Med 32:1915–1922. https://doi.org/10.1177/0363546504265005

Ma D, Wu L, He Z (2013) Effects of walking on the preservation of bone mineral density in perimenopausal and postmenopausal women: a systematic review and meta-analysis. Menopause 20:1216–1226. https://doi.org/10.1097/GME.0000000000000100

Maas O, Joseph GB, Sommer G et al (2015) Association between cartilage degeneration and subchondral bone remodeling in patients with knee osteoarthritis comparing MRI and (99m)Tc-DPD-SPECT/CT. Osteoarthr Cartil 23:1713–1720. https://doi.org/10.1016/j.joca.2015.05.014

Madaleno FO, Santos BA, Araújo VL et al (2018) Prevalence of knee osteoarthritis in former athletes: a systematic review with meta-analysis. Braz J Phys Ther 22:437–451. https://doi.org/10.1016/j.bjpt.2018.03.012

Maffulli N, Binfield PM, King JB (2003) Articular cartilage lesions in the symptomatic anterior cruciate ligament-deficient knee. Arthroscopy 19:685–690. https://doi.org/10.1016/s0749-8063(03)00403-1

Maffulli N, Khan KM, Puddu G (1998) Overuse tendon conditions: time to change a confusing terminology. Arthroscopy 14:840–843. https://doi.org/10.1016/s0749-8063(98)70021-0

Maffulli N, Wong J (2003) Rupture of the Achilles and patellar tendons. Clin Sports Med 22:761–776. https://doi.org/10.1016/s0278-5919(03)00009-7

Martyn-St James M, Carroll S (2008) Meta-analysis of walking for preservation of bone mineral density in postmenopausal women. Bone 43:521–531. https://doi.org/10.1016/j.bone.2008.05.012

McIntyre J, Moelleken S, Tirman P (2001) Mucoid degeneration of the anterior cruciate ligament mistaken for ligamentous tears. Skelet Radiol 30:312–315. https://doi.org/10.1007/s002560100336

Menard D, Stanish WD (1989) The aging athlete. Am J Sports Med 17:187–196. https://doi.org/10.1177/036354658901700208

Mesiha M, Zurakowski D, Soriano J et al (2007) Pathologic characteristics of the torn human meniscus. Am J Sports Med 35:103–112. https://doi.org/10.1177/0363546506293700

Mintz DN, Hooper T, Connell D et al (2005) Magnetic resonance imaging of the hip: detection of labral and chondral abnormalities using noncontrast imaging. Arthroscopy 21:385–393. https://doi.org/10.1016/j.arthro.2004.12.011

Möller M, Kälebo P, Tidebrant G, Movin T, Karlsson J (2002) The ultrasonographic appearance of the ruptured Achilles tendon during healing: a longitudinal evaluation of surgical and nonsurgical treatment, with comparisons to MRI appearance. Knee Surg Sports Traumatol Arthrosc 10(1):49–56. https://doi.org/10.1007/s001670100245. Epub 2001 Dec 18. PMID: 11819022

Morley JE (2000) The aging athlete. J Gerontol A Biol Sci Med Sci 55:M627–M629. https://doi.org/10.1093/gerona/55.11.m627

Visser M, Goodpaster BH, Kritchevsky SB et al (2005) Muscle mass, muscle strength, and muscle fat infiltration as predictors of incident mobility limitations in well-functioning older persons. J Gerontol A Biol Sci Med Sci 60:324–333

Narici M, Franchi M, Maganaris C (2016) Muscle structural assembly and functional consequences. J Exp Biol 219:276–284. https://doi.org/10.1242/jeb.128017

Narvekar A, Gajjar S (2004) Mucoid degeneration of the anterior cruciate ligament. Arthroscopy 20:141–146. https://doi.org/10.1016/j.arthro.2003.11.030

Nelson AE, Stiller JL, Shi XA et al (2016) Measures of hip morphology are related to development of worsening radiographic hip osteoarthritis over 6 to 13 year follow-up: the Johnston County Osteoarthritis Project. Osteoarthr Cartil 24:443–450. https://doi.org/10.1016/j.joca.2015.10.007

Nepple JJ, Vigdorchik JM, Clohisy JC (2015) What is the association between sports participation and the development of proximal femoral cam deformity? A systematic review and meta-analysis. Am J Sports Med 43:2833–2840. https://doi.org/10.1177/0363546514563909

Nichols JF, Rauh MJ (2011) Longitudinal changes in bone mineral density in male master cyclists and nonathletes. J Strength Cond Res 25:727–734. https://doi.org/10.1519/JSC.0b013e3181c6a116

Øiestad BE, Engebretsen L, Storheim K, Risberg MA (2009) Knee osteoarthritis after anterior cruciate ligament injury: a systematic review. Am J Sports Med 37:1434–1443. https://doi.org/10.1177/0363546509338827

O'Neill PJ, Cosgarea AJ, Freedman JA et al (2002) Arthroscopic proficiency: a survey of orthopaedic sports medicine fellowship directors and orthopaedic surgery department chairs. Arthroscopy 18:795–800. https://doi.org/10.1053/jars.2002.31699

Peh WC, Khong PL, Yin Y et al (1996) Imaging of pelvic insufficiency fractures. Radiographics 16:335–348. https://doi.org/10.1148/radiographics.16.2.8966291

Pessis E, Drapé J-L, Ravaud P et al (2003) Assessment of progression in knee osteoarthritis: results of a 1 year study comparing arthroscopy and MRI. Osteoarthr Cartil 11:361–369. https://doi.org/10.1016/S1063-4584(03)00049-9

Potter HG, Ho ST, Altchek DW (2004) Magnetic resonance imaging of the elbow. Semin Musculoskelet Radiol 8:5–16. https://doi.org/10.1055/s-2004-823011

Potter HG, Jain SK, Ma Y et al (2012) Cartilage injury after acute, isolated anterior cruciate ligament tear: immediate and longitudinal effect with clinical/MRI follow-up. Am J Sports Med 40:276–285. https://doi.org/10.1177/0363546511423380

Puddu G, Ippolito E, Postacchini F (1976) A classification of Achilles tendon disease. Am J Sports Med 4:145–150. https://doi.org/10.1177/036354657600400404

Rausch Osthoff A-K, Niedermann K, Braun J et al (2018) 2018 EULAR recommendations for physical activity in people with inflammatory arthritis and osteoarthritis. Ann Rheum Dis 77:1251–1260. https://doi.org/10.1136/annrheumdis-2018-213585

Risberg MA, Oiestad BE, Gunderson R et al (2016) Changes in knee osteoarthritis, symptoms, and function after anterior cruciate ligament reconstruction: a 20-year prospective follow-up study. Am J Sports Med 44:1215–1224. https://doi.org/10.1177/0363546515626539

Roemer FW, Neogi T, Nevitt MC et al (2010) Subchondral bone marrow lesions are highly associated with, and predict subchondral bone attrition longitudinally: the MOST study. Osteoarthr Cartil 18:47–53. https://doi.org/10.1016/j.joca.2009.08.018

Roubenoff R (2000) Sarcopenia and its implications for the elderly. Eur J Clin Nutr 54(Suppl 3):S40

Runhaar J, Luijsterburg P, Dekker J, Bierma-Zeinstra SMA (2015) Identifying potential working mechanisms behind the positive effects of exercise therapy on pain and function in osteoarthritis; a systematic review. Osteoarthr Cartil 23:1071–1082. https://doi.org/10.1016/j.joca.2014.12.027

Saberi Hosnijeh F, Zuiderwijk ME, Versteeg M et al (2017) Cam deformity and acetabular dysplasia as risk factors for hip osteoarthritis. Arthritis Rheumatol 69:86–93. https://doi.org/10.1002/art.39929

Sanders TL, Kremers HM, Bryan AJ et al (2016) Is anterior cruciate ligament reconstruction effective in preventing secondary meniscal tears and osteoarthritis? Am J Sports Med 44:1699–1707. https://doi.org/10.1177/0363546516634325

Schepsis AA, Jones H, Haas AL (2002) Achilles tendon disorders in athletes. Am J Sports Med 30:287–305. https://doi.org/10.1177/03635465020300022501

Schmitt H, Hansmann HJ, Brocai DR, Loew M (2001) Long term changes of the throwing arm of former elite javelin throwers. Int J Sports Med 22:275–279. https://doi.org/10.1055/s-2001-13814

Sepúlveda F, Sánchez L, Amy E, Micheo W (2017) Anterior cruciate ligament injury: return to play, function and long-term considerations. Curr Sports Med Rep 16:172–178. https://doi.org/10.1249/JSR.0000000000000356

Shelbourne KD, Muthukaruppan Y (2005) Subjective results of nonoperatively treated, acute, isolated posterior cruciate ligament injuries. Arthroscopy 21:457–461. https://doi.org/10.1016/j.arthro.2004.11.013

Shepherd JA, Baim S, Bilezikian JP, Schousboe JT (2013) Executive summary of the 2013 International Society for Clinical Densitometry Position Development Conference on body composition. J Clin Densitom 16:489–495. https://doi.org/10.1016/j.jocd.2013.08.005

Sofu H, Oner A, Camurcu Y et al (2016) Predictors of the clinical outcome after arthroscopic partial meniscectomy for acute trauma-related symptomatic medial meniscal tear in patients more than 60 years of age. Arthroscopy 32:1125–1132. https://doi.org/10.1016/j.arthro.2015.11.040

Soto-Quijano DA (2017) The competitive senior athlete. Phys Med Rehabil Clin N Am 28:767–776. https://doi.org/10.1016/j.pmr.2017.06.009

Sowers MF, Hayes C, Jamadar D et al (2003) Magnetic resonance-detected subchondral bone marrow and cartilage defect characteristics associated with pain and X-ray-defined knee osteoarthritis. Osteoarthr Cartil 11:387–393. https://doi.org/10.1016/s1063-4584(03)00080-3

Steadman JR, Matheny LM, Singleton SB et al (2015) Meniscus suture repair: minimum 10-year outcomes in patients younger than 40 years compared with patients 40 and older. Am J Sports Med 43:2222–2227. https://doi.org/10.1177/0363546515591260

Stenholm S, Harris TB, Rantanen T, Visser M et al (2008) Sarcopenic obesity: definition, cause and consequences. Curr Opin Clin Nutr Metab Care 11(6):693–700

Strasser EM, Draskovits T, Praschak M et al (2013) Association between ultrasound measurements of muscle thickness, pennation angle, echogenicity and skeletal muscle strength in the elderly. Age (Dordr) 35:2377–2388

Strobel MJ, Weiler A, Schulz MS et al (2003) Arthroscopic evaluation of articular cartilage lesions in posterior-cruciate-ligament-deficient knees. Arthroscopy 19:262–268. https://doi.org/10.1053/jars.2003.50037

Sturnieks DL, Besier TF, Mills PM et al (2008) Knee joint biomechanics following arthroscopic partial meniscectomy. J Orthop Res 26:1075–1080. https://doi.org/10.1002/jor.20610

Tarpenning KM, Hamilton-Wessler M, Wiswell RA, Hawkins SA (2004) Endurance training delays age of decline in leg strength and muscle morphology. Med Sci Sports Exerc 36:74–78. https://doi.org/10.1249/01.MSS.0000106179.73735.A6

Thomas GER, Palmer AJR, Batra RN et al (2014) Subclinical deformities of the hip are significant predictors of radiographic osteoarthritis and joint replacement in women. A 20 year longitudinal cohort study. Osteoarthr Cartil 22:1504–1510. https://doi.org/10.1016/j.joca.2014.06.038

Thorlund JB, Holsgaard-Larsen A, Creaby MW et al (2016) Changes in knee joint load indices from before to 12 months after arthroscopic partial meniscectomy: a prospective cohort study. Osteoarthr Cartil 24:1153–1159. https://doi.org/10.1016/j.joca.2016.01.987

Ticinesi A, Meschi T, Narici MV et al (2017) Muscle ultrasound and sarcopenia in older individuals: a clinical perspective. J Am Med Dir Assoc 18:290–300. https://doi.org/10.1016/j.jamda.2016.11.013

Tran G, Smith TO, Grice A et al (2016) Does sports participation (including level of performance and previous injury) increase risk of osteoarthritis? A systematic review and meta-analysis. Br J Sports Med 50:1459–1466. https://doi.org/10.1136/bjsports-2016-096142

Tsujii A, Nakamura N, Horibe S (2017) Age-related changes in the knee meniscus. Knee 24:1262–1270. https://doi.org/10.1016/j.knee.2017.08.001

Tuite MJ (2003) MR imaging of sports injuries to the rotator cuff. Magn Reson Imaging Clin N Am 11:207–219, v. https://doi.org/10.1016/s1064-9689(03)00025-4

van Meer BL, Oei EHG, Meuffels DE et al (2016) Degenerative changes in the knee 2 years after anterior cruciate ligament rupture and related risk factors: a prospective observational follow-up study. Am J Sports Med 44:1524–1533. https://doi.org/10.1177/0363546516631936

Vanhoenacker FM (2021) Bone marrow edema in sports injuries/general concept. Med Radiol https://doi.org/10.1007/174_2020_241

Wluka AE, Wang Y, Davies-Tuck M et al (2008) Bone marrow lesions predict progression of cartilage defects and loss of cartilage volume in healthy middle-aged adults without knee pain over 2 yrs. Rheumatology 47:1392–1396. https://doi.org/10.1093/rheumatology/ken237

Wolf BR, Amendola A (2005) Impact of osteoarthritis on sports careers. Clin Sports Med 24:187–198. https://doi.org/10.1016/j.csm.2004.08.005

Yoon MA, Hong SJ, Ku MC, Kang CH, Ahn KS, Kim BH (2018) Multiparametric MR imaging of age-related changes in healthy thigh muscles. Radiology 287(1):235–246

Yusuf E, Kortekaas MC, Watt I et al (2011) Do knee abnormalities visualised on MRI explain knee pain in knee osteoarthritis? A systematic review. Ann Rheum Dis 70:60–67. https://doi.org/10.1136/ard.2010.131904

Zanetti M, Bruder E, Romero J, Hodler J (2000) Bone marrow edema pattern in osteoarthritic knees: correlation between MR imaging and histologic findings. Radiology 215:835–840. https://doi.org/10.1148/radiology.215.3.r00jn05835

Zanetti M, Pfirrmann CWA, Schmid MR et al (2003) Patients with suspected meniscal tears: prevalence of abnormalities seen on MRI of 100 symptomatic and 100 contralateral asymptomatic knees. AJR Am J Roentgenol 181:635–641. https://doi.org/10.2214/ajr.181.3.1810635

Zaraiskaya T, Kumbhare D, Noseworthy MD (2006) Diffusion tensor imaging in evaluation of human skeletal muscle injury. J Magn Reson Imaging 24(2):402–408

Zehnacker CH, Bemis-Dougherty A (2007) Effect of weighted exercises on bone mineral density in postmenopausal women. A systematic review. J Geriatr Phys Ther 30:79–88. https://doi.org/10.1519/00139143-200708000-00007

Zhao J, Li X, Bolbos RI et al (2010) Longitudinal assessment of bone marrow edema-like lesions and cartilage degeneration in osteoarthritis using 3 T MR T1rho quantification. Skelet Radiol 39:523–531. https://doi.org/10.1007/s00256-010-0892-6

Zhao R, Zhao M, Xu Z (2015) The effects of differing resistance training modes on the preservation of bone mineral density in postmenopausal women: a meta-analysis. Osteoporos Int 26:1605–1618. https://doi.org/10.1007/s00198-015-3034-0

Zlatkin MB, Rosner J (2004) MR imaging of ligaments and triangular fibrocartilage complex of the wrist. Magn Reson Imaging Clin N Am 12(301–331):vi–vii. https://doi.org/10.1016/j.mric.2004.02.012

Part III

Monitoring of Sports Injury Repair

Natural History and Monitoring of Fractures and Microfractures

Apostolos H. Karantanas

Contents

Abstract

Musculoskeletal injuries are common in elite athletes of highly competitive sports and among recreational or "weekend" athletes. Delay in diagnosis could lead to improper treatment and development of complications. Imaging with plain radiographs, CT, MR imaging, and scintigraphy provides valuable information which allows an early diagnosis. The requests for MR imaging in patients with sports-related injuries are increasing because of its superb contrast resolution. Ultrasonography is a reliable diagnostic modality for imaging sports-related injuries, with wide availability and relatively low cost, more efficient though for soft tissues rather than osseous structures. Each modality has advantages and limitations in imaging fractures and microfractures in athletes. Knowledge of their natural history will aid in understanding the significance of imaging in both diagnosis and treatment planning. Monitoring of the above injuries is meaningful only when imaging data will alter patient's management.

1 Introduction

Over the last three decades there has been an increasing number of people participating in recreational or organized sporting activities. Sports

A. H. Karantanas (✉)
Department of Radiology, University Hospital, Crete, Greece
e-mail: akarantanas@gmail.com

https://doi.org/10.1007/174_2020_271, © Springer Nature Switzerland AG
Published Online: 12 March 2021

injuries represent 4–9% of attendances of accident and emergency departments. The annual healthcare expenditure in the USA has been estimated to be $680 million (Burt and Overpeck 2001). Musculoskeletal injuries are common both in elite athletes of highly competitive sports and among recreational or "weekend" athletes. Delay in diagnosis could lead to improper treatment and development of complications. Imaging with plain radiographs, computed tomography (CT), magnetic resonance imaging (MRI), and scintigraphy provides valuable information which results in an early diagnosis (Overdeck and Palmer 2004). The requests for MRI in patients with sports-related injuries are increasing (Livstone et al. 2002). Ultrasonography is a reliable diagnostic modality for imaging sports-related injuries, with wide availability and relatively low cost, more efficient though for soft tissues rather than osseous structures (Torriani and Kattapuram 2003; Sofka 2004). Each modality has advantages and limitations in imaging fractures and microfractures in athletes. Knowledge of the natural history of sports-related fractures and microfractures will aid in understanding the significance of imaging. Monitoring of the above injuries is meaningful only when the imaging diagnosis will alter patient's management.

Box 1: Plain Radiographs

- Initial imaging for fractures and avulsions.
- Two views are needed for long bones.
- Evaluation of fracture healing.
- Exclusion of preexisting osseous lesion in young athletes.
- Limited accuracy in depicting microfractures.

Box 2: MRI

- Method of choice for soft tissues and bone marrow injuries.
- Diagnosis and grading of stress and osteochondral injuries.
- Monitoring physeal injuries and occult fractures.

2 Fractures

2.1 Osseous Fractures

A fracture is defined as a disruption in the continuity of cortical bone. With an estimated six million fractures occurring annually in the USA and a 5–10% of them complicated with nonunion, it is obvious that management of patients with fractures is of major importance in any national health system (Einhorn 1995).

Sports-related fractures occur in children older than 10 years and in young adults participating in highly competitive sports. Different kinds of athletic activities are often associated with fractures at specific locations, i.e., scaphoid in football, hook of the hamate in golf and baseball, lateral process of the talus in snowboard, tibia in children in skiing, vertebral transverse process in football and hockey, proximal fibula (Maisonneuve fracture) following twisting injuries in any sport, maxillofacial in football, forearm and ankle in skateboarding, and distal radius in football and skiing. The occurrence of a fracture may influence the athlete's future further career. Lawson et al. (1995) reported that only 72.5% of athletes with distal radial fracture returned to their previous level of competition.

The main clinical concerns with regard to a fractured bone refer to normal or abnormal healing, complete or incomplete healing, and timing for its safe use with regard to specific sport and level of activity. In general, fractures of the long bones in athletes correlate to the type of sport activity and heal in the same way as in every healthy subject. In a young injured athlete, the interpreter of plain films should always exclude a preexisting lesion which might predispose to a pathologic fracture.

2.1.1 Natural History

Bone healing occurs in three stages: (1) inflammatory, (2) reparative, and (3) remodeling of the bone to normal or near-normal shape (Crues and Dumont 1975; Frost 1989a, b; Harwood et al. 2010). These phases comprise, respectively, 10%, 40%, and 70% of the fracture union period, significantly overlapping each other. The inflammatory phase peaks at 2–3 weeks after injury and is

defined radiographically by a loss of fracture line definition due to the locally increased osteoclastic activity (Islam et al. 2000). The reparative phase consists of vascular dilatation, neovascular proliferation, and collagen production. The remodeling phase is characterized by periosteal and endosteal calcium deposition and growth of new osteoid tissue. Remodeling in the growing skeleton is able to correct deformities if (a) the fracture is close to the end of a long bone, (b) the deformity parallels the movement plane of the nearest joint, or (c) 2 or more years of growth remains in the injured patient. Remodeling is not able to correct (a) intra-articular fractures with displacement, (b) significantly displaced or rotated diaphyseal fractures, and (c) displaced fractures with growth plate involvement at right angles. Nonunion is defined as the fracture which shows no signs of healing for at least 3 months and persists for a minimum of 9 months (Borges et al. 2020). History of smoking, diabetes, and nonsteroid anti-inflammatory drugs and the presence of open fracture and specific anatomical location (scaphoid, tibia) increase the risk of nonunion (Tzioupis and Giannoudis 2007). However, there is no standard clinical test to evaluate fracture healing (Cunningham et al. 2017) and thus imaging plays an important role in patient management. Elderly female patients with low estrogen levels and patients with metabolic and endocrine abnormalities may show reduced capacity for fracture healing (Calori et al. 2007). Growth plate injuries with associated epiphyseal or metaphyseal fractures have been classified by Salter and Harris (1963). This radiographic classification highly correlates with the morbidity of these injuries. For type II Salter-Harris fractures, return to sports is possible in 12 weeks, whereas for types III and IV, sports-related loading of the lower extremity joints is sustained for at least 6 months (Stanitski 1998a).

2.1.2 Monitoring

The question of return to full athletic or any kind of normal activities should be individualized (i.e., type of fracture, age, specific sport activity, occupation, lifestyle) and decision should be based on clinical criteria. For instance, for clinical union of a clavicular fracture in an adult, a period of 3–4 weeks is required, whereas for a femoral shaft fracture that period would extend to 12–14 weeks (Heppenstall 1980).

Plain radiographs are able to demonstrate the normal healing process of the long-bone fractures and remain the mainstay of its evaluation (Figs. 1, 2, 3, 4, and 5). Early radiological signs of repair include blurring of the opposing fracture surfaces, widening of the fracture line, and peripheral callus formation. In a fracture less than 5–7 days old the well-defined fracture line is seen. In a fracture between 2 and 3 weeks old, callus formation close to but separate from the cortex is noted. By 3–4 weeks the separated osseous surfaces start to bridge and the fracture line is not well defined. In most patients, a widened fracture gap corresponds to bone resorption and is obvious radiographically at 3–6 weeks (Fig. 2). A fracture with marginal sclerosis and callus still separable from cortex is probably between 3 and 11 weeks old. A fracture with periosteal new bone inseparable from the cortex is usually older than 6 weeks (Heppenstall 1980). A partial or whole bridge at the fracture site is expected radiographically at about 10 weeks or more after injury where the callus reaches its peak (Islam et al. 2000). The remodeling stage lasts from 3 months to 2 years and is faster in children (Chapman 1992). Radiological criteria for fracture healing include demonstration of solid callus and trabecular bone bridging the fracture site. Fracture union is established (a) radiologically when there is continuous external bridging callus across the fracture line seen in two orthogonal radiographic projections and (b) clinically when there is no pain or motion at the fractured bones (Heppenstall 1980). Since there is concern that radiographic definition of union is not very reliable, two radiographic scoring systems for the hip (RUSH) and the tibia (RUST), respectively, have been shown to increase the agreement among observers in assessing healing (Whelan et al. 2010; Chiavaras et al. 2013).

Plain radiographs cannot be considered as a valid imaging investigation for detecting occult fractures of the scaphoid (Low and Raby 2005). Avascular necrosis is a common complication of

Fig. 1 7-Year-old male with slightly displaced fracture of the distal tibia and fibula during skiing (*left*). In 8 weeks after casting, periosteal reaction is obvious and early bridging of the fracture sites with diminished definition of the fracture line (*middle*). Complete bridging of the fracture sites occurs at 12 weeks with mature callus formation (*arrows*, *right*)

these fractures. Delayed diagnosis may contribute to such a complication (Fig. 6).

Physeal fractures, particularly Salter-Harris IV and V, have increased risk for growth arrest and poor prognosis. MRI is the method of choice for demonstrating the physeal bar (Fig. 7). If no deformity is depicted at a 2-year follow-up, growth arrest is rather unlikely.

In general, computed tomography (CT) is superior to plain radiographs in the assessment of normal healing of fractures. Advances in software allow optimization of the scanning technique for reducing the metallic artifacts (Krestan et al. 2006). The increased radiation though limits its use in clinically questionable cases.

Although ultrasonography was considered for decades as totally unable to assess the osseous structures, it is now accepted as capable of detecting and evaluating callus formation in fractures (Nicholson et al. 2019). Its low cost, wide availability, and lack of radiation will enhance its role in fracture assessment.

Virtual stress testing is a new technique assessing and grading fracture union by use of finite element analysis, based on CT data (Petfield et al. 2017; Dailey et al. 2019).

Despite the development of newer techniques and advanced imaging tools, the clinical examination remains the primary method of depicting fracture union as shown with the capability for full weight bearing.

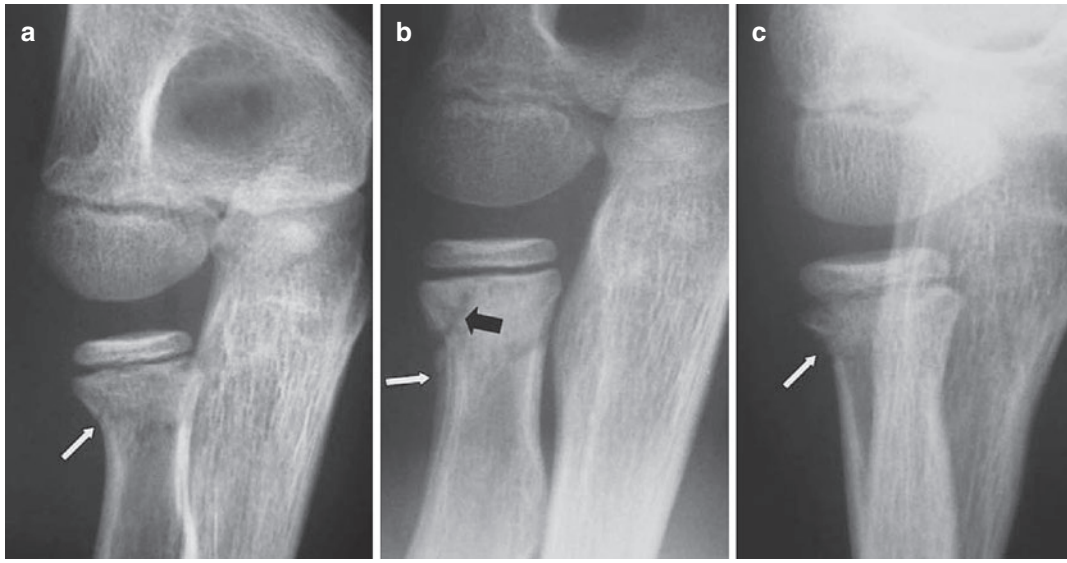

Fig. 2 (**a–c**) Fracture of the proximal radial metaphysis after fall during tennis playing, treated conservatively with casting. (**a**) The fracture is demonstrated as a lucent thin line without any displacement (*arrow*) extending to the growth plate (Salter-Harris II lesion). (**b**) In a 4-week period, the fracture line looks widened (*black arrow*) and callus formation separate from the cortex has developed (*white arrow*). (**c**) Eight weeks after fracture, there is still some discontinuity of the cortex (*arrow*) but both the callus and the fracture line are not seen, in keeping with healing

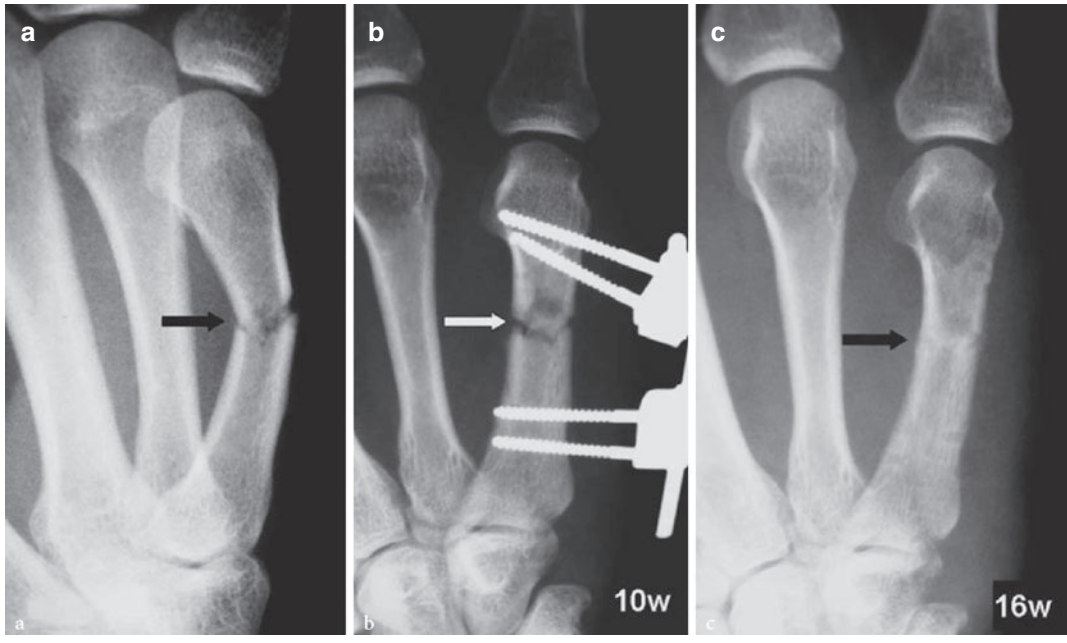

Fig. 3 (**a–c**) Fracture of the fifth metacarpal diaphysis during karate. (**a**) The fracture is horizontal involving the cortex bilaterally and is associated with displacement and angulation (*arrow*). (**b**) Ten weeks after external fixation, there is neither remarkable periosteal reaction nor fracture bridging (*arrow*). (**c**) Sixteen weeks postoperatively, the fracture has completely healed (*arrow*) and the fixation was removed

Fig. 4 (**a**) Initial AP and (**b**) lateral radiographs in a 19-year-old male showing the complete and markedly displaced fractures of the tibia and fibula (arrows). (**c**) Postoperative AP and (**d**) lateral radiographs following reduction and external fixation 2 days after the accident. (**e**) The AP and **f** lateral radiographs 14 months after the operation show a very good result with callus formation in both bones, new bone formation filling the gaps of the fractures, and restoration of the alignment

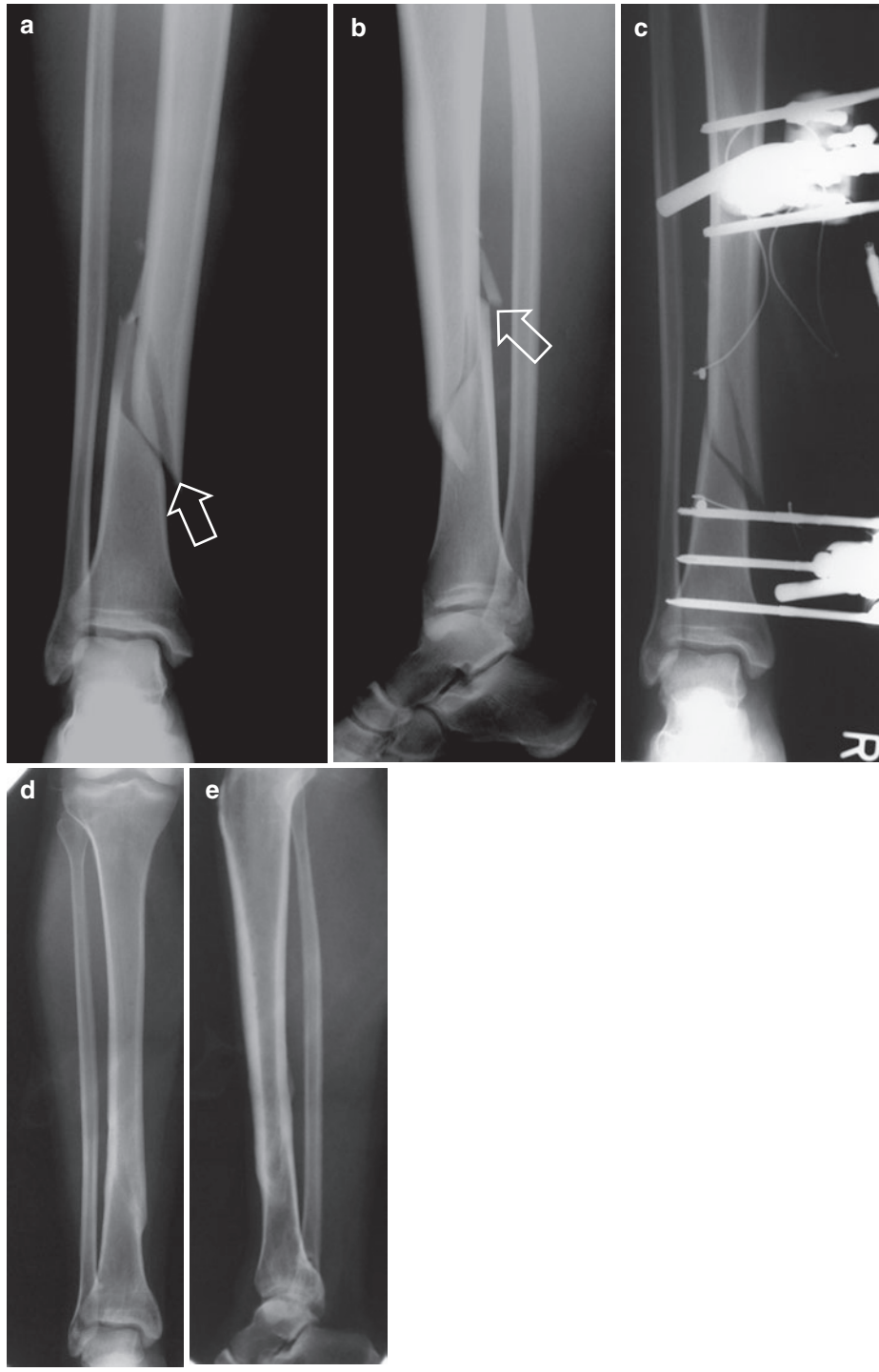

Fig. 5 (**a**) AP and (**b**) lateral radiographs in a 26-year-old male patient following motor vehicle accident, showing the complete oblique comminuted fracture of the tibia (arrows). (**c**) Postoperative radiograph shows the fracture reduction and restoration of the alignment as well as the external fixation; (**d**) AP and (**e**) lateral radiographs 18 months after the accident show complete healing with callus formation and restoration of the alignment

Fig. 6 Scaphoid fracture in a 23-year-old male secondary to ball contact during a basketball competitive game 40 days ago. Persistent pain during training and rest forced the patient to seek medical care. MDCT reveals a fracture of the scaphoid waist (*thin arrow*) without any periosteal reaction. The proximal pole of the scaphoid is hyperdense compared to surrounding bones (*thick arrow*) suggesting nonunion and early avascular necrosis. A "cyst"-like change is obvious in the nonunion site

Fig. 7 Ten-year-old girl with a previous Salter-Harris fracture (III in tibia and I in fibula) during waterskiing 18 months ago. The postoperative plain film (*left*) shows focal sclerosis and growth plate deformity (*black arrow*). The coronal 2D multi-echo gradient echo MR image (*right*) shows directly the bone bar as a low-signal-intensity zone replacing the cartilage (*white arrow*)

2.2 Avulsion Fractures

Avulsion fractures occur during sports activities, are the result of failure of the apophysis, and thus are more common in adolescents than in adults, because of the inherent weakness of the growing skeleton apophysis (Zarins and Cuillo 1983). Diagnosis can be difficult in children before formation of the secondary ossification centers (Shiller et al. 2017). Usually there is a definite history of injury. There are cases though where the athlete does not disclose a history of a single traumatic event. Therefore, radiographic findings without the appropriate history might be confusing and lead to further imaging, biopsy, and an incorrect clinical diagnosis (Brandser et al. 1995). Patients with acute injuries present with severe pain and loss of function (El-Khoury et al. 1997). Chronic avulsion injuries result from repetitive microtrauma or overuse and usually occur during organized sports activities (Micheli and Fehlandt Jr. 1992). Multiple avulsions may be seen in different stages of healing. Cheerleaders, sprinters, and gymnasts as well as football, baseball, and track athletes are especially prone to avulsion injuries (Tehranzadeh 1987; Brandser et al. 1995).

Avulsion fractures are diagnosed with plain radiographs in the context of a reliable and informative history. Avulsions in the healing process may demonstrate radiographic characteristics of an aggressive lesion. Chronic avulsion injuries may frequently show bone formation (Fig. 8). MRI is generally not required for the evaluation of avulsion per se, as its main usefulness is the evaluation of associated muscular, tendinous, and ligamentous disorders. Ultrasonography may play a role both for the initial diagnosis and for assessing healing. Its value however is limited by its inability to image deeply located structures such as the hamstring insertion.

2.2.1 Natural History

Avulsion injuries of the greater tuberosity of the humerus are rare lesions and occur in high-energy contact sports such as rugby. These may be occult on initial radiographs and detected at MRI (Zanetti et al. 1999) (Fig. 9). An anterior dislocation of the shoulder may be an associated injury. Clinical examination alone is not able to distinguish these injuries from rotator cuff tears. Incomplete avulsion injuries can result either from a single traumatic event or from overuse

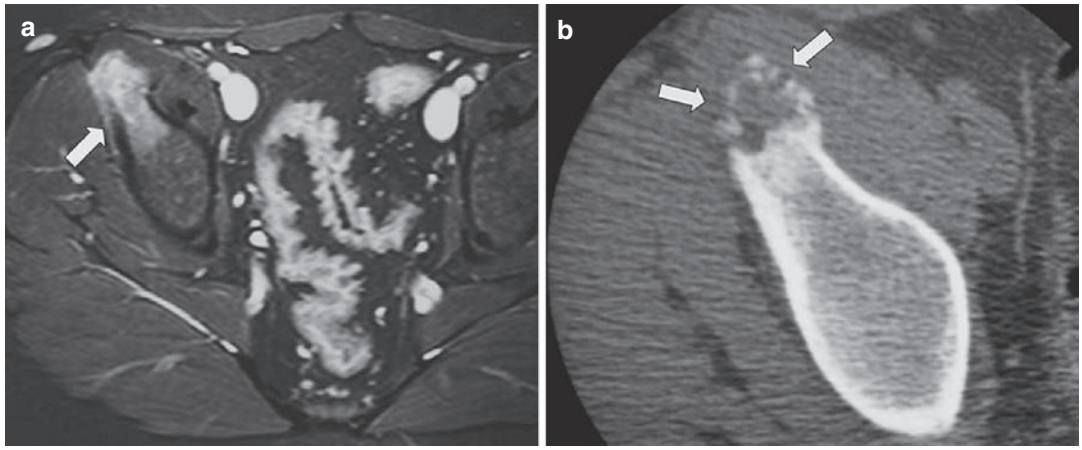

Fig. 8 (**a**, **b**) 12-Year-old male participating in organized football activities (junior's football academy) with pain during the last 3 months over the right anterior and lower pelvis. There was no history of contact or other injury. (**a**) Contrast-enhanced fat-suppressed T1-weighted MR image demonstrates diffuse bone marrow enhancement. There is also periosteal enhancement (*arrow*). (**b**) CT image shows the typical fragmentation of the ossifying subacute avulsion injury of the anterior inferior iliac spine (*arrows*)

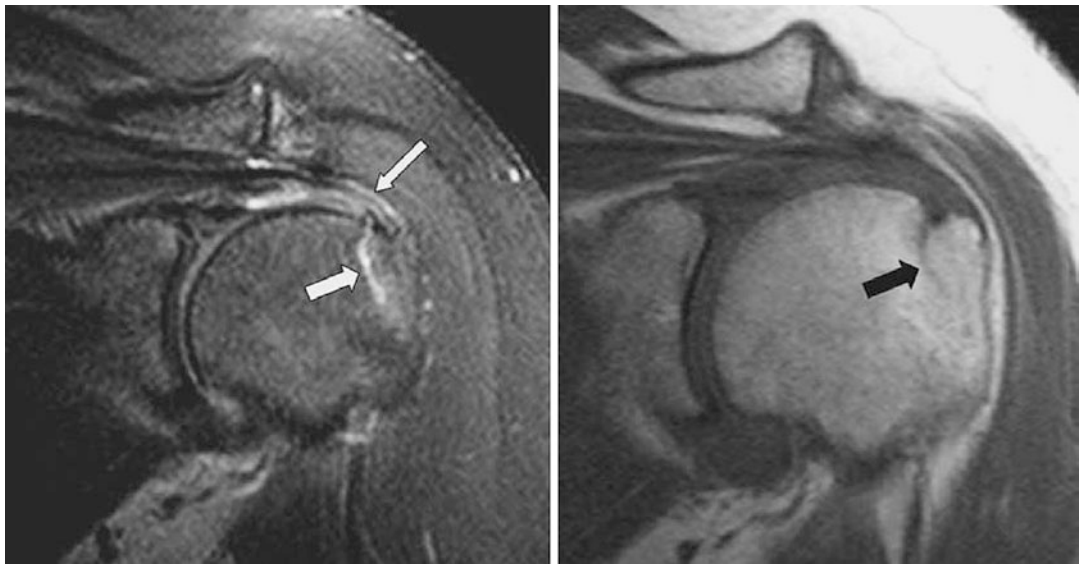

Fig. 9 Occult avulsion injury of the greater tuberosity. Oblique coronal fat-suppressed T2-weighted MR image (*left*) shows the fracture line (*thick arrow*) with partial healing caudally. There is also reactive effusion in the subacromial bursa (*thin arrow*). The oblique coronal T1-weighted MR image (*right*) shows the fracture line (*black arrow*) and normal marrow in the most caudal part of the lesion

activity. Imaging is important since rotator cuff tears require surgical treatment whereas non-displaced avulsion fractures can heal by immobilization alone. Avulsion injuries of the lesser tuberosity of the humerus are rare and occur during wrestling and similar sports. The avulsed fragment may be obvious on plain radiographs or may be erroneously diagnosed as calcific tendinitis secondary to hydroxyapatite deposition disease.

The most common site of avulsion injuries in the pelvis is the ischial tuberosity where the hamstring muscles are inserted. The above injury is observed in runners or dancers (Metzmaker and

Pappas 1985). If the radiologically obvious fragment is displaced more than 2 cm, fibrous union with associated disability may occur. Avulsion injuries of the anterior superior iliac spine occur in sprinters and usually heal without any sequelae after rest. Avulsion injuries of the anterior inferior iliac spine are less common. Athletes with the latter injuries may fully start their activities in about 5–6 weeks. Avulsion injuries in the symphysis pubis and inferior pubic ramus usually result from chronic overuse and are rarely acute following contact sports. These injuries are not obvious on plain radiographs because osseous fragments are not usually seen. MRI can be diagnostic as it demonstrates bone marrow changes on fat-suppressed images in the pubic bones, but it does not have any impact on treatment. The chronic form of this injury may simulate infection or Ewing's sarcoma. Avulsion of the greater trochanter of the femur can be minimally displaced and thus plain radiographs may be negative. These lesions in the middle-aged and elderly patients should raise the suspicion of metastatic disease or renal osteodystrophy.

Avulsion injuries around the knee include the Segond fracture, fibular head avulsion, Gerdy's tubercle avulsion, avulsion of the tibial eminence, and avulsion of the posterior cruciate ligament at the tibial insertion. Osgood-Schlatter disease represents a chronic avulsion injury resulting from repetitive microtrauma at the insertion site of the patellar tendon. Sports related to this disorder include tennis, soccer, and jumping. Acute avulsion injuries of the tibial tubercle are rare and commonly occur in athletes, usually in basketball often superimposed on a preexisting Osgood-Schlatter. In this case, the fracture pattern determines return to sports ranging from 2 to 6 months (Stanitski 1998b). Chronic avulsion in young adults on a preexisting Osgood-Schlatter is known as "unresolved" and typically shows bone marrow edema together with retropatellar bursitis and surrounding soft-tissue edema (Fig. 10).

2.2.2 Monitoring

Plain radiographs are generally sufficient for the diagnosis and follow-up of avulsion injuries. MRI is not recommended because it may demonstrate extensive soft-tissue and bone marrow edema, misinterpreted as an aggressive lesion. When symptoms persist despite treatment, follow-up radiographs are required for assessing possible significant displacement.

Subacute injuries may have an aggressive radiographic appearance due to coexistence of mixed lytic and sclerotic areas. Chronic or old inactive injuries may be associated with an osseous mass, simulating a neoplastic or infectious process. In case of equivocal plain radiographic findings or when the injury is not in the acute phase, CT might provide the correct diagnosis.

2.3 Osteochondral Lesions and Focal Osseous Indentations

Osteochondral fractures are intra-articular fractures involving both the articular cartilage and the bone. These fractures may be acute or chronic. The latter, also known as osteochondritis dissecans, can be caused by repetitive microinjuries. Osteochondritis dissecans is demonstrated on plain radiographs as an oval radiolucency of the articular surface, which may contain a central bony fragment. About 70% of acute osteochondral fractures will be diagnosed correctly by plain radiography (Pettine and Morrey 1987) and most of them with CT (Anderson et al. 1989). However, MRI is the method of choice for assessing these injuries since it can better depict the articular cartilage as well as the subchondral bone (Bohndorf 1999).

2.3.1 Natural History

Acute osteochondral lesions consist of abnormalities of the subchondral bone marrow, subchondral bone, and articular cartilage. They are commonly found at the knee, associated with anterior cruciate ligament ruptures (Rosen et al. 1991) (Fig. 11), and at the talar dome, associated with ankle sprains (Shea and Manoli II 1993; Stone 1996). Osteochondral lesions of the talus are often missed initially because many athletes with "ankle sprains" are not treated by specialists.

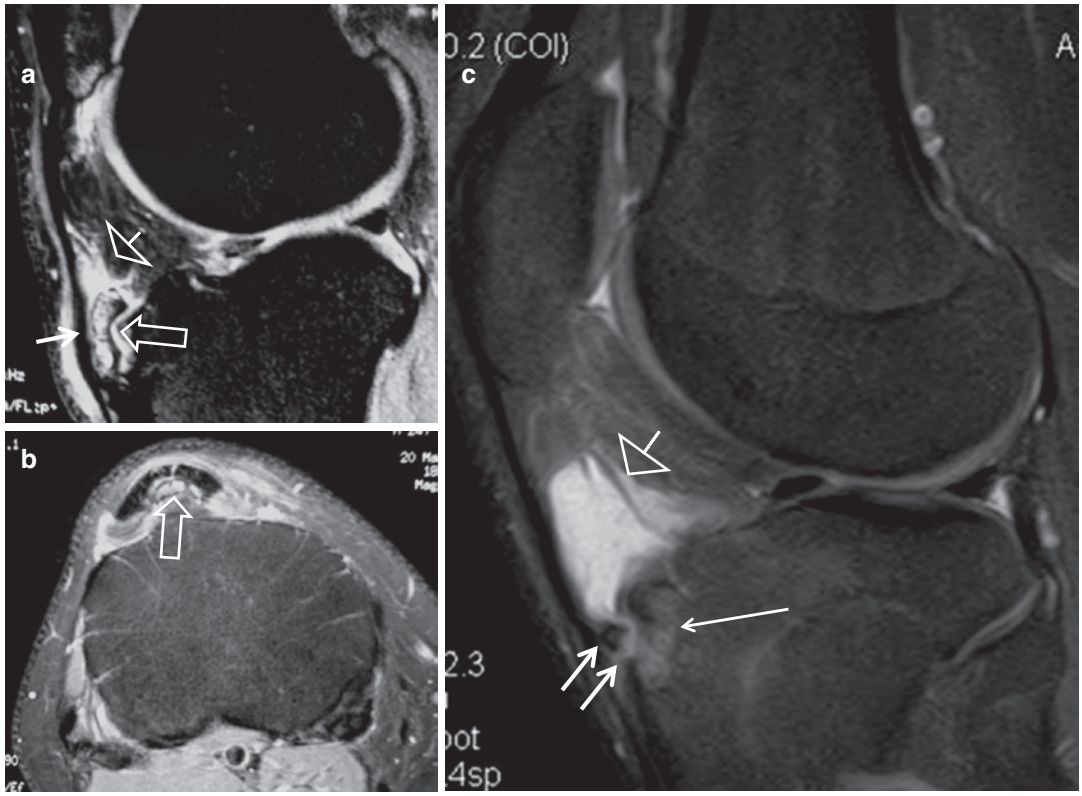

Fig. 10 Unresolved Osgood-Schlatter disease in a 25-year-old male (**a**, **b**) and 20-year-old male (**c**) volleyball athletes. (**a**, **c**) Sagittal fat-suppressed PD-w and (**b**) axial fat-suppressed PD-w MR images showing the avulsed bone (thin arrows), bone marrow edema within the avulsed fragment (open arrow in **a**), reactive bone marrow edema in the anterior tibia (long thin arrow), prepatellar bursitis, and retropatellar bursitis (arrowheads). Bone marrow edema in the lower pole of the patella and edema within the superior Hoffa's fat pad are also shown in **a**, suggesting abnormal friction upon the trochlea

The most widely accepted classification applied in both radiology and arthroscopy practice is the one suggested by Berndt and Harty (1959). This staging schema, though, is limited by the inability to predict prognosis and guide treatment. Lesions with flattening on clinical presentation are considered clinically stable, whereas lesions with fragments are unstable (Takahara et al. 2000). MRI is useful in demonstrating instability of the lesion by depicting fluid signal and/or cystic changes at its deep margin (De Smet et al. 1996). MR arthrography can be useful when development of granulation tissue in the deep surface may simulate fluid and may lead to an erroneous diagnosis of an unstable lesion. On conventional MRI the presence of fatty marrow and contrast enhancement suggests viability of the fragment (Linklater 2004). Activity of the lesion with potential further progression and displacement is suggested by the presence of surrounding bone marrow edema, the extent of which correlates closely to the degree of clinical symptoms (Morrison 2003) (Fig. 12). Stable osteochondral lesions in patients with open physes are usually treated with rest and splinting, whereas unstable lesions are treated surgically. It has been shown that minimally symptomatic osteochondral lesions of talus do not progress over time with nonoperative treatment (Klammer et al. 2015). The surgical options include drilling, fixation or debridement of the fragment, and performance of autologous osteochondral transfer, autologous chondrocyte implantation, or osteochondral allografting (Peterson et al. 2000; Rubin

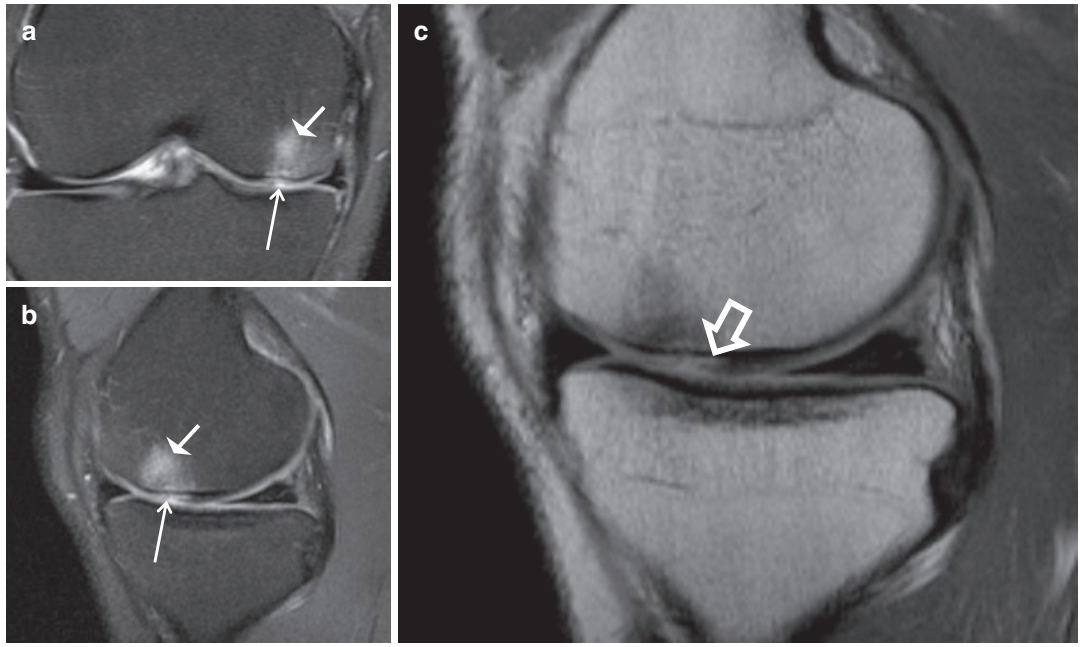

Fig. 11 (**a**–**c**) A 44-year-old male with a football injury 3 weeks prior to imaging. (**a**) Coronal and (**b**) sagittal fat-suppressed PD-w MR images showing the bone marrow edema (*arrowheads*) and the abnormal signal intensity of the corresponding articular cartilage (*thin arrows*). The sagittal PD-w MR image shows to better advantage the articular cartilage disruption with delamination (*open arrow*)

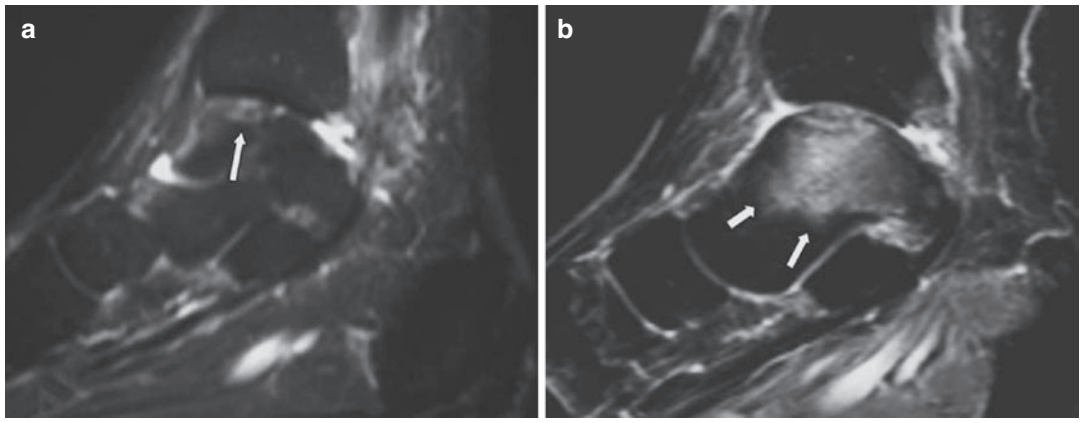

Fig. 12 (**a**, **b**) Active osteochondral lesion in a 46-year-old weekend athlete. (**a**) The fat-suppressed MR image in the sagittal plane shows an osteochondral lesion in the talar dome (*arrow*). (**b**) Eight months later, the symptoms deteriorated despite conservative treatment and MR image shows diffuse bone marrow edema in keeping with the activity of the lesion (*arrows*)

et al. 2000). Traumatic osteochondral lesions have to be differentiated from subchondral insufficiency fractures, avascular necrosis, and osteoarthritis-related osteochondral abnormalities (Gorbachova et al. 2018). The pattern of the lesion on MRI, the patient's demographics, and the clinical presentation allow in most of the cases the correct diagnosis.

Extra-articular focal osseous indentations commonly occur in shoulder instability and dis-

locations. The Hill-Sachs impaction injury is located in the superolateral aspect of the humeral head. This defect is a compression fracture occurring during anterior dislocation after impaction of the humeral head over the anteroinferior glenoid rim. The presence of subchondral bone marrow edema suggests that the lesion is acute or subacute. Increasing size of this defect in follow-up imaging suggests that the patient sustains recurrent dislocations. A "reverse" Hill-Sachs defect results from posterior dislocation. In overhead athletes such as throwers, swimmers, and tennis players, an internal (posterosuperior) impingement syndrome may occur (Giaroli et al. 2005). This entity is characterized by supraspinatus tendinopathy resulting from repetitive contact with the posterosuperior labrum between the supra- and infraspinatus tendon interval. A common finding in these athletes is a focal indentation in the cortex of the posterior greater tuberosity (Fig. 13) with or without focal bone marrow "edema"-like and degenerative cystic changes (Nakagawa et al. 2001). It has been suggested in a limited number of patients that these bony cyst-like changes disappear, presumably due to improved mechanics, after a successful surgical treatment (Giaroli et al. 2005).

2.3.2 Monitoring

All patients with persistent symptoms 6–12 weeks after an ankle sprain should undergo CT or even better MRI, in order to exclude a possible osteochondral lesion of the talus. Patients with a stable osteochondral lesion and persisting symptoms beyond 3 months of treatment may require MRI to determine if the stage of the lesion has changed. Patients with symptoms beyond 6 months should undergo arthroscopy. MRI is the method of choice for the assessment of the progress of osteochondral lesions and the response to treatment. Unstable fragments will usually progress and become a loose body. Two factors determine the treatment strategy for osteochondritis dissecans lesions, namely the stability of the lesion and the skeletal maturity of the patient (Gorbachova et al. 2018). Conservative management is the treatment of choice for stable lesions in children (Ghahremani et al. 2014). If failed, or in cases with unstable lesions, loose bodies, and meniscal tears, surgery is indicated. Postoperative

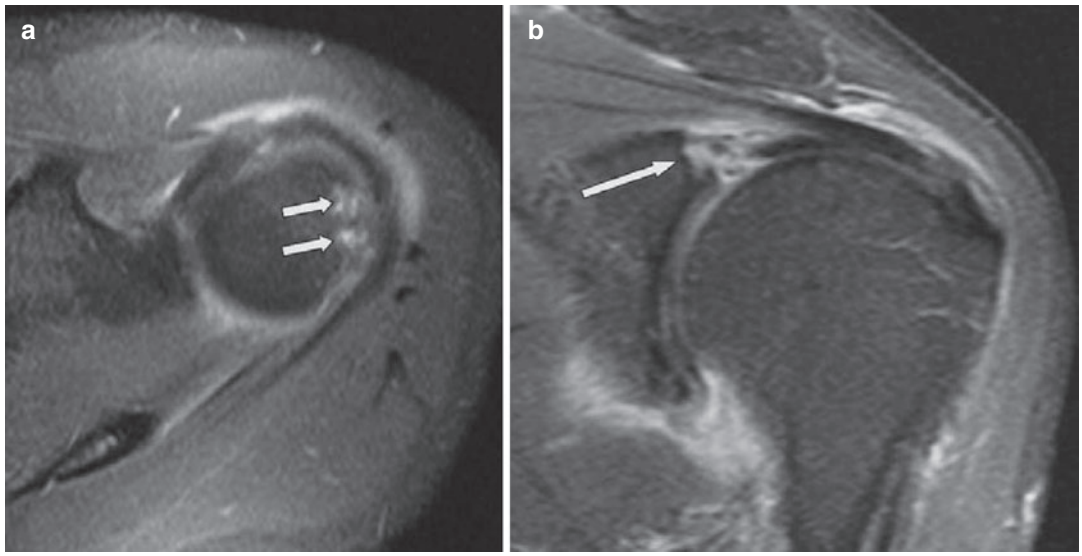

Fig. 13 (**a**, **b**) Indirect MR arthrogram in a 30-year-old tennis player with posterosuperior impingement. (**a**) The axial fat-suppressed T1-weighted SE MR image shows a focal notch with small cysts in the posterolateral greater tuberosity (*arrows*). (**b**) The oblique coronal fat-suppressed T1-weighted SE MR image shows disruption of the superior labrum (*arrow*)

assessment of healing and incorporation can be evaluated with contrast-enhanced MRI (Sanders et al. 2001). Osseous indentations do not require monitoring with imaging.

3 Microfractures

Before the advent of MRI, microfractures were referred to as osseous injuries in the pediatric population not associated with a fracture line in plain radiographs. These injuries, also known as incomplete linear fractures, include *bowing fractures* which usually heal without any periostitis, and *greenstick* and *torus* fractures. Scintigraphy was able to demonstrate increased uptake of the injured bone. The application of musculoskeletal MRI allowed depiction of various similar disorders in adults. These include the spectrum of *stress reactions and fractures*, *bone bruises*, *acute occult fractures*, and *physeal microfractures*. *Transient osteoporosis-transient bone marrow edema* and *regional migratory osteoporosis* can be included in this group.

3.1 Stress Reactions and Fractures

Stress reactions and fractures result from repetitive stress to an otherwise normal bone and represent a variety of osseous and associated soft-tissue injuries (Ánderson and Greenspan 1996). They are common injuries caused by prolonged activities such as marching or running and are usually encountered in the lower extremities, especially tibia, femoral neck, and metatarsals (Coady and Micheli 1997). The importance of early diagnosis of a stress lesion has been highlighted by Ohta-Fukushima et al. (2002) who showed that athletes with an early diagnosis of stress injury return to their sport within 10.4 weeks as opposed to 18.4 weeks in those with a diagnosis later than 3 weeks after the onset of symptoms. Close correlation between imaging and clinical findings is important since MRI is so sensitive that it can show marrow edema-like changes even in asymptomatic runners (Lazzarini et al. 1997; Bergman et al. 2004).

Shin splints, or *medial tibial stress syndrome*, and *thigh splints* or *adductor insertion avulsion syndrome* are terms representing an early form of the stress injury spectrum (Fredericson et al. 1995; Anderson et al. 1997, 2001; Hwang et al. 2005).

In the spectrum of stress fractures, there are additional entities which belong to the so-called insufficiency fractures, i.e., those resulting from repetitive normal loading on a weakened bone. These include the *microtrabecular osteoporotic fractures*, *bisphosphonate-related fractures*, and the complex of *transient osteoporosis-regional migratory osteoporosis*.

3.1.1 Natural History and Monitoring

Plain radiographs are not a sensitive method for depicting early stress injuries (Matheson et al. 1987). The earliest imaging findings of stress injuries are the stress reactions, demonstrated with bone marrow edema on MRI (Fig. 14). Stress fractures are demonstrated radiologically 2–4 weeks after the onset of pain, as a sclerotic line perpendicular to the long axis of the trabeculae. Depending upon the duration of symptoms, a periosteal reaction may be present. Indeed, periostitis may be the only radiological manifestation of the underlying injury. Follow-up radiographs demonstrate the evolution and healing of the injury, thus eliminating the need for a biopsy in cases where clinical history is not helpful and an aggressive lesion is suspected. Multi-detector CT with its multiplanar capability and bone algorithm reconstructions is able to detect the fracture lucent line or the periosteal reaction in specific anatomic locations such as the tibia (Fig. 15), sacrum, spine, and tarsal navicular. Bone scintigraphy has been used as the gold standard for assessing stress injuries (Ánderson and Greenspan 1996). The low specificity though of this imaging modality together with the radiation

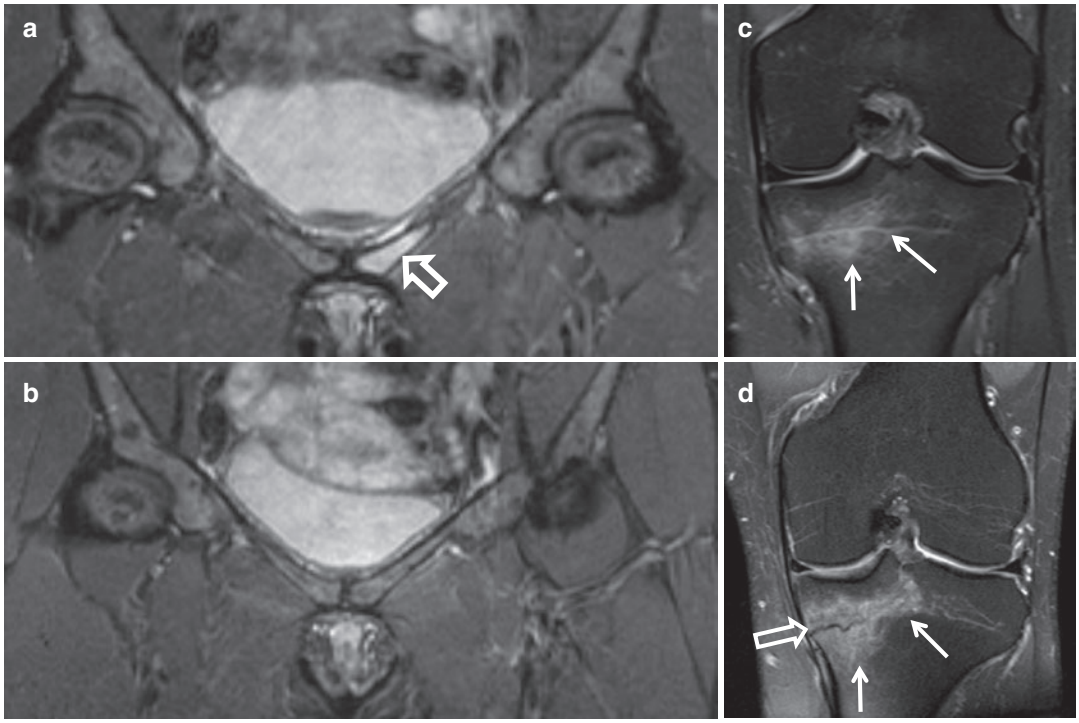

Fig. 14 (**a**) Coronal STIR MR image of a 42-year-old female long-distance runner presenting with groin pain on training for 3 months prior to imaging shows bone marrow edema in the left pubic bone in keeping with stress reaction (open arrow). (**b**) The corresponding image 9 weeks later shows resolution of the edema, matching the clinical improvement. (**c**) Coronal fat-suppressed PD-w MR image of a 39-year-old female runner with pain for 3 weeks prior to imaging shows bone marrow edema in the medial proximal meta-epiphysis of the tibia, in keeping with stress reaction (arrows). There was clinical improvement within 2 weeks following cessation of jogging. (**d**) Coronal fat-suppressed PD-w MR image of a 45-year-old female long-distance runner shows a stress fracture (open arrow) surrounded by bone marrow edema (arrows)

risk and lack of anatomic detail limits its role in the management of stress injuries. In addition, follow-up which is important in elite athletes is further limited by the fact that uptake may be present for several months (Ánderson and Greenspan 1996).

MRI applying STIR and T2-weighted fat-suppressed sequences has emerged as the imaging technique of choice, providing excellent sensitivity and specificity together with superb anatomical detail (Fredericson et al. 1995; Arendt and Griffiths 1997; Yao et al. 1998). MRI findings precede by weeks those of plain radiographs also demonstrating associated soft-tissue injuries. MRI is better than scintigraphy at depicting early stress injuries, possibly due to absence of significant osteoblastic response at this stage, and lacks ionizing radiation which is of consideration when applied to young athletes and in follow-up studies (Deutsch et al. 1997; Gaeta et al. 2005).

Bone marrow changes may be present on MRI of asymptomatic athletes undertaking intensive physical activity. These stress reactions reflect high training load and resolve or continue as asymptomatic changes on imaging regardless of continuation of intensive physical training (Kiuru et al. 2005). Bergman et al. (2004) have shown that tibial stress reactions detected on MRI in asymptomatic runners are not associated with future symptomatic tibial stress injuries.

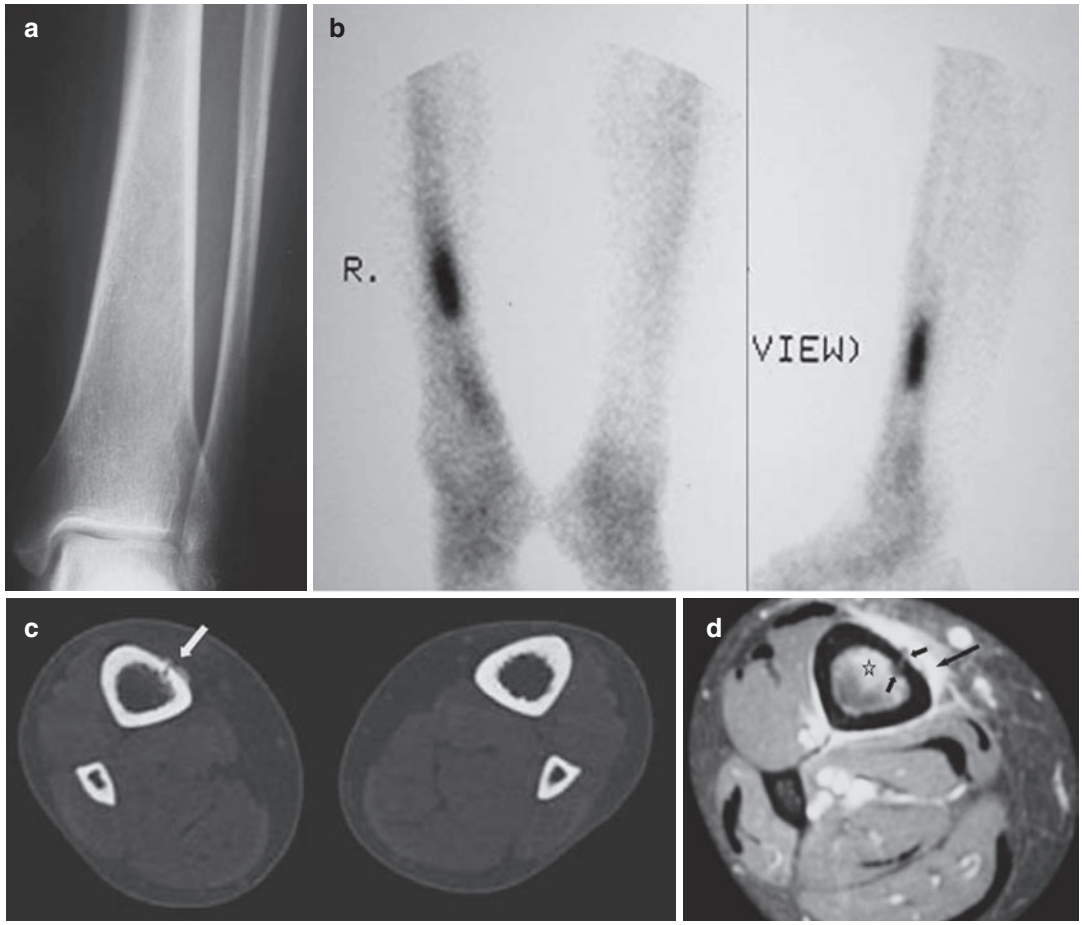

Fig. 15 (**a–d**) Stress fracture in a runner. (**a**) The plain film is normal. (**b**) Scintigraphy reveals increased uptake in the tibia. (**c**) CT shows the lucent fracture line and the callus formation in the anterior cortex (*arrow*). (**d**) Contrast-enhanced fat-suppressed SE T1-weighted MR image shows the soft-tissue enhancement (*long arrow*), periosteal and endosteal new bone formation at the fracture site (*small arrows*), and bone marrow edema (*asterisk*)

Therefore, these findings are not clinically important and there is no need for unnecessary rest or modification of the training program.

A recent study showed that PET-MRI is superior to plain MRI for detecting early stress reaction in the lower extremity (Crönlein et al. 2015).

Symptomatic patients with stress injuries present with localized pain in the end rather than at the onset of the athletic activity. Patients' complaints tend to occur following increase or change in sports activity. The pain is typically relieved at rest and can recur with the onset of the activity. With increased severity of the injury, the pain may persist at rest. A suggested 2- to 3-week period of rest or decrease in training may be curative. No follow-up imaging in *shin splint* and *thigh splint* syndromes is needed.

Patients with sacral stress fractures recover quickly with rest and return to sports within 4–6 weeks. Stress fractures of the pubic rami heal successfully after 6–10 weeks of rest. Femoral neck stress fractures need to be diagnosed early because of their tendency for a frank complete fracture with displacement, particu-

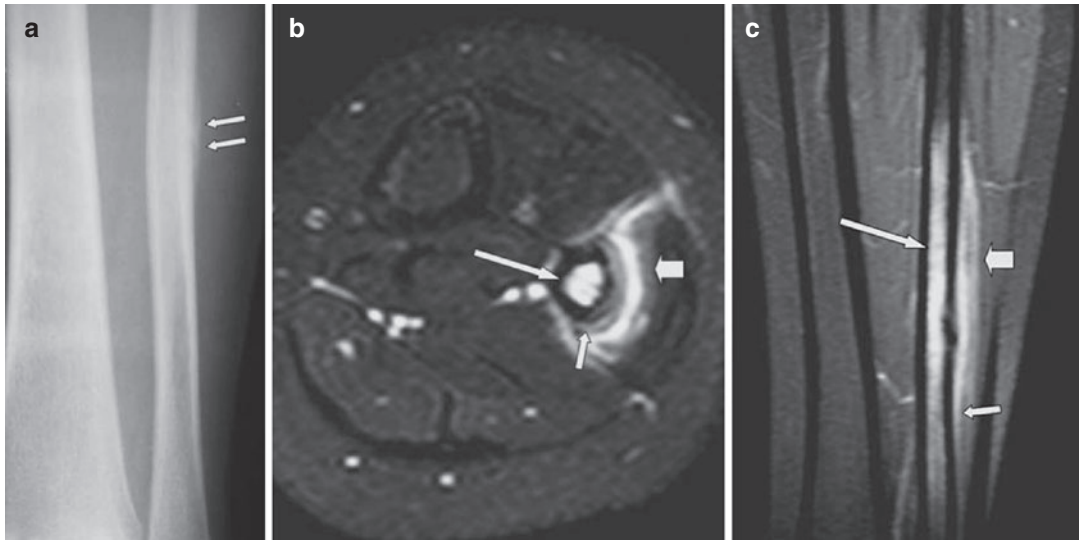

Fig. 16 (**a**–**c**) A 7-year-old girl with calf pain but no history of trauma or sports activity and a biopsy-proven stress fracture of the fibula. (**a**) The plain film shows a periosteal new bone formation (*arrows*). (**b**) The axial fat-suppressed T2-weighted MR image shows the soft-tissue changes (*thick arrow*), periosteal new bone formation (*arrow*), and bone marrow changes (*long white arrow*). (**c**) Contrast-enhanced fat-suppressed SE T1-weighted MR image in the coronal plane shows extensive soft-tissue enhancement (*thick arrow*), subperiosteal enhancement (*arrow*), and bone marrow changes (*long arrow*).

larly when located laterally (Spitz and Newberg 2003). A high degree of clinical suspicion for its presence should be followed by a prompt MRI examination. Most fractures, however, occur medially where the risk for displacement is lower. Most patients with femoral shaft stress fractures are able to resume full sport activity by 12 weeks.

Spondylolysis is considered a non-united stress fracture of the pars interarticularis in children and young adult elite athletes across a wide range of sports (Cheung et al. 2018). Athletes with asymptomatic spondylolysis require no treatment or follow-up imaging. For symptomatic patients with acute spondylolysis, treatment consists of restriction of sports activity varying from 6 weeks to 6 months that should generally continue until the athlete becomes asymptomatic. The treatment is different in patients with a bilateral pars defect, due to the risk of spondylolisthesis. In athletes with stress-induced spondylolysis, fat-suppressed MRI and SPECT-CT can demonstrate if this lesion is active and therefore responsible for the symptoms. Most athletes become asymptomatic and develop no long-term sequelae although only 30–50% of stress fractures demonstrate bony healing radiologically.

Fredericson et al. (1995) classified stress injuries in four grades according to MRI findings. Patients with grade I injuries return to controlled athletic activities within 2–3 weeks, patients with grade II injuries within 4–6 weeks, and patients with grade III in 6–9 weeks. Patients with grade IV injuries, on the other hand, should be treated with a cast for 6 weeks and restrain from impact activities for another 6 weeks. The presence of a medullary line or a cortical abnormality in keeping with grade IV was shown by Yao et al. (1998) to correlate with a longer period of recovery. In pediatric stress fractures, there is often extensive periosteal reaction and bone marrow changes which might lead to an erroneous diagnosis of a neoplastic process (Horev et al. 1990; Ánderson and Greenspan 1996) (Fig. 16). In these cases, MRI can be applied for the diagnosis with direct evaluation of bone marrow edema and for the evaluation of the healing process due to its inherent lack of radiation (Fig. 17).

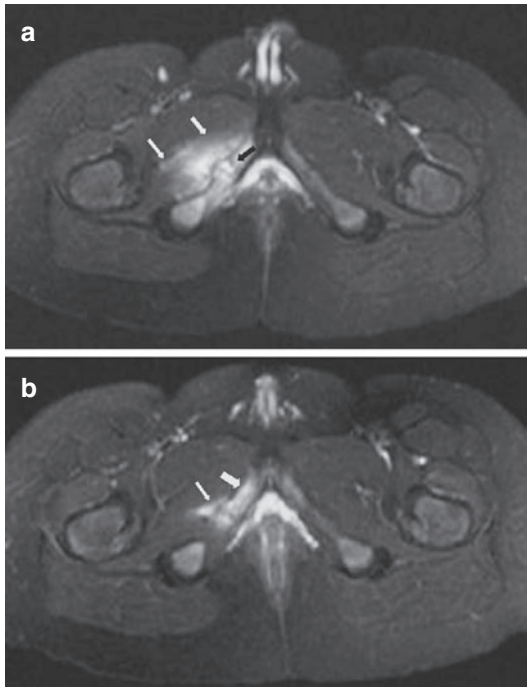

Fig. 17 (**a**, **b**) A 14-year-old male with a stress fracture of the pubic bone. (**a**) The fat-suppressed T2-weighted MR image 1 week after the onset of symptoms shows the stress fracture (*black arrow*) and the muscular strain (*white arrows*). (**b**) A repeat MR imaging examination 1 month later shows resolution of the muscular strain (*thin arrow*) and of the fracture line with residual bone marrow edema (*arrow*).

Low-risk stress fractures are considered those located at the posterior or medial aspect of the tibia, fibula, and lateral malleolus. Treatment consists of a rest period of 2–8 weeks with limited weight bearing, progressing gradually to full athletic activities.

High-risk stress fractures are considered those located at the femoral neck, anterior midtibia, medial malleolus, tarsal navicular, talus, fifth metatarsal, base of second metatarsal, patella, and great toe sesamoids (Mandell et al. 2017). High-risk fractures may require longer recovery period and often surgical intervention.

Osteoporotic microfractures are often seen in the spine and pelvis (Figs. 18a and 19). MRI is the method of choice for prompt diagnosis. Clinical improvement is obvious within few weeks from the onset of symptoms, unless a collapse of a vertebral body complicates the initial bone marrow involvement. Monitoring is usually not required unless a new pain syndrome appears, raising suspicion of a new fracture.

Bisphosphonate treatment, usually in the context of osteoporosis, Paget's disease, and metastatic disease, is related to the presence of factures, typically located in the femoral diaphysis (Rheinboldt et al. 2014). These fractures result from a combination of suppressed bone turnover and tensile forces along the lateral femoral cortex. The natural progression of these fractures starts with focal cortical thickening and ends to a displaced complete fracture (Png et al. 2019). MRI shows the bone marrow edema whereas plain radiographs and CT detect the intracortical fracture line which may be indistinct and suspected only because of focal demineralization of the cortex (Fig. 18b, c). After the focal thickening of the cortex and eventually the presence of a "black" cortical line, monitoring is feasible with plain radiographs (Png et al. 2019).

The *transient bone marrow edema syndrome*, also known as *transient osteoporosis*, is a self-limiting disorder which resolves with conservative treatment. It is seen more commonly in middle-aged males (76.4%) and in females during the third trimester of pregnancy or during the postpartum period. Klontzas et al. showed that DEXA of the spine reveals osteopenia or osteoporosis in the vast majority of patients (30/31). Migration of the bone marrow edema may occur in 19.4%, also known as *regional migratory osteoporosis* (Klontzas et al. 2015). Osteopenia or osteoporosis was also observed in patients with acute nontraumatic bone marrow edema syndrome in the knee and articular collapse (Karantanas et al. 2008). Thus, there is growing evidence that the nontraumatic bone marrow edema syndromes are the result of trabecular microfractures. The method of choice for early diagnosis is MRI (Fig. 18d–f). The natural history is resolution of symptoms and imaging findings within 4–9 months after initial presentation (Vassalou et al. 2019). Typically, migration of the

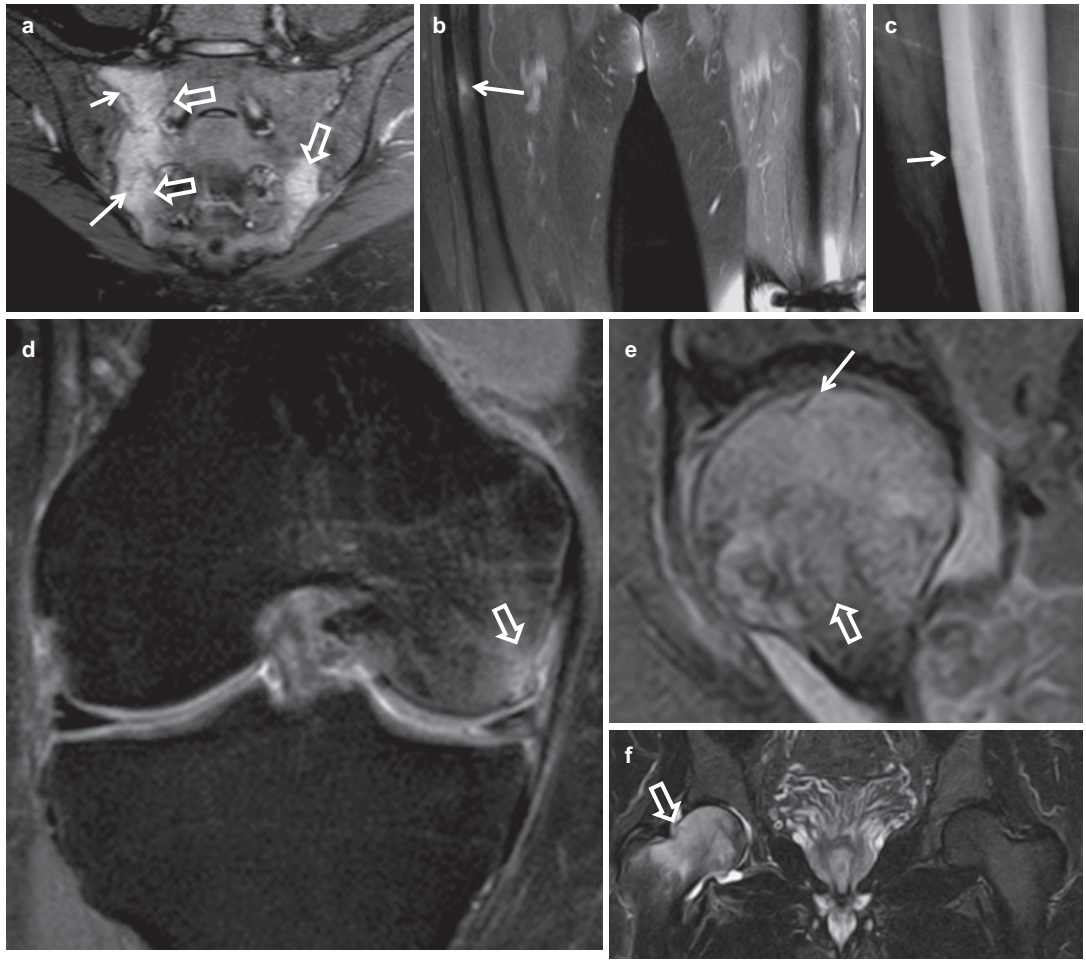

Fig. 18 (**a**–**e**) Insufficiency fractures. (**a**) Coronal oblique STIR MR image in a 36-year-old female patient with pregnancy-induced osteopenia, showing microtrabecular fractures (arrows) surrounded by bone marrow edema (open arrows). (**b**) Coronal fat-suppressed T2-w MR image and (**c**) AP radiograph of the right femoral bone in a 77-year-old female with a history of bisphosphonate treatment, showing the bone marrow edema and the subtle cortical fracture line (arrows). (**d**) Coronal fat-suppressed PD-w MR image of a 57-year-old male with sudden non-traumatic knee joint pain, showing bone marrow edema in the medial femoral condyle (arrow), in keeping with microtrabecular insufficiency fracture. (**e**) Sagittal and (**f**) coronal fat-suppressed PD-w MR images of the hips 13 months after initial knee joint involvement, showing bone marrow edema (open arrows) and a microtrabecular subchondral fracture line (arrow) in keeping with transient osteoporosis/regional migratory osteoporosis. A DEXA of the spine showed severe osteoporosis.

BME to the contralateral hip or the ipsilateral knee and ankle occurs within 12 months of the initial presentation. Monitoring of these disorders is not required by imaging. However, in a patient with a new painful joint location, MRI is required to confirm the diagnosis of migratory osteoporosis.

3.2 Acute Subchondral Injury: Bone Bruise

Bone bruise and *bone contusion* are synonymous terms to describe the occult injury of the trabecular bone resulting in hemorrhage, edema, and infarction (Bohndorf 1999; Ryu et al. 2000; Mandalia

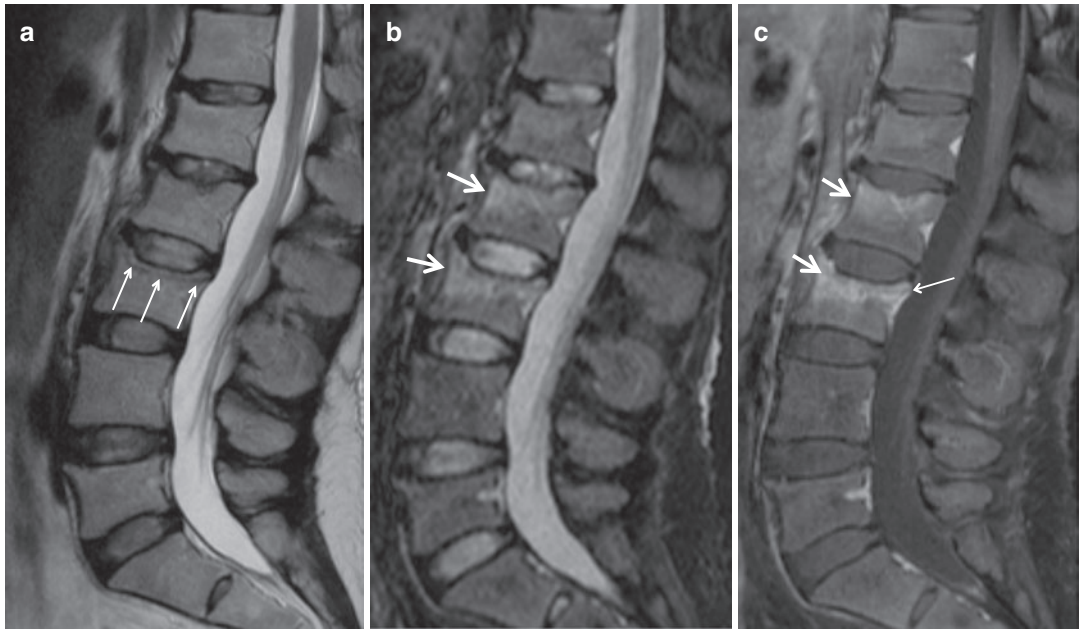

Fig. 19 A 35-year-old female patient presenting with acute back pain, 3 weeks after delivery of her third child. DEXA of the spine showed osteoporosis. (**a**) Sagittal T2-w, (**b**) STIR, and (**c**) fat-suppressed contrast-enhanced T1-w MR images showing bone marrow edema in the L2 and L3 vertebral bodies (arrows), mild depression of the superior end plate, and microtrabecular fractures (thin arrows)

et al. 2005). MRI is very sensitive in detecting bone bruises and understanding the mechanism and severity of injury (Sanders et al. 2000).

3.2.1 Natural History and Monitoring

There might be an increase with MRI in the volume of bone bruise within a few weeks following injury (Davies et al. 2004). Various studies have addressed the rate and degree of resolution of the bruised bone, mainly after knee injuries (Ariyoshi et al. 1997; Bretlau et al. 2002; Davies et al. 2004). It appears that in most patients there is a significant decrease or complete resolution of the lesion within 12–18 weeks (Vanhoenacker et al. 2005) (Fig. 20); however, patients with persisting MRI abnormalities for up to 2 years have been reported. Athletes with isolated bone bruises appear to return to previous sports activities within 3 months on average (Wright et al. 2000).

Bone bruises might indicate an overlying osteochondral injury. This should be particularly suspected when the pattern of resolution on follow-up studies occurs towards the articular surface (Davies et al. 2004). Long-term cartilage degeneration might occur even without imaging findings of acute chondral injury during the acute phase (Nakamae et al. 2006) (Fig. 21). This may be due to either microinjury of the chondrocytes or inadequate weight-bearing protection during resolution which might induce increased load to the articular cartilage.

3.3 Acute Occult Fractures

Acute occult fractures are defined as those not detected by plain radiographs. They may be seen on MRI as fracture lines either associated with

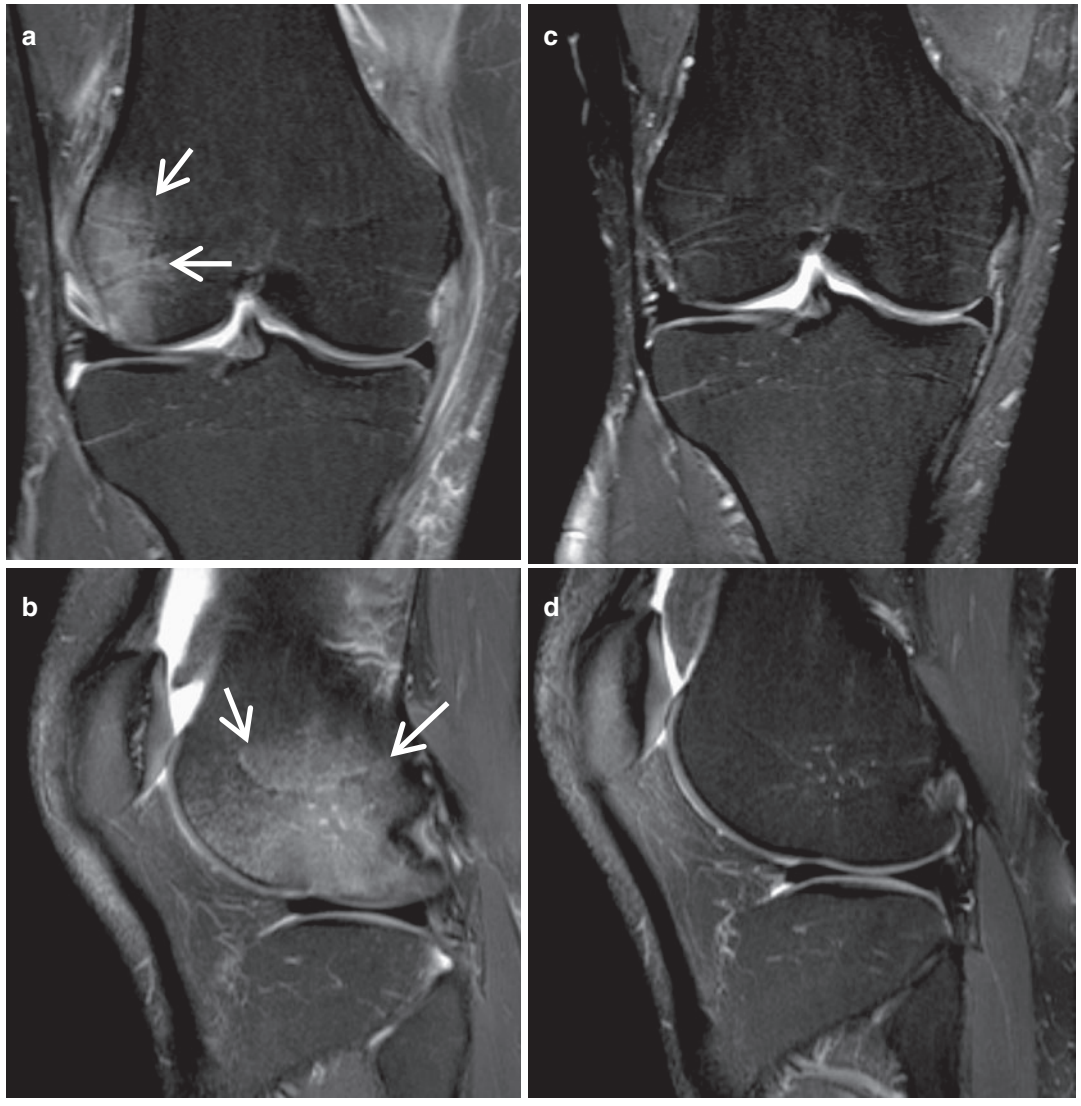

Fig. 20 (**a**–**d**) Resolution pattern of bone bruise in a 26-year-old male mountain skiing athlete, with lateral patella dislocation prior to imaging. (**a**) Coronal and (**b**) sagittal fat-suppressed PD-w MR images of the right knee immediately after injury and (**c**, **d**) 30 weeks later. Extensive impaction bone marrow edema at the lateral femoral condyle is shown (*arrows*). There is complete resolution of the marrow edema on the follow-up MRI

bone bruises or without any bone marrow changes (Figs. 22 and 23). Usually they are detected with MRI in the subacute stage, due to persistent symptoms. Common sites for occult fractures include proximal tibia, distal femur, talar neck, scaphoid, anterior calcaneal process, and lateral talar process, also known as *snowboarder's* fracture. In one study, it was found that in patients with presumed scaphoid fracture and normal radiographs, scintigraphy was able to demonstrate abnormal

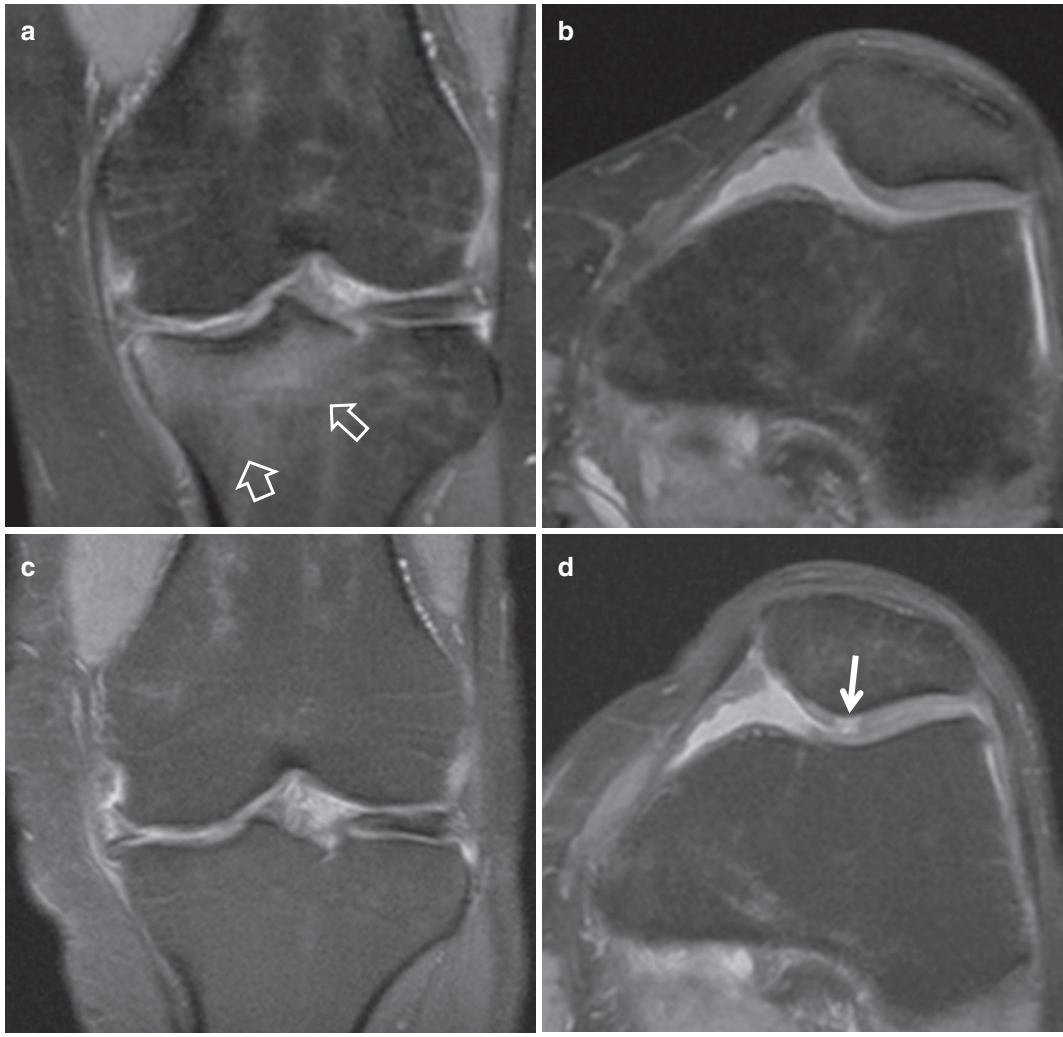

Fig. 21 (**a–d**) A 53-year-old female patient presenting with a painful knee following an injury during dancing. (**a**, **c**) Fat-suppressed PD-w in coronal and (**b**, **d**) axial planes. Bone marrow edema is shown (**a**) suggesting bone bruise (open arrows). The patellar articular cartilage shows thinning on the medial surface. A follow-up MRI 11 months later shows complete resolution of the bone bruise (**c**) and a cartilage full-thickness defect (arrow in **d**) of the previously intact articular cartilage. Degenerative tear of the medial meniscus is also shown

uptake in 45% and CT depicted a fracture in 27.4% of the cases (Groves et al. 2005).

3.3.1 Natural History and Monitoring

The true incidence of long-bone occult fractures cannot be estimated, as these injuries are not detected with plain radiographs. Most of these injuries will resolve after 6–8 weeks and therefore no radiological monitoring is required. Nonunion is unlikely since no major cortical disruption occurs.

Acute scaphoid fractures are of particular interest because in up to 65% of cases they remain radiographically occult immediately after injury, and disrupted blood supply may result in proximal pole osteonecrosis. In addition, these fractures may not be painful enough to demand medical care and therefore late diagnoses with nonunion and/or osteonecrosis are common (Fig. 4). Focal radiolucent areas may develop at the site of previous microfractures (Rennie and

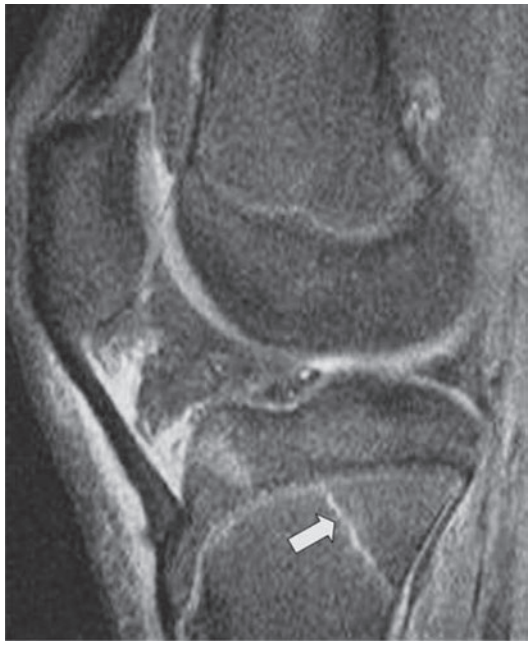

Fig. 22 A 15-year-old football player with a normal radiograph after injury (not shown). The sagittal fat-suppressed PD MR image shows the fracture line extending from the physis to the posterior cortex (*arrow*). There is also post-traumatic edema surrounding the patellar tendon

Fig. 23 A 55-year-old male patient with a valgus direct impaction upon the knee 1 week prior to imaging. The coronal fat-suppressed PD-w MR image shows the bone bruise (*open arrows*) and an occult microfracture in the subarticular medial tibial epiphysis (*thin arrow*). Grade II injury of the medial collateral ligament is also shown (*thick arrow*)

Finlay 2003). Occult fractures are best appreciated with MRI (Rosner et al. 2004). Early use of MRI may prove to be cost effective if early confirmation of the presence of a scaphoid fracture would affect treatment and the patient's returning to sports activities. Gadolinium-enhanced MRI is the method of choice for the preoperative assessment of the vascular status and healing potential of a given fracture as well as for postoperative assessment of graft viability (Cerezal et al. 2000; Dailiana et al. 2004).

3.4 Physeal Microfractures

Growth plate or physis in the growing skeleton represents a thin layer of cartilage located between the metaphysis and epiphysis or apophysis. Most of the physeal injuries occur during sports activities, more commonly in males with a median age of 13 years. The most frequently injured bones are the distal femur, radius, tibia, ulna, fibula, and proximal humerus.

Before the advent of MRI, the growth plate was indirectly evaluated on plain radiographs, seen as a radiolucent line. Acute injury of the growth plate was diagnosed when there was decreased or increased width of the physis with or without displacement of the surrounding fractured osseous structures. Acute physeal injuries without osseous changes (types I and V Salter-Harris) commonly occur in children and may be obvious exclusively with MRI (Fig. 24). An injured growth plate can be associated with a subperiosteal hematoma extending up to the diaphysis where the bony attachment of the periosteum is not firm enough (Fig. 25).

3.4.1 Natural History

Repair of growth plate injury occurs quickly if there is no cartilage cell layer or vascular supply disruption and normal growth occurs in 3 weeks. Good prognosis is the rule for most of the physeal fractures. About 15% of all physeal fractures lead to growth arrest with a bony bridge formation across the physis. This may cause limb shortening or angular deformity depending upon several factors (Oeppen and Jaramillo 2003).

Fig. 24 A 10-year-old male with a water skiing injury. The coronal fat-suppressed T2-weighted MR image shows bone bruise in the tibial metaphysis and epiphysis and a physeal injury demonstrated with high signal intensity without any widening of the physis (*arrows*). There are also soft-tissue edematous and hemorrhagic changes

Growth arrest results from vascular compromise in the epiphyseal site and is much more common at the distal ends of long bones and in the lower extremities. Patients close to skeletal maturity are less likely to develop deformity. A fracture parallel to the physis is at greater risk for growth arrest, especially when the juxtaepiphyseal layer, which includes the germinal zone, rather than the juxtametaphyseal layer, is involved. For type I Salter-Harris fractures, return to sports is possible within 12 weeks (Stanitski 1998a).

Chronic physeal stress injuries are commonly found in young gymnasts, involving the distal radius and ulna bilaterally where the surrounding structures are stronger than the physis. Repetitive stress from overuse causes shearing microfractures locally. Chronic physeal injuries have also been described in skateboarders and adolescent runners with involvement of the distal femoral, proximal tibial, and distal fibular sites. Plain radiographs may show widened physis along with sclerosis and rarely lucent metaphyseal changes. Cessation of the sports activity allows for a full recovery in 6 months. Undiagnosed chronic physeal injuries of the distal radius may cause premature fusion and ulnar positive variance in adulthood.

3.4.2 Monitoring

MRI can be used to depict an acute physeal fracture in very young children with unossified epiphyses but as a rule it is not routinely performed in acute physeal injuries. Radiological follow-up is essential in order to assess normal growth and guide surgical management in cases of suspected growth disturbance. Even the most benign type I Salter-Harris injuries may produce growth arrest. Comparative radiographs of both sides at quarterly intervals for a year should be performed. Most growth arrests are evident by 2 years after a severe physeal injury. When a bony bridge is suspected on the plain radiographs, MRI can assess the central or peripheral location as well as the physeal area involved. Gradient echo 3D with fat suppression sequences can be applied to demonstrate the bony bridge as a low-signal-intensity structure surrounded by the hyperintense physeal cartilage and to calculate the area with its multiplanar capabilities. Bony bridges involving less than 50% of the physeal area are associated with resumption of growth if resected (Peterson 1984).

4 Deep Learning

Deep learning is one of the most widely used forms of artificial intelligence which induce new tools aiming at automatic extraction of features out of imaging data (Lecun et al. 2015). The convolutional neural network (CNN) has been the main network architecture used in medical imaging (Kijowski et al. 2019). Regarding detection of fractures based on plain X-rays, multiple deep learning methods have been used, mainly using open-source CNNs. The machine's capability for depicting fractures

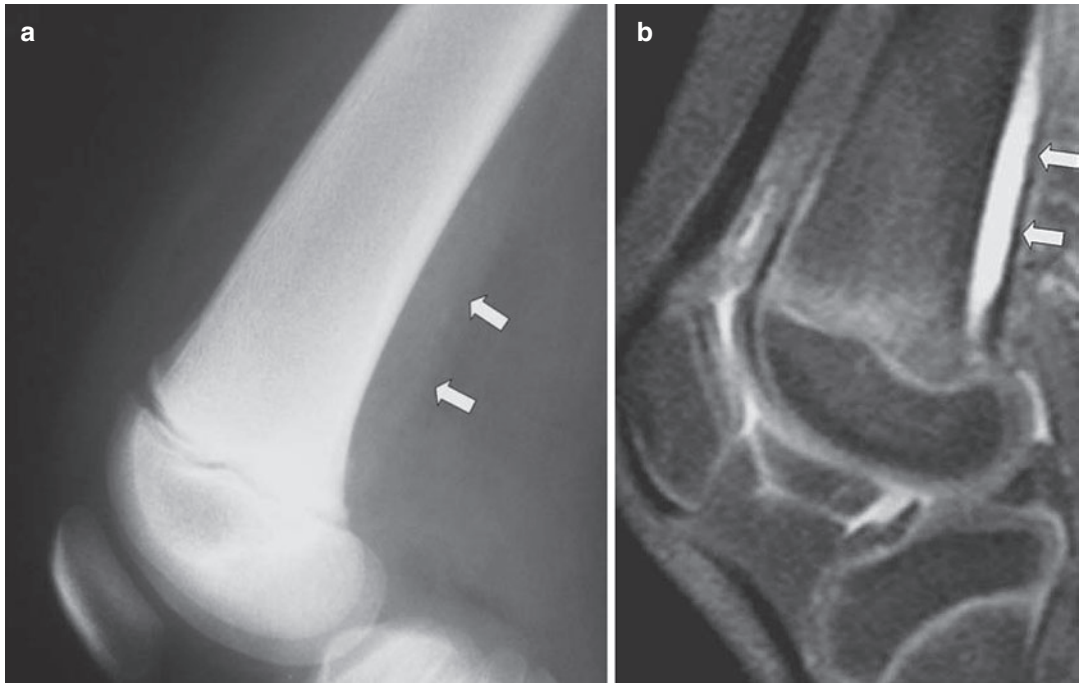

Fig. 25 (**a**, **b**) A 9-year-old girl with a skiing injury. (**a**) The lateral plain film shows a soft-tissue opacity posterior to the femoral metadiaphysis (*arrows*). (**b**) The sagittal fat-suppressed PD MR image shows that the opacity represents a subperiosteal hematoma (*arrows*), presumably secondary to an occult physeal fracture. There is also a shearing injury of the Hoffa's fat pad

on plain radiographs showed an area under curve of 0.99 (Lindsey et al. 2018). The same study using CT for spinal fracture detection showed that there was a 47% reduction in the misinterpretation rate by clinicians. Up to the present, the literature has focused on deep learning and fracture detection. Thus, an open field for research is available to those who wish to explore the value of deep learning in monitoring fracture healing and complications.

5 Conclusions

Evaluation of sports- and trauma-related fractures and microfractures is heavily dependent on imaging. With increased participation of children and adults in organized or recreational sports activities, radiologists are frequently asked to assist in the diagnosis and management of these patients. Plain radiographs are important in depicting and monitoring osseous fractures, avulsion injuries, and osteochondral lesions. MRI is extremely valuable for assessing, grading, and monitoring healing of osteochondral lesions and microfractures in the context of both acute trauma and stress injury.

Things to Remember

1. Evaluation of sports-related fractures and microfractures is heavily dependent on imaging.
2. Plain radiographs are important in depicting and monitoring osseous fractures and avulsion injuries.
3. CT can depict most of the osteochondral fractures and is able to differentiate subacute avulsion injury and stress fracture from a malignant lesion.
4. MRI is extremely valuable for assessing and grading the osteochondral lesions and microfractures.
5. Monitoring of the healing process of microfractures is better performed with MRI.

References

Ánderson MW, Greenspan A (1996) Stress fractures. Radiology 199:1–12

Anderson IF, Crichton KJ, Grattan-Smith T et al (1989) Osteochondral fractures of the dome of the talus. J Bone Joint Surg Am 71:1143–1152

Anderson MW, Ugalde V, Batt M et al (1997) Shin splints: MR appearance in a preliminary study. Radiology 204:177–180

Anderson MW, Kaplan PA, Dussault RG (2001) Adductor insertion avulsion syndrome (thigh splints): spectrum of MR imaging features. AJR Am J Roentgenol 177:673–675

Arendt EA, Griffiths HJ (1997) The use of MR imaging in the assessment and clinical management of stress reactions of bone in high-performance athletes. Clin Sports Med 16:291–306

Ariyoshi M, Nagata K, Sato K et al (1997) Hemarthrosis of the knee and bone contusion. Kurume Med J 44:135–139

Bergman AG, Fredericson M, Ho C et al (2004) Asymptomatic tibial stress reactions: MRI detection and clinical follow-up in distance runners. AJR Am J Roentgenol 183:635–638

Berndt AL, Harty M (1959) Transchondral fractures (osteochondritis dissecans) of the talus. J Bone Joint Surg 41:988–1020

Bohndorf K (1999) Imaging of acute injuries of the articular surfaces (chondral, osteochondral and subchondral fractures). Skelet Radiol 28:545–560

Borges CS, Ruchel PH, Pignataro MB (2020) Scaphoid reconstruction. Orthop Clin N Sm 51:65–76

Brandser EA, El-Khoury GY, Kathol MH (1995) Adolescent hamstring avulsions that simulate tumors. Emerg Radiol 2:273–278

Bretlau T, Tuxoe J, Larsen L et al (2002) Bone bruise in the acutely injured knee. Knee Surg Sports Traumatol Arthrosc 10:96–101

Burt CW, Overpeck MD (2001) Emergency visits for sports related injuries. Ann Emerg Med 37: 301–308

Calori GM, Albisetti W, Agus A, Iori S, Tagliabue L (2007) Risk factors contributing to fracture nonunions. Injury 38(2):S11–S18

Cerezal L, Abascal F, Canga A et al (2000) Usefulness of gadolinium-enhanced MR imaging in the evaluation of the vascularity of scaphoid nonunions. AJR Am J Roentgenol 174:141–149

Chapman S (1992) The radiological dating of injuries. Arch Dis Child 67:1063–1065

Cheung KK, Dhawan RT, Wilson LF et al (2018) Pars interarticularis injury in elite athletes—the role of imaging in diagnosis and management. Eur J Radiol 108:28–42

Chiavaras MM, Bains S, Choudur H et al (2013) The radiographic union score for hip (RUSH): the use of a checklist to evaluate hip fracture healing improves agreement between radiologists and orthopedic surgeons. Skelet Radiol 42:1079–1088

Coady C, Micheli L (1997) Stress fractures in the pediatric athlete. Clin Sports Med 16:225–238

Crönlein M, Rauscher J, Neer AJ et al (2015) Visualization of stress fractures of the foot using PET-MRI: a feasibility study. Eur J Med Res 20:99–105

Crues RL, Dumont J (1975) Fracture healing. Can J Surg 18:403–413

Cunningham BP, Brazina S, Morshed S, Miclau TIII (2017) Fracture healing: a review of clinical, imaging and laboratory diagnostic options. Injury Suppl 1:S69–S75

Dailey HL, Schwarzenberg P, Daly CJ et al (2019) Virtual mechanical testing based on low-dose computed tomography scans for tibial fracture: a pilot study of prediction of time to union and comparison with subjective outcomes scoring. J Bone Joint Surg Am 101:1193–1202

Dailiana ZH, Zachos V, Varitimidis S et al (2004) Scaphoid nonunions treated with vascularised bone grafts: MRI assessment. Eur J Radiol 50:217–224

Davies NH, Niall D, King LJ et al (2004) Magnetic resonance imaging of bone bruising in the acutely injured knee—short-term outcome. Clin Radiol 59:439–445

De Smet AA, Ilahi OA, Graf BK (1996) Reassessment of the MR criteria for stability of osteochondritis dissecans in the knee and ankle. Skelet Radiol 25:159–163

Deutsch AL, Coel MN, Mink JH (1997) Imaging of stress injuries to bone: radiography, scintigraphy, and MR imaging. Clin Sports Med 16:275–290

Einhorn TA (1995) Enhancement of fracture-healing. J Bone Joint Surg Am 77:940–956

El-Khoury GY, Daniel WW, Kathol MH (1997) Acute and chronic avulsive injuries. Radiol Clin N Am 35:747–766

Fredericson M, Bergman G, Hoffman KL et al (1995) Tibial stress reaction in runners: correlation of clinical symptoms and scintigraphy with a new MRI grading system. Am J Sports Med 23:472–481

Frost HM (1989a) Biology of fracture healing: an overview for clinicians. Part I. Clin Orthop Relat Res 248:293–293

Frost HM (1989b) Biology of fracture healing: an overview for clinicians. Part II. Clin Orthop Relat Res 248:294–309

Gaeta M, Minutoli F, Scribano E et al (2005) CT and MR imaging findings in athletes with early tibial stress injuries: comparison with bone scintigraphy findings and emphasis on cortical abnormalities. Radiology 235:553–561

Ghahremani S, Grigg R, Hall T et al (2014) Osteochondral lesions in pediatric and adolescent patients. Semin Musculoskelet Radiol 18:505–512

Giaroli EL, Major NM, Higgins LD (2005) MRI of internal impingement of the shoulder. AJR Am J Roentgenol 185:925–929

Gorbachova T, Melenevsky Y, Cohen M, Cerniglia BW (2018) Osteochondral lesions of the knee:

differentiating the most common entities at MRI. Radiographics 38:1478–1495
Groves AM, Cheow H, Balan K et al (2005) 16-MDCT in the detection of occult wrist fractures: a Comparison with skeletal scintigraphy. AJR Am J Roentgenol 184:1470–1474
Harwood PJ, Newman JB, Michael ALR (2010) An update on fracture healing and non-union. Orthop Traumatol 24:9–23
Heppenstall RB (1980) Fracture healing. In: Heppenstall RB (ed) Fracture treatment and healing. Saunders, Philadelphia, pp 35–64
Horev G, Koreneich L, Ziv N et al (1990) The enigma of stress fractures in the pediatric age: clarification or confusion through the new imaging modalities. Pediatr Radiol 20:469–471
Hwang B, Fredericson M, Chung CB et al (2005) MRI findings of femoral diaphyseal stress injuries in athletes. AJR Am J Roentgenol 185:166–173
Islam O, Soboleski D, Symons S et al (2000) Development and duration of radiographic signs of bone healing in Children. AJR Am J Roentgenol 175:75–78
Karantanas AH, Drakonaki E, Karachalios T et al (2008) Acute non-traumatic marrow edema syndrome in the knee: MRI findings at presentation, correlation with spinal DEXA and outcome. Eur J Radiol 67:22–33
Kijowski R, Liu F, Caliva F, Pedoia V (2019) Deep learning for lesion detection, progression, and prediction of musculoskeletal disease. J Magn Reson Imaging 52:1607–1619
Kiuru MJ, Niva M, Reponen A et al (2005) Bone stress injuries in asymptomatic elite recruits: a clinical and MRI study. Am J Sports Med 33:272–276
Klammer G, Maquieira GJ, Spahn S et al (2015) Natural history of nonoperatively treated osteochondral lesions of the talus. Foot Ankle Int 36(1):24–31
Klontzas ME, Vassalou EE, ZIbis AH et al (2015) MR imaging of transient osteoporosis of the hip: an update on 155 hip joints. Eur J Radiol 84:431–436
Krestan CR, Noske H, Vasilevska V et al (2006) MDCT versus digital radiography in the evaluation of bone healing in orthopedic patients. AJR Am J Roentgenol 186:1754–1760
Lawson GM, Hajducka C, McQueen MM (1995) Sports fractures of the distal radius-epidemiology and outcome. Injury 26:33–36
Lazzarini KM, Troiano RN, Smith RC (1997) Can running cause the appearance of marrow edema on MR images of the foot and ankle? Radiology 202:540–542
Lecun Y, Bengio Y, Hinton G (2015) Deep learning. Nature 521:436–444
Lindsey R, Daluiski A, Chipra S et al (2018) Deep neural network improves fracture detection by clinicians. Proc Natl Acad Sci U S A 115:11591–11596
Linklater J (2004) Ligamentous, chondral, and osteochondral ankle injuries in athletes. Semin Musculoskelet Radiol 8:81–98
Livstone BJ, Parker L, Levin DC (2002) Trends in the utilization of MR angiography and body MR imaging in the US Medicare population: 1993–1998. Radiology 222:615–618
Low G, Raby N (2005) Can follow-up radiography for acute scaphoid fracture still be considered a valid examination? Clin Radiol 60:1106–1110
Mandalia V, Fogg AJ, Chari R et al (2005) Bone bruising of the knee. Clin Radiol 60:627–636
Mandell JC, Khurana B, Smith SE (2017) Stress fractures of the foot and ankle, part 2: site-specific etiology, imaging, and treatment, and differential diagnosis. Skeletal Radoil 46:1165–1186
Matheson GO, Clement DB, McKenzie DC et al (1987) Stress fractures in athletes; a study of 320 cases. Am J Sports Med 15:46–58
Metzmaker JN, Pappas AM (1985) Avulsion fractures of the pelvis. Am J Sports Med 13:349–358
Micheli LJ, Fehlandt AF Jr (1992) Overuse injuries to tendons and apophyses in children and adolescents. Clin Sports Med 11:713–726
Morrison WB (2003) MRI of sports injuries of the ankle. Top Magn Reson Imaging 14:179–197
Nakagawa S, Yoneda M, Hyashida K et al (2001) Greater tuberosity notch: an important indicator of articular-side partial rotator cuff tears in the shoulders of throwing athletes. Am J Sports Med 29:762–770
Nakamae A, Engebretsen L, Bahr R et al (2006) Natural history of bone bruises after acute knee injury: clinical outcome and histopathological findings. Knee Surg Traumatol Arthrosc 14:1252–1258
Nicholson JA, Tsang STJ, MacGillivray TJ et al (2019) What is the role of ultrasound in fracture management? Diagnosis and therapeutic potential for fractures, delayed unions, and fracture-related infection. Bone Joint Res 8:304–312
Oeppen RS, Jaramillo D (2003) Sports injuries in the young athlete. Top Magn Reson Imaging 14:199–208
Ohta-Fukushima M, Mutoh Y, Takasugi S et al (2002) Characteristics of stress fractures in young athletes under 20 years. J Sports Med Phys Fitness 42:198–206
Overdeck KH, Palmer WE (2004) Imaging of hip and groin injuries in athletes. Semin Musculoskelet Radiol 8:41–55
Peterson HA (1984) Partial growth plate arrest and its treatment. J Pediatr Orthop 4:246–258
Peterson L, Minas T, Brittberg M et al (2000) Two- to 9-year outcome after autologous chondrocyte transplantation of the knee. Clin Orthop 374:212–234
Petfield JL, Hayeck GT, Kopperdahl DL (2017) Virtual stress testing of fracture stability in soldiers with severely comminuted tibial fractures. J Orthop Res 35:805–811
Pettine KA, Morrey B (1987) Osteochondral fractures of the talus. A long term follow-up. J Bone Joint Surg (Br) 69:89–92
Png MA, Mohan PC, Koh JSB et al (2019) Natural history of incomplete atypical femoral fractures in patients after a prolonged and variable course of bisphosphonate therapy—a long-term radiological follow-ip. Osteoporos Int 30:2417–2428

Rennie WJ, Finlay DB (2003) Posttraumatic cystlike defects of the scaphoid: late sign of occult microfracture and useful indicator of delayed union. AJR Am J Roentgenol 180:655–658

Rheinboldt M, Harper D, Stone M (2014) Atypical femoral fractures in association with bisphosphonate therapy: a case series. Emerg Radiol 21:557–562

Rosen M, Jackson D, Berger P (1991) Occult osseous lesions documented by magnetic resonance imaging associated with anterior cruciate ligament ruptures. Arthroscopy 7:45–51

Rosner JL, Zlatkin MB, Clifford P et al (2004) Imaging of athletic wrist and hand injuries. Semin Musculoskelet Radiol 8:57–79

Rubin DA, Harner CD, Costello JM (2000) Treatable chondral injuries in the knee: frequency of associated focal subchondral edema. AJR Am J Roentgenol 174:1099–1106

Ryu KM, Jin W, Ko YT et al (2000) Bone bruises: MR characteristics and histological correlation in the young pig. Clin Imaging 24:371–380

Salter RB, Harris R (1963) Injuries involving the epiphyseal plate. J Bone Joint Surg 45A:587–622

Sanders TG, Medynski MA, Feller JF et al (2000) Bone contusion pattern of the knee at MR imaging: footprint of the mechanism of injury. Radiographics 20:S135–S151

Sanders TG, Mentzer KD, Miller M et al (2001) Autogenous osteochondral "plug" transfer for the treatment of focal chondral defects: postoperative MR appearance with clinical correlation. Skelet Radiol 30:570–578

Shea MP, Manoli A II (1993) Osteochondral lesions of the talar dome. Foot Ankle 14:48–55

Shiller J, DeFroda S, Blood T (2017) Lower extremity avulsion fractures in the pediatric and adolescent athete. J Am Acad Otrhop Surg 25:251–259

Sofka CM (2004) Ultrasound in sports medicine. Semin Musculoskelet Radiol 8:17–27

Spitz D, Newberg A (2003) Imaging of stress fractures in the athlete. Magn Reson Imaging Clin N Am 11:323–339

Stanitski CL (1998a) Epiphyseal fractures about knee. Oper Techn Sports Med 6:234–242

Stanitski CL (1998b) Acute tibial tubercle avulsion fractures. Oper Techn Sports Med 6:243–246

Stone JW (1996) Osteochondral lesions of the talar dome. J Am Acad Orthop Surg 4:63–73

Takahara M, Ogino T, Takagi M et al (2000) Natural progression of osteochondritis dissecans of the humeral capitellum: initial observations. Radiology 216:207–212

Tehranzadeh J (1987) The spectrum of avulsion and avulsion-like injuries of the musculoskeletal system. Radiographics 7:945–974

Torriani M, Kattapuram SV (2003) Musculoskeletal ultrasound: an alternative imaging modality for sports-related injuries. Top Magn Reson Imaging 14:103–111

Tzioupis C, Giannoudis PV (2007) Prevalence of long-bone non-unions. Injury 38:S3–S9

Vanhoenacker FM, Snoeckx A, Vandaele L et al (2005) Bone marrow changes in sports injuries. JBR-BTR 88:332–335

Vassalou EE, Spanakis K, Tsifountoudis IP, Karantanas AH (2019) MR imaging of the hip: an update on bone marrow edema. Semin Musculoskelet Radiol 23:276–288

Whelan DB, Bhandari M, Stephen D et al (2010) Development of the radiographic union score for tibial fractures for the assessment of tibial fracture healing after intramedullary fixation. J Trauma 68:629–632

Wright RW, Phaneuf MA, Limbird TJ et al (2000) Clinical outcome of isolated subcortical trabecular fractures (bone bruise) detected on magnetic resonance imaging in knees. Am J Sports Med 28:663–667

Yao L, Johnson C, Gentili A et al (1998) Stress injuries of bone: analysis of MR imaging staging criteria. Acad Radiol 5:34–40

Zanetti M, Weishaupt D, Jost B et al (1999) MR imaging for traumatic tears of the rotator cuff: high prevalence of greater tuberosity fractures and subscapularis tendon tears. AJR Am J Roentgenol 172:463–467

Zarins B, Cuillo JV (1983) Acute muscle and tendon injuries in athletes. Clin Sports Med 2:167–182

Monitoring of Muscle and Tendon Repair

Iris Kilsdonk, Danoob Dalili,
Anne D. van der Made, and Mario Maas

I. Kilsdonk
Department of Radiology and Nuclear Medicine, OLVG Hospital Amsterdam, Amsterdam, The Netherlands

D. Dalili
Department of Musculoskeletal Radiology, Nuffield Orthopaedic Centre, Oxford University Hospitals NHS Foundation Trust, Oxford, UK

A. D. van der Made
Department of Orthopaedic Surgery, Amsterdam Movement Sciences, Amsterdam UMC, University of Amsterdam, Amsterdam, The Netherlands

Academic Center for Evidence-Based Sports Medicine (ACES), Amsterdam UMC, Amsterdam, The Netherlands

Amsterdam Collaboration for Health and Safety in Sports (ACHSS), AMC/VUmc IOC Research Center, Amsterdam, The Netherlands

M. Maas (✉)
Academic Center for Evidence-Based Sports Medicine (ACES), Amsterdam UMC, Amsterdam, The Netherlands

Amsterdam Collaboration for Health and Safety in Sports (ACHSS), AMC/VUmc IOC Research Center, Amsterdam, The Netherlands

Department of Radiology & Nuclear Medicine, Amsterdam Movement Sciences, Amsterdam UMC, University of Amsterdam, Amsterdam, The Netherlands

Amsterdam Movement Sciences, Amsterdam UMC, Amsterdam, The Netherlands
e-mail: m.maas@amsterdamumc.nl

Contents

Abstract

The use of magnetic resonance imaging (MRI) has taken a prominent place in the diagnosis and classification of sports-related muscle injury. However, its role in follow-up and monitoring of muscle and tendon repair is still debated. Muscle injuries have a common nature and are most often self-limiting; therefore they are usually evaluated clinically and do not need further follow-up imaging. However, in certain high-stake cases, for instance in elite athletes, follow-up MRI visualizing the repair process of the damaged muscle and/or tendon would be of added value. This chapter gives an up-to-date overview on the role of conventional and advanced MR techniques in the process of monitoring muscle and tendon repair, in order to plan and guide optimal rehabilitation of the athlete.

Med Radiol Diagn Imaging (2021)
https://doi.org/10.1007/174_2020_264, © Springer Nature Switzerland AG
Published Online: 16 March 2021

1 Introduction

At the moment of acute injury, the use of magnetic resonance imaging (MRI) has taken a prominent role in the diagnosis and classification of sports-related muscle injury (Mueller-Wohlfahrt et al. 2013; Pollock et al. 2014; Wangensteen et al. 2018). However, its role in follow-up and monitoring of muscle and tendon repair is still debated. Muscle injuries have a common nature and are most often self-limiting with adequate nonoperative treatment. Therefore, they are usually evaluated clinically and do not need further follow-up imaging. However, in certain high-stake cases, for instance in elite athletes, follow-up MRI visualizing the repair process of the damaged muscle and/or tendon would be of added value (Kerkhoffs et al. 2013). Ideally, it should provide additional information which might help the treating physician decide on management, monitor treatment effects, prevent reinjury or exacerbation, and most importantly assist in return-to-play (RTP) decision-making. Currently, there is an increasing demand for MRI in this process of monitoring muscle repair, of which this chapter will give an up-to-date overview. The chapter focuses on muscle injury including the muscle belly itself (mostly based on direct injury, consisting of a blow to the muscle) and injury to the myotendinous and myofascial junctions as well as injury of the free/intramuscular tendon (all mostly caused by indirect injury: tearing due to excessive eccentric loading) (Garrett 1990).

The most commonly affected muscles in sports-related injury are located in the lower extremity: hamstrings, adductor muscles, quadriceps, and gastrocnemius muscles, probably because they cross two joints (Ekstrand et al. 2011). Most of the information regarding follow-up, prognosis, and RTP of muscle injury originates from studies on hamstring muscle injury; this forms the basis of our current knowledge and the information written in this chapter (Slavotinek 2007).

2 Healing Process of Muscle and Tendon Injury

To be able to understand the MR features and to understand the advanced MR techniques it is important to appreciate the pathophysiology of the healing process of muscle injury, which can be divided into three phases (Järvinen et al. 2005). It starts with the "destruction" or "inflammatory phase" starting after the injury, in which there is rupture of myofibers, the main components of a muscle giving it its contractility. A hematoma fills the gap, the damaged myofibers undergo necrosis, and an inflammatory reaction is initiated. Inflammatory cells appear in the area by direct influx from damaged blood vessels and by activation of macrophages and fibroblasts in the damaged myofibers. The destruction phase is followed by a second repair phase starting at days 2–3 and a third remodeling phase, which generally show overlap in time. During the repair phase, necrotized muscle tissue undergoes phagocytosis and there is ingrowth of capillary vessels into the damaged tissue. Myofibers regenerate and connective (scar) tissue is formed. With time, the size of the scar diminishes, and the ends of the ruptured muscle approach each other. It still is not clear whether there will ever be a fusion or always be a remaining connective tissue in between. Lastly, in the remodeling phase the regenerated myofibers mature and the scar tissue reorganizes so that the function of the muscle will be restored. There is a gradual resolution of edema. The injured muscle revascularizes and there is regeneration of intramuscular nerves.

Concerning the normal response to tendon injury, there are similarities with the healing response following muscle injury (Sharma and Maffulli 2005). In the inflammatory phase, there is an influx of neutrophils followed by monocytes and phagocytes. Necrotic debris is cleared by phagocytosis, and angiogenesis and proliferation of tenocytes are initiated by vasoactive and chemotactic factors. These tenocytes are derived from either epi/endotenon or surrounding

sheet/synovium, and synthesize type III collagen, which peaks in the following (proliferative) phase, lasting for several weeks. It should be noted that water content is high during this phase, which has consequences for interpretation of imaging. Subsequently, the final (remodeling) phase is subdivided into a consolidation and maturation stage and is characterized by decreased cellularity and more fibrous repair tissue. In the consolidation phase, tenocytes and collagen align in the direction of tensile forces. It is at this stage that a higher proportion of type I collagen is synthesized. In the maturation phase, the fibrous tissue matures over the course of months, and tendon vascularity decreases.

3 What the Radiologist Needs to Know

3.1 MR Protocol

Most muscle injuries can be visualized with a dedicated surface coil. Images should be acquired in at least a transverse and a longitudinal plane (coronal or sagittal depending on the affected muscle), with optional use of multiplanar reconstructions. Preferably, at least one of these sequences includes images of the contralateral side. This is important to compare anatomy as well as atrophy and fatty infiltration of the affected muscle with the asymptomatic side. We recommend to place a skin marker at the site of maximal tenderness as indicated by the athlete (typically a cod-liver oil capsule). To obtain full transverse coverage in thigh injuries, two separate axial acquisitions should be performed. The MR protocol to monitor muscle repair should be the same as the protocol used in the diagnostic setting and contain at least the following conventional MR sequences (Fig. 1):

- T1-weighted (W) sequence: ideal to evaluate anatomy and assess tendon continuity. Furthermore, T1-W images (WI) allow the detection of (sub)acute hemorrhage or hematoma, fatty infiltration, muscle atrophy, and scar tissue formation.
- PD/T2-W fat-suppressed fluid-sensitive sequences: sensitive to muscle damage by the

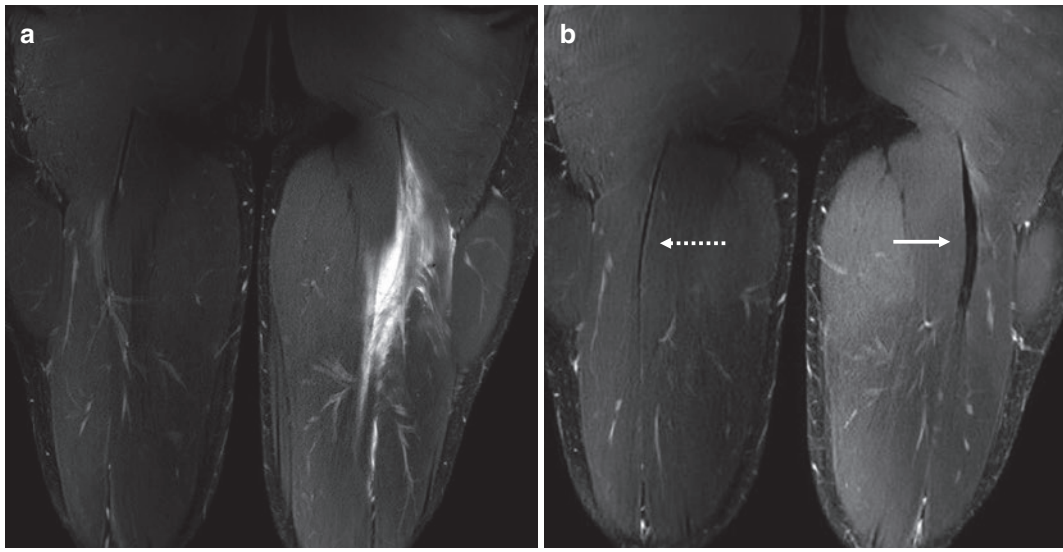

Fig. 1 (**a**, **b**) 19-Year-old male with left-sided partial-thickness conjoined semitendinosus-biceps femoris tendon injury. (**a**) Coronal T2 DIXON image at the time of injury showing high-signal-intensity intramuscular hematoma and edema. (**b**) Coronal T2 DIXON image at RTP showing almost complete resorption of edema and a thickened fibrous tendon (closed arrow) compared to the asymptomatic right side (dashed arrow)

detection of edematous changes/infiltration as high signal. In our institution, we prefer DIXON chemical shift imaging to obtain homogeneous fat suppression (Maas et al. 1999). Alternatively, a STIR sequence can be used. In low-grade muscle injuries fluid-like signal may be seen at the MTJ dispersing alongside the muscle fascicles in a classical feathery distribution. In higher grade injuries where there is distortion of muscle fibers, more organized intramuscular and intratendinous focal areas of high signal appear. Depending on the exact location of the injury, edema can collect along the myotendinous junction or the peripheral myofascial junction.

3.2 What to Look for at Follow-Up

It is not yet possible to use conventional MR sequences to image the microstructural changes within the healing muscle as described previously. During the process of muscle healing, MR imaging using conventional sequences will show a series of characteristics that the radiologist should mention in his/her report. We highly advocate that the radiologist uses the same terminology and grading system used by the referring physician. Generally speaking, the most important imaging changes that may occur during the process of healing muscle are:

1. *Regression of the acute-stage findings:* Assess the reduction of fluid between the muscle fascicles and perimysial fluid. This amount of edema is measured in a simple and reproducible manner by assessing caudocranial length. Follow local preferences; also cross-sectional area or volume of T2 hyperintensity can be used as a measure for edema reduction. Furthermore, assess gap size; in normal healing of high-grade muscle injury it reduces over time as fibers begin to oppose one another (Figs. 1, 2, and 3).
2. *Formation of scar tissue:* Fibrosis can be seen on MR as low signal intensity at T1-WI and high signal intensity at T2-WI in the first few weeks (Connell et al. 2004). As the scar develops, T2 signal of scar tissue becomes hypointense on all MR sequences and its size gradually decreases (Figs. 1, 2, and 3). It is important to recognize areas of fibrosis, because recurrent tears can occur nearby (Koulouris and Connell 2005) (Fig. 3c). It is believed that the site of fibrosis alters elasticity of the muscle and contraction mechanics during movement and therefore may contribute to reinjury risk (Silder et al. 2008). Keep in mind to always look at the T1-WI when

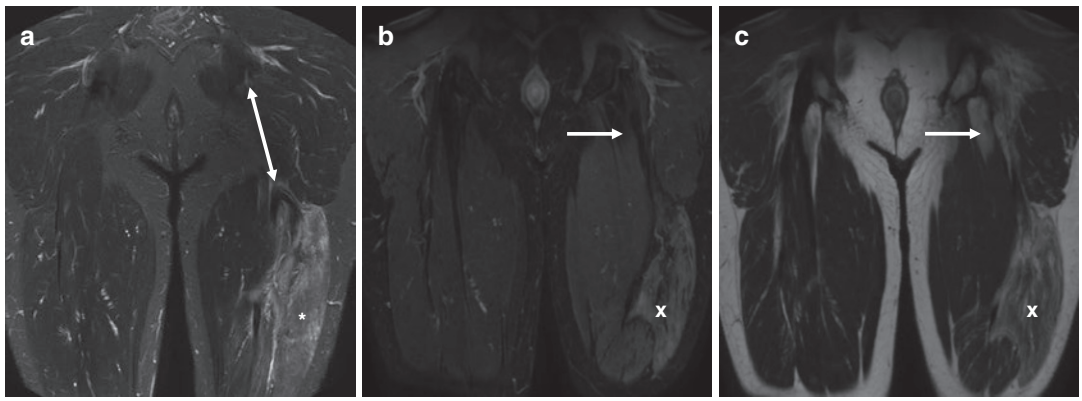

Fig. 2 (**a**–**c**) 39-Year-old male with complete avulsion of proximal hamstring tendons of the left leg. (**a**) Coronal T2 DIXON image showing rupture and retraction (arrow) of the proximal hamstring tendon with surrounding intramuscular edema (*). (**b**) Coronal T2 DIXON and (**c**) coronal T1-weighted images at follow-up after 1 year showing thickened fibrotic tendon (arrow) and fatty infiltration and muscle atrophy (x) as complication

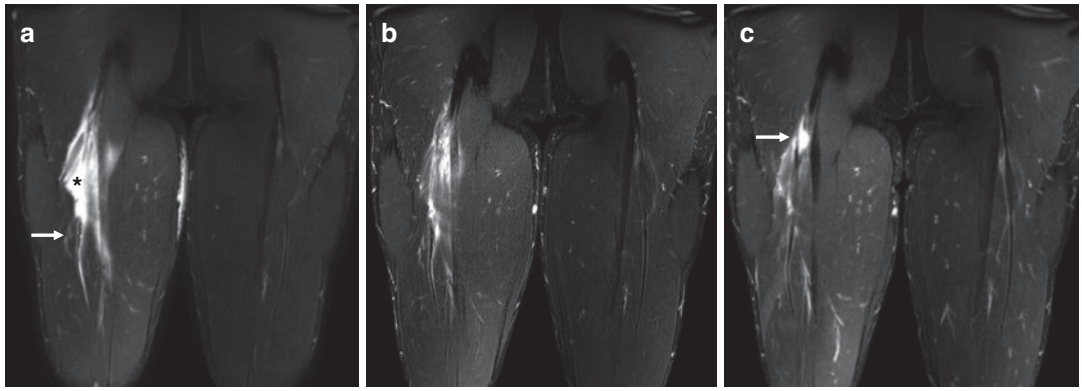

Fig. 3 (**a–c**) 19-Year-old male with full-thickness conjoined semitendinosus-biceps femoris tendon injury. (**a**) Coronal T2 DIXON image at the time of injury showing tendon disruption and waviness (arrow), intramuscular hematoma, and edema (*). (**b**) Coronal T2 DIXON image at RTP showing resorption of hematoma, edema, as well as resolution of waviness of the tendon which is now thickened (arrow). (**c**) Coronal T2 DIXON image after 1 year showing a re-tear (arrow)

interpreting the (size of a) scar, because on fat-saturated PD/T2-WI, part of the hypointense signal can be caused by perifocal fatty atrophy of the muscle, which will be hyperintense on T1-WI. Failure to correlate with T1-WI may lead to overestimation of scar tissue.

3. *Phases of hematoma:* Intramuscular and perifascial hematomas have a range of signal characteristics varying with the age of the hematoma. They resolve over time in a typical fashion. In the acute period (<48 h) hematomas are typically isointense on T1-WI. In the subacute stage (<30 days) hematomas have a T1- and T2-hyperintense signal due to the accumulation of methemoglobin. Signal intensities in a chronic hematoma are heterogeneous, but a typical hypointense rim will appear based on the deposition of hemosiderin and fibrosis. These fibrotic margins will contract the lesion over time. The blood degradation products will be absorbed and the hematoma will shrink, resolving after 6–8 weeks (Blankenbaker and Tuite 2010). The radiologist should keep in mind that this predictable pattern of blood degradation is only true for focal hematomas; hemorrhage infiltrating the muscle does not evolve in this predictable manner (Davis 2008). It is important to note that the size of an intramuscular hematoma does not correlate necessarily with clinical status nor functional deficit. In some instances, the elite athlete can engage in athletic activity without pain and be asymptomatic, even with a large hematoma present.
4. *Detection of complications:* The injured muscle heals mostly by repair (scar formation) instead of regeneration. This causes certain complications, of which the radiologist should be aware of:
   (a) Atrophy and fatty infiltration: Muscle injury may cause changes in the affected muscle, namely a loss of muscle volume and infiltration of fatty tissue (Fig. 3).
   (b) Myositis ossificans: A common complication of direct muscle injury by blunt trauma in the athlete, resulting from an aberrant healing response leading to formation of bone instead of scar tissue. The intramuscular hematoma goes through an inflammatory, pseudotumor, and chronic healing phase, in which MR signal characteristics are at first nonspecific and can even be confused with soft-tissue tumors (Fig. 4a). Additional testing to rule out malignancies can be warranted. At the chronic stage, a peripheral calcified rim around the lesion appears due to lamellar organization of osteoid material (Fig. 4b).

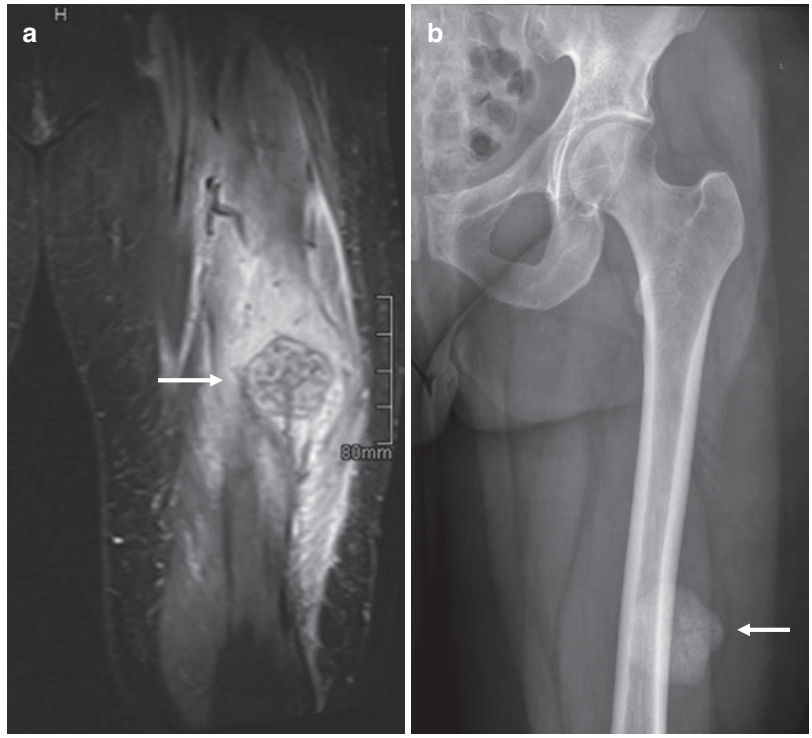

Fig. 4 (**a**, **b**) 47-Year-old female with myositis ossificans as complication after partial m. rectus femoris injury. (**a**) Coronal TIRM showing mass lesion (arrow) with surrounding edema. (**b**) Anteroposterior X-ray showing peripheral calcification (arrow) which is pathognomonic for myositis ossificans

This can be seen on conventional X-ray of CT after 6 weeks.

(c) Muscle herniation: A focal defect in the muscle fascia through which the muscle herniates, causing cramping sensation, pain, and a palpable mass during exertion.

(d) Tethering of adjacent nerves by scar tissue formation resulting in (traction) neuropathy: This can be seen as increased intratendinous signal intensity on fluid-sensitive sequences and swelling. This MR phenomenon may be subclinical, and the imaging findings should thus be correlated with the clinical symptoms.

3.3 Advanced MR Techniques

Conventional MR techniques are not convincingly able to predict RTP and risk for reinjury (Reurink et al. 2014; Van Heumen et al. 2017). Furthermore, imaging characteristics during the healing process of muscle injury do not reflect the physical status of the athlete; at RTP most athletes still show increased T2 signal at the site of injury and MR abnormalities have not completely resolved (Sanfilippo et al. 2013; Silder et al. 2013; Reurink et al. 2014).

Currently, we monitor the repair process of muscle injury in terms of regression of the MR abnormalities found at the moment of acute injury (Slavotinek 2007). We evaluate morphology and signal changes of the injured muscle as well as any complications, as described above. The major challenge ahead is to visualize the invisible: to go beyond imaging resolution and try to monitor muscle structure, function, and metabolism quantitatively. Quantitative MR techniques such as T2 mapping, diffusion-weighted/tensor imaging (DWI, DTI), and MR spectroscopy are emerging. They are subject of many scientific studies and have already shown their clinical value in monitoring disease progress and treatment efficiency in chronic muscle injury, (neuro) muscular disorders such as dystrophies, or ischemia-induced muscle damage. Further scientific effort is needed to translate

these findings into the field of acute sports-related muscle injury. As for free tendon injury, the role of advanced imaging as T2 mapping and DWI remains challenging, due to low water content of tendons.

In theory, monitoring the healing process of acute muscle injury will benefit from the use of quantitative imaging techniques since they are more reproducible. Interpretation of conventional MR imaging is prone to inter- and intra-reader variation, whereas quantitative techniques are more accurate in measuring changes over time. These comparative studies will be of great importance in monitoring the healing of muscle injury. Ideally a reproducible and sensitive technique needs to be developed to indicate in which phase of muscle recovery the athlete resides, so that a more powerful prediction can be made in terms of RTP and reinjury risk.

3.3.1 T2 Mapping

T2 mapping quantifies T2 relaxation times in a particular tissue; this T2 value provides information on the tissues' water content. T2 values correlate to the degree of activation of muscles, with proportionally higher T2 values with higher activity in involved muscles (Kinugasa et al. 2006). In this way, T2 mapping has shown to be able to recognize muscle activation patterns and subtle muscle damage (Ganal et al. 2016; Guermazi et al. 2017). In a recent animal study, increased T2 values also correlated to the degree of muscle damage and inflammatory infiltration at histopathological verification (Fu et al. 2019).

Furthermore, T2 mapping can be applied for quantitative assessment of fatty degeneration of muscles, as a complication of acute muscle or tendon injury (Matsuki et al. 2014). Fat deposition and restricted motion of water molecules increase the T2 value of the injured muscle. For instance, the most commonly used semiquantitative method in determining fatty infiltration of rotator cuff muscle on T1-WI, the Goutallier method, is not able to detect subtle differences and remains subject to significant intra- and interobserver variability. A more accurate method to quantify fatty infiltration would be of help in monitoring the repair process of muscle injury. A challenge is that patients may show concomitant edema and inflammatory changes in addition to fatty infiltration, which both lead to increased T2 values (Azzabou et al. 2015; Klupp et al. 2017). The use of fat-saturated and fat-suppressed T2 mapping techniques has been proved to solve this (Arpan et al. 2013).

Despite the technical challenges, T2 maps can be used theoretically to monitor the repair process of muscle injury over time by quantification of (microstructural) edema and inflammatory changes, as well as fatty degeneration. When we are able to quantify subclinical healing patterns in a more reproducible and sensitive manner than by using conventional T2-WI, this might help in providing objective measures for predicting at-risk athletes for reinjury or help in determining RTP in the future.

3.3.2 Diffusion-Weighted/Diffusion Tensor Imaging

DWI is an MR technique that measures differences in the extent and direction of diffusion of water molecules within a tissue (Le Bihan et al. 1986). Water diffusion in muscles is restricted due to the parallel orientation of fibers, which creates a physical diffusion barrier. In muscle injury, myocyte damage leads to disorganization of these barriers and loss of fiber structure and hence an increase in diffusion of water molecules and a decrease in anisotropy. The formation of muscle edema enhances this process, which can be quantified by using DTI. The increased diffusivity in the injured muscle is reflected by an increase in apparent diffusion coefficient (ADC) and a decrease in fractional anisotropy (FA) (Yanagisawa et al. 2011; Froeling et al. 2015).

DWI of muscle can help detect minor lesions and subclinical changes in muscles after exercise that would remain undetected on conventional MRI (Froeling et al. 2015). Hereby, it may improve early diagnosis, but may also be a more reliable marker for monitoring subtle (subclinical) changes during the healing process of muscle injury. In a recent study Agten et al. quantified diffusion in athletes with delayed-onset muscle soreness (DOMS) (Agten et al. 2017). The study showed subtle temporal changes in ADC and FA,

but it furthermore showed a strong inverse correlation between FA and pain, and a normalization of FA values when the pain subsided. This shows that DTI values might better reflect underlying muscle damage compared to edema at conventional fluid-sensitive MR sequences, because intramuscular and perifascial edema at T2-WI/STIR may persist long after the resolution of clinical symptoms and RTP (Silder et al. 2008; Sanfilippo et al. 2013; Reurink et al. 2014).

The stages of the muscle-healing process as described above correlate to temporal changes in FA in several animal studies (Esposito et al. 2013; Hata et al. 2018). During the inflammatory phase FA sharply decreases since most of the anisotropic structure of skeletal muscle is lost in injury (already at day 1). During the regeneration phase FA elevates to above basal level (days 5–7) and during the remodeling phase FA recovers back to basal level as the muscle fibers mature (Esposito et al. 2013; Hata et al. 2018).

Besides quantitative measurements, DTI can be used for muscle fiber tracking. Especially in traumatic muscle injuries where fiber orientation is disrupted, the use of post-processing can create 3D images of muscle fiber architecture that might assist in defining severity and healing status of the injured muscle.

Translating these results to sports imaging, in the near future diffusivity measures might be applied to monitor the phases of the healing muscle more accurately, as well as the correlation with symptoms/physical status of the athlete making DWI/DTI a potential clinically relevant marker in determining prognosis and RTP and monitoring treatment (Froeling et al. 2015; Oudeman et al. 2016).

3.3.3 Spectroscopy

Recent studies demonstrate the added value of spectroscopy in the assessment of function (Crema et al. 2015), as well as the healing process of muscles, ligaments, and tendons (Ban et al. 2016). Collagen is one of the key components in tendons and ligaments and plays an important role in modulating the mechanical properties of these structures, which are directly linked to the risk of tears, as well as influence the healing process (Liu 2008). MR spectroscopy has been used to evaluate various metabolites related to collagen secretion among tendon and ligament fibroblasts. Lactate is involved in tendon and ligament development, and many studies have shown that it acts as a mediator promoting collagen secretion from tendon and ligament fibroblasts.

Muscle metabolites involved in the energy production process utilize mitochondrial ATP, and therefore contain phosphorus (Johansen and Quistorff 2003). 31P-MR spectroscopy is therefore better suited than the widely available 1H-MR spectroscopy to assess their muscular concentrations in vivo and monitor changes over time (Taylor 2000). In addition, its quantitative and qualitative properties allow early and accurate detection of metabolic abnormalities in tendons, ligaments, and muscles during rest, exercise, and recovery and compare these values over time (Johansen and Quistorff 2003; Pesta et al. 2013). This technology allows coaches, doctors, physiotherapists, rehab specialists, and athletes to better understand the underlying functional changes affecting the muscles, compare with the contralateral side where relevant, and modulate the training protocols to prevent injuries and achieve optimal rehabilitation.

Limitations include the need to perform comparative studies on the same scanner and under the same scanning parameters to allow reproducibility of results without the need for recalibration. Also, cost and time remain relative limitations, albeit less relevant in high-level athletic settings due to the relevant risk-benefit values.

Being a noninvasive technique renders MR spectroscopy a valuable tool in elite athletes and can be repeatedly used for follow-up during the healing phase, as well as in the quantitative assessment of various treatments and interventions in research and clinical settings.

3.3.4 Ultrahigh-Field MRI

In 2017, the EU and US Food and Drug Administration cleared the first 7T MR scanners for clinical use (Medgadget.com 2017; Megadget.com 2017). Over the past decade, the introduction of 7T MR scanners has reached a worldwide level of more than 40, most of which are used for research (Trattnig 2013). In general, the increased signal-to-noise ratio (SNR) of ultrahigh-field 7T scanners offers higher resolution images and shorter acquisition times. In the field of MSK radiology, 7T MRI has shown its advantage in depicting greater morphological detail in cartilage and in trabecular bone imaging (Krug et al. 2009).

Concerning the repair process of muscle injury, 7T imaging might further improve diagnostic confidence, but the question is whether it will improve accuracy regarding morphological imaging alone. Nevertheless, to a greater extent, quantitative imaging techniques will probably profit from increasing field strengths. At the moment clinical implementation of advanced MR techniques at clinical field strengths, such as T2 mapping and DTI is challenging in traumatology and sports radiology, in contrast to brain imaging where it is widely used to tract white matter integrity. Muscle T2 values are typically shorter and water proton density is less than that of brain. Especially FA measurements and fiber tracking suffer from (partial volume) artifacts. The increased SNR and resolution of ultrahigh-field MR imaging can improve this. Another drawback of quantitative imaging is long acquisition times (De Mello et al. 2019). Patient movement causes artifacts and limits FOV in large injuries, which can be solved by the more rapid scanning which is possible at 7T.

In addition to SNR improvements, spectral resolution at 7T is also increased, which contributes to more reliable quantification of MRS data at 7T, and the ability to perform non-proton imaging.

4 Conclusion: Outlook for the Future

Till now, using MRI in assessing RTP and reinjury risk has been challenging, if not impossible, for the individual athlete. Functional recovery precedes structural recovery at imaging; therefore complete regression of (conventional) MR abnormalities is not necessarily required for a successful return to play. This illustrates the importance of the search for sensitive MR markers to follow the muscle repair process and to be able to provide a prognosis as well as play a part in RTP decision-making in sports-related muscle and tendon damage. As described in this chapter, in the future there might be a more prominent role for advanced MR sequences and a shift to ultrahigh-field MRI for more accurate monitoring of different (stages of) tissue changes in the repair process. This will likely complement conventional MRI with T1-WI and T2-WI that might be kept to evaluate anatomy and classify muscle injury in the more acute stage.

Things to Remember

1. The role of MRI in follow-up and monitoring of muscle and tendon repair is still debated, but can be of added value in certain high-stake cases, for instance in elite athletes.
2. The MR protocol for follow-up MRI includes T1-W and PD/T2-W fluid-sensitive images with multiplanar reconstructions, a dedicated surface coil, and imaging of the asymptomatic contralateral side.
3. Important things to look for at follow-up MRI are regression of the acute-stage findings, formation of scar tissue, phases of hematoma, and possible complications.
4. Quantitative MR techniques and ultrahigh-field MRI might play a more prominent role in the future, for more accurate monitoring of different (stages of) tissue changes in the repair process.

5 Imaging Boxes

Box 1: Conventional MRI

- Used to monitor the repair process of muscle injury (in elite athletes)
- Functional recovery precedes structural recovery at imaging
- Shows reduction of edema and gap size, development of hematoma, and formation of scar tissue
- Shows possible complications such as fatty infiltration, muscle atrophy, myositis ossificans, muscle herniation, and (traction) neuropathy

Box 2: Advanced MRI

- Such as T2 mapping, diffusion-weighted/tensor imaging (DWI, DTI), MR spectroscopy and ultra-high field MRI are emerging
- Is in theory more reproducible and less prone to inter- and intra-reader variation, and therefore more accurate in measuring changes over time
- Might play a more prominent role in more accurate monitoring of different (stages of) tissue changes in the repair process

References

Agten CA, Buck FM, Dyer L et al (2017) Delayed-onset muscle soreness: temporal assessment with quantitative MRI and shear-wave ultrasound elastography. Am J Roentgenol 208:402–412

Arpan I, Forbes SC, Lott DJ et al (2013) T2 mapping provides multiple approaches for the characterization of muscle involvement in neuromuscular diseases: a cross-sectional study of lower leg muscles in 5–15-year-old boys with Duchenne muscular dystrophy. NMR Biomed 26:320–328. https://doi.org/10.1002/nbm.2851

Azzabou N, De Sousa PL, Caldas E, Carlier PG (2015) Validation of a generic approach to muscle water T2 determination at 3T in fat-infiltrated skeletal muscle. J Magn Reson Imaging 41:645–653. https://doi.org/10.1002/jmri.24613

Ban HY, Shin JW, Chun S-I et al (2016) Distinguishing tendon and ligament fibroblasts based on 1H nuclear magnetic resonance spectroscopy. Tissue Eng Regen Med 13:677–683. https://doi.org/10.1007/s13770-016-0128-5

Blankenbaker DG, Tuite MJ (2010) Temporal changes of muscle injury. Semin Musculoskelet Radiol 14:176–193. https://doi.org/10.1055/s-0030-1253159

Connell DA, Schneider-Kolsky ME, Hoving JL et al (2004) Longitudinal study comparing sonographic and MRI assessments of acute and healing hamstring injuries. Am J Roentgenol 183:975–984. https://doi.org/10.2214/ajr.183.4.1830975

Crema MD, Yamada AF, Guermazi A et al (2015) Imaging techniques for muscle injury in sports medicine and clinical relevance. Curr Rev Musculoskelet Med 8:154–161

Davis KW (2008) Imaging of the hamstrings. Semin Musculoskelet Radiol 12:28–41

De Mello R, Ma Y, Ji Y et al (2019) Quantitative MRI musculoskeletal techniques: an update. Am J Roentgenol 213:524–533

Ekstrand J, Hägglund M, Waldén M (2011) Epidemiology of muscle injuries in professional football (soccer). Am J Sports Med 39:1226–1232. https://doi.org/10.1177/0363546510395879

Esposito A, Campana L, Palmisano A et al (2013) Magnetic resonance imaging at 7T reveals common events in age-related sarcopenia and in the homeostatic response to muscle sterile injury. PLoS One 8. https://doi.org/10.1371/journal.pone.0059308

Froeling M, Oudeman J, Strijkers GJ et al (2015) Muscle changes detected with diffusion-tensor imaging after long-distance running. Radiology 274:548–562. https://doi.org/10.1148/radiol.14140702

Fu C, Xia Y, Meng F et al (2019) MRI quantitative analysis of eccentric exercise-induced skeletal muscle injury in rats. Acad Radiol 27(4):e72–e79. https://doi.org/10.1016/j.acra.2019.05.011

Ganal E, Ho CP, Wilson KJ et al (2016) Quantitative MRI characterization of arthroscopically verified supraspinatus pathology: comparison of tendon tears, tendinosis and asymptomatic supraspinatus tendons with T2 mapping. Knee Surgery Sport Traumatol Arthrosc 24:2216–2224. https://doi.org/10.1007/s00167-015-3547-2

Garrett WE (1990) Muscle strain injuries: clinical and basic aspects. Med Sci Sports Exerc 22:436–443. https://doi.org/10.1249/00005768-199008000-00003

Guermazi A, Roemer FW, Robinson P et al (2017) Imaging of muscle injuries in sports medicine: sports imaging series. Radiology 282:646–663. https://doi.org/10.1148/radiol.2017160267

Hata J, Mizuno S, Haga Y et al (2018) Semiquantitative evaluation of muscle repair by diffusion tensor imaging in mice. JBMR Plus 2:227–234. https://doi.org/10.1002/jbm4.10040

Järvinen TAH, Järvinen TLN, Kääriäinen M et al (2005) Muscle injuries: biology and treatment. Am J Sports Med 33:745–764

Johansen L, Quistorff B (2003) 31P-MRS characterization of sprint and endurance trained athletes. Int J Sports Med 24:183–189. https://doi.org/10.1055/s-2003-39085

Kerkhoffs GMMJ, van Es N, Wieldraaijer T et al (2013) Diagnosis and prognosis of acute hamstring injuries in athletes. Knee Surg Sport Traumatol Arthrosc 21:500–509

Kinugasa R, Kawakami Y, Fukunaga T (2006) Mapping activation levels of skeletal muscle in healthy volunteers: an MRI study. J Magn Reson Imaging 24:1420–1425. https://doi.org/10.1002/jmri.20772

Klupp E, Weidlich D, Schlaeger S et al (2017) B1-insensitive T2 mapping of healthy thigh muscles using a T2-prepared 3D TSE sequence. PLoS One 12:e0171337. https://doi.org/10.1371/journal.pone.0171337

Koulouris G, Connell D (2005) Hamstring muscle complex: an imaging review. Radiographics 25:571–586

Krug R, Stehling C, Kelley DAC et al (2009) Imaging of the musculoskeletal system in vivo using ultra-high field magnetic resonance at 7T. Investig Radiol 44:613–618

Le Bihan D, Breton E, Lallemand D et al (1986) MR imaging of intravoxel incoherent motions: application to diffusion and perfusion in neurologic disorders. Radiology 161:401–407. https://doi.org/10.1148/radiology.161.2.3763909

Liu H (2008) In vivo evaluation of the stiffness of the patellar tendon. ProQuest, Miami

Maas M, Dijkstra PF, Akkerman EM (1999) Uniform fat suppression in hands and feet through the use of two-point Dixon chemical shift MR imaging. Radiology 210:189–193. https://doi.org/10.1148/radiology.210.1.r99ja35189

Matsuki K, Watanabe A, Ochiai S et al (2014) Quantitative evaluation of fatty degeneration of the supraspinatus and infraspinatus muscles using T2 mapping. J Shoulder Elb Surg 23:636–641. https://doi.org/10.1016/j.jse.2014.01.019

Medgadget.com (2017) EU gives first approval for ultra-high-field MRI scanner, The Siemens Magnetom Terra. https://www.medgadget.com/2017/08/eu-gives-first-approval-ultra-high-field-mri-scanner-siemens-magnetom-terra.html

Megadget.com (2017) FDA Gives First Clearance to Siemens High-Field 7 Tesla MRI Scanner

Mueller-Wohlfahrt HW, Haensel L, Mithoefer K et al (2013) Terminology and classification of muscle injuries in sport: the Munich consensus statement. Br J Sports Med 47:342–350. https://doi.org/10.1136/bjsports-2012-091448

Oudeman J, Nederveen AJ, Strijkers GJ et al (2016) Techniques and applications of skeletal muscle diffusion tensor imaging: a review. J Magn Reson Imaging 43:773–788

Pesta D, Paschke V, Hoppel F et al (2013) Different metabolic responses during incremental exercise assessed by localized 31P MRS in sprint and endurance athletes and untrained individuals. Int J Sports Med 34:669–675. https://doi.org/10.1055/s-0032-1327648

Pollock N, James SLJ, Lee JC, Chakraverty R (2014) British athletics muscle injury classification: a new grading system. Br J Sports Med 48:1347–1351. https://doi.org/10.1136/bjsports-2013-093302

Reurink G, Goudswaard GJ, Tol JL et al (2014) MRI observations at return to play of clinically recovered hamstring injuries. Br J Sports Med 48:1370–1376. https://doi.org/10.1136/bjsports-2013-092450

Sanfilippo JL, Silder A, Sherry MA et al (2013) Hamstring strength and morphology progression after return to sport from injury. Med Sci Sports Exerc 45:448–454. https://doi.org/10.1249/MSS.0b013e3182776eff

Sharma P, Maffulli N (2005) Tendon injury and tendinopathy: healing and repair. J Bone Jt Surg Ser A 87:187–202

Silder A, Heiderscheit BC, Thelen DG et al (2008) MR observations of long-term musculotendon remodeling following a hamstring strain injury. Skelet Radiol 37:1101–1109. https://doi.org/10.1007/s00256-008-0546-0

Silder A, Sherry MA, Sanfilippo J et al (2013) Clinical and morphological changes following 2 rehabilitation programs for acute hamstring strain injuries: a randomized clinical trial. J Orthop Sports Phys Ther 43:284–299. https://doi.org/10.2519/jospt.2013.4452

Slavotinek JP (2007) Monitoring of muscle, tendon and ligament repair. In: Imaging of Orthopedic Sports Injuries. Springer, Berlin, Heidelberg

Taylor DJ (2000) Clinical utility of muscle MR spectroscopy. Semin Musculoskelet Radiol 4:481–502. https://doi.org/10.1055/s-2000-13172

Trattnig S (2013) "Special section: Emerging clinical applications with 7 Tesla. Editorial." Eur J Radiol 82(5):707

Van Heumen M, Tol JL, De Vos RJ et al (2017) The prognostic value of MRI in determining reinjury risk following acute hamstring injury: a systematic review. Br J Sports Med 51:1355–1363

Wangensteen A, Guermazi A, Tol JL et al (2018) New MRI muscle classification systems and associations with return to sport after acute hamstring injuries: a prospective study. Eur Radiol 28:3532–3541. https://doi.org/10.1007/s00330-017-5125-0

Yanagisawa O, Kurihara T, Kobayashi N, Fukubayashi T (2011) Strenuous resistance exercise effects on magnetic resonance diffusion parameters and muscle-tendon function in human skeletal muscle. J Magn Reson Imaging 34:887–894. https://doi.org/10.1002/jmri.22668

Part IV

Addenda

Imaging-Guided Intervention of Sports Injuries

Davide Orlandi, Matteo De Cesari,
Carmelo Messina, and Luca Maria Sconfienza

Contents

Abstract

Dynamic high-resolution ultrasonography (US) has emerged as the first-choice imaging modality to guide musculoskeletal (MSK) percutaneous procedures in many articular, tendon, and muscle pathologies. The main advantages of this imaging modality are the lack of ionizing radiations, the real-time visualization of the target structure and the needle during the entire procedure, and the global low cost of the whole procedure.

US guidance also allows for careful avoidance of crucial structures such as neurovascular bundles, thus reducing the risk of complications and improving patient outcome in terms of pain reduction during and after the procedure.

Sports medicine is a clinical field in which ultrasound-guided percutaneous procedures are well applied both in muscle injuries (10–55% of all sport-related lesions are muscular contusions and strains) and in tendon damage besides the traditional conservative treatments (rest, ice, compression, elevation (RICE) protocols, nonsteroidal anti-inflammatory drugs, physical therapy, and functional rehabilitation). In this setting, an appropriate ultrasound-guided aspiration procedure (i.e., in hematoma) or ultrasound injection procedure with platelet-rich plasma (PRP) or stem cells may improve the healing process and ensure a rapid return to preinjury muscle functionality with an important impact especially on professional athletes (Orlandi et al., Br J Radiol 89:20150484, 2016).

D. Orlandi
Servizio di Radiologia, Ospedale Evangelico Internazionale, Genova, Italy

M. De Cesari
Struttura complessa di radiologia, ASL 4, presidio di Lavagna, Via Don Giovanni Battista Bobbio, Lavagna, Italy

C. Messina · L. M. Sconfienza (✉)
IRCCS Istituto Ortopedico Galeazzi, Milano, Italy

Dipartimento di Scienze Biomediche per la Salute, Università degli Studi di Milano, Milano, Italy
e-mail: io@lucasconfienza.it

Med Radiol Diagn Imaging (2021)
https://doi.org/10.1007/174_2020_263, © Springer Nature Switzerland AG
Published Online: 07 February 2021

1 Basic Clinical Information

A preliminary accurate medical history of the patient is recommended. In particular, referring to traumatic muscle injuries, it is important to know:

- When the trauma happened
- Elucidate the dynamics of the trauma

Further considerations should be focused on:

- Possible history of drug allergies
- Assumption of anticoagulant/antiplatelet drugs or presence of blood-thinning pathologies that could cause severe bleeding after the procedure

Past medical history, family medical history, and personal/social medical history could be helpful to correctly evaluate the patient (Orlandi et al. 2016).

2 Contraindications, Complications, and Informed Consent

Ultrasound-guided interventional MSK maneuvers are minimally invasive and associated with a low complication rate; however the patient must be given details about the contraindications and potential complications related to the planned procedure.

The patients must be clearly informed about:

- Pain/soreness during the procedure
- Pain/soreness after the procedure and the possibility of steroid flare
- Post-procedural indications/rehabilitation
- Potential risk of infection
- Potential risk of tendon rupture

After receiving this information, the patient must formally agree to the procedure by providing both verbal and written informed consent (Sconfienza et al. 2011).

3 Patient Positioning

The patient must be placed on the examination table in a comfortable position in order to avoid any potential movements during the procedure.

4 Antisepsis

Antisepsis includes skin antisepsis, equipment, and operator sterility:

- Skin antisepsis: Transient microorganisms are removed from the skin using chemical solutions for disinfection; our antisepsis procedure consists of two steps. In the first step a brown water-based povidone-iodine solution is used and after 3–5 min, in the second step, a transparent solution of 70% isopropyl alcohol and 2% chlorhexidine is applied. Both steps are recommended for adequate skin decontamination prior to the insertion of an invasive device.
- Aseptic non-touch technique minimizes the risk of infection by ensuring that only uncontaminated objects/fluids make contact with sterile/susceptible sites. The only part of sterile equipment that may be handled is that which will not be exposed to the susceptible site. Reusable equipment employed during an aseptic procedure should be cleaned with wipes and must be fit for purpose, i.e., a steel dressing trolley for dressing changes. All packs/single-use equipment, i.e., dressing packs, cannula packs, and syringe packs, must be intact, with a still-valid expiration date, and without visible signs of contamination.
- Surgical field: Delimitation of the area to be operated on is performed by the operator using sterile technique, including adhesive sterile towels.
- Probe antisepsis: We recommend using a sterile probe cover to ensure complete sterility during the procedure. Alternatively, probe disinfection may be obtained using specific cleaning solutions.
- US contact gel: Conventional US contact gel should not be used for aseptic US-guided

procedures. However, contact gel is not generally used in short procedures (i.e., simple injections), as simple skin wetting using antiseptic solution is generally sufficient to ensure optimal contact. For longer procedures, sterile contact gel can be applied.

- Operator sterility: Accurate and effective hand hygiene is the most important component of good infection prevention and control, given that the hands are a common route of infection transmission. Sterile gloves and gowns are also mandatory (Sconfienza et al. 2011).

5 Probe Selection

The choice of the probe is based on the depth of the target structure. During MSK interventional procedures, linear phased array high-frequency probes (5–12 MHz up to 18 MHz) are usually preferred because they allow a high-resolution visualization of superficial structures. Deep muscle injuries, athletes with large muscular mass, or obese patients may require the use of a convex probe (3–5 MHz) (Orlandi et al. 2016).

6 Interventional Equipment

Needle choice should be based mainly on the depth of the anatomic structure to treat and on the density of the drug to inject and/or of the fluid to aspirate.

The choice of syringe size strictly depends on the amount of fluid to inject or drain (Orlandi et al. 2016).

7 Basic Principles of Ultrasound Guidance

The interventional maneuvers can be performed using two main approaches: longitudinal/in-plane and coaxial/out-of-plane.

- In the longitudinal/in-plane approach, the needle is placed and inserted parallel to the ultrasound beam, on the short side of the probe. This approach has the advantage of excellent visibility of the needle during the entire procedure, allowing the operator to reach the precise site of injection/aspiration. An example of this approach is reported in Fig. 1a.

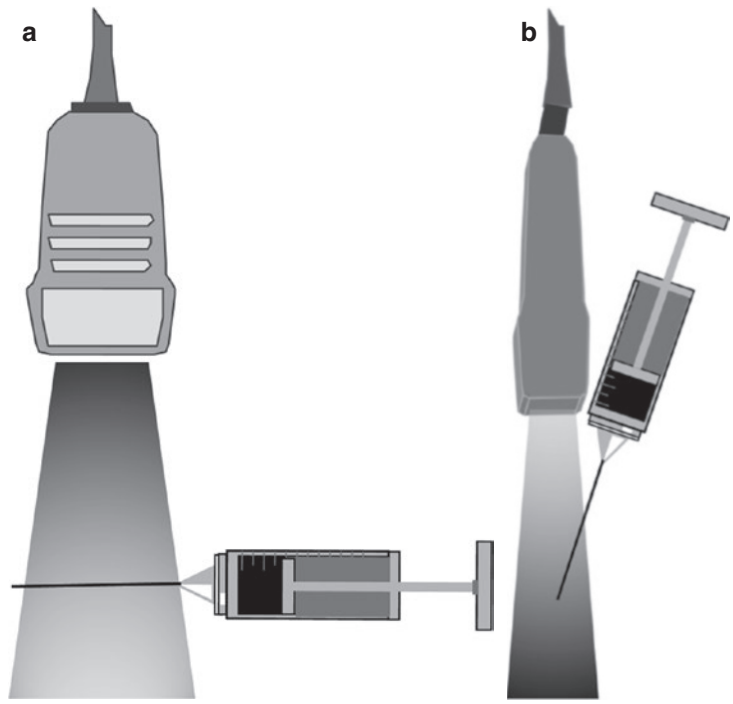

Fig. 1 Examples of (**a**) longitudinal/in-plane and (**b**) coaxial/out-of-plane approaches for performing ultrasound-guided procedures in the musculoskeletal system

- The coaxial/out-of-plane approach is burdened by reduced needle visibility; it can be used when the space around the target is greatly restricted (Sconfienza et al. 2011). An example of this approach is reported in Fig. 1b.

8 Ultrasound-Guided Treatment of Traumatic Sports Injuries

Contusive and/or strain muscular traumas account for the majority of sport-related traumatic injuries. Usually, they are managed with a conservative approach and heal spontaneously after a variable amount of time, with complete restitutio ad integrum. In some cases, complications may occur that can induce many clinical manifestations which variably modify patient outcome and management during rehabilitation period: chronic hematomas may delay the healing process inducing focal muscle atrophy or myositis ossificans phenomena; a predominant scar tissue may increase the risk of recurrences also leading to chronic pain during contraction (Orlandi et al. 2016).

Ultrasound-guided percutaneous procedures play an important role in some of those cases, such as hematomas and muscle strain injuries.

8.1 Hematomas

Hematomas can be divided according to the location into subcutaneous, intrafascial, subfascial, and intramuscular.

Muscle hematomas represent the direct consequence of muscle strain or contusions and could be less frequently intramuscular (if they are confined between the fibers of a single muscle) or more frequently intermuscular if located between two or more muscles (along fascial planes).

According to their ultrasound characteristics, muscle hematomas can be further classified into different stages of maturation. Initially, hematoma may demonstrate variable appearance with muscle swelling and edema, ranging from anechoic or hypoechoic to hyperechoic. As the organization progresses in the subsequent 2–3 days, the walls become more evident and the amount of fluid becomes progressively hypoechoic or anechoic: this is the ideal time for ultrasound examination to detect hematomas in case of low-grade muscular strain. In the weeks following the injury, the amount of fluid progressively decreases and its echogenicity increases; meanwhile, its walls thicken towards the center until the fluid closes. Frequently the fluid component does not appear as homogeneously hypoanechoic but may present increased central echogenicity and fluid/debris levels. A preliminary ultrasound evaluation before ultrasound-guided percutaneous aspiration of a hematoma is therefore mandatory in order to characterize the correct location and timing for drainage.

Ultrasound-guided percutaneous aspiration is the first-line approach in order to drain symptomatic hematomas and chronic muscular hematomas that do not resolve in few weeks and predispose to complications such as partial calcification, cyst formation, myositis ossificans, and neural compression. Chronic hematomas are frequently seen in the triceps surae muscle in tennis leg setting, as a consequence of a tear involving the aponeurosis between the soleus and gastrocnemius muscles. Another common location is the vastus intermedius muscle, which is particularly prone to developing hematomas after direct trauma owing to its location just over the femur.

In clinical practice, the ideal timing to drain a hematoma is between 1 and 2 weeks after injury when the hematoma has sufficiently liquefied evaluating its internal echotexture and compressibility with the pressure of the transducer.

Morel-Lavallée lesions are post-traumatic hemolymphatic collections occurring after a shearing injury with disruption of interfascial planes between the subcutaneous fat tissue and deep fascia and muscle with most common location in the thigh at the level of the greater trochanter or more rarely around the knee, calf, and trunk.

When not treated in acute setting, Morel-Lavallée lesions may develop an inflammatory reaction and, subsequently, a fibrous capsule, which contributes to the self-perpetuation and eventual slow growth of such processes. Various

treatment options are reported and include conservative approaches such as compression banding, aspiration, surgical drainage, incision, and evacuation with or without sclerosing agents and radical surgery. The Mayo Clinic experience proposed operative intervention in the presence of fluid collection >50 mL.

When the lesions are <50 mL, not associated with bone fractures and/or infections, and the skin is viable, percutaneous aspiration under ultrasound guidance is possible.

At ultrasound examination, Morel-Lavallée lesions have different possible presentations ranging from well-defined hypo-anechoic fluid collection called seroma to inhomogeneous echogenicity lesion in chronic organizing and/or expanding hematoma (Orlandi et al. 2016).

Procedure

Ultrasound-guided needle aspiration of the hematoma or Morel-Lavallée lesion can easily be performed with a freehand technique; in the first case a 10 mL syringe and an 18–20 G needle are typically used, while in the second case a 10 mL syringe and an 18–20 G needle or cannula are used considering the possible significant dimensions of this kind of lesion.

In order to promote the complete emptying of the collection, which is essential to reduce the risk of infection and recurrence, it may be helpful to press the tissues around it in order to increase the amount of fluid to be aspirated. When dealing with intrafascial or subfascial hematomas, 1 mL of long-acting steroid (triamcinolone acetonide or methylprednisolone acetate 40 mg/mL) is then injected in the empty cavity of the hematoma in order to reduce inflammation.

After the procedure, a thigh elastic dressing must be performed in order to reduce the risk of recurrences and a period of mild rest of about 24–48 should be recommended.

One week after the treatment, it is useful to perform an ultrasound follow-up and, in case of recurrence, it is possible to repeat the procedure. Such recurrences are more frequent in the case of large collections, not completely emptied or with the presence of fibrotic capsule (especially in Morel-Lavallée lesions) (Orlandi et al. 2016).

In brief

Ultrasound-guided aspiration is the first-line approach in order to drain the fluid collected in chronic muscular hematomas (1–2 weeks after injury).

The procedure can easily be performed with a freehand technique; 10–20 mL syringe and 18–20 G needle or cannula are generally used. A 1 week follow-up/re-aspiration is useful to prevent recurrences. A small amount of corticosteroid is also injected in the empty cavity of the hematoma, especially when a thick fibrous capsule is present, in order to reduce inflammation.

8.2 Muscle Strain Injuries

When a muscular injury is suspected, it is very important to start with a precise anamnesis followed by a careful clinical examination of the muscles and an accurate imaging evaluation.

Imaging evaluation allows confirming the lesion, determining its extent and its severity, also providing a comprehensive assessment of the muscle-tendon-bone chain status and finally helping the physician to establish a precise prognosis reducing the risk of recurrence. In this setting, panoramic and highly sensitive MRI imaging and high-resolution ultrasound aided with dynamic scans during isometric contraction of the injured muscular group (against appropriate resistance opposed by the operator) allow evaluating the appearance of muscle fibers and the site and size of injury (calculated as the percentage of cross-sectional area of the muscle and/or as the longitudinal length of the tear) (Corazza et al. 2014).

The healing process is achieved through the regeneration of muscle fibers and the formation of a fibrotic scar tissue; the balance between these two mechanisms (acting simultaneously and competitively) represents a crucial point because the formation of a dense scar correlates with a slower recovery of muscle function and an increased risk of recurrence.

Several biological factors such as the platelet-rich plasma (PRP) and stem cells can be directly injected under ultrasound guidance at the site of the lesion to facilitate muscle regeneration, improve the healing process, and also reduce the risks of dense scar formation (Orlandi et al. 2016).

8.2.1 Platelet-Rich Plasma (PRP)

PRP is a platelet-rich preparation obtained from centrifugation of peripheral blood. Nowadays PRP is applied in various clinical settings including sports medicine, where it has been proposed for the treatment of muscle and tendon injuries, tendinopathies, ligamentous injuries, peripheral neuropathies, and plantar fasciitis. A recent meta-analysis emphasized that PRP was associated with a significant pain reduction at 2 months compared with hyaluronic acid, but no differences were observed at 6- and 12-month follow-up (Ye et al. 2018).

The rationale behind PRP use is the ability to stimulate the process of tissue regeneration through angiogenesis, innervation, and release of multiple GFs and cytokines from platelets while the local immune response and fibrinogenesis are modulated (Orlandi et al. 2016).

The most common PRP types are:

1. Pure PRP (P-PRP) with low content of leukocytes
2. Leukocyte- and platelet-rich plasma (L-PRP): preparation with leukocyte and with low-density fibrin network; greater concentration of platelets than P-PRP
3. Pure platelet-rich fibrin (P-PRF): preparation without leukocytes and with a high-density fibrin network (Allen et al. 2019)

Procedure

The most frequent PRP preparations used in sports medicine are L-PRP with 5× to 8× platelets and leukocytes concentration than peripheral blood. The preparation may be obtained by using disposable kit (with predetermined PRP concentration, almost no risk of contamination but higher cost) or obtained from the transfusion medicine service of the hospital. The second method of preparation starts by collecting a whole venous blood sample (40–50 mL) from a patient usually from the cubital vein, and it is mixed with citrate to prevent early clotting. Then, it is centrifuged for about 15 min (depending on the centrifugation method), and a small sample is taken in order to determine the absence of contamination. The centrifugation separates and concentrates platelets and, depending on the type of preparation, leukocytes from other blood components. In the end, usually 4–10 mL of PRP solution is obtained. Unactivated PRP must be injected in the site of fiber injury as soon as possible after centrifugation in order to prevent gelification and will be activated by the contact with collagen and other tissue factors.

Sometimes the release of platelet granules is induced by using exogenous substances such as the simultaneous injection of 1–2 mL of calcium gluconate solution by a two-way syringe.

In our experience, we recommend the use of inactivated PRP in larger lesions and/or in particular involving the epimysium and/or the fascial planes, where up to 10 mL of PRP may be injected seeking endogenous physiological activation through its contact with collagen and other inflammatory mediators into the site of the injury while exogenously activated 2–6 mL of PRP may be used in particular in small, focal intramuscular strain, where its potential role in the promotion of the fibrin clot may help to speed up the regenerative process. After the procedure a plaster and an ice pack are applied.

Finally, early rehabilitative mobilization protocol should be considered in order to promote the mechanical stimuli which are essential to the optimal injury recovery (myogenesis stimulation, correct alignment of new fires, and proper innervation promotion) (Orlandi et al. 2016).

In brief

PRP treatment of muscle tears consists of 1–3 injections performed weekly after muscular injury and is usually considered for those lesions involving the myotendinous junction which are usually affected by a delayed recovery and high risk of recurrence. Following a proper diagnosis and preoperative ultrasound planning, in large lesions and/or lesions involving the epimysium and/or the fascial planes, PRP treatment is performed by direct US-guided injection in the rupture site using 10 mL of L-PRP, while small intramuscular and focal lesions are treated using 2–6 mL of L-PRP usually activated with calcium gluconate by simultaneous injection with a two-way syringe.

After the procedure early rehabilitative mobilization protocol is encouraged in order to promote optimal injury recovery.

9 Ultrasound-Guided Treatment of Nontraumatic Sports Injuries

Nontraumatic sports injuries mainly affect tendons and joints and are associated with mechanical, chronic-degenerative, and inflammatory pathogenic causes.

The diagnosis of these pathologies is often clinical, but imaging evaluation is fundamental for their confirmation to exclude other associated pathologies and as a guidance for percutaneous therapies.

9.1 Cysts and Articular Ganglia Drainage

Ganglia are tumorlike conditions arising from the juxta-articular soft tissue. Synovial herniation and tissue degeneration, as well as repeated traumas, are suggested as causes. Although the location suggests their origin as the result of synovial herniation through a defect in the joint capsule or tendon sheath, a patent communication between the ganglia and its origin site is quite uncommon. Juxta-articular ganglia (or cysts) could also arise from a meniscal tear (especially those located over the anterior horn of the lateral meniscus) or from a glenoid/acetabular labrum tear.

In this setting, ganglia can grow, diminish in size, or resolve spontaneously and because of their size and location could be painful, could cause impingement syndromes, and could compress nerves (e.g., posterior glenohumeral joint ganglion compressing suprascapular nerve).

Ultrasound-guided treatment of ganglia is generally performed for mass reduction or therapeutic pain relief. In case of recurrence, surgery is advised (Ju et al. 2017).

Procedure

The patient is positioned according to the anatomical location of the ganglion and a US scan is made to identify the structure and to assess its anatomical extension.

A needle connected to a syringe is inserted with an in-plane approach until the needle tip enters the bursa or cyst. The content may be very dense and drainage could be extremely challenging. In these cases, the operator may inject in the bursa or in the cyst a small amount of local anesthetic (5 mL) to dilute the content and aspirate it more easily. A larger shielded cannula and application of a manual compression may also be helpful. A biopsy handle may also be used to obtain a more effective vacuum effect.

When the cyst is completely drained, a small amount of steroid (1 mL) is then injected, visualized with a cloudy hyperechoic appearance. This aims to both reduce inflammation and help the walls to remain collapsed. The needle is then removed, local compression is applied, and a plaster is placed over the puncture site. The

patient is kept in observation for about 10 min. Pain after treatment may occasionally occur and it could be managed using oral NSAIDs.

In brief

Ganglia are very common, accounting for around 40% of all soft-tissue masses, and up to 70% of all ganglia are located around the wrist.

Other common locations are the shoulder (glenohumeral joint), the hip, and the ankle (subtalar joint).

Ganglion may grow, diminish in size, or resolve spontaneously.

US-guided treatment of ganglia is generally performed for diagnostic purposes or therapeutic pain relief. Simple ultrasound-guided aspiration and steroid injection helps reducing the mass safely.

9.2 Tendinopathies

Tendinopathy is referred to as a general umbrella term for pain and swelling of a tendon but depending on biomechanical characteristics the tendons may be affected by various diseases (D'Addona et al. 2017).

Tendons can be distinguished into anchor tendons, which are coated with connective tissue called peritenonium (such as the Achilles tendon) and sliding tendons, covered with a synovial sheath that facilitates their action (such as flexor or extensor tendons of the wrist and foot).

Inflammatory and degenerative tendinopathy of anchor tendons are characterized by degenerative-structural changes in collagen fibers associated with fibrotic phenomena and nonconstant presence of inflammatory signs, both intratendinous and of the peritenonium (Maffulli et al. 2004).

This condition may affect the tendon enthesis or the preinsertional tendon portion, resulting in a fusiform thickening of the tendon body with focal areas of intra-tendinous degeneration, depending on the degree of tendinopathy. When the degenerative disease chronically affects the tendon enthesis, it is often associated with the presence of bony spurs and intra-tendinous enthesopathic lamellar calcifications (Ferrero et al. 2012; Tagliafico et al. 2014; Uygure et al. 2017).

Sliding tendons are susceptible to tenosynovitis, with or without inflammatory or degenerative pathology of the underlying tendon. Acute tenosynovitis is characterized by a fluid effusion within the compartment or the tendon sheath, while in chronic tenosynovitis there is synovial thickening or proliferation.

9.2.1 Scarification of the Tendons (Dry Needling)

Dry needling is an ultrasound-guided procedure for the treatment of anchoring tendons consisting of multiple fenestration of the affected tendon which could be performed alone or combined with simultaneous intra-tendinous PRP injection.

The purpose of the treatment is to cause local hyperemia and bleeding into the tendon, thus promoting post-procedural platelet-induced recovery phenomena (Sconfienza et al. 2011).

Procedure

A 20 G needle is inserted under in-plane ultrasound guidance in the affected portion of the tendon to be treated. Anesthetic (up to 5 mL) is injected along the path of the needle and in the peritendinous soft tissues avoiding intratendinous injection, which could slow the regenerative action of the procedure.

The procedure consists of performing 15–20 small punctures along the entire thickness of the tendon and, when the enthesis is involved, also hitting the periosteum in order to promote a mild bleeding (Fig. 2).

At the end of the procedure a plaster and ice pack are applied and the patient is asked to assume paracetamol in case of pain within 48 h and to reduce his/her sport activity for 1–2 weeks (Sconfienza et al. 2011).

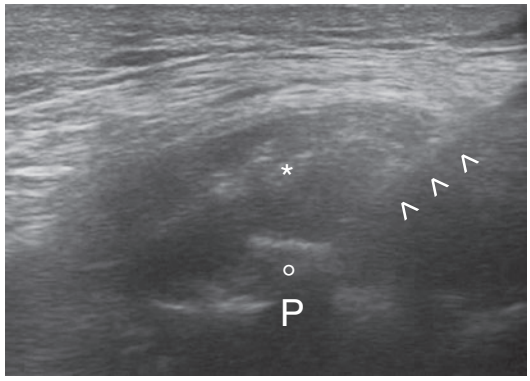

Fig. 2 Pubic symphysis dry needling treatment for chronic adductor enthesopathy in a professional athlete. P: pubis; ^ needle; ° calcification; * common adductor tendon

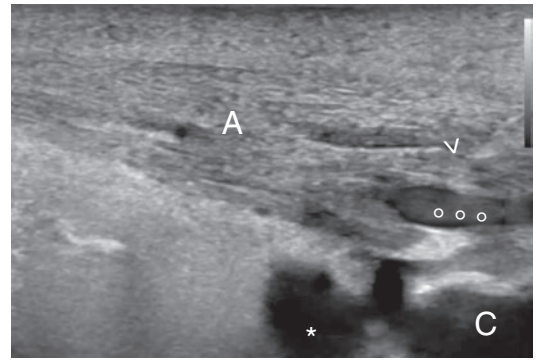

Fig. 3 Platelet-rich plasma (PRP) injection treatment for Achilles tendon enthesopathy with longitudinal intrasubstance partial tear. C: calcaneus; A: Achilles tendon; ^ needle tip; ° PRP; * deep retrocalcaneal bursitis

9.2.2 Regenerative Treatments

The rationale in the use of PRP or adipose-derived mesenchymal stem cells (ASCs) for the treatment of intra-tendinous tendinopathies is the same as that described in the treatment of muscle strain injuries. In the case of PRP the purpose is to speed up the physiological tissue regeneration tendon while in the case of ASCs it is to participate directly in the process of tendon regeneration, being able to differentiate into different types of cells. In this setting the administration of ASCs within their stromal vascular fraction (SVF) has recently been shown to be safe in orthopedic setting for the regenerative treatment of Achilles tendinopathy and plantar fasciitis (Fig. 3).

In non-insertional tendinopathy of the Achilles tendon, studies agree on the reduction of pain after regenerative treatments, but still have discrepancies on the pathogenic mechanisms; it seems that in the initial stages there is a treatment-induced local inflammation with regional hyperemia and mild thickening of the tendon and then, after a few months, a thickness reduction of the regenerated tendon (Albano et al. 2017).

ASC Preparation and Injection Procedure

A small amount of subcutaneous adipose tissue (50 mL) is manually lipoaspirated with a blunt 19 cm, 13 G aspiration cannula.

The adipose tissue is then processed with a dedicated kit, resulting in 10–12 cc of autologous micro-fractured lipoaspirate. The disrupted portion of the tissue, including the SVF, is then centrifuged for 10 min at 400 × g. In the last stage of preparation 4 mL of ASC with SVF is transferred into a syringe ready to be injected.

A 20 G needle is then inserted under in-plane ultrasound guidance in the affected portion of the structure to be treated. Anesthetic (up to 5 mL) is injected along the path of the needle and in the peritendinous soft tissues avoiding intra-tendinous injection, which could slow the regenerative action of the procedure. Care must be taken to inject SVF into the thickest part of the affected structure, covering the entire degenerated area.

After treatment, the patient is advised to walk on crutches for 24 h and to use paracetamol in case of pain within 48 h.

No specific physical therapy is prescribed after the treatment and patients could progressively resume their normal life and sport activities after 1–2 weeks (Albano et al. 2017).

9.2.3 High-Volume Injection

Many studies have focused on non-insertional tendinopathy of the Achilles tendon, a condition that mainly affects runners and in which conservative treatments such as anti-inflammatory drugs and eccentric exercises have limited efficacy.

High-volume injection procedure is based on peritendinous injection of a large amount (up to 40 mL) of several substances (isolated or in combination) such as saline solution, local anesthetic, corticosteroid, or hyaluronates in cases of inflammatory tendinopathy with high intra- and/or peritendinous vascularity.

In this setting, all the previous substances injected into the peritoneum have been shown to significantly reduce pain and improve tendon functionality in the short and medium terms. The rationale of the procedure would be due to the stretching, rupture, or occlusion of the nerves and vessels responsible for inflammation causing the patient pain (Maffulli et al. 2013; Boesen et al. 2017).

Procedure

A 21 G needle is inserted from the lateral aspect of the tendon under real-time ultrasound guidance between the deep aspect of the Achilles tendon and Kager's fat pad. Then, 5 mL of local anesthetic and up to 40 mL of saline solution are injected. Finally, 1 mL of long-acting steroid could be injected in the same space (Fig. 4). At the end of the procedure a plaster and ice pack are applied.

Patients could walk on the injected leg immediately, but are advised strictly to refrain from high-impact activity, such as running or jumping, for 72 h.

After 72 h, patients are instructed to restart heavy eccentric loading under the guidance of a certified physiotherapist (Maffulli et al. 2013).

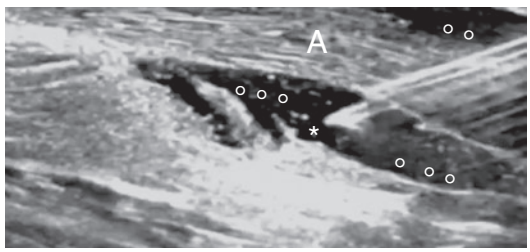

Fig. 4 Ultrasound-guided high-volume injection for Achilles tendinopathy. A: Achilles tendon * needle tip; ° saline solution

9.2.4 Tendon Synovial Sheath Injection

Ultrasound guidance is used in the treatment of tenosynovitis to guide the injection of steroid anti-inflammatory drugs or low-molecular-weight hyaluronic acid into the space between the synovial sheath and the tendon; it is very important to avoid intra-tendinous steroid injection as it is associated with an increased risk of tendon rupture (Orlandi et al. 2014).

A special treatment is reserved for stenosing tenosynovitis (such as trigger finger or De Quervain's disease), those diseases in which inflammation is partly sustained by the rubbing of the tendon with thickened stabilization structures such as retinacula or pulleys. In these cases a first intra-sheath steroid injection is followed by a 1–2-week delayed second treatment consisting of forced injection of low-weight hyaluronic acid into the synovial sheath, which determines mechanical stretching and release of the stabilization structures for up to 12 months (Orlandi et al. 2015; Callegari et al. 2011).

Procedure

Ultrasound-guided synovial sheath injection is generally performed using small-caliber needles (27–29 G) in order to minimize the pain perceived by the patient during the procedure.

At the end of the procedure a plaster is applied and the patient is asked to assume NSAIDs for few days in case of post-procedural pain.

References

Orlandi D, Corazza A, Arcidiacono A et al (2016) Ultrasound-guided procedures to treat sport-related muscle injuries. Br J Radiol 89:20150484

Sconfienza LM, Serafini G, Silvestri E (eds) (2011) Ultrasound-guided musculoskeletal procedures. Springer-Verlag, Milano

Corazza A, Orlandi D, Baldari A et al (2014) Thigh muscles injuries in professional soccer players: a one year longitudinal study. Muscles Ligaments Tendons J 3:331–336

Ye Y, Zhou X, Mao S et al (2018) Platelet rich plasma versus hyaluronic acid in patients with hip osteoarthritis: a meta-analysis of randomized controlled trials. Int J Surg 53:279–287

Allen G, Obradov M, Chianca V et al (2019) Ultrasound-guided musculoskeletal interventions for the most common hip and pelvis conditions: a step-by-step approach. Semin Musculoskelet Radiol 23:58–67

Ju BL, Weber KL, Khoury V (2017) Ultrasound-guided therapy for knee and foot ganglion cysts. J Foot Ankle Surg 56:153–157

D'Addona A, Maffulli N, Formisano S et al (2017) Inflammation in tendinopathy. J Royal College Surg Edinburgh Ireland 15:297–302

Maffulli N, Sharma P, Luscombe KL (2004) Achilles tendinopathy: aetiology and management. J R Soc Med 97:472–476

Ferrero G, Fabbro E, Orlandi D et al (2012) Ultrasound-guided injection of platelet rich plasma in chronic Achilles and patellar tendinopathy. J Ultrasound 15:260–266

Tagliafico A, Russo G, Boccalini S et al (2014) Ultrasound-guided interventional procedures around the shoulder. Radiol Med 119:318–326

Uygure E, Aktas¸ B, Ozkut A, Erinç S, Yılmazoglu EG (2017) Dry needling in lateral epicondylitis: a prospective controlled study. Int Orthop. 41:2321–2325

Albano D, Messina C, Usuelli FG et al (2017) Magnetic resonance and ultrasound in Achilles tendinopathy: predictive role and response assessment to platelet-rich plasma and adipose-derived stromal vascular fraction injection. Eur J Radiol 95:130–135

Maffulli N, Spiezia F, Longo UG et al (2013) High volume image guided injections for the management of chronic tendinopathy of the main body of the Achilles tendon. Phys Ther Sport 14:163–167

Boesen AP, Hansen R, Boesen MI et al (2017) Effect of high-volume injection, platelet-rich plasma, and sham treatment in chronic midportion Achilles tendinopathy: a randomized double-blinded prospective study. Am J Sports Med 45:2034–2043

Orlandi D, Corazza A, Silvestri E et al (2014) Ultrasound-guided procedures around the wrist and hand: How to do. Eur J Radiol 83:1231–1238

Orlandi D, Corazza A, Fabbro E et al (2015) Ultrasound-guided percutaneous injection to treat de Quervain's disease using three different techniques: a randomized controlled trial. Eur Radiol 25:1512–1519

Callegari L, Spanò E, Bini A et al (2011) Ultrasound-guided injection of a corticosteroid and hyaluronic acid: a potential new approach to the treatment of trigger finger. Drugs R D 11:137–145

Postoperative Imaging of Joints in the Sportive Patient

Dimitri Nicolas Graf and Tobias Johannes Dietrich

Contents

Abstract

Postoperative shoulder: Normal postoperative MRI findings after rotator cuff repair in sportive patients include increased signal of the rotator cuff tendons and peribursal soft tissues on fluid-sensitive sequences as well as small dehiscences of the rotator cuff tendons. The postoperative glenoid labrum may be rounded or even slightly frayed after Bankart repair; however, the labrum should be closely attached to the underlying glenoid without undercutting joint fluid or contrast medium (so-called watertight labrum).

Postoperative hip: Labral tears, cartilage defects, and anterior capsular defects are frequent MRI findings in both symptomatic and asymptomatic patients 1 year after arthroscopic treatment of femoroacetabular impingement. Undercorrection of the underlying intra-articular impingement abnormality, secondary conversion to total hip arthroplasty due to osteoarthritis, and intra-articular adhesions at the osteochondroplasty site are common indications for revision surgery in FAI patients.

Postoperative knee: The most frequent surgical error causing persistent knee instability after ACL reconstruction is incorrect placement of the femoral and/or tibial tunnels. Recurrent trauma causes late ACL graft failure due to ACL graft tear. MR imaging criteria for a retear of the repaired meniscus or after partial meniscectomy are fluidlike signal at the repair site with communication

D. N. Graf (✉)
Department of Radiology, Balgrist University Hospital, Zurich, Switzerland

Faculty of Medicine, University of Zurich, Zurich, Switzerland
e-mail: dimitri.graf@balgrist.ch

T. J. Dietrich
Faculty of Medicine, University of Zurich, Zurich, Switzerland

Radiology and Nuclear Medicine, Kantonsspital St. Gallen, St. Gallen, Switzerland
e-mail: tobias.dietrich@kssg.ch

Med Radiol Diagn Imaging (2021)
https://doi.org/10.1007/174_2020_243, © Springer Nature Switzerland AG
Published Online: 23 February 2021

to the articular surface, a displaced meniscal fragment, presence of a new parameniscal cyst, and a new meniscal tear without a preexisting tear on preoperative images. Imaging findings after cartilage repair may be reported according to the MOCART 2.0 classification.

1 Postoperative Shoulder

1.1 Impingement and Rotator Cuff

1.1.1 Objective of Surgery

Surgery in subacromial impingement and rotator cuff tear is mainly indicated to increase strength and active range of motion as well as to avoid irreversible changes to the rotator cuff, including tear enlargement and muscle degeneration (Tashjian 2012). Subacromial impingement symptoms and rotator cuff tears frequently coexist; thus therapeutic surgical procedures in these patients commonly consist of both objectives (Pierce et al. 2016):

- Subacromial decompression with subacromial bursectomy and acromioplasty (Pierce et al. 2016)
- Debridement and repair of partial- and full-thickness tears of the rotator cuff (Pierce et al. 2016)

1.1.2 Surgical Procedure of Subacromial Decompression

It is hypothesized that subacromial impingement symptoms such as pain are caused by contact between rotator cuff tendons, osseous spurs of the acromion, osseous and capsular hypertrophy of the acromioclavicular joint, as well as subacromial soft-tissue structures such as bursa or coracoacromial ligament (Beard et al. 2018). As a consequence, subacromial decompression aims to increase the subacromial space by resection and debridement of osseous and soft-tissue structures to reduce subacromial impingement symptoms (Beard et al. 2018).

1.1.3 Normal Postoperative Imaging Findings

Postoperatively, the undersurface of the acromion appears flattened at the anterior part of the acromion; in particular bony spurs may have been resected (Pierce et al. 2016; Mohana-Borges et al. 2004). The acromioclavicular joint appears widened (1–2 cm) after acromioclavicular joint resection (so-called Mumford procedure) (Mohana-Borges et al. 2004). Decreased signal intensity in the acromion on T1-weighted or proton density-weighted and T2-weighted images represents fibrosis in the bone marrow. Fluid may leak from the subacromial space into the acromioclavicular joint similar to the "geyser sign" due to releasement of acromioclavicular joint capsule (Pierce et al. 2016; Mohana-Borges et al. 2004). Subacromial granulation tissue frequently develops after subacromial bursectomy and may persist for years. Corresponding normal MR imaging findings for this subacromial granulation tissue are a layer of fluidlike signal and should not be confused with inflammation, bursitis, or rotator cuff disease (Pierce et al. 2016; Jacobson et al. 2011).

1.1.4 Abnormal Postoperative Imaging Findings

A cause of persistent shoulder pain after subacromial impingement surgery is incomplete decompression (Pierce et al. 2016); therefore postoperative images should be evaluated for residual acromioclavicular joint osteoarthritis and subacromial spurs (Pierce et al. 2016; Mohana-Borges et al. 2004). It was shown that a persistent spur from the undersurface of the acromion has a high association with residual impingement symptoms (sensitivity: 84%, specificity: 87%) (Magee et al. 1997).

1.1.5 Surgical Procedure of Rotator Cuff Repair

Anterior, lateral, and posterior portals are commonly placed for arthroscopic rotator cuff reconstruction. Suture anchors implanted in the humeral head and related anchor fibers connected to the tendon reattach the rotator cuff tendon with the humeral head to enable

transmission of muscular strength. Compared to arthroscopy, open or mini open techniques are less frequently used in sportive patients due to the lower return-to-play time (Pierce et al. 2016). Either single- or double-row sutures are placed along the medial or lateral margin of the greater tuberosity to reattach the tendon to the humeral head. Surgical rotator cuff repair techniques are mainly influenced by the individual training of the shoulder surgeon as well as the size and morphologic aspect of the tendon tear (Beltran et al. 2014). Major contributors of vascularization of the rotator cuff repair are the suture anchor sites and peribursal tissues, which may explain in part the better rotator cuff repair healing in patients treated with double-row techniques (Adler 2013). The larger the tear the more advantageous are double-row techniques.

1.1.6 Normal Postoperative Findings

Imaging findings of postoperative rotator cuff tendons are highly variable. The surfaces of the postoperative tendon may appear smoothed after debridement. Sutures, granulation tissue, and fibrosis may cause increased signal intensity on fluid-sensitive MRI sequences for several years and do not necessarily represent a recurrent abnormality (Pierce et al. 2016; Mohana-Borges et al. 2004; Beltran et al. 2014).

Solely 10% of repaired rotator cuff tendons demonstrate a low signal on T2-weighted MR images at any time after surgery (Spielmann et al. 1999). Thinning and increased signal on T2-weighted images may be detectable in asymptomatic patients and do not represent reliable imaging characteristics for a retear of the rotator cuff repair (Pierce et al. 2016) (Fig. 1). Moreover, small residual defects of <1 cm are not obligatorily associated with persistent clinical symptoms (Zanetti et al. 2000). A postoperative rotator cuff is not necessarily watertight; thus contrast leakage into the subacromial bursa on CT or MR arthrogram images can be considered as normal (Mohana-Borges et al. 2004; Zanetti et al. 2000). Bone marrow edema in the humeral head adjacent to anchor screws in particulate adjacent to bioabsorbable anchor screws is a common MR imaging finding and should not be misinterpreted as a Hill-Sachs lesion (Pierce et al. 2016). It has to be considered that some areas of a rotator cuff tear were not surgically repaired; thus comparison between preoperative imaging, surgical report, and postoperative images enables a more specific radiological report.

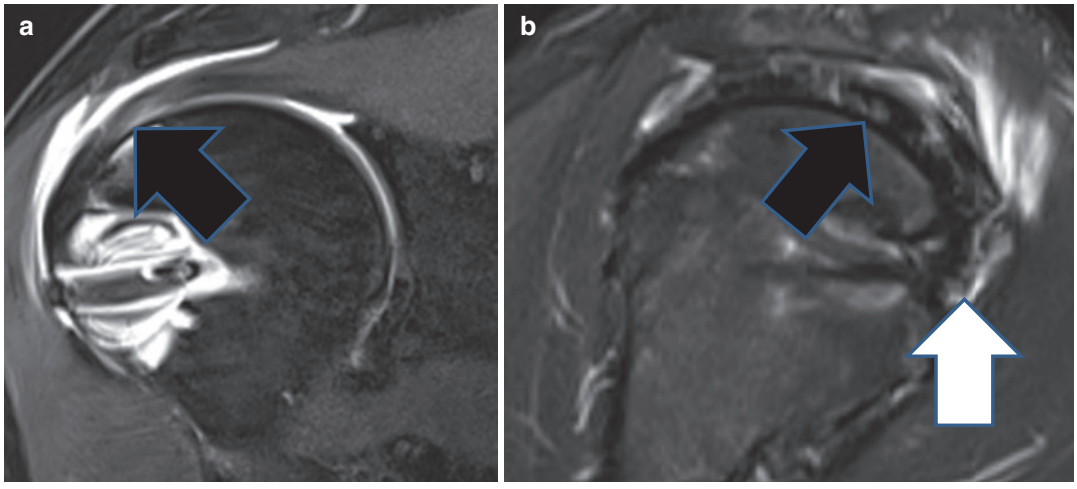

Fig. 1 (**a** and **b**) 45-year-old female patient underwent reconstruction of the supraspinatus and subscapularis tendon 12 months ago. (**a**) Postoperative coronal proton density-weighted and (**b**) sagittal STIR MR images demonstrate intact supraspinatus (black arrows) and subscapularis (white arrow) tendon reconstruction with increased fluid signal in the tendon without neither a cleft nor a discontinuation

1.1.7 Abnormal Postoperative Imaging Findings

An anchor screw dislocation also known as anchor screw pullout represents a typical, however rare, imaging finding of a failed rotator cuff repair (Pierce et al. 2016) (Fig. 2). Recurrent rotator cuff tears after reconstruction are also related to fixation failure at the bone such as suture breakage (Pierce et al. 2016). The MRI criteria for diagnosing recurrent full-thickness rotator cuff tears are similar to those of tears on preoperative images: a tendon dehiscence and the presence of fluid or contrast material on arthrograms in the tendinous gap (Mohana-Borges et al. 2004) (Fig. 3). Partial-thickness recurrent tears are difficult to distinguish from granulation

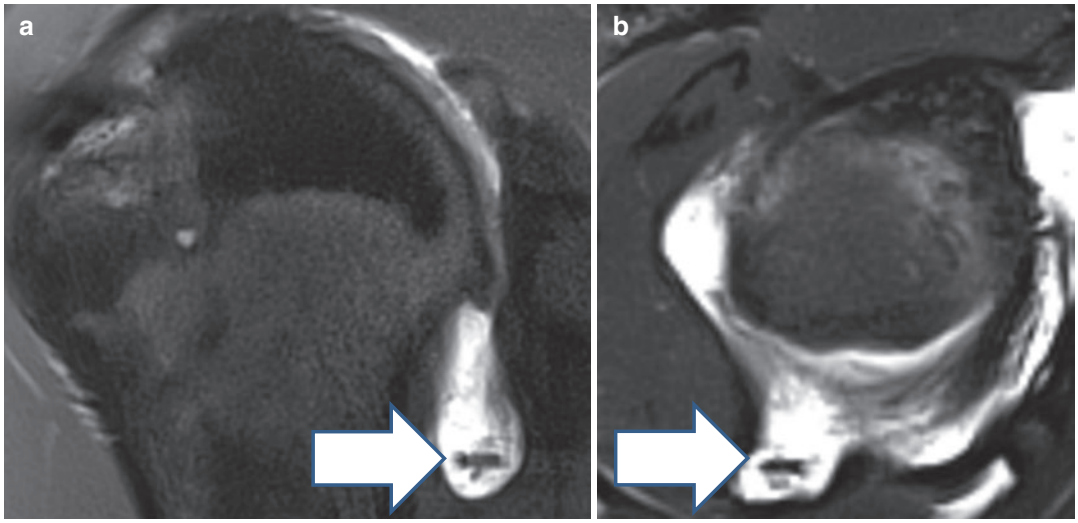

Fig. 2 (**a** and **b**) 24-year-old male underwent SLAP and rotator cuff repair. Patient reported persistent pain 2 years after surgery. (**a**) Postoperative coronal proton density-weighted coronal image and (**b**) sagittal fat-suppressed T2-weighted MR images demonstrate a dislocated supraspinatus anchor in the axillary recess (arrows). Anchor dislocation frequently implicates a failure of the surgical treatment

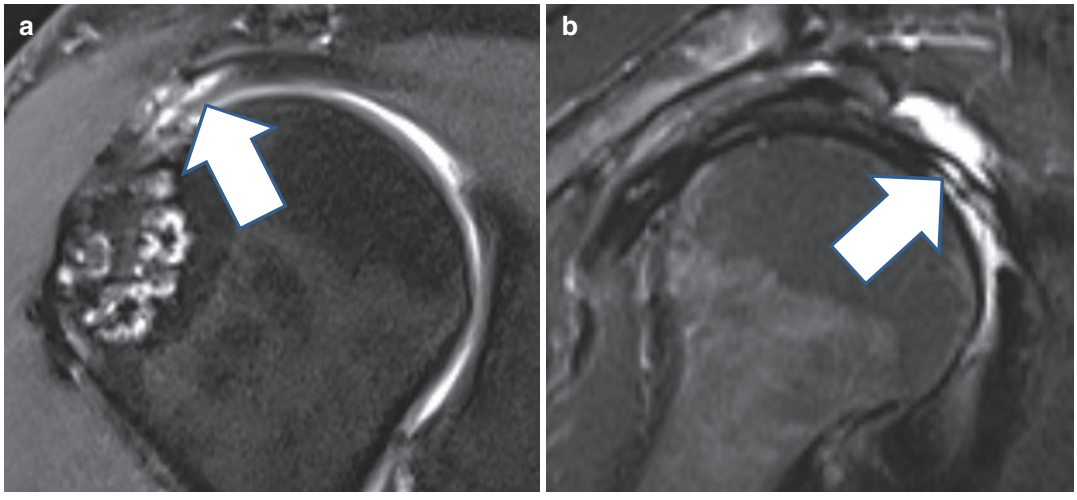

Fig. 3 (**a** and **b**) 53-year-old male patient underwent rotator cuff repair (supraspinatus). Patient reported persistent pain. (**a**) 24-Month postoperative coronal fat-suppressed T1-weighted and (**b**) sagittal STIR MR arthrography images demonstrate linear and articular sided contrast within the tendon reconstruction (arrows) representing a recurrent articular sided and interstitial partial-thickness tear of the supraspinatus tendon

tissue or fluid trapped in sutures. A specific sign for a retear after rotator cuff repair is contrast media penetration within a dehiscence of a tendon repair of more than 1 cm, because granulation tissue is not replaced by contrast media (Mohana-Borges et al. 2004; Zanetti et al. 2000). Not surprisingly, recurrent full-thickness tears (sensitivity 84%, specificity 91%) are more accurately diagnosed compared with partial-thickness tears on MRI arthrography (sensitivity 83%, specificity 83%) (Pierce et al. 2016; Magee et al. 1997).

Things to Remember

The normal postoperative rotator cuff and peribursal soft tissues frequently demonstrate increased signal on fluid-sensitive sequences and small tendon dehiscences of the rotator cuff. CT arthrography and MR arthrography increase the diagnostic accuracy for the assessment of the repaired rotator cuff.

1.2 Shoulder Instability

1.2.1 Objective of Surgery

The primary objective of surgery in patients with recurrent shoulder dislocations is restoration of shoulder stability (Zimmermann et al. 2016).

1.2.2 Surgical Procedure

Arthroscopic Bankart soft-tissue repair and open coracoid transfer according to Latarjet (so-called Latarjet procedure) are the most frequent surgical approaches to regain stability in the shoulder (Zimmermann et al. 2016).

Labral repair (so-called Bankart soft-tissue repair), frequently in combination with capsulorrhaphy: Arthroscopic refixation of the torn glenoid labrum by absorbable tacks (so-called Warren procedure), transglenoid sutures (Caspari procedure), or suture anchors (Snyder procedure) (Mohana-Borges et al. 2004). Capsulorrhaphy is a soft-tissue reconstruction procedure to tighten the capsule, for instance by a T-shaped incision and subsequent overlapping sutures (Mohana-Borges et al. 2004).

Osseous reconstruction: The glenoid is augmented by transferring the coracoid process to the anteroinferior glenoid with an associated screw fixation (so-called Latarjet-Bristow procedure) (Pierce et al. 2016). Comparing the Bristow and Latarjet techniques, the osteotomy of the coracoid process is closer to the basis in the Latarjet procedure, while the Bristow technique transfers rather the coracoid tip (Figs. 4 and 5). As a consequence, the coracoid bone block is larger in the Latarjet procedure compared to the Bristow procedure. The coracoid bone block transfer includes a transfer of the short head of the biceps and coracobrachialis tendons (so-called conjoint tendon). The Latarjet-Bristow procedure regains stabilization of the shoulder by restoration of the osseous shape of the glenoid, a sling effect of the transferred conjoint tendon, and shoulder capsule repair (Pierce et al. 2016).

An engaging Hill-Sachs lesion is a risk factor for recurrent shoulder dislocations (Soterios et al. 2013). A remplissage procedure aims to restore the humeral head anatomy of the Hill-Sachs lesion by an infraspinatus tenodesis and the posterior capsule (Pierce et al. 2016). Bone graft filling of the Hill-Sachs lesion is a further surgical approach as a treatment of engaging Hill-Sachs lesions.

1.2.3 Normal Imaging Findings

The labrum at the anteroinferior glenoid margin appears hypointense to intermediate signal intense on MR images after Bankart soft-tissue repair (Pierce et al. 2016; Sugimoto et al. 2002). The labral contour may be rounded or even slightly frayed. The labrum after Bankart repair should be closely attached to the underlying glenoid without undercutting joint fluid or contrast medium (Pierce et al. 2016) (so-called watertight labrum). A small amount of contrast may undercut the periphery of the labrum, but the majority of the repaired labrum has to be reattached to the glenoid. The inferior glenohumeral ligament and anteroinferior capsule may be more restricted after capsulorrhaphy.

1.2.4 Abnormal Postoperative Imaging Findings

Detachment or displacement of the reattached labrum is an evidence of labral repair failure (Fig. 6). Suture anchors may stick out over the glenoid cartilage surface and cause humeral head

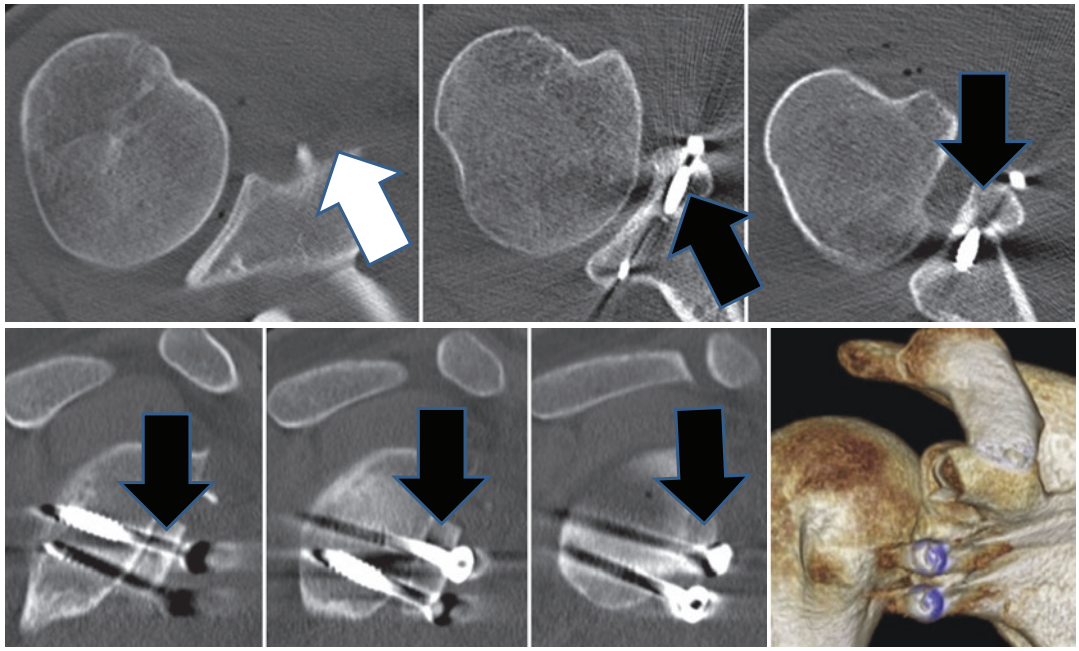

Fig. 4 21-Year-old male patient underwent a Latarjet procedure. Postoperative transversal (upper row) and sagittal (bottom row) CT images as well as 3D reconstruction (bottom right) demonstrate the osteotomy site of the coracoid process (white arrow) and the correct position of the transferred bone block (black arrows)

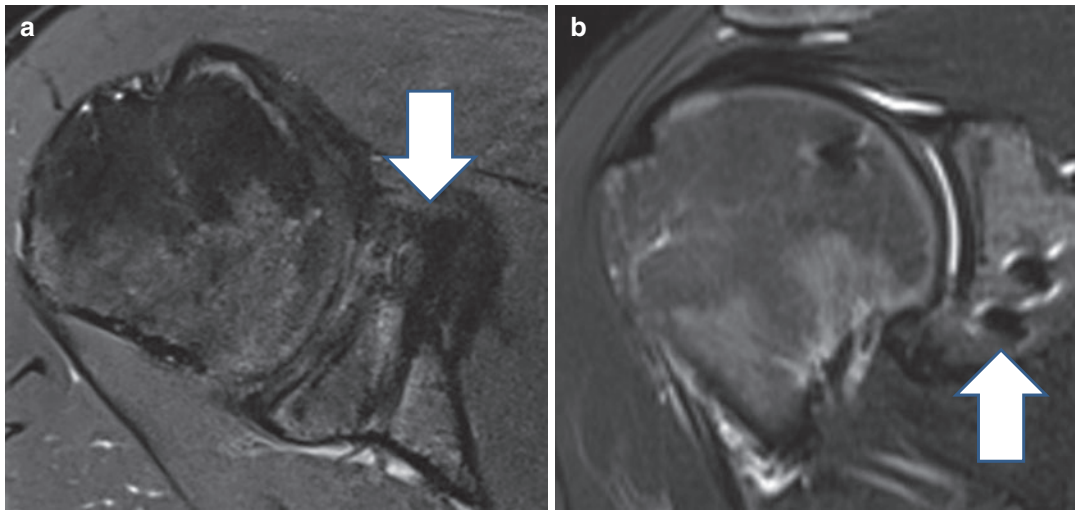

Fig. 5 29-Year-old male underwent Latarjet procedure. (**a**) Transversal proton density-weighted and (**b**) coronal STIR MR images demonstrate the correct position of the bone block and its screws (arrows)

cartilage defects. Suture anchors may even fully dislocate and cause synovitis (Pierce et al. 2016).

Complications of Latarjet procedure occur between 7% and 30% and include infection, recurrent instability (up to 8%) (Dauzère et al. 2016), fracture or nonunion of the bone graft, and loosening of screws (Pierce et al. 2016). A too medial (=deep) transferred bone block is a major risk factor for recurrent shoulder instability (Pierce et al. 2016). Too much lateral overhang of

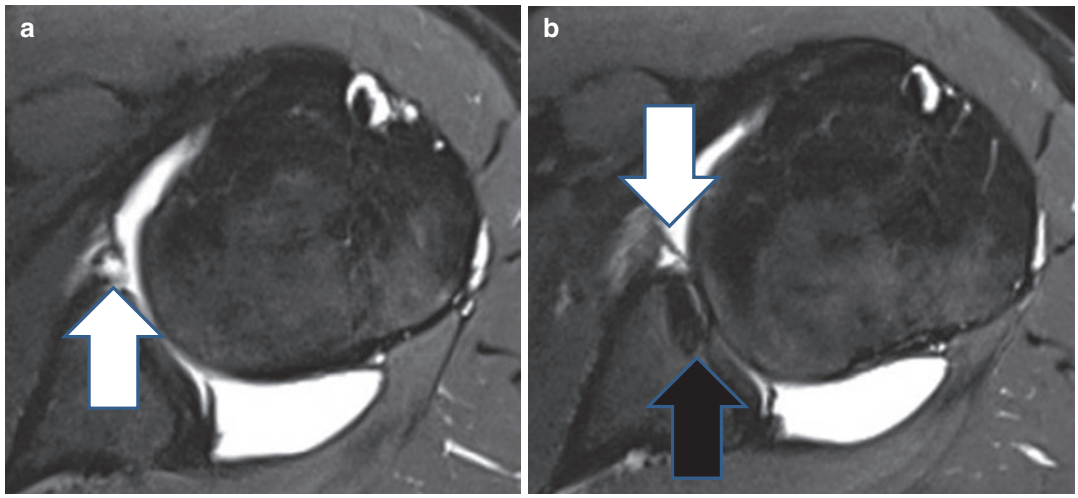

Fig. 6 33-Year-old male snowboarder underwent labral refixation. Patient reported painful shoulder after postoperative trauma. 12-Month transversal T1-weighted MR arthrography images demonstrate labral fragmentation and dislocation (white arrows) representing a recurrent labral tear. Labral anchor in correct position (black arrow)

the transferred bone block or fixation screws predisposes to impingement and subsequent osteoarthritis.

Things to Remember

The normal postoperative labral contour may be rounded or even slightly frayed after Bankart repair. The labrum after Bankart repair should be closely attached to the underlying glenoid without undercutting joint fluid or contrast medium (so-called watertight labrum).

1.3 Long Head of the Biceps Tendon and SLAP Lesion

1.3.1 Objective of Surgery

Surgical procedures due to SLAP (superior labrum anterior to posterior) lesions and long head biceps tendon disorders are common in sportive patients and represent a common cause of shoulder pain, in particular in overhead throwing athletes (Cvetanovich et al. 2019).

1.3.2 Surgical Procedure

SLAP lesions and long head biceps tendon disorders can be surgically treated by debridement, repair of the SLAP lesion, tenodesis, or tenotomy of the long head of the biceps tendon.

In tenotomy procedures the long head of the biceps tendon is cut and the released tendon retracts distally. A tenodesis procedure attaches the long head of the biceps tendon stump to the humerus proximal to the pectoralis major insertion (Pierce et al. 2016). Long head biceps tenodesis is more favored in sportive patients due to diminished symptoms during lifting activities (Gill et al. 2001; Hsu et al. 2011).

A type I SLAP tear (labral fraying) is treated with labral debridement; type II with repair, tenotomy, or tenodesis; type III is treated with debridement of the labral bucket handle tear; and type IV with debridement and tenotomy or tenodesis of the long head of the biceps tendon (Popp and Schöffl 2015). Type II lesions are most common in sportive patients and athletes (Pierce et al. 2016; Popp and Schöffl 2015).

1.3.3 Normal Postoperative Findings

The biceps anchor after SLAP debridement or SLAP repair may appear more diminutive and slightly frayed; however no contrast should extend into the repaired superior labrum (Pierce et al. 2016; Popp and Schöffl 2015).

Normal postoperative findings after long head biceps tenotomy include retraction of the biceps tendon into the bicipital groove. In contrast, after long head biceps tenodesis suture anchors or screws are found at the level of or adjacent to the bicipital groove. The intra-articular segment of the biceps tendon is absent after both tenotomy and tenodesis of the long head of the biceps tendon. Thus an empty rotator cuff interval after tenotomy or tenodesis should not be misinterpreted as a long head biceps tear. Moreover implants of radiolucent anchors on conventional radiographs should not be mistaken as an osseous lesion (Pierce et al. 2016).

1.3.4 Abnormal Postoperative Findings

Undercutting joint fluid or contrast medium on arthrograms represent imaging findings of a SLAP repair failure. Tendon pullout due to a dislodged biceps tenodesis screw/anchor is not uncommon. Humeral fractures at the tenodesis site have been reported rarely (Virk and Nicholson 2016). Groove pain may be present at the site of the fixation of the tendon (Fig. 7).

Things to Remember

Undercutting joint fluid or contrast medium on arthrograms represents an imaging finding of a SLAP repair failure. Tendon pullout due to a dislodged long head biceps tenodesis is not an uncommon complication.

2 Postoperative Hip

2.1 Femoroacetabular Impingement Surgery

2.1.1 Objective of Surgery

The main objectives of joint preservation surgery in femoroacetabular impingement patients are pain reduction, increasing the range of motion and prevention of early osteoarthritis of the hip.

2.1.2 Surgical Procedures

Open surgical hip dislocation, surgical minimal invasive direct approaches, hip arthroscopy, reverse periacetabular osteotomy, and combinations are common surgical interventions to correct the underlying abnormality of the

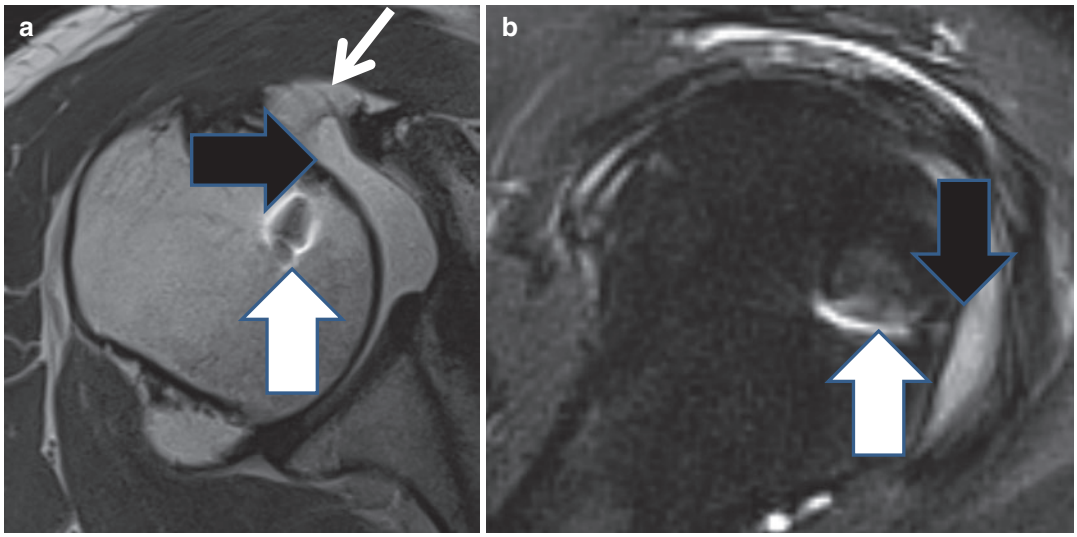

Fig. 7 (**a** and **b**) 46-year-old male patient underwent long head biceps tenodesis. The patient reported recent trauma. (**a**) 20-Month postoperative transversal proton density-weighted and (**b**) sagittal STIR MR arthrography images demonstrate a tendon pullout with a displaced suture stump from the suture anchor (black arrows). Tenodesis anchor in correct position (white bold arrows). Additional full-thickness tear of the subscapularis tendon (white narrow arrow)

femur and/or acetabulum in femoroacetabular impingement (FAI) patients (Dietrich et al. 2013a, b, 2017).

2.1.3 Normal Postoperative Findings

Correction of the underlying osseous abnormality in FAI patients can be assessed by comparison between preoperative and postoperative conventional radiographs and cross-sectional images, preferentially MRI and MR arthrography (Fig. 8) (Dietrich et al. 2013a, b, 2017).

In general, cam-type deformity is pronounced at the femoral-head neck junction anterosuperiorly (Sutter et al. 2012a; Zingg et al. 2013). Thus, radial CT or MR images are recommended for evaluation of the resection site (so-called osteochondroplasty) of the cam-type deformity, because radial cross-sectional images enable a better evaluation of the preoperative and/or postoperative cam-type deformity compared to transverse, coronal, or sagittal cross-sectional images (Sutter et al. 2012a).

Variants of the labrum and cartilage such as sublabral recess, capsular synovial plicae, or supra-acetabular fossa as a pseudodefect of the acetabular cartilage are common and may be

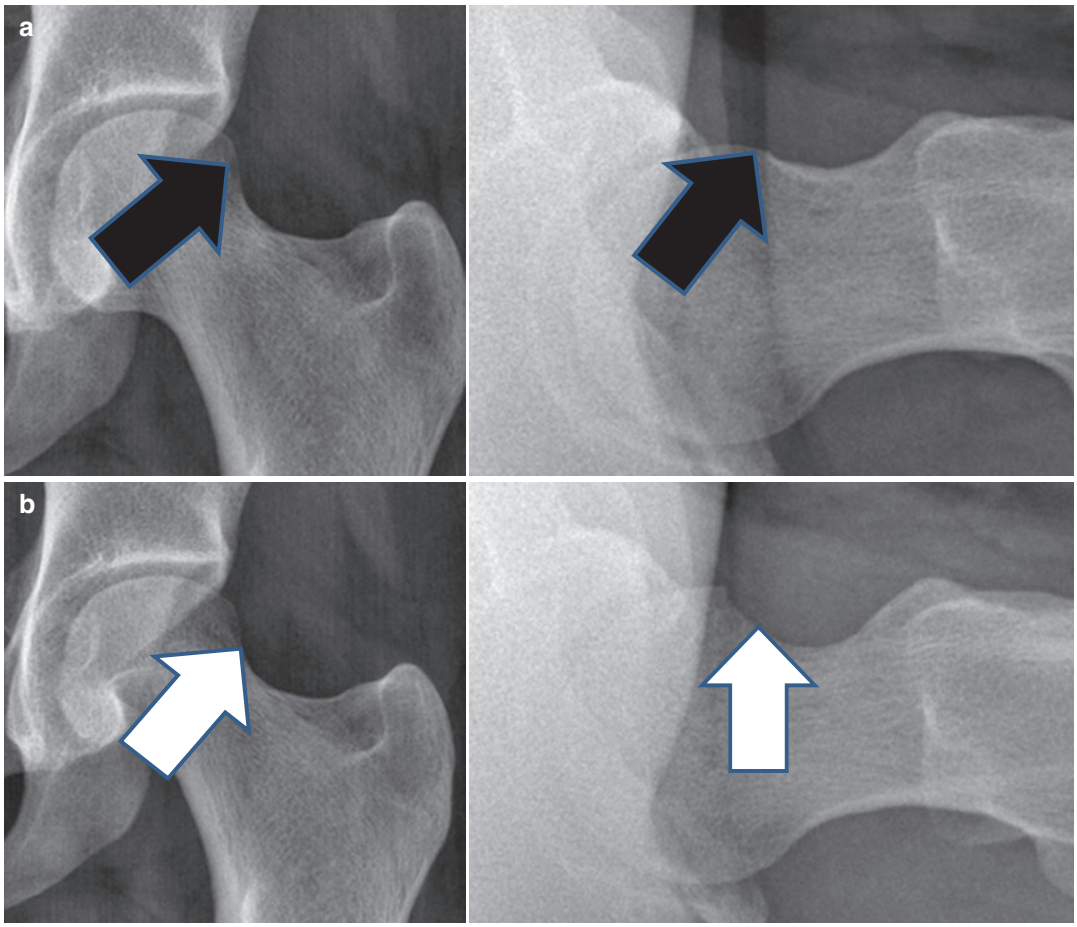

Fig. 8 (**a** and **b**)18-Year-old female patient underwent arthroscopy for treatment of FAI symptoms. (**a**) Preoperative anteroposterior and cross-table lateral radiographs demonstrate bony cam-type FAI deformity (black arrows). (**b**) 6-Week postoperative radiographs illustrate technical successful and sufficient arthroscopic resection of the cam-type deformity (white arrows) (so-called osteochondroplasty)

identified in the postoperative FAI patient (Studler et al. 2008; Omoumi and Vande 2017; Dietrich et al. 2012). A congenital absence of the ligamentum teres has a low prevalence; nevertheless this rare variant should not be reported as an iatrogenic injury after arthroscopy (Omoumi and Vande 2017). In contrast a missing ligamentum teres is a normal postoperative finding after open surgical hip dislocation.

Pincer-type impingement configuration on MR images such as cranial retroversion of the acetabulum was observed in approximately one-third of all asymptomatic volunteers (Bensler et al. 2019). A wide overlap of acetabular depth measurements on MRI between asymptomatic volunteers and patients with pincer- or mixed-type FAI was also found (Bensler et al. 2019). Thus, MR images are limited for the discrimination of asymptomatic volunteers from pincer-type FAI patients (Bensler et al. 2019).

Interestingly, a high prevalence was shown for labral tears (52%), acetabular cartilage defects (47%), and femoral cartilage defects (30%) in FAI patients without previous surgery (Tresch et al. 2017). Moreover, intra-articular adhesions, labral tears, cartilage defects, and anterior capsular defects are frequent findings on MR images in both symptomatic and asymptomatic patients 1 year after arthroscopic treatment of femoroacetabular impingement (Kim et al. 2017): Adhesions between the joint capsule and the femoral neck anteriorly were found in 35% whereas obliteration and bandlike adhesions of the paralabral sulcus were detected between 94% and 100% of both asymptomatic and symptomatic postoperative FAI patients 1 year after arthroscopic treatment for FAI (Kim et al. 2017). Residual labral tears were found between 35% and 53% whereas acetabular and femoral cartilage defects were found between 12% and 41% of both asymptomatic and symptomatic postoperative FAI patients 1 year after surgical treatment of FAI. Between 47% and 77% of all asymptomatic and symptomatic postoperative FAI patients demonstrated anterior capsular defects with a mean capsular defect size between 21 mm and 27 mm (Fig. 9). It has to be stated that a uniform distribution between symptomatic and

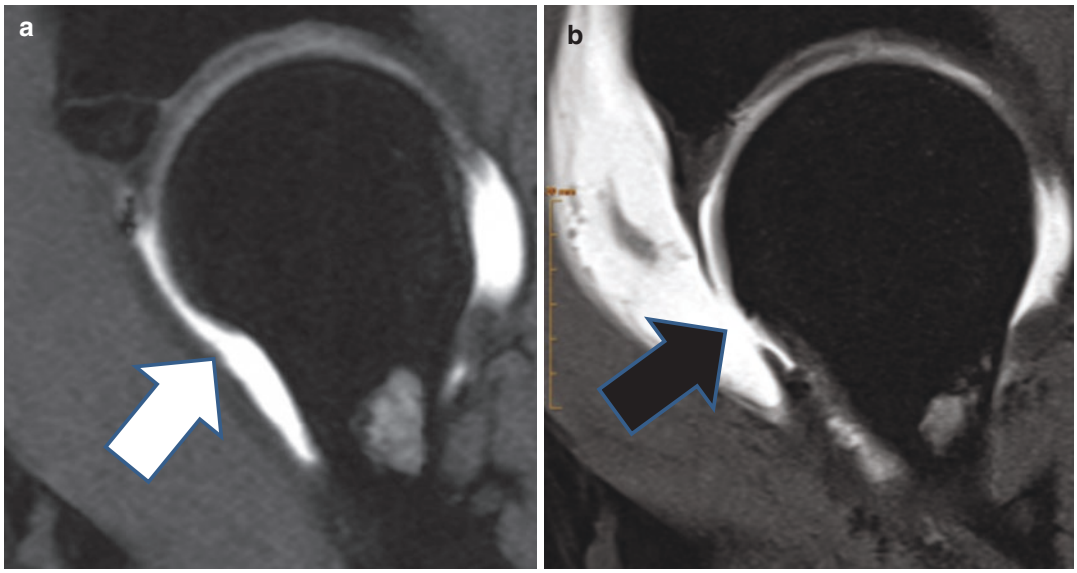

Fig. 9 (**a** and **b**) 18-year-old male patient underwent arthroscopy for treatment of FAI symptoms. (**a**) Preoperative sagittal fat-suppressed proton density-weighted MR image demonstrates intact anterior joint capsule (white arrow). (**b**) 4-Year postoperative sagittal fat-suppressed proton density-weighted MR image demonstrates anterior capsular defect (black arrow). Anterior capsular defects after arthroscopic treatment of FAI are frequent findings on MR images in both symptomatic and asymptomatic patients

asymptomatic patients 1 year after arthroscopic FAI treatment was found without significant differences for the aforementioned apparent abnormal MR imaging findings (Kim et al. 2017). Thus, the presence of intra-articular adhesions, labral tears, cartilage defects, and anterior capsular defects on postoperative MR arthrography is not necessarily associated with symptoms in postoperative FAI patients (Dietrich et al. 2017; Kim et al. 2017).

2.1.4 Abnormal Postoperative Findings

Undercorrection

Undercorrection of the underlying mechanical conflict is the most common surgical failure and most frequent indication for revision surgery within the first 2 years after FAI surgery (Fig. 10) (Dietrich et al. 2013a, b, 2017). Residual cam-type, pincer-type, and mixed-type FAI

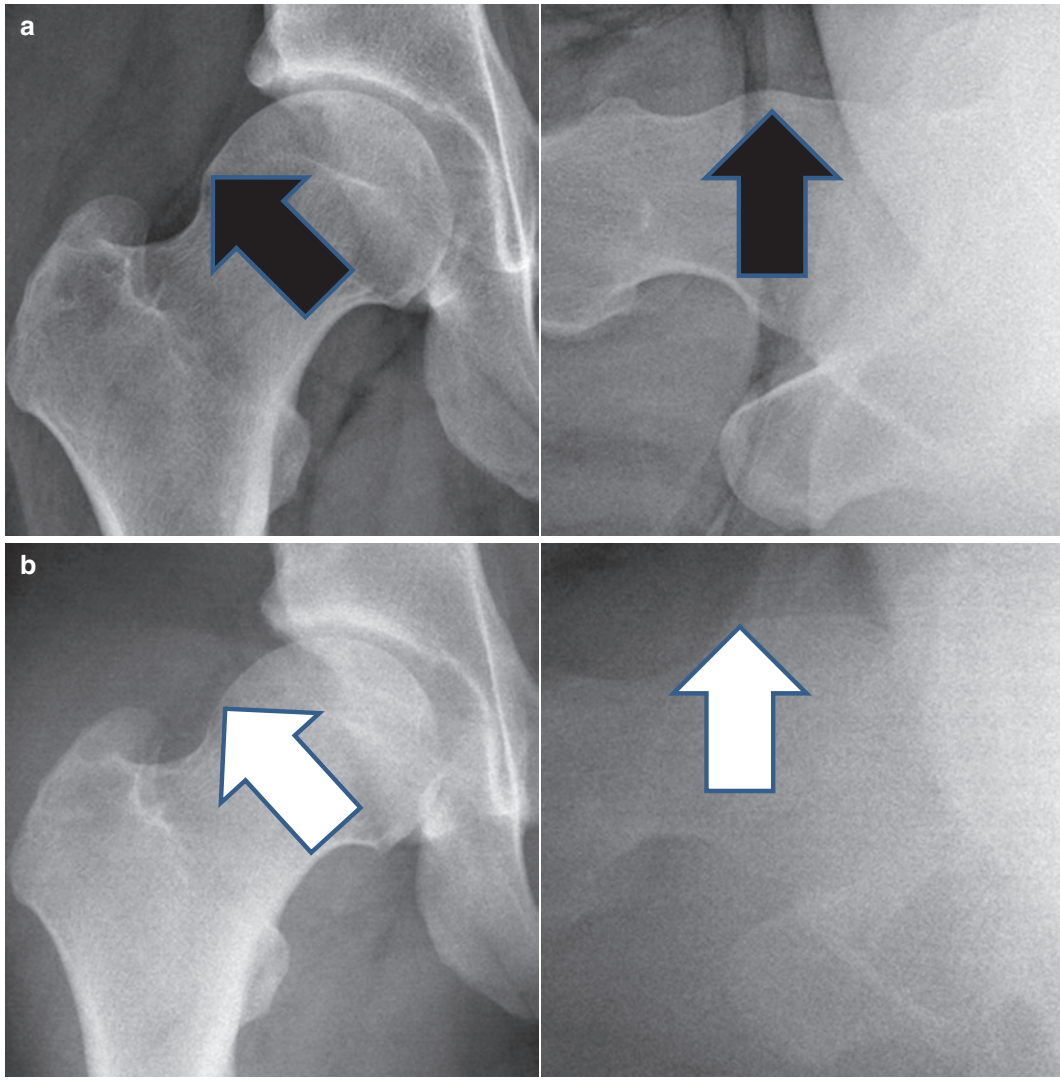

Fig. 10 (**a** and **b**) 21-year-old male patient underwent arthroscopy for treatment of FAI symptoms. (**a**) Preoperative anteroposterior and cross-table lateral radiographs of the cam-type deformity demonstrate bony cam-type FAI deformity (black arrows). (**b**) Intraoperative radiographs illustrate undercorrection with a residual cam-type deformity at the arthroscopic resection site (white arrows) (so-called osteochondroplasty). Subsequently, the patient underwent revision arthroscopy due to residual FAI symptoms

configuration or extra-articular contributors to FAI symptoms such as subspine impingement configuration, ischiofemoral impingement, abnormal femoral antetorsion, and spinopelvic parameters should be evaluated on images in patients with persistent or recurrent hip and/or groin pain after FAI surgery (Dietrich et al. 2013a, b, 2017; Sutter and Pfirrmann 2013; Sutter et al. 2012a, b, 2015; Mascarenhas et al. 2018).

Mean alpha angles of 38° after arthroscopic correction (compared to a preoperative alpha angle of 59°) as well as 39° after open surgical correction (compared to a preoperative alpha angle of 57°) of the osseous cam-type abnormality on cross-table lateral radiographs were reported (Zingg et al. 2013). On MRI, the preoperative mean alpha angle of 60° in both the arthroscopic group and open surgery group was reduced to 43° in arthroscopically treated patients compared to a higher mean alpha angle of 48° in open surgery group patients (Zingg et al. 2013).

The mean preoperative alpha angle on Dunn view radiographs was significantly reduced from 70° preoperatively to 43° at 2 weeks and 2 years after arthroscopic resection of the cam-type deformity at the femoral head-neck junction (Gupta et al. 2014). Thus, it was concluded that no recurrence of cam-type configuration occurred at 2-year follow-up after arthroscopic treatment of femoroacetabular impingement (Gupta et al. 2014).

One may recommend determining routinely femoral antetorsion values in FAI patients because increased or decreased femoral antetorsion values are contributors to FAI symptoms (Sutter and Pfirrmann 2013; Sutter et al. 2012a, b, 2015). Normal femoral antetorsion values in an asymptomatic volunteer population with an age between 20 and 50 years (mean age: 34.4 years) were 17° ± 10.6 for females and 9° ± 7.4 for males (Sutter et al. 2012a, b). Pathological femoral antetorsion measurements may influence surgery; for instance a more extensive femoral excision osteochondroplasty may be indicated in FAI patients with abnormally decreased femoral antetorsion values to avoid postoperative hip and groin pain compared to FAI patients with normal femoral antetorsion values (Sutter and Pfirrmann 2013; Dietrich et al. 2017). Scout-like MR image quality is sufficient for femoral antetorsion measurements. The additional acquisition time for these scout-like MR images is between 1 and 2 min (Sutter et al. 2012a, b; Dietrich et al. 2016).

Spinopelvic parameters were significantly different in symptomatic FAI patients compared to asymptomatic volunteers. FAI patients demonstrated significantly more anterior pelvic tilt, significantly higher sacral slope (41° ± 6° versus 48° ± 6°) and significantly higher pelvic incidence (47° ± 7 versus 51° ± 7°) compared to asymptomatic volunteers (Mascarenhas et al. 2018). Spinopelvic parameters can be measured on MRI, upright whole-spine radiographs obtained with a standard digital radiography system, or low-dose biplanar X-ray unit (Mascarenhas et al. 2018; Dietrich et al. 2013b).

Overcorrection

Extensive acetabular rim trimming, in particular in borderline dysplastic hips, may cause microinstability/instability of the hip due to an insufficient acetabular coverage of the femoral head. Moreover, extensive acetabular rim trimming contributes to premature osteoarthritis of the hip (Dietrich et al. 2017; Steppacher et al. 2014).

Excessive osteochondroplasty at the femoral head-neck junction decreases the weight-carrying capacity of the femur. Non-displaced stress or insufficiency femoral neck fractures were observed between 0.1% and 1.9% as an early complication 4 ± 4 weeks postoperatively in surgically treated FAI patients. Postoperative FAI patients with stress/insufficiency femoral neck fractures demonstrated significant smaller alpha angels compared to postoperative FAI patients without a femoral fracture (35° ± 4° versus 41° ± 6°) (Dietrich et al. 2017; Zingg et al. 2014).

Osteoarthritis

One specific objective of joint preservation surgery in FAI patients is to prevent premature osteoarthritis of the hip. Continuation of hip joint degeneration and subsequent early postoperative osteoarthritis with conversion to total hip arthroplasty implicate a failure of the joint preservation

Fig. 11 41-Year-old male patient underwent conversion to total hip arthroplasty due to continuation of hip joint degeneration (=osteoarthritis) after surgical treatment of FAI symptoms

surgery in FAI patients (Fig. 11) (Dietrich et al. 2017). Secondary conversion rate to total hip arthroplasty was 2.9% after hip arthroscopy in a systematic review with more than 6000 FAI patients and a mean follow-up of 2 years (Harris et al. 2013). Patients presenting with substantial osteoarthritis (Kellgren-Lawrence grade 3), a joint space of 2 mm or less on preoperative conventional radiographs, as well as patients demonstrating severe cartilage defects, acetabular subchondral edema, and cysts on MR images are linked with a poorer clinical outcome after FAI surgery and are more likely to undergo early secondary conversion to total hip arthroplasty (Steppacher et al. 2014; Herrmann et al. 2016; Krych et al. 2016).

Adhesions

Intra-articular adhesions between the joint capsule and the femoral head-neck junction anteriorly at the osteochondroplasty site are considered as a postoperative scar tissue which may cause limited range of motion, soft-tissue impingement, and pain in the postoperative FAI patient (Fig. 12) (Dietrich et al. 2013a, b, 2017). As a consequence, intra-articular adhesions are one of the indications for revision surgery to perform an adhesiolysis. Painful intra-articular adhesions were diagnosed in 9 of 42 revision hip arthroscopy FAI patients (Newman et al. 2016).

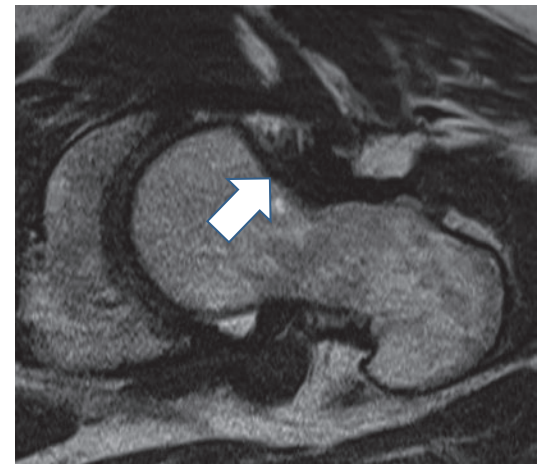

Fig. 12 34-Year-old female patient underwent open surgery for treatment of FAI symptoms. 1-Year postoperative transverse T2-weighted MR image demonstrates intra-articular adhesions between the joint capsule and the femoral head-neck junction anteriorly at the osteochondroplasty site (white arrow)

One may recommend injecting intra-articular contrast media during an arthrography procedure at the femoral head rather than at the femoral neck to enable an easy intra-articular contrast media administration and to avoid intra-articular contrast media injection into adhesions between the joint capsule and the femoral neck anteriorly in postoperative FAI patients. A contrast media injection into adhesions complicates both diagnosis of adhesions between the joint capsule and the femoral neck anteriorly and a successful intra-articular contrast agent administration (Dietrich et al. 2017).

Avascular Necrosis of the Femoral Head, Heterotopic Ossification, and Iatrogenic Intra-articular Injuries

Avascular necrosis of the femoral head has never been reported after open surgical dislocation (Ganz technique) of the hip for treatment of FAI (Dietrich et al. 2017). Avascular necrosis of the femoral head after hip arthroscopy is very uncommon; a systematic review reported 10 cases of avascular necrosis of the femoral head in an observational cohort of 6134 patients (Harris et al. 2013).

Heterotopic ossifications were observed in approximately one-third of all patients in the early days of hip joint preservation surgery (Ganz et al. 2001). Routine administration of nonsteroidal anti-inflammatory drugs prevents heterotopic ossifications in hip arthroscopy patients. Both selective and nonselective nonsteroidal anti-inflammatory drugs decrease the frequency and amount of heterotopic ossifications (Zhang et al. 2019). Thus, less than 5% of hip arthroscopy patients treated with nonsteroidal anti-inflammatory drugs to prevent heterotopic ossifications demonstrate heterotopic ossifications on conventional radiographs (Beckmann et al. 2015). Moreover, revision surgery due to heterotopic ossifications in hip arthroscopy patients treated with nonsteroidal anti-inflammatory drugs to prevent heterotopic ossifications is exceedingly rare (Dietrich et al. 2017).

Iatrogenic intra-articular injury of the femoral head cartilage or acetabular labrum during portal placement or exchange of the instruments (so-called scope trauma) is infrequent and occurs in approximately 1% (Dietrich et al. 2017).

Things to Remember

Labral tears, cartilage defects, and anterior capsular defects are frequent findings on MR images in both symptomatic and asymptomatic patients 1 year after arthroscopic treatment of femoroacetabular impingement. Undercorrection of the underlying intra-articular impingement abnormality, osteoarthritis with secondary conversion to total hip arthroplasty, and intra-articular adhesions between the joint capsule and the femoral head-neck junction anteriorly at the osteochondroplasty site are common indications for revision surgery in postoperative FAI patients.

3 Postoperative Knee

3.1 Anterior Cruciate Ligament Reconstruction

3.1.1 Objective of Surgery

The primary objective of anterior cruciate ligament (ACL) reconstruction is restoration of the function, specifically anteroposterior and rotational stability of the knee after an ACL rupture. Moreover, ACL reconstruction should avoid or at least decelerate posttraumatic osteoarthritis of the knee (Krause et al. 2018; Musahl and Karlsson 2019). ACL reconstruction is widely acknowledged as the reference standard of treatment for regaining knee stability, as well as increasing knee function and quality of life after an ACL injury, in particular in young athletes with the ambition to keep up in their demanding sport activities (Krause et al. 2018; Musahl and Karlsson 2019).

It has to be considered that conservative treatment of a torn ACL is an alternative (Krause et al. 2018). A recent systematic review retrieved exclusively two prospectively randomized controlled trials comparing conservative treatment and ACL reconstruction (Krause et al. 2018;

Frobell et al. 2013, 2010; Tsoukas et al. 2016). These both randomized controlled trials reported conflicting knee stability scores after surgical treatment in comparison with conservative treatment of an ACL rupture (Krause et al. 2018; Frobell et al. 2013, 2010; Tsoukas et al. 2016). In addition, literature does not provide definitive scientific evidence for a potential protective effect of anterior cruciate ligament reconstruction regarding prevention of long-term posttraumatic osteoarthritis of the knee after an ACL rupture (Harris et al. 2017). For instance, a higher proportion of patients (41%) presented with osteoarthritis of the knee after ACL reconstruction compared to a lower percentage of patients (31%) with osteoarthritis of the knee after conservative treatment at 12-year follow-up (Fig. 13) (Harris et al. 2017). In conclusion, although research for decades was conducted in the field of treatment after an ACL injury, one may admit a lack of high-quality investigations to identify the best treatment concept of a torn ACL in adults (Krause et al. 2018; Smith et al. 2014).

3.1.2 Surgical Procedures

Bone-patellar tendon-bone autografts and hamstring autografts of the semitendinosus and gracilis tendons are most frequently used grafts for anterior cruciate ligament reconstruction.

3.1.3 Normal Postoperative Findings

The radiographic quadrant method, an assessment technique for determination of the optimal placement of the intra-articular opening of the femoral tunnel on lateral radiographs, was proposed by Bernard et al. (1997). First, a rectangle with its sides along the Blumensaat's line, the distal, proximal, and posterior contour of the femoral condyles is created. Subsequently the rectangle is divided into a grid by quartering the long and short axes (Fig. 14a) (Bernard et al. 1997; Srinivasan et al. 2018). An optimal

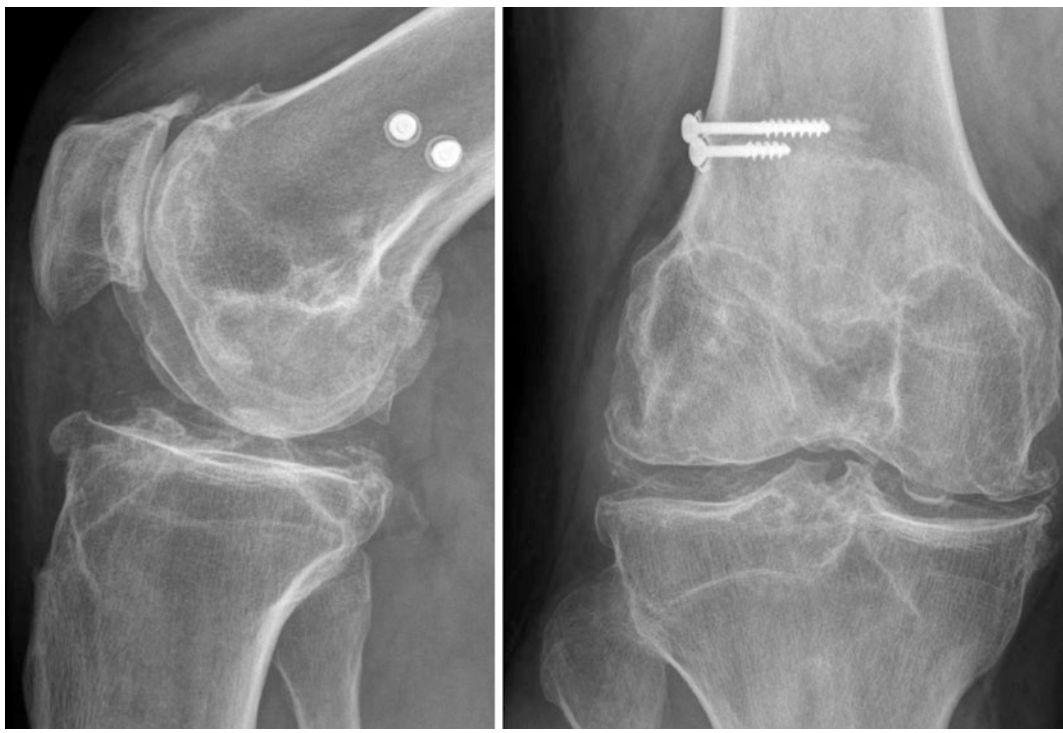

Fig. 13 49-Year-old male patient underwent ACL reconstruction. 20-Year postoperative lateral and anteroposterior radiographs demonstrate osteoarthritis of the knee

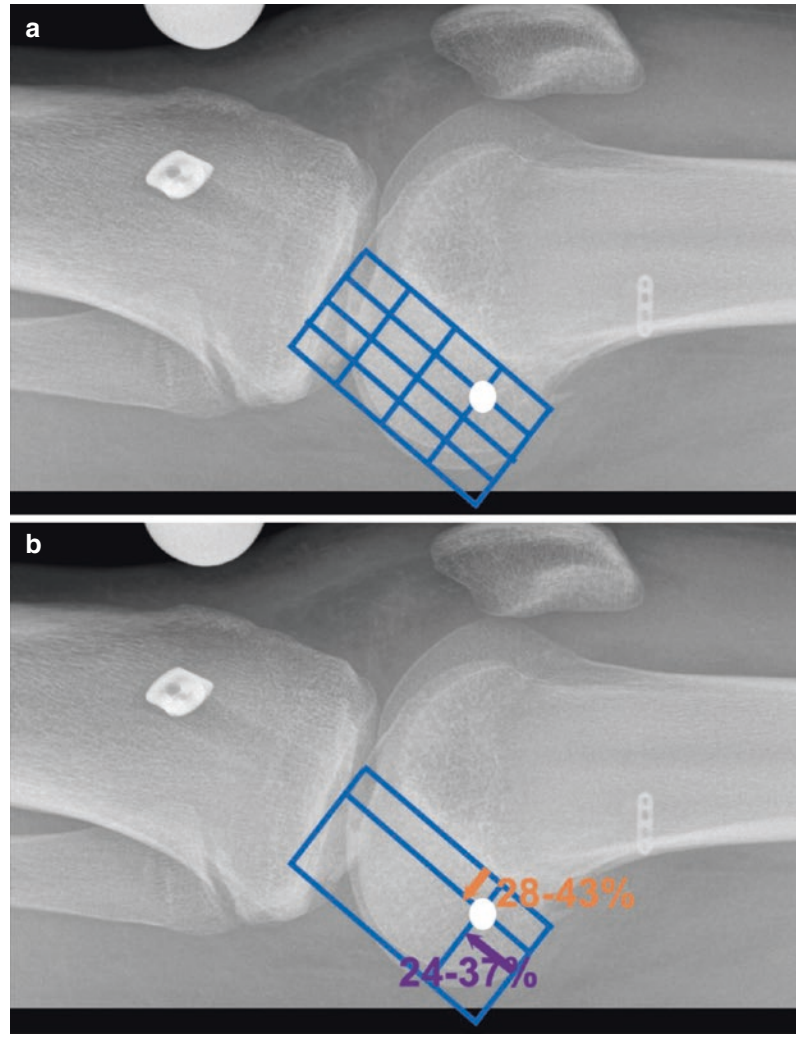

Fig. 14 (**a** and **b**) Radiographic quadrant method by Bernard et al. on a horizontal beam lateral radiograph. The sides of the rectangle are along the Blumensaat's line, the distal, proximal, and posterior contour of the femoral condyles. Rectangle is divided into a grid by quartering the long and short axes (**a**). An optimal positioning of the femoral intra-articular tunnel opening is at the intersecting lines of the most proximal and anterior quadrant (white dot) (**a**). Normal values range between 24% and 37% for the x-axis and between 28% and 43% for the y-axis (white dot) (**b**)

positioning of the femoral intra-articular tunnel opening is located at the intersecting lines of the most proximal and anterior quadrant; however a range of normal values between 24% and 37% for the x-axis and between 28% and 43% for the y-axis are proposed in the literature (Fig. 14b) (Srinivasan et al. 2018; Parkar et al. 2017).

Ideally, the tibial tunnel is placed parallel to the Blumensaat's line and the intra-articular opening of the tibial tunnel is found directly posterior to the intersection of the Blumensaat's line and the tibial plateau in a full-extended knee on a horizontal beam lateral radiograph, MRI, or CT image (Fig. 15) (Srinivasan et al. 2018). On imaging, the center of the intra-articular opening of the tibial tunnel should be at approximately 43% of the anteroposterior distance of the tibial head (Fig. 16); however a small range of normal values between 39% and 46% were proposed by various authors (Srinivasan et al. 2018; Parkar et al. 2017). On anteroposterior radiographs the intra-articular opening of the tibial tunnel should be just lateral to the midway of the tibial plateau (=51.5% of the medial to lateral tibial plateau distance) (Fig. 15) (Dhawan et al. 2016).

It is generally accepted that a mature ACL graft should be composed of low signal intensity on all MRI sequences. Nevertheless, it was reported that small areas of increased signal intensity within the ACL graft are frequent: Between

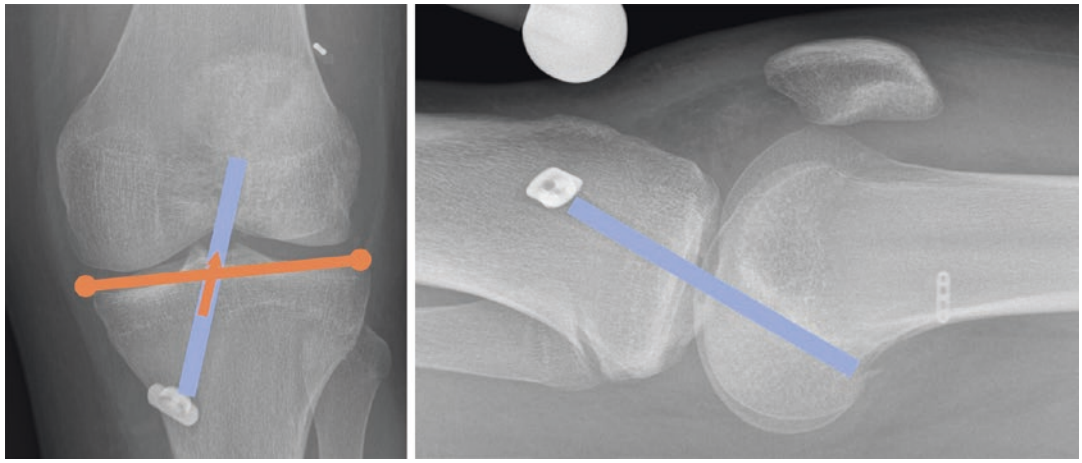

Fig. 15 Optimal intra-articular opening of the tibial tunnel on a anteroposterior radiograph is just lateral to the midway of the tibial plateau (orange arrow) (=51.5% of the medial to lateral tibial plateau distance). Optimal tibial tunnel placement parallel to the Blumensaat's line (blue line) and ideal intra-articular opening of the tibial tunnel is directly posterior to the intersection of the Blumensaat's line and the tibial plateau in a full-extended knee on a horizontal beam lateral radiograph (blue line)

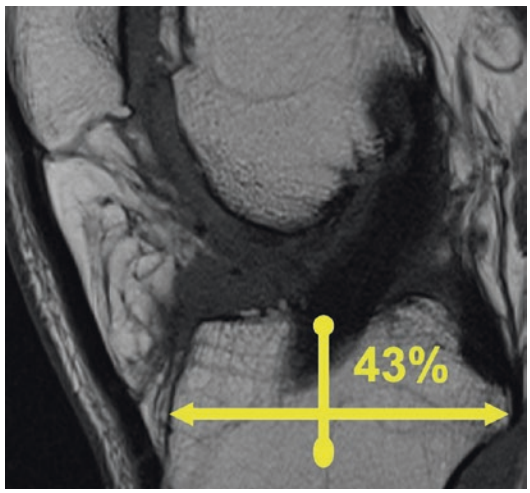

Fig. 16 The center of the intraarticular opening of the tibial tunnel should be at approximately 43% of the anteroposterior distance of the tibial head

64% and 70% of $n = 47$ ACL autografts demonstrated small amounts of increased signal intensity on intermediate-weighted and T2-weighted MR images at long-term follow-up of 4 years and longer (Fig. 17) (Saupe et al. 2008). These small areas of increased signal intensity within the ACL graft on fluid-sensitive sequences did not influence the function or stability scores of the knee after ACL reconstruction (Saupe et al. 2008). Thus, small amounts of increased signal intensity on fluid-sensitive sequences within an ACL graft can be considered as normal, even at long-term follow-up (Saupe et al. 2008).

3.1.4 Abnormal Postoperative Findings

Persistent or recurrent postoperative knee joint instability occurs between 8% and 50% of all patients after ACL reconstruction (Krause et al. 2018). Early graft failure develops within the first 6 months after surgery and is most likely due to a poor surgical technique (Bencardino et al. 2009). The most frequent surgical error is incorrect placement of the femoral and tibial graft tunnels (Musahl and Karlsson 2019; Srinivasan et al. 2018). The length and tension of the ACL graft should be constant (=isometry) during the full range of motion, in particular during flexion and extension of the knee (Srinivasan et al. 2018; Bencardino et al. 2009). Potential isometry of the ACL graft is mainly influenced by the positions of the femoral and tibial tunnel. Hence, proper tunnel positioning is essential and should be evaluated on imaging.

Button-based ACL graft fixation dislocation such as button migration into the femoral or tibial

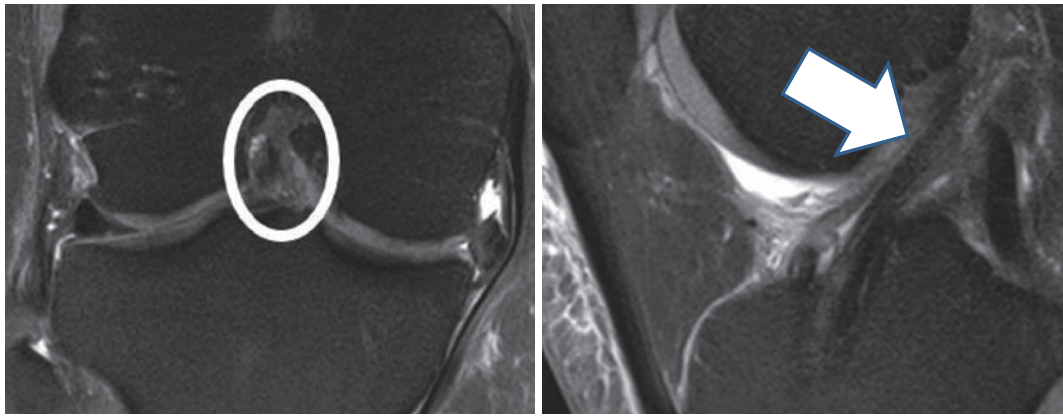

Fig. 17 18-Year-old female patient underwent ACL reconstruction. 26-Month postoperative coronal and sagittal fat-suppressed proton density-weighted MR images demonstrate small amounts of increased signal intensity on fluid-sensitive sequences within an ACL graft; these imaging findings can be considered as normal

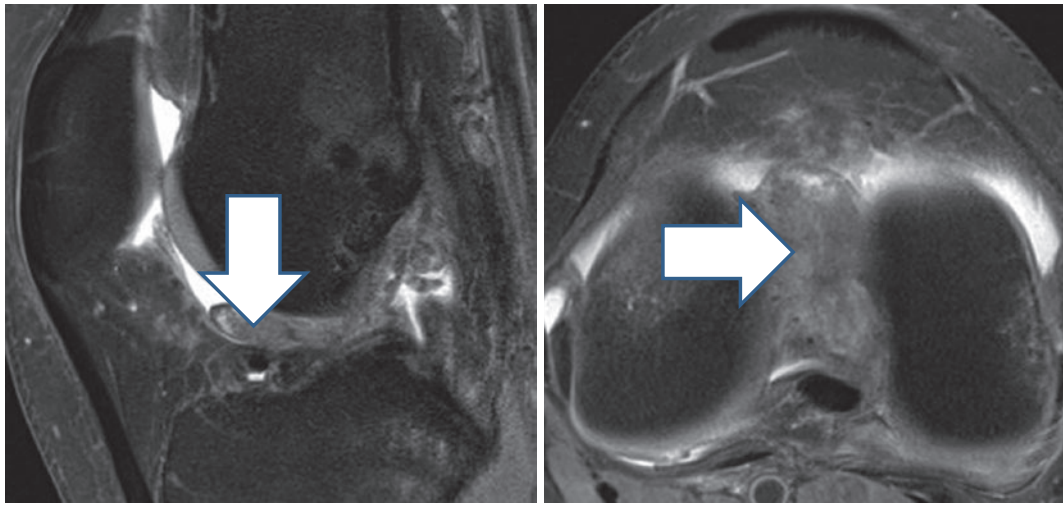

Fig. 18 20-Year-old male patient underwent ACL reconstruction. Postoperative sagittal and transverse fat-suppressed proton density-weighted MR images demonstrate a full-thickness tear of the ACL graft after a recurrent trauma. The fibers of the torn ACL graft are dislocated anteriorly and mimic a cyclops lesion (arrows). This specific imaging appearance of a torn ACL graft is also known as a "pseudocyclops lesion"

tunnel occurs infrequently; however these imaging findings implicate improper ACL graft fixation and presumably implicate persistent postoperative instability and may implicate revision surgery.

Late ACL graft failure at 1 year or later after surgery is frequently due to trauma recurrence and consecutive ACL graft tearing (Bencardino et al. 2009). Fibers of an ACL graft partial-thickness or full-thickness tear may mimic an anteriorly localized fibrous and granulation tissue (=cyclops lesion) after ACL repair (Fig. 18) (Simpfendorfer et al. 2015). This specific imaging appearance of torn ACL graft is also known as a "pseudocyclops lesion" and was originally described as a case report of two ACL graft partial tears (Simpfendorfer et al. 2015).

Focal nodules consisting of fibrous and granulation tissue, firmly attached to the ACL graft and localized in the intercondylar notch, predominantly anterior the ACL graft are named as cyclops lesions (Facchetti et al. 2017).

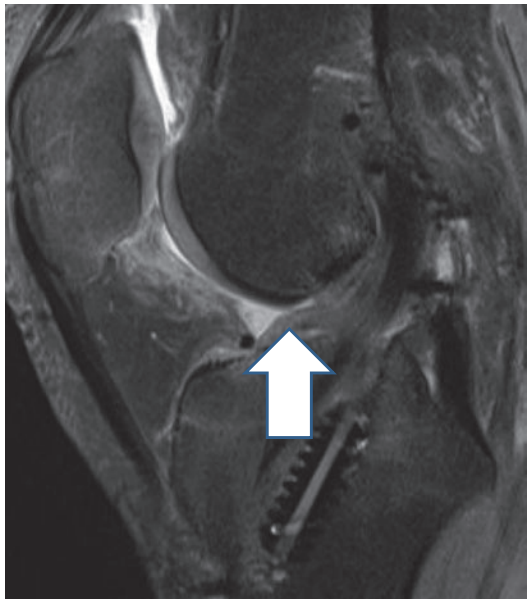

Fig. 19 24-Year-old male patient underwent ACL reconstruction. Postoperative sagittal fat-suppressed proton density-weighted MR image demonstrates a small cyclops lesion. No restriction of terminal knee extension was noted

Fig. 20 30-Year-old male patient underwent ACL reconstruction. Postoperative sagittal gradient-echo MR image demonstrates a small cyclops lesion. The patient suffered from restriction of terminal knee extension

Cyclops lesions are most frequently localized anteriorly to the ACL graft. It was found that cyclops lesions develop in approximately 25% of all patients with an average long axis of 14 mm on MRI within the first 6 months after ACL reconstruction (Fig. 19) (Facchetti et al. 2017). Later on, no significant cyclops lesion size change was found at 1-year or 2-year follow-up after surgery compared to 6-month measurements. Interestingly, clinical outcome assessed as function and overall clinical outcome was not significantly different in the study cohort with cyclops lesions compared to study participants without cyclops lesions within 2 years after ACL repair (Facchetti et al. 2017). A large cyclops lesion may cause a mechanical conflict such as restriction of terminal knee extension and may require revision arthroscopy (Fig. 20) (Noailles et al. 2019).

Arthrofibrosis is a poorly defined clinical diagnosis. Clinical symptoms of arthrofibrosis are relevant limitation of the range of motion, for both flexion and extension of the knee (Ekhtiari et al. 2017). A wide range of frequency of arthrofibrosis between 4% and 38% after ACL reconstruction is provided in the literature (Ekhtiari et al. 2017). Imaging criteria for arthrofibrosis are formation of irregular extensive fibrous scar tissue located anterior to the graft, in the Hoffa fat pad, along the extensor mechanism and the ACL graft, in the posterior compartment as well as thickening of the joint capsule (Bencardino et al. 2009).

Things to Remember

The most frequent surgical error is incorrect placement of the femoral and tibial graft tunnels. Late ACL graft failure at 1 year or later after surgery is most commonly due to trauma recurrence and consecutive ACL graft tearing.

3.2 Meniscus Repair

3.2.1 Objective of Surgery

The objective of meniscal tear surgery is to relieve pain and to restore the full range of motion of the knee joint as well as preserve the integrity of the menisci for long-term knee function (Fuchs et al. 2018).

3.2.2 Surgical Procedure of Meniscus Repair

Arthroscopic meniscal surgery includes repair, partial resection, or allograft replacement (Walz 2016). Meniscus repair yields a better functional outcome and lower degree of radiologic degeneration of the knee than partial meniscectomy (Paxton et al. 2011). In contrast a systematic review found a higher long-term revision surgery rate in patients after meniscal repair of approximately 21% (30 of 145 patients) compared to approximately 4% (52 of 1319) of all patients after partial meniscectomy (Paxton et al. 2011). The reparability of a meniscus tear depends on its location and orientation. A tear in the outer 20–30% of the meniscus (the so-called red zone) has the potential to heal after meniscus repair (Baker et al. 2018). Partial meniscectomy is the most commonly performed orthopedic surgery in the USA (Mather et al. 2015). Resection of torn meniscal tissue is usually successful to reduce knee pain and restore the range of motion; however associated modification of the biomechanics may contribute to early post-meniscectomy knee pain or subsequent osteoarthritis of the knee (Beaufils and Pujol 2017). A meniscal allograft replacement is an infrequent procedure to address persisting pain after meniscal repair and/or partial resection.

3.2.3 Normal Postoperative Findings

Patients after arthroscopic surgery of a torn meniscus may develop new symptoms such as pain, clicking, locking, or swelling in the treated knee. A meta-analysis found a meniscal repair failure in 131 of 566 patients (23.1%) at a minimum of 5 years or longer postoperatively. These data implicate that medical imaging, in particular conventional radiographs and MRI, is frequently requested in patients after meniscal tear surgery (Nepple et al. 2012).

MR imaging after meniscal surgery is sufficient in most patients. However, MR arthrography can be considered in challenging cases and CT arthrography is valuable in patients who are not suitable for MR imaging (Walz 2016). It was shown that the sensitivity of 78% and specificity of 75% for 3-T MRI in diagnosis of a meniscal retear in the postoperative knee after partial meniscectomy were lower compared to a sensitivity of 88% and specificity of 100% for 3-T MR arthrography using arthroscopy as the reference standard (Magee 2014).

Postoperative menisci may demonstrate increased signal intensity on T2-weighted MR images as a false-positive mimicker of a residual tear or retear (Hoffelner et al. 2011; Miao et al. 2011) (Fig. 21). Explanations of increased signal intensity on T2-weighted MR images are preexisting meniscal degeneration or healing response of the meniscus (Barber and McNally 2013). Persistent intermediate to high signal on fluid-sensitive MR image sequences within the first 1–2 years after surgery in a healing meniscus can be related to fibrovascular granulation tissue (Hoffelner et al. 2011; Miao et al. 2011). It has to be stated that complete resolution of the former tear site is rare (Mather et al. 2015).

The normal partially resected meniscus may appear more diminutive with blunted rather than sharp edges (Walz 2016). Low-volume partial meniscectomy (<25%) may demonstrate an apparent normal postoperative meniscus with or without marginal changes regarding meniscal shape and size (Walz 2016). Normal MR imaging findings of a meniscus allograft within the first postoperative year are meniscus extrusion, shrinkage, and increased signal intensity on T2-weighted images (Walz 2016).

3.2.4 Abnormal Postoperative Findings

MR imaging criteria for a retear of the repaired meniscus or after partial meniscectomy preserving more than 75% of the original meniscus are fluidlike signal at the repair site with communication to the articular surface, a displaced meniscal fragment, presence of a new parameniscal cyst, and a new meniscal tear without a preexisting tear on preoperative images (Walz 2016; Baker et al. 2018) (Fig. 22).

Intermediate-to-high signal on fluid-sensitive sequences after partial meniscectomy preserving less than 75% of the original meniscus may represent a meniscal tear, scar, or also meniscal degeneration. The higher the signal intensity in

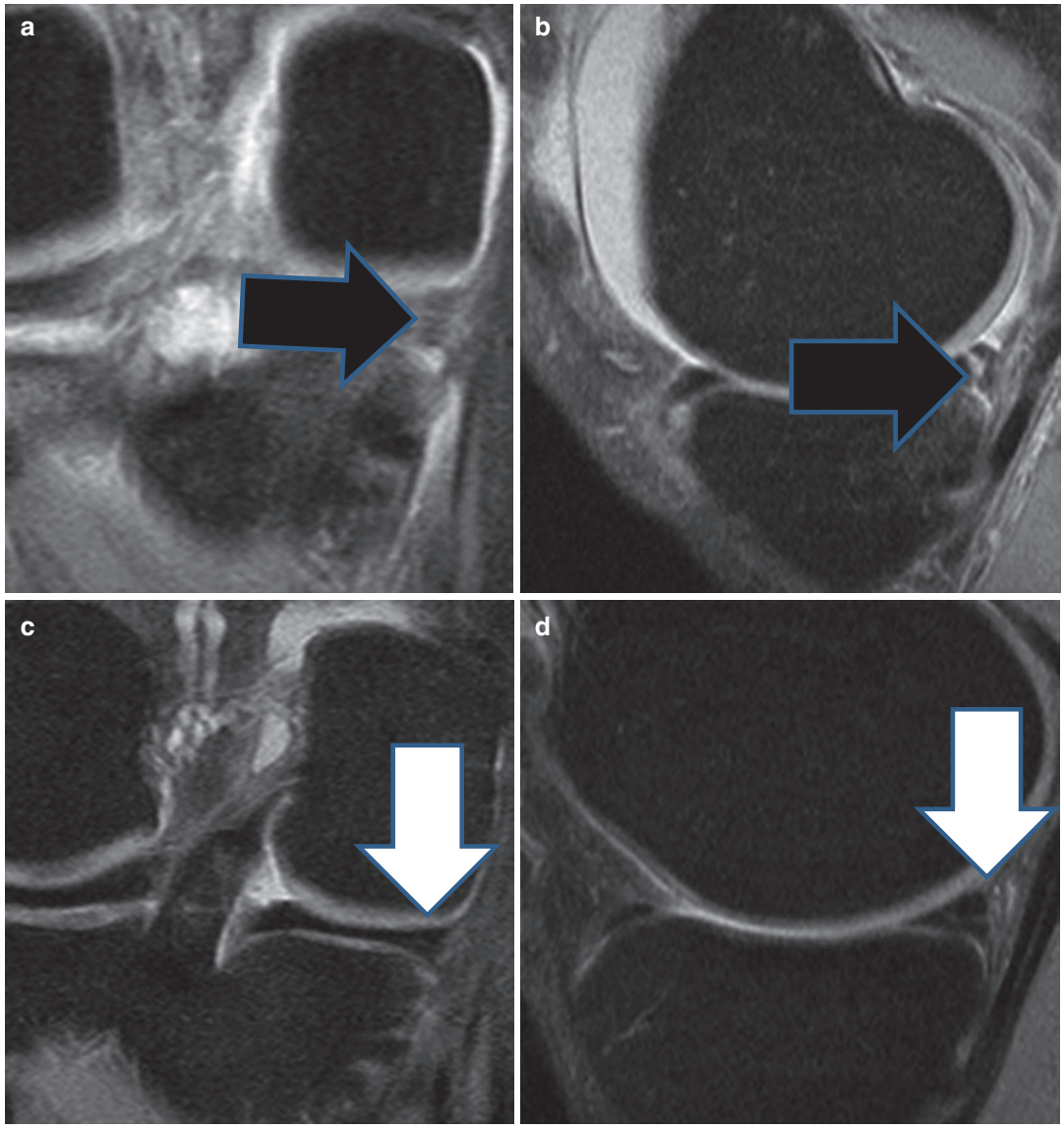

Fig. 21 (**a** and **d**) 18-year-old female snowboarder underwent meniscus repair. Preoperative (**a** and **b**) and 1-year postoperative (**c** and **d**) coronal fat-suppressed proton density-weighted (**a** and **c**) and sagittal fat-suppressed proton density-weighted (**b** and **d**) MR images. The preoperative images demonstrate a vertical tear of the medial meniscus (black arrows). The images on the lower row show normal postoperative meniscus with mild increased signal in the posterior medial meniscus (white arrows)

the postoperative meniscus after partial meniscectomy on fluid-sensitive images the higher the probability for a retear (Boutin et al. 2014).

Classic MR arthrography findings of meniscal retears are penetration of gadolinium-based contrast material into the substance of the meniscus. However, 10 of 94 meniscal retears diagnosed on arthroscopy did not demonstrate contrast material tracking into the meniscus on MR arthrography images (Magee 2014). Moreover, these false-negative ten meniscal retears on MR arthrography were diagnosed as retears on MRI without intra-articular contrast agent administration (Magee 2014). Based on

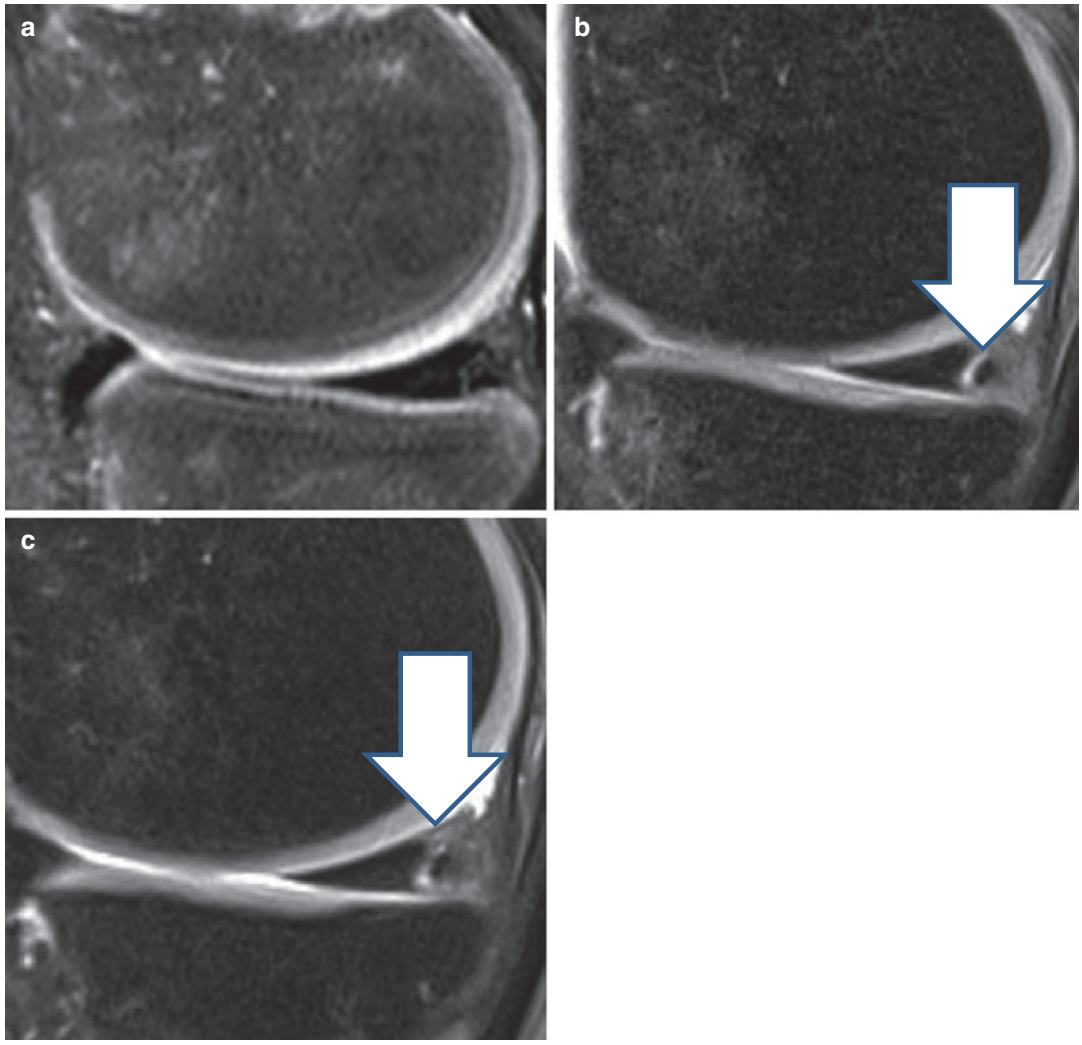

Fig. 22 (**a–c**) 18-year-old male underwent meniscus repair. 3 months (**a**), 42 months (**b**), and 48 months (**c**) postoperative sagittal fat-suppressed proton density-weighted MR images. Increasing vertical fluid signal over time represents a retear of the meniscus (white arrows)

the fact that intra-articular contrast agent does not necessarily penetrate into the retear after partial meniscectomy on MR arthrography images it was concluded that MR arthrography images in combination with MR images without previous intra-articular contrast agent allow a high diagnostic accuracy in the detection of meniscal retears after partial meniscectomy (Magee 2014).

Displaced meniscal fragments, fluid-filled clefts, and morphologic change are indicators of tears of the meniscal allograft transplantation (Walz 2016; Verdonk et al. 2006). (Fig. 23). However poor correlation between MR imaging and clinical findings after meniscal allograft implantation was reported (Barber and McNally 2013; Verdonk et al. 2006).

Things to Remember

MR imaging criteria for a retear of the repaired meniscus or after partial meniscectomy preserving more than 75% of the original meniscus are fluid-like signal at the repair site with communication to

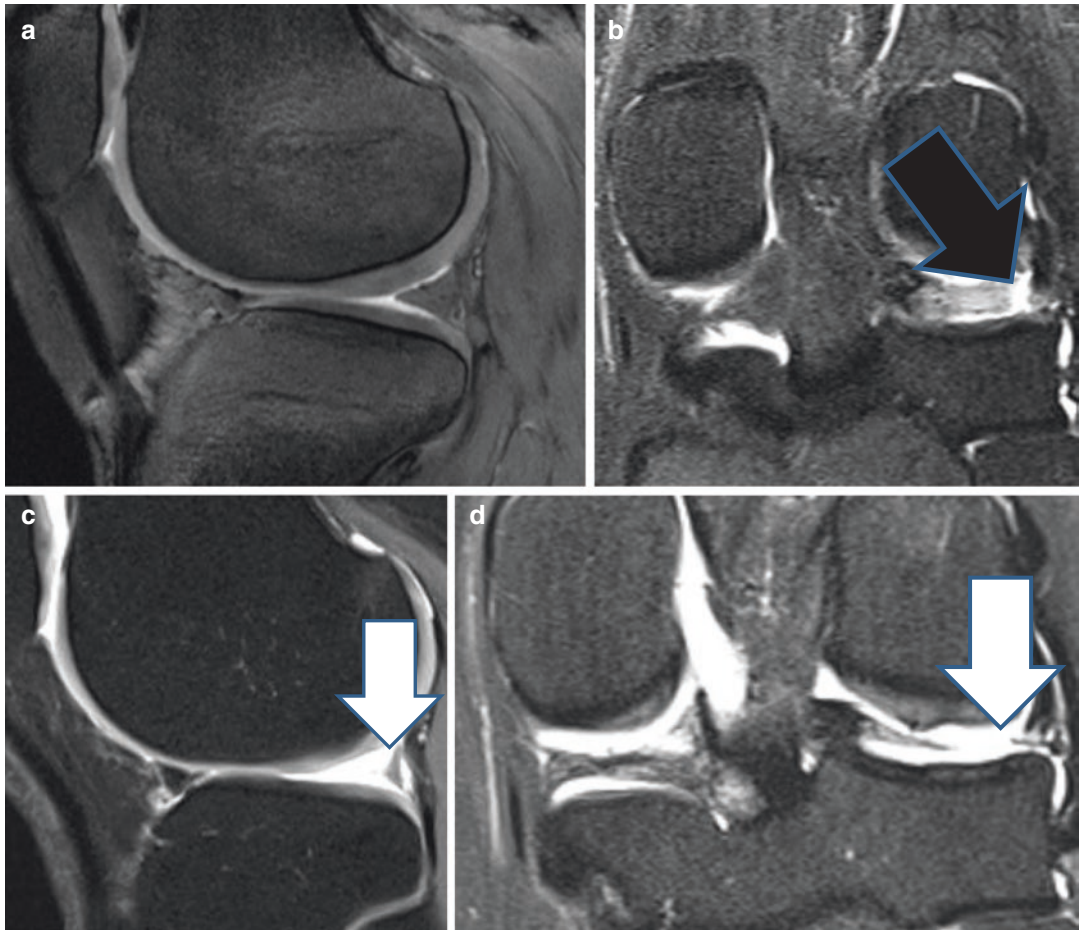

Fig. 23 (**a**–**d**) 29-year-old female underwent meniscusallograft implantation. (**a** and **b**) 1-year and (**b** and **d**) 3-year (**b** and **c**) sagittal trueFISP (left) and coronal STIR (right) MR images. The 1-year postoperative coronal image shows a tear of the meniscus (black arrow). The 3-year postoperative images demonstrate an ongoing deconfiguration and diminution of the allograft (white arrows)

the articular surface, a displaced meniscal fragment, presence of a new parameniscal cyst, and a new meniscal tear without a preexisting tear of preoperative images. Granulation tissue may mimic a retear and may persist for 2 years after surgery.

3.3 Cartilage Repair

3.3.1 Objectives of Surgery

The aim of cartilage repair procedures in athletes is prevention of premature osteoarthritis of the knee and reduction of pain (Houck et al. 2018).

3.3.2 Surgical Procedure

Cartilage repair surgery includes bone marrow stimulation techniques (for instance microfracture, drilling), osteochondral allograft, osteochondral autograft, and autologous chondrocyte implantation techniques (Walz 2016).

An arthroscopic bone marrow stimulation technique uses a microfracture awl or a drill to create multiple 2–4 mm deep osteochondral defects. These osteochondral holes promote vascularization, release cytokines, and finally stimulate the growth of fibrocartilage. Osteochondral allograft procedures use cadaveric donor tissue grafts to

restore the defect of the cartilage surface (Walz 2016; Forney et al. 2014). Osteochondral autograft fills the articular surface defect by harvesting tissue grafts from the same patient in a non-weight-bearing area such as intercondylar notch or trochlear groove (Walz 2016; Forney et al. 2014). Frequently used names for osteochondral autograft procedures are autogenous osteochondral transfer (AOT), mosaicplasty, and osteochondral autograft transfer system (OATS) (Forney et al. 2014). Autologous chondrocyte implantation (ACI) techniques are two-step surgical interventions. First, cartilage is harvested from a non-weight-bearing portion of the knee, subsequently the donor tissue is cultured ex vivo for approximately 3–4 weeks to increase the number of chondrocytes, and finally the graft fills the articular surface defect during a second surgical intervention in the same patient (Forney et al. 2014).

3.3.3 Normal and Abnormal Imaging Findings

MRI, MR arthrography, and CT arthrography are useful for the assessment of cartilage repair (Walz 2016). The MOCART (Magnetic Resonance Observation of Cartilage Repair Tissue) 2.0 knee score and atlas were developed for the assessment of cartilage repair of the knee joint and may be used with or without modification as a template in daily clinical radiology in postoperative patients after cartilage repair (Schreiner et al. 2019) (Fig. 24).

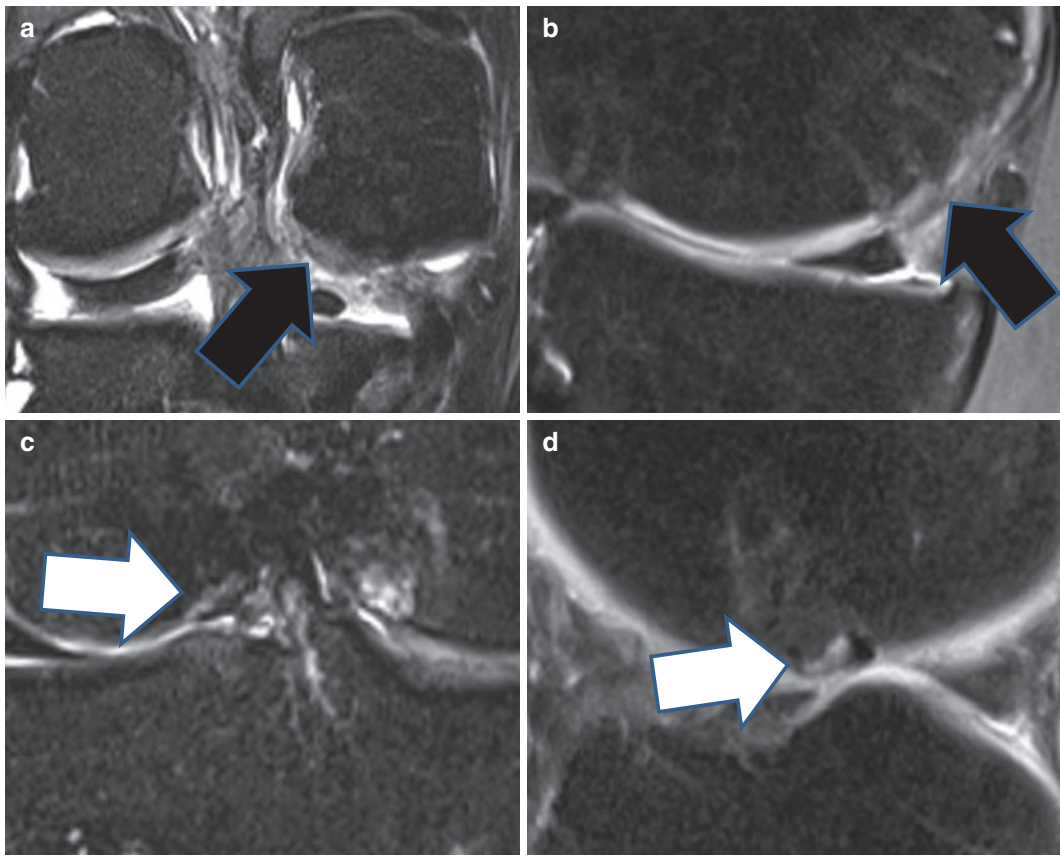

Fig. 24 (**a–d**) 32-year-old male underwent osteochondral autograft transfer. 48-Month postoperative coronal STIR (**a** and **c**) and sagittal fat-suppressed proton density-weighted (**b** and **d**) MR images. The images (**a**) and (**b**) present an integrated osteochondral autograft transfer with deep fissures (black arrows). The images (**c**) and (**d**) demonstrate the normal donor site at the lateral femoral condyle with a residual osteochondral defect (white arrows)

Volume of cartilage defect filling	The first parameter "volume of cartilage defect filling" according to MOCART 2.0 classification describes the volume of cartilage defect filling in relation to the adjacent native reference cartilage. The description is provided as a percentage in relation of the hypothetical volume of intact cartilage that would cover the defect
Integration into adjacent cartilage	The second MOCART 2.0 parameter entitled "integration into adjacent cartilage" assesses the integration of the cartilage repair tissue into the adjacent native cartilage by evaluating the interface between both tissues
Surface of the repair tissue	The third MOCART 2.0 parameter "surface of the repair tissue" determinates distinguishable cartilage surface irregularities, regardless of perfect filling, present hypertrophy, or underfilling
Structure of the repair tissue	The fourth MOCART 2.0 parameter "structure of the repair tissue" assesses the signal intensity of the repaired tissue as homogeneous or heterogeneous, depending on whether typical cartilage layers are detectable or not
Signal intensity of the repair tissue	The fifth MOCART 2.0 parameter "signal intensity of the repair tissue" classifies the signal intensity on turbo spin-echo PD-weighted MR images of the repair tissue as "normal," "minor abnormal," or "severely abnormal"
Bony defect or bony overgrowth	The sixth MOCART 2.0 parameter "bony defect or bony overgrowth" evaluates the extent of osseous defects and intrachondral osteophytes at the cartilage repair site
Subchondral changes	The final MOCART 2.0 parameter "subchondral changes" differentiates a normal subchondral lamina and normal subchondral bone from subchondral bone marrow edema, subchondral cysts of 5 mm or larger, and osteonecrosis-like MRI signal

Additional non-repair site findings such as donor-site appearance, cartilage defects, and meniscus and ligament disorders may be integrated in the radiology report (Walz 2016; Forney et al. 2014).

Things to Remember

The MOCART 2.0 score was developed for the assessment of cartilage repair and may be used with or without modification as a template in daily clinical radiology in postoperative patients after cartilage repair. The MOCART 2.0 score consists of the following seven parameters: "volume of cartilage defect filling," "integration into adjacent cartilage," "surface of the repair tissue," "structure of the repair tissue," "signal intensity of the repair tissue," "bony defect or bony overgrowth," and "subchondral changes."

Box 1

Conventional radiography remains the basic imaging modality for routine postoperative imaging. Cross-sectional imaging such as CT/CT arthrography and MR/MR arthrography is valuable for the closer evaluation of patients with persistent or recurrent pain and symptoms such as joint instability.

References

Adler RS (2013) Postoperative rotator cuff. Semin Musculoskelet Radiol 17:12–19

Baker JC, Friedman MV, Rubin DA (2018) Imaging the postoperative knee meniscus: an evidence-based review. AJR Am J Roentgenol 211:519–527

Barber BR, McNally EG (2013) Meniscal injuries and imaging the postoperative meniscus. Radiol Clin N Am 51:371–391

Beard DJ, Rees JL, Cook JA, Rombach I, Cooper C, Merritt N, Shirkey BA, Donovan JL, Gwilym S, Savulescu J, Moser J, Gray A, Jepson M, Tracey I, Judge A, Wartolowska K, Carr AJ, CSAW Study Group (2018) Arthroscopic subacromial decompression for subacromial shoulder pain (CSAW): a multicentre, pragmatic, parallel group, placebo-controlled, three-group, randomised surgical trial. Lancet 391:329–338

Beaufils P, Pujol N (2017) Management of traumatic meniscal tear and degenerative meniscal lesions. Save the meniscus. Orthop Traumatol Surg Res 103:237–244

Beckmann JT, Wylie JD, Potter MQ, Maak TG, Greene TH, Aoki SK (2015) Effect of naproxen prophylaxis on heterotopic ossification following hip arthroscopy: a double-blind randomized placebo-controlled trial. J Bone Joint Surg Am 97:2032–2037

Beltran LS, Bencardino JT, Steinbach LS (2014) Postoperative MRI of the shoulder. J Magn Reson Imaging 40:1280–1297

Bencardino JT, Beltran J, Feldman MI, Rose DJ (2009) MR imaging of complications of anterior cruciate ligament graft reconstruction. Radiographics 29:2115–2126

Bensler S, Dietrich TJ, Zubler V, Pfirrmann CWA, Sutter R (2019) Pincer-type MRI morphology seen in over a third of asymptomatic healthy volunteers without femoroacetabular impingement. J Magn Reson Imaging 49:1296–1303

Bernard M, Hertel P, Hornung H, Cierpinski T (1997) Femoral insertion of the ACL. Radiographic quadrant method. Am J Knee Surg 10:14–21; discussion 21–22

Boutin RD, Fritz RC, Marder RA (2014) Magnetic resonance imaging of the postoperative meniscus: resection, repair, and replacement. Magn Reson Imaging Clin N Am 22:517–555

Cvetanovich GL, Gowd AK, Agarwalla A, Forsythe B, Romeo AA, Verma NN (2019) Trends in the management of isolated SLAP tears in the United States. Orthop J Sports Med 7:232596711983399. https://doi.org/10.1177/2325967119833997

Dauzère F, Faraud A, Lebon J, Faruch M, Mansat P, Bonnevialle N (2016) Is the Latarjet procedure risky? Analysis of complications and learning curve. Knee Surg Sports Traumatol Arthrosc 24:557–563

Dhawan A, Gallo RA, Lynch SA (2016) Anatomic tunnel placement in anterior cruciate ligament reconstruction. J Am Acad Orthop Surg 24:443–454

Dietrich TJ, Suter A, Pfirrmann CW, Dora C, Fucentese SF, Zanetti M (2012) Supra-acetabular fossa (pseudodefect of acetabular cartilage): frequency at MR arthrography and comparison of findings at MR arthrography and arthroscopy. Radiology 263:484–491

Dietrich TJ, Dora C, Pfirrmann CW (2013a) Postoperative imaging in femoroacetabular impingement. Semin Musculoskelet Radiol 17:272–278

Dietrich TJ, Pfirrmann CW, Schwab A, Pankalla K, Buck FM (2013b) Comparison of radiation dose, workflow, patient comfort and financial break-even of standard digital radiography and a novel biplanar low-dose X-ray system for upright full-length lower limb and whole spine radiography. Skelet Radiol 42:959–967

Dietrich TJ, Fucentese SF, Pfirrmann CW (2016) Imaging of individual anatomical risk factors for patellar instability. Semin Musculoskelet Radiol 20:65–73

Dietrich TJ, Grob K, Kim CO (2017) Postoperative imaging after impingement surgery. Semin Musculoskelet Radiol 21:529–538

Ekhtiari S, Horner NS, de Sa D, Simunovic N, Hirschmann MT, Ogilvie R, Berardelli RL, Whelan DB, Ayeni OR (2017) Arthrofibrosis after ACL reconstruction is best treated in a step-wise approach with early recognition and intervention: a systematic review. Knee Surg Sports Traumatol Arthrosc 25:3929–3937

Facchetti L, Schwaiger BJ, Gersing AS, Guimaraes JB, Nardo L, Majumdar S, Ma BC, Link TM, Li X, UCSF-P50-ACL Consortium; AF-ACL Consortium (2017) Cyclops lesions detected by MRI are frequent findings after ACL surgical reconstruction but do not impact clinical outcome over 2 years. Eur Radiol 27:3499–3508

Forney MC, Gupta A, Minas T (2014) Magnetic resonance imaging of cartilage repair procedures. Magn Reson Imaging Clin N Am 22:671–701

Frobell RB, Roos EM, Roos HP, Ranstam J, Lohmander LS (2010) A randomized trial of treatment for acute anterior cruciate ligament tears. N Engl J Med 363:331–342

Frobell RB, Roos HP, Roos EM, Roemer FW, Ranstam J, Lohmander LS (2013) Treatment for acute anterior cruciate ligament tear: five year outcome of randomised trial. BMJ 346:f232

Fuchs A, Kloos F, Bode G, Izadpanah K, Südkamp NP, Feucht MJ (2018) Isolated revision meniscal repair - failure rates, clinical outcome, and patient satisfaction. BMC Musculoskelet Disord 19:446

Ganz R, Gill TJ, Gautier E, Ganz K, Krügel N, Berlemann U (2001) Surgical dislocation of the adult hip a technique with full access to the femoral head and acetabulum without the risk of avascular necrosis. J Bone Joint Surg Br 83:1119–1124

Gill TJ, McIrvin E, Mair SD, Hawkins RJ (2001) Results of biceps tenotomy for treatment of pathology of the long head of the biceps brachii. J Shoulder Elb Surg 10:247–249

Gupta A, Redmond JM, Stake CE, Finch NA, Dunne KF, Domb BG (2014) Does the femoral cam lesion regrow after osteoplasty for femoroacetabular impingement? Two-year follow-up. Am J Sports Med 42:2149–2155

Harris JD, McCormick FM, Abrams GD, Gupta AK, Ellis TJ, Bach BR Jr, Bush-Joseph CA, Nho SJ (2013) Complications and reoperations during and after hip arthroscopy: a systematic review of 92 studies and more than 6,000 patients. Arthroscopy 29:589–595

Harris KP, Driban JB, Sitler MR, Cattano NM, Balasubramanian E, Hootman JM (2017) Tibiofemoral osteoarthritis after surgical or nonsurgical treatment of anterior cruciate ligament rupture: a systematic review. J Athl Train 52:507–517

Herrmann SJ, Bernauer M, Erdle B, Südkamp NP, Helwig P, Hauschild O (2016) Osteoarthritic changes rather than age predict outcome following arthroscopic treatment of femoroacetabular impingement in middle-aged patients. BMC Musculoskelet Disord 17:253

Hoffelner T, Resch H, Forstner R (2011) Arthroscopic all-inside meniscal repair–does the meniscus heal? A clinical and radiological follow-up examination to verify meniscal healing using a 3-T MRI. Skelet Radiol 40:181–187

Houck DA, Kraeutler MJ, Belk JW, Frank RM, McCarty EC, Bravman JT (2018) Do focal chondral defects of the knee increase the risk for progression to osteoarthritis? A review of the literature. Orthop J Sports Med 6:232596711880193. https://doi.org/10.1177/2325967118801931

Hsu AR, Ghodadra NS, Provencher MT, Lewis PB, Bach BR (2011) Biceps tenotomy versus tenodesis: a review of clinical outcomes and biomechanical results. J Shoulder Elb Surg 20:326–332

Jacobson JA, Miller B, Bedi A, Morag Y (2011) Imaging of the postoperative shoulder. Semin Musculoskelet Radiol 15:320–339

Kim CO, Dietrich TJ, Zingg PO, Dora C, Pfirrmann CWA, Sutter R (2017) Arthroscopic hip surgery: fre-

quency of postoperative MR Arthrographic findings in asymptomatic and symptomatic patients. Radiology 283:779–788

Krause M, Freudenthaler F, Frosch KH, Achtnich A, Petersen W, Akoto R (2018) Operative versus conservative treatment of anterior cruciate ligament rupture. Dtsch Arztebl Int 115:855–862

Krych AJ, King AH, Berardelli RL, Sousa PL, Levy BA (2016) Is subchondral acetabular edema or cystic change on MRI a contraindication for hip arthroscopy in patients with femoroacetabular impingement? Am J Sports Med 44:454–459

Magee T (2014) Accuracy of 3-Tesla MR and MR arthrography in diagnosis of meniscal retear in the post-operative knee. Skelet Radiol 43:1057–1064

Magee TH, Gaenslen ES, Seitz R, Hinson GA, Wetzel LH (1997) MR imaging of the shoulder after surgery. AJR Am J Roentgenol 168:925–928

Mascarenhas VV, Rego P, Dantas P, Caetano AP, Jans L, Sutter R, Marques RM, Ayeni OR, Consciência JG (2018) Can we discriminate symptomatic hip patients from asymptomatic volunteers based on anatomic predictors? A 3-dimensional magnetic resonance study on cam, pincer, and spinopelvic parameters. Am J Sports Med 46:3097–3110

Mather RC 3rd, Garrett WE, Cole BJ et al (2015) Cost-effectiveness analysis of the diagnosis of meniscus tears. Am J Sports Med 43:128–137

Miao Y, Yu JK, Ao YF (2011) Diagnostic values of 3 methods for evaluating meniscal healing status after meniscal repair: comparison among second-look arthroscopy, clinical assessment, and magnetic resonance imaging. Am J Sports Med 39:735–742

Mohana-Borges AV, Chung CB, Resnick D (2004) MR imaging and MR arthrography of the postoperative shoulder: spectrum of normal and abnormal findings. Radiographics 24:69–85

Musahl V, Karlsson J (2019) Anterior cruciate ligament tear. N Engl J Med 380:2341–2348

Nepple JJ, Dunn WR, Wright RW (2012) Meniscal repair outcomes at greater than five years: a systematic literature review and meta-analysis. J Bone Joint Surg Am 94:2222–2227

Newman JT, Briggs KK, McNamara SC, Philippon MJ (2016) Outcomes after revision hip arthroscopic surgery in adolescent patients compared with a matched cohort undergoing primary arthroscopic surgery. Am J Sports Med 44:3063–3069

Noailles T, Chalopin A, Boissard M, Lopes R, Bouguennec N, Hardy A (2019) Incidence and risk factors for cyclops syndrome after anterior cruciate ligament reconstruction: a systematic literature review. Orthop Traumatol Surg Res 105:1401–1405

Omoumi P, Vande BB (2017) Hip imaging: Normal variants and asymptomatic findings. Semin Musculoskelet Radiol 21:507–517

Parkar AP, Adriaensen MEAPM, Vindfeld S, Solheim E (2017) The anatomic centers of the femoral and tibial insertions of the anterior cruciate ligament: a systematic review of imaging and cadaveric studies reporting normal center locations. Am J Sports Med 45:2180–2188

Paxton ES, Stock MV, Brophy RH (2011) Meniscal repair versus partial meniscectomy: a systematic review comparing reoperation rates and clinical outcomes. Arthroscopy 27:1275–1288

Pierce JL, Nacey NC, Jones S, Rierson D, Etier B, Brockmeier S, Anderson MW (2016) Postoperative shoulder imaging: rotator cuff, labrum, and biceps tendon. Radiographics 36:1648–1671

Popp D, Schöffl V (2015) Superior labral anterior posterior lesions of the shoulder: current diagnostic and therapeutic standards. World J Orthop 6:660–671

Saupe N, White LM, Chiavaras MM, Essue J, Weller I, Kunz M, Hurtig M, Marks P (2008) Anterior cruciate ligament reconstruction grafts: MR imaging features at long-term follow-up—correlation with functional and clinical evaluation. Radiology 249:581–590

Schreiner MM, Raudner M, Marlovits S, Bohndorf K, Weber M, Zalaudek M, Röhrich S, Szomolanyi P, Filardo G, Windhager R, Trattnig S (2019) The MOCART (Magnetic Resonance Observation of Cartilage Repair Tissue) 2.0 Knee Score and Atlas. Cartilage 17. https://doi.org/10.1177/1947603519865308

Simpfendorfer C, Miniaci A, Subhas N, Winalski CS, Ilaslan H (2015) Pseudocyclops: two cases of ACL graft partial tears mimicking cyclops lesions on MRI. Skelet Radiol 44:1169–1173

Smith TO, Postle K, Penny F, McNamara I, Mann CJ (2014) Is reconstruction the best management strategy for anterior cruciate ligament rupture? A systematic review and meta-analysis comparing anterior cruciate ligament reconstruction versus non-operative treatment. Knee 21:462–470

Soterios G, Yemin A, Beltran L, Babb J (2013) Engaging Hill-Sachs lesion: is there an association between this lesion and findings on MRI? Am J Roentgenol 201:W633–W638

Spielmann AL, Forster BB, Kokan P, Hawkins RH, Janzen DL (1999) Shoulder after rotator cuff repair: MR imaging findings in asymptomatic individuals—initial experience. Radiology 213:705–708

Srinivasan R, Wan J, Allen CR, Steinbach LS (2018) Knee imaging following anterior cruciate ligament reconstruction: the surgeon's and radiologist's perspectives. Semin Musculoskelet Radiol 22:386–397

Steppacher SD, Huemmer C, Schwab JM, Tannast M, Siebenrock KA (2014) Surgical hip dislocation for treatment of femoroacetabular impingement: factors predicting 5-year survivorship. Clin Orthop Relat Res 472:337–348

Studler U, Kalberer F, Leunig M, Zanetti M, Hodler J, Dora C, Pfirrmann CW (2008) MR arthrography of the hip: differentiation between an anterior sublabral recess as a normal variant and a labral tear. Radiology 249:947–954

Sugimoto H, Suzuki K, Mihara K, Kubota H, Tsutsui H (2002) MR arthrography of shoulders after suture-anchor Bankart repair. Radiology 224:105–111

Sutter R, Pfirrmann CW (2013) Atypical hip impingement. AJR Am J Roentgenol 201:W437–W442

Sutter R, Dietrich TJ, Zingg PO, Pfirrmann CW (2012a) How useful is the alpha angle for discriminating between symptomatic patients with cam-type femoroacetabular impingement and asymptomatic volunteers? Radiology 264:514–521

Sutter R, Dietrich TJ, Zingg PO, Pfirrmann CW (2012b) Femoral antetorsion: comparing asymptomatic volunteers and patients with femoroacetabular impingement. Radiology 263:475–483

Sutter R, Dietrich TJ, Zingg PO, Pfirrmann CW (2015) Assessment of femoral Antetorsion with MRI: comparison of oblique measurements to standard transverse measurements. AJR Am J Roentgenol 205:130–135

Tashjian RZ (2012) Epidemiology, natural history, and indications for treatment of rotator cuff tears. Clin Sports Med 31:589–604

Tresch F, Dietrich TJ, Pfirrmann CWA, Sutter R (2017) Hip MRI: prevalence of articular cartilage defects and labral tears in asymptomatic volunteers. A comparison with a matched population of patients with femoroacetabular impingement. J Magn Reson Imaging 46:440–451

Tsoukas D, Fotopoulos V, Basdekis G, Makridis KG (2016) No difference in osteoarthritis after surgical and non-surgical treatment of ACL-injured knees after 10 years. Knee Surg Sports Traumatol Arthrosc 24:2953–2959

Verdonk PC, Verstraete KL, Almqvist KF (2006) Meniscal allograft transplantation: long-term clinical results with radiological and magnetic resonance imaging correlations. Knee Surg Sports Traumatol Arthrosc 14:694–706

Virk MS, Nicholson GP (2016) Complications of proximal biceps tenotomy and tenodesis. Clin Sports Med 35:181–188

Walz DM (2016) Postoperative imaging of the knee: meniscus, cartilage, and ligaments. Radiol Clin N Am 54:931–950

Zanetti M, Jost B, Hodler J, Gerber C (2000) MR imaging after rotator cuff repair: full-thickness defects and bursitis-like subacromial abnormalities in asymptomatic subjects. Skelet Radiol 29:314–319

Zhang AH, Chen X, Zhao QX, Wang KL (2019) A systematic review and meta-analysis of naproxen for prevention heterotopic ossification after hip surgery. Medicine (Baltimore) 98:e14607

Zimmermann SM, Scheyerer MJ, Farshad M, Catanzaro S, Rahm S, Gerber C (2016) Long-term restoration of anterior shoulder stability: a retrospective analysis of arthroscopic Bankart repair versus open Latarjet procedure. J Bone Joint Surg Am 98:1954–1961

Zingg PO, Ulbrich EJ, Buehler TC, Kalberer F, Poutawera VR, Dora C (2013) Surgical hip dislocation versus hip arthroscopy for femoroacetabular impingement: clinical and morphological short-term results. Arch Orthop Trauma Surg 133:69–79

Zingg PO, Buehler TC, Poutawera VR, Alireza A, Dora C (2014) Femoral neck fractures after arthroscopic femoral neck osteochondroplasty for femoroacetabular impingement. Knee Surg Sports Traumatol Arthrosc 22:926–931

Imaging of Sports Lesions in Soccer Players

Tineke De Coninck, M. Shahabpour, and F. M. Vanhoenacker

Contents

T. De Coninck (✉)
Department of Radiology, AZ Groeninge, Kortrijk, Belgium
e-mail: tinekedeconinck@gmail.com

M. Shahabpour
Department of Radiology, Universitair Ziekenhuis Brussel, Brussels, Belgium
e-mail: maryam.shahabpour@uzbrussel.be

F. M. Vanhoenacker
Department of Radiology, AZ Sint-Maarten Mechelen, Mechelen, Belgium

Department of Radiology, Antwerp University Hospital, University of Antwerp, Antwerp, Belgium

Faculty of Medicine and Medical Sciences, Ghent University, Ghent, Belgium
e-mail: filip.vanhoenacker@telenet.be

Abstract

Soccer is one of the world's most popular sports, but is physically demanding and acute and overuse injuries occur rather frequently. It is a typical low-extremity sport, with the lower limb region most frequently injured. Through a structured approach focused on injury epidemiology, relevant anatomy, mechanism, and appearance on medical imaging, the radiologist can gain familiarity with the common and important injuries experienced by soccer players and in turn assist the player and referring clinician towards the goal of appropriate treatment and timely return to play. This chapter reviews the most commonly observed and most important injuries in soccer players.

Med Radiol Diagn Imaging (2021)
https://doi.org/10.1007/174_2020_262, © Springer Nature Switzerland AG
Published Online: 12 March 2021

1 Introduction

Soccer is the world's most popular sport, fascinating hundreds of millions of participants of all ages and sexes each year. It is a physically demanding contact sport, requiring coordination, velocity, and physical skills. Injuries occur rather frequently compared to most other sports and range from common and relatively benign low-grade muscle strains to potentially career-ending ligamentous injuries in elite soccer players (De Loes 1995). The nature of the injury or degree of disability sometimes warrants further assessment with diagnostic imaging. Through a structured approach focused on injury epidemiology, relevant anatomy, mechanism, and appearance on medical imaging, the radiologist can gain familiarity with the common and important injuries experienced by soccer players and in turn assist the player and referring clinician towards the goal of appropriate treatment and timely return to play. In this chapter we review the most frequently observed and most important injuries in soccer players.

2 Groin Injuries

Groin injuries are a common problem in both elite and recreational soccer players (10–15% of all soccer injuries), are often disabling, and can even be career-ending. Unfortunately, chronic groin pain remains a poorly understood clinical condition and diagnosis and management can be challenging (De Loes 1995; Tak 2014). Imaging findings are common in soccer players, but often do not correlate well with symptoms. The term athletic groin pain was established as a unifying name and it comprises four distinct clinical entities related to the anatomy, patterns of injury, and clinical presentation (Weir et al. 2015; Chopra and Robinson 2016):

- Adductor-related groin pain
- Pubic-related groin pain
- Inguinal-related groin pain
- Iliopsoas-related groin pain

For a more detailed overview of groin injuries we refer to Prasad et al. (2021).

2.1 Adductor-Related Groin Pain

Adductor-related groin pain is the most frequently encountered groin problem in soccer players and results from sliding, passing, kicking, or pivoting. The kicking leg is most often affected and subsequently the players switch to submaximal kicking to avoid pain, but eventually they have to entirely stop training or playing matches (Tak and Langhout 2014). The adductor longus is predominantly affected at its musculotendinous junction, and injuries are less commonly reported at the gracilis, adductor magnus, adductor brevis, and iliacus origins. A combination of adductor longus and rectus abdominis strains often occurs; the injury then extends through the adductor aponeurosis at the symphysis pubis to the lower part of the rectus abdominis muscle.

Imaging

Ultrasound is the first-line imaging modality, demonstrating hypoechogenic signal of the adductor insertion, tendon thickening, and convex tendon bulging, accompanied by cortical irregularities, peritendinous fluid, and calcifications (Fig. 1). These cortical irregularities and calcifications are often asymptomatic in athletes; they are sequelae of enthesopathy or due to incomplete fusion of the secondary ossification centers (up to age 26) (Pesquer et al. 2015). It is often difficult to determine if the enthesopathy is recent or not; color Doppler can demonstrate hyperemia, but is often not observed.

In case of a tear, disruption of the tendon fibers and intratendinous fluid clefts are observed on longitudinal images. In acute rupture of the adductor longus, the muscle is significantly retracted (more than 2 cm from its bony attachment) and hyperemia is observed. The extent of the rupture depends on its spread posteriorly towards the muscular attachment; the rupture is

therefore greater if the muscular insertion is affected (Pesquer et al. 2015).

MR imaging provides a more detailed overview. Key imaging findings are:

- *Adductor origin tendinopathy at the aponeurosis (± partial or complete tear):* Adductor tendinopathy results in high signal intensity on T1- and T2-weighted MR images; the high signal commences peripherally and then spreads to the central tendon without apparent fluid. Acute injuries can be categorized as minor strains/contusions (grade 1) demonstrating edema while maintaining their feathered structure. Partial tears (managed nonoperatively) demonstrate an intramuscular and epifascial hematoma formation with disruption of the muscle fibers (grade 2). Complete tears or avulsions (sometimes in necessity of operative repair) are characterized by discontinuity of the entire cross section, and retraction is possible (grade 3).
- *Pubic bone marrow edema (BME)*: BME of the anteroinferior part of the pubic bone adjacent to the adductor attachment can be the only sign of aponeurosis involvement in early stage (Fig. 2). However, BME has a high prevalence in asymptomatic elite athletes and it has been demonstrated that the presence of pubic BME and adjacent rectus-adductor aponeurosis capsular edema does not differ substantially between players with and without history of previous injury (Madani and Robinson 2019).
- *Bony remodeling of the pubic symphysis*.
- *Secondary cleft sign*: This reflects unilateral extension of the lesion on the rectus-adductor

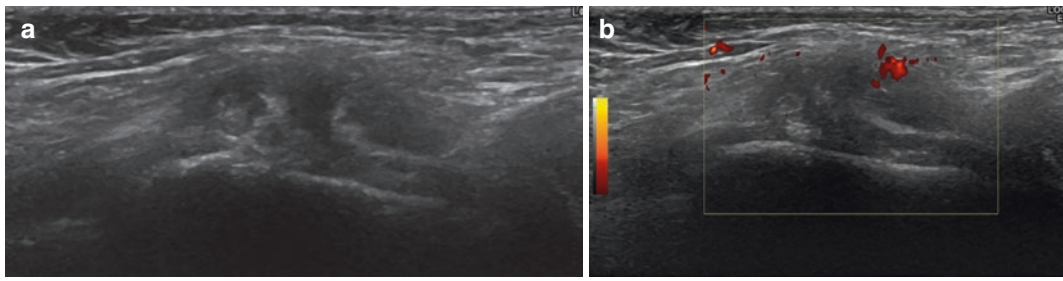

Fig. 1 Adductor tendinopathy. (**a**) Ultrasound image demonstrating a hypoechogenic thickened insertion of the adductor longus tendon with calcifications. (**b**) Increased vascularity on power Doppler indicating an active enthesopathy

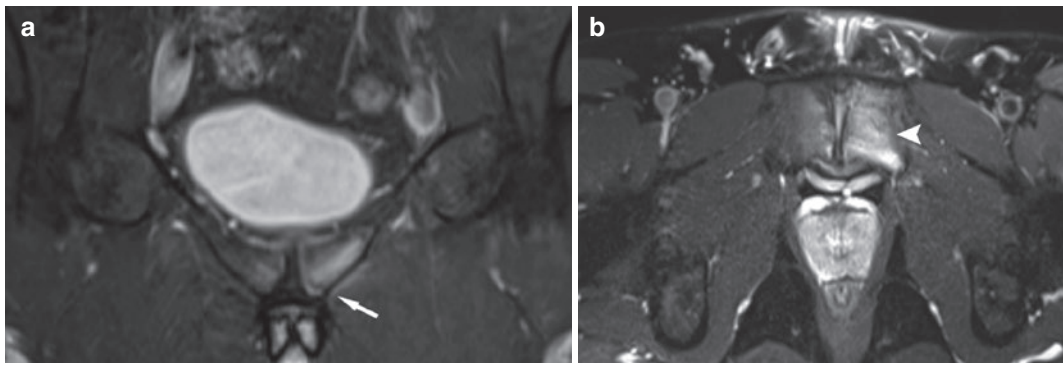

Fig. 2 Adductor tendinopathy. (**a**) Coronal and (**b**) axial fat-saturated (FS) PD-weighted image (WI) showing secondary cleft sign (arrow) and adjacent para-articular BME (arrowhead) in the left pubic bone. Note also subtle BME at the right pubic bone

aponeurosis towards the capsule in depth, inferiorly towards the adductors and in continuity with the central physiological cleft (Pesquer et al. 2015). The central physiological cleft presents as a vertical linear hyperintense signal on fluid-sensitive MR images. The secondary cleft presents as linear oblique high signal on water-weighted images that extends inferolaterally from the central symphysial cleft, most easily detected in the coronal plane (Fig. 2). Grading can be done in terms of edema intensity (mild to severe) and distribution (superior, anterior, inferior to the level of the pubic body).

2.2 Iliopsoas-Related Groin Pain

Iliopsoas-related groin pain is uncommon, has an insidious onset, and is caused by raising the hip from a squatting or seating position. In acute iliopsoas bursitis, MR imaging will show a fluid-filled thin-walled iliopsoas bursa communicating with the hip joint and demonstrating homogeneous low signal intensity on T1-weighted images (WI) and high signal intensity on T2-WI (Fig. 3). In chronic bursitis, the bursal wall will be thickened and the content will be more complex and inhomogeneous. Ultrasound will demonstrate similar findings and is useful for guidance of therapeutic injection (Madani and Robinson 2019).

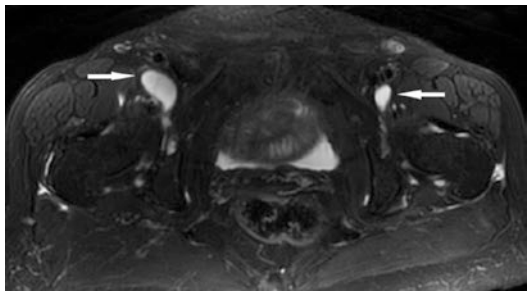

Fig. 3 Iliopsoas bursitis. Axial FS T2-WI demonstrating a bilateral fluid distension in the iliopsoas bursa (arrows)

2.3 Inguinal-Related

Inguinal-related groin pain is situated around the inguinal canal and is triggered by Valsalva or cough tests. Gilmore described the groin disruption syndrome which includes injury to the internal oblique aponeurosis, conjoined tendon-pubic tubercle attachment, and dehiscence between the conjoined tendon-inguinal ligament. These have all been grouped together as inguinal wall and superficial inguinal ring disorders. Posterior inguinal wall deficiency occurs as a result of injury to the transversalis fascia or conjoined tendon, which is formed by the medial portion of the internal oblique and transversus abdominis muscles (Caudill et al. 2008).

Imaging

To exclude a true inguinal or femoral hernia, ultrasound has a high sensitivity and specificity. In the athletic population—however—true groin herniations are rarely diagnosed (Madani and Robinson 2019). In soccer players, inguinal hernias are direct inguinal hernias, with a sac protruding medially to the epigastric arteries (Pesquer et al. 2016). In posterior wall deficiency, pain can be caused by irritation of the cutaneous branches of the ilioinguinal nerve within the inguinal canal (Tyler et al. 2010). Dynamic ultrasound imaging is obligatory; one has to look for excessive movement, laxity, or convex anterior bulging or ballooning of the inguinal canal at the superficial inguinal ring (Caudill et al. 2008). These findings are also nonspecific and also observed in asymptomatic athletes. In most cases, static MR imaging is disappointing in demonstrating pathology at the inguinal canal. Rarely in an acute setting edema can be observed at the inguinal ligament.

2.4 Pubic-Related

Pubic-related pain is suspected when athletes suffer from pain in the pubic area combined with local tenderness on palpation of the pubic symphysis, painful resisted bilateral hip adduction, and presence of para-articular pubic BME

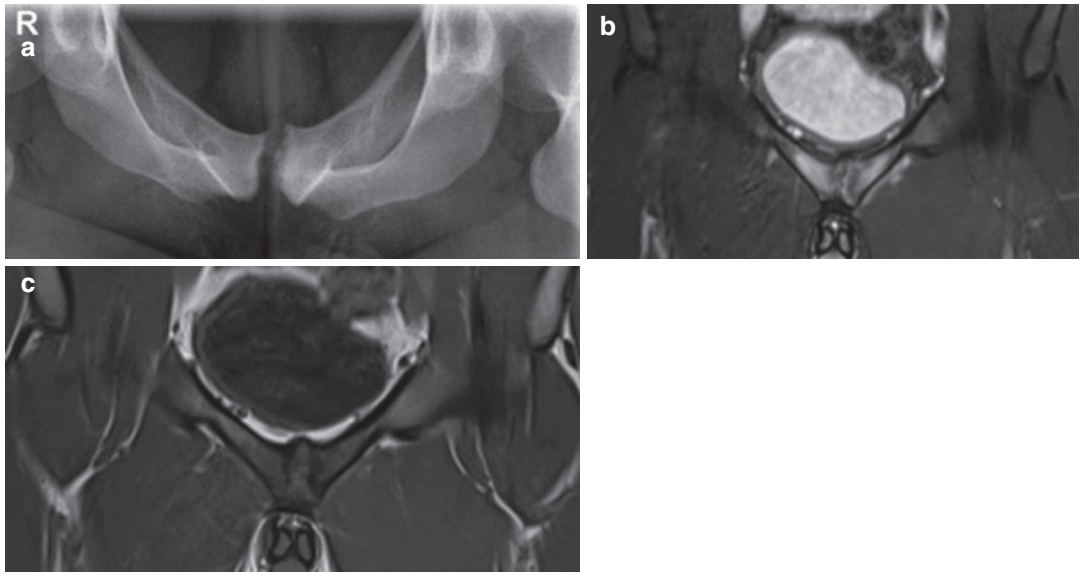

Fig. 4 Pubic-related groin pain. (**a**) Radiography demonstrating irregular sclerotic margins of the pubic symphysis. (**b**) Axial FS PD-WI demonstrates BME in pubic bones. (**c**) Coronal T1-WI demonstrating irregular margins and sclerosis

on MR imaging, remote from the adductor muscle attachment (Cunningham et al. 2007; Zoga et al. 2008; Branci et al. 2013). BME is a commonly observed finding in both symptomatic and asymptomatic elite athletes and it is thought to reflect a response to the chronic loading during training and matches (Madani and Robinson 2019).

Imaging

In the (sub)acute stage (pain <6 months) MRI demonstrates subchondral and periarticular BME away from the adductor attachment and fluid within the symphysis pubis joint (Fig. 4). The distribution of BME (diffuse in the body or focal anteromedial), the BME intensity (mild to severe), and if there are any adjacent soft-tissue changes all have to be reported. In the chronic stage, degenerative changes can be observed: joint surface erosions and irregularities, subchondral sclerosis and cyst formation, joint space widening or narrowing, central disc herniation, and bony proliferation at the superior margins of the joint (Branci et al. 2013).

3 Pelvis and Hip-Related Groin Pain

For a more detailed overview on pelvic and hip pathology we refer to Mascarenhas et al. (2020).

3.1 Femoroacetabular Impingement

Femoroacetabular impingement (FAI) results from an incongruence between the acetabulum and femoral head–neck junction, causing secondary impingement of the chondrolabral complex and progressive associated chondrolabral injury due to repetitive microtrauma (Di Pietto et al. 2018). Predisposing anatomic deformities can be distinguished at the acetabulum, i.e., the pincer-type morphology, at the proximal end of the femur, i.e., the cam-type morphology, or in both anatomical sites. Mixed-type FAI is more common in male (62%) than female (38%) athletes (Di Pietto et al. 2018). The participation in high-level soccer during skeletal immaturity itself is

not associated with a higher risk of development of cam deformity in the young adult years (Johnson et al. 2012).

In *cam-type* impingement, an osseous bump at the anterosuperior margin of the femoral head leads to a nonspherical bony extension of the femoral head and loss of normal concavity, called the "pistol-grip" deformity. This bony prominence abuts the acetabulum and injures the labral and acetabular cartilage during hip movement (Di Pietto et al. 2018). Males demonstrate a higher prevalence of cam deformity than do females (Johnson et al. 2012).

Pincer-type impingement occurs in the setting of overcoverage of the femoral head. This acetabular overcoverage may be due to either acetabular retroversion or increased acetabular depth, as in coxa profunda and protrusio acetabuli (Pfirrmann et al. 2006), and is more common in women.

While playing soccer, the underlying labrum and cartilage are continuously pinched between the acetabular rim and the femoral neck, resulting in a shallow cartilage defect adjacent to the acetabular labrum and subsequent labral tears (Di Pietto et al. 2018).

Imaging workup includes plain radiographs, computed tomography (CT), and MR imaging, all further discussed in Mascarenhas et al. (2020).

3.2 Labral Tears

Acetabular labral tears are often a source of pain in athletes, especially in soccer, tennis, and golf players (Di Pietto et al. 2018). Most labral tears are a combination of cam-type FAI combined with anterosuperior labral tears. Athletes who have FAI without pain can go through intermittent pain when a partial acetabular labral tear occurs due to repetitive stimuli, which also leads to a degenerative tear that causes constant pain. Labral tears can be undersurface (partial thickness), detached (full thickness), or complex. The diagnosis of labral tears should always be correlated with the clinical findings, as labral tears can also be identified in asymptomatic volunteers (Schmitz et al. 2012).

3.3 Stress Fractures

Stress fractures are less commonly observed as they represent 0.5% of all injuries in soccer players. The risk of a stress fracture increases after a long series of matches, and the femoral neck and pubic rami are the most vulnerable anatomic injury sites. A sudden change in a player's training regime is a risk factor for developing a stress fracture (Di Pietto et al. 2018). Medial femoral neck stress fractures are due to a repetitive compressive force and have a lower risk for complications and dislocation than lateral femoral neck stress fractures (Di Pietto et al. 2018).

In the early phase radiographs are often false negative; a few weeks after the onset of symptoms, a horizontal sclerotic band perpendicular to the osseous trabeculae or a periosteal reaction can be observed. Bone scan and MRI have a higher sensitivity in the early phase. The primary finding on MRI is BME centered around the stress fracture; typically a hypointense line on T1-WI, T2-WI, and intermediate-weighted images can be observed with surrounding BME. In the very early phase the fracture line may not be evident on MRI and the BME alone may appear to be a simple stress reaction. If—however—mechanical stress to the bone persists, the athletes will develop an evident stress fracture (Di Pietto et al. 2018).

3.4 Ischiofemoral Impingement

Ischiofemoral impingement refers to the impingement of soft tissues between the lesser trochanter and the ischial tuberosity, and the quadratus femoris muscle is primarily affected. The distance between these two osseous landmarks (= ischiofemoral space) is narrowed leading to edematous changes in the quadratus femoris muscle and less frequently the hamstring tendons. It can manifest as buttock pain, groin pain, or snapping of the hip.

A typical MR imaging finding is high signal intensity on T2-WI in the involved muscles with narrowing of the ischiofemoral space and

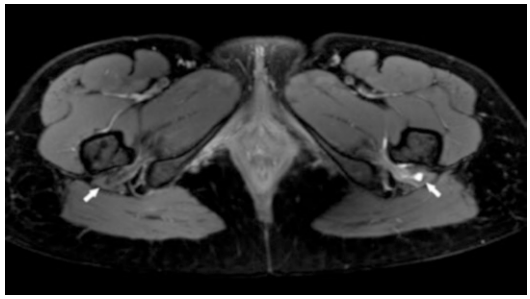

Fig. 5 Ischiofemoral impingement. Axial FS PD-WI demonstrates edema in the quadratus femoris muscle bilateral (arrows), more pronounced on the left side compared to right, with narrowing of the ischiofemoral space

eventually the development of atrophic muscle (Fig. 5). It has been reported—however—that athletes can present with a narrowed ischiofemoral space and edema in the quadratus femoris muscle bilaterally (up to 62.5%) while being asymptomatic (Papavasiliou et al. 2014). A threshold of 15 mm can be used to diagnose a narrowed ischiofemoral space with a 77% sensitivity and 88% specificity (Di Pietto et al. 2018).

3.5 Subspine Impingement

During hip movement there can be direct contact between the anterior inferior iliac spine (AIIS) and the femoral head–neck junction. This can be caused by defective healing of an avulsed AIIS fragment at a caudally dislocated position with secondary enlargement of the AIIS, but can also be caused by chronic overloading of traction forces on the rectus femoris tendon (Di Pietto et al. 2018). This phenomenon is called subspine or anterior inferior iliac spine impingement (Sutter and Pfirrmann 2013).

Athletes typically present with a limited range of motion during hip flexion and anterior hip pain aggravated by the movement. Radiography demonstrates the avulsed AIIS, calcifications within the direct or indirect tendon of the rectus femoris origin, or extension of the AIIS below the acetabular surface. MR imaging additionally may demonstrate soft-tissue abnormalities with tendon and muscle edema and peritendinous fluid (Sutter and Pfirrmann 2013).

3.6 Snapping Hip

Snapping hip, or coxa saltans, presents as an audible or palpable snap that occurs in or around the hip during movement. Prevalence is estimated to be 10% in the general population, but it has been especially described in soccer players, resulting from repetitive overuse movements performed by soccer players during their training and matches (Lee et al. 2013). Snapping hip may be divided into two distinct categories: *extra-articular and intra-articular*, with extra-articular snapping accounting for most of the patients presenting with this symptom. *Extra-articular snapping* hip can be further divided into *external* and *internal* causes. The *external form* is the most common cause and is associated with snapping of the iliotibial band or the gluteus maximus over the greater trochanter, typically during return to full extension of the hip.

The most common *internal cause* is the abnormal snapping of the iliopsoas tendon over the iliopectineal eminence. The snapping occurs while the leg returns to neutral position after an abduction, flexion, and external rotation movement, like while climbing stairs, getting out of a car, or standing from a chair.

Intra-articular snapping hip is caused by the presence of intra-articular bodies, fracture fragments, synovial folds, and labral tears with paralabral cysts.

Imaging

In patients with extra-articular snapping hip, radiography is often normal, but sometimes an underlying coxa vara or hip dysplasia can be detecting and contributes to snapping hip.

Ultrasound is of significant diagnostic value and can detect bursitis, tendinitis, and synovitis. With dynamic ultrasound, abrupt movement of the involved tendon can be observed. In external snapping hip, either a thickened posterior iliotibial band or an anterior gluteus maximus muscle

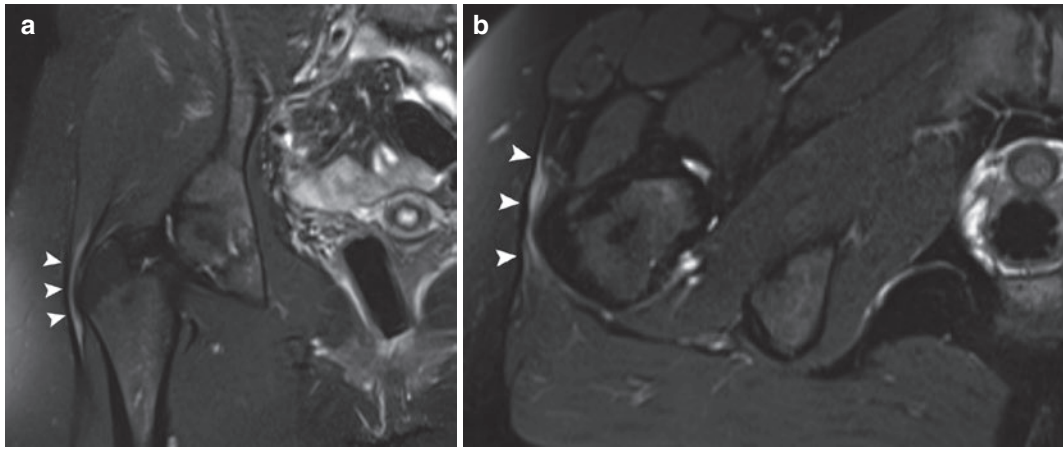

Fig. 6 External hip impingement. (**a**) Coronal and (**b**) axial FS PD-WI image demonstrates fluid between the iliotibial tract and the greater trochanter (arrowheads) in a 26-year patient with lateral hip pain and snapping during movement

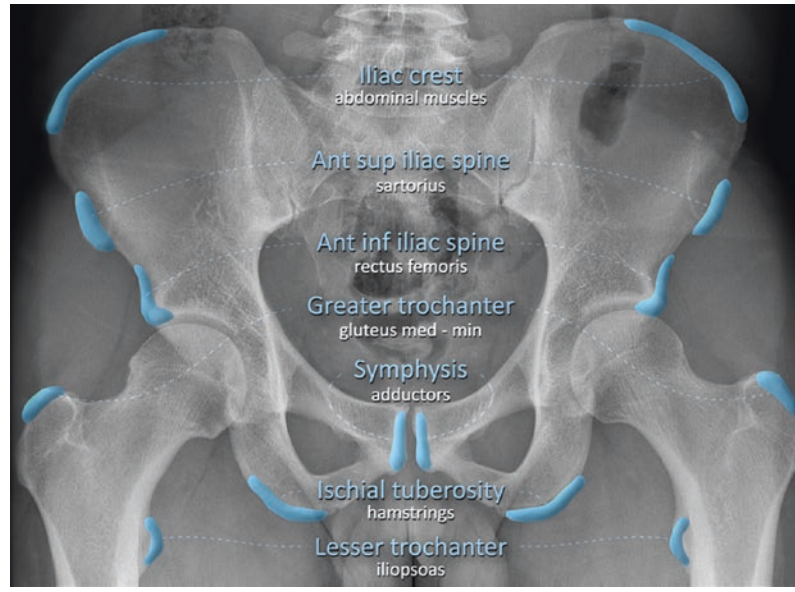

Fig. 7 Illustration of the locations of the apophyses of the pelvis indicated in blue

can be seen abruptly moving anteriorly over the greater trochanter during hip movement from extension to flexion or vice versa.

In internal snapping, snapping of the iliopsoas tendon over the iliopectineal eminence may be observed during the provocative maneuver of hip flexion-abduction-external rotation (Lee et al. 2013).

MR imaging may demonstrate associated soft-tissue changes in the involved tendon or bursae (Fig. 6).

3.7 Apophysitis or Avulsion Fractures

3.7.1 Acute Avulsion Injuries

Avulsion fractures of the apophyses and spines of the pelvis are almost exclusively seen in adolescent athletes involved in high-level sport activities; they result from a sudden forceful eccentric contraction of the attached musculotendinous unit, and the cartilaginous growth plate is the most commonly involved structure (Figs. 7 and 8).

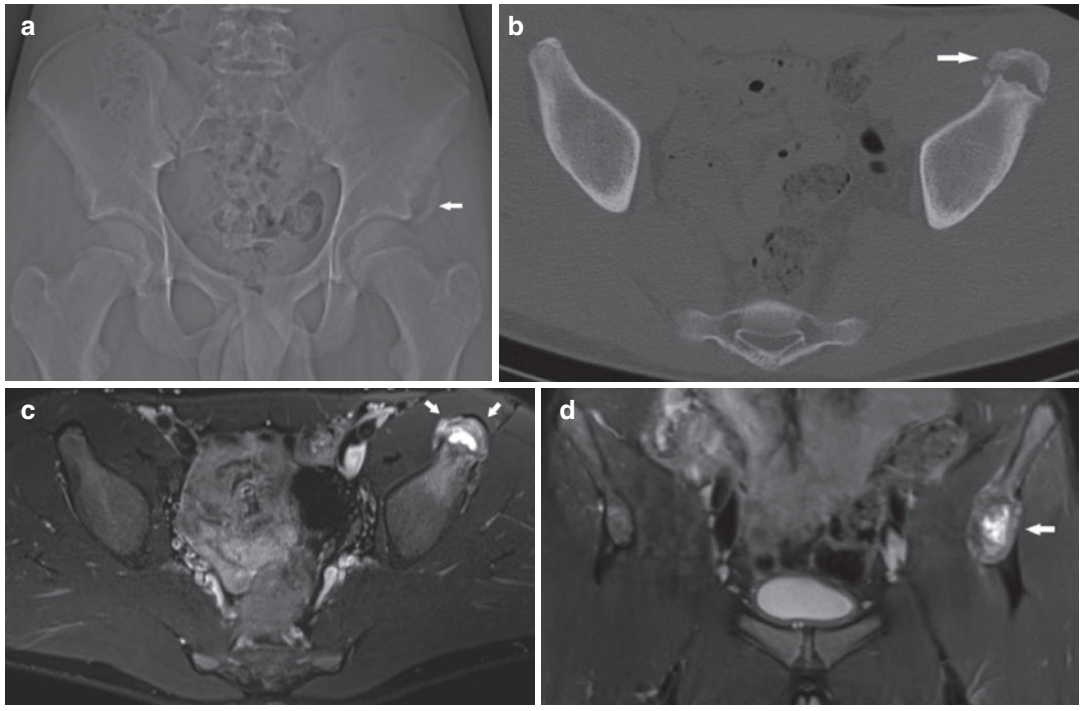

Fig. 8 Avulsion apophysis AIIS. (**a**) CT scout view demonstrating avulsion of the left AIIS (arrow). (**b**) CT image demonstrating immature callus (arrow) of the avulsed AIIS, suggesting the subacute character of the avulsion. (**c**) Axial and coronal (**d**) FS PD-WI demonstrating fluid in the cleft between the iliac bone and the avulsed apophysis of the AIIS (arrow) and surrounding BME

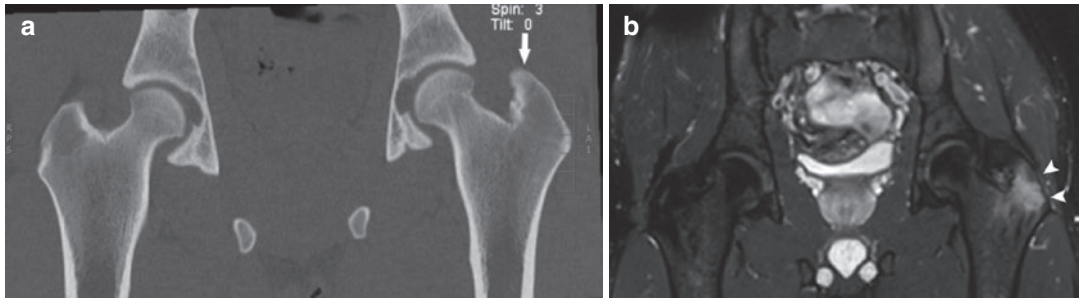

Fig. 9 Small avulsion fracture of the greater trochanter in an elite soccer player. (**a**) Coronal CT image demonstrating cortical irregularity of the medial side of the greater trochanter (arrow). (**b**) Coronal FS PD-WI demonstrating accompanying BME at the greater trochanter (arrowheads)

Separation and retraction of the partially ossified apophysis can occur.

Injuries to the anterior superior and anterior inferior iliac spine in soccer generally result from an excessive upward movement of the leg in "kicking the air" or a powerful shot at goal with maximum flexion of the hip and extension of the knee (Rossi and Dragoni 2001). Avulsion of the iliac spine apophysis is quite commonly observed in adolescent soccer players, but very rare in skeletally mature players (Figs. 9 and 10). It can occur in goalkeepers, involving the transition zone at the interface of the straight and reflected tendons of the rectus femoris. These tendons

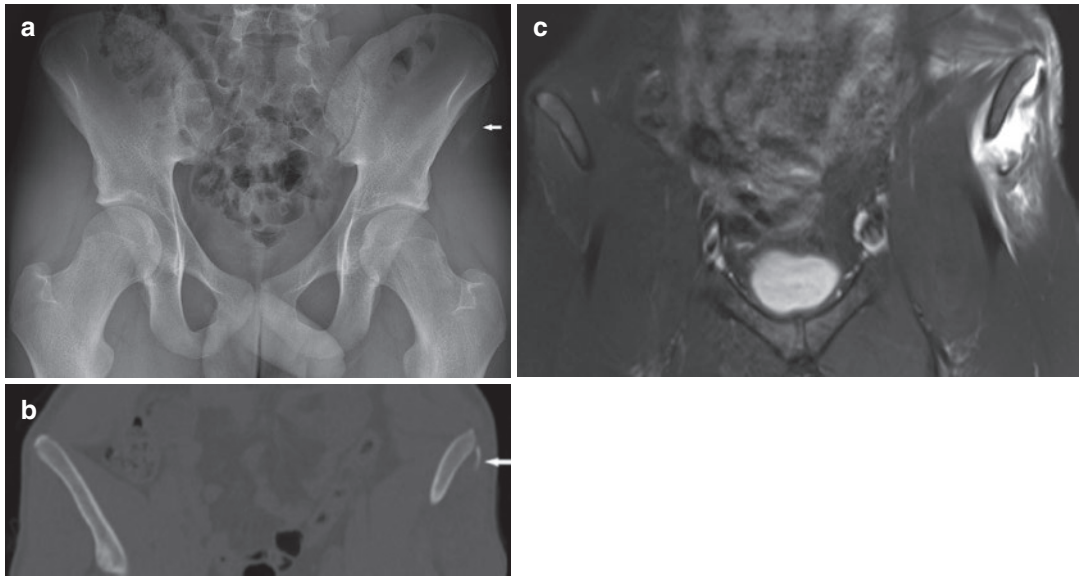

Fig. 10 Avulsion apophysis ASIS. (**a**) Radiograph and (**b**) coronal CT image demonstrating osseous avulsion of the apophysis of the left ASIS (arrow). (**c**) Coronal FS PD-WI demonstrating the avulsed ASIS apophysis with accompanying periapophyseal fluid and extensive edema in the sartorius muscle

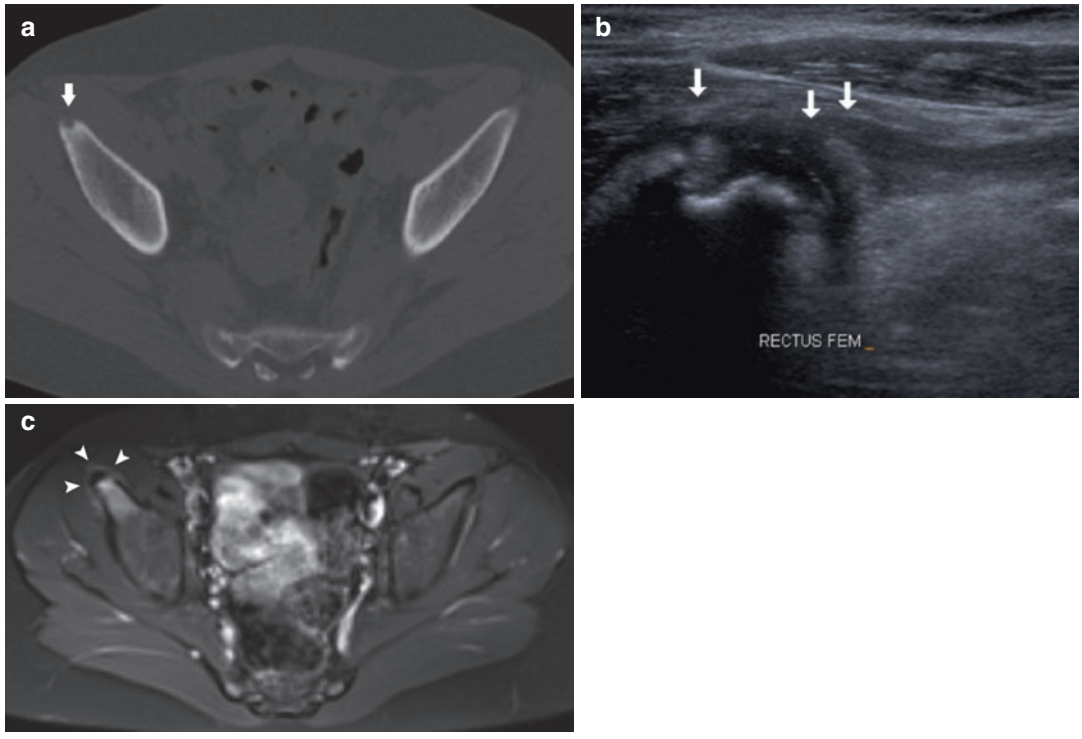

Fig. 11 Traction apophysitis AIIS. (**a**) Axial CT image demonstrating blurring and cortical irregularity of the apophysis of the AIIS (arrow). (**b**) Focal thickening and heterogeneous echogenicity of the right rectus femoris tendon (arrow). Note widening and irregular delineation of the growth plate adjacent to the apophysis of the AIIS. (**c**) Axial FS PD-WI demonstrating BME of the AIIS and subtle periosseous fluid (arrowheads)

arise from the inferior iliac spine (straight) and acetabulum (reflected), but their footprints overlap by about 10%. When taking a goal kick, the goalkeeper strikes the dead ball from the goal area into the opposition half, thereby hyperextending the kicking leg at the hip and flexing at the knee and resulting in severe eccentric tension on both the straight and reflected tendon components of the rectus femoris and making them susceptible to injury (Robinson and White 2005).

3.7.2 Chronic Traction Injuries/ Apophysitis

During long-standing and intensive sport training, chronic apophyseal injuries can occur with a spectrum ranging from apophysitis to avulsion fractures (Fig. 11). When severe, they can lead to growth disturbance.

Imaging

On radiographs apophysitis can be demonstrated in some patients by blurring and widening of the apophysis. When obtaining radiographs, comparison with the contralateral pelvis is mandatory. With chronic avulsions, the apophysis often looks larger than normal due to periosteal reaction and exuberant new bone formation associated with healing of such an injury; this may create an appearance that can be confused with a malignant neoplasm. Computed tomography may be helpful to ensure the correct diagnosis in such cases. MR imaging demonstrates edema of the apophysis and surrounding soft-tissue structures (Paterson 2009).

4 Knee Injuries

Knee injuries are common in soccer players (both male and female); although they are not as common as thigh strains or ankle sprains in higher level players, they can have a more deleterious effect on return to play and post-injury level of play, and can put the athletes at risk for accelerated knee osteoarthritis.

In amateur soccer players knee ligament sprains are the most commonly observed injury.

The knee joint undergoes stress from sprinting, jumping, cutting-in, and direct-impact forces, leading to internal derangement of the knee joint. During landing on one leg after jumping, translational forces are produced across the athlete's knee joint; if the soccer player then immediately pushes off in another direction, this requires a forceful contraction of the thigh muscles, resulting in further femur rotation and ligament stress. The hamstring muscles are particularly under stress trying to decrease anterior tibial translation. Injury or hamstring fatigue can make the knee joint more susceptible for a serious injury during landing, because then more force is transmitted directly through the ligaments instead of partly through the hamstring muscles (Robinson and White 2005).

4.1 Patellar Tendinopathy/ Jumper's Knee

Jumper's knee or patellar tendinopathy refers to a spectrum of disorders located at the proximal insertion site of the patellar tendon and is associated with anterior knee pain. It is recognized in skeletally mature soccer players and considered to be the adult form of Sinding-Larsen-Johansson disease. Repetitive traction and overload of the knee extensor mechanism during jumping and landing lead to a high mechanical load transfer to the proximal enthesis of the patellar tendon. The inflammatory changes occur in the patellar tendon close to its insertion onto the patellar apex, especially in the posterior fibers, and can progress to mucoid degeneration of the tendon, fibrosis, neovascularization, and eventually partial- or full-thickness tears and even avulsion of the patellar apex.

Ultrasound demonstrates tendon thickening and heterogeneously hypoechogenic signal of the tendon fibers with disruption of the normal fibrillar pattern (Fig. 12). Doppler may demonstrate increased vascularity, and the adjacent Hoffa's fat pad may demonstrate hyperechoic signal with increased vascularity. Peritendinous fluid can be observed. In case of a tear, a fluid-containing cleft can be observed within the tendon fibers.

On *MR imaging* focal tendon thickening and increase in proximal patellar tendon signal on both T1- and T2-WI can be observed (Fig. 13) (Paterson 2009). Edema may be observed in the patellar bone apex and the adjacent Hoffa's fat pad, with irregular hyperintense signal on T2-WI replacing the normal fat signal (Yu et al. 1995).

Sinding-Larsen-Johansson disease is the analogue of jumper's knee in skeletally immature athletes and often referred to as traction apophysitis, because there is still unossified cartilage at the patellar margin in some children. Similar imaging findings to jumper's knee can be observed. *Radiography* shows thickening of the proximal patellar tendon and osseous fragments in the proximal ligament, due to avulsed patellar margins (cortex or cartilage that ossifies) or dystrophic osseous fragments due to long-standing overuse (Fig. 14).*MRI findings* are similar to those of jumper's knee. The degree of swelling is often greater than that of jumper's knee and intratendinous bone fragments may be present. It is supposed to be a self-limiting condition, resolving within 1–1.5 year, but many patients remain symptomatic into adulthood and continue to demonstrate radiologic abnormal findings (Davis 2012).

Fig. 12 Jumper's knee. Ultrasound image demonstrating hypoechogenic thickening of the proximal patellar tendon with intratendinous calcification

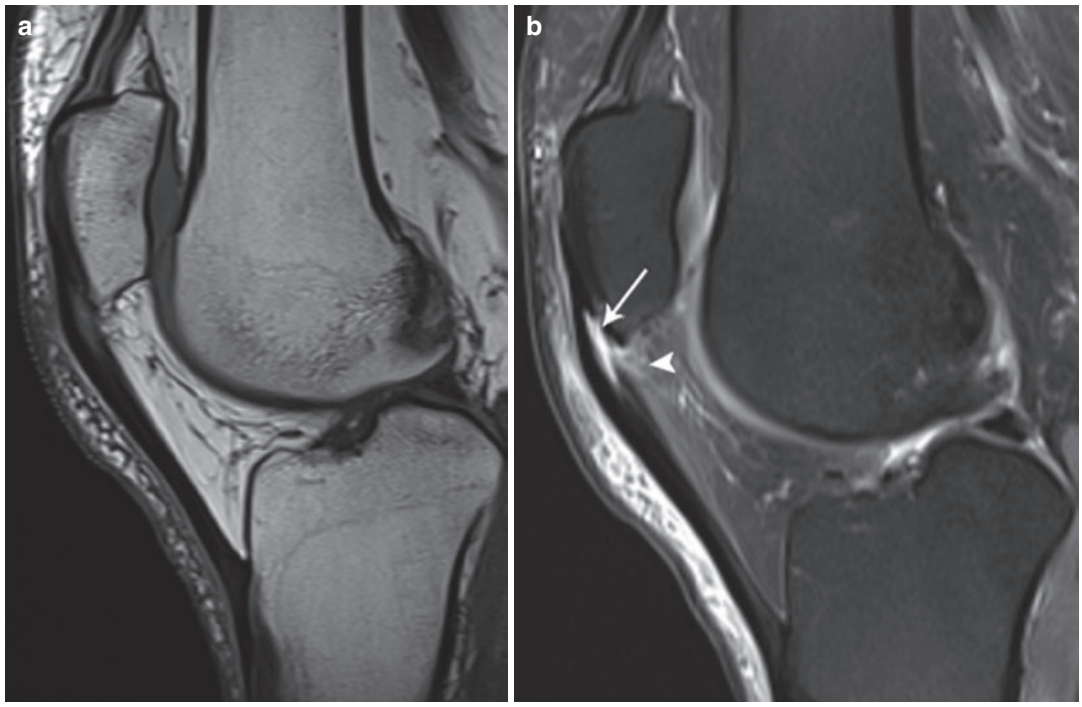

Fig. 13 Proximal patellar tendon tendinopathy. (**a**) Sagittal T1-WI demonstrating thickening of the proximal patellar tendon with central hypointense signal reflecting tendinosis. (**b**) Sagittal FS PD-WI demonstrates a fluid cleft within the tendon, in keeping with an intrasubstantial tear (arrow). Adjacent mild inflammation of the adjacent Hoffa's fat pad (arrowhead)

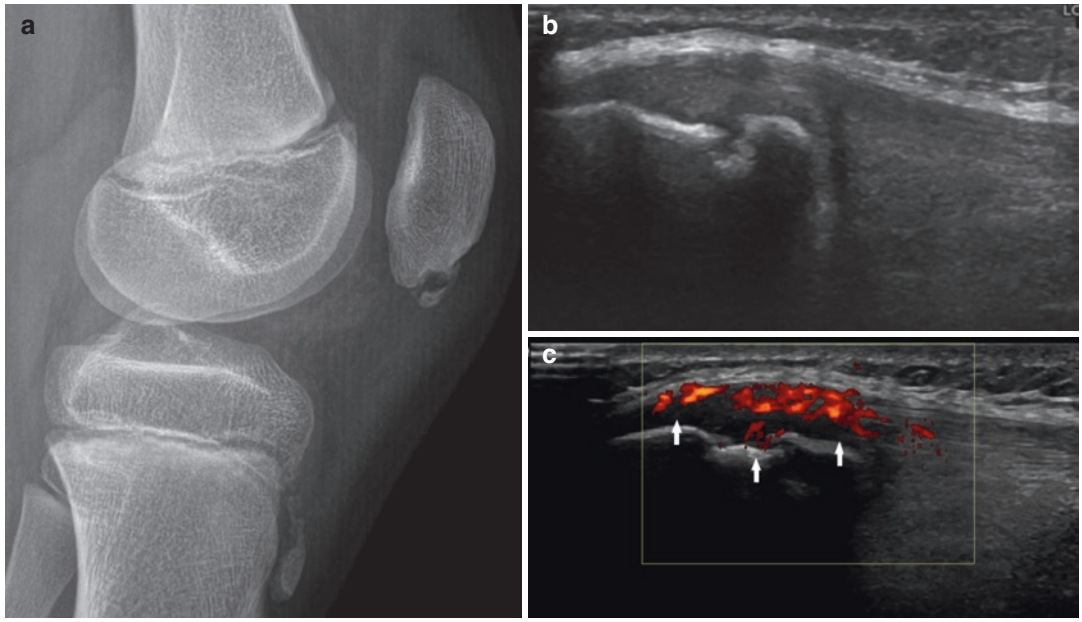

Fig. 14 Sinding-Larsen-Johansson disease in a 10-year-old soccer player. (**a**) Radiograph demonstrating fragmentation of the apophysis of the distal patellar pole. (**b**) Ultrasound of the same patient showing hypoechogenic swelling of the proximal patellar tendon with (**c**) increased vascularization of the tendon on power Doppler (arrows)

4.2 Osgood-Schlatter Disease

The disease of Osgood-Schlatter is an identical pathology affecting the distal part of the patellar tendon. It is more common than Sinding-Larsen-Johansson disease and produces similar radiological findings at the distal part of the patellar tendon and has a similar clinical course (Fig. 15). About half of the patients demonstrate intratendinous ossicles, but one has to be aware however that sometimes these osseous fragments can be present as a normal variant. Thus, one cannot diagnose Osgood-Schlatter disease solely on the basis of isolated bone fragments; swelling and clinical findings must also be present (Davis 2012).

4.3 Anterior Cruciate Ligament Tear

The anterior cruciate ligament (ACL) is one of the most commonly injured knee ligaments and the most commonly reconstructed knee ligament. It is the most common non-osseous injury among children who play soccer and more prevalent in girls and women (Faude et al. 2005; Paterson 2009; Brophy et al. 2010). This higher incidence could be due to a decreased intercondylar notch size, a decreased ACL size, differences in lower extremity alignment, a greater knee joint laxity, and the influence of female hormones (Faude et al. 2005; Paterson 2009).

Most ACL injuries are noncontact injuries that occur during landing after a jump or turning, just when the player is sharply decelerating. The knee is usually semi-flexed in combination with a rotational force applied to the lower leg. Often this knee twist occurs suddenly without the athlete having appropriate muscle strength to counteract this twisting. The injured player often fills a pop during the acute trauma, which is actually the bone bruise that happens when the tibia slips forwards and contacts the anterolateral part of the femoral condyle (Naraghi and White 2016).

Several noncontact mechanisms have been described in ACL injuries, with the pivot shift mechanism being one of the most common. The pivot shift injury is composed of a valgus force,

Fig. 15 Osgood-Schlatter disease. Radiograph demonstrating fragmentation of the tibial tuberosity apophysis and subtle adjacent soft-tissue swelling of the distal patellar tendon (arrowheads)

quadriceps loading, and a planted foot with relative internal rotation of the tibia in relation to the femur (Naraghi and White 2016). This produces the characteristic osseous contusions of the lateral femoral condyle, posterior aspect of the lateral tibial plateau, and less commonly medial sided contusions. A varus force combined with internal rotation of the tibia can also result in an ACL injury and has been implicated in the etiology of the Segond fracture, involving the lateral tibial rim. A minority of the ACL injuries are contact injuries, including a clip injury (valgus force applied to the partly flexed knee) or a hyperextension injury. Clip injuries are associated with medial collateral ligament **sprains** and medial meniscal tears (when all three combined it is called O'Donoghue's unhappy triad) and are often associated with lateral osseous contusion.

An ACL tear is associated with a longer return to play than any other typical soccer knee injury, averaging 194 days in the UEFA injury study (compared to an average of 52 days for posterior cruciate ligament injuries and 23 days for collateral ligament injuries) (Lundblad et al. 2013). They require surgical treatment more frequently, and despite early and expert management, ACL tears can be career-ending, more than any other soccer knee injury (Söderman et al. 2002; Paterson 2009).

Imaging

In the acute phase of an ACL injury, radiographs often only demonstrate joint capsule distension. One of the most common causes of acute hemarthrosis in athletes is an ACL injury. In pivot shift injuries a subtle deformity of the posterior rim of the lateral tibial plateau or a deep lateral femoral notch sign can be observed; this is a cortical depression on the lateral femoral condyle at the terminal sulcus (consisting of the junction between the weight-bearing tibial articular surface and the patellar articular surface of the femoral condyle). A Segond fracture can be diagnosed during a flexion–varus injury.

In youth soccer players, an avulsion fracture of the distal ACL footprint can sometimes be diagnosed on radiographs (Naraghi and White 2016).

MR imaging in complete ACL rupture demonstrates either focal discontinuity or diffuse swelling and increased signal intensity within the ACL (Naraghi and White 2016). Abnormal fiber orientation with posterior bowing or vertical oriented proximal fibers and horizontal oriented distal fibers can be observed. Ligamentous tears should be distinguished from avulsion fractures of the distal ligament insertion, because these avulsions require surgical repair (Naraghi and White 2016). Secondary MR imaging signs of ACL injury are anterior translation of the lateral tibial plateau in relation to the lateral femoral condyle, uncovering of the posterior horn of the lateral meniscus, and buckling of the PCL (Naraghi and White 2016).

In partial tears, the anteromedial bundle is most often torn. Increased intrasubstance signal, distortion, fiber attenuation, and abnormal fiber orientation are indicative of a partial tear, but MR imaging still has diminished accuracy in diagnos-

ing partial ACL tears (Van Dyck et al. 2012). 3T MR imaging however appears to have an increased sensitivity, specificity, and accuracy for diagnosing partial tears (Van Dyck et al. 2011). When bone contusions are diagnosed, this is associated with a higher grade partial tear.

For more extensive review of ACL injuries we refer to McNally and Thompson (2020).

4.4 Meniscus Injury

We refer to De Smet et al. (2020) for a more extensive review on meniscus injuries. Soccer players frequently sustain acute traumatic meniscal tears, isolated or associated with ligamentous or articular surface injuries. Axial loading combined with rotational forces results in shear stress on the meniscus, causing meniscal tears.

Approximately 87% of lateral meniscal injuries are due to sport activities, with the majority occurring in pivot-contact sports like soccer.

The MR imaging criteria for a meniscal tear, in the absence of previous surgery, are meniscal distortion or increased intrasubstance signal intensity unequivocally extending to and contacting the articular surface of the meniscus on at least two consecutive MR images (= the two-touch slice rule) (Huysse et al. 2008).

Meniscal tears can be classified based on morphological characteristics (tear length—depth—location) or tear pattern: vertical longitudinal, radial, horizontal, flap, or complex (116).

Horizontal tears are most often degenerative, occurring in older patients with mucoid meniscus degeneration and often associated with meniscal cysts (Huysse et al. 2008). A ***radial tear*** involves the free edge of the meniscus, runs perpendicular to the tibial plateau and long axis of the meniscus, and divides the meniscus into an anterior and posterior portion. A radial tear gives an interruption of the bow-tie configuration on a sagittal MR image, and blunting of the free apical margin on a coronal MR image (Rosas 2014). They can be associated with trauma.

Vertical longitudinal tears mostly affect younger patients after trauma and are highly associated with tears of the ACL (Huysse et al. 2008; Rosas 2014). They course parallel to the long axis of the meniscus and perpendicular to the tibial plateau (Fig. 16). When the tear has a length of 10 mm or more, it is considered unstable. Sagittal images are best suited to demonstrate these tears. Coronal imaging is used to assess extension into the meniscal body.

A ***parrot-beak*** or ***flap tear*** is a vertical free-edge tear, consisting of a central radial component and a longitudinal peripheral component. They are unstable, and preoperative identification is essential, because displaced fragments may be difficult to visualize arthroscopically. On at least one MR image the free edge is blunted and it has a flap, whereas on sequential images a vertically oriented longitudinal tear becomes visible (Huysse et al. 2008; Rosas 2014).

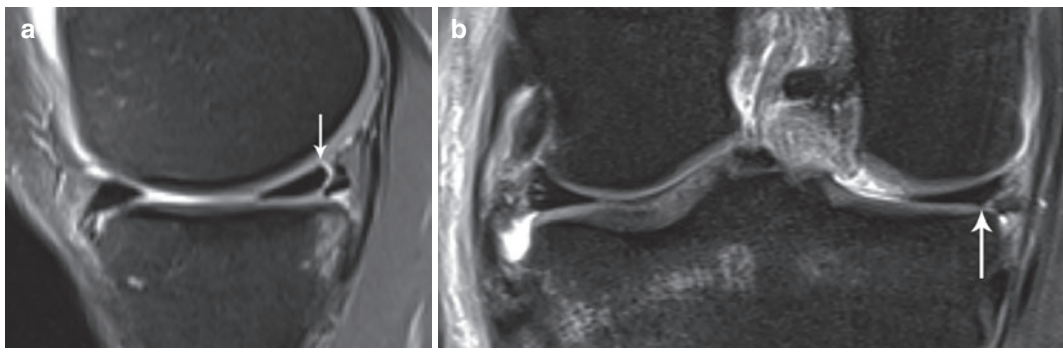

Fig. 16 Peripheral vertical longitudinal tear of the medial meniscus. (**a**) Sagittal and (**b**) coronal FS PD-WI demonstrating longitudinal fluid-containing cleft in the body and posterior horn of the medial meniscus in the peripheral red zone (arrows)

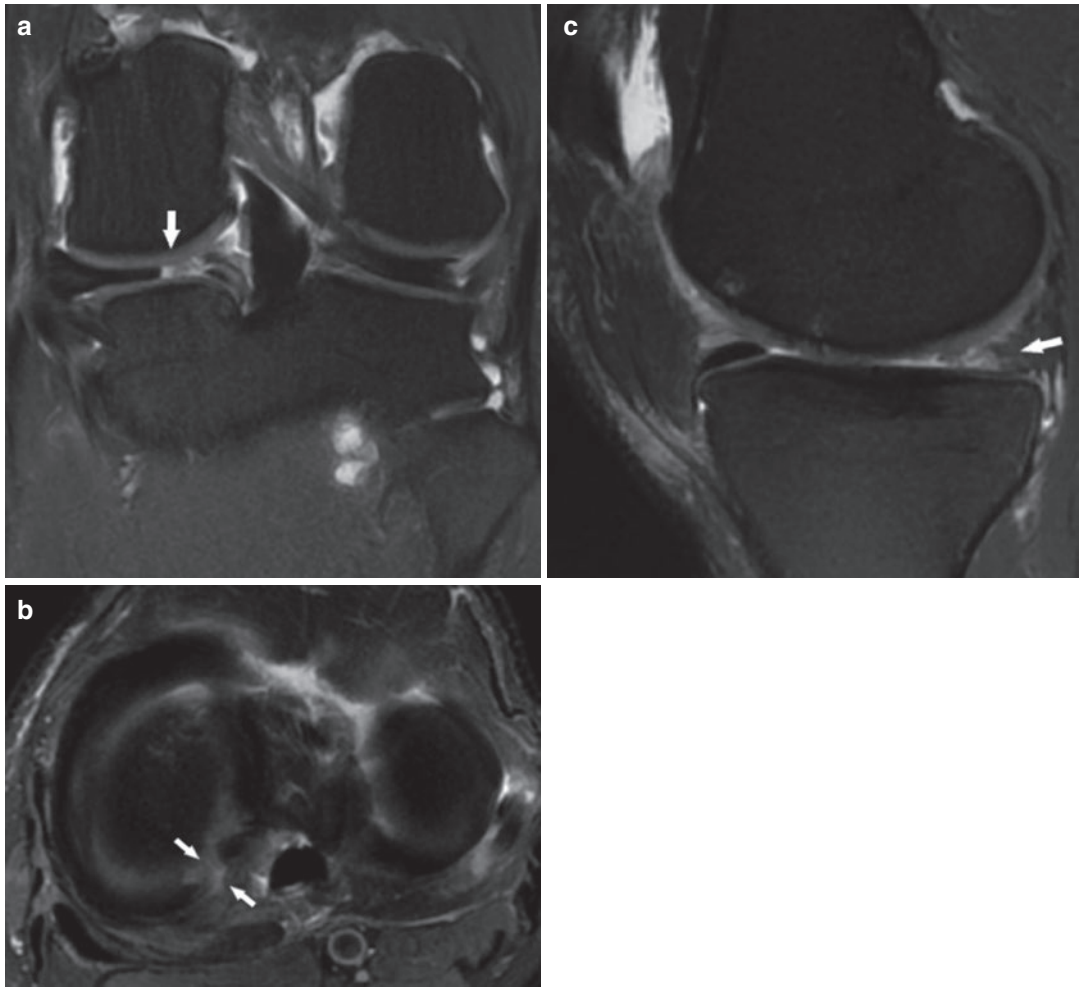

Fig. 17 Radial root tear of the posterior horn of the medial meniscus in the right knee. (**a**) Coronal and (**b**) axial FS PD-WI demonstrating a radial tear in the meniscal root (arrows). (**c**) Sagittal FS PD-WI with ghost meniscus (arrow) in keeping with a large root tear

A ***root tear*** represents a radial type of tear located up to 9 mm from the root attachment, and extends through the entire thickness of the meniscus (Fig. 17). It significantly alters the native biomechanics of the posterior meniscal root and results in alteration of the circumferential hoop stresses, causing meniscal extrusion, increased tibiofemoral contact forces, and accelerated degenerative changes in the knee (Bhatia et al. 2014).

Acute root injuries can be associated with ACL tears, hyperflexion injuries, and grade 3 medial collateral ligament tears with intact meniscocapsular attachment (Naraghi and White 2016). Underdiagnosis of root tears on both MR imaging and arthroscopy has led to increased attention in the surgical and radiological literature and to alterations in the imaging evaluation of this region. In patients younger than 30 years, particularly patients with concomitant ACL injuries, any abnormal signal within the posterior root of the lateral meniscus indicates a tear. The posterior roots should be scrutinized, especially in the setting of an ACL tear or meniscal extrusion (Rosas 2014). 3T MR imaging has a high negative predictive value to

detect posterior meniscal root tears; that is, the absence of posterior meniscal root pathology on 3T MRI is a good indicator of the absence of pathology on arthroscopy. The positive predictive value is low indicating that many root tears classified as torn or avulsed on 3T MRI were later determined to be intact on arthroscopic probing. Sensitivity was higher for medial **posterior** root tears, indicating a higher risk of missing lateral root tears on MRI (224).

On MR imaging, fluid can track through the root tear defect. Coronal and fluid-sensitive sequences result in better delineation of the roots and partially compensate for the magic-angle artifacts. On coronal images, the roots should be identified draping over the tibial plateau on at least a single image. On sagittal images, if the posterior root of the medial meniscus is not clearly visualized on the image immediately medial to the posterior cruciate ligament, one should suspect a tear. If recognized preoperatively, this situation can alter the surgical technique, because the posterior roots are not easily accessible at the time of arthroscopy and require placement of additional portals for adequate visualization and treatment. Root tears through the vascular posterior root can be surgically repaired, but radial tears through the posterior horn adjacent to the root may not be reparable (Naraghi and White 2016).

4.5 Medial Collateral Ligament

The medial collateral ligament (MCL) is the most frequently injured structure among all levels of players and all age groups (Fig. 18). The MCL is considered the weakest of the three main knee-stabilizing ligaments, apart from the injury mechanisms inherent to soccer that already place the MCL at risk. The UEFA injury study subgroup found that MCL injuries are the second most common severe injury after hamstring injuries (Lundblad et al. 2013). MCL injuries are sustained more frequently during matches than during training sessions (ratio of 9:1), with the dominant leg being afflicted in more than half of the MCL injuries. More than two-thirds of MCL injuries are a result of direct player contact. About half of the MCL injuries that are sustained during matches occur during the last 15 minutes of first or second half, attributed to the combination of player fatigue, situational urgency, and related increased match intensity.

Fig. 18 Sprain (grade 3) of the medial collateral ligament. Coronal FS PD-WI of the right knee demonstrating disruption of the distal fibers of the deep and superficial components of the MCL with hyperintense signal of the distal fibers and thickening of the MCL (arrowheads). Accompanying fluid superficial and deep of the MCL fibers

5 Ankle Injuries

5.1 Ligament Injuries

We refer to Van Royen et al. (2020) for a more extensive review on ankle ligament injuries.

Ankle inversion injuries frequently occur in soccer and lead to lateral capsular and ligament lesions. Muscle recruitment and scar tissue can luckily compensate for the loss in ligament function, even in complete ligament tears. Imaging is often only indicated when players experience instability or symptoms after treatment in the

acute phase, and also allows to diagnose concomitant injuries such as sinus tarsi syndrome or peroneal tendon or retinaculum injury, which may warrant surgical repair.

Injuries to the medial ligaments and syndesmosis are not so frequent as lateral ligament injuries (Robinson and White 2005).

MR imaging offers a more global assessment compared to ultrasound, including concomitant osteochondral and osseous injuries. Ultrasound is often sufficient because the referring clinician is confident of his/her clinical diagnosis.

Sometimes diagnostic problems can occur when imaging demonstrates an intact ligament (that can be thickened or attenuated) but the patients suffer from mechanical instability. The other way around, a torn ATFL and CFL does not necessarily imply mechanical instability, and complete tears can be an incidental finding in the athletic population. Only 10–15% of athletes suffer from impaired athletic function after an acute ligament injury.

5.2 Osteochondral Lesions

Osteochondral injuries arise from shearing and impaction forces on both talus and tibia, but are **more frequently** observed on the talar dome. Symptomatic lesions have a poor prognostic outcome for the athlete's recovery.

The Berndt and Harty classification (graded 1–4) is still the most widely accepted classification on radiographs and CT. The most accurate imaging assessment for osteochondral injuries and associated soft-tissue abnormalities is done with MR imaging (Fig. 19). High-resolution CT arthrography is now being evaluated for osteochondral injuries with some studies suggesting accuracy equivalent or even better than that of MR imaging (Schmid et al. 2003; Pirimoglu et al. 2019).

MR staging is nowadays usually done by the Anderson classification, which is a modification of the Berndt and Harty staging system (Anderson et al. 1989).

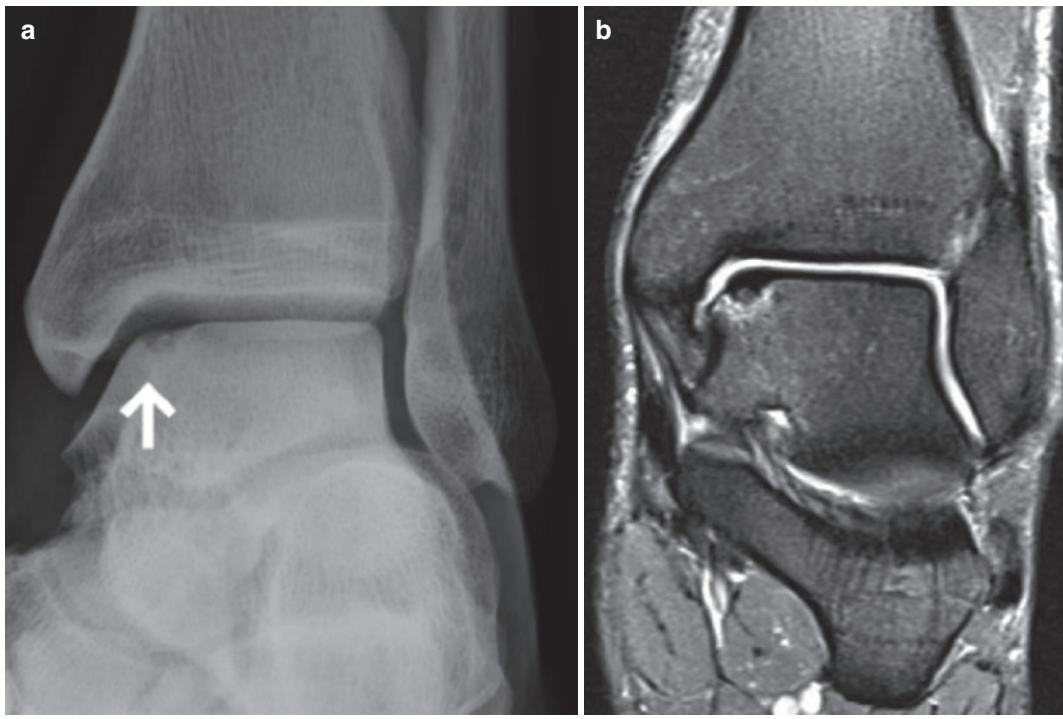

Fig. 19 Osteochondral lesion of the medial talar dome. (**a**) Radiography showing a translucent sharply demarcated subchondral lesion on the medial talar dome (arrow). (**b**) Coronal FS PD-WI demonstrating the subchondral bone sclerosis with surrounding BME; there is no subchondral cyst formation

- Grade 1: subchondral trabecular compression; plain radiograph normal but positive bone scan, BME on MRI
- Grade 2a: formation of subchondral cyst and surrounding BME
- Grade 2b: incomplete separation of fragment, surrounding BME
- Grade 3: completely detached, undisplaced fragment with presence of synovial fluid (around fragment and surrounding BME)
- Grade 4: displaced fragment with adjacent BME

It can sometimes be difficult to differentiate on T2-WI between high-signal BME at the fragment margin (grade 2b) and free fluid tracking along the osteochondral fracture line indicative of an undisplaced but potentially free fragment (grade 3). To demonstrate this difference, both CT and MR arthrography have improved accuracy compared with conventional MR imaging to demonstrate free flow of contrast and differentiate between grade 2 and grade 3 lesions.

Grade 1 and 2 lesions get conservative or functional treatment initially, and grade 3 and 4 lesions often necessitate surgery. Some authors also advocate functional treatment for medial talar grade 3 lesions. Surgical treatment consists of debridement of the injury and drilling of the defect to stimulate a healing response. Surgery can significantly decrease pain and functional impairment in chronic lesions. Surgical techniques are still developing and improving every day, and repair techniques now involve chondrocyte implantation and mosaicplasty. MR imaging has additional value for these surgical techniques by defining appropriate areas for cartilage harvesting within the ankle or knee (Robinson and White 2005).

5.3 Impingement Syndromes

Both osseous and soft-tissue ankle impingement syndromes are commonly observed in soccer players. All types of impingement can occur (anterolateral, anterior, posterior, and posteromedial).

Anterior impingement can often be diagnosed on radiographs, demonstrating the tibiotalar spurs that develop due to repeated direct microtrauma.

Anterolateral and posteromedial impingements originate from an initial inversion injury, which results in tensile stress to the anterolateral capsule and compression of the posteromedial capsule between the talus and medial malleolus. In soccer players, the posterior capsular structures are subject to constant stress from kicking and push-off maneuvers. This repeated microtrauma results in capsular hemorrhage and focal hypertrophy, on its turn resulting in painful limitation of movement (Robinson and White 2005).

In soccer players impingement often presents 2–4 weeks after an acute injury, with the area of impingement frequently being remote from the initial site of acute injury, for example posterior impingement arising after a lateral ankle sprain.

MR imaging can accurately assess the soft-tissue abnormalities but can also define significant concomitant injuries like osteochondral lesions that can influence therapy (Fig. 20).

Intravenous gadolinium-enhanced MR imaging can demonstrate pericapsular inflammation but can also have an indirect arthrographic effect from any preexisting effusion. Indirect MR arthrography demonstrates soft-tissue abnormalities with enhancement on fat-suppressed T1-WI and can resolve subtle changes related to capsular and synovial inflammation (Robinson and White 2005). Ultrasound combined with MR imaging may improve correlation of imaging findings with symptoms and aid management. Ultrasound can define capsular abnormalities with focal and nodular thickening of mixed echogenicity. Increased Doppler signal and intra-articular fluid are not always present, but dynamic maneuvers may reproduce deformity and impingement of the thickened tissues. Ultrasound-guided injection of a steroid (triamcinolone) and bupivacaine into the abnormal capsular tissues can be performed, often allowing players to return to full training within 2–3 weeks without surgical intervention (Robinson and White 2005).

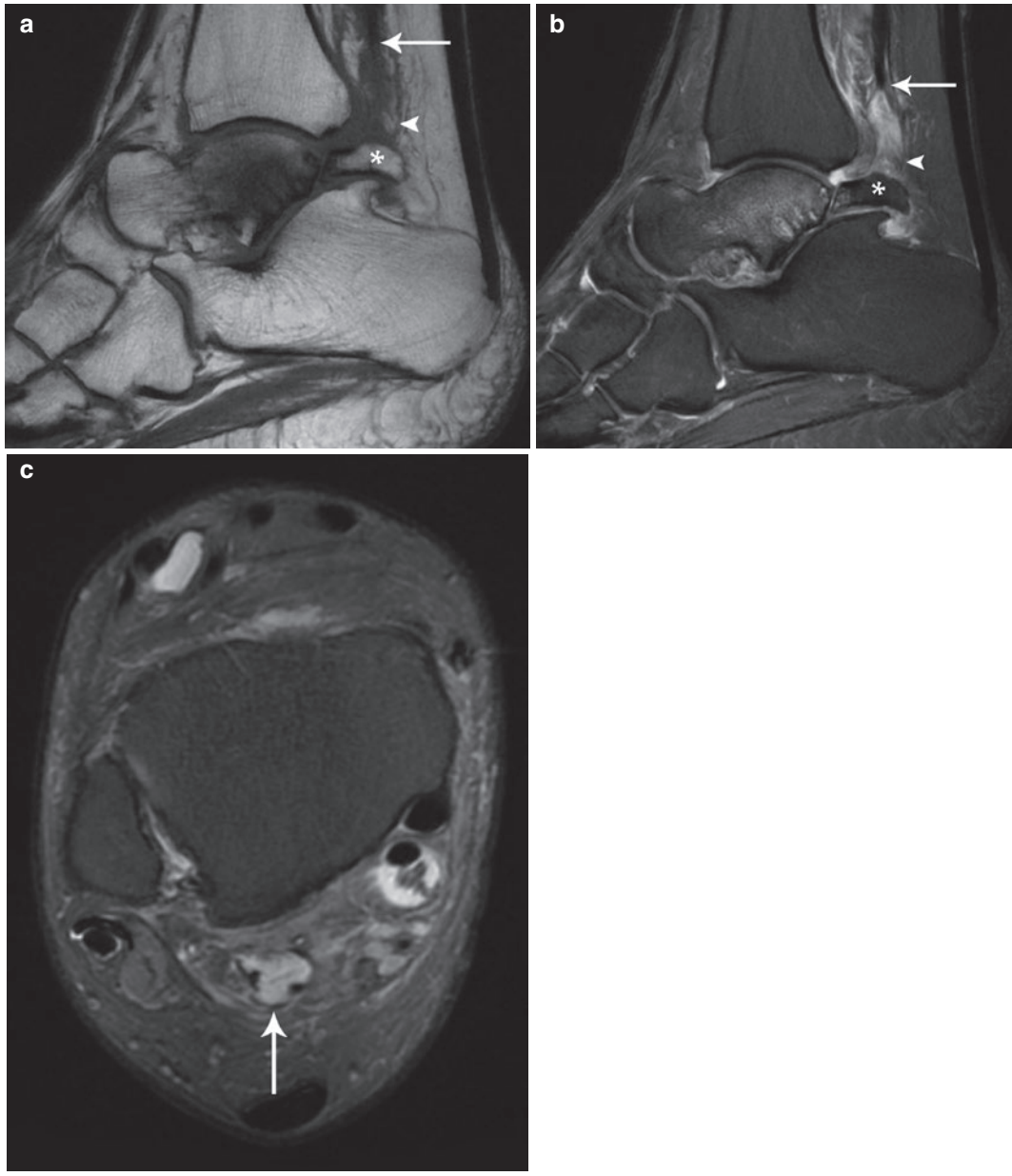

Fig. 20 Posterior ankle impingement. (**a**) Sagittal T1-WI and (**b**) FS PD-WI demonstrating a large os trigonum with BME in the os trigonum (asterisk), in the synchondrosis, and in the lateral tubercle of the posterior talar process. Chronic stress reaction with full-thickness cartilage defects and subchondral geodes in the posterior subtalar facet. Posterior capsular thickening and fluid in the posterior recess (arrowheads). Complete rupture of the flexor hallucis longus tendon (arrow) with absence of the tendon in the synovial sheath. (**c**) Axial FS PD-WI demonstrating a complete rupture of the flexor hallucis longus tendon (arrow) with absence of the tendon in the synovial sheath

5.4 Calcaneal Apophysitis

Calcaneal apophysitis or Sever's disease is a painful inflammation of the calcaneal apophysis. As the calcaneal apophysis fuses to the main calcaneal body between 12 and 15 years, Sever's disease cannot occur in youth soccer players beyond this age range. They present with intermittent or

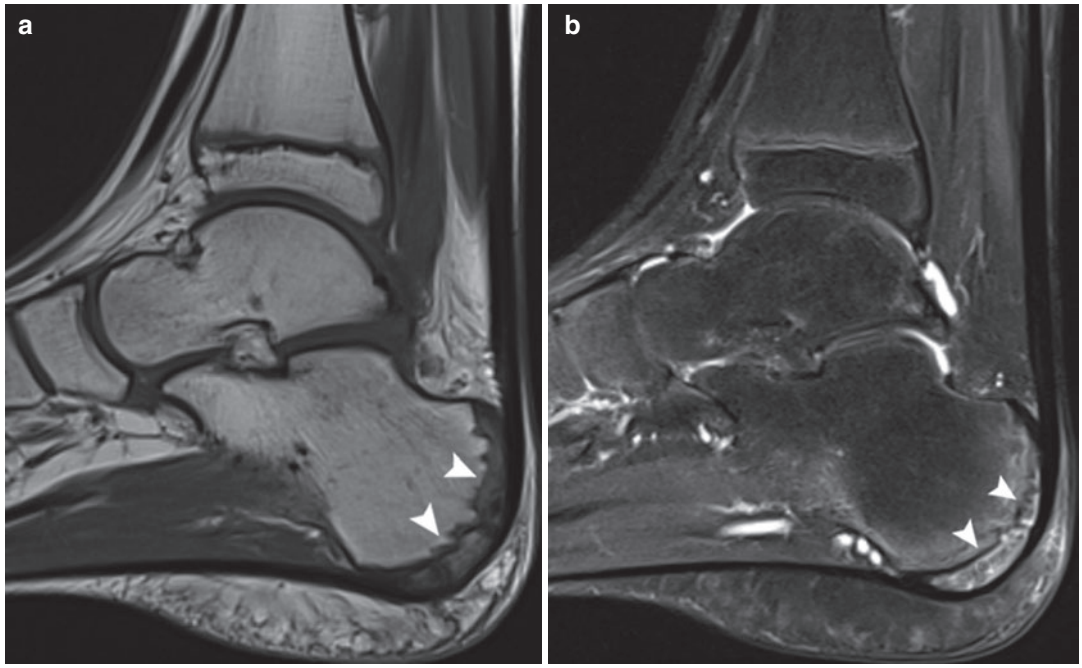

Fig. 21 Sever apophysitis. (**a**) Sagittal T1-WI and (**b**) sagittal FS PD-WI demonstrating BME within the calcaneal apophysis (arrowheads), extending into the adjacent calcaneal tuberosity

continuous posterior heel pain, aggravated by physical activity. They have a positive Achilles squeeze test on physical examination.

It is thought to occur because of reduced flexibility of the Achilles, and posterior tibial and peroneal tendons, possibly associated with tightening of the plantar fascia. Limited ankle flexibility can then place abnormal stress on the calcaneal apophysis during repetitive heel loading as occurs during running. The diagnosis is a clinical one, though a calcaneal radiograph is occasionally beneficial to exclude other causes of heel pain. MR imaging is not indicated, but may show BME within the calcaneal apophysis that can extend into the adjacent calcaneal tuberosity (Fig. 21). The treatment is symptomatic (Paterson 2009).

5.5 Achilles Tendinopathy and Rupture

The Achilles tendon is subject to tendinopathy and tears in soccer athletes. Tendon fibers are not organized in a linear way, but all three tendon components (two heads of gastrocnemius and soleus) rotate medially so that the soleus component moves from deep to medial. The hypothesis is that during soccer, the repetitive twisting and untwisting of the tendon lead to stress concentration in the area of maximal rotation, being 4–6 cm proximal to the calcaneus. This area is also the relatively most avascular region of the Achilles tendon, also predisposing the tendon to injury at this location. Soccer players often also present with heel valgus, increasing the stress on the medial aspect of the tendon. These biomechanical factors combined lead to paratenonitis and tendinopathy usually first being observed at the medial aspect of the tendon. This area is also a relative avascular area as mentioned before, further limiting the ability to repair this mechanically induced damage.

Due to improved insight in the biomechanics of the Achilles tendon, injuries have decreased in recent years because modifications have been made to the training schedule in the preseason

training. Still chronic overuse tendon injuries remain common (Robinson and White 2005).

Ultrasound shows fusiform thickening of the tendon in the affected region, with loss of the normal concave aspect and now convex bulging of the tendon. Hypoechoic regions presenting mucoid degeneration can be present within the tendon, distorting the normal fibrillar texture. Doppler ultrasound may demonstrate neovascularization, which is a negative prognostic sign and associated with a poorer clinical outcome. Adjacent inflammation of the Kager's fat pad may present as hyperechoic signal within the fat pad. The adjacent paratenon can appear thickened and hypoechoic. Partial tears present fluid-containing clefts within the tendon fibers. MR imaging depicts these changes even better, and can diagnose subtle intrasubstantial tears.

5.6 Turf Toe

Turf toe is an acute dorsiflexion injury of the first metatarsophalangeal (MTP) joint and its associated capsular complex, and is common among American football and soccer players. It is a capsular sprain of the first MTP joint due to hyperextension of the first MTP complex.

It results from axial loading forces being applied to the forefoot while the first MTP joint in the tiptoe (equinovarus) position. Injuries can range from low-grade capsular sprains to high-grade capsular and ligamentous tears (Schein et al. 2015).

Plantar plate injuries can accurately be identified with MR imaging. A normal plantar plate is a dense low-signal-intensity band that connects the hallux sesamoids to the plantar base of the proximal phalanx. It is best seen on sagittal and short-axis images. Imaging findings depend on the severity and acuity of the injury. Sprains and partial-thickness tears can both demonstrate thinning or thickening of an ill-defined plantar plate.

Full-thickness tears demonstrate a focal disruption of the fibers of the plantar plate with retraction and a fluid gap (Fig. 22). A caveat is a plantar plate recess, a normal variant at the proximal phalangeal attachment, which can be mistaken for a partial tear (Schein et al. 2015; Nery et al. 2017).

Proximal retraction of the sesamoids is expected in cases of complete plantar plate tear and may be detected with lateral radiographs with the great toe stressed in dorsiflexion (Nery et al. 2017). Acute injuries will usually demonstrate associated soft-tissue edema, while chronic injuries usually lack edema.

Heterotopic ossification along the plantar plate suggests chronic injury. Chronic injury may also result in the development of an osteophyte at the dorsum of the first metatarsal head, which can cause hallux rigidus. It is important to evaluate the chondral surfaces of the first MTP joint complex to assess for the presence of a chondral injury, which may affect management (Schein et al. 2015).

6 Muscle Injuries

Professional soccer players frequently miss training or matches each season due to muscle injuries. The most injured muscles in elite soccer players are muscles of thigh (hamstrings and quadriceps) and calf (gastrocnemius-soleus complex), accounting for more than one-third of all injuries, with the hamstrings most commonly affected (Robinson and White 2005). Most elite soccer players are skeletally mature and have no previous tendon degeneration; excessive tensile forces then lead to failure at the myotendinous junction. Adolescents on the contrary fail at the apophysis and in more mature players with tendinosis, the diseased tendon fails before the myotendinous junction.

Older players, players with previous hamstring injuries, high-level players, and athletic

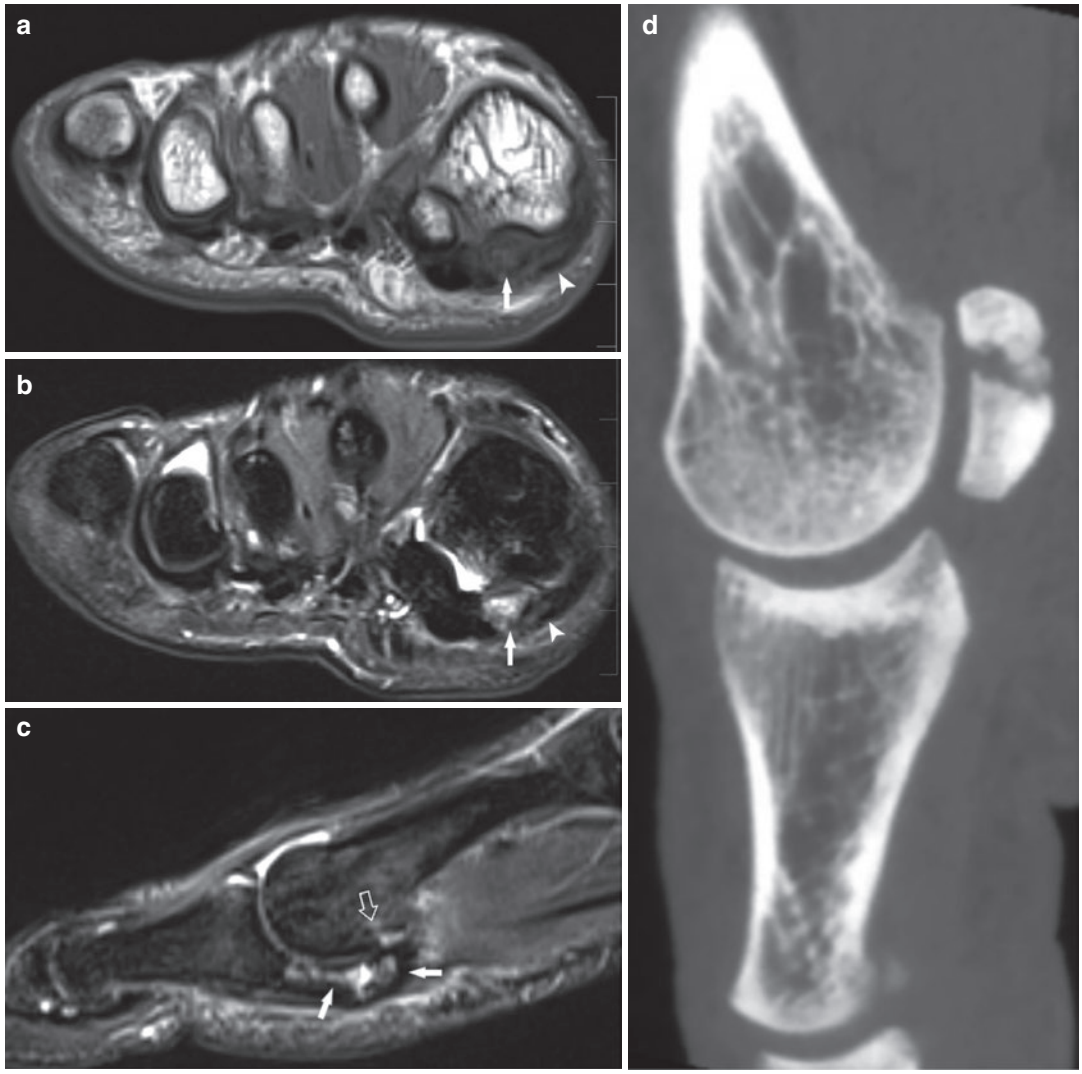

Fig. 22 Turf toe. (**a**) Coronal T1-WI and (**b–c**) coronal and sagittal FS T2-WI demonstrating disruption of the capsuloligamentous structures (arrowheads) with articular cartilage damage (open arrow) and BME (arrow). (**d**) Sagittal CT image showing the associated medial sesamoidal fracture

fatigue (end of game half) are more prone to acute injuries. Almost most muscle injuries are the consequence of an indirect trauma mechanism, often resulting in a muscle tear. Acute injuries commonly occur at the distal myotendinous junction of rectus femoris, proximal or distal myotendinous junction of biceps femoris, and myotendinous junction of the gastrocnemius-soleus (De Smet and Best 2000). Muscles that show high peak levels of stress are more vulnerable to injury: the rectus femoris muscle during shooting and the biceps femoris muscle during sprinting.

Clinically, acute muscle strains can be divided into three grades. For a more extensive overview on muscle injuries we refer to Gielen et al. (2021).

Imaging

Grade 1 injuries can appear normal at ultrasound, or may demonstrate a focal area of minimal fiber disruption (<5% cross-sectional area of the muscle) exhibiting ill-defined areas of increased echogenicity within the muscle (Peetrons 2002). MR imaging has a higher sensitivity to detect these lesions; a small area of ill-defined high signal representing interstitial edema and hemorrhage around the myotendinous junction on fluid-sensitive sequences can be observed, with a classic feathery appearance (Figs. 23 and 24). There is no substantial disruption of the muscle fibers (Robinson et al. 2017).

Grade 2 injuries are partial tears of the muscle fibers around the myotendinous junction with hematoma formation (Lee et al. 2012). On ultrasound partial muscle fiber disruption (>5% but <100% of the cross-sectional area of the muscle) is observed (Robinson et al. 2017). In the first 48 h, the intramuscular hematoma appears as an ill-defined muscle laceration separated by hypoechoic fluid and with increased reflectivity in the surrounding muscle. After 48–72 h, the hematoma will develop into a well-defined hypoechoic fluid collection with an echogenic margin, gradually enlarging and potentially filling the hematoma in a centripetal

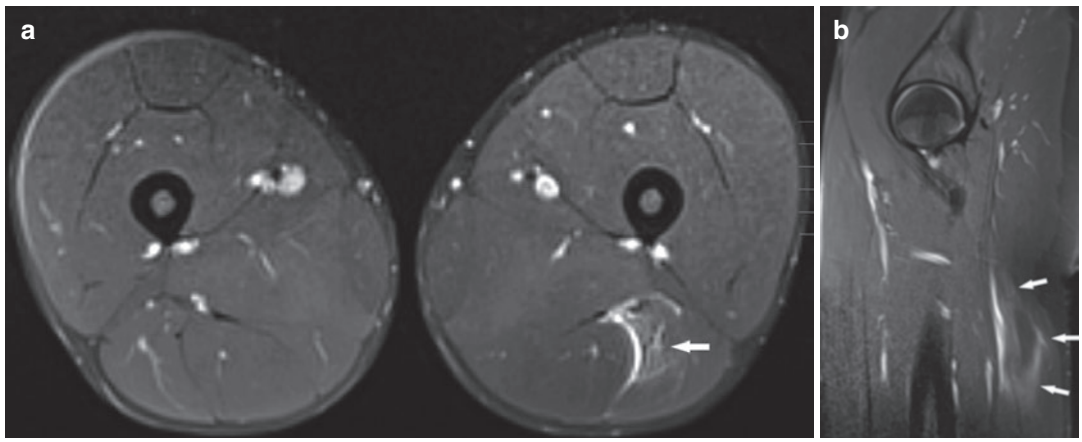

Fig. 23 Sprain (grade 1) hamstrings in an elite soccer player. (**a**) Axial FS PD-WI and (**b**) sagittal FS PD-WI demonstrating feather-like muscle edema and perifascial fluid (arrow), indicative of a grade 1 sprain, without muscle fiber disruption

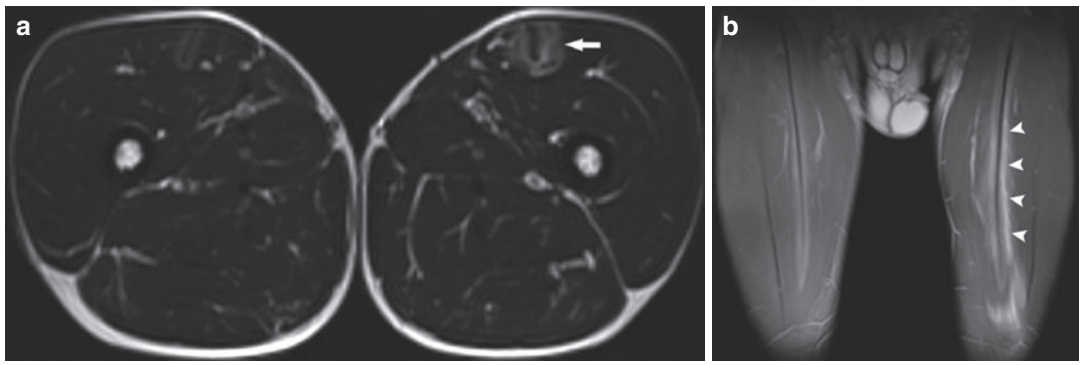

Fig. 24 Sprain (grade 1) along the myotendinous junction of the rectus femoris muscle. (**a**) Axial T1-WI demonstrating hyperintense signal intensity along the myotendinous junction of the rectus femoris muscle, reflecting hemorrhage (arrow). (**b**) Coronal FS T2-WI demonstrating edema along the entire length of the myotendinous junction (arrowheads)

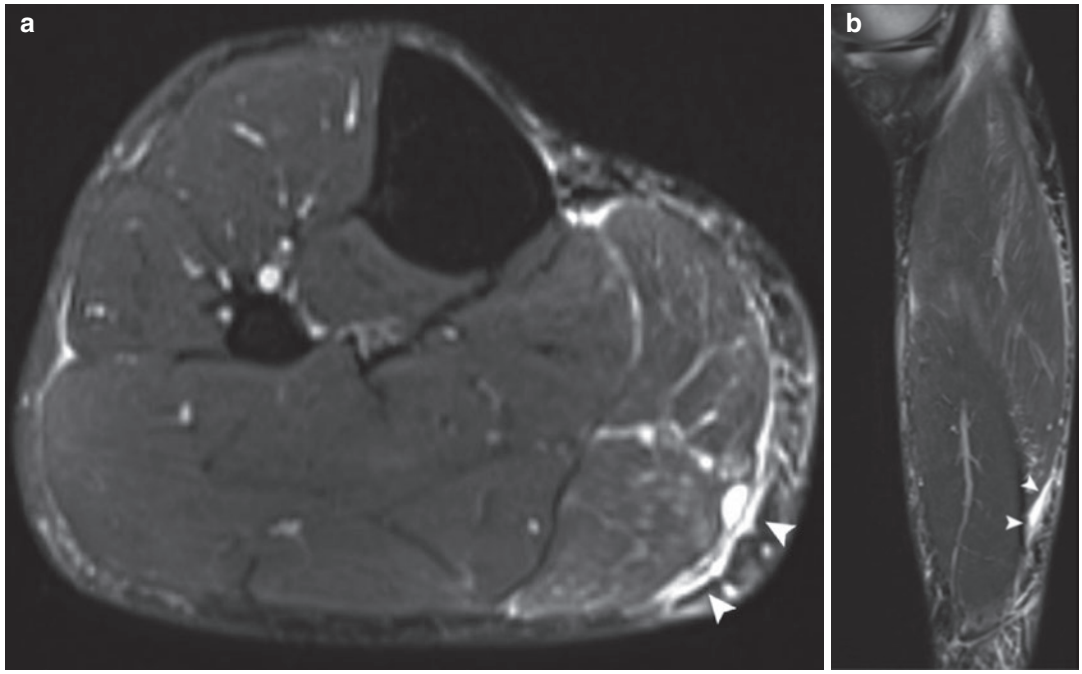

Fig. 25 Tear of the myotendinous junction of the medial gastrocnemius muscle. (**a**) Axial and (**b**) sagittal FS T2-WI demonstrating rupture of the medial gastrocnemius myotendinous junction, with proximal fiber retraction and perifascial fluid (arrowheads)

fashion (Lee et al. 2012). On MR imaging the partial fiber disruption is depicted as a focal area of well-defined high signal intensity on fluid-sensitive sequences (Fig. 25). The tendon adjacent to the myotendinous junction may be thickened and display features of laxity, and even partial tendon disruption may be depicted (Robinson et al. 2017).

Grade 3 injuries are a complete discontinuity or disruption of the muscle fibers with different degrees of muscle retraction. They are often clinically evident with a palpable gap between the retracted muscle ends. Ultrasound may demonstrate perifascial fluid, with possible increased echogenicity due to the presence of extravascular blood, but most often being hypoechoic because most ultrasound examinations occur more than 24 h after the injury. Ultrasound can increase the accuracy to differentiate between partial and complete tears by performing dynamic muscle maneuvers.

MR imaging depicts a complete disruption of the myotendinous junction with a local hematoma filling the gap created by the tear (Figs. 26 and 27) (Robinson et al. 2017).

Fig. 26 Avulsion of the proximal hamstrings complex. Coronal T2-WI of an avulsion of the proximal hamstrings (arrow) with distal retraction of the tendon fibers and fluid-filled gap

Imaging is important to grade the muscle injury, to describe the proportion and volume of the muscle injury, and to describe the length of

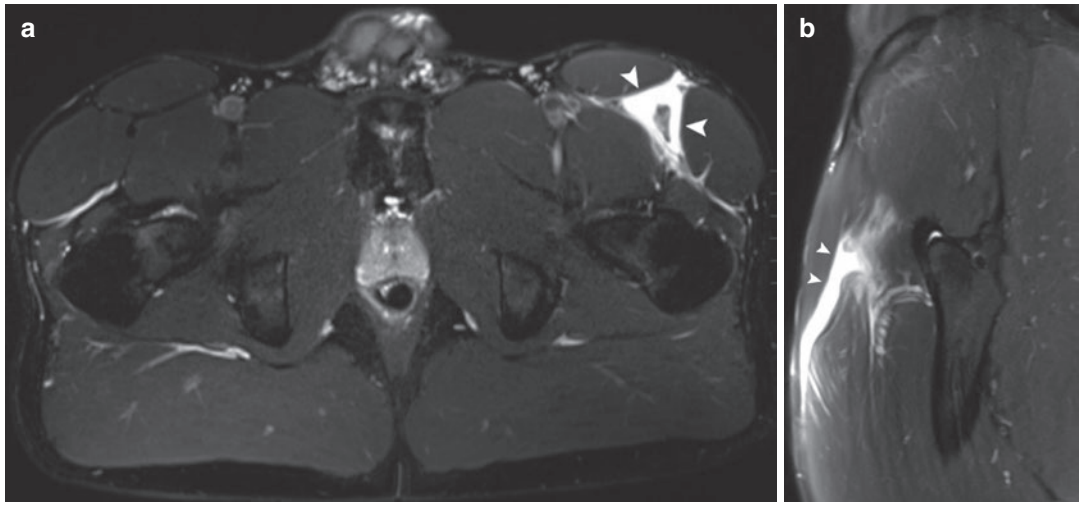

Fig. 27 Tear and avulsion of the rectus femoris insertion. (**a**) Axial and (**b**) sagittal FS T2-WI demonstrating a complete tear of the proximal insertion of the rectus femoris tendon of the AIIS, with distal retraction of the tendon and a fluid-filled gap (arrowheads)

the tear, all predictors for the time it will take for the player to return to competition. The longitudinal length of the muscle injury has the highest prognostic value, with an injury length of 10 mm correlating to approximately 30 days before return to competition (Thierfelder et al. 2019). A previous injury of a high-risk muscle increases the risk of another injury of the same muscle. In elite soccer players, 16% of muscle injuries are reinjuries, which imply a 30% longer layoff time (Thierfelder et al. 2019). An underestimated injury and the subsequent premature return to play are common reasons for recurrent muscle injuries. Also, an inadequate rehabilitation is a risk factor for muscle injuries in soccer players (Thierfelder et al. 2019). Currently there is no strong evidence that MR imaging is useful for predicting the time to return to sports following hamstring injury (Svensson et al. 2016). Recently it has been documented that the extent of edema in hamstring injuries does not have prognostic value in predicting the time to return to play (Crema et al. 2018).

Things to Remember

- Adductor-related groin pain is the most frequently encountered groin problem in soccer players, with the adductor longus being predominantly affected.
- Avulsions of the anterior superior and anterior inferior iliac spine in soccer, commonly observed in adolescent players, result from an excessive upward movement of the leg in "kicking the air" or a powerful shot at goal with maximum flexion of the hip and extension of the knee (Rossi and Dragoni 2001).
- An anterior cruciate ligament tear is the most common non-osseous injury among children who play soccer and more prevalent in girls and women. An ACL tear is associated with a longer return to play than any other typical soccer knee injury.
- Professional soccer players frequently miss training or matches each season due to muscle injuries. The most injured muscles in elite soccer players are muscles of thigh (hamstrings and quadriceps) and calf (gastrocnemius-soleus complex).

References

Anderson IF, Crichton KJ, Grattan-Smith T et al (1989) Osteochondral fractures of the dome of the talus. J Bone Joint Surg Am 71:1143–1152

Bhatia S, LaPrade CM, Ellman MB, LaPrade RF (2014) Meniscal root tears: significance, diagnosis, and treatment. Am J Sports Med 42:3016–3030. https://doi.org/10.1177/0363546514524162

Branci S, Thorborg K, Nielsen MB, Hölmich P (2013) Radiological findings in symphyseal and adductor-related groin pain in athletes: a critical review of the literature. Br J Sports Med 47:611–619. https://doi.org/10.1136/bjsports-2012-091905

Brophy RH, Backus S, Kraszewski AP et al (2010) Differences between sexes in lower extremity alignment and muscle activation during soccer kick. J Bone Jt Surgery Am 92:2050–2058. https://doi.org/10.2106/JBJS.I.01547

Caudill P, Nyland J, Smith C et al (2008) Sports hernias: a systematic literature review. Br J Sports Med 42: 954–964. https://doi.org/10.1136/bjsm.2008.047373

Chopra A, Robinson P (2016) Imaging athletic groin pain. Radiol Clin N Am 54:865–873. https://doi.org/10.1016/j.rcl.2016.04.007

Crema MD, Godoy IRB, Abdalla RJ (2018) Hamstring injuries in professional soccer players: extent of MRI-detected edema and the time to return to play. Sports Health 10:75–79. https://doi.org/10.1177/1941738117741471

Cunningham PM, Brennan D, O'Connell M et al (2007) Patterns of bone and soft-tissue injury at the symphysis pubis in soccer players: observations at MRI. AJR Am J Roentgenol 188:W291–W296. https://doi.org/10.2214/AJR.06.0051

Davis KW (2012) Imaging of the knee extensor mechanism. www.radiology.wisc.edu/people/davis/files/

De Loes M (1995) Epidemiology of sports injuries in the Swiss organization "Youth and Sports" 1987–1989. Injuries, exposure and risks of main diagnoses. Int J Sports Med 16:134–138. https://doi.org/10.1055/s-2007-972980

De Smet AA, Best TM (2000) MR imaging of the distribution and location of acute hamstring injuries in athletes. Am J Roentgenol 174:393–399. https://doi.org/10.2214/ajr.174.2.1740393

De Smet E, Van Dyck P, Gielen J, Vanhoenacker FM (2020) Sports-related meniscal injury. Med Radiol https://doi.org./10.1007/174_2020_244

Di Pietto F, Chianca V, Zappia M, Romano S (2018) Articular and peri-articular hip lesions in soccer players. The importance of imaging in deciding which lesions will need surgery and which can be treated conservatively? Eur J Radiol 105:227–238. https://doi.org/10.1016/j.ejrad.2018.06.012

Faude O, Junge A, Kindermann W, Dvorak J (2005) Injuries in female soccer players: a prospective study in the German national league. Am J Sports Med 33:1694–1700. https://doi.org/10.1177/0363546505275011

Gielen JLMA, Robinson P, Van Dyck P, Van der Stappen A, Vanhoenacker FM (2021) Muscle injuries. Med Radiol https://doi.org./10.1007/174_2020_247

Huysse WCJ, Verstraete KL, Verdonk PC, Verdonk R (2008) Meniscus imaging. Semin Musculoskelet Radiol 12: 318–333. https://doi.org/10.1055/s-0028-1100639

Johnson AC, Shaman MA, Ryan TG (2012) Femoroacetabular impingement in former high-level youth soccer players. Am J Sports Med 40:1342–1346. https://doi.org/10.1177/0363546512439287

Lee JC, Mitchell AWM, Healy JC (2012) Imaging of muscle injury in the elite athlete. Br J Radiol 85:1173–1185

Lee KS, Rosas HG, Phancao JP (2013) Snapping hip: imaging and treatment. Semin Musculoskelet Radiol 17:286–294. https://doi.org/10.1055/s-0033-1348095

Lundblad M, Waldén M, Magnusson H et al (2013) The UEFA injury study: 11-year data concerning 346 MCL injuries and time to return to play. Br J Sports Med 47:759–762. https://doi.org/10.1136/bjsports-2013-092305

Madani H, Robinson P (2019) Top-ten tips for imaging groin injury in athletes. Semin Musculoskelet Radiol 23:361–375. https://doi.org/10.1055/s-0039-1694754

Mascarenhas VV, Castro MO, Diana Afonso P (2020) Hip, pelvis and sacro-iliac joints. Med Radiol https://doi.org./10.1007/174_2020_256

McNally E, Thompson G (2020) Knee: ligaments and tendons. Med Radiol https://doi.org./10.1007/174_2020_255

Naraghi AM, White LM (2016) Imaging of athletic injuries of knee ligaments and menisci: sports imaging series. Radiology 281:23–40. https://doi.org/10.1148/radiol.2016152320

Nery C, Baumfeld D, Umans H, Yamada AF (2017) MR imaging of the plantar plate normal anatomy, turf toe, and other injuries. Magn Reson Imaging Clin N Am 25(1):127–144. https://doi.org/10.1016/j.mric.2016.08.007

Papavasiliou A, Siatras T, Bintoudi A et al (2014) The gymnasts' hip and groin: a magnetic resonance imaging study in asymptomatic elite athletes. Skelet Radiol 43:1071–1077. https://doi.org/10.1007/s00256-014-1885-7

Paterson A (2009) Soccer injuries in children. Pediatr Radiol 39:1286–1298. https://doi.org/10.1007/s00247-009-1416-1

Peetrons P (2002) Ultrasound of muscles. Eur Radiol 12:35–43. https://doi.org/10.1007/s00330-001-1164-6

Pesquer L, Poussange N, Sonnery-Cottet B et al (2016) Imaging of rectus femoris proximal tendinopathies. Skelet Radiol 45:889–897. https://doi.org/10.1007/s00256-016-2345-3

Pesquer L, Reboul G, Silvestre A et al (2015) Imaging of adductor-related groin pain. Diagn Interv Imaging 96:861–869. https://doi.org/10.1016/j.diii.2014.12.008

Pfirrmann CWA, Mengiardi B, Dora C et al (2006) Cam and pincer femoroacetabular impingement: characteristic MR arthrographic findings in 50 patients. Radiology 240:778–785. https://doi.org/10.1148/radiol.2403050767

Pirimoglu B, Ogul H, Polat G et al (2019) The comparison of direct magnetic resonance arthrography with volumetric interpolated breath-hold examination sequence and multidetector computed tomography arthrography techniques in detection of talar osteochondral lesions. Acta Orthop Traumatol Turc 53:209. https://doi.org/10.1016/J.AOTT.2019.03.012

Prasad R, Abdullah O, Robinson P (2021) Athletic groin pain. Med Radiol https://doi.org./10.1007/174_2020_254

Robinson P, Crema MD, Regatte RR et al (2017) Imaging of muscle injuries in sports medicine: sports imaging series. Radiology 282:646–663. https://doi.org/10.1148/radiol.2017160267

Robinson P, White LM (2005) The biomechanics and imaging of soccer injuries. Semin Musculoskelet Radiol 9:397–420

Rosas HG (2014) Magnetic resonance imaging of the meniscus. Magn Reson Imaging Clin NA 22:493–516. https://doi.org/10.1016/j.mric.2014.07.002

Rossi F, Dragoni S (2001) Acute avulsion fractures of the pelvis in adolescent competitive athletes: prevalence, location and sports distribution of 203 cases collected. Skelet Radiol 30:127–131. https://doi.org/10.1007/s002560000319

Schein AJ, Skalski MR, Patel DB et al (2015) Turf toe and sesamoiditis: what the radiologist needs to know. Clin Imaging 39:380–389. https://doi.org/10.1016/j.clinimag.2014.11.011

Schmid MR, Pfirrmann CWA, Hodler J et al (2003) Cartilage lesions in the ankle joint: comparison of MR arthrography and CT arthrography. Skelet Radiol 32:259–265. https://doi.org/10.1007/s00256-003-0628-y

Schmitz MR, Campbell SE, Fajardo RS, Kadrmas WR (2012) Identification of acetabular labral pathological changes in asymptomatic volunteers using optimized, noncontrast 1.5-T magnetic resonance imaging. Am J Sports Med 40:1337–1341. https://doi.org/10.1177/0363546512439991

Söderman K, Pietilä T, Alfredson H, Werner S (2002) Anterior cruciate ligament injuries in young females playing soccer at senior levels. Scand J Med Sci Sports 12:65–68

Sutter R, Pfirrmann CWA (2013) Atypical hip impingement. Am J Roentgenol 201

Svensson K, Alricsson M, Eckerman M et al (2016) The correlation between the imaging characteristics of hamstring injury and time required before returning to sports: a literature review. J Exerc Rehabil 12:134–142

Tak I, Langhout R (2014) Groin injury in soccer. Aspeter Sport Med J 3:272–277

Thierfelder KM, Gerhardt JS, Gemescu IN et al (2019) Imaging of hip and thigh musscle injury: a pictorial review. Insights Imaging 10:1–9

Tyler TF, Silvers HJ, Gerhardt MB, Nicholas SJ (2010) Groin injuries in sports medicine. Sports Health 2:231–236. https://doi.org/10.1177/1941738110366820

Van Dyck P, De Smet E, Veryser J et al (2012) Partial tear of the anterior cruciate ligament of the knee: injury patterns on MR imaging. Knee Surg Sport Traumatol Arthrosc 20:256–261. https://doi.org/10.1007/s00167-011-1617-7

Van Dyck P, Vanhoenacker FM, Gielen JL et al (2011) Three tesla magnetic resonance imaging of the anterior cruciate ligament of the knee: can we differentiate complete from partial tears? Skelet Radiol 40:701–707. https://doi.org/10.1007/s00256-010-1044-8

Van Royen A, Shahabpour M, Al Jahed D, Abid W, Vanhoenacker F, De Maeseneer M (2020) Injuries of the ligaments and tendons in ankle and foot. Med Radiol https://doi.org./10.1007/174_2020_257

Weir A, Brukner P, Delahunt E et al (2015) Doha agreement meeting on terminology and definitions in groin pain in athletes. Br J Sports Med 49:768–774. https://doi.org/10.1136/bjsports-2015-094869

Yu JS, Popp JE, Kaeding CC, Lucas J (1995) Correlation of MR imaging and pathologic findings in athletes undergoing surgery for chronic patellar tendinitis. Am J Roentgenol 165:115–118. https://doi.org/10.2214/ajr.165.1.7785569

Zoga AC, Kavanagh EC, Omar IM et al (2008) Athletic pubalgia and the "sports hernia": MR imaging findings. Radiology 247:797–807. https://doi.org/10.1148/radiol.2473070049